

Wireless Communications and Mobile Computing

# Internet of Things in Multimedia Communication Systems

Lead Guest Editor: Deepak Gupta

Guest Editors: Rohit Sharma, Danda B. Rawat, and Amiya Nayak





---

# **Internet of Things in Multimedia Communication Systems**



Wireless Communications and Mobile Computing

---

## **Internet of Things in Multimedia Communication Systems**

Lead Guest Editor: Deepak Gupta

Guest Editors: Rohit Sharma, Danda B. Rawat, and  
Amiya Nayak





Copyright © 2023 Hindawi Limited. All rights reserved.

This is a special issue published in “Wireless Communications and Mobile Computing.” All articles are open access articles distributed under the Creative Commons Attribution License, which permits unrestricted use, distribution, and reproduction in any medium, provided the original work is properly cited.

# Chief Editor

Zhipeng Cai , USA

## Associate Editors

Ke Guan , China  
Jaime Lloret , Spain  
Maode Ma , Singapore

## Academic Editors

Muhammad Inam Abbasi, Malaysia  
Ghufran Ahmed , Pakistan  
Hamza Mohammed Ridha Al-Khafaji ,  
Iraq  
Abdullah Alamoodi , Malaysia  
Marica Amadeo, Italy  
Sandhya Aneja, USA  
Mohd Dilshad Ansari, India  
Eva Antonino-Daviu , Spain  
Mehmet Emin Aydin, United Kingdom  
Parameshchhari B. D. , India  
Kalapraveen Bagadi , India  
Ashish Bagwari , India  
Dr. Abdul Basit , Pakistan  
Alessandro Bazzi , Italy  
Zdenek Becvar , Czech Republic  
Nabil Benamar , Morocco  
Olivier Berder, France  
Petros S. Bithas, Greece  
Dario Bruneo , Italy  
Jun Cai, Canada  
Xuesong Cai, Denmark  
Gerardo Canfora , Italy  
Rolando Carrasco, United Kingdom  
Vicente Casares-Giner , Spain  
Brijesh Chaurasia, India  
Lin Chen , France  
Xianfu Chen , Finland  
Hui Cheng , United Kingdom  
Hsin-Hung Cho, Taiwan  
Ernestina Cianca , Italy  
Marta Cimitile , Italy  
Riccardo Colella , Italy  
Mario Collotta , Italy  
Massimo Condoluci , Sweden  
Antonino Crivello , Italy  
Antonio De Domenico , France  
Floriano De Rango , Italy

Antonio De la Oliva , Spain  
Margot Deruyck, Belgium  
Liang Dong , USA  
Praveen Kumar Donta, Austria  
Zhuojun Duan, USA  
Mohammed El-Hajjar , United Kingdom  
Oscar Esparza , Spain  
Maria Fazio , Italy  
Mauro Femminella , Italy  
Manuel Fernandez-Veiga , Spain  
Gianluigi Ferrari , Italy  
Luca Foschini , Italy  
Alexandros G. Fragkiadakis , Greece  
Ivan Ganchev , Bulgaria  
Óscar García, Spain  
Manuel García Sánchez , Spain  
L. J. García Villalba , Spain  
Miguel Garcia-Pineda , Spain  
Piedad Garrido , Spain  
Michele Girolami, Italy  
Mariusz Glabowski , Poland  
Carles Gomez , Spain  
Antonio Guerrieri , Italy  
Barbara Guidi , Italy  
Rami Hamdi, Qatar  
Tao Han, USA  
Sherief Hashima , Egypt  
Mahmoud Hassaballah , Egypt  
Yejun He , China  
Yixin He, China  
Andrej Hrovat , Slovenia  
Chunqiang Hu , China  
Xuexian Hu , China  
Zhenghua Huang , China  
Xiaohong Jiang , Japan  
Vicente Julian , Spain  
Rajesh Kaluri , India  
Dimitrios Katsaros, Greece  
Muhammad Asghar Khan, Pakistan  
Rahim Khan , Pakistan  
Ahmed Khattab, Egypt  
Hasan Ali Khattak, Pakistan  
Mario Kolberg , United Kingdom  
Meet Kumari, India  
Wen-Cheng Lai , Taiwan







Jose M. Lanza-Gutierrez, Spain  
Pavlos I. Lazaridis , United Kingdom  
Kim-Hung Le , Vietnam  
Tuan Anh Le , United Kingdom  
Xianfu Lei, China  
Jianfeng Li , China  
Xiangxue Li , China  
Yaguang Lin , China  
Zhi Lin , China  
Liu Liu , China  
Mingqian Liu , China  
Zhi Liu, Japan  
Miguel López-Benítez , United Kingdom  
Chuanwen Luo , China  
Lu Lv, China  
Basem M. ElHalawany , Egypt  
Imadeldin Mahgoub , USA  
Rajesh Manoharan , India  
Davide Mattera , Italy  
Michael McGuire , Canada  
Weizhi Meng , Denmark  
Klaus Moessner , United Kingdom  
Simone Morosi , Italy  
Amrit Mukherjee, Czech Republic  
Shahid Mumtaz , Portugal  
Giovanni Nardini , Italy  
Tuan M. Nguyen , Vietnam  
Petros Nicolitidis , Greece  
Rajendran Parthiban , Malaysia  
Giovanni Pau , Italy  
Matteo Petracca , Italy  
Marco Picone , Italy  
Daniele Pinchera , Italy  
Giuseppe Piro , Italy  
Javier Prieto , Spain  
Umair Rafique, Finland  
Maheswar Rajagopal , India  
Sujan Rajbhandari , United Kingdom  
Rajib Rana, Australia  
Luca Reggiani , Italy  
Daniel G. Reina , Spain  
Bo Rong , Canada  
Mangal Sain , Republic of Korea  
Praneet Saurabh , India





Hans Schotten, Germany  
Patrick Seeling , USA  
Muhammad Shafiq , China  
Zaffar Ahmed Shaikh , Pakistan  
Vishal Sharma , United Kingdom  
Kaize Shi , Australia  
Chakchai So-In, Thailand  
Enrique Stevens-Navarro , Mexico  
Sangeetha Subbaraj , India  
Tien-Wen Sung, Taiwan  
Suhua Tang , Japan  
Pan Tang , China  
Pierre-Martin Tardif , Canada  
Sreenath Reddy Thummaluru, India  
Tran Trung Duy , Vietnam  
Fan-Hsun Tseng, Taiwan  
S Velliangiri , India  
Quoc-Tuan Vien , United Kingdom  
Enrico M. Vitucci , Italy  
Shaohua Wan , China  
Dawei Wang, China  
Huaqun Wang , China  
Pengfei Wang , China  
Dapeng Wu , China  
Huaming Wu , China  
Ding Xu , China  
YAN YAO , China  
Jie Yang, USA  
Long Yang , China  
Qiang Ye , Canada  
Changyan Yi , China  
Ya-Ju Yu , Taiwan  
Marat V. Yuldashev , Finland  
Sherali Zeadally, USA  
Hong-Hai Zhang, USA  
Jiliang Zhang, China  
Lei Zhang, Spain  
Wence Zhang , China  
Yushu Zhang, China  
Kechen Zheng, China  
Fuhui Zhou , USA  
Meiling Zhu, United Kingdom  
Zhengyu Zhu , China


# Contents


**Retracted: A Detailed Research on Human Health Monitoring System Based on Internet of Things**  
Wireless Communications and Mobile Computing  
Retraction (1 page), Article ID 9863259, Volume 2023 (2023)

**Retracted: Research on the Difficulties and Countermeasures of the Practical Teaching of Ideological and Political Theory Courses in Colleges and Universities Based on Wireless Communication and Artificial Intelligence Decision Support**  
Wireless Communications and Mobile Computing  
Retraction (1 page), Article ID 9841638, Volume 2023 (2023)


**Intrusion Detection System on IoT with 5G Network Using Deep Learning**  
Neha Yadav , Sagar Pande , Aditya Khamparia , and Deepak Gupta   
Research Article (13 pages), Article ID 9304689, Volume 2022 (2022)




**Application of Cable Climbing Robot Automation Control Technology in Bridge Cable Measuring System**  
Weihua Zhou , Junqi Bao , Zhenzhi Liu , and Zhengda Chen   
Research Article (7 pages), Article ID 2453144, Volume 2022 (2022)

**Security-Level Improvement of IoT-Based Systems Using Biometric Features**  
Masoud Moradi, Masoud Moradkhani , and Mohammad Bagher Tavakoli  
Research Article (15 pages), Article ID 8051905, Volume 2022 (2022)

**Application of the Blockchain Technology in the Vertical Value Chain Management of Enterprises**  
Yang Wang , Yiqi Wang, and Yi Zhang  
Research Article (13 pages), Article ID 2408027, Volume 2022 (2022)

**Acclimatization of Nanorobots in Medical Applications Using the Artificial Intelligence System with the Data Transfer Approach**  
Hariprasath Manoharan, Yuvaraja Teekaraman , Ramya Kuppusamy , Arun Radhakrishnan , and K. Hariprasath Venkatachalam  
Research Article (8 pages), Article ID 5877042, Volume 2022 (2022)

**Design of the Secure Smart Home System Based on the Blockchain and Cloud Service**  
Kun Liao   
Research Article (12 pages), Article ID 4393314, Volume 2022 (2022)

**Foundation Reinforcement Method of Railway Logistics Center Station Based on Deformation Control and Thermodynamics**  
Zhiping Peng , Xiumiao Liu , and Kuangying Zhao   
Research Article (10 pages), Article ID 6340064, Volume 2022 (2022)


**Application of Blockchain Technology in Value Chain of Procurement in Manufacturing Enterprises**  
Yang Wang , Sichun Men, and Tingting Guo  
Research Article (8 pages), Article ID 1674412, Volume 2021 (2021)

### **Research on Video Quality Diagnosis Technology Based on Artificial Intelligence and Internet of Things**

Zhidong Sun , Jie Sun , and Xueqing Li 






Research Article (6 pages), Article ID 2460916, Volume 2021 (2021)

### **Simulation Research on Risks of Entrepreneurship Platform Organization Complex Network**

Chun Huang 

Research Article (12 pages), Article ID 3606812, Volume 2021 (2021)

### **IoT-Enabled Big Data Analytics Architecture for Multimedia Data Communications**

Muhammad Babar , Mohammad Dahman Alshehri , Muhammad Usman Tariq, Fasee Ullah , Atif Khan , M. Irfan Uddin , and Ahmed S. Almasoud


Research Article (9 pages), Article ID 5283309, Volume 2021 (2021)

### **Wireless Image Transmission Interference Signal Recognition System Based on Deep Learning**

Zhijun Guo  and Shuai Liu


Research Article (7 pages), Article ID 8024953, Volume 2021 (2021)

### **Drive System Design for Small Autonomous Electric Vehicle: Topology Optimization and Simulation**

Zhongming Wu , Mufangzhou Zhu, Yu Guo, Li Sun, and Yuchen Gu

Research Article (12 pages), Article ID 7192484, Volume 2021 (2021)

### **A New Method of Identifying Graphite Based on Neural Network**

Guangjun Liu , Xiaoping Xu, Xiangjia Yu, and Feng Wang

Research Article (10 pages), Article ID 4716430, Volume 2021 (2021)

### **A Novel, Efficient, and Secure Anomaly Detection Technique Using DWU-ODBN for IoT-Enabled Multimedia Communication Systems**

M. Sathya , M. Jeyaselvi, Lalitha Krishnasamy , Mohammad Mazyad Hazzazi , Prashant Kumar Shukla, Piyush Kumar Shukla , and Stephen Jeswinde Nuagah 








Research Article (12 pages), Article ID 4989410, Volume 2021 (2021)

### **Evaluating Technological Innovation of Media Companies from the Perspective of Technological Ecosystem**

Kui Yi , Ligang Zhang , Xiulan Mao , Yi Li , and Jiaxuan Bao 

Research Article (8 pages), Article ID 4170619, Volume 2021 (2021)

### **Current-Fed Bidirectional DC-DC Converter Topology for Wireless Charging System Electrical Vehicle Applications**



Partha Sarathi Subudhi , M. Thilagaraj , C. S. Sundar Ganesh , S. Diwakaran , P. Naveen , Saravanakumar Gurusamy , and M. Pallikonda Rajasekaran 

Research Article (15 pages), Article ID 1144453, Volume 2021 (2021)




# Contents

## **An Improved Simulated Annealing Particle Swarm Optimization Algorithm for Path Planning of Mobile Robots Using Mutation Particles**

Jianzhang Lu  and Zhihao Zhang 


Research Article (12 pages), Article ID 2374712, Volume 2021 (2021)

## **[Retracted] Research on the Difficulties and Countermeasures of the Practical Teaching of Ideological and Political Theory Courses in Colleges and Universities Based on Wireless Communication and Artificial Intelligence Decision Support**

Chaozhen Tang 


Research Article (7 pages), Article ID 3229051, Volume 2021 (2021)

## **Positioning Control Algorithm of Vehicle Navigation System Based on Wireless Tracking Technology**

Leibing Yan 


Research Article (11 pages), Article ID 8620409, Volume 2021 (2021)

## **Optimization of Hotel Financial Management Information System Based on Computational Intelligence**

Hongmei Ma 



Research Article (11 pages), Article ID 8680306, Volume 2021 (2021)

## **Research on Enterprise Financial Customer Classification Method and Preference Based on Intelligent Algorithm**

Ze Fu, Bo Zhang , Lingjun Ou, Kaiyang Sun, Xinyi Sun, and Ningyan Chen

Research Article (11 pages), Article ID 6585486, Volume 2021 (2021)

## **A Vehicle Detection Model Based on 5G-V2X for Smart City Security Perception**

Teng Liu, Cheng Xu , Hongzhe Liu , Xuwei Li, and Pengfei Wang




Research Article (11 pages), Article ID 5237568, Volume 2021 (2021)

## **Evaluation Method of Chemical Technology Safety Practical Operation Ability Based on Stochastic Model**

Xiaotong Wang 

Research Article (8 pages), Article ID 7060339, Volume 2021 (2021)

## **Polygon Number Algorithm for Peak-to-Average Ratio Reduction of Massive 5G Systems Using Modified Partial Transmit Sequence Scheme**

Hayder Alkatrani, Muhammad Ilyas , Salam Alyassri, Ali Nahar, Fadi Al-Turjman , Jawad Rasheed , Ali Alshahrani, and Basil Al-Kasasbeh


Research Article (10 pages), Article ID 7498240, Volume 2021 (2021)

## **Optimization Method of Art Design Resource Scheduling for 6G Network Environment in Colleges and Universities**

Meng Zhou  and Dong Yang


Research Article (8 pages), Article ID 3380867, Volume 2021 (2021)

**Automatic Roadblock Identification Algorithm for Unmanned Vehicles Based on Binocular Vision**

Liang Fang , Zhiwei Guan, and Jinghua Li



Research Article (7 pages), Article ID 3333754, Volume 2021 (2021)

**Green Product Market Development Strategy of Mobile Network Group Buying Community: Based on Three-Party Evolutionary Game and Simulation Analysis**

Zhihong Ai 






Research Article (11 pages), Article ID 4746723, Volume 2021 (2021)

**Research on the Application of Internet of Things and VR Technology in the Protection and Development of Shouzhou Kiln**

Xuelian Yu  and Yajun Zhang 




Research Article (9 pages), Article ID 2352988, Volume 2021 (2021)

**A Real-Time and Long-Term Face Tracking Method Using Convolutional Neural Network and Optical Flow in IoT-Based Multimedia Communication Systems**

Hanchi Ren, Yi Hu , San Hlaing Myint, Kun Hou , Xiuyu Zhang, Min Zuo, Chi Zhang , Qingchuan Zhang , and Haipeng Li 

Research Article (15 pages), Article ID 6711561, Volume 2021 (2021)

**Internet of Things-Based Smart Electricity Monitoring and Control System Using Usage Data**

Mohammad Kamrul Hasan , Musse Mohamud Ahmed, Bishwajeet Pandey , Hardik Gohel, Shayla Islam , and Izzul Fitrie Khalid


Research Article (16 pages), Article ID 6544649, Volume 2021 (2021)

**A Recommendation Model for College Career Entrepreneurship Projects Based on Deep Learning**

Yuan Feng and Weixian Huang 

Research Article (13 pages), Article ID 1418333, Volume 2021 (2021)

**Resource Sharing of Smart City Based on Blockchain**

Tao Huang 



Research Article (11 pages), Article ID 5886024, Volume 2021 (2021)

**Synchronized Information Acquisition Method for Virtual Geographic Scene Image Synthesis in Cities Based on Wireless Network Technology**

Tianfang Ma  and Shuoyan Liu


Research Article (7 pages), Article ID 9357427, Volume 2021 (2021)

**An Effective Fault-Tolerant Intrusion Detection System under Distributed Environment**

Bo Hong , Hui Wang , and Zijian Cao

Research Article (9 pages), Article ID 2716881, Volume 2021 (2021)

**Lightweight Automatic Identification and Location Detection Model of Farmland Pests**

Kunpeng Li, Junsheng Zhu, and Nianqiang Li 

Research Article (11 pages), Article ID 9937038, Volume 2021 (2021)

# Contents

## **Dynamic Gesture Contour Feature Extraction Method Using Residual Network Transfer Learning**

Xianmin Ma and Xiaofeng Li 


Research Article (11 pages), Article ID 1503325, Volume 2021 (2021)

## **Influence of Hayao Miyazaki's Animation on the Cross-Cultural Spread of Japanese Traditional Culture under the Background of 5G and Wireless Communication**

Chenmei Li 







Research Article (5 pages), Article ID 1640983, Volume 2021 (2021)

## **The Application of Virtual Reality Technology on Intelligent Traffic Construction and Decision Support in Smart Cities**

Gongxing Yan and Yanping Chen 


Research Article (9 pages), Article ID 3833562, Volume 2021 (2021)

## **An Efficient Method for Choosing Digital Cluster Size in Ultralow Latency Networks**

Alexander Paramonov , Mashael Khayyat , Natalia Chistova, Ammar Muthanna , Ibrahim A. Elgendy , Andrey Koucheryavy , and Ahmed A. Abd El-Latif 


Research Article (9 pages), Article ID 9188658, Volume 2021 (2021)

## **Key Technologies of Cache and Computing in 5G Mobile Communication Network**

Yanfang Zha 

Research Article (11 pages), Article ID 3099272, Volume 2021 (2021)

## **A Machine Learning Approach for Improving the Movement of Humanoid NAO's Gaits**

Fatmah Abdulrahman Baothman 

Research Article (14 pages), Article ID 1496364, Volume 2021 (2021)

## **Study and Analysis of Multiconnectivity for Ultrareliable and Low-Latency Features in Networks and V2X Communications**

Alexander Paramonov , Jialiang Peng , Dmitry Kashkarov, Ammar Muthanna , Ibrahim A.

Elgendy , Andrey Koucheryavy , Yassine Maleh , and Ahmed A. Abd El-Latif 

Research Article (10 pages), Article ID 1718099, Volume 2021 (2021)

## **[Retracted] A Detailed Research on Human Health Monitoring System Based on Internet of Things**

Lei Ru , Bin Zhang , Jing Duan , Guo Ru , Ashutosh Sharma , Gaurav Dhiman, Gurjot Singh Gaba , Emad Sami Jaha, and Mehedi Masud 

Research Article (9 pages), Article ID 5592454, Volume 2021 (2021)



## Retraction

# Retracted: A Detailed Research on Human Health Monitoring System Based on Internet of Things

### Wireless Communications and Mobile Computing

Received 8 August 2023; Accepted 8 August 2023; Published 9 August 2023

Copyright © 2023 Wireless Communications and Mobile Computing. This is an open access article distributed under the Creative Commons Attribution License, which permits unrestricted use, distribution, and reproduction in any medium, provided the original work is properly cited.

This article has been retracted by Hindawi following an investigation undertaken by the publisher [1]. This investigation has uncovered evidence of one or more of the following indicators of systematic manipulation of the publication process:

- (1) Discrepancies in scope
- (2) Discrepancies in the description of the research reported
- (3) Discrepancies between the availability of data and the research described
- (4) Inappropriate citations
- (5) Incoherent, meaningless and/or irrelevant content included in the article
- (6) Peer-review manipulation

The presence of these indicators undermines our confidence in the integrity of the article's content and we cannot, therefore, vouch for its reliability. Please note that this notice is intended solely to alert readers that the content of this article is unreliable. We have not investigated whether authors were aware of or involved in the systematic manipulation of the publication process.

In addition, our investigation has also shown that one or more of the following human-subject reporting requirements has not been met in this article: ethical approval by an Institutional Review Board (IRB) committee or equivalent, patient/participant consent to participate, and/or agreement to publish patient/participant details (where relevant).

Wiley and Hindawi regrets that the usual quality checks did not identify these issues before publication and have since put additional measures in place to safeguard research integrity.

We wish to credit our own Research Integrity and Research Publishing teams and anonymous and named external

researchers and research integrity experts for contributing to this investigation.

The corresponding author, as the representative of all authors, has been given the opportunity to register their agreement or disagreement to this retraction. We have kept a record of any response received.

### References

- [1] L. Ru, B. Zhang, J. Duan et al., "A Detailed Research on Human Health Monitoring System Based on Internet of Things," *Wireless Communications and Mobile Computing*, vol. 2021, Article ID 5592454, 9 pages, 2021.

## Retraction

# Retracted: Research on the Difficulties and Countermeasures of the Practical Teaching of Ideological and Political Theory Courses in Colleges and Universities Based on Wireless Communication and Artificial Intelligence Decision Support

### Wireless Communications and Mobile Computing

Received 1 August 2023; Accepted 1 August 2023; Published 2 August 2023

Copyright © 2023 Wireless Communications and Mobile Computing. This is an open access article distributed under the Creative Commons Attribution License, which permits unrestricted use, distribution, and reproduction in any medium, provided the original work is properly cited.

This article has been retracted by Hindawi following an investigation undertaken by the publisher [1]. This investigation has uncovered evidence of one or more of the following indicators of systematic manipulation of the publication process:

- (1) Discrepancies in scope
- (2) Discrepancies in the description of the research reported
- (3) Discrepancies between the availability of data and the research described
- (4) Inappropriate citations
- (5) Incoherent, meaningless and/or irrelevant content included in the article
- (6) Peer-review manipulation

The presence of these indicators undermines our confidence in the integrity of the article's content and we cannot, therefore, vouch for its reliability. Please note that this notice is intended solely to alert readers that the content of this article is unreliable. We have not investigated whether authors were aware of or involved in the systematic manipulation of the publication process.

In addition, our investigation has also shown that one or more of the following human-subject reporting requirements has not been met in this article: ethical approval by an Institutional Review Board (IRB) committee or equivalent, patient/participant consent to participate, and/or agreement to publish patient/participant details (where relevant).

Wiley and Hindawi regrets that the usual quality checks did not identify these issues before publication and have since put additional measures in place to safeguard research integrity.

We wish to credit our own Research Integrity and Research Publishing teams and anonymous and named external researchers and research integrity experts for contributing to this investigation.

The corresponding author, as the representative of all authors, has been given the opportunity to register their agreement or disagreement to this retraction. We have kept a record of any response received.

### References

- [1] C. Tang, "Research on the Difficulties and Countermeasures of the Practical Teaching of Ideological and Political Theory Courses in Colleges and Universities Based on Wireless Communication and Artificial Intelligence Decision Support," *Wireless Communications and Mobile Computing*, vol. 2021, Article ID 3229051, 7 pages, 2021.

## Research Article

# Intrusion Detection System on IoT with 5G Network Using Deep Learning

Neha Yadav <sup>1</sup>, Sagar Pande <sup>1</sup>, Aditya Khamparia <sup>2</sup>, and Deepak Gupta <sup>3</sup>

<sup>1</sup>*School of Computer Science, Lovely Professional University, Phagwara, Punjab, India*

<sup>2</sup>*Department of Computer Science, Babasaheb Bhimrao Ambedkar University (Central University), Satellite Centre, Amethi, UP, India*

<sup>3</sup>*Department of Computer Science and Engineering, Maharaja Agrasen Institute of Technology, Delhi, India*

Correspondence should be addressed to Deepak Gupta; [deepakgupta@mait.ac.in](mailto:deepakgupta@mait.ac.in)

Received 15 June 2021; Revised 14 February 2022; Accepted 17 February 2022; Published 10 March 2022

Academic Editor: Carles Gomez

Copyright © 2022 Neha Yadav et al. This is an open access article distributed under the Creative Commons Attribution License, which permits unrestricted use, distribution, and reproduction in any medium, provided the original work is properly cited.

The Internet of Things (IoT) cyberattacks of fully integrated servers, applications, and communications networks are increasing at exponential speed. As problems caused by the Internet of Things network remain undetected for longer periods, the efficiency of sensitive devices harms end users, increases cyber threats and identity misuses, increases costs, and affects revenue. For productive safety and security, Internet of Things interface assaults must be observed nearly in real time. In this paper, a smart intrusion detection system suited to detect Internet of Things-based attacks is implemented. In particular, to detect malicious Internet of Things network traffic, a deep learning algorithm has been used. The identity solution ensures the security of operation and supports the Internet of Things connectivity protocols to interoperate. An intrusion detection system (IDS) is one of the popular types of network security technology that is used to secure the network. According to our experimental results, the proposed architecture for intrusion detection will easily recognize real global intruders. The use of a neural network to detect attacks works exceptionally well. In addition, there is an increasing focus on providing user-centric cybersecurity solutions, which necessitate the collection, processing, and analysis of massive amounts of data traffic and network connections in 5G networks. After testing, the autoencoder model, which effectively reduces detection time as well as effectively improves detection precision, has outperformed. Using the proposed technique, 99.76% of accuracy was achieved.

## 1. Introduction

Deep learning frameworks became an active field for the role of network intrusion detection in cybersecurity. While many excellent surveys cover a growing research field on this topic, the literature fails to make an impartial comparison of different deep learning models, especially in recent datasets for intrusion detection, in a controlled setting. Cybersecurity is a critical issue in today's world [1, 2]. Firewalls, for example, have long been used to secure data confidential information [1]. IDS analyses network traffic or a specific computer environment to detect signs of malicious action [2]. The rapid growth in interest in artificial intelligence (AI) development has resulted in major advances in mechanisms including pattern recognition and anomaly detection.

For these issues, neural networks are a suitable option, so their use is no longer limited. This is largely due to higher in the number of computing resources available. This situation caused researchers to make changes to neural network architectures to incorporate or improve IDS [3–5].

*1.1. Internet of Things Devices Using 5G Networks.* 5G is a key to the Internet of Things although it provides a faster network with greater capacity to meet connectivity needs. The 5G spectrum broadens the frequencies used by mobile communication technologies to transmit data. Because there is a wide range available for use, a whole bandwidth of mobile networks rises, enabling more devices to connect. To resolve current issues, 5G certainly requires control of the response period of the network and network infrastructure. Notice that



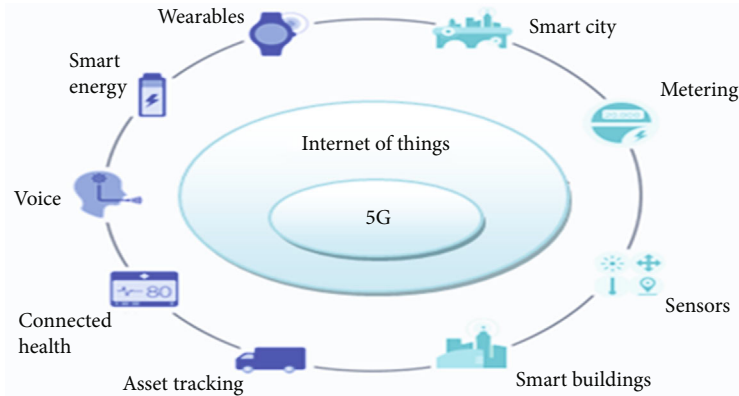


FIGURE 1: Applications of Internet of Things [5].

the model Internet of Things has a different system of interaction technology, including wireless sensor networks. Therefore, in this case, the role of fog calculation is also evident. Fog computing or fogging mostly consists of effective distribution of data, transmission, stocking, and applications between data sources and the cloud, through a decentralized networking and computing framework. Various applications of 5G network are depicted in Figure 1 which was reproduced from the article [5].

*1.2. The Architecture of 5G Technology.* 5G has an integrated infrastructure that usually updates network modules and terminals to include a new scenario. Advanced technology may often be used by service companies to easily take advantage of value-added offers. However, upgradability is based on cognitive radio technology which has many important characteristics such as the ability of devices to recognize their place, voice, sensors, health, energy, environment, temperature, etc. In its working environment, cognitive radio equipment works as a transceiver (beam) that can collect radio signals perceptually and respond to them. Furthermore, it detects changes in its environment automatically and thus responds to continuous continuity.

As soon as 4G becomes publicly accessible, package companies will be forced to adopt a 5G network [6]. To satisfy customer demands and resolve conflicts in the 5G environment, a fundamental change in the 5G wireless cellular technology growth is needed. According to the researchers' major findings in [7], the majority of wireless customers spend essentially 80% of their time indoors and 20% of their time outdoors (2018)). That is a narrow blend of both NFV and SDN innovations which are efficiently detected by 5G networks and cyberattacks that mitigate them. To address this challenge, a new concept or design technique for planning the 5G cellular architecture has emerged: distinguishing between outside and inside setups [8]. The accessibility loss across the building's boundaries will be slightly decreased with this design technique. The user details would be filtered by other user computers as in the device-to-device communications, so the anonymity of this information is the key concern. Closed access ensures the confidentiality of programs at the system stage. The sys-

tem lists such trustworthy devices as consumers situated near you or in your place of business, you know; otherwise, a trusted entity, e.g., an organization, will easily link and maintain a degree of confidentiality, whereas devices that are not included in this list can interact on the macrocell phase.

One of the important issues in 5G network lies in the component which is used in the designing as well as at the deployment phase, as every element needs authentication with all of the other elements in the network architecture even before initiating any operation, whereas in physical layer phase the network, components are also required to be developed through the trusty worthy network components. As the traffic on internet is growing continuously, the domain is also constantly updating 5G and IoT technologies, lot of security breaches are there which can be easily affected due to intrusion-based attacks like Denial-of-Service Attacks (DDoS) which can not only affect the application layer of the Open Systems Interconnection (OSI) model but also affects the network layer as well. In this paper, the dataset used for the implementation purpose consists of all such kinds of attacks which are feasible on not only 5G networks but also IoT-based system. Hence, a novel technique to detect such type of attacks is elaborated in Section 3 of this paper.

### 1.3. The Contribution of the Paper Is as Follows

- (i) Autoencoder-based novel deep learning technique is implemented for the detection of network attacks
- (ii) Several machine learning algorithms are used for implementation purposes
- (iii) A recent benchmark dataset is used for the implementation purpose
- (iv) A comparative analysis of the work with the existing framework has been provided

*1.4. The Structure of This Paper Is as Follows.* Section 2 outlines the literature review based upon various intrusion detection systems. The third section reveals the research

TABLE 1: Comparative analysis of various existing frameworks.

Year	Performance evaluation parameters	Dataset	Algorithm/technique/ approach	Findings
2017 [10]	Accuracy, precision, recall, F1	RedIRIS	RNN and CNN	In this work, the authors have improvised the existing deep learning algorithms by modifying the hidden layers.
2017 [11]	Accuracy, precision, recall, F1, FAR	KDD 99 Cup	GRU and RF	Minimizing the loss function has helped the researchers to achieve better results.
2018 [12]	Accuracy, precision, recall, F1 score, MR, FAR, detection time	UNSW_NBI5	BLSTM RNN	In this work, feature normalization and conversion of categorical features to numeric values have helped them to generate improvised results.
2018 [13]	Accuracy, precision, recall, F1 measure	NSL-KDD	DNN	In this work, SGD was used to minimize the loss function of DNN.
2019 [14]	Accuracy, precision, recall	CICIDS2017	MLP, 1d-CNN, LSTM, and CNN+LSTM	In this work, researchers have balanced the dataset by performing data processing in which they have duplicated the records.
2019 [15]	Precision, recall (TPR), F1 score	NSL-KDD	DBN	In this work, deep neural network was optimized by assigning a cost function to each layer of their proposed model.
2019 [16]	Accuracy, precision, recall, F1 measure	NSL-KDD	SDPN	SMO algorithm is used for optimal selection of features.
2020 [17]	Accuracy, precision, recall, F1 measure	NSL-KDD	RF	In this work, Weka tool was used for evaluation purposes.
2021 [18]	Accuracy, precision, recall, F1 measure	NSL-KDD, KDD99	ANN	In this work, the stack-based feature selection technique has been proposed to optimize the computation time.
2021 [19]	F1 score	Bot-IoT	RF, NB, and MLP	In this work, a hierarchical approach was used for intrusion detection.
2021 [20]	Accuracy, precision, recall, F1 measure	CICIDS2017	HW-DBN	In this work, low frequency attack was detected.

methodology by providing a theoretical description of IDS and deep neural network (DNN) concepts along with the details of the proposed model. Following that, the fourth section provides the results and discussion of intrusion detection with system configuration and comparative analysis. The fifth section provides the conclusion based upon the presented work along with its future scope.

## 2. Literature Survey

**2.1. Intrusion Detection System-Based Detection Systems.** To identify possible computer intrusions, intrusion detection calls for monitoring and analysing running networks and networking traffic. The IDS system is a collection of methods and mechanisms for this purpose. In general, most IDSs have standard capabilities to secure the network [9]. An IDS starts with data collection from the observed incidents. It does detailed logging and compares operations with event-related data from different networks. The detector which employs various methods and related techniques is at the core of an IDS, depending on the situation.

There would also be mitigation capability. It is here that the process of identification and avoidance of intrusion is called as Intrusion Detection and Prevention System.

**2.2. Anomaly-Based Detection Strategy.** In anomaly-based recognition methods, different patterns, like generative, discriminatory, and hybrid structures, can be used. Where the assault is allocated to one form of attack, clustering should be binary if normal and until behaviours are to be distinguished. Divide into multisubclass hierarchical structures may be further broken down into many classes. Any studies utilizing hierarchical datasets have been performed. The detector often operates online or offline to support applications in real time. In the last several years, various research articles have been published on intrusion detection techniques, many of which are focused on the detection of network attacks using various machine learning and deep learning approaches. In Table 1, various existing frameworks are compared.

**2.3. Summary of the Related Work.** After reviewing various research papers based upon the intrusion detection system, it can be observed that commonly used datasets NSL-KDD and KDD99 were utilized for the implementation purpose. No doubt both the datasets are benchmark dataset seems to be outdated, and hence, work needs to be carried out on new dataset. Also, very few researchers have implemented the system based upon the Internet of Things and 5G network [20–24]. In this work, the UNSW-NB15 benchmark dataset which was created by the IXIA PerfectStorm tool in the Cyber Range Lab of UNSW Canberra was used [25, 26].

## 3. Proposed Methodology

**3.1. Background of Deep Learning Architectures.** Deep learning is one of the popular techniques of data mining. Tiefskin’s learning is a valuable algorithm for modelling abstract subjects and relationships over two neural layers [27]. Deep learning is currently being studied in several

Generic	39496
Normal	19488
Exploits	16187
DoS	1791
Fuzzers	1731
Reconnaissance	1703
Analysis	564
Worms	114
Backdoor	99

Name: attack\_cat, dtype: int64

FIGURE 2: Attack category.

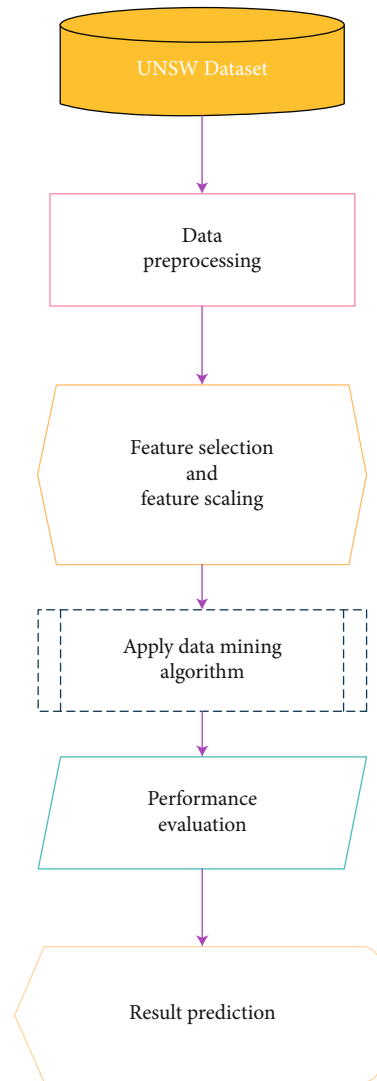


FIGURE 3: Generalized system flow chart.

areas, including the identification of images, speech, natural language processing, social network filtering, and so forth. In addition to finding correlations between vast data from different sources to carry out attribute learning, classification, or classification tasks at the same time, deep-sea learning algorithms vary in their ability. Various deep

Input Given: Complete Dataset  $D=(a_1, a_2, \dots, a_n)$  where  $a_i \rightarrow X$   
 Output: Prediction result for binary class label denoted by variable  $b$   
 Step 1: Data Pre-processing ( $S$ )  $\rightarrow S'$   
 Step 2: Correlated sample Obtained was  $S''$   
 Step 3: Training using AE ( $S, F_\varphi, G_\theta$ )  $\rightarrow$  Cust AE  
 Step 4: Apply AE ( $S',$  Cust AE)  $\rightarrow$  Full\_AE  
 Step 5:  $S''' = S'$ , Where Full AE  $\rightarrow$  Correlated Features  
 Step 6: Training using DNN ( $S'''$ )  $\rightarrow$  Cust DNN  
 Step 7: Add Cust DNN after Cust AE to form Cust AE+ Cust DNN  
 Step 8: Input Testing Data to generate class label  $b$ .

ALGORITHM 1: Proposed customized AE and DNN detection input.

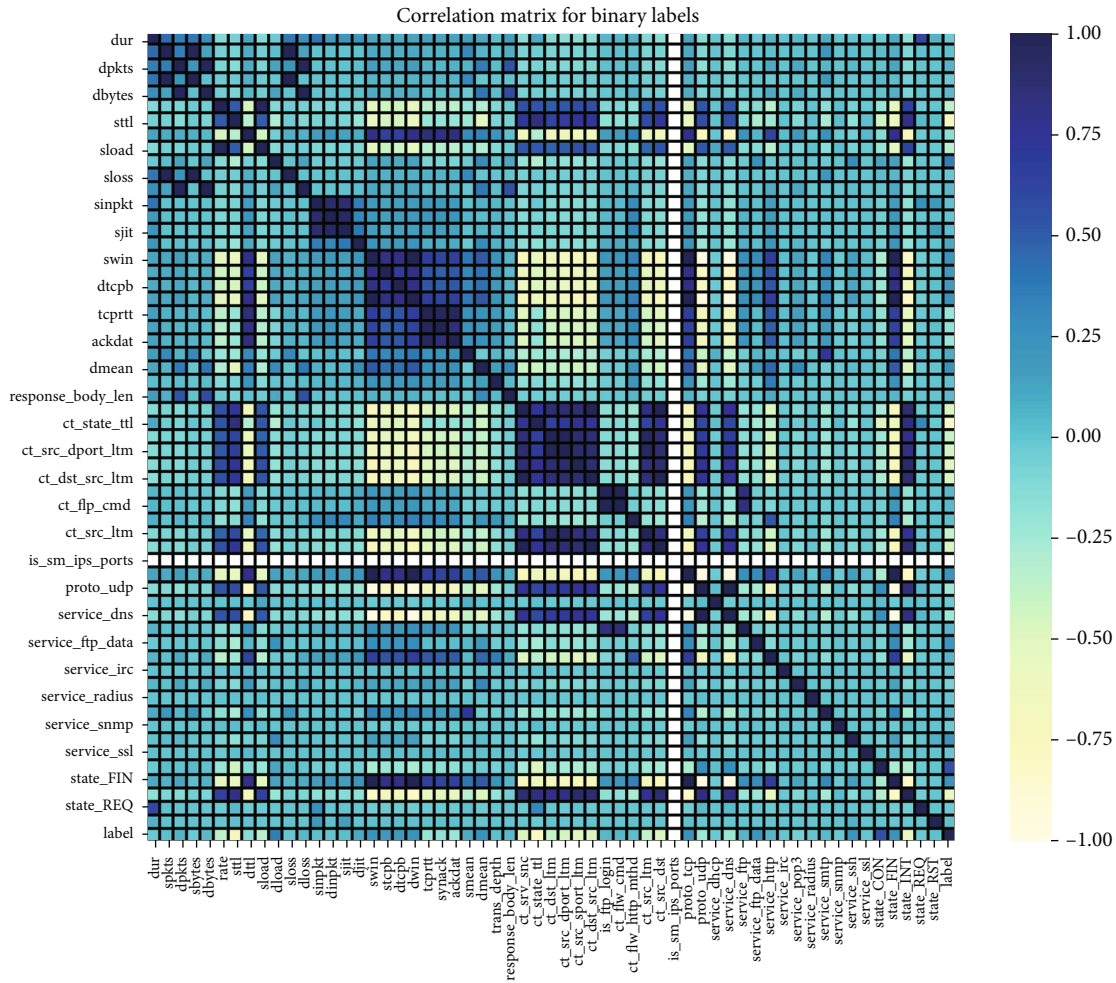


FIGURE 4: Heatmap for binary classification.

learning techniques which are used by different researchers for the development of intrusion detection system are discussed as follows:

(i) *Generative Architectures*. Unlisted raw data dynamically train algorithms to carry out different activities. This is the most general architecture in the architectural class category.

(ii) *Autoencoder (AE)*. Gao et al. [28] is a massive neural network widely used to minimize dimensionality by having improved data representation compared to raw inputs. The AE contains layers of the same number of feature vectors, in addition to a hidden layer with a low-dimensional representation. An AE incorporates and trains an encoder and decoder with a backpack. As knowledge is

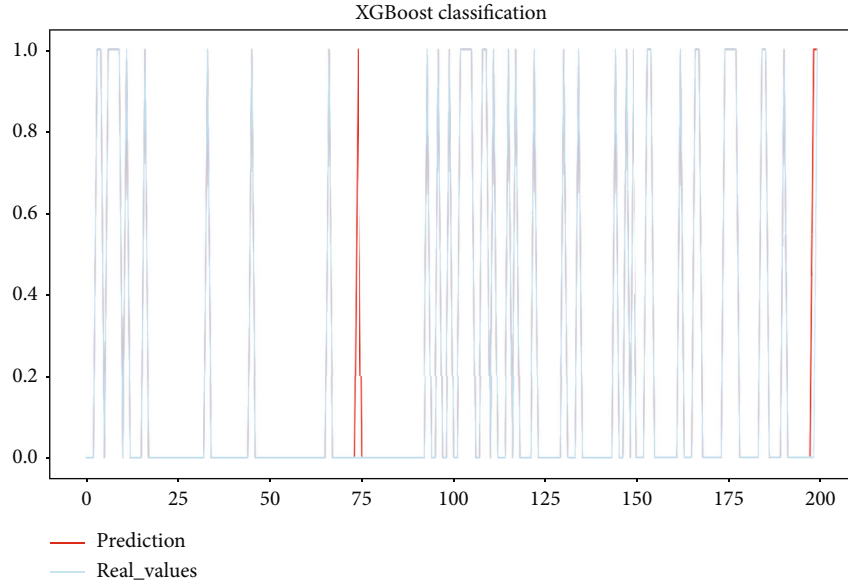


FIGURE 5: XGboost classification results.

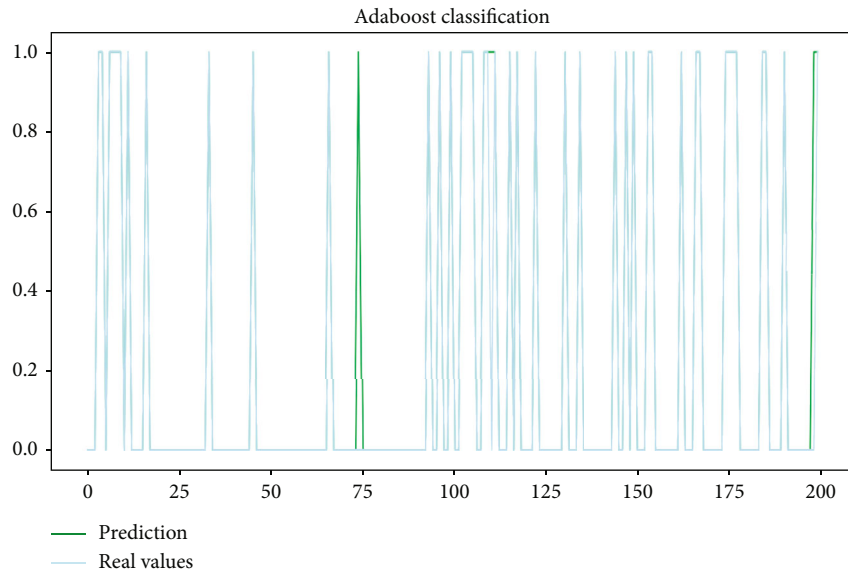


FIGURE 6: Adaboost classification results.

translated into small abstraction, it captures brutal characteristics and learns the representation of details. Afterward, the decoder receives small displays and reconstructs original functions [29]. Some AE extensions like AE (SAE), sparse AE, and denoise AE are available.

- (iii) *SAE*. Cascade through a vast network and SAE via more than one hidden sheet. The features used to create a new data display are more thoroughly studied [30].
- (iv) *Sparse AE*. Units covered in scarce AE are of a little sparse size. While there are many hidden units available to research data representations, AE

remains valuable. Sparsity constraints are intended to ensure that most neurons are inactive [31] in the low average output.

- (v) *Denoising AE*. Denoise is built on the use of skewed data for refined data view where hidden layers only use stable characteristics vectors [32].
- (vi) *Restricted Boltzmann Machine (RBM)*. As a probabilistic neural network, the Boltzmann (BM) was created by Hinton and Sejnovsk. A BM network consists of binary units symmetrically connected which specifies which units are permitted. Several interactions between units, however, contribute to very slow learning [33]. RBM is the unidirectional



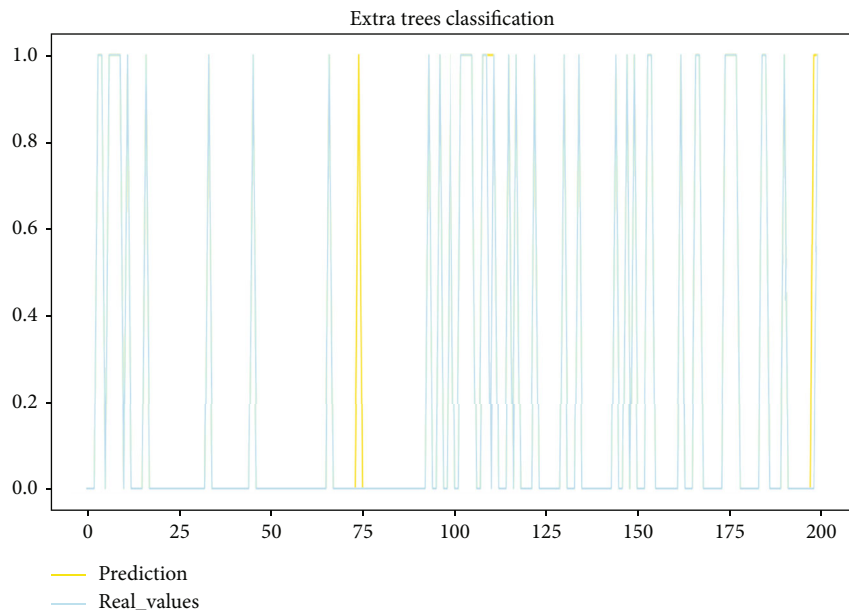


FIGURE 7: ExtraTreeClassifier results.

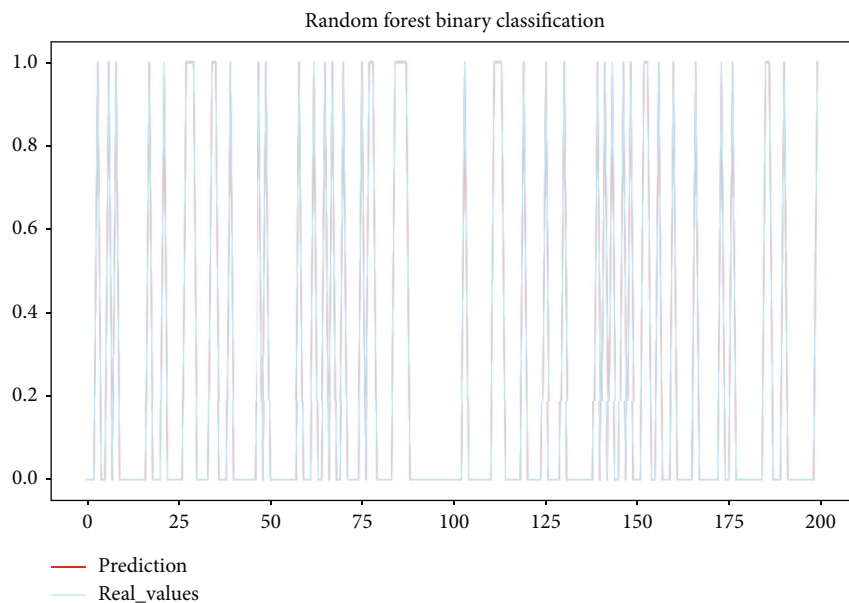


FIGURE 8: Random Forest Classifier results.

paradigm of Smolensky 1986 which solves BM’s uncertainty. The principle of RBM is that neuronal connections are removed on the same sheet. RBM contains a translucent layer and an occult layer of latent (hidden) variables for initial input variables. Both units are connected to the hidden layer in a clear layer with corresponding weights. The feature distribution learns the units covered by the input variables. As an initial stage, RBM is typically employed as a preprocessing feature extractor or for initializing other network parameters, for

another learning network. RBM may be used as a grouping model as well. A nonlinear, autonomous classification of Larochell and Bengaio was taught to be the discriminatory Boltzmann (DRBM) device. If some of the Boltzmann press are waterfalls, this is called a deeper Boltzmann (DBM).

(vii) *Deep Belief Network (DBN)*. The DBN consists of stacked RBMs, which have been trained in a pessimistic way. In comparison to the previous RBM, each RBM is trained and represents a contribution

Model : "sequential\_2"

Layer (Type)	Outout shape	Param #
Dense_features (Densefeature)	Multiple	0
Dense_6 (Dense)	Multiple	22912
Dense_7 (Dense)	Multiple	16512
Dense_8 (Dense)	Multiple	129
Total params : 39, 553		
Trainable params : 39, 553		
Non-trainable params : 0		

FIGURE 9: Model summary for DNN.

to the hidden layer of the RBM. The algorithm for profound learning is efficient and rapid to move. In case an additional layer of bias is applied, DBN is generalized for both dimensional reduction and independent classification for practical applications.

- (viii) *Recurrent Neural Network (RNN)*. Holand suggested RNN is a dynamic network of nerve feed in 1982. In normal transmission, depending upon the neural network architecture and its dependency, the output of each layer will consist of the same unit of the neuron. The discrepancy in the neural feed system feeds from hidden layers to RNNs. Various models of the memory unit such as long, temporary memory were extended, and the recurrent gated unit can be used.
- (ix) *Long Shorter Memory Time (LSTM)*. The RNN gradient is addressed by LSTM. It will learn long-term dependencies by utilizing the gate scheme. Every LSTM device is equipped with a memory cell containing old states.
- (x) *Gated System Recurrent (GRU)*. Lightweight is the GRU version of the LSTM. The architecture has been streamlined, the doors merged, and the states integrated.
- (xi) *Neural Classic Network (NCN)*. The perceptron is multilayered and is further known as the fully connect network. The model must be modified to binary entries in simple records.
- (xii) *Linear Function (LF)*. Rightly called, it is a single line multiplying the input by a constant multiplier.
- (xiii) *Nonlinear Function (NLF)*. Furthermore, the nonlinear function is split into three subsets: curve sigmoid, which is an S-shaped feature with several zeros to 1. The S-shaped curve with a scale of -1 to 1 relates to the hyperbolic tangent (tanh).

3.2. *Proposed Architecture*. In this work, UNSW 2015 benchmark dataset was used. Initially, the dataset was analysed in

Model : "functional\_1"

Layer (Type)	Outout shape	Param #
Input-1 (InputLayer)	((None, 14))	0
Dense (Dense)	(None, 14)	210
Dense_1 (Dense)	(None, 7)	105
Dense_2 (Dense)	(None, 7)	56
Dense_3 (Dense)	(None, 14)	112
Total params : 483		
Trainable params : 483		
Non-trainable params : 0		

FIGURE 10: Proposed model summary.

No.	Name	Type	Description	
0	1	Srcip	Nominal	Source IP address
1	2	Sport	Integer	Source port number
2	3	Dstip	Nominal	Destination IP address
3	4	Dsport	Integer	Destination port number
4	5	Proto	Nominal	Transaction Protocol

FIGURE 11: Sample feature description.

Pie chart distribution of normal and abnormal labels

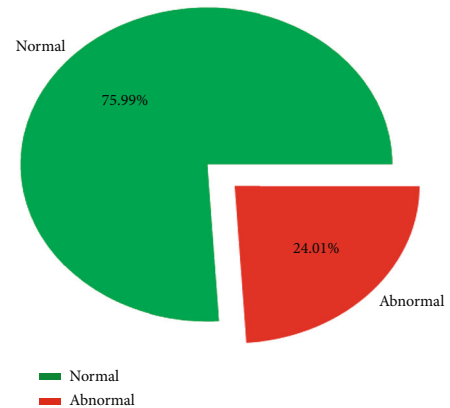


FIGURE 12: Dataset distribution.

the data preprocessing phase where the null value-based columns were dropped. Further, the updated dataset was provided to feature selection and feature scaling phase. In this phase, important features were considered using the Pearson correlation technique. Attack category used for the analysis purpose is depicted in Figure 2. After obtaining the important features, the categorical features were

TABLE 2: Results obtained using various deep learning approaches.

Sr. No.	Algorithm	Accuracy (%)
1.	Deep neural network	91.72
2.	Recurrent neural network+convolutional neural network [10]	96.12
2.	Gated recurrent neural networks [11]	98.91
3.	Bidirectional long short-term memory recurrent neural network [12]	95.71
4.	Distributed deep model [13]	99.20
5.	Convolutional neural network+long short-term memory [14]	97.16
6.	Spider monkey optimization+stacked-deep polynomial network [16]	99.02
7.	Random Forest [17]	99.70%
8.	Artificial neural network [18]	99.00%
9.	Hybrid Weighted Deep Belief Network [20]	99.38
10.	Proposed methodology	99.76

TABLE 3: Results obtained using various machine learning algorithms.

Sr. No.	Algorithm	Accuracy	R2 score	Precision	Recall	F1 score	MAE	MSE	RMSE
1.	XGboostClassifier	0.984	0.910	0.98	0.99	0.99	0.015	0.015	0.125
2.	AdaboostClassifier	0.983	0.910	0.98	0.99	0.99	0.016	0.0164	0.128
3.	ExtraTreeClassifier	0.983	0.910	0.98	0.99	0.99	0.016	0.016	0.128
4.	Random Forest Classifier	0.986	0.924	0.99	0.99	0.99	0.013	0.013	0.117

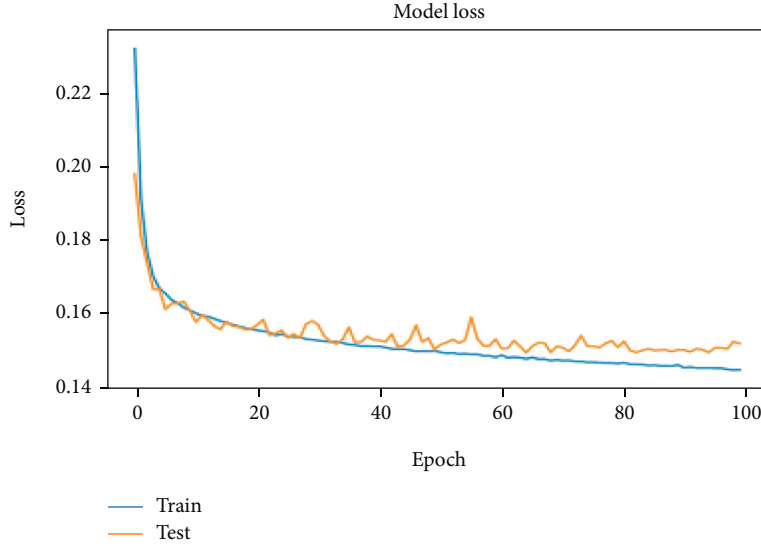


FIGURE 13: Training validation accuracy of the proposed model for 100 epochs.

converted to the numeric features using the one-hot encoding technique. Later for scaling, the feature normalization and standardization techniques were used. Finally, various machine learning and deep learning algorithms were used for training the model. In the training phase, 80% of the dataset was utilized, while for testing the model, remaining 20% of the dataset was used. The proposed autoencoder technique has outperformed compared to other models. Ini-

tially, a deep neural network and proposed model were implemented using 100 epochs. Finally, the proposed model has got more promising results when it was trained with 5000 epochs. The generalized flow chart of the proposed model is depicted in Figure 3. The proposed system algorithm has been represented in Algorithm 1 as follows:

For identifying the highly correlated features in the dataset, Pearson correlation technique was used. The

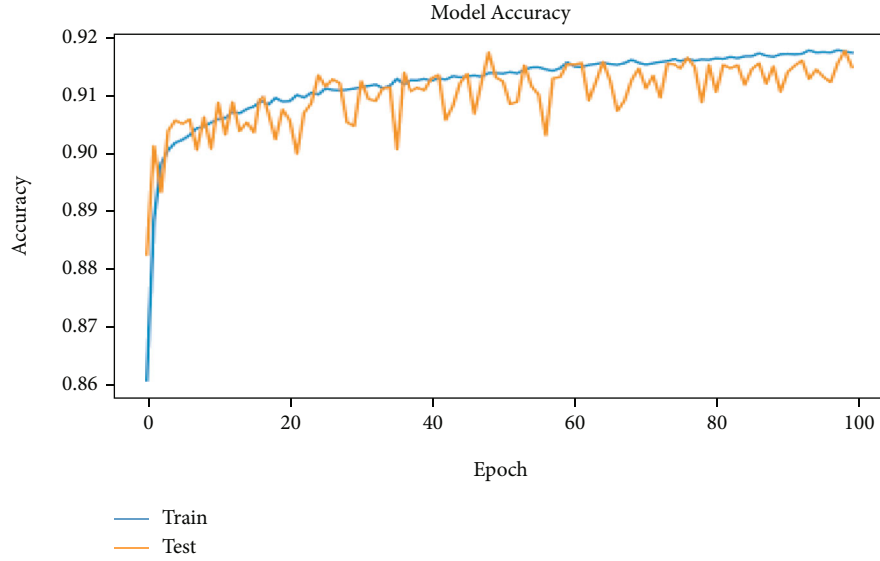


FIGURE 14: Training validation loss of the proposed model for 100 epochs.

correlated features were analysed through heatmap as provided in Figure 4.

For implementation purpose, ensemble-based machine learning techniques were considered. XGboost, Adaboost, ExtraTreeClassifier, and Random Forest Classifier were used for implementation purpose. Results obtained through various machine learning algorithms are depicted in Figures 5–8.

Figures 9 and 10 represent the model summary of deep neural network and the proposed methodology, respectively.

## 4. Results and Discussions

**4.1. Dataset Description and Preprocessing.** In this work, the UNSW-NB15 dataset was used for the implementation. This dataset consists of a total of 175341 rows and 45 attributes. In the dataset preprocessing step, initially, the null values were dropped. Due to this, the dataset was converted into almost half of its size. Further, to handle the categorical features, encoding techniques were used. Later for performing feature scaling, the normalization technique was applied. Figure 2 provides the details of the attack category available in the dataset. The sample of feature description is depicted in Figure 11. Dataset distribution after splitting in training and testing samples is depicted in Figure 12. For generating efficient results of the proposed model, the implementation is done with high configuration architecture which is comprised of AMD RYZEN 9 processor with 8 cores, 64-bit Windows 10 OS, 16 GB of RAM, and 6 GB GTX 1660 TI GPU. The complete model script was implemented on Jupyter Notebook tool using python programming language.

**4.2. Evaluation Metrics.** The main aim of the evaluation metrics is to depict the implications of enriching the IDS with the proposed model using some of the following important parameters:

- (i) Maximize detection rate (DR)

$$\text{Detection rate} = \frac{\text{true positive}}{(\text{true positive} + \text{false negative})} \quad (1)$$

- (ii) Maximize accuracy (AC)

$$\text{False alarm rate} = \frac{\text{false positive}}{(\text{false positive} + \text{true positive})} \quad (2)$$

- (iii) Minimize false alarm rate (FA)

$$\text{Maximize accuracy} = \frac{\text{true positive} + \text{true negative}}{(\text{true negative} + \text{true positive} + \text{FN} + \text{false positive})} \quad (3)$$

Our model obtained higher accuracy compared to the existing model as depicted in Table 2. The proposed model was tested on various performance metrics, and classification accuracy was used as a comparison parameter with the existing model.

Table 3 provides the details of the results obtained using various machine learning algorithms. Results obtained using the deep learning algorithm and proposed methodology are provided in Table 2. In Table 2, only results obtained from those researchers are considered who have used accuracy as their comparative parameter.

In Figures 13 and 14, the accuracy results and loss results of the proposed methodology computed for 100 epochs are depicted. An appendix of all the acronyms is given in Table 4.

TABLE 4: Appendix of all the acronyms.

Sr. No.	Term	Acronym
1	Internet of Things	IoT
2	Intrusion detection system	IDS
3	Denial of Service	DoS
4	Artificial intelligence	AI
5	Deep neural network	DNN
6	Wireless sensor network	WSN
7	Recurrent neural network	RNN
8	Convolutional neural network	CNN
9	Gated recurrent unit	GRU
10	Bidirectional long short-term memory recurrent neural network	(BLSTM RNN)
11	False alarm rate	FAR
12	Stochastic gradient descent	SGD
13	Multilayer perceptron	MLP
14	Long short-term memory	LSTM
15	Spider monkey optimization	SMO
16	Stacked-deep polynomial network	SDPN
17	Artificial neural network	ANN
18	Random Forest	RF
19	Naïve Bayes	NB
20	Autoencoder	AE
21	Sparse AE	SAE
22	Restricted Boltzmann machine	RBM
23	Boltzmann	BM
24	Discriminatory Boltzmann	DRBM
25	Deeper Boltzmann	DBM
26	Deep belief network	DBN
27	Recurrent neural network	RNN
28	Neural classic networks	NCN
29	Fully connect network	FCN
30	Linear function	LF
31	Nonlinear function	NLF
32	Mean absolute error	MAE
33	Mean squared error	MSE
34	Root mean squared error	RMSE
35	Miscalculation rate	MR
36	Hybrid Weighted Deep Belief Network	HW-DBN
37	Denial-of-Service Attacks	DDoS
38	Open Systems Interconnection	OSI

## 5. Conclusion and Future Scope

The proposed algorithm is trained using the SoftMax classifier to identify the attack types in the dataset. The benchmark dataset, UNSW-NB15, was used for training and testing the model. For training the hidden layers, there are many options, such as linear, SoftMax, sigmoid, and corrected linear functionality which can be used as an activation function. A novel autoencoder technique was used for training and testing the model. The proposed model has achieved

comparatively high accuracy than the existing system. Several machine learning and deep learning approaches were used for implementation purposes. Further, to extend the work, stack-based autoencoder technique can be used for reducing the computational resources. Also, more focus can be given to optimizing the computational time.

### Data Availability

No data were used to support this study.

## Conflicts of Interest

The authors declare that there is no conflict of interest regarding the publication of this paper.

## References

- [1] B. Susilo and R. F. Sari, "Intrusion detection in IoT networks using deep learning algorithm," *Information*, vol. 11, no. 5, p. 279, 2020.
- [2] A. Aldweesh, A. Derhab, and A. Z. Emam, "Deep learning approaches for anomaly-based intrusion detection systems: a survey, taxonomy, and open issues," *Knowledge-Based Systems*, vol. 189, p. 105124, 2020.
- [3] L. Fernández Maimó, A. Huertas Celdrán, M. Gil Pérez, F. J. García Clemente, and G. Martínez Pérez, "Dynamic management of a deep learning-based anomaly detection system for 5G networks," *Journal of Ambient Intelligence and Humanized Computing*, vol. 10, no. 8, pp. 3083–3097, 2019.
- [4] V. Yihua Liao, "Rao Vemuri, Use of K-nearest neighbor classifier for intrusion detection11An earlier version of this paper is to appear in the Proceedings of the 11th USENIX Security Symposium, San Francisco, CA, August 2002," *Computers & Security*, vol. 21, no. 5, pp. 439–448, 2002.
- [5] N. Abdullah, *Advances in Cyber Security: Third International Conference, ACeS 2021, Penang, Malaysia, August 24–25, 2021, Revised Selected Papers*, Springer Nature, Penang, Malaysia, 2021, <https://link.springer.com/book/10.1007/978-981-16-8059-5>.
- [6] E. Hodo, X. Bellekens, A. Hamilton, C. Tachtatzis, and R. Atkinson, "Shallow and deep networks intrusion detection system: a taxonomy and survey," 2017, <https://arxiv.org/abs/1701.02145>.
- [7] Y. Bengio, "Learning Deep Architectures for AI," *Found. Trends Mach. Learn. Foundations and Trends® in Machine Learning*, vol. 2, no. 1, pp. 1–127, 2009.
- [8] J. Cannady, "Artificial neural networks for misuse detection," *InNational information systems security conference*, vol. 26, pp. 443–456, 1998.
- [9] A. Khamparia, S. Pande, D. Gupta, A. Khanna, and A. K. Sangaiah, "Multi-level framework for anomaly detection in social networking," *Library Hi Tech*, vol. 38, no. 2, pp. 350–366, 2020.
- [10] M. Lopez-Martin, B. Carro, A. Sanchez-Esguevillas, and J. Lloret, "Network traffic classifier with convolutional and recurrent neural networks for Internet of Things," *IEEE Access*, vol. 5, pp. 18042–18050, 2017.
- [11] M. Kumar, *Deep Learning Approach for Intrusion Detection System (IDS) in the Internet of Things (IoT) Network Using Gated Recurrent Neural Networks (GRU)*, Wright State University, 2017, [https://corescholar.libraries.wright.edu/etd\\_all/1848/](https://corescholar.libraries.wright.edu/etd_all/1848/).
- [12] B. Roy and H. Cheung, "A deep learning approach for intrusion detection in internet of things using bi-directional long short-term memory recurrent neural network," in *2018 28th International Telecommunication Networks and Applications Conference (ITNAC)*, pp. 1–6, Sydney, NSW, Australia, November 2018.
- [13] A. A. Diro and N. Chilamkurti, "Distributed attack detection scheme using deep learning approach for Internet of Things," *Future Generation Computer Systems*, vol. 82, pp. 761–768, 2018.
- [14] M. Roopak, G. Y. Tian, and J. Chambers, "Deep learning models for cyber security in IoT networks," in *2019 IEEE 9th annual computing and communication workshop and conference (CCWC)*, pp. 452–457, Las Vegas, NV, USA, January 2019.
- [15] G. Thamilarasu and S. Chawla, "Towards deep-learning driven intrusion detection for the internet of things," *Sensors*, vol. 19, no. 9, p. 1977, 2019.
- [16] Y. Otoum, D. Liu, and A. Nayak, "DL-IDS: a deep learning-based intrusion detection framework for securing IoT," *Transactions on Emerging Telecommunications Technologies*, article e3803, 2019.
- [17] S. Pande, A. Khamparia, D. Gupta, and D. N. H. Thanh, "DDoS Detection Using Machine Learning Technique," in *Recent Studies on Computational Intelligence. Studies in Computational Intelligence*, A. Khanna, A. K. Singh, and A. Swaroop, Eds., vol. 921, Springer, Singapore, New Delhi, India, 2021.
- [18] S. Pande, A. Khamparia, and D. Gupta, "An intrusion detection system for health-care system using machine and deep learning," *World Journal of Engineering*, 2021.
- [19] G. Bovenzi, G. Aceto, D. Ciuonzo, V. Persico, and A. Pescapé, "A hierarchical hybrid intrusion detection approach in IoT scenarios," in *GLOBECOM 2020 - 2020 IEEE Global Communications Conference*, pp. 1–7, Taipei, Taiwan, December 2020.
- [20] Z. K. Maseer, R. Yusof, S. A. Mostafa, N. Bahaman, O. Musa, and B. A. Al-rimy, "DeepIoT.IDS: hybrid deep learning for enhancing IoT network intrusion detection," *CMC-Computers, Materials & Continua*, vol. 69, no. 3, pp. 3945–3966, 2021.
- [21] T. O'Shea and J. Hoydis, "An Introduction to deep learning for the physical layer," *IEEE Transactions on Cognitive Communications and Networking*, vol. 3, no. 4, pp. 563–575, 2017.
- [22] G. Aceto, D. Ciuonzo, A. Montieri, and A. Pescapé, "Mobile encrypted traffic classification using deep learning: experimental evaluation, lessons learned, and challenges," *IEEE Transactions on Network and Service Management*, vol. 16, no. 2, pp. 445–458, 2019.
- [23] Y. Mirsky, T. Doitshman, Y. Elovici, and A. Shabtai, "Kitsune: an ensemble of autoencoders for online network intrusion detection," 2018, <https://arxiv.org/abs/1802.09089>.
- [24] M. Almiyani, A. AbuGhazleh, Y. Jararweh, and A. Razaque, "DDoS detection in 5G-enabled IoT networks using deep Kalman backpropagation neural network," *International Journal of Machine Learning and Cybernetics*, vol. 12, no. 11, pp. 3337–3349, 2021.
- [25] N. Moustafa and J. Slay, "The evaluation of network anomaly detection systems: statistical analysis of the UNSW-NB15 dataset and the comparison with the KDD99 dataset," *Information Security Journal: A Global Perspective*, vol. 25, no. 1–3, pp. 1–14, 2016.
- [26] A. Bhardwaj, V. Mangat, and R. Vig, "Hyperband tuned deep neural network with well posed stacked sparse autoencoder for detection of DDoS attacks in cloud," *IEEE Access*, vol. 8, pp. 181916–181929, 2020.
- [27] L. Yuancheng, M. Rong, and J. Ruhai, "A hybrid malicious code detection method based on deep learning," *Journal of Security and Its Applications*, vol. 9, no. 5, pp. 205–216, 2015.
- [28] N. Gao, L. Gao, Q. Gao, and H. Wang, "An intrusion detection model based on deep belief networks," in *2014 Second*

- International Conference on Advanced Cloud and Big Data*, pp. 247–252, Huangshan, China, November 2014.
- [29] C. Zhou and R. C. Paffenroth, “Anomaly detection with robust deep autoencoders,” in *InProceedings of the 23rd ACM SIGKDD international conference on knowledge discovery and data mining*, pp. 665–674, New York, NY, United States, August 2017.
- [30] M. Abadi and D. G. Andersen, “Learning to protect communications with adversarial neural cryptography,” 2016, <https://arxiv.org/abs/1610.06918>.
- [31] A. L. Buczak and E. Guven, “A survey of data mining and machine learning methods for cyber security intrusion detection,” *IEEE Communications Surveys & Tutorials*, vol. 18, no. 2, pp. 1153–1176, 2016.
- [32] D. Kwon, H. Kim, J. Kim, S. C. Suh, I. Kim, and K. J. Kim, “A survey of deep learning-based network anomaly detection,” *Cluster Computing*, vol. 22, pp. 1–13, 2019.
- [33] M. Usama, J. Qadir, A. Raza et al., “Unsupervised machine learning for networking: techniques, applications and research challenges,” 2017, <https://arxiv.org/abs/1709.06599>.



## Research Article

# Application of Cable Climbing Robot Automation Control Technology in Bridge Cable Measuring System

Weihua Zhou <sup>1</sup>, Junqi Bao <sup>2</sup>, Zhenzhi Liu <sup>2</sup> and Zhengda Chen <sup>2</sup>

<sup>1</sup>College of Electrical Engineering, Zhejiang University, Hangzhou 318000, China

<sup>2</sup>Hangzhou Changchuan Technology Co., Ltd., Hangzhou 310056, China

Correspondence should be addressed to Weihua Zhou; dididi@zju.edu.cn

Received 30 September 2021; Accepted 4 December 2021; Published 26 February 2022

Academic Editor: Deepak Gupta

Copyright © 2022 Weihua Zhou et al. This is an open access article distributed under the Creative Commons Attribution License, which permits unrestricted use, distribution, and reproduction in any medium, provided the original work is properly cited.

According to the traditional bridge cable measurement system, the accuracy of the bridge cable measurement is low, and the measurement time is long. Based on the automatic control technology of the climbing robot, a new bridge cable measurement system is designed. We design system hardware through CIS drive circuit, main controller, and communication module; design system software on the basis of hardware design; obtain the motion control equation of orthogonal joint cable climbing robot through DH transformation; and apply this equation to the bridge cable measurement system. The bridge cable measurement model is constructed, and the bridge cable measurement system design is completed through the system hardware design and software design. The simulation results show that the designed system has higher accuracy in measuring bridge cables and shorter measuring time.

## 1. Introduction

As a new type of bridges, cable-stayed bridges are being used more and more in actual production. They have beautiful appearance, relatively low cost, and good seismic resistance. With the continuous improvement of design theories, the continuous updating of materials, the widespread use of electronic computers, the continuous accumulation of construction experience, and the continuous improvement of construction technology, the span of cable-stayed bridges is also increasing, which also indicates that cable-stayed bridges will play an increasingly important role in the future bridge construction [1]. The main force-bearing component of a cable-stayed bridge is a cable, but it is exposed to the atmosphere for a long time and is corroded by wind, sun, rain, and environmental pollution, and its surface will be severely damaged. The main load-bearing part of the bridge is about 25%–30% of the cost of the whole bridge. The damage of the cable surface means that the safety of the cable-stayed bridge will be greatly affected [2]. In order to

reduce the loss caused by the uncertain damage of the cable, it is necessary to carry out internal and external measurement, painting, or repair of the cable regularly to improve the safety and image of the bridge [3]. The cable-stayed bridge is mainly composed of a bridge tower under pressure, a cable under tension, and a beam body under bending. In its normal operation, the stay cable will be repeatedly affected by the dynamic load of the bridge deck, wind and rain vibration, sunshine, and corrosive gas, and it is prone to damage to the outer sheath and local steel wire corrosion. The damage of the stay cable sheath causes the internal steel wire to be exposed to the air, and the oil stains attached to the surface of the stay cable may penetrate into the cable, accelerating the corrosion of the steel wire. If it is not regularly maintained, this will eventually lead to the failure of the steel wire corrosion and lead to accidents such as cable failure or even bridge deck collapse. As the main load-bearing structure of cable-stayed bridges and suspension bridges, the effective metal bearing area of the cable is directly related to the safety and service life of the bridge, so it is necessary to

measure the bridge cable. In order to ensure the accuracy of the measurement and the safety of the personnel, the automation technology of the bridge cable measurement is now being studied at home and abroad [4].

Literature [5] designed a long-distance monitoring system for bridge cable force based on LoRa; designed a low-power, low-collision star-shaped wireless network structure using LoRa wireless communication technology; introduced the principle of measuring cable force by vibration frequency method; gave the overall structure and modular design of the monitoring system; and finally carried out the cable force monitoring test experiment. The experimental results show that the developed cable force remote monitoring system has perfect functions and strong real-time performance, which provides an efficient and convenient implementation method for remote and long-term bridge monitoring and has a relatively broad application prospects. However, the bridge cable measurement accuracy of this system is low. Cui proposed a cable-stayed bridge cable anchoring measurement system based on data transmission [6]. Based on the establishment of bridge construction control network and main tower linear monitoring, certain technical means were used to transfer plane coordinate datum and elevation coordinate datum to the main tower. For the construction section, according to the accuracy requirements of the measurement location and the conditions of the instrument's visibility, the absolute station method of the total station, the relative station method, or the method of combining the total station and the vertical cast point is selected to realize the rapid and high construction of the cable anchor system [6]. Yi et al. designed an ultrasonic testing system for axial force of cable clamp screw of suspension bridge [7]. First, the ultrasonic probe was fixed on one end of the screw to excite the ultrasonic wave. The ultrasonic wave propagated in the screw shaft along the axial direction to the other end surface to be reflected. The ultrasonic probe received the reflected wave and then used it. The software system measured the change in ultrasonic echo sound to obtain the screw axial force. After the system was tested and the coefficient was calibrated, the system was applied to the cable clamp screw axial force detection of the Wuhan Yangsigang Yangtze River Bridge. The results show that the system has good performance. The reliability of the test is about 3.5% under the condition that the stress-free echo sound is clear. The test of the single screw axial force in the Wuhan Yangsigang Yangtze River Bridge screw test took less than 1 min [7]. Real bridge detection is convenient and quick. However, the bridge cable measurement time of the last two systems is long.

In order to solve the defects of low measurement accuracy and long time of traditional bridge cable measurement system, an automatic control technology of cable climbing robot based on bridge cable measurement system is designed, and the effectiveness of the system is verified by simulation experiments. This method can be applied to the regular measurement of bridge cables. Through the rapid and accurate detection of bridge cables, the risk factors can be found in time to maintain the safety of the bridge.

## 2. Design of Bridge Cable Measurement System Based on Automatic Control Technology of Cable Climbing Robot

*2.1. System Hardware Design.* The hardware design part of the bridge cable measurement system includes the CIS drive circuit, the main controller, and the communication module.

*2.1.1. CIS Drive Circuit.* The driving circuit of CIS mainly includes the provision of CIS working clock (CLK) and start pulse (SP). The recommended operating clock frequency of the linear solid-state image sensor SV200A4-10 is 250 kHz, and the duty cycle is 25%–50%. If the clock frequency is too high or the duty cycle is too large, the integration time of the photosensitive element integration circuit will be reduced, and the output signal amplitude of the CIS will be too small. Under the excitation of the start pulse, the CIS starts a frame of scanning, and the width of the start pulse must be at least not less than one working clock. The clock signal (CLK) and the start pulse signal (SP) of the CIS can be generated by the timer of the DSP by dividing the frequency of the internal clock or can be provided by an external programmable logic device or other circuits. In the system, in order to reduce the complexity of the circuit, the drive signal of the CIS is provided by the multifunction serial port of the DSP [8].

TMS320C32 is equipped with a serial port, which can send and receive 8-bit, 16-bit, 24-bit, and 32-bit data in both directions by setting the registers. In the continuous working mode, it can continuously send and receive any number of words without the need for a new synchronization pulse. TMS320C32 provides eight memory-mapped control registers to control serial port operations. They include an overall control register, two port control registers, three transmit/receive timer registers, one data receiving buffer register, and one sending buffer register [9]. Among them, the overall control register is used to control the overall function of the serial port and determine the operation mode of the serial port; the two port control registers are used to control the functions of the six serial ports; the transmit buffer is used to buffer the next word to be sent; and the receive buffer is used to buffer the last received word. The TMS320C32 serial port has a strong load capacity. Its sending clock pin CLKX and sending frame synchronization pin FSX can directly drive the CIS without any bus enhancement circuit. The interface circuit is very simple. The connection diagram of DSP and CIS is shown in Figure 1.

*2.1.2. Main Controller.* The function of the main controller is as follows: the wireless serial port communicates with the host computer, connects to the CAN bus, and then processes the large amount of data fed back. In order to facilitate the realization of these two points, when designing the master controller, combined with the characteristics of the slave controller, this article selects STM32F103, which can fully meet these functional requirements. STMicroelectronics STM32 series chips are based on the ARM Cortex-M3 core

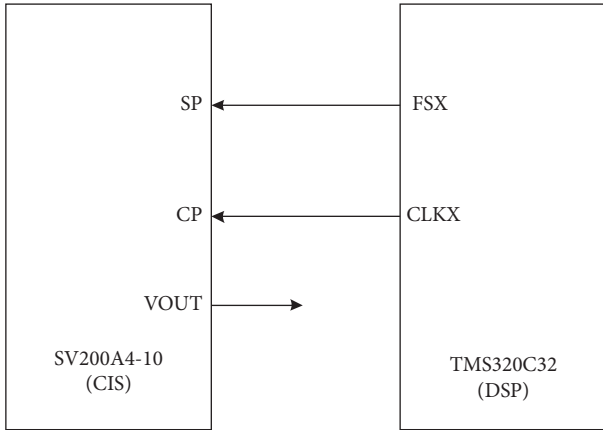


FIGURE 1: Connection diagram between DSP and CIS.

and are cost-effective 32-bit processors that can meet the needs of high-performance, low-cost, and low-power embedded applications [10].

The STM32F103 selected in this article belongs to the “enhanced” series of STM32, with a clock frequency of 72 MHz. The specific model of the prototype developed in this article is the STM32F103C8T6 main controller with 64 KB of flash storage space, 20 KB of SRAM space, and seven timers. The timer of the MCU can generate 30 PWM outputs and up to 9 communication interfaces. The specific performance is shown in Table 1. The package has a small size and good versatility, which is convenient for the development of the main controller used in this article.

The design block diagram of the main controller is shown in Figure 2. Its volume requirement is very small, so the design is compact. The power supply of the whole controller is 1A low dropout voltage stabilizer AMS1117. The stable output voltage is 3.3 V. The main controller is in low-level reset mode and can be freely selected in JTAG or SWD mode, which is convenient for software code writing and debugging [11].

**2.1.3. Communication Module.** The communication mainly includes the communication between the ground PC and the master controller and the communication between the master and slave controllers in the prototype. The ground PC communicates with the main controller through the 2.4 G wireless communication module, the prototype body adopts master-slave distributed control, and the main controller communicates with the slave controllers through the CAN bus [12]. The communication topology is shown in Figure 3.

- (1) Ground PC to the main controller: the wireless communication between the ground PC and the main controller is realized through the 2.4 G wireless serial port module. An RS232-TTL converter is connected to the DB9 serial port of the PC to realize the full-duplex TTL of the physical layer. In asynchronous serial communication, the data link layer is a commonly used duplex 8N1 (8 data bits, no parity, 1 stop bit) serial frame with a baud rate of 9600, and the main controller interrupts the receiving wireless

TABLE 1: Specific parameters of STM32F103C8T6.

Series to which IC belongs	STM32 F1
Core processor	ARM® Cortex™-M3
Core size	32 bits
Speed	72 MHz
Connectivity	CAN, I <sup>2</sup> C, IrDA, LIN, SPI, UART/USART, USB
Peripheral equipment	DMA, PWM, PDR, POR, PVD, PWM, temperature sensor, WDT
Number of inputs/outputs	37
Program memory capacity	64 KB (64 K × 8)
Program memory type	Flash memory
RAM capacity	20 K × 8
Voltage-power (V <sub>cc</sub> /V <sub>dd</sub> )	2 V~3.6 V
Data converter	A/D 2 × 10 × 12b
Oscillator type	Internal
Operating temperature	-40°C~85°C
Encapsulation/shell	48-LQFP

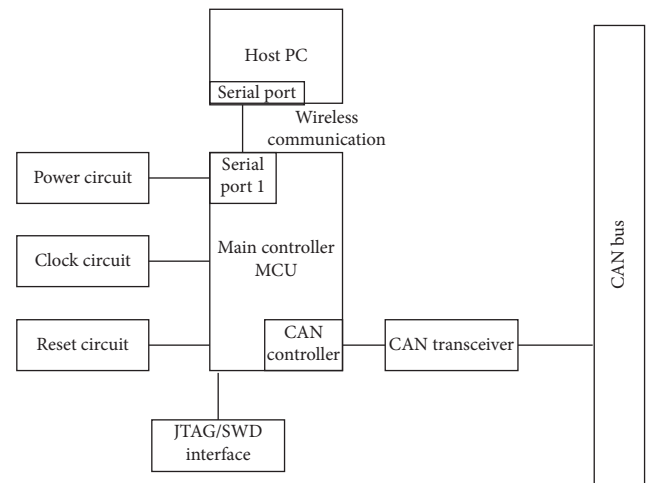


FIGURE 2: Design block diagram of the main controller.

serial port. The information is bridged with the CAN bus, and at the same time, its own information and the sensor information obtained on the bus are sent back to the ground PC through the wireless serial port to realize status monitoring [13].

- (2) Master controller to slave controller: due to the mechanical size of the robot body, the CAN node circuit should avoid complexity, and the circuit board size should be as small as possible. Therefore, the on-chip integrated CAN controller can be efficiently processed with the minimum CPU load. The STM32F103 series processors with a large number of received messages are used as MCUs. The physical layer is the topological structure of the CAN bus, and the data link layer is a half-duplex message that can be framed, arbitrated, acknowledged, and calibrated at a rate of 1 Mbps. Its function is in the hardware of the CAN controller. At the same time, the software sets CAN parameters (working mode, baud rate, filter), sends message requests, processes message reception, manages interruptions, and obtains

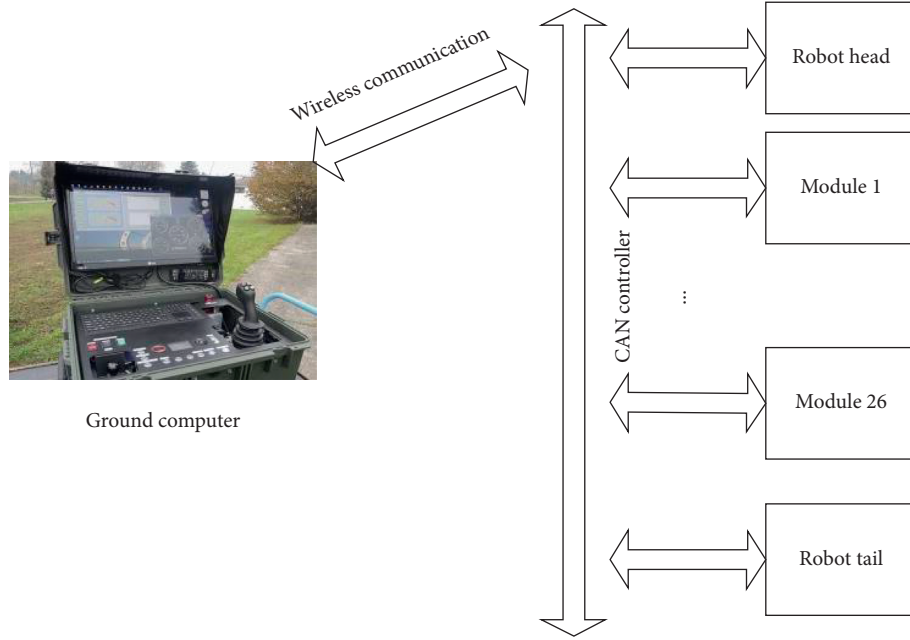


FIGURE 3: Communication topology.

diagnostic information through registers such as status, control, and configuration [14].

**2.2. System Software Design.** Because the rope climbing robot is similar to a biological snake without limbs and wheels, the force when it moves comes from the friction between the surface of its body and the contact object (e.g., ground). The rotation of the module joints inside the body will cause the friction of all parts of the body. The magnitude and direction of the force are different, and the imbalance of the force produces a movement trend, forming various movement patterns. The rope climbing robot can imitate the movement of some biological snakes and create a movement pattern that biological snakes do not have [15]. At present, the prototypes of cable climbing robots made by domestic and foreign scholars can move in two-dimensional space, and some even made attempts to move in three-dimensional space. The basic motion modes of the rope climbing robot are meandering motion, traveling wave motion, side shifting motion, and rolling motion. Winding motion, traveling wave motion, and lateral motion are all imitating the motion patterns of biological snakes, and traveling wave motion can be understood as a meandering motion in the vertical direction [16]. In order to obtain the spatial pose (position and posture) of the joint points of each module of the cable climbing robot, it is necessary to perform kinematics modeling for its high-redundancy system [17]. Because the cable climbing robot prototype in this paper adopts a serial modular structure, Denavit–Hartenberg transformation can be used to establish the kinematics model of the cable climbing robot through the simplified spatial linkage model. In the kinematics analysis of joint robots, the DH matrix is the most widely used. First, a coordinate system is fixed on each link of the robot, and then a homogeneous

transformation matrix is used to represent the relative poses of two adjacent links. The multiplication transformation can finally derive the pose of the end joint point relative to the base coordinate system, thereby establishing the kinematics equation of the robot [18].

In this paper, the motion control equation of the orthogonal joint cable climbing robot can be obtained through DH transformation, and the bridge cable can be measured according to this equation. We use the DH transformation to establish the DH coordinate system for the prototype of the cable climbing robot with the modular structure in series, establish the base coordinate system  $O_0X_0Y_0Z_0$  near the head of the robot, and take the center of the rotation axis of the joint (steering gear) in each module as the origin  $O_1, O_2, \dots, O_n$  of each coordinate system.  $Z_i$  axis is set as the rotation axis of each steering gear, looking from the head end to the end, which follows the body axis and rotates counterclockwise around it.  $X_i$  axis is set as the male perpendicular of the  $Z_i$  axis, looking from the steering gear  $i$  to the steering gear  $i + 1$ , of which the direction is set as the positive direction of the  $X_i$ -axis. The  $Y_i$ -axis is determined by the right-hand screw rule. The link DH coordinate system of the rope climbing robot is shown in Figure 4.

According to the establishment of the DH coordinate system of the rope climbing robot, the DH matrix of each module can be obtained as

$$T_i = \begin{bmatrix} s\theta_i & c\theta_i & 0 & 0 \\ c\theta_i & -s\theta_i & 0 & L_0 \\ 0 & 0 & 1 & 0 \\ 0 & 0 & 0 & 1 \end{bmatrix}. \quad (1)$$

In the formula,  $L_0$  is the distance between the joint axis of the first module and the base coordinate system, 3 cm;  $L$  is

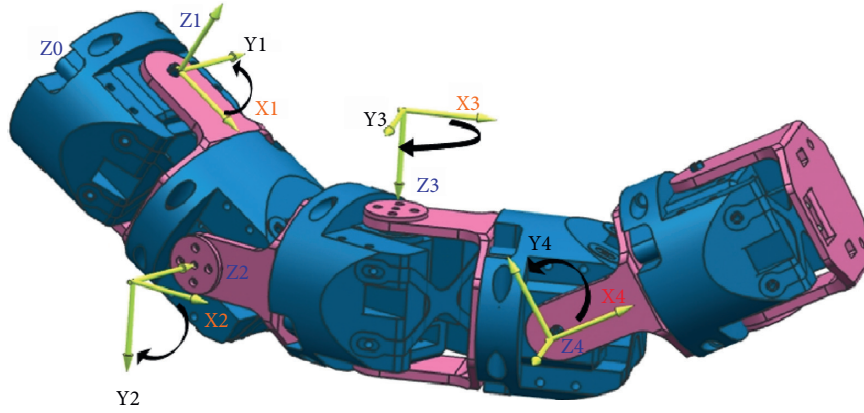


FIGURE 4: Link DH coordinate system of rope climbing robot.

the length of the module, 7 cm; and  $\theta_i$  is the rotation angle of each steering gear in the module. The transformation matrix of the module can be obtained by multiplying the DH matrices of first  $i$   ${}^0T_i$  and the space position of the  $i$ -th module can be obtained from the space coordinate by  $T_i$ , so the space position of each module can be obtained, and the kinematics model of the climbing robot can be established as

$$T_1 = P_0 \cdot {}^0T_i. \quad (2)$$

In the formula,  $P_0$  is the homogeneous coordinate of the head end of the rope climbing robot in the base marking system, which can be at the origin of the base marking system or in other positions. Therefore, the space coordinate of the  $i$ -th module is  $P_i(X_i, Y_i, Z_i)$ ; when  $P_0$  and  $\theta_i$  are known, the spatial configuration of the rope climbing robot can be obtained.

The robot part of the prototype in this paper is composed of orthogonally connected modules. According to the connection characteristics, they can be divided into two groups: pitch modules and yaw modules. The rotation axis of the pitch module and the rotation axis of the yaw module are perpendicular to each other. In the initial state, the rotation axes of all pitch modules are parallel to the horizontal plane, and the rotation axes of all yaw modules are perpendicular to the horizontal plane. If the rope climbing robot rotates around its body axis by  $0 \pm 90^\circ$ , the pitch module and the yaw module swap positions. If the first module is a yaw module, the second and even-numbered modules are both pitch modules, and the odd-numbered modules are yaw modules. The motion control equation of the orthogonal joint cable climbing robot is

$$E_i = A_i \cdot \text{SIN}(\omega \cdot t + k \cdot t) + \gamma_i. \quad (3)$$

In the formula,  $i$  represents the module number,  $A_i$  represents the maximum rotation angle of the  $i$ -th module,  $\omega$  represents the frequency of the module angle change,  $k$  represents the motion control parameter, and  $\gamma_i$  represents the angle compensation amount.

We apply the motion control equation of the orthogonal joint cable climbing robot to the bridge cable measurement system to construct the bridge cable measurement model:

$$Q_i = \frac{E_i}{T_1 L}. \quad (4)$$

### 3. Simulation Experiment Analysis

**3.1. Introduction to Experimental Environment.** In order to verify the application of the cable climbing robot automation control technology in the cable measurement system, firstly, the simulation environment of the cable climbing robot is established using the Webots mobile robot simulation software, and the simulation platform is built according to the prototype in a 1:1 ratio. The i7 is simulated and tested in a computer with 5600U@2.6 GHz, memory 8GB1600MHz.

Webots is professional multifunctional mobile robot simulation software that integrates modeling, programming, simulation, and program migration developed by the Swiss Federal Institute of Technology. Based on VRML (virtual reality language), the modeling environment of robots is more convenient for its development. At present, nearly 400 universities and research institutions at home and abroad have applied Webots series software to carry out related research on robot technology. Webots software is based on OpenGL technology with a built-in 3D compiler, which can perform 3D modeling of the operating environment and robots. The scene tree is used to display the properties of objects in the simulation environment. The parameters can be edited in combination with the model. The code area is the code of the controller. The code area is the code of the controller, which supports programming language supports C/C++, Python, Java, and other IDEs, such as visual studio. The console displays debugging information and controller output parameters. Webots provides a wealth of sensor and driver models. The available sensors include cameras, distance sensors, light sensors, position and force sensors, and GPS. It provides humanoid robots, simulated robots, mobile robots, and connecting rod joints. The research and development of robots facilitate the learning and application of the platform. The simulation cable climbing robot built in the Webots environment is shown in Figure 5.



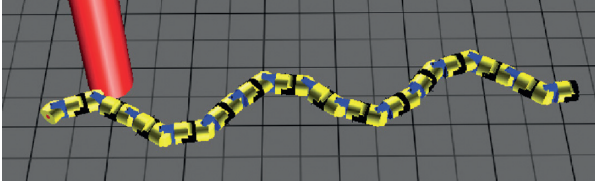


FIGURE 5: A simulation platform of a rope climbing robot based on Webots.

The entire rope climbing robot is composed of 30 orthogonal 30 modules, which are driven by Servo. The motion control of the robot in the simulation environment is to assign values to the Servo parameters at each moment, and different rotation angles have different motion modes for the rope climbing robot. First, click controller in the general node in the scene tree, select the associated controller code file, click “Edit” to enter the code writing interface, then call the necessary precompiled header files, and set and initialize the relevant values; in the control program by obtaining keyboard commands to dynamically select the motion mode, Servo rotates the angle calculated by the control equation with time as a function to perform the simulation.

**3.2. Comparison of Measurement Accuracy of Different Systems.** Under the above-mentioned simulation platform, the bridge cable measurement system based on cable climbing robot automatic control technology designed in this paper, the cable-stayed bridge cable anchor measurement system based on datum transfer designed in literature [6], and the suspension bridge cable clamp designed in literature [7] are adopted. The screw axial force ultrasonic testing system measures the bridge cables to verify the measurement accuracy of the three systems. The comparison results are shown in Figure 6.

According to Figure 6, it can be seen that the cable measurement accuracy of the cable climbing robot automatic control technology designed in this paper is up to 99%, which is better than the cable-stayed bridge cable anchor measurement system based on datum transfer designed in [6], and [7] designed the suspension bridge cable clamp screw axial force ultrasonic testing system to measure the bridge cable with high accuracy.

**3.3. Comparison of Measurement Time of Different Systems.** Using the bridge cable measurement system designed in this paper based on the automatic control technology of the climbing robot, the cable-stayed bridge cable anchor measurement system based on datum transfer designed in literature [6], and the ultrasonic testing system of the screw axial force of the suspension bridge cable clamp designed in literature [7], a comparative analysis of the bridge cable measurement time was conducted, the comparison result is shown in Table 2.

According to the analysis in Table 2, the shortest measurement time of cable-stayed bridge cable anchor measurement system designed in [6] is 240.7 s, the shortest measurement time of suspension bridge cable clamp screw

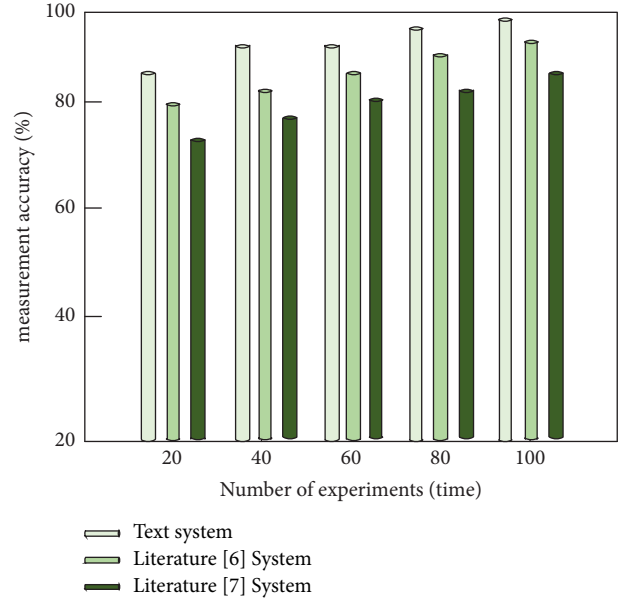


FIGURE 6: Comparison results of the bridge cable measurement accuracy of the three systems.

TABLE 2: Comparison results of bridge cable measurement time of different systems.

Number of experiments/time	Average bridge cable measurement time (s)		
	Text system	Literature [6] system	Literature [7] system
10	541.8	550.7	556.5
20	458.5	510.5	540.7
30	401.6	485.6	498.5
40	387.7	420.4	405.2
50	312.0	398.0	351.6
60	247.2	374.8	298.7
70	198.4	320.2	255.1
80	102.9	291.6	196.3
90	105.7	240.7	152.0
100	124.0	340.4	275.1

axial force ultrasonic detection system designed in [7] is 152.0 s, and the shortest measurement time of bridge cable measurement system designed in this paper based on cable climbing robot automatic control technology is 102.9 s. This shows that the bridge cable measurement system based on the automatic control technology of cable climbing robot designed in this paper takes a short time in cable measurement, has good performance, and can achieve the purpose of design.

## 4. Conclusion

With the rapid development of society, bridges have become an indispensable part of modern transportation. As the key load-bearing structure of cable-stayed bridge and suspension bridge, the effective metal bearing area of cable is directly related to the safety and service life of the bridge. Aiming at remedying the shortcomings of low measurement accuracy and long time of traditional bridge cable

measurement system, a new bridge cable measurement system based on automatic control technology of climbing robot is designed in this paper. The CIS driving circuit, main controller, and communication module in the hardware are designed; the motion control equation of the orthogonal joint cable climbing robot is obtained by calculating the DH transformation; the bridge cable measurement model is constructed; and the design of the new bridge cable measurement system is completed. By comparing this system with two traditional systems for simulation experiments, it is concluded that the cable measurement accuracy of the system designed in this paper is as high as 99% and the shortest measurement time is 102.9 s, which verifies the effectiveness of the system, achieves the purpose of system design in this paper, brings significant social and economic benefits, and lays a good foundation for bridge engineering in our country.

### Data Availability

The datasets used and/or analyzed during the current study are available from the corresponding author on reasonable request.

### Conflicts of Interest

The authors declare that there are no conflicts of interest.

### References

- [1] Y. B. Liang, S. J. Cai, and Q. Feng, "The PE appearance detection technology of the bridge cables of Wuhan Tianxingzhou Yangtze River Bridge based on drone aerial photography," *Geodesy and Geodynamics*, vol. 39, no. 11, pp. 1207–1210, 2019.
- [2] Y. P. Ou, J. G. Shi, and J. Zhang, "Design and realization of anthropomorphic climbing robot based on single chip microcomputer," *Industrial Technology Innovation*, vol. 40, no. 5, pp. 42–49, 2020.
- [3] M. L. Che, "Application design of remote control in measuring robot," *Electronic World*, vol. 15, pp. 177–178, 2019.
- [4] X. Liu, "Application of intelligent control technology in the field of industrial robot control," *Technological Innovation and Application*, vol. 10, no. 15, pp. 177–178, 2020.
- [5] L. X. Wu and Y. G. Sun, "Design of remote monitoring system for bridge cable force based on lora," *Software*, vol. 41, no. 1, pp. 216–219, 2020.
- [6] W. Cui, "Cable-stayed bridge cable anchor measurement technology based on datum transfer," *Modern Surveying and Mapping*, vol. 42, no. 1, pp. 57–59, 2019.
- [7] J. J. Yi, X. M. Peng, and B. Wang, "Ultrasonic testing technology for axial force of suspension bridge cable clamp screw," *Bridge Construction*, vol. 49, no. z1, pp. 68–73, 2019.
- [8] H. Welch and S. Mondal, "Analysis of magnetic wheel adhesion force for climbing robot," *Journal of Mechatronics and Robotics*, vol. 3, no. 1, pp. 534–541, 2019.
- [9] D. Cruz-Ortiz, M. Ballesteros-Escamilla, I. Chairez, and A. Luviano, "Output second-order sliding-mode control for a gecko biomimetic climbing robot," *Journal of Bionics Engineering*, vol. 16, no. 4, pp. 633–646, 2019.
- [10] P. Zhao, M. T. Wu, and J. X. Gu, "Design and production of a climbing robot for climbing rope," *Electronic Design Engineering*, vol. 26, no. 23, pp. 121–129, 2018.
- [11] S. Yu, C. Ye, G. Tao, J. Ding, and Y. Wang, "Design and analysis of a modular rope-climbing robot with the finger-wheeled mechanism," *Journal of Mechanical Science and Technology*, vol. 35, no. 5, pp. 2197–2207, 2021.
- [12] D. N. Badodkar and T. A. Dwarakanath, "Machines, mechanism and robotics, lecture notes in mechanical engineering," in *Proceedings of the iNaCoMM 2017, Design and Analysis of Spring-Based Rope Climbing Robot*, pp. 453–462, Springer, Berlin, Germany, 2019.
- [13] S. Yoo, I. Joo, J. Hong, J. Kim, H. S. Kim, and T. Seo, "Mechanical and empirical parameter design on a multi-wound differential pulley winch for a wall-climbing robot," *International Journal of Precision Engineering and Manufacturing*, vol. 21, no. 5, pp. 857–867, 2020.
- [14] R. S. Bisht, P. M. Pathak, and S. K. Panigrahi, "Experimental investigations on permanent magnet based wheel mechanism for safe navigation of climbing robot," *Procedia Computer Science*, vol. 133, pp. 377–384, 2018.
- [15] H. J. Zhuang, J. Li, and W. Wang, "Research on power tower climbing robot system," *Automation & Instrumentation*, vol. 246, no. 4, pp. 205–210, 2020.
- [16] C. C. Yan, H. H. Zhang, and H. Han, "Design and implementation of intelligent climbing robot based on single chip microcomputer," *Science and Technology Information*, vol. 17, no. 7, p. 2, 2019.
- [17] Y. J. Lv, L. T. Wang, and F. Su, "Design and kinematic model simulation of XY-DELTA redundant robot," *Machine Tool & Hydraulics*, vol. 489, no. 15, pp. 77–80, 2019.
- [18] P. Li, X. Duan, G. Sun, X. Li, Y. Zhou, and Y. Liu, "Design and control of a climbing robot for inspection of high mast lighting," *Assembly Automation*, vol. 39, no. 1, pp. 77–85, 2019.

## Research Article

# Security-Level Improvement of IoT-Based Systems Using Biometric Features

Masoud Moradi,<sup>1</sup> Masoud Moradkhani ,<sup>2</sup> and Mohammad Bagher Tavakoli<sup>1</sup>

<sup>1</sup>Department of Electrical Engineering, Arak Branch, Islamic Azad University, Arak, Iran

<sup>2</sup>Department of Electrical Engineering, Ilam Branch, Islamic Azad University, Ilam, Iran

Correspondence should be addressed to Masoud Moradkhani; moradkhani.m@ilam-iau.ac.ir

Received 22 July 2021; Revised 14 December 2021; Accepted 27 December 2021; Published 25 February 2022

Academic Editor: Deepak Gupta

Copyright © 2022 Masoud Moradi et al. This is an open access article distributed under the Creative Commons Attribution License, which permits unrestricted use, distribution, and reproduction in any medium, provided the original work is properly cited.

The Internet of Things (IoT) is reported as a main research topic in the current decade. It will be possible to connect smart devices to each other using IoT, a platform such as the Internet. However, the expansion and intrusion of such a large network raises some new security issues and risks related to the disclosure of user confidential information where these devices are subject to hacker threats and intrusions. Traditional security systems were password based. In this paper, after reviewing the actions taken in this regard, the improvement level of biometric security compared with traditional password-based methods will be proven in section three using the Markov model. By considering the results of the evaluation, the probability of occurrence of security problems is decreased by 90.71% by applying biometric features. Then, multi-layer security architecture with biometric features and coding systems is suggested to increase security. In the first layer, the fingerprint recognition algorithm is dependent on the module, and the U.are.U 5100 module provides more security than others. In the second layer, the Hash mechanism of the MD5 algorithm is, on average, 63.21% more efficient. By determining the properties of the first two architectural layers and ultimately for the IoT application layer, empirical methods and hardware platforms for the Internet of things are used. Concerning the simulation results, the suggested mechanism enhances the system security by 120.38% on average, which is 106.23, 110.45, and 144.46% of relative improvement compared with IoT sensors, controller layer mechanisms, and application layer mechanisms, respectively.

## 1. Introduction

Internet of Things (IoT) [1] is one of the new popular technologies in the modern era whose security and confidentiality is still a controversial topic in this field. IoT primarily requires the precise mechanisms of confidentiality, integrity, authentication, and access control model. The current Internet is constantly under attack due to technical, legal, and human problems. This issue leads to hundreds of new security challenges that should be addressed in detail. Another challenge in this area is that the IoT applications are on the rise. In this article, a brief review of security issues related to IoT and the impact of this technology on the digital divide are presented. According to a May 2014 report by the Pew Research Center, the IoT will have significantly grown by 2025. According to a research by the Gartner Institute in

2020, nearly 26 billion identifiable devices could be part of this global computer network. According to Gartner, more than 50% of Internet connections are accomplished through IoTs. The market value of IoT equipment increased from less than \$ 1 billion in 2015 to \$ 48 billion in 2025. HIS Research also reports a 6-fold increase in sales of IoT products over the next decade. According to the agency forecasts, the supply of products, e.g., sensors for pedestrian identification and traffic status applications, estimates of the state, and amount of water and air pollution in 2026, will be 1.4 billion units. IHS predicts that the IoT market will grow from a base cost of 15.4 billion devices in 2015 to 30.7 billion in 2020 and 75.4 billion in 2025 [2]. Given the rapid growth in the number of IoT devices according to International Data Corporation (IDC), the market for IoT is expected to reach \$ 41 billion by 2020 [3]. The security and privacy of IoT [4] are intended to



protect against malicious attacks and any unauthorized use of users' private information on the Internet, which has always been a major challenge in cyberspace. Theft of confidential information from the business servers, private photos from private clouds, and video content from IP-connected home cameras are typical examples of Internet hackers destroying security. Sharing personal shopping habits, disclosing people's residential information, and giving personal details to unauthorized people are behaviors that affect privacy. The impact of the challenge will be certainly enhanced by increasing the number of IoT-connected devices and services. As security threats increase, users need new authentication techniques to increase security. Many applications and services have emerged in various monitoring, medical, military care, etc. Fields using IoT technology. Moreover, the rapid growth of the sensor industry in mobile and smart devices entails users' permanent connection as a standard feature in the near future. As a result, the importance of IoT security and privacy is reported as an urgently necessary requirement, specifically for the IoT infrastructure with high level of security. Fingerprint is a reliable biometric feature that is addressed in a wide range of applications requiring authentication. Biometric systems such as fingerprints provide tools to create reliable reports and protect the privacy of authorized users [5].

In this paper, one or more of the biometric features such as fingerprint and multi-layer security architecture can be used to increase security and reliability of system from the security risk perspective. On the other hand, for the implementation of the proposed approach, the partial method and the Arduino hardware platform are used. This controller's performance can be upgraded based on the algorithms to support a variety of IoT sensors and communication platforms. Furthermore, another improvement is the simultaneous use of biometric sensors and back-up communication paths to address security threats in each layer of the IoT. The main contributions of this paper are as follows:

- (i) Security improvement by combining sensors for biometric features identification such as fingerprint sensors and voice biometric systems. The system can also be upgraded by other biometric features such as the user's face.
- (ii) IoT Controller section theory, where the Arduino controller is used with the capability of intelligence algorithms to resolve possible errors.
- (iii) Security improvement in the IoT communication layer by applying redundant mechanisms for transferring information from the Arduino controller to the Internet infrastructure.
- (iv) Security enhancement for user authentication and confirmation, a combination of password and biometric features are used to identify the person and allow access to the IoT. Along with simulating and implementing biometric identification models, cryptographic models are used to increase system

security with the secure storage of biometric data. Biometric templates must be stored with a hash-based private key to merely provide access for the registered user.

- (v) Recording biometric features should be done in a secure part of the reliable hardware so that it is not accessible to other users except the system administrator. The encrypted form of the biometric data is merely stored in the system. Moreover, once a user is erased, their biometric data are also erased from the device where rooting the device should not compromise the biometric data.
- (vi) Using Markov model for improvement biometric authentication.
- (vii) Combine hash algorithm with biometric technique for more security improvement.

The rest of this paper is structured as follows. Section 2 contains the research related to authentication and cryptography in the context of the Internet of Things. Using the Markov model, the improvement level of biometric securities compared with conventional password-based methods will be proven in Section 3. The proposed method and the related models are presented in Section 4. Simulation and details of simulation are given in Section 5 Finally, the conclusion is proposed in section six.

## 2. Related Work

In this section, the research study is reviewed from different perspectives of IoT security-related research based on fingerprint biometrics and the applied research in the area, such as medical research, is initially reviewed [6]. Then, the studies associated with IoT authentication and encryption are addressed accompanied by the reviewing the practical uses of security-sensitive applications Different types of platforms associated with security, such as cloud computing, the Arduino platform, and the cloud platform are reviewed.

In Ref. [7], a prototype-based framework for IoT-enabled health care systems is presented. The solution uses smart gateway architecture to facilitate data storage and processing, as well as the cloud as a support infrastructure for analysis and decision-making. The security of this solution depends on the security features and capabilities of the operating system. Another solution is suggested in Ref. [8]. In this context, Raspberry Pi devices are used as fog nodes. It is also guaranteed through the use of an authentication process based on the role of data confidentiality. In this context, the cloud environment is used to some extent for data storage. Also Ref. [9] discusses the hierarchical framework for use in the field of health along with the security of its data. In this method, information related to the analysis of health data is stored separately in the cloud and fog infrastructure. The solution also uses the MAPE-K-based model to support computations related to running various programs as well as data encryption. In addition, Ref. [10] suggests a low-energy health monitoring framework. This method is used to facilitate and secure the process of sending

the analyzed IoT data to the fog environment. In this solution, IoT devices also have processing power and are able to process raw data. They also have the ability to discharge data to different nodes in order to reduce energy consumption. In the fog layer is a distributed database for classifying and securing data. Hu [11] Provides a security framework for use in face recognition systems. In this solution, a central cloud is responsible for managing all available resources. Small tasks are also unloaded to process the fog infrastructure. Upon completion of tasks in fog, only the results will be sent back to the cloud for analysis and storage. In Ref. [12], another framework has been developed to provide data-sharing capabilities for users. In this proposed framework, each user operation is managed by the core of the Spark platform embedded in the cloud environment. In this method, encryption and authentication techniques have been used to provide security. Finally, an one-pass architecture is proposed that proposes PaaS capability for combining fog nodes and IoT devices [13]. This method helps with messaging communications as well as authentication. This solution supports horizontal integration between gateways and cloud data centers as well as task migration. Table 1

The authors in Ref. [14] suggested a system including NodeMCU ESP8266 microcontroller with a Wi-Fi connection for IoT driver applications. Android applications have features such as history control, navigation, registration menu, and speech recognition control. In this research, system security consists of a unique biometric and speech authentication mechanism. However, compared with the mechanism in our paper, the suggested mechanism is proposed only in the layer of IoT sensors. Authors in their study designed a low-cost biometric system for IoT devices using limited resources to be able to save the memory and computation costs [15]. The suggested system utilizes an algorithm based on the block logic operation to reduce biometric property measurement. However, the introduced mechanism is only proposed in the layer of IoT sensors compared with the suggested one in our article.

In their study, Karimian et al. discuss the cost of using biometric systems and suggest frameworks for their improvement [16]. In this regard, Srianusha et al. proposed a system for fingerprint engine start. This system allows only authorized users to drive the vehicle via scanning their fingerprints. Users can enter the system and register by letting the system scan their fingerprints. In this research, Atmega 328 and esp8266 wifimodule microcontrollers are used. We can refer to the single-layer security mechanism approach in the sensors layer as one of the limitations of this study. In this paper, by considering the reviews regarding the related activities, in contrast with traditional security systems, we seek to utilize biometric properties on the platform of multi-layer security architecture. In other words, a multi-layer security architecture, including biometric features and coding systems, is proposed. In the first, second, and application IoT layers, fingerprint recognition algorithm, Hash algorithm, and hardware platforms for the Internet of things are used, respectively.

In Ref. [17] a lightweight algorithm is presented to ensure the security of the cloud computing environment. The proposed algorithm uses the 16 byte block encryption technique to encrypt the data. In this algorithm, Faistel network with permutation and replacement architecture are used to complicate the cryptographic process. This solution has the power to run with the length of the private key and the number of different cycles. The results of the evaluation indicate that the implementation time of the solution is low. But the problem with these private key-based solutions is that they require an encryption key exchange, which can compromise security and privacy. In Ref. [18] several different encryption techniques have been used to secure cloud storage space. For this purpose, an encryption system based on AES algorithm and asynchronous key transfer system for data or information exchange is provided. Elliptic curve encryption technique has also been used to exchange information between the user and the server. The solution has been able to achieve a relatively good execution time in the process of sending and receiving data, although in this evaluation, the volume of data is considered very small. The authors in Ref. [19] presented a two-step encryption solution to secure data storage in the cloud. In this solution, the main data are divided into two parts, which are encrypted by a common key. The cryptographic key is based on the model of chaos theory. This solution can increase the encryption time while increasing security, but the required time for splitting and combining data has not been investigated. In Ref. [20], blockchain is used for a security solution based on cloud computing. Accordingly, to ensure data security, data are stored in the form of blockchain blocks. For any data to be stored in block form, it will require the approval of more than half of the servers, so it will be virtually impossible to make unwanted changes. But this type of security will have problems; for example, if the user wants to delete or change the data, it will be very costly. Another problem is how to store different types of data in the form of blockchain blocks because the blockchain is originally designed to store data related to transactions. In Ref. [21], the performance of some symmetric cryptographic algorithms has been studied in terms of runtime parameters and memory consumption. The results show that DES and Blowfish algorithms are more efficient in encryption and decryption time as well as memory consumption. The articles [22, 23] provide an overview of the most important cryptographic solutions that can be used in cloud computing and the Internet of Things. The results of these studies indicate the need for algorithms and solutions that can create a kind of compromise between security and service quality parameters, so that due to the limited resources of processing nodes in the IoT devices, the use of encryption technique has the least negative impact on providing services.

Authors in Ref. [24] provides a secure decision-making solution for the Internet of Things based on cloud computing. Accordingly, machine learning alongside IoT based on fog computing has been used to provide a safe experience in healthcare systems. Blockchain has also been used to secure the framework. In this solution, data related to patients' physiological signals are first collected using

TABLE 1: Shows summarizing the metrics and limitations of various methods.

Method	Decentralized management	Security features			Platform independence	Ability to integrate in...		
		Security	Authentication	Integrity		Cloud	Fog	IoT
Rahmani [7]	✓	✓	✓	✗	✗	✓	✓	✓
Dubey [8]	✓	✓	✓	✗	✗	✗	✓	✓
Azimi [9]	✓	✓	✓	✗	✗	✓	✓	✓
Gia [10]	✓	✓	✓	✗	✗	✗	✓	✓
Hu [11]	✗	✗	✗	✗	✗	✓	✓	✓
Suneetha et al. [12]	✗	✗	✓	✗	✗	✓	✓	✓
Jaberi, et.al. 2021	✗	✗	✓	✓	✓	✗	✓	✓
Proposed	✓	✓	✓	✓	✓	✓	✓	✓

intelligent devices and sent to fog nodes. In this case, the fog nodes use their processing power to use machine learning to examine the physiological signals received and to make decisions about patients who may have problems. After the diagnosis of this group of patients, a warning message is sent to the relevant doctor. In this case, blockchain is used to secure the data stream. The authors in Ref. [25] provided a survey on IoT-based healthcare system. For this purpose, a comprehensive review of the applications, problems, and challenges of these systems has been conducted. The result of this study is the need for the development of traditional health models with the help of IoT infrastructure. In this way, a permanent connection can be established between the patient and the medical centers through IoT sensors. But, in the meantime, there are security and privacy challenges that require new research and solutions to provide secure algorithms that require low resources.

Also in Table 2 contribution of some related works are shown.

### 3. Biometric Security Using Markov Model

In the traditional systems, security depended on password-based approaches. In this section, the level of security improvement in biometric-based systems compared with traditional password methods will be proven.

In order to evaluate the security, we introduce a Markov process to describe a security attack model based on the Markov transition matrix. A security threat is a stochastic process; therefore, we model it as a Markov chain.

**3.1. Two-State Markov Model.** The probability of transition from one state to another is defined based on the vulnerabilities present in the current state. An attacker misuses various vulnerabilities to reach a security threat state and, ultimately, reaches the ultimate failure. Not applying security measures, the system has two states, as shown below:

- (i) S state for secure state
- (ii) F state for failure state

**3.1.1. Two-State Markov Model in the State of Inability for Recovering Security Threat.** In the Markov model shown below, “a” probability indicates the probability of

transition from a secure state to a failure state. Since in this model, recovering the security threat is not possible, the system enters the failure state (fault state) during the security threat. In the Markov chain, the sum of probabilities of outgoing edges from each state is equal to one (see Figure 1).

**3.1.2. Two-State Markov Model Able to Recover Security Threat.** In this Markov chain, since recovering the security threat is possible, there is a “b” probability for a system in failure state to return and recover from security error state to a secure state (see Figure 2).

- (i) “a” probability: it indicates the transition probability from a secure state to a threat state.
- (ii) “b” probability: it indicates the return and recovery probability of the system from a security error state to a secure state (detection and correction of security threat).

**3.2. Three-State Markov Model.** By applying the suggested mechanism, we focus on the observable and measurable states and develop three states [27].

- (i) State “S” for the secure state of the system
- (ii) State “T” for the threat state of the system
- (iii) State “F” for the failure state of the system

Figure 3 presents the suggested pattern of Markov for modeling security threats and attacks with the probability of transition between states.

The probabilities of transition between states in the Markov model are as follows:

- (i) Probability “a”: indicates the probability of transition from a secure state of the system to a threat state.
- (ii) Probability “b”: indicates the probability of threat elimination and return of the system from a threat state to a secure state.
- (iii) Probability “c”: indicates the probability of transition from the system’s threat state to failure state and occurrence of security error (in the case of not identifying the security threat).

TABLE 2: Related works in the field of IoT security.

Reference paper	Year	Contribution
[17]	2021	In this solution, a lightweight algorithm based on block cryptography is used to provide security in fog computing.
[19]	2020	A two-step encryption solution is provided to secure the data stored in the cloud. In this solution, the main data are divided into two parts, which are encrypted by a common key.
[22]	2020	In this article, the authors provide an overview of the most important cryptographic solutions that can be used in fog computing. The results of these studies indicate the need for algorithms and solutions that can create a kind of compromise between security and service quality parameters.
[24]	2020	A framework for use in health care systems along with machine learning for decision-making based on patient data is provided. Also, blockchain has been used to secure the data stream.
[26]	2020	This paper first examines the infrastructure, protocol, and application of the Internet of Things. Then, security problems in the IoT environment are expressed. It also identifies some emerging techniques that can be used to address IoT security issues. In this study, the authors conclude that machine learning, blockchain, and artificial intelligence are the new approaches to solving the problem of IoT security.
[14]	2020	The authors provided a system including a microcontroller with android application that has features for history control and speech recognition. For securing this system, they are using a unique biometric and speech authentication mechanism.
[15]	2019	Authors in this paper provided a low-cost biometric system for IoT devices that used limited resources to reduce memory and computation costs. The proposed system utilizes an algorithm based on the block logic operation to reduce biometric property measurement.
[21]	2019	A number of symmetric cryptographic algorithms have been investigated in terms of performance. Solutions in terms of runtime parameters and memory consumption have been investigated. The purpose of this study was to determine the capabilities and limitations of each cryptographic algorithm.
[18]	2018	In this research, an encryption system based on AES algorithm and asynchronous key transfer system for data exchange is presented. This solution can be used to secure infrastructure with limited processing resources.
[20]	2018	Blockchain has been used as a security solution based on cloud computing. To ensure data security, data are stored in the form of blockchain blocks.

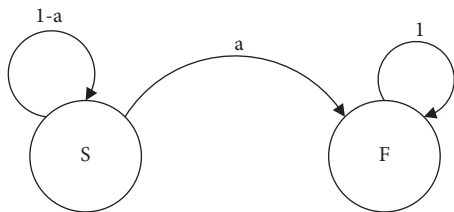


FIGURE 1: Markov model before the proposed mechanism and impossibility of security threat.

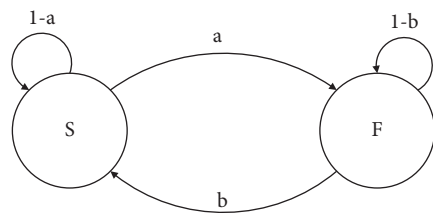


FIGURE 2: Markov model before the suggested mechanism.

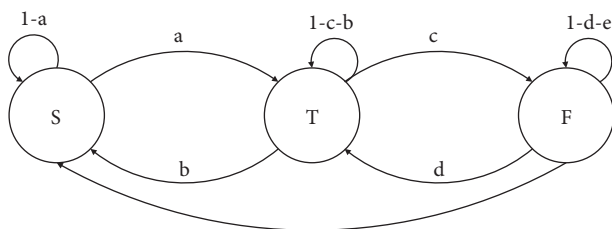


FIGURE 3: Three-state Markov model.

- (iv) Probability “d”: indicates the probability of return of the system from security error occurrence state to threat state (detection of security threat).
- (v) Probability “e”: indicates the probability of return and recovery of the system from security error occurrence to secure state (detection and correction of security threat).

This security model contains every element of a security attack, including attack, defense, and system recovery. In this article, due to some reasons, we will not introduce the direct transition from state S to state F, because several stages exist for the detection and correction of security threats in the proposed mechanism.

Since security threats, as error occurrence factors, lead to the system entering an undesired state, there are two states of detection and correction to deal with security threats.

In the above model, probabilities “b” and “d” indicate the correction probabilities of the security threats (probability “b” indicates the probability for system return from a threat state to a secure state after correction of the threat state and probability “d” indicates the probability of system return from security error occurrence to threat state in the case of error correction of the threat state).

3.3. Transition Probability Matrix for States of Security Evaluation. The transition probability matrix for a Markov chain with  $n$  states is a  $n \times n$  matrix in which the element

$p[i, j]$  is the probability of transition from state  $i$  to state  $j$  in the range [1, 28].

3.3.1. *Transitions Probability Matrices of the Two-State Markov Model in the Mode of the Impossibility of Security Threat Recovery.* In the transition probability matrix, the sum of values of each row is equal to one. Hence, based on the Markov chain, the transition probability matrix is obtained, as shown in Figure 4.

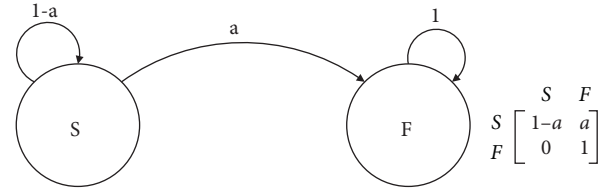


FIGURE 4: The Markov chain and transitions probability matrix before suggested mechanism and impossibility of security threat recovery.

3.3.2. *Transition Probability Matrix of the Two-State Markov Model with the Possibility of Threat Recovery.* In this case, in the Markov chain, there is a probability of  $b$  for recovery of the security threat. Therefore, the transition probability matrix is obtained (see Figure 5).

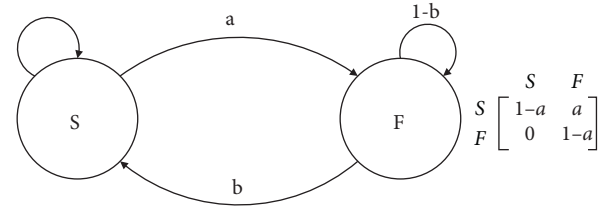


FIGURE 5: Markov chain and transitions probability matrix before the suggested mechanism and the possibility for recovery of the security threat.

3.3.3. *Transition Probability Matrix of the Three-State Markov Model.* Figure 6 presents the suggested pattern for modeling security threats and attacks based on the Markov chain and the transition probability matrix.

3.4. *The Failure Probability of the System and Security Hacking.* Based on the Markov chain and transition probability matrix, the probability of the system failure and security hacking is shown as  $P(F)$  and obtained by the below equations:

- (a) The probability of system failure and security hacking in the first Markov model

$$P(F) = P(S).a + P(F).1$$

$P(S)$ : The probability of the system being at the secure state

$P(F)$ : The probability of the system being at the hacking state and failure of the firewall

- $b$ . The probability of system failure and security hacking in the second Markov model

$$P(F) = P(S).a + P(F).(1 - b)$$

- $c$ . The probability of system failure and security hacking in the third Markov model

$$P(F) = P(S).a.P(T).c + P(F).(1 - d - e)$$

$P(T)$ : The probability of the system being at the threat state

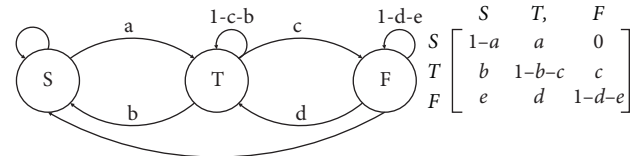


FIGURE 6: The Markov chain and transition probability matrix with the suggested mechanism.

## 4. The Proposed Mechanism

Security improvement in different systems is based on the following three mechanisms:

- (i) Authentication Algorithm
- (ii) Hash Algorithm
- (iii) Encryption Algorithm

The proposed mechanism in this paper is based on a combination of Hash and Authentication mechanisms.

4.1. *First Layer of Security Architecture: Authentication.* If the fingerprint is accepted by the controller, the confirmation signal is sent through the transmitter module to the IoT system, which can also include a wireless receiver pair and a similar controller. The flowchart of the IoT platform transmitter function is shown in Figure 7. In this algorithm, the fingerprint is initially received by the relevant module via the IoT controller for receiving and authentication of the user and after comparing the received data, the data are compared with the approved biometric features database. If the user authentication is verified, the connection to the infrastructure will be established.

As shown in Figure 8, a fingerprint image is captured by a scanner or sensor and the sensor converts it into a data format.

The Next Scenario is similar to the baseline scenario based on the hardware perspective except that the VeriFinger fingerprint identification algorithm is used. A set of minutiae points is used in the VeriFinger fingerprint identification algorithm. The first step in fingerprint authentication is fingerprint image sampling. In the fingerprint sensor, the characteristics of the points with the matched fine lines are taken from the fingerprint image, and they are referred to as minutiae points. In biometrics and fingerprint scanning, minutiae refer to specific plot points on a fingerprint. This includes characteristics such as ridge bifurcation or a ridge ending on a fingerprint. These features store

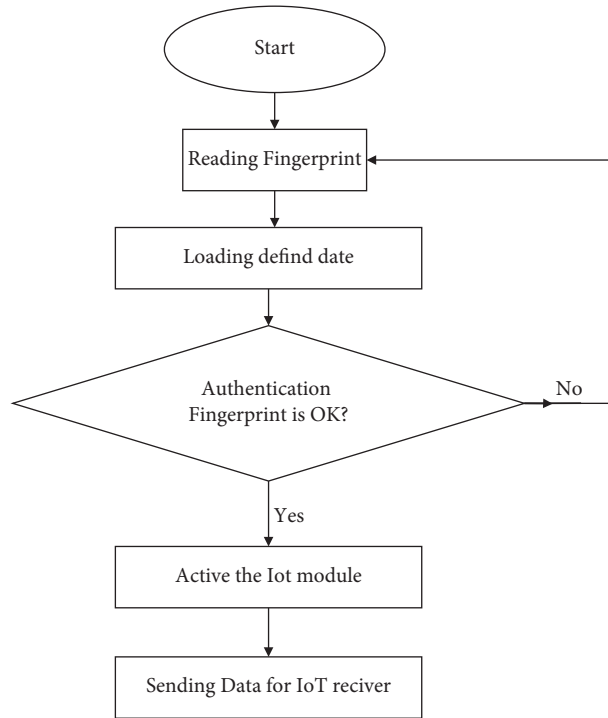


FIGURE 7: System failure probability in the first Markov model.

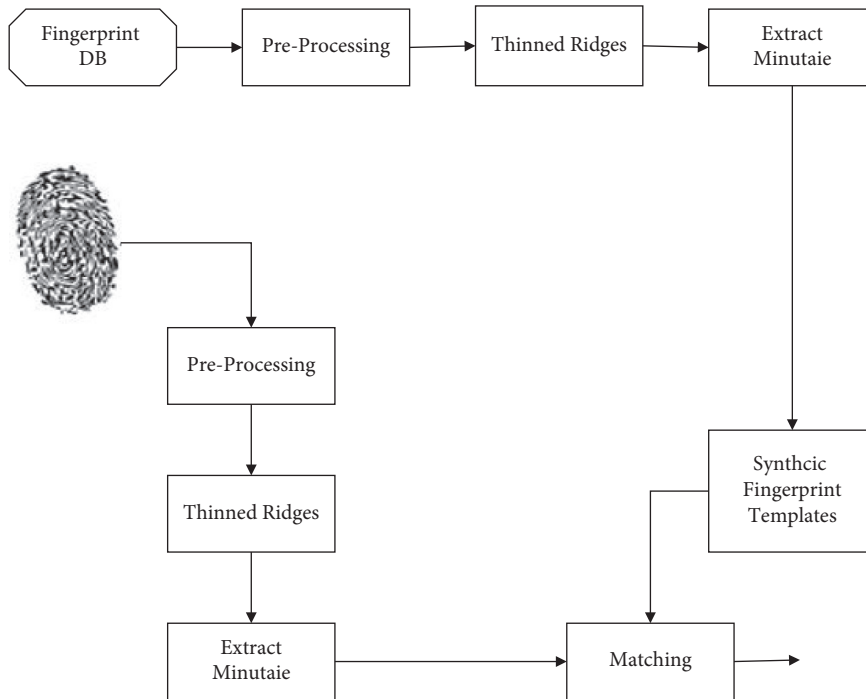


FIGURE 8: System failure probability in the second Markov model.

each individual finger in a database and differentiate them from other recorded fingerprints. Fingerprint is initially matched with the entries in the database which have general features similar to the tested fingerprint. If the matching operation with this group does not produce a positive result, the next record with the most similar general features would

be selected and the process continues with the same basis until either the successful result is achieved or the end of the database is announced.

Three fingerprint samples are taken from one finger to produce more accurate and higher quality results. Each of the three images is processed to extract its features. The

three sets of features are then analyzed and subdivided into a single set of features written in the database. Accordingly, the recorded features will be more reliable and the fingerprint identification quality is significantly enhanced. The flowchart in Figure 9 illustrates the VeriFinger fingerprint identification algorithm step by step.

**4.2. Second Layer of Security Architecture: Hashing.** In subsequent scenarios, in addition to security enhancement by the fingerprint sensor at the IoT sensor layer, hash and encoding algorithms are used. Figure 10 schematically illustrates the mechanism of combining hash and biometric fingerprint encoding algorithms.

The fingerprint sensor and encryption in this scenario are combined with the MD5 algorithm. The MD5 algorithm returns a 128-bit digital fingerprint as an output where the message means the biometric feature of the IoT user (see Table 3).

**4.3. Third Layer of Architecture: IoT Controller.** User authentication based on each one of the biometric properties, such as voice biometric and cryptosystem, is according to the below items:

IoT controller supports below elements regarding encryption algorithms.

- (i) Authenticated encryption with associated data (AEDA): GCM, EAX, ChaChaPoly
- (ii) Encrypted blocks: AES256, AES192, AES128
- (iii) Encryption modes: XTS, GCM, EAX, CTR
- (iv) Hash algorithms: BLAKE2b, BLAKE2s, SHA3\_512, SHA3\_256, SHA512, SHA256
- (v) Extendable output functions: SHAKE256, SHAKE128
- (vi) Message authentication: MAC-, GHASH, Poly1305
- (vii) Public-key algorithms: P521, Ed26619, Curve25519
- (viii) Random number generation: RNG

Based on the statistics of Ref. [6], the application of some of these algorithms is listed as follows:

Encryption algorithms  
Hash algorithms  
Authentication algorithms

**4.4. Combining Biometric and Hashing.** Multiple authentication to enhance user authentication along with coding mechanisms has been proposed as a new approach in this study. Primary authentication is done using biometric identification, which demonstrates the highest level of security compared to other methods of identification. The main advantage of this approach is reported to provide unique information, i.e., the biological features of the individuals, and remove the problem of replay attacks. The use

of encryption-based systems also prevents replay attacks and eavesdropping. The proposed architecture includes the following components:

- (i) Biometric authentication by scanning the relevant biological features
- (ii) Sending the scan result to the database
- (iii) Encrypting the data to the database
- (iv) Comparing the encrypted data with the samples in the database
- (v) Performing the compliance and authenticity steps
- (vi) Approving and allowing the user to communicate in case of matching
- (vii) Monitoring of the IoT data

To improve security, the security threats are classified as follows:

- (i) Security threats in the identification layer
- (ii) Security threats of the control algorithms
- (iii) Security threats in the network communications layer (IoT Infrastructure)

Figure 11 shows how to combine biometric and hashing features to increase security:

## 5. Evaluation

**5.1. System Configuration.** The details and configuration of hardware's instrument are shown in Table 4.

Also, the raspberry Pi 4 details are described in Table 5.

**5.2. Simulation Details.** The simulated data are extracted from the Arduino IDE (A compiler of commands for programming IoT sensors) and Fritzing V0.9.2 b (simulating the hardware needs to communicate with the sensors) simulation software and the proposed algorithm is evaluated with different benchmark test structures. Then, the IoT security models are analyzed. The Arduino controller is an open source platform. This unique feature contributes to find relevant libraries for each module or sensor. User authentication is based on each of the biometric features such as audio biometric and cryptographic system to increase security. To analyze and evaluate the proposed method, various simulation scenarios are presented related to the security of IoT-based systems. In Scenario 1, the level of security is checked by the fingerprint sensor authentication mechanism. The components of this scenario can be seen in Figure 12:

Schematic of IoT implementation based on fingerprint biometrics is illustrated in Figure 13:

Considering the evaluation results, the VeriFinger algorithm and encryption algorithms both affect the security authentication on the Internet of things. These parameters are selected based on the interactions between security, efficiency, and system cost. From the perspective of VeriFinger algorithm modules, U.are.U 5100 and Verifier 300 modules have the most and least level of security. For



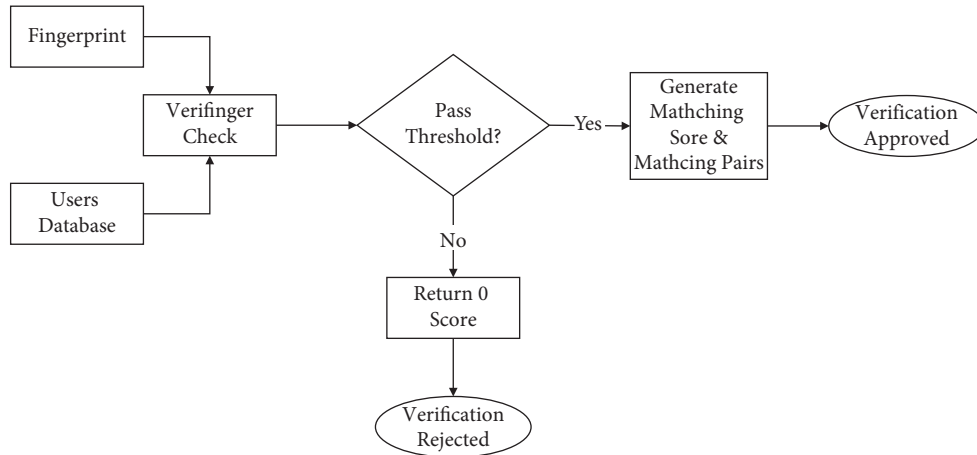


FIGURE 9: The transmitter module flowchart.

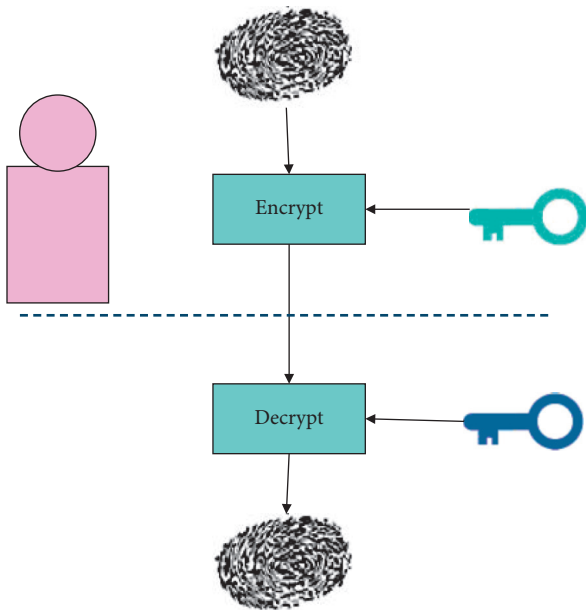


FIGURE 10: Biometric data matching steps.

TABLE 3: Comparing the characteristics of MD5 and SHA1 algorithms.

Function	MD5	SHA1
Block length	512 bit	512 bit
Algorithm length	128 bit	160 bit
Rotation steps	64 steps	80 steps
Initialization variables	4	5
Collision complexity	$2^{54}$	$2^{80}$

moderate security purposes, the FS80 module can be used based on efficiency and costs.

The fingerprint identification algorithm of VeriFinger is evaluated regarding authentication mechanisms; on the other hand, the efficiency and security of this algorithm are dependent on other fingerprint modules. In this regard, based on the agreement accuracy and agreement speed of fingerprint reading, U.are.U 5100 module has

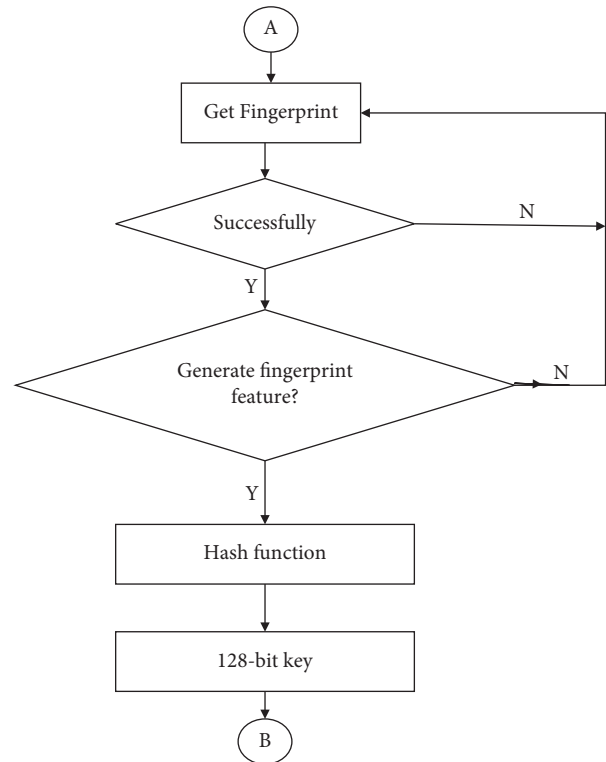


FIGURE 11: VeriFinger fingerprint identification algorithm.

more security than modules FS80 and Verifier 300. Hence, in the following sections, the fingerprint recognition authentication mechanisms are simulated based on the U.are.U 5100 module. Concerning Hash mechanisms, the strongest Hash mechanism is based on security evaluation in different conditions of algorithms, namely, MD5 and SHA1.

To check the performance of the MD5 and SHA1 encoding algorithms, the encoding time parameter is used, which is a function of the fingerprint file size (see Figure 14).

Comparing the computation time required for MD5 algorithm coding relative to SHA1 is 63.21% on average (see Table 6).

TABLE 4: Details and configuration of hardware's instrument.

IoT Device	Finger Pulse Oximeter Jumper JPD-450F, 1.6 V, with Bluetooth v4.2.
Master node	Laptop dell E6520, intel core i7- CPU 2760QM @ 2.40 GHz, 8 GB RAM DDR3
Worker node	Raspberry pi 4, ARM Cortex-A72

TABLE 5: Raspberry Pi 4 details.

Broadcom BCM2711, Quad core Cortex-A72 (ARM v8) 64 bit SoC @ 1.5 GHz
4 GB LPDDR4-3200 SDRAM
2.4 GHz IEEE 802.11ac wireless, bluetooth 5.0, BLE
2-Lane MIPI CSI camera port
Gigabyte ethernet 10/100/1000 Mbit/s
2-Lane MIPI CSI camera port
OpenGL ES 3.1, vulkan 1.0
5V DC via USB-C connector

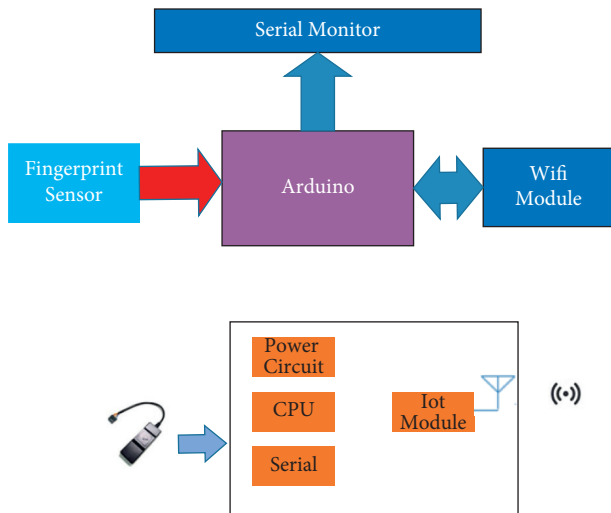


FIGURE 12: Combining hash and fingerprint biometric encryption algorithms.

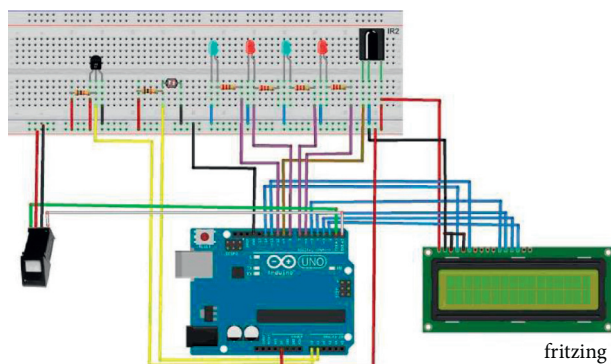


FIGURE 13: Comparison of the performance of MD5 and SHA1 encoding algorithms by the fingerprint file size.

Thus, by applying the biometric properties and a combination of applied innovations in IoT layers, the probability of security problems reduced by 90.71% on average. On the other

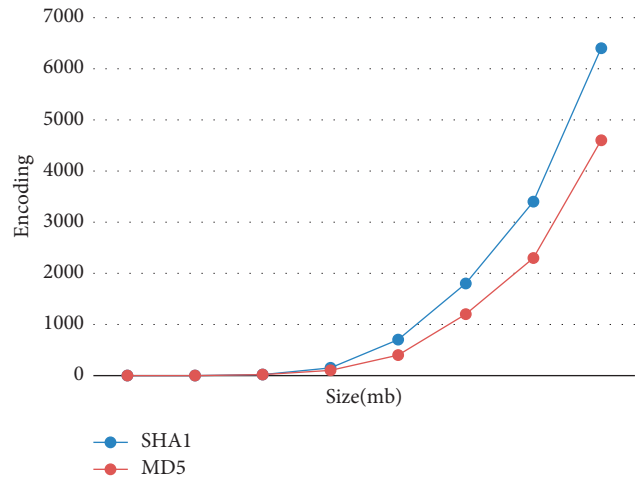


FIGURE 14: Increasing security by combining biometric and hashing features.

TABLE 6: Summary of comparing the time required for coding.

File size(KB)	Time MD5/SHA1 (%)
8	67.65
16	69.35
32	36.63
64	74.07
128	52.85
256	66.88
512	67.56
1024	70.70
Average	63.21

hand, to keep the efficiency of these MD5 and SHA1 algorithms from the perspective of the time required for coding, using the MD5 algorithm, leads to a 63.21% reduction in the delay time of system efficiency improvement.

5.3. Evaluation of the Two Proposed Methods. Based on the study [29], the security resulted from traditional systems, such as password compared with biometric properties, like the fingerprint, as shown in Table 7.

5.3.1. Evaluation of Security of the Two-State Markov Model in the State of the Impossibility of Security Threat Recovery. Before the suggested mechanism and impossibility of security threat, concerning the obtained equation, the probability of the system being at the hacking state and firewall failure is obtained from the below relationship:

$$P(F) = P(s_0) \cdot A + (F_0) \cdot 1. \tag{1}$$

TABLE 7: Evaluation of Users' accounts.

Security rating	Password (%)	Fingerprint (%)
Very secure	23.4	31.9

Based on different values of  $a$ , which is the occurrence probability of security threat, and initial value of  $P(S0)$ , which according to the security results of traditional systems, is assumed as password and biometric property, two tables are generated, as shown below. It should be noted that the initial value of  $P(F0)$  is the supplement of state  $P(S0)$ . See Tables 8 and 9.

The probability of system failure and security hacking of the first Markov model in two states of using password compared with using fingerprint biometric can be observed in Figure 15.

**5.3.2. Evaluation of the Two-State Markov Model Security with the Possibility of Security Threat Recovery.** Before applying the proposed mechanism and with security threat recovery, considering the acquired equation, the probability of the system being at hacking state and firewall failure is obtained from the below relationship:

$$P(F) = P(s0) \cdot a + P(F0) \cdot (1 - b). \quad (2)$$

By considering the probability of security threat occurrence and initial values  $P(S0)$ , which are assumed based on the security results from traditional systems, such as password and biometric property, Tables 10–13 are obtained based on different values of  $a$  and  $b$ .

The probability of system failure and security hacking of the second Markov model using password compared with using fingerprint biometric can be observed in Figure 16.

**5.3.3. Security Evaluation of the Three-State Markov Model.** By applying the proposed mechanism, which is measured based on the initial values of states  $P(s0)$ ,  $P(T0)$ ,  $P(F0)$ , and coefficients of  $e$ ,  $d$ ,  $c$ , and  $a$ :

$$P(F) = P(s0)a \cdot P(T0) \cdot c + P(F0) \cdot (1 - d - e). \quad (3)$$

The result was much higher than the first and second models, which were obtained using fingerprint biometrics instead of passwords, thus reducing the probability of system hacking by an average of 83.12%.

#### 5.4. Evaluation Results of Different Markov Models

**5.4.1. Evaluation Result of Security Failure Probability in the First Markov Model.** As seen in Table 14, applying the biometric fingerprint leads to an average decrease of 94.99% in the probability of system hacking compared with using a password.

**5.4.2. Evaluation Result of Security Failure Probability in the Second Markov Model.** Averaging the evaluation results

TABLE 8: Evaluation of security in the first model of Markov with the assumption of using password.

$a$	$P(S0)$	$P(F0)$	$P(F)$
0.10	23.4	76.6	78.94
0.20	23.4	76.6	81.28
0.30	23.4	76.6	83.62
0.40	23.4	76.6	85.96
0.50	23.4	76.6	88.3
0.60	23.4	76.6	90.64
0.70	23.4	76.6	92.98
0.80	23.4	76.6	95.32
0.90	23.4	76.6	97.66

TABLE 9: Evaluation of security in the first model of Markov with the assumption of using fingerprint biometric.

$a$	$P(S0)$	$P(F0)$	$P(F)$
0.10	31.9	68.1	71.29
0.20	31.9	68.1	74.48
0.30	31.9	68.1	77.67
0.40	31.9	68.1	80.86
0.50	31.9	68.1	84.05
0.60	31.9	68.1	87.24
0.70	31.9	68.1	90.43
0.80	31.9	68.1	93.62
0.90	31.9	68.1	96.81

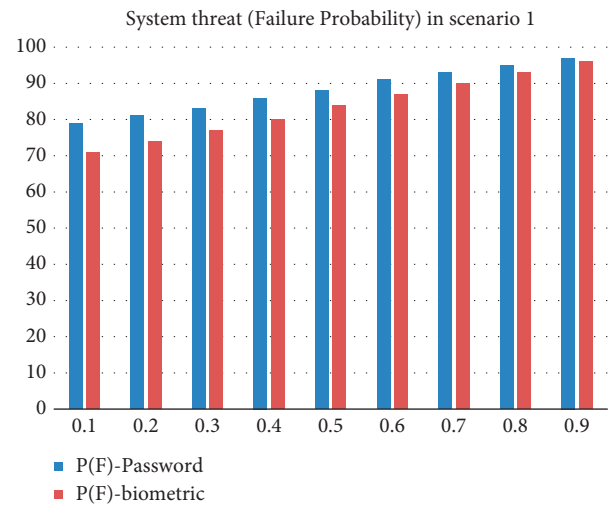


FIGURE 15: Block Diagram of Scenario Modules 1 (fingerprint sensor authentication in IoT).

shows that using biometric fingerprint reduces the probability of system hacking by 94.02% on average.

**5.4.3. Evaluation Result of Security Failure Probability in the Third Markov Model.** Applying the biometric fingerprint reduces the system hacking probability by 83.12% on average.

**5.5. Evaluation Result of Security Failure Probability.** Overall, the probability of security problem occurrence in three Markov models reduces by 90.71% on average by applying the biometric properties (see Table 15).

TABLE 10: Evaluation of security in the second Markov model with the assumption of using a password (constant value of  $b$  and variable  $a$ ).

$a$	$b$	$P(S)$	$P(F)$	$P(F)$
0.10	0.90	23.4	76.6	10
0.20	0.90	23.4	76.6	12.34
0.30	0.90	23.4	76.6	14.68
0.40	0.90	23.4	76.6	17.02
0.50	0.90	23.4	76.6	19.36
0.60	0.90	23.4	76.6	21.7
0.70	0.90	23.4	76.6	24.04
0.80	0.90	23.4	76.6	26.38
0.90	0.90	23.4	76.6	28.72

TABLE 11: Evaluation of security in the second Markov model with the assumption of using a password (constant value of  $a$  and variable  $b$ ).

$a$	$b$	$P(S)$	$P(F)$	$P(F)$
0.10	0.10	23.4	76.6	71.28
0.10	0.20	23.4	76.6	63.62
0.10	0.30	23.4	76.6	55.96
0.10	0.40	23.4	76.6	48.3
0.10	0.50	23.4	76.6	40.64
0.10	0.60	23.4	76.6	32.98
0.10	0.70	23.4	76.6	25.32
0.10	0.80	23.4	76.6	17.66
0.10	0.90	23.4	76.6	10

TABLE 12: Evaluation of security in the second Markov model with the assumption of using biometric (constant value of  $b$  and variable  $a$ ).

$a$	$b$	$P(S)$	$P(F)$	$P(F)$
0.10	0.90	31.9	68.1	10
0.20	0.90	31.9	68.1	13.19
0.30	0.90	31.9	68.1	16.38
0.40	0.90	31.9	68.1	19.57
0.50	0.90	31.9	68.1	22.76
0.60	0.90	31.9	68.1	25.95
0.70	0.90	31.9	68.1	29.14
0.80	0.90	31.9	68.1	32.33
0.90	0.90	31.9	68.1	35.52

TABLE 13: Evaluation of security in the second Markov model with the assumption of using biometric (constant value of  $a$  and variable  $b$ ).

$a$	$b$	$P(S)$	$P(F)$	$P(F)$
0.10	0.10	31.9	68.1	64.48
0.10	0.20	31.9	68.1	57.67
0.10	0.30	31.9	68.1	50.86
0.10	0.40	31.9	68.1	44.05
0.10	0.50	31.9	68.1	37.24
0.10	0.60	31.9	68.1	30.43
0.10	0.70	31.9	68.1	23.62
0.10	0.80	31.9	68.1	16.81
0.10	0.90	31.9	68.1	10

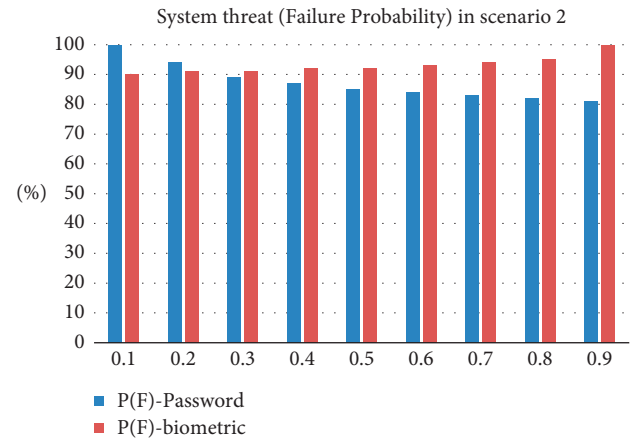


FIGURE 16: Schematic of implementing the IoT application.

TABLE 14: Evaluation result of security failure probability in the first Markov model.

$a$	$P(F)$ -Password	$P(F)$ -Biometric	System threat (failure probability) in model 1 (%)
0.10	78.94	71.29	90.31
0.20	81.28	74.48	91.63
0.30	83.62	77.67	92.88
0.40	85.96	80.86	94.07
0.50	88.3	84.05	95.19
0.60	90.64	87.24	96.25
0.70	92.98	90.43	97.26
0.80	95.32	93.62	98.22
0.90	97.66	96.81	99.13
Average			94.99

TABLE 15: Security failure probability by applying the biometric properties.

System threat (failure probability) (%)	
Model 1	94.99
Model 2	94.02
Model 3	83.12
Average	90.71

5.6. *Simulation Scenarios.* As mentioned in previous sections of the article, we assume the below scenarios by considering the schematic of Figure 13:

- (i) Facing security threats by fingerprint recognition in the first layer of IoT
- (ii) Facing security threats by the hash mechanism in the second layer of IoT
- (iii) Facing security threats by software and hardware mechanisms in the application layer of IoT
- (iv) Facing security threats by applying the suggested mechanism in the article, including the aggregation of the above mode in all three architectural layers of IoT

In the following, we examine the results of each scenario from the security perspective and study the improvement level of the suggested system.

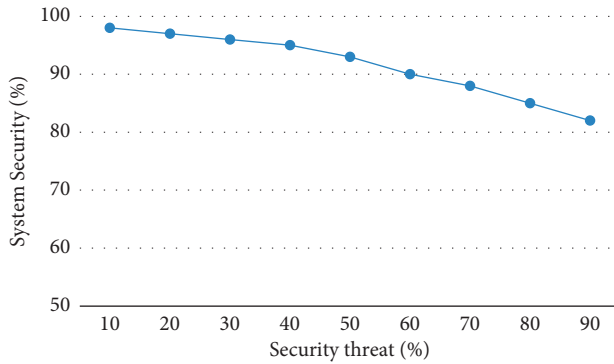


FIGURE 17: System security in the first scenario for different levels of security threats.

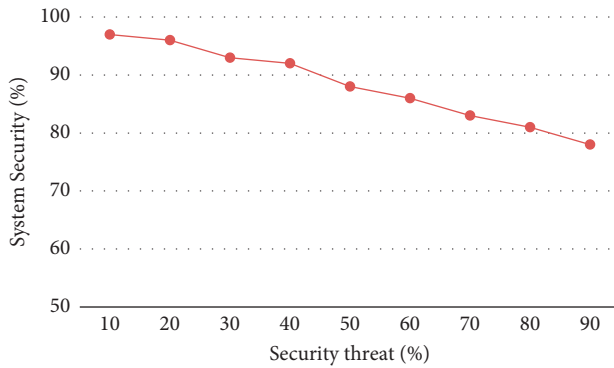


FIGURE 18: System security in the second scenario for different levels of security threats.

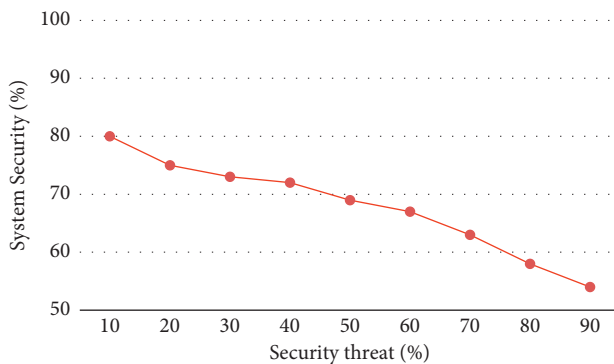


FIGURE 19: System security in the third scenario for different levels of security threats.

5.6.1. *First Scenario: Facing the Security Threats by Fingerprint Recognition in the First Layer of IoT.* In this case, biometric properties are applied only in the sensors' layer, and on average, the system security is 91.34% (see Figure 17).

5.6.2. *Second Scenario: Facing the Security Threats by the Hash Mechanism in the Second Layer of IoT.* In this case, the hash mechanism in the second IoT layer is used to face

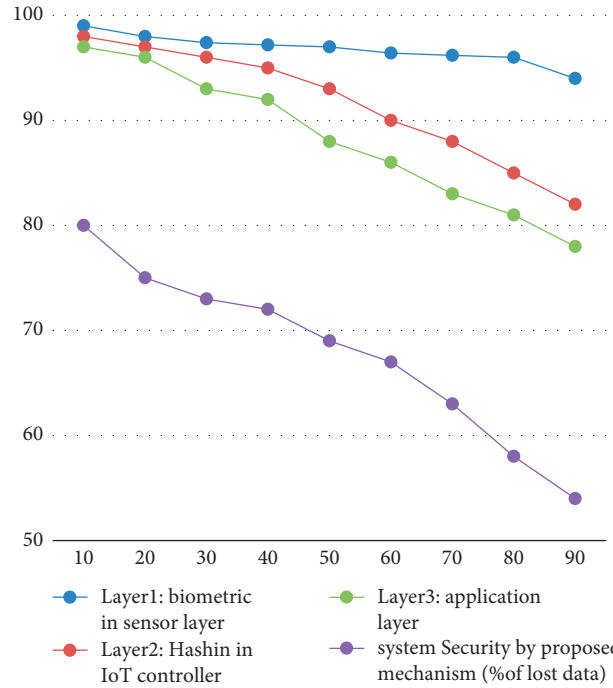


FIGURE 20: Comparison of system security in the suggested mechanism with available scenarios.

TABLE 16: Comparison results.

Security threat (%)	System security improvement (relative to each layer)		
	Layer 1: Biometric in sensor layer	Layer 2: Hashing in IoT controller	Layer 3: Application layer
10	101.33	101.33	122.80
20	102.32	103.29	130.58
30	102.08	105.84	133.46
40	102.72	106.20	136.66
50	105.14	109.91	139.73
60	107.13	111.98	143.80
70	108.75	116.25	154.07
80	112.41	119.26	164.19
90	114.22	120.04	174.83
Average	106.23	110.45	144.46

security threats, and the system security is 88.02% on average (see Figure 18).

5.6.3. *Third Scenario: Facing Security Threats with Software and Hardware Mechanisms in the Application Layer of IoT.* In this scenario, security measures are applied in the application layer. Due to the weakness of this layer, system security is 67.89% on average (see Figure 19).

5.6.4. *Fourth Scenario: Facing the Security Threats by Applying the Suggested Mechanism in the Article, Including the Aggregation of above Mode in All Three Architectural Layers of IoT.* In this case, which is suggested by

this paper, a combination of three above scenarios is proposed, and the system security is 96.82%, on average, and the improvement level of security in this scenario compared with previous modes can be seen in Figure 20:

The relative comparison of results is observed in Table 16:

## 6. Conclusion

IoT is expected to expand user connectivity and ease daily life; however, serious security challenges are considered in using this technology for distributed authentication. Moreover, integrating with biometrics in IoT design raises concerns about the cost and implementation of a user-friendly design. Furthermore, user authentication in the IoT environment is one of the most important challenges, especially in accessing important data. Current user authentication approaches on the IoT are either less flexible or inflexible. For authentication, the security of password-based systems decreases over time due to human error and the complexity of malicious attacks. According to the proposed mechanism in this paper, which is a combination of biometrics and coding, the security of the system has been improved by an average of 96.82%. Based on simulation states, the proposed method improves the system security by 120.38% on average, which shows 106.23, 110.45 and 144.46% improvement for the IoT sensor layer, controller layer and application layer, respectively [30–35].

## Data Availability

The data are available upon request to the corresponding author.

## Conflicts of Interest

The authors declare that they have no conflicts of interest.

## References

- [1] P. Aufner, "The IoT security gap: a look down into the valley between threat models and their implementation," *International Journal of Information Security*, vol. 19, no. 1, pp. 3–14, 2019.
- [2] Gartner, "Gartner Says the Internet of Things Will Transform the Data Center, (2014)<http://www.gartner.com/newsroom/id/2684616>.
- [3] IoT. Analytics, "Why the Internet of Things Is Called Internet of Things: Definition, History, Disambiguation," (2014) <https://iot-analytics.com/internetof-things-definition>.
- [4] D. Ferraris and C. Fernandez-Gago, "TrUStAPIS: a trust requirements elicitation method for IoT," *International Journal of Information Security*, vol. 19, 2019.
- [5] M. Trik, S. Pour Mozafari, and A. M. Bidgoli, "An adaptive routing strategy to reduce energy consumption in network on chip," *Journal of Advances in Computer Research*, vol. 12, no. 3, pp. 1–12, 2021.
- [6] H.-T. Nguyen, Q.-D. Ngo, and V.-H. Le, "A novel graph-based approach for IoT botnet detection," *International Journal of Information Security*, vol. 19, 2019.
- [7] A. M. Rahmani, "Exploiting smart e-Health gateways at the edge of healthcare Internet-of-Things: a fog computing approach," *Future Generation Computer Systems*, vol. 78, pp. 641–658, 2018.
- [8] H. Dubey, "Fog computing in medical internet-of-things: architecture, implementation, and applications," *Handbook of Large-Scale Distributed Computing in Smart Healthcare*, Springer, Berlin, Germany, 2017.
- [9] I. Azimi, "HiCH: hierarchical fog-assisted computing architecture for healthcare IoT," *ACM Transactions on Embedded Computing Systems*, vol. 16, pp. 1–20, 2017.
- [10] T. N. Gia, "Low-cost fog-assisted health-care IoT system with energy-efficient sensor nodes," in *Proceedings of the 2017 13th International Wireless Communications and Mobile Computing Conference (IWCMC)*, Valencia, Spain, June 2017.
- [11] P. Hu, "Fog computing based face identification and resolution scheme in internet of things," *IEEE Transactions on Industrial Informatics*, vol. 13, pp. 1910–1920, 2016.
- [12] V. Suneetha, S. Suresh, and J. Viswa, "A novel framework using Apache spark for privacy preservation of healthcare big data," in *Proceedings of the 2020 2nd International Conference on Innovative Mechanisms for Industry Applications (ICIMIA)*, Bangalore, India, March 2020.
- [13] S. Jebri, "lightweight Algorithm to secure data transmission in IoT systems," *Wireless Personal Communications*, vol. 116, pp. 2321–2344, 2021.
- [14] F. Afandi and R. Sarno, "Android application for advanced security system based on voice recognition, biometric authentication, and internet of things," in *Proceedings of the 2020 International Conference on Smart Technology and Applications (ICoSTA)*, pp. 1–6, Surabaya, Indonesia, February 2020.
- [15] W. Yang, S. Wang, G. Zheng, J. Yang, and C. Valli, "A privacy-preserving lightweight biometric system for internet of things security," *IEEE Communications Magazine*, vol. 57, no. 3, pp. 84–89, 2019.
- [16] N. Karimian, M. Tehranipoor, D. Woodard, and D. Forte, "Unlock your heart: next generation biometric in resource-constrained healthcare systems and IoT," *IEEE Access*, vol. 7, pp. 49135–49149, 2019.
- [17] F. Thabit, "A new lightweight cryptographic algorithm for enhancing data security in cloud computing," *Global Transitions Proceedings*, vol. 2, pp. 91–99, 2021.
- [18] A. Hussain, C. Xu, and M. Ali, "Security of cloud storage system using various cryptographic techniques," *International Journal of Mathematics Trends and Technology*, vol. 60, pp. 45–51, 2018.
- [19] R. F. Abdel-Kader, S. H. El-Sherif, and R. Y. Rizk, "Efficient two-stage cryptography scheme for secure distributed data storage in cloud computing," *International Journal of Electrical and Computer Engineering*, vol. 10, pp. 3–1, 2020.
- [20] C. Esposito, "Blockchain: a panacea for healthcare cloud-based data security and privacy," *IEEE Cloud Computing*, vol. 5, pp. 31–37, 2018.
- [21] Wani and Q. P. Abdul Raouf, "Performance evaluation and analysis of advanced symmetric key cryptographic algorithms for cloud computing security," *Soft Computing: Theories and Applications*, Springer, Berlin, Germany, 2019.
- [22] V. Agarwal, A. K. Kaushal, and L. Chouhan, "A survey on cloud computing security issues and cryptographic techniques," *Social Networking and Computational Intelligence*, Springer, Berlin, Germany, 2020.
- [23] B. Umapathy, "A survey ON cryptographic algorithm for data security IN cloud storage environment," *European Journal of Molecular & Clinical Medicine*, vol. 7, no. 9, 2020.

- [24] A. Banerjee, "A secure IoT-fog enabled smart decision making system using machine learning for intensive care unit," in *Proceedings of the 2020 International Conference on Artificial Intelligence and Signal Processing (AISP)*, Amaravati, India, January 2020.
- [25] K. Jaiswal and V. Anand, "A survey on IoT-based healthcare system: potential applications, issues, and challenges," *Advances in Biomedical Engineering and Technology*, Springer, Berlin, Germany, 2021.
- [26] B. K. Mohanta, "Survey on IoT security: challenges and solution using machine learning, artificial intelligence and blockchain technology," *Internet of Things*, vol. 11, p. 100227, 2020.
- [27] N. T. Le and D. B. Hoang, "Security threat probability computation using Markov chain and common vulnerability scoring system," in *Proceedings of the 28th International Telecommunication Networks and Applications Conference (ITNAC)*, Sydney, Australia, November 2018.
- [28] H. A. Kholidy, A. Erradi, S. Abdelwahed, and A. Azab, "A finite state hidden Markov model for predicting multistage attacks in cloud systems," in *Proceedings of the 2014 IEEE 12th International Conference on Dependable, Autonomic and Secure Computing*, pp. 14–19, Dalian, China, August 2014.
- [29] H. Wimberly and L. M. Liebrock, "Using Fingerprint Authentication to Reduce System Security: An Empirical Study," in *Proceedings of the IEEE Symposium on Security and Privacy*, Berkeley, CA, USA, May 2011.
- [30] V. A. Bharadi and G. M. DSilva: Online Signature Recognition Using Software as a Service (SaaS) Model on Public Cloud. 2015 International Conference on Computing Communication Control and Automation, (2015).
- [31] D. Choi, S. Seo, Y. Oh, and Y. Kang, "Two-factor fuzzy commitment for unmanned IoT devices security," *IEEE Internet of Things Journal*, vol. 6, no. 1, pp. 335–348, 2019.
- [32] A. F. Jabeen, "Development and implementation using Arduino and Raspberry Pi based Ignition control system," *Advances in Computational Sciences and Technology*, vol. 10, no. 7, pp. 1989–2004, 2017.
- [33] M. Mehrnezhad, E. Toreini, S. F. Shahandashti, and F. Hao, "Stealing PINs via mobile sensors: actual risk versus user perception," *International Journal of Information Security*, vol. 17, no. 3, pp. 291–313, 2017.
- [34] R. Vijaysanthi, N. Radha, M. J. Shree, and V. Sindhujaa, "Fingerprint authentication using raspberry Pi based on IoT," in *Proceedings of the 2017 International Conference on Algorithms, Methodology, Models and Applications in Emerging Technologies (ICAMMAET)*, India, Chennai, February 2017.
- [35] M. Trik, S. Pour Mozaffari, and A. M. Bidgoli, "Providing an adaptive routing along with a hybrid selection strategy to increase efficiency in NoC-based neuromorphic systems," *Computational Intelligence and Neuroscience*, vol. 2021, Article ID 8338903, 8 pages, 2021.



## Research Article

# Application of the Blockchain Technology in the Vertical Value Chain Management of Enterprises

Yang Wang , Yiqi Wang, and Yi Zhang

School of Management, China University of Mining and Technology-Beijing, Beijing 100083, China

Correspondence should be addressed to Yang Wang; wangyang.som@cumtb.edu.cn

Received 30 September 2021; Revised 15 November 2021; Accepted 30 November 2021; Published 22 January 2022

Academic Editor: Deepak Gupta

Copyright © 2022 Yang Wang et al. This is an open access article distributed under the Creative Commons Attribution License, which permits unrestricted use, distribution, and reproduction in any medium, provided the original work is properly cited.

This paper studies how the blockchain technology applies the enterprise's vertical value chain management and specifically studies how the blockchain technology is applied to the management of various transaction information involved in the enterprise's vertical value chain management. This paper first analyzes the basic needs of the enterprise vertical value chain management, analyzes the decentralization, integrity, and authenticity of relevant transaction information in management, and designs and implements enterprise value chain management solution based on the blockchain technology, including the design and implementation of organizations, consensus mechanisms, data structures, and business processes. The simulation data is used for testing, and finally, the solution is evaluated in terms of security, transparency, efficiency, and scalability. The research in this paper shows that the blockchain technology can be applied to the enterprise's vertical value chain management, which can ensure the authenticity, transparency, tamper resistance, and security of various transaction information of enterprises, thus improving the quality and reliability of the vertical value chain management of enterprises.

## 1. Introduction

On November 1, 2008, Satoshi Nakamoto first proposed the concept of blockchain in *Bitcoin: A Peer-to-Peer Electronic Cash System*, which attracted wide attention from the general public. Blockchain technology attracts investors with its decentralized characteristics and is considered to be a potential technology that will bring about major changes to human society in the future.

In *Bitcoin: A Peer-to-Peer Electronic Cash System* published by Satoshi Nakamoto in 2008, it is pointed out that blockchains are data structures used to record the history of bitcoin transactions. In addition, Wikipedia likens blockchain technology to a distributed database technology, which can maintain a continuously growing and tamper-resistant data record by maintaining the chain structure of data blocks [1].

The concept of a value chain was first proposed by Michael Porter in his book *Competitive Advantage* in 1985 [2], who held that an enterprise is a collection of interrelated but separated activities, all of which constitute the value creation of an enterprise, and that formation and change of the value chain are caused by the market demand [3]. The

competitiveness of an enterprise is reflected on all the activities in the value chain, but not all links of the value chain can produce value; only a few specific links can [4]. Porter classified the value chain into two categories: basic activities, which include the activities of internal logistics, production, marketing external logistics, and service, and ancillary activities, which include enterprise infrastructure, technology development, procurement, and human resources. These separate and interrelated activities constitute the dynamic process of corporate value creation, which is called the value chain [5]. Value chain analysis methods can be divided into three types: vertical value chain analysis, horizontal value chain analysis, and internal value chain analysis [6].

Unlike Porter's emphasis on internal value chains, vertical value chains are defined as a chain of value creation and value transfer between suppliers, businesses, and buyers, each providing a variety of activity links that form a chain [7], ranging from the initial supplier of raw materials to the final buyer of final products. For an enterprise, its vertical value chain is represented by the relationship between the enterprise and upstream suppliers and downstream buyers or consumers [8]. The vertical value chain and the internal value chain of

an enterprise are interrelated and interdependent, which form an organic whole and serve the strategic objectives of the enterprise together [9].

Since the information related to the transaction is held by each transaction participant separately, there is a technical single point of risk in the traditional vertical value chain management. Transaction information is low in transparency, easy to be tampered with, and difficult to be traced and has a low degree of trust. This paper designs a solution for enterprise value chain management based on blockchain technology by using the characteristics of blockchain's decentralization, immutability, and untrustworthiness. This solution can not only fundamentally solve the technical single-point risk in traditional vertical value chain management but also help improve the quality and reliability of enterprise vertical value chain management.

## 2. Design of Solutions to Enterprise Vertical Value Chain Management Based on the Blockchain Technology

*2.1. Demand Analysis of Enterprise Vertical Value Chain Management Based on the Blockchain Technology.* In the demand analysis of vertical value chain management, the enterprise is regarded as a link in the value production process of the whole industry to analyze the relationship between the upstream and downstream enterprises, to discover the demand in optimizing the relationship with them.

Vertical value chain management involves the management of various transactions, including the management of its procurement, sales, logistics, and funds. Purchasing management and sales management are the core content of vertical value chain management, and the vertical value chain of an enterprise can be optimized based on them.

In the traditional transaction model, the accounting process of the enterprise transaction involved in the vertical value chain management is independently completed by transaction participants, so that it is difficult to discover the omission of transaction information and multiple recorded errors among transaction participants in time. They are often discovered when the transaction information is found inconsistent with the actual books or the auditing is performed. Therefore, the independent custody of transaction information by all parties is a risk that the traditional transaction model cannot solve.

Longitudinal value chain management is applied to blockchain technology, which allows a set of ledgers to be maintained by both parties involved in purchasing management and sales management. Moreover, all relevant transaction information, including purchasing, sales, logistics, and cash flow, can only be written into the blockchain ledger with the unanimous consent of the relevant parties. Trading participants can query related transactions at any time without restrictions from other parties, including historical transaction information, historical update information, and historical deletion of transaction information. For transaction participants, the blockchain ledger is a transparent, tamperproof, traceable, and trustworthy shared ledger endorsed, thus ensuring the consistency, tamper resistance, and transparency of

transaction information between related parties in the vertical value chain from the source and eliminating the risk of inconsistency and tampering of ledgers caused by traditional independent accounting.

As the information in the blockchain ledger is shared and trustworthy, there is no need to reconcile between the relevant parties when entering relevant transaction information, thus improving transaction efficiency.

In addition, enterprises can use programmable smart contracts to implement their business logic in the blockchain platform. Because the programming language of smart contracts is Turing complete and can access the various resources of the enterprise as needed, which enables them to implement various complex business logic and automatically execute smart contract codes written in advance and related businesses, including procurement, sales, logistics, cash settlement, and other businesses, as well as high-level businesses such as data analysis, statistics, and early warning, it can ensure business security while greatly providing business efficiency. Improving the level of vertical value chain management.

The demand for vertical value chain management of enterprises based on blockchain technology analyzed in this paper includes the following contents:

*2.1.1. Decentralization of Transaction Information.* In the traditional transaction mode, the accounting process of transactions is carried out by two or more parties of the buyer and the supplier, each of which has an independent set of ledgers. The transaction participants each have a set of independent ledgers, and they only maintain their own ledgers.

Blockchain technology, such as consortium blockchain, enables buyers and suppliers to distribute their own nodes in the consortium blockchain network, which can be freely connected to exchange transaction data, information, and assets, to maintain a set of ledgers together. Transaction information recorded in the ledgers is endorsed by relevant parties and recorded in each node of the consortium blockchain to achieve true decentralization.

*2.1.2. Integrity of Transaction Information.* Enterprises need to manage and maintain all necessary information with suppliers, sellers, transporters, and banks, including purchase and sale transaction information, logistics information, cash flow information, and related contracts.

Ensuring the integrity of transaction information is an important responsibility for an enterprise to safeguard the security of transactions and the legal rights and interests of the enterprise.

*2.1.3. Authenticity of Transaction Information.* The authenticity of transaction information, including the authenticity of transaction information content. The correctness of transaction data and the trustworthiness of transaction data are an important basis for enterprise accounting, enterprise decision-making, and management and an objective basic requirement for the quality of enterprise accounting information.

*2.1.4. Tamper Resistance of Transaction Information.* The immutability of transaction information means that the relevant participants cannot hide or individually modify the transaction information that has occurred. The transaction information queried by each participant is the same information that was originally recorded.

*2.1.5. Traceability of Transaction Information.* Trading information traceability refers to the ability of trading participants to trace the relevant transaction history information and to query and obtain the transaction history information without restriction by others.

*2.1.6. Transparency of Transaction Information.* Transparency of transaction information means that the transaction information is open, transparent, and accessible to the participants and the participants are not restricted by other parties to obtain transaction information.

*2.1.7. Efficiency of Transaction Information.* Transaction efficiency refers to the comparison of the cost and time to complete an exchange with the results achieved. The transaction system can realize the basic functions of the transaction procedure and has low cost of learning and maintenance.

*2.1.8. Application of Transaction Information.* The application of transaction information refers to providing support for further decision-making, improving the efficiency and level of enterprise management and further enhancing the enterprise value through data analysis and information discovery based on various transaction information recorded in the course of the transaction.

*2.2. Enterprise Vertical Value Chain Management Solution Based on the Blockchain Technology.* Based on the basic needs of enterprise vertical value chain management, this paper designs and implements an enterprise value chain management solution based on the blockchain technology, including the design and implementation of transaction organization, consensus mechanism, data structure, and business process. The application of the blockchain technology to the management of the enterprise's vertical value chain can ensure the transparency, traceability, immutability, and authenticity of various transaction information of the enterprise, thereby improving the quality and reliability of the enterprise's vertical value chain management.

*2.2.1. Design of the Organizational Structure.* The organization referred to in this paper refers to a consortium of some nodes with transaction, accounting, and endorsement functions in the vertical value chain, where "node" usually represents one or more servers with transaction, accounting, or endorsement functions and usually jointly assumes the corresponding functions of an enterprise or a department in an enterprise, such as purchasing and sales.

Enterprises in the vertical value chain are interrelated by purchasing and selling activities. Therefore, the vertical value chain management involves buyers, suppliers, transporters, and banks. The typical transactions involved in the vertical value chain management cannot be separated from the par-

ticipation of these four parties. According to the different functions of participants in the transaction, four organizations are set up in this paper: buyer organization, supplier organization, transporter organization, and banking organization. These four organizations participate in the consensus and maintenance of the blockchain ledgers.

*2.2.2. Design of the Consensus Mechanism.* As the block chain studied in this paper is a coalition block chain, consensus mechanism is reached between alliance participants. Every transaction can be recorded in the blockchain ledger after the alliance participants reach consensus.

When wanting to reach a consensus on a certain transaction, each participant first writes the information related to the transaction into their own temporary ledgers. As a consensus initiator, one of the participants first sends relevant information and endorsement request to its endorsement node, and then the endorsement node sends it to the endorsement node of others. Next, the endorsement nodes of other participants will verify the information with the information in their own temporary ledgers. Finally, after the endorsement node of the consensus initiator collects all the information with the signatures of the participants, it is included in the blockchain ledger. The specific process is shown in Figure 1.

*2.2.3. Design of the Data Structure.* The following data structure is designed in this paper according to the participants and related transactions involved in vertical value chain management:

The structure of transaction data, a common standard for the records of the transaction between the buyer and the supplier, is mainly used to record the format of the transaction information that is convenient for the exchange of the transaction information between the buyer and the supplier. The transaction data includes the transaction number, transaction creation time, logistics number, cash flow number, transaction status and remarks, and other transaction information.

The structure of logistics data, a common standard for the records of the logistics among the buyer, the transport enterprise, and the supplier, is mainly used to record the logistics information in a form that is convenient for the exchange of the logistics information among the buyer, the transport enterprise, and the supplier. The logistics data includes the logistics number, logistics creation time, cash flow number, logistics status and remarks, and other logistics information.

The structure of cash flow data, a common standard for the records of the cash flow among the buyer, the bank, and the supplier, is mainly used to record the cash flow information in a form that is convenient for the exchange of the cash flow information among the buyer, the bank, and the supplier. The cash flow data includes the cash flow number, cash flow creation time, bank statement number, cash flow status and remarks, and other cash flow information.

The structure of organization information data is a format used to record organization information, which facilitates the identification and maintenance of identity information

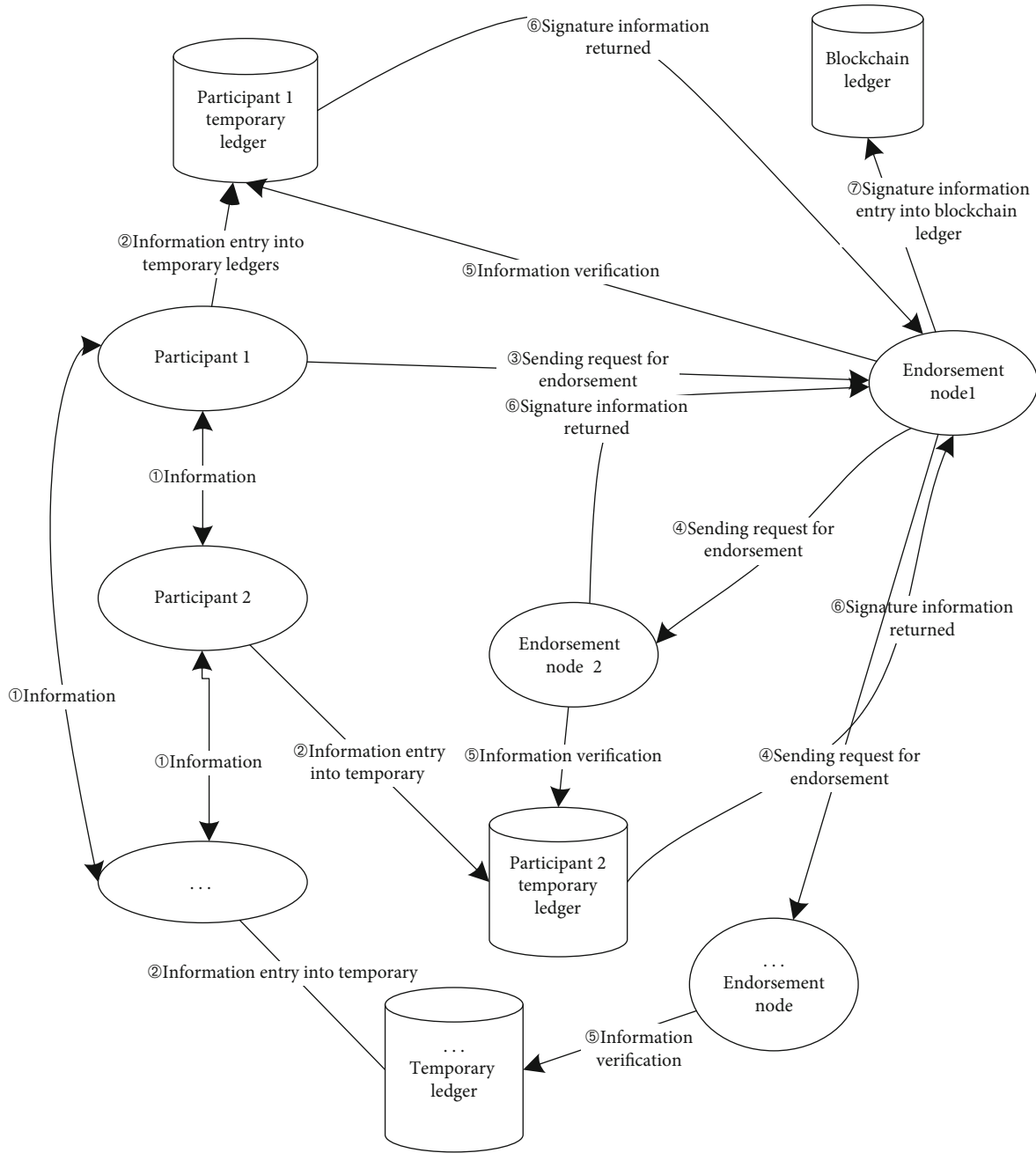


FIGURE 1: Information consensus process based on the blockchain technology.

between the buyer, the supplier, the transporter, and the bank. The organization information data mainly includes the organization number, organization name, organization domain name, organization address, organization creation time, organization modification time, organization status, and other organization information.

Taking the transaction data structure as an example, the implementation code is

*2.2.4. Design of the Business Process.* The vertical value chain management process in this paper involves four main bodies: the supplier, buyer, transporter, and bank. In a typical

vertical value chain, the enterprise is both the supplier and the buyer. Therefore, this paper mainly studies the content of related processes that the enterprise as a supplier involves upstream vertical value chain management and as a buyer involves downstream vertical value chain management.

In this paper, the business involved in enterprise vertical value chain management based on the blockchain technology is divided into three tiers; the upper tier is based on its lower tier, and the next tier provides services for its upper tier. At the bottom is the business related to the reading and writing of blockchain ledgers, at the middle is the business related to basic transactions, and at the top is the business related to purchasing

```

// Transaction information structure
type Transaction struct {
Transaction ID string //Transaction ID e.g. tx0001
Logistics ID string //Logistics ID e.g. pd0001
Cash Flow ID string //Cash Flow ID e.g. fd0001
Create Time int64 //Transaction creation time Unix time
Change Time int64 //Transaction modification time Unix time
State string //Transaction status
Type string //Transaction type
Mode string //Transaction method
Remark string //Transaction Remarks
Product ID string //Product ID
Product Name string //Product Name
Unit string //Unit
Count int //Quantity
Price int //Unit price
Total int //Total price
Attrs map[string]string //Other attributes
}

```

CODE 1 .

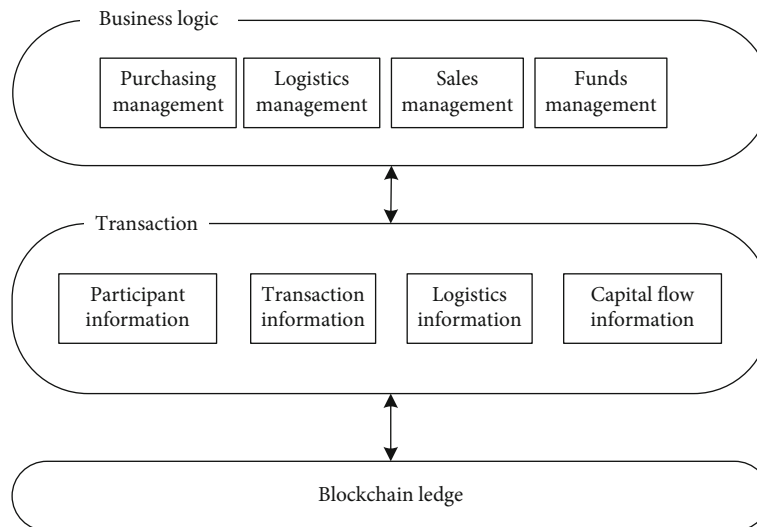


FIGURE 2: The three-tier structure of the business processes.

management, logistics management, sales management, and fund management. The three-tier structure is shown in Figure 2.

**2.2.5. Design of the Transaction Process.** In traditional transactions, the buyer-seller transaction generally involves the supplier, the buyer, the transporter, and the bank. The transaction request can be initiated by the buyer or the supplier, mostly by the buyer, which is also the case in this paper. After the purchaser generates the product demand, it sends the product demand information to the supplier and initiates the transaction request. After negotiation, the supplier signs a sales contract with the buyer to conclude the transaction and entrusts the transportation enterprise to transport the products. The transportation enterprise delivers the products to the buyer who entrusts the bank to pay, and

the bank pays to the supplier, in which the supplier delivers the goods first or the buyer pays first depending on the contract between the two parties. For the convenience of research, this paper considers the case that the supplier delivers goods first. The transaction process is shown in Figure 3.

In the traditional transaction model, the accounting process of the transaction is completed by the buyer and seller separately. So the both parties are prone to errors, omissions, and multiple records of the transaction information, which are difficult to be discovered by both parties to the transaction until the account books are unbalanced or audited. Once errors are found, not only a large number of manpower, financial, and material resources are needed but also problems such as inconsistent accounting of transaction information may be difficult to be traced and dealt with. Therefore, the transaction information is kept independently



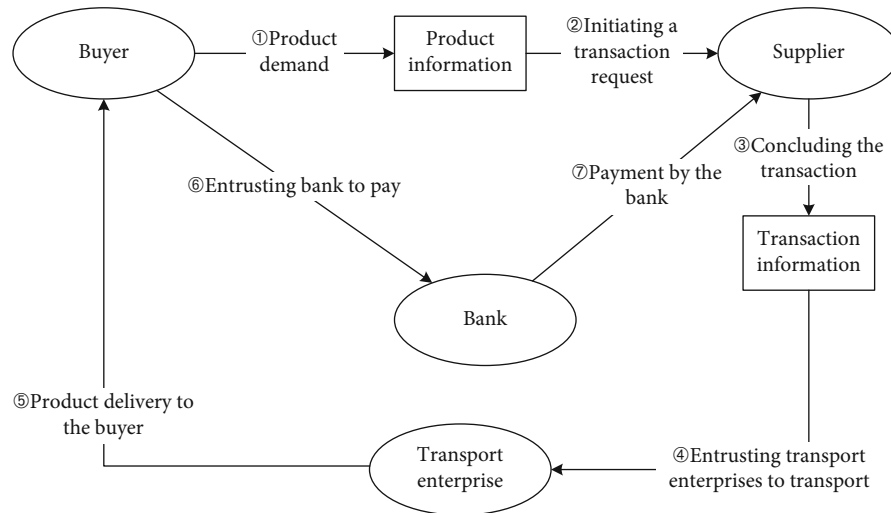


FIGURE 3: Traditional transaction process.

by all parties, which makes it difficult for the traditional transaction mode to solve the technical single-point risk.

Longitudinal value chain management is applied to blockchain technology, which allows a set of ledgers to be maintained by both or many parties involved in purchasing management and sales management. Moreover, all relevant transaction information, including purchasing, sales, logistics, and cash flow, must be unanimously approved by the relevant parties before it can be written into and updated to the blockchain ledger. Trading participants can query related transactions at any time without restrictions from other parties. For transaction participants, the blockchain ledger is a transparent, tamperproof, traceable, and trustworthy shared ledger endorsed, thus ensuring the consistency, tamper resistance, and transparency of transaction information between related parties in the vertical value chain from the source and eliminating the risk of inconsistency and tampering of ledgers caused by traditional independent accounting. As the information in the blockchain ledger is shared and trustworthy, there is no need to reconcile between the relevant parties when entering relevant transaction information, thus improving transaction efficiency.

In the transaction process of vertical value chain management based on the blockchain technology, the buyer, the transporter, and the supplier jointly maintain the ledgers related to logistics in the transaction. The transaction information included in the logistics ledgers is signed by the buyer, the transporter, and the supplier and cannot be tampered with by any single party and is transparent and traceable to any of them.

The buyer, the bank, and the supplier jointly maintain the ledgers related to the transactional capital in the transaction. The transaction information included in the capital ledgers is signed by the buyer, the transporter, and the supplier and cannot be tampered with by any single party and is transparent and traceable to any of them.

The transporter, the bank, and the supplier jointly maintain the ledgers related to the capital for the transport transac-

tion in the transaction. The transaction information included in the transport capital ledgers is signed by the transporter, the bank, and the supplier and cannot be tampered with by any single party and is transparent and traceable to any of them.

*2.2.6. Design of the Organization Information Maintenance Process.* The buyer sends the latest information after the initialization, updating, and deletion of organization information to the supplier for endorsement confirmation. Each party will write the latest buyer organization information to the temporary ledgers. Upon confirmation of endorsement by the supplier and the buyer, the latest buyer organization information will be recorded in the blockchain ledger.

The supplier sends the latest information after the initialization, updating, and deletion of organization information to the supplier for endorsement confirmation. Each party will write the latest supplier organization information to the temporary ledgers. Upon confirmation of endorsement by the supplier and the buyer, the latest supplier organization information will be recorded in the blockchain ledger.

The transporter sends the latest information after the initialization, updating, and deletion of organization information to the buyer and supplier for endorsement confirmation. Each party will write the latest transporter organization information to the temporary ledgers. Upon confirmation of endorsement by the supplier, the buyer, and the transporter, the latest transporter organization information will be recorded in the blockchain ledger.

The bank sends the latest information after the initialization, updating, and deletion of organization information to the buyer and supplier for endorsement confirmation. Each party will write the latest bank organization information to the temporary ledgers. Upon confirmation of endorsement by the supplier, the buyer, and the bank, the latest bank organization information will be recorded in the blockchain ledger.

The transaction process using the blockchain technology is shown in Figure 4.

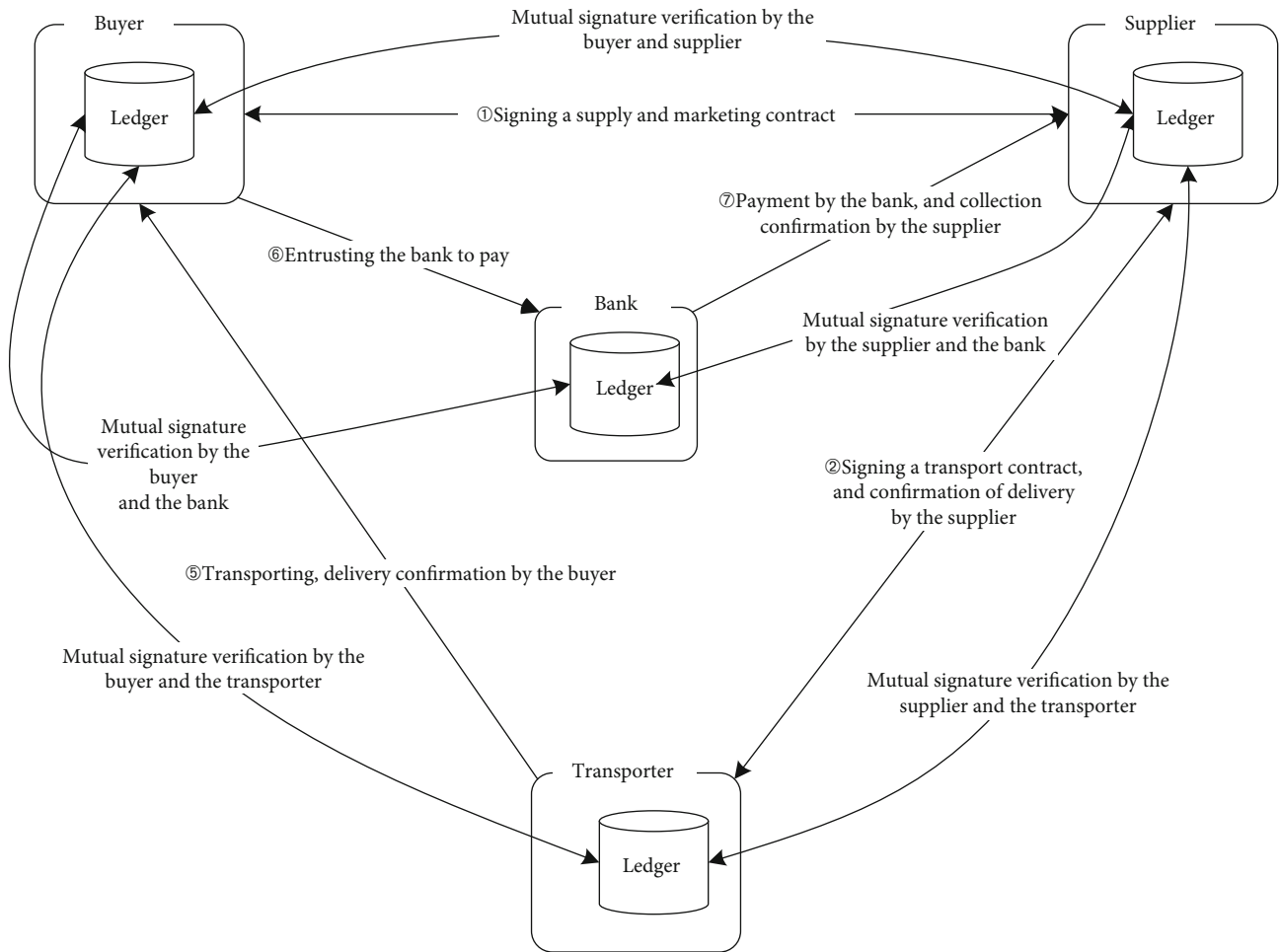


FIGURE 4: Transaction process using the blockchain technology.

2.2.7. *Design of the Business Logic.* Business logic is based on transactions between buyers and suppliers. On the basis of the data generated by transactions, business logic of enterprises provides a higher level of application, including purchasing management, supply management, logistics management, and fund management. Due to the need for research purposes and limited space, this paper only lists some basic business logic as follows:

(I) The business logic content of purchasing management

- (1) Query for purchase: enter the transaction number to query the purchase of certain goods or the time period parameter to query good purchase in a certain time period
- (2) Query for exchange: enter the transaction number to query the exchange of certain goods or the time period parameter to query good exchange in a certain time period
- (3) Query for return: enter the transaction number to query the return of certain goods or the time period parameter to query good return in a certain time period

- (4) Query for purchasing logistics: enter the transaction number to query the purchasing logistics of certain goods or the time period parameter to query purchasing logistics in a certain time period.
- (5) Query for the payment for purchasing: enter the transaction number to query the payment of certain goods or the time period parameter to query the payment for goods in a certain time period
- (6) Purchasing statistics: query the purchasing information of certain goods in a certain time period according to the commodity information
- (7) Query purchase per day: count the purchase of goods on a certain day

(II) The business logic content of sales management

- (1) Sales query: enter the transaction number to query the sales of certain goods or the time period



- parameter to query commodity sales in a certain time period
- (2) Query for exchange: enter the transaction number to query the exchange of certain goods or the time period parameter to query good exchange in a certain time period
  - (3) Query for return: enter the transaction number to query the return of certain goods or the time period parameter to query good return in a certain time period
  - (4) Query for distribution logistics: enter the transaction number to query the distribution logistics of certain goods or the time period parameter to query distribution logistics in a certain time period
  - (5) Query for the payment for sales: enter the transaction number to query the payment of certain goods or the time period parameter to query the payment for goods in a certain time period
  - (6) Sales statistics: to query the sales information of certain goods in a certain time period according to the commodity information
  - (7) Query sales per day: count the sales of goods on a certain day
- (III) The business logic content of logistics management
- (1) Query for logistics: enter the logistics number to query the logistics of certain goods or the time period parameter to query logistics in a certain time period
  - (2) Logistics expenses statistics: count the logistics cost in a certain time period
  - (3) Logistics time inquiry: enter the logistics number to query logistics updating of specific goods
  - (4) Logistics time statistics: count the logistics time in a certain time period
- (IV) The business logic content of cash management
- (1) Query for cash flow: enter the cash flow number to query the cash flow of certain goods or the time period parameter to query cash flow in a certain time period
  - (2) Statistics of cash flow expenses: count the cash flow expenses in a certain period of time
  - (3) Cash flow time inquiry: enter the cash flow number to query the cash flow updating of certain goods
  - (4) Statistics of cash flow time: count the time consumption of the cash flow in a certain period of time
  - (V) The business logic content of organizational information management
    - (1) Query for organizational information: enter the organizational number to query the current information of a certain organization
    - (2) Statistics of organizational information: count the change in organizational information in a certain period of time
    - (3) Query for historical organizational information: enter the organizational number to query all the historical information of a certain organization

### 3. Realization of Solutions to the Vertical Value Chain Management of Enterprises Based on the Blockchain Technology

The Hyperledger Fabric platform is set up in the Ubuntu system by using Docker environment, in which the version is v1.3.0.

- (1) Organizational structure configuration which includes the ordering organization, bank organization, shipper organization, buyer organization, and seller organization is set up. There are three consortiums configured under the consortium node. The first is the Transaction Consortium, which consists of two organizations, the supplier and buyer. The second is the Logistics Consortium, which consists of three organizations, the shipper, seller, and buyer. The third is the Cash Flow Consortium, which consists of three organizations, the bank, seller, and buyer
- (2) The application channel configuration template contains three channels, which enable specific peer nodes and applications in the blockchain network to interact. The first application channel is the Transaction Orgs Channel, in which a transaction consortium is configured, including two organizations, the supplier and the buyer. The second application channel is the logistics channel, in which a logistics alliance is configured, including the transporter, the supplier, and the buyer. The third application channel is the capital flow channel, in which the capital flow alliance is configured, including the bank (bank), the supplier (seller), and the buyer (buyer). Default parameters are configured in the three application channels
- (3) In Docker, the mirrors and containers required by the Hyperledger Fabric environment are defined by docker-compose.yaml. Docker can use docker-Compose.yaml to start containers required by multiple

Hyperledger Fabric environments. Docker Compose.yaml mainly consists of two parts, networks and services

- (4) In this paper, the function of the Hyperledger Fabric client is realized through fabric-sdk-go, by firstly installing the package related to fabric-sdk-go so that fabric-sdk-go is installed via `go get—u http://github.com/hyperledger/fabric-sdk-go`, secondly encapsulating the relevant API of fabric-sdk-go for client use, and finally initializing fabric-sdk by writing config.yaml
- (5) Chaincode is a program written in Go, node.js, or Java that implements a specified interface and runs in a secure Docker container isolated from supporting peer-to-peer processes, which initializes and manages the ledger status through transactions submitted by the application

In this paper, the chaincode of basic business logic required in this paper is mainly implemented in Go language and the transaction information structure is implemented in the datastruct folder; the transaction process is implemented in each folder under chaincode/transaction; the logistics process is implemented in each folder under chaincode/logistics; the cash flow process is implemented in each folder under chaincode/capitalflow; the information maintenance process is implemented in files ending Invoke.go in various folders under chaincode (Table 1).

#### 4. Testing and Evaluation on Solutions to Enterprise Vertical Value Chain Management Based on the Blockchain Technology

*4.1. Testing on Solutions to Enterprise Vertical Value Chain Management Based on the Blockchain Technology.* Due to the nonforeseeability of the formal system and the limitation of the code language, there are some flaws in the software [10]. Software testing, as an important part of the whole software development process [11], is to find out the defects and errors in the design and operation process of the software through various tests of the software, analyze and sort out the test results specifically, to evaluate the software, and provide evidence for the reliability of the system [12], with a view to ensure the high quality and reliability of software.

The test in this paper is designed to verify whether the solution achieves the functions described above and meets the requirements of enterprise vertical value chain management described above.

##### (1) Testing environment

The hardware environment for testing in this paper is as follows: CPU: Intel core i5-3,210 M; memory: 8 G; and hard disk: 1 T. The software environment is as follows: operating system: Ubuntu 18.04.1 LTS, Docker version 18.06.1-ce, build e68fc7a, Go language version: go1.10.4 Linux/AMD64, Hyperledger Fabric version: v1.3.0.

##### (2) Testing process

Testing processes are as follows:

- (a) Start the completed Hyperledger Fabric environment platform
- (b) Run channel creation and chaincode installation client
- (c) Generate simulated transaction data
- (d) Run data test client

##### (3) Test case

In this paper, the transaction process between the buyer and the supplier is divided into three main categories: payment before delivery, delivery before payment, prepayment before delivery, and final payment. According to the completion of the transaction, each of the three categories can be further divided into 4 types: normal completion, return, exchange, and cancellation, totaling 12 types of transaction processes. For each of these twelve scenarios, transaction data generated randomly and six products, namely, A, B, C, D, E, and F, are prepared for each transaction (Table 2).

Transaction test data, logistics test data, cash flow test data, and organizational information maintenance test data are generated based on the above product data simulation. Take transaction test data as an example (Table 3).

The transaction data of the tamperproof test for related transactions are carried out by selecting data modified unilaterally by one party. If the data can not complete the relevant transaction, the tamperproof test is successful, whereas the tamperproof test fails. In this paper, the transaction data is tampered with by prefixing the product name with “tamper.” The new transaction tamperproof test data, logistics tamperproof test data, cash flow tamperproof test data, and organization information tamperproof test data are generated. Take transaction tamperproof test data as another example (Table 4).

##### (4) Test result

Chaincode test results are as follows, taking transaction chaincode test results as an example (Table 5).

In Table 5, the consensus and writing test results are passed, indicating that any transaction information has passed the consensus of the transaction participants and been successfully written into the blockchain ledger. The passing of the tamperproof modification test indicates that any party to the transaction cannot unilaterally tamper with the transaction information. The pass of the transparency test indicates that any party to the transaction can query transaction information. The traceability test result passed, indicating that any party to the transaction can query historical transaction information.

The test results of the business layer are as follows, taking the test results of the purchasing management business as an example (Table 6).

TABLE 1: Information structure implementation.

Items	Structure	Files
Structure of transaction information	Transaction	TransactionStruct.go
Structure of cash flow information	CapitalFlow	CapitalFlowStruct.go
Structure of logistics information	Logistics	LogisticsStruct.go
Structure of organization information	Organization	OrganizationStruct.go

TABLE 2: Product test data.

Product no.	Product name	Unit price (Yuan)	Freight (Yuan/piece)	Number of transaction (piece/time)
pd001	Product A	80–120	0.1–0.3	100–300
pd002	Product B	200–300	0.2–0.5	50–500
pd003	Product C	180–250	0.1–0.3	200–600
pd004	Product D	300–400	0.3–0.6	100–200
pd005	Product E	500–800	0.3–0.5	30–300
pd006	Product F	20–40	0.1–0.5	500–1000

The test results show that the enterprise vertical value chain management solution based on the blockchain technology achieves the expected goals using Go language based on the Hyperledger Fabric platform.

#### 4.2. Evaluation on Solutions to Enterprise Vertical Value Chain Management Based on the Blockchain Technology

- (1) In terms of security, the blockchain ledger uses distributed storage and relies on a consensus mechanism to ensure consistency between nodes. Each piece of transaction information that is entered in the blockchain ledgers cannot be tampered with without the consent of all nodes, thus ensuring the reliability and security of the transaction information stored in the distributed ledgers
- (2) In terms of transparency and traceability, the data information of each transaction is entered in the blockchain ledger in the order of transaction time. The latter purchase transaction will record the previous hash value, so that the purchase transaction data entered into the blockchain ledger is continuous, accurate, and unique and cannot be tampered with. Therefore, every purchase transaction data information entered in the blockchain ledger can be retrospectively queried to facilitate the management of participants
- (3) In terms of efficiency, each transaction data entered in the blockchain ledger is shared and trusted by the transaction participants through the consensus and endorsement of the transaction participants. So, they do not need to check the transaction data in the later stage, saving a lot of time and human, material, and financial resources of the enterprise
- (4) In terms of expandability, enterprises can use the blockchain technology to record various transaction

information and organization information in the blockchain ledger, which can be used as a basis to expand the related applications, for example, data analysis, customer management, and vendor management to support purchasing and sales decisions of enterprises and to expand the related applications of vertical value chain management

## 5. Research Conclusions and Suggestions

5.1. *Research Conclusions.* Through the above research, the following conclusions are drawn:

- (1) The application of the blockchain technology in vertical value chain management of enterprises can solve the problem of inconsistency and opacity between transaction information in vertical value chain management and one party. Each piece of transaction information must be unanimously approved by all the parties and endorsed by their signatures before it can be entered in the blockchain ledger, eliminating the technical single-point risk in the vertical value chain management of the enterprise
- (2) The blockchain technology can ensure the authenticity, transparency, tamper resistance, and security of enterprise purchase transaction information, sales transaction, logistics information, and cash flow information, thus improving the quality and reliability of vertical value chain management
- (3) The application of blockchain in enterprise vertical value chain management enables core enterprises to share a set of trustworthy and transparent blockchain ledgers with upstream and downstream enterprises, so that they can connect more closely, optimize the transaction process between them, enhance mutual trust and transaction security, and reduce enterprise costs

TABLE 3: Transaction test data.

Transaction no.	Logistics no.	Cash flow no.	Product no.	Product name	Unit	Quantity	Unit price
tx00001	lg00001	cf00001	pd003	Product C	kg	355	180
tx00002	lg00002	cf00002	pd001	Product A	kg	273	90
tx00003	lg00003	cf00003	pd004	Product D	kg	149	395
tx00004	lg00004	cf00004	pd006	Product F	kg	741	33
tx00005	lg00005	cf00005	pd005	Product E	kg	91	663
tx00006	lg00006	cf00006	pd003	Product C	kg	434	235
tx00007	lg00007	cf00007	pd006	Product F	kg	942	31
tx00008	lg00008	cf00008	pd003	Product C	kg	557	221
tx00009	lg00009	cf00009	pd005	Product E	kg	99	762
tx00010	lg00010	cf00010	pd004	Product D	kg	101	318
tx00011	lg00011	cf00011	pd003	Product C	kg	454	229
tx00012	lg00012	cf00012	pd001	Product A	kg	102	100

TABLE 4: Transaction tamperproof test data.

Transaction no.	Logistics no.	Cash flow no.	Product no.	Product name	Name of tampered product	Unit	Quantity	Unit price
newtx00001	lg00001	cf00001	pd003	Product C	tamper-Product C	kg	355	180
newtx00002	lg00002	cf00002	pd001	Product A	tamper-Product A	kg	273	90
newtx00003	lg00003	cf00003	pd004	Product D	tamper-Product D	kg	149	395
newtx00004	lg00004	cf00004	pd006	Product F	tamper-Product F	kg	741	33
newtx00005	lg00005	cf00005	pd005	Product E	tamper-Product E	kg	91	663
newtx00006	lg00006	cf00006	pd003	Product C	tamper-Product C	kg	434	235
newtx00007	lg00007	cf00007	pd006	Product F	tamper-Product F	kg	942	31
newtx00008	lg00008	cf00008	pd003	Product C	tamper-Product C	kg	557	221
newtx00009	lg00009	cf00009	pd005	Product E	tamper-Product E	kg	99	762
newtx00010	lg00010	cf00010	pd004	Product D	tamper-Product D	kg	101	318
newtx00011	lg00011	cf00011	pd003	Product C	tamper-Product C	kg	454	229
newtx00012	lg00012	cf00012	pd001	Product A	tamper-Product A	kg	102	100

TABLE 5: Transaction chaincode test results.

Type of test	Test items	Test methods	Number of passes	Number of failures	Test result	Time per request (msec)
Consensus and writing	Initializing transaction information	Init transaction	12	0	Pass	2443
Tamperproofness	Initializing transaction information	Init transaction	12	0	Pass	18
Consensus and writing	Updating transaction information	Update transaction	25	0	Pass	2458
Tamperproofness	Updating transaction information	Update transaction	25	0	Pass	18
Transparency	Querying updating transaction information	Query transaction	74	0	Pass	15
Transparency	Rich query of updating transaction information	Rich query transactions	25	0	Pass	18
Traceability	Query of historical information	Query transaction history	25	0	Pass	11

TABLE 6: Purchasing management business test results.

Test items	Number of passes	Number of failures	Test result	Time per request (msec)
Query purchase by transaction ID	1	0	Pass	147
Query purchase by time range	1	0	Pass	23
Query purchase exchange by transaction ID	1	0	Pass	20
Query purchase exchange by time range	1	0	Pass	17
Query buyer, return by transaction ID	1	0	Pass	16
Query buyer return by time range	1	0	Pass	16
Query purchase logistics by transaction ID	1	0	Pass	41
Query purchase cash flow by transaction ID	1	0	Pass	37
Query purchase product by time range	1	0	Pass	16
Query purchase daily	1	0	Pass	22

5.2. *Suggestions.* When applying blockchain technology, enterprises should pay attention to distinguish the application scenarios of different blockchain types, determine the type of blockchain that they should use according to their own actual needs, and select a suitable blockchain platform.

Before and after applying blockchain technology in vertical value chain management, enterprises should communicate with upstream and downstream enterprises to improve their cooperation ability and jointly develop and maintain the blockchain.

Enterprises should realize that while improving the security and transparency of transactions, blockchain also has disadvantages such as slow transaction speed and high requirements for enterprise computer hardware and network configuration.

When using the Hyperledger Fabric platform, enterprises should plan the channel design, isolate unrelated nodes, prevent data leakage, and design endorsement strategy to ensure effective transactions. They should also set up and configure peer-to-peer nodes and sorting nodes reasonably to ensure business security and improve efficiency.

Due to the research purpose and space limitation, this paper only analyzes and realizes some basic requirements involved in the process of enterprise vertical value chain management based on blockchain technology and other specific, special, or complex needs should be analyzed and realized by readers themselves.

In this paper, the implementation of solutions to enterprise vertical value chain management based on the blockchain technology is only applicable to the relevant software and hardware environments used herein. Please pay attention to the relevant software and hardware versions when inspecting and using.

The test results in this paper may vary depending on the software and hardware environments tested.

## 6. Prospect

According to the research of the blockchain technology in the enterprise's vertical value chain management in this paper, it only includes the value transmission activities between the enterprise and the upstream and downstream and does not include the internal value creation and transmission process of the enterprise. In the next step of research, we will combine

internal and external value chain activities to conduct research on full value chain management and explore how the blockchain technology can be used in full value chain management and how to use the blockchain technology to improve the value of the entire chain. Doing these helps companies improve their management and decision-making capabilities.

## Data Availability

The datasets used and/or analyzed during the current study are available from the corresponding author upon reasonable request.

## Conflicts of Interest

It is declared by the authors that this article is free of conflict of interest.

## Acknowledgments

This work was supported, in part, by the funds for the "Undergraduate Teaching Reform and Innovation Project" of Beijing Higher Education in 2020 and "Undergraduate Teaching Reform and Research Project" of China University of Mining and Technology (Beijing) in 2020 (J20ZD18).

## References

- [1] B. Yang and C. Chang, *Principle, Design and Application of Blockchain*, China Machine Press, Beijing, 2017.
- [2] W. W. Dai and Z. J. Wang, "A brief exploration on real time control of value chain accounting," *China Management Informatization*, vol. 1, pp. 3-4, 2007.
- [3] L. Cen, "Optimization analysis of enterprise cost control based on value chain," *Business Times*, vol. 27, pp. 86-87, 2012.
- [4] S. L. Liu, *Research on Strategic Cost Management of Growing Small and Mediumsized Enterprises Based on Value Chain*, Hunan University of Technology, 2015.
- [5] J. Duan, *Research on Internal Control of Company a from the Perspective of Value Chain Management*, East China Jiaotong University, 2017.
- [6] M. Li, *Analysis of Longitudinal Value Chain Based on Improving the Competitiveness of Core Enterprises*, Beijing Forestry University, 2005.

- [7] Z. Gao and R. C. Jiang, "Enterprise competitive strategy based on vertical value chain: cooperative game perspective," *Management Modernization*, vol. 2, pp. 36–38, 2014.
- [8] M. Wang and J. Q. Wang, "Research on decision-making methods of management accounting based on value chain," *Research of Finance and Economics*, vol. 9, pp. 18–24, 2012.
- [9] X. J. Han, *Research on Cost Management of Construction Enterprises Based on Value Chain Theory*, Liaoning Technical University, 2012.
- [10] Z. Z. Wang, "Preliminary framework of software testing theory," *Computer Science*, vol. 41, no. 3, 2014.
- [11] L. Lin, "Use case design method for aerospace embedded software based on black box testing," *Computer Engineering and Design*, vol. 33, no. 6, pp. 2272–2276, 2012.
- [12] H. F. Xu and K. X. Zhao, "Software testing and quality assurance," *Modern Radar*, vol. 10, pp. 98–100, 2006.



## Research Article

# Acclimatization of Nanorobots in Medical Applications Using the Artificial Intelligence System with the Data Transfer Approach

**Hariprasath Manoharan,<sup>1</sup> Yuvaraja Teekaraman ,<sup>2</sup> Ramya Kuppusamy ,<sup>3</sup>  
Arun Radhakrishnan ,<sup>4</sup> and K. Hariprasath Venkatachalam<sup>5</sup>**

<sup>1</sup>Department of Electronics and Communication Engineering, Panimalar Institute of Technology, Chennai 600 123, India

<sup>2</sup>Department of Electronic and Electrical Engineering, The University of Sheffield, Sheffield S1 3JD, UK

<sup>3</sup>Department of Electrical and Electronics Engineering, Sri Sairam College of Engineering, Bangalore City 562 106, India

<sup>4</sup>Faculty of Electrical & Computer Engineering, Jimma Institute of Technology, Jimma University, Ethiopia

<sup>5</sup>Department of Electronics and Communication Engineering, Audisankara College of Engineering and Technology, Gudur, Andhra Pradesh 524 101, India

Correspondence should be addressed to Yuvaraja Teekaraman; [yuvarajastr@ieee.org](mailto:yuvarajastr@ieee.org)  
and Arun Radhakrishnan; [arun.radhakrishnan@ju.edu.et](mailto:arun.radhakrishnan@ju.edu.et)

Received 28 September 2021; Accepted 23 December 2021; Published 20 January 2022

Academic Editor: Deepak Gupta

Copyright © 2022 Hariprasath Manoharan et al. This is an open access article distributed under the Creative Commons Attribution License, which permits unrestricted use, distribution, and reproduction in any medium, provided the original work is properly cited.

This article deliberates various issues that are present in the integration of nanorobots in medical applications when real-time arrangements are used. In the current generation, there is a need for a device to recognize different diseases in a fast mode of operation where data transfer should be highly accurate. Even though many devices are existing, valuable information is not provided on the detection segment that has been delivered. Therefore, the technology of nanorobots can be implemented for detecting and providing solutions to various diseases in the human body. These nanorobots operate with gesture actions and they are applied in two different surfaces. Since the robotic technology is implemented in the proposed method, it is necessary to integrate an artificial intelligence (AI) technique in amalgamation with a neural network system which feeds the input in multiple ways using hidden layers. If such arrangements are processed, then, a data transfer path will be communicated with the media access control (MAC) design where the results can be analyzed in a real-time environment using online analysis, and in turn, the outcomes are simulated using MATLAB. Subsequently, comparing the MATLAB exploration with the existing method, it can be observed that the proposed method in the application of the medical field can be prominently improved for an average of 68%.

## 1. Nanorobots in Medical Applications: An Indication

In the previous generation, nearly one-third of the population in the world is facing various issues related to health care and needs early diagnosis which is necessary for proper surgical methods. In case if the diseases are not diagnosed properly at early stages, then, there is a high probability that it may lead to an individual death which should be avoided at any cause. Even though many image processing algorithms are present for early detection of nerves and materials, not even a single method is able to provide high

effective results. In addition, a sensor-based technology is also introduced in medical applications which require installation of nanosensors inside the body where severe affects will raise inside the body. Therefore, to avoid such causes, a technology needs to be introduced which needs to be minuscule in size. Moreover, if nanosized particles are introduced in the field of medical applications, then, more amount of blocks will be transferred; this type of problems can be solved using single injection cases.

To solve the problem of implementation using conventional techniques in the field of medical applications, a diverse technique is needed and it is proposed that nanorobots can



be introduced in the field of treatment for every inspection of time. It is also perceived that during such installation cases, early diagnosis can be done, thus preventing loss of lives among a group of people. Further, nanorobots differ from conventional methods in terms of ease of installation and the cost of connecting equipment will vary with respect to the designed considerations. If nanorobots are implemented, then, people can monitor their health at their remote locations which provides high modicum in fast-moving conditions. Most of the nanorobotic technology focuses on monitoring various parameters that are related to lost tissues thereby improving the productivity of medical tests and devices.

*1.1. Relevant Works.* In this section, the mechanisms that are related to nanorobots are discussed where all basic parametric evaluation has been perceived in a complete modus. For assessing the proposed method, a study case has been examined by using magnetic control systems where a microbotic technology has been used for treatment of medical circumstances [1]. Since the robots are navigated in different directions, an innovative formulation for magnetic radiation has been instigated and mechanical designs with open discussion and solutions are presented. However, a magnetic control system requires a moving torque inside the robots which makes the study case to be implemented only at most necessary circumstances. When this study case has been determined, an evaluation has been made for all biomedical applications [2] in a versatile mode by linking sensing devices with nanorobots. In this case, the robots are developed using different chemical components as they vary depending on morphology and consistency. Even though high amount of consistency has been acquired, a lot of chemical parameters has been used which makes the process to be implemented in a real-life environment as it may cause hazardous actions. In real-time simulation, a three dimensional clinical database address has been protected where most of the communicating nanorobots have been integrated in basic segments [3]. This type of contrivance usually includes a satellite surveillance system that focuses on saving the lives of many people from epidemic diseases. In the absence of a satellite surveillance system, the movement of nanorobots inside blood vessels is observed [4] with an adaptive control algorithm where the destination can be reached instantaneously with high accurate measurements. But this system is not suitable under real-time applications as installation of nanorobots is a difficult task and it is not possible to keep these robots in neighboring nodes. Several basic parameters have been evaluated with rigid body trajectory paths which provide a high intelligent system for a precise design of controllers. Since the robots are constructed with supporting tissues, a high power line communication is required [5] with reliable communication rates that vary between 100 and 1000 microns. Even at high power, there is a high possibility that all constructed tissues will be unexploited if the distance of separation is maximized. Therefore, for better construction at high frequency ranges, only few neighboring nodes will be allocated that provides a good tradeoff in terms of construction and management.

Further, advanced diagnosis on medical applications has been developed that provides an exceptional capability to minimize the risk of operation where all complex tasks can be performed at a small-scale operation [6]. High technological implications can create a better opportunity for future concocts to implement nanorobots in the medical field with high image capturing proficiency. The methodology implemented in [7] suggests that if future development is needed, then, adjacent collaboration is needed with miscellaneous energy modes. However such advances are not developed and after realizing the benefits of Nano robots in medical applications such intriguing technologies are developed. If high energy is touched, then, the mode of adaptability will be increased in considered regions for all different applications with low cost of implementation. In case of gesture activities, it is required to identify a collaborative mechanism between nanorobots and different communities on medical research. Even detoxification and the approach on synthesis will be provided with rapid changes on all cutting edge technologies.

If nanorobots are applied in medical applications, the velocity of blood vessels that are flowing deep inside the body can be easily recognized [8]. The aforementioned method is demonstrated with the help of online tool analysis where all navigation information will be provided with a two-stage state estimation procedure. Conversely, the same model has been replaced by the Fourier series procedure where the movement of blood vessels is estimated with an observable behavior (i.e., if zero is present, then the system will not be observed whereas in case of 1, the system remains in observable condition so that any flow during this period will be calculated). By extending this observable concept, the authors [9] have formulated a magnetic method which makes the nanorobots be ambitious using magnetic field configurations. In this way, interactions will happen and an actuation mechanism can be added to describe the effect of nanorobots in case of emergency situations. In addition, three steps will be followed for the design of magnetic-driven robots such as understanding the design concept with different topologies, indulgent functionalities, and high automotive devices. Further, the magnetic system perception can be applied in the self-propagation mode with immediate delivery of targets [10]. This method is directly applied as an automotive technique for tumor treatment using different gesture paths.

In the current generation, the nanorobotic technology has been extended to check the DNA of individual persons and it is used for treatment of cancer with high radiation [11]. But still now, such technologies are under testing mode since the addition of targets will happen which can able to detect other diseases in the entire body. If drugs are delivered for any disease, the variety in engrossment is calculated using noninvasive techniques [12]. Since drugs are delivered at a proper time, most of the diseases can be eradicated within a short period of time, and if any side effects are found, those also will be treated immediately at a remote location in the presence of nanotechnology. Even after invention of nanorobots, AI-based technique is not integrated as devices are not precise due to the low micron size

[13]. Due to the presence of low micron size Nanorobots are termed as controllable machines where any defected parts can be easily identified and controlled, and they can be used in all biomedical applications [14]. Furthermore, the speed of identification will be increased at low cost as compared to wearable devices. Nevertheless, the amount of fabrication needed for the emerging purposed is not mentioned due to negative impulse response variants [15]. The aforementioned works are developed with respect to nanotechnology fields and all interventions are tested with some limitations.

**1.2. Research Gap and Motivation.** Most of the existing works focuses only on the implementation of conventional devices that will not help the people to monitor themselves at their remote locations. However, if any sudden discomfort occurs, people can visit nearby infirmaries and they can check their vigor after waiting for a long period of time. Even the same method exists in all parts of the world, and societies still believe the same way which is organized like the older day periods. But on the other side, a number of technologies have been developed with many devices which are very minute in sizes, and the usage of such intellectual devices is lesser.

Therefore, this research article identifies the gap that is not present in an existing conventional device and discovers a new way to nanorobotic solution for applying in medical applications. However, at initial stage of installation, some motions are difficult to detect but after equivalent training models, the proposed work on nanorobots performs much better than existing case studies [1, 2]. The foremost impetus of the projected work is to implement such artificial intelligent nanorobots at low cost for all individuals in the society to detect the presence of diseases at the early stage.

**1.3. Objectives.** The major objective of the proposed research is to introduce a nanorobot in the field of medical diagnosis by combining multisensing models for early diagnosis of both tissues and muscles by solving the ensuing basic robotic parameters.

- (i) To measure the motion of a nanorobot using corresponding weights for external control process
- (ii) To detect the motion error for allocating sufficient resources at corresponding intervals
- (iii) To maximize the transmission capability of nanorobots for transferring the information at maximum possible routed ways

For implementing the abovementioned objectives, an AI technique has been introduced where training data has been incorporated at starting stages with a set of predetermined values. Once the values are obtained, a neural network has been introduced with different weightage process that detects the ailment of different individuals.

## 2. Problem Formulation

In this section, a new flanged mathematical formulation that is used for calculating the exact scenarios of nanorobots is provided with high benefits of integration at corresponding

segments. In this case, as a first segment, transmission of signals is calculated from the reference path using different weights as follows

$$R_i = \sum_{i=1}^n a_n x_n, \quad (1)$$

where  $a_n$  and  $x_n$  denote the corresponding nanorobots that are installed with larger encumbrances.

In the proposed method, nanorobots are designed in such a way where the moment is restricted to either a flat or perpendicular level. For both directions, discrete equations should be framed and it can be represented in terms of error as

$$e_i = \begin{cases} x_t - x_m & \text{for flat,} \\ y_t - y_m & \text{for perpendicular,} \end{cases} \quad (2)$$

where  $x_t$  and  $x_m$  indicate the motion of nanorobots for a flat surface in both curved and gesture paths, respectively.  $y_t$  and  $y_m$  indicate the motion of nanorobots for a perpendicular surface in both curved and gesture paths, respectively.

Equation (2) indicates that there will be some system error with respect to different motions in nanorobots and they can be installed in both surfaces in a precise method. This equation is framed in order to reduce the error during arrival of different motion paths. Therefore, oscillation of nanorobots should be calculated using negative force values with integral values using equation (3).

$$F_i = \int_{S \in i}^n \rho_i \varphi_i d\varphi, \quad (3)$$

where  $\rho_i$  denotes the density of flux over the given surface area.  $\varphi_i$  represents the area covered in all directions with finite integral values.

Since in equation (3), the flux density is represented, a power line communication for transmission of signals should be inserted in the body surface of nanorobots. Therefore, the power line communication at corresponding time periods can be expressed using equation (4) as follows

$$P_i = \frac{1}{2} \sum_{i=1}^n \aleph(F_i * \vartheta_i), \quad (4)$$

where  $\aleph(F_i * \vartheta_i)$  represents the average power with respect to time that entails force and velocity parameters.

Equation (4) indicates the transmission power capability of only standard nanorobots. But the same equation will be varied for spherical nanorobots, and the design constellation will also differ for such robots that are not examined in the proposed method. If the power supplied to nanorobots are higher, then, constraint on heat will become complex, and to avoid such complexities, equation (5) is framed with spherical power density as

$$SP_i = \frac{P_i}{\text{surface area of sphere}}, \quad (5)$$

where the surface area of sphere =  $(4/3)\pi r^3$  should be calculated for avoiding of the complex condition related to temperature relationships.

Equation (5) can also be expanded using the thermal relationship on spherical conditions that satisfies the temperature constraint using the dispersion equation as follows

$$T_i = \frac{\circ F_i}{\circ C_i} \nabla_i^2, \quad (6)$$

where  $\circ F_i$  and  $\circ C_i$  denote the outer tissue that contains thermal and heat capacity of nanorobots, respectively.

Equation (6) represents that maximum endurable limits should be established before insertion of tissues inside the nanorobots. In addition, a steady-state temperature should be established for any boundary that exceeds within a certain limit as warning indications can be given at a short period of time. Therefore, the susceptibility of nanorobots can be given using equation (7) as

$$\omega(i) = \sum_{i=1}^n \frac{M_i}{\epsilon_i}, \quad (7)$$

where  $M_i$  and  $\epsilon_i$  denote the corresponding applied mass and external electric field, respectively, in order to get physical representation for the type of magnetic penetrability in robots.

Equation (7) indicates that the supplied external electric field should be minimized; therefore, aggregate vulnerability characteristics of nanorobots can be minimized. In addition, another important parameter is the cost of installing tissue around the robots which gives a complete round off values using equation (8).

$$C_i = \sum_{i=1}^n \partial_i \gamma_i, \quad (8)$$

where  $\partial_i$  and  $\gamma_i$  denote the tissues and weight, respectively, of tissues that are covered at the outer end of robots.

It is factual that the cost of implementation depends only on tissue values, and therefore, for each flat of the perpendicular surface, the measurement should be precise which in turn leads to minimization of the cost.

### 3. Optimization Algorithm

Since nanorobots are designed with tissues, it is necessary to implement a set of rules for passing the information from the transmitting to the receiving station. In this case, an infrastructureless network has been designed using ad hoc wireless network since the robots are present at different nodes that move with respect to time. In addition, since wireless networks are used as communication module, it is necessary to implement a media access control (MAC) protocol that uses a common clock for synchronizing the packets with respect to each other. Moreover, the designed network uses the distributed mode of operation in the absence of concealed and exposed stations. The parameters

for designing the MAC protocol for the operation of the nanorobot can be expressed in mathematical form as

$$K_1 = \sum_{i=1}^n \frac{\theta_1}{2} * \beta_i + TR_{xi}, \quad (9)$$

where  $\theta_1$  denotes the single time period frame.  $\beta_i$  represents the duration of the preamble.  $TR_{xi}$  denotes the transmission and reception power of MAC protocols.

If equation (9) is designed correctly, then, even at low bandwidth and power, the robots is able to transfer information to all corresponding neighboring nodes. Further, resources will also be allocated for avoiding the delay in the entire network which can be expressed as

$$d_i = \sum_{i=1}^n \frac{\theta_i}{2} (t_d + t_{ea} + t_{da}), \quad (10)$$

where  $t_d$ ,  $t_{ea}$ , and  $t_{da}$  denote the time taken for data transfer, early acknowledgment, and data transfer acknowledgement at different phases.

Since the robotic technology is used, an artificial intelligence (AI) technique [16, 17] is integrated for further process verification using multihop networks. Therefore, a multilayer feed forward mechanism is implemented where it is easier to implement an omnidirectional antenna for data transfer in one direction. When such multiple layers are designed, then, errors in data should be minimized. This can be integrated with equation (2) as follows

$$E_i = \sum_{i=1}^n \frac{1}{2} (O_i - \widehat{O}_i), \quad (11)$$

where  $O_i$  and  $\widehat{O}_i$  denote the observed output and predicted output values, respectively, for a single time period.

If errors are minimized, then, binary classification can be applied for all packets that are transmitted to the destination. The binary classification can be modeled using a binary number as expressed in equation (12).

$$O_i = \begin{cases} 1 & \text{if error} = 0, \\ 0 & \text{if error} = 1. \end{cases} \quad (12)$$

The predicted output is related to the activation function of different neurons which can be expressed in mathematical form using equation (13).

$$\widehat{O}_i = \frac{E_T}{\sum_{i=1}^n E_i}, \quad (13)$$

where  $E_T$  denotes the total error after combining equation (2) and (11).

The major advantage of implementing the multilayer feed forward mechanism in AI is that it can be integrated with many problem domains in different areas as their topology is very easy to implement. Moreover, a universal

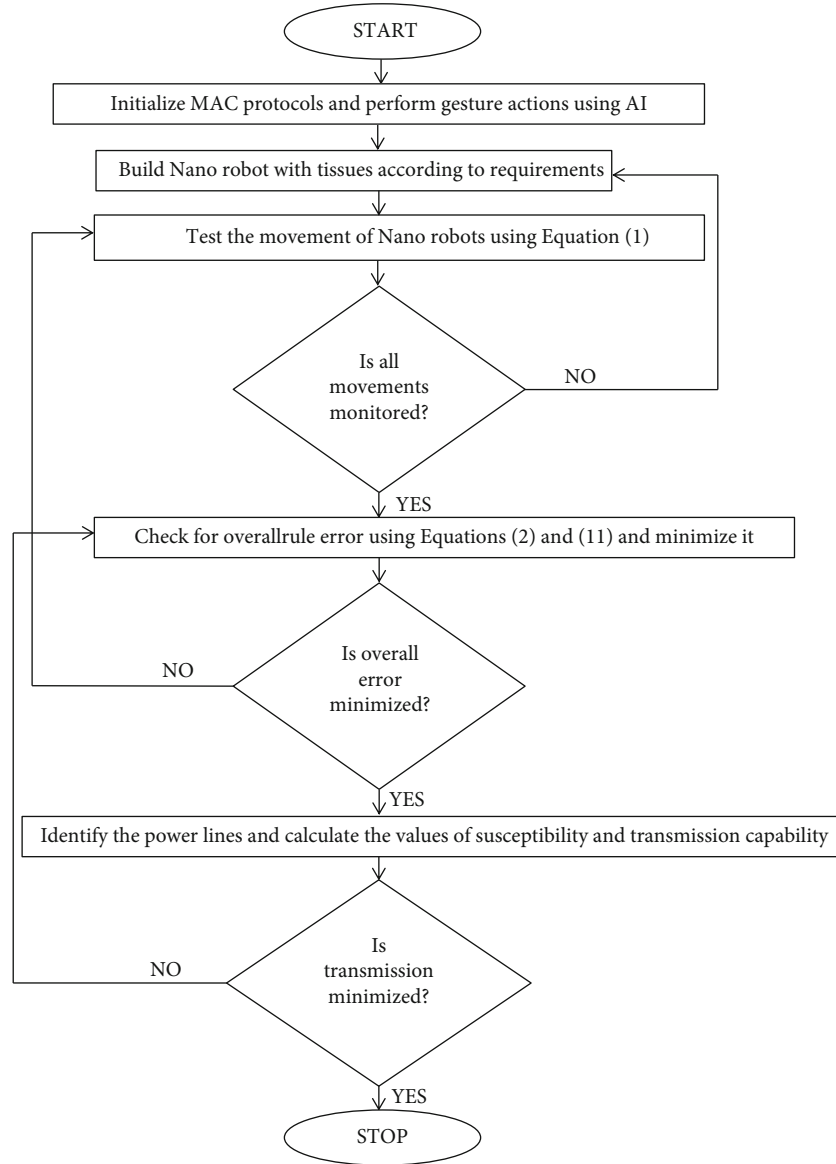


FIGURE 1: Process of assimilating nanorobots for medical applications using AI.

approximation problem can be solved using this type of algorithm where all nonlinear dynamic systems can be activated using composite materials. In the multilayer perceptron mechanism, the images can be easily classified by different robots since the input variables are not limited in their topology even though they are present in complex networks. The cost of implementing such networks can be integrated with equation (8) as

$$C_i(w_i, b_i) = \frac{1}{2V} (|a|), \quad (14)$$

where  $w_i$  and  $b_i$  indicate the corresponding weights and input biases of feed forward networks, respectively.  $|a|$  denotes the output vector from multiple layers.

Equation (14) denotes that cost function of the integrated algorithm is calculated with respect to weights and

biases that are supplied from three different layers such as input, hidden, and output layers.

Also, the aforementioned equation represents the weighted least square mechanism that is universally used for all neural network algorithms for nanorobotic technology. Figure 1 shows the step-by-step process of designing nanorobots for medical applications using AI.

#### 4. Results and Discussion

In this section, real-time analysis on the performance of microrobots for medical applications has been verified by measuring different parameters. The purpose of measuring different parameters will assure better quality of service, and in turn, these values can be observed using an online monitoring system. In addition, for all these scenarios, a set of rules have been defined that provides support for high-reliability and scalability measures. All the observed



parametric values are considered as different scenarios as follows—scenario 1: motion of the nanorobot, scenario 2: motion error, scenario 3: transmission capability, scenario 4: susceptibility, and scenario 5: cost of implementation.

To provide better understanding, all scenarios are plotted in MATLAB where three dimensional images are strategized. Also, an additional assumption has been considered for achieving a high-performance operation where the size of each robot should be much higher. This assumption is made in order to provide a self-organizing capability since the nodes are in moving position with respect to each other. By following the assumption for five different scenarios, descriptions on plots have been provided as follows.

**4.1. Scenario 1.** In this scenario, the motion of nanorobots with respect to different weights has been observed. The major reason for elucidating this scenario is that an artificial force will be present as an external controller where the user is not able to control the motion of robots if they are going in the wrong direction. Therefore, it is necessary to use an omnidirectional antenna for calculating the motion of nanorobots as energy is spread equally in all the directions even in the presence of an external controller. In the first step, an obstacle-free path should be identified under real-time applications, and by using the desired arrangement, all the shortest paths should be identified within a short period of time. Therefore, the motion of nanorobots is difficult to design, and in the proposed method, a new topology has been used and the corresponding motion has been identified and plotted using Figure 2.

In Figure 2, it can be observed that the motion of nanorobots is observed for different meters according to the corresponding weights in kilograms. Also, from the contour plot, a distance in hundred meters can be extended as a maximum time period for wave motion. Therefore, from the observed results for different weights, the proposed method proves to be much efficient than the existing method [3]. For example, if the weight of the nanorobot is 30000 kg, then, the motion of the nanorobot is observed as 1691 meters for the proposed method whereas with same amount of weight, the existing method has limited the motion of nanorobots to 1004 meters which is much less than the proposed method.

**4.2. Scenario 2.** Once the motion of nanorobots is maximized, then, in the next case, error values in terms of micrometers should be observed under two different surfaces such as flat and perpendicular. Error values will be calculated from equation (2) using two different paths such as gesture and curved. In addition, the overall error values are calculated from equation (11) where predicted output values will be observed. In the proposed method, an infrastructureless network has been designed where error values should be minimized (i.e., gesture paths should be chosen correctly in accordance with resources that are allocated at the first stage). The observed error values are plotted in Figure 3 under offline analysis.

In Figure 3, error values in terms of micrometers are plotted at different time periods ranging from 5 seconds to 50 seconds. For different time periods, the error values

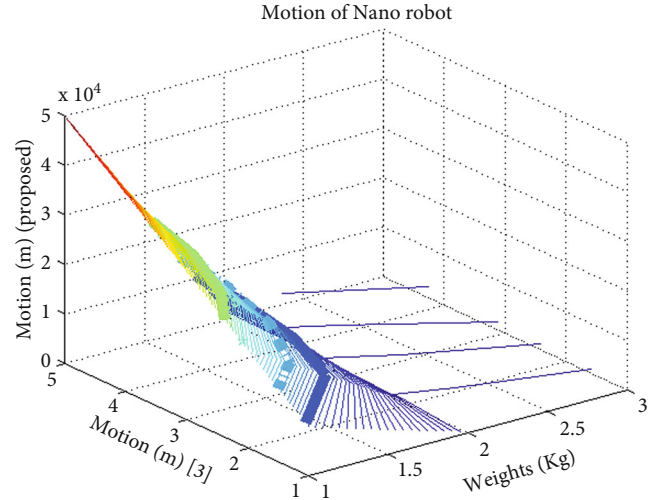


FIGURE 2: Motion of nanorobots.

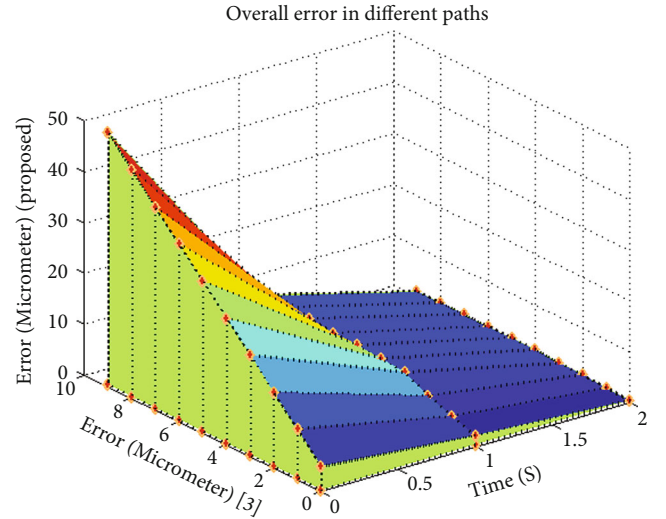


FIGURE 3: Motion errors of nanorobots.

should decrease or it should remain at a constant rate. If the aforementioned condition is satisfied, then, it is much easier to observe the motion of robots and even it can be controlled at a corresponding time period. The mesh plot indicates that error values for the proposed method are much lesser than the existing method [3]. For example, if the time period is 30 seconds, then, the overall error rate can be observed as 8.6 micrometers for the existing method whereas for the proposed method, the error rate remains constant after 30 seconds until the maximum time period is accomplished.

**4.3. Scenario 3.** In this scenario, the minimum transmission capability of the designed nanorobots in medical applications has been observed. Transmission capability defines the rate of how deep an image can be captured and reported to the neighboring nodes under mobility. If the transmission capability of nanorobots is lesser, then, a clear image can be captured, and if any problem occurs inside the human body,

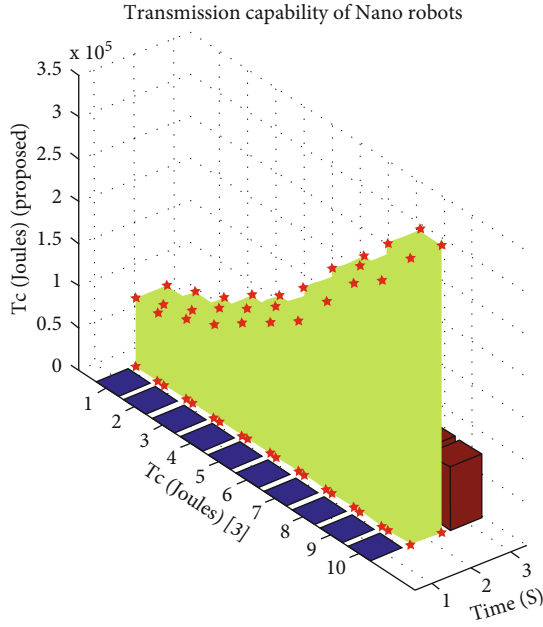


FIGURE 4: Capability of transmission.

it will be detected within a short period of time. But if the designed robots are having high transmission capability, identification of diseases will take a long period of time which in turn makes the designed methodology inefficient. After observing the minimum capability rate, the results are simulated in offline analysis and are shown in Figure 4.

In the three-dimensional bar graph in Figure 4, it is implicit that the transmission capability of the proposed method using nanorobots is much lower which is expressed in Joules. For a clear view, the time period is considered from 5 to 50 seconds where within the corresponding time period, transmission capability remains constant for the proposed method from 45 seconds. Moreover, if the time period is 30 seconds, then, the transmission capability is observed to be 178000 Joules for the existing method, but for same time period, the proposed method provides low capability rate which is equal to 68000 Joules. This proves that even the capability rate can be minimized or it can be kept constant for the designed nanorobots.

**4.4. Scenario 4.** In this scenario, the vulnerability rate of response received from nanorobots has been observed at a corresponding distance. If the distance is increased or decreased, the vulnerability rate should be either maximized or minimized depending on gesture actions. But in the design of nanorobots, the vulnerability rate should always be minimized since the nanorobots are designed with high-end tissues where gesture actions will always be accurate. Therefore, for different gesture actions with high distance, the rate of vulnerability is observed and plotted in Figure 5.

Figure 5 is plotted by considering 31 different data sets which varies with respect to distance and time periods. It can be observed in Figure 5 that as the distance of separation increases, the susceptibility rate which is measured in micrometer per kilogram is increased, and for the proposed

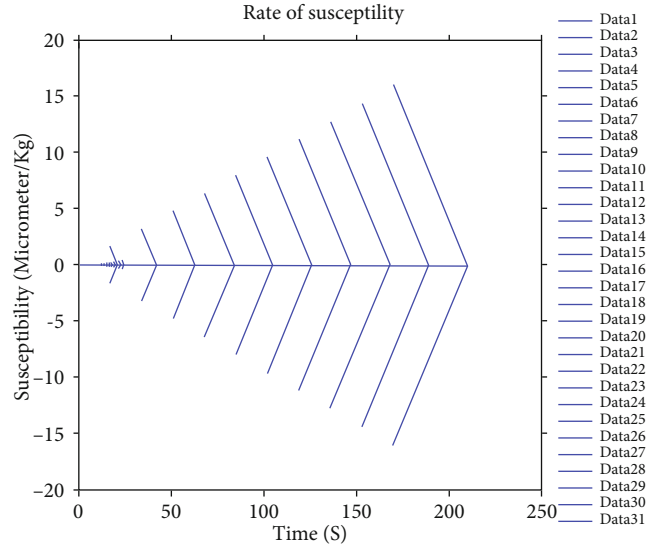


FIGURE 5: Vulnerability rate for 31 datasets.

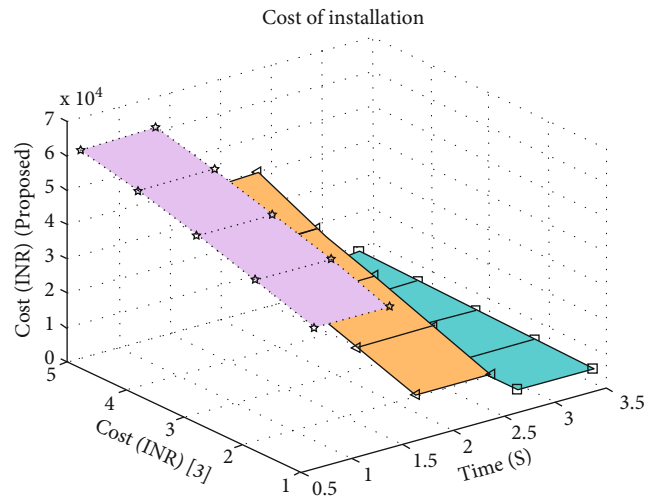


FIGURE 6: Cost of implementation.

method, after a distance of 80 meters, the vulnerability rate is observed to be constant even though the data is varied to maximum extent. But for the existing method [3], even though data varies, the susceptibility rate increases to maximum extent which does not guarantee proper operation rate even for 200 meters.

**4.5. Scenario 5.** The aforementioned scenario focuses on hypothetical segments that are necessary for the operation of nanorobots. But in this scenario, the cost of implementing nanorobots according to the designed parameters is calculated. Since in the proposed method, nanorobots are designed for medical applications, only few parameters are considered, and as a result, the cost of implementation will be lesser than those of standard methods. The cost of implementation is measured in Indian Rupees, and the same is plotted using the ribbon plot in Figure 6.

In Figure 6, it can be observed that cost of installation is much lesser for the proposed method and is calculated using equations (8) and (14). It is apparent that as time varies, the cost of implementation becomes lesser, and depending on the transmission capability between 41000 and 61000, the cost will be varying and maximum Rs. 8500 can be consumed for building such nanorobots. This proves that the proposed method is highly valuable during real-time implementation of different networks under the presence of MAC protocol.

## 5. Conclusions

The proposed work uses a new flanged technology on the nanorobotic mechanism in medical applications where its performance is tested under basic parametric values. In case of pandemic circumstances, a real-time application on medical diagnosis is always necessary for saving the life of humans. Even if diseases cannot be cured, at least, it should be identified and spread rate should be controlled at a higher proportion. With such high technologies on nanorobots, medical applications can be developed and any disease can be identified within a short period of time. Moreover, many developed methods provide high advantage on real-time applications but a highly efficient algorithm integration is not provided in any advanced technologies. But the proposed method integrates an AI technique with the MAC protocol for designing a set of rules with the data transfer stage. If these technologies are integrated with each other, then, automatic monitoring of robots can be created at low cost with different tissues, and in real time, this technology can be installed using different gesture actions. The proposed technology is tested under five different scenarios, and overall parametric values are also calculated where the proposed method proves to be much efficient even if it is installed in real time.

## Data Availability

The data used to support the findings of this study are available from the corresponding author upon request.

## Conflicts of Interest

The authors declare that they have no conflicts of interest.

## References

- [1] Y. Shao, A. Fahmy, M. Li, C. Li, W. Zhao, and J. Sieng, "Study on magnetic control systems of micro-robots," *Frontiers in Neuroscience*, vol. 15, pp. 1–15, 2021.
- [2] L. Wang, Z. Meng, Y. Chen, and Y. Zheng, "Engineering magnetic micro/nanorobots for versatile biomedical applications," *Advanced Intelligent Systems*, vol. 3, no. 7, article 2000267, 2021.
- [3] A. Cavalcanti, B. Shirinzadeh, M. Zhang, and L. C. Kretly, "Nanorobot hardware architecture for medical defense," *Sensors*, vol. 8, no. 5, pp. 2932–2958, 2008.
- [4] A. Farahani and A. Farahani, "An adaptive controller for motion control of nanorobots inside human blood vessels," *Bioscience Biotechnology Research Communications*, vol. 9, no. 3, pp. 546–552, 2016.
- [5] T. Hogg and R. A. Freitas, "Acoustic communication for medical nanorobots," *Nano Communication Networks*, vol. 3, no. 2, pp. 83–102, 2012.
- [6] F. Soto and R. Chrostowski, "Frontiers of medical micro/nanorobotics: in vivo applications and commercialization perspectives toward clinical uses," *Frontiers in Bioengineering and Biotechnology*, vol. 6, pp. 1–12, 2018.
- [7] C. Yamamuro, J.-K. Zhu, and Z. Yang, "乳鼠心肌提取 HHS public access," *Physiology & Behavior*, vol. 176, no. 12, pp. 139–148, 2017.
- [8] M. Fruchard, L. Arcese, E. Courtial et al., *Estimation of the Blood Velocity for Nanorobotics to Cite This Version : HAL Id : Hal-01071275 Estimation of the Blood Velocity for Nanorobotics*, 2014.
- [9] H. Zhou, C. C. Mayorga-Martinez, S. Pané, L. Zhang, and M. Pumera, "Magnetically driven micro and nanorobots," *Chemical Reviews*, vol. 121, no. 8, pp. 4999–5041, 2021.
- [10] S. S. Andhari, R. D. Wavhale, K. D. Dhobale et al., "Self-propelling targeted magneto-nanobots for deep tumor penetration and PH-responsive intracellular drug delivery," *Scientific Reports*, vol. 10, no. 1, pp. 1–16, 2020.
- [11] R. Devasena Umair, P. Brindha Devi, and R. Thiruchelvi, "A review on Dna nanobots – a new technique for cancer treatment," *Asian Journal of Pharmaceutical and Clinical Research*, vol. 11, no. 6, pp. 61–64, 2018.
- [12] P. Khulbe, "Nanorobots: a review," *International Journal of Pharmateutical Sciences and Research*, vol. 5, no. 6, pp. 2164–2173, 2014.
- [13] A. Kumar and S. Roy, *Amandeep Kumar, Ramya CB, Surashree Roy* 8, vol. 3, no. 2, pp. 1725–1729, 2014.
- [14] R. B. Durairaj, J. Shanker, and M. Sivasankar, "Nano robots in bio medical application," in *IEEE-International Conference on Advances in Engineering, Science and Management, ICAESM-2012*, Nagapattinam, India, 2012.
- [15] F. Novotny, H. Wang, and M. Pumera, "Nanorobots: machines squeezed between molecular motors and micromotors," *Chem*, vol. 6, no. 4, pp. 867–884, 2020.
- [16] G. F. Luger, "Artificial intelligence: structures and strategies for complex problem solving," *Zywnienie Czlowieka I Metabolizm*, vol. 5th, 2005 <http://www.amazon.com/dp/0321545893>.
- [17] G. Lample, *Deep Learning for Symbolic Mathematics*, pp. 1–24, International Conference on Learning Representations (ICLR), 2020.



## Research Article

# Design of the Secure Smart Home System Based on the Blockchain and Cloud Service

**Kun Liao** 

*Art College, Chongqing Technology and Business University, Chongqing 400067, China*

Correspondence should be addressed to Kun Liao; 2012a42@ctbu.edu.cn

Received 19 August 2021; Revised 2 September 2021; Accepted 30 December 2021; Published 17 January 2022

Academic Editor: Deepak Gupta

Copyright © 2022 Kun Liao. This is an open access article distributed under the Creative Commons Attribution License, which permits unrestricted use, distribution, and reproduction in any medium, provided the original work is properly cited.

In this paper, a variety of cloud service combinations is used to form the control core of a smart home, realize data forwarding, storage, and analysis in the cloud, and complete the remote management of smart home devices. This paper studies the secure access control of smart home data combined with the blockchain technology and password technology to realize the secure and efficient access control of smart home data. The system can achieve the goal of independent research and development. Aiming at the problem that the access control of a smart home is generally managed by third-party authorized institutions and there is an unauthorized access, a blockchain-based smart home (BSH) access control scheme is proposed. The scheme extends the attribute-based access control model (ABAC) and applies the blockchain technology to the smart home ABAC model to realize fine-grained access control. In the scheme, the resource provider first publishes the access control policy of the resource to the blockchain. If the resource visitor wants to access the resource, he needs to submit an access request to the blockchain and use an SM2 threshold signature to process the transaction proposal. The endorsement peer node in the blockchain runs the access control policy smart contract to decide whether to grant access rights. This scheme can ensure that resource providers can participate in all the processes of access control and avoid the risk of unauthorized access caused by the centralized management of the third party. Finally, the simulation experiment is carried out on the Hyperledger Fabric alliance chain development platform. The results show that the BSH access control scheme has good applicability in the smart home scenario.

## 1. Introduction

In modern society, the smart home has become the trend of intelligent life. In order to build a good smart home interconnection system and provide users with more valuable services, it is usually necessary to share smart home data with the outside world. However, these shared data often contain a large number of user sensitive privacy data and there is still a lack of an effective smart home data access control scheme to ensure the security of user data, which will become the bottleneck of the development of the smart home field. At present, more than 90% of smart home network access is carried out through mobile smart terminals. These terminal devices generally have the characteristics of scattered network topology and limited resources and are vulnerable to external attacks resulting in key leakage. In addition, the traditional smart home access control system

is a centralized management, which does not include all participants in the access control decision-making process, and the data owner lacks the right to speak in the access control policy formulation and decision-making process. This enables the data requester to access the data of smart home devices without the authorization of the data provider, and there is a risk of ultra vires access.

Smart home is becoming more and more popular in recent years, because it brings us comfort and convenience of life; it has been recognized and widely used by people [1]. Its main core is to embed intelligence into sensors and actuators to integrate devices. When people apply, there may be multiple users visiting home devices at the same time or at different times, which requires no one to participate in data processing and exchange. On the one hand, the rise of a smart home improves our quality of life; on the other hand, because its information system mainly shares information

through smart devices (IoT) and embedded sensors [2], there are some potential safety hazards. Mainly in the process of data transmission, privacy or user's privacy information will be exposed. A new secure smart home system solution based on blockchain is proposed, which aims at dealing with the security constraints in the blockchain method and uses the combination of Hyperledger Fabric and Hyperledger Composer. The popularity of a smart home in the Internet of things will increase the cost of security requirements [3]. How to use a relatively low-end design to strengthen the research on network security in families is very meaningful. This paper puts forward the method of localization by using the private blockchain technology and trilateral measurement. After our investigation, it is found that using private blockchain has great advantages. Blockchain plays a great role in the field of Internet of things [4], and it can also solve security problems. We apply it to a smart home, which can effectively optimize security, attacks, user privacy, and so on. It is found that blockchain plays three roles in smart home applications [5]. The superiority of a smart home is self-evident, and it can fundamentally improve our quality of life. However, we also find that its data storage security cannot meet our needs for privacy security.

## 2. Blockchain Technology

*2.1. Key Features.* Blockchain uses distributed ledgers to maintain stored data [6], so blockchain has the following key characteristics [7]:

- (1) Decentralization. Blockchain abandons the traditional and centralized network architecture and uses distributed computing methods and decentralized storage mode to ensure that any node in blockchain is equal to each other and every data block in the chain needs the participation and maintenance of each node
- (2) Transparency. The data stored on the blockchain is open and transparent, and the nonprivate information can query the data stored on the blockchain in an open interface and develop related applications
- (3) Autonomy. In order to avoid human intervention and exclude the trust of "people," blockchain uses consensus-based norms and protocols and any human intervention will not work
- (4) As long as the information is added to the blockchain through verification, it cannot be tampered with and will be stored permanently. Under special circumstances, more than 51% nodes in the control system can be modified at the same time
- (5) Anonymity. The exchange of data between nodes follows a fixed algorithm. Blockchain data exchange and even transactions can be conducted anonymously

*2.2. Blockchain Structure.* Blockchain is a distributed ledger, and internal blocks are connected by hash values in chronological order. As the basic technology of digital cryptocur-

rency, blockchain stores information blocks with digital signatures in distributed networks [8].

Blocks in the blockchain are linked to each other through parent blocks. Each block header consists of meta-data, including a version number, parent block hash, Merkle tree root hash, nBits, and random number, as shown in Table 1.

The block body of blockchain consists of two parts, namely, trading counter and trading. As shown in Figure 1.

Because of its unique open attribute, the public blockchain can attract many users and is particularly active. Alliance blockchain is used in commercial applications, and Hyperledger is developing the blockchain framework of business alliance [9]. Ethereum also provides tools for building alliance blockchain.

*2.3. Consensus Process.* In blockchain, how to reach an agreement among untrusted nodes is a transformation of the Byzantine General (BG) problem. How to reach consensus in an environment lacking trust is a challenge. Because the blockchain network is distributed [10], it is also a challenge for blockchain. We need protocols to ensure that the distributed books of different nodes are consistent. Then, the common ways to reach consensus in blockchain are as follows:

*2.3.1. Proof of Workload (PoW).* The consensus technology is to identify nodes in the existing chain that add new block rights by providing sufficient evidence to prove their workload. In fact, each node tries to broadcast the block of authentication transaction and chaos will occur. PoW can try to solve the difficulty adjustment problem by attaching a new block to the current chain. This process is called miner digging, where miners are responsible for selecting verified transactions and then forming a block. And add some additional information to the block, such as the hash value and timestamp in the parent block. Then, all the information in the block header is converted into a hash value by the SHA-256 hash function.

Such a scene can be considered. Several miners found random numbers that met the requirements almost simultaneously. When the miner node  $M_1$  digs out the block  $Block_{21}$  based on the block  $Block_1$ , it broadcasts to the whole network. However, since the miner node  $M_2$  is far away from the miner  $M_1$ , it does not receive the block  $Block_{21}$  for a period of time and digs out the block  $Block_{22}$  at the same height as the block  $Block_{21}$  and broadcasts to the whole network. According to the blockchain protocol, when different miners generate different blocks of the same height at the end of the blockchain, each node separately selects which block to receive. In the absence of other factors, nodes typically receive the first block they see. This creates an obvious problem, as different nodes receive the same height blocks  $Block_{21}$  and  $Block_{22}$  separately, resulting in the main chain of the blockchain being bifurcated. There will also be a rare continuous fork in the blockchain. As shown in Figure 2, at the fifth height of the block chain, when the branch blocks  $Block_{51}$  and  $Block_{52}$  have not been solved, the branch blocks  $Block_{61}$  and  $Block_{62}$  at the sixth height appear. The block interval depends on various parameter settings, such as

TABLE 1: Block header attributes.

Block header attribute	Definition
Version number	Used to indicate which set of block validation rules to follow
Parent block hash	256-bit hash value pointing to the previous block
Merkle root hash	Hash value of all transactions in the block
Time stamp	The current timestamp is from 1970-01-01T00: 00UTC seconds
nBits	Target value corresponding to mining difficulty
Random number	A 4-byte field, usually starting from 0, is incremented by each hash calculation

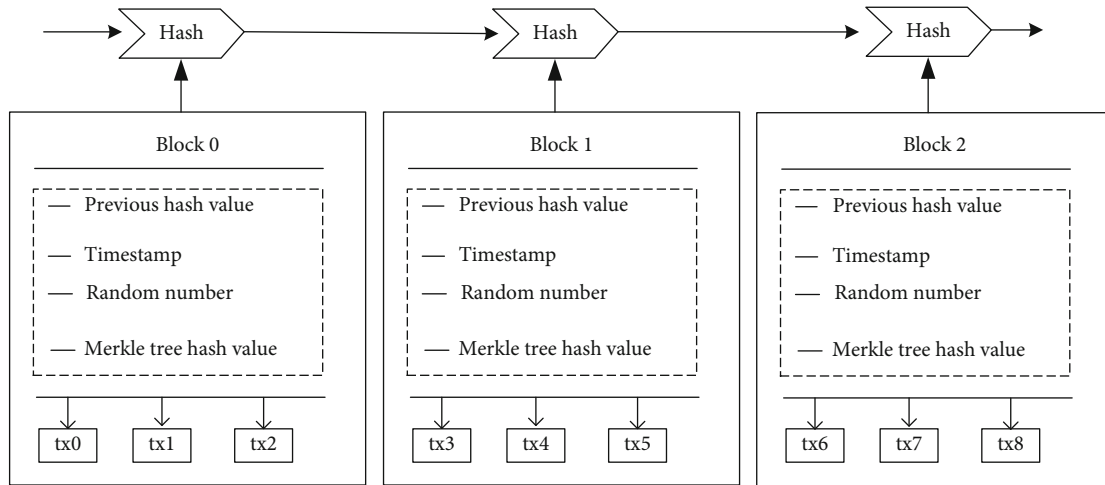


FIGURE 1: Blockchain structure.

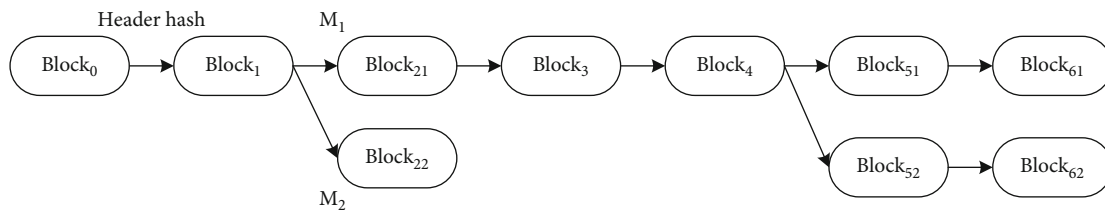


FIGURE 2: Blockchain bifurcation process.

generating Bitcoin blocks every 10 minutes and Ethernet blocks every 17 seconds [11].

The main problem with the PoW algorithm is that miners need to spend a lot of computing resources to solve this problem. In addition, only one miner succeeded in the end and the process was unsustainable.

**2.3.2. Certificate of Equity (PoS).** In this consensus algorithm, miners do not need to waste a lot of computing resources to solve mathematical problems. Since the selection of verifiers is based on equity relationships, the richest nodes may be given more opportunities to verify a block, thus becoming more advantageous in the network, which may lead to unfairness or concentration of rights. Because the mining cost and workload are much lower than PoW, PoS is more vulnerable to malicious attacks.

**2.3.3. Certificate of Entrusted Equity (DpoS).** It is a selective consensus process. In order to ensure efficiency, network

parameters, such as the block size, can also be adjusted. However, it has the tendency of centralization, which is also its limitation. Equity ownership can not only vote for itself but also manipulate others. However, dishonest witnesses will be voted down by shareholders because they will do anything malicious.

**2.4. Intelligent Contract.** Smart contracts are usually executed by system nodes, so it is impossible for a single entity to bypass the rules defined in this code, because this requires the consent of most consensus nodes. The main advantage of intelligent contract is that it can automate the business logic of the organization. The shift to automation eliminates the impact of possible legal disputes due to human error and misunderstanding. Legal contracts may have personal explanations, but blockchain intelligent contracts realized by software algorithms are decisive, and there is no possibility of subjective explanations. In the scheme proposed in this

paper, the intelligent contract stores the data owner list, and when the data user searches, the data owner list will be provided to the data user. The specific functions of smart home access control and data sharing scheme need to be realized by executing smart contract functions.

*2.5. Hyperledger Fabric.* Hyperledger Fabric is implemented by an open-source blockchain platform [12]. It provides a modular architecture to implement various functional modules by utilizing well-known and proven technologies. The core artifacts in Hyperledger Fabric [13] are described in Figure 3.

- (1) Organize peer node channel: in Hyperledger Fabric, peer node is the node that hosts blockchain and runs intelligent contract. Peer stores critical data and executes specific programs. The stored data mainly include books and smart contracts, and the executed procedures mainly include endorsement and smart contract execution. The functions of the following node can be divided into the submission node and endorsement node. All nodes in the blockchain network are submission nodes, which are responsible for recording complete blockchain data information and verifying the correctness of each transaction. They are nodes that package transactions into blocks and add them to the blockchain. Nodes with smart contracts are called endorsement nodes, which are mainly responsible for accepting transaction requests, executing smart contracts and sending signed data back to clients after verifying that transactions are valid. There can be one or more peer nodes in an organization. As shown in Figure 3, organization 1 manages two peer nodes, P1 and P2, and one peer node can be added to one or more channels, such as P1, P3, and P7 in the same channel
- (2) Membership service provider (MSP): MSP provides certificates to each peer node, so that the nodes connect to the blockchain network and trade. Organizations can have separate MSPs and get services
- (3) Sorting service: subscription service refers to the transactions that are approved first, which are sorted by the consensus protocol, and finally, the designated peer nodes get the results
- (4) Chain code: chain code is similar to smart contract. These are programs written in traditional programming languages such as Go, Java, and node.js, which can operate blockchain
- (5) Blockchain data structure: blockchain contains two different data structures in Hyperledger Fabric: state database and distributed ledger. The blockchain is modeled as key value storage (KVS) to store its latest state. It is maintained and managed by the peer node and can be operated by the chain code triggered by the transaction. On the other hand, distributed books store verifiable historical data of all failed

attempts and successful changes as a completely ordered hash chain of transaction blocks

### 3. SM2 Elliptic Curve Cryptography Algorithm

SM2 elliptic curve cryptography [14] is composed of the digital signature algorithm, public key encryption algorithm, and public key exchange protocol. The digital signature algorithm and public key encryption algorithm are used in this paper. Before the algorithm is executed, all parties need to set the public security parameters, including the scale  $q$  of finite field  $F_q$ , the parameters of elliptic curve equation, and the basic point  $G = (x_G, y_G)$  on the elliptic curve, and select cryptographic hash algorithm  $H_{256}$  and hash algorithm  $H_v$ .

*3.1. SM2 Digital Signature Algorithm.* The key generation is as follows:

- (1) The signer randomly selects  $d$  as the private key,  $d \in [1, q - 1]$ . After that, the public key is calculated

$$P = dG. \quad (1)$$

The public key  $P$  is made public and the private key  $D$  is kept secretly.

- (2) The signer selects the random number  $k \in [1, q - 1]$  and calculates

$$kG = (x_1, y_1). \quad (2)$$

- (3) The subscriber's placement is as follows:

$$\bar{M} = Z_A || M. \quad (3)$$

Among them,

$$Z_A = H_{256}(\text{ENTL}_A || ID || a || b || x_G || y_G || x_1 || y_1). \quad (4)$$

$\text{ENTL}_A$  is two bytes converted from the integer  $\text{entlen}_A$ ,  $a$  and  $b$  are the parameters of the elliptic curve, and  $(x_G, y_G)$  is the coordinates of the  $G$  point.

Calculate later

$$e = H_v(M). \quad (5)$$

The data type of  $E$  is converted to an integer according to the method given in the SM2 elliptic curve public key cryptography algorithm.

- (4) The signer calculates through the message  $M$  to be signed

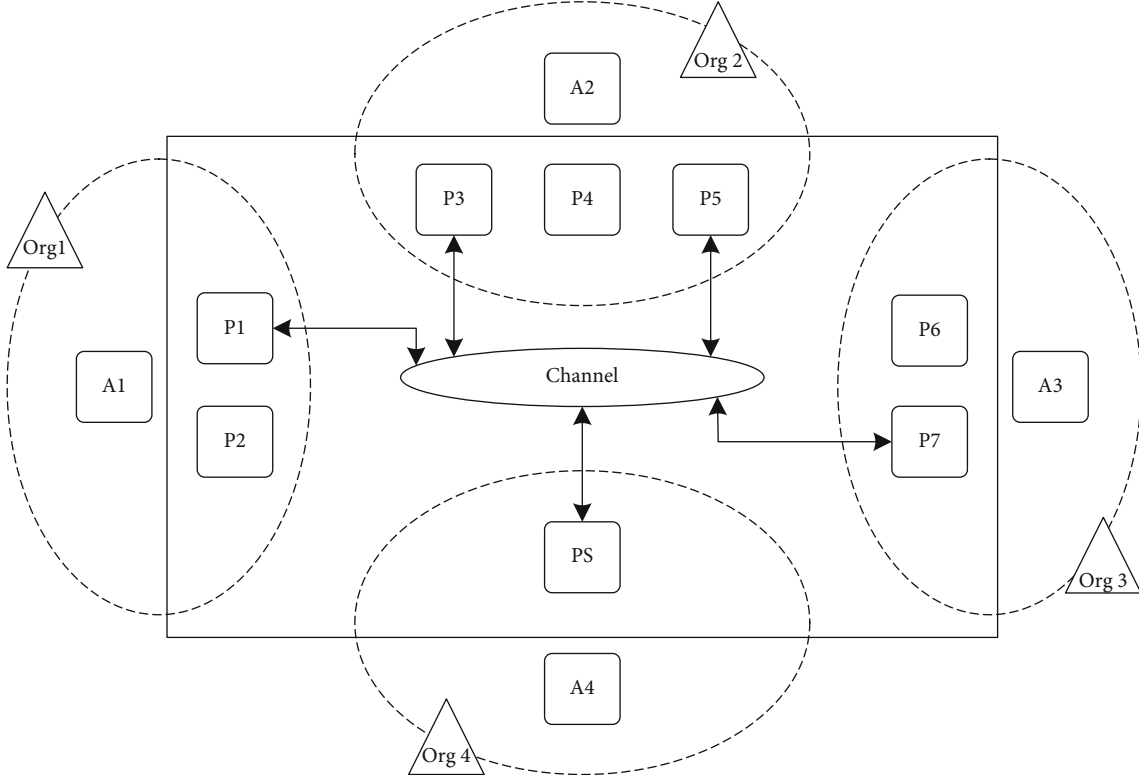


FIGURE 3: Peer node organization channel diagram.

$$r = (e + x_1) \bmod q. \quad (6)$$

If  $r = 0$  or  $r + k = q$ , the signer needs to reselect the random number  $k$ .

(5) The calculation is

$$s = (1 + d)^{-1}(k - rd) \bmod q. \quad (7)$$

If  $s = 0$ , choose a new random number  $k$ . If  $s = (1 + d)^{-1}(k - rd) \bmod q$ , the signer outputs  $(r, s)$  as the signature result.

(6) When the signature verifier receives the message  $M$  and the signature  $(r, s)$ , the signature verifier first checks whether  $r, s \in [1, q - 1]$  and  $r + s \neq q$  is true. Then, calculate  $e' = Hv(m)$ , and then, calculate

$$(x'_1, y'_1) = sG + (r + s)P. \quad (8)$$

(7) Calculate  $r' = (e + x_1') \bmod q$ , and judge whether  $r' = r$  is true. If the equation is true, the verification passes; otherwise, the verification fails

3.2. SM2 Public Key Cryptography Algorithm. The bit length of the plaintext  $M$  is  $m\text{len}$  and KDF is the key derivation function.

The encryption algorithm is

(1) Choose the random number  $l \in [1, q - 1]$ , and then, calculate

$$\begin{aligned} C1 &= lG = (x_2, y_2), \\ lp &= (x_3, y_3). \end{aligned} \quad (9)$$

(2) Calculate later

$$e = \text{KDF}(x_3 || y_3, m\text{len}). \quad (10)$$

Recalculate

$$C_3 = \text{hash}(x_3 || M || y_3). \quad (11)$$

(3) Finally, output ciphertext



$$C = C_1 \| C_3 \| C_2. \quad (12)$$

The decryption algorithm is as follows:

- (1) First, the decrypter needs to verify whether  $C_1$  is on the elliptic curve and calculate

$$dC1 = (x_3, y_3). \quad (13)$$

- (2) After that, the decrypter needs to calculate  $e = \text{KDF}(x_3 \| y_3, \text{mlen})$  and calculate

$$M = C2 \oplus e. \quad (14)$$

- (3) The decrypter calculates  $C'_3 = \text{hash}(x_3 \| M \| y_3)$  and passes the verification formula

$$C'_3 = C_3. \quad (15)$$

Determine whether the decryption is correct. If not, exit the decryption process. If true, output message plaintext  $m$ .

**3.3. Signature Scheme.** When nonmembers of the group want to join the group and become members of the group, they need to perform an interactive registration process with the home gateway HG. The specific process is as follows:

- (1) Group member  $U_i$  sends a registration request to  $\text{HG}_i$

$$\text{Req}_{\text{enroll}} = \text{Enc}_{\text{SM2}}(\text{ID}_i, pk_{\text{HG}_i}). \quad (16)$$

$\text{Enc}_{\text{SM2}}$  is the SM2 public key encryption algorithm, and  $\text{ID}_i$  is the identity information of group member  $U_i$ . After receiving the registration request,  $\text{HG}_i$  uses its own private key  $sk_{\text{HG}_i}$  to decrypt the registration request message  $\text{Req}_{\text{enroll}}$ , thus obtaining the true identity information of  $U_i$ . After that,  $\text{HG}_i$  needs to check whether the member has been registered in the local identity list, and if the member has been registered, it will refuse its registration request. Otherwise, it will randomly select  $u \in Z^*_p$  for the group member  $U_i$  applying for registration and obtain the first anonymous identity  $\text{ID}_{i1}$  of  $U_i$  by the following calculation:

$$\begin{aligned} U &= uG = (x_u, y_u), \\ \text{ID}_{i1} &= (x_u + sk_{\text{HG}_i})h(\text{ID}_i) + u \text{ mod } p. \end{aligned} \quad (17)$$

Thereafter, the  $\text{HG}_i$  sends response information  $M_H^1 : \{U, \text{ID}_{i1}, T_H^1\}$  to the group member  $U_i$ , where  $T_H^1$  is the current timestamp

- (2) After receiving the response information from  $\text{HG}_i$ ,  $U_i$ , a group member, first checks the freshness of  $T_H^1$ . After that, verify whether the equation  $\text{ID}_{i1}G = (x_uG + pk_{\text{HG}_i})h(\text{ID}_i) + U$  holds. If not,  $U_i$  needs to repeat step (1). Otherwise,  $U_i$  will generate part of the private key  $sk_{u_i}^{x_i} \in Z^*_p$  and calculate the corresponding pub  $pk_{u_i}^{x_i} = sk_{u_i}^{x_i}G$  lic key. After that, the  $U_i$  selects the random number  $v \in Z^*_p$  and obtains the second anonymous identity  $\text{ID}_{i2}$  of the  $U_i$  by the following calculation:

$$\begin{aligned} V &= vG = (x_v, y_v), \\ \text{ID}_{i2} &= (x_v + sk_{u_i}^{x_i})h(\text{ID}_{i1}) + v \text{ mod } p. \end{aligned} \quad (18)$$

After that, a response message  $M_U^1 : \{sk_{u_i}^{x_i}, V, \text{ID}_{i2}, T_U^1\}$  is sent to the  $\text{HG}_i$ .

**3.4. Cloud Server Technology.** At present, the standard definition of the cloud server refers to “virtual servers” running on the same physical hardware which are independent of traditional servers. Compared with the characteristics, cloud services are a cluster and their functions need to be coordinated with each other. Because there is no need to install hardware equipment, the cost performance of the cloud server will be higher and the host configuration and business scale of the cloud server can be configured according to the needs of users, so users are more flexible in cost control. Cloud servers can enable clients such as smart phones, PCs, or tablets to access the server through public networks. Common servers include Alibaba Cloud, Tencent Cloud, Jinshan Cloud, and Baidu Cloud, which support Internet applications such as e-commerce, enterprise or personal websites, social networking services (SNS), cloud storage, and office automation (OA), such as office software collaboration tools and forums.

## 4. Smart Home

**4.1. Smart Home System Model.** In Figure 4, the main actors in the system and the system components are introduced in turn.

**4.1.1. Participating Roles.** The data collected from participants equipped with smart home devices varies according to different devices and comes from the sensing data in the home, including the temperature, humidity, and luminosity, even from medical data generated by wearable devices, images generated by monitoring systems, and audio and video data.

Any party accessing the data of smart home devices is the requester. Usually, the party that relies on smart home data to provide different services is regarded as the data requester.

**4.1.2. System Components.** The role of the router is as the network coordinator and connection gateway. The gateway is a channel to connect with external networks. It can not

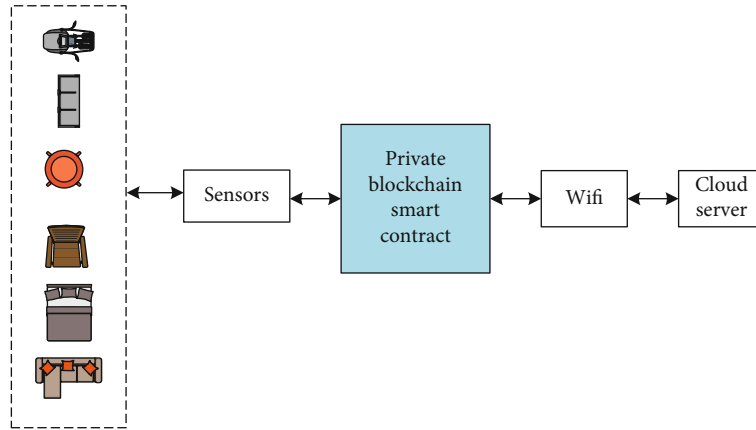


FIGURE 4: Smart home system model diagram.

only have its own IP but also connect to the cloud of the public interface. As the manager of all available information in intelligent home networks, multiple local smart home networks can exist at the same time and each network represents a home, office, school, etc. equipped with smart home devices.

All verified attributes and access control policies are stored in the blockchain. It can also be used as the execution point of the access request policy for specific smart home resources. Blockchain provides a unified access control platform for the whole smart home network.

**4.2. Attribute-Based Access Control (ABAC) Model.** Attribute-based access control (ABAC) is a logical approach to access control [15]. Attributes are the core concept of this model. In the attribute-based access control model, attributes are usually represented in quadruple (S, O, P, and E):

- (1) S (subject attribute): the attribute of the entity in the system that initiated the access request, such as the organization, identity, and rank
- (2) O (object attribute): attributes of entities that provide resources and can be accessed in the system, such as the name, type, and format of resources
- (3) P (permission attribute): various operations on object resources, such as querying, writing, creating, and deleting
- (4) E (environment attribute): the environment information in which the access control process is going on, such as the time, place, network location, and concurrent access restrictions when the access requester initiates the access. This attribute is independent of the access request subject and the accessed resource object

The basic framework of the attribute-based access control (ABAC) model [16] is shown in Figure 5. The basic steps of the authorization process of the access control policy are as follows:

- (1) The subject sends the access request to the object through the system: the access request subject sends

the access request information to the policy enforcement point PEP, and then, the PEP forwards the access request information from the requesting subject to the policy decision point PDP

- (2) PDP carries out policy decision evaluation: the policy decision point receives the access request information from the main body of the access request from the policy execution point, then, obtains all the attributes in the attribute library and the environment attribute library, then, matches the access control policies satisfying the conditions in the policy library, evaluates according to the access control policies, and finally sends the evaluation results to the policy execution point PEP
- (3) Policy enforcement point execution decision result: after the policy enforcement node PEP receives the evaluation result, if the return value of the result is true, then, the subject returns the evaluation result to the object and grants the permission to access the object resources. If the evaluation result is false, this access of the principal will be denied and the result will be sent to the principal

It can be seen from the above access control process that the ABAC model authorizes access control decisions based on the attributes of access objects and has nothing to do with the identity information of subjects. Therefore, it can ensure the anonymity of smart home users and ensure that their privacy is not leaked. In the ABAC model, access control policies can be changed according to users' needs. Based on the attributes of access entities, the model can enter fine-grained access control and dynamic authorization, which enhances the scalability of the model and makes it have high application value in smart home scenarios.

### 4.3. Simulation Experiment

**4.3.1. Smart Home Network.** A smart home network test platform is realized by FIWARE [17]. FIWARE is an open-source experimental platform of the Internet of things created in Europe, which provides a general API for intelligent



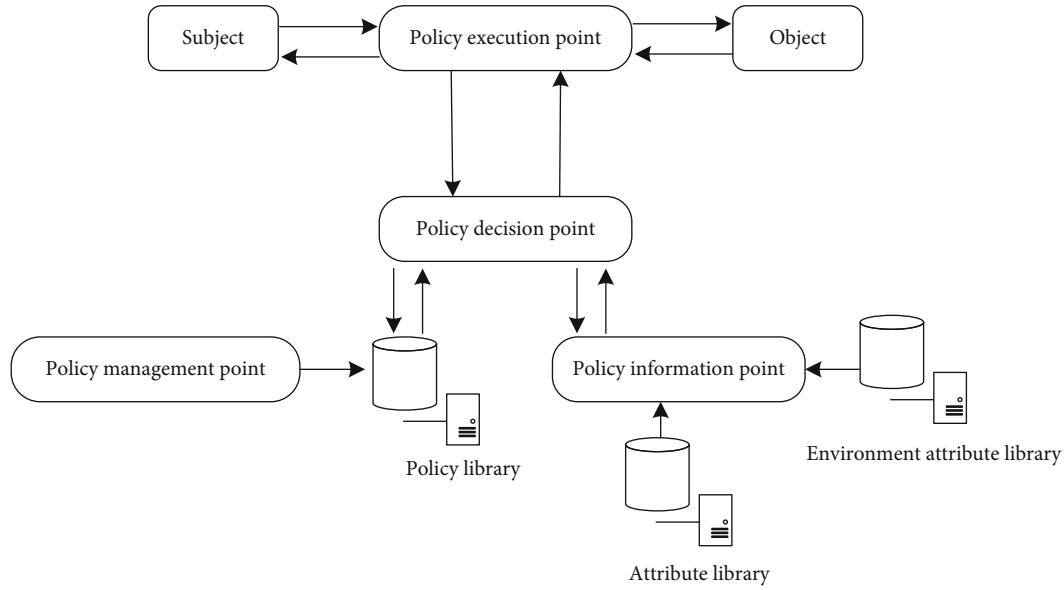


FIGURE 5: ABAC model frame diagram.

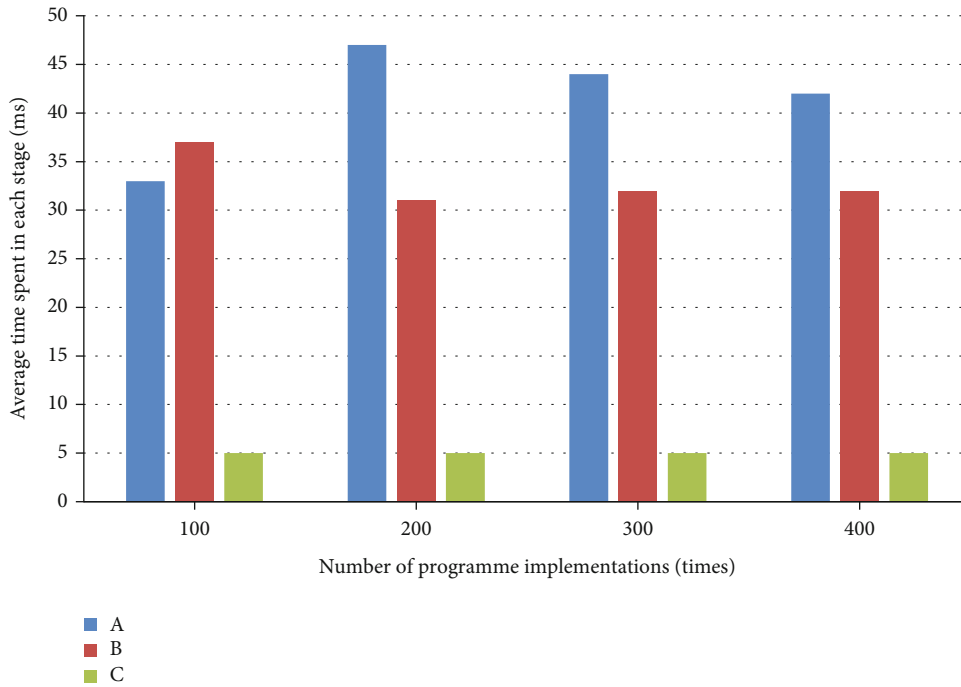


FIGURE 6: Average result of the signature scheme test performed by the mobile terminal device.

application development. The platform integrates many basic components in the smart home network, for example, the integrated temperature, illumination and humidity sensors, and IEEE 802.15.4 radio-integrated antennas. On the smart home network test bench, the sensors are divided into three groups: each group has four FIWARE devices, among which three are smart home terminal devices and one is a router. Using Java to write an independent gateway program, using the MySQL database to store the routing table, resource directory, and data table, each group constitutes an independent smart home network. Device discovery

and resource discovery in smart home networks are based on the IEEE 802.15.4 standard [18]. Each group represents a home, school, or office equipped with smart home equipment in real life.

Firstly, the adaptability of the signature scheme in a smart home environment is analyzed. According to the scheme proposed in this paper, the hardware of the smart home simulation system consists of an intelligent mobile terminal device and a home gateway server. The SM2 threshold group signature scheme is uplink on these devices, and the simulation test results in the following figure are obtained.

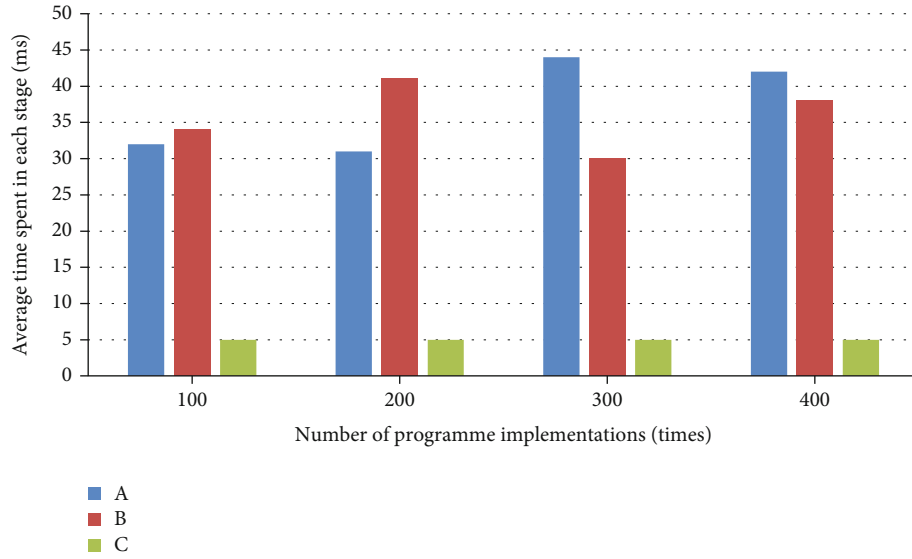


FIGURE 7: Average results of the signature scheme test performed by the home gateway server.

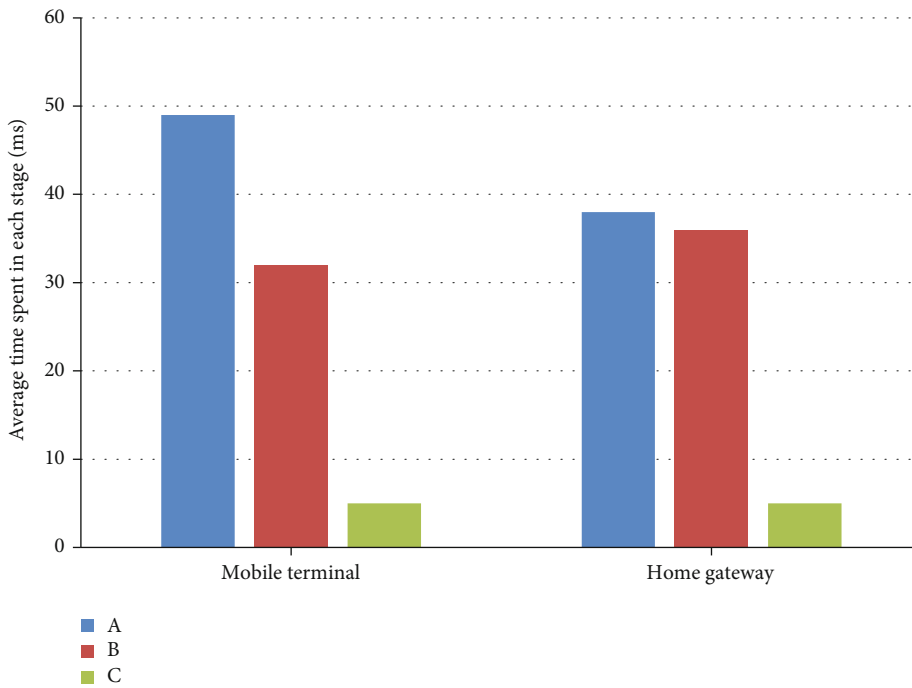


FIGURE 8: Average results of the signature scheme test performed by various devices in the smart home.

In Figures 6 and 7, the ordinate is the average time spent in different stages of the scheme during execution of 100, 200, 300, and 400 times and the abscissa A, B, and C represent the three stages of key generation, signature generation, and signature verification in the signature scheme, respectively. Figure 8 shows the total average time spent on each of the three phases performed on the two devices.

It can be clearly seen in Figures 6 and 7 that the time spent by the terminal equipment executing each stage of the signature scheme is similar to the average time spent in Figure 8, indicating that the signature scheme has good sta-

bility and is within the acceptable time range of practical application scenarios. It can be seen in Figure 8 that the signature scheme proposed in this paper has good performance on the premise of satisfying security characteristics and computational overhead. Therefore, the threshold group signature scheme based on SM2 proposed in this paper can meet the application requirements of smart home scenarios and has a good application prospect.

Next, in order to prove the practicability of the proposed scheme, a smart home access control system based on blockchain is implemented by using the simulation platform. In

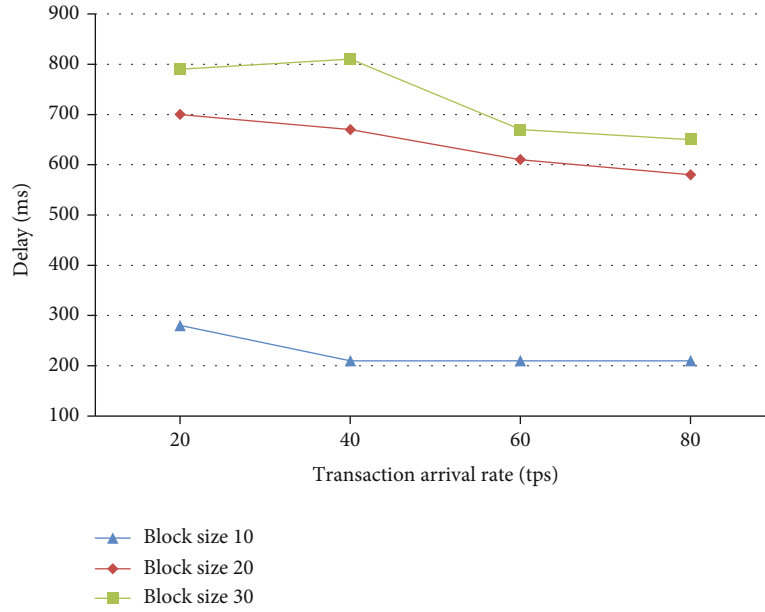


FIGURE 9: Property creation transaction delay.

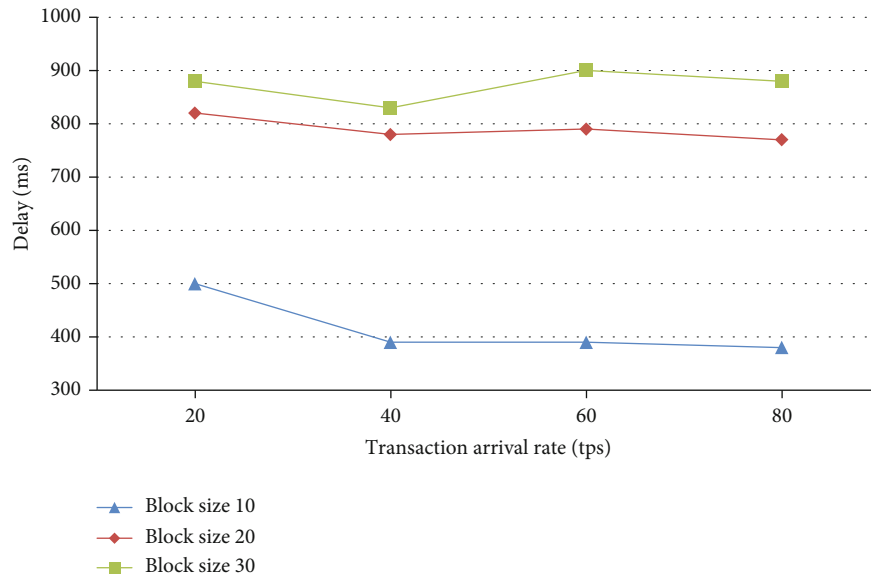


FIGURE 10: Attribute assignment transaction delay.

this section, we first introduce the implementation details, that is, the implementation of blockchain and a smart home platform. Then, the performance of the system is evaluated by simulation experiments.

4.3.2. *Experimental Results.* In the blockchain experiment, the timeout is set to 1 second. Examine the latency of attribute creation, attribute assignment, and policy creation operations for block size values of 10, 20, and 30 for four different transaction arrival rates (20, 40, 60, and 80 transactions per second).

It can be seen in Figures 9–11 that the delay increases as the block size increases. In Figure 9, if the arrival rate of the

attribute generation is 40, the latency increases from 390 milliseconds to 830 milliseconds if the block size increases from 10 to 30. This is because the retained transactions will delay the writing speed of transactions within the blockchain as the block size increases and has to wait longer on the message queue.

Experimental results show that between attribute creation, attribute assignment, and policy creation, attribute assignment takes longer than the other two operations.

The experimental results of the test platform show that the access control performance of the blockchain network can be improved by finding the best parameter values of the blockchain network. The optimal parameters obtained

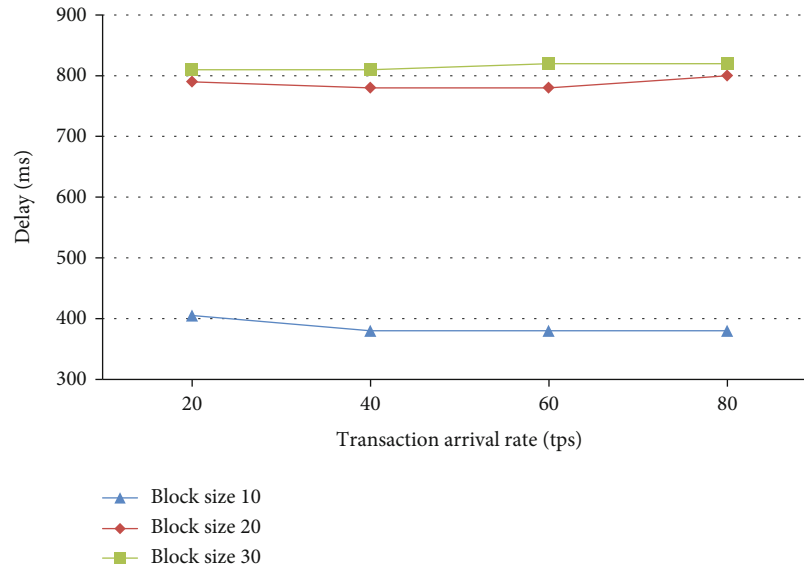


FIGURE 11: Policy creation transaction delay.

by experiments are block size 20 and 40 transactions per second, and the delay of data resource access is about 1 s.

## 5. Conclusion

Compared with the public blockchain, the scheme based on Hyperledger Fabric Alliance Chain proposed in this paper can serve smart home resource access requests faster. In addition, the more authentication peer nodes in the endorsement policy, the higher the security level of the system and the greater the communication and computational overhead. By setting appropriate security parameters, the balance between security and practicality can be realized in the smart home access control system. From the simulation results, the access control scheme proposed can meet the practical application requirements within the appropriate security parameters. Future research work will be in-depth study on parameter optimization, and multi-intelligent optimization algorithms will be applied to blockchain and cloud services to improve system performance.

## Data Availability

The experimental data used to support the findings of this study are available from the corresponding author upon request.

## Conflicts of Interest

The author declared that there are no conflicts of interest regarding this work.

## References

- [1] A. Mukherjee, M. Balachandra, C. Pujari, S. Tiwari, A. Nayar, and S. R. Payyavula, "Unified smart home resource access along with authentication using blockchain technology," *Global Transitions Proceedings*, vol. 2, no. 1, pp. 29–34, 2021.
- [2] M. Ammi, S. Alarabi, and E. Benkhelifa, "Customized blockchain-based architecture for secure smart home for light-weight IoT," *Information Processing & Management*, vol. 58, no. 3, article 102482, 2021.
- [3] B. E. Sabir, M. Youssfi, O. Bouattane, and H. Allali, "Towards a new model to secure IoT-based smart home mobile agents using blockchain technology," *Engineering, Technology and Applied Science Research*, vol. 10, no. 2, pp. 5441–5447, 2020.
- [4] M. Abunaser and A. A. Alkhatib, "Advanced survey of blockchain for the Internet of things smart home," in *2019 IEEE Jordan International Joint Conference on Electrical Engineering and Information Technology (JEEIT)*, pp. 58–62, Amman, Jordan, 2019.
- [5] Y. Ren, Y. Leng, J. Qi et al., "Multiple cloud storage mechanism based on blockchain in smart homes," *Future Generation Computer Systems*, vol. 115, pp. 304–313, 2021.
- [6] D. Schmelz, K. Pinter, S. Strobl, L. Zhu, P. Niemeier, and T. Grechenig, "Technical mechanics of a trans-border waste flow tracking solution based on blockchain technology," in *2019 IEEE 35th international conference on data engineering workshops (ICDEW)*, pp. 31–36, Macao, China, 2019.
- [7] L. Liu and B. Xu, "Research on information security technology based on blockchain," in *2018 IEEE 3rd International Conference on Cloud Computing and Big Data Analysis (ICCCBDA)*, pp. 380–384, Chengdu, China, 2018.
- [8] A. A. Monrat, O. Schelen, and K. Andersson, "A survey of blockchain from the perspectives of applications, challenges, and opportunities," *IEEE Access*, vol. 7, pp. 117134–117151, 2019.
- [9] X. Zhu, "Research on blockchain consensus mechanism and implementation," *IOP Conference Series: Materials Science and Engineering*, vol. 569, no. 4, p. 042058, 2019.
- [10] K. J. Kim and S. P. Hong, "Study on rule-based data protection system using blockchain in P2P distributed networks," *International Journal of Security and its Applications*, vol. 10, no. 11, pp. 201–210, 2016.
- [11] S. J. Syscoin, "A peer-to-peer electronic cash system with blockchain-based services for E-business," in *2017 26th*

- International Conference on Computer Communication and Networks (ICCCN)*, Vancouver, BC, Canada, 2017.
- [12] W. S. Park, D. Y. Hwang, and K. H. Kim, "A TOTP-based two factor authentication scheme for hyperledger fabric blockchain," in *Tenth International Conference on Ubiquitous and Future Networks (ICUFN)*, pp. 817–819, Prague, Czech Republic, 2018.
- [13] P. Thakkar, S. Nathan, and B. Viswanathan, "Performance benchmarking and optimizing hyperledger fabric blockchain platform," in *2018 IEEE 26th international symposium on modeling, analysis, and simulation of computer and telecommunication systems (MASCOTS)*, pp. 264–276, Milwaukee, WI, USA, 2018.
- [14] W. Li, J. Liu, and G. Bai, "High-speed implementation of SM2 based on fast modulus inverse algorithm," in *2018 China semiconductor technology international conference (CSTIC)*, Shanghai, China, 2018.
- [15] H. Tian, X. Li, H. Quan, C. C. Chang, and T. Baker, "A light-weight attribute-based access control scheme for intelligent transportation system with full privacy protection," *IEEE Sensors Journal*, vol. 21, no. 14, pp. 15793–15806, 2020.
- [16] A. A. Jabal, E. Bertino, J. Lobo et al., "Polisma - a framework for learning attribute-based access control policies," in *Computer Security–ESORICS 2020. ESORICS 2020*, L. Chen, N. Li, K. Liang, and S. Schneider, Eds., vol. 12308 of Lecture Notes in Computer Science, , Springer, Cham, 2020.
- [17] M. Fazio, A. Celesti, F. G. Márquez, A. Glikson, and M. Villari, "Exploiting the FIWARE cloud platform to develop a remote patient monitoring system," in *2015 IEEE symposium on computers and communication (ISCC)*, pp. 264–270, Larnaca, Cyprus, 2015.
- [18] R. Pass, L. Seeman, and A. Shelat, "Analysis of the blockchain protocol in asynchronous networks," in *Advances in Cryptology–EUROCRYPT 2017. EUROCRYPT 2017*, J. S. Coron and J. Nielsen, Eds., vol. 10211 of Lecture Notes in Computer Science, , Springer, Cham, 2017.

## Research Article

# Foundation Reinforcement Method of Railway Logistics Center Station Based on Deformation Control and Thermodynamics

Zhiping Peng <sup>1</sup>, Xiumiao Liu <sup>1</sup>, and Kuangying Zhao <sup>2</sup>

<sup>1</sup>Foundation Department, Hebei Vocational College of Rail Transportation, Shijiazhuang 050000, China

<sup>2</sup>President's Office, Hebei Vocational College of Rail Transportation, Shijiazhuang 050000, China

Correspondence should be addressed to Xiumiao Liu; [kjy001@heuet.edu.cn](mailto:kjy001@heuet.edu.cn)

Received 30 September 2021; Revised 3 December 2021; Accepted 14 December 2021; Published 17 January 2022

Academic Editor: Deepak Gupta

Copyright © 2022 Zhiping Peng et al. This is an open access article distributed under the Creative Commons Attribution License, which permits unrestricted use, distribution, and reproduction in any medium, provided the original work is properly cited.

In view of the existing methods of foundation reinforcement considering the deformation of the site and the poor effect of the foundation reinforcement, a method of the foundation reinforcement of a railway logistics center station based on deformation control and thermodynamics is proposed. The basic principle of thermodynamics is introduced, and the influence of temperature on the soil properties of foundation is analyzed. Based on the analysis of the engineering geology and hydrogeological conditions of the site, the deformation of the site is calculated, the bearing capacity of the surrounding environment of the foundation pit to the additional deformation is analyzed, and the reinforcement mechanism of the yard foundation in the railway logistics center is proposed to realize the reinforcement of the yard foundation. The experimental results show that this method can use the least tamping pit filler under the same conditions, with a minimum of 7.34 m<sup>3</sup> to realize foundation reinforcement, the maximum ground settlement is only 5.98 mm, and the maximum lateral displacement of pile top is only 6 mm, which can meet the actual requirements and has high practical value.

## 1. Introduction

Deformation control is one of the core contents in the design of deformation control for the foundation reinforcement project of a railway logistics center. If the deformation of the retaining structure caused by deep foundation pit excavation and its influence on the surrounding environment can be predicted comprehensively and accurately, economic and reasonable retaining scheme and construction measures can be adopted, accidents of a deep foundation pit can be reduced, or resources can be avoided effectively [1–3]. However, due to the high complexity and regional characteristics of the city railway logistics center yard foundation strengthening project, although there are a lot of railway logistics center yard foundation strengthening project practices, there is no systematic understanding of its deformation characteristics of theoretical research, coupled with the foundation pit itself is a theory seriously lagging behind the practice of the subject, design, to be more accurate and reliable to predict its deformation is often more difficult. Through analyzing the factors affecting the construction of metro stations, the comprehensive evaluation

index system of the construction risk of a metro station foundation pit is established [4, 5]. Based on the hierarchical structure of these factors, a three-stage fuzzy comprehensive evaluation model is proposed. The AHP method is used to determine the weights of the factors in each stage, and the fuzzy set method is used to determine the degree of membership and to sort the risks. Based on the practice of the railway logistics center yard, the deformation characteristics of the deep foundation pit of the railway logistics center yard are studied deeply and systematically, and the deformation control method is put forward. The research of the deep foundation pit design based on deformation control starts late [6–8]. As far as the research and engineering practice at home and abroad are concerned, there are four problems in this field: (1) The design of the deep foundation pit based on deformation control lacks reliable theoretical guidance, and it is difficult to achieve the scientific design. At present, the experience based engineering analogy method is widely used in deep foundation pit design in our country. Because of the characteristics of the deep foundation pit and the diversity of geological conditions, the guidance function of the system



theory is less than that of other technical fields, so that the design of the deep foundation pit is too conservative under some conditions and causes waste, while in other cases, there are greater safety risks to the construction and safe use of the deep foundation pit [9–11]. (2) The understanding of the ground deformation law and mechanism caused by deep foundation pit excavation is not clear enough, and it is difficult to achieve refined design and construction. Previous studies on the deformation of the foundation pit mainly focus on the estimation of the maximum deformation, but the dynamic description of the deformation process is relatively deficient. Many of the formulas obtained are preliminary and not comprehensive. (3) Ignoring the space-time law of foundation pit deformation, a two-dimensional plane strain model to design and calculate is used, which causes the waste of stiffness design of the retaining structure near the pit angle; on the other hand, it increases the difference deformation between the middle of foundation pit and the pit angle and is unfavorable to the deformation control of the surrounding environment. (4) The deformation control index is single, and the standard is absolute, which is difficult for meeting the complex and sensitive environmental requirements around the deep foundation pit.

Because of the high complexity and regional characteristics of the foundation reinforcement project of the city railway logistics center, although there are a lot of practices of the foundation reinforcement project of the railway logistics center in various regions, there is no systematic theoretical research on its deformation characteristics, and the foundation pit project itself is a subject whose theory lags behind the practice seriously; it is often difficult to predict its deformation accurately and reliably in design. However, the design concept of deep excavation based on deformation control has not been put forward for a long time and is obviously different from the conventional strength control method. Lei et al., using laboratory model test and numerical simulation PFC2D, systematically analyze a new vacuum preloading method. Alternating vacuum preloading method is used to reinforce super-soft soil filled by dredging [12]. The study shows that the alternating movement of soil particles in the alternating vacuum preloading method can effectively restrain the formation of silted mud layer and the phenomenon of “soil column” and make the overall reinforcement effect more uniform and effective. Compared with the conventional vacuum preloading method, the displacement of the alternating vacuum preloading method increases 14.92%, the settlement increases 11.80%, the shear strength of the reinforced soil cross slab increases 21.65%, the water content decreases 26.74%, the density of the silt plugged layer decreases, the porosity of the area formed by the silt layer increases more than 30%, and the effect of breaking silt is obvious. But the foundation deformation is not statistically analyzed, and the reinforcement effect is not ideal. Based on the purpose of improving the construction level of geotechnical engineering, the application of the method of strengthening the foundation is simply discussed. From the point of view of ground control, the reinforcement effect is ensured. However, there is no detailed discussion on the foundation deformation [12–14].

Therefore, it is of great significance to study the deformation characteristics of deep foundation pit of railway logistics center, find out the corresponding deformation law, and apply it to the design of deep foundation pit based on deformation control and thermodynamics. In order to improve the effect of foundation reinforcement, a foundation reinforcement method of the railway logistics center station based on deformation control and thermodynamics is proposed in this paper. The basic principle of thermodynamics is introduced, and the influence of temperature on the properties of foundation soil is analyzed. Based on the analysis of the engineering geological and hydrogeological conditions of the site, the deformation of the site is calculated, the bearing capacity of the surrounding environment of the foundation pit to the additional deformation is analyzed, the reinforcement mechanism of the station foundation of the railway logistics center is put forward, the reinforcement of the station foundation is realized, and the effectiveness of the design method is verified by experiments.

## 2. Basic Theory of Thermodynamics

The process of heat conduction is a process of thermal motion in which objects with different temperatures contact or have different internal temperatures. Heat conduction can occur in solid, liquid, and gas, and heat convection often occurs in gas and liquid. Where the temperature of the object is higher, the microparticles have more energy. In the process of continuous collision between particles, the particles with higher energy will transfer energy to the particles with lower energy. From the macro point of view, when there is a temperature gradient, the heat will transfer from high temperature to low temperature.

## 3. Analysis of Foundation Reinforcement Conditions for Railway Logistics Center Yard

*3.1. Influence of Temperature on the Properties of Foundation Soil.* The influence of temperature on the properties of the soil mass is as follows: (1) The influence of temperature on the internal structure of foundation soil is the volume change of the upper particles and pore water caused by thermal expansion. (2) The influence of temperature on the physical and mechanical parameters of the foundation soil is mainly considered as shear strength, consolidation coefficient, and permeability coefficient. (3) The temperature has an effect on the thermal parameters of the soil, such as the resistance of the upper body.

*3.2. Choice of Pavement Type.* The selection of pavement types for the stacking yard of a road or railway logistics center shall be determined by comprehensively considering the characteristics of port loading and unloading operations, the requirements of the types of goods on the surface layer, and other conditions. Heavy container stacking area is located in the southeast of the logistics center, with wide terrain, large load, and large foundation settlement; construction conditions are not limited by objective factors; interlocking block pavement is selected. The dismantling and loading yard,

empty container yard, road, gate area, sinking loading and unloading area, and auxiliary yard are located on the stacking yard and road of the existing railway logistics center, and the foundation settlement is relatively small, so the concrete pavement can be selected [15, 16].

### 3.3. Settlement Standard

**3.3.1. Settlement Control Indicators.** The settlement control indexes of the foundation of a storage yard mainly include differential settlement, overall settlement, and inclination (angle variable). The bearing capacity of additional deformation is closely related to the type of foundation, the type of foundation, the type of structure, the size of the building, the age of construction, the load, and the function of use. The bearing capacity of the whole settlement, differential settlement, and tilt (angle variable) is different even for the foundation of the same yard. Therefore, it is necessary to conduct a systematic study to determine the scientific and appropriate control standards, in order to avoid excessive damage to the surrounding yard foundation at the same time to prevent the blindly controlled waste of funds. Overall settlement, differential settlement, and inclination (angle variable) are the earliest parameters used as the foundation deformation control parameters of storage yard, and they are also the most widely used parameters so far. Therefore, they are introduced into the index system in this paper. Compared with the strain and the crack, the settlement value of the pile foundation is more easily obtained by monitoring and measuring. Numerous studies have shown that differential settlement is an important factor causing the pile site foundation inclination (angle variable), and differential settlement increases with the increase of overall settlement. When inquiring into the data of reinforced concrete frame structure and brick and concrete structure affected by excavation, the author found that, for the reinforced concrete frame structure, when the total settlement of the pile site foundation is greater than that of the pile site, the foundation of the pile site is damaged to some extent. The following can be found from the research on the influence data of foundation pit excavation on the pile foundation in the Middle East: (1) Old buildings with a construction time of more than one year are generally prone to damage, while recent buildings less than one year old have no major damage. (2) Compared with other foundation forms, the independent column foundation is more prone to differential settlement and is also more sensitive to stratum deformation. (3) The overall settlement of the clay soil layer pile foundation should be controlled within. When the overall settlement of the sand layer is greater than that, slight and moderate deformation may occur. (4) When the differential settlement is smaller, the slope is generally smaller, and the pile site foundation is not damaged; when the differential settlement is larger, a larger slope may occur. When it is tilted, the damage to the foundation of the general stacking site is slight, and if it is greater than that, moderate or severe damage occurs. Therefore, the inclination of general buildings should be controlled within, and its control index can be determined when considering the safety factor. And accord-

ing to the damage investigation results of the pile site foundation, when the tilt is greater than that of the load-bearing wall and the partition wall of the frame-type stacking site base may crack, and if it is greater than that, structural damage may occur. It is recommended to use it as a control index for tilt.

**3.3.2. Crack Control Index.** The appearance and development of cracks are the precursors and intuitive manifestations of the destruction of the foundation structure of the pile site, for brittle materials such as concrete, gun body, stone, and brick wall. Because the compressive capacity is significantly greater than the tensile capacity, uneven settlement, horizontal deformation, and inclination will cause excessive tensile and shear stress in the wall to be the main reason for the formation of cracks. According to the monitoring results of various structural cracks on the railway logistics center site, the form, direction, and distribution of the cracking of the pile yard foundation caused by the excavation of the foundation pit are relatively complicated. In summary, there are two main types: (1) the pile yard foundation caused by uneven foundation settlement vertical cracks formed by tension of load-bearing walls; (2) oblique cracks formed by shearing corners of components such as doors and windows due to local stress concentration. The crack width is one of the important parameters for evaluating the damage of the pile site foundation. According to the width and distribution of the cracks, the extent of damage to the pile site foundation can be judged by the excavation of the foundation pit, and whether its bearing capacity and use function are greatly affected, and whether protective measures are required.

**3.4. Site Conditions.** A container railway logistics center station is built in the southwest corner of a railway logistics center station in a city in northern China, and some building materials are stacked in the south central station. In its northwest, there is a concrete pavement with a thickness of 0.15 m and coke accumulation. However, the concrete pavement is unevenly sinking, and the concrete pavement has been damaged and has been soaked in water for a long time. A large amount of construction and domestic waste are piled on the surface of the southeast, and the surface of the northeast is covered with a layer of white alkali residue, and the surface is low-lying water. In addition, the existing railway logistics center yards are in operation, and land acquisition and demolition need further coordination. There are 3 in-use alkali slag pipelines in the heavy tank site, running across the north and south. This alkali slag pipeline has been in use for 30 years. The pipe wall is rusty, and there are many small holes leaking alkali slag. Due to the tight schedule, the new alkali slag pipe cannot be built when the foundation is reinforced, and the old alkali slag pipe should continue to be used. If the design is not properly considered, deviations in the foundation settlement control during the construction process will cause the alkali slag pipe to distort and damage roads, a large amount of alkali slag leakage, and the shutdown of alkali plants and other immeasurable serious consequences.

- (1) According to the engineering geological survey data, the soil layers of the railway logistics center area are distributed from top to bottom. Miscellaneous fill (mainly alkali slag, bricks, and furnace ash slag), silty clay, silt, silt, and silty clay. The surface miscellaneous fill soil is thin and cannot play the role of a holding layer; the silt or silty clay layer below about 20 m thick has high water content, large void ratio, and flow plasticity. It belongs to medium and high compressibility soil with low strength, and the settlement deformation is large. Therefore, the main purpose of foundation reinforcement is to improve the strength and bearing capacity of the soil, control the settlement of the foundation, and ensure the stability of the railway logistics center yard during construction and use. After investigation, a soda plant is located on the south side of the railway logistics center yard. About 1 km north of the railway logistics center yard is the alkali slag mountain, which is formed by the accumulation of alkali slag discharged from the alkali plant for 30 years. This is the reason for the existence of the alkali slag pipe. This area is formed by dredging and reclamation of the port [17]. In order to save investment and use waste, the alkali slag is turned over in the sun and filled with dredging soil. The plastic alkali slag on the surface is caused by the leakage of the alkali slag pipe. Before the foundation reinforcement is carried out, the alkali residue, construction waste, domestic garbage, and rot plants on the surface should generally be removed. In this project, nearly 200,000 m<sup>2</sup> is covered by alkali residue, and the thickness is 1.4~3.8 m. The removal cost will cost 20~30 million yuan. Because the alkali residue has good reinforcement characteristics, the alkali residue layer can be considered as a part of the foundation for reinforcement treatment, rather than for removal and disposal

## 4. Calculation Method of Yard Deformation

### 4.1. Calculation of Vertical Deformation of Stratum in Central Section

4.1.1. *Calculation of Surface Settlement in Central Section.* According to the actual measurement data collected by the author on the ground settlement of the deep foundation pit of the railway logistics center, the distribution function is used to estimate the distribution of the ground settlement outside the pit. Calculated as follows:

$$M = \alpha f_c A e_a + (\alpha - \alpha_t) f_y A_s N, \quad (1)$$

$$A_s = f_y r_s \frac{(\sin \pi \alpha + \sin \pi \alpha_t)}{\pi} + \frac{(r_1 + r_2)}{N}. \quad (2)$$

In the formula,  $\alpha$  represents the proportion of the cross-sectional area of the foundation structure of the railway logistics center's stack yard affected by the slope of the foun-

ation to the cross-sectional area of the entire model;  $\alpha_t$  represents the cross-sectional area of the foundation structure of the railway logistics center's stack yard affected by the vertical tension of the foundation occupies the entire model. The ratio of the cross-sectional area of the model:  $f_c$  and  $f_y$ , respectively, represent the compression index and rebound index of the foundation structure of the railway logistics center yard under the influence of the slope of the foundation;  $A$  represents the circular cross-sectional area of the foundation structure of the railway logistics center yard; and  $A_s$  represents the model. The area of all longitudinal steel bars in the horizontal section:  $r_1$  and  $r_2$  represent the inner and outer radii of the circular planar section of the foundation structure of the railway logistics center storage yard, respectively;  $r_s$  represents the outer radius of all longitudinal bars in the model, generally  $r_1/r_2 \geq 0.5$ ; and  $e_0$  represents the foundation slope. The degree of eccentricity of the model ring section:  $e_a$  represents the additional eccentricity of the base structure of the railway logistics center stacking yard, and  $N$  represents the number of longitudinal steel bars in the plane section of the model ring structure, usually  $N \geq 6$ .

### 4.1.2. Calculation of Deep Soil Settlement in Central Section.

It can be seen from the previous text that the formation deformation has certain stratification, but the overall deformation trend is obvious [18]. The settlement of deep soil above the bottom of the pit is caused by excavation and unloading, and the settlement is transmitted downward from the surface. Then, the expression of the settlement process of the deep soil in the central section is as follows:

$$B = \frac{M_k}{M_q(\theta - 1) + M_k} B_s, \quad (3)$$

$$B_s = \frac{\eta E_s A_s h_0^2}{1.15\psi + 0.2 + 6\alpha_E \rho / (1 + 3.5r_f)}, \quad (4)$$

$$\psi = 1.1 - 0.65 \frac{f_{tk}}{\rho_{te} \sigma_s}. \quad (5)$$

Among them,  $\psi$  represents the uneven coefficient of tensile strain of the foundation structure of the railway logistics center yard under the influence of the foundation slope;  $\alpha_E$  represents the ratio of the elastic modulus  $E_s$  of the steel bar in the model to the elastic modulus  $E_c$  of the tunnel concrete structure;  $\rho$  represents the railway logistics center yard reinforcement ratio of the steel in the foundation structure;  $r_f$  represents the ratio between the model's annular flat section and the effective section of the model web under the influence of the foundation slope;  $M_k$  represents the standard compression moment of the model;  $M_q$  represents the model under the influence of foundation slope compressive bending moment;  $\theta$  represents the influence coefficient of the deflection of the model under the long-term influence of the foundation slope;  $f_{tk}$  represents the axial compressive strength of the tunnel concrete structure;  $\rho_{te}$  represents the reinforcement ratio of the tunnel structure's compressive

effective steel bar affected by the foundation slope;  $\sigma_s$  represents the reinforcement stress of the tunnel structure affected by the slope of the foundation; and  $\rho'$  represents the reinforcement ratio of the compressed reinforcement of the model under the impact of the slope of the foundation.

**4.1.3. Calculation of Horizontal Lateral Displacement of Central Section Retaining Wall.** According to the statistics of the deformation characteristics of the deep foundation pit wall of the railway logistics center yard and the analysis of the basic law of deformation, it can be seen that for deep foundation pits with greater rigidity such as the internal support system of bored piles, the side of the retaining structure the axial deformation is usually convex. Therefore, a polynomial is used to fit the horizontal lateral displacement of the retaining wall, and the expression is

$$\omega_{\max} = \frac{\Psi l^4}{8EL}. \quad (6)$$

Among them,  $l$  represents the effective length of the longitudinal bolts in the tunnel structure model;  $[\tau]$  represents the compressive strength of the longitudinal bolts in the model under the influence of the slope of the foundation; and  $EL$  represents the bending stiffness of the longitudinal bolts in the model.

**4.1.4. Calculation of Deformation at Any Position of 3D Deep Foundation Pit.** The deformation of the deep foundation pit has obvious spatial effect. The deformation of the pit corner is much smaller than that of the middle part, but the spatial effect only changes the magnitude of the deformation and does not change the shape of the deformation [19]. Therefore, the deformation at other positions can be estimated from the deformation of the main section according to the law of spatial deformation. The distribution function of the surface deformation parallel to the direction of the foundation pit wall is obtained.

$$b_i = \sum_{i=1}^m \omega_i \times s_{ij} = \min \left\{ 1, \sum_{i=1}^m \omega_i \times s_{ij} \right\}. \quad (7)$$

In the formula,  $i = 1, 2, \dots, m$ ,  $j = 1, 2, \dots, n$ ,  $b_i$  represents the deformation value of the interface type of the foundation pit in the  $j$  logistics center,  $s_{ij}$  represents the  $j$  structural factor of foundation structure factor of  $i$  yard, and  $\omega_i$  represents the interface type of foundation pit in  $i$  logistics center;

**4.2. The Tolerance of the Surrounding Environment of the Foundation Pit to Additional Deformation.** The foundation structure of any pile site has a certain strength and can resist certain additional deformation. The allowable deformation of the pile yard foundation structure refers to the limit value of the deformation that can be used normally under the influence of the ground deformation [20]. The severity of the consequences of damage to the foundation of the stack is the main basis for the classification of the foundation protection. The “generalized” pile yard foundation damage level

is divided according to the function damage of the pile yard foundation, which belongs to the definition of “qualitative” [21, 22]. It is generally divided into four levels: pile yard foundation, functional damage, structural damage, and collapse. The pile yard foundation affects the appearance of the pile yard foundation, resulting in visible appearance or “aesthetic” damage, generally manifested as slight deformation or cracking of the filling wall or decoration [22]. Wide cracks in gypsum walls and wide cracks in brick-concrete or plain walls are considered to be the upper limit of damage to the pile site foundation. Under normal circumstances, minor repairs may be required. Functional damage affects the use of the structure and the realization of its functions, resulting in usability or functional damage, manifested as follows: crack development, broken water pipes, and inclined walls and floors. Under normal circumstances, intermediate repairs may be required. All functions of the structure can be restored after repairs that are not related to the structure. Structural damage affects the stability and safety of the structure. It usually means that major load-bearing components such as beams, columns, and load-bearing walls have large cracks or deformations, resulting in structural or stability damage, and generally require major repairs. The load-bearing capacity of the pile yard’s foundation has declined, and it has become a dilapidated building that needs to be reinforced, and some parts need to be overhauled. Part or all of the collapsed house collapsed and need to be rebuilt. The classification according to the degree of damage to the foundation of the heap site belongs to the definition of “quantity.”

## 5. Reinforcement Mechanism of Pile Yard Foundation of Railway Logistics Center

After completing the calculation of the deformation index of the storage yard, the obtained data is counted. The main function of the deformation control method is replacement. The poor foundation soil is forced to be discharged by the pile forming machine and replaced with good performance gravel. The pile-earth railway logistics center pile yard foundation is formed as shown in Figure 1.

Since the stiffness of the gravel is greater than the stiffness of the cohesive soil around the pile, the stress in the foundation will be redistributed according to the material deformation modulus.

The ratio of the pile body stress to the cohesive soil stress between the piles, that is, the pile-soil stress ratio, is generally about one, and most of the load will be borne by the gravel pile [23]. Secondly, the replacement pile can also be used as a drainage sand well. When the selected pile material meets certain grading requirements, the gravel pile can form a good drainage channel in the clay foundation, greatly shorten the horizontal seepage path of pore water, and accelerate the drainage consolidation of soft soil and stabilize the foundation settlement. However, it should be noted that the grading requirements need to comprehensively consider many conditions such as gravel volume, pile material, loose bulk density, maximum particle size, and the actual situation of the pile yard. It is a dynamic standard, and the grading



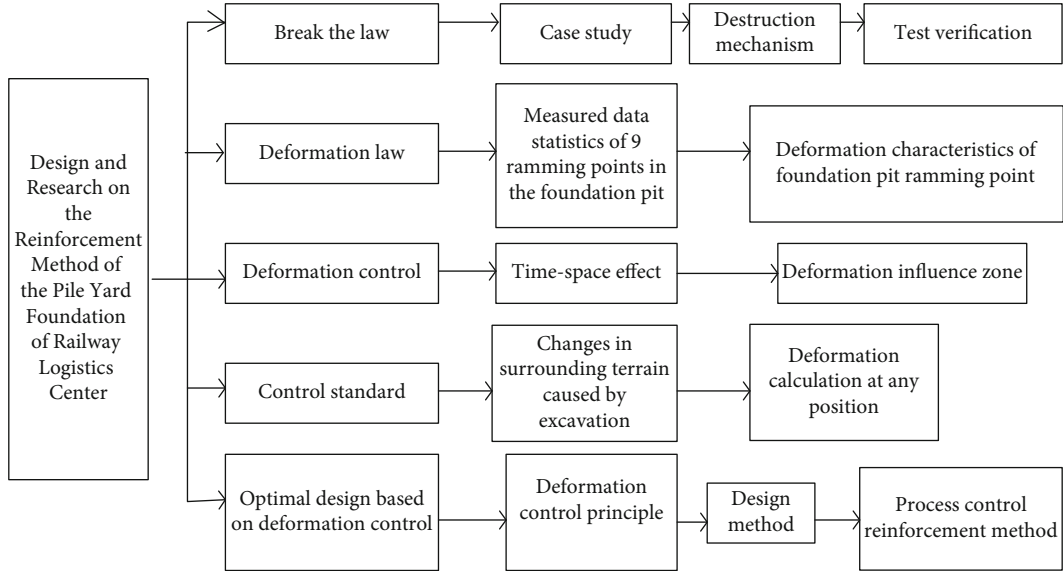


FIGURE 1: Reinforcement ideas of railway logistics center pile yard based on deformation control.

requirements need to be put forward after careful consideration of various conditions. At the same time, in this paper, in order to achieve the actual effect, the pile material required by grading needs to meet the requirements of strong structural strength and strong deformation resistance. Thirdly, the deformation control method also has the effect of dynamic consolidation. In the process of pile formation, due to vibration, squeezing, and other reasons, there will be a large additional pore water pressure in the soil between the piles, resulting in a decrease in the strength of the original foundation soil. After the pile is completed, on the one hand, the structural strength of the original foundation soil will gradually recover over time; on the other hand, the pore water pressure will transfer to the pile body and dissipate. As a result, the effective stress increases, and the strength increases and recovers and exceeds the original soil strength [24]. The main damage of the gravel pile is bulging damage. Because the gravel pile is composed of loose particles, it will not only produce vertical deformation but also radial deformation after bearing the load and cause the surrounding cohesive soil to produce passive resistance. If the strength of the cohesive soil is too low to allow the gravel pile to obtain the required radial support force, the pile body will be bulged and damaged, the gravel will be squeezed into the surrounding soft soil, and the foundation reinforcement effect will be poor. The replacement rate of several factors that affect the reinforcement effect of the deformation control method is determined by the distance between the ramming points and the diameter of the pile body, which directly affects the bearing capacity of the foundation of the railway logistics center. The depth of reinforcement is the length of the pile, which directly affects the sliding stability, settlement deformation, and allowable bearing capacity. The performance of crushed stone affects the internal friction angle and drainage effect of crushed stone [25]. Therefore, during construction, the construction procedures that

affect the above three important factors should be strictly monitored to make the construction quality meet the requirements of the design. The schematic diagram of the shear characteristics of the pile site foundation is shown in Figure 2.

The intersection angle between the shear surface and the horizontal plane at a certain depth of the foundation of the railway logistics center of the logistics center is  $\theta$ . If both the gravel pile and the soil between the piles are considered to exert the shear strength, the shear resistance of the foundation of the stack can be obtained. The intensity can be calculated as

$$T_s = \frac{F_m}{Wt} \cos \theta. \quad (8)$$

Among them,  $T_s$  represents the tensile strength,  $F_m$  represents the maximum tensile force recorded,  $W$  represents the width of the narrow part of the cutter, and  $t$  represents the thickness of the waterproof material. When the waterproof material is used in the foundation pit of the railway logistics center, the waterproof membrane will have a certain breaking elongation [26], and the breaking elongation can be expressed as

$$E_b = \frac{100(L_b - L_0)}{L_0}. \quad (9)$$

Among them,  $L_b$  represents the test length of the waterproof material when it breaks, and  $L_0$  represents the length of the initial waterproof material. The components of the foundation pit of the railway logistics center are combined with each other, the waterproof material produces a certain amount of extrusion [27, 28], the waterproof material is uniformly loaded with a force of 2400 N, and the compressive

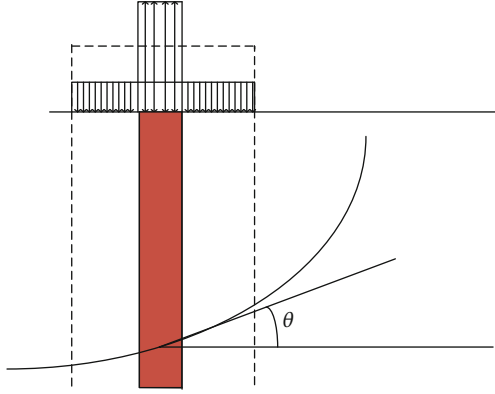


FIGURE 2: Schematic diagram of the shear characteristics of the pile site foundation.

strength of the waterproof material specimen is calculated, which can be expressed as

$$R_c = \frac{F_c}{A}. \quad (10)$$

Among them,  $F_c$  represents the load value when the waterproof material is destroyed, and  $A$  represents the compression area of the waterproof specimen. After the physical performance testing indicators are determined, according to the physical performance testing platform built, the water seepage calculation formula is constructed, which can be expressed as

$$\frac{Q}{S} = -\frac{k \Delta P}{\mu L}. \quad (11)$$

Among them,  $Q$  represents the total flow through the waterproof material per unit time,  $S$  represents the cross-sectional area of the solution through the waterproof material,  $k$  represents the absolute permeability,  $\mu$  represents the dynamic viscosity coefficient of the solution,  $\Delta P$  represents the pressure difference on both sides of the waterproof material, and  $L$  represents the solution on the waterproof material that occupies the length of the waterproof material [29].

## 6. Experimental Analysis

In order to be able to deal with the foundation reinforcement treatment of the large railway logistics center yard, we select a certain area as a test base for comparison of foundation reinforcement methods. The foundation reinforcement methods suitable for a certain area are compared in terms of applicable conditions, reinforcement bearing capacity, maximum reinforcement depth, reinforcement construction period, and cost, so as to obtain large-area foundation treatment effective experience.

This foundation pit protection system adopts fully enclosed deep-house stirring piles as the water-proof scheme of the foundation pit, which extends into the relative waterproof layer of the soil layer. Except for the section (excava-

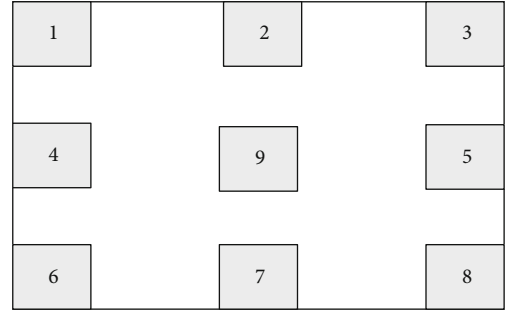


FIGURE 3: Reinforcement layout of supporting plane soil.

TABLE 1: Filling amount of ram pit at the first ramming point.

Tamping point number	Filling amount of ramming pit (m <sup>3</sup> )		
	The proposed method	Literature [12] method	Literature [14] method
1	10.89	12.63	13.54
2	10.56	12.96	13.98
3	10.58	12.65	13.45
4	10.34	12.87	13.67
5	9.98	12.54	13.58
6	9.56	12.67	13.69
7	10.24	12.58	13.57
8	10.32	11.63	13.56
9	10.69	11.97	13.94

tion location) which is supported by soil nails, the section uniformly uses cast-in-place piles and prestressed anchor cables to form a foundation pit support system. The reinforcement layout of the supporting plane soil is shown in Figure 3.

**6.1. Comparison of Ramming Pit Filler.** In order to determine the effective replacement depth of the deformation control method and the dynamic consolidation effect of the soil between piles, the test area is specially arranged in the early stage of the project. Tamping pit filling amount statistics the first ramming point, the second ramming point tamping pit filling amount construction statistics as shown in Tables 1 and 2.

As shown in Tables 1 and 2, the proposed method uses the least amount of ramming pit filler under the same conditions, which can minimize the cost and has high practical applicability.

**6.2. Analysis of Surface Settlement.** The surface deformation rate decreases with the increase of time. During the excavation of the foundation pit, the settlement speed is greater; the ground settlement continues to increase during the dismantling process; the surface deformation rate is slow during the construction of the internal structure; and with the internal structure strength gradually increasing, the settlement decreases slightly, the surface deformation tends to be stable, and the deformation is mainly caused by the creep of the



TABLE 2: Filling amount of ramming pit at the second ramming point.

Tamping point number	Filling amount of ramming pit (m <sup>3</sup> )		
	The proposed method	Literature [12] method	Literature [14] method
1	8.65	10.21	11.31
2	8.34	10.56	11.54
3	8.69	10.45	11.47
4	8.57	10.57	11.59
5	7.56	10.57	11.54
6	7.58	10.58	11.67
7	7.34	10.34	11.57
8	8.12	10.24	11.52
9	8.01	10.54	11.57

TABLE 3: Statistics of surface settlement of the proposed reinforcement methods.

Tamping point number	Standard settlement (mm)	Depth of surface settlement (mm)	
		24 hours later	48 hours later
Northeast corner	30	10.34	5.34
Northwest corner	30	10.36	5.28
Southeast corner	30	10.87	5.12
Southwest corner	30	10.98	5.98
East	30	12.54	5.64
West	30	10.35	5.37
South	30	10.46	5.84
North	30	10.34	5.64
Intermediate	30	10.54	5.12

soil. Statistics on the settlement of the proposed method is shown in Table 3.

As shown in Table 3, in different areas of the deep foundation pit pile foundation, the settlement of the proposed reinforcement method is within the standard settlement range, which meets the actual demand. The surface settlement gradually shrinks with the development of time, and the settlement gradually stabilizes during the excavation of the foundation pit.

**6.3. Analysis of Pile Top Lateral Displacement.** The horizontal displacement of the pile top of the cross-section develops with time. Like ground settlement, the horizontal displacement of the pile top decreases with the development of time. The amount of lateral displacement of the pile top is shown in Figure 4.

As shown in Figure 4, within one month, the pile top offset of the proposed reinforcement method is within the standard range, the maximum is only 6 mm, and the pile top offset shrinks with the increase of time. During and after the construction, the ground pile top offset is controlled within the allowable range, the pile foundation settlement is well controlled, the deformation control effect is good,

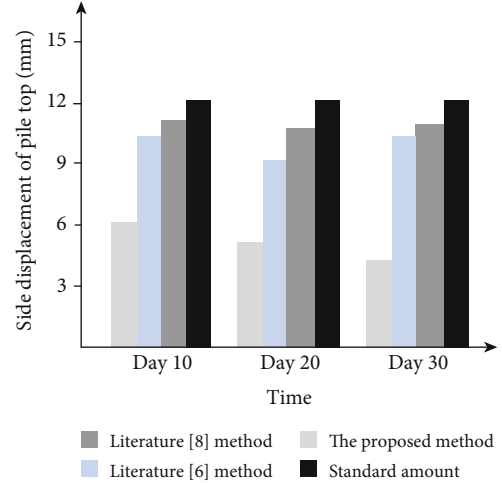


FIGURE 4: Offset of pile top.

and the reinforcement effect is stable. The pile top offset of the other two methods far exceeds that of the design method in this paper, with the maximum of 10 and 11 mm, and does not show the trend of shrinkage. Therefore, it can be seen that the design method in this paper has good effect and certain application value.

## 7. Conclusion

The railway logistics center stack yard foundation reinforcement project is an important part of the construction project. When the railway logistics center stack yard foundation reinforcement plan, if it can comprehensively and accurately predict the deformation of the enclosure structure caused by the deep foundation pit excavation and the impact on the surrounding environment, and then adopting economical and reasonable support plans and construction measures can effectively reduce deep foundation pit accidents or avoid waste of resources. Therefore, in this paper, a method based on deformation control and thermodynamics is proposed to reinforce the pile field of the railway logistics center. Through the analysis of the engineering geology and hydrogeological conditions of the site, the deformation of the station is calculated, and the bearing capacity of the surrounding environment of the foundation pit for additional deformation is analyzed. The mechanism of the reinforcement of the railway logistics center yard foundation has realized the reinforcement of the yard foundation. The experimental results show that this method can use the least tamping pit filler, at least 7.34 m<sup>3</sup>, to realize foundation reinforcement under the same conditions; the maximum ground settlement is only 5.98 mm; and the maximum lateral displacement of the pile top is only 6 mm, which can improve the stability of the basic structure and maximize the project quality on the premise of ensuring the stability of the foundation construction, and has a certain application prospect. However, because more pile foundation differences of the railway logistics center are not considered in the design process of this paper, the reinforcement effect may be affected. Therefore, this will be used as

the starting point for in-depth research in the next research, so as to better improve the stability of pile foundation.

## Data Availability

The datasets used and/or analyzed during the current study are available from the corresponding author on reasonable request.

## Conflicts of Interest

It is declared by the authors that this article is free of conflict of interest.

## References

- [1] H. Dong, B. Zhao, and Y. Deng, "Instability phenomenon associated with two typical high speed railway vehicles," *International Journal of Non-Linear Mechanics*, vol. 105, pp. 130–145, 2018.
- [2] N. Lu, H. Wang, K. Wang, and Y. Liu, "Maximum probabilistic and dynamic traffic load effects on short-to-medium span bridges," *Cmes-Computer Modeling in Engineering & Sciences*, vol. 127, no. 1, pp. 345–360, 2021.
- [3] Y. Luo, H. Zheng, H. Zhang, and Y. Liu, "Fatigue reliability evaluation of aging prestressed concrete bridge accounting for stochastic traffic loading and resistance degradation," *Advances in Structural Engineering*, vol. 24, no. 13, pp. 3021–3029, 2021.
- [4] L. Li, Y. Wang, and X. Li, "Tourists forecast Lanzhou based on the Baolan high-speed railway by the Arima model," *Applied Mathematics and Nonlinear Sciences*, vol. 5, no. 1, pp. 55–60, 2020.
- [5] Y. S. Shen, P. Wang, M. P. Li, and Q. W. Mei, "Application of subway foundation pit engineering risk assessment: a case study of Qingdao rock area, China," *China. KSCE journal of civil engineering*, vol. 23, no. 11, pp. 4621–4630, 2019.
- [6] Y. Jiang and X. Li, "Broadband cancellation method in an adaptive co-site interference cancellation system," *International Journal of Electronics*, vol. 102, no. 1, pp. 1–21, 2021.
- [7] J. Xu, L. Zhou, Y. Li, and J. Ding, "Experimental study on uniaxial compression behavior of fissured loess before and after vibration," *International Journal of Geomechanics*, vol. 22, no. 2, 2022.
- [8] A. A. Mousavi, C. Zhang, S. F. Masri, and G. Gholipour, "Structural damage detection method based on the complete ensemble empirical mode decomposition with adaptive noise: a model steel truss bridge case study," *Structural Health Monitoring*, vol. 84049609, 2021.
- [9] Y. Lv, "Numerical simulation and model of deformation features of destabilized mining slope under fault-controlled conditions," *Earth Sciences Research Journal*, vol. 24, no. 1, pp. 61–69, 2020.
- [10] B. Liu and X. Jiang, "Consolidation and deformation characteristics of soft rock foundation in hydrological wetland environment," *Earth Sciences Research Journal*, vol. 24, no. 2, pp. 183–190, 2020.
- [11] Y. Yang, Q. Wang, and J. Ma, "Application of post-grouting in bridge foundation reinforcement: a case study," *Journal of Geo-Engineering*, vol. 14, no. 3, pp. 155–165, 2019.
- [12] H. Lei, C. Li, J. Liu, and L. Wang, "Experimental and numerical simulation study of alternate vacuum preloading for reinforcement of super-soft soil," *Journal of Rock Mechanics and Engineering*, vol. 38, no. 10, pp. 2112–2125, 2019.
- [13] Y. Liu, K. Wang, and C. E. Rodriguez, "The research on the effect of intercity railway project on housing price nearby," *Journal of Mechanical Engineering Research and Developments*, vol. 39, pp. 173–177, 2016.
- [14] Y. Zhou and K. Meng, "Field test and effect evaluation of reinforcement and blowing of mixed land foundation by vibration scour method," *Construction Engineering Technology and Design*, vol. 11, pp. 3892–3893, 2018.
- [15] A. T. Vanli, I. Unal, and D. Ozdemir, "Normal complex contact metric manifolds admitting a semi symmetric metric connection," *Applied Mathematics and Nonlinear Sciences*, vol. 5, no. 2, pp. 49–66, 2020.
- [16] M. A. Medvedeva, T. E. Simos, and C. Tsitouras, "Sixth-order, p-stable, Numerov-type methods for use at moderate accuracies," *Mathematical Methods in the Applied Sciences*, vol. 44, no. 8, pp. 6923–6930, 2021.
- [17] Y. S. Wong, "Analysis of treatment method for foundation reinforcement in geotechnical engineering," *Low carbon world*, vol. 9, no. 10, pp. 136–137, 2019.
- [18] M. Zhou, X. Su, and J. Lei, "Foundation reinforcement and deviation rectifying of the leaning pagoda of Dinglin Temple," *Geotechnical Engineering*, vol. 173, no. 6, pp. 1–32, 2019.
- [19] X. Huang, S. Hou, and M. Liao, "Bearing capacity evaluation and reinforcement analysis of bridge piles under strong earthquake conditions," *KSCE Journal of Civil Engineering*, vol. 22, no. 4, pp. 1295–1303, 2018.
- [20] S. Aria, S. K. Shukla, and A. Mohyeddin, "Numerical investigation of wraparound geotextile reinforcement technique for strengthening foundation soil," *International Journal of Geomechanics*, vol. 19, no. 4, article 04019003, 2019.
- [21] W. Zhang, Z. Tang, Y. Yang, and J. Wei, "Mixed-mode debonding behavior between CFRP plates and concrete under fatigue loading," *Journal of Structural Engineering*, vol. 147, no. 5, article 04021055, 2021.
- [22] L. Zhu, C. Zhang, X. Guan, B. Uy, L. Sun, and B. Wang, "The multi-axial strength performance of composite structural B-C-W members subjected to shear forces," *Steel and Composite Structures*, vol. 27, no. 1, pp. 75–87, 2018.
- [23] J. Li, "An effective system layout planning method for railway logistics centre in the background of big data," *International Journal of Reasoning-based Intelligent Systems*, vol. 10, no. 1, p. 11, 2018.
- [24] M. Zmen and E. K. Aydoan, "Robust multi-criteria decision making methodology for real life logistics center location problem," *Artificial Intelligence Review*, vol. 53, no. 1, p. 45, 2019.
- [25] L. Xue, X. Huang, Y. Wu, X. Yan, and Y. Zheng, "Grade setting of a timber logistics center based on a complex network: a case study of 47 timber trading markets in China," *Information (Switzerland)*, vol. 11, no. 2, p. 107, 2020.
- [26] Q. Li, W. Di, X. Chen, L. Lei, Y. Yu, and G. Wei, "Nonlinear vibration and dynamic buckling analyses of sandwich functionally graded porous plate with graphene platelet reinforcement resting on Winkler-Pasternak elastic foundation," *International Journal of Mechanical Sciences*, vol. 148, pp. 596–610, 2018.

- [27] K. Hatami and G. Raymond, "Influence of soil strength on optimal embedment depth of geosynthetic reinforcement layer in granular-reinforced foundations," *Transportation Research Record*, vol. 1975, no. 1, pp. 155–162, 2018.
- [28] M. A. Medvedeva, T. E. Simos, and C. Tsitouras, "Variable step-size implementation of sixth-order Numerov-type methods," *Mathematical Methods in the Applied Sciences*, vol. 43, no. 3, pp. 1204–1215, 2020.
- [29] R. J. Mei, L. Ding, X. M. An, and P. Hu, "Modeling for heterogeneous multi-stage information propagation networks and maximizing information project supported by the National Natural Science Foundation of China (grant no. 61873194)," *Chinese physics B*, vol. 28, no. 2, article 028701, 2019.

## Research Article

# Application of Blockchain Technology in Value Chain of Procurement in Manufacturing Enterprises

**Yang Wang** , **Sichun Men**, and **Tingting Guo**

*School of Management, China University of Mining and Technology-Beijing, Beijing 100083, China*

Correspondence should be addressed to Yang Wang; wangyang.som@cumtb.edu.cn

Received 30 September 2021; Revised 16 November 2021; Accepted 28 November 2021; Published 31 December 2021

Academic Editor: Deepak Gupta

Copyright © 2021 Yang Wang et al. This is an open access article distributed under the Creative Commons Attribution License, which permits unrestricted use, distribution, and reproduction in any medium, provided the original work is properly cited.

Blockchain technology, as a database which combines encryption algorithm, smart contract, consensus mechanism, time stamp, and other technologies, has received wide attention from all walks of life and can be used to solve such problems as asymmetric, incomplete, and untimely information in both interenterprise transactions and enterprise internal control management as a good solution owing to its characteristics of decentralization, traceability, and tamper-proofness. Consequently, it is worthy of studying how to apply blockchain technology to daily business activities of enterprises. In this paper, some problems existing in the value chain activities of the enterprise internal procurement are analyzed by designing the solutions to requisition, warehousing, and payment based on blockchain technology, in which the Hyperledger Fabric platform is selected as an implementation tool to simulate some purchasing data for testing procedures. After the successful test, the research conclusions and research prospects of this paper are thus proposed, proving the feasibility of applying the blockchain technology to the internal value chain management of the enterprise, which provides reference for the construction of the internal value chain management of the enterprise by the blockchain.

## 1. Introduction

In 2008, the concept of blockchain was first proposed in “Bitcoin: A Peer-to-Peer Electronic Cash System” published by Satoshi Nakamoto who believed that blockchain technology can be applied in fields such as financial technology and business development [1]. The first large-scale and well-known typical application of blockchain technology is Bitcoin that has been popular in recent years. Blockchain provides a very valuable idea for people to create a mechanism of distrust. Although people can now transmit data and information on the Internet, the information that can ensure value still needs a reliable and trusted central organization, such as banks and stock exchanges. The emergence of blockchain has a great impact on people’s existing concepts, and the creation of distrust information transmission circles has been supported by more and more scholars. As of the beginning of 2019, there are more than 20,000 companies involved in blockchain business in China, and more than 500 listed companies with shares have published businesses related to blockchain.

Blockchain, as an emerging database technology, is open and traceable in peer-to-peer data communication, in which each node consciously maintains the authenticity and integrity of ledgers, which makes blockchain technology have unique advantages in accounting and auditing. Besides Internet finance, blockchain technology currently has been applied in many other fields such as Internet of Things [2], transportation [3], and supply chain management [4] and has shown great prospects [5]. The internal control of an enterprise covers the organizations, plans, procedures, and methods for various restrictions and adjustments implemented within the unit in order to improve the operation efficiency, fully and effectively obtain and use various resources, and achieve the established management objectives. With the continuous improvement of blockchain technology, whether it can be applied in enterprise internal control is a question worthy of study. In this paper, blockchain technology will be used to design a set of internal control optimization scheme based on enterprise purchasing value chain to verify the feasibility of blockchain application in enterprise internal management process and to provide

reference for the enterprise to solve the problems of execution efficiency and information distortion.

## 2. Value Chain in Traditional Procurement

At present, the purchase and payment process of an enterprise, whether it is the requisition, warehousing, or payment, needs to be approved by the departments step by step. For example, the procurement application process needs to be approved level by level, from the initiator of the application department to the head of the application department, to the head of the warehouse management department and relevant departments, then to the deputy general manager in charge of approval, and finally to the top authority. The whole process is too complicated and tedious to guarantee efficiency. Upon the arrival of goods, the warehousing department will check the quantity and quality according to the purchase order and warehouse them after inspection. In this process, it is only the warehousing department that determines whether the quantity and quality of the goods meet the purchase standards or not [6]. In terms of raw material quality, the employees of the warehousing department can not judge the quality of goods to a high degree due to professional reasons, but it is too late to find slight defects in raw materials until the production staff carries out production. In terms of raw material quantity, the staff of warehousing department may not find the shrinkage of quantity in time if they do not inspect the quantity rigorously or even substitute the inferior products for the superior ones without authorization, which seriously damages the interests of the enterprise [7]. In addition, whether intentionally or unintentionally, accounting fraud occurs from time to time, and there are always cases of accounting information fraud in the procurement process, such as fraud in procurement contracts, fictitious purchasing transaction, improper inventory losses and gains, and inaccurate related document information, which seriously affects the normal interests of the enterprise and increases the workload of auditors [8].

In the above processes, the confirmation of purchase plan, acceptance and warehousing of raw materials, and payment are prone to errors in the internal procurement and payment of enterprises. Therefore, the solution that conforms to blockchain logic is designed for some problems that appear in these three processes at present.

## 3. Design Ideas for Solutions

Blockchain technology has the characteristics of partial decentralization, tamper-proof modification, traceability, and distrust, which should be met in the purchasing business information when designing solutions [9].

*3.1. Partial Decentralization of Business Information.* In traditional procurement, business is carried out through a longitudinal approval process between departments, each of which has its own authority and only maintains its own information as a center. Each department has its own node in the consortium blockchain which is established between

departments and departments by using the blockchain technology, and all the nodes can freely enter the channel according to the business classification to exchange relevant information. Each transaction can only be executed with endorsement of all nodes in the business channel to achieve partial decentralization, so that all nodes can maintain a set of ledgers together [10]. Therefore, the following partial decentralization needs are put forward:

- (1) Reasonable node setting, including reasonable number and distribution of nodes. Although the more nodes are able to bring higher security, the maintenance cost gets higher and the consensus speed gets slower. The cost, transaction speed, and security should be considered when setting the number of nodes. Nodes should not concentrate on a particular trading participant but should be reasonably distributed [11]
- (2) Each node can communicate with each other
- (3) Each node jointly maintains a set of ledgers

*3.2. Tamper-Proofness of Business Information.* In traditional enterprise internal information management, information of various businesses can be revised after auditing or, in serious cases, directly revised without canceling audits, which is unfavorable for the maintenance of enterprise information [12]. The following tamper-proofness requirements are therefore proposed:

- (1) Each node can query the relevant information on the ledgers
- (2) Each node cannot hide the business information that has happened
- (3) Each node cannot modify the business information that has happened separately
- (4) The information available to each node should be consistent

*3.3. Traceability of Business Information.* The traceability of business information is not only the guarantee of business development but also the important safeguard of querying historical information. Therefore, the following integrity requirements are proposed:

- (1) Record the requisition completely, including the name, quantity, unit price, supplier, latest payment date, and payment method of raw material
- (2) Record the warehousing information completely, including whether the quantity of raw materials is accurate and the quality meets the standards
- (3) Record payment information completely, including name of counterparty, payment amount, and payment date

*3.4. Authenticity of Business Information.* The authenticity of business information is the basis of enterprise accounting



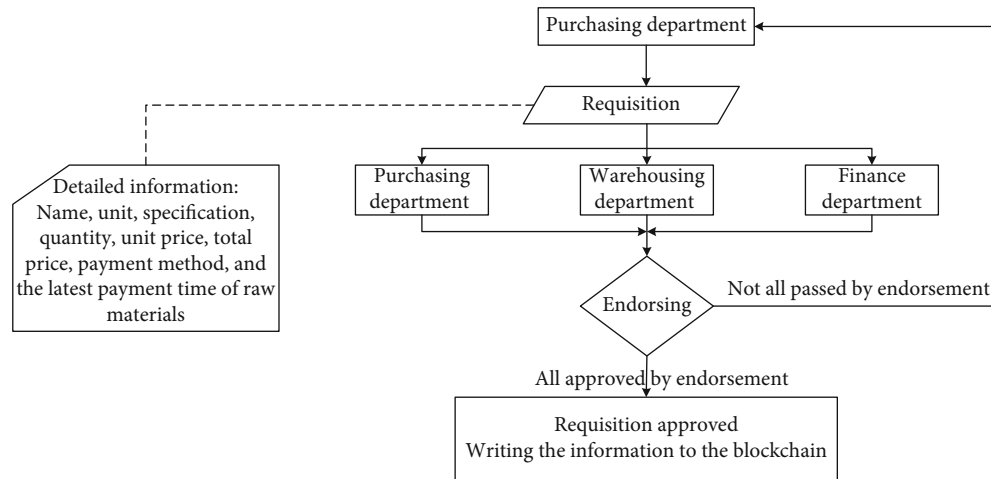


FIGURE 1: Flow chart of the requisition process.

and the basic requirement to ensure the quality of accounting information. Therefore, the following authenticity requirements are proposed:

- (1) Record the requisition truly, including the name, quantity, unit price, supplier, latest payment date, and payment method of raw material
- (2) Record the warehousing information truly, including whether the quantity of raw materials is accurate and the quality meets the standards
- (3) Record payment information truly, including name of counterparty, payment amount, and payment date

#### 4. Design Content of the Solution

**4.1. Design Content of Business Process Solution.** In the requisition process, the purchasing department, warehousing department, and finance department are responsible for the ledger maintenance of the requisition business. The requisition plan determined by the purchasing department no longer needs to be examined and approved in the order of the warehousing department and the financial department; instead, it is approved by each department simultaneously for the content related to the department in each business information and endorsed by default for other information. After determining the purchase plan, the purchasing department initiates the purchase request and sends the purchase information to the warehousing department and the financial department. Each party writes the initial purchase information into the temporary ledger. The purchasing department, as the business initiator, approves all the contents of the requisition information by endorsement. The warehousing department examines and approves the quantity and specifications of raw materials in the requisition information on the basis of the actual inventory quantity and the production plan for a certain period of time in the future. After approval, it agrees to endorse and other information is agreed by default. The finance department approves the amount of requisition, the latest payment date, and the payment method in the requisition information

based on the future cash flow of the enterprise and then agrees to endorse after the approval, while other information is agreed by default. After all of them are agreed, the initial requisition information will be written into the blockchain ledger. If a return or discount occurs, which is equivalent to a negative requisition, the quantity or unit price of the purchase will be negatively counted and the business process will proceed as described above. The flow chart is as shown in Figure 1.

In the warehousing process, the purchasing department, warehousing department, and quality control department are responsible for the ledger maintenance of the warehousing business. After the arrival of raw materials, the purchasing department, warehousing department, and quality control department inspect the raw material information jointly, and each department simultaneously approves the content related to this department in each of business information and approves other information by default by endorsement. The warehousing department initiates the warehousing request after the arrival of raw materials and sends the warehousing information to the purchasing department and the quality control department. Each party writes the initial warehousing information into the temporary ledger. The warehousing department, as the business initiator, approves all the contents of the warehousing information by endorsement. The purchasing department examines and approves the quantity, specifications, and quality of raw materials in the warehousing information according to the contract. After approval, it agrees to endorse and other information is agreed by default. Then, the quality control department examines and approves the quantity, specifications, and quality of raw materials in the warehousing information according to the contract. After approval, it agrees to endorse and other information is agreed by default. After all of them are agreed, the initial warehousing information will be written into the blockchain ledger. If a return or discount occurs, which is equivalent to a negative requisition, the quantity or unit price of the raw materials to be warehoused will be negatively counted and the business process will proceed as described above. The flow chart is as shown in Figure 2.

In the payment process, the purchasing department, warehousing department, and finance department are



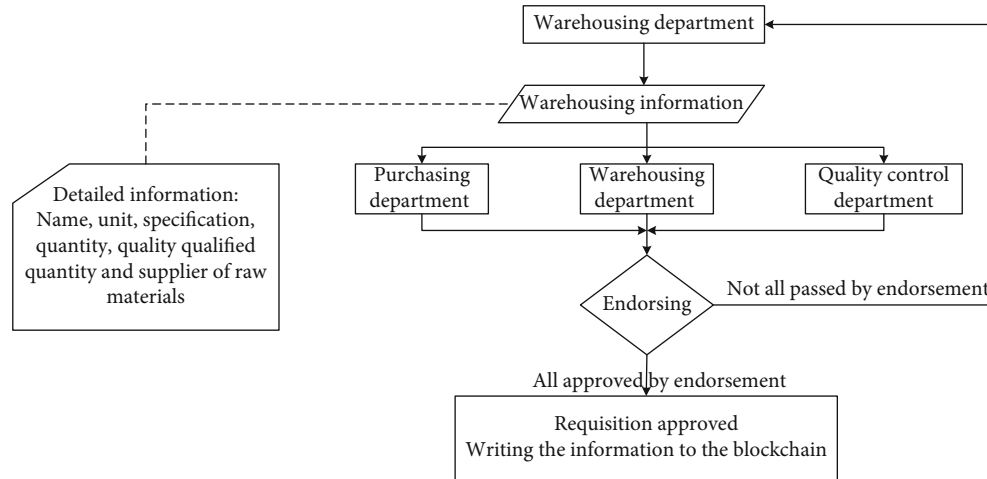


FIGURE 2: Flow chart of the warehousing process.

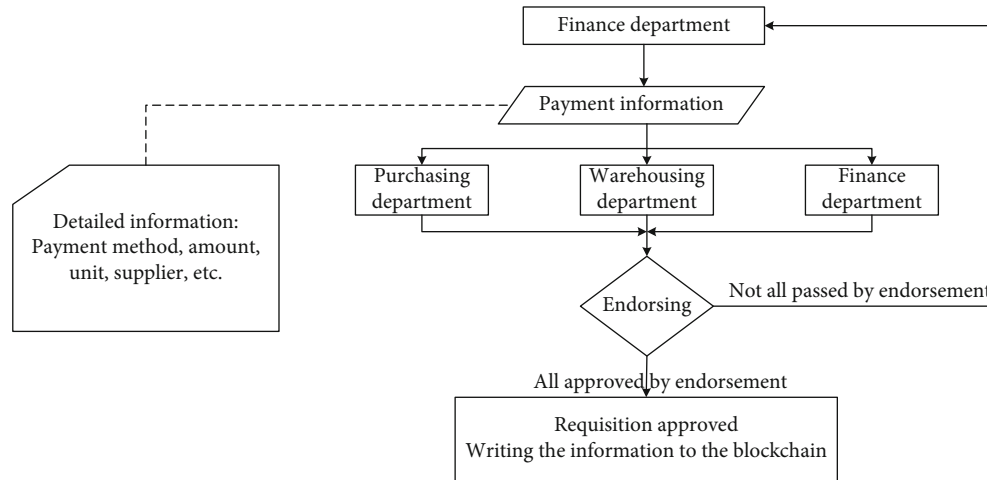


FIGURE 3: Flow chart of the payment process.

responsible for the ledger maintenance of the payment business. The finance department initiates payment request according to the contract amount before the date specified in the contract. Each department simultaneously approves the content related to this department in each payment information and approves other information by default by endorsement. Then, the finance department issues a payment request when it is ready to make a payment before the payment deadline and sends the initial payment information to the purchasing department and the warehousing department. The finance department, as the business initiator, approves all the contents of the payment information by endorsement. The purchasing department examines and approves whether the payment amount conforms to the purchasing contract. After approval, it agrees to endorse and other information is agreed by default. The warehousing department examines and approves whether the payment amount is in line with the warehouse entry. After approval, it agrees to endorse and other information is agreed by default. After all of them are agreed, the initial payment information will be written into the blockchain ledger. If a

return or discount occurs, which is equivalent to a negative requisition, the quantity or unit price of the raw materials to be paid will be negatively counted and the business process will proceed as described above. The flow chart is as shown in Figure 3.

*4.2. Design Content of Consensus Mechanism.* The most important part of the creation of the chain code is the formation of a consensus mechanism, which is the main content of the chain [13]. At present, the well-known consensus mechanisms mainly include proof of work (PoW), proof of stake (PoS), and Delegated Proof of Stake (DPoS) [14], which are limited to the application in public blockchains and can not solve the dependence on virtual tokens, so they can not be well applied to the design of consensus mechanism within enterprises. Since consensus mechanisms can be designed separately in the design of consortium blockchains and private blockchains, taking into account the true operating principle within the enterprise that a business must be completed with the consent of all departments or personnel involved, this paper uses a full

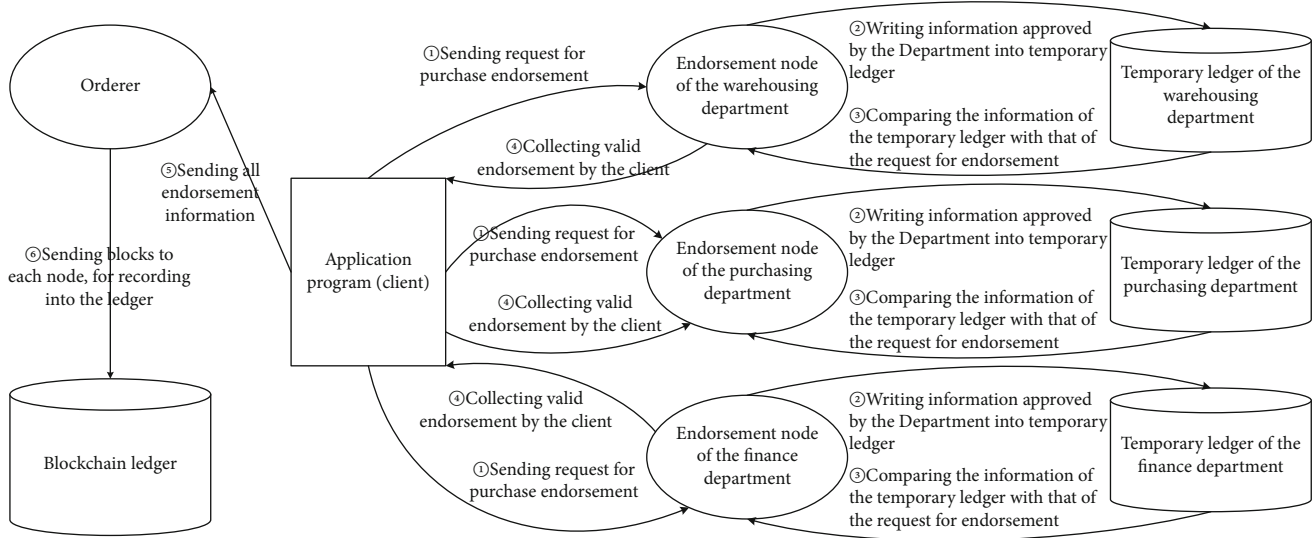


FIGURE 4: Consensus process of requisition.

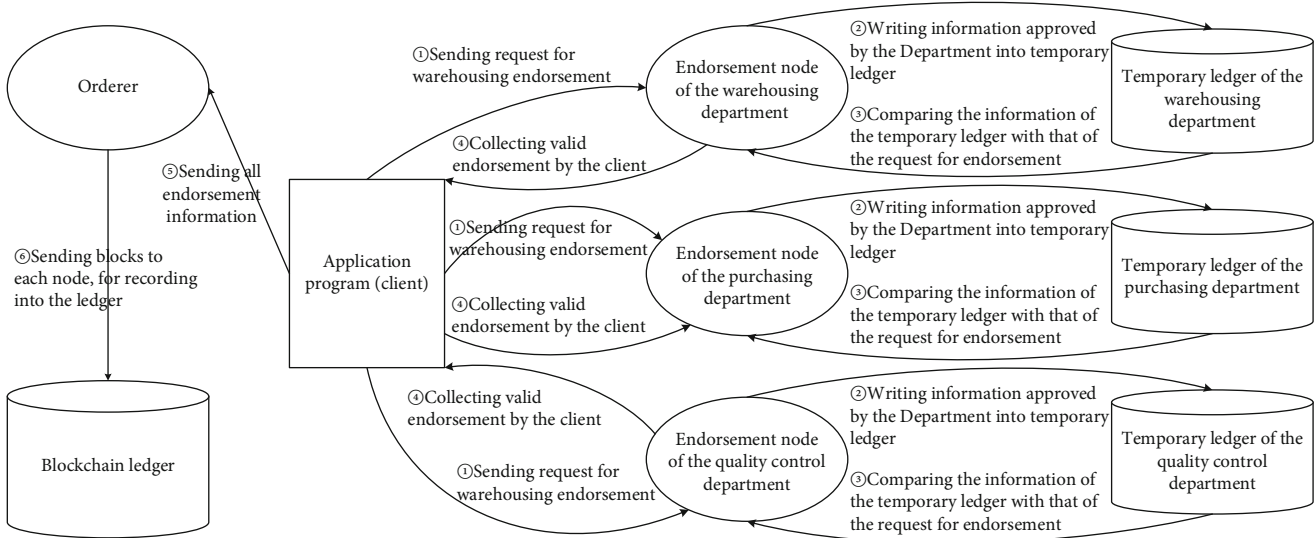


FIGURE 5: Consensus process of warehousing requisition.

consensus mechanism to complete the processing of related business, that is, the initiation of each business must be carried out with the endorsement consent of all endorsement nodes involved in the business. The design basis of the consensus mechanism is as follows:

The consensus mechanism of requisition uses the full consensus mechanism, i.e., the initialization, change, completion, and cancellation of requisition need to be endorsed by all endorsement nodes before they can be written into the blockchain ledger. The detailed flow chart is shown in Figure 4.

The consensus mechanism of warehousing uses the full consensus mechanism, i.e., the initialization, change, completion, and cancellation in the warehousing information need to be endorsed by all endorsement nodes before they can be written into the blockchain ledger. The detailed flow chart is shown in Figure 5.

The consensus mechanism of payment uses the full consensus mechanism, i.e., the initialization, change, completion, and cancellation of payment in the payment information need to be endorsed by all endorsement nodes before they can be written into the blockchain ledger. The detailed flow chart is shown in Figure 6.

## 5. Solution Enablement

5.1. *Programming Environment Setup.* First, clone the fabric-samples project from GitHub using the git tool at the address of <http://github.com/hyperledger/fabric-samples.git>, then check out version v1.3.0. Execute “scripts/bootstrap.sh”: the Ubuntu system will automatically install the Docker and Hyperledger Fabric related mirrors and automatically run the “first-Network” of Hyperledger Fabric,

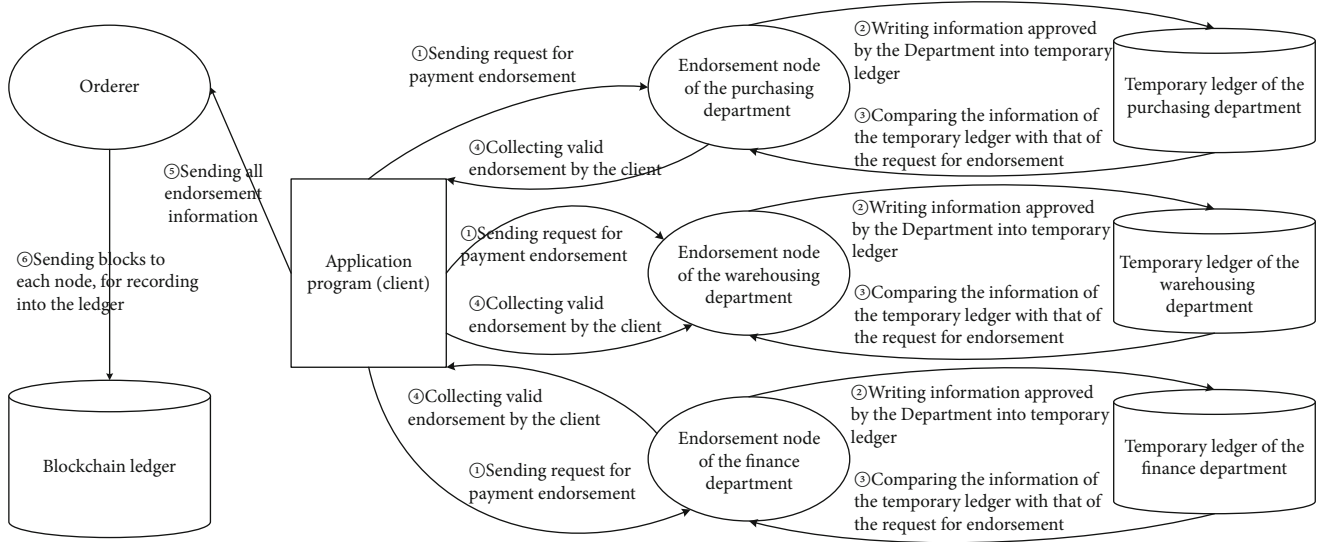


FIGURE 6: Consensus process of payment requisition.

TABLE 1: Test data of requisition.

No.	Raw material No.	Raw material name	Quantity	Unit	Unit price	Suppliers
pr0001	pd001	Material A	78	kg	225	Supplier A
pr0002	pd001	Material A	21	kg	163	Supplier C
pr0003	pd002	Material B	63	kg	211	Supplier D
pr0004	pd002	Material B	45	kg	141	Supplier B
pr0005	pd003	Material C	86	kg	156	Supplier A
pr0006	pd003	Material C	91	kg	228	Supplier C
pr0007	pd004	Material D	42	kg	286	Supplier D
pr0008	pd004	Material D	11	kg	173	Supplier B

and then close and remove all Docker containers. The basic environment of Hyperledger Fabric has been completed. The following is to build the Hyperledger Fabric environment on this basis to implement the enterprise vertical value chain management solution based on blockchain technology.

Hyperledger Fabric configures the organizational information through `crypto-conFigureyaml` and generates configuration files of the organization through `cryptogen`. The configuration file of `crypto-conFigureyaml` generally consists of two parts, namely, `OrdererOrgs` and `PeerOrgs`. The former defines the organizations that manage the orders, while the latter defines the nodes that manage peer. According to the design of the previous chapter, the internal purchasing management of the enterprise involves four organizations: pur-

chasing department, warehousing department, finance department, and quality control department. The specific organizations are set up according to the requirements of the Hyperledger Fabric environment platform [15].

**5.2. Chain Code Enablement.** Hyperledger Fabric's smart contract is written by using chain codes, which are called by an application outside the application when the application needs to interact with the account book. Chain codes run in a protected Docker container and are isolated from the operation of endorsement nodes. Chain codes are written in Go language in this paper. Chain code mainly realizes the data structure and business functions. The data structure includes the business information structure of purchase, warehousing, and payment processes. The business functions include functions such as initializing business information, updating business information, and querying business information.

## 6. Solution Test

**6.1. Testing Environment.** The hardware conditions of this test are as follows:

CPU: Intel core i5-6,300HQ; memory: 16 G; hard disk: 1 T.

The software conditions of this test are as follows:

Operating system: Ubuntu 18.04.1 LTS, Docker version 18.06.1-ce, build e68fc7a, go language version: go1.10.4 linux/amd64, Hyperledger Fabric version: v1.3.0.

**6.2. Testing Process**

- (1) Start the Hyperledger Fabric network enabled in this paper
- (2) Modify the relevant configuration in programming environment setup

TABLE 2: Results of the requisition chain code test.

Type of test	Test items	Test methods	Number of passes	Number of failures	Test results
Consensus and writing	Information initialization	initPurchasereq	8	0	Pass
Tamper-proofness	Information initialization	initPurchasereq	8	0	Pass
Transparency	Information query	queryPurchasereq	16	0	Pass
Transparency	Information rich query	richQueryPurchasereq	8	0	Pass
Traceability	History query	queryPurchasereqHistory	8	0	Pass

TABLE 3: Results of requisition management test.

Test items	Test methods	Number of passes	Number of failures	Test results
Requisition content query	QueryPurchaseByPurchasereqID	1	0	Pass
Requisition content query	QueryPurchaseByTimeRange	1	0	Pass
Warehousing query	QueryPurchaseWarehouseByPurchasereqID	1	0	Pass
Payment query	QueryPurchasePaymentByPurchasereqID	1	0	Pass
Requisition daily report	QueryPurchasePerDay	1	0	Pass

- (3) Start temporary ledgers and execute `templledger/Server.go`
- (4) Execute `test/testdata/datagen_test.go` to generate related chain code documents
- (5) Install chain codes and execute `client/chaincodeinstall/chaincodeinstall.go`
- (6) Run test, and execute `test/testdata.go` [16].

**6.3. Test Case.** This test involves the relevant data of the requisition process, the warehousing process, and the payment process. The data required by each process is generated according to the random function `rand` function in the Go language.

In this test, the basic information of some raw materials is simulated and then some businesses such as purchase, warehousing, and payment are simulated. The raw material information is as shown in Table 1.

**6.4. Test Result.** The test results are divided into chain code test results and business layer test results.

Chain code test results include requisition chain code, warehousing chain code, payment chain code, and organization information maintenance chain code. For example, the results of the requisition chain code test are as shown in Table 2.

The business layer test results include the requisition management business, the warehousing management business, the payment management business, and the organization information maintenance business. For example, the results of the requisition management business test are as shown in Table 3.

**6.5. Solution Evaluation.** In terms of efficiency, introducing blockchain technology into the internal procurement management of enterprises changes some processes from level-to-level approval of a business among the departments originally to concurrent approval while ensuring the security and transparency of the information, which will save a lot of time because the total time spent by each department in

completing a decision is immeasurable in serial decision-making, but there is only one delay in parallel decision-making, which can save a lot of time cost compared with serial decision-making [17].

In terms of information integrity, either party can query any business information through the requisition ID, warehousing ID, or payment ID as well as statistical information according to time in the requisition management, warehousing management, and payment management.

From the perspective of tamper-proofness, business information in the requisition management, warehousing management, and payment management will be recorded in the ledgers of the blockchain after reaching a consensus. It is impossible for a single department to tamper with the information.

From the view of extensibility, this paper uses the Hyperledger Fabric platform to complete the basic application of requisition management, warehousing management, payment management, and organization information management in the procurement process. The main applications of requisition management, warehousing management, payment management, and organization information management can be fully completed by or based on Hyperledger Fabric chain codes. Because chain code is an intelligent contract and programmable, it can access information related to transactions within their respective rights and can complete a variety of rich applications of purchase management, warehousing management, payment management, and organization information management, making the solution scalable.

## 7. Conclusions

First, the current status of blockchain research and the concept of blockchain are introduced, and then, the value chain management requirements of the internal procurement based on blockchain technology are analyzed, involving partial decentralization, tamper-proof modification, information integrity, authenticity, and maintainability. After that, an enterprise internal procurement management solution based on blockchain technology is designed, including business organizations,

consensus mechanism, data structure, and business process. Next, the solution is implemented based on the Hyperledger Fabric platform, including the Hyperledger Fabric environment setup, chain code enablement, temporary ledger and Hyperledger Fabric client enablement, and business layer enablement. Then, the completed solution is tested, including the chain code layer test and business layer test. Finally, the solution is analyzed from four aspects of efficiency, tamper-proofness, information integrity, and expandability. The conclusions in the paper are as follows:

- (1) The paper realize the internal procurement value chain management solution based on blockchain technology through code, which confirms the partial decentralization, immutability, information integrity, security, and expandability of blockchain technology
- (2) The application of blockchain technology to the management of the enterprise's internal procurement value chain can reduce the risk of individual personnel making false accounts and fictitious business. All businesses must be agreed by all departments involved in this business before they can be written into the blockchain ledger
- (3) Blockchain technology is applied to the management of the enterprise's internal procurement value chain. In interdepartmental decision-making, it has become a parallel decision based on the previous serial decision, which can speed up the efficiency of departmental decision-making and save a lot of time and cost
- (4) Blockchain technology is applied to the management of the enterprise's internal procurement value chain. Because of its immutability, it makes the business information of the enterprise more transparent, and the transaction data is more authentic. The focus of the work of internal auditors will transform from the authenticity of the business information to the business. The rationality of the process of information on the chain has also reduced the workload in disguised form

The above contents can reflect the feasibility of blockchain technology in enterprise internal application. The design and enablement of the solution in this paper can provide ideas for other scholars, improve their respective solutions, and provide guidance and reference for future blockchain implementation and enterprise practice.

### Data Availability

The datasets used and/or analyzed during the current study are available from the corresponding author on reasonable request.

### Conflicts of Interest

It is declared by the authors that this article is free of conflict of interest.

### Acknowledgments

This work was supported, in part, by the funds for "Undergraduate Teaching Reform and Innovation Project" of Beijing Higher Education in 2020 and "Undergraduate Teaching Reform and Research Project" of China University of Mining and Technology (Beijing) in 2020 (J20ZD18).

### References

- [1] N. Satoshi, "Bitcoin: a peer-to-peer electronic cash system," Social Science Electronic Publishing, 2009.
- [2] K. Christidis and M. Devetsikiotis, "Blockchains and smart contracts for the internet of things," *IEEE Access*, vol. 4, pp. 2292–2303, 2016.
- [3] J. Kang, R. Yu, X. Huang et al., "Blockchain for secure and efficient data sharing in vehicular edge computing and networks," *IEEE Internet of Things Journal*, vol. 6, no. 3, pp. 4660–4670, 2019.
- [4] S. Saberi, M. Kouhizadeh, J. Sarkis, and L. Shen, "Blockchain technology and its relationships to sustainable supply chain management," *International Journal of Production Research*, vol. 57, no. 7, pp. 2117–2135, 2019.
- [5] Y. Yuan and F. Y. Wang, "Blockchain technology development status and prospect," *Acta Automatica Sinica*, vol. 42, no. 4, pp. 481–494, 2016.
- [6] Z. B. Xie, "Design ideas and application of internal control system with purchasing and payment as example," *Modern Economic Information*, vol. 5, p. 191, 2013.
- [7] J. Y. Huang and Y. Zhao, "Research on internal control of enterprise procurement and payment," *Special Economic Zone*, vol. 2, pp. 235–236, 2014.
- [8] Q. L. Zhang and X. K. You, *Construction and Evaluation of Enterprise Internal Control*, Economic Science Publishing, Beijing, China, 2011.
- [9] Z. T. Li, J. W. Kang, R. Yu, D. Ye, Q. Deng, and Y. Zhang, "Consortium blockchain for secure energy trading in industrial internet of things," *IEEE Transactions on Industrial Informatics*, vol. 14, no. 8, pp. 3690–3700, 2018.
- [10] B. H. Yang and C. Chen, *Principle, Design and Application of Blockchain*, China Machine Press, Beijing, China, 2017.
- [11] Q. W. An, *Research and Application of Decentralized Transaction Key Technology Based on Blockchain*, Donghua University, 2017.
- [12] K. Jia, "Research on blockchain governance: technology, mechanism and policy," *Administrative Forum*, vol. 2, pp. 80–85, 2019.
- [13] Z. Zheng, S. Xie, H. Dai, X. Chen, and H. Wang, "An overview of blockchain technology: architecture, consensus," in *2017 IEEE International Congress on Big Data (BigData Congress)*, pp. 557–564, Honolulu, HI, USA, 2017.
- [14] F. T. Li, "Consensus mechanism in blockchain," *China New Communications*, vol. 21, no. 21, p. 12, 2019.
- [15] J. Zou, H. Zhang, Y. Tang et al., *Blockchain Technology Guide*, China Machine Press, Beijing, China, 2016.
- [16] X. Feng, T. Liu, S. Wu, and G. Zhou, *Blockchain Development Practice: Hyperledger Fabric Key Technologies and Case Analysis*, China Machine Press, Beijing, China, 2018.
- [17] P. Cheng and S. Wang, "Research on big accounting of procurement activities based on blockchain technology," *Friends of Accounting*, vol. 2, pp. 153–158, 2020.



## Research Article

# Research on Video Quality Diagnosis Technology Based on Artificial Intelligence and Internet of Things

Zhidong Sun <sup>1</sup>, Jie Sun <sup>2</sup>, and Xueqing Li <sup>1</sup>

<sup>1</sup>School of Software, Shandong University, Shandong, China

<sup>2</sup>Affiliated Hospital of Qingdao Binhai University, Shandong, China

Correspondence should be addressed to Xueqing Li; [xqli@sdu.edu.cn](mailto:xqli@sdu.edu.cn)

Received 29 September 2021; Revised 2 November 2021; Accepted 9 November 2021; Published 29 December 2021

Academic Editor: Deepak Gupta

Copyright © 2021 Zhidong Sun et al. This is an open access article distributed under the Creative Commons Attribution License, which permits unrestricted use, distribution, and reproduction in any medium, provided the original work is properly cited.

The remote video diagnosis system based on the Internet of Things is based on the Internet of Things and integrates advanced intelligent technology. To better promote a harmonious society, constructing a video surveillance system is accelerating in our country. Many enterprises and government agencies have invested much money to build video surveillance systems. The quality of video images is an important index to evaluate the video surveillance system. However, as the number of cameras continues to increase, the monitoring time continues to extend. In the face of many cameras, it is not realistic to rely on human eyes to diagnose video-solely quality. Besides, due to human eyes' subjectivity, there will be some deviation in diagnosis through human eyes, and these factors bring new challenges to system maintenance. Therefore, relying on artificial intelligence technology and digital image processing technology, the intelligent diagnosis system of monitoring video quality is born using the computer's efficient mathematical operation ability. Based on artificial intelligence, this paper focuses on studying video quality diagnosis technology and establishes a video quality diagnosis system for video definition detection and noise detection. This article takes the artificial intelligence algorithm in the diagnosis of video quality effect. Compared with the improved algorithm, the improved video quality diagnosis algorithm has excellent improvement and can well finish video quality inspection work. The accuracy of the improved definition evaluation function for the definition detection of surveillance video and noise detection is as high as 95.56%.

## 1. Introduction

The video monitoring system is being constructed in China in order to promote the development of a harmonious society. Many enterprises and government agencies have invested much money to build video monitoring systems. The quality of video images is an important index to evaluate the video monitoring system. However, with the increasing number of cameras, the monitoring time is constantly extended. It is not realistic to rely on human eyes to diagnose the quality of the video. Besides, there will be some deviation through human eye diagnosis due to the human eye's subjectivity. These factors all bring new challenges to system maintenance. Therefore, the intelligent diagnosis system of monitoring video quality based on the computer efficient mathematical operation ability relies on artificial intelligence technology and digital image processing technology. This

paper focuses on video quality diagnosis technology based on artificial intelligence and establishes a video quality diagnosis system of video definition detection, video color deviation detection, and video noise detection. The artificial intelligence algorithm adopted in this paper has a pronounced effect on video quality diagnosis. The improved optical frequency quality diagnosis algorithm has a more significant improvement than the improved algorithm, which can better complete video quality inspection work.

A video monitoring system's video image quality is the most critical performance index of a monitoring system [1, 2]. Good quality monitoring video can bring great convenience to users and improve their work efficiency. However, the video image quality in the case will be seriously reduced when failure of monitoring equipment happens while with no timely maintenance. It is undoubtedly a devastating disaster for the monitoring system. Therefore, accurate time



detection and maintenance monitoring equipment are essential for people. However, with the increasing number of surveillance cameras, the monitoring time is constantly extended. The existing manual detection camera has a huge workload, low efficiency, and high human cost, making traditional video image quality diagnosis relying on human eyes quantity no longer realistic. Therefore, based on computer image vision technology and artificial intelligence technology, intelligent video quality diagnosis algorithms with the help of a powerful computer's powerful processing ability emerges. Intelligent video quality diagnosis algorithm is a branch of artificial intelligence research. It establishes the relationship between images through computer image vision technology and extracts valuable information from video images, thus analyzing and processing video images. Using a video quality diagnosis algorithm, we can simultaneously analyze thousands of video devices and screen out the places of interest. Therefore, it can significantly improve the efficiency of maintenance personnel, greatly ease the human cost, and improve the ability to handle emergency affairs.

Intelligent video quality diagnosis technology originated in the 1990s, an essential branch of intelligent video analysis technology. An intelligent video quality diagnosis algorithm is an integral part of the video monitoring system, and it is an essential tool for the video monitoring system's maintenance personnel. The popularization of the modern video monitoring network, the construction of a safe city at home and abroad, the development of cities, the rapid expansion of cities, frequent accidents in some security fields, and military use all promote the accelerated development of video monitoring. It also makes people realize the importance of the video quality diagnosis function to the video monitoring industry [3].

Video quality diagnosis system is an intelligent video fault analysis and early warning system. It is mainly used in the control center of the large-scale monitoring system. By controlling the video switching output of the monitoring center's matrix host or connecting the digital video streaming media management server, the video signal of all the cameras in the front end is obtained. The standard camera failures such as snowflake, rolling screen, blur, color deviation, picture freezing, gain imbalance, and malicious behavior of blocking and damaging the monitoring equipment are judged accurately. The alarm information is sent out. The video quality diagnosis system uses video image analysis to detect the monitoring system's common video faults. From the current common faults, the detection is mainly carried out from the following aspects: camera interference detection, video definition detection, video interference detection, video signal missing detection, video brightness anomaly detection, and video color deviation detection.

*Camera interference detection* [4, 5]: automatically detects camera lens when artificial or because some unexpected events are moved or blocked, making the camera deviate from the monitoring area. This function can diagnose whether the camera position changes or whether the camera lens is blocked.

*Video definition detection* [6]: automatically detects the image blur of the central part of the field of vision caused by improper focus and lens damage in the video; the func-

tion evaluates the clarity of the real-time video picture and the content of information.

*Video interference detection* [7]: automatically detects noise phenomena such as video image distortion, snowflake, jitter, or rolling screen; the main monitoring objects are dot, prick, and strip interference on the video screen due to aging of the line, transmission failure, poor contact, or electromagnetic interference.

*Video brightness detection* [8]: automatically detects the phenomenon of over dark, over bright, or black screen of the picture caused by camera failure, gain control disorder, and abnormal lighting conditions; this function will diagnose the brightness and darkness of video. Because the diagnostic plan and monitoring threshold can be changed in different periods, the brightness anomaly detection can play a role in day and night.

*Video color deviation detection* [9]: automatically detects screen color deviation caused by poor line contact, external interference, or camera failure, mainly including the color deviation of the whole screen with single color or mixed colors; the function analyzes the color information of video, and its feature is that when there is rich color in the video, it can distinguish them from natural scenes or from camera fault, which makes camera color detection practical.

*Video freeze detection* [10, 11]: automatically detects the freezing phenomenon of video pictures caused by the failure of video transmission and dispatching system can avoid missing real-time video image.

*Video signal missing detection*: automatically detects intermittent or continuous video loss caused by the operation abnormality, damage, evil human intention, or video transmission link failure of front-end platform and camera.

This paper focuses on the video definition detection and video noise detection in video quality detection.

## 2. Video Definition Detection

When the playing picture of a video exceeds 24 frames/s, according to the principle of visual retention, the human eye cannot distinguish every single static picture, which appears to be a smooth and continuous visual effect. Objects in a video are usually divided into static and moving categories. Objects that remain static in a continuous multiframe frame can be regarded as the static background. In contrast, objects whose positions change in a continuous multiframe frame can be regarded as the moving foreground. Therefore, every frame in a real-time video image can be divided into two areas: the static background and the moving foreground. It is challenging to detect real-time video images' sharpness because of the unexpected change of moving foreground area in video sequence image, which causes the random change of pixel gradient value. This paper's algorithm uses the static background area in the real-time video image to detect the clarity of the visual composition sequence image; that is, it consists of background extraction and definition detection.

This algorithm is roughly divided into three steps:

- (1) Intercept a real-time video image to obtain the initial background image

The calculation formula of background image is as follows:

$$\text{ImageBack}(x, y) = \frac{\sum_{i=1}^N g_i(x, y)}{N}, \quad (1)$$

where  $N$  is the number of frames captured in a video sequence and  $g_i(x, y)$  is the gray value of an image pixel  $(x, y)$ .

- (2) The current real-time video image is used to update the initial background to detect the background image
- (3) Calculate the sum of the edge gradient values of the background image according to the Sobel operator, judge the background image's sharpness according to the threshold value, and get the sharpness evaluation value of the real-time video image. The Sobel operator can be expressed by formula (2):

$$G = \sqrt{g_x^2 + g_y^2} = \sqrt{(f(x, y) \times S_x^2) + (f(x, y) \times S_y^2)}, \quad (2)$$

where  $f(x, y)$  is gradation of image and  $g_x$  and  $g_y$  are finished by convolution template.

$$S_x = \begin{pmatrix} -1 & 0 & 1 \\ -2 & 0 & 2 \\ -1 & 0 & 1 \end{pmatrix}, \quad (3)$$

$$S_y = \begin{pmatrix} -1 & -2 & -1 \\ 0 & 0 & 0 \\ 1 & 2 & 1 \end{pmatrix}.$$

The implementation steps of the algorithm are as follows:

A video image with a length of 1 min was intercepted from the real-time video image, sampled every 5 seconds, and a total of 12 frames of images were obtained. The sampled 12 frames of images are converted from RGB space to gray space because of reducing the amount of calculation. The gray value  $f(x, y)$  of each pixel in the image is accumulated and averaged to get the real-time video image's initial background image. The calculation formula is

$$\text{Background}_0(x, y) = \frac{\sum_{i=1}^{12} f_i(x, y)}{12}. \quad (4)$$

The current frame image in the real-time video image needs to update the background image to achieve real-

time monitoring constantly. The calculation formula of background update is as follows:

$$\text{Background}(n+1) = \text{background}(n) + \frac{1}{n+1} \cdot [\text{image}(n+1) - \text{background}(n)], \quad (5)$$

where  $\text{Image}(n+1)$  is the latest frame image in a live video image and  $\text{background}(n)$  and  $\text{background}(n+1)$  are the background image before and after updating, respectively.

According to the gray value of the pixels in the background image, the Sobel operator is used to detect the image's edge. Complete the detection of the sharpness of the real-time video image. The detection process is as follows:

- (1) According to the edge detection theory of the Sobel operator and the template of four directions as shown in Figure 1, neighborhood convolution calculation is carried out for each pixel point in the image to extract the edge components of pixel points in four directions:

$$F_1 = f(x, y) \times s_1, F_2 = f(x, y) \times s_2, F_3 = f(x, y) \times s_3, F_4 = f(x, y) \times s_4 \quad (6)$$

The gradient value of each pixel in the image is

$$F(x, y) = \sqrt{F_1^2 + F_2^2 + F_3^2 + F_4^2}. \quad (7)$$

- (2) If  $|F| \geq T_N$ , the pixel point is an edge point; if  $|F| \leq T_N$ , the pixel point is a nonedge point. The edge gradient energy value and the edge gradient energy value are taken as the evaluation value of image sharpness detection by adding the gradient values of image edges:

$$\text{value} = \sum_{k=1}^n |F_k(x, y)|^2, \quad (8)$$

where  $n$  is the number of edge points. We compared value with the sharpness detection range value of a clear real-time video image background. If  $\text{value} \in T(\alpha_1, \alpha_2)$ , the live video image is clear; if  $\text{value} \in T(\alpha_1, \alpha_2)$ , the live video image is blurry

In order to compare the effect of the Sobel operator and other algorithms in clarity detection, the article selected 6 real-time video images. The first three are transparent images; the latter three are fuzzy images and analyzed the effect of the Sobel operator and square gradient method. The comparison results are shown in Table 1.

$$\begin{array}{cc}
\begin{pmatrix} -1 & -2 & -1 \\ 0 & 0 & 0 \\ 1 & 2 & 1 \end{pmatrix} & \begin{pmatrix} -1 & -2 & -1 \\ 0 & 0 & 0 \\ 1 & 2 & 1 \end{pmatrix} \\
\text{(a) } 0^\circ \text{ gradient direction template } (s_1) & \text{(b) } 45^\circ \text{ gradient direction template } (s_2) \\
\begin{pmatrix} -1 & 0 & 1 \\ -2 & 0 & 2 \\ -1 & 0 & 1 \end{pmatrix} & \begin{pmatrix} 0 & 1 & 2 \\ -1 & 0 & 1 \\ -2 & -1 & 0 \end{pmatrix} \\
\text{(c) } 90^\circ \text{ gradient direction template } (s_3) & \text{(d) } 135^\circ \text{ gradient direction template } (s_4)
\end{array}$$

FIGURE 1: Sobel operator convolution template of four directions.

TABLE 1: Comparison of different calculated clarity detection.

Algorithm	Picture 1	Picture 2	Picture 3	Picture 4	Picture 5	Picture 6	Computation time (ms)
Sobel	0.9153	0.8501	0.6447	0.5914	0.4305	0.2138	62.4004
Square gradient	0.9092	0.8341	0.4015	0.2051	0.1689	0.1128	328.5043

As shown in Table 1, the changing trend of the clarity evaluation value of Sobel operator clarity detection and square gradient algorithm is consistent with the facts observed by the naked eye. The more blurred the video sequence image, the smaller the clarity evaluation value. The further comparative analysis found that Sobel operator clarity detection accuracy was higher than in the square gradient method. In addition, the Sobel operator detects faster than the square gradient method.

### 3. Video Color Bias Detection

Traditional noise detection algorithms include the grayscale interpolation method and spatial neighborhood method. To better detect the noise of the image and effectively eliminate the false positives generated by noise detection of nonnoise points in the picture, this paper proposes to use the “image smoothing region” module to describe the noise in the video image.

The “image smoothing area” is a particular area in the video picture, which has the following two characteristics. The first is the channel change between the values of all pixels in the smooth area. The second is the high similarity of all pixels in the smooth area to the pixels in the surrounding neighborhood. The video image area that satisfies the above two points is called the “image smoothing area.”

The algorithm flow is as follows:

- (1) The user requests video diagnosis, and the video diagnosis platform finds the idle algorithm analysis unit and sends a message to VAM requesting the establishment of the association between the algorithm analysis unit and the camera
- (2) The user starts setting diagnostic rules, including the items to be detected and the thresholds for the items to be detected
- (3) The user requests “start diagnosis” through the video quality diagnosis platform. After receiving

$$\begin{array}{cc}
\begin{bmatrix} 0 & 0 & 0 & 0 & 0 \\ 0 & 0 & 0 & 0 & 0 \\ 1 & 1 & -4 & 1 & 1 \\ 0 & 0 & 0 & 0 & 0 \\ 0 & 0 & 0 & 0 & 0 \end{bmatrix} & \begin{bmatrix} 0 & 0 & 0 & 0 & 0 \\ 0 & 0 & 0 & 0 & 0 \\ 1 & 1 & -4 & 1 & 1 \\ 0 & 0 & 0 & 0 & 0 \\ 0 & 0 & 0 & 0 & 0 \end{bmatrix} \\
\text{Template 1} & \text{Template 2} \\
\begin{bmatrix} 0 & 0 & 0 & 0 & 0 \\ 0 & 0 & 0 & 0 & 0 \\ 1 & 1 & -4 & 1 & 1 \\ 0 & 0 & 0 & 0 & 0 \\ 0 & 0 & 0 & 0 & 0 \end{bmatrix} & \begin{bmatrix} 0 & 0 & 0 & 0 & 0 \\ 0 & 0 & 0 & 0 & 0 \\ 1 & 1 & -4 & 1 & 1 \\ 0 & 0 & 0 & 0 & 0 \\ 0 & 0 & 0 & 0 & 0 \end{bmatrix} \\
\text{Template 3} & \text{Template 4}
\end{array}$$

FIGURE 2: Template of “Image Smoothing Area.”

the request, VAM will send the diagnosis items, diagnosis threshold, and related information to the corresponding algorithm analysis unit according to the diagnosis rules

- (4) After receiving the diagnosis request, the video quality algorithm analysis unit finds the corresponding diagnosis algorithm according to the diagnosis item. If it is video noise detection, the noise detection algorithm is selected as the diagnosis algorithm, and the corresponding threshold value is set for the algorithm
- (5) The video quality algorithm analysis unit obtains the camera ID to be detected according to the associated camera list, and the algorithm analysis unit obtains the video code stream to be detected through the interface provided by the video monitoring platform according to the camera ID
- (6) Use OpenCV computer image vision function to extract the current video image frame data, and judge whether the current frame data is YUV data; if not, the current picture gray processing is used, so as to obtain Y, U, and V data

TABLE 2: Software environment tested.

Number	Software	Application
1	Video and video surveillance platform ishot6000	Platform service program
2	Network monitoring system of the video monitoring platform	Platform service program
3	Video monitoring platform VQCS6000 module	Platform service program
4	Video monitoring platform VQCC video diagnosis client	Platform service program
5	Video diagnostic analysis module VAM	Diagnostic system analysis module

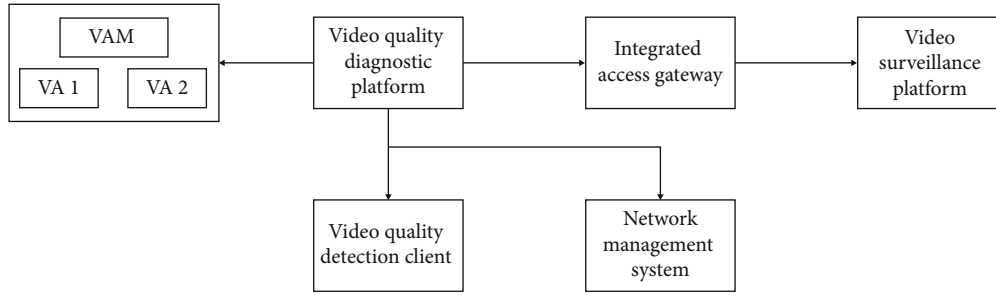


FIGURE 3: Video quality diagnostic algorithm test topology.

TABLE 3: Test items and results.

Algorithm	Sobel operator	Square gradient method	Improved algorithm
Number of correctly detected	28	32	42
Detection rate of the algorithm	68.22%	71.11%	93.33%
Number of false positives	12	5	2
The false-positive rate of the algorithm	26.67%	11.11%	4.44%
Algorithm	Gray scale difference method	Spatial neighborhood method	Improved algorithm
Number of correctly detected	20	37	43
Detection rate of the algorithm	44.44%	82.22%	95.56%
Number of false positives	5	10	2
The false-positive rate of the algorithm	11.11%	22.22%	4.44%

- (7) First, the current frame image data is transmitted to the video image analysis module. Then, the current frame image data is sent to the video image noise anomaly analysis algorithm unit according to the currently selected diagnostic items. The algorithm in the analysis unit analyzes the image data. The implementation process of the algorithm is from Step 4 to Step 8
- (8) A template of “Image Smooth Area” is designed to scan the pixel points of the current video picture. As shown in Figure 2, the template of “Image Smooth Area” designed in this paper is composed of four templates with different vector directions
- (9) According to the template of “Image Smooth Area” designed in this paper, each pixel of the current video image frame is scanned successively from left to right and from top to bottom. In other words, the Y value of the current pixel is multiplied by each element value in the four modules to obtain the four “scan” values of the current pixel corresponding to the four

templates: Value1, Value2, Value3, and Value4;  $\text{MinValue} = \text{Min} [\text{Value1}, \text{Value2}, \text{Value3}, \text{Value4}]$ .

- (10) Calculate the MinValue corresponding to each pixel in the current video image according to Step 4. When the MinValue of a pixel is 0, it is judged that this pixel is in the smooth area of the image. We call it “smooth pixel”; otherwise, this pixel should be a noise point
- (11) The method in Step 6 is used to calculate the total number of “smooth pixel points” in the current video picture, and then, the total number of “smooth pixel points” is compared with the total number of pixel points in the current video picture. When this ratio is less than the noise threshold value of 0.9, it is determined that the current video image has noise abnormality
- (12) The total number of frames with abnormal video noise in a certain period of time is counted, and the ratio of the total number of frames with noise

in the video to the total number of frames in the video picture in this period of time is used. When the ratio is greater than 0.4, the video is judged to have abnormal noise

- (13) After being processed by the video noise diagnosis algorithm, if the current video is found to be noisy, alarm information will be sent to the video quality analysis module immediately, and the alarm information will be uploaded to the network management system
- (14) Upload the warning information to the network management system

#### 4. Video Quality Diagnostic System Testing

**4.1. Construction of Test Environment.** The software environment tested by this algorithm is shown in Table 2.

**4.2. Construction of Test Environment.** The testing process of the quality diagnosis algorithm in this paper is as follows.

Firstly, the video code stream to be analyzed is obtained through the video monitoring platform's video media interface. Secondly, the received video code stream is connected to the video diagnosis and analysis management device, simultaneously managing the VA's multiple video analysis algorithm units. Finally, the video analysis algorithm unit VA is used to analyze the quality of the specified video quality diagnosis items. Each VA can independently complete the diagnostic analysis of all the videos. Finally, the VQCC video quality diagnosis client is used to browse the alarm results obtained by analyzing each route VA's specified video quality diagnosis algorithm. The test topology for this article is shown in Figure 3.

**4.3. Analysis of Test Result.** To verify the text's accuracy improved diagnostic algorithm, this paper uses the above test topology to test and compare the commonly used diagnostic algorithm and the improved diagnostic algorithm.

Table 3 shows the results of video detection using different definition evaluation algorithms and noise detection algorithms. From the detection rate results of the algorithm, it can be seen that the accuracy of the improved definition evaluation function for the definition detection of surveillance video and noise detection is as high as 95.56%, which is much higher than the detection rate of other definition evaluation functions. It can more accurately judge the clarity of images. As can be seen from the algorithm's false-positive rate results, the false-positive rate of the improved evaluation function for the definition detection of surveillance video and noise detection is 4.44%, which is much lower than other evaluation functions. It can be seen that the improved algorithm is a reliable evaluation function of video definition and video noise.

#### Data Availability

The datasets used and/or analyzed during the current study are available from the corresponding author on reasonable request.

#### Conflicts of Interest

The authors declared no potential conflicts of interest with respect to the research, authorship, and/or publication of this article.

#### References

- [1] L. Xi, "Analysis of current situation and development trend of network video surveillance," *China Computer & Communication*, vol. 14, 2017.
- [2] F. Zhu, H. Y. Tian, Z. Y. Zhou, and Y. Q. Gong, "The full digitalization and development trend of video monitoring," *Science and Technology of West China*, vol. 2, 2011.
- [3] L. Q. Guo, "The application of the video surveillance technology in the mid-route of the south-to-north water," *Applied Mechanics & Materials*, vol. 170-173, pp. 2037-2042, 2012.
- [4] Z. Buchta, P. Jedlicka, M. Matejka et al., "White-light interference fringe detection using color CCD camera," in *AFRICON 2009*, Nairobi, 2009.
- [5] A. Schwarz, Y. Sanhedrai, and Z. Zalevsky, "Digital camera detection and image disruption using controlled intentional electromagnetic interference," *IEEE Transactions on Electromagnetic Compatibility*, vol. 54, no. 5, pp. 1048-1054, 2012.
- [6] Y. G. Sui, "Method for optimally controlling crossing vehicle signal under high definition video detection condition: CN, CN101976510 A," 2011.
- [7] D. Alonso-Caneiro, D. R. Iskander, and M. J. Collins, "Computationally efficient interference detection in videokeratometry images," in *2008 IEEE 10th Workshop on Multimedia Signal Processing*, Cairns, QLD, Australia, 2008.
- [8] Z. Rui, S. Zhang, and S. Yu, "Moving objects detection method based on brightness distortion and chromaticity distortion," *IEEE Transactions on Consumer Electronics*, vol. 53, no. 3, pp. 1177-1185, 2007.
- [9] L. V. Alphen and J. G. Lourens, "Detection of colour biases in video images," *IEEE Transactions on Broadcasting*, vol. 37, no. 2, pp. 69-74, 2002.
- [10] V. Zlokolica, V. Pekovic, N. Teslic, T. Tekcan, and M. Temerinac, "Video freezing detection system for end-user devices," in *2011 IEEE International Conference on Consumer Electronics (ICCE)*, Las Vegas, NV, USA, 2011.
- [11] R. Grbi, D. Stefanovi, M. Vranje, and M. Herceg, "Real-time video freezing detection for 4K UHD videos," *Journal of Real-Time Image Processing*, vol. 17, no. 5, pp. 1211-1225, 2020.



## Research Article

# Simulation Research on Risks of Entrepreneurship Platform Organization Complex Network

Chun Huang 

College of Business Administration, Zhejiang University of Finance and Economics, Hangzhou 310018, China

Correspondence should be addressed to Chun Huang; [huangchun2021222@163.com](mailto:huangchun2021222@163.com)

Received 27 September 2021; Accepted 15 November 2021; Published 27 December 2021

Academic Editor: Deepak Gupta

Copyright © 2021 Chun Huang. This is an open access article distributed under the Creative Commons Attribution License, which permits unrestricted use, distribution, and reproduction in any medium, provided the original work is properly cited.

The risks of entrepreneurship platform are considered one of the most significant factors that affect regional economic development. However, the complexity of the constitutive relationship and the dynamics of the research process have made it difficult for studies to analyse the evolution and risks from the quantitative perspective. According to the analysis perspective of complex networks, this study determined the coupling relationship between the entrepreneurship platform network structure and complex network model. With the results studied and described in the paper, this study had constructed a platform structure model portraying the evolution process of the platform structure under two types of risks by using the simulation method. Three main conclusions are being drawn from the study: Firstly, endogenous and exogenous risks showed substantial results in affecting the changes in microentities and network relationship of enterprises within the platform, causing the robustness of platform to risk to differ significantly. Secondly, based on exogenous risks, the robustness distribution scaling from highest to lowest among three types of platforms studied is hub-and-spoke > mixed > market. Lastly, based on endogenous risk, the robustness distribution scaling from highest to lowest among the three types of platform studies is market > mixed > hub-and-spoke.

## 1. Introduction

As a new form of network formation being generalised and commonly used by the majority in the market, platform organizations have now become a potential economic mover for resource integration and optimization [1–4]. Moreover, cluster entrepreneurship platform helps in enhancing the value of products by leveraging on its powerful sharing effects for building networks, speeding up the formation and growth of the organizations, reflecting on the influencing values of platform networks and organizations [5–7]. The Alibaba Group that pioneered the e-commerce industry in China has created a remarkable and sustainable success in leveraging the power of network formation by creating and managing a strong entrepreneurship platform for its users to utilise their respective business organizations within the platform itself. The company has enhanced the communication for business arrangements in B2B e-commerce market with simplified resource management processes and monetary transaction, and created a breakthrough in transforming

the traditional trading business model. However, as entrepreneurship platform produces positive results in network formations, it also increases the network risks in the system. For example, the bike-sharing industry in China is encountering decline in profitability and growth due to several frequent problems in platform-type enterprises, as evidenced by Ofo, Mobike, Wukong Bicycle, and Xiaoming Bike as representatives. In the Sino-US trade war, Huawei's 5G technology is a potential systematic risk in both global and domestic information technology industries, which might create uncertainties in the growth of industrial development. As such, it is necessary to conduct a comprehensive research investigation on the risks in entrepreneurship platform organizations and network, as there are lots of platforms available in the market today. This is to advocate a healthy development of sustainable industrial economy and markets.

Platform organization allows multiple connections to be built between users within a platform, fulfilling the user's needs and promoting more interactions among users that



create the much needed influential values. Theoretically, while entrepreneurship platform organization facilitates bilateral networking results and instant resources matching and business matching effects [5, 8–10], it also mirrors certain negativity as well. It may restrict businesses in a constraint relationship of vested interest, or prevent the enterprise from seeking a more effective external partner, thereby causing a certain measure of risks [3, 10–13]. Most of the studies inferred platform risk based on the external environment of platforms, such as macropolicies and market environment, and the internal environment of platforms (management risk, innovation risk, etc.). Unfortunately, scholars of these studies focused only on singular influencing factor to lay out potential platform risks in their evaluation. This is due to, firstly, the relationship structure among enterprises differing among platforms, and thus, the platform structures demonstrate significant differences. In addition, the complexity of the influencing factors in reality makes it difficult for researchers to extract general models and perform empirical studies on the overall network structure of the platform. Secondly, the structural growth of the platform network is a dependent variable of time, resulting in having more uncertainties to take place in real-time situation and unpredicted statistics to be shown. Due to the limitations in the existing research methods, it is challenging for researchers to produce accurate risk analysis from a quantitative perspective.

Organization network should be the structural basis of platform organization [5, 8]. Additionally, it also reflects on the internal structure of the platform organization as well as the relationship between businesses through network connection and contact referrals [3, 9]. Based on the abovementioned studies, this paper regarded the platform network structure as a complex network structure as discovered by Lee et al. [14]. Through the construction of a complex network structure model and simulation using computers, the robustness of distribution of platform risks can be obtained, in order to verify relevant propositions.

## 2. Platform Network Structures and Platform Risks

*2.1. Three Types of Platforms and Their Network Structures.* The current literature related to entrepreneurial platforms mainly includes corporate entrepreneurship and platform-based organizations. Corporate entrepreneurship refers to innovative behaviours such as the development of new services, technologies, and products that are carried out within the firm [15]. Platform-based organizations are easy to achieve rapid business growth and scale up and can respond to the environment and market with agility, and high-speed innovation behaviours are done through low-cost trial and error, giving the company to develop new competitive advantages [16]. The concept of entrepreneurial platform is closely related to the more developed literature on the entrepreneurial ecosystem. The two concepts both try to explain how system conditions influence actors' entrepreneurial agency to create value [17]. Markusen [18], who had studied the industrial districts of various countries, proposed that

industrial platforms can be divided into four different types: marshallian, hub-and-spoke, satellite, and state-anchored platform. Years later, when more researches had been conducted, Evans [19] divided it into market-makers, audience-makers, and demand-coordinators. However, in today's urbanised society, reality has proven that platforms can be a hybrid of centralised types, or they may now belong to one and over time become the other. For the use of metricsm, this paper used two indicators as the criteria for categorizing platform functions: "reciprocity" was used to depict the network effect for value cocreation within the platform network achieved through bilateral/multilateral cooperation, whereas "heterogeneity" was used to depict the equivalence of enterprise cooperation within the platform. In several literatures, it can be found that Jacobides et al. have also used similar indicators to depict platform characteristics [1, 20–22]. It is viable then that we explore based on the internal network structure of the platform, specifically categorising them based on the standards laid in the references mentioned; the theories and research description have been concluded and reviewed accordingly, leading us to study in this paper, on platforms with three respective types: market-based [19, 23], hub-and-spoke [24, 25], and mixed platforms [26].

For market-based entrepreneurship platform, each enterprise uses peer-to-peer partnership to cocreate value through horizontal connections, to achieve bilateral/multilateral win-win. The heterogeneity is low, and therefore, the equivalence of enterprise within the platform is high; the overall network effect of the platform is relatively weak.

For hub-and-spoke entrepreneurship platform, this platform is established using platform-type enterprise as the core and other enterprises as the periphery. Platform-type enterprise is the resource agglomeration point and a central position, whereas the other enterprises are peripheral and mainly obtain resources like platform fund, professional technology, or dedicated information service through the platform. The enterprise–platform-type enterprise cooperation within this platform has high stability and strong network effect.

For mixed entrepreneurship platforms, this platform is between the market-based and hub-and-spoke platforms thus having the characteristics of both platforms. The enterprise heterogeneity within this platform is moderate; moreover, the multilateral characteristic of its platform enterprise partnership is significant, and the equivalence and network effect are moderate.

A comparison between the types of entrepreneurship platform structure is given in Table 1.

*2.2. Offensive Nature of Two Entrepreneurship Platform Risks.* The main types of entrepreneurship platform risks include endogenous and exogenous risks [27]. The endogenous risk refers to the risk accumulated by the internal forces of the platform such as network risks [11–13, 27]. It takes the organization and network built within the platform and the collection of such data as research subject, or in simpler terms, it takes the relationship between enterprises and businesses in the platform as the research subject, and

TABLE 1: Comparison of three types of entrepreneurship platform network structure.

Indicator	Platform type		
	Market-based entrepreneurship platform	Hub-and-spoke entrepreneurship platform	Mixed entrepreneurship platforms
Heterogeneity	Low	High	Moderate
Reciprocity	Low	High	Moderate

TABLE 2: Characteristics of the two platform risk types.

Risk type	Characteristics		
	Properties	Object of action	Mode of action
Endogenous risk	Microscopic entities	Platform-type enterprise	Specific
Exogenous risk	Macroscopic population	Platform enterprise	Random

studies the microscopic entities so as to particularly understand further the risks exist from within the platform. For example: Jing and Benner [28] believed that a negative effect of the network organization in platforms would be generated during the development and expansion of platform due to restrictive and limited use of information and other resources, affecting the business collaboration and cooperation within the platform [29] and surfacing higher and more risks in general. As we observed in recent research reports, research on endogenous risks is giving much focus to the cyber risks caused by microindividuals, especially those caused by platform-based companies, which often referred as “self-fertility.” Concrete evidence would be this: the risks of platform enterprises such as the Zhonghuatai Automobile, Lifan Automobile, Zhongtai Automobile, etc. have led to the rise of the new energy vehicles (NEV) risks. This is in addition to the quake of the Chinese photovoltaic industry caused by the collapse of the Suntech platform photovoltaic company in Wuxi back in 2013.

Exogenous risk refers to the risk caused by external forces of the platform, including structural and periodic risks [30]. Exogenous risk is caused by the external forces that affect the overall progress and performances of the platforms, which include the economic and political changes termed as cyclical risks. Not to forget that the life cycle of platforms is the structural risk that is part of the consideration as the commonly faced by enterprises within the platforms are important information to the study in order to objectively analyse the overall platform risks truthfully. Fritz et al. studied the risk caused by periodic fluctuation in the external economy, while Wu and Han [31] studied the platform risk caused by changes in macropolicies. Taking the integrated circuit and television industries in Japan as an example, Zhu [32] studied the problem of the decline of the industrial competitiveness due to changes in the lifecycle of platform core technology in the industry. The characteristics of the two platform risks are as listed in Table 2.

As we understood from the recent literature, it can be clearly seen that exogenous risks are paying much concern on the overall risks of cluster entrepreneurship platforms, especially network risks caused by cluster entrepreneurship platform system risks that occur after the overall macroimpact. For instance, the financial crisis that happened in 2008 has led to the decline of the textile industry in Shaoxing

County of Zhejiang, China. Looking at the cluster size of such industry, the total output value of the textile industry in Shaoxing County had exceeded 100 billion yuan in 2008, and the percentage increase in the output value from 5.53% in 2006 to 34.76% in 2007. However, the growth rate has declined sharply since 2008 as it dropped to -29.41% in 2009. In contrast, in analysing the cluster benefits, the total profit and tax increased from 4.302 billion yuan in 2005 to 6.118 billion yuan in 2007. The percentage for total profit and tax increased rapidly from 5.53% in 2006 to 34.76% in 2007 and fell drastically to -13.95% in 2009 [33, 34]. To illustrate the data described better, Figure 1 shows the changes in the scale of the output value in percentage, while Figure 2 shows the changes in the scale of the increase in profit and taxes in percentage, both figures showing the changes in graph range between 2005 and 2009.

*2.3. Robustness Analysis of Risks of the Three Types of Entrepreneurship Platform.* Different entrepreneurship platforms differ in structures. Therefore, observing and analysing the risks of network structure are vital as it is an important indicator that differentiates between various types of entrepreneurship platforms, and it represents the connection mode between individuals, including network connections, network configuration, and layout (with special attention to describing connection forms in terms of density, connectivity, and hierarchy) [35]. Structural differences have an important impact on entrepreneurship platform development. Wang [36] from Dongguan’s IT industry believed that low-density network structures are not conducive to the development of cluster entrepreneurship platforms, while Shi [37] who did a research Wenzhou’s light industry confirmed that high-density network structure is the main cause of the platform’s dilemma. Though there have been scholars commenting on the risks analyses on network structures, it is not sufficient to understand the current changes in the high digital evolution of network structures and platforms performing in the demands today and the risk robustness of various platforms. In fact, very few literatures have reported and compared the risk robustness of different types of platforms. Nonetheless, there are still some useful insights that we can discover from the case studies in existing literature as we look more in-depth into the matter. This can be better understood in referring to a recent study done by a

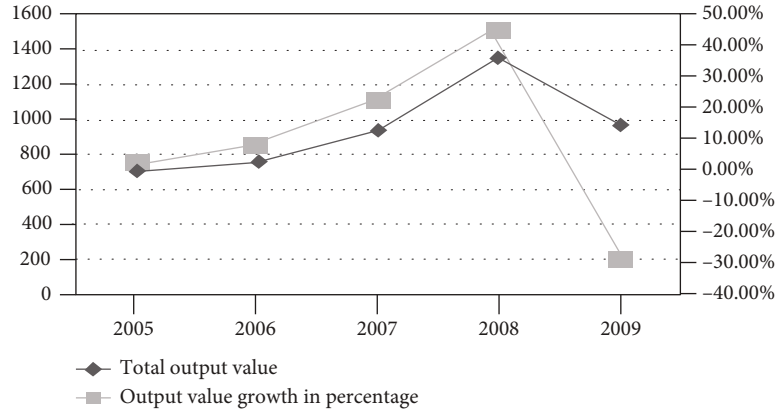


FIGURE 1: The changes in scale of the total output value of textile industry in Shaoxing County, Zhejiang by percentage, between 2005 and 2009.

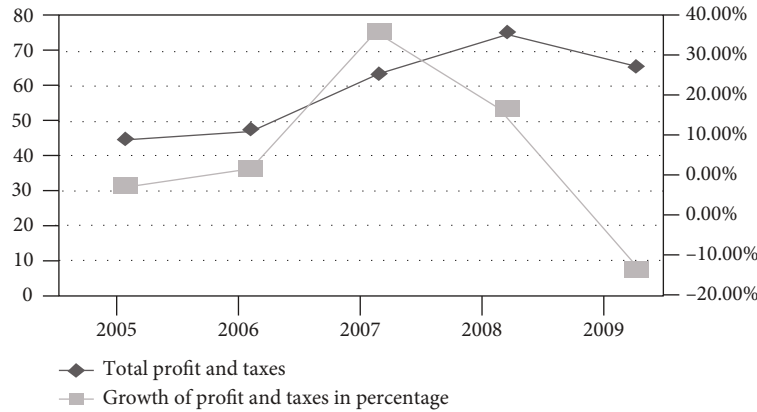


FIGURE 2: The changes in scale of the increase in profit and taxes of textile industry in Shaoxing County, Zhejiang by percentage between 2005 and 2009.

Chinese scholar, Yu [38] who had considered two Chinese household appliances industry platforms: Qingdao, a household appliance industry platform (an industrial hub-and-spoke platform that uses the platform-type enterprise Haier), as the core, and Ningbo, another household appliance industry platform, (an industrial market-based platform based on the cooperation of household electrical appliances association and several small and medium platform enterprises) as the research object. In the depiction of the two platforms, Yu found that Qingdao was less affected by exogenous risk when foreign household appliances entered the domestic market in mass in the 1990s, whereas Ningbo household appliance industry platform became more successful after experiencing an endogenous risk, that is, the emergence of digital television, a new technology [39]. Another similar research was reported by Morgan [40], where the research analysed the differences in network risk across various platforms in risk perspectives.

Encouragingly, in another study conducted much earlier by a Western scholar, Saxenian took two high-tech industrial regions in the United States—namely, Silicon Valley [40], a mixed entrepreneurship platforms consisting of platform-type enterprises such as Fairchild, Intel, and Texas Instruments and many small and medium start-up enter-

prises, and Route 128, a hub-and-spoke-platform that mainly consists of large platform-type enterprises such as Wang Laboratories and Massachusetts Institute of Technology, to evaluate the platform risks between the two based on their platform structures. In its depiction of the two entrepreneurship platforms, the author found that Route 128 was less affected by exogenous risk, which is the effect of the Japanese semiconductor industry on the US electronics industry towards the end of the 1970s, as compared to Silicon Valley [40], whereas Silicon Valley was more successful than Route 128 after experiencing an endogenous risk, where the US electronics industry shifted from semiconductors to microcomputers. After further portraying the network structure of the two entrepreneurship platforms, Acebrón et al. concluded that the two platforms differ in robustness to risk at different stages [41].

Based on the understanding from the literature mentioned above, we can conclude two different results of risks robustness as compared in its respective different situations as the following:

- (1) Hub-and spoke entrepreneurship platform has higher exogenous risk when compared to market-based and mixed platforms

- (2) Hub-and-spoke entrepreneurship platform has lower endogenous risk when compared to market-based and mixed platforms

Therefore, we can draw a few potential rationale and solutions to the risks described above. First of all, in the accord of taking different types of entrepreneurship platform as the subject of study, the construction of the overall network structure requires a large amount of sample data. Next, the risks and attack processes are dynamically faced in all three different entrepreneurship platforms, and thus, sufficient timespan for observation must be established in order to develop reliable evaluation. Another reason is that it is challenging to identify the victim of attacks in the platform as well as to observe the intensity of the attacks when happened in real time, making it tougher to study the overall effects of the overall attacks and risks on the platform. Consequently, the accuracy to describe the risks dynamics on platform network structure is challenged, and it is hard to be analysed quantitatively using the conventional research methods that we are familiar with. It is not only reflected in the data collection and analysis; the shortcomings of the indicator descriptions and model constructions are also echoed. Therefore, in this paper, we had used complex network theory to analyse different entrepreneurship platform types as defined, while constructing a macroscopic perspective by studying through the specific behaviours in the micro-entities, so as to effectively identify variables for detailed quantitative study of risks in entrepreneurship platform organization.

### 3. Research Design

Based on the complex network perspective, the network structure within the entrepreneurship platform consists of nodes (representing the enterprises within the platform) in the network and network edges (representing the relationship between the enterprises). With these nodes and edges, the platform reveals cluster, nonlinearity, and interaction characteristics between the heterogeneous entities and portrays them through resource sharing, open information, knowledge interaction, multilateral network effects, cocreation, and the complex relationship between behavioural entities and structural evolution [3, 18, 42–44]. There have been researches done by other scholars who observed the changes in activities of variables in constructing a dynamic network model, such as the degree distribution, mean path length, clustering coefficient, and network density. There are also other scholars who had analysed the cause of one or malfunctions of one or more nodes in relative effects of other nodes and edges, and how the transmission of the malfunctioning affects the whole network chains, resulting in the collapse in the entire network [45].

In this study, we observed the coupling relationship between the structure of the entrepreneurship platform network and complex network, so as to identify several network metrics that is commonly used, such as degree distribution, mean path length, and relative value of maximal connected subgraph for portraying platform network and risks. Also,

Lagrange method was used in our model, because this method can obtain dynamic equations from the dynamic equations from the view of energy, which does not need to calculate the internal force. The calculation will be convenient. With these, we established here a research model for all as reference in analysing the entrepreneurship platform network structure.

**3.1. Relevant Attribute Indicators.** To ensure the validity and reliability of the measuring tools, this study had used the most common indicators in the complex network theory and supplemented it appropriately according to the research objectives for this computer simulation research.

**3.1.1. Degree Distribution ( $P$ ).** The degree of node  $i$ ,  $k_i$  is the number of nodes that node  $i$  is connected to. The degree distribution of the nodes in the network can be portrayed using distribution function  $P(k)$ , which represents the probability that the degree of a randomly selected node is  $k$ .

$$P_k = \sum_{k'=k}^{\infty} P(k'). \quad (1)$$

The formula represents the probability distribution of nodes with degree  $\geq k$ . Degree distribution reflects the overall structure of the network; the higher the degree distribution of few nodes, the more uneven is the network structure, and the higher the homogeneity of the degree distribution between nodes, the more even is the network structure.

**3.1.2. Mean Path Length ( $L$ ).** The distance  $d_{ij}$  between two nodes  $i$  and  $j$  in the network is defined as the shortest path length connecting these two nodes. The mean path length  $L$  of the network is defined as the average distance between any two nodes, that is,

$$L = \frac{1}{(1/2)N(N-1)} \sum_{i \geq j} d_{ij}, \quad (2)$$

where  $N$  is the number of nodes in the network, without considering the distance between node and self. In the network, there are multiple paths between nodes  $i$  and  $j$ , cutting some of the paths may increase the distance  $d_{ij}$  between these two nodes; simultaneously, the mean path length  $L$  of the entire network will also be increased.

**3.1.3. Relative Value of Maximal Connected Subgraph ( $G$ ).** This parameter measures the number of nodes in the maximal connected subnetwork in the network after eliminating the malfunctioning nodes. The relative value  $G$  of the maximal connected subgraph is defined as

$$G = \frac{N'}{N}, \quad (3)$$

where  $N'$  represents the number of nodes included in the maximal connected subgraph of the network after ending

TABLE 3: Coupling evaluation of the ER model and market-based platform.

Model	Properties	
	Property 1	Property 2
ER model	Even degree distribution	Connected probability
Market-based platform	High commonality	Low reciprocity

TABLE 4: Coupling evaluation of the BA model and hub-and-spoke platform.

Model	Properties	
	Property 1	Property 2
BA model	Has “large” nodes with higher connectivity	Preferential attachment
Hub-and-spoke platform	Low commonality	High reciprocity

the malfunction. The parameter  $G$  denotes the network performance.

*3.2. Research Model Establishment.* This study first analysed the network characteristics of market-based, hub-and-spoke, and mixed platforms, bringing forth the analyses to perform coupling comparison with classic complex network models, namely Erdős-Rényi (ER) model [46], Barabási-Albert (BA) model [47], and local-world evolving network model. Subsequently, through the connection rules of various models, this study used computer simulation model to construct the network structure of the three platforms.

- (i) MP-ER model (Table 3 shows the market-based platform and ER model): ER model is a completely random network, it was developed by Erdős and Rényi [46], and the degree distribution of the network nodes is approximated by the Poisson distribution. The model has two significant properties:

- (1) The degree distribution tends to become average
- (2) The edging connection between nodes occurred as probabilistic events

This study coupled the network structure of the ER model with the market-based platform network structure (MP-ER model). The probability of new entrant enterprises connecting to original enterprises in the MP-ER model is

$$\prod_i = \frac{1}{N(t)}, \quad (4)$$

where  $N$  is the total number of enterprises at time  $t$  (i.e., the total number of network nodes).

- (ii) HP-BA model (Table 4 shows the hub-and-spoke platform and BA model): BA model is a scale-free network model proposed by Barabasi and Albert [47]. The network connection degree distribution

function has a power-law form; it has two significant properties:

- (1) Growth characteristics (i.e., the scale of the network is constantly expanding)
- (2) Preferential attachment characteristics (i.e., new nodes tend to connect to “large” nodes with higher connectivity) [47]

This study coupled the network structure of BA model with hub-and-spoke platform network structure (HP-BA model). The probability of new entrant enterprises connecting to original enterprises in the HP-BA model is

$$\prod_i = \frac{k_i}{\sum_j k_j}, \quad (5)$$

where  $k_i$  and  $k_j$  denotes the degree of nodes  $i$  and  $j$ , respectively.

- (iii) SP-LN model (Table 5 shows the satellite model and local-world evolving network model): The local-world evolving network model is an improvement of the BA scale-free network model; it was proposed by Li and Chen [48]. Each node has its own local-world (local and world is connected by probability); therefore, it only occupies or uses the local connectivity information of the network. The model has two significant properties:

- (1) Growth (i.e., the scale of the model is constantly expanding)
- (2) Local-world preferential attachment (i.e., new nodes connect to specific nodes to form local world)

This study coupled the network structure of local-world evolving network model and mixed platforms network structure (SP-LN model). The probability of new entrant



TABLE 5: Coupling evaluation of the local-world evolving network model and mixed platforms.

Model	Properties	
	Property 1	Property 2
Local-world evolving network model	Preferential attachment within the local world	Local and world is connected by probability
Satellite model	Hub-and-spoke platform characteristics	Market-based platform characteristics

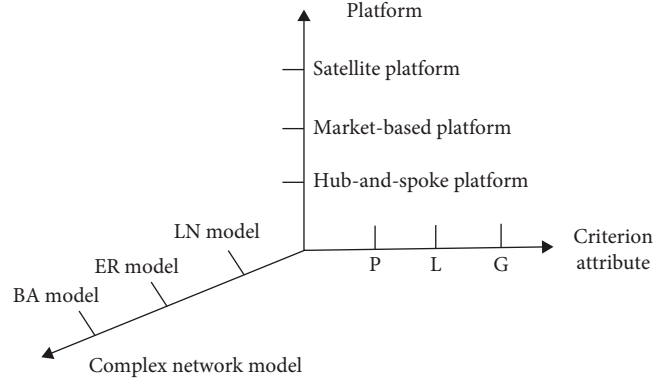


FIGURE 3: Construct diagram of the theoretical model.

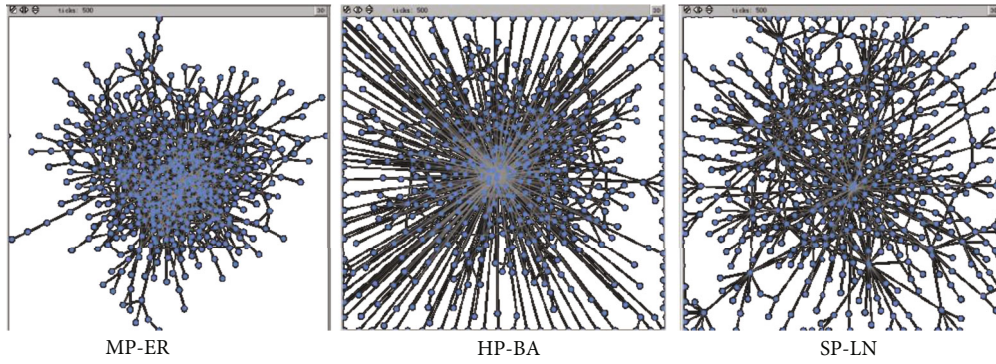


FIGURE 4: Platform network structure model (simulation; 500 agents in random connection).

enterprises connecting to original enterprises in the SP-LN model is

$$\prod_{\text{Local}} (k_i) = \frac{M}{m_0 + t} \frac{k_i}{\sum_{j \in \text{Local}} k_j}, \quad (6)$$

where  $M$  denotes the selection of  $M$  number of nodes from among the existing nodes in the network ( $M \geq m$ ) as the local-world of the new nodes,  $m_0$  is the initial number of nodes in the network,  $k_i$  is the degree of node  $i$ , and  $k_j$  is the degree of node  $j$ .

Figure 3 presents the simulation diagram of the three model simulations. We had used simulation to first distinguish the network structure of each of the three platforms and thus established the three models: MP-ER, HP-BA, and SP-LN models (as shown in Figures 4 and 5). We assumed that the enterprises within the platform were connected through the enterprise relationship. The platform network under normal circumstances operated in a free-

flow state [49], and it remains an undirected graph, regardless of the intensity of the relationship between the enterprises; that is, the weight between the connected edges is equal. In place of the effort aimed in constructing a specific concrete model, we started by constructing a network with an initial node, and following each platform's network structure to connect nodes based on the connection probability rules, and each time a node is added, until 500 nodes were reached.

#### 4. Result Analysis and Discussion

We had compared the evolution of network structure of the three models using computer simulation to study how risks are evaluated with attacks and obtained the distribution of risk robustness of different platforms as it developed throughout the process (Figure 6 shows the details). There are two attack strategies adopted in this study: random attack and deliberate attack. Random attack involves removing nodes in the network completely randomly; in the



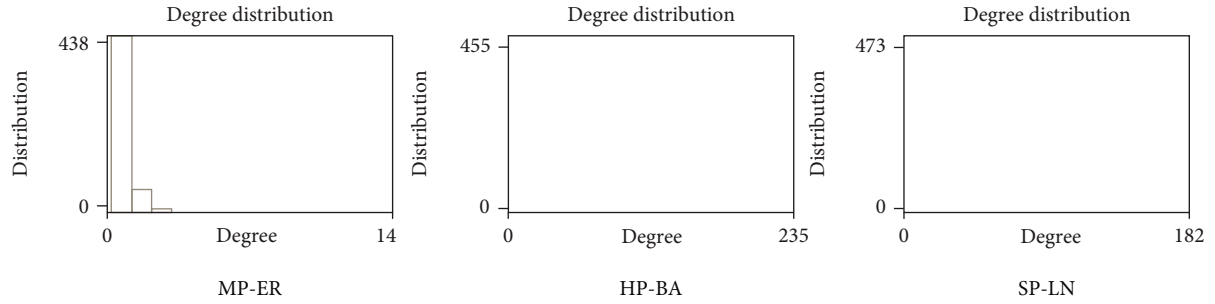


FIGURE 5: Degree distribution of platform network structure model (simulation; 500 agents in random connection).

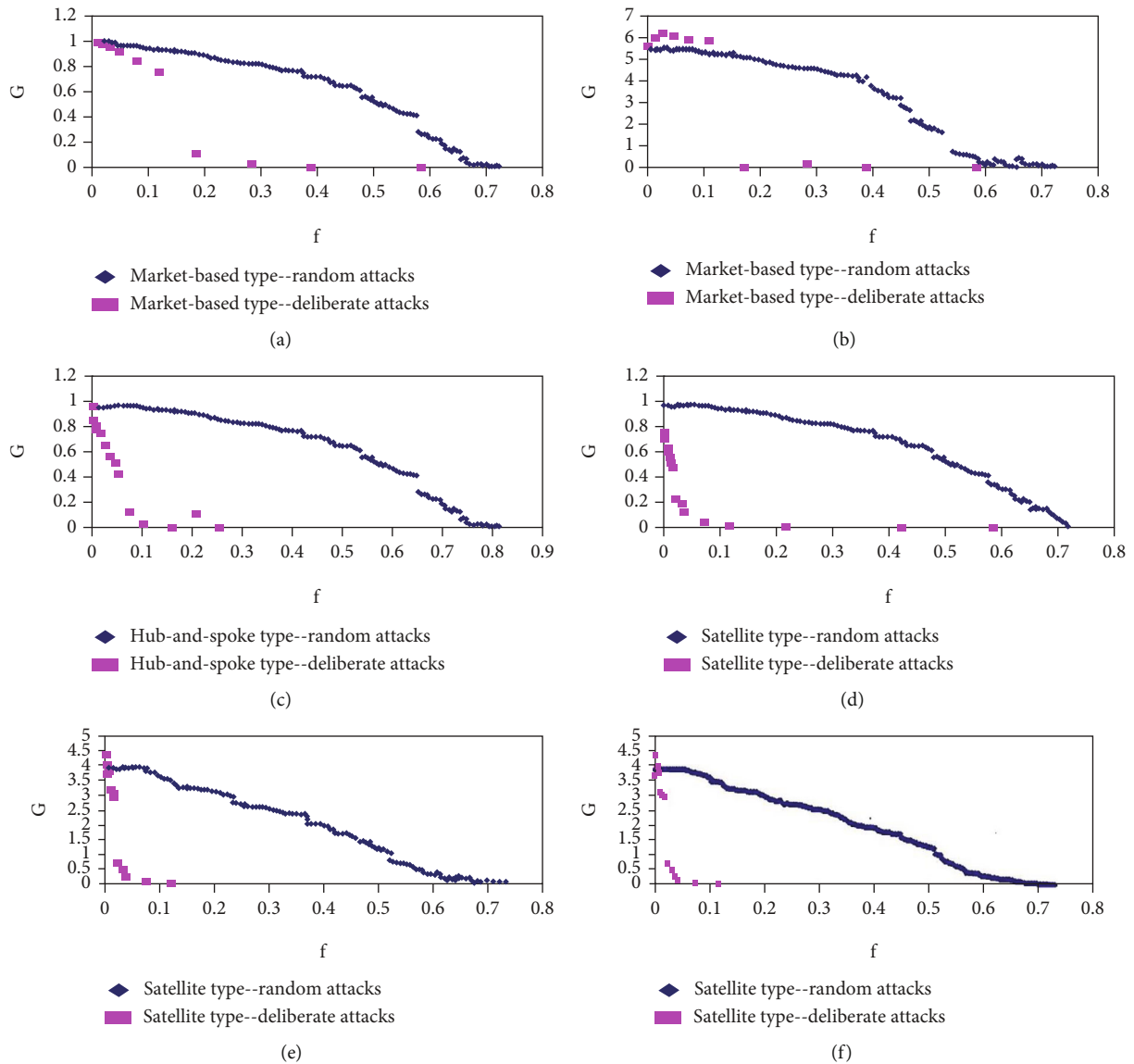


FIGURE 6: Robustness and vulnerability of the MC-ER, CC-BA, and IC-LN models. Note: curves (a) and (b) correspond to the MC-ER model, (c) and (d) to the CC-BA model, and (e) and (f) to the IC-LN model; in all curves; triangles and squares correspond to deliberate and random attacks, respectively.

current experiment, only one node was attacked at a time. Deliberate attack involves removing the nodes with the highest degrees in the network consciously and gradually; in the current experiment, each attack targeted all nodes to the

same extent. Simultaneously, the attacked node and the edges that connected the node to other nodes were removed, until the connectivity of the entire network became zero. Assuming that the ratio of the number of removed nodes

to the original total number of network nodes was  $f$ , the relationship between  $f$  and the relative value of the maximal connected subgraph  $G$  and the mean path length  $L$  can be used to measure the robustness of the network. The simulation results are as follows.

*4.1. Model Evolution Simulation.* The relative value of maximal connected subgraph reflects the overall connectivity of the network. The speed of change of connected subgraph can reflect, on a certain level, the robustness of the model after attack. The three maximal connected subgraph diagrams of Figure 5 illustrate that under the circumstances of other conditions being identical, the development process and the results of the three models differed significantly.

- (i) Random attack: the maximal connected subgraphs of MP-ER model was the first to reach zero, followed by the SP-LN model, and finally, the HP-BA model. Thus, under random attack, the robustness comparison of the three models is HP-BA model > SP-LN model > MP-ER model
- (ii) Deliberate attack: the maximal connected subgraphs of HP-BA model was the first to reach zero, followed by SP-LN model, and finally, the MP-ER model. Thus, under deliberate attack, the robustness comparison of the three models is MP-ER model > SP-LN model > HP-BA model

Another observation that we can draw from the study is that the mean path length reflects the network connectivity efficiency. The change in length of the mean path length can reflect the robustness of the model after an attack at certain level. The three mean path length diagrams of Figure 5 demonstrated that under the circumstances of other conditions being identical, the evolution process and results of the three models differed significantly

- (i) Random attack: the mean path length of the MP-ER model was the first to reach zero, followed by the SP-LN model, and finally, the HP-BA model. Thus, under random attack, the robustness comparison of the three models is HP-BA model > SP-LN model > MP-ER model
- (ii) Deliberate attack: the mean path length of the HP-BA model dropped to zero after a relatively high  $f$ , followed by the SP-LN model, and finally, the MP-ER model. Simultaneously, the mean path length of the HP-BA model was the first to reach zero, followed by the SP-LN model, and finally, the MP-ER model. Thus, under deliberate attack, the robustness comparison of the three models is MP-ER model > SP-LN model > HP-BA model

#### 4.2. Entrepreneurship Platform Risk and Structural Evolution Analysis

*4.2.1. Entrepreneurship Platform Risk and Structural Evolution.* As shown with the analysis study that is conducted and discussed above, we can now better understand

TABLE 6: Comparison of robustness of platform to risks.

Risk type	Platform type		
	Market-based	Hub-and-spoke	Satellite
Endogenous risk	Strong	Weak	Moderate
Exogenous risk	Weak	Strong	Moderate

that endogenous risk uses a specific mode of action on the microenterprise entities within the entrepreneurship platform. Therefore, deliberate attacks can be considered a manifestation of the endogenous risk. The exogenous risk uses a random mode of action on the macroenterprises within the platform. In other words, random attacks can be regarded as a manifestation of exogenous risk. The two types of risk could affect the changes in the microscopic entities of enterprises and network relationships within the platform, which led to the development of the platform network structure. In the model studied, the changes in the microscopic entities of enterprises within the platform are manifested in the form of attacks on the network nodes, that is, changes in the relative value of maximal connected subgraph. The changes in network relationship are manifested as attacks on the network edges, that is, changes in the mean at the shortest path. Thus, we can conclude that the model characterises the evolution of the entrepreneurship platform structure through two indicators: the maximum number of connected subgraphs and the average shortest path.

*4.2.2. Entrepreneurship Platform Risk Robustness Comparison.* The evolution process and results of entrepreneurship platform network structure are different, causing significant differences in the platform risk robustness. According to the analysis of the relative value of maximal connected subgraph and mean path length, this study considers that when platform networks are subjected to exogenous risk (random attack), market-based platform is highly vulnerable to random attack, hub-and-spoke platform has high robustness, and mixed platforms falls in-between the two. Thus, the robustness distribution of the three platforms is as such hub-and-spoke platform > mixed platforms > market-based platform. When platform networks are subjected to endogenous risk (deliberate attack), hub-and-spoke platform is highly vulnerable to deliberate attack, market-based platform has high robustness, and mixed platforms falls in-between the two. Therefore, the robustness distribution of the three platforms is market-based platform > mixed platforms > hub-and-spoke platform (Table 6 shows the details).

*4.2.3. Analysis of Comparison Results.* This article applies the complex network theory to the description of the entrepreneurship platform network structure and implies the reality scenarios at global states based on the ER and BA models, aimed at clearly defining the internal network composition relationship of the three types of entrepreneurship platforms and distinguish the variation of platforms. The network structure provides a new perspective for the application of complex network theory in platform research. In distinguishing between two types of risk situations, endogenous

risk and exogenous risk, the two types of attack strategies (random attack and deliberate attack) of network failures generated in complex network theory are organically combined with platform risks to distinguish the two. Using the dynamic perspective to treat the entire process of cluster risk as a function of time, it is concluded that the break in the network relationship between the network node enterprise and other enterprises is the root cause of platform risk, thus laying a foundation for quantitative description of platform risk.

Consequently, we can now draw a few significant conclusive understandings of the analysis study to better describe the risk performance of the platform network organization and structure. First, the high robustness of hub-and-spoke platform against random attacks originating from the extreme unevenness of the degree distribution of the network nodes; that is, a small number of nodes had relatively large degree, and most of the nodes had very small degree. When  $f$  is smaller, the randomly selected nodes were nodes with smaller degree, and the elimination of these nodes will not have a large effect on the connectivity of the network. However, this extreme jaggedness made the hub-and-spoke platform highly vulnerable to deliberate attacks; the attacks gradually removed the largest nodes in the network and had strongly affected the connectivity of the network.

Next, the high robustness of market-based platform against deliberate attacks originating from the high evenness of the degree distribution of the network nodes; that is, most of the nodes had similar degree. The gradual removal of the largest nodes in the network during the attacks did not have much of an effect on the connectivity of the network. However, this high evenness made market-based platforms relatively vulnerable to random attacks.

Lastly, the moderate robustness of mixed platforms against random attacks and deliberate attacks are attributable to the properties of local-world connection and moderate degree distribution of the network nodes; therefore, regardless of the type of attack, its robustness will always fall in-between that of the other two platforms.

## 5. Conclusions

As a complex network system, the interrelationship caused by platform risk in the evolution process of network structure is extremely complex and changeable. Therefore, quantitatively analysing the entrepreneurship platform network structure from a dynamic perspective to determine the robustness and vulnerability of the three platforms to risks is a field that is theoretically worthy of exploration. With the conduct of simulation, we have showed a result using quantitative research on the dynamic evolution of the model under different attack strategies, followed by an examination of the robustness and vulnerabilities of different platforms to risks; the following main conclusions were obtained:

- (1) Deliberate and random attacks can be considered the manifestations of endogenous and exogenous attacks, respectively. These two risks affected the

enterprise entities and the relationship between enterprises within the platform, leading to the evolution of platform network structure; however, the differences in evolution process and the corresponding results made the robustness distribution of platform risk vary

- (2) When a platform network was subjected to exogenous risk (random attack aimed at all the enterprises within the platform), the robustness distribution of the three platforms was central satellite > satellite > market-based
- (3) When a platform network was subjected to endogenous risk (deliberate attack aimed at focus enterprise within the platform), the robustness distribution of the three platforms was market-based > mixed satellite > central satellite

Our study makes several novel contributions. Firstly, our study incorporates complex network theory and platform network structure in the investigation of ER and BA platform networks' evolution. Our simulation model inspects the internal network composition relationship of the three entrepreneurship platforms and distinguishes the network structure of different types of platforms. Thus, this study has successfully provided a new perspective on the application of complex network theory in platform research. Secondly, our study endogenous and exogenous risks were distinguished, while random and deliberate attack strategies for network failure were generated in complex network theory with entrepreneurship platform network risk to distinguish the essence of attack of the two types of platform risks. Thirdly, we adopted the dimension of dynamic perspective. To gain a more complete picture, we call for investigating how the relationship between the enterprises within the platform evolve in different levels of dynamism that are characterised by different levels and combinations of robustness and vulnerability dimensions of platform risk.

Our paper provides several avenues for future research. Firstly, our model is relatively different from the actual entrepreneurship platform structure. Future studies could conduct more in-depth discussion from the following three aspects. The first aspect is the expansion and improvement of the theoretical model. Not only do different types of risks have different effects on the platform, even the same risk could affect the platform differently. Secondly, this study is specifically focusing on different types of risks, however, in terms of investigating possible ways to improve the model reflecting the effects of different risks attack intensities on the three entrepreneurship platforms shall be reported in future papers for this study. The second aspect is the problem of research subject matters. Platform risks affect not only enterprises but also the relationship between enterprises; in complex network theory, this can be reflected by the change in nodes; it can also be reflected by the connection of the edges. Moreover, the load and capacity of different nodes are different, and the robustness to risk is also different. The difference in connection strength, connection mode, and connection direction also manifested differently

to risk. The effect of this type of change between the two on the model is also a problem that requires further research. At last, this study only conducted a simulation experiment based on the theoretical models. We suggest that future studies should select empirical cases corresponding to the three types of entrepreneurship platforms as the research subject, analyse the network structure, perform evolution experiment on this basis, and track actual cases on long-term basis for dynamic study of comparative analysis.

## Data Availability

The datasets used and/or analysed during the current study are available from the corresponding author on reasonable request.

## Conflicts of Interest

It is declared by the author that this article is free of conflict of interest.

## Acknowledgments

This work was supported by the Project of Zhejiang Philosophy and Social Planning under Grant Number 18NDJC146YB and Number 22YJRC09ZD-1YB.

## References

- [1] T. R. Eisenmann, G. Parker, and M. W. Van Alstyne, "Strategies for two sided markets," *Harvard Business Review*, vol. 84, no. 10, 2006.
- [2] A. Gawer and M. A. Cusumano, "Industry platforms and ecosystem innovation," *Journal of Product Innovation Management*, vol. 31, no. 3, pp. 417–433, 2014.
- [3] D. P. McIntyre and A. Srinivasan, "Networks, platforms, and strategy: emerging views and next steps," *Strategic Management Journal*, vol. 38, no. 1, pp. 141–160, 2017.
- [4] Y. Chao and T. Derdenger, "Mixed bundling in two-sided markets in the presence of installed base effects," *Management Science*, vol. 59, no. 8, pp. 1904–1926, 2013.
- [5] K. J. Boudreau and L. B. Jeppesen, "Unpaid crowd complementors: the platform network effect mirage," *Strategic Management Journal*, vol. 36, no. 12, pp. 1761–1777, 2014.
- [6] F. Zhu and M. Iansiti, "Entry into platform-based markets," *Strategic Management Journal*, vol. 33, no. 1, pp. 88–106, 2012.
- [7] D. B. Yoffie and K. Mary, "With friends like these: the art of managing complementors," *Harvard Business Review*, vol. 84, no. 9, 2006.
- [8] C. Cennamo and J. Santalo, "Platform competition: strategic trade-offs in platform markets," *Strategic Management Journal*, vol. 34, no. 11, pp. 1331–1350, 2013.
- [9] F.-B. Wang, X. P. Wang, and C. Zhang, "Ultra-modular architecture in platform and customized support for intrapreneurship: an embedded case study of Haier's transformation to platform organization," *Management World*, vol. 35, no. 2, pp. 121–150, 2019.
- [10] J. C. Rochet and J. Tirole, "Tying in two-sided markets and the honor all cards rule," *International Journal of Industrial Organization*, vol. 26, no. 6, pp. 1333–1347, 2008.
- [11] D. Acemoglu, A. E. Ozdaglar, and A. Tahblaz-Salehi, "Systemic risk in endogenous financial networks," *SSRN Electronic Journal*, pp. 15–17, 2015.
- [12] C. Aymanns and C. P. Georg, "Contagious synchronization and endogenous network formation in financial networks," *Journal of Banking & Finance*, vol. 50, pp. 273–285, 2015.
- [13] H. Dewachter and R. Wouters, "Endogenous risk in a DSGE model with capital-constrained financial intermediaries," *Journal of Economic Dynamics & Control*, vol. 43, pp. 241–268, 2014.
- [14] E. Lee, J. Lee, and J. Lee, "Reconsideration of the winner-take-all hypothesis: complex networks and local bias," *Management Science*, vol. 52, no. 12, pp. 1838–1848, 2006.
- [15] F. J. van Rijnsvoever, "Meeting, mating, and intermediating: how incubators can overcome weak network problems in entrepreneurial ecosystems," *Research Policy*, vol. 49, no. 1, pp. 138–157, 2020.
- [16] E. G. Carayannis, M. Provance, and E. Grigoroudis, "Entrepreneurship ecosystems: an agent-based simulation approach," *Journal of Technology Transfer*, vol. 41, no. 3, pp. 631–653, 2016.
- [17] A. Cavallo, A. Ghezzi, and R. Balocco, "Entrepreneurial ecosystem research: present debates and future directions," *International Entrepreneurship and Management Journal*, vol. 15, no. 4, pp. 532–560, 2019.
- [18] A. Markusen, "Sticky places in slippery space: a typology of industrial districts," *Economic Geography*, vol. 72, no. 3, pp. 293–313, 1996.
- [19] D. S. Evans, "Governing bad behavior by users of multi-sided platforms," *Berkeley Technology Law Journal*, vol. 27, pp. 1201–1250, 2012.
- [20] M. G. Jacobides, C. Cennamo, and A. Gawer, "Towards a theory of ecosystems," *Strategic Management Journal*, vol. 39, no. 8, pp. 2255–2276, 2018.
- [21] N. J. Foss and T. Saebi, *Business Model Innovation: The Organizational Dimension*, OUP Oxford, 2015.
- [22] V. Agarwal, S. Goyal, S. Mittal, and S. Mukherjee, "MobVine: a middleware layer to handle fragmentation of platform interfaces for mobile applications," in *Proceedings of the 10th ACM/IFIP/USENIX International Conference on Middleware (Companion)*, p. 24, Urbana Illinois, USA, 2009.
- [23] P. Ballon, "The platformisation of the European mobile industry," *Communications and Strategies*, vol. 75, pp. 15–34, 2010.
- [24] G. Parker and M. Van Alstyne, "Innovation, openness & platform control," in *Proceedings of the 11th ACM Conference on Electronic Commerce*, pp. 95–96, Cambridge Massachusetts, USA, 2010.
- [25] H. J. Xiao and P. Li, "Ecological governance of platform enterprises' CSR," *Management World*, vol. 35, no. 4, 2019.
- [26] X. H. Zhu, H. S. Chen, and T. Zhang, "Iterative innovation in the construction of platform-based enterprises in the era of knowledge economy: a comparative case study from the dynamic capabilities perspective," *Management World*, vol. 35, no. 3, pp. 142–156, 2019.
- [27] G. Q. Sun and Y. L. Zhu, "Research risk and evaluation of modular network organization-empirical evidences from FAW group network," *China Industrial Economics*, vol. 8, pp. 139–148, 2011.
- [28] R. Jing and M. Benner, "Institutional regime, opportunity space and organizational path constitution: case studies of



- the conversion of military firms in China,” *Journal of Management Studies*, vol. 53, no. 4, pp. 552–579, 2016.
- [29] Y. S. Du and C. H. Yang, “A situation-paradigm model for platform network management,” *Foreign Economics & Management*, vol. 38, no. 8, pp. 27–45, 2016.
- [30] O. M. Fritz, H. Mahringer, and M. T. Valderrama, *A Risk-Oriented Analysis of Regional Clusters*, Clusters and Regional Specialization Press, London, UK, 1998.
- [31] Z. G. Wu and Z. R. Han, “Platform enterprise risk management analysis,” *Economic Research Guide*, vol. 35, pp. 13–16, 2017.
- [32] R. B. Zhu, “Analysis on mechanism of resistance industry cluster’s endogenous risk by modulization,” *China Industrial Economy*, vol. 5, pp. 54–60, 2004.
- [33] N. Cai, C. Huang, and W. Sun, “Theory construction on self-organization of industry cluster risk: an exploratory case study perspective,” *China Industrial Economics*, vol. 7, pp. 54–64, 2008.
- [34] J. B. Wu and B. Guo, “Coevolution of firm’s adaptation, networking and industrial clusters: a longitudinal case study on the growth of the textile industrial cluster in Shaoxing County,” *Management World*, vol. 2, pp. 141–155, 2010.
- [35] J. Nahapiet and S. Ghoshal, “Social capital, intellectual capital and the organizational advantage,” *Academy of Management Review*, vol. 23, no. 2, pp. 242–266, 1998.
- [36] Q. C. Wang, *Space for Innovation: Enterprise Cluster and Regional Development*, Beijing University Press, 2001.
- [37] J. C. Shi, “An analysis of the historical system of the Wenzhou model—observation from the perspective of personalized and depersonalized transactions,” *Zhejiang Social Sciences*, vol. 2, no. 16, p. 2, 2004.
- [38] J. G. Yu, *Study on the Development Strategy of Transformation and Upgrading of Ningbo Home Appliance Industry-Based on the Comparison of Competitiveness with Foshan*, Qingdao and Hefei. Ningbo Economy (Sanjiang Forum), 2015.
- [39] G. Q. Sun and Y. X. Qiu, “The risks and its governance of network organization: from the perspective of risk paradox,” *On Economic Problems*, vol. 1, p. 16, 2016.
- [40] K. Morgan, “Regional advantage: culture and competition in Silicon Valley and route 128: AnnaLee Saxenian, (Harvard University Press, Cambridge, MA, 1994) 226 pp; Price £19.95, ISBN 0 674 75339 9,” *Research Policy*, vol. 25, no. 3, pp. 484–485, 1996.
- [41] J. A. Acebrón, S. Lozano, and A. Arenas, “Amplified signal response in scale-free networks by collaborative signaling,” *Physical Review Letters*, vol. 99, no. 12, article 128701, 2007.
- [42] H. C. Bozduman and E. Afacan, “Simulation of a homomorphic encryption system,” *Applied Mathematics and Nonlinear Sciences*, vol. 5, no. 1, pp. 479–484, 2020.
- [43] Y. Qin, Y. Luo, J. Lu, L. Yin, and X. Yu, “Simulation analysis of resource-based city development based on system dynamics: a case study of Panzhihua,” *Applied Mathematics and Nonlinear Sciences*, vol. 3, no. 1, pp. 115–126, 2018.
- [44] X. N. Zhang, “A literature review on platform strategy,” *Economic Management*, vol. 3, pp. 190–199, 2014.
- [45] D. S. Callaway, M. E. Newman, S. H. Strogatz, and D. J. Watts, “Network robustness and fragility: percolation on random graphs,” *Physical Review Letters*, vol. 85, no. 25, pp. 5468–5471, 2000.
- [46] P. Erdős and A. Rényi, “On the evolution of random graphs,” *Publications of the Mathematical Institute of the Hungarian Academy of Sciences*, vol. 5, no. 1, pp. 17–60, 1960.
- [47] A. L. Barabási and R. Albert, “Emergence of scaling in random networks,” *Science*, vol. 285, no. 5349, pp. 509–512, 1999.
- [48] X. Li and G. Chen, “A local-world evolving network model,” *Physica A: Statistical Mechanics and its Applications*, vol. 328, no. 1–2, pp. 274–286, 2003.
- [49] T. Nishikawa, A. E. Motter, Y. C. Lai, and F. C. Hoppensteadt, “Smallest small-world network,” *Physics Review E*, vol. 66, no. 4, article 046139, 2002.

## Research Article

# IoT-Enabled Big Data Analytics Architecture for Multimedia Data Communications

Muhammad Babar <sup>1</sup>, Mohammad Dahman Alshehri <sup>2</sup>, Muhammad Usman Tariq,<sup>3</sup>  
Fasee Ullah <sup>4</sup>, Atif Khan <sup>5</sup>, M. Irfan Uddin <sup>6</sup>, and Ahmed S. Almasoud<sup>7</sup>

<sup>1</sup>Department of Computer Science, Allama Iqbal Open University, Islamabad, Pakistan

<sup>2</sup>Department of Computer Science, College of Computers and Information Technology, Taif University, P.O. Box 11099, Taif 21944, Saudi Arabia

<sup>3</sup>Abu Dhabi School of Management, Abu Dhabi, UAE

<sup>4</sup>Department of Computer Science and IT, Sarhad University of Science and Information Technology, Peshawar, Pakistan

<sup>5</sup>Department of Computer Science, Islamia College Peshawar, Peshawar 25120, Pakistan

<sup>6</sup>Institute of Computing, Kohat University of Science and Technology, Kohat, Pakistan

<sup>7</sup>Prince Sultan University, College of Computer and Information Sciences, Saudi Arabia

Correspondence should be addressed to Fasee Ullah; fasee.csit@suit.edu.pk

Received 27 September 2021; Accepted 24 November 2021; Published 17 December 2021

Academic Editor: Deepak Gupta

Copyright © 2021 Muhammad Babar et al. This is an open access article distributed under the Creative Commons Attribution License, which permits unrestricted use, distribution, and reproduction in any medium, provided the original work is properly cited.

The present spreading out of the Internet of Things (IoT) originated the realization of millions of IoT devices connected to the Internet. With the increase of allied devices, the gigantic multimedia big data (MMBD) vision is also gaining eminence and has been broadly acknowledged. MMBD management offers computation, exploration, storage, and control to resolve the QoS issues for multimedia data communications. However, it becomes challenging for multimedia systems to tackle the diverse multimedia-enabled IoT settings including healthcare, traffic videos, automation, society parking images, and surveillance that produce a massive amount of big multimedia data to be processed and analyzed efficiently. There are several challenges in the existing structural design of the IoT-enabled data management systems to handle MMBD including high-volume storage and processing of data, data heterogeneity due to various multimedia sources, and intelligent decision-making. In this article, an architecture is proposed to process and store MMBD efficiently in an IoT-enabled environment. The proposed architecture is a layered architecture integrated with a parallel and distributed module to accomplish big data analytics for multimedia data. A preprocessing module is also integrated with the proposed architecture to prepare the MMBD and speed up the processing mechanism. The proposed system is realized and experimentally tested using real-time multimedia big data sets from authentic sources that discloses the effectiveness of the proposed architecture.

## 1. Introduction

Internet of Things (IoT) is one of the latest concepts in the current age. The future of this globe is IoT which will be going to alter today's world objects into intelligent and smart objects [1]. The term IoT was introduced in the late 1990s, yet any other components like semiconductors and wireless networks exist for quite a long time [2]. The Internet of Things is comprised of hardware and software tools. The hardware consists of the associated devices with sensors hav-

ing a network among them, and a software component comprises data storage and analytics programs that help in presenting information for users. The IoT involves communication between different objects in an intelligent fashion. The IoT comprises a network of sensors connected with various devices, which gives information that can be evaluated to initiate different actions. IoT is mainly used to define smart devices equipped for sending data back remotely to a specific application or a computer server to provide some assistance in making people make smarter decisions. IoT



keeps monitoring machines and sensors, even when they are placed in immensely remote locations or places with extremely tough climate conditions [3]. The latest advancement in technologies, computing powers, storage sizes, and energy sources provides better ingredients for the IoT world [4]. IoT is aimed at connecting the physical structure, the IT requirements, the business, and the social requirements to influence the mutual intelligence of the city [5]. With the growth of IoT data growing at a frightening hop, the impending of IoT is also dignified [6].

The multimedia big data (MMBD) vision is also gaining prominence with the increase of IoT. The IoT devices generate gigantic multimedia data. The massive data is termed big data that plays a great part in the information management of intelligent applications. The multimedia data refers to the various media types including videos and animations along with text and audio. Multimedia communications change the lifestyle of people, thus changing the way we use devices present in a technological environment. Multimedia data communications have been evolved naturally, and it will be mixed between user experience and the adoption of the user by technology which unites to take advantage of living in a smart environment and government and corporate putting employs mechanisms to make multimedia communications in living easier and more livable [7]. Multimedia communications involve big data when there are more vital problems. Traditional data analytics of multimedia data face a lot of bottlenecks to process the heterogeneous data of the IoT environment. Therefore, the incorporation of IoT with big data plays a vital part in the direction of multimedia data computation. The multimedia big data management in the IoT setting is serving to solve the challenges associated with people and society including lighting automation, controlling traffic, and automation of building.

Big data management systems provide computing, analysis, storage, and control to resolve the issues of sustainability. Multimedia data generated in the IoT environment is the big data. The interactions among all the components involved in the IoT setting create a new type of big data collection of various types of applications and services. The IoT is regarded as the fourth basic need for human beings in the near future. Everything surrounding human being gets connected to the network every second. The IoT paradigm allowed us to connect through these different types of IoT devices in multiple ways that generate different types of data. Big data analytics is combined with IoT application development to truthful processing and computation of the generated multimedia data. Parallel and distributed processing platforms are used for processing big data followed by intelligent decision-making. Big data analytics of multimedia data has released a sphere of possibilities and opportunities in the industry including retail, energy, healthcare, transportation financial services, and manufacturing. In addition, some researches have been carried out to understand the conviction of community that covers health management, waste management, water controlling, traffic controlling, parking management, and so forth [8]. The MMBD has fascinated attention by providing an image of the worldwide infrastructure of multimedia communication.

Consequently, processing the immense data has turned out to be a need for smart community development. However, there are challenges featured by big data and IoT that are interoperability issues, heterogeneity problems, data valuing challenges, data format issues, normalization of data, incompleteness data, data filtration, scaling the data, etc. [9, 10]. A scalable infrastructure will be required to handle the massive influx of devices for multimedia communications. This article proposes a generic parallel and distributed framework to process the huge data efficiently and overcome the processing issue. The proposed scheme is a layered framework with a parallel and distributed module using big data analytics. A preprocessing module is also integrated with the proposed architecture to speed up the processing mechanism in the IoT-enabled environment. Specific datasets are utilized to realize the proposed multimedia big data management architecture to optimize the processing method of data.

## 2. Literature Review

The multimedia big data generation is growing rapidly day by day as industries and societies move towards the IoT applications that generate various types of data. This increase demands an efficient computational and analytics of multimedia data. An efficient architecture for MMBD management is a key pillar for the quality of IoT-enabled multimedia systems. It is bound to enhance the services including healthcare, traffic, parking, smart home, and surveillance. IoT-enabled multimedia information deals with sensor technologies that generate different types of multimedia data. In the most recent decade, academia and researchers both have extensively studied the IoT-enabled systems [11, 12]. Therefore, the concept is considerably raised in the entire world for linking various diverse devices, objects, or “things” with the Internet. The IoT-based applications generated MMBD that require to be computed to have resourceful decision management. As relocation to built-up endures better occupation chances, a more efficient system is required in handling challenges in the major areas.

A massive data is created by sensors and other digital devices resulting in big data. Traditional databases are ineffective for storing, processing, and evaluating purposes; that is why big data terminology has been introduced in the IT field [13]. The traditional approaches lack efficient cluster management and processing. Numerous sensor data are processed in a household and office environment that collects run-time data in an appropriate and inappropriate format [14]. The collected data was not preprocessed properly to remove the anomalies and aggregate in a uniform format. Many organizations use different analytical techniques, i.e., genetic algorithms, neural networks, and sentiment analysis, to learn the behavior of different types of data that helps in process discovery and analysis [15]. Big data brings altogether not only a large data volume but several data types that never would have been considered together previously.

The impression of objects connected through the internet is expanded with the implausible expansion of multimedia information that brought up IoT as an important gesture

[16]. Furthermore, the IoT environment allows both a static and mobile object to link to any object anywhere and anytime, which eventually produces any type of data [17]. Hence, the vital objective of such environments is to build up a model that could be used for the processing of heterogeneous information. The “things” are linked with the web employing various technologies such as ZigBee and Bluetooth that is another factor of having the distributed, heterogeneous, and diverse multimedia data. Although offline processing can assist in designing the MMBD processing framework, it lacks real-time decision-making. The hurried expansion of automation takes away the concentration of scientists in the way of effective designs. The customary processing design could present advantages to the researchers and industry.

The majority of investigative research depends on the new technologies of multimedia, and now, the societies are completely dependent on these technologies [18, 19]. To design a generic and efficient smart community schema, it is essential to vigilantly examine the big data collected from the community [20]. Several methods are designed to analyze the data based on the Hadoop processing mechanism for the betterment of the societies. For instance, the CiDAP (City Data and Analytics Platform) architecture is proposed that is used for data processing [21]. This architecture consists of an IoT broker and IoT agent that achieve higher throughput. Similarly, various other proposals are proposed to tackle this issue [22, 23]. These proposals help in different perspectives and provide methods to process data; however, they are not explicitly accessible for further use of research and lack an efficient processing mechanism. MMBD is very significant to regulate technology relevant to IoT because the IoT is a new-fangled technology that generates big data with a variety of formats [24]. Rapidly, this technology has been taken up by several groups, organizations, associations, and firms for better expansion of IT. There are a couple of IoT-based architectures that have been designed based on big data analytics [25, 26].

Unluckily, no model portrays a general configuration that could be utilized by all and sundry. In the same way, an inclusive architecture is required to grip data of diverse things and compute accordingly. The literature renders some notable challenges that require to be considered, that is, proper collection of the data from various IoT devices, noise removal, data analytics, and decision-making in the smart community development. To improve the storage and processing issues of MMBD generated in the IoT-enabled environment, we propose a specific architecture that overcomes the challenges faced in the IoT-enabled infrastructure. The proposed architecture is based on distributed and parallel processing that would be performing efficient processing using a multimedia big data analytics mechanism.

### 3. Proposed Framework

The proposed parallel and distributed architecture are connected with multimedia big data sources. The data sources comprised of multimedia big data such as weather, water,

traffic, health, and parking. The workflow of the proposed parallel and the distributed scheme is provided in Figure 1. Data gathering is done by the respective units collected from various devices. To devise effective parallel and distributed architecture, the data must be sensibly scrutinized before computation. The data is generated by different devices such as environmental monitoring sensors, security monitoring sensors, power monitoring sensors, facility monitoring sensors, traffic, and transportation monitoring sensors. The data is properly collected by the various departments such as the smart health monitoring department, water management department, traffic controlling authorities, and weather monitoring department. This process is known as edge caching. The predefined data is given to the proposed parallel and distributed architecture to process using proposed modules. This overall data collection is a part of a distributed system known as caching. It involves the overall data management including the aggregation, collection, and storage for the diverse multimedia data.

The data is also preprocessed before injecting into the proposed scheme to remove noise and make uniform format and anomalies for speeding up the processing activities. Afterward, the data is divided into different chunks for parallel processing. The distributed storage mechanism is also taken into consideration to assist the parallel processing. The preferred technique for storage is the Hadoop distributed file system (HDFS). The map-reduce parallel processing paradigm for big data processing is preferred that requires distributed storage. Hence, we preferred the HDFS storage technique. Premediated algorithms (e.g., capacity algorithms, DP algorithms) are applied for data processing in the cluster. The processed data are sent for the decision-making to the corresponding services providers, which are finally provided to the users. Afterward, the Hadoop processing unit is used to process the data which is stored in the distributed storage. Lastly, the analyzed data is operated for multimedia system planning. The data is collected from the smart community multimedia systems, and the decisions are sent back to the same systems.

The proposed architecture is connected with several multimedia sources that are smart home, smart water management system, electricity management system, smart environment, smart surveillance system, and so forth. The objective is to realize a scheme to perform efficient processing of multimedia big data. The multimedia systems are the data sources for the proposed system and a mediator between system and user. Architecturally, the anticipated solution consists of 3 modules which are data management, processing, and service management that are shown in Figure 2.

*3.1. Multimedia Big Data (MMBD) Management.* The MMBD management module involves the overall data organization including big data aggregation, acquisition and collection, and big data storage. The data is distributed across various devices for computation to get the load from the central server or cloud. Intelligent applications are supported by acquiring data via the Internet from various devices. Various devices including sensors, cameras, and

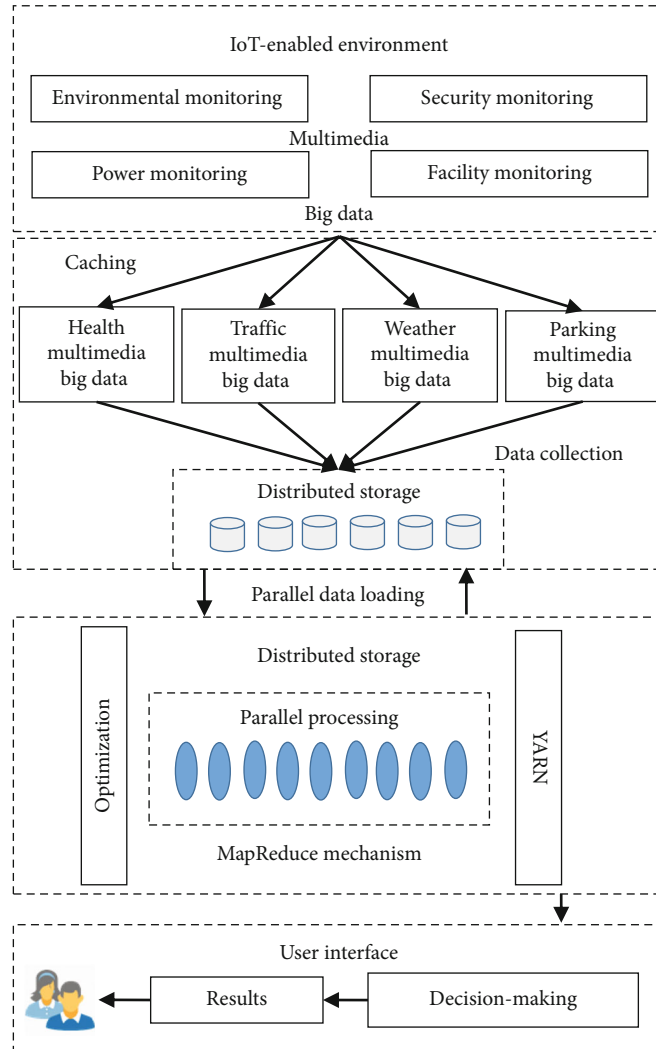


FIGURE 1: Workflow of the proposed framework.

object-mounted devices record the information of the environment in the different domains. This MMBD is later utilized for analysis to get insights and produce intelligent decisions. This layer is responsible for MMBD collection from various sources that are used to manage the multimedia systems and services. A practical community does not only hold a huge quantity of data but also includes versatile and wide-ranging processing areas. The multimedia systems implementation is dependent on all types of big data processing with heterogeneous environment. Data collection is used to transform signals that are assessed in practical circumstances and convert outcomes to the digital form for processing. The MMBD collection is done by a special system that pulls out the data using various environmental objects to collect real-time MMBD. The data collection layer further includes the data aggregation, where the data are grouped based on the identification of the connected devices. This aggregation is applied because the data is gigantic and need to be grouped for efficient processing.

**3.2. Multimedia Big Data (MMBD) Processing.** The multimedia big data processing involves the distribution of MMBD into various splits for the parallel processing using multiple nodes in the cluster. The storage and processing of the MMBD are done using the Apache Spark distributed and parallel big data analytics platform. The process of computation from the distributed environment is based on the specific algorithms available in the distributed environment. On the other hand, cluster management is the particular activity in the system architecture. We utilized the specific utility called Yet Another Resource Negotiator (YARN) for cluster management. This layer is the central processing unit and is accountable for processing including training and inferencing. Initially, raw multimedia data that may include the irrational data combination, missing values, and values beyond the range are managed before processing the data. If the data is not inspected for such problems, there could be misleading results during decision-making. Therefore, the conversion is also performed to scale the data to a

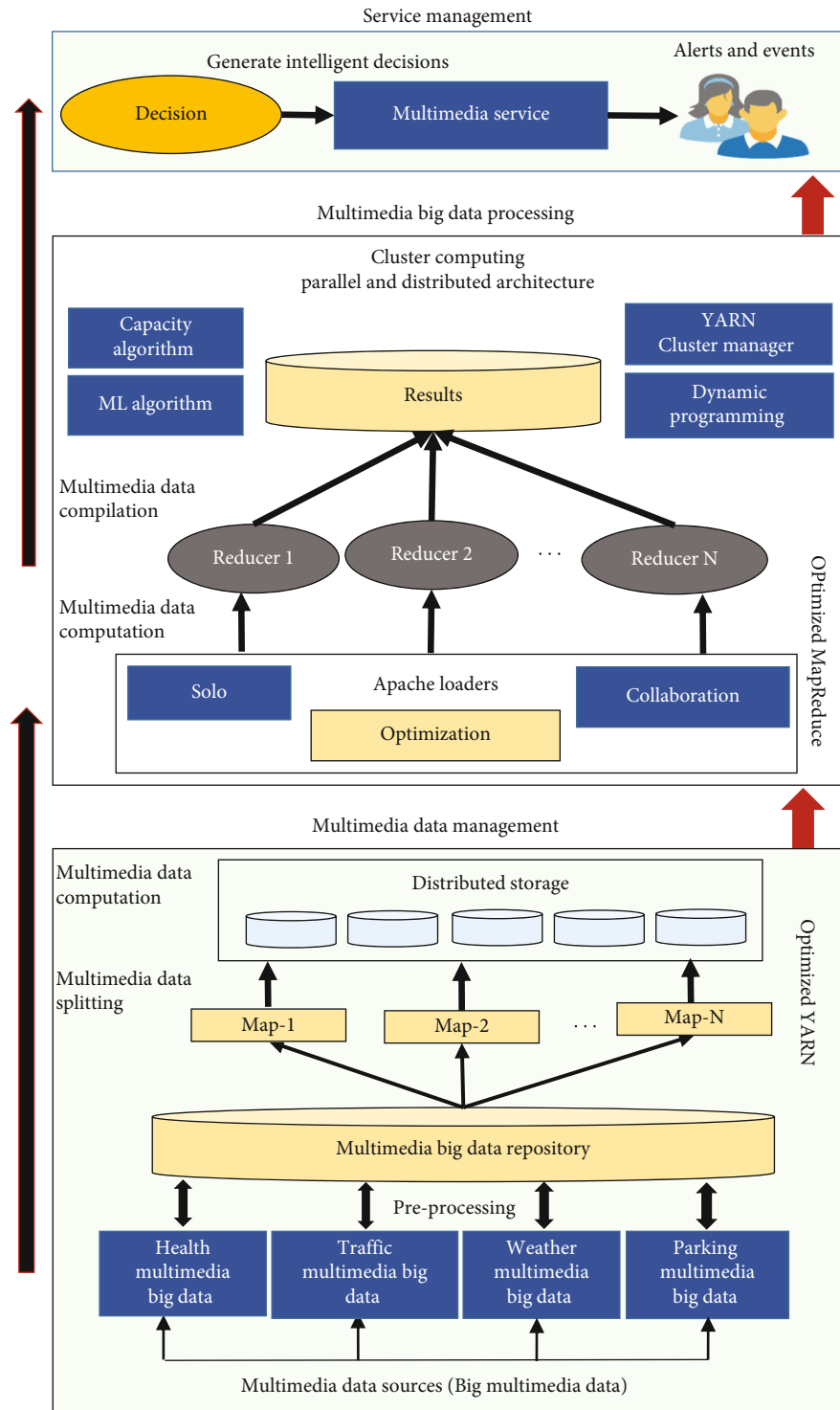


FIGURE 2: Proposed architecture.

particular specified scale. Subsequently, data is taken by a parallel and distributed processing unit that is the backbone of the proposed architecture.

The parallel and distributed processing unit processes huge data distributed and parallel form. It uses MapReduce programming that carries work in mapping and reducing processes. The storage obligation is supported using the distributed filing system. The proposed architecture is based on a parallel and distributed computing paradigm that is utilized for processing and computation. An optimized map-reduce model is introduced to implement the MMBD analytics. The proposed optimized model processes huge datasets in parallel. It executes the analytics processes in a distributed manner with high availability. The proposed architecture also overcomes the machine failures, machine's performance issues, and effective communications. The job distribution in the computing cluster is performed using the YARN cluster management framework. The YARN model is equipped with dynamic programming for job distribution and resources management in the cluster. The earlier versions of the parallel and distributed platforms (e.g., traditional Hadoop) utilized MapReduce for both processing and cluster management, which created the communication overhead and decreases the performance. On the other hand, the Yet Another Resource Negotiator (YARN) is favored as it performs cluster management separately. A detailed explanation is provided in the revised manuscript.

In the context of YARN-based cluster management, the job is a YARN application. The Application Master implementation in the YARN-based solution is provided by MRAppMaster. There could be many tasks in the phase of mapping or reducing stage for every split of MMBD. In addition, the map and reduce phases can be interleaved; therefore, the reduce phase may start before the end of the map phase. When an application is submitted to YARN considering the edge information, some additional information is given to YARN infrastructure particularly a configuration, a JAR file, and input/output information. The configuration might be limited as some parameters might not be specified in that case; for job execution, the default values are utilized. If the data file size is too large (larger than the block size of HDFS (256 MB in proposed architecture), then there would be two or more two map splits related to the same input file. For stream processing, running map-reduce is not a good idea. Additional utilities (e.g., Apache Spark) can be added with optimized MapReduce to process the data in memory (RAM) rather than put it on a disk, etc.

The predefined method called `getSplits()` of the predefined class called `FileInputFormat` is customized with information for implementing map-reduce jobs using dynamic programming algorithms. The MRAppMaster requests for containers to the resource manager required executing the job. After the setup of the system, for every  $\langle k, v \rangle$  tuple enclosed in a split of the map, the `map()` method is called. Therefore, `map()` accepts a specific key, a specific value, and a specific mapper context. We utilized the parallel and distributed platform. We preferred the use of the capacity scheduling algorithm for parallel processing. Similarly, the DP (dynamic programming) is utilized for recursion as the

huge data is divided into chunks repeatedly for parallel processing. The DP is one of the best algorithms for resolving a problem by recursively breaking it down into simpler sub-problems and producing the optimal solution. The Apache loader is the utility that loads the Apache Hadoop files and libraries for map-reduce and other operations.

The output of the optimized mapper is stored to a particular buffer using the context. When the overall optimized-map split has been processed and executed, the clean method is called by a run. There is no action performed by default but the user might decide to override it. MapReduce is the batch-processing mechanism. The concept behind MapReduce is that data of a particular edge is first grouped into small portions. After that, these edge-map splits or portions are processed in a distributed manner to create desired results. MapReduce is the extension of the traditional MapReduce model which is easy and generally useful for various diverse applications such as bioinformatics, web mining, and machine learning technologies. On the other hand, stream processing is meant for processing and executing the data record-wise as the data is pulled in and updated incrementally. The result is reorganized with each new record of the data. Stream processing queries run continuously and are never ending.

**3.3. Service Management.** This layer exists on top of the proposed architecture and is responsible for making decisions and communicating the corresponding decision to the corresponding departments of the smart community. It is the end-user or application layer. The intelligent decisions and results are sent to the management centers. Afterward, the events are classified and the corresponding users are informed accordingly. First of all, the sophisticated actions are kept at community development departmental glassy and then dispatched to the users. The application interfaces are responsible for the subservice selection and the classification of the events. Moreover, the decision-making process is carried out using a properly maintained rule engine, where several rules based on particular thresholds are defined. IoT-enabled MMBD applications could be education that involves people in dynamic learning environments to adjust to the rapid changes of society, traffic lights that improve the transportation systems and overall traffic patterns, smart grid that improves the productivity and supply of electric power, healthcare that monitors and analyzes health issues daily or on-demand basis, smart energy that helps in management related to the providing the intensity of power with the definite claim of the citizens, and smart environment that provides weather info to improve the country's agriculture and other possible harmful circumstances.

## 4. Results and Discussion

We utilized the open-source platform Apache Hadoop version 3.0 (parallel and distributed platform) for the validation of the proposed framework. Additionally, Apache Spark is configured with the Hadoop version 3.0 for real-time stream processing and computation. The discussion about the results is provided in this section. Results are produced by



utilizing various authentic multimedia big data sets to assess the proposed MMBD framework using parallel and distributed paradigms and premeditated algorithms. The pre-processing mechanism is carried out before the core processing to remove the anomalies and noise from multimedia big data sets. Thus, notable efficiency is achieved in the processing time and throughput. The proposed architecture is implemented using Hadoop and Apache Spark parallel and distributed framework along with optimized premeditated algorithms. The datasets include transportation and vehicular data, pollution data, and water data [27–29]. These datasets are preferred due to the utilization of this dataset in the literature. We deliberately executed almost the similar kind of queries for the processing time and throughput comparison of the proposed IoT-enabled MMBD system using optimized map-reduce and YARN for parallel and distributed processing.

The utilization of the water is assessed to accomplish sustainable management and control of the water consumption in the region. The unpredictable depletion of water can be a catastrophe for society. The dataset used in the proposed research includes the data of the city of Surrey, Canada. The data is collected for various sources that contain the intake of water by houses. The information is processed using our suggested processes. The outcomes are revealed in Figure 3. It demonstrates the families spent water more than 83500 liters a month. The well-defined threshold is 83500 according to the defined rule. The water consumption higher than the threshold or TLV is specifically emphasized that could cause scary circumstances for the consultants. It is perceived that almost 55% of the users utilized more water than the TLV. The users above TLV limit usages have utilized water between 115000 and 120500 liters that is pretty frightening. Current production approaches can be utilized by the industry to govern the challenges of the users.

Furthermore, the traffic dataset is also experimentally tested with the proposed optimized MMBD architecture. The average speed is exposed in Figure 4. The average speed is observed in the pretty similar complete day, excluding from 12:50 to 17:50 for a few automobiles.

Similarly, the pollution dataset is also experimentally tested with the proposed optimized MMBD framework using customized map-reduce and YARN for parallel and distributed processing. The dataset of the pollution is thoroughly investigated. The pollution of a specific day is also shown in Figure 5.

The selection criteria of the parameters for the analysis of the results were the parameters of the base papers. We preferred the same set of queries utilized by base papers. We also preferred the same datasets for comparison. Moreover, a similar configuration (storage, CPU, cluster, and nodes) is preferred for comparison. Equally, a comparison to related architectures is also provided concerning system processing time in Figure 6. The proposed architecture processing time is better than the existing solutions provided in the literature for smart city planning. The performance improvement is due to the customization in the YARN cluster management and utilizing MapReduce. The YARN and MapReduce are the extensions of the traditional YARN

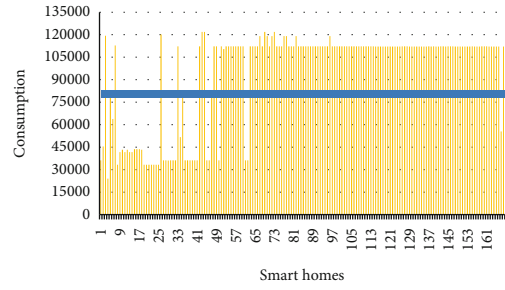


FIGURE 3: Consumption of water in smart homes.

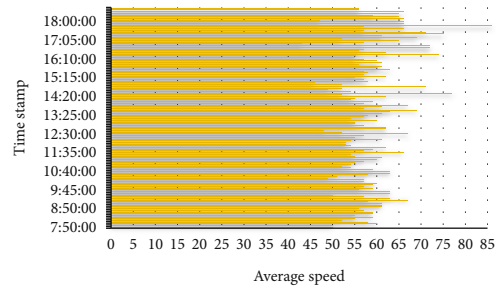


FIGURE 4: Average speed.

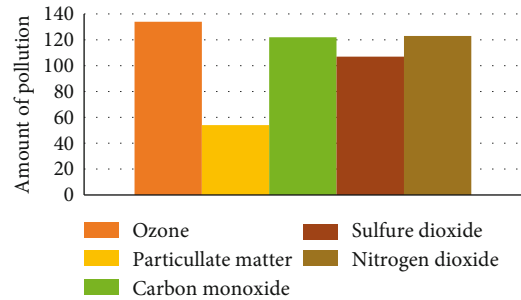


FIGURE 5: Pollution.

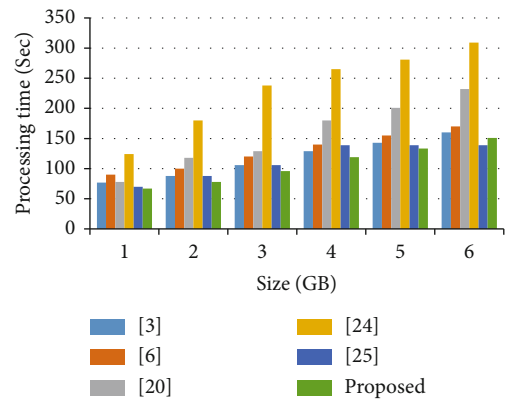


FIGURE 6: Processing time comparison with existing solutions.



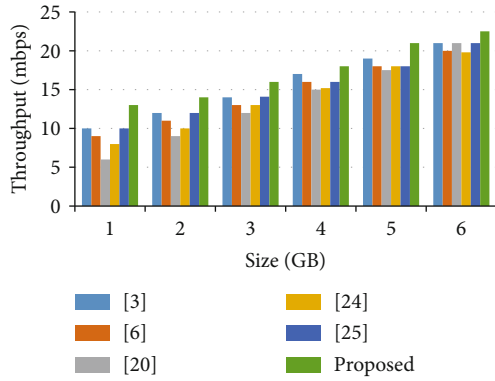


FIGURE 7: Throughput comparison with existing solutions.

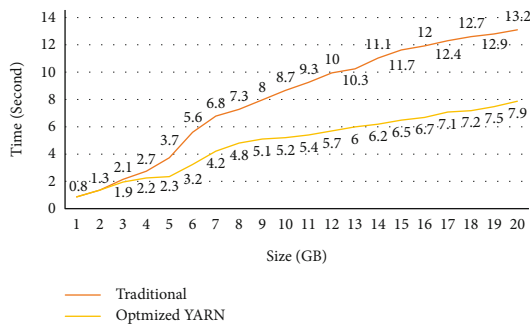


FIGURE 8: Traditional vs. optimized cluster management.

and MapReduce for edge computing. The results show that the proposed architecture is better than existing architectures in the context of processing time.

Finally, a comparison to related architectures is also provided about throughput in Figure 7. The proposed architecture throughput is much better than the existing solutions provided in the literature for planning due to the customization of the traditional distributed framework. Figure 8 highlights the effectiveness of optimized YARN. The throughput increases due to the decrease in the processing time. The processing time decreases because the parallel processing platform is optimized with different block sizes, replica numbers, and the use of the configured utility.

## 5. Conclusion

This paper proposes a generic scheme to process data in the parallel and distributed mechanism to overcome the processing issues. Parallel processing is utilized to perform big data processing. This research intends the explicit apprehension of multimedia communication to make possible efficient data processing and decision-making. Multimedia systems provide computing, storage, and analysis, to solve the challenges. However, it becomes challenging to tackle with the diverse IoT settings. The proposed architecture is a layered framework with a parallel and distributed architecture using big multimedia data analytics. A preprocessing module is also integrated with the proposed architecture to speed up the processing mechanism of big data produced

by IoT devices in the IoT-enabled environment. Specific datasets are utilized to realize the proposed architecture to optimize the processing of data. The proposed system is realized using real-time datasets from various sources. The proposed architecture is experimentally tested with authentic datasets that reveal the effectiveness of the proposed architecture.

## Data Availability

The data used to support the findings of the study are included within the article.

## Conflicts of Interest

The authors declare that they do not have conflict of interest.

## Acknowledgments

This study was supported by Taif University Researchers Supporting Project (number TURSP-2020/126), Taif University, Taif, Saudi Arabia.


## References

- [1] Z. Liao, S. Nazir, H. U. Khan, and M. Shafiq, "Assessing security of software components for Internet of Things: a systematic review and future directions," *Networks*, vol. 2021, article 6677867, 22 pages, 2021.
- [2] M. Ahmad, T. Younis, M. A. Habib, R. Ashraf, and S. H. Ahmed, *Recent Trends and Advances in Wireless and IoT-enabled Networks*, Springer Nature Switzerland AG, 2019.
- [3] M. Babar, F. Arif, M. A. Jan, Z. Tan, and F. Khan, "Urban data management system: towards Big Data analytics for Internet of Things based smart urban environment using customized Hadoop," *Future Generation Computer Systems*, vol. 96, pp. 398–409, 2019.
- [4] M. Elkhodr, B. Alsinglawi, and M. Alshehri, "Data provenance in the internet of things," in *2018 32nd International Conference on Advanced Information Networking and Applications Workshops (WAINA)*, pp. 727–731, Krakow, Poland, 2018.
- [5] L. Ru, B. Zhang, J. Duan et al., "A detailed research on human health monitoring system based on Internet of Things," *Wireless Communications and Mobile Computing*, vol. 2021, Article ID 5592454, 9 pages, 2021.
- [6] M. Babar and F. Arif, "Real-time data processing scheme using big data analytics in internet of things based smart transportation environment," *Journal of Ambient Intelligence and Humanized Computing*, vol. 10, no. 10, pp. 4167–4177, 2019.
- [7] H. Gao, Y. Duan, L. Shao, and X. Sun, "Transformation-based processing of typed resources for multimedia sources in the IoT environment," *Wireless Networks*, vol. 27, no. 5, pp. 3377–3393, 2021.
- [8] W. Shang, J. Chen, H. Bi, Y. Sui, Y. Chen, and H. Yu, "Impacts of COVID-19 pandemic on user behaviors and environmental benefits of bike sharing: a big-data analysis," *Applied Energy*, vol. 285, 2021.
- [9] Z.-N. Li, M. S. Drew, and J. Liu, "Network services and protocols for multimedia communications," in *Fundamentals of Multimedia*, pp. 535–582, Springer, 2021.

- [10] L. Tan, K. Yu, F. Ming, X. Chen, and G. Srivastava, "Secure and resilient Artificial Intelligence of Things: a HoneyNet approach for threat detection and situational awareness," *IEEE Consumer Electronics Magazine*, vol. 2021, p. 1, 2021.
- [11] K. Yu, Z. Guo, Y. Shen, W. Wang, J. C. Lin, and T. Sato, "Secure Artificial Intelligence of Things for implicit group recommendations," *IEEE Internet of Things Journal*, vol. 2021, 2021.
- [12] Z. Guo, K. Yu, Y. Li, G. Srivastava, and J. C.-W. Lin, "Deep learning-embedded social internet of things for ambiguity-aware social recommendations," *IEEE Transactions on Network Science and Engineering*, vol. 2021, 2021.
- [13] M. Khan, J. Iqbal, M. Talha, M. Arshad, M. Diyan, and K. Han, "Big data processing using internet of software defined things in smart cities," *International Journal of Parallel Programming*, vol. 48, no. 2, pp. 178–191, 2020.
- [14] B. Anthony Jnr, S. Abbas Petersen, D. Ahlers, and J. Krogstie, "Big data driven multi-tier architecture for electric mobility as a service in smart cities," *International Journal of Energy Sector Management*, vol. 14, no. 5, pp. 1023–1047, 2020.
- [15] E. Carter, P. Adam, D. Tsakis, S. Shaw, R. Watson, and P. Ryan, "Enhancing pedestrian mobility in smart cities using big data," *Journal of Management Analytics*, vol. 7, no. 2, pp. 173–188, 2020.
- [16] A. Al-Fuqaha, M. Guizani, M. Mohammadi, M. Aledhari, and M. Ayyash, "Internet of Things: a survey on enabling technologies, protocols, and applications," *Communications Surveys and Tutorials*, vol. 17, no. 4, pp. 2347–2376, 2015.
- [17] M. A. Razzaque, M. Milojevic-Jevric, A. Palade, and S. Clarke, "Middleware for internet of things: a survey," *IEEE Internet of Things Journal*, vol. 3, no. 1, pp. 70–95, 2016.
- [18] Y. Gong, L. Zhang, R. Liu, K. Yu, and G. Srivastava, "Nonlinear MIMO for industrial Internet of Things in cyber-physical systems," *IEEE Transactions on Industrial Informatics*, vol. 17, no. 8, pp. 5533–5541, 2021.
- [19] S. Uppoor, O. Trullols-Cruces, M. Fiore, and J. M. Barcelo-Ordinas, "Generation and analysis of a large-scale urban vehicular mobility dataset," *IEEE Transactions on Mobile Computing*, vol. 13, no. 5, pp. 1061–1075, 2014.
- [20] M. Khan, B. N. Silva, and K. Han, "Internet of things based energy aware smart home control system," *IEEE Access*, vol. 4, pp. 7556–7566, 2016.
- [21] B. Cheng, S. Longo, F. Cirillo, M. Bauer, and E. Kovacs, "Building a big data platform for smart cities: experience and lessons from Santander," in *2015 IEEE International Congress on Big Data*, pp. 592–599, New York, NY, USA, 2015.
- [22] "FIWARE open source platform," <https://www.fiware.org/>.
- [23] "SCOPE a smart-city cloud-based open platform and ecosystem," <https://www.bu.edu/hic/research/highlighted-sponsored-projects/scope/>.
- [24] M. Khan, B. N. Silva, and K. Han, "A Web of Things-based emerging sensor network architecture for smart control systems," *Sensors*, vol. 17, no. 2, p. 332, 2017.
- [25] M. Babar, A. Rahman, F. Arif, and G. Jeon, "Energy-harvesting based on internet of things and big data analytics for smart health monitoring," *Sustainable Computing: Informatics and Systems*, vol. 20, pp. 155–164, 2018.
- [26] A. Ahmad, A. Paul, S. Din, M. M. Rathore, G. S. Choi, and G. Jeon, "Multilevel data processing using parallel algorithms for analyzing big data in high-performance computing," *International Journal of Parallel Programming*, vol. 46, no. 3, pp. 508–527, 2018.
- [27] "T. Dataset, Dataset collection," <http://iot.ee.surrey.ac.uk:8080/datasets.html#traffic>.
- [28] "P. Dataset, Dataset collection," <http://iot.ee.surrey.ac.uk:8080/datasets.html#pollution>.
- [29] "Dataset water meters," <http://data.surrey.ca/dataset/water-meters>.

## Research Article

# Wireless Image Transmission Interference Signal Recognition System Based on Deep Learning

Zhijun Guo <sup>1,2</sup> and Shuai Liu<sup>1,2</sup>

<sup>1</sup>*Institute of Information Science and Technology, Hunan Normal University, Changsha 410081, China*

<sup>2</sup>*Hunan Xiangjiang Artificial Intelligence Academy, Changsha 410081, China*

Correspondence should be addressed to Zhijun Guo; [guozhijun@hunnu.edu.cn](mailto:guozhijun@hunnu.edu.cn)

Received 18 September 2021; Accepted 13 November 2021; Published 16 December 2021

Academic Editor: Deepak Gupta

Copyright © 2021 Zhijun Guo and Shuai Liu. This is an open access article distributed under the Creative Commons Attribution License, which permits unrestricted use, distribution, and reproduction in any medium, provided the original work is properly cited.

In the process of wireless image transmission, there are a large number of interference signals, but the traditional interference signal recognition system is limited by various modulation modes, it is difficult to accurately identify the target signal, and the reliability of the system needs to be further improved. In order to solve this problem, a wireless image transmission interference signal recognition system based on deep learning is designed in this paper. In the hardware part, STM32F107VT and SI4463 are used to form a wireless controller to control the execution of each instruction. In the software part, aiming at the time-domain characteristics of the interference signal, the feature vector of the interference signal is extracted. With the support of GAP-CNN model, the interference signal is recognized through the training and learning of feature vector. The experimental results show that the packet loss rate of the designed system is less than 0.5%, the recognition performance is good, and the reliability of the system is improved.

## 1. Introduction

The emergence of wireless image transmission technology makes it convenient, fast, accurate, and real time for people in need to obtain remote image information, which provides convenience for special industry applications [1]. In recent years, the related technologies of wireless image transmission system have developed rapidly, but there are still some limitations, such as limited transmission bandwidth, inflexible transmission mode, and communication and image transmission quality assurance mechanism. Therefore, the research on these related aspects has extremely important social and economic value [2–4].

The existing wireless image acquisition and transmission system can only be used in the place where the line is laid in advance, and its application range is greatly limited. At present, many of them use GPRS/CDMA (General Packet Radio Service and Code Division Multiple Access) technology to achieve wireless image acquisition and transmission system,

which uses the cellular network transmission mode, so the transmission signal must rely on the base station. In a bad environment, such as catastrophic weather and special circumstances, when the base station fails, the whole communication network will be destroyed. Even if it is not damaged, there will be a lot of interference in the transmission signal, which will affect the performance of wireless image transmission [5–7]. Although the JPEG image can be received in any area covered by the signal, the transmission of image data is not very stable. In addition, the user has to bear the communication cost. The existing underlying communication protocol of the Internet of things consumes too much power in the application of wireless image sensing system and cannot support sudden big data transmission (image data transmission) [8–10]. Therefore, according to the network transmission requirements of the above different application fields, the research and development of a low-power, low-cost, self-relaying narrow-band communication network system for rapid deployment without power

supply infrastructure will help to rapidly promote the scale of related Internet of things applications and promote the application in intelligent power grid, intelligent transportation, industry and automation control, etc. Application promotion of IoT in the field of environment and safety inspection [11–13]. The realization of this reliable network communication is inseparable from the identification of interference signals. Only by accurately identifying the interference signals in wireless transmission can we further ensure the quality of wireless transmission.

Signal recognition technology originated in the early last century; with the early application in radio signal interference, information interception, and other military-related fields, after long-term research and development, the relevant signal recognition technology has been proposed. The early recognition technology is relatively primitive and relies more on manual work. Nowadays, the research on signal recognition is mostly modulation pattern recognition, and this traditional recognition pattern is far from enough [14]. In recent years, signal recognition technology has a very good development, and professionals have improved. After the system design is completed, the traditional identification system is introduced, and a large number of comparative experiments are carried out image transmission, the traditional identification system includes Fang et al., which integrates the multidimensional domain characteristic parameters of typical interference signals such as single-tone interference, broadband noise interference, multitone interference, and sweep interference, such as time domain, frequency domain, and transform domain [15]. The jamming signal recognition method based on decision tree algorithm and the range velocity composite deception jamming recognition technology based on space-time frequency feature fusion are proposed by Yang et al. This method completes the jamming signal recognition by extracting the spatial and frequency domain features of echo traces, respectively, and fusing the extracted spatial and frequency domain features in time domain [16]. These traditional recognition systems can meet some basic recognition requirements. However, as the image attributes become more and more complex, the service signal adopts more complex multiple modulation, so it is difficult for the recognition system to accurately identify the target signal, and the reliability of the system needs to be further improved. In order to solve the above problems and improve the effect of target signal recognition, a wireless image transmission interference signal system based on deep learning is proposed in this paper. In the hardware part, stm32f107vt and si4463 are used to form a wireless controller to control the execution of each instruction. In the software part, aiming at the time-domain characteristics of the interference signal, the feature vector of the interference signal is extracted. With the support of GAP-CNN model, the interference signal is recognized through the training and learning of feature vector. Through the above steps, the identification of interference signals is completed, and through the experimental link, the effect of the design system is proved, in order to provide some help to improve the identification effect of interference signals.

## 2. Hardware Design of Wireless Image Transmission Interference Signal Recognition System Based on Deep Learning

According to the characteristics of wireless image transmission, the wireless network controller is designed in the hardware design part of the system. Wireless network controller (WNC) consists of “micro control unit (MCU)” and “wireless module.” The main function of micro control unit is to control business logic and implement wireless communication protocol and network communication protocol. Among them, the role of wireless module is to complete the wireless signaling and data transceiver function [17, 18]. The wireless module and wireless protocol interact with WIS to complete the transmission of image data from WIS to WNC. WNC interacts with the “image monitoring platform” through Ethernet to execute the commands issued by it. WNC plays a role of bridge between the “image monitoring platform” and WIS and completes the conversion of information between wireless and network transmission media [19].

Wireless network controller (WNC) is composed of STM32 series 107 MCU, wireless module, and Ethernet PHY chip. The MCU of STM32F 107 has an Ethernet controller, which only needs to expand PHY chip of Ethernet to realize Ethernet communication. The hardware block diagram of the wireless network controller (WNC) is shown in Figure 1.

The WNC board controller is STM32F107VT, with the main frequency of 72 MHz and the Ethernet MAC controller with 10/100 M on the chip and is compatible with the MII and RMII interfaces. Through RMII interface, it can realize seamless connection with PHY chip DM9161CI. The network transformer HX2019 mainly enhances the anti-interference and load capacity of network port [20]. The SPI interface of WNC is connected with the wireless module. The system realizes airport communication, receives image data and uplink control signaling, and sends downlink control signaling.

MCU module is composed of the smallest system of STM32F107. Its function is connected with other modules through various interfaces to complete the control of other modules. The wireless module is a wireless transceiver module composed of SI4463 chip. It is connected with the MCU module through SPI interface. MCU controls the wireless module to send and receive packets through SPI to complete the task of wireless communication. Network interface module is composed of network controller in MCU and HX2019 chip. It is responsible for the basic sending and receiving of the network to complete the network communication task. The SD card is composed of card reader interface. Its function is to cache the image information collected from WIS to transmit the image upward when the network is not busy.

According to the above contents, the power consumption of main devices is counted, and the WNC power supply is designed. The details are shown in Table 1.

At present, the commonly used power management chips are linear power supply (LDO power supply) and DCDC switching power supply. So far, the hardware design of the identification system has been completed, and on this basis, the software part is designed.



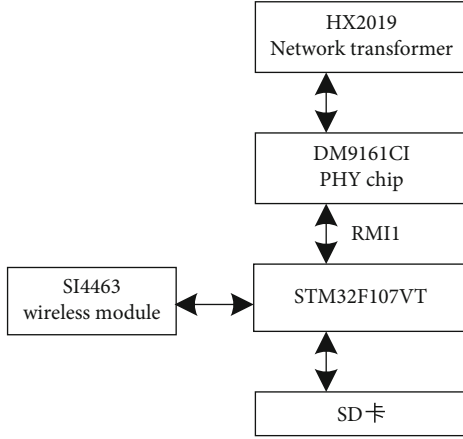


FIGURE 1: Hardware block diagram of wireless network controller.

TABLE 1: Power consumption of main components of WNC.

Main chip	Supply voltage (V)	Power consumption (mW)	Supply current (mA)
STM32F107VT	3.3	350	106.06
DM9161CI	3.3	290	87.88
SI4463	3.3	270	81.82
Other	3.3	100	30.30

### 3. Software Design of Wireless Image Transmission Interference Signal Recognition System Based on Deep Learning

**3.1. Feature Extraction of Interference Signal.** In deep learning, supervised CNN architectures for classification, such as AlexNet, GoogLeNet, and ResNet, all take the Softmax layer as the output layer, which is connected with the convolution layer or full connection layer. The input of Softmax layer is the feature vector of the original input signal  $y(n)$ , so it can be considered that the function of the convolution layer in CNN is to map  $y(n)$  to the feature space, that is, to extract the feature vector. In the convolution layer, each convolution kernel can be considered as a linear system for extracting a certain feature. But before the network training, the operation parameters of the whole system are unknown. Therefore, the weight parameters of convolution kernel are randomly initialized, and the parameters of the system can only be optimized and updated by BP algorithm to reduce the value of the objective function. After the training, the system can be used to extract the input features. The concatenation of convolution layers makes the input signal  $y(n)$  be abstractly mapped layer by layer, and finally, the feature vector needed by the classifier is obtained. But before network training, the operating parameters of the whole system are unknown. Therefore, the weight parameters of convolution kernel are also initialized randomly. In this case, in order to reduce the value of the objective function, the system parameters need to be optimized and updated by the BP algorithm. After training, the system can be used to extract

the input features, and then, the input signal  $y(n)$  is abstractly mapped layer by layer through the superposition of convolution layers, so as to finally obtain the feature vector required by the classifier, so as to overcome the influence of unknown operating parameters.

In the process of feature extraction of jamming signal, the time-domain feature of jamming signal is taken as the extraction target. It is assumed that  $x(n)$  is the discrete time-domain sequence of jamming signal, and the characteristic parameter reflecting the steepness of amplitude distribution of time-domain signal  $x(n)$  is the time-domain moment kurtosis. The expression is as follows:

$$\alpha_1 = \frac{p(x(n) - \varepsilon)}{\eta^4}. \quad (1)$$

In the formula,  $\varepsilon$  is the mean value of time-domain signal and  $\eta$  is the standard deviation of time-domain signal. It can be seen from formula (1) that the characteristic parameter  $\alpha_1$  is a fourth-order statistic and generally takes the kurtosis of moment in the time domain of normal distribution signal as the comparison standard. If the kurtosis of the moment in time domain is less than 3, the time-domain distribution of the signal is relatively flat, which is called flat peak distribution. If the kurtosis of the time-domain moment is greater than 3, the time-domain distribution of the signal is relatively steep, which is called the peak distribution. In order to further characterize the fluctuation of amplitude distribution in time domain, the normalized amplitude standard deviation of target signal is calculated. The smaller the value, the distribution is relatively balanced, otherwise, the greater the amplitude of the signal changes. The calculation formula is as follows:

$$x_0(u) = \frac{x(u) - \varepsilon}{\varepsilon},$$

$$\alpha_2 = \left( \frac{1}{N-1} \sum_{i=1}^n \left( |x_0(u)| - \frac{1}{N} \sum_{i=1}^n |x_0(u)| \right)^2 \right)^{1/2}. \quad (2)$$

In the formula,  $x_0(u)$  represents the normalized value of amplitude sequence  $x(n)$ , and  $N$  represents the number of sequences. After the target is determined, the feature vector of interference signal is extracted by encoder and decoder. In the encoder stage, after the convolution layer mapping, the signal is downsampled through the pooling layer to compress the size of the output feature map. After several times of the same operation, the convolution layer at the bottom is reached, and the output at the bottom can be regarded as the abstraction of the original input signal  $y(n)$ . In the decoder stage, these abstract features are sampled continuously by the deconvolution layer and finally reach the top output layer. The goal of CAE is to output and input consistently, and its extraction process can be described as “compress before refactoring.” After obtaining the feature vector of the interference signal, the interference signal is recognized in the wireless transmission signal.



**3.2. Identify Jamming Signal.** In order to recognize the interference signal by deep learning, it is necessary to generate the signal training set before recognition, so as to provide the necessary data for signal recognition. Moreover, the signal training set is mainly completed through software simulation and hardware acquisition. The interference signals to be identified are commonly used digital modulation signals, including MPSK, MQAM, MFSK, and GMSK modulation types. The hardware acquisition adopts NI-USRP 2920 software radio signal receiving and receiving platform, which is in the same way as the real communication to modulate the code elements, and then, it is filtered and mixed to high frequency and transmitted. At the receiving end, the captured signal is mixed to it by analog frequency and then is collected and processed by digital downconversion. Finally, the complex baseband signal is obtained. The signal collected by hardware contains all the modulation information of the signal and is very close to the characteristics of the signal in real communication. However, due to the limitations of NI-USRP equipment, there are many problems in signal acquisition, such as non-real-time and complicated operation, and it is difficult to simulate various complex outdoor channels. Therefore, in order to make up for these shortcomings, this paper also uses software simulation to supplement the training set data. The training set includes the baseband signal after shaping filtering at the transmitter, the baseband signal after digital downconversion at the receiver, and the modulation type. After the Recovery-Net training, the collected output data is stored in the training set.

In the recognition of interference signal, CNN and GAP-CNN models in deep learning are combined. In order to make the structure of the model concise and learn the characteristics of the interference signal well, we built the CNN and GAP-CNN model structure. The model has the following characteristics: in the convolution process, the space size becomes smaller and the output depth increases layer by layer. In deep learning, more convolution kernels can learn more features, but the number of convolution kernels should be kept within a reasonable range, because the unreasonable number of convolution kernels will interfere with the recognition and affect the recognition effect. When the size of convolution kernel is fixed, the number of convolution kernel must be proportional to the depth of input and output of the convolution layer. Under the above requirements, the convolution pooling layer in CNN is usually connected with one or more fully connected layers, and the fully connected layer transforms the input feature spectrum into vectors to complete the dimension reduction of the input and provide input for subsequent recognition. However, when the parameters are too large, it is difficult for the CNN network to support the identification service alone. Therefore, in order to reduce the network parameters and the risk of over fitting, the convolution layer is used to replace the full connection layer, and the large convolution core is used to connect with a small number of nodes in the back layer. Gap is not directly used to replace the full connection layer. In the design, GAP-CNN layer is introduced to replace the flattening layer to reduce the input quantity of the full con-

TABLE 2: Parameter configuration of NI-USRP 2920.

Parameter number	Project	Parameter
Q01	I/Q sampling rate	500k sample/s
Q02	Oversampling multiple	4
Q03	Symbol rate	125k symbol/s
Q04	Carrier frequency	915 MHz
Q05	Transmit/receive gain	10 dB/20 dB
Q06	Transmit/receive antenna	$T \times 1/R \times 2$
Q07	Roll-off factor	0.4
Q08	Filter order	20
Q09	Shaping/matched filter	Root raised cosine filter

nection layer. Other structures are designed by CNN. After the design of the GAP-CNN model structure, the training set is used as the input to complete the learning process. Then, the target to be identified is input into the model to complete the recognition of interference signal of wireless image transmission. So far, the design of wireless image transmission interference signal recognition system based on deep learning is completed.

## 4. Experimental Study on the Interference Signal Recognition System of Wireless Image Transmission Based on Deep Learning

**4.1. Building Experimental Platform.** Through the construction of wireless communication transceiver platform, the verification of wireless image transmission interference signal recognition system is carried out in the real environment. NI-USRP 2920 is based on the public version of software radio platform USRP Radio by NI instrument company. It is a part of the external circuit transformation. NI-USRP hardware has a common software-defined radio (SDR) architecture. In its FPGA digital signal processing logic, the communication transmitter modulates the user data into digital baseband data, and the output becomes analog baseband signal  $I/Q$  through high-speed DAC. After the high-order harmonics and spurious are filtered by low-pass filter, the analog baseband signal is up converted to the carrier frequency 915 MHz by analog RF quadrature, and the communication transmission is completed by power amplification and antenna. At the communication receiving end, the weak wireless communication signal received by the antenna is modulated by low-noise amplifier, and then, the analog RF orthogonal downconversion is completed. Output  $I/Q$  baseband signal to high-speed ADC; quantize  $I/Q$  data stream to FPGA digital signal processing logic. The FPGA digital signal processing logic is used to realize the digital downconversion (DDC) at the receiving end and the digital upconversion (DUC) at the transmitting end. Through the experimental platform, the interference signal and normal

TABLE 3: Experimental signal parameters.

	Center frequency	Sampling rate	Code rate	Signal intensity	Modulation depth	Inter frequency
AM signal	300	192	—	-40	50~100	—
FM signal	300	192	—	-40	—	4-10
PSK signal	300	192	20-80	-40	—	—

TABLE 4: Experimental results of packet loss rate of different identification systems.

	Transmission interval	Packet loss rate	Number of images	Number of images in question
Traditional identification system 1	3 s	12.5%	1000	12
	5 s	14.6%	1000	9
	8 s	17.2%	1000	14
Traditional identification system 2	3 s	9.2%	1000	4
	5 s	8.7%	1000	8
	8 s	11.6%	1000	9
The proposed recognition system	3 s	0.3%	1000	0
	5 s	0.4%	1000	0
	8 s	0.2%	1000	0

signal of wireless image transmission can be effectively distinguished.

In the experiment, the transceiver parameters of NI-USRP 2029 digital transceiver that need to be adjusted are shown in Table 2.

The table, respectively, lists the specific parameters required by the equipment as signal generator and signal receiver, including the carrier frequency, symbol rate, modulation type, transceiver gain, and other parameters of the signal. In the experiment, the receiver is set to display and store the  $I/Q$  signal sequence to the hard disk every 50 ms; then, the sequence is processed into the format required by the subsequent work by the software and finally added to the data set.

**4.2. Generation of Data Set.** The experimental data used in the experiment are all generated and collected by the signal receiving and receiving equipment in the previous section. The experiment collects six kinds of experimental data: AM modulation signal, FM modulation signal, BPSK modulation signal, QPSK modulation signal, 8PSK modulation signal, and noise. Among them, the parameter range set in the signal generator to generate 5 modulation signals is shown in Table 3.

For the binary signals received by the receiver, the time-domain data set is obtained by reading every 16-bit binary signal as a real number. The SNR is added or interfered by the data specified by MATLAB simulation program, which makes the original regular signal start to spread randomly after noise.

**4.3. Experimental Results and Analysis of Packet Loss Rate.** After the preparation of experimental data, two widely used traditional recognition systems 1 and 2 (literature [15] and literature [16] systems) are compared with the designed system. Under the same experimental conditions, the packet

loss rate experiment and the recognition performance experiment are carried out, respectively. In the two groups of experiments, the data set in the above is taken as the target.

In the experiment of packet loss rate, different wireless image transmission intervals are set. In the process of identifying interference signals, the third-party plug-in is used to supervise the working process of the system. After the transmission, the packet loss rate, the total number of images, and the number of images with problems are output. The more the number of images with problems is, the higher the packet loss rate is. The experimental results are shown in Table 4.

According to the data in Table 3, with the change of transmission interval, the packet loss rate of the system has different changes. The highest packet loss rate of the two traditional recognition systems reaches 17.2%, and a certain number of problematic images appear, which indicates that the transmission reliability of the system is not guaranteed in the recognition process. In contrast, the packet loss rate of the designed recognition system based on deep learning is less than 0.5%, and there is no problem image when processing the same number of images, which indicates that the transmission reliability of the system is guaranteed. The reason why the design system has such a good effect is that the design system optimizes and updates the system parameters through the BP algorithm. After training, the system can be used to extract the input features. Then, through the superposition of convolution layers, the input signals are abstractly mapped layer by layer, and finally, the feature vector required by the classifier is obtained, which not only overcomes the influence of unknown operating parameters. It also ensures the integrity of information transmission and reduces the packet loss rate.

**4.4. Experimental Results and Analysis of Recognition Expressiveness.** Different recognition systems are used to

BPSK	0.89	0.0	0.0	0.0	0.0	0.0	0.0	0.0
QPSK	0.0	0.84	0.0	0.0	0.0	0.0	0.0	0.0
8PSK	0.0	0.02	0.71	0.0	0.0	0.0	0.0	0.0
16PSK	0.0	0.0	0.04	0.69	0.04	0.02	0.0	0.0
16QAM	0.0	0.0	0.03	0.06	0.76	0.04	0.0	0.0
64QAM	0.0	0.0	0.0	0.0	0.07	0.62	0.0	0.0
256QAM	0.0	0.0	0.0	0.0	0.02	0.05	0.59	0.0
GMSK	0.0	0.0	0.0	0.0	0.0	0.0	0.0	0.53
	BPSK	QPSK	8PSK	16PSK	16QAM	64QAM	256QAM	GMSK

(a) Experimental results of traditional recognition system 1

BPSK	0.92	0.0	0.0	0.0	0.0	0.0	0.0	0.0
QPSK	0.0	0.91	0.0	0.0	0.0	0.0	0.0	0.0
8PSK	0.0	0.01	0.74	0.0	0.0	0.0	0.0	0.0
16PSK	0.0	0.03	0.06	0.85	0.06	0.0	0.0	0.0
16QAM	0.0	0.0	0.0	0.0	0.79	0.04	0.0	0.0
64QAM	0.0	0.0	0.0	0.0	0.05	0.83	0.0	0.0
256QAM	0.0	0.0	0.0	0.0	0.02	0.04	0.62	0.0
GMSK	0.0	0.0	0.0	0.0	0.0	0.0	0.0	0.54
	BPSK	QPSK	8PSK	16PSK	16QAM	64QAM	256QAM	GMSK

(b) Experimental results of traditional recognition system 2

BPSK	1.0	0.0	0.0	0.0	0.0	0.0	0.0	0.0
QPSK	0.0	0.98	0.0	0.0	0.0	0.0	0.0	0.0
8PSK	0.0	0.0	0.95	0.0	0.0	0.0	0.0	0.0
16PSK	0.0	0.0	0.0	0.92	0.0	0.0	0.0	0.0
16QAM	0.0	0.0	0.0	0.0	0.94	0.0	0.0	0.0
64QAM	0.0	0.0	0.0	0.0	0.0	0.96	0.0	0.0
256QAM	0.0	0.0	0.0	0.0	0.0	0.0	0.97	0.0
GMSK	0.0	0.0	0.0	0.0	0.0	0.0	0.0	0.91
	BPSK	QPSK	8PSK	16PSK	16QAM	64QAM	256QAM	GMSK

(c) Experimental results of the proposed recognition system

FIGURE 2: Experimental results of recognition expressiveness of different recognition systems.

process the signals in the experimental data set, and the recognition performance of the recognition system is analyzed according to the recognition level of different types of signals. The signals in the experimental data set are completed by NI-USRP2920. Before the experiment, MATLAB is used to interfere with the signals, and then, different recognition systems are used to identify them. The recognition results are shown in the form of confusion matrix, and the specific content is shown in Figure 2.

Compared with the experimental results, it can be seen that BPSK and GMSK are the most easily recognized signal types, and their accuracy is the highest among all the results. The experimental result of the proposed recognition system is the best, reaching 100%. Among other signals, the traditional recognition system has the worst recognition effect on 256QAM and GMSK signals, only about 50%, while the recognition accuracy of the proposed recognition system is more than 90%. And it can be seen from the results in the figure that the traditional recognition system has a certain deviation for the recognition of some signals, so it is difficult to correctly identify the signal type, but the proposed signal recognition system can maintain a more accurate recognition effect. This is because the design system not only uses STM32F107VT and SI4463 to form a wireless controller to control the execution of each instruction but also takes the time-domain characteristics of the interference signal as the target to extract the characteristic vector of the interfer-

ence signal. With the support of the GAP-CNN model, the interference signal is recognized through the training and learning of the feature vector. Through multiple guarantees, the signal recognition effect is improved.

Combined with the experimental analysis of the system packet loss rate, it can be seen that the designed wireless image transmission interference signal recognition system based on deep learning is more reliable, and the performance of interference signal recognition is also very good. The overall reliability of the system is better than the traditional recognition system.

## 5. Conclusion

With the emergence of a large number of wireless communication signals, signal service identification has become a new requirement in the field of signal identification. In the field of wireless image transmission, signal recognition is very important. It is an important link to ensure the quality of image transmission. On this basis, based on a large number of literature research, a wireless image transmission interference signal recognition system based on deep learning is proposed, the development and design of the whole system are completed from two aspects of hardware and software, and a large number of comparative experiments are carried out. The reliability of the designed system is verified by experiments. This shows the effect and function of the

system designed in this paper in the field of interference signal recognition. However, the interference signals are not classified during the design, which may affect the identification effect. In the next research process, we will conduct in-depth research on this point to better improve the interference signal identification effect of the design system.

### Data Availability

The data sets used and/or analyzed during the current study are available from the corresponding author on reasonable request.

### Conflicts of Interest

It is declared by the authors that this article is free of conflict of interest.

### Acknowledgments

This study was financially supported by the Natural Science Foundation of Hunan Province with No. 2020JJ4434 and Hunan Provincial Science and Technology Department Project Foundation (2018TP1018, 2018RS3065).

### References

- [1] X. LI, J. LI, Y. QU, and D. HE, "Semi-supervised gear fault diagnosis using raw vibration signal based on deep learning," *Chinese Journal of Aeronautics*, vol. 33, no. 2, pp. 418–426, 2020.
- [2] S. Y. Lee, C. Tsou, and P. W. Huang, "Ultra-high-frequency radio-frequency-identification baseband processor design for bio-signal acquisition and wireless transmission in healthcare system," *IEEE Transactions on Consumer Electronics*, vol. 66, no. 1, pp. 77–86, 2020.
- [3] C. F. Yee, M. Mohamad Isa, A. Abdullah al-Hadi, and M. K. Md Arshad, "Techniques of impedance matching for minimal PCB channel loss at 40 GBPS signal transmission," *Circuit World*, vol. 45, no. 3, pp. 132–140, 2019.
- [4] A. L. Yi, L. S. Yan, H. J. Liu et al., "Modulation format identification and OSNR monitoring using density distributions in Stokes axes for digital coherent receivers," *Optics Express*, vol. 27, no. 4, pp. 4471–4479, 2019.
- [5] W. P. Tang, A. Q. Wang, S. Ramkumar, and R. K. R. Nair, "Signal identification system for developing rehabilitative device using deep learning algorithms," *Artificial Intelligence in Medicine*, vol. 102, 2020.
- [6] A. H. Tan and K. R. Godfrey, "Direct synthesis signal sets for multi-input system identification," *Systems & Control Letters*, vol. 124, pp. 92–98, 2019.
- [7] S. S. Miriyala and K. Mitra, "Deep learning based system identification of industrial integrated grinding circuits," *Powder Technology*, vol. 360, pp. 921–936, 2020.
- [8] G. Singh, S. Agrawal, and B. S. Sohi, "Handwritten Gurmukhi digit recognition system for small datasets," *Traitement du Signal*, vol. 37, no. 4, pp. 661–669, 2020.
- [9] X. D. Yan and X. G. Song, "An image recognition algorithm for defect detection of underground pipelines based on convolutional neural network," *Traitement du Signal*, vol. 37, no. 1, pp. 45–50, 2020.
- [10] H. Qu, T. Feng, Y. Wang, and Y. Zhang, "AdaBoost-SCN algorithm for optical fiber vibration signal recognition," *Applied Optics*, vol. 58, no. 21, 2019.
- [11] E. Agliari, F. Alemanno, A. Barra, M. Centonze, and A. Fachechi, "Neural networks with a redundant representation: detecting the undetectable," *Physical Review Letters*, vol. 124, no. 2, article 028301, 2020.
- [12] R. Supekar and T. Peacock, "Interference and transmission of spatiotemporally locally forced internal waves in non-uniform stratifications," *Journal of Fluid Mechanics*, vol. 866, pp. 350–368, 2019.
- [13] K. Takahashi, T. Yamada, and Y. Takemura, "Circuit parameters of a receiver coil using a Wiegand sensor for wireless power transmission," *Sensors*, vol. 19, no. 12, p. 2710, 2019.
- [14] W. H. W. Hassan, S. M. Idrus, H. King, S. Ahmed, and M. Faulkner, "Idle sense with transmission priority in fibre-wireless networks," *IET Communications*, vol. 14, no. 9, pp. 1428–1437, 2020.
- [15] F. Fang, Y. Li, Y. Niu, and Y. Wang, "Interference signal recognition based on decision tree algorithm," *Communication Technology*, vol. 52, no. 11, pp. 2617–2623, 2019.
- [16] L. Yang, X. Zhang, L. Li, and G. Wang, "Research on range velocity composite deception jamming identification technology based on space-time frequency feature fusion," *Systems engineering and electronic technology*, vol. 41, no. 12, pp. 2684–2691, 2019.
- [17] A. Lund, S. J. Dyke, W. Song, and I. Bilonis, "Global sensitivity analysis for the design of nonlinear identification experiments," *Nonlinear Dynamics*, vol. 98, no. 1, pp. 375–394, 2019.
- [18] T. F. Bernard Marie, D. Han, and B. An, "Pattern recognition algorithm and software design of an optical fiber vibration signal based on  $\Phi$ -optical time-domain reflectometry," *Applied Optics*, vol. 58, no. 31, pp. 8423–8432, 2019.
- [19] R. Hercik, Z. Machacek, J. Koziorek, J. Vanus, M. Schneider, and W. Walendziuk, "Continuity detection method in binary image signal," *Elektronika ir Elektrotechnika*, vol. 26, no. 6, pp. 4–9, 2020.
- [20] W. Lejmi, A. B. Khalifa, and M. A. Mahjoub, "A novel spatio-temporal violence classification framework based on material derivative and LSTM neural network," *Traitement du Signal*, vol. 37, no. 5, pp. 687–701, 2020.

## Research Article

# Drive System Design for Small Autonomous Electric Vehicle: Topology Optimization and Simulation

Zhongming Wu , Mufangzhou Zhu, Yu Guo, Li Sun, and Yuchen Gu

Department of Mechanical and Electrical Engineering, Jinling Institute of Technology, Nanjing 211169, China

Correspondence should be addressed to Zhongming Wu; wuzhming0926@163.com

Received 30 September 2021; Accepted 3 November 2021; Published 16 December 2021

Academic Editor: Deepak Gupta

Copyright © 2021 Zhongming Wu et al. This is an open access article distributed under the Creative Commons Attribution License, which permits unrestricted use, distribution, and reproduction in any medium, provided the original work is properly cited.

High driving efficiency remains challenging in autonomous electric vehicles, especially in small electric vehicle subtype. Here, we reported investigation of the structure and requirements of the drive system for those vehicles, while the motor-drive axle combined integrated driving scheme has been chosen. In the study, the power matching of drive motor as well as transmission ratio has been calculated based on the performance of the small electric vehicles, and the total gear ratio of 8.124 was determined. For better comprehensive performance and efficiency, the two-stage retarder has been designed, in which elements including high-speed shaft, low-speed shaft, gears, and differential have been examined to ensure their proof strength when the motor outputs reached the maximum torque. Notably, by utilizing topology optimization, Gear 4, the transmission unit with the heaviest weight percentage has been modified in a lightweight way, achieving a 41% reduction of the mass in emulation analysis and turned up to the target of optimization eventually.

## 1. Introduction

Energy conservation and environmental protection remain a great global social concern, with great attention on the development and applications of energy-saving and emission reduction technology in the industry and daily life. It is widely accepted in the reduction of carbon emission, and thus, particular carbon emission management has been established in some countries and regions. Fossil fuels are the common energy resources for traditional vehicles, which has been identified as the pivotal field for carbon emission governance. Currently, energy-saving and emission reduction technology leads the development of vehicles, in which technology for new energy vehicles holds priority by research institutions and auto enterprises. Compared to conventional fossil-fueled cars, electric vehicles hold various advantages, such as zero-carbon, heralding vast potentials for application, and considerable market prospects, whereas the rapid technology development has been achieved by auto industries.

The drive system, one of the essential units in electric vehicles, directly influences the vehicles' performance and efficiency, indicating the necessity of the particular optimization

in compacting structure for better match of the driving motor. Ample of studies have shown the simpler and more compact driving system in electric cars than in patrol-driven cars.

Hence, the study was designed to reduce the mass and volume of the driving system for the improvement of transmission efficiency and further reduction of energy consumption under the ensurance of reliable properties. Based on previous studies, we designed the transmission system of the electric vehicles and optimized the driving system by reducing the weight of transmission units following the requirements, for further enhancement of dynamic performance of the vehicles [1–3].

## 2. Requirements for Vehicle Performance and Matching of Driven Parameters

Partial transmission scheme, one of the schemes for electric vehicles, has a simple structure. It utilized a centralized driven method through a single reduction gear with constant speed ratio and limited adjustment. Within this scheme, the request for a driving cycle was completely dependent on motor speed regulation, contributing to the dynamic



underperformance of electric vehicles at medium-high speed. Hence, for a superior balance between cost and performance, the two-stage retardation method in power transmission with motor-drive integrated driving formulation has been investigated.

*2.1. Technical Parameters of Electric Vehicles A Subsection.* The technical parameters and design requirements of a small electric car have been listed in Table 1.

*2.2. Selection and Matching of Driving Motor.* Driving motor has been employed in electric cars at present, including DC motor, AC asynchronous motor, permanent-magnet synchronous machine, and switched reluctance machine. The features of those motors vary. DC motor has been used in electric vehicles at an early stage and gradually been replaced due to its complicated large structure along with frequently high-cost maintenance. Permanent-magnet synchronous machine, among the AC motors, has competitive overload capacity, with higher load efficiency and power factors than others, but inferior in constant power factor. Even though, the permanent-magnet synchronous machine, which is small in size, holds advantages of torque performance, high efficiency, and reliability was used in our study.

*2.2.1. Power Matching of Driving Motor.* It is known that driving motor plays a decisive role in the performance of the vehicle. Driving motors with low power cannot afford valid dynamic properties and in turn make themselves overloaded for a long time, which negatively influences their lifetime. On the other hand, high-power motors provide great reserve capability with increased mass and volume, affecting the overall efficiency of vehicles, and hence, they are not the economical option for electric cars [4–6].

To find a suitable driving motor for electric vehicles, several factors including rated output, peak power, rated revolution, and the maximum revolution, should be taken under consideration.

First, the rated output and peak power of the motor was determined, in which rated output should support the long-term steady run of the car at the highest speed. Rolling resistance and air resistance impact when cars are on the road. In accordance with those factors, under the maximum speed ( $V_{\max}$ ), the required power of the vehicle can be calculated based on the following formula.

$$P_{V_{\max}} = \left( mgf + \frac{C_D AV_{\max}^2}{21.15} \right) \frac{V_{\max}}{3600\eta_T}. \quad (1)$$

In the formula,  $m$  represents complete vehicle curb mass (kg);  $g$  represents gravitational acceleration ( $m/s^2$ );  $f$  represents the coefficient of rolling resistance;  $C_D$  represents the coefficient of air resistance;  $A$  represents frontal area;  $V_{\max}$  represents maximum speed (km/h), and  $\eta_T$  represents transmission efficiency.

The rated power of driving motor in electrical vehicles should be more than 90% of the required power when the vehicles driving on the horizontal road at highest speed. In another word, the minimum power for electrical vehicles

TABLE 1: Technical parameters of electric vehicles.

Name of parameters	Value
Complete vehicle curb mass ( $m$ )	950
Maximum loading capacity (kg)	210
Frontal area $A$ ( $m^2$ )	1.94
The rolling radius of the tire $R$ ( $m$ )	0.329
Transmission efficiency $\eta_T$	0.86
Coefficient of air resistance $C_D$	0.3
Correction coefficient of mass $\delta$	1.04
Coefficient of rolling resistance $f$	0.011
Maximum speed $V_{\max}$	110 km/h
Maximum gradeability $i_{\max}$ 25 km/h	25%
Driving mileage $s$	150 km
Acceleration time (0-50 km/h)	8 s
Acceleration time (0-100 km/h)	14 s

to run at maximum speed on the horizontal road can be set as the minimum value of the rated power. In addition, taking the requirement from accessories of vehicles into consideration, the final calculated rated power is 20 kW and peak power is 40 kW (based on Formula (2)).

Further, the peak power of the motor was determined by the  $V_{\max}$ , maximum gradeability and the acceleration time, which has been given in the following formula.

$$P_{mas} \geq \max (P_{V_{\max}}, P_{i_{\max}}, P_t). \quad (2)$$

Apart from the rolling resistance and air resistance, grade resistance should be considered. When the stabilized speeding for climbing is 25 km/h, the related power can be calculated as per the following equation.

$$P_{i_{\max}} = \left( mgf \cos \alpha_{\max} + mg \sin \alpha_{\max} + \frac{C_D AV_s^2}{21.15} \right) \frac{V_s}{3600\eta_T}. \quad (3)$$

In the equation,  $\alpha_{\max}$  represents the maximum angle of gradient;  $V_s$  represents stabilized speed (km/h).

The acceleration time of the vehicle was confirmed on a horizontal road, thus, the required power for accelerating time in the absence of grade resistance can be calculated by the following equation.

$$P_t = \left( mgf + \frac{C_D AV^2}{21.15} + \delta m \frac{dv}{dt} \right) \frac{V}{3600\eta_T}. \quad (4)$$

In the equation,  $v$  represents running speed (km/h);  $\delta$  represents the correction coefficient of mass.

Subsequently, the equivalent fitting has been employed to the procedure from standstill to acceleration of the vehicle, simplifying the calculation of the connection between speed and acceleration time, which has been revealed in the following equation.

$$V = V_m \left( \frac{t}{t_m} \right)^a. \quad (5)$$

In the equation,  $V_m$  indicates the speed at the end of acceleration (km/h);  $t_m$  represents accelerating time (s);  $a$  represents fit coefficient (in general,  $a = 0.5$ ).

Equation (6) shown below can be obtained when plugging Equation (5) into Equation (4):

$$P_t = \left( mgf \frac{V_m}{1.5} + \frac{C_D A V_m^3}{52.875} + \frac{\delta m V_m^2}{7.2 t_m} \right) \frac{1}{3600 \eta_T}. \quad (6)$$

In accordance with acceleration time mentioned in Table 1, 50 km/h and 100 km/h were taken as  $V_m$  separately, while 8 s and 14 s were taken as  $t_m$ , respectively. After the calculation, the power required for 0-50 km/h acceleration is 15.40 kW, whereas 37.42 kW is needed for 0-100 km/h acceleration.

Further, to sustain the highest speed, the minimum power of the motor is 15.47 kW, and also the minimum motor power for climbing is 19.21 kW. Taken together, the peak power for acceleration time is the largest among those various conditions. Based on Equation (2), the motor peak power should be no less than 37.42 kW. With a certain overload capacity, motors within electric cars have the rated power which is more than 90% of the power needed for the highest running speed on the level road [7]. In addition, attachments such as electronic devices and air conditioners consume amounts of power in the car. Thus, in this paper, we took the power required for cars running with the highest speed on the horizontal road as the lower limit for the rated power of the driving motor, which means the minimum rate power is 15.47 kW.

**2.2.2. Options for Driving Motors.** The permanent-magnet synchronous machines have a maximum speed from 4000 to 10000 r/min in general, belonging to medium speed motors. The coefficient of expanded power zone ( $\beta$ ), which is around 2 to 4, has been identified by the ratio between the highest speed and rated speed of the motor. The higher the maximum speed of the driving motor, the stricter production along with higher cost would be, in which higher quality of gear and bearing units within the transmission system needs to be reinforced, especially in impact resistance and fatigue endurance [8]. Here, we set the initial rated speed of the motor as 2500 r/min, the highest speed as 8000 r/min, and  $\beta$  value as 3.2.

Under the condition, the rated power of the driving motor was 20 kW and peak power was 40 kW, while calculated rated torque and peak torque equaled  $76 \text{ N} \cdot \text{m}$  and  $152 \text{ N} \cdot \text{m}$ , respectively. The parameters for the motor have been given in Table 2.

### 3. Design of Transmission System

**3.1. Options for the Transmission Scheme.** The transmission scheme of electric cars has been roughly divided into mechanical drive layout, motor-drive axle integral, and distributed layout, in which mechanical drive layout is out of

TABLE 2: Parameters of driving motor.

Parameters	Value
Rated power	20 kW
Peak power	40 kW
Rated speed	2500 r/min
Peak speed	8000 r/min
Rated torque	$76 \text{ N} \cdot \text{m}$
Peak torque	$152 \text{ N} \cdot \text{m}$

date. Distributed electric drive has attracted massive attention recently; however, its further full-fledged application remains challenging. Currently, the motor-drive axle combined scheme, used in almost electric vehicles on the market, is simple in structure but with high efficiency, which exerts the similar driving performance of traditional fuel cars and has lower development cost compared to the integral scheme. Thus, it has been chosen by various companies and put on the front axle of the vehicle for cost control.

In the motor-drive combined scheme, the transmission box has several formulations, including constant speed ratio retarder and multidrive. Multidrive has increased gears, which could raise the operating time of motors while running with high efficiency, improving the dynamic and economic properties of the vehicle. Nevertheless, there is a limitation of the gears, and excessive gears complicate transmission with increased mass and cost. It is well accepted that two-speed transmission is available for existing electric vehicles, where additional gears will not bring obvious improvements of the performance other than the reduction of efficiency. Further, the transmission system directly impacts on the dynamic properties and mechanical efficiency. Therefore, the fixed speed ratio retarder, which has a simple structure, lightweight, compact size, and low cost, has been employed in current electric vehicles to slow down and increase torque. Furthermore, small electric vehicles we investigated declared low dynamic properties, while the permanent magnet synchronous motor chosen for them was equipped with excellent wide-range low-speed torque [9]. Hence in the study, to reduce the cost, the fixed speed ratio retarder has been adopted with conventional differential to make up the deceleration system. As shown in Figure 1, the double reduction was composed of four gears, in which Gear4 was integrated with the differential to reduce install size and weight. Back motion can be achieved by motor reversal. In addition, the motor was connected with a high-speed shaft through splines. For compact structure, in integrated Gear4-differential, the bevel gear of the differential was placed at the right end of Gear4 and assembled inside the retarder shell with splash lubrication.

**3.2. Design of Transmission Ratio.** The transmission ratio plays a pivotal role in the dynamic and economic properties of vehicles [10]. The allowed minimum and maximum transmission ratio value should be calculated, so a suitable total transmission ratio can be chosen.

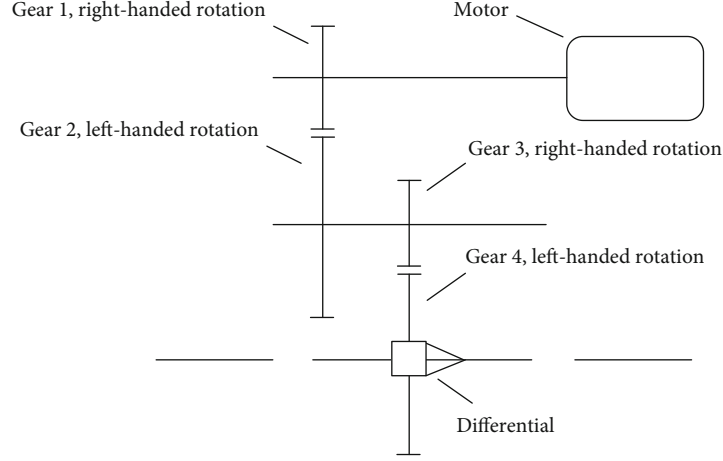


FIGURE 1: Two-dimension diagram of deceleration system.

The maximum transmission ratio enables vehicles to climb at a steady speed when the motor outputs the maximum torque, as shown in the following formula.

$$i_0 \cdot i_g \geq \frac{[mg(f \cos \alpha_{\max} + \sin \alpha_{\max}) + (C_D AV_s^2/21.15)]}{T_{\max} \cdot \eta_T}. \quad (7)$$

In the formula,  $i_0$  represents transmission ratio of the main retarder,  $i_g$  represents transmission ratio of differential,  $r$  represents rolling radius of the tire (m), and  $T_{\max}$  represents peak torque of motor ( $N \cdot m$ ). And also, in Formula (8), the maximum driving force should be no more than the adhesive rate.

$$i_0 \cdot i_g \leq \frac{F_Z \cdot \phi \cdot r}{T_{\max} \eta_T}. \quad (8)$$

In the formula,  $F_Z$  represents the normal reaction of the ground to the driving wheel, and  $\phi$  represents the coefficient of adhesion (0.8 has been used in the study). After calculation, the range of  $i_{\max}$  is from 5.987 to 9.373.

Then, minimum transmission ratio has a relation with the maximum speed and running resistance of the vehicle, which has been shown in Formula (9).

$$i_0 \cdot i_g \leq \frac{0.377r \cdot n_{\max}}{V_{\max}}. \quad (9)$$

In the formula,  $n_{\max}$  represents the maximum speed of the motor, and  $V_{\max}$  represents maximum speed (km/h), complied with the following formula.

$$i_0 \cdot i_g \geq \frac{(mgf + C_D AV_{\max}^2) \cdot r}{T_{\max} \eta_T}. \quad (10)$$

The estimated range for  $i_{\min}$  is 1.096 to 9.021.

Taken together, the total range of the designed transmission ratio in the study has been shown in the following formula.

TABLE 3: Transmission parameters.

Parameters	Value
First transmission ratio	2.789
Peak power of the motor	40 kW
Peak torque of the motor	152 $N \cdot m$
Input torque of the high-speed shaft	152 $N \cdot m$
Input power of the high-speed shaft	40 kW
Input torque of the low-speed shaft	415.449 $N \cdot m$
Input power of the low-speed shaft	39.20 kW

TABLE 4: Gear parameters for differential.

Parameters	Axle shaft gear	Planetary gear
The number of teeth	20	16
Module	3 mm	3 mm
Helix angle	51.340°	38.660°
Reference diameter	60 mm	48 mm
Gear width	12 mm	12 mm
Pressure angle	22°30'	22°30'

$$\begin{cases} 5.987 \leq i_{\max} \leq 9.373, \\ 1.096 \leq i_{\min} \leq 9.021. \end{cases} \quad (11)$$

Due to the high speed of the driving motor, a relatively small ratio of transmission should be excluded from the design. Based on the abovementioned calculation,  $i_{\max}$  should be no more than 9.021 while  $i_{\min}$  should be no less than 5.987. Thus, the initial transmission ratio was set as 8.1. Generally, the equal speed ratio principle was employed in the two-stage transmission ratio [11].

### 3.3. Design and Modeling of the Transmission Case

**3.3.1. Parameter Calculation.** Both first and second gear in retarder were driven by helical cylindrical gear, and their parameters have been exhibited in Table 3.

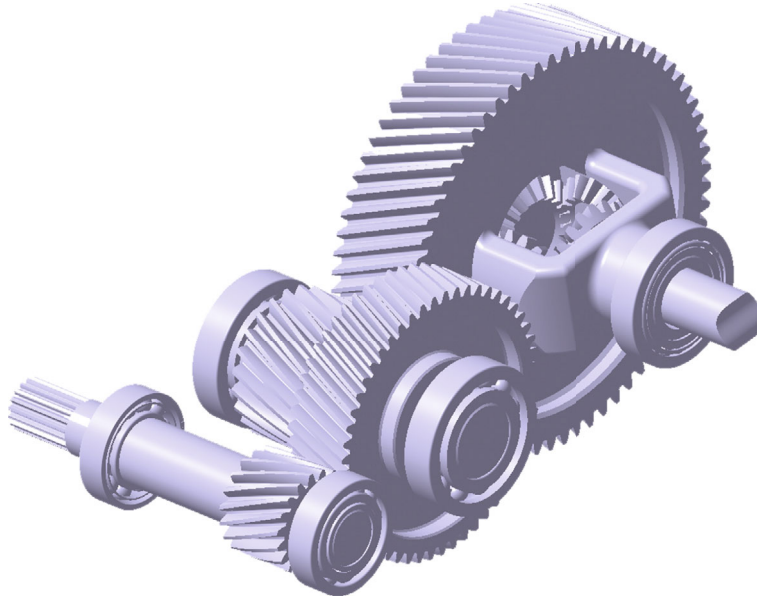


FIGURE 2: Structure model of the transmission case.

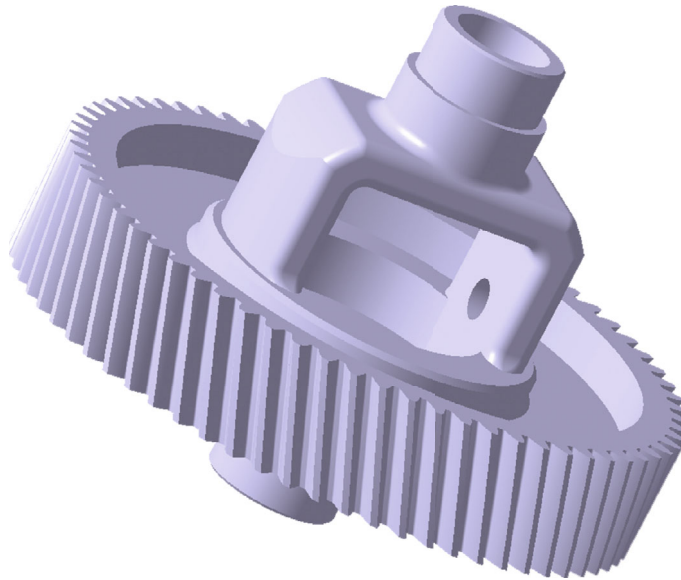


FIGURE 3: Model after web thickness reduction.

As per the design manual, the first transmission-related parameters have been examined and displayed as follows: the number of Gear 1 teeth ( $z_1 = 19$ ), the number of Gear 2 ( $z_2 = 53$ ), module (2.5 mm), center distance (97 mm), helix angle ( $21.90^\circ$ ), reference diameter of Gear 1 (51.194 mm), reference diameter of Gear 2 (142.805 mm), gear width ( $b_1 = 40$  mm,  $b_2 = 38$  mm), and transmission ratio (2.789). Similarly, second gear was driven by helical cylindrical gear, in which the number of teeth in pinion ( $z_3$ ) was 23 and in rack wheel ( $z_4$ ) was 67 along with the coefficient of face width as 0.7, followed by serious parameters including standard module ( $m_2 = 3.0$ ), center distance (146 mm), helix angle ( $22.392^\circ$ ), reference diameter of Gear 3 (74.627 mm),

reference diameter of Gear 4 (217.391 mm), gear width ( $b_3 = 60$  mm,  $b_4 = 55$  mm), and transmission ratio (2.913).

In accordance with the bearing requirement of small electric vehicles, the planetary gear number was set as 2. The spherical radius of planetary gear ( $R_b$ ) can be roughly determined by empirical in the following formula.

$$R_b = K_b \sqrt[3]{T_d}. \quad (12)$$

In the formula,  $T_d$  represents calculated torque of differential,  $K_b$  represents spherical radius coefficient of planetary gear, and  $K_b = 3.0$  has been taken in the study. Added,  $R_b$



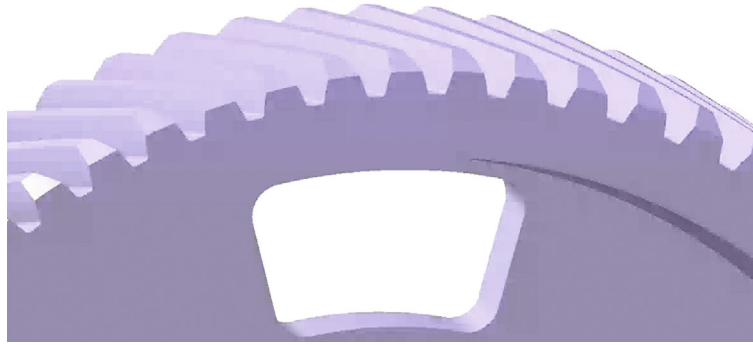


FIGURE 4: Structure of the through-hole.

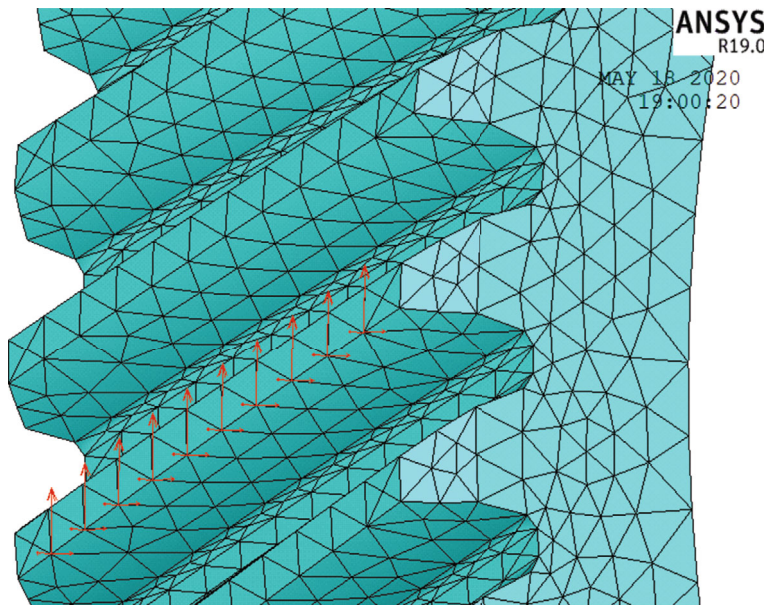


FIGURE 5: Position of applied force.

was set as 31.744 mm, and thus, pitch cone of planetary gear ( $A_0$ ) might be 31.11 mm and 31.43 mm based on the equation  $A_0 = (0.98 \sim 0.99)/R_b$ . The differential was connected directly to the final output axis, which has been identified as an axle shaft, under large torque force, and thus, greater module ( $m = 3$  mm) was adopted for assurance of strength. Generally, the teeth number of planetary gear ( $z_1$ ) should be no less than 10, whereas the teeth number of axle shaft gear ( $z_2$ ) should be between 14 to 25, with a teeth ratio ( $z_2/z_1$ ) between 1.5 and 2.0 [12]. For engagement of those four bevel gears simultaneously, the number of their teeth should be even ( $z_1 = 16$ ,  $z_2 = 20$ , shown in Table 4).

20CrMnTi has been well studied as the conventional materials used in vehicles' gearbox shafts. Here, we reported the design and examination of the important units of retarder, including high-speed shaft, low-speed shaft, transmission gears, bearing units, and other retarder components, to make sure the reliable strength under the motor's maximum torque output. As the high-speed shaft was designed

to have a straightforward connection with the motor, the minimum diameter of the high-speed shaft was defined as 30 mm while 40 mm for the low-speed shaft in diameter.

*3.3.2. Modeling of the Driving System.* The model of retarder assembled by CATIA has been shown in Figure 2.

#### 4. Light-Weight Design of Transmission Case

Driving mileage has a decisive impact on the development of electric vehicles, whose weight in turn influences their driving mileage. Hence, under the condition of safety concerns, utilization of advanced materials along with novel technology could cut down the weight of the car, extending the vehicle's driving mileage, which could also improve the dynamic and economic properties by saving materials and resources. As has been exhibited in Figure 2, Gear 4, the biggest gear in the transmission case, reached 12.725 kg in weight, whose light-weight design holds particular significance.



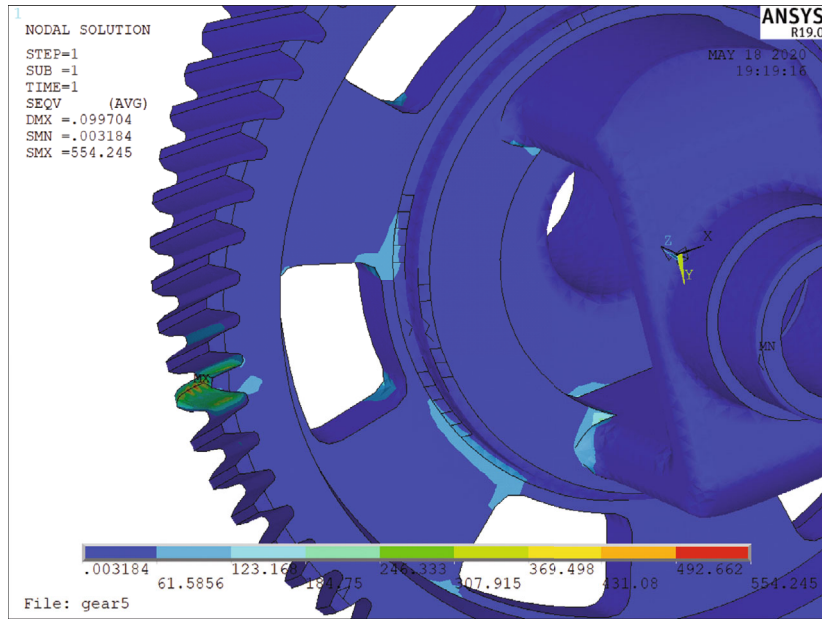


FIGURE 6: Simulated stress nephogram.

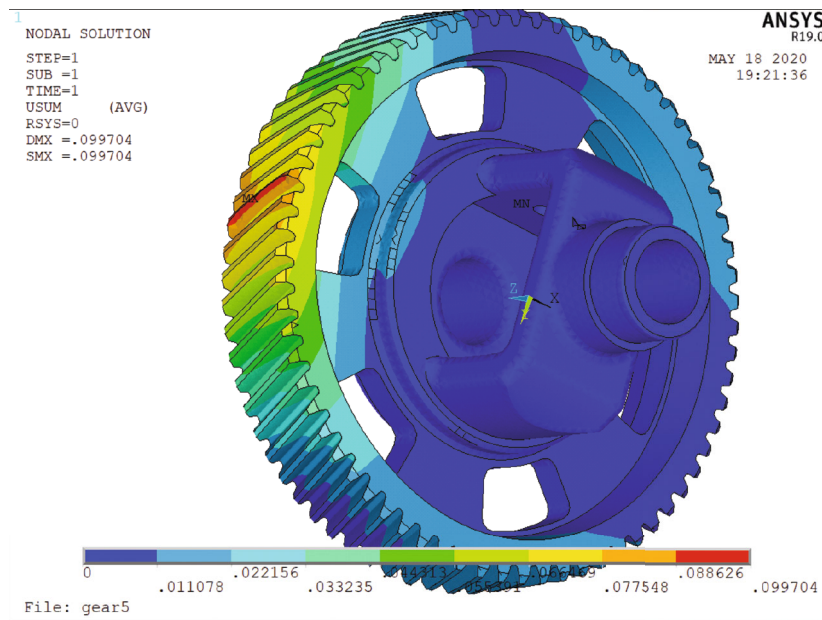


FIGURE 7: Simulated displacement nephogram.

*4.1. Method for Light-Weight Design.* Conventional mechanical design has been used in the gears. In other words, root bending fatigue limit and contact fatigue limit of tooth surface provided the basis of gear design, in which excessive safety coefficient leads to much more redundancy in gear size [1]. 20CrMnTi, used in the study, has a considerable high tensile strength of more than 1080 MPa, offering opportunities for size optimization. Gears comprise hub, rim, and web in common. However, due to the presence of differential, Gear 4 did not have the structure of hub, and also chances for light-weight improvement of differential

are less. Further, the rim of the gear was determined by its basic parameters, which has been almost fixed in structure. Therefore, the optimization was focused on Gear 4 [13] by reduction of coefficient of gear width followed with spoke type improvement.

In the transmission case, the initial coefficient of face width was 0.7 and the face width was 55 mm. And the target coefficient of face width and the face width was 0.56 and 44 mm, respectively. Under the circumstance, in accordance with the conventional gear design, the corresponding reference diameter of Gear 3, which was engaged

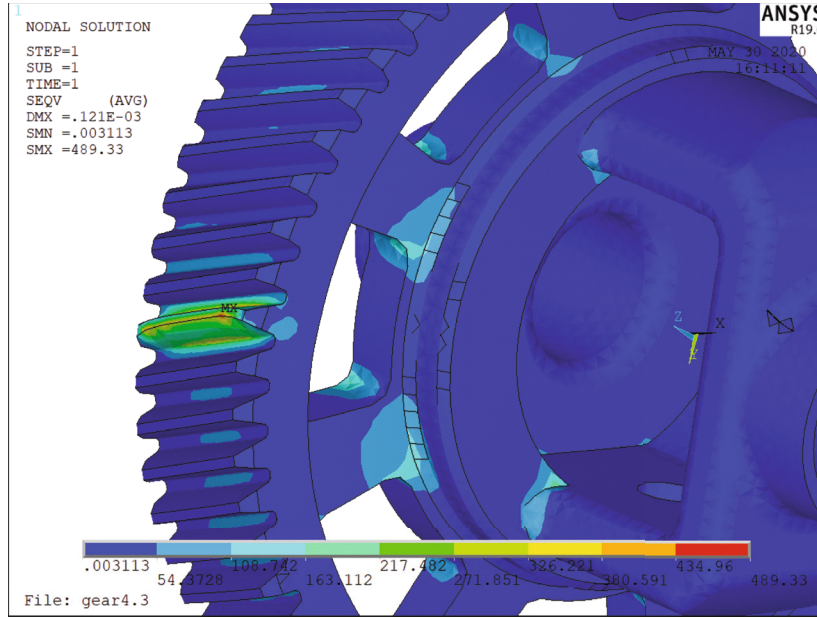


FIGURE 8: Simulated stress nephogram.

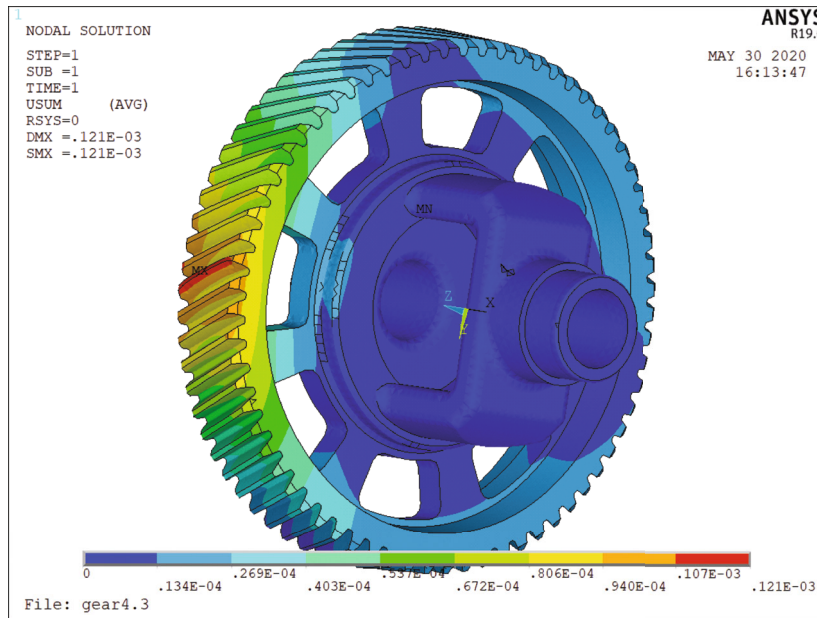


FIGURE 9: Simulated displacement nephogram.

with Gear 4, should be more than 42.35 mm following by module (more than 2.192 mm). So, the gear reached the strength requirements.

Hence, in the study, the main work of the optimization was to improve and examine the spoke type of Gear 4 for light-weight design.

**4.2. Light-Weight Design of Gear Structure.** Due to concern of the structure, the optimization design of the overall transmission system is mainly carried on Gear 4, which has the largest weight proportion, by reducing the tooth width coefficient and optimizing the spoke structure. The principle of optimal design contains two parts. One side, the strength

should meet the requirement. On the other side, there is no possibility of resonance when transmission gears are working after modal analysis. Therefore, lightweight design, in which FEM from ANSYS was used to analyze the gradually optimized structure, has been applied in the optimization of gear structure. The main process was as follows:

- (1) *Thickness Reduction of the Web.* Regularly, gear structure can be divided into several types, including solid, web, and spoke type. As has been mentioned in Section 3.3.1, the reference diameter for Gear 4 was 217.4 mm, and the web type was used. As per the manual of mechanical design, the thickness of the

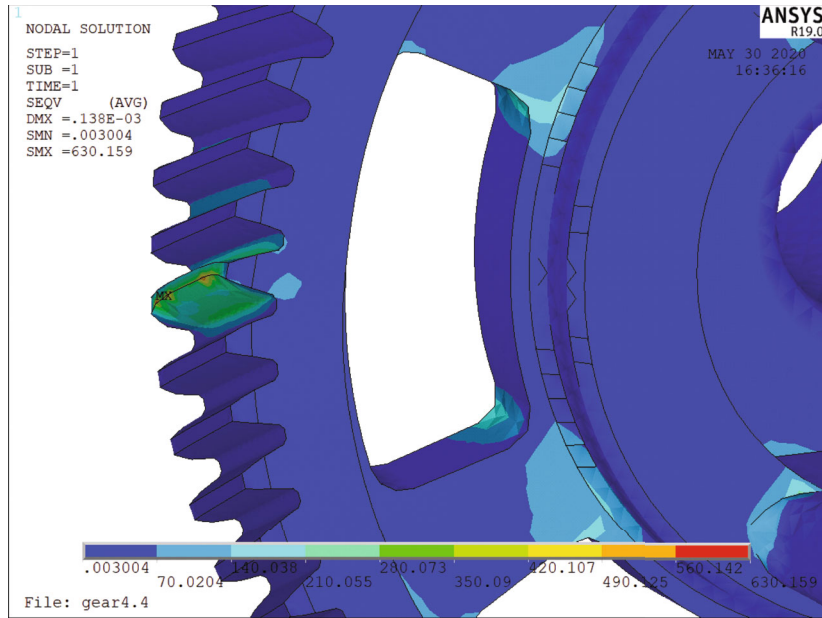


FIGURE 10: Simulated stress nephogram.

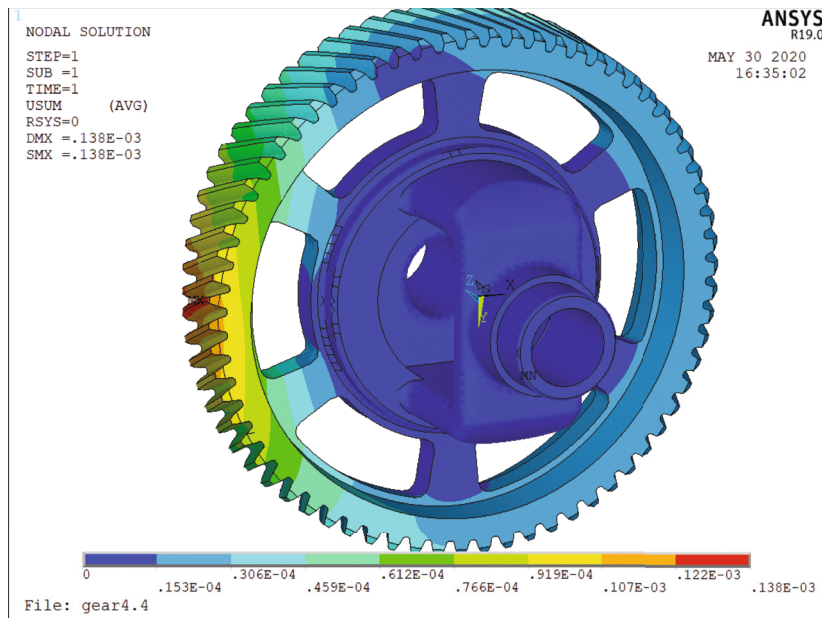


FIGURE 11: Simulated displacement nephogram.

web should be no less than 10 mm. Therefore, based on references, 13 mm of thickness was defined. The structure was shown in Figure 3

(2) *Optimization of Web Topology.* In general, topological optimization indicates the investigation of best material distribution scheme, which could bear the load, within the design area. Thus, the stress distribution on the web of the gear under the working condition could be quickly determined through

topological optimization, from which the optimized scheme could be picked. In another word, the proportion in system for light-weight optimization could be confirmed. Therefore, few steps should be followed. The finite element model should be set up firstly, followed by gear material selection. Then, the corresponding load can be applied to the model with settled boundary conditions, and the topology optimized results can be achieved in Ansys/Workbench. Huang and colleagues analyzed gear topology optimization based on Ansys/Workbench. The outward of those gears' web was reported to have

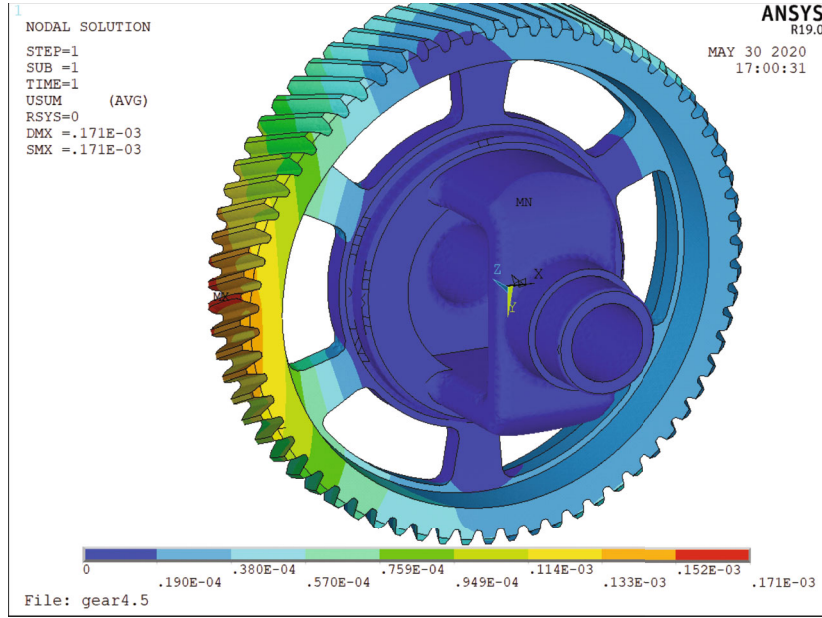


FIGURE 12: Simulated stress and displacement nephogram.

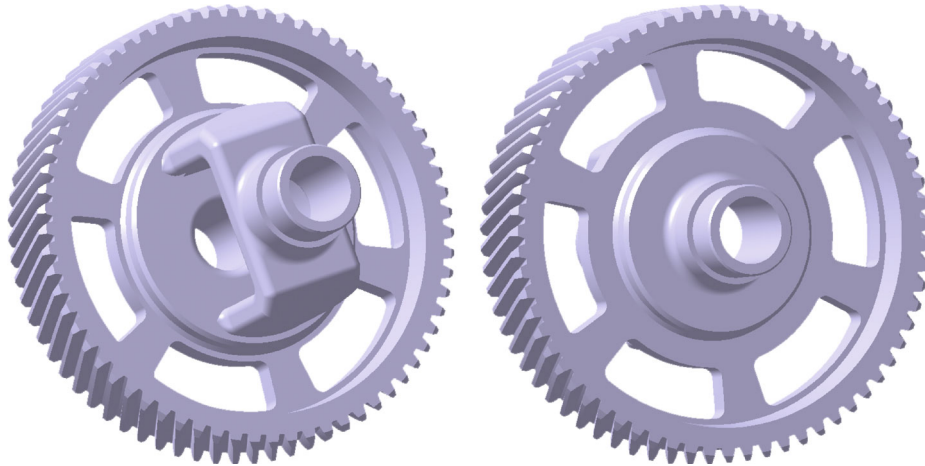


FIGURE 13: Optimized structure of Gear 4.

considerable residual strength, which could be hollowed out for light-weight purposes [14]. In addition, the equivalent stress on spoke-plate gears was less compared to circular hole structures with the same material. Taken together, six through-holes were made on the outward of the web at first. The area of a single through-hole was  $9.932 \text{ cm}^2$ , while the total area of the through-hole was  $59.592 \text{ cm}^2$ . The specific structure has been displayed in Figure 4

Based on the analysis of dedendum bending stress, the peak stress of gear engagement emerged at the place of through holes. Thus, mesh division was applied to the model, followed by circumferential force, radial force, and axial force on the addendum circle of the through-hole (Figure 5).

In Figure 6, the acceptable maximum stress (554 MPa) appeared on the tooth surface, which is within the limit contact stress of 20CrMnTi (745 MPa). However, in Gear 4, at

TABLE 5: Modal frequency of nonupdated Gear 4.

Oder	Intrinsic frequency (Hz)
1	901.23
2	1492.5
3	1924.4
4	2307.3
5	2314.9
6	2351.1

the root of differential shell and inner ring of the web, stress concentration came up with the value around 130 MPa, indicating the further improvement could be achieved considering the materials' features. Nevertheless, in Figure 7, the maximum displacement (0.0997 mm) took place on the tooth surface where force was applied, confirmed to safety standards.



TABLE 6: Modal frequency of updated Gear 4.

Oder	Intrinsic frequency (Hz)
1	1103.4
2	1208.5
3	1342.7
4	1668.1
5	1768.6
6	1797.2

As has been mentioned above, the stress on the web was far less than the limit when there were six through-holes, thus, more through-holes (up to eight) were further studied. The total area of eight through holes reached  $79.456 \text{ cm}^2$ , and the corresponding simulated stress and displacement nephogram has been exhibited in Figures 8 and 9, respectively.

It is shown that the stress is employed mainly on the inner ring with the maximum value of 163 MPa (Figure 8). In comparison with the six-through-hole structure, the stress on the inner ring increased in this updated safe 8-through-hole model. Inconsistent with the results, the maximum displacement augmented to 0.121 mm (Figure 9). Compared to the earlier one, the whole structure enlarged.

For manufacturing and technological feasibility, decreased number of through-holes with the increased area was authorized. In the simulation, the number of through-holes decreased to 6, and the single area of those holes increased to  $15.004 \text{ cm}^2$ . The total area of through-holes was  $90.024 \text{ cm}^2$ , larger than what has mentioned in the eight-through-hole structure.

Under the same condition, the maximum stress increased up to 210 MPa within the web (Figure 10) whereas the maximum displacement reached 0.138 mm (Figure 11). This newly light-weighted structure confirmed the strength requirement.

- (3) Later, the thickness of the web was reduced to a critical size of 10 mm referred to the design manual. As displayed in Figure 12, no significant enhancement of maximum stress was shown on the web, while the area under large force was raised. On the other hand, the maximum displacement increased by 0.171 mm after the thickness reduction. However, the gear deformation should be no more than 0.15 mm on account of engineering experience and mechanical design manual. In this way, the present designed structure underwent a rather large displacement. Hence, the thickness of web was determined as 13 mm

Taken together, the finalized structure of Gear 4 has been shown in Figure 13. In CATIA, its mass was measured and shown as 7.498 kg, which was 41% of the previous design.

**4.3. Modal Analysis of Gear Optimization.** The intrinsic frequency has been determined by the structure of the gear.

Thus, the probability of the occurrence of resonance in light-weighted Gear 4 during work has been analyzed.

In the beginning, the prior six modes of the initially designed structure in Gear 4 have been analyzed, in which all the degrees of freedom at bearing positions were restricted. And the relative modal frequency has been listed in Table 5, while the same feature examined in the updated structure has been exhibited in Table 6.

Compared with the nonupdated structure, the relevant modal frequency had few differences. Interestingly, obvious diversity in mode of vibration was shown in the last three modes. The first-stage intrinsic frequency was raised, while others declined to some extent but within the safety zone, which will not induce resonance normally.

## 5. Conclusion

In summary, this study investigated the structure of the transmission system in small electric vehicles and optimized the gear in retarder, one of the units for the transmission system, by reducing 20% of face width along with a novel spoke structure. Also, the finite element method was used to analyze the strength of gear structure for safety concerns. The total weight of the initial design was 12.725 kg, of which roughly 41% of weight has been diminished based on CATIA analysis. Thus, the final weight reached 7.489 kg, and the safe light-weight target was achieved perfectly [15].

In the future, further following investigations can be processed. One side, optimizing the overall structure of the transmission case by utilizing novel materials and manufacturing technology to further cut down its weight. On the other side, particular updates, especially the improvement of the device structure, can be processed on transmission structure within the transmission case. By approaching the demand for transmission power, the model system could be established to enhance the efficiency of the transmission case for better choices [16].

## Data Availability

The datasets used and/or analyzed during the current study are available from the corresponding author on reasonable request.

## Conflicts of Interest

It is declared by the authors that this article is free of conflict of interest.

## Acknowledgments

The study presented in this article was substantially supported by Natural Science Foundation of China (no. 51505172). The supports are gratefully acknowledged.

## References


- [1] J. Shen, S. L. Zheng, and J. Z. Feng, "Light weight design of gear sets in wheel driving deceleration system of electric vehicle



- based on load spectrum,” *Journal of Mechanical Strength.*, vol. 39, no. 4, pp. 835–841, 2017.
- [2] G. X. Zhao, *Research on Electric Vehicle Powertrain Matching and Global Optimization*, Jiangsu University, 2017.
  - [3] C. W. Huang, S. L. Zheng, J. Z. Feng, and J. Shen, “Lightweight design of gear webs in wheel-side deceleration system of electric vehicle,” *Agricultural Equipment & Vehicle Engineering.*, vol. 55, no. 4, pp. 1–5, 2017.
  - [4] X. Y. Xu, “Development of transmission technology for energy-saving vehicles and new energy resource vehicle,” *Journal of Automotive Safety and Energy.*, vol. 8, no. 4, pp. 323–332, 2017.
  - [5] C. J. Liang, “Analysis of the influence of transmission system on the performance of electric vehicles,” *Shanghai Auto.*, vol. 9, p. 4-8+27, 2018.
  - [6] B. H. Zhang, *Parameter matching design and optimization of power system for pure electric*, Chongqing Jiaotong University, 2017.
  - [7] J. Li, *Parameters Design and Optimization of Powertrain for Battery Electric Vehicle*, Chang’an University, 2017.
  - [8] J. H. Liu, “Matching design of powertrain parameters of pure electric vehicle. Auto,” *Manufacturing Engineering*, vol. 3, p. 57-58+61, 2018.
  - [9] J. M. Wang, *Design and optimization of driving system of battery electric vehicle*, Jilin University., 2019.
  - [10] Z. S. Yu, *Automobile Theory*, China Mechine Press, Beijing, Edition 5 edition, 2009.
  - [11] L. Wang, *Structure Design and Anylsis of Pure Electric Vehicle Gear Box*, Jilin University, 2015.
  - [12] W. Y. Wang, *Automobile Design. Edition 4*, China Mechine Press, Beijing, 2004.
  - [13] C. Zou, “Research on gear lightweight based on ANSYS workbench,” *Mechanical Engineering*, vol. 5, pp. 34–36, 2015.
  - [14] Y. Li, *Simulation and Design Method Research of Large Gear Lightweight of Ball Mill*, Northeastern University, 2013.
  - [15] P. D. Walker and S. A. Rahman, *Modelling, simulations, and optimisation of electric vehicles for analysis of transmission ratio selection*, Hindawi Publishing Corporation., 2013.
  - [16] J. J. Hu and H. L. Ran, “Parameter design and performance analysis of shift actuator for a two-speed automatic mechanical transmission for pure electric vehicles,” *Advances in Mechanical Engineering*, vol. 8, no. 8, 2016.

## Research Article

# A New Method of Identifying Graphite Based on Neural Network

Guangjun Liu <sup>1</sup>, Xiaoping Xu,<sup>1</sup> Xiangjia Yu,<sup>1</sup> and Feng Wang<sup>2</sup>

<sup>1</sup>School of Sciences, Xi'an University of Technology, Xi'an 710054, China

<sup>2</sup>School of Mathematics and Statistics, Xi'an Jiaotong University, Xi'an 710049, China

Correspondence should be addressed to Guangjun Liu; liuguangjun202106@126.com

Received 30 September 2021; Accepted 16 November 2021; Published 15 December 2021

Academic Editor: Deepak Gupta

Copyright © 2021 Guangjun Liu et al. This is an open access article distributed under the Creative Commons Attribution License, which permits unrestricted use, distribution, and reproduction in any medium, provided the original work is properly cited.

The unique physical properties of graphite enable it to be applied in various fields of the national economy and people's livelihood, which has very important industrial value. Many countries have listed graphite as a key mineral. To promote the transformation of the mining industry to informatization and intelligence, the realization of the intelligent recognition of graphite is particularly critical. Aiming at the problems of long time and low efficiency in manually identifying graphite, an improved AlexNet convolution neural network is proposed for graphite image recognition. First, we perform image preprocessing on the data set by means of random cropping, horizontal flipping according to probability, and normalization processing to achieve the purpose of data enhancement. Then we use the activation function ReLU6 to compress the dynamic range to make the algorithm more robust, using the batch standardization algorithm for normalization to speed up the convergence speed, modifying the size of the convolution kernel to enhance the generalization ability, and adding dropout regularization to the fully connected layer to further prevent overfitting. Finally, in the simulation experiment, compared with the existing method, the given method reduces the loss value and improves the average accuracy of identifying graphite.

## 1. Introduction

At present, graphite has become an important raw material of new composite materials in the field of high technology and has an important strategic position in the national economy [1, 2]. With the rapid development of science and technology, graphite is known as "the strategic resource supporting the development of high and new technology in the 21st century," which has good high temperature resistance, conductivity, chemical stability, and thermal shock resistance [3]. It is not only the key raw material in new energy, new materials, aerospace, and other fields but also the important raw material in traditional industries such as refractories, electrode brushes, and pencils [4]. In the development of high-tech industry, graphite is becoming more and more important. Its unique physical characteristics make it applicable in various fields of the national economy and people's livelihood, which has very important industrial value [5, 6].

The deep learning algorithm represented by convolution neural network (CNN) has developed rapidly in the era of

big data, and has attracted much attention in the research fields of machine learning and computer vision [7, 8]. As a kind of deep feedforward neural network, CNN has made a great breakthrough in the field of image recognition [9]. Compared with the traditional classification method, the convolution network-based automatic classification method breaks away from the tedious of human identification. At the same time, the back propagation algorithm is used to automatically optimize the model parameters to obtain the optimal model under the current conditions. The concept of deep learning was put forward by Hinton and Salakhutdinov in 2006 [10]. It can describe the attributes and features of objects more abstractly and deeply, and design the AlexNet network. Since then, a wave of deep learning upsurge has been set off.

As a powerful algorithm in the field of image recognition [8, 9], few researchers have applied CNN to the graphite image recognition task. Compared with more advanced models such as GoogleNet and ResNet, AlexNet has a simpler network structure and fewer network parameters [9]. Compared with the existing lightweight network, the

depth is deep, the training is not very difficult, the representation ability is strong, it is more convenient to make different improvements, it can save a lot of model training time, and it is not easy to overfit [8]. Therefore, this paper presents an image recognition technology based on AlexNet and deep learning to recognize and sort graphite and nongraphite. In view of the characteristics of a graphite image and the small data set, the data set is preprocessed to achieve the purpose of data enhancement, and the activation function, normalization layer, convolution kernel, dropout layer, and optimizer are replaced and updated. Compared with the related algorithms, simulation results show that the proposed method has low complexity and less parameters, improves the convergence speed of the network, reduces the loss rate, and effectively realizes the graphite image recognition target.

## 2. Traditional AlexNet Network Model

*2.1. Convolutional Neural Network.* AlexNet is a kind of CNN, and CNN is an artificial neural network, which has been widely used in image recognition and other machine learning fields [8]. Because its network structure adopts the way of weight sharing, it is more similar to the biological neural network. Compared with the general neural network, it reduces the number of network weights. The biggest advantage of CNN is to reduce the network parameters through receptive field and shared weight, that is, parameter reduction and weight sharing. This method makes the training faster and needs fewer samples. The basic network structure of CNN is shown in Figure 1, which is divided into four parts: input layer (input), convolution layer (conv), full connection layer (FC), and output layer (output).

The biggest difference between convolution neural network shown in Figure 2 and other neural network models is that convolution neural network connects convolution layer in front of input layer of neural network, so convolution layer becomes data input layer of convolution neural network. Convolution layer is a unique network structure in convolution neural network, which is mainly used for image feature extraction. The purpose of pooling layer is to sparse the feature map and reduce the amount of data computation. The full join layer plays the role of ‘‘Classifier’’ in the whole convolution neural network. It maps the learned ‘‘content’’ to the sample label space (synthesizes the previously extracted features).

In Figure 2,  $f_x$  represents a digital filter,  $b_x$  is an offset, Sigmoid is an activation function,  $C_x$  represents the characteristic map of the convolution layer,  $W_{x+1}$  represents the weight of downsampling,  $b_{x+1}$  represents the corresponding weight, and  $S_{x+1}$  represents the lower sampling layer.

It can be seen that the  $C$  layer is used for feature extraction as convolution layer. Each neuron connects with a small receptive field in the upper layer, and then moves the receptive field to correspond the new receptive field to another neuron in  $C$  layer. The activation function is used to make the process displacement invariant. Here, as long as the size of input layer and local receptive field are determined, the size of  $C$  layer is also determined. The  $S$  layer is the lower

sampling layer, and its purpose is to change multiple pixels of the  $C$  layer into one pixel. Because the weights on the mapping surface are shared, that is to say, the weights of each neuron are the same, so the parameters of the whole network are greatly reduced and the complexity is reduced.

*2.2. AlexNet Convolution Neural Network.* AlexNet is the champion network of the ISLVR 2012 (ImageNet Large Scale Visual Recognition) competition. The classification accuracy has been improved from more than 70% to more than 80%. Its network structure is shown in Figure 3.

The network consists of eight layers, including five layers of convolution layer (conv) and three layers of full connection layer (FC). There are also three pooling layers in the AlexNet network, and the convolution layer and pooling layer are connected alternately.

In AlexNet network, the five-layer convolution layer uses convolution kernel of  $11 \times 11$ ,  $5 \times 5$ ,  $3 \times 3$ ,  $3 \times 3$ , and  $3 \times 3$  to extract the feature. AlexNet abandons Sigmoid or Tanh functions, which are commonly used before, and uses ReLU as the activation function. Since there is no interval in the range of values obtained by the ReLU function, AlexNet proposes local response normalization (LRN) to normalize the data obtained by ReLU, suppressing small neurons and improving the generalization ability of the model.

## 3. Improved AlexNet Network Model

*3.1. Data Enhancement.* In order to improve the generalization ability of the model, the best way is to use a large sample data set for training. For small sample data sets, data enhancement can be used in deep learning to solve the problem of insufficient data [11]. Here, we use the image preprocessing package transform of Python to preprocess the images in the data set as shown in Figure 4.

Firstly, the test set is cut randomly to get the image pixel of  $224 \times 224$ , and the image is flipped horizontally according to the probability (setting  $p = 0.5$ ). Finally, the processed data set is normalized to achieve the purpose of data enhancement.

*3.2. Activation Function.* In the AlexNet network, although the ReLU function as the activation function effectively overcomes the shortcomings of the Sigmoid and Tanh function gradient disappearing and slow convergence speed, the linear activation of the ReLU in the region  $x > 0$  of the network may cause the value after activation to be too large and affect the stability of the model, which will reduce the training speed of the network, and even reduce the generalization performance of the network. In order to counteract the linear growth of ReLU, this paper uses the ReLU6 function.

$$\text{ReLU6}(x) = \min(\max(x, 0), 6) \in [0, 6]. \quad (1)$$

Compared with the ReLU function, the model uses ReLU6 as the nonlinear layer, which can compress the dynamic range in a low precision calculation, and the algorithm is more robust. The ReLU6 function is shown in Figure 5.

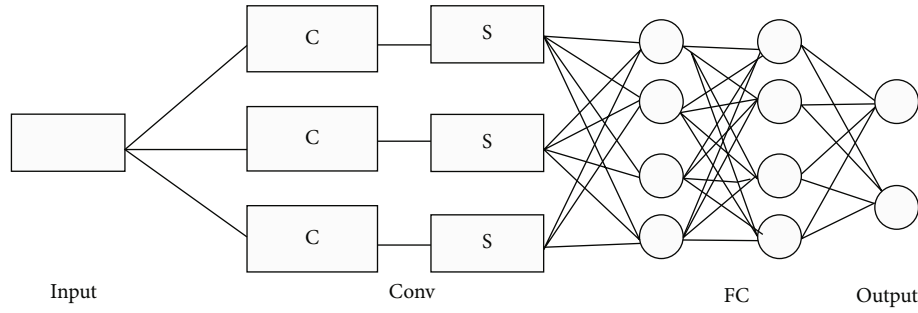


FIGURE 1: Basic CNN network structure.

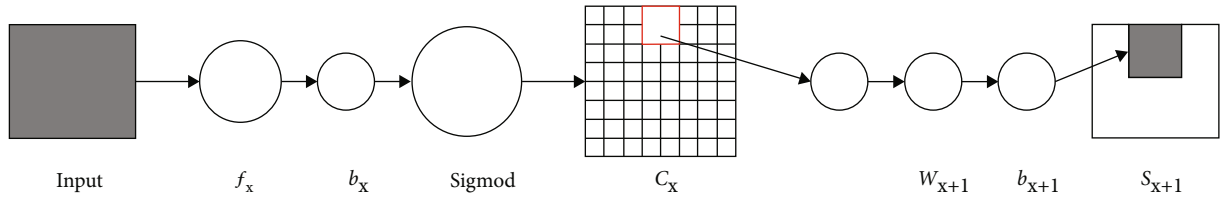


FIGURE 2: Convolution neural network connection process.

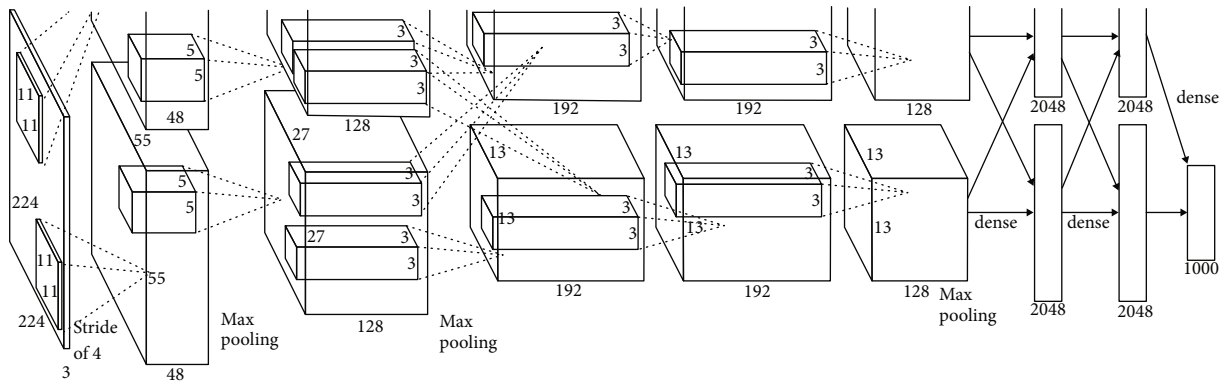


FIGURE 3: Traditional AlexNet network junction.

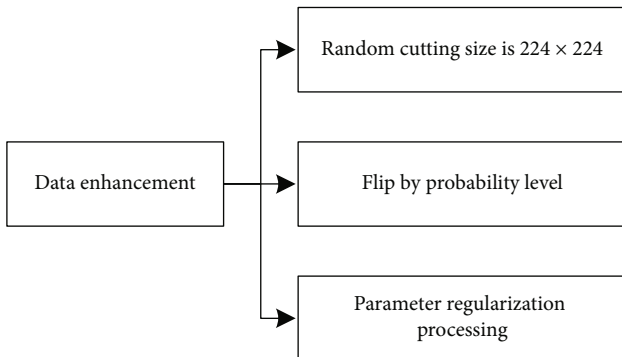


FIGURE 4: Data enhancement operation.

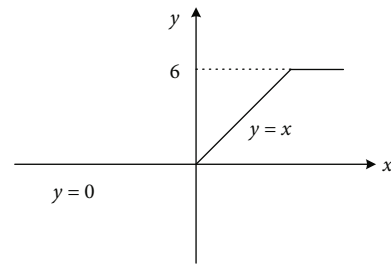


FIGURE 5: Graph of ReLU6 function.

3.3. *Batch Normalization Algorithm.* In the traditional AlexNet, LRN is used to normalize the first and second layers to enhance the generalization performance of the model. However, the actual improvement effect of LRN algorithm on the model is limited, and the training time of the model will be

greatly increased. The batch normalization (BN) algorithm proposed in reference [12] can reduce the data offset caused by the activation function and effectively solve the problem of inconsistent data distribution in the training process. The BN algorithm achieves the goal of feature normalization by calculating the mean and variance of small batches.

Given a batch  $B = \{x_1, x_2, \dots, x_m\}$  of size  $n$  initially, then, in order to normalize the data, the mean  $\mu_B$  and variance  $\sigma_B^2$

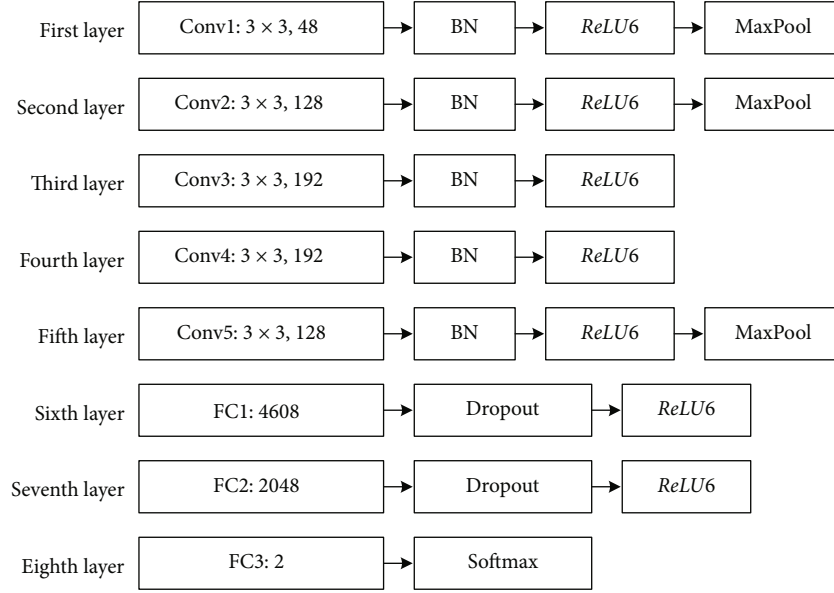


FIGURE 6: Improved AlexNet network model.

of each batch are recorded by using the following Equations (2) and (3) in the training process.

$$\mu_B = \frac{1}{m} \sum_{i=1}^m x_i, \quad (2)$$

$$\sigma_B^2 = \frac{1}{m} \sum_{i=1}^m (x_i - \mu_B)^2. \quad (3)$$

In this way, the following Equation (4) can be used to normalize the data in the actual test.

$$\hat{x}_i = \frac{x_i - \mu_B}{\sqrt{\sigma_B^2 + \varepsilon}}, \quad (4)$$

where  $\varepsilon$  is a coefficient used to increase the stability of the value.

The key of the BN algorithm is to transform and reconstruct, and introduce stretch parameter  $\gamma$  and offset parameter  $\beta$  to correct as the following equation.

$$y_i = \gamma \hat{x}_i + \beta = BN_{\gamma, \beta}(x_i), \quad (5)$$

where  $\gamma^{(i)} = \sqrt{D[x^{(i)}]}$  and  $\beta^{(i)} = E[x^{(i)}]$ ; the two parameters are updated with the update of network weight, and the normalized sample value is  $y_i$ .

**3.4. Convolution Layer.** The VGG (visual geometry group) network is a deep convolution neural network developed by Oxford University Computer Vision Group and Google DeepMind. The network structure uses a convolution kernel to expand the number of channels to extract more complex and expressive features and has strong scalability and good generalization ability. Therefore, this paper uses the advan-

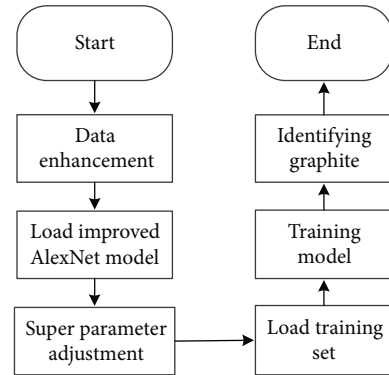


FIGURE 7: Flow chart of image classification using improved AlexNet.

tages of VGG network as a reference and modifies all convolutional cores in AlexNet to small convolutional cores  $3 \times 3$ , which greatly reduces the number of parameters and extracts more specific features.

**3.5. Improved AlexNet Convolution Neural Network.** In this paper, the Adam optimizer is selected, and the initial learning rate is 0.0002. The cross-entropy is selected as the loss function to avoid the problem that the learning rate gradually decreases due to the mean square error. Because a large number of parameters are introduced into the full connection layer of the AlexNet network, dropout is added after the full connection layer, which reduces the complex coadaptation of neurons and makes the model fusion more effective. The improved AlexNet network model is shown in Figure 6.

This paper uses the improved AlexNet network model to complete the task of automatic classification of data sets. The overall framework of the model is shown in Figure 7.





FIGURE 8: Images of graphite and nongraphite samples.

#### 4. Experimental Parameters and Data Sets

**4.1. Experimental Environment and Parameter Setting.** In this paper, in the Python compiler environment, we use the 1.5.0 version of the Python framework to complete the experimental simulation and realize the image data preprocessing through transformation. The experimental environment is Mac OS 10.14.6 operating system, processor is 1.6 GHz Intel Core i5, and without GPU acceleration; running a network consumes 9000-10000 seconds on average. The weight attenuation is set to 0.01 to prevent overfitting. The epoch is 100, and a batch size is set to 32. All the weight parameters are initialized to Gaussian distribution with mean value of 0 and standard deviation of 0.01. At the same time, the images of the training set are randomly scrambled before input to reduce the influence of image order on the model.

**4.2. Sample Collection and Expansion.** In this paper, the image samples were collected from the existing graphite samples in the laboratory, cleaned, and dried, and the sample images were captured from different directions and angles by using the iPhone rear camera; then, the video was processed by frame, and a total of 166 sample images were obtained. At the same time, 180 nongraphite ore images were collected on the internet, and finally, the images were divided into graphite and nongraphite categories; 346 color images are obtained. Figure 8 shows the sample images of graphite and nongraphite.

In general, the more abundant the data set, the better the training effect of the model, and its generalization ability is enhanced. In order to solve the problem of insufficient training samples, the above data sets are expanded. The collected images are processed by center clipping, sample rotation (180° and 90°, respectively), flipping around a coordinate axis and mean value blur. Finally, 1857 images are obtained. 955 (80%) of the data sets are randomly selected as the training set according to the proportion to train the network, and 902 (20%) were used as test sets to verify the performance of the network. The training set and the test set are processed separately. The classification of data sets is shown in Table 1.

TABLE 1: Graphite data set.

Category	Graphite	Nongraphite
Data set	955	902
Training set	764	722
Test set	191	180

**4.3. Data Set Preprocessing.** In order to reduce the imbalance of samples and solve the overfitting phenomenon caused by a too small data set, this paper carries out data augmentation (DA) operation on the data set to improve the accuracy of network classification. In the DA operation, common methods include scale transformation, image contrast adjustment, image clipping, affine transformation, and horizontal or vertical flipping. Different enhancement methods can be selected for different data sets. Based on the characteristics of the ore image, the training set images are randomly scrambled before input to reduce the influence of image order on the model. Each image in the training set is randomly cropped, the image pixels are unified, and the image is flipped horizontally according to the probability (setting  $p=0.5$ ). Finally, the data of each channel is regularized with the mean value of 0.5 and the standard deviation of 0.5, so as to achieve the purpose of data expansion and data enhancement.

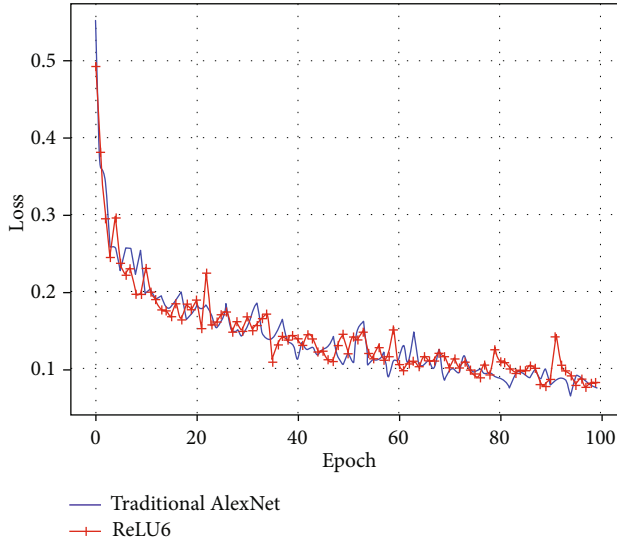
#### 5. Experimental Results and Analysis

**5.1. Evaluating Index.** In this paper, the training effect of a network is evaluated by two indexes: accuracy acc and loss value loss. Test accuracy acc refers to the ratio of the model output correct results in the test set, which can reflect the use effect of a network and is a very important index. The definition formula is shown in the following equation.

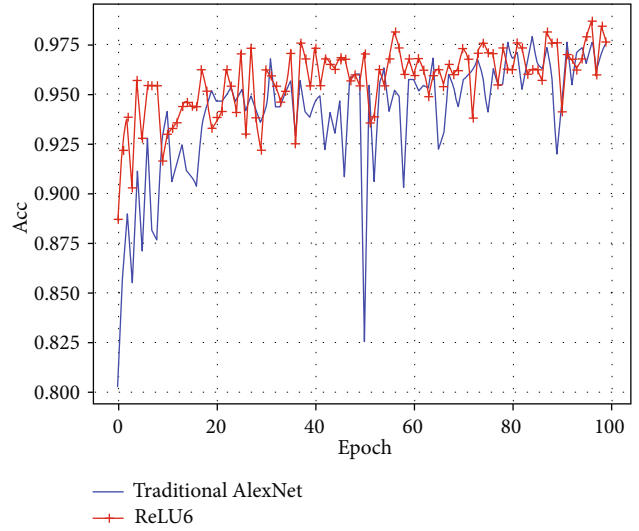
$$\text{acc} = \frac{n_{\text{correct}}}{n}, \quad (6)$$

where  $n_{\text{correct}}$  is the number of correct network identification in the test set and  $n$  is the number of samples in the test set.

The training process of neural network is to minimize the loss function, and loss is the value of the loss function.

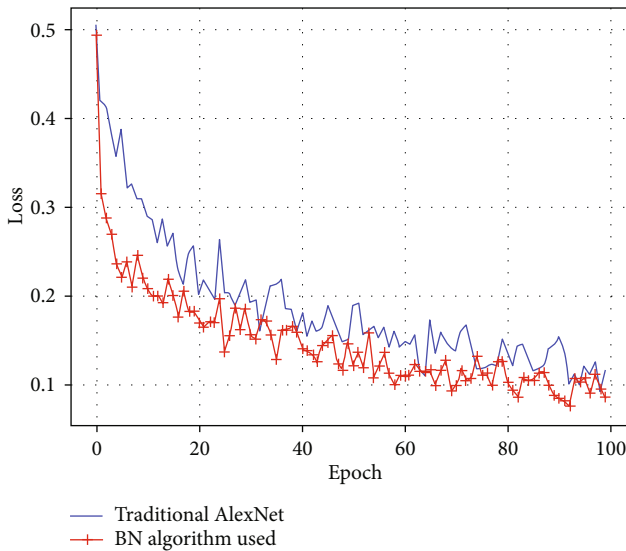


(a) Loss

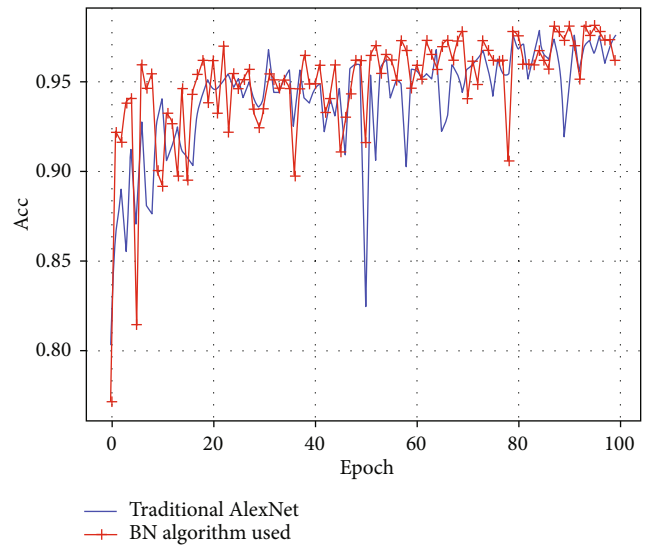


(b) Acc

FIGURE 9: Comparison curves of different activation function models.



(a) Loss



(b) Acc

FIGURE 10: Model comparison curves of using BN algorithm or not.

In fact, the loss function calculates the mean square error (MSE) of the model on the test set.

$$\text{MSE} = \frac{1}{n} \sum_i (y^{\wedge \text{test}} - y^{\text{test}})_i^2. \quad (7)$$

**5.2. Experimental Result.** In this paper, the improved AlexNet model and the traditional AlexNet model are used to train the data set. Figure 9 shows the curves of loss and accuracy of using the ReLU6 function and ReLU function. The experimental results show that the loss value can be reduced from 0.0925 to 0.0772 by using the ReLU6 function, which is relatively small.



FIGURE 11: Feature extraction graphite sample image.

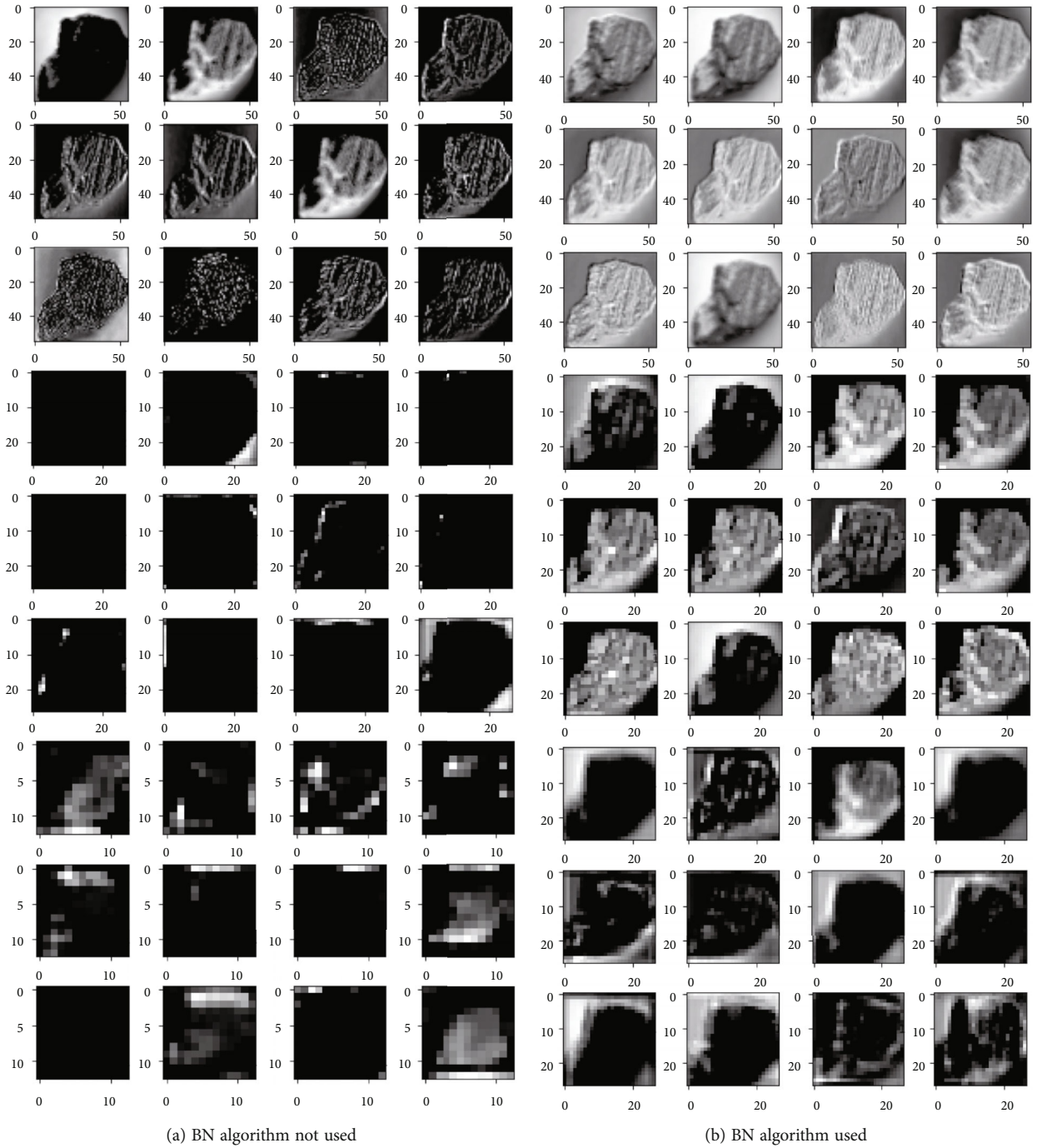


FIGURE 12: Convolution layer feature extraction using BN algorithm or not.

For the normalization layer, this paper compares the two cases of using the BN algorithm and not using the BN algorithm for simulation, and the results are shown in Figure 10.

The results in Figure 10 show that the BN algorithm can effectively reduce the loss value of model testing and avoid the risk of the model falling into overfitting. In order to further observe the feature extraction of the convolution layer before and after using the BN algorithm, a picture in the data set is randomly extracted, as shown in Figure 11, which is classified as graphite.

TABLE 2: Comparison of loss and accuracy of using BN algorithm or not.

Method	Loss	Acc
BN algorithm not used	0.0925	94.0377%
BN algorithm used	0.0750	94.8976%

Then, the feature extraction diagram of the first 11 channels of Figure 11 in conv1, conv2, and conv3 is printed out in sequence, as shown in Figure 12.

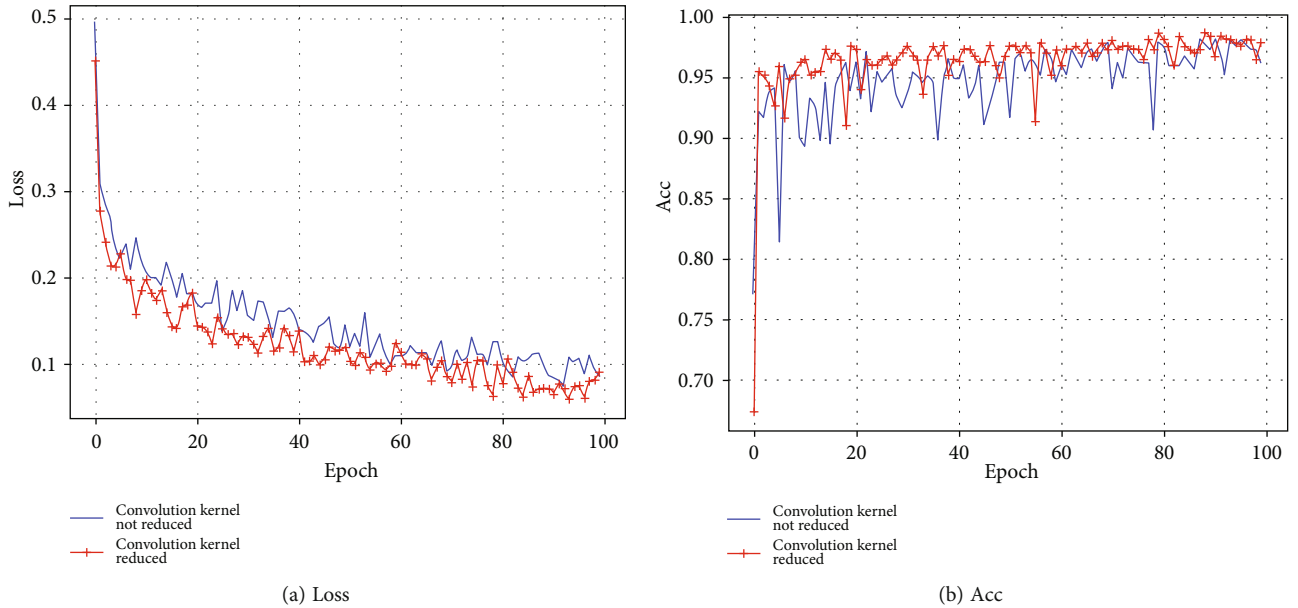


FIGURE 13: Model comparison curves of reducing convolution kernel or not.

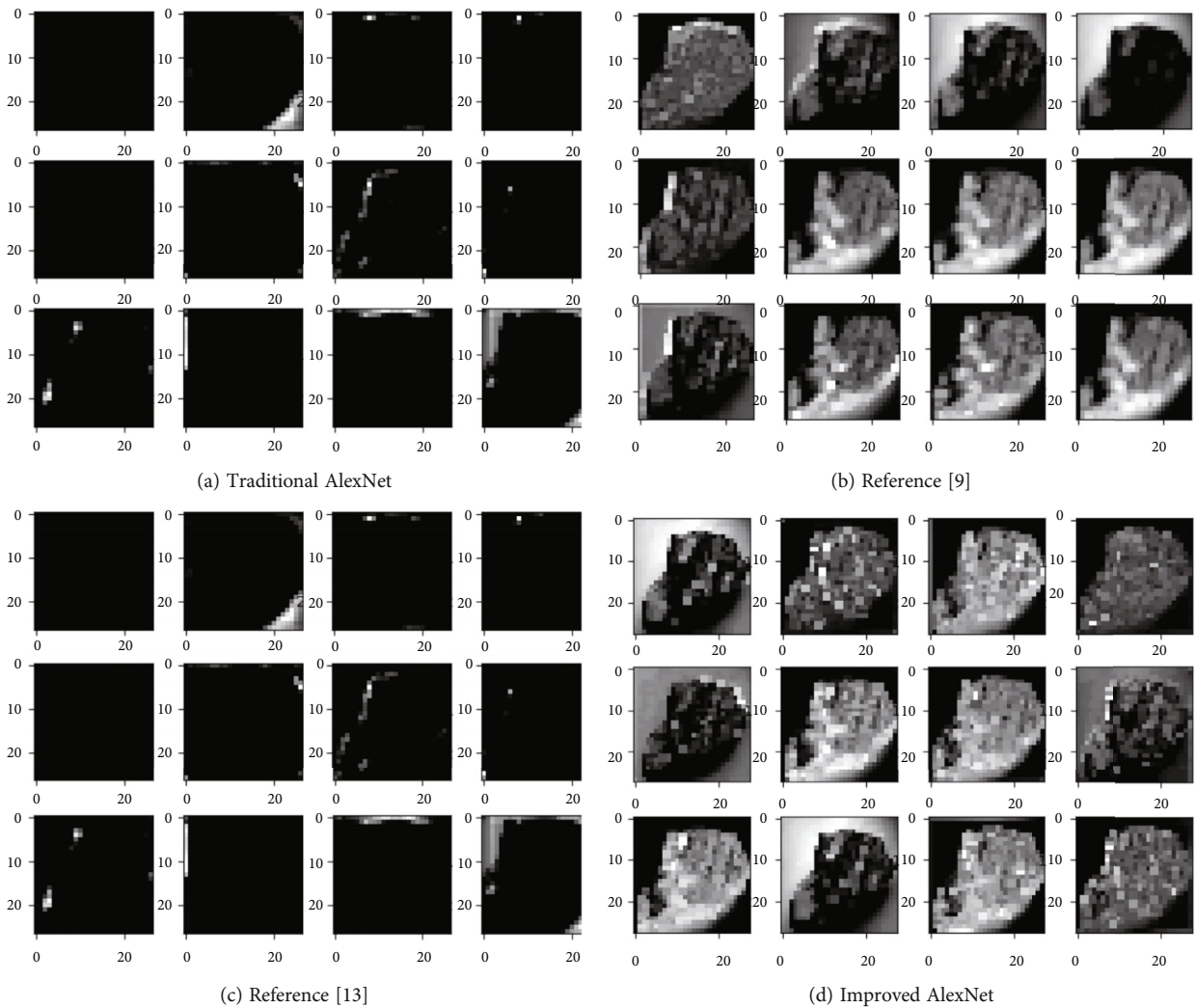


FIGURE 14: Feature extraction of conv2 under different models.



TABLE 3: Comparison of loss and acc.

Method	Loss	Maximum acc	Average acc
Traditional AlexNet	0.0925	97.8437%	94.0377%
Reference [9]	0.0806	98.1132%	94.7709%
Reference [13]	0.0867	97.8437%	94.9973%
Improved AlexNet	0.0599	98.6523%	96.3639%

It can be seen from Figure 12 that the features extracted by the traditional AlexNet network in the third volume layer are fuzzy, and the learning ability is not very good. Compared with the model using the BN algorithm, the feature extraction ability is enhanced, which can ensure that the network learns quickly and fully. The loss and acc of image recognition before and after using the BN algorithm are shown in Table 2.

In addition to the improvement of the activation function and normalization layer, this paper also modifies the size of the convolution kernel, as shown in Figure 13, to show whether to reduce the image recognition loss and acc of the convolution kernel.

Figure 13 shows the comparison between the loss value and the accuracy rate using the small convolution kernel on the basis of the above improvements. It is obvious that the use of the small volume core improves the generalization ability of the model and reduces the loss value of the model in the test set.

In order to evaluate the recognition performance of the improved AlexNet network on the graphite classification data set, the traditional AlexNet network and the AlexNet network of Reference [9] and Reference [13] are compared, and the situation of conv2 is extracted, as shown in Figure 14.

It can be seen from Figure 14 that the features in the second convolution layer using the improved AlexNet network are clearer than the other two models, and more features are extracted and learned. Finally, the comparison curves of models' loss and acc are obtained, which further verifies the effectiveness of the improved AlexNet network proposed in this paper.

Through the experiment on the test set, the traditional AlexNet network, Reference [9], and Reference [13] are compared, and the comparison of the loss and acc with the method in this paper is shown in Table 3.

It can be seen from Table 3 that the improved AlexNet network proposed in this paper is better than the other two cases, which effectively verifies the feasibility and effectiveness of the network model proposed in this paper.

## 6. Conclusion

In this paper, the improved AlexNet convolution network is used to identify graphite. This process does not need to extract the image features of graphite manually. It has a high degree of intelligence, and the training process is relatively simple. By optimizing the activation function, normalization layer, and super parameters of AlexNet, the robustness of the whole model is improved, and the overfitting problem is

avoided without increasing the computational complexity of the model. The experimental results show that the average accuracy of the improved algorithm is improved, the loss value is reduced, and the model has strong generalization. Moreover, the improved AlexNet convolution network model is applied to graphite image recognition, which increases the automation degree of the beneficiation process and reduces the workload of manual sorting. But in this paper, the data set is a small data set and the graphite sample is a block. Increasing the types of graphite to expand the data set and identifying most of the flowing graphite in the market are the next research direction.

## Data Availability

The data sets used and/or analyzed during the current study are available from the corresponding author on reasonable request.

## Conflicts of Interest

It is declared by the authors that this article is free of conflicts of interest.

## Acknowledgments

This work is supported by the Innovation Capability Support Program of Shaanxi Province of China (Grant No. 2020PT-023), National Natural Science Foundation of China (Grant No. 11801438), and Natural Science Basic Research Plan in Shaanxi Province of China (Grant No. 2018JQ1089).

## References

- [1] C. Y. Wang, J. L. Zhao, and X. H. Du, "Hydrogen production from ammonia borane hydrolysis catalyzed by non-noble metal-based materials: a review," *Journal of Materials Science*, vol. 56, no. 4, pp. 1–23, 2021.
- [2] M. Q. Liu, Y. Y. Jiao, J. C. Qin, Z. Li, and J. Wang, "Boron doped  $C_3N_4$  nanodots/nonmetal element (S, P, F, Br) doped  $C_3N_4$  nanosheets heterojunction with synergistic effect to boost the photocatalytic hydrogen production performance," *Applied Surface Science*, vol. 541, article 148558, 2021.
- [3] B. Sun and Q. Y. Kong, *Ordinary miracle graphite*, Shandong science and Technology Press, Jinan, China, 2019.
- [4] Z. N. Liu, S. F. Shen, H. Y. Liu, J. L. Wang, and Z. B. Qian, "Progress of graphite beneficiation technology and equipment," *Modern Mining*, vol. 36, no. 8, pp. 143–146, 2020.
- [5] X. D. Zhang, Y. L. Qiu, Y. M. Wu, S. J. Wang, and L. Y. Zhang, "Effect of raw material characteristics and preparation process on thermal conductivity of flexible graphite film," *Silicate Bulletin*, vol. 38, no. 12, pp. 3988–3992, 2019.
- [6] H. M. Gao, L. Y. Zhang, J. F. Guan, Y. P. Qian, and Z. J. Ren, "Progress in mineral processing and purification technology of graphite, quartz and fluorite," *Metal Mines*, vol. 10, pp. 58–69, 2020.
- [7] A. Krizhevsky, I. Sutskever, and G. Hinton, "ImageNet classification with deep convolutional neural networks," *Advances in Neural Information Processing Systems*, vol. 25, no. 2, pp. 1–9, 2012.



- [8] S. Cuiping, T. Cong, Z. Jiang, and Z. Kexin, "Facial expression recognition based on improved AlexNet convolutional neural network," *Telecommunication Technology*, vol. 60, no. 9, pp. 1005–1012, 2020.
- [9] L. Gan, Z. H. Guo, and Y. Wang, "Image recognition method of gastric tumor cells based on radial transform and improved AlexNet," *Computer Applications*, vol. 39, no. 10, pp. 2923–2929, 2019.
- [10] G. E. Hinton and R. R. Salakhutdinov, "Reducing the dimensionality of data with neural networks," *Science*, vol. 313, no. 5786, pp. 504–507, 2006.
- [11] P. D. Faris, W. A. Ghali, R. Brant et al., "Multiple imputation versus data enhancement for dealing with missing data in observational health care outcome analyses," *Journal of Clinical Epidemiology*, vol. 55, no. 2, pp. 184–191, 2002.
- [12] S. Loffe and C. Szegedy, "Batch normalization: accelerating deep network training by reducing internal covariate shift," <https://arxiv.org/abs/1502.03167>.
- [13] J. Wang, H. Zheng, Y. Huang, and X. Ding, "Vehicle type recognition in surveillance images from labeled web-nature data using deep transfer learning," *IEEE Transactions on Intelligent Transportation Systems*, vol. 19, no. 9, pp. 2913–2922, 2018.

## Research Article

# A Novel, Efficient, and Secure Anomaly Detection Technique Using DWU-ODBN for IoT-Enabled Multimedia Communication Systems

M. Sathya <sup>1</sup>, M. Jeyaselvi,<sup>2</sup> Lalitha Krishnasamy <sup>3</sup>, Mohammad Mazyad Hazzazi <sup>4</sup>, Prashant Kumar Shukla,<sup>5</sup> Piyush Kumar Shukla <sup>4,6</sup> and Stephen Jeswinde Nuagah <sup>7</sup>

<sup>1</sup>Department of Information Science and Engineering, AMC Engineering College, Bangaluru, India

<sup>2</sup>Department of Computer Science and Engineering, SRM Institute of Science and Technology, Chennai, India

<sup>3</sup>Department of Information Technology, Kongu Engineering College, Tamil Nadu, India

<sup>4</sup>Department of Mathematics, College of Science, King Khalid University, Abha, Saudi Arabia

<sup>5</sup>Department of Computer Science and Engineering, K L University, 29-36-38, Museum Rd, Governor Peta, Vijayawada, Andhra Pradesh 520002, India

<sup>6</sup>Computer Science & Engineering Department, University Institute of Technology, Rajiv Gandhi Proudyogiki Vishwavidyalaya, (Technological University of Madhya Pradesh), Bhopal 462033, India

<sup>7</sup>Department of Electrical Engineering, Tamale Technical University, Ghana

Correspondence should be addressed to Stephen Jeswinde Nuagah; [jeswinde@tatu.edu.gh](mailto:jeswinde@tatu.edu.gh)

Received 19 September 2021; Revised 28 October 2021; Accepted 19 November 2021; Published 14 December 2021

Academic Editor: Paolo Barsocchi

Copyright © 2021 M. Sathya et al. This is an open access article distributed under the Creative Commons Attribution License, which permits unrestricted use, distribution, and reproduction in any medium, provided the original work is properly cited.

The Internet of Things (IoT) is enhancing our lives in a variety of structures, which consists of smarter cities, agribusiness, and e-healthcare, among others. Even though the Internet of Things has many features with the consumer Internet of Things, the open nature of smart devices and their worldwide connection make IoT networks vulnerable to a variety of assaults. Several approaches focused on attack detection in Internet of Things devices, which has the longest calculation times and the lowest accuracy issues. It is proposed in this paper that an attack detection framework for Internet of Things devices, based on the DWU-ODBN method, be developed to alleviate the existing problems. At the end of the process, the proposed method is used to identify the source of the assault. It comprises steps such as preprocessing, feature extraction, feature selection, and classification to identify the source of the attack. A random oversampler is used to preprocess the input data by dealing with NaN values, categorical features, missing values, and unbalanced datasets before being used to deal with the imbalanced dataset. When the data has been preprocessed, it is then sent to the MAD Median-KS test method, which is used to extract features from the dataset. To categorize the data into attack and nonattack categories, the features are classified using the dual weight updation-based optimal deep belief network (DWU-ODBN) classification technique, which is explained in more detail below. According to the results of the experimental assessment, the proposed approach outperforms existing methods in terms of detecting intrusions and assaults. The proposed work achieves 77 seconds to achieve the attack detection with an accuracy rate of 98.1%.

## 1. Introduction

Considering the rapid development of IoT (Internet of Things) [1] technology, researchers and developers are urged to look at new smart services that can extract vital information from IoT data [2]. When physical objects such

as mobile devices, home appliances, vehicles, and buildings are implanted with electronics, software, sensors, and network connectivity, the Internet of Things (IoT) came into effect. The Internet of Things (IoT) enables these objects to collect and exchange data with one another. By using the existing network infrastructure, the Internet of Things

allows things to be detected, identified, and controlled from a distance. When the Internet of Things is combined with sensors and actuators, it becomes an example of cyber-physical systems, which also incorporate concepts such as intelligent grids, intelligent homes, intelligent cities, and intelligent transportation systems. The IoT has developed as a highly technical area in the current scenario [3]. In many applications, IoT devices have been implemented, including intelligent vehicles, healthcare, environmental monitoring, and personal wearable devices which have increased the volume, variety, speed, and veracity of data that are handled with connected systems (including sensitive data like personal information) [4–11]. The Internet of Things (IoT) builds on the idea of expanding everyday activities via computing and Internet connections to detect, compute, communicate, and control the environment [5, 6]. Along with the growth of IoT ecosystems, the extent and intensity of adverse actions have increased, focused on the resilience of the system, and thus affected latency-sensitive applications [6]. The poor physical safety of the devices [8] enables inside attacks against IoT nodes. It provides useful suggestions about the safety of industrial IoT systems [9]. As attackers tried to reveal the integrity of data and equipment [10], security issues emerged because of the rapid growth of hacking techniques. However, there will be data anomalies [11] and attacks like man-in-the-middle, message changes, authentication attacks, denial-of-service attacks, replay attacks, and eavesdropping which may threaten the viability of the Internet of Things [12]. The bulk of these attacks are slight differences in previously reported incursions (around 99 percent mutations). Security and privacy problems must be solved before IoT devices can be extensively utilized, especially in mission-critical scenarios involving sensitive data [13]. Anomalies or outliers are uncommon, but they can still be important in the event of a credit card transaction; for example, the aberrant conduct of credit card transactions may suggest that a credit card is stolen, whereas strange network traffic patterns can indicate that illegal network access is available [14]. According to the 2019 threat report SonicWALL, in 2018 in Gatlan (2019), more than 327 million threats from the Internet of Things (IoT) were detected globally [15]. As a consequence, assaults on and detection of abnormalities in IoT infrastructure in the IoT industry become an increasing cause of concern [16].

In the past, a wide variety of techniques for attack detection were proposed with various scenarios [17]. Computer algorithms based on artificial intelligence (AI) methods and machine learning (ML) have been extensively used to detect anomalous patterns of traffic in the network. While some excellent work has been done on the security issues related to the Internet of Things [18], many solutions designed to prevent security threats cannot be able to protect from new attacks [19]. Consequently, new kinds of attacks or novel variants in current attacks might not be identified [20]. In this paper, an effective anomaly detection system based on DWU-ODBN is proposed to solve the issues that presently exist. The fundamental goal of this work is to develop a new architecture for the IoT to defeat energy-related threats. A denial-of-sleep attack occurs when the

nodes remain awake even when there is no traffic, resulting in the battery's energy being depleted and the node dying as a result of the assault. The lifespan of the IoT will be reduced as a result of this action. The primary goal of this research endeavour is to develop effective defence approaches for identifying and defending against DDoS attacks to prevent them from occurring. The following are the objectives: A review of different IDS in WSN and MANET, identify the steps for launching a denial-of-service attack, and develop and deploy an innovative technique for identifying and isolating rogue agents. Intruders from inside the network are responsible for the energy drain assaults. Aa DWU-ODBN with intrusion detection and prevention was designed and implemented. Attack prevention is made possible by the introduction of a new malicious node alert (MNA). Nodes in the network are alerted using this strategy. It is necessary to build a method that comprises a lightweight monitoring system module and detector module for detecting and preventing sleep deprivation in IoT.

The rest of the paper is organized as follows: Section 3 of this article explains the proposed approach, Section 4 of the paper includes a test assessment of the proposed methodology, and Section 5 of the paper ends the study with future improvements.

## 2. Literature Survey

Based on the SDx paradigm, Zarei and Fotohi [21] presented a comprehensive framework for the internet of things software-defined (SD-IoT). In addition to the SD-IoT controller package, the frame contained SD-IoT switches coupled to an IoT gateway and IoT devices connected via an IoT gateway. Then, an algorithm for detecting and mitigating DDoS attacks was created utilizing the SD-IoT platform. The cosine similarity of packet-in message rate vectors at border SD-IoT switch ports has been used to evaluate if DDoS assaults have occurred in the IoT. Last but not least, test results showed that the algorithm provided was very good and the framework offered was changed to enhance security in the Internet of Things while dealing with a variety of vulnerable devices. Since it was intended to be used only with directed vectors, the cosine similarity function could not be utilized for normal values.

Liu et al. [22] presented a new safe things architecture internet, in which the ensemble machine learning technique can detect IoT sensor risks based on their results. In an Internet of Things environment, the gradient boosting technique was selected with minimum modifying hyper-parameters and applied to identify discriminant attacks. In total, the system included a variety of processes, including internet data collection of the things sensor networks (IoT sensor networks), data clearing (data visualization), vectorization, ensemble learning (ensemble learning), and attack detection. First, the feature selection method was utilized to decrease the dataset size, which improved the attack and detection environment. The feature selection method was then utilized to decrease the dataset size. To get the best results, the ensemble gradient boosting technique was employed after the previous stage with only a little

hyperparameter adjusting. Attacks on the environment of the IoT sensor were more correctly identified by the model with an accuracy of 99.40%, precision of 99%, and an F1 scoring of 99%, which showed that the model was more efficient. The ensemble method utilized throughout the process required more time to train for learning.

The novel lightweight random neural network (RaNN) prediction model has been suggested according to Latif et al. [23]. The collection and monitoring of datasets were the first stages in developing this architecture. The dataset was compiled and assessed according to its data type at this point. Dataset preprocessing was performed in the following step, including data cleansing, visualization, feature engineering, and vectorization. All of these techniques have been utilized to extract data from the data collection. These characteristic vectors were separated into two groups: a training set and a test set, where the two sets split 80 percent to 20 percent. The recommended random neural network was utilized to study the training set employed along with the proposed random neural network. To investigate RaNN-based prediction model performance, a variety of evaluation parameters were calculated and compared with traditional artificial neural network (ANN) performance, the support vector system (SVM), and decision-tree prediction models (DT). The results of this evaluation showed that the proposed RaNN model achieved a 99.20-percent accuracy with a learning rate of 0.01 and a prediction time of 34.51 milliseconds while training with a learning rate of 0.01. The precision of the system was hindered by the random character of the functioning of the network.

Chang et al. [24] presented a three-hierarchy joint local-global anomaly detection framework (HADIoT) that provides Internet of Things devices with sensory information generated and transferred to the local edge servers for local data anomaly recognition including data framing, standardization, analysis of principal components, and symbol mapping. The gated recurrent unit was used to focus local AD on the data consistency of certain devices and then sent the processed data from the edge servers for global AD to the cloud server. In the analysis of data pattern correlations between different Internet of Things devices, which were the focus of global AD, the conditional random fields were used. Simulations using a real dataset, the 2012 Information Security Center of Excellence (ISCX) dataset, were also utilized to evaluate the proposed method's performance for the study. Compared to three benchmarking schemes, the results of the simulation indicated that the proposed framework has been more effective than the benchmarks in terms of true positive rates, false positive rates, precision, exactness, and  $F$  score. Due to the low learning efficiency of the GRU, a longer training time was necessary.

Guo et al. [25] investigated uncontrolled anomaly detection on Internet multidimensional time series data of things systems and developed a Gaussian GRU-based VAE mixture technique which, in brief, was called GGM-VAE. Specifically utilized to identify correlations between time series data include the gated recurrent unit (GRU), whereas Gaussian mixture priors were used in latent space to characterize multimodal data, which is subsequently used to find correlations

between time series data. During the training phase, further development was undertaken under the Bayesian inference criterion (BIC) to select the model best suited to estimate the latent distribution of the Gaussian mixture. According to the results of extensive simulations carried out on four datasets, the approach detected the latest abnormality. Due to the lack of flexibility in the Gaussian model mixing, many calculation errors occurred when creating the multimodal data.

### 3. Proposed Anomaly Detection System Model

Every security vulnerability of different Internet of Things devices that has been deployed in real time may be very difficult to detect and address. This is because many Internet of Things devices are designed with little attention to their safety implications. It is thus important to create ways to prevent these dangers or attacks and to protect IoT devices from malfunctioning or failure. Current IDS and other attack detection methods could not detect attacks that were started dynamically or during the online procedure. To solve the attack issues, efficient secure anomaly detection has been proposed for an IoT context, as detailed in the article. The proposed system is split into four phases: preprocessing, feature extraction, selection of features, and classification. The first of these procedures is preprocessing. Initially, the input data is handled using four steps called NaN value handling, categorical features, missing values, and an imbalanced dataset. The random sampling method is used to handle the imbalanced dataset. Then, the most important features are chosen from the preprocessed data and compared to the originals using the median absolute deviations in the mid-based Kolmogorov-Smirnov test (MAD Median-KS test). The most important properties are then selected from the gathered functions, using the optimization technique based on robust confidence interval chimp, which is explained in full below (RCI-ChOA). Once this is done, we will apply the selected features to the optimum deep faith network based on dual weight update (DWU-ODBN) to translate the categorized output into the attack and nonattack data. Figure 1 shows a block diagram with each block indicating a step.

*3.1. Preprocessing.* Initially, the data is preprocessed, which includes handling of NaN values, categorical features, unbalanced datasets, and missing values, which occurs both randomly and nonrandomly. After that, the data is processed further. The preprocessing step assists us in obtaining healthier data while also reducing the difficulties associated with the data, which inhibits the flow of data traffic. The following are the stages involved in the preprocessing process.

In handling NaN values, NaN is an abbreviation that stands for "Not a Number," and it is one of the most often used symbols to indicate a missing value in data. To improve the accuracy of attack detection, the input data for an attack detection system must be devoid of NaN values. The following is the procedure for dealing with NaN values in the input data:

$$d_n^{\text{hand}(\text{NaN})} = \psi_{\text{hand\_NaN}}(d_n), \quad (1)$$

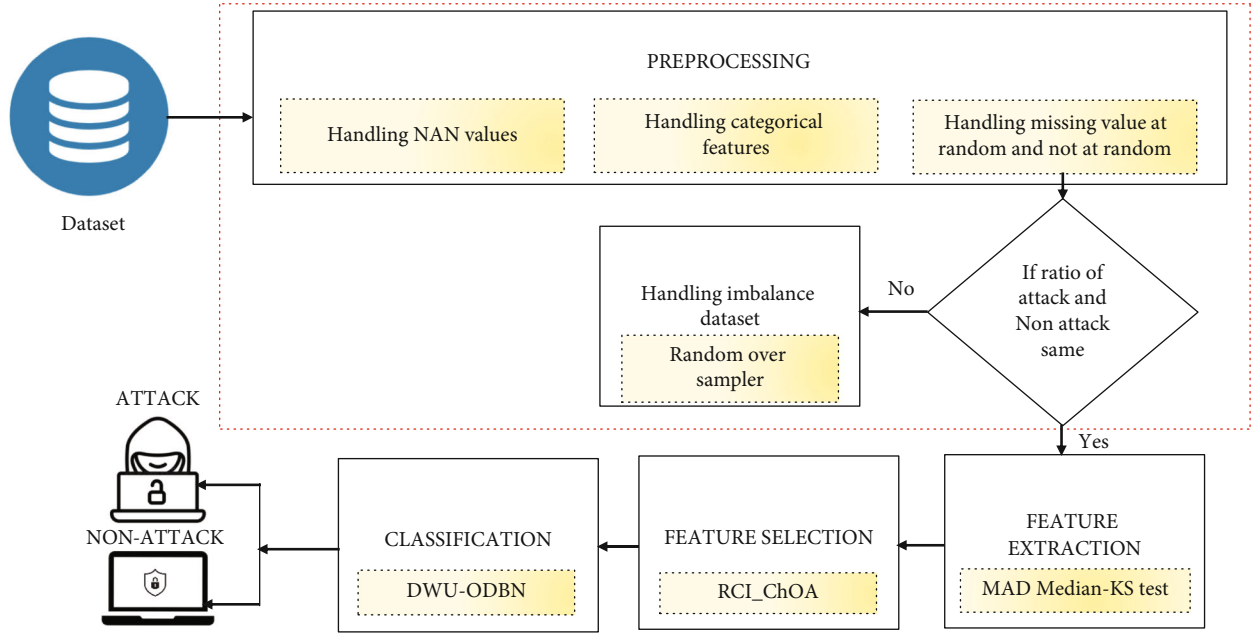


FIGURE 1: Block diagram of the proposed methodology.

where  $d_n$  is the input data,  $\psi_{\text{hand\_NaN}}$  is the method that handles the NaN values, and  $d_n^{\text{handl(NaN)}}$  is the data obtained after handling of NaN values.

In handling categorical features, handling categorical characteristics comes next once dealing with NaN values has been completed successfully. Categorical data must be processed in this phase before it can be fed into the machine learning models, which is the last step. Because machine learning models are considered mathematical models, they will not function properly with data that is stored in the texture format. The categorical characteristics may be handled in the following ways:

$$d_n^{\text{handl(ctg)}} = \xi_{\text{hand\_ctg}}(d_n), \quad (2)$$

where  $\xi_{\text{hand\_ctg}}$  denotes the method that handles the categorical data values and  $d_n^{\text{handl(ctg)}}$  is the data obtained after handling of categories.

In handling of missing values, in this step, the missing value at random and the missing values not at random are handled. Missing the values from some subsamples of data is considered as missing values at random. If the missing data has a specific structure, then it is known as missing values, not at random. The missing values can be handled as

$$d_n^{\text{handl(mis\_val)}} = \zeta_{\text{hand\_mis}}^{\text{(ran,not-ran)}}(d_n), \quad (3)$$

where  $\zeta_{\text{hand\_mis}}^{\text{(ran,not-ran)}}$  is the method that handles the missing values and  $d_n^{\text{handl(mis\_val)}}$  is the data obtained after handling of missing values.

Thus, the final set of preprocessed data is obtained as

$$d_n^{\text{PP}} = \{d_1, d_2, d_3, \dots \dots d_N\}, \quad (4)$$

where  $d_n^{\text{PP}}$  denotes the preprocessed data and  $N$  is the number of data. Then, the ratio of attacked and nonattacked data is checked to get the balanced and imbalanced data as

$$d_n^{\text{PP}} = \begin{cases} d_n^{\text{bal}} & \text{if } (A(d_n^{\text{PP}}) = \text{NA}(d_n^{\text{PP}})), \\ d_n^{\text{imbal}} & \text{if } (A(d_n^{\text{PP}}) \neq \text{NA}(d_n^{\text{PP}})), \end{cases} \quad (5)$$

where  $d_n^{\text{bal}}$  shows the balanced data,  $d_n^{\text{imbal}}$  shows the imbalanced data,  $A$  describes the attacked data, and  $\text{NA}$  describes the nonattacked data. From the obtained data, the balanced data is contributed to the next phase and the imbalanced data is handled using a random over sampler.

In handling of imbalanced dataset, here, the imbalanced data  $d_n^{\text{imbal}}$  is balanced with the help of a random oversampler. The random oversampler produces the balanced data using arbitrarily repeating the instances from the minority class and extreme them to the exercise input. The oversampling of data is

$$d_n^{\text{imbal}} \xrightarrow{\text{oversampling}} d_n^{\text{bal}}. \quad (6)$$

After that, the balanced data obtained with the help of oversampling is subjected to the feature extraction phase.

**3.2. Feature Extraction.** Following that, to gain knowledge of the balanced data, the work has developed a median absolute deviation around the median-based Kolmogorov-Smirnov test (MAD Median-KS test) that passages techniques from the net and uses arithmetical examination to detect abnormalities originating from compromised IoT devices. The MAD Median-KS test takes into account the distribution similarity and eliminates the repeated distribution data, and it applies to both continuous and discrete data. It is



important to note that the current Kolmogorov-Smirnov test only focuses on the highest difference value, which is affected by outliers and decreases the accuracy of identifying the attack. To get around this, the researchers utilized median absolute deviations around the median in their research.

In the MAD median-KS test, the features for the input data is computed as

$$\sigma_{ks} = \alpha \cdot \Lambda_n \left| \partial \left( d_n^{\text{bal}} \right) - \Lambda_i \left( \Gamma \left( d_n^{\text{bal}} \right) \right) \right|, \quad (7)$$

where  $\alpha$  is the constant that disregards the abnormality induced by the outliers,  $\Lambda_n$  denotes the median of the distribution functions,  $\partial, \Gamma$  are the two distribution functions of the sample  $d_n^{\text{bal}}$ ,  $\Lambda_i$  is the median of  $\Gamma$  which observes the features of the data. The extracted features such as duration, protocol type, service, flag, root\_shell, count, server\_count, and etcare denoted as

$$d_n^f = \left\{ d_1^{f(1)}, d_1^{f(2)}, d_1^{f(3)}, \dots, \dots, d_n^{f(k)} \right\}, \quad (8)$$

where  $f$  denotes the number of features extracted from the input data and  $f(k)$  denotes the  $k^{\text{th}}$  feature of  $n^{\text{th}}$  data.

**3.3. Feature Selection.** To maintain a superior computational speed and accuracy, the robust confidence interval-based chimp optimization method is used to extract and select important features after feature extraction (RCI-ChOA). The random updation of parameters in the existing chimp optimization algorithm leads to inaccurate model driving and chasing of prey, which results in the selection of features that are not relevant to the problem; therefore, to overcome this problem, the work has used robust confidence interval to update the parameters.

The ChOA algorithm simulates the social behavior of individual intelligence as well as the sexual drive of chimpanzees throughout a hunting expedition.

According to the retrieved characteristics, the chimp population that lives in a fission-fusion society is divided into four groups: (a) drivers, (b) barriers, (c) chasers, and (d) attackers (see Figure 1). This procedure is divided into two phases: the exploration stage and the exploitation stage, which are both important stages in the chimpanzees' hunting process. The exploration stage consists of driving, blocking, and pursuing, while the exploitation stage consists of assaulting the target and completing the mission.

When driving, the drivers simply follow the prey and do not make any effort to capture them. To impede the prey's entrance, the chimpanzees took up positions in trees and obstructed the prey's path. If you are pursuing something, you are trying to catch that something. In exploitation, the attackers [26] forecast the most advantageous path to take to assault the victim.

The driving and chasing of the prey can be modeled mathematically as

$$R = \left| v \cdot \chi_p(q) - \vartheta \cdot \chi_c(q) \right|, \quad (9)$$

$$\chi_c(q+1) = \chi_p(q) - v \cdot R, \quad (10)$$

where  $v$  and  $v$  are the coefficient vectors  $v = 2\varphi_2$ ,  $\vartheta$  is the chaotic vector computed concerning various chaotic maps, and  $\chi_p(q)$  and  $\chi_c(q)$  are the position of the prey and a chimp at the number of current iterations  $q$ . The chaotic vector  $\vartheta$  expresses the effect of the sexual motivation of chimps during the hunting process. The coefficient vectors are calculated as

$$v = \mathfrak{F}(2\varphi_1 - 1), \quad (11)$$

$$v = 2\varphi_2, \quad (12)$$

where  $\mathfrak{F}$  is the parameter that reduces nonlinearly from 2.5 to 0 in both exploration and exploitation stages and  $\varphi_1, \varphi_2$  are the parameters updated using robust confidence intervals  $\text{Con.Int}(H, F)$ . The robust confidence intervals are calculated as

$$\text{Con.Int}(H, F) = \text{med} \pm \varepsilon_{(\gamma/2, n-1)} \frac{\sigma}{\sqrt{n}}, \quad (13)$$

where  $\gamma$  denotes the confidence coefficient,  $\varepsilon$  is the percentage point of the confidence interval,  $\sigma$  is the sample standard deviation, and  $\text{med}$  denotes the sample median. Then, the fitness is evaluated based on the computation time and accuracy of the system.

For attacking the prey, the attackers find the position of the prey with the help of a driver, barrier, and chasers. The chimps also attack the prey based on chaotic strategy. Here, two approaches are employed as exploring the location of the prey and encircling the prey. Since the initial position of the prey was unknown, the attacker, driver, barrier, and chaser update the position of the prey. The position updation can be expressed as

$$R_{\text{attacker}} = |v_1 * \chi_A - \vartheta_1 * \chi|, \quad (14)$$

$$R_{\text{barrier}} = |v_3 * \chi_B - \vartheta_3 * \chi|, \quad (15)$$

$$R_{\text{chaser}} = |v_2 * \chi_{Ch} - \vartheta_2 * \chi|, \quad (16)$$

$$R_{\text{driver}} = |v_4 * \chi_D - \vartheta_4 * \chi|. \quad (17)$$

The four optimal solutions are stored, and other chimps are required to update their solutions. If the random vectors of  $v$  lies in  $[1, -1]$ , then the next position of the chimp can be at any location in the middle of its current position and the position of prey. The location of the chimp can be updated as

$$\chi(1) = \chi_A - v_1 \cdot R_{\text{attacker}}, \quad (18)$$

$$\chi(2) = \chi_{Ch} - v_2 \cdot R_{\text{chaser}}, \quad (19)$$

$$\chi(3) = \chi_B - v_3 \cdot R_{\text{barrier}}, \quad (20)$$

$$\chi(4) = \chi_D - v_4 \cdot R_{\text{driver}}. \quad (21)$$

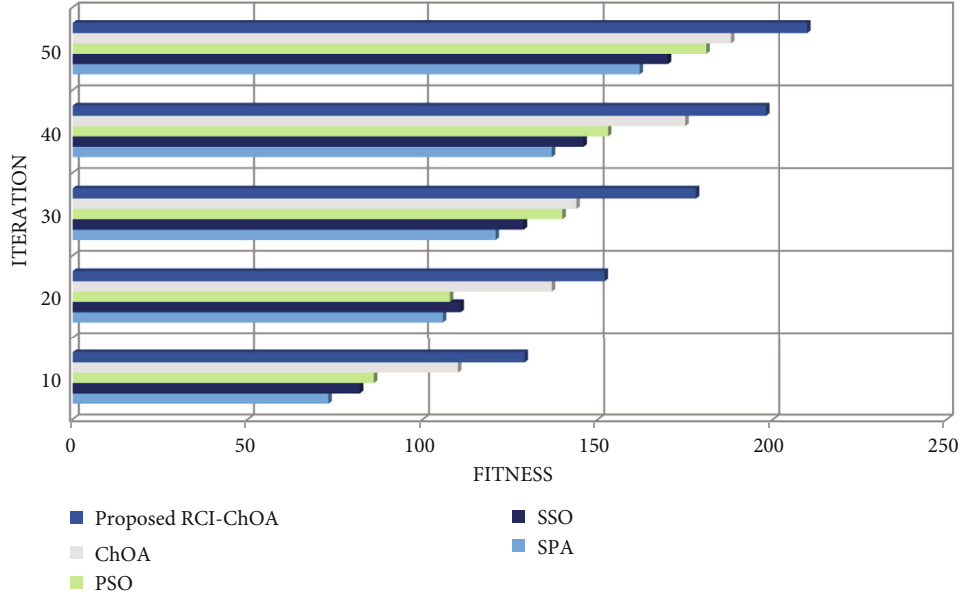


FIGURE 2: The performance of proposed RCI-ChOA based on fitness vs. iteration.

From the obtained locations, the position of the Chimp can be updated as

$$\chi(q+1) = \frac{\chi(1) + \chi(2) + \chi(3) + \chi(4)}{4}. \quad (22)$$

The hunting process of chimps can be affected by social benefits like support and sex. This motivates chimps to forget their contribution to the hunting process. So, the chaotic maps are used in the final stage of attacking the prey which helps chimps to lessen the local optima and slow convergence rate problems. The probability of choosing the normal position updation and chaotic map-based position updation is determined by the parameter  $\eta \in (0, 1)$  as

$$\chi_c(q+1) = \begin{cases} \chi_p(q+1) - \vartheta.R, & \text{if } (\eta < 0.5), \\ \varsigma_{m(\text{pos})}, & \text{if } (\eta > 0.5), \end{cases} \quad (23)$$

where  $\varsigma_m$  denotes the chaotic map-based position updation process. Based on the updated position, the prey has been attacked by the attackers [27]. The hunting process will be stopped when the movement of the prey was stopped. The pseudocode of the RCI-ChOA method is shown in Figure 2,

Algorithm 1 explains the steps involved in the RCI-ChOA method. In the same way as the hunting behavior of the chimps, the optimal features  $d_n^{\text{opt}}$  are selected from the extracted features.

**3.4. Classification.** The last stage involves training and evaluating the selected features over a dual weight updation-based optimal deep belief network (DWU-ODBN) classification system to detect and classify attacks [28]. Semisupervised classification algorithms, in contrast to supervised classification techniques, are capable of coping with adversarial attacks as well as uncertain attacks, which makes them more

robust. As a result of the technique's low error rate as well as its low false alarm rate (FAR), it can detect assaults more quickly and reliably. There are two RBM layers in the DBN, each of which consists of a single observable coating and one concealed coating. There are three RBM layers in the DBN. MLP is composed of three layers: the input layer, a hidden layer, and a final output layer. The input layer is the smallest of the three layers, and it is composed of the hidden layer and the final output layer. Only between the visible layer neurons and the hidden layer neurons does the connection form in DBN; the link does not form between the visible layer neurons and the hidden layer neurons in other words. However, there is no joining amid the visible nerve cell in the brain and the hidden neurons in other parts of the body.

Dual weight updation is used to enhance the accuracy of the classification process while simultaneously reducing the error rate of the classification process. Examples of weight updates in the proposed classification technique include stochastic gradient descent with momentum (SGDM), which has a higher convergent rate than gradient descent, and weight updates in the proposed classification technique include the best neighbor direction-based seagull optimization algorithm, which has a higher convergent rate than gradient descent (BND-SOA). Due to inaccuracy in the existing seagull optimization, the construction of the best neighbor direction results in high variance and standard deviation, which may result in poor convergence for updating weight as well as a long computation time for the update weight to be done. To overcome this barrier, the best neighbor direction based on Euclidean distance is determined.

The selected characteristics are presented as the input to the visible layer of the first RBM in DBN, which is the visible layer of the first RBM at the start of the simulation. The output of the visible layer is then mapped to the hidden layer of the first RBM, and the process is repeated until the output of

```

Input: Extracted features  $d_n^f$ 
Output: Selected features  $d_n^{f, \text{opt}}$ 
Begin
  Initialize population  $d_n^f$ , coefficient vectors  $\nu, \vartheta, \nu$ , maximum number of iteration
   $q_{\text{max}}$ 
  Calculate fitness for each chimps
  Set  $q = 0$ 
  While ( $q \leq q_{\text{max}}$ )
    Update  $\nu, \vartheta, \nu$ 
    Update position using  $R_{\text{attacker}}, R_{\text{chaser}}, R_{\text{barrier}}, R_{\text{driver}}$ 
    Evaluate fitness of the position of chimps
    If ( $\mu < 0.5 \& \nu \in (0, 1)$ ) {
      Update position of the chimps using  $\chi_p(q + 1) - \vartheta.R$ 
    }
    Else
      {
        Update position of the chimps using  $c_{m_{\text{pos}}}$ 
      }
    } End if
    Update  $\nu, \vartheta, \nu$ 
    Calculate fitness of the current position of the chimp
    Set  $q = q + 1$ 
  } End while
  Return selected features  $d_n^{f, \text{opt}}$ 
End

```

ALGORITHM 1: Pseudocode of the RCI-CHOA method

the visible layer is no longer visible. These modifications to RBM weights are accomplished via the use of SGDM.

$$\omega_i = \lambda \omega_{i-1} + (1 - \lambda) G^{(-i)}, \quad (24)$$

$$h^{i+1} = h^i - \tau \omega_i, \quad (25)$$

where  $\lambda$  is the momentum coefficient,  $\tau$  is the step size,  $h^{i+1}$  is the intermediate model parameter, and  $G^{(-i)}$  is the gradient of the weight values. The output of the hidden layer is expressed as

$$\Phi_{\text{hid\_out}}^1 = \mathfrak{R} \left( B_s^1 + \sum_i \Phi_{\text{vis\_out}}^1 \omega_{i(\text{vis\_hid})}^1 \right), \quad (26)$$

where  $\mathfrak{R}$  is the activation function,  $B_s^1$  represents the bias of the hidden units,  $\Phi_{\text{vis\_out}}^1$  is the output of the visible layer, and  $\omega_{i(\text{vis\_hid})}^1$  is the weight values between the visible and hidden neurons using the SGDM method.

$$\Phi_{\text{hid\_out}}^2 = \mathfrak{R} \left( B_s^2 + \sum_i \Phi_{\text{hid\_out}}^1 \omega_{i(\text{vis\_hid})}^2 \right), \quad (27)$$

where  $\omega_{\text{hid\_vis}}$  is the weight values between the visible and hidden neurons of the second RBM,  $\Phi_{\text{hid\_out}}^1$  is the output from the previous RBM, and  $B_s^2$  denotes the bias of the hidden units. Then, the output obtained from the second RBM is inputted to the MLP.

The MLP contains two weight vectors between the input and hidden layer and amid the hidden and output layer. In the MLP layer, the optimal weight values are updated using the BND-SOA method. The SOA method is the inspiration for migrating and attacking behaviors of the seagulls. During migration, a group of seagulls shifts their position to another position. In this migration process, it needs to consider three conditions which are detailed below:

- (i) Collision avoidance: to avoid collision between the search agents, the position of the new search agent is computed as

$$D_{\text{SA}} = E \times C_{\text{SA}}^p(z), \quad (28)$$

where  $E$  is the variable that represents the search agent's movement behavior and reduces from its maximum frequency to zero,  $C_{\text{SA}}^p$  denotes the current position of new search agent, and  $D_{\text{SA}}$  is the position of the search agents which does not involve in collision with other search agents

- (ii) The movement regards the best neighbor's direction: once the collision has been avoided, the search agents move by facing the direction of the best search agent. The movement of the search agents is expressed using the Euclidian distance as

$$\text{Mt}_{\text{SA}} = 2 \times E^2 \times Q \sqrt{\sum_{z=1}^{z_{\text{max}}} \left( C_{\text{BSA}(z)}^p - C_{\text{SA}(z)}^p \right)^2}, \quad (29)$$

where  $Q \in (0, 1)$  is the random parameter and  $C_{SA(z)}^p$  is the position of search agent towards the position  $Mt_{SA}$  of the best search agent  $C_{BSA(z)}^p$  at  $z$

- (iii) *Endure close to the best search agent*: the position of the search agent is updated regarding the position of the best search agent as

$$L_{SA} = |D_{SA} + Mt_{SA}|, \quad (30)$$

where  $L_{SA}$  is the distance between  $D_{SA}$  and  $Mt_{SA}$ .

After that, in the attacking action, the seagulls change the speed and angle of attack continuously. The change can be done using their weights and wings and makes spiral movement behavior in the air. The spiral movement behavior is defined in  $Xx$ ,  $Yy$ , and  $Zz$  plane as

$$Xx = \text{rad} \times \cos(u), \quad (31)$$

$$Yy = \text{rad} \times \sin(u), \quad (32)$$

$$Zz = \text{rad} \times u, \quad (33)$$

where each turn in the spiral contains a certain radius and is denoted as  $\text{rad}$  and  $u \in (0, 2\pi)$  is the random number. Then, the fitness is evaluated based on the error rate of the MLP layer. The updated position can be calculated using the spiraling action as

$$C_{SA}^p(z) = (L_{SA} \times Xx \times Yy \times Zz) + C_{BSA}^p(z), \quad (34)$$

where  $C_{SA}^p(z)$  is responsible for storing the best position of the search agents and updating the position of other search agents. In this way, the weight values for the MLP layer  $\omega_i^{\text{MLP}}$  are selected.

Concerning the input values, the output of the hidden layer in MLP is denoted as

$$\Phi_{\text{hid\_out}}^{\text{MLP}} = \left( \sum_{i=1}^K \Phi_{\text{hid\_out}}^2 \omega_{i(\text{ip\_hid})}^{\text{MLP}} \right) B_s^{\text{MLP}}, \quad (35)$$

where  $\omega_{i(\text{ip\_hid})}^{\text{MLP}}$  is the weight value between the input and hidden layers of the MLP,  $K$  is the number of neurons in the hidden layer, and  $B_s^2$  is the bias of the hidden neuron in MLP. Based on the output of the hidden layer, the output vector is calculated as

$$\Phi_{\text{op\_out}}^{\text{MLP}} = \left( \sum_{k=1}^K \omega_{k(\text{hid\_out})}^{\text{MLP}} \Phi_{\text{hid\_out}}^{\text{MLP}} \right) B_r, \quad (36)$$

where  $\omega_{k(\text{hid\_out})}^{\text{MLP}}$  is the weight value between the hidden and output layer. The output unit contains two classes of data as attack and nonattack. The proposed system detects adversarial attacks and uncertain attacks as well. Adversarial attacks mean the data are modified in such a way that, they cannot be detectable to the human eye.

TABLE 1: Evaluation of proposed RCI-ChOA based on fitness vs. iteration.

Techniques/iteration	10	20	30	40	50
SPA	73	106	121	137	162
SSO	82	111	129	146	170
PSO	86	108	140	153	181
ChOA	110	137	144	175	188
Proposed RCI-ChOA	129	152	178	198	210

## 4. Results and Discussion

In this part, the efficacy of the suggested irregularity discovery outline for use in the Net of Belongings setting is assessed using case studies. The experiments for assessing the suggested system are carried out using the Python programming language's working platform.

*4.1. Database Description.* The NSL-KDDCUP99 dataset is utilized in this study for experimental assessment. KDD Cup'99 is a dataset that is often used in the development of intrusion detection systems. Per network connection, the dataset includes a total of 41 characteristics. The characteristics are divided into several categories. Eighty percent of the data in the dataset is utilized for training, whereas only twenty percent of the data is used for testing.

*4.2. Performance Evaluation of Feature Selection Technique.* Based on the fitness vs. iteration trade-off, this section evaluates the performance of the proposed RCI-ChOA technique. The suggested technique is compared to the current SPA, SSO, particle swarm optimization (PSO), and chimp optimization algorithm (ChOA) methods to determine its suitability for the task at hand.

In discussion, fitness versus iteration is used to assess the performance of the proposed and current techniques, as shown in Table 1. The number of iterations required for the analysis is shown in Table 1 and ranges from 10 to 50. The suggested technique has a fitness value of 129 for the 10 number iterations that are included in the analysis. For 10 iterations, the current SSO and PSO techniques have fitness values of 82 and 86, respectively, while the existing SPA and ChOA methods have fitness values of 73 and 110, respectively. When the suggested technique is evaluated for its fitness throughout the remaining number of iterations, it scores 152 for 20 iterations, 178 for 30 iterations, 198 for 40 iterations, and 210 for 50 iterations, according to the findings. According to the suggested approach, current methods have poorer fitness for the number of iterations in comparison to the new method. The discussion demonstrates that the suggested approach outperforms the current methods in terms of overall performance. Figure 2 depicts a graphical depiction of the fitness versus iteration analysis in terms of fitness,

*4.3. Performance Evaluation of Classification Technique.* The accuracy, sensitivity, specificity, precision,  $F$  measure, FPR, FNR, and MCC of the proposed DWU-ODBN technique are compared to the current ENN, CNN, SVM, and DBN

TABLE 2: Performance analysis of proposed DWU-ODBN based on quality metrics.

Performance metrics/techniques	ENN	CNN	SVM	DBN	Proposed DWU-ODBN
Accuracy	92.14	91.51	94.84	93.26	97.34
Specificity	86.67	87.57	85.82	93.39	93.42
Sensitivity	89.69	90.48	85.54	91.62	95.61
Precision	92.37	90.62	87.63	95.83	97.43
<i>F</i> measures	93.52	93.39	89.29	94.62	97.72
FPR	46.46	44.25	59.42	31.51	11.04
FNR	42.93	49.64	56.58	38.58	8.39
MCC	85.44	82.87	80.52	88.28	94.65

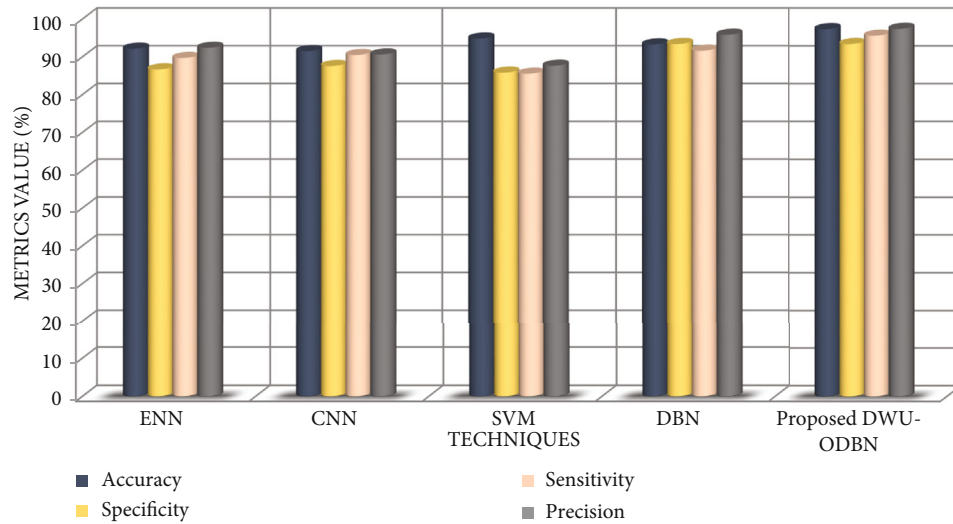


FIGURE 3: The performance analysis of the proposed DWU-ODBN based on accuracy, specificity, sensitivity, and precision.

methods in this section, as well as the existing ENN, CNN, SVM, and DBN methods. Following that, a comparison of the calculation time and attack detection time of the proposed and current techniques is provided.

In discussion, several quality indicators are used to assess the presence of the planned and current techniques, which are summarised in Table 2. For a classifier to be efficient, its accuracy, sensitivity, specificity, precision, *F* measure, and MCC values should all be greater than their current levels. The FPR and FNR are negative numbers that are often lower to achieve better categorization. As seen in the above table, the current SVM achieves low-level performance. Additionally, the current ENN, CNN, and DBN techniques have medium-level performance, according to the researchers. However, the suggested DWU-ODBN approach outperforms all other methods in terms of performance measures. In addition, it should be highlighted that the suggested approach exhibits improvement across all measures and outperforms the current ENN, CNN, SVM, and DBN methods in terms of overall performance.

In discussion, in the above Figure 3, the accuracy, sensitivity, specificity, and precision of the proposed and current techniques are evaluated about one another. The proposed method achieves classification accuracy of 97.34 percent,

whereas the existing ENN, CNN, SVM, and DBN methods achieve accuracy of 92.14 percent, 91.51 percent, 94.84 percent, and 93.26 percent, respectively, which is lower than the proposed DWU-ODBN method. The proposed method outperforms the existing methods by a wide margin. The suggested approach also has better sensitivity, specificity, and precision than the current methods, with 95.61 percent, 93.42 percent, and 97.43 percent, respectively, compared to the existing methods. It is apparent from the above study that the suggested DWU-ODBN technique outdoes the other current methods in terms of overall performance.

*In discussion*, on the right, you can see how the proposed and current techniques compare in terms of *F* measure, FPR, FNR, and MCC in Figure 4. While the proposed method has an FPR of 11.04 percent and an FNR of 8.39 percent, existing ENN, CNN, SVM, and DBN methods have FPRs of 46.46 percent, 44.25 percent, 59.42 percent, and 31.51 percent, respectively, and FNRs of 42.93 percent, 49.64 percent, 56.58 percent, and 38.58 percent, respectively, which are higher than the proposed DWU-ODBN method. Similarly, the *F* measure and MCC of the suggested approach are 97.72 percent and 94.65 percent, respectively, which are greater than those of the current methods. According to the findings of the preceding study, the



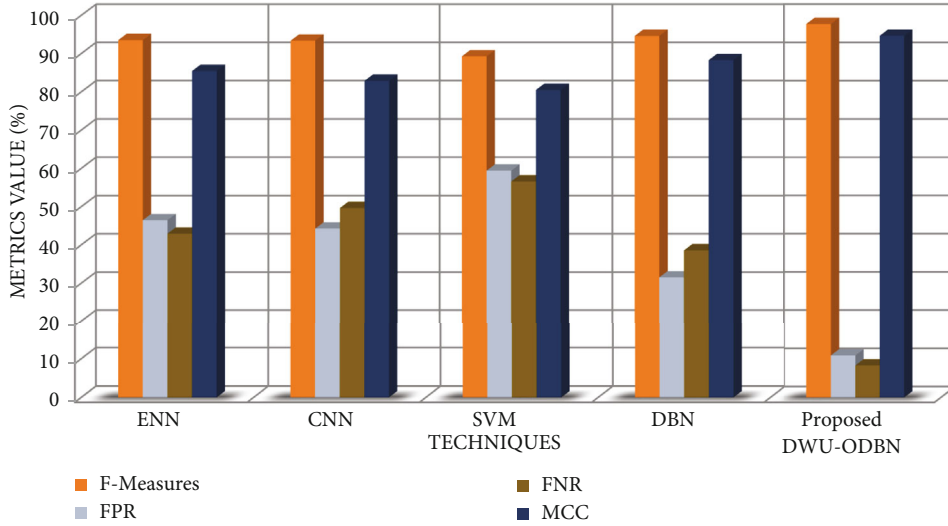


FIGURE 4: The performance of the proposed DWU-ODBN concerning *F* measure, FRR, FNR, and MCC.

suggested approach produces superior outcomes for all metrics than the current methods.

In discussion, Figure 5 compares the detection rates of the proposed and current techniques for detecting attacks. This study estimates the rate at which attacks are detected for two types of information: attack data and nonattack data. For the assault data, the proposed approach achieves a detection rate of 98.06 percent, while the current methods achieve a detection rate of 76.25 percent for ENN, 88.29 percent for CNN, 77.15 percent for SVM, and 86.36 percent for DBN, respectively. The suggested approach obtains a detection rate of 99.88 percent in the case of data that is not subjected to an assault. In comparison, the current ENN, CNN, SVM, and DBN techniques obtained rates of 77.76 percent, 87.56 percent, 78.65 percent, and 90.60 percent in the study, respectively. According to the results of the study, the suggested approach achieved the greatest detection rate for both attack data and nonattack data, whereas the detection rates of the current methods were much lower than the proposed method's detection rate. According to the results of the study, the suggested approach outperforms the current methods in terms of performance.

In discussion, Figure 6 compares the calculation times of the proposed DWU-ODBN technique with those of the current ENN, CNN, SVM, and DBN methods, among others. The study is carried out on several different datasets, including KDD99, NSL-KDDCUP99, CIDDS-001, and UNSW-NB15. The calculation time should be kept to a minimum for an efficient classifier. The suggested approach takes 77 seconds to compute for the KDD99 dataset, 78 seconds to compute for the NSL-KDDCUP99 dataset, 71 seconds to compute for the CIDDS-001 dataset, and 62 seconds to compute for the UNSW-NB15 dataset. When compared to the suggested approach, the current methods need a longer calculation time for all datasets. The results of the study indicate that the suggested approach is more effective at detecting assaults than the already available techniques.

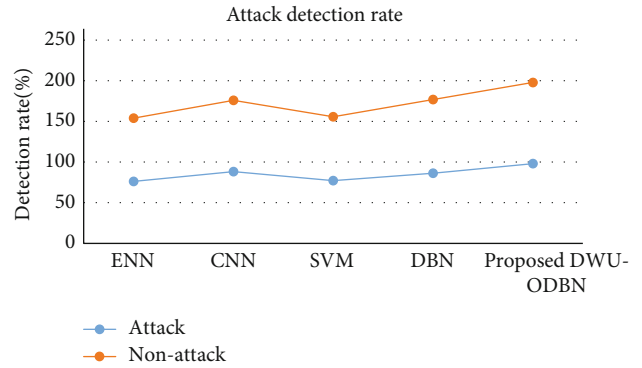


FIGURE 5: The attack detection rate of the proposed and existing methods.

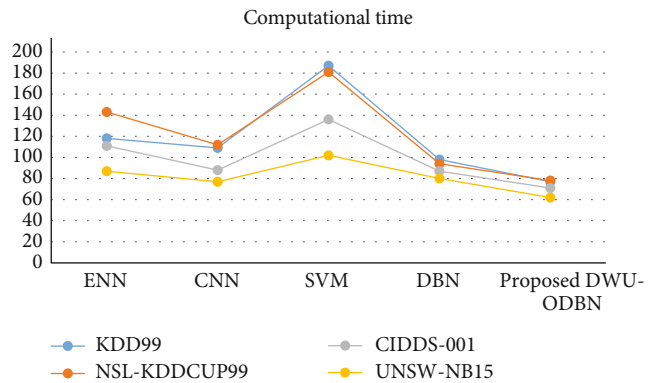


FIGURE 6: The computation time of the proposed and existing methods.

The result and analysis consider the feature selection, classification based on the performance metrics such as accuracy, sensitivity, specificity, precision, *F* measure, FPR, FNR, and MCC, attack detection rate, and computation time. These parameters were broadly compared against

existing techniques. Further, the parameters would be designed based on the real-time scenario. This will be incorporated in the future work of this article.

## 5. Conclusion

Typically, IoT devices are resource-constrained, and those that do have the limited onboard capability for security operations may result in data breaches due to a lack of available functionality. In turn, it makes it more difficult for the system to detect cyberattacks from the network promptly before they impair smart city operations. This article presents a dual weight updating-based optimum deep belief network for attack detection to protect Internet of Things devices from a variety of security threats. The suggested technique is divided into four stages. It is essential to evaluate the presentation of the suggested system in command to use the KDD99 dataset. It is determined how well the suggested RCU-ChOA and DWU-ODBN techniques perform when compared to the already available methods. Although the suggested DWU-ODBN technique is more accurate than the current methods, the accuracy of the proposed method is greater than that of the existing methods. The suggested system has a calculation time of 77 seconds, which is much shorter than the current techniques. In this way, it is concluded that the suggested method outstrips the present approaches in footings of performance. The proposed system attains a 98% accuracy rate in detecting the attack from the malicious node. As we compared various dataset analyses through our proposed work, the proposed work detects the attack within 71 seconds. The proposed method achieves classification accuracy of 97.34 percent, whereas the existing ENN, CNN, SVM, and DBN methods achieve accuracy of 92.14 percent, 91.51 percent, 94.84 percent, and 93.26 percent, respectively, which is lower than the proposed DWU-ODBN method.

## Data Availability

The data that support the findings of this study are available on request from the corresponding author.

## Conflicts of Interest

The authors of this manuscript declared that they do not have any conflict of interest.

## Acknowledgments

King Khalid University Researchers Supporting Project Number (R. G. P. 2/150/42), King Khalid University, Saudi Arabia, supported this work.

## References

- [1] Y. Cheng, X. Yan, H. Zhong, and Y. Liu, "Leveraging semi-supervised hierarchical stacking temporal convolutional network for anomaly detection in IoT communication," *IEEE Internet of Things Journal*, vol. 99, pp. 1–11, 2021.
- [2] X. Rongbin, Y. Cheng, Z. Liu, Y. Xie, and Y. Yang, "Improved long short-term memory based anomaly detection with concept drift adaptive method for supporting IoT services," *Future Generation Computer Systems*, vol. 112, pp. 228–242, 2020.
- [3] M. Roopak, G. Y. Tian, and J. Chambers, "Multi-objective-based feature selection for DDoS attack detection in IoT networks," *IET Networks*, vol. 9, no. 3, pp. 120–127, 2020.
- [4] G. De La Torre, P. R. Parra, K.-K. R. Choo, and N. Beebe, "Detecting Internet of Things attacks using distributed deep learning," *Journal of Network and Computer Applications*, vol. 163, p. 102662, 2020.
- [5] P. Dymora and M. Mazurek, "Anomaly detection in IoT communication network based on spectral analysis and Hurst exponent," *Applied Sciences*, vol. 9, no. 24, pp. 5319–5320, 2019.
- [6] A. Protogerou, S. Papadopoulos, A. Drosou, D. Tzovaras, and I. Refanidis, "A graph neural network method for distributed anomaly detection in IoT," *Evolving Systems*, vol. 12, no. 1, pp. 19–36, 2021.
- [7] A. A. Diro and N. Chilamkurti, "Distributed attack detection scheme using deep learning approach for Internet of Things," *Future Generation Computer Systems*, vol. 82, pp. 1–12, 2018.
- [8] D. B. Gothawal and S. V. Nagaraj, "Anomaly-based intrusion detection system in RPL by applying stochastic and evolutionary game models over IoT environment," *Wireless Personal Communications*, vol. 110, no. 3, pp. 1323–1344, 2020.
- [9] C. Wang, "IoT anomaly detection method in intelligent manufacturing industry based on trusted evaluation," *The International Journal of Advanced Manufacturing Technology*, vol. 107, no. 3, pp. 993–1005, 2020.
- [10] M. Keshk, E. Sitnikova, N. Moustafa, H. Jiankun, and I. Khalil, "An integrated framework for privacy-preserving based anomaly detection for cyber-physical systems," *IEEE Transactions on Sustainable Computing*, vol. 6, no. 1, pp. 66–79, 2021.
- [11] W. Di, Z. Jiang, X. Xie, X. Wei, Y. Weiren, and R. Li, "LSTM learning with bayesian and gaussian processing for anomaly detection in industrial IoT," *IEEE Transactions on Industrial Informatics*, vol. 16, no. 8, pp. 5244–5253, 2019.
- [12] Z. A. Baig, S. Sanguanpong, S. N. Firdous, V. N. Vo, T. G. Nguyen, and C. So-In, "Averaged dependence estimators for DoS attack detection in IoT networks," *Future Generation Computer Systems*, vol. 102, pp. 198–209, 2020.
- [13] A. Y. Khan, R. Latif, S. Latif, S. Tahir, G. Batool, and T. Saba, "Malicious insider attack detection in IoTs using data analytics," *IEEE Access*, vol. 8, pp. 11743–11753, 2019.
- [14] I. Razzak, K. Zafar, M. Imran, and X. Guandong, "Randomized nonlinear one-class support vector machines with bounded loss function to detect of outliers for large scale IoT data," *Future Generation Computer Systems*, vol. 112, pp. 715–723, 2020.
- [15] R. Vangipuram, R. K. Gunupudi, V. K. Puligadda, and J. Vinjamuri, "A machine learning approach for imputation and anomaly detection in IoT environment," *Expert Systems*, vol. 37, no. 5, pp. 1–16, 2020.
- [16] M. Hasan, M. Milon Islam, M. I. I. Zarif, and M. M. A. Hashem, "Attack and anomaly detection in IoT sensors in IoT sites using machine learning approaches," *Internet of Things*, vol. 7, p. 100059, 2019.
- [17] D. H. Hoang and H. D. Nguyen, "A PCA-based method for IoT network traffic anomaly detection," in *International*

- Conference on Advanced Communications Technology (ICACT)*, Chuncheon, Korea (South), 2018.
- [18] Y. An, F. Richard YuJianqiang Li, J. Chen, and V. C. M. Leung, "Edge intelligence (EI)-enabled http anomaly detection framework for the internet of things (IoT)," *IEEE Internet of Things Journal*, vol. 8, no. 5, pp. 3554–3566, 2020.
  - [19] V. Kumar, A. K. Das, and D. Sinha, "UIDS a unified intrusion detection system for IoT environment," *Evolutionary Intelligence*, vol. 14, no. 1, pp. 47–59, 2019.
  - [20] Y. Ebazadeh and R. Fotohi, "A reliable and secure method for network-layer attack discovery and elimination in mobile ad-hoc networks based on a probabilistic threshold," *Security and Privacy*, no. article e183, 2021.
  - [21] S. M. Zarei and R. Fotohi, "Defense against flooding attacks using probabilistic thresholds in the internet of things ecosystem," *Security and Privacy*, vol. 4, no. 3, article e152, 2021.
  - [22] Y. Liu, S. Garg, J. Nie et al., "Deep anomaly detection for time-series data in industrial IoT: a communication-efficient on-device federated learning approach," *IEEE Internet of Things Journal*, vol. 8, no. 8, pp. 6348–6358, 2021.
  - [23] S. Latif, Z. Zou, Z. Idrees, and J. Ahma, "A novel attack detection scheme for the industrial internet of things using a lightweight random neural network," *IEEE Access*, vol. 4, pp. 1–14, 2016.
  - [24] H. Chang, J. Feng, and C. Duan, "HADIoT a hierarchical anomaly detection framework for IoT," *IEEE Access*, vol. 4, pp. 1–10, 2016.
  - [25] Y. Guo, T. Ji, Q. Wang, Y. Lixing, G. Min, and P. Li, "Unsupervised anomaly detection in IoT systems for smart cities," *IEEE Transactions on Network Science and Engineering*, vol. 7, no. 4, pp. 2231–2242, 2020.
  - [26] B. Butani, P. K. Shukla, and S. Silakari, "An exhaustive survey on physical node capture attack in WSN," *International Journal of Computer Applications*, vol. 95, no. 3, pp. 32–39, 2014.
  - [27] A. K. Saxena, S. Sinha, and P. Shukla, "Design and development of image security technique by using cryptography and steganography: a combine approach," *Graphics and Signal Processing (IJIGSP)*, vol. 10, no. 4, pp. 13–21, 2018.
  - [28] A. Kothari, P. Shukla, and R. Pandey, "Trust centric approach based on similarity in VANET," in *2016 International Conference on Signal Processing, Communication, Power and Embedded System (SCOPEs)*, pp. 1923–1926, Paralakhemundi, India, 2016.

## Research Article

# Evaluating Technological Innovation of Media Companies from the Perspective of Technological Ecosystem

Kui Yi <sup>1</sup>, Ligang Zhang <sup>2</sup>, Xiulan Mao <sup>3</sup>, Yi Li <sup>1</sup> and Jiaxuan Bao <sup>1</sup>

<sup>1</sup>College of Economics and Management, East China Jiaotong University, Jiangxi 330013, China

<sup>2</sup>School of Literature and Law, East China University of Technology, Jiangxi 330013, China

<sup>3</sup>College of Economics and Management, Jiangxi Industry Polytechnic College, Jiangxi 330039, China

Correspondence should be addressed to Ligang Zhang; [levox@ecut.edu.cn](mailto:levox@ecut.edu.cn)

Received 28 September 2021; Revised 15 November 2021; Accepted 17 November 2021; Published 10 December 2021

Academic Editor: Deepak Gupta

Copyright © 2021 Kui Yi et al. This is an open access article distributed under the Creative Commons Attribution License, which permits unrestricted use, distribution, and reproduction in any medium, provided the original work is properly cited.

The evaluating indicators on the benefits of innovative technology to media companies are preliminarily analyzed and evaluated, according to the research review and evaluating criteria of self-organization and ecosystem selection. Factor analysis and structural equation modeling are used to further explore and select the indicators. According to the results, from the perspective of technology ecosystem, innovative technology performance of media companies can be measured through a two-factor structure—the input of innovative technology and its output. On this basis, ANP (analytic network process) is used to establish a weighted evaluation of indicators. At the end of the paper, a complete set of evaluation systems was created to measure the performance of technology innovation.

## 1. Introduction

Media technology is evolving faster than we could imagine. With the gradual entry into the era of rationality, the role of media technology has become increasingly prominent. Media technology has created a new entertainment environment and makes life more colorful, influencing the trend of social civilization and the social lifestyle, as well as people's aesthetic and spiritual pursuit. Nowadays, the construction of spiritual civilization is the top priority of China's development. As early as in the "Twelfth Five-Year Plan" period, the development of cultural industry was put forward as a pillar industry. After that, a series of measures were put forward to promote the development of the media industry, which further accelerated the change of people's lives by science and technology. The new technology represented by the Internet, new media, cloud technology, and big data has become new driving forces for the development of media companies.

## 2. Analysis of Technological Ecological Mechanism of Media Companies

To maintain a favorable position in market competition, companies often rely on dominant technologies for innovation [1]. In formulating a technological innovation strategy, it is particularly important to identify the law of technological evolution [2]. With the rapid growth of consumers' demand on the renewal of science and technology in the new era, an accurate understanding of technology development trends and ecological characteristics of technology will promote the sustainable development of a company's innovative ability. Therefore, the analysis of the technological ecosystem is helpful to further understand the relationship between media company technology and technology and the technology and environment of media companies and provide a theoretical basis for the study of innovation and development of media companies.

On the basis of the research on the technological ecological characteristics of companies [3], it is understood that the technological ecosystem of media companies has two mechanisms, namely, the self-organization mechanism of the technology system and the selection mechanism of the technological ecosystem.

### 2.1. Self-Organization Mechanism of Technology System.

Firstly, technology is inclusive, which is best reflected in media technology. For example, science, optics, chemistry, and other technologies lead to the invention of video and audio. Meanwhile, the inclusiveness of its technology system guarantees that media products will always stay ahead of the time and keep up with time and meet the basic audio-visual needs of consumers. For example, the early phonograph recording technology replaced the musical instrument dubbing, and the emergence of 3D media in the new era is gradually replacing the traditional 2D media technology. Therefore, taking the opportunity of technology evolution is key to the technological innovation and development of the media companies and will ensure the return of technology.

The technology system has the characteristics of nonlinear interaction, which is represented by the nonlinear characteristics of technology in the production and development stage and the interaction between technology and technology. It is mainly reflected in the synergy of technologies and the new functions and effects produced by the interaction between technologies. For example, optical lens recording technology and 3D stereo imaging technology form prototype of stereo film, creating a powerful combination beyond a single technology.

Finally, the evolution of technology system is an automatic process. Any technology of a media enterprise is composed of technical factors, which plays a major part, and technological environment. It is an automatic process in which the technology is able to come into being, adapt to the surrounding system, and become stabilized without external instructions. Therefore, media technology is affected by both the internal and external factors. The innovation of media companies also depends on the quality of innovators and the application rate of innovative resources.

### 2.2. Selection Mechanism of Technological Ecosystem.

Under the organization of media technology, companies could obtain premium benefits through innovation that subverts the existing technology. However, consumers and the market may not favor all technological innovations during this process. For example, a magic movie with an investment of 200 million yuan used full-scale 3D live shooting and the state-of-art technology of dynamic capture in its making, but its audience score was poor. When a disruptive technology is created, the selection mechanism of the technological ecosystem plays a leading role in market efficiency, and it is a significant other-organizational process. For example, Chinese consumers did not accept dynamic capture technology when it was first launched and so did European and American consumers when they first encountered the 3D technology. Thus, the application of innovative technology needs to adapt to the market. And technological innovation

needs to constantly integrate with media products and make improvements. At this stage, the new technology of media needs to be dynamically adjusted to fit the market and meet the demand of consumers.

The environment of technological innovation is the major player in the ecosystem selection. Media companies need to cater to the demand of the consumer market, which is the major player, and the innovation, which creates market impact, serves as the manifestation. When the media technology first enters the market, it will be influenced by many factors, among which the market is the most crucial one. The technological innovation of media is constantly evolving to meet the market demand. Therefore, the success of innovation and its return are the direct results of market selection. Meanwhile, the market choice can be divided into rational and emotional choices of consumers, so the media technology innovation is influenced by multiple factors.

In conclusion, the self-organization mechanism of technology system and the selection mechanism of the technical ecosystem can fully demonstrate the performance of the technological innovation in the media enterprise. Therefore, in this paper, the technological performance evaluation of media companies is carried out on this basis.

## 3. Research Review and Hypotheses

### 3.1. Research Review.

As there is no research on technology evaluation of benefits to media companies, based on the technological ecological mechanism of the media companies and its features, this study will review and summarize the existing research and make relevant hypotheses.

For the understanding of technological innovation in companies, previous studies have put emphasis on the effect of technology innovation input. In Nelson's view [4], the investment in technological innovation in early days will promote the sustainability of innovation, thus conducive to the allocation of innovative resources. Scherer [5] held that the content of enterprise technology innovation input is broad and innovative activities are constantly changing and have different forms. Therefore, researches on enterprise technological innovation should adopt multiple evaluation indicators. Innovative indicators proposed by Scherer include R&D investment, the number of major technological innovations, and the number of new products. Hagedoorn [6] believed that R&D investment is crucial for accelerating the application of innovative technologies and the effective output of new products. With further research on R&D investment, Acs and Audretsch [7] discovered that patents represent the most significant new technical knowledge, processes, and new industrial products of a firm. Griliches and Mairesse [8] argued and found that R&D investment is directly related to the output of technological innovations and could increase the innovative abilities and performance of a firm.

As research goes on, scholars proposed more direct measures of returns on innovative technologies for firms. Many scholars use the commercialization of new product as a measure for innovative performances [9]. Meanwhile, scholars found that using patent data as an innovation indicator has



some limitations. However, high-tech companies can use patent propensity rates to measure innovation performance to some extent [10]. In this regard, scholars put forward a number of relevant indicators: Fischerchose to use the sales revenue of new products, product innovation degree, and the percentage of innovative process as indicators of innovation returns [11]. Hagedoorn included R&D inputs, patent counts, and patent citations to new product announcements into the indicators of innovative performance of companies summarize the existing research [12]. Laursen and Foss argued that the technical returns in the innovative performance of companies should be measured from the number of patent filed and licensed [13]. In the measurement research, Beneito added the indicators such as the growth of innovative performance, the number of new products and patents, R&D input, and investment return as indicators [14]. Kesidou and Romijn thought that patent counts and R&D input can reflect the technological returns from innovative activities [15].

Based upon data and papers from foreign studies or databases, Chinese scholars gradually deepened their understanding of innovation measurement. Chen and Wang took product innovation as the first-level indicator and established a performance evaluation system for technology innovation, which was divided into innovation output and performance dimensions during innovation [16]. He also put forward a series of indicators including the number of new products, improved products, new standards, patent applications, technical know-how, technical documents, scientific papers, technical innovation proposals and competitive intelligence analysis reports, frequency of communication between the R&D department and customers, between R&D departments in companies, between R&D department and manufacturing department, between R&D departments and universities and research institutes, R&D/sales ratio, proportion of R&D staff, number of technical leaders, number of rewarded technicians, average training cost for each technician, and number of technicians attending conferences at home and abroad, as well as industrial technical forums. Yin and Yang used the Balanced Scorecard (BSC) to study the technological innovation performance of enterprises [17]. In their design, the effects of technological innovation, innovation management, innovation input, finance, and social benefit are the second-level indicators of the evaluation system. They continued to divide the abovementioned dimensions, such as technological innovation effects, innovation management, and technology innovation input, into subcategories such as the number of new products, sales rate and profit margin of new products, the number of new standards, patent counts, productivity rate, number of scientific papers, proportion of R&D personnel, number of technical leaders and rewarded technicians, number of technical personnel attending conferences at home and abroad, exchanges between R&D departments and other institutions, market penetration rate of a new technology, the rate of innovative products and their success rate, product life cycle, proportion of R&D investment to sales revenue, expenses of acquiring external technologies, expenses on human capital development and training, input on university-industry collaboration on inno-

vation, and the quality of equipment compared with peers. Cao et al. took the number of patent applications, the number of patents, implementation level of technological innovation, and the sales of new products as the indicators of enterprise innovation in their research on assessment model and evaluation index for the effect of tacit knowledge conversion on technology transfer [18]. Wang and Deng set up an innovation evaluation system for Jiangxi companies based on innovation process, in which knowledge output and economic performance are regarded as the first-level indicators, input factor, and output factor as the third-level indicators [19]. Items including number of scientific and technical personnel, R&D personnel, funds for scientific and technological activities, and R&D expenditure are the input factors under the indicator of knowledge output; patent licenses, application rate of innovative resources, scientific and technical publications, and scientific and technological achievements and awards are output factors under the indicator of economic performance. In the research on the coupling indicator system of enterprise patent management and innovation performance, Cao and Su believed that the following factors could be taken as second-level indicators for technological innovation performance, and they are the number of staff in R&D and training activities, R&D expenditure, the amount of sophisticated equipment, patent information utilization, market penetration of the product, frequency of communication between patent R&D departments, number of patent applications and licenses, number of corporate patent regulations, patent risk assessment, the number and volume of patent disputes, the term of patents, the number of participating standards, core patents, technical files and scientific papers, and improvement of R&D personnel skills, as well as external networking [20]. Wei and Liang proposed to use the performance of organization and management skills as well as technical ability as the second-level indicator to evaluate innovation [21]. Each second-level indicator will further extend to third-level indicators. There are nine third-level items in total, including innovative management skills on company strategies, methods and institutions, improvement of new product, cleanliness of production process, the input-output ratio of exploring new market and introducing new resources, the conversion rate of new techniques, and the input-output ratio of environmental technological achievements.

*3.2. Research Hypotheses.* This study has carried out an expert review of indicators (a total of 6 experts, including 4 academic experts (all of whom are professors of management) and 2 industrial experts (a CCTV program director and a president assistant from a media company)), which has mentioned above, based on the feature of technological ecosystem in media companies (as shown in Table 1). The chosen indicators must meet the following criteria: (1) suitable to the mechanism of technological ecosystem, (2) relevant to returns generated by innovative activities by media companies, (3) with concise and easy-to-understand language, (4) clear in meaning, and (5) related to innovation. The expert review has selected 14 indicators that fit the media companies from existing ones, and they are the number of technically improved media products, the application

TABLE 1: Preliminary establishment of technological innovation indicators for media companies.

Dimensions	Proposed indicators	Features of related technical ecosystem
Technological innovation	The application rate of a new media technology	Openness
	The number of major technological innovations	
	The output rate of innovative technologies by media companies	
	The conversion rate of new techniques	
	The frequency of new product announcements	
	R&D inputs of media companies	
	The implementation of innovative media technology	Nonlinear interaction
	The application rate of new media technology	
	The number of staff in technological innovation	Self-organization
	The application rate of innovative resources	
	The number of technically improved media products	
	The life cycle of media products	Ecosystem selection
The market penetration rate of a new media technology		
The success rate of innovative products		

rate of innovative resources, the number of staff in technological innovation, the frequency of new product announcements, the conversion rate of new techniques, the output rate of innovative technologies by media companies, the application rate of a new technology, the number of major technological innovations, R&D inputs of media companies, the life cycle of media products, the implementation of innovative media technology, the success rate of innovative media products, the application rate of new media technology, and the market penetration rate of a new media technology.

Technological performance usually refers to the margin of economic results, and labor inputs after technological policies and measures are implemented and applied. Technological performance of media firms reflects the return of input during the creation of film and television products. The technological performance of media innovation is to explore such relation from the perspective of innovation, in order to help media companies, achieve rapid and sound development with low cost. On this basis, this study also takes into account the ecosystem selection of media companies and uses academic classification methods, the evaluation indicators of innovative technology of media companies to divide the indicators of technological innovation performance of media companies into two dimensions: the performances of technology input and output.

Firstly, the performance of technology output generally refers to higher returns brought about by technological innovation and improvements to media companies. As the media companies belong to strategic emerging industries, the application of innovative technologies will greatly affect the revenue of companies.

Secondly, the performance of technology input generally refers to the returns of technological innovation and improvements to media companies, which reflects the revenues generated by innovation in production process by media companies.

#### 4. Quantitative Analysis and Discussion

Descriptive statistics, exploratory factor analysis, and confirmatory factor analysis were used in the statistical research,

and a questionnaire was distributed. A total of 656 questionnaires were collected during one month, and 626 questionnaires were screened out with an effective rate of 95.42%. The questionnaires were randomly divided into two parts, each of which consisted of 313 questionnaires, to ensure the validity and randomness of sample selection. They were used, respectively, for exploratory factor analysis and confirmatory factor analysis. Factors of the sample are as shown in Table 2.

*4.1. Exploratory Factor Analysis.* Through the analysis and research review of technological ecosystem, it can be concluded that the technological performance of Chinese media companies includes 14 measurements. The KMO value and Bartlett spherical test of 313 effective samples were carried out. The results showed that the KMO's test had a high value of 0.921. The Bartlett value of the spherical test was 1,904.697 and a level of significance of less than 0.001. Secondly, the reliability analysis was carried out. The result showed that the correlation coefficient of the single item to the total item in all items was greater than 0.5. Finally, a consistency analysis was performed, and the results showed an Alpha value of 0.902. In summary, the reliability of the scale is very good, in line with the exploratory factor analysis standard.

The screening of items was carried out with principles that were agreed upon by scholars. The analysis principles are as follows: (1) the common factor load should be greater than 0.50; (2) the common factor load can only be one and more than 0.50; (3) the common factor load should have a large difference.

Based on the principles, factor analysis was operated as follows: constructing covariance matrix, extracting factors with principal component analysis, rotating with the maximum variance method, and converging after 3 rotations. The technological benefit indicator shows a clear two-factor structure.

Conclusions are as follows: items T1, T4, T8, and T13 with a common degree of less than 0.50 were deleted; T7

TABLE 2: Demographic variables for questionnaires.

Exploratory analysis phase ( $n = 313$ )				Confirmatory analysis phase ( $n = 313$ )			
Gender	Male	99	31.6%	Gender	Male	113	31.6%
	Female	214	68.4%		Female	200	68.4%
Education background	Graduate	4	1.3%	Education background	Graduate	6	1.3%
	Undergraduate	288	92%		Undergraduate	268	92%
	Junior college student	20	6.4%		Junior college student	38	6.4%
	Below junior college	1	0.3%		Below junior college	1	0.3%
Age	20-30	121	38.7%	Age	20-30	100	38.7%
	30-40	190	60.7%		30-40	210	60.7%
	40-50	2	0.6%		40-50	3	0.6%
	Above 50	0	0		Above 50	0	0
Identity	Technician	109	34.8%	Identity	Technician	101	32.3%
	Management	71	22.7%		Management	92	29.4%
	Consumer	133	42.5%		Consumer	120	38.3%
Employment duration	1-2 yrs	51	16.3%	Employment duration	1-2 yrs	73	16.3%
	3-5 yrs	170	54.3%		3-5 yrs	164	54.3%
	6-10 yrs	91	29.1%		6-10 yrs	72	29.1%
	Over 10 yrs	1	0.3%		Over 10 yrs	4	0.3%

TABLE 3: Results of exploratory factor analysis of innovative technology for efficiency scale of media companies ( $N = 313$ ).

Items/name of factors	Technology output performance	Technology input performance
T6: the output rate of innovative technologies by media companies	0.748	
T10: life cycle of media products	0.737	
T11: the implementation of innovative media technology	0.760	
T12: success rate of innovative products	0.791	
T14: the market penetration rate of a new media technology	0.677	
T2: the application rate of innovative resources		0.754
T3: the number of staff in technological innovation		0.785
T5: the conversion rate of new techniques		0.689
T9: R&D inputs of media companies		0.797
Characteristic value	6.198	1.566
Variance contribution ratio (%)	30.249	25.203
Cumulative variance contribution ratio (%)	30.249	55.452

was deleted because it has 2 common factors with loads exceeding 0.50. The total explained variance ratio is 55.452%, and the results are shown in Table 3.

In view of the meaning of the abovementioned items and combining with the review and classification criteria of the characteristics of innovation technological ecological mechanism and innovative technology performance characteristics of media companies, the above 2 factors are named.

Factor 1 is named as technology output performance with variance contribution ratio of 30.249%, consisting 5 items: T6, T10, T11, T12, and T14.

Factor 2 is named as technology input performance with variance contribution ratio of 25.203%, consisting 4 items: T2, T3, T5, and T9.

The two-factor structure shows that the investment by media companies will affect innovation activities, which can increase the output of the companies, thus enhancing the technological performance of media companies in all aspects.

*4.2. Confirmatory Factor Analysis.* During the exploratory factor analysis, it was found that the innovative technology performance of media companies was composed of two factors. Therefore, the second-order confirmatory factor analysis was carried out (shown in Figure 1 and Table 4). The results show that all factors of indicators for the innovative technology performance had significant levels.

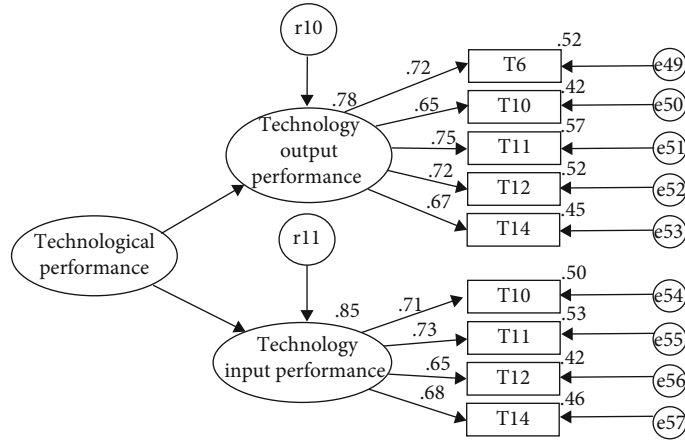


FIGURE 1: Confirmatory factor analysis model.

TABLE 4: Factor load coefficient of the indicators model for innovative and social performances for media companies ( $N = 313$ ).

Items/factors	Technology output performance	Technology input performance	
T6: the output rate of innovative technologies by media companies	0.722		
T10: the life cycle of media products	0.650		
T11: the implementation of innovative media technology	0.753		
T12: the success rate of innovative products	0.723		
T14: the market penetration rate of a new media technology	0.673		
T2: the application rate of innovative resources		0.709	
T3: the number of staff in technological innovation		0.726	
T5: the conversion rate of new techniques		0.651	
T9: R&D inputs of media companies		0.680	
Second-order factor load coefficient	0.885	0.924	First-order factor load coefficient

TABLE 5: Overall fitness of the indicator system of innovative technology efficiency of media companies ( $N = 313$ ).

Model fitness	Fitted value	Fitting standard
$X^2/df$	1.996	Less than 3, good fit
GFI	0.964	Greater than 0.9, good fit
AGFI	0.938	Greater than 0.9, good fit
CFI	0.975	Greater than 0.9, good fit
RFI	0.934	Greater than 0.9, good fit
IFI	0.976	Greater than 0.9, good fit
NFI	0.952	Greater than 0.9, good fit
NNFI (TLI)	0.966	Greater than 0.9, good fit
ECVI	0.228	The smaller the better
RMSEA	0.057	Less than 0.1, good fit
RMR	0.034	Less than 0.1, good fit

Table 5 shows that the overall fitness of the indicator model for innovative technology performance is very good,  $x^2/df$  is 1.996 ( $<3$ ), which is within the acceptable range of

the test value. All indicators of CFI, NNFI, IFI, RFI, NFI, GFI, and AGFI are greater than 0.9, RMSEA and RMR are less than 0.1, and ECVI value is smaller, indicating a very good fit. Therefore, it is judged through confirmatory factor analysis on the verification model of indicators for innovative technology performance of media companies has a high degree of fit, and all the indices are valid.

4.2.1. *Weight Establishment.* To further improve the construction of the indicator system for innovative technology performance of Chinese media companies and scientifically evaluate the technological innovation activities of media companies, the Super Decisions software is used to analyze the weight of the indicator system on the basis of dimension empirical test. Firstly, a structural model of the indicator system of innovative technology performance of Chinese media companies is drawn, as shown in Figure 2. The model consists of two levels:

Control level: technological benefit ( $B_3$ ).

Network level: technology output performance ( $C_1$ ), technology input performance ( $C_2$ ), the output rate of

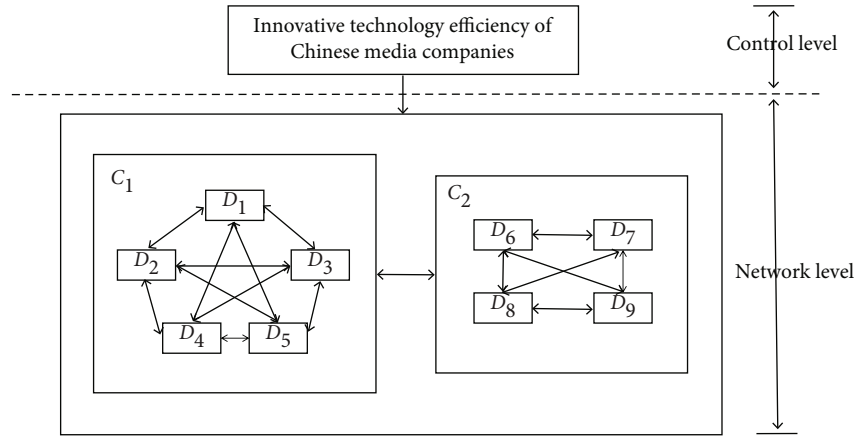


FIGURE 2: Network level structure model of innovative technology efficiency indicator system for Chinese media companies.

TABLE 6: Weight system of innovative technology efficiency evaluation indicators for Chinese media companies.

First-level indicators	Second-level indicators	Third-level indicator element			
		Indicators	The weight of the element to the overall system (retaining 3 decimal places)	Actual rating	
Technological benefit	Technology output performance	Technology innovation output rate of media companies	0.063		
		Life cycle of media products	0.257		
		Implementation of innovative media technology	0.084		
		The success rate of innovative products	0.111		
		The market penetration rate of a new media technology	0.152		
	Technology input performance	Technology input performance	The application rate of innovative resources	0.088	
			The number of staff in technological innovation	0.058	
			The conversion rate of new techniques	0.118	
			R& D investment by companies	0.069	

innovative technologies by media companies ( $D_1$ ), the life cycle of media products ( $D_2$ ), the implementation of innovative media technology ( $D_3$ ), the success rate of innovative products ( $D_4$ ), the market penetration rate of a new media technology ( $D_5$ ), the application rate of innovative resources ( $D_6$ ), the number of staff in technological innovation ( $D_7$ ), the conversion rate of new techniques ( $D_8$ ), and investment in R& D by companies ( $D_9$ ).

This study explicit the innovative technology efficiency of media company, the process includes innovations on inner sensational experiences, in terms of input and output to abstract the words of implantation and expression, which explains the innovating process of media companies; the words of output and input contain a more general conation.

In this study, the analytic network process (ANP) was used comprehensively, and the one-time test was used to calculate and form a complete weight system for indicators of innovative technology performances of Chinese media companies, as shown in Table 6.

## 5. Conclusions and Suggestions

**5.1. Conclusions.** The application of the technological ecosystem can well explain the overall characteristics of technological innovation in media companies. The self-organized technology system is the driving force of innovation in media companies and is crucial for companies to generate returns. The market selection in the technological ecosystem determines whether a newly applied media technology can adapt to the consumer market and whether a disruptive technology could dominate the market.

The ecosystem of technology tends to follow a fixed path of accumulation and time evolution. Such a path for media technologies is especially unique. Transitions from black and white to color, silent to sound, 2D to 3D, fully reflect the interaction and fierce competition among old and new media technologies. Upon achieving self-organization and selection by technological ecosystem, new media technologies will always replace the old ones and realize a



technological leap. In market competition, new disruptive media technology needs to compete with dominant technologies for advantageous positions in the consumer market. A new disruptive media technology will not only meet the blockade from the old but also the selection and feedback from the market. After continuous evolving, new media technology will finally trump the old by leapfrogging to a new level and making paradigm changes.

Therefore, in this paper, evaluation forms for innovative technology performance of media companies are designed based on the characteristics of the technological ecosystem, to provide a methodological guide for innovation and the improvement of technical performance for media companies. The forms follow a two-factor structure: technology output performance and technology input performance.

**5.2. Suggestions.** Through the research, it concluded that the utilization of innovative resources and the number of staff in technical innovation would significantly affect the performance of media technology. Therefore, innovative talents and resources are still the key to the success in innovation competition of media companies in the new era. The output rate of innovative technology, implementation of innovative technology, and the success rate of technological innovation are more significant in the output performance of media technology. Therefore, media companies should pay more attention to details in innovation and understand the characteristics of the ecosystem.

Generally speaking, from the perspective of the technological ecosystem, the technological innovation of media companies' progresses in stages. Media companies or media-related departments should better identify each stage during the application of new technology, take targeted measures in different stages, to promote the application of the new technology and the paradigm transformation of media technology.

## Data Availability

The raw data supporting the conclusions of this article will be made available by the authors, without undue reservation.

## Conflicts of Interest








It is declared by the authors that this article is free of conflict of interest.

## References

- [1] H. Taskin, M. Adali Rizaersin, and E. Ersin, "Technological intelligence and competitive strategies: an application study with fuzzy logic," *Journal of intelligence manufacturing*, vol. 15, no. 4, pp. 417–429, 2004.
- [2] A. Momeni and K. Rost, "Identification and monitoring of possible disruptive technologies by patent- development paths and topic modeling," *Technology Forecasting & Social Change*, vol. 104, pp. 16–29, 2016.
- [3] K. Wang and J. A. Wang, "Analysis framework of technological evolution from the perspective of technological eco-system," *Management and Management*, vol. 5, pp. 100–102, 2017.
- [4] W. Nelson, *An Evolutionary Theory of Economic Change*, Harvard University Press, Cambridge, 1982.
- [5] F. Scherer, *Research and Development Resource Allocation under Rivalry: Innovation and Growth*, The MIT Press, Cambridge Mass, 1984.
- [6] J. Hagedoorn, *The Dynamic Analysis of Innovation and Diffusion*, Pinter Publishers, London, 1989.
- [7] Z. J. Acs and D. B. Audretsch, "Patents as a measure of innovative activity," *Kyklos*, vol. 42, no. 2, pp. 171–180, 1989.
- [8] Z. Griliches and J. Mairesse, "R&D and productivity growth: comparing Japanese and US manufacturing firms," in *Productivity Growth in Japan and the United States*, pp. 113–116, University of Chicago Press, 1990.
- [9] M. A. Hitt, R. E. Hoskisson, R. A. Johnson, and D. D. Moesel, "The market for corporate control and firm innovation," *Academy of Management Journal*, vol. 39, no. 5, pp. 1084–1119, 1996.
- [10] A. Arundel and J. Kabla, "What percentage of innovations are patented? Empirical estimates for European firms," *Research Policy*, vol. 27, no. 2, pp. 127–141, 1998.
- [11] M. Fischer, J. R. Diez, and F. Snickars, *Metropolitan Innovation Systems: Theory and Evidence from Three Metropolitan Regions in Europe*, Springer, Berlin, 2010.
- [12] J. Hagedoorn and M. Cloudt, "Measuring innovative performance: is there an advantage in using multiple indicators?," *Research Policy*, vol. 32, no. 8, pp. 1365–1379, 2003.
- [13] K. N. Laursen and J. Foss, "New human resource management practices, complementarities and the impact on innovation performance," *Cambridge Journal of Economics*, vol. 27, no. 2, pp. 243–263, 2003.
- [14] P. Beneito, "The innovative performance of in-house and contracted R&D in terms of patents and utility models," *Research Policy*, vol. 35, no. 4, pp. 502–517, 2006.
- [15] E. Kesidou and H. Romijn, "Do local knowledge spillovers matter for development? An empirical study of Uruguay's software cluster," *World Development*, vol. 36, no. 10, pp. 2004–2028, 2008.
- [16] J. Chen and H. X. Wang, *Evolutionary Economics*, Tsinghua University Press, Beijing, 2008.
- [17] J. H. Yin and J. H. Yang, "Research on the performance indicator system of enterprise technological innovation based on the enhanced balanced score method," *Scientific Research Management*, vol. 1, pp. 1–7, 2008.
- [18] Y. Cao, L. Zhao, and F. J. Su, "Research on coupling measurement model and evaluation indicator of enterprise patent management and technological innovation performance," *Scientific Research Management*, vol. 10, pp. 55–63, 2011.
- [19] Y. Y. Wang and Q. Z. Deng, "Performance evaluation of Jiangxi province's technological innovation based on input-output perspective," *Science and Technology Management Research*, vol. 1, pp. 64–68, 2013.
- [20] Y. Cao and F. J. Su, "Empirical study on the impact of technological innovation investment on innovation performance in high-tech industries: a comparative analysis based on panel data of the whole industry and its five subordinate industries," *Scientific Research Management*, vol. 9, pp. 22–31, 2012.
- [21] J. Z. Wei and L. L. Liang, "Design of performance evaluation indicator for enterprise environmental innovation," *Journal of Liaoning University of Engineering and Technology*, vol. 1, pp. 160–164, 2012.

## Research Article

# Current-Fed Bidirectional DC-DC Converter Topology for Wireless Charging System Electrical Vehicle Applications

Partha Sarathi Subudhi <sup>1,2</sup>, M. Thilagaraj <sup>3</sup>, C. S. Sundar Ganesh <sup>3</sup>, S. Diwakaran <sup>4</sup>,  
P. Naveen <sup>5</sup>, Saravanakumar Gurusamy <sup>6</sup> and M. Pallikonda Rajasekaran <sup>4</sup>

<sup>1</sup>Department of Electrical and Electronics Engineering, Faculty of Engineering and Architecture, Nisantasi University, Istanbul, Turkey

<sup>2</sup>Department of Electrical Engineering, Bajaj Institute of Technology, Wardha, Maharashtra, India

<sup>3</sup>Department of Electronics and Instrumentation Engineering, Karpagam College of Engineering, Coimbatore, India

<sup>4</sup>Department of Electronics and Communication Engineering, Kalasalingam Academy of Research and Education, Srivilliputhur, India

<sup>5</sup>Department of Electronics and Communication Engineering, Sri Eshwar College of Engineering, Coimbatore, India

<sup>6</sup>Department of Electrical and Electronics Technology, Ethiopian Technical University, Addis Ababa, Ethiopia

Correspondence should be addressed to Saravanakumar Gurusamy; [saravanakumar.gurusamy@etu.edu.et](mailto:saravanakumar.gurusamy@etu.edu.et)

Received 30 September 2021; Revised 28 October 2021; Accepted 30 October 2021; Published 8 December 2021

Academic Editor: Deepak Gupta

Copyright © 2021 Partha Sarathi Subudhi et al. This is an open access article distributed under the Creative Commons Attribution License, which permits unrestricted use, distribution, and reproduction in any medium, provided the original work is properly cited.

This paper compares the efficiency of a modified wireless power transfer (WPT) system with a current-fed dual-active half-bridge converter topology and a complete bridge converter topology for a current-fed resonate compensation network with current sharing and voltage doubler. Full-bridge topologies are widely used in current WPT structures. The C-C-L resonate compensation networks for dual-active half-bridge converter and full-bridge converter topologies are built in this paper on both the transmitter and receiver sides. Due to higher voltage stress around inverter switches, series-parallel (S-P) tanks are not recommended for current-fed topologies because they are not ideal for medium power applications. A series capacitor is connected to reduce the reactive power absorbed by the loosely coupled coil. As a consequence, the C-C-L network is used as a compensation network. Dual-active half-bridge topology is chosen over full-bridge topology due to the system's component count and overall cost. Soft-switching of the devices is obtained for the load current. The entire system is modelled, and the effects are analysed using MATLAB simulation.

## 1. Introduction

The revolution in the development of electric vehicles has brought many modifications in charging strategies. Initially, the plug-in electric vehicle battery charging strategy was popular for two, three decades. However, users may get shocked during adverse climatic conditions such as rain and snowfall. The cost of the charging cable also adds more manufacturing cost to the plug-in electric vehicle. These limitations of plug-in vehicles motivated researchers to concentrate on the wireless charging system. Wireless power transfer (WPT) is aimed at making electrical power transfer

simpler, reducing complexity, and making it flexible for users and less costly.

Battery charging for electric vehicles (EVs) [1–10], mobile devices, biomedical implants [11], and lighting applications [6] have been the subject of a recent WPT study. Revolution in WPT technique started with the invention of the microwave power transfer (MPT) technique. In this technique, the user had the capability to transfer power for a wider range [12]. MPT used rectennas that were connected at the sending and receiving end of the power transfer system. The rectenna facilitates conversion of microwave signal to electric power and vice versa. This power transfer technique was very famous

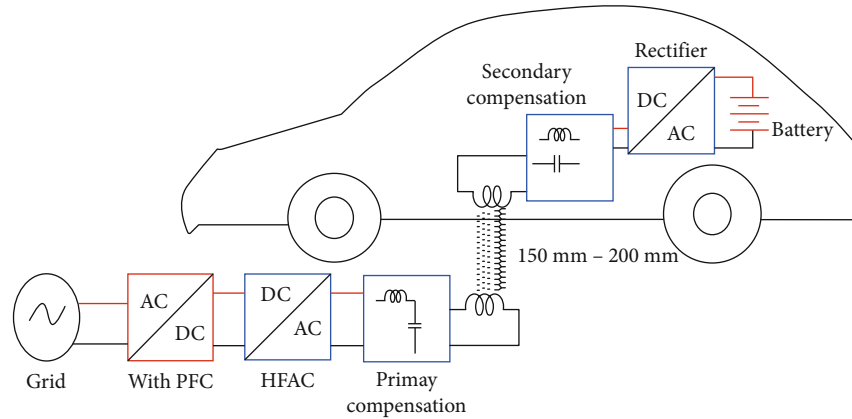


FIGURE 1: Basic block diagram.

among users as it was able to transfer a higher range of power for a larger range of air gap [13]. However, MPT uses a high-frequency power transfer system, which is not safe for living beings. These power transferring paths must be sealed with protective covers. This arrangement increases the system cost and reduces the reliability of the WPT system [14].

Further research in WPT area motivated researchers to develop the inductive power transfer (IPT) technique [15–17]. This technique employs a lower range frequency compared to MPT technique for transferring power wirelessly. This WPT technique has been used in a range of applications over short distances. On the other hand, the performance begins to plummet after a certain distance between the coupling coils. With the increase in distance between the power transferring points and the increase in the misalignment between coils, the power transfer efficiency reduces drastically due to the increase in leakage inductance between the coupling coils [18, 19].

In order to compensate for the leakage inductance in IPT technique, there are resonating capacitors connected to both sides of the WPT coupling coils.

These resonating capacitors compensate the leakage inductance between the power transfer coils. A basic block diagram of IPT technique is depicted in Figure 1. Generally, IPT technique operates in a frequency range of few kilohertz to 300 MHz to balance converter size, performance, and manufacturing cost of the system [6].

As per the connection of resonating capacitor at both sides of the WPT coils, the WPT technique is divided into two compensation techniques. These techniques are series compensation and parallel compensation technique. WPT using parallel compensation technique is discussed in [8–10]. Basically, current source inverters (CSI) are used for parallel compensation of WPT technique. The parallel compensation technique provides various advantages such as it provides necessary reactive power to the coil; the parallel capacitors show lower impedance to higher-order harmonics. This feature reduces the voltage and current across the power transferring terminals of WPT coils. The parallel compensation circuit employs a series inductor connected with the WPT coils [20–23]. This inductor reduces the fault current during inverter fault conditions in CSI. This is a very

significant advantage of the WPT technique employing parallel compensation capacitors.

Conversely, this series inductor is of big size, which limits the application of this technique to the area where the source produces a stiff rise in current, such as solar power generation system. The parallel LC tank used in WPT technique increases the impedance of the circuit, which can be solved by connecting a series capacitor in series with the compensating circuit. This series capacitor supplies a fraction of reactive power, which is needed by the coupling network [24, 25].

The literature review found that using the CCL compensation technique in the primary side coil and LC compensation technique in the secondary coil increases the reliability of the WPT system. This technique is adopted in this proposed system.

This paper proposes a soft-switching nonisolated duplex CCL compensation resonant circuit. Circuit diagram of the proposed system is shown in Figure 2. It is a front-end half-bridge boost converter followed by an associate in CCL compensation resonant circuit and voltage electronic device at high-voltage facet. The planned converter has the subsequent merits: (1) zero voltage switch (ZVS) stimulation of all switches in each directions, (2) zero current switching (ZCS) stimulation and turn-off of all diodes in each directions, (3) voltage level decreases across all the components used to fabricate the system, (4) use of extra snubber circuit is avoided in this system, (5) high improvement and step down ratio, and (6) reduced volume of geophysical science.

Contributions of this work are as follows:

- (i) Soft-switching nonisolated duplex CCL compensation resonant circuit is proposed in this work
- (ii) The proposed converter uses half-bridge boost converter in the front-end of the network, and CCL resonant circuit is used in this system in order to maximise the power output
- (iii) The proposed converter uses ZVS and ZCS switching techniques which reduce the switching voltage of the converter

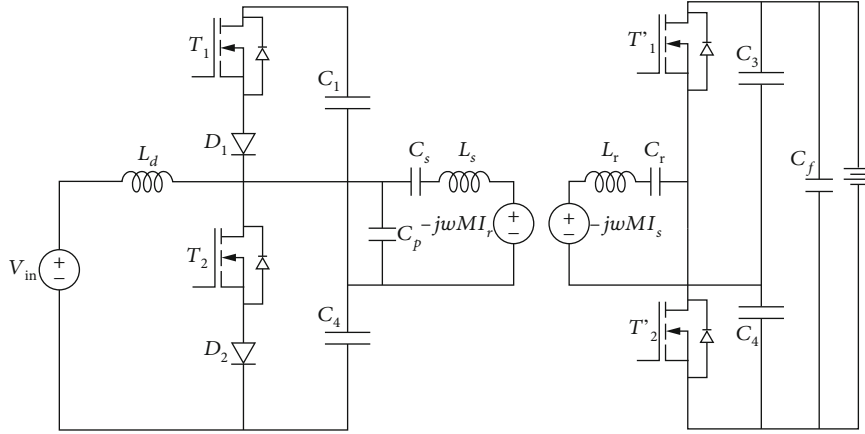


FIGURE 2: Circuit diagram of the proposed bidirectional resonant DC/DC converter.

- (iv) This converter also has high step up and step down voltage output capacity

## 2. Working of the Proposed Bidirectional DC/DC Converter

The CCL compensation resonant circuit enhances the voltage magnitude at the output of the converter and provides ZVS and ZCS for front-end devices and diodes, respectively. Half-bridge converter connected at the primary side of the compensating network increases the voltage across its output terminals. The CCL compensation technique adopted at the primary coil further increases the voltage level based on the resonant and switching frequency ratio. This voltage at the output of the compensation network is doubled by employing a voltage doubler circuit at the output of the compensation network. This is how the circuit behaves during the boost operation of the system. Circuit behavior during buck operation is provided in the following paragraph.

While the user wants to reduce the converter's output voltage, the capacitors of the half-bridge converter are used to divide the input voltage to equal magnitude.  $M_3$  and  $M_4$  switches are also modulated to allow for a high step down ratio. ZVS of switches  $M_3$  and  $M_4$  and ZCS of diodes  $D_1$  and  $D_2$  are aided by the CCL compensation resonant circuit.

$M_1$  and  $M_2$ 's gating signals complement one another, with a sufficiently dead band for boost activity.  $M_3$  and  $M_4$  are switched off.  $M_3$  and  $M_4$  are run in tandem with enough dead time to allow for buck activity.  $M_1$  and  $M_2$  do not have any modulation. The converter's steady-state functions while increasing the output voltage and while decreasing the output voltage are explained in the following subsection.

**2.1. Converter Behavior while Increasing the Output Voltage Compared to the Input Voltage.** Steady-state operating waveforms and the operation of the converter in boost mode are shown in Figures 3 and 4, respectively. Devices  $M_3$  and  $M_4$  are not triggered and remain in OFF-state for the entire boost operation.

**Mode 1 [ $t_0 < t < t_1$ ]:** The converter is operating as a boost converter. Switch  $M_2$  is conducting, and inductor  $L$  is storing energy. Working of the converter during this mode

is depicted in Figure 4(a). Switch  $M_1$  and diodes  $D_1$  and  $D_3$  remain OFF during this mode. Load is fed by output capacitors,  $C_7$  and  $C_8$ .

**Mode 2 [ $t_1 < t < t_2$ ]:** During this mode,  $t = t_2$ ; switch  $M_2$  is in OFF state. Now, both the switches  $M_1$  and  $M_2$  are OFF. Inductor current  $i_L$  and resonant current  $i_{L_r}$  jointly start discharging and charging the parasitic device capacitances  $C_1$  and  $C_2$ , respectively. Working of the converter during this mode is depicted in Figure 4(b). Before the next interval,  $C_1$  discharges the stored charge in it and  $C_2$  is fully charged. This is quick, and the duration is concise. At the end of this mode,  $i_{M_1}(t_2) = 0$ ,  $i_{M_2}(t_2) = 0$ ,  $v_{M_1}(t_2) = 0$ , and  $v_{D_4}(t_2) = 0$ . Switch  $M_2$  voltage is given by the following:

$$v_{M_2(t_1)} = \frac{V_L}{1-D}, \quad (1)$$

where  $D = T_{ON}/T_s$ ,  $T_{ON}$  is the main switch conduction period, and  $T_s$  is the switching period.

$$i_L(t) = i_L(t_3) - \frac{v_{C_s}(t_2) - v_{C_p}(t_2)}{L}(t - t_3). \quad (2)$$

Voltage across diode  $D_3$  is given by the following:

$$v_{D_3} = V_H. \quad (3)$$

**Mode 3 [ $t_2 < t < t_3$ ]:** Now, the body diode  $D_1$  starts conducting by  $i_L - i_{L_r}$  causing zero voltage across  $M_1$ . Diode  $D_4$  is forward biased, and current starts flowing through resonant inductor  $L_r$  and capacitor  $C_p$  starts charging output capacitor  $C_8$ . Working of the converter during this mode is depicted in Figure 4(c). Final values are  $i_{M_1}(t_3) = 0$ ,  $i_{M_2}(t_3) = 0$ ,  $v_{M_1}(t_3) = 0$ , and  $v_{M_2}(t_3) = V_L/1 - D$

$$i_{D_1}(t_3) = i_L(t_3) - i_{L_r}(t_3). \quad (4)$$

**Mode 4 [ $t_3 < t < t_4$ ]:** At  $t = t_3$ ,  $M_1$  starts conducting with ZVS. The equivalent resonant circuit is shown in Figure 5(a). Antiparallel body diode  $D_4$  conducts to charge capacitor  $C_8$ ,

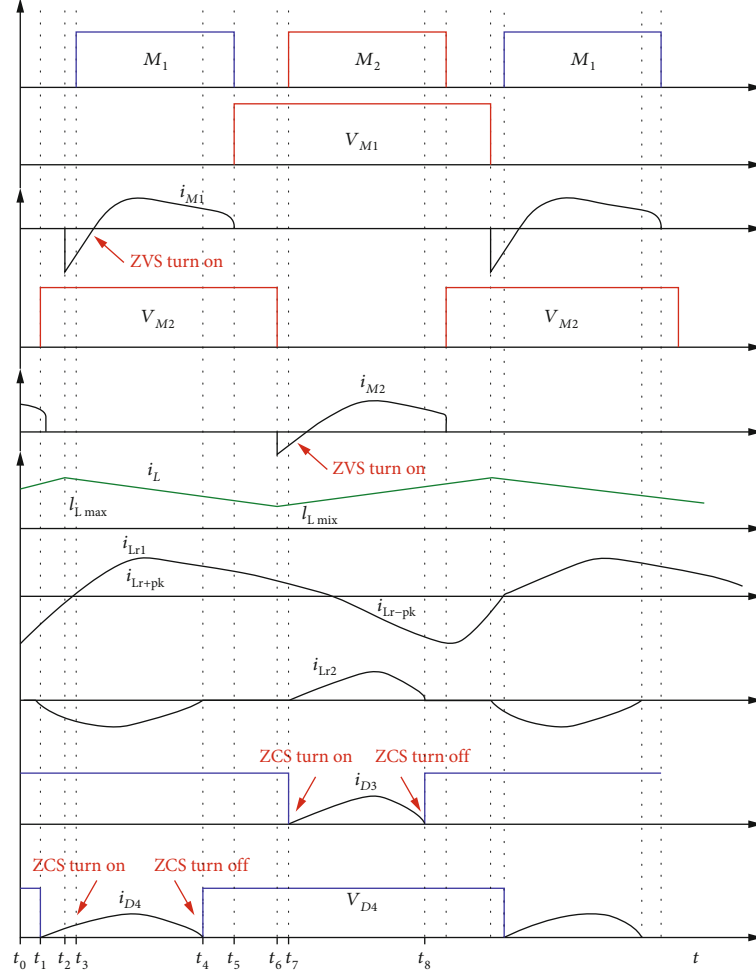


FIGURE 3: Voltage and current waveforms of the components while the converter is used to step up the output voltage compared to the input voltage.

while diode  $D_3$  is reverse biased. Before the next interval, the diode  $D_4$  turns off with ZCS as the resonant inductor current  $i_{Lr2}$  discontinues to zero. Working of the converter during this mode is shown in Figure 4(d). The equations for this interval are as follows:

$$i_{Lr1}(t) = \frac{v_{C_s}(t_3) - v_{C_p}(t_3)}{Z_r} \cdot \sin \omega_r(t - t_3), \quad (5)$$

where

$$\omega_r = \sqrt{\frac{C_5 + C_p}{L_{r1} C_p C_s}},$$

$$z_r = \sqrt{\frac{L_{r1} (C_p + C_s)}{C_p + C_s}}, \quad (6)$$

$$i_L(t) = i_L(t_3) - \frac{v_{C_s}(t_2) - v_{C_p}(t_2)}{L} (t - t_3),$$

$$i_{M1}(t) = i_{Lr1}(t) - i_L(t).$$

Voltage across antiparallel diode  $D_3$  is follows:

$$v_{D_3} = V_H, \quad (7)$$

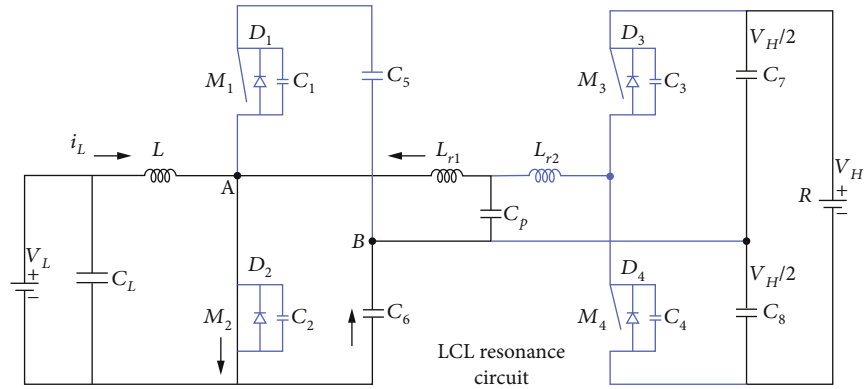
where  $Z_r$  is known as characteristic impedance offered by the circuit formed by resonant tank  $L_{r1}$ ,  $C_p$ , and capacitor  $C_5$  as shown in Figure 5(a).

Mode 5 [ $t_4 < t < t_5$ ]: Current continues to flow through switch  $M_1$ , and body diodes do not conduct. Load is fed by energy stored in output capacitor  $C_7$  and  $C_8$ . At  $t = t_4$ , switch  $M_1$  stops conducting. At the end of this mode,  $v_{D_3}(t_5) = 0$ ,  $v_{D_4}(t_5) = 0$ , and  $v_{M_2}(t_5) = V_L/1 - D$ . Working of the converter during this mode is depicted in Figure 4(e).

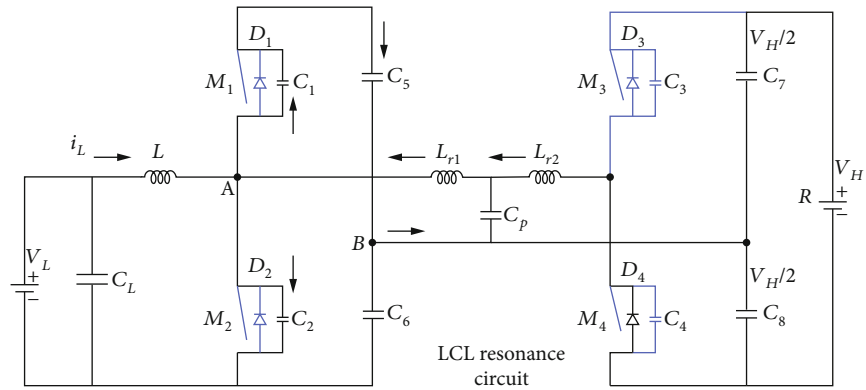
Mode 6 [ $t_5 < t < t_6$ ]: Parasitic capacitance  $C_1$  is charged, and capacitance  $C_2$  is discharged by  $i_{Lr1} - i_L$ . High-side body diodes are reverse biased. Before next interval, capacitance  $C_2$  is discharged completely, and  $C_1$  is charged to  $V_H/1 - D$ . Working of the converter during this mode is depicted in Figure 4(f).

Mode 7 [ $t_6 < t < t_7$ ]: In this interval, diode  $D_2$  starts conducting through a difference of  $(i_{Lr} - i_L)$  and  $M_2$  can now use for ZVS turn-on. Working of the converter during this

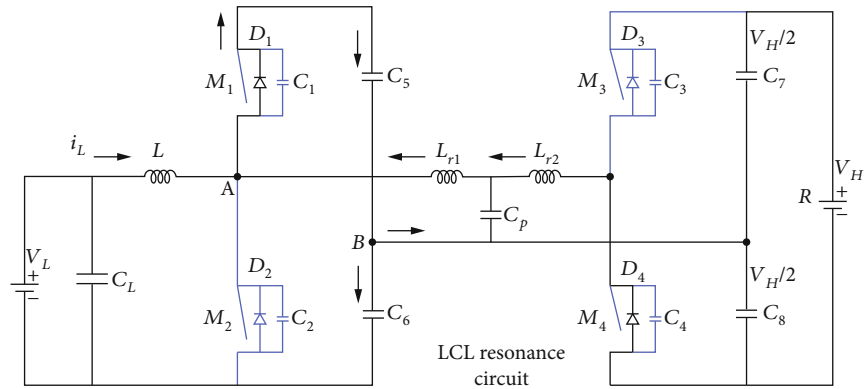




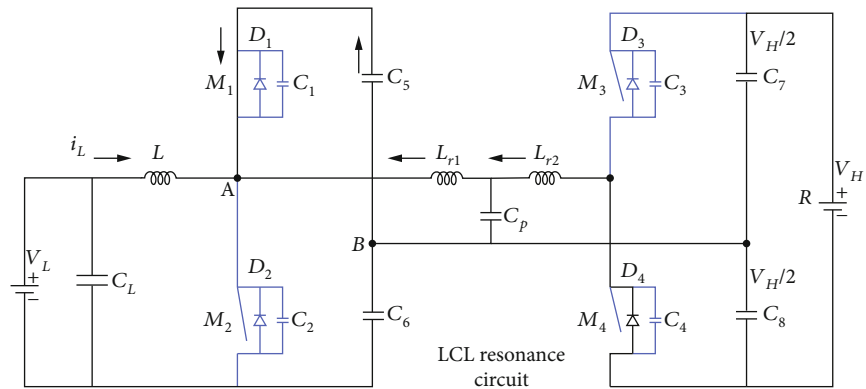
(a)



(b)

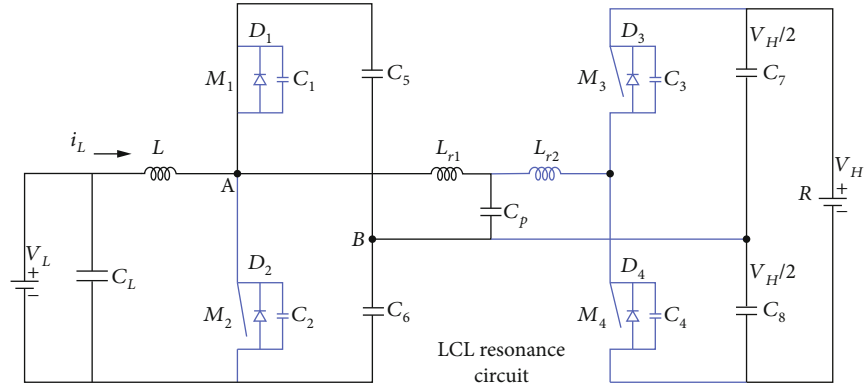


(c)

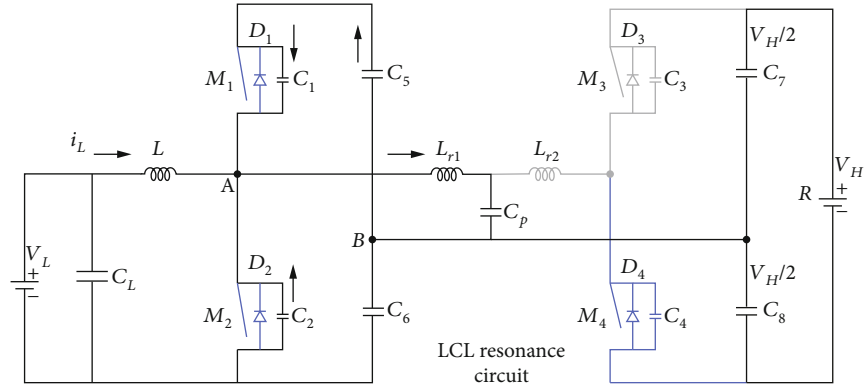


(d)

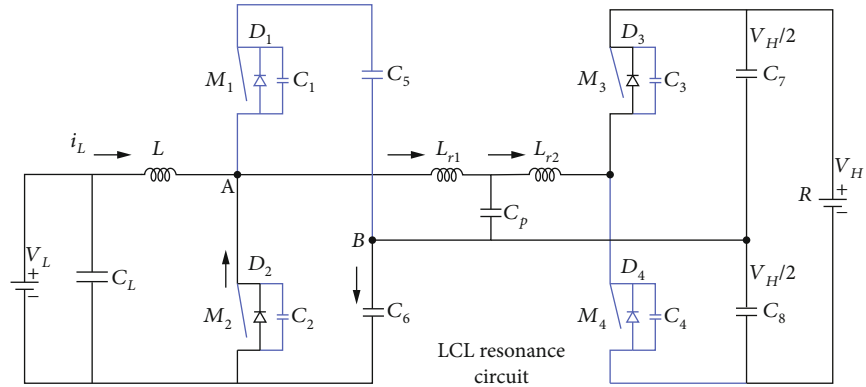
FIGURE 4: Continued.



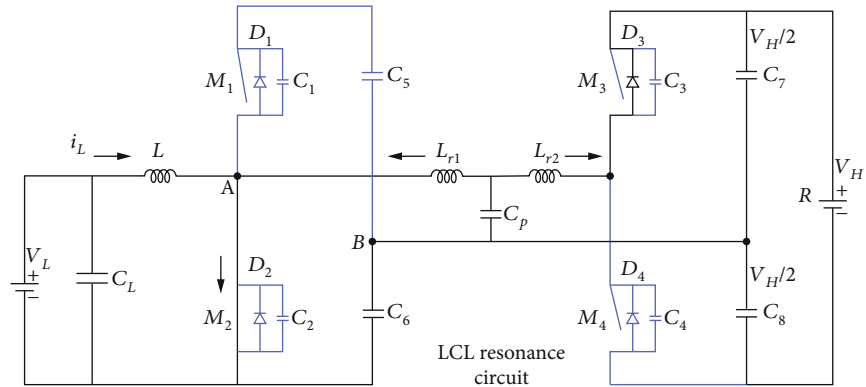
(e)



(f)



(g)



(h)

FIGURE 4: Equivalent circuits during different intervals of operation of the proposed converter in boost operation.

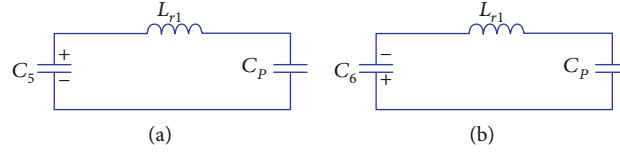


FIGURE 5: Equivalent circuit for resonant operation in (a) interval 3 and (b) interval 7.

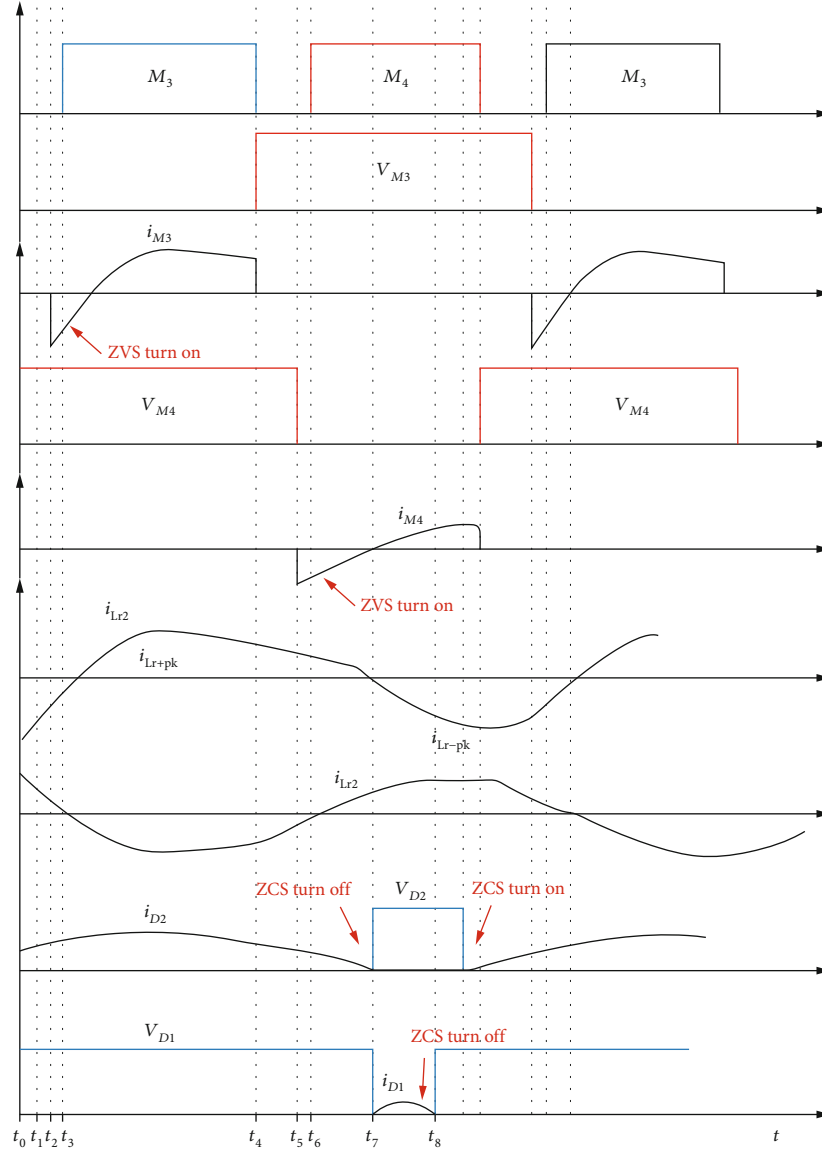


FIGURE 6: Voltage and current waveforms of the components. The converter is used to step down the output voltage compared to the input voltage.

mode is depicted in Figure 4(g). Diode  $D_4$  is reverse-biased while  $D_3$  conducts. Final values are  $i_{M_1}(t_7) = 0$ ,  $i_{M_2}(t_7) = 0$ ,  $v_{M_1}(t_7) = 0$ , and  $v_{M_2}(t_7) = V_{in}/1 - D$ .

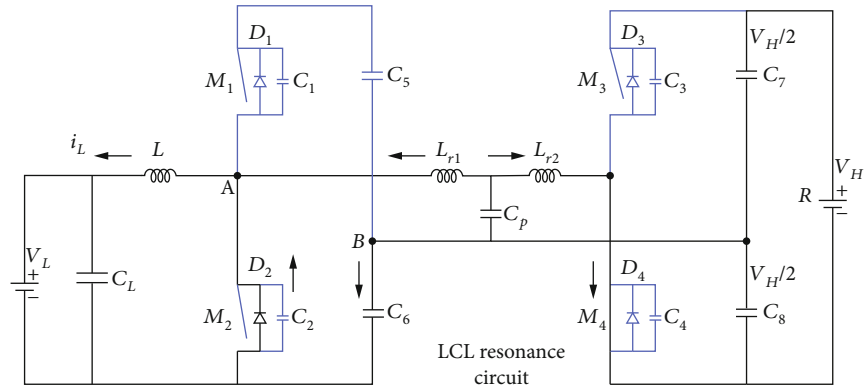
$$i_{D_2}(t_7) = i_L(t_7) - i_{L_{r1}}(t_7). \quad (8)$$

Mode 8 [ $t_7 < t < t_8$ ]: At  $t = t_7$ , switch  $M_2$  conducts with ZVS. Resonant inductor  $L_r$ , capacitor  $C_p$ , and  $C_4$  resonate

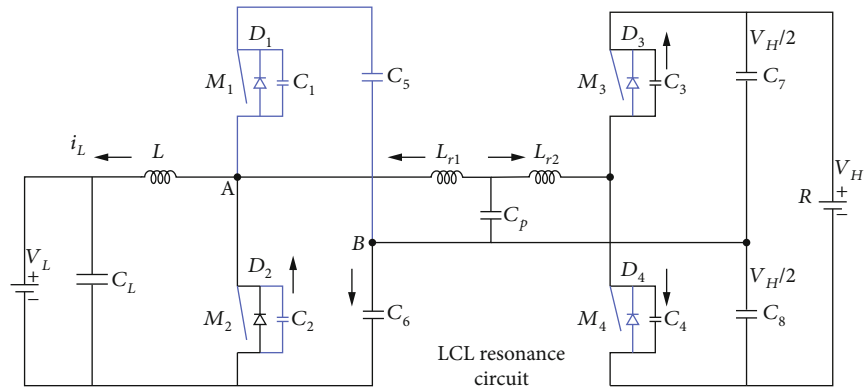
together as shown in Figure 5(b). Working of the converter during this mode is depicted in Figure 4(h). Before the next interval  $t = t_8$ , body diode  $D_3$  turns off with ZCS. The current through  $L_r$  is given by the following:

$$i_{L_{r1}} = -\frac{v_{C_6}(t_7) + v_{C_p}(t_7)}{Z_r} \sin w_r(t - t_7), \quad (9)$$

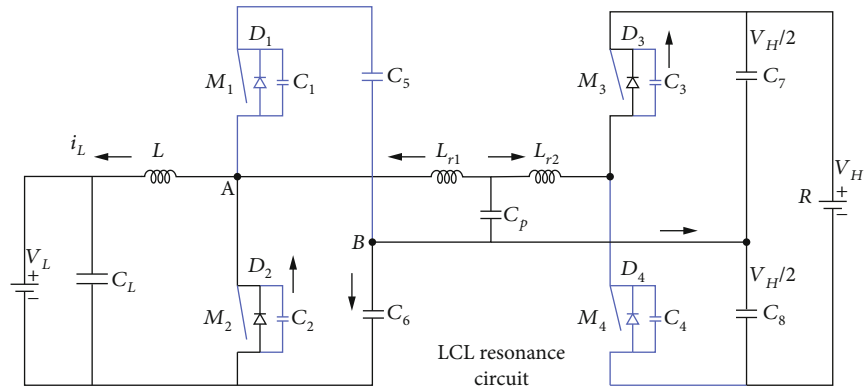
for  $C_5 = C_6$ .



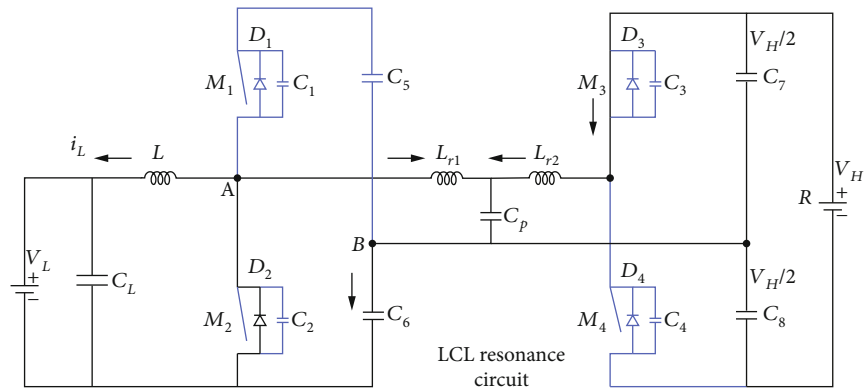
(a)



(b)

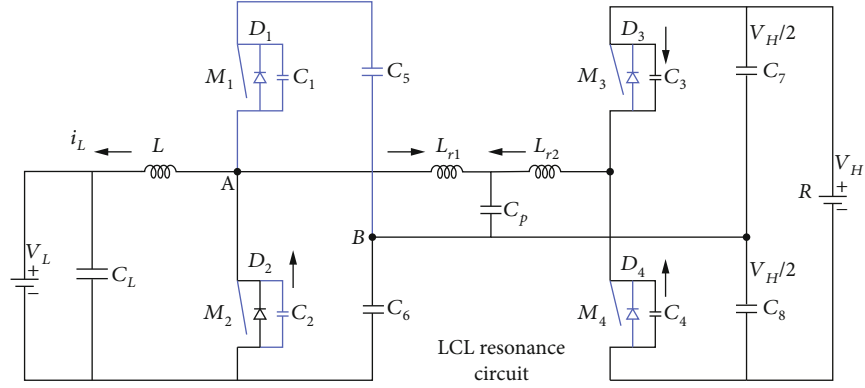


(c)

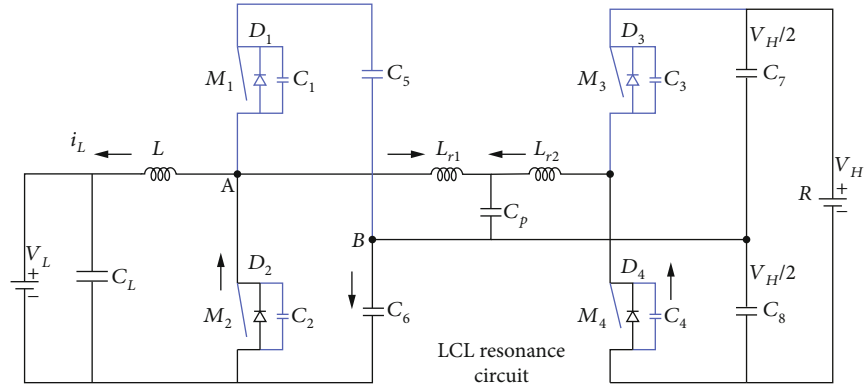


(d)

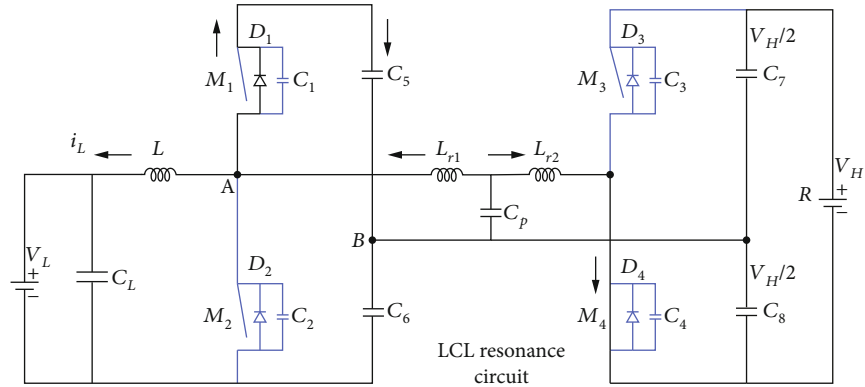
FIGURE 7: Continued.



(e)



(f)



(g)

FIGURE 7: Equivalent circuits during different intervals of buck operation.

TABLE 1: List of the components used in the system.

Sl. No.	Component	Specification
1	MOSFET	200 V, 30 A
2	Inductor	101 mH, 20 A
3	Capacitor	100 $\mu$ F, 500 V
4	Diode	20 A
5	Coupled inductor	100 mH, 20 A

Here, characteristic impedance  $Z_r$  is offered by the circuit formed by  $L_{r1}$ ,  $C_p$ , and capacitor  $C_6$  as shown in Figure 5(b).  $i_L$  is given by the following:

$$i_L(t) = i_L(t_7) + \frac{V_L}{L}(t - t_7). \quad (10)$$

$i_{M_2}$  is given by the following:

$$i_{M_2} = i_L(t - t_7) - i_{L_{r1}}(t - t_7). \quad (11)$$



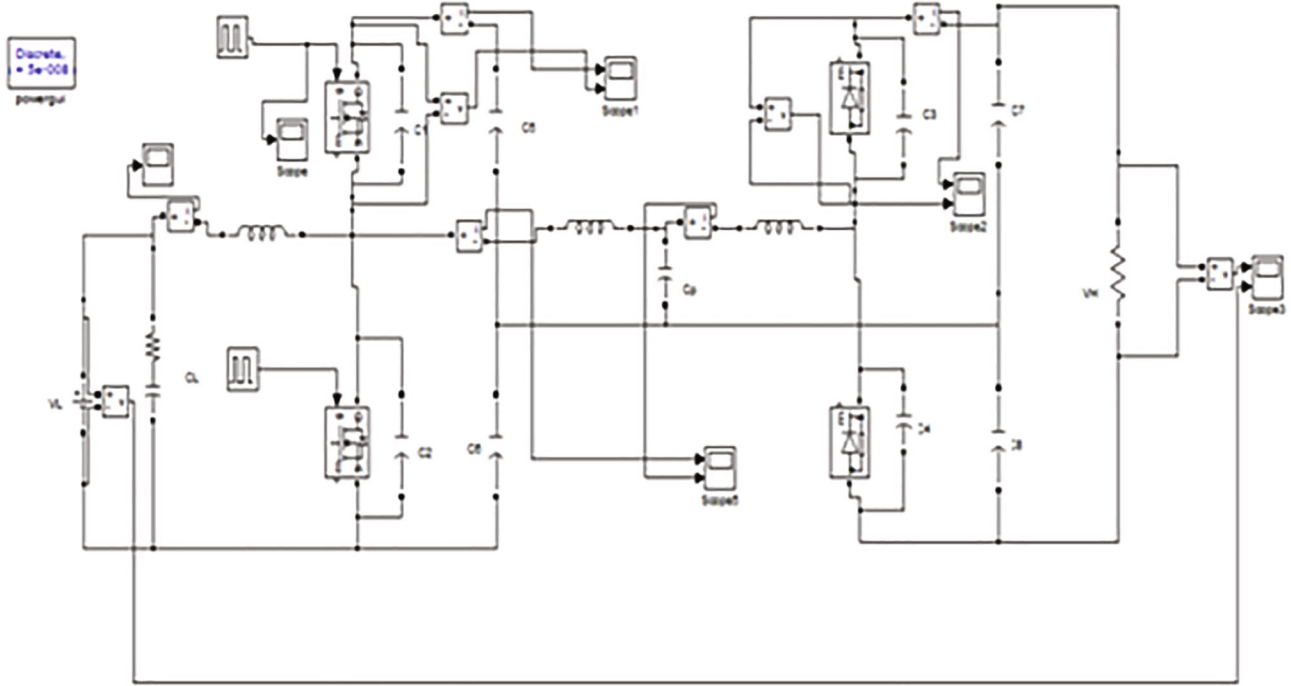


FIGURE 8: Simulation model of proposed DC-DC converter in boost mode.

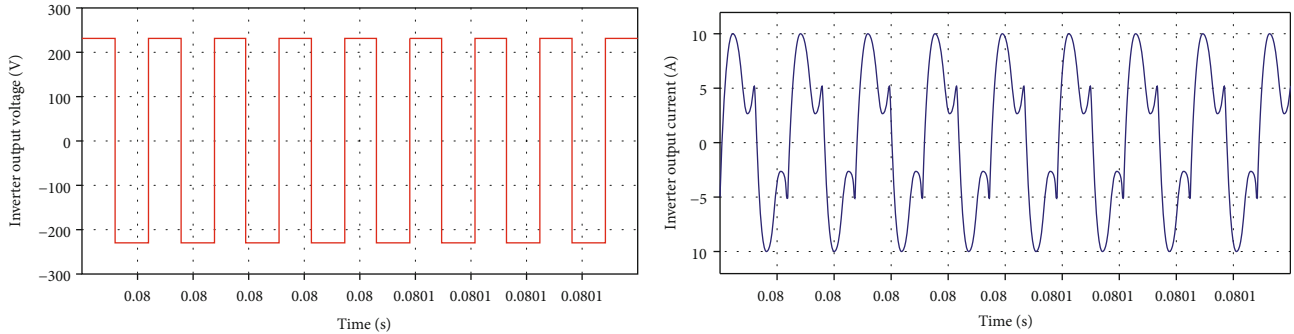


FIGURE 9: Voltage and current waveforms of inverter.

Then, the next half cycle repeats in order to complete the full cycle.

**2.1.1. Converter Behavior while Decreasing the Output Voltage Compared to the Input Voltage.** The converter waveforms and the current flow during different intervals of operation for the buck mode are shown in Figures 6 and 7, respectively.  $M_1$  and  $M_2$  are not triggered for the entire buck operation.

Interval 1  $[t_0 < t < t_1]$ : It is identical to buck or voltage-fed operation. Current through switch  $M_4$  flows and power flows to low voltage side through the resonant circuit and body diode  $D_2$ . Resonant current flows in the circuit.

Interval 2  $[t_1 < t < t_2]$ : At  $t = t_1$ , switch  $M_4$  is turned off. Parasitic capacitances  $C_3$  and  $C_4$  start charging and discharging, respectively, by resonant current  $i_{Lr_2}$ . At the end of this interval,  $C_3$  and  $C_4$  are fully discharged and charged (to  $V_H$ ),

respectively. This is a quick and short interval. Current  $i_{Lr_1}$  is given by the following:

$$i_{Lr_1}(t) = \frac{v_{C_5}(t_1) + v_{C_6}(t_1)}{Z_r} \cdot \sin \omega_r(t - t_1), \quad (12)$$

where  $C_5 = C_6$ ;  $i_L$  is given by the following:

$$i_L(t) = i_L(t_1) - \frac{V_L}{L}(t - t_1). \quad (13)$$

$i_{D_2}$  is given by the following:

$$i_{D_2}(t - t_1) = i_{Lr_1}(t - t_1) - i_L(t - t_1). \quad (14)$$

Final values are  $i_{M_3}(t_2) = 0$ ,  $i_{M_4}(t_2) = 0$ ,  $v_{M_3}(t_2) = V_H$ , and  $v_{M_4}(t_2) = 0$ .

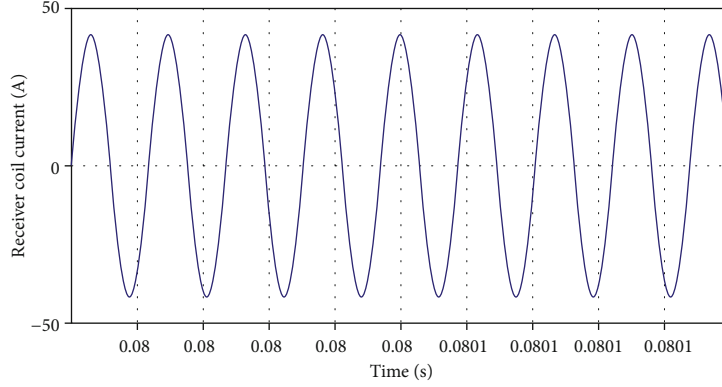


FIGURE 10: Currents of resonant inductors.

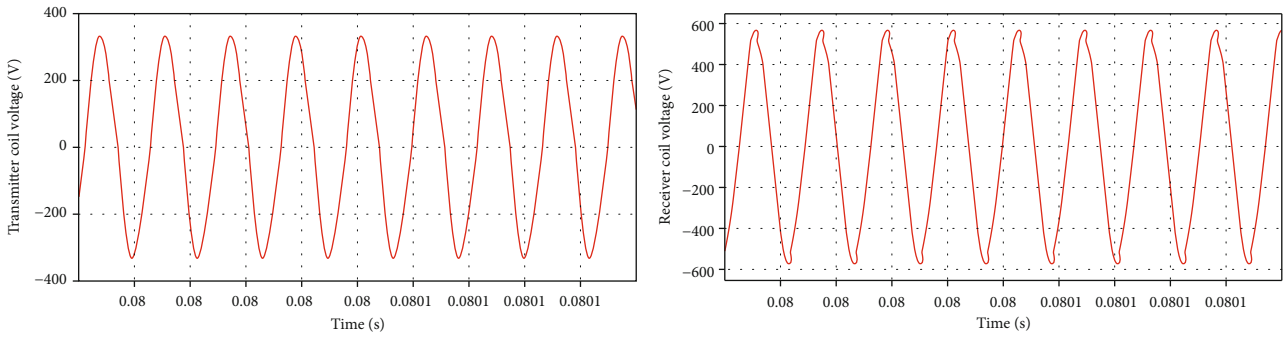


FIGURE 11: The output voltage and input voltage of transmitter, receiver coil.

Interval 3 [ $t_2 < t < t_3$ ]: The resonant inductor current  $i_{L_{r2}}$  flows through the diode  $D_3$ , which results voltage across switch  $M_3$  to 0 and it results for ZVS turn-on.  $i_{L_{r2}}$  is given by the following:

$$i_{L_{r2}} = \frac{v_{C_p}(t_2) + 0.5V_H}{Z_{rb}} \cdot \sin \omega_{rb}(t - t_2), \quad (15)$$

where current  $i_{D_3}$  is given by the following:

$$i_{D_3}(t) = i_{L_{r2}}(t). \quad (16)$$

Final values are  $i_{M_3}(t_3) = 0$ ,  $i_{M_4}(t_3) = 0$ ,  $v_{M_3}(t_3) = 0$ , and  $v_{M_4}(t_3) = V_H$ .

Interval 4 [ $t_3 < t < t_4$ ]: At  $t = t_3$ , switch  $M_3$  turns on. Voltage  $V_H/2$  is applied across resonant circuit through switch  $M_3$ . Resonant inductor  $L_{r2}$  and capacitor  $C_p$  resonate with capacitor  $C_7$ . This interval ends at  $t = t_4$  when switch  $M_3$  is turned off.

Interval 5 [ $t_4 < t < t_5$ ]: In this interval, both the switches  $M_3$  and  $M_4$  are off. Parasitic capacitances  $C_4$  and  $C_3$  start discharging and charging, respectively, by resonant current  $i_{L_{r2}}$ . At  $t = t_5$ ,  $C_4$  is discharged completely and  $C_3$  is fully charged to  $V_H$ . Final values are  $i_{M_3}(t_5) = i_{M_4}(t_5) = 0$ ,  $v_{M_3}(t_5) = V_H$ , and  $v_{M_4}(t_5) = 0$ .

Interval 6 [ $t_5 < t < t_6$ ]: Antiparallel diode  $D_4$  starts conducting, and  $M_4$  is used for ZVS turn-on. Before next inter-

val, antiparallel diode  $D_2$  turns off with ZCS.  $i_{L_{r2}}$  is given by the following:

$$i_{L_{r2}}(t) = \frac{v_{C_p}(t_5) + 0.5V_H}{Z_{rb}} \cdot \sin \omega_{rb}(t - t_5), \quad (17)$$

where current through antiparallel diode  $D_3$  is given by the following:

$$i_{D_4} = i_{L_{r2}}. \quad (18)$$

Final values are  $i_{M_3}(t_6) = i_{M_4}(t_6) = 0$ ,  $v_{M_4}(t_6) = 0$ , and  $v_{M_3}(t_6) = V_H$ .

Interval 7 [ $t_6 < t < t_7$ ]: At  $t = t_6$ , switch  $M_4$  turns on with ZVS. Therefore,  $i_{L_{r2}}$  flows through switch  $M_4$ . Diode  $D_1$  is forward biased and starts charging capacitor  $C_5$ . At  $t = t_7$ , diode  $D_1$  turns off with ZCS.

Then, the next half cycle starts with the same operation cycle in order to complete the other half cycle.

### 3. Voltage Gain and Soft-Switching Conditions

#### 3.1. Voltage Gain

- (1) Boost mode: The converter operates in three stages that contribute to the voltage gain of the system:
  - (1) front-end boost converter gain =  $V_{in}/(1-D)$ ,
  - (2) resonant circuit gain, and
  - (3) voltage doubler

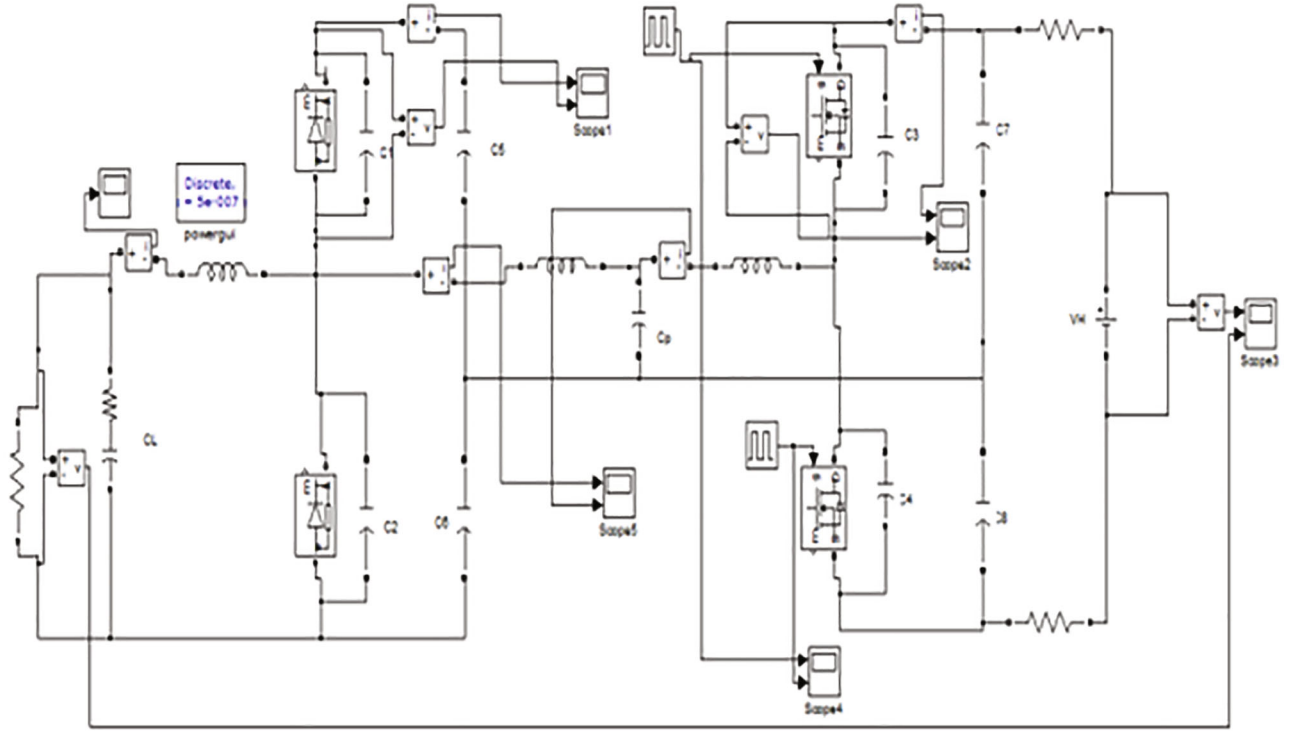


FIGURE 12: Simulation model of the proposed DC-DC converter in buck mode.

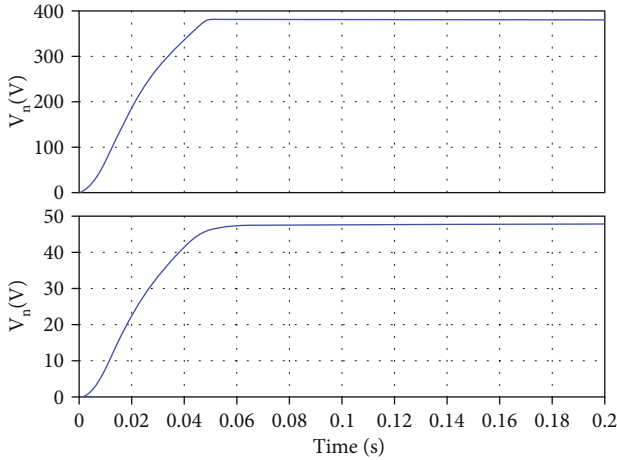


FIGURE 13: Output voltage and input voltage of boost mode.

gain =  $2 \times$ . The overall converter gain is the multiplication of the gains offered by the individual circuits and is given by the following:

$$V_H = \frac{V_L \cdot G_{\text{boost}} \cdot 2}{1 - D}, \quad (19)$$

where  $D$  is the duty cycle,  $f_s$  is the switching frequency, and  $R_{\text{ac}}$  is effective ac load resistance and is given by  $R_{\text{ac}} = X_{C_p}, X_{L_{r_1}}, X_{L_{r_2}}, X_{C_6}$  which are reactances of  $C_p, L_{r_1}, L_{r_2}$ , and  $C_6$ , respectively. It is straightforward to derive using standard complex ac analysis.

(2) Buck mode: In the buck mode,  $V_H/2$  is applied across the coupling circuit due to the half-bridge inverter capacitors. The step down ratio is given by the following:

$$V_L = \frac{1}{2} V_H \cdot D_{\text{Buck}} G_{\text{Boost}}. \quad (20)$$

3.2. ZVS Conditions. Power stored in inductor  $L_{r_1}$  at  $t = t_1$  must be bigger than the power stored in system capacitance of switches  $M_1$  and  $M_2$  to facilitate ZVS of  $M_1$ .

$$\frac{1}{2} L_{r_1} I_{L_{\text{avg}}}^2 - \frac{1}{2} L_{r_1} i_{r_1}^2(t_1) > \frac{1}{2} (C_1 + C_2) \left( \frac{V_{\text{in}}}{1 - D} \right). \quad (21)$$

The variance between the power stored in the inductor  $L_{r_1}$  and the power stored in the inductor  $L$  must be adequate to charge and discharge system capacitances  $C_1$  and  $C_2$  as shown as follows:

$$\frac{1}{2} L_{r_1} I_{L_{\text{avg}}}^2 - \frac{1}{2} L_{r_1} i_{r_1}^2(t_5) > \frac{1}{2} (C_1 + C_2) \left( \frac{V_{\text{in}}}{1 - D} \right)^2. \quad (22)$$

In order to adjust the motor speed to the required set point, a controller is used. An error signal is produced to adjust the speed generated by the difference of real motor speed with the reference speed, which facilitates the closed loop control of the motor. The error signal's magnitude and polarity are directly proportional to the real and

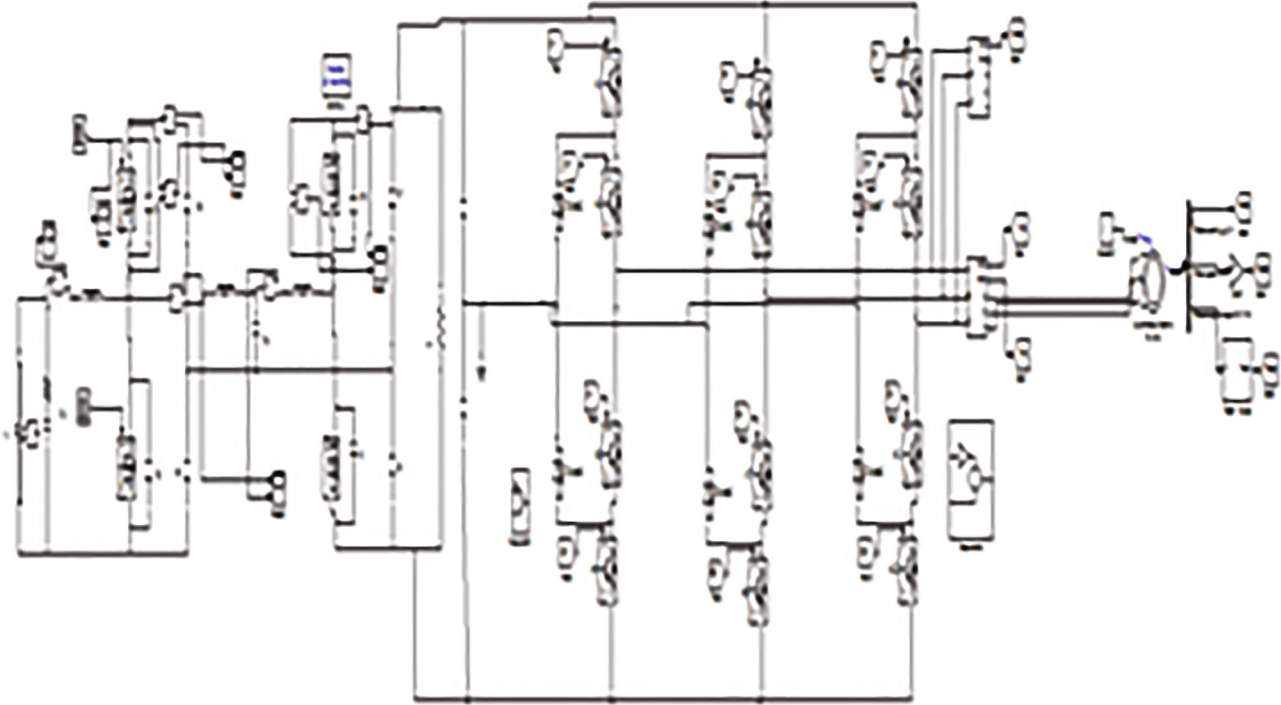


FIGURE 14: Simulation model of proposed DC-DC converter in boost mode with induction motor drive.

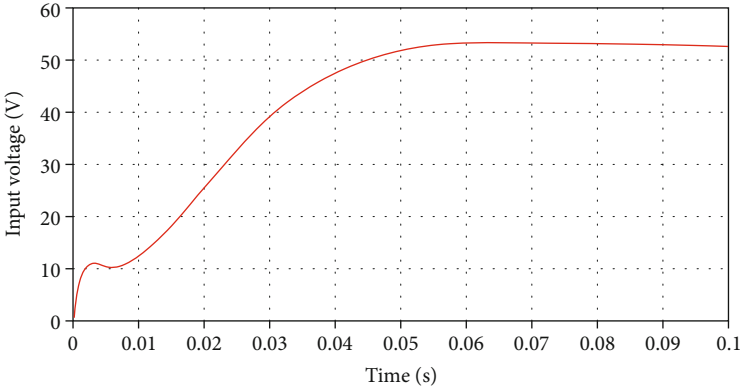


FIGURE 15: Performance of load voltage.

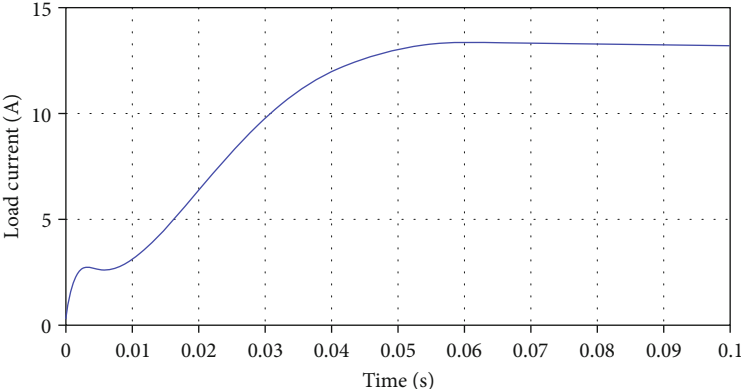


FIGURE 16: Performance of load current.

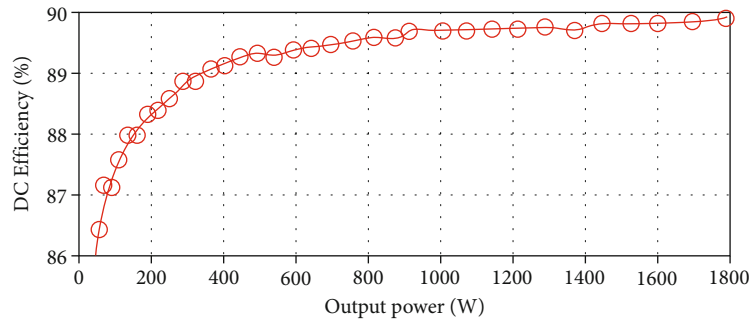


FIGURE 17: Measured output power and efficiency property.

necessary speed change. The PI controller is in charge of generating the data.

#### 4. Simulation Analysis of the Proposed System

Simulation analysis of the proposed system is described in this section. MATLAB software is used in order to carry the simulation of the system. The components used in order to carry out the simulation are listed in Table 1. The simulation model of the proposed system is depicted in Figure 8. Voltage and current waveform at the output terminal of the inverter is depicted in Figure 9.

Waveform of the current passing through the resonant inverter is shown in Figure 10. Voltage across the transmitter coil and receiver coils used in order to transfer power wirelessly is depicted in Figures 11 and 12, respectively.

Simulation model of the proposed system in buck mode is depicted in Figure 12. Output and input voltage waveform of the converter in boost mode is shown in Figure 13.

In boost mode, induction motor drive is used as the load in the proposed system. Simulation model of the system in boost mode is shown in Figure 14. Waveforms of the load current and load voltage during this mode are depicted in Figures 15 and 16, respectively.

The output power of the system is varied and it is compared to the efficiency of the overall system. The comparison is plotted as shown in Figure 17. It is observed that, in this proposed system, when the output power of 400 W is achieved, the efficiency of the system corresponds to 89%.

#### 5. Future Extension of the Proposed System

- (i) The converter can be redesigned in order to reduce power conversion stages
- (ii) Capacitive power transfer technique can be followed in the improved system in order to reduce manufacturing loss and complexity of the system
- (iii) New wireless power techniques can be developed in order to increase the power transfer distance and efficiency of the system
- (iv) New controller and cooling techniques can be developed in order to reduce overall system losses

#### 6. Conclusion

This paper explains the design and analysis of a nonisolated bidirectional soft-switching current-fed resonant DC/DC converter. The converter is able to achieve high step up/step down ratio, high efficiency, and the low voltage across the components used to manufacture the converter. ZCS and ZVS turn-on of the system is achieved, which is a great achievement of the proposed converter compared to the existing topologies. The output voltage of the converter is clamped without the use of any snubber circuit. The proposed system is linked to an induction motor drive, and the drive's output is controlled. The simulation analysis of the proposed converter resembles the theoretical explanation of the system proving the efficacy of the WPT system.

#### Abbreviations

AC:	Alternating current
DC:	Direct current
WPT:	Wireless power transfer
MOSFET:	Metal oxide semiconductor field effect transistor
MPT:	Microwave power transfer
IPT:	Inductive power transfer
ICPT:	Inductively coupled power transfer
EV:	Electric vehicle
ZVS:	Zero voltage switching
ZCS:	Zero current switching.

#### Data Availability

The available data will be distributed to readers based on the request.

#### Conflicts of Interest

The authors declare that they have no conflicts of interest.

#### References

- [1] G. A. Covic and J. T. Boys, "Inductive power transfer," *Proceedings of the IEEE*, vol. 101, no. 6, pp. 1276–1289, 2013.
- [2] A. Kurs, A. Karalis, R. Moffatt, J. D. Joannopoulos, P. Fisher, and M. Soljacic, "Wireless power transfer via strongly coupled magnetic resonances," *Science*, vol. 317, no. 5834, pp. 83–86, 2007.



- [3] F. Musavi and W. Eberle, "Overview of wireless power transfer technologies for electric vehicle battery charging," *IET Power Electronics*, vol. 7, no. 1, pp. 60–66, 2014.
- [4] A. Khaligh and S. Dusmez, "Comprehensive topological analysis of conductive and inductive charging solutions for plug-in electric vehicles," *IEEE Transactions on Vehicular Technology*, vol. 61, no. 8, pp. 3475–3489, 2012.
- [5] D. Patil, M. Ditsworth, J. Pacheco, and W. Cai, "A magnetically enhanced wireless power transfer system for compensation of misalignment in mobile charging platforms," in *2015 IEEE Energy Conversion Congress and Exposition (ECCE)*, pp. 1286–1293, Montreal, QC, Canada, 2015.
- [6] C. J. Kaufman, *Private Communication*, Rocky Mountain Research Lab., Boulder, CO, 1995.
- [7] Y. Yorozu, M. Hirano, K. Oka, and Y. Tagawa, "Electron spectroscopy studies on magneto-optical media and plastic substrate interface," *IEEE Translation Journal on Magnetism in Japan*, vol. 2, no. 8, pp. 740–741, 1987.
- [8] K. Aditya and S. Williamson, "A review of optimal conditions for achieving maximum power output and maximum efficiency for a series-series resonant inductive link," *IEEE Transactions on Transportation Electrification*, vol. 3, no. 2, pp. 303–311, 2017.
- [9] D. Patil, M. Sirico, G. Lei et al., "Maximum efficiency tracking in wireless power transfer for battery charger: phase shift and frequency control," in *2016 IEEE Energy Conversion Congress and Exposition (ECCE)*, Milwaukee, WI, USA, 2016.
- [10] B. Mangu and B. G. Fernandes, "Multi-input transformer coupled DC-DC converter for PV-wind based stand-alone single phase power generating system," in *2014 IEEE Energy Conversion Congress and Exposition (ECCE)*, Pennsylvania, USA, 2014.
- [11] Susheela and P. S. Kumar, "Analysis and comparison of various pulse width modulation strategies for hybrid inverter with reduced number of components," *International Journal of Inventions in Engineering & Science Technology*, vol. 3, no. 3, pp. 12–26, 2017.
- [12] P. Patra, S. Samanta, A. Patra, and S. Chattopadhyay, "A novel control technique for single-inductor multiple-output DC-DC buck converters," in *2006 IEEE International Conference on Industrial Technology*, Mumbai, India, 2006.
- [13] S. Samanta, A. K. Rathore, and S. K. Sahoo, "Current-fed full-bridge and half-bridge topologies with CCL transmitter and LC receiver tanks for wireless inductive power transfer application," in *2016 IEEE Region 10 Conference (TENCON)*, Singapore, 2016.
- [14] V. Ravikiran, R. K. Keshri, and M. Bertoluzzo, "Efficient wireless charging of batteries with controlled temperature and asymmetrical coil coupling," in *2018 IEEE International Conference on Power Electronics, Drives and Energy Systems (PEDES)*, Chennai, India, 2018.
- [15] P. S. Subudhi, K. Subramanian, and B. B. J. D. Retnam, "Wireless electric vehicle battery-charging system for solar-powered residential applications," *International Journal of Power and Energy Systems*, vol. 39, no. 3, pp. 130–140, 2019.
- [16] P. S. Subudhi and S. Krithiga, "PV and grid interfaced plug-in EV battery charger operating in P-VG, P-V and V-G modes," *International Journal of Recent Technology and Engineering*, vol. 8, no. 2, pp. 3431–3443, 2019.
- [17] P. S. Subudhi and K. S., "Wireless power transfer topologies used for static and dynamic charging of EV battery: a review," *International Journal of Emerging Electric Power Systems*, vol. 21, no. 1, pp. 1–34, 2020.
- [18] C.-T. Truong and S.-J. Choi, "Single-stage duty-controlled half-bridge inverter for compact capacitive power transfer system," *IEEE Access*, vol. 9, pp. 119250–119261, 2021.
- [19] X.-J. Ge, Y. Sun, Z.-H. Wang, and C.-S. Tang, "A single-source switched-capacitor multilevel inverter for magnetic coupling wireless power transfer systems," *Electrical Engineering*, vol. 101, no. 4, pp. 1083–1094, 2019.
- [20] R. A. Sekar and S. Sasipriya, "Implementation of FIR filter using reversible modified carry select adder," *Concurrency and Computation: Practice and Experience*, vol. 31, no. 14, 2019.
- [21] A. Arasan, R. Sadaiyandi, F. al-Turjman, A. S. Rajasekaran, and K. Selvi Karuppuswamy, "Computationally efficient and secure anonymous authentication scheme for cloud users," *Personal and Ubiquitous Computing*, vol. 25, 2021.
- [22] J. Subramani, M. Azees, A. Sekar, and F. Al-Turjman, "Lightweight privacy and confidentiality preserving anonymous authentication scheme for WBANs," *IEEE Transactions on Industrial Informatics*, 2021.
- [23] J. Subramani, A. Maria, R. B. Neelakandan, and A. S. Rajasekaran, "Efficient anonymous authentication scheme for automatic dependent surveillance-broadcast system with batch verification," *IET Communications*, vol. 15, no. 9, pp. 1187–1197, 2021.
- [24] A. Iqbal, A. S. Rajasekaran, G. S. Nikhil, and M. Azees, "A secure and decentralized blockchain based EV energy trading model using smart contract in V2G network," *IEEE Access*, vol. 9, pp. 75761–75777, 2021.
- [25] J. Subramani, T. N. Nguyen, A. Maria, A. S. Rajasekaran, and K. Cengiz, "Lightweight batch authentication and privacy-preserving scheme for online education system," *Computers & Electrical Engineering*, vol. 96, article 107532, 2021.

## Research Article

# An Improved Simulated Annealing Particle Swarm Optimization Algorithm for Path Planning of Mobile Robots Using Mutation Particles

Jianzhang Lu  and Zhihao Zhang 

Chongqing University-University of Cincinnati Joint Co-op Institute, Chongqing University, Chongqing 400000, China

Correspondence should be addressed to Zhihao Zhang; 20186101@cqu.edu.cn

Received 30 September 2021; Revised 3 November 2021; Accepted 6 November 2021; Published 6 December 2021

Academic Editor: Deepak Gupta

Copyright © 2021 Jianzhang Lu and Zhihao Zhang. This is an open access article distributed under the Creative Commons Attribution License, which permits unrestricted use, distribution, and reproduction in any medium, provided the original work is properly cited.

Artificial intelligence technology has brought tremendous changes to human life and production methods. Mobile robots, UAVs, and autonomous driving technology have gradually entered people's daily life. As a typical issue for a mobile robot, the planning of an optimal mobile path is very important, especially in the military and emergency rescue. In order to ensure the efficiency of operation and the accuracy of the path, it is crucial for the robot to find the optimal path quickly and accurately. This paper discusses a new method and MP-SAPSO algorithm for addressing the issue of path planning based on the PSO algorithm by combining particle swarm optimization (PSO) algorithm with the simulated annealing (SA) algorithm and mutation particle and adjusting the parameters. The MP-SAPSO algorithm improves the accuracy of path planning and the efficiency of robot operation. The experiment also demonstrates that the MP-SAPSO algorithm can be used to effectively address path planning issue of mobile robots.

## 1. Introduction

*1.1. The Purpose and Significance of the Research.* As modular and intelligent thinking gradually penetrates into business and traditional manufacturing, the application of cutting-edge technologies has become much more efficient, and a large number of digital and intelligent high-end technology products have entered human daily life with lower cost and higher quality. The mobile robot, the object of this thesis, is a microcosm of this change. Path planning is the key to the autonomous control module of a robot. The path planning problem is an NP-hard problem, which allows the robot to automatically calculate the best path from the start point to the end point in minimum time [1]. To solve the path planning problem, two issues need to be tackled. One is to build an environment model that can simulate the robot's working scenario, and the other is to establish the rules for the robot to search the path in the environment model and find the optimal path for the robot in the envi-

ronment model. In this way, the path planning problem for robots is transformed into a combinatorial optimization problem. The common path planning methods include swarm intelligence algorithm, graph search algorithm, RRT algorithm, Artificial Potential Field algorithm, BUG obstacle avoidance algorithm, and incremental heuristic algorithm. Swarm intelligence algorithm is a popular category in current research, and the more mature algorithms include particle swarm optimization algorithm and ant colony algorithm, although the particle swarm optimization algorithm is relatively simple in implementation. However, compared to other algorithms, there are problems such as premature convergence and more likely to fall into local optimal solutions. To address these shortcomings [2], this paper combines particle swarm optimization algorithm and simulated annealing algorithm, introduces the concept of mutation factor, and proposes a new robot path planning scheme for path planning under a known environment model. Compared with the traditional classical particle swarm

optimization algorithm, this algorithm can effectively avoid premature convergence, improve the efficiency of the algorithm, and provide a new idea for robot path planning.

*1.2. Mobile Robot Path Planning Problem.* According to the different perception degrees of robot to its own environment model, common path planning methods are divided into global path planning with a known environment model and local path planning methods using sensor, SLAM radar, and other technologies. This paper mainly studies the global path planning algorithm under the known environment model. Similar to the research of Katrakazas et al. [3] on path planning for mobile robot, the global path planning for robots should include the following problems:

- (1) How to implement path planning in actual robot tasks

If the path planning strategy violates the hardware structure and dynamics of the robot, the path planning strategy is inaccurate. This can be achieved through personalized modeling of the environment model and personalized adjustment of path planning strategy for different robots.

- (2) How to obtain the optimal solution of path planning

There are many paths from the start point to the end point, but due to the efficiency and power of the robot, it is necessary to find a feasible optimal path.

- (3) How to avoid collision between the robot and obstacles on the planned path

The robot may deal with a variety of situations when performing tasks. Collision with obstacles in the environment will have a certain impact on the robot and surrounding obstacles. Collision will also adversely affect the execution path of the robot, thereby reducing work efficiency.

*1.3. Development Trend of Robot Path Planning Algorithm.* Some works are focused on the path planning to solve the above problems. Figure 1 shows some of the algorithms used in path planning.

The key to building an environment model is to make the state of robot in the environment model consistent with the real environment; the path planning algorithm focuses on optimizing the robot path based on the known environment model. For the second point, robot path planning algorithm has attracted the attention of many experts and scholars. There are also many solutions and achievements in this field. Roberge et al. combine genetic algorithm and particle swarm optimization algorithm to solve the path planning problem of UAV in a complex three-dimensional environment [4]. Mo and Xu proposed a global path planning method, which combines BBO, PSO, and approximate Voronoi boundary network (AVBN) in a static environment [5]. Yu and Rus proposed a centralized algorithm framework to solve the multirobot path planning problem in a general two-dimensional continuous environment [6]. Li et al. developed an effective Improved Artificial Potential Field-

based Simultaneous Forward Search (Improved APF-based SIFORS) method in a known environment [7]. Jiao et al. performed an improved quantum particle swarm optimization algorithm to solve the path planning model [8]. Tharwat et al. proposed a new chaos particle swarm optimization algorithm to optimize the control points of Bezier curve [9]. Li et al. proposed a new adaptive learning mechanism to select the most suitable search strategy adaptively in different stages of the optimization process, which improves the searchability of particle swarm optimization algorithm [7]. Das et al. performed an improved particle swarm optimization (IPSO) algorithm combined with differential disturbance velocity (DV) algorithm to determine the optimal path of multirobot in a clutter environment [10]. Zeng et al. aimed to propose a particle swarm optimization (PSO) algorithm based on nonhomogeneous Markov chain and differential evolution for path planning of intelligent robot when encountering obstacles in the environment [11].

We can see particle swarm optimization has not only strong local searchability but also global exploration ability. Moreover, the proportion of local search and global search can be controlled by adjusting the parameters. Therefore, it is suitable to be used as a path optimization algorithm for mobile robot.

## 2. Establishment and Optimization of the Model

*2.1. Establishment of Environmental Model.* The application problem discussed in this paper needs to simulate the environment with obstacles and give a visual expression of the improved algorithm, so a direct and specific environment model is needed. For the path planning algorithm, the solution is only limited to the two-dimensional plane space of the robot movement, so a two-dimensional space model is established.

*2.1.1. Polygon Obstacle Environment Model.* When the environment model is a two-dimensional space, a polygonal obstacle environment is the clearest and most direct representation of obstacles [12]. The image displayed by this environment model can be regarded as the top view of the two-dimensional obstacle environment in a three-dimensional space (as shown in Figure 2). It can not only clearly display the state of the obstacle environment and facilitate the adjustment of the obstacle environment but also prepare for the optimization path of the visualization algorithm.

*2.1.2. Improvement of Polygon Obstacle Environment Model.* In the actual process of robot movement, due to the limitation of its own mechanical structure, the robot cannot fully adapt to the movement of the edges and corners of obstacles. Therefore, considering the protection of the robot itself and the needs of practical application, the polygon obstacles were regarded as a noncontact space containing multiangle obstacles in the environment model, and it is stated that as long as the mobile body does not enter the space, it is regarded as effective movement and can be realized in the path; The noncontact space is built following the principle of

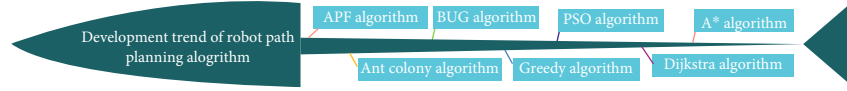


FIGURE 1: The development of path planning algorithm.

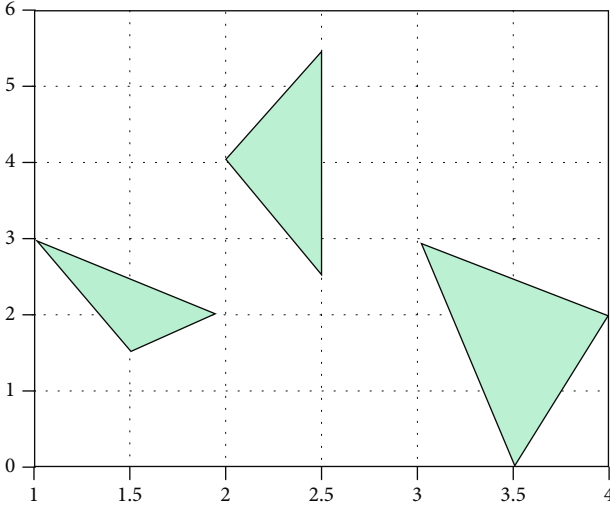


FIGURE 2: Polygon obstacle environment.

minimum enclosing circle, and the space of the obstacle is defined as the minimum circular space that can completely cover the obstacle. To find the minimum enclosing circle, we need to get the vertices of the obstacle and form the point set  $P$ . By iterating in  $P$ , we can find three vertices, so as to determine a minimum circle that completely covers all the vertices of the obstacle. Let these three points be  $p_1(x_1, y_1)$ ,  $p_2(x_2, y_2)$ , and  $p_3(x_3, y_3)$ . Then, the midpoint of the line  $l_1$  with  $p_1(x_1, y_1)$ ,  $p_2(x_2, y_2)$  is

$$(x_{\text{mid}}, y_{\text{mid}}) = \left( \frac{x_1 + x_2}{2}, \frac{y_1 + y_2}{2} \right). \quad (1)$$

The equation of the vertical line  $l_1$  is  $A_1x + B_1y = C_1$ , where

$$\begin{aligned} A_1 &= -B = x_2 - x_1, \\ B_1 &= A = y_2 - y_1, \end{aligned} \quad (2)$$

$$C_1 = -B * x_{\text{mid}} + A * y_{\text{mid}} = \frac{(x_2^2 - x_1^2) + (y_2^2 - y_1^2)}{2}.$$

Two midperpendicular lines are obtained using the above-mentioned method, and their intersection point is the center of the minimum enclosing circle, and the noncontact space that completely covers the obstacle can be obtained, as shown in Figure 3.

If the result of the robot entering the obstacle space occurs in the loop iteration of the algorithm, the violation is output and marked with “\*” as shown in Figure 4.

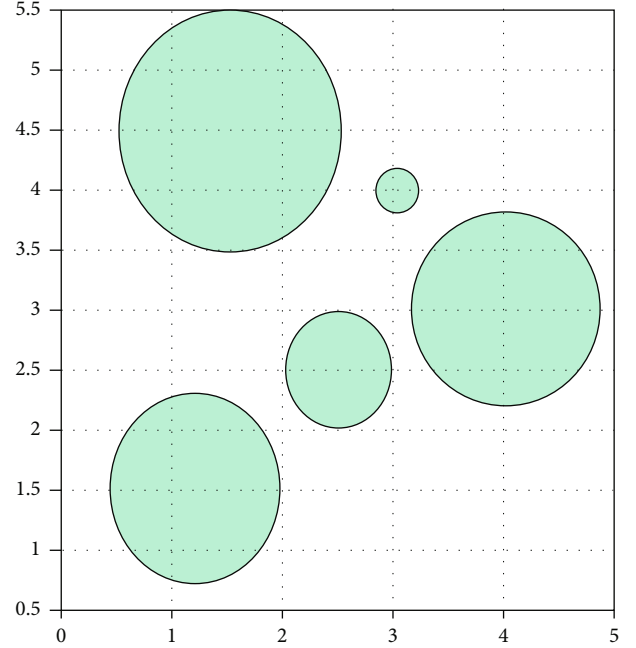


FIGURE 3: Improvement of multilateral obstacle model.

## 2.2. Basic Particle Swarm Optimization Algorithm

**2.2.1. Overview of Particle Swarm Optimization Algorithm.** Particle swarm optimization (PSO, hereinafter referred to as “PSO”) is a kind of evolutionary computing technology, which affects the simple behavior of individuals through the sharing of information among individuals in the group. It simulates the evolution process of the group from disorder to order in the space via iteration and obtains the optimal solution. By controlling the inertia parameter, acceleration parameter, and fitness algorithm, the group behavior can be influenced and converged to the desired direction. On the premise that the computing platform supports large-scale parallel computing, particle swarm optimization has higher efficiency and faster computing speed. Compared with other evolutionary algorithms, particle swarm optimization has the advantages of high accuracy, fewer iterations, and rapid convergence. It is a mature and feasible solution to apply particle swarm optimization algorithm to the path planning of robots.

**2.2.2. Equations of the Basic Particle Swarm Optimization Algorithm.** The core of particle swarm optimization algorithm lies in two equations velocity update equation and position update equation. In each iteration, each particle updates its position and velocity according to the velocity update equation and the position update equation and

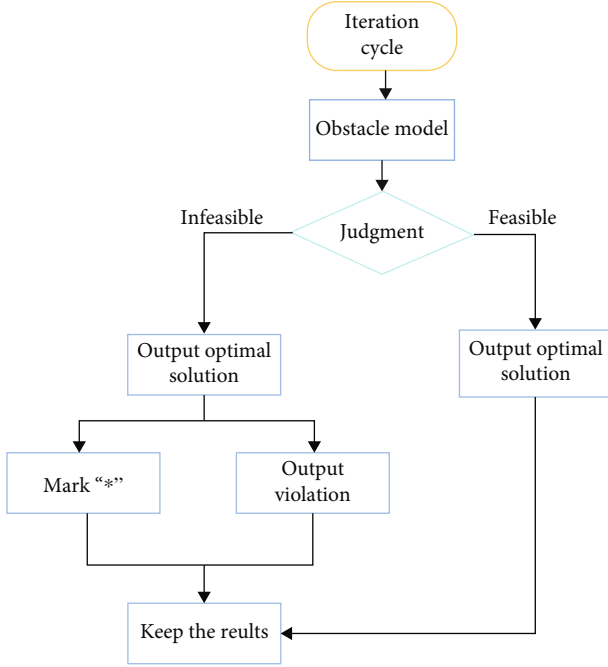


FIGURE 4: Flow chart of space violation judgment.

updates the individual optimal solution and the global optimal solution. Through several iterations, the particle swarm in the solution space converges to the optimal solution and finally converges to the optimal solution.

Velocity update equation

$$v_i = \omega \times v_i + c_1 \times \text{rand}() \times (\text{pbest}_i - x_i) + c_2 \times \text{rand}() \times (\text{gbest}_i - x_i). \quad (3)$$

Location update equation

$$x_i = x_i + v_i. \quad (4)$$

In the equations,  $v_i$  is the velocity of the particles,  $\omega$  is the weighted inertia, and  $x_i$  is the location for the particles.  $\text{pbest}_i$  is the local optimal solution.  $\text{gbest}_i$  is the global optimal solution.  $\text{rand}()$  is a random number between 0 and 1, and  $c_1$  and  $c_2$  are learning factors. Usually,  $c_1 = c_2 = 2$ .

**2.2.3. Defects of Basic Particle Swarm Optimization Algorithm.** The basic particle swarm optimization algorithm has the advantages of fast convergence speed, few adjustment parameters, and simple implementation. The speed displacement model and the small amount of calculation have attracted the attention of many researchers. However, with more and more research, researchers have gradually found the defects of particle swarm optimization algorithm. The defects of particle swarm optimization are mainly manifested in two aspects: (1) the accuracy of particle swarm optimization is not high. Since the PSO only uses the global optimal solution and local optimal solution in each iteration, it does not use all the information of each iteration. Therefore, even if the convergence speed of PSO is fast, it is diffi-

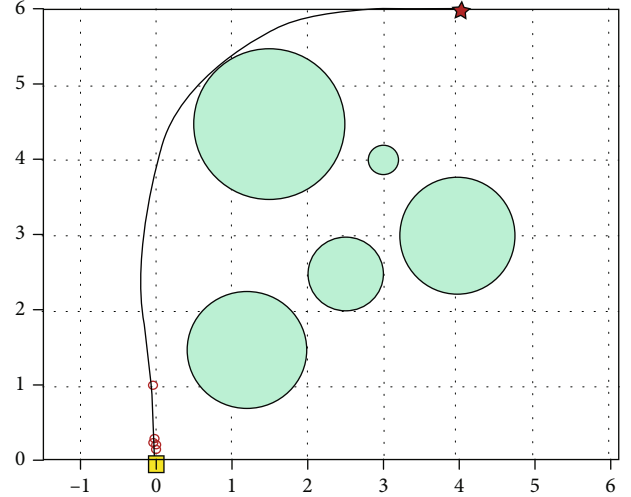


FIGURE 5: PSO path planning result.

cult to guarantee the accuracy of the algorithm. (2) Local optimization, premature convergence, and the inability to find the global optimal solution are likely to occur in the search process of particle swarm optimization. This may be because the particle swarm optimization algorithm cannot get a complete proof of convergence in theory [13]. For more complex multimodel function optimization, the global optimal solution may not be obtained; in addition, if the parameter selection is wrong, particles quickly lose diversity, and the global optimal solution cannot be obtained.

In order to solve these problems, Zhou et al. proposed an improved adaptive PSO algorithm, where the Bezier curve was incorporated and larger control parameters were used to improve the smoothness and efficiency of path planning [14]. The adaptive particle swarm optimization algorithm based on simulated annealing (SAPSO) proposed by Yan et al. has also achieved good results [15].

However, the current PSO algorithm still has the problems of slow convergence and is easy to fall into local optimal solution, so its application in robot path planning is not ideal.

For example, the particle swarm algorithm is applied to the optimized environment model, and the following results are obtained (Figure 5):

It can be seen that the path planning result is not ideal, obviously not the optimal path, and even if the number of iterations is increased, the result will not be significantly improved.

In order to solve the above problems, this paper puts forward the following improvements in the algorithm and its practical application: firstly, by incorporating the concept of mutation factor in simulated annealing algorithm and genetic algorithm, on the improvement of parameters, the paper tries to deal with the linear differential decreasing of weighted inertia, optimize the convergence factor and acceleration factor, and make a comparison. A Simulated Annealing Particle Swarm Optimization Algorithm with Mutation Particles (MP-SAPSO) was proposed in the paper, and Figure 6 illustrates the basic flow of the MP-SAPSO.



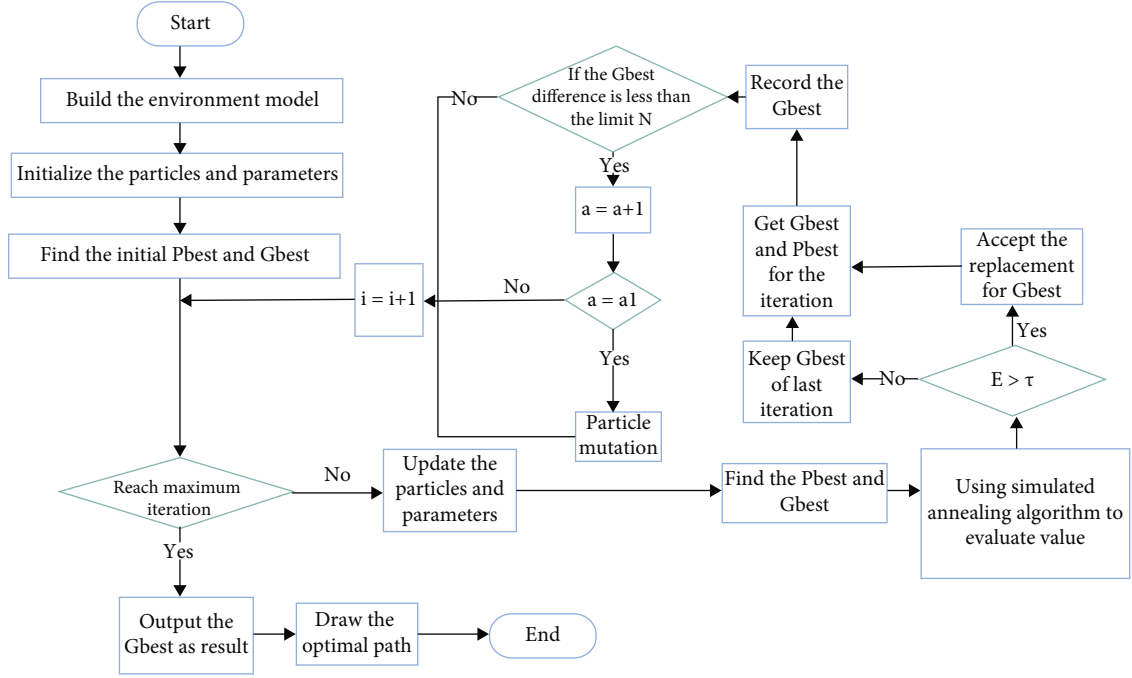


FIGURE 6: MP-SAPSO flow chart.

2.3. *Improvement and Optimization of PSO Algorithm (Simulated Annealing Particle Swarm Optimization Algorithm with Mutation Particles)*. Aiming at the shortcomings of premature convergence of traditional particle swarm optimization, this paper incorporates the concept of population mutation factor in simulated annealing algorithm (SA) and genetic algorithm [16], assembles the optimization for adaptive annealing particle swarm optimization algorithm, and adjusts the original parameters and application parameters in order to apply to the actual path planning application. The following will be divided into two parts, algorithm and parameters, to introduce the kernel logic.

### 2.3.1. For the Optimization of the Algorithm

(1) *The Combination of Simulated Annealing (SA) and Particle Swarm Optimization (PSO)*. Simulated annealing algorithm (SA) is one of the best algorithms for solving the local optimal solution in deep learning [17]. The algorithm is derived from the crystal cooling process. If the temperature drops too fast, an amorphous with high energy will be produced, and if the temperature drops slowly, regular crystals with high density and low energy will be formed. Combined with the actual results of the algorithm, the noncrystal corresponds to the local optimal solution, and the regular crystal corresponds to the global optimal solution.

In simulated annealing, the process of applying energy to the amorphous to form crystal can be understood as jumping out of the local optimal solution and then continuing to search. The Metropolis algorithm, which is used to accept the new state by probability instead of using the standard rules, is a great choice for the local optimal solution in particle swarm optimization [18].

In each iteration of PSO, the value of each particle is evaluated, and the best choice  $\alpha$  of each particle in the group is recorded, which will be compared with the global optimal particle  $\beta$  recorded at this time. If it is better than  $\beta$ , it is replaced and the next iteration is carried out. For this optimization method, we choose to add probability. For each particle  $I$  in the  $n$ th iteration, it has the optimal solution substitution expectation  $E$  and the substitution tolerance  $\tau$ , where

$$E = e^{-(\alpha(i) - \beta(i)) / \alpha(i)},$$

$$\tau = \text{rand}() \times \frac{n_{\max} - n}{n_{\max}}, \quad (5)$$

random rational numbers with  $\text{rand}()$  being (0,1).

If  $E > \tau$ , the replacement of the particle optimal solution is accepted, otherwise it is rejected.

The convergence trend after optimization is shown in Figures 7 and 8.

It can be seen from the curve that the introduction of “annealing” probability can effectively reduce the number and time of searching for the local optimal solution, and at the same time, it can quickly jump out of the local optimal solution.

(2) *The Embodiment of Population Variation in PSO*. Although SA algorithm can reduce the time and times of falling into the local optimal solution, it cannot change the trend of large-scale particles gathering in the local optimal solution. Therefore, the premature convergence characteristic of the particle swarm algorithm cannot be fundamentally changed solely from the probability.

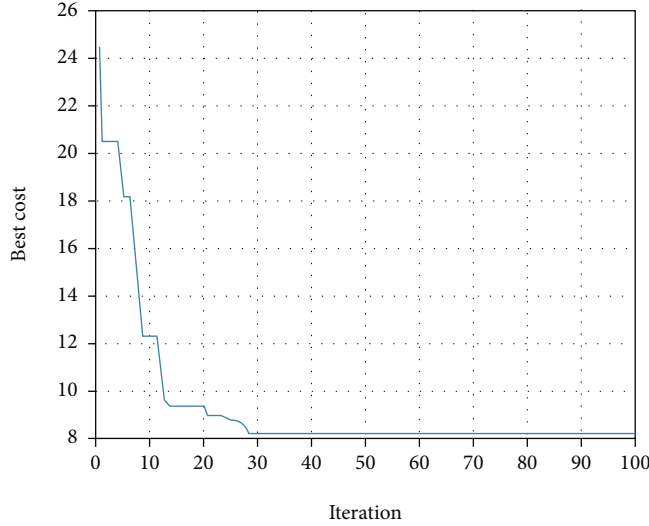


FIGURE 7: Convergence curve of traditional particle swarm optimization.

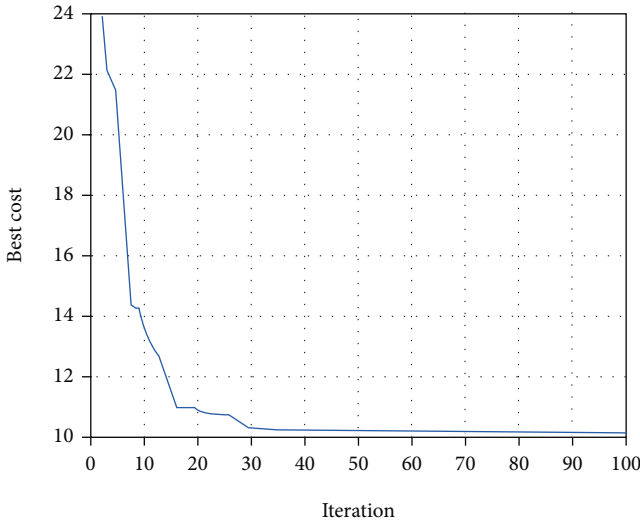


FIGURE 8: Convergence curve after SA optimization.

Considering that particle swarm optimization is also a branch of swarm intelligence, it can also be applied to the treatment of swarm intelligence. So we think of the classic genetic algorithm. The algorithm processing process of genetic algorithm is shown in Figure 9.

Since a single particle does not have many characteristics of chromosome, it consumes too much computational power for calculation, which deviates from the application. So we only use the mutation module to optimize the population [19]. When the state difference between the  $n$ th iteration and the  $n - 1$  iteration is less than the limit  $n$ , record once. When the number of times reaches  $n_1$ , the population variation of particle swarm is simulated. In the application of path planning, the inherent attributes of particles are position  $(x, y)$  and velocity  $(v)$ .

So we reinitialize the particles of population mutation and bring them into the next iteration to simulate the mutation, as shown in Figure 10.

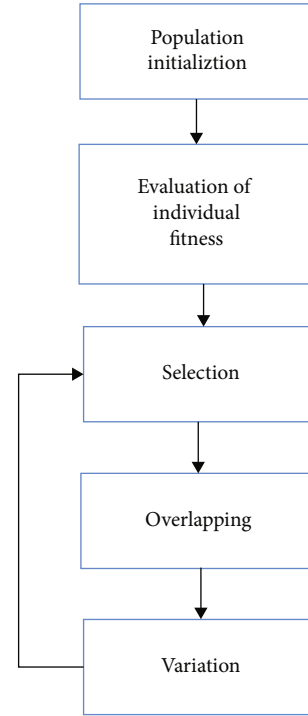


FIGURE 9: Genetic algorithm process.

Specifically, in the mathematical model, we set the randomly selected particles from the original particle swarm number  $L$  as mutation particle swarm  $L_1$  and reinitialize the velocity and position of each particle  $i$ .

$$\begin{aligned}
 \text{Particle}(i).\text{position} &= \text{create random solution}(\text{model}), \\
 &\downarrow \\
 (x, y) &= (x_0, y_0), \\
 v &= v_0.
 \end{aligned}$$

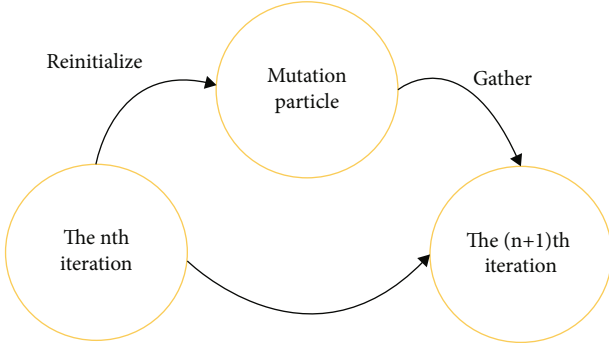


FIGURE 10: Simulation of mutation process.

Substituting the mutation particle swarm into the traditional particle swarm, the comparison is shown in Figures 11 and 12.

We can interpret from Figures 11 and 12 that the addition of mutation particles not only changes the state of being trapped in the local optimal solution for a long time but also successfully updates the global optimal solution even in the later iteration. At the same time, the global optimal solution obtained has a better evaluation value, which is more effective in the obstacle environment model.

**2.3.2. Adjustment and Introduction of Parameters.** In the particle swarm optimization, not only the algorithm needs to be improved, but also the adjustment of parameters is indispensable. The characteristics of particle swarm optimization requires discretion on the selection of parameters. Attention needs to be paid first to the global search and to the local search, so as to avoid premature local optimal solution and premature convergence. For the optimization of particle swarm optimization parameters, we try two optimization strategies.

*(1) Linear Differential Decreasing: Optimization Strategy of Weighted Inertia  $w$ .* Larger weight inertia is conducive to global search, and smaller weight is conducive to local search [20]. At the same time, due to the aggregation property of particles, the rate of reducing the search range of obstacle environment is proportional to the number of iterations. So for  $W$ , linear differential decreasing can satisfy this function relation.

$$\begin{aligned} \frac{dw}{dt} &= \frac{2 \cdot (w_{\max} - w_{\min})}{t_{\max}^2} \cdot t, \\ \int_{w(t)}^{w_m} dw &= \frac{2 \cdot (w_{\max} - w_{\min})}{t_{\max}^2} \int_0^t \pi \tau, \\ w &= w_{\max} - \frac{w_{\max} - w_{\min}}{t_{\max}^2} \cdot t^2, \end{aligned} \quad (7)$$

where  $t$  is the number of iterations.

*(2) Convergence Factor: Acceleration Factor  $c_1$  and  $c_2$  Optimization Strategy.* In order to ensure the convergence, Clerc

and Kennedy introduce a convergence factor  $K$  [21] and cancel the introduction of weighted inertia:

$$\begin{aligned} V_i &= K[V_i + \varphi_1 \times \text{rand}() \times (\text{pbest}_i - x_i) \\ &\quad + \varphi_2 \times \text{rand}() \times (\text{gbest}_i - x_i)], \\ K &= \frac{2}{\left| 2 - \varphi - \sqrt{\varphi^2 - 4\varphi} \right|}, \\ \varphi &= \varphi_1 + \varphi_2, \quad \varphi > 4. \end{aligned} \quad (8)$$

For the comparison of the two strategies, we also substitute into the obstacle environment model to observe the convergence curve and the final result, as shown in Figures 13 and 14.

In terms of convergence speed, although the two strategies are faster than the traditional PSO, the application of convergence factor makes the convergence speed not limited by the number of iterations, resulting in the fact that mutation particles cannot directly reflect the role, and the curve presents the trend of premature convergence (lack of fluctuations about the approximate solution). In contrast, linear differential decrement has a better search process and is compatible with the optimization of mutation jump out of local optimal solution. So we finally adopt the linear differential decreasing scheme.

### 3. Simulation Results of Path Planning

**3.1. Algorithm Parameter Setting.** In order to reflect the superiority of the MP-SAPSO algorithm over the traditional PSO algorithm, we apply them to the same environmental model for path planning and solution and analyze the results.

The parameter settings of the two algorithms are shown in Table 1.

In view of the uncomplicated environment model, the adjusted number of iterations is 100 times, and the population size is 150 times, which can reflect the convergence process and tend to be stable. At the same time, we know that when the inertia weight is within  $[-4, 4]$  and the learning coefficient is within  $[1.25, 2]$ , the results can converge quickly and the global optimal solution can be obtained relatively easily [15]. In order to dynamically adjust the inertia weight, we introduced a damping coefficient of 0.8 to effectively make the inertia weight as superior as possible in the iteration [20]. To ensure convergence, we set the constant  $\varphi$  to 4.1 and then calculate the convergence factor  $K$  to 0.729 (Table 2) [21].

#### 3.2. Results and Analysis

**3.2.1. Analysis of Path Results.** By substituting MP-SAPSO into the obstacle environment model and drawing the abscissa of the particle swarm as the global optimal solution, we get the simulation results of path planning for the specified starting point and end point, as shown in Figures 15 and 16.

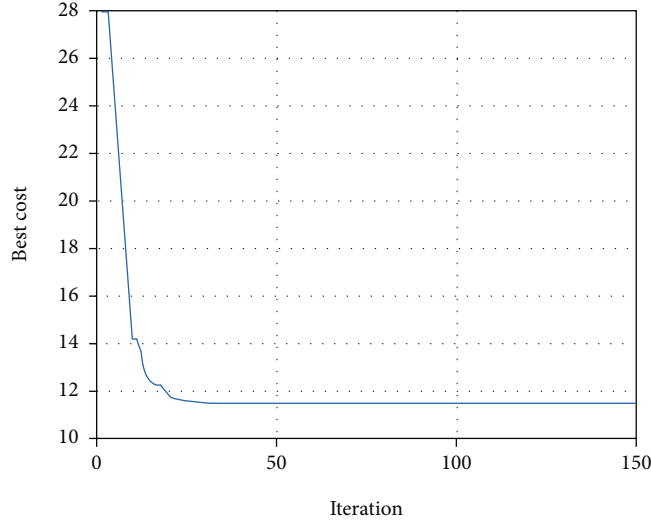


FIGURE 11: 150 times iteration curve of traditional particle swarm optimization.

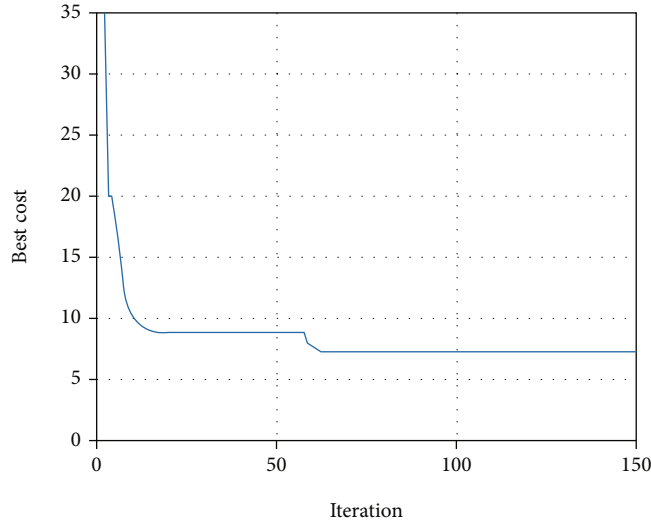


FIGURE 12: Variation particle swarm optimization curve.

As can be seen from Figure 15, the traditional particle swarm optimization fell into premature convergence, causing the calculation to stop in the early iteration. The convergence result shows a steep drop and several invalid iterations; in the 20th iteration, it was basically the same as the final result, and no optimization route planning was carried out. More importantly, the planned route does not achieve the result of crossing the obstacle model but finally shows the route out of the model.

It can be seen from Figure 16 that after MP-SAPSO is applied, the convergence of PSO is continuous. In the 30th iteration, PSO successfully jumps out of the local optimal solution, realizes the optimization function of mutation particle, and obtains the result that is more in line with the best route (through obstacles).

**3.2.2. Algorithm Complexity Analysis.** Since the core calculation process of the traditional PSO algorithm needs to

update the position of each individual in each iteration of the particle swarm, we can get

$$T(n) = O(I_{\max} \times P_{\text{size}}), S(n) = O(I_{\max} \times P_{\text{size}}). \quad (9)$$

Compared with MP-SAPSO, we found that the mutation factor needs to judge individual particles after a single iteration, and the substitution expectation  $E$  for this iteration needs to be calculated. Both have no effect on the number of iterations and the calculation of the population size. Therefore, the traditional PSO algorithm has the same complexity as the MP-SAPSO algorithm, and the introduction of parameters does not affect the solution time and the required calculation space.

**3.2.3. Analysis of Algorithm Superiority.** In order to fully prove the superiority of the MP-SAPSO algorithm from the perspective of statistical analysis, we use the method of

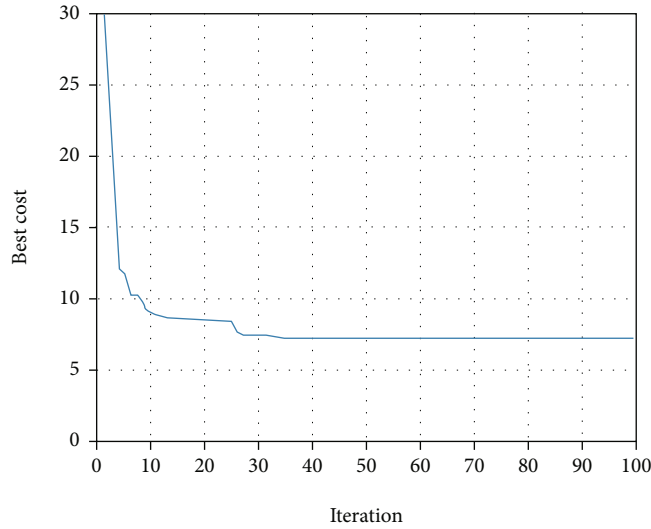
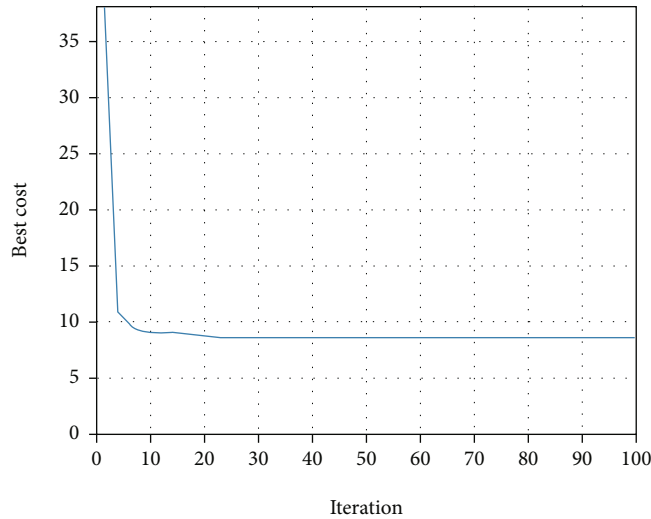
FIGURE 13: Linear differential decreasing  $w$  optimization.

FIGURE 14: Convergence factor optimization.

TABLE 1: Parameter setting.

Parameter	Description	Traditional PSO	MP-SAPSO
$I_{\max}$	Maximum number of iteration	100	100
$P_{\text{size}}$	Population size	150	150
$w$	Inertia weight	1	1
$w_{\text{dr}}$	Inertia weight damping ratio	0.8	0.8
$c_1$	Personal learning coefficient	1.5	\
$c_2$	Global learning coefficient	1.5	\
$\varphi$	Constant	\	4.1
$K$	Convergence factor	\	0.729

TABLE 2: Algorithm complexity analysis.

Algorithm	Time complexity $T(n)$	Spatial complexity $S(n)$
Traditional PSO	$O(I_{\max} \times P_{\text{size}})$	$O(I_{\max} \times P_{\text{size}})$
MP-SAPSO	$O(I_{\max} \times P_{\text{size}})$	$O(I_{\max} \times P_{\text{size}})$

running the algorithm multiple times to extract data, use the two algorithms to solve the set environment model for multiple paths, and calculate the output cost function. After analysis, the preliminary results are shown in Table 3.

Since the final iteration will tend to stabilize and fluctuate and the standard deviations of the two algorithms in multiple experiments are known, the cost function results of the two algorithms can be sorted again by the approximate normal distribution, and the paired-sample  $T$ -test is used for statistical analysis (Table 4).



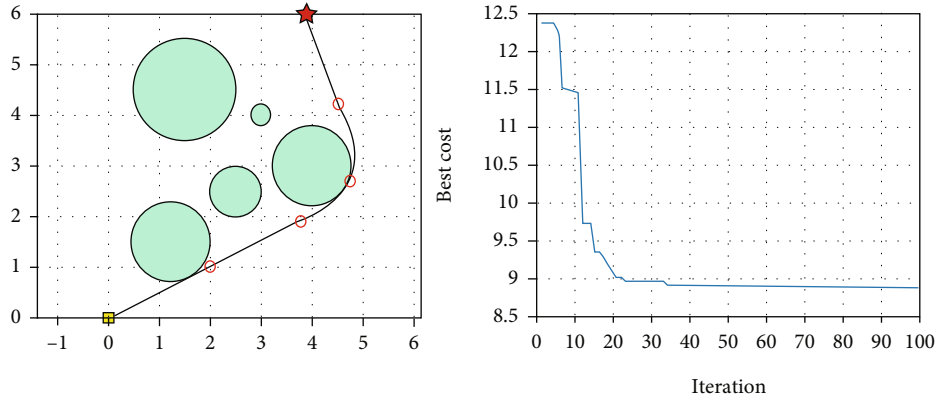


FIGURE 15: Simulation results of traditional particle swarm optimization.

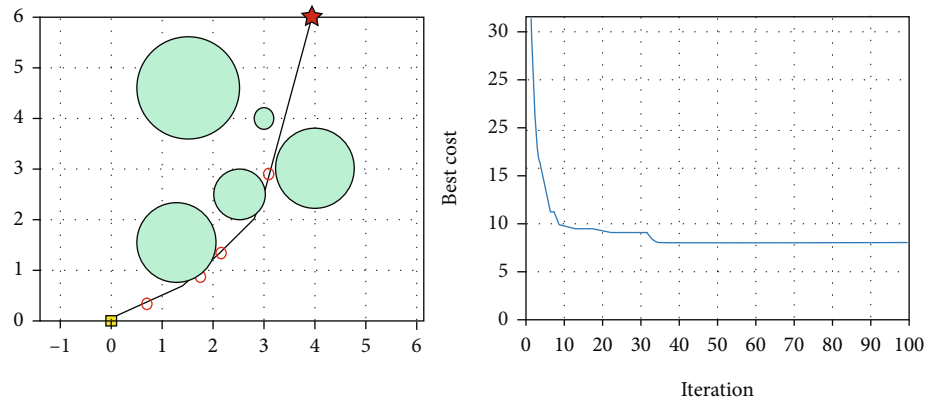


FIGURE 16: MP-SAPSO optimization results.

TABLE 3: Statistical analysis.

Algorithm	Best cost	Average cost	Standard deviation
Traditional PSO	8.6559	8.6790	0.0054
MP-SAPSO	7.6826	7.7608	0.0079

TABLE 4: Paired-sample  $T$ -test analysis.

Paired-sample $T$ -test	Standard deviation	Mean value of standard error	$P$ (significance)
PSO_ MP-SAPSO	0.0030	0.0004	$9.4306E-125$

It can be seen that  $P < 0.001$ , so the reduction in the output value of the cost function is very much related to the application of MP-SAPSO. It is proved that MP-SAPSO reduces the value of the cost function, which further reflects the advantage of MP-SAPSO to plan more accurate and better paths easily.

**3.3. Advantages and Further Research of the Algorithm.** Compared with the traditional particle swarm optimization algorithm, the MP-SAPSO algorithm can obtain the valid

path in the obstacle environment more accurately. The simulated annealing algorithm (SA) is combined with the concept of population mutation factor in genetic algorithm to solve the premature convergence problem of traditional particle swarm algorithm. When there are multiple routes, the algorithm can jump out of invalid iterations and find more feasible routes. This helps the robot to improve the accuracy of path selection in obstacle environments. According to the complex calculation and statistical analysis, it can be concluded that after several rounds of experimental verification, the MP-SAPSO algorithm does not significantly increase the calculation time compared with the traditional algorithm, and the calculation space does not take up too much. The reduction of the cost function is proved to be significantly correlated with the application of the improved algorithm by the paired-sample  $t$ -test. This proves the superiority of the present algorithm to the traditional algorithm.

Although the establishment of the obstacle environment can avoid the influence of the edges and corners of the obstacle itself on the path selection of the robot, many specific environmental parameters (obstacle size, robot size) are not taken into consideration, including the discussion in a three-dimensional space. Therefore, further research and exploration are needed for more complex obstacle environments.

## 4. Conclusion

In this paper, an improved particle swarm optimization algorithm MP-SAPSO is proposed to solve the robot path planning problem. In building a mathematical model, considering the complexity of the obstacle model, and to facilitate the operation in practical application, we build the untouchable space as the obstacle environment model, which is easy to operate in practical application. At the same time, MP-SAPSO can make a better path planning strategy in the obstacle environment by screening the result of annealing probability and introducing mutation particles; by introducing linear differential decreasing inertia weight  $w$ , the convergence speed is not affected by the introduction of the new algorithm. Finally, without sacrificing the efficiency of the algorithm, the accuracy of path planning and the efficiency of robot operation are improved.

The simulation results show that compared with the existing methods, the application of this algorithm can make the robot find a better mobile path faster. It has a great application prospect in application scenarios such as UAV, rescue robot, cleaning robot, and military robot that need to ensure operational efficiency and accuracy. However, due to the simple design of the model, the complex situation in the actual application scenario is not covered in this paper. Some real parameters are not available, and the research of some specific application scenarios needs to be further deepened to strengthen the ability of this algorithm to deal with specific problems, which will be further explored in future research.

## Data Availability

The datasets used and/or analyzed during the current study are available from the corresponding author on reasonable request.

## Conflicts of Interest

The authors declare that they have no conflicts of interest to report regarding the present study.

## References

- [1] M. Nazarahari, E. Khanmirza, and S. Doostie, "Multi-objective multi-robot path planning in continuous environment using an enhanced genetic algorithm," *Expert Systems with Applications*, vol. 115, pp. 106–120, 2019.
- [2] R. Eberhart and J. Kennedy, "A new optimizer using particle swarm theory," in *MHS'95. Proceedings of the sixth international symposium on micro machine and human science*, pp. 39–43, Nagoya, Japan, 1995.
- [3] C. Katrakazas, M. Quddus, W. H. Chen, and L. Deka, "Real-time motion planning methods for autonomous on-road driving: state-of-the-art and future research directions," *Transportation Research Part C: Emerging Technologies*, vol. 60, pp. 416–442, 2015.
- [4] V. Roberge, M. Tarbouchi, and G. Labonte, "Comparison of parallel genetic algorithm and particle swarm optimization for real-time UAV path planning," *IEEE Transactions on industrial informatics*, vol. 9, no. 1, pp. 132–141, 2013.
- [5] H. Mo and L. Xu, "Research of biogeography particle swarm optimization for robot path planning," *Neurocomputing*, vol. 148, pp. 91–99, 2015.
- [6] J. Yu and D. Rus, *An effective algorithmic framework for near optimal multi-robot path planning* September 2021, <https://arc.cs.rutgers.edu/files/YuRus15ISRR.pdf>.
- [7] G. Li, S. Tong, G. Lv et al., "An improved artificial potential field-based simultaneous FORWARD search (improved APF-based SIFORS) method for robot path planning," in *2015 12th international conference on ubiquitous robots and ambient intelligence (URAI)*, pp. 330–335, Goyangi, Korea (South), 2015.
- [8] M. H. Jiao, H. X. Wei, B. W. Zhang, J. Q. Jin, Z. Q. Jia, and J. L. Yan, "Path planning of escort robot based on improved quantum particle swarm optimization," in *2019 Chinese control and decision conference*, Nanchang, China, 2019.
- [9] A. Tharwat, M. Elhoseny, A. E. Hassanien, T. Gabel, and A. Kumar, "Intelligent Bézier curve-based path planning model using chaotic particle swarm optimization algorithm," *Cluster Computing*, vol. 22, no. S2, pp. 4745–4766, 2019.
- [10] P. K. Das, H. S. Behera, S. Das, H. K. Tripathy, B. K. Panigrahi, and S. K. Pradhan, "A hybrid improved PSO-DV algorithm for multi-robot path planning in a clutter environment," *Neurocomputing*, vol. 207, pp. 735–753, 2016.
- [11] N. Zeng, H. Zhang, Y. Chen, B. Chen, and Y. Liu, "Path planning for intelligent robot based on switching local evolutionary PSO algorithm," *Assembly Automation*, vol. 36, no. 2, pp. 120–126, 2016.
- [12] B. Ames, A. Beveridge, R. Carlson et al., "A leapfrog strategy for pursuit-evasion in a polygonal environment," *International Journal of Computational Geometry and Applications*, vol. 25, no. 2, pp. 77–100, 2015.
- [13] W. J. Yang, H. B. Wang, and J. H. Wang, "Research on path planning for mobile robot based on grid and hybrid of GA/SA," in *Advanced Materials Research*, vol. 479–481, pp. 1499–1503, 2012.
- [14] Z. Y. Zhou, P. A. Mu, and R. J. Zhang, "Application of PSO optimization algorithm in smooth path planning," *Software Guide*, vol. 20, no. 3, pp. 67–72, 2021.
- [15] Q. M. Yan, R. Q. Ma, Y. X. Ma et al., "An adaptive simulated annealing particle swarm optimization algorithm," *J Xi'an U Electron Sci Te*, vol. 48, no. 4, pp. 120–127, 2021.
- [16] F. Javidrad and M. Nazari, "A new hybrid particle swarm and simulated annealing stochastic optimization method," *Applied Soft Computing*, vol. 60, pp. 634–654, 2017.
- [17] R. Da Silva, E. V. Filho, and A. Alves, "A thorough study of the performance of simulated annealing in the traveling salesman problem under correlated and long tailed spatial scenarios," *Physica A*, vol. 577, article 126067, 2021.
- [18] S. Stefan and J. Wolfhard, "Accelerating polymer simulation by means of tree data-structures and a parsimonious Metropolis algorithm," *Computer Physics Communications*, vol. 256, article 107414, 2020.
- [19] A. Jamali, R. Mallipeddi, M. Salehpour, and A. Bagheri, "Multi-objective differential evolution algorithm with fuzzy inference-based adaptive mutation factor for Pareto optimum design of suspension system," *Swarm and Evolutionary Computation*, vol. 54, article 100666, 2020.

- [20] P. C. Cai and D. M. Zhang, "Improved gray wolf algorithm based on dynamic inertia weight and adaptive search," *Journal of Physics: Conference Series*, vol. 1802, no. 3, article 032122, 2021.
- [21] M. Clerc and J. Kennedy, "The particle swarm - explosion, stability, and convergence in a multidimensional complex space," *IEEE transactions on Evolutionary Computation*, vol. 6, no. 1, pp. 58–73, 2002.

## Retraction

# Retracted: Research on the Difficulties and Countermeasures of the Practical Teaching of Ideological and Political Theory Courses in Colleges and Universities Based on Wireless Communication and Artificial Intelligence Decision Support

### Wireless Communications and Mobile Computing

Received 1 August 2023; Accepted 1 August 2023; Published 2 August 2023

Copyright © 2023 Wireless Communications and Mobile Computing. This is an open access article distributed under the Creative Commons Attribution License, which permits unrestricted use, distribution, and reproduction in any medium, provided the original work is properly cited.

This article has been retracted by Hindawi following an investigation undertaken by the publisher [1]. This investigation has uncovered evidence of one or more of the following indicators of systematic manipulation of the publication process:

- (1) Discrepancies in scope
- (2) Discrepancies in the description of the research reported
- (3) Discrepancies between the availability of data and the research described
- (4) Inappropriate citations
- (5) Incoherent, meaningless and/or irrelevant content included in the article
- (6) Peer-review manipulation

The presence of these indicators undermines our confidence in the integrity of the article's content and we cannot, therefore, vouch for its reliability. Please note that this notice is intended solely to alert readers that the content of this article is unreliable. We have not investigated whether authors were aware of or involved in the systematic manipulation of the publication process.

In addition, our investigation has also shown that one or more of the following human-subject reporting requirements has not been met in this article: ethical approval by an Institutional Review Board (IRB) committee or equivalent, patient/participant consent to participate, and/or agreement to publish patient/participant details (where relevant).

Wiley and Hindawi regrets that the usual quality checks did not identify these issues before publication and have since put additional measures in place to safeguard research integrity.

We wish to credit our own Research Integrity and Research Publishing teams and anonymous and named external researchers and research integrity experts for contributing to this investigation.

The corresponding author, as the representative of all authors, has been given the opportunity to register their agreement or disagreement to this retraction. We have kept a record of any response received.

### References

- [1] C. Tang, "Research on the Difficulties and Countermeasures of the Practical Teaching of Ideological and Political Theory Courses in Colleges and Universities Based on Wireless Communication and Artificial Intelligence Decision Support," *Wireless Communications and Mobile Computing*, vol. 2021, Article ID 3229051, 7 pages, 2021.

## Research Article

# Research on the Difficulties and Countermeasures of the Practical Teaching of Ideological and Political Theory Courses in Colleges and Universities Based on Wireless Communication and Artificial Intelligence Decision Support

Chaozhen Tang 

*School of Marxism, Guangxi Vocational and Technical Institute of Industry, Guangxi 53001, China*

Correspondence should be addressed to Chaozhen Tang; [tang\\_chaozhen@outlook.com](mailto:tang_chaozhen@outlook.com)

Received 29 September 2021; Revised 27 October 2021; Accepted 30 October 2021; Published 6 December 2021

Academic Editor: Deepak Gupta

Copyright © 2021 Chaozhen Tang. This is an open access article distributed under the Creative Commons Attribution License, which permits unrestricted use, distribution, and reproduction in any medium, provided the original work is properly cited.

The rapid development of wireless communication technology has caused the computing speed and performance of information terminals to increase exponentially. Artificial intelligence technology emerged in this context. As an efficient work system, artificial intelligence has been introduced into many areas of social life. Especially in the field of education, it has made outstanding contributions. At this stage, the conflict between Eastern and Western civilizations is intensifying. As the most active ideological group, college students have not yet formed a scientific understanding of the pros and cons of Eastern and Western civilizations, and it is easy for them to fall into confusion in this kind of ideological turmoil. This requires that the ideological and political education in our country's colleges and universities effectively play a role, strengthen ideological guidance, and create a new system of practical teaching of college ideological and political theory courses under the background of wireless communication. Ideological and political education, as one of the courses with outstanding characteristics in our country's university education courses, has a guiding role that cannot be ignored for university students. This paper uses a questionnaire survey method to conduct an online survey of 500 college students from 6 universities in Shanghai to obtain first-hand information on the current ideological and political practice courses of Chinese universities and then sort out the emergence of artificial intelligence-based decision support systems in China. The practical class encountered difficulties and explored strategies to alleviate this dilemma, hoping to provide a useful reference for the development of ideological and political teaching in China in the future.

## 1. Introduction

With the rapid development and maturity of wireless communication and artificial intelligence technology, decision support systems based on artificial intelligence have become a new hot research field. The decision support system (DSS) is a system based on operation research and management, cybernetics, and behavioral sciences, using computer simulation and other technical means, comprehensively using existing data, information, and models to assist decision-makers in improving the efficiency and accuracy of decision-making [1]. The application of artificial intelligence-based decision

support systems in the field of education plays an important role in education reform in the information age.

In recent years, my country has continuously strengthened the ideological-oriented function of ideological and political practice courses in colleges and universities and made joint efforts in many aspects such as the staffing of teachers, the promotion of advanced characters, and the interpretation of the Marxist-Leninist era [2, 3]. In 2017, the current state of ideological and political education in colleges and universities with the largest scale since the founding of the People's Republic of China started and ended successfully at the end of that year. After



investigation, it is found that after years of hard work, the recognition of ideological and political teaching and ideological and political teachers by college students in our country is very high [4]. After years of hard work, the current ideological and political education has become one of the courses that college students quite like. Both the students' recognition of ideological and political courses and the recognition of ideological and political teachers have been greatly improved. It shows that the achievements of ideological and political education in colleges and universities in our country are remarkable [5, 6].

At the level of theoretical research, many scholars have carried out deep research in this field and put forward a series of valuable viewpoints. Feng Weiya believes that ideological and political practice courses in colleges and universities are a useful supplement to theoretical courses. With the help of the development of information technology, microclasses and other forms can better highlight the key points of teaching and have more flexibility in the selection of teaching subjects and sharing of teaching resources [7, 8]. Therefore, colleges and universities should strengthen cooperation and realize the sharing of microcourse resources, which has a very significant effect on the development of ideological and political practice courses. Zhang Jinliang and Jiang Dong use VR technology to combine red tourism and other forms with ideological and political education through practical research, effectively alleviating the defects of traditional ideological and political practice courses such as solidification and single form, allowing the ideological and political practice courses to be issued, giving new life [9]. From the perspective of improving the teaching effect of ideological and political courses, Wang Yuehui put forward suggestions such as "equal emphasis on theory and practice," perfecting the guarantee system, and innovating the assessment mechanism [10]. These representative studies have studied ideological and political teaching in contemporary colleges and universities from multiple levels, but how to carry out this work in the context of wireless communication and artificial intelligence decision-making and the students' attitudes towards existing teaching reforms are not analyzed in depth.

In addition to theoretical research, many colleges and universities are also actively exploring artificial intelligence decision support in college ideological and political practice courses in the context of wireless communication [11, 12]. For example, some colleges and universities have closely followed the antiepidemic theme in the ideological and political practice classes, starting with discovering antiepidemic heroes around them, to why major countries are actively developing vaccines and other drugs with independent intellectual property rights, and then why countries will adopt measures in the face of the epidemic [13]. Different strategies, etc., conducted research based on artificial intelligence decision support. Through independent analysis, students deepen their scientific understanding of current affairs, thereby enhancing their scientific understanding of ideological and political theories. Some universities uploaded the ideological and political classroom records to the website through live webcasts, which received a large number of

clicks from college students, and successfully realized the scientific sharing of teaching resources with the help of wireless communication technology [14, 15]. This paper wants to comb out the current situation of artificial intelligence-based ideological and political practice courses, analyzed the difficulties encountered in the practice courses, and discussed strategies to alleviate this dilemma, hoping to provide useful references for the development of ideological and political education in China in the future.

## 2. Artificial Intelligence Decision Support System

The decision support system involves management, computer, information, and other disciplines. Its objects include decision information and decision models, decision problems and their environment, organizational structure and decision-makers, and related computer, information, and communication technologies. Among them, decision information, decision models, and decision-makers are the three basic elements of a decision support system. The structure of DSS three libraries is shown in Figure 1.

*2.1. Architecture of Artificial Intelligence Decision Support System.* Artificial intelligent decision support systems (IDSS) are a product of the combination of decision support systems (DSS) and artificial intelligence (AI) technologies. Intelligent decision support systems (IDSS) are formed by integrating artificial intelligence expert systems on the basis of decision support systems (DSS). The decision support system is mainly composed of problem processing and human-computer interaction system (composed of language system and problem processing system), model library system (composed of model library management system and model library), database system (composed of database management system and database), and other composition. The expert system is mainly composed of the knowledge base, inference engine, and knowledge base management system. The decision support system and the expert system are integrated into an intelligent decision support system, as shown in Figure 2.

*2.2. Characteristics of Artificial Intelligence Decision Support System.* The artificial intelligence decision support system has the following characteristics: selecting a suitable decision model, tracking the problem-solving process, assisting in diagnosing the boundary conditions and environment of the problem, simulating the thinking of the decision-maker, etc., as shown in Table 1.

- (1) IDSS has a reasoning mechanism that can simulate the thinking process of decision-makers, so it can guide decision-makers to choose a suitable decision model according to the needs of decision-makers, through conversation, analysis of problems, and application of relevant knowledge
- (2) The reasoning mechanism of IDSS can track the problem-solving process, so as to prove the

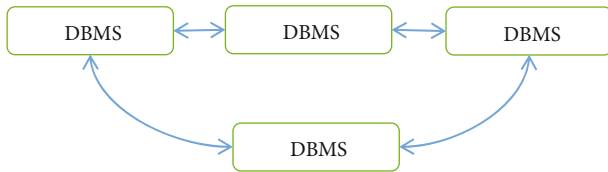


FIGURE 1: DSS three-database structure.

correctness of the model and increase the credibility of the decision-maker to the decision-making plan

- (3) When decision-makers use DSS to solve semistructured and unstructured problems, sometimes they are not very clear about the boundary or conditions of the problem itself, but IDSS can assist in diagnosing the boundary conditions and environment of the problem by asking the decision-maker
- (4) IDSS can track and simulate the thinking and thoughts of decision-makers, so that decision-makers not only know the conclusion but also know why such a conclusion is reached. The intelligent decision support system gives full play to the expert system's characteristic of solving qualitative analysis problems in the form of knowledge reasoning, and the decision support system's characteristic of solving quantitative analysis problems with model calculation as the core, and fully achieves the organic combination of qualitative analysis and quantitative analysis, making a big development in the ability and scope of problem-solving

**2.3. Evaluation of AI Decision Support Results.** The patterns and rules discovered in the decision support stage are evaluated, and redundant and irrelevant patterns are eliminated. If the model does not meet the user requirements, then the entire discovery process needs to return to the discovery stage before reselecting the data, adopting a new data transformation method, setting new data mining parameter values, or changing a mining algorithm to recalculate and extract rules. For those valuable and correct results, the information is presented to users in a graphical way. The system flow chart is shown in Figure 3. First, the initial data is cleaned and integrated, then the data is sorted through selection and transformation, then decision-making support is given to a specific data set, and finally, the decision-making result is evaluated.

### 3. Investigation of the Status Quo of Ideological and Political Classrooms in Colleges and Universities Based on the *K*-Means Clustering Algorithm Model

This article first collects the current situation of ideological and political classrooms in colleges and universities in the form of questionnaire surveys, hoping to grasp the true feelings of students about the ideological and political classrooms in colleges and universities through students'

responses to the questionnaire, and provides strong evidence for the discovery of key issues. Then, the artificial intelligence decision support system was used to filter, process, and analyze the data.

**3.1. Research Purpose.** Improving the effectiveness of ideological and political classrooms in colleges and universities is our key goal in recent years. The purpose of this research is to better respond to the challenges posed by the global spread of the new crown epidemic and to explore ways to improve the effectiveness of the ideological and political classroom by making full use of the technological dividends brought by "cloud computing." It is hoped that through research, students will be guided to take a scientific view of the development of ideological and political courses in the new era and meet the needs of students for ideological and political courses.

**3.2. Research Object.** The questionnaire selected in this article is mainly distributed to 500 sophomores from six universities in Shanghai. The selection and design of the questions in the questionnaire have been thoroughly and scientifically demonstrated. After uploading to the questionnaire star, the class counselor will organize the students to answer. The questionnaire is anonymous. After summarizing, the six colleges and universities submitted a total of 487 valid answer sheets, with an effective rate of over 97%, indicating that college students have a strong willingness to cooperate.

**3.3. Research Tools.** The research tools used in this study mainly include online questionnaires, information capture tool python, and data statistics tool SPSS12.0.

**3.3.1. Online Questionnaire.** Due to the impact of various factors such as the epidemic situation, this study chose the online questionnaire in the questionnaire distribution method, which is to organize students to answer and submit online in the form of online questionnaires. This not only saves research time and funds to a certain extent but also speeds up the questionnaire issuance and recovery. Answering papers through information terminals is in line with the current living habits of college students, allowing them to use fragmented time to answer, ensuring their enthusiasm for participation.

**3.3.2. Information Grabbing Tool Python.** Python is what we often call "crawler," and it is a very practical tool for crawling network information at this stage. After the questionnaire is retrieved, by searching for several keywords, such as "recognition" and "teacher ability," the data proportion of each item can be clearly displayed, so that this research can conduct a more adequate horizontal comparison.

**3.3.3. Data Statistics Tool SPSS13.0.** In terms of data operation, this article chooses the *K*-Means Clustering Algorithm Model as the main operation tool and uses this *K*-Means Clustering Algorithm Model to comprehensively process the data to find out the deep-level associations between the questionnaire data. After the preliminary data analysis and comparison work, the research uses SPSS13.0 to perform

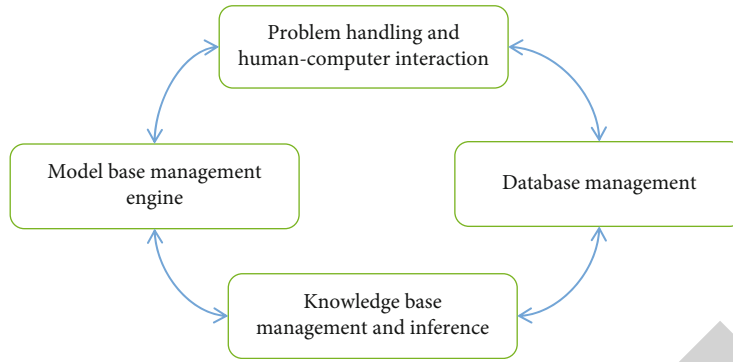


FIGURE 2: Architecture diagram of intelligent decision support system.

TABLE 1: Characteristics of artificial intelligence decision support system.

Features	Description
Choose the right decision model	According to the needs of decision-makers, through conversations, analysis of problems, and application of relevant knowledge to guide decision-makers to choose a suitable decision model
Tracking the problem-solving process	Track the problem-solving process, prove the correctness of the model, and increase the credibility of the decision-maker for the decision-making plan
Boundary conditions and environment to assist in diagnosing problems	When the decision-maker is not clear about the boundary or conditions of the problem itself, he can assist in diagnosing the boundary conditions and environment of the problem by asking the decision-maker
Simulate the thinking of decision-makers	So that decision-makers not only know the conclusion but also why they came to such a conclusion

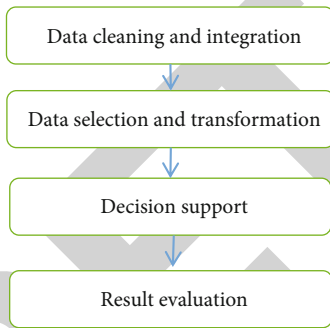


FIGURE 3: Flow chart of artificial intelligence decision-making.

terminal processing on the data. The reason for using SPSS13.0 is that it can support the retrieval of ultralong bytes, and the obtained data is carried out in the form of graphs. Intuitive display is helpful for the further development of research.

#### 4. Analysis and Discussion of Research Results

##### 4.1. The Current Dilemma Faced by the Practical Teaching of Ideological and Political Courses in Colleges and Universities

4.1.1. The Mismatch between the Lack of Faculty and Student Expectations. Through investigation, it is found that many students have a very clear understanding of the important

value of ideological and political courses. In recent years, China has attached great importance to ideological and political courses and has made a lot of efforts in reforming the teaching content and teaching mode of ideological and political courses in colleges and universities. Contemporary ideological and political teaching has shifted from the memorization of classical theories in the past to the analysis of practical problems. This change has made students highly affirm the effectiveness and orientation of the ideological and political courses. Students have moved from passive learning under academic pressure in middle and high school to regard it as important for future life development. The subjects of guiding significance come to learn. This kind of learning attitude and the improvement of learning desire are very beneficial to the development of ideological and political practice teaching. Therefore, almost the vast majority of students have high expectations for the teaching of ideological and political courses.

However, judging from reality, there is a big gap between the current state of ideological and political teaching in our country and the expectations of students. The main reason for this phenomenon is the lack of teachers. Although the registered ideological and political teachers in my country's colleges and universities have exceeded the 100,000 mark by the end of 2020, it is still difficult to meet the needs of college ideological and political education. At the same time, the abilities of existing ideological and political teachers are also uneven. As a result, there is a big gap between the



students' expectations of ideological and political courses and their realistic feelings.

It can be seen from Table 2 that there is a big gap between the expected value of the ideological and political teachers' abilities and the practicality of the curriculum and the actual scores of college students in our country. The average expectation of students is as high as 4.8 points, which shows that college students generally have higher expectations for ideological and political teachers. However, judging from the students' actual scores, it is only 4.0 points. It proves that there is still a lot of room for improvement in the teaching level of ideological and political teachers in our country.

*4.1.2. The Contradiction between the Massive Resources in the Cloud and the Solidification of the Content of Ideological and Political Courses.* At this stage, students are using information terminals for longer and longer, which enables them to be more closely linked with society. Their thoughts are more active, they have their own unique insights into heroic images, and they hope to find shining points from ordinary people around them. After the outbreak of the new crown epidemic, the people of the whole country are committed to a city, and many ordinary people have shown their heroic glory. These can become excellent materials for our ideological and political theory practice courses. However, under the influence of traditional utilitarian thinking, ideological and political education in my country's colleges and universities still pays too much attention to its role in political construction and economic development services, resulting in a disconnect between instrumental and educational features and neglecting the satisfaction of the needs of the student era.

For example, in practical classes, teachers use class time mainly to illustrate national current affairs and politics and analysis of national policies, but they rarely organize teaching content according to the actual needs of students. In order to show the openness of the classroom, teachers usually take the form of letting students have group discussions, expounding their own understanding of specific content. This teaching model is a considerable improvement compared with the simple teacher teaching in the past; in fact, the subject of the classroom is still planned by the teacher in advance, and the student's dominant position has not been truly realized.

It can be seen from Table 3 that at this stage, the classroom themes of the ideological and political theory and practice courses in various universities are still based on the teachers' self-design, accounting for 84% of the total. Only 16% of the ideological and political classrooms are based on the collective wishes of the students. Although this kind of established classroom content can better realize the control of teaching, it ignores the advantage of stimulating students' interest in topics that interest students, thus turning ideological and political classrooms into formal innovations, but internally. It is still the traditional model of "teaching as the mainstay."

## 4.2. Countermeasures to Develop High-Efficiency Ideological and Political Theory and Practice Courses

*4.2.1. Improve the Professional Ability of Ideological and Political Teachers in Colleges and Universities.* The funda-

TABLE 2: Comparison of college students' expectations and actual scores for ideological and political courses.

Category	Expected value	Actual score
Teacher ability	4.8	4.1
Course practicality	4.9	4.0

TABLE 3: Analysis of sources of ideological and political topics in colleges and universities.

The source of teaching themes	Teachers' self-imposition	Students' collective agreement
Proportion	84%	16%

mental research that causes a large gap between the expected value of learning and the actual score is that the professional ability of ideological and political teachers in colleges and universities is uneven. Therefore, to alleviate this contradiction, we must start with improving their professional ability. At this stage, college ideological and political teachers generally have higher academic qualifications and have a higher level of theoretical cultivation. What they lack is the ability to combine theoretical cultivation with politics.

In this regard, a coordinated improvement method can be adopted at multiple levels. The education department organizes outstanding experts to demonstrate and explain and upload the video to the cloud for ideological and political teachers to learn. Colleges and universities with similar majors can also form teaching and research groups together to gather the strength of teachers and work together to improve in the form of joint lesson preparation.

At the same time, it is necessary to strengthen the use of information terminals for ideological and political teachers. The survey shows that ideological and political teachers generally lack the ability to use information terminals. At this stage, the influence of information terminals on students is increasing, and students are gradually accustomed to learning through information terminals. Ideological and political teachers must also follow this trend, pay attention to improving their own ability to combine in this area, and use information equipment to enhance teacher-student interaction in the teaching process.

*4.2.2. Broaden the Scope of Materials for Practical Topics.* In the design of the theme of the practical class, ideological and political teachers should adopt a more open attitude and way to introduce the current political topics that students are concerned about into the classroom and replace the teacher's explanation with the discussion and speech of the students, so as to enhance the students' understanding of the classroom, attention, and participation. For example, Fudan University and Shanghai University have introduced epidemic fighting and prevention and control into the classroom, encouraging students to tell the deeds of antiepidemic heroes around them, and then, the teacher summarizes, analyzes the spiritual essence, finds the inner connection, and integrates the content, returning to teaching materials to realize the combination of ideological and political

education theory and practice. Broadening the range of subject matter selection in class can help students get rid of the constraints of fixed thoughts and recognize the close connection between social life and ideological education, so as to take a long-term view of learning and take the initiative to use what they have learned when encountering social problems, thinking about theoretical knowledge,

## 5. Conclusion

With the further deepening of economic and cultural exchanges between countries in the world, the deep-seated conflicts between Eastern and Western civilizations have gradually emerged. Various decadent trends of thought have caused very serious negative effects on the healthy development of my country's society, economy, and culture. At the same time, my country's tendency to one-sidedly attach importance to economic construction after reform and opening up has also caused us to pay a very heavy price. In order to reverse this trend, my country has vigorously promoted the development of ideological and political education in recent years and strengthened the status of ideological and political education in schools at all levels, especially colleges and universities, so that the marginalized ideological and political education has gradually become the favorite of students. As one of the courses, especially in the context of cloud computing, ideological and political education can be more closely integrated with students' daily lives. Relying on the K-Means Clustering Algorithm Model, this article investigates the true feelings of some sophomores in six universities in Shanghai about the current ideological and political theory practice courses, finds out the difficulties faced by the further development of ideological and political courses, and proposes targeted solutions. I hope to more calmly face the new challenges brought by the development of the times to ideological and political education. Therefore, colleges and universities must pay sufficient attention to the teaching of ideological and political theory and practice courses; comprehensively exert their efforts in curriculum design, teacher construction, and other fields; and seek opportunities and methods to break through difficulties in active innovation, so that ideological and political education can be effective for colleges and universities. The guiding role of students in the growth process has been better brought into play.

## Data Availability

The datasets used and/or analyzed during the current study are available from the corresponding author on reasonable request.

## Conflicts of Interest

It is declared by the author that this article is free of conflict of interest.

## Acknowledgments

The study was funded by the 2021 Guangxi Vocational Education Teaching Reform Research Project, "Research and Practice on the Practical Teaching System of Ideological and Political Courses from the Perspective of Quality Improvement and Excellence—Taking Guangxi's "Double High Plan" colleges as an example" (GXGZJG2021B029).

## References

- [1] Q. Dong, *Innovation and prospects of ideological and political education in colleges and universities in the era of big data*, Management Observation, 2019.
- [2] X. F. Liu and M. G. Wang, "The basic requirements of case teaching method and case selection in college ideological and political courses," *Literature Education*, vol. 7, no. 14, pp. 144-145, 2020.
- [3] H. F. Tao and Y. Mo, "Research on the innovation path of ideological and political education in colleges and universities from the perspective of big data," *China Audio-visual Education*, vol. 8, 2019.
- [4] H. Zhou and Q. Q. Gong, "Analysis of the integration path of new media technology and ideological and political courses in colleges and universities," *Audio-visual Education Research*, vol. 10, 2020.
- [5] Z. T. Wang, "Research on the experience path of improving the affinity of ideological and political courses in colleges and universities in the new era," *China Higher Education*, vol. 7, pp. 45-47, 2020.
- [6] Y. W. Song and Y. Wang, "Research on the transformation of ideological and political theory course textbook system to teaching system in colleges and universities," *China Higher Education*, vol. 3, no. 6, pp. 57-58, 2019.
- [7] L. Qin and J. D. Zhu, "Artificial intelligence: the trend of the times and coping strategies of ideological and political education in colleges and universities—based on the visual threshold of complexity science," *Jiangsu Higher Education*, vol. 2, pp. 102-106, 2020.
- [8] C. Chen and J. P. Zhong, "On the "micro-era" university ideological and political education innovation research—comment on "the "micro-era" university ideological and political education innovation research"," *Educational Development Research*, vol. 2, 2020.
- [9] N. N. Wang, "On the influence of emotional education on ideological and political education in colleges and universities," *Journal of Jiaozuo University*, vol. 3, 2020.
- [10] B. D. Han, "Research on student evaluation strategies of ideological and political courses in colleges and universities under the background of curriculum ideological and political," *Modern Education Forum*, vol. 2, no. 11, 2020.
- [11] X. W. Kong, X. Z. Tang, and Z. M. Wang, "Research review on the interpretability of artificial intelligence decision-making," *Systems Engineering Theory and Practice*, vol. 2, pp. 526-532, 2021.
- [12] G. S. Zhang and C. D. Yang, "The impact, challenges and prospects of artificial intelligence on organizational decision-making," *Shandong Social Sciences*, vol. 9, pp. 100-105, 2020.
- [13] C. Liu and X. F. Li, "AI+public decision-making": theoretical changes, system elements and action strategies," *Journal of*



## Research Article

# Positioning Control Algorithm of Vehicle Navigation System Based on Wireless Tracking Technology

Leibing Yan 

*School of Electronic Information Engineering, Henan Institute of Technology, Xinxiang 453003, China*

Correspondence should be addressed to Leibing Yan; [leibingy@hait.edu.cn](mailto:leibingy@hait.edu.cn)

Received 22 September 2021; Revised 29 October 2021; Accepted 9 November 2021; Published 6 December 2021

Academic Editor: Deepak Gupta

Copyright © 2021 Leibing Yan. This is an open access article distributed under the Creative Commons Attribution License, which permits unrestricted use, distribution, and reproduction in any medium, provided the original work is properly cited.

To improve the accuracy and reliability of the on-board navigation system positioning, the positioning control algorithm of vehicle navigation system based on wireless tracking technology is proposed. By using modern information fusion technology, the accurate positioning of vehicle integrated navigation is realized, and the design goal of omnidirectional, all weather, and self-contained positioning function is realized. Finally, the test shows that the accuracy and reliability of the positioning control algorithm of vehicle navigation system based on wireless tracking technology are improved than existing point system, speed measurement accuracy can reach 0.02 m/s, and positioning accuracy is about 18 meters. The vehicle operation efficiency and safety are greatly improved, and the traffic capacity is improved. And the traffic congestion is effectively alleviated, which provides reliable guarantee for the realization of traffic management automation and intelligent vehicle driving.

## 1. Introduction

With the acceleration of social development, there are many problems in road traffic in recent years, which makes intelligent transportation system get widespread attention. As an important part, intelligent vehicle is a comprehensive intelligent vehicle system which integrates many functions such as environmental perception, planning, decision-making, and auxiliary driving and is the future development direction. The further study of it can help to reduce the incidence of traffic accidents, and to some extent, it can effectively alleviate the current traffic situation. Real-time acquisition of high precision navigation and positioning information is an important part of intelligent vehicle system and also the primary goal to ensure its safety. Vehicle navigation and positioning technology has achieved some scientific research results as one of the key technologies of intelligent vehicle system. Lin and Liao [1] proposed a design scheme of Beidou/GPS-based vehicle positioning monitoring system, which receives satellite positioning information via dual-mode positioning module, analyzes and displays it on the LCD (liquid crystal display) screen, and uses 4G wireless communication to upload monitoring data to the monitor-

ing center for remote monitoring management. The positioning system is relatively stable, but the positioning accuracy is not high. Su et al. [2] analyzed three common satellite navigation and positioning methods. Key research on differential techniques is performed. After the comparison analysis, it is found that the carrier phase difference positioning accuracy can reach the cm level positioning, and this technology is applied to the on-board navigation terminal equipment. The positioning of this method is better reliable, but the speed measurement accuracy cannot meet the actual needs. Hu et al. [3] proposed the combined navigation scheme in the vehicle combined navigation system. Using the zero lateral and celestial velocity of the vehicle during normal driving, the combined navigation filter measurement equation is obtained when the satellite signal fails; considering the difficulty to obtain the measured noise covariance matrix during the Kalman filtering, a new adaptive Kalman filtering (ADKF) algorithm is derived, which calculates the actual covariance of the new interest sequence, and adjusts the noise covariance matrix size using the fuzzy inference system (FIS) to adjust the noise covariance to navigate the vehicle position. The navigation method is highly adaptable to the environment, but the positioning accuracy

is not ideal enough. Based on this, it is of great significance to develop a complete navigation and positioning system which is suitable for intelligent vehicle platform and existing laboratory equipment.

In order to improve the accuracy and reliability of the navigation positioning system, the vehicle navigation system positioning control algorithm based on wireless tracking technology is designed. The positioning control algorithm of vehicle navigation system is the core of this paper, including lane tracking algorithms and lane departure algorithms.

The innovation point of this paper is that it does not rely on one kind positioning and navigation system control algorithm, but instead combines multiple algorithms to make the positioning more accurate. Based on the equipment configuration of the current intelligent vehicle platform, the paper designs a new algorithm based on loose combination and decentralized extended Kalman filter, which makes full use of the complementary characteristics of GPS and inertial system in navigation and positioning information; second, in order to make the navigation and positioning of intelligent vehicles more accurate, a more detailed GPS coordinate conversion algorithm is adopted to replace the traditional GPS localization protocol used in the document [1], and the information preprocessing mechanism of GPS positioning system and inertial system is introduced; third, in order to realize the visualization effect of intelligent vehicle navigation and positioning, the software integrates the secondary development of MapX map control and draws the vehicle position and driving path in real time by using the dynamic layer principle and map matching algorithm; finally, the above algorithm is tested in the intelligent vehicle platform [4]. The feasibility of the algorithm is verified by real vehicle control, and the whole design intention of establishing a complete navigation and positioning system is achieved. Experiments also demonstrate that the present design has higher system accuracy and reliability compared to existing literature methods.

## 2. The Positioning Control Algorithm of Vehicle Navigation System

*2.1. Positioning Function Optimization of Vehicle Navigation System.* With the increasing number of urban vehicles, how to effectively command, dispatch, and manage public service vehicles and some special vehicles in the city has become an important problem faced by transportation departments and urban planning departments. Therefore, vehicle navigation and positioning system have attracted more attention. With the development of wireless communication and mobile communication network, vehicle navigation and positioning technology are developing rapidly [5]. The basic function block diagram of modern vehicle navigation and positioning is shown in Figure 1.

At present, the main application types of vehicle navigation and positioning technology are automatic navigation system, fleet management system, consultant navigation system, information storage system, and portable system [6]. There are three types of vehicle navigation and positioning system: autonomous, nonautonomous, and combined. The

autonomous vehicle navigation and positioning system uses the inertial principle of navigation; uses the distance sensor, direction sensor, and other sensors to measure the displacement and heading information of the vehicle; and calculates the position of the vehicle. In the research of intelligent vehicle safety assistant driving system, navigation and positioning module is one of the most important parts [7]. It is responsible for providing accurate location information for the vehicle and informing the vehicle of the path and direction to be driven. After obtaining the information, it is transmitted to the information processing module through various interfaces. Only when the components in the navigation and positioning module work stably and reliably, the functions of auxiliary driving and vehicle control can play a role [8]. In this paper, the differential GPS and inertial navigation elements are used to provide relevant information for the vehicle, and the vehicle position is informed in real time, so that it will not be lost in the road. This chapter will mainly introduce the working principle and characteristics of differential GPS and inertial navigation system, as well as the integrated navigation and positioning mode as Figure 2.

The basic positioning principle of GPS is the satellite sends its own ephemeris parameters and time information continuously [9]. After receiving the information, the user calculates and calculates the three-dimensional position, three-dimensional direction, motion speed, and time information of the receiver. Suppose that the GPS time and satellite clock time of satellite signal are expressed in  $t$ , respectively. The GPS time and receiver clock time when the receiver receives the satellite signal are expressed by  $T_G$  and  $T_R$ , respectively [10]. Therefore, the satellite clock deviation  $\Delta t_S^j$  and the clock deviation of the receiver  $\Delta t_R$  can be calculated as follows:

$$\begin{cases} \Delta t_S^j = t_S^j - t_G^j, \\ \Delta t_R = T_R - T_G, \\ \tau_R^j = (T_G - t_G^j) + \Delta t_R - \Delta t_S^j. \end{cases} \quad (1)$$

In formula (1),  $t_S^j$  expresses the satellite time when the receiver receives the satellite signal  $j$ ,  $t_G^j$  expresses the GPS time when the receiver receives the satellite signal  $j$ ,  $\tau_R^j$  expresses the GPS time deviation of the receiver receiving the satellite signals.

Inertial navigation system (INS) is a kind of navigation method which uses the internal information of vehicle to calculate the position and attitude information of vehicle through inertial sensors, such as gyroscope, accelerometer, and angle sensor [11]. Navigation and positioning system mainly provides accurate vehicle position and attitude information for vehicle navigation control, such as vehicle position coordinates, heading angle, front wheel angle, and driving speed [12]. In this study, the Futian Ou Bao 4040 tractor is taken as the research object. The heading angle sensor, the angle sensor, and the speed sensor are installed on the tractor, respectively. The angle sensor is a multicircle

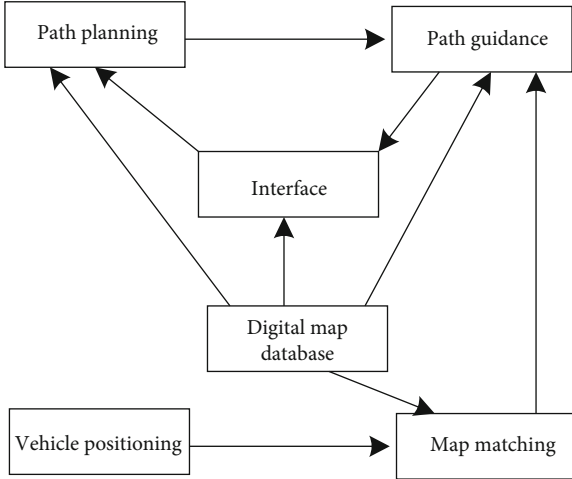


FIGURE 1: Functional block diagram of vehicle navigation and positioning.

hollow angle sensor, using Witterson technology “magnetic-Angle displacement detection.” Even if the mechanical displacement is generated after power loss, a high-reliability measurement of the real-time absolute angle can be achieved after recharging. The speed sensor has embedded precision integrated circuit for equipment fault absolute vibration speed measurement. The vehicle status information detected by the sensor is input into the computer through a certain interface, and the vehicle position coordinates are calculated by the computer [13]. The hardware structure of the test system is shown in Figure 3.

The heading angle sensor is the MTI (“MTI” is the brand name of the US sensor) type sensor produced by *x* sense company of the Netherlands. The sensor is a microelectro mechanical system integrating gyroscope, acceleration sensor, and geomagnetic sensor. Its internal low-energy signal processing system can provide zero drift 3D (3-Dimension) direction information, 3D acceleration, and 3D angular velocity information, which can be used in robot, aerospace, navigation, and other fields. There are good application prospects in the fields of navigation and autonomous vehicles.

The sensor is suitable for the PC equipped with serial port. By integrating the 3D acceleration signal, 3D angular velocity, and 3D geomagnetic field signal detected by the internal sensor, three Euler angles of the sensor dynamic coordinate system are obtained: roll, pitch, and yaw. The sensor base is bolted to the tractor, and the measured yaw angle is the vehicle heading angle. The sensor is equipped with geomagnetic sensor. Because the earth magnetic field is weak and the sensor and it is easy to be affected by the surrounding magnetic field, the sensor should be far away from the strong magnetic field as far as possible and suitable position shall be selected for installation [14]. The selected heading angle sensor has an angular resolution of 0.050, a static precision of less than 0.50, and a dynamic precision of less than 20. It can measure all the angle values in the 3D range. The sampling frequency can be adjusted to 120 Hz at the maximum according to the needs of the user. When measuring vehicle speed, the sensor is installed on the engine fly-

wheel housing, and the sensor is kept at a proper distance from the flywheel [15]. When the engine is rotating, the concave and convex changes of the tooth on the flywheel make the output voltage of the sensor change. Through the internal amplifying and shaping circuit, the sensor outputs a square wave signal with stable amplitude, and the engine speed  $n_1$  can be obtained by measuring the frequency  $P$  of square wave high and low voltage change in a certain time  $R$  interval of  $T_4$ . If the throttle is kept constant, the transmission ratio  $K_1$  of engine speed  $n_1$  and wheel speed  $n_2$  remains basically the same [16]. Without considering the vehicle sliding, the sensor obtains engine speed, and wheel speed and vehicle speed are calculated as follows:

$$\begin{cases} v = 2n_2\pi R, \\ n_2 = n_1K_1, \\ n_1 = \frac{\Delta tz}{p}. \end{cases} \quad (2)$$

The course deviation measured in eight directions is made into a curve, and the output course angle of the sensor is corrected by using the curve to obtain the accurate course angle value, as shown in Table 1.

According to the geometric relationship between the virtual front wheel angle and the real front wheel angle, the functional relationship between them can be obtained as follows:

$$\text{ctg}\alpha = \text{ctg}\beta + \frac{B}{2L}, \quad (3)$$

where  $B$  is the center distance between the left and right front wheels, and  $L$  is the distance between the front and rear axles of the tractor. Using the formula, the virtual front wheel angle can be calculated according to the detected right front wheel angle. The measurement of vehicle speed is realized through the detection of engine speed:

$$v = 2\pi RK_1 n_1. \quad (4)$$

If the tire pressure is constant, the rear wheel radius  $R$  of the vehicle remains unchanged. In the same gear,  $K$  is the constant value, so that  $K = 2\pi zRK$ ,  $K$  are also fixed values, the calculation formula of vehicle speed can be obtained as follows:

$$v = Kn_1. \quad (5)$$

Let a linear time invariant continuous time system be

$$\begin{cases} \dot{x} = Ax + Bu, \\ y = Cx. \end{cases} \quad (6)$$

After discretization, the difference equation of the system is obtained as follows:

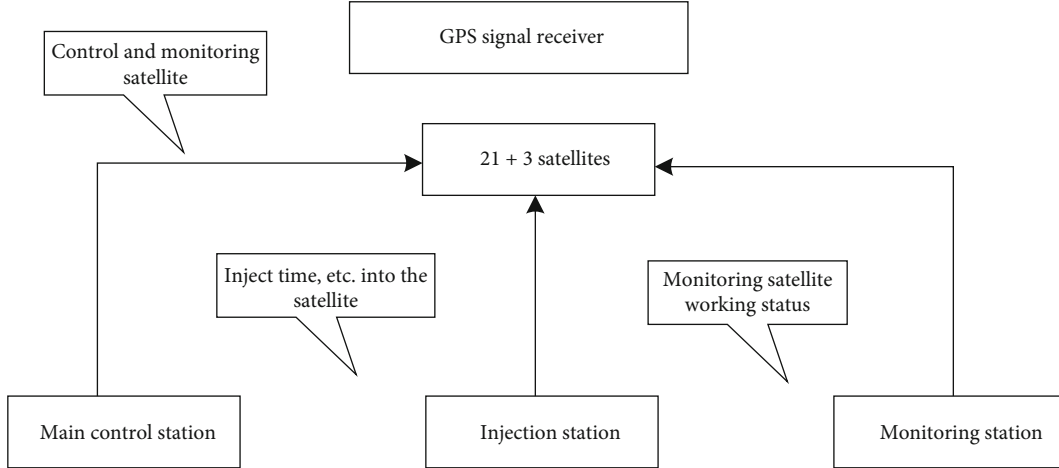


FIGURE 2: Composition of GPS positioning system.

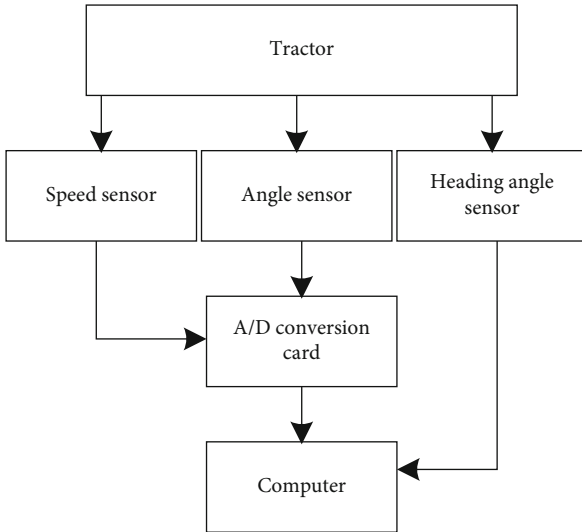


FIGURE 3: Composition block diagram of navigation and positioning system.

$$\begin{cases} x_k = G_d x_{k-1} + H_d u_{k-1}, \\ y_k = C x_k. \end{cases} \quad (7)$$

According to the above formula, as long as the initial state of the system is known, the state parameters and output values at any time can be predicted, but there are always interference and noise in practice, which makes the calculated values deviate from the actual state. Considering the system input noise and measurement noise, the equation can be rewritten as

$$\begin{cases} x_k = G_d x_{k-1} + H_d u_{k-1} + \omega_{k-1}, \\ y_k = C x_k + v_{r,k}. \end{cases} \quad (8)$$

*2.2. Positioning Data Processing Algorithm of Vehicle Navigation System.* The processing of vehicle navigation

and positioning data plays an important role in the navigation and positioning system. It is not only the basis of map matching but also the data source of the whole positioning process, which affects the effect of map matching to a large extent. The current navigation and positioning system mainly include GPS positioning system and Dr positioning system, but each of them has its advantages and disadvantages. A single positioning system cannot guarantee good positioning effect [17]. Therefore, how to make it better and make up for short is the key problem to solve the problem of vehicle navigation and positioning data processing. GPS is a passive ranging system. In passive ranging system, users measure the propagation delay by comparing the received satellite signals and local reference signals; if the satellite clock and the user clock are synchronized, that is, the two clocks are synchronized in the same frequency or known difference, the measured propagation delay  $t$  is proportional to the distance  $d$  between the satellite and the user, i.e., the distance  $d$  between the satellite and the user:

$$d = ct. \quad (9)$$

In fact, there is an unknown clock difference  $4t$  between the user clock and the satellite clock. At this time, the measured propagation delay  $t$  and the corresponding distance  $P$  are not the real radio wave propagation delay  $T$  and the distance  $d$  from the satellite to the user. At this time,  $P$  is called pseudorange:

$$\rho = d + c\Delta t. \quad (10)$$

To minimize the localization distance bias caused by the aforementioned signal propagation time delay, lateral auxiliary control of the lane deviation is required. The premise and basis of lateral assistant control of lane departure are to judge whether the vehicle has lane departure or not, that is, to judge whether the error between the vehicle trajectory and the expected track is less than the allowable threshold of vehicle safe driving [18]. The process of lane departure judgment is mainly divided into two stages: lane line recognition

TABLE 1: Secondary calibration data of sensor (unit: degree).

	1	2	3	4	5	6	7	8
Actual heading angle	0	40.4	88.7	143.1	178.5	217.1	269.7	316.3
Sensor output	1.1	37.2	86.1	141.5	176.8	215.9	272.2	320.2
Deviation value	1.1	-3.2	-2.6	-1.6	-1.7	-1.2	2.5	3.9

and tracking, and lane departure judgment. The following is a detailed analysis.

The first stage task is lane recognition and tracking.

Lane departure means that vehicles are not within the range of lane line, so lane line recognition and tracking are very important [19]. The specific process of lane recognition and tracking is as follows:

*Step 1.* Arrange cameras on the vehicle to collect sequence image information.

*Step 2.* Preprocess the acquired image sequence, including graying, image filtering, and lane edge point filtering.

*Step 3.* Vanishing point detection, that is, to detect the lane feature points from the lane feature map.

*Step 4.* According to the detected vanishing points, the image is clipped to obtain the region of interest.

*Step 5.* In the region of interest, collect the four points in the lane edge line.

*Step 6.* Make the confidence judgment and lane width information to supplement the lane line under the condition of fuzzy, shadow, or vehicle occlusion, so as to realize the detection of lane line.

*Step 7.* Lane tracking. According to the identified lane line, the lane line is recognized again in the next frame, namely, lane line tracking. In this link, the Kalman filter tracking method is used to realize the lane tracking operation.

Second stage task is deviation judgment.

In this stage, a lane departure algorithm is selected to judge the lane departure and realize the departure warning. At present, lane departure algorithms mainly include the following, as is shown in Table 2.

According to the above table, each lane departure algorithm has some shortcomings [20]. Therefore, the algorithm based on the current position of the vehicle and the algorithm based on the time of vehicle crossing the lane line are combined to judge the lane departure. The principle formula is as follows:

$$S = S_{CCP} \cup S_{TLC} = \begin{cases} 1, S_{CCP} = 1 \text{ or } S_{TLC} = 1, \\ 0, \text{ other.} \end{cases} \quad (11)$$

Among them:

$$S_{CCP} = \begin{cases} 1, d_L \leq T_{CCP} \text{ or } d_R \leq T_{CCP}, \\ 0, \text{ other,} \end{cases} \quad (12)$$

$$S_{TLC} = \begin{cases} 1, t_{TLC} \leq T_{TLC}, \\ 0, \text{ other,} \end{cases} \quad (13)$$

where  $S_{CCP}$  represents the output result of the algorithm based on the current position of the vehicle;  $S_{TLC}$  represents the output result of the algorithm based on the time of vehicle crossing the lane line;  $d_L$  represents the lateral distance from the left wheel of the vehicle to the left lane line;  $d_R$  represents the lateral distance between the right lane and the right lane of the vehicle;  $T_{CCP}$  represents the distance threshold;  $t_{TLC}$  represents the time to cross the lane line;  $T_{TLC}$  represents the time threshold. When there is deviation trend, it will send early warning signal to the control system in time to trigger the lateral control procedure of lane keeping and correct the deviation in time to make it return to the safe range and ensure the safety of vehicles.

*2.3. Realization of Positioning Control in Vehicle Navigation System.* In the lateral assistant control of vehicle lane departure, the algorithm depends on vehicle system model and driver model, so it is necessary to establish appropriate vehicle model and driver model before the implementation of the control algorithm. The former is to determine the desired vehicle motion state, and the latter is to obtain the required optimal steering wheel angle. The formula of the model equation is as follows:

$$\begin{bmatrix} \dot{\beta} \\ \dot{\omega} \end{bmatrix} = \begin{pmatrix} a_{11} & a_{12} \\ a_{21} & a_{22} \end{pmatrix} \begin{bmatrix} \beta \\ \omega \end{bmatrix} + \begin{bmatrix} (2 \cdot C_f / m \cdot v) \\ 2 \cdot C_f \cdot l_f / I_z \end{bmatrix}, \quad (14)$$

where

$$a_{11} = -\frac{2(C_r + C_f)}{m \cdot v}, \quad (15)$$

$$a_{12} = -1 + \frac{2(l_r C_r - l_f C_f)}{m \cdot v^2}, \quad (16)$$

$$a_{21} = \frac{2(l_r C_r - l_f C_f)}{I_z}, \quad (17)$$

$$a_{22} = -\frac{2(l_r^2 C_r + l_f^2 C_f)}{I_z \cdot v}. \quad (18)$$



TABLE 2: Comparison of lane departure algorithms.

Algorithm	Definition	Characteristic
Algorithm based on vehicle current position	According to the distance between the vehicle tire and the left and right lane lines, it can judge whether the vehicle deviates	The advantages are high precision; the disadvantage is that the reserved reaction time is short
Algorithm based on future preview offset	By comparing the lateral position of the vehicle in the forward-looking time with the virtual boundary, the deviation problem can be judged	The advantage is that the structure of the algorithm is simple; the disadvantage is that the virtual lane is difficult to determine
Algorithm based on vehicle crossing lane time	According to the time of the vehicle crossing the lane line to judge whether the vehicle touches the boundary	The advantages are simple algorithm, easy parameter measurement, low false alarm rate, long reserved reaction time, and low accuracy.
Algorithm based on prediction trajectory	The evaluation is based on the deviation between the predicted trajectory and the target trajectory after a period of time	The advantage is that the algorithm is easy to implement; the disadvantage is that it is more suitable for straight deviation judgment

Driver control model:

$$\delta_d = \arctan \left[ \frac{2L}{L_p^2} (\Delta y_p - L_p \beta) \right], \quad (19)$$

$$L_p = uT_p. \quad (20)$$

In the formula, the parameters of vehicle system model and driver model are shown in Table 3.

Both electric power steering control and differential braking control are important algorithms for lateral auxiliary control of vehicle lane departure. Among them, the former control idea is to determine whether the deviation problem occurs through deviation detection. In case of deviation, early warning is given and control signal is output to automatically control the steering wheel rotation of the vehicle, so as to maintain the lateral position deviation of the vehicle within the specified range and turn the vehicle back to the right track of the lane. In this process, the key lies in the role of BP (back propagation) neural network PID (proportion integral differential) controller. The optimal steering wheel angle is obtained through the driver model, and then it is input into the BP neural network PID controller. After the BP neural network PID controller operation, the target auxiliary torque is obtained. The specific calculation formula of the target auxiliary torque is as follows:

$$J = \frac{1}{2} \sum_{k=1}^n [r(k) - r_d(k)]^2. \quad (21)$$

In formula (21),  $r(k)$  expresses the ideal pendulum velocity in the input PID controller,  $r_d(k)$  expresses the actual pendulum angle velocity, and  $k$  indicates the wheel-base of the vehicle [21].

Finally, the man-machine coordinated control is realized by combining the actual operation torque of the driver and the lateral position deviation of the vehicle relative to the lane centerline. The latter control idea is to first determine the desired vehicle motion state, that is, the ideal yaw rate, based on the driver model, and then take the ideal yaw rate

as the input of BP neural network PID controller. After calculation, the ideal yaw moment is obtained. Finally, this parameter is reasonably distributed to the four wheels of the vehicle, and the braking system controls the vehicle to return to the normal lane.

Although both of the above methods can realize the control of vehicle deviation, both methods are difficult to meet the control requirements under various conditions. The electric power steering control is more suitable for the deviation correction in straight road, and differential braking control is more suitable for deviation correction in curve. Therefore, this chapter combines the two and proposes an extension joint lateral auxiliary control method. The method is based on the road adhesion coefficient and the initial steering wheel angle. The extension set is divided into four regions, namely, classical domain, extension domain, and nondomain. Different control strategies are adopted for each area as shown in Table 4.

The principle equation of extension joint lateral auxiliary control is as follows:

$$u(t) = \begin{cases} u(DBC), K(S) \geq 0, \\ (1 + K(S))u(DBC) - K(S)u(EPs), -1 \leq K(S) < 0, \\ u(EPs), K(S) < -1, \end{cases} \quad (22)$$

where  $u(t)$  represents the controller output;  $u(DBC)$  represents the output of differential braking control;  $(1 + K(S))u(DBC) - K(S)u(EPs)$  represents the output under the cooperative operation of differential braking control and electric power steering control;  $u(EPs)$  represents the control output of electric power steering;  $K(S)$  represents the value of the correlation function obtained by the characteristic state  $S$ . GPS/DR integrated navigation mode. When GPS signal is lost and cannot be located, the GPS position calculation system can continue to work and the reliability of the system is improved. However, when the vehicle is in the urban area with dense roads, it is impossible to use the digital map matching technology to further correct the GPS

TABLE 3: Parameter description of vehicle system model and driver model.

Parameter	Meaning	Parameter	Meaning
$m$	Vehicle mass	$L$	Wheelbase
$v$	Vehicle longitudinal speed	$L_p$	Preview range
$I_z$	Moment of inertia of vehicle around vertical axis	$\beta$	Sideslip angle of mass center
$C_f, C_r$	Equivalent cornering stiffness of front and rear tires	$\Delta y_p$	Lateral deviation at preview point
$l_f, l_r$	Distance from the center of mass of the whole vehicle to the front and rear axles	$T_p$	Preview time
$\delta_d$	Optimal steering wheel angle	$u$	Vehicle longitudinal speed

TABLE 4: Extension joint lateral auxiliary control strategy.

Extension set	State characteristics	Control strategy
Classical domain	The road adhesion coefficient is large and the initial steering angle is small	Differential braking control
Nondomain	When the road adhesion coefficient is small and the initial steering wheel angle is large	Electric power steering control
Extension field	Between nondomain and classical domain	Coordinated operation of differential braking control and electric power steering control

positioning information and the positioning information of the GPS positioning system, as is shown in Figure 4.

GPS/DR/M integrated navigation mode. It overcomes the disadvantages of GPS/MM and GPS/DR, which is an ideal independent combination. But the matching map must have high precision, so it can achieve high positioning accuracy and navigation system reliability. Although it is possible to apply all the positioning technologies to vehicle positioning, due to the cost and coverage, the low-cost GPS receiver and the inertial sensor with the increasing performance price ratio and the increasingly widespread digital map make GPS/DR/MM technology become the mainstream of vehicle combination positioning technology.

### 3. Analysis of Experimental Results

Taking CarSim as a tool and based on the collected information, the system model and driver model of intelligent vehicle are built by using simulation software CarSim and MATLAB. The basic data required are shown in Table 5.

In order to further explain the characteristics of integrated navigation positioning mode, the test of sports car is carried out by using the designed system proposed by Lin and Liao [1], the designed system proposed by Su et al. [2], and GPS/GLONASS/mm integrated navigation (design of this article) to verify the accuracy and reliability of integrated navigation positioning. GPS/GLONASS integrated navigation and positioning has 24 parallel channels and simultaneously receives 24 satellites from GPS/GLONASS two systems. The two systems backup each other and are no longer subject to the constraints and control of the U.S. military. The coverage of satellites is expanded, and the number of satellites that can be used for positioning calculation is increased, so that the strength of satellite geometry is better. Moreover, GLONASS satellite system has no SA impact,

GPS/GLONASS does not need difference, and the accuracy of single machine positioning can be about 15 m, which can get rid of the trouble of SA or differential communication. The speed measurement accuracy can be as high as 0.02 m/s, even better than that of differential GPS. This is because the system designed in this paper combines multiple systems to make full use of the complementarity of GPS and inertial systems in navigation and positioning information, using a more detailed GPS coordinate conversion algorithm, using dynamic layer principle and map matching algorithm in real time, thus, has higher system accuracy and reliability. In this way, it is more conducive to uninterrupted positioning in multiocclusion environment and realize full field tracking measurement. At the same time, RAIM is enhanced, which can benefit from two independent global positioning systems, increase the geometric strength of satellites and the number of positioning combinations, and effectively judge the health status of satellites, so as to improve the integrity of the whole system. GPS/GLONASS/mm three integrated navigation and positioning can make up for the inherent defects of GPS and GLONASS single system, eliminate the problem of perfection, and use digital map matching technology to further correct GPS/GLONASS integrated positioning information, so as to improve the accuracy of its navigation and positioning. The performances of the designed system proposed by Lin and Liao [1], the designed system proposed by Su et al. [2], and GPS/GLONASS/mm integrated navigation (design of this article) are tested, respectively. Roadcar test curves result for three navigation systems as shown in Figure 5.

From the graph and curve, the positioning accuracy of GPS/GLONASS integrated navigation is higher than the designed systems proposed by Lin and Liao [1] and Su et al. [2], especially when driving at the corner and under the overpass, the positioning accuracy of GPS/GLONASS

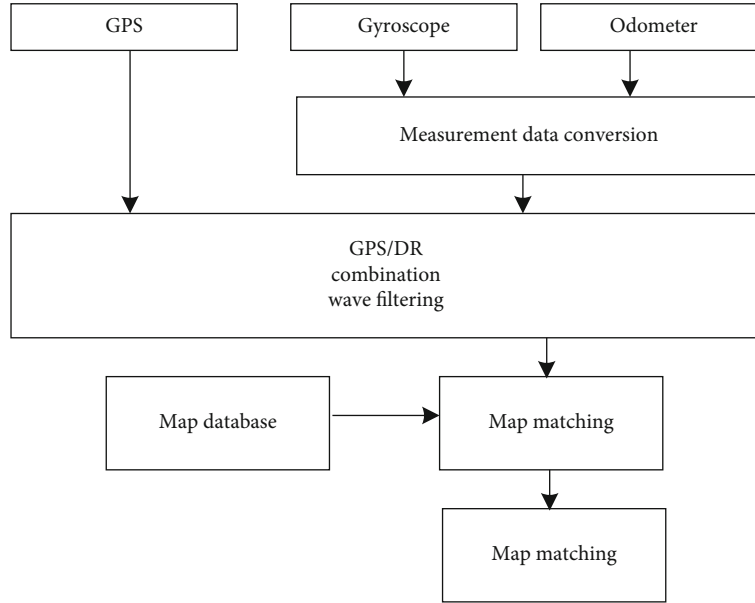


FIGURE 4: GPS/DR/M integrated navigation and positioning control steps.

TABLE 5: Intelligent vehicle information.

Parameter name	Numerical value	Parameter name	Numerical value
Vehicle mass (kg)	1231	Front wheel track (mm)	1481
Sprung mass (kg)	1111	Rear wheel track (mm)	1486
Vehicle width (mm)	1695	Kingpin inclination (deg)	13.7603
Car height (mm)	1535	Caster angle (deg)	3.000056
Wheelbase (mm)	2600	Left and right front wheel brake pressure (Nm/MPa)	250
Distance from centroid to front axle (mm)	1040	Left and right rear wheel brake pressure (Nm/MPa)	150
Distance from centroid to ground (mm)	540	Tire size	185/65R15
Wheelbase (m)	2.6	Sideslip angle of mass center	35°
Preview range (m)	16	Lateral deviation at preview point (m)	0.5
Preview time (s)	0.5	Vehicle longitudinal speed (m/s)	100

integrated navigation is more obvious than the designed systems proposed by Lin and Liao [1] and Su et al. [2], and its positioning accuracy is generally about 18 m. This is because this paper designs a new algorithm based on loose combination and decentralized extended Kalman filtering, using a more detailed GPS coordinate conversion algorithm, replacing the traditional GPS localization scheme, and the software design integrates the secondary development of MapX map control, which significantly improves the positioning accuracy of the system. The figure shows the test curve of GPS/GLONASS/mm three integrated navigation for sports car, as is shown in Figure 6.

The scale of digital map is 1:6000. In the GPS/DR/mm integrated navigation mode, digital map is not only a digital traffic map, behind the digital map is a geographic information database, which should contain all the geographic codes. These geographic information should be corresponding to the two-dimensional or three-dimensional coordinates, because GPS positioning adopts the coordinate mode, and people often only know the destination of the

vehicle rather than the coordinates. The matching accuracy of coordinate point and address should be within 15 m, so that the driver can easily and accurately find the target. When the coordinate value of the positioning system deviates from the road chain of the digital map, the digital map should find the nearest road chain according to a certain algorithm and match the vehicles back. With the driving of the vehicle, the shape of the route should be determined according to the change of the direction of the vehicle and the journey, and it should match with the road network on the map. Map matching algorithm requires high accuracy of the map itself, and map matching is also used to smooth the noise of positioning sensor or positioning system. The system should also be able to determine the best driving route according to the best route algorithm, driving time, driving distance, and other special criteria based on the digital road map. The determination of the best route is not a simple calculation of the shortest route; it needs a lot of map information. The digital map must contain the driving direction and turning limit of each road chain, so as to avoid

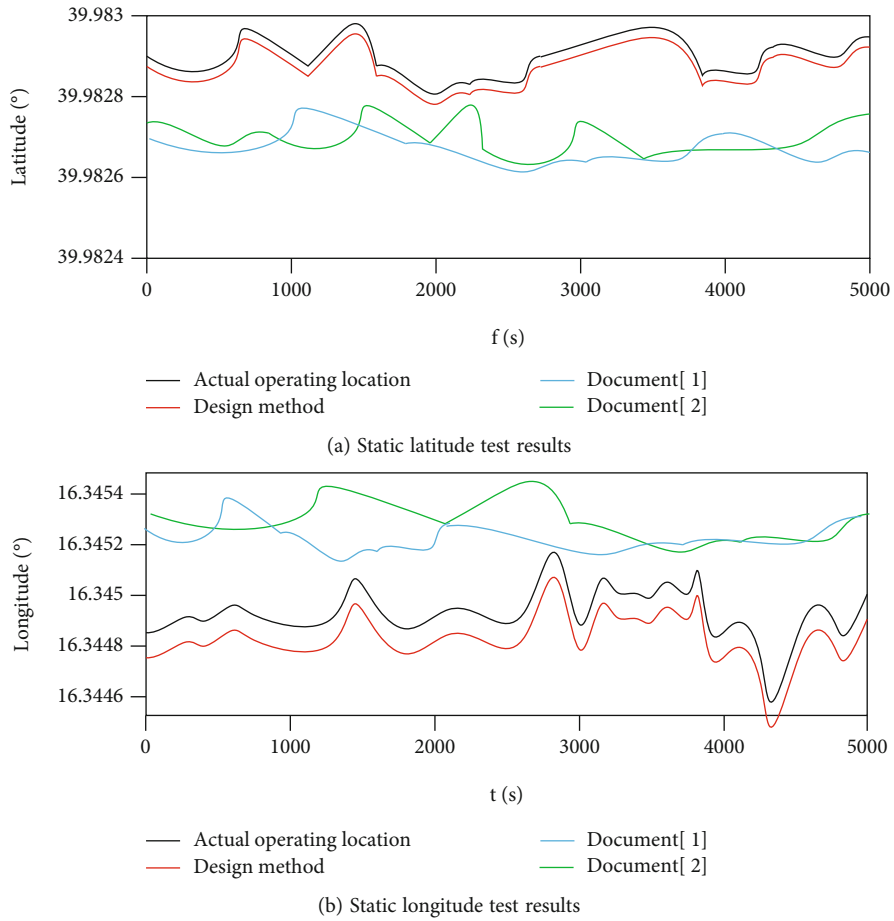


FIGURE 5: Static control test results of GS/GLONASS integrated navigation system.

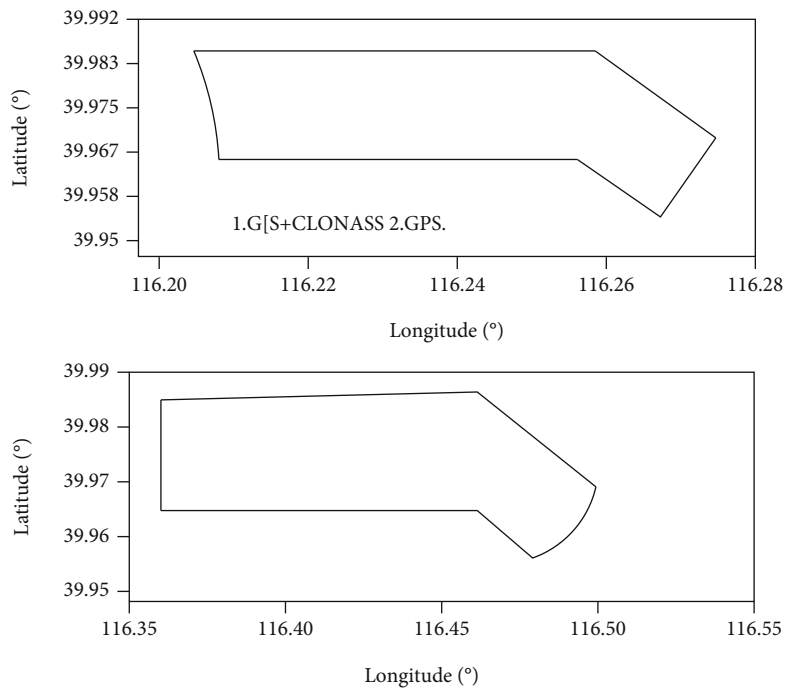


FIGURE 6: Positioning control test curve of GPSGLONASSMM integrated navigation sports car.

the consequences of illegal turning and entering one-way road. The display of the map should have the display function of general graphics, such as local magnification, roaming, and layering. The position of the vehicle shall be indicated on the screen with a certain symbol. For the vehicle positioning and navigation system, the realization of many functions depends on some special features of the geographic information in the digital map, which also shows that the success of vehicle positioning and navigation is directly related to the accuracy and integrity of the digital map and its information.

#### 4. Conclusions

To enhance the positioning accuracy of the vehicle positioning control system, in this paper, the navigation and positioning technology of intelligent vehicle is studied, and the common methods of vehicle positioning and the configuration characteristics and functional characteristics of existing intelligent vehicle navigation and positioning sensors are analyzed. A combined localization algorithm based on loose combination and decentralized extended Kalman filter is designed and matched with the map to display the accurate driving route in the map in real time. According to the function of each module, the communication mode between each module is set, and the positioning information is shared with other control terminals. Finally, through MATLAB simulation and real vehicle test, the design method can improve the accuracy and reliability of the vehicle positioning control and further improve the vehicle operation efficiency and safety. However, due to the limited conditions, the localization system studied in this paper mainly improves the localization accuracy and reliability, but does not significantly improve the localization speed, and future studies can further reduce the localization time.

#### Data Availability

The data used to support the findings of this study are available from the corresponding author upon request.

#### Conflicts of Interest

The authors declare that there is no conflict of interest regarding the publication of this paper.

#### Acknowledgments

This work was supported by the Key Scientific and Technological Project of Henan Province (grant number 212102210558) and Doctoral Research Start Project of Henan Institute of Technology (grant number KQ1852).

#### References

- [1] J. Lin and P. Liao, "Design of vehicle positioning monitoring system for construction machinery based on Beidou/GPS," *Manufacturing Automation*, vol. 41, no. 10, pp. 53–57, 2019.
- [2] X. G. Su, L. L. Yang, X. Q. Peng et al., "Application of carrier phase difference technology in vehicle navigation," *Modern Navigation*, vol. 4, pp. 262–267, 2019.
- [3] J. Hu, Y. J. Yan, and J. H. Wang, "Vehicle integrated navigation based on velocity constraint and fuzzy adaptive filtering," *Acta Armamentarii*, vol. 41, no. 2, pp. 231–238, 2020.
- [4] W. Cai, R. Q. Yao, and Z. Y. Wang, "Temperature field modeling and model universal analysis of a civil car hood," *Computer Simulation*, vol. 36, no. 8, pp. 122–128, 2019.
- [5] S. Yabui, T. Atsumi, and T. Inoue, "Coupling controller design for miso system of head positioning control systems in HDDs," *IEEE Transactions on Magnetics*, vol. 56, no. 5, pp. 1–9, 2020.
- [6] J. Kim, M. Park, and Y. Bae, "A low-cost, high-precision vehicle navigation system for deep urban multipath environment using TDCP measurements," *Sensors*, vol. 20, no. 11, p. 3254, 2020.
- [7] V. Ilci and C. Toth, "High definition 3D map creation using GNSS/IMU/LiDAR sensor integration to support autonomous vehicle navigation," *Sensors*, vol. 20, no. 3, p. 899, 2020.
- [8] A. B. Toropov, A. V. Loparev, and A. E. Pelevin, "Comparing underwater vehicle positioning algorithms using single-beacon navigation," *Journal of Physics: Conference Series*, vol. 1864, no. 1, p. 012028, 2021.
- [9] Y. Ji, Y. Tanaka, and Y. Tamura, "Adaptive motion planning based on vehicle characteristics and regulations for off-road UGVs," *IEEE Transactions on Industrial Informatics*, vol. 15, no. 1, pp. 599–611, 2019.
- [10] C. Yang, J. Strader, and Y. Gu, "Cooperative navigation using pairwise communication with ranging and magnetic anomaly measurements," *Journal of Aerospace Information Systems*, vol. 8, no. 3, pp. 1–10, 2020.
- [11] R. B. Issa, M. Das, and M. S. Rahman, "Double deep Q-learning and faster R-Cnn-based autonomous vehicle navigation and obstacle avoidance in dynamic environment," *Sensors*, vol. 21, no. 4, p. 1468, 2021.
- [12] M. Moussa, S. Zahran, and M. Mostafa, "Optical and mass flow sensors for aiding vehicle navigation in GNSS denied environment," *Sensors*, vol. 20, no. 22, p. 6567, 2020.
- [13] L. Barker, M. V. Jakuba, and A. D. Bowen, "Scientific challenges and present capabilities in underwater robotic vehicle design and navigation for oceanographic exploration under-ice," *Remote Sensing*, vol. 12, no. 16, p. 2588, 2020.
- [14] R. Abdallah, J. Vilà-Valls, and G. Pagès, "Robust LCEKF for mismatched nonlinear systems with non-additive noise/inputs and its application to robust vehicle navigation," *Sensors*, vol. 21, no. 6, p. 2086, 2021.
- [15] A. Stateczny, W. Kazimierski, and D. Gronska-Sledz, "The empirical application of automotive 3D radar sensor for target detection for an autonomous surface vehicle's navigation," *Remote Sensing*, vol. 11, no. 10, p. 1156, 2019.
- [16] K. W. Chiang, D. T. Le, and T. T. Duong, "The performance analysis of INS/GNSS/V-SLAM integration scheme using smartphone sensors for land vehicle navigation applications in GNSS-challenging environments," *Remote Sensing*, vol. 12, no. 11, p. 1732, 2020.
- [17] P. Z. Schulte and D. A. Spencer, "State machine fault protection architecture for aerospace vehicle guidance, navigation, and control," *Journal of Aerospace Information Systems*, vol. 17, no. 3, pp. 1–16, 2020.
- [18] M. Maaref and Z. M. Kassas, "Autonomous integrity monitoring for vehicular navigation with cellular signals of



- opportunity and an IMU,” *IEEE Transactions on Intelligent Transportation Systems*, vol. 99, pp. 1–16, 2021.
- [19] L. Castigliola, F. Causa, and M. Grassi, “Navigation architecture for hypersonic aircraft,” *MATEC Web of Conferences*, vol. 304, no. 5, p. 04008, 2019.
- [20] D. C. Guastella and G. Muscato, “Learning-based methods of perception and navigation for ground vehicles in unstructured environments: a review,” *Sensors*, vol. 21, no. 1, p. 73, 2021.
- [21] Y. B. Yan, Z. Y. Zhang, X. W. Xu et al., “PID control of independent drive electric vehicle stability based on neural network,” *Mechanical Science and Technology for Aerospace Engineering*, vol. 38, no. 10, p. 8, 2019.

## Research Article

# Optimization of Hotel Financial Management Information System Based on Computational Intelligence

Hongmei Ma 

*School of Business Administration, Tourism College of Zhejiang, Hangzhou 311231, China*

Correspondence should be addressed to Hongmei Ma; [mhm@tourzj.edu.cn](mailto:mhm@tourzj.edu.cn)

Received 30 August 2021; Revised 30 October 2021; Accepted 1 November 2021; Published 30 November 2021

Academic Editor: Deepak Gupta

Copyright © 2021 Hongmei Ma. This is an open access article distributed under the Creative Commons Attribution License, which permits unrestricted use, distribution, and reproduction in any medium, provided the original work is properly cited.

Nowadays, the hotel management concept cannot keep pace with the times. Traditional concepts are often adopted to manage hotel financial personnel, for the hotel financial personnel cannot take timely and effective training. All these lead to the hotel financial staff designing the hotel's related business without sufficient understanding of the hotel industry and judging and deciding if they do not master the hotel's professional knowledge, which makes the participating projects unable to give correct and reasonable answers to the substantive problems of the hotel. This leads to the hotel management not going up; extensive management makes the hotel benefit not go up. Hotel intelligent technology can solve these problems and not only save manpower and material resources but also intelligently predict the financial crisis of hotels. In the context of the accelerated development of globalization and informatization, there are still many problems in the financial management process of my country's hotel industry. Based on these questions, the article draws on foreign advanced experience, puts forward effective suggestions in financial management, and uses computational intelligence technology to design a centralized and intelligent financial management system. The research results show the following: (1) the financial crisis model is created by using the principle of support vector machine and logistic regression method, which greatly reduces the financial crisis of the enterprise. (2) The system can straightforwardly summarize the data for easy query. Taking three domestic hotels as an example, a comprehensive study has been carried out on the three aspects of pricing assessment risk, financial integration risk, and debt risk. In 2016, the financial leverage coefficient has been relatively high, the quick ratio has fluctuated greatly, and the interest protection coefficient has shown a downward trend. (3) The performance of the system is compared with traditional development mode, framework development mode, and intelligent optimization mode. The intelligent optimization system has the lowest response time and the highest success rate. The new system has reduced response time by about 57% compared with the original response time, and the access success rate has been greatly improved.

## 1. Introduction

The arrival of the information age has given new meaning to hotels. Traditional hotel financial management models can no longer meet today's needs, so it is inevitable to apply intelligence to hotel financial management. Literature [1] pointed out the problems existing in the financial management process of the hotel industry in our country. According to these problems, we need to reform and innovate the existing financial management system and continuously optimize the hotel's financial management system. Literature [2] explains the basic principles of financial management in the hotel industry. Literature [3] proposed an intelligent financial

management system. This system is a system designed based on Python. It has many potential benefits. It can help the hotel better control costs, improve the hotel's core competitiveness, and lay the foundation for the hotel's long-term development. At present, most hotels have applied information management to all parts of the hotel, especially in terms of financial management. Whether the hotel has a complete financial management system is directly related to the long-term development of the hotel. Literature [4] proposed a fuzzy-based analytic hierarchy process (FAHP) to consider user perception to access decision-making. Use computing intelligence to extract hotel information, establish customer models, realize the hotel's "customer-centric" concept,

improve the hotel's core competitiveness, and lay a solid foundation for the hotel's long-term development. Literature [5] develops a powerful and reliable model for evaluating the quality of hotel websites. The resulting model can evaluate the hotel's website in an all-round way, which is a very important task for enterprises. Literature [6] tested the application of smart technology in the hotel industry. We conducted a survey of many top hotels in five surrounding cities in China and found that the intelligence of hotels can be divided into three levels. Literature [7] developed a wireless ordering system based on Android phones for the needs of high-end hotel brand marketing services. Literature [8] used sustainable growth models and applied profit and risk graphs based on DuPont equations to investigate whether there is a connection between hotel financial management and management decision-making. We conducted a data analysis on two domestic hotels and calculated the profit of the hotel. The results of the study showed that the management of the manager has a great relationship with the financial situation of the hotel. The article pointed out the methods that the hotel can increase profitability. Literature [9] investigates the core financial analysis capabilities that hotel managers must possess. The literature [10] pointed out that recent reports focusing on the future of the global hotel industry have determined that key management issues include the impact of new technologies, lack of capital investment, and increasing attention to the future of the environment. The role of hotel finance director is very important for hotels. In recent years, people's perception of the role of hotel finance director has also changed tremendously. This position is also involved in the hotel's management team. The status in people's hearts has gradually increased. Literature [11] introduces some results of a research project, investigating the role of financial controller in the 10 years up to 1990. Literature [12] introduced the compilation method and indicator analysis of the cash flow statement. Literature [13] examines the combined impact of management response and online comments on hotel financial performance. We have collected a lot of data in the management responses to the online reviews of many online consumers. The research found that a high response rate can improve the financial performance of the hotel, while nonreplying will have a slight impact on the performance of the hotel, so more information should be provided. Reply more to improve the performance of the hotel. Literature [14] investigates the relationship between comprehensive quality management elements and customer attention and financial performance. Literature [15] investigates the relationship between the acquisition amount, the number of acquisition target hotels, and the financial performance of the hotel group after the acquisition. The research results show that the size of the acquisition has a significant impact on the financial performance of the acquirer's hotel, and the degree of impact varies according to different indicators of the company's financial performance. As an important part of hotel operation management, financial management not only involves hotel internal management, cost control, and payment but also affects hotel operation decision. Compared with large hotels, the management of small and medium-sized hotels has cer-

tain limitations, poor antirisk ability, and weak financial management awareness of managers, which easily constrains the development of hotels. Science and technology drive the development of human life in the future. Intelligent hotels can meet customer needs in all directions and realize the concept of hotel service first and customer first. In today's society with expensive human and material resources, intelligent technology has become the future trend of hotel development. Pujie Technology uses artificial intelligence to bring new vitality and new development to the hotel industry and meets the unique experience needs of customers with the principle of customer first.

## 2. Research Background

*2.1. Research Significance.* Different from hotels in the economically backward era, their main function is to provide customers with catering and accommodation services. On this basis, today's hotels are more comprehensively developed into very comprehensive social service organizations. The services provided by hotels are also increasing. Hotels have gradually become an indispensable part of people's lives. Hotels have driven my country's economic development and become my country's third emerging industry, which is closely related to the development of tourism. On the other hand, in large and medium-sized cities, hotel business is a common place for business negotiations and fitness sessions, and the demand for high-quality services is very necessary. The financial management of the hotel means that the financial staff is responsible for the statistics, summary, comprehensive analysis of the results, and conclusions of the various currency and capital exchanges and values collected by various financial institutions or units in the hotel's operating activities, and it is the hotel's general managers who provide information closely related to the management business in order to make correct business decisions. The popularization and development of information technology have opened up a new idea for the financial management of my country's tourism catering service industry. If this information technology is widely used in the financial management of tourism catering companies, it can provide tourism catering companies with more intelligent and automated financial management, including some daily financial and peacetime accounting management; if you make full use of the computer to manage it, on the one hand, you can effectively avoid financial management omissions; on the other hand, it is also for the convenience of inspection. The use of information technology to manage hotel financial data can share and manage the financial data of branches in multiple locations in real time under the premise of ensuring safety, which is very critical and important for hotel group management.

*2.2. The Necessity of Hotel Financial Management.* In the development of China's hotel industry for decades, although it is concentrated in the two aspects of catering and accommodation, the hotel has undergone revolutionary innovation and transformation in many aspects [16]. Any department and hotel operation management are any part of this

process, including project management, accounting, capital management, fixed asset management, material and supply management, office supplies and equipment for various functional departments, hotel procurement and leasing contract management, and management of large warehouses, from the purchase of raw materials to processing and later sales of the hotel; any department and hotel management are any part of this process, including project management, accounting, capital management, and fixed asset management. In supply management of materials and supplies, office supplies and equipment of various functional departments, hotel procurement and lease contract management, and large warehouse procurement management, from the purchase of raw materials to processing and later sales of the hotel, all the details are required because we need financial management, mainly manifested in the following aspects: the financial management of the hotel is related to the development of the hotel. The hotel's financial management is directly related to whether a hotel company can truly obtain long-term operations. Each department of the hotel also has traces of financial management. Any activity or action in the hotel is also inseparable from hotel finance. With the help and support of management, at the same time, by predicting the cost and benefit of various business activities, the hotel can clearly understand and master its own overall financial situation.

- (a) The financial management of the hotel is related to the development of the hotel. The hotel's financial management is directly related to whether a hotel company can truly obtain long-term operations. Each department of the hotel also has a trace of financial management. Any activity or some action in the hotel is also inseparable from hotel finance. With the help and support of management, at the same time, by predicting the cost and benefit of various business activities, the hotel can clearly understand and master its own overall financial situation
- (b) Financial management can reflect hotel operations, and hotel revenue, costs, and fluctuations can be reflected in the hotel's financial management activities [17]. The hotel management staff should formulate the company's development strategy according to the hotel's operating conditions to achieve the long-term development of the hotel
- (c) Conducive to hotel cost control. The hotel's financial system can effectively control the various activities carried out by the hotel and ensure the rational use of hotel funds and the regeneration of funds [18]

*2.3. Analysis of the Status Quo of Hotel Financial Management.* The traditional corporate finance department is mainly responsible for recording and managing the various expenditures of the enterprise, while the corporate finance department of the new era has more functions, including observation of the market where the enterprise is located and the management of the enterprise based on the existing financial information. Provide strategic advice on

future development. The settings include in-depth exploration of financial data and discovering some invisible corporate conditions on the surface. Many corporate financial management systems have been developed abroad. These corporate financial management systems include improvements to accounting and provide good support for voucher management and bank reconciliation. Some systems can even be connected with other companies in the production chain in the industry, such as Oracle's Financial Analyzer system, which can provide a very friendly management function for traditional corporate finance. The hotel's financial management department has a weak sense of supervision, and many problems have arisen in the hotel's operation process because the hotel's related systems are not perfect and cannot regulate and restrict employees.

*2.4. Countermeasures and Suggestions for Hotel Financial Management.* For some modern commercial hotel companies, financial management was an important management content at the time, and it was also regarded as an effective guarantee for the hotel companies' competitiveness in the international market. When our hotel companies want to further improve their own operating efficiency, they need to further enhance their own awareness of financial management significance and importance, and continue to strengthen the supervisory function of financial management workers and the sense of responsibility of employees, so that all employees of our hotel can fully realize the importance of financial management. It is clarified that the financial management work is closely related to the corporate procurement department and its market administrative department, further strengthens the management concept of the corporate financial department, builds a stricter operation and management system, further optimizes the business process of the hotel company, and implements financial supervision, to ensure that the operation and management of hotel companies have more extensive supervision powers and to promote communication and cooperation between other operation and management departments and the financial departments of hotel companies, so as to ensure that the hotel operation and management system and financial management work can be carried out in a regular manner. Moreover, financial management work will also be implemented, helping hotel business management and development work to play a practical effect.

*2.5. Hotel Financial Management System Design.* The financial part should judge the feasibility of decision-making based on conditions such as market and cost control and maximize the profit of the hotel as much as possible [19]. The financial management department divides positions according to parts and performs their duties. The financial department sets up cashier positions to control the turnover of funds. The issue of reserve funds should be managed by the procurement department. Under the conditions of analyzing the production needs of the hotel, the funds should be reasonably controlled to promote the turnover rate of funds. Set up a tax planning system. Form an asset flow management system to reduce waste of inventory and increase capital turnover [20].

## 2.6. Financial Model Construction

**2.6.1. Optimized Quantitative Model of Business Model.** Assuming  $p$  variable  $X_1, X_2, \dots, X_p$ , each variable has  $n$  pairs of measured values, and assuming that the measured values of  $X_1, X_2, \dots, X_p$ , vary independently, the statistical distance from any point  $P = (X_1, X_2, \dots, X_p)$  to any fixed point  $Q = (y_1, y_2, \dots, y_p)$  is [21]

$$d(p, Q) = \sqrt{\frac{(x_1 - y_1)^2}{S_{11}} + \frac{(x_2 - y_2)^2}{S_{22}} + \frac{(x_p - y_p)^2}{S_{pp}}}. \quad (1)$$

If  $S_k$  is the sample standard deviation, then

$$S_k^2 = S_{kk} = \frac{1}{n} \sum_{j=1}^k (x_{jk} - \bar{x}_k)^2, \quad k = 1, 2, \dots, p. \quad (2)$$

$\bar{X}_k$  is the mean value of the  $k$ th variable; there are

$$\bar{X}_k = \frac{1}{n} \sum_{j=1}^k X_{jk}. \quad (3)$$

When the coordinate values are not independent, the original coordinate system needs to be rotated by the angle  $\theta$ , and the statistical distance from any point  $P = (X_1, X_2, \dots, X_p)$  to any fixed point  $Q = (y_1, y_2, \dots, y_p)$  is [22]

$$d(p, Q) = [a_{11}(x_1 - y_1)^2 + 2a_{12}(x_1 - y_1)(x_2 - y_2) + \dots]^{1/2}. \quad (4)$$

Solve

$$\begin{aligned} d^2(p, Q) &= d(p, Q) \\ &= [a_{11}(x_1 - y_1)^2 + 2a_{12}(x_1 - y_1)(x_2 - y_2) + \dots] \\ &= (X - Y)TA(X - Y), \end{aligned} \quad (5)$$

where

$$\begin{aligned} A &= (a_{ij}), \quad i, j = 1, 2, \dots, 5, \\ (X - Y)^T &= [x_1 - y_1, x_2 - y_2, \dots, x_5 - y_5]. \end{aligned} \quad (6)$$

Find the first derivative of formula (5), and the other is 0; there are

$$\frac{\partial[(X - Y)TA(X - Y)]}{\partial(X - Y)} = 2A(X - Y) = 0. \quad (7)$$

Any point  $p$  on the objective function satisfies

$$y = x_1 \times x_2 \times x_3 \times x_4 \times x_5. \quad (8)$$

**2.6.2. Construction of Financial Crisis Early Warning Model.** Support vector machine [23] is applied to two clas-

sifications, and the specific classification is shown in Figure 1.

We set the dividing line of the support vector machine to  $g(x)$ :

$$g(x) = (a_1x + b_1) = 0. \quad (9)$$

Among them,  $\{y \mid (-1 \leq y \leq 1)\}x \in R_1$  is  $g(x) > 0, y = 1$ . When  $x \in R_2$ ,  $g(x) < 0, y = -1$ . The function can be expressed as

$$\begin{aligned} (a_1x) + b_1 &= -k, \\ (a_1x) + b_1 &= k. \end{aligned} \quad (10)$$

To transform the above formula, there are

$$\begin{cases} g(x) = (a_1x + b_1) = 0, \\ (a_1x) + b_1 = -1, \\ (a_1x) + b_1 = 1. \end{cases} \quad (11)$$

And because

$$\|a\| = \frac{\|a\|}{k}, \quad (12)$$

find the minimum value of  $\|a\|$  and turn the problem into a constrained optimization problem:

$$\text{s.t. } yi\{(a_1x) + b_1\} \geq 1. \quad (13)$$

Introduce the Lagrangian multiplier

$$L(a, \alpha) = \frac{1}{2} \|a\|^2 - \sum_i^n \alpha_i y_i (ax + b) + \sum_i^n \alpha_i. \quad (14)$$

Finally,

$$y(x) = \text{sgn} \sum_{i=1}^n \alpha_i y_i x_i^T x + b. \quad (15)$$

Assuming there is  $a$  sample, for each sample  $b$  description indicators, we can use a matrix to represent the sample:

$$x = \begin{pmatrix} x_{11} & \dots & x_{1b} \\ \vdots & \ddots & \vdots \\ x_{a1} & \dots & x_{ab} \end{pmatrix}. \quad (16)$$

The data standardization processing formula is

$$x = \frac{x_{ab} - \bar{x}_b}{\sqrt{\text{Var}(x_a)}}, \quad a \in (1, n), b \in (1, p). \quad (17)$$



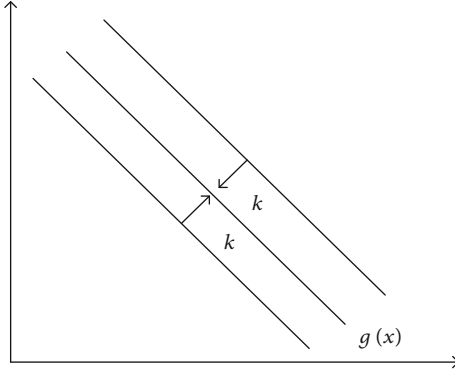


FIGURE 1: Schematic diagram of support vector machine.

Calculate the covariance:

$$\Sigma = \begin{cases} \text{Var}(x_1) & \text{Cov}(x_1, x_2) & \cdots & \text{Cov}(x_1, x_p), \\ \text{Cov}(x_2, x_1) & \text{Var}(x_2) & \cdots & \text{Cov}(x_2, x_p), \\ \vdots & & & \\ \text{Cov}(x_n, x_1) & \text{Cov}(x_n, x_2) & \cdots & \text{Var}(x_p). \end{cases} \quad (18)$$

Introduce the eigenvalues and eigenvectors of the matrix:

$$\begin{aligned} e &= (e_1, e_2, e_3 \cdots e_p), \\ \lambda &= \text{diag}(\lambda_1, \lambda_2, \lambda_3 \cdots \lambda_p). \end{aligned} \quad (19)$$

The main component results obtained are

$$\begin{cases} F_1 = e_{11}x_1 + e_{21}x_2 + e_{31}x_3 + \cdots + e_{p1}x_p, \\ F_2 = e_{12}x_1 + e_{22}x_2 + e_{32}x_3 + \cdots + e_{p2}x_p, \\ \vdots \\ F_p = e_{1p}x_1 + e_{2p}x_2 + e_{3p}x_3 + \cdots + e_{pp}x_p. \end{cases} \quad (20)$$

The linear model is used for fitting, and the following formula is obtained according to the principle:

$$P_i = f(\beta_0 + \beta_1 X_{i1} + \beta_2 X_{i2} + \cdots + \beta_n X_{in}), \quad (21)$$

where

$$f = \frac{ex}{1 + ex}. \quad (22)$$

Express  $Y_i$  in another way:

$$P(Y_i) = \pi_i y_i (1 - \pi)^{1 - y_i}. \quad (23)$$

The logarithms obtained by using the method of maximum similarity function are

$$\text{Ln}L = \sum_{i=1}^n y_i \ln \pi_i + (1 - y_i) \ln (1 - \pi_i),$$

$$\pi_i = \exp(\beta_0 + \beta_1 X_{i1} + \cdots + \beta_n X_{in}) A + \exp(\beta_0 + \beta_1 X_{i1} + \cdots + \beta_n X_{in}). \quad (24)$$

TABLE 1: Comparison table of property rights' rate of 3 top hotels in China.

Project	2016	2015	2014	2013
Hotel one	116.01%	165.78%	64.18%	66.69%
Hotel two	188.58%	192.22%	23.313%	54.18%
Hotel three	85.08%	124.29%	92.20%	84.14%
Average value	129.89%	162.10%	59.56%	68.34%

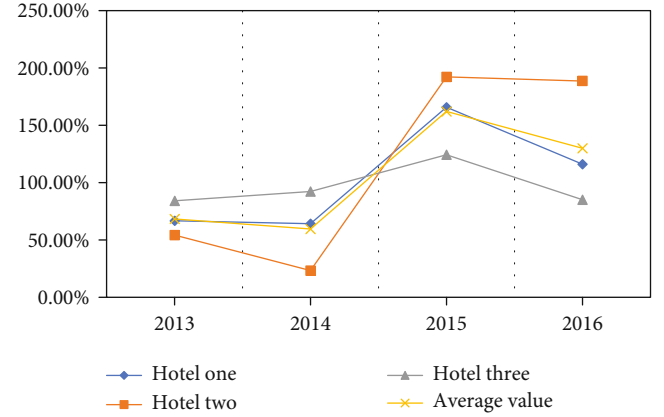


FIGURE 2: Change in equity ratio.

TABLE 2: Financial leverage coefficient comparison.

Project	2016	2015	2014	2013
Hotel one	1.58	1.75	1.17	1.18
Hotel two	1.69	1.40	1.10	1.08
Hotel three	1.08	1.05	1.07	1.02
Average value	1.45	1.40	1.11	1.09

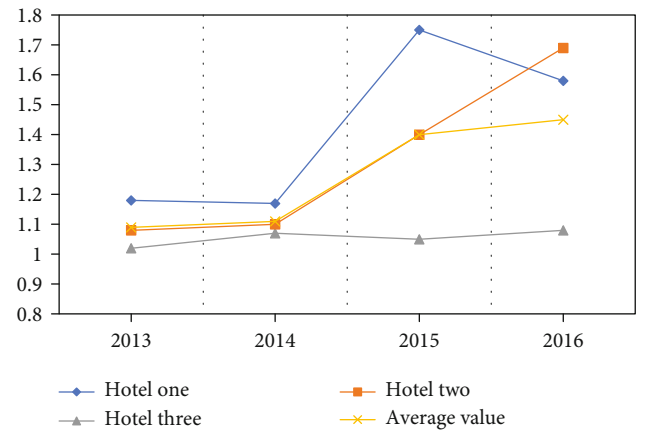


FIGURE 3: Changes in financial leverage coefficient.

TABLE 3: Quick ratio comparison table.

Project	2016	2015	2014	2013
Hotel one	0.23	0.21	0.93	0.92
Hotel two	0.80	0.77	1.93	0.36
Hotel three	1.18	0.67	0.55	0.34
Average value	0.74	0.55	1.14	0.54

The following equation is obtained:

$$LnL = \sum_{i=1}^n y_i (\beta_0 + \beta_1 X_{i1} + \dots + \beta_n X_{in}) - \ln [1 + \exp (\beta_0 + \beta_1 X_{i1} + \dots + \beta_n X_{in})]. \quad (25)$$

The linear regression model is used to find the linear relationship coefficient  $\beta$  between dependent variable  $Y$  and independent variable  $X$ , which satisfies  $Y = X\beta$ . At this time, the dependent variable  $Y$  is required to be continuous, so it is a regression model. If the dependent variable  $Y$  is discrete, we need to do another function transformation for this  $Y$  to become  $G(Y)$ . If the value of  $G(Y)$  is Class A when it is in a real number interval, Class B when it is in another real number interval, and so on, we get a classification model. In credit risk control, the value of default probability is changeable. By constructing dummy variable  $Y$  and setting critical value, the value of default probability is transformed into two variables. When the default probability is greater than the critical value, the value is 1; that is, the customer will default; when the default probability is less than the critical value, the value is 0; that is, the customer will not default. Assuming that the probability of dependent variable  $y = 1$  is  $p$  under the given condition of independent variable  $x$ , which is denoted as  $p = P(y = 1 | x)$ , then the probability of  $y = 0$  is  $1 - p$ , the probability ratio  $p/(1 - p)$  of dependent variable taking 1 and 0 is called dominance ratio, and the natural logarithm of dominance ratio is taken; then, sigmoid function can be obtained.

This paper puts forward two methods; one is the business model optimization quantification model; the other is the financial crisis early warning model; the financial crisis early warning model is obtained by the principle of support vector machine and principal component analysis.

### 3. Simulation Experiment

*3.1. Experimental Environment and Data Sources.* The article selects 4 top hotels in China, analyzes the hotel's financial operating conditions over the past 4 years, and calculates the hotel's property rights ratio, as shown in Table 1 and Figure 2.

*3.2. Simulation Experiment.* The analysis of financial leverage coefficient is shown in Table 2 and Figure 3.

From Figure 3, we can see that from 2013 to 2015, the financial leverage of hotel one has been higher than that of the other two hotels. This shows that the financial risk of hotel one is greater than that of the other two hotels, and the hotel should take relevant measures to reduce it (financial risk).

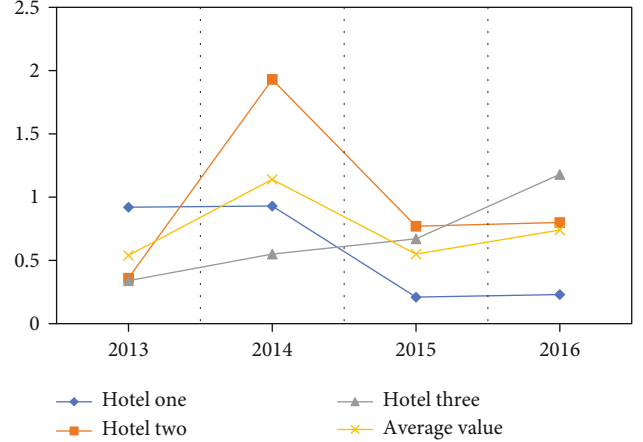


FIGURE 4: Hotel quick ratio change graph.

TABLE 4: Comparison of cash flow ratio.

Project	2016	2015	2014	2013
Hotel one	0.19	0.21	0.93	0.92
Hotel two	0.19	0.77	1.93	0.36
Hotel three	1.18	0.67	0.55	0.34
Average value	0.74	0.55	1.14	0.54

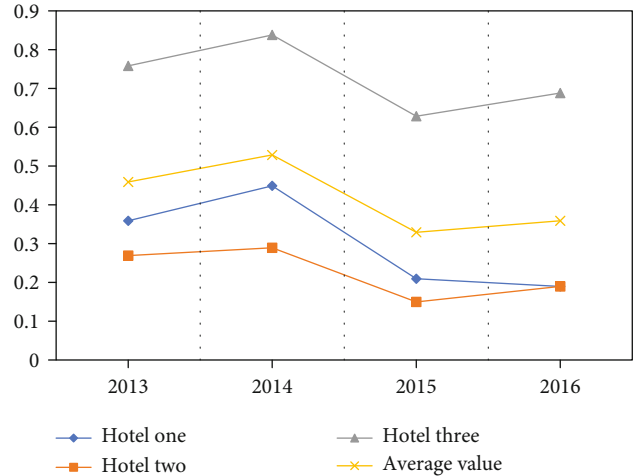


FIGURE 5: Cash flow ratio chart.

TABLE 5: Comparison table of interest coverage multiples.

Project	2016	2015	2014	2013
Hotel one	2.72	2.34	6.93	6.69
Hotel two	2.44	3.49	11.02	13.67
Hotel three	13.20	19.97	16.15	49.37
Average value	6.12	8.60	11.73	23.24

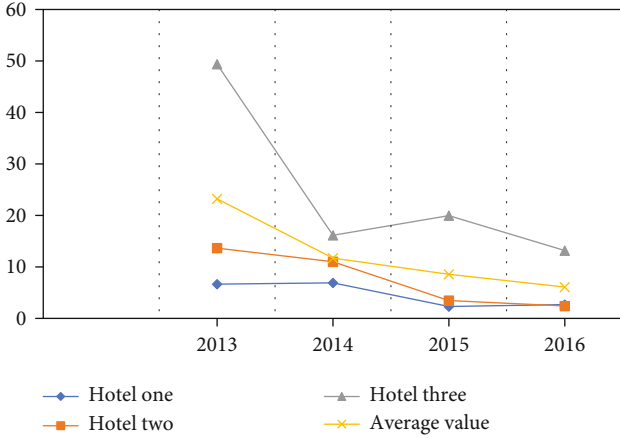


FIGURE 6: Changes in interest coverage multiples.

3.3. Debt Repayment Risk Identification

3.3.1. Analysis of Short-Term Solvency

(a) Analysis of quick ratio index

Adding that the quick ratio is significantly reduced at a certain moment, it proves that the short-term payment ability of the company may be insufficient, and the company may face a greater debt repayment risk [24]. The specific values are shown in Table 3 and Figure 4.

(b) Cash flow ratio analysis

Cash flow represents the liquidity of corporate assets. The higher the cash ratio, the stronger the corporate asset liquidity [25]. The specific values are shown in Table 4 and Figure 5.

According to Figure 5, we can conclude that the change trend of hotel 1’s cash flow ratio is roughly the same as that of quick ratio. There was an upward trend in 2013-2014 and a downward trend in 2015-2016. Compared with the other two hotels, the cash ratio has changed significantly.

3.3.2. Analysis of Long-Term Solvency

(a) Analysis of interest guarantee multiple index

The value of the interest protection multiple represents the risk of the company’s debt repayment, and the value of the value represents the level of the company’s debt repayment risk. The specific values are shown in Table 5 and Figure 6.

We can see from Figure 6 that in the three years from 2013 to 2016, the interest coverage multiples of the three hotels have shown a downward trend as a whole, which indirectly proves the increasingly fierce competition among hotel mayors.

(b) Asset-liability ratio index analysis

The higher the asset-liability ratio index, the greater the proportion of the company’s borrowed funds in the total funds. The specific data is shown in Table 6 and Figure 7.

TABLE 6: Asset-liability ratio comparison table.

Project	2016	2015	2014	2013
Hotel one	59.50	64.50	39.74	40.44
Hotel two	67.60	68.64	23.19	38.15
Hotel three	45.80	55.28	47.94	45.69
Average value	57.63	62.81	36.96	41.43

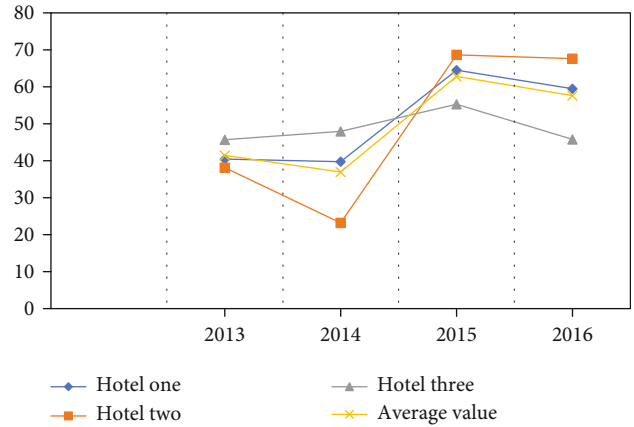


FIGURE 7: Change in asset-liability ratio.

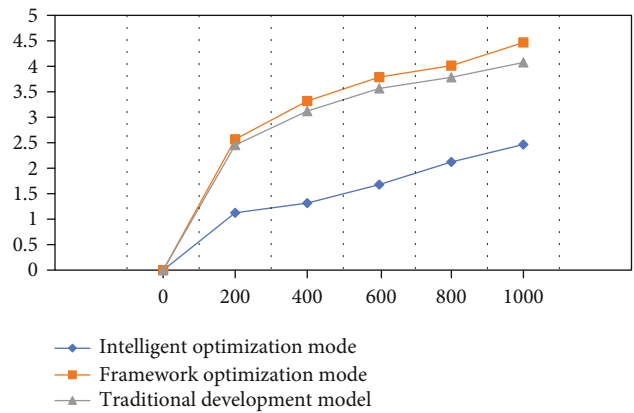


FIGURE 8: Response time vs. number of user drawing table.

Financial risk refers to the additional risks that enterprises bear by sovereign capital under the uncertain future income due to the use of debt funds. If the business is in good condition and if the enterprise’s investment return rate is greater than the debt interest rate, it will get the positive effect of financial leverage. If the enterprise’s operating condition is poor, making the enterprise’s investment return rate less than the debt interest rate, it will get the negative effect of financial leverage and even lead to the bankruptcy of the enterprise. This uncertainty is the financial risk that the enterprise bears by using debt. The size of enterprise financial risk mainly depends on the level of financial leverage coefficient. Under normal circumstances, the greater the financial leverage coefficient, the greater the elasticity of

TABLE 7: System query test results.

System	Number of requests	2000	2500	3000	3500	4000	4500	5000
Intelligent optimization mode	Average response time (MS)	33	45	55	95	135	205	279
	Success rate (%)	100	100	100	100	100	100	100
Framework optimization mode	Average response time (MS)	35	45	76	130	190	380	400
	Success rate (%)	100	99.7	99.6	99.5	99.4	98.4	99.3
Traditional development model	Average response time (MS)	42	55	90	200	380	350	500
	Success rate (%)	100	99.4	99.3	99.2	99.2	99.1	99

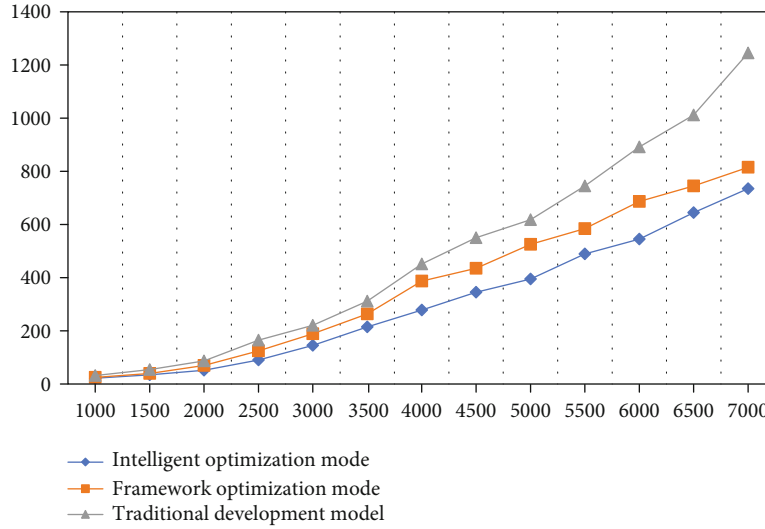


FIGURE 9: Request curve.

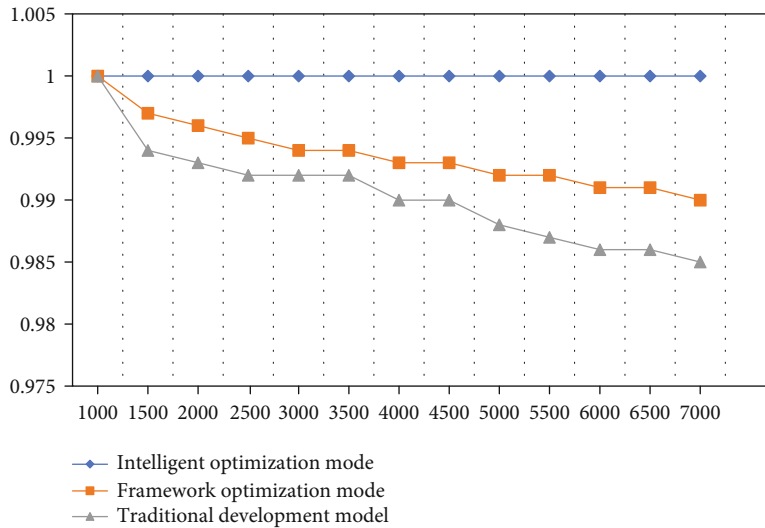


FIGURE 10: Success rate curve.

sovereign capital return rate to EBIT. If EBIT rate rises, the sovereign capital return rate will rise at a faster speed. If EBIT falls, then sovereign capital margins fall at a faster rate, and therefore, the risk is greater. On the con-

trary, the financial risk is smaller. The essence of the existence of financial risks is that the part of operating risks borne by liabilities is passed on to equity capital because of debt management.

TABLE 8: Business transaction processing function test.

System	Number of requests	60	90	120	150	180	210	240
Intelligent optimization mode	Average response time (MS)	75	190	250	350	500	700	820
	Success rate (%)	100	100	100	100	100	100	100
Framework optimization mode	Average response time (MS)	95	200	330	450	650	1050	1400
	Success rate (%)	100	99.5	99.4	99.4	99.3	99.2	99.1
Traditional development model	Average response time (MS)	150	250	400	500	800	1300	160
	Success rate (%)	99.6	99.4	99.3	99.2	99.1	89.9	89.7

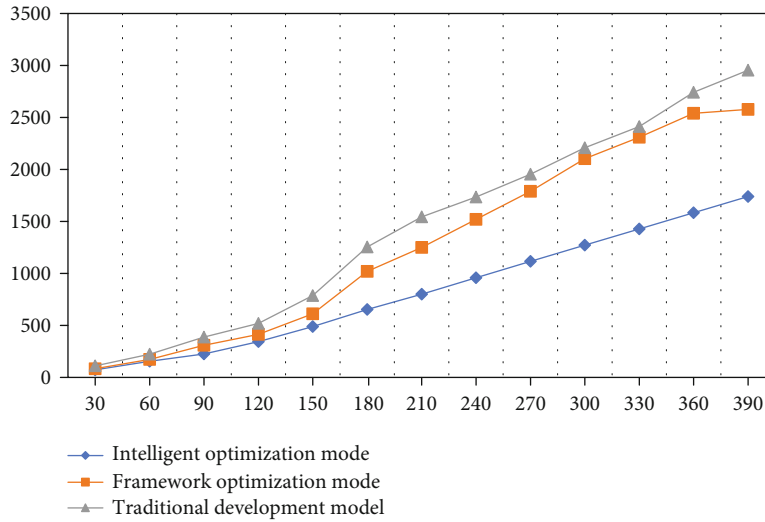


FIGURE 11: ART-concurrent completed transaction volume curve.

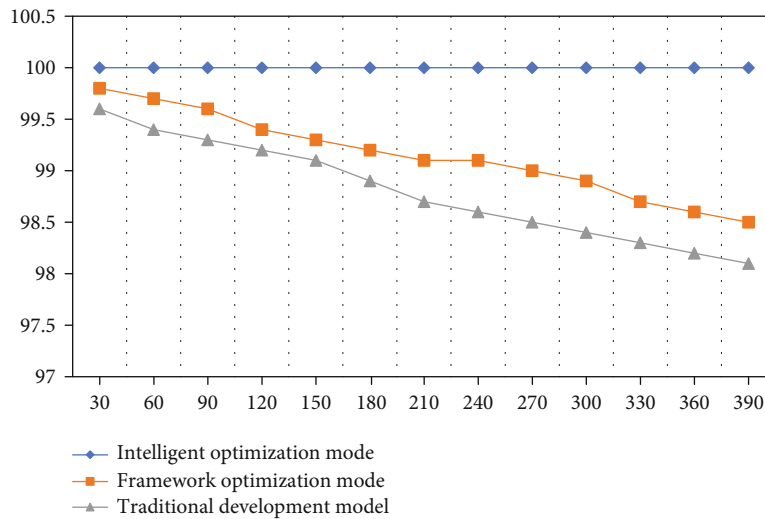


FIGURE 12: ART-concurrent business transaction success rate.

### 3.4. System Performance Test

3.4.1. *System Specific Function Test.* Detect with two indicators: the number of concurrent users and the response time. For the working status of a domestic hotel, the detection sys-

tem draws a graph of response time and the number of users, and the result is shown in Figure 8.

3.5. *Comparison of Specific Functions of the Block System.* The system response time is tested, compared with other



systems, and the test results are shown in Table 7 and Figures 9 and 10.

Judging from the query time and success rate of concurrent information in Figures 9 and 10, the intelligent optimization system can have a very low average response time and the highest query success rate. The average response time will increase as the amount of concurrency increases, but the success rate shows a downward trend.

**3.5.1. Business Transaction Processing Function Test.** Test the business transaction processing function of the system. Compared with other system users, the test results are shown in Table 8 and Figures 11 and 12.

Judging from the response time and success rate of completing business transactions in Figures 11 and 12, the intelligent optimization system can have a very low average response time and the highest query success rate.

#### 4. Conclusion

Speed up and strengthen the hotel's financial management business, establish a sound financial management system, reduce management expenses and costs, and increase the hotel's revenue to comply with the fierce market competition. In the operation and management of large-scale tourism enterprises in my country, managers must be good at discovering existing problems and actively explore and take effective measures to completely solve these problems. New corporate management concepts should be implemented in various management tasks. Our hotel is ready for future socioeconomic sustainability.

Under the condition of market economy, the challenges and pressures brought to the hotel industry are enormous. If you want to be in an invincible position in this fierce competition, you must strengthen the management in all aspects, keep learning, and keep exploring and innovating, and then, you can build a boutique hotel. Strengthen the cultivation of talents, and improve service quality: talent is the most precious resource of enterprises, which has become the consensus of people of insight. Hotel competition is the competition of talents, and talents are the root of hotel survival and development. With the advent of the globalization of Chinese economy, the goal of hotel service in China has gradually changed from nationalization to globalization, and the diversification of customers means the need for diversified professionals. Hotel enterprises need to be employee-centered on the premise of customer satisfaction, because service quality, customer satisfaction, and enterprise performance all depend on employees, and all services are delivered by employees. "There are no satisfied customers without satisfied employees" is the consensus of successful hotel managers. Recruiting and retaining talents are the most concerned issue in any industry.

#### Data Availability

The experimental data used to support the findings of this study are available from the corresponding author upon request.

#### Conflicts of Interest

The author declared that there are no conflicts of interest regarding this work.

#### Acknowledgments

This work was sponsored by Project of Department of Education of Zhejiang Province (Zhejianghan[2021]47) and Project of Tourism College of Zhejiang (2019GCC13).

#### References

- [1] L. I. Lin, "Innovation and development of financial management in modern hotel industry," *Management & Technology of SME*, vol. 27, no. 1, pp. 6–6, 2019.
- [2] Bagaeva Ksenia Olegovna source: Corporate Financial, *Financial Management in the Hotel Business: Basic Approach and Foreign Experience Application*, Корпоративные финансы, 2011.
- [3] T. C. Canada, "Tourism, that's your business. A programme of financial management for the Canadian hotel industry," *Study Guide*, vol. 52, no. 12, pp. 22–36, 1983.
- [4] Q. Wang and B. Zhang, "Research and implementation of the customer-oriented modern hotel management system using fuzzy analytic hierarchical process (FAHP)," *Journal of Intelligent and Fuzzy Systems*, vol. 40, no. 4, pp. 8277–8285, 2021.
- [5] A. Akincilar and M. Dagdeviren, "A hybrid multi-criteria decision making model to evaluate hotel websites," *International Journal of Hospitality Management*, vol. 36, pp. 263–271, 2014.
- [6] W. Xiong and W. U. Yuanmei, "The influence of intelligence application on hotel performance in luxury hotels: a case study in the Pearl River Delta," *Tourism Tribune*, vol. 22, pp. 22–36, 2018.
- [7] X. U. Chaohui, "Design of intelligent ordering system based on Android mobile phone," *Machine Design and Manufacturing Engineering*, vol. 25, no. 23, pp. 11–16, 2016.
- [8] G. Tildikova, "The impact of sustainable growth indicators on hotel's financial management," *Jyväskylä Ammattikorkeakoulu*, vol. 2, no. 3, pp. 1–9, 2014.
- [9] Y. Yang, *A study of hotel management financial competencies with the focus on revenue and cost management*, [Ph.D. thesis], Kent State University, 2014.
- [10] C. Burgess, "The hotel financial manager - challenges for the future," *International Journal of Contemporary Hospitality Management*, vol. 12, no. 1, pp. 6–12, 2000.
- [11] C. L. Burgess, "The hotel financial controller: a member of the management team," in *Accounting and finance for the international hospitality industry*, Butterworth-Heinemann, 1998.
- [12] X. G. Ding, "Application of cash flow statement in hotel financial management," *Journal of Shaanxi Normal University (Natural Science Edition)*, vol. 23, no. 2, pp. 55–75, 2001.
- [13] K. L. Xie, K. So, and W. Wang, "Joint effects of management responses and online reviews on hotel financial performance: a data-analytics approach," *International Journal of Hospitality Management*, vol. 62, no. 62, pp. 101–110, 2017.
- [14] S. Al-Shourah and A. A. Shourah, "An examination between total quality management and hotel financial performance: evidence from Jordanian international hotels," *International Journal of Information and Decision Sciences*, vol. 23, no. S1, pp. 418–431, 2020.

- [15] Y. Yang, "Effects of the size of acquisition on a hotel group's financial performance," *Journal of Hospitality Financial Management*, vol. 27, no. 1, pp. 6–6, 2019.
- [16] Y. Li, "Analysis on how to promote the refined construction of hotel enterprise financial management," *Manager*, vol. 11, pp. 22–52, 2011.
- [17] A. Banerjee, V. Mukherjee, and S. P. Ghoshal, "Seeker optimization algorithm for load-tracking performance of an autonomous power system," *International Journal of Electrical Power & Energy Systems*, vol. 43, no. 1, pp. 1162–1170, 2012.
- [18] K. Ikeda, T. M. Baduge, T. Umedu, H. Yamaguchi, and T. Higashino, "ALMware: a middleware for application layer multicast protocols," *Computer Communications*, vol. 34, no. 14, pp. 1673–1684, 2011.
- [19] Z. Jia, "Problems and countermeasures in financial management of a star hotel in Shenzhen," *Research on Communication Power*, vol. 3, no. 6, pp. 185–187, 2019.
- [20] Sun Microsystems Inc, *Core J2EE Patterns*2022, <http://sun.com/blueprints/coreJ2EEpatterns/index.html>.
- [21] S. Mingxia, *Research and application of component-based software reuse technology*, [Ph.D. thesis], Wuhan University of Technology, 2009.
- [22] H. Qinghua and Y. Liqing, "The research and application of Struts architecture in talent training system," *Software Guide*, vol. 12, pp. 22–36, 2010.
- [23] G. Chen, X. Xie, and S. Li, "Research on complex classification algorithm of breast cancer chip based on SVM-RFE gene feature screening," *Complexity*, vol. 2020, Article ID 1342874, 12 pages, 2020.
- [24] W. Ling, "Research on the financial management innovation of hotel enterprises under the new situation," *China's Foreign Trade*, vol. 16, pp. 22–36, 2011.
- [25] C. Szyperki, D. Gruntz, and S. Murer, *Component software: beyond object-oriented programming*, Pearson Education, 2003.

## Research Article

# Research on Enterprise Financial Customer Classification Method and Preference Based on Intelligent Algorithm

Ze Fu,<sup>1</sup> Bo Zhang ,<sup>2</sup> Lingjun Ou,<sup>3</sup> Kaiyang Sun,<sup>4</sup> Xinyi Sun,<sup>5</sup> and Ningyan Chen<sup>6</sup>

<sup>1</sup>Yiwu Innovation Institute, Yiwu Industrial & Commercial College, Yiwu 322000, China

<sup>2</sup>School of Information and Communication Engineering, Communication University of China, Beijing 100024, China

<sup>3</sup>Aston University, Birmingham B47ET, UK

<sup>4</sup>Monash University, Melbourne, VIC 3800, Australia

<sup>5</sup>Navigation College, Dalian Maritime University, Dalian 116026, China

<sup>6</sup>South China Normal University, Zhaoqing 526000, China

Correspondence should be addressed to Bo Zhang; zhangbo2015@cuc.edu.cn

Received 22 September 2021; Accepted 11 November 2021; Published 28 November 2021

Academic Editor: Deepak Gupta

Copyright © 2021 Ze Fu et al. This is an open access article distributed under the Creative Commons Attribution License, which permits unrestricted use, distribution, and reproduction in any medium, provided the original work is properly cited.

Compared with the past questionnaire survey, this paper applies the intelligent algorithm developed rapidly in recent years to identify the tendency of customers to buy financial products in the market. In addition, for the single state customer classification indicators based on the previous demographic information and action information, it is proposed to combine the action of market activities with demographic information; that is, the static integrated customer classification index is further combined with the improved neural network model to study the classification and preference of enterprise financial customers. Firstly, the enterprise financial customer classification model based on neural network algorithm is studied. Aiming at the shortcomings of easy falling into the local optimal solution of neural network algorithm, slow convergence speed of algorithm, and difficult setting of network structure, combined with the characteristics of genetic algorithm, the concept of adaptive genetic neural network algorithm is proposed. Then, the design of adaptive genetic neural network model is studied. Secondly, combined with the customer data of a financial enterprise and the characteristics of enterprise finance, this paper analyzes the risk influencing factors of enterprise financial customers, analyzes the customer data, evaluates the enterprise financial customers through the adaptive genetic neural network model, and realizes the classification of enterprise financial customers. Through an example, it is proved that the enterprise financial customer classification and preference model based on the adaptive genetic neural network algorithm discussed in this paper has better customer classification accuracy and can provide better method support for enterprise financial customer management.

## 1. Introduction

Customers in modern society have more choices. Customers' needs have been personalized. The competition among enterprises will also become fierce [1]. At the same time, with the progress of production technology, the differences between commodities become smaller, and the focus of competition changes from "product-centered" to "customer-centered" [2]. Only the enterprises that meet the needs of customers as quickly as possible can realize the sales of products. Only financial enterprises that can quickly respond to the individuation and change of customers can survive and develop in the fierce mar-

ket competition. The most important index of enterprise management has changed from profit and cost to customer satisfaction. Customer relationship management is an important means for financial enterprises to gain competitive advantage. Therefore, this paper uses the improved self-adaptive genetic neural network customer classification model, which can distinguish the customers with different purchasing tendencies of financial enterprises and provide financial enterprises with different customers as the target, differentiated, and effective marketing services, which not only reduces the cost but also improves the operating profit and facilitates the financial customer relationship management of enterprises [3].

The effective classification of customers is the key to maintain and manage customer relationships in various fields, so it has attracted much attention. This paper puts forward a new method of customer value classification based on BP-AdaBoost, which is based on BP and AdaBoost algorithm, and analyzes the characteristics of different customers according to the designed evaluation system. AdaBoost algorithm is used to form a strong classifier, so as to improve the accuracy of traditional BP network [4]. Experiments show that this method is also effective for the application of financial customer classification, and the accuracy is satisfactory.

By collecting 2000 social media reviews of financial banks on the Internet, we studied the research framework for establishing financial bank data sets. In today's intelligent network, the role of social media in various fields cannot be ignored, including financial institutions. It can provide ways and channels to analyze needs and understand how to improve product quality and service, so that financial institutions can tailor personalized needs for customers. This framework uses various machine learning methods and technologies to classify emotions [5]. With fierce market competition, many financial institutions have to take sales as the first premise and use the quickest way to focus on "possible" customers. At the same time of competition, although financial institutions have a series of documents and methods to control risks, the borrower's intention is not obvious, which leads to a great reduction in the controllability of risks. In view of this serious phenomenon, we study the method of machine learning to promote handwriting analysis, which reflects a certain degree of intention from the unique properties of handwriting, and the recognized handwriting association is helpful to map individuals to corresponding personality types. When using machine learning technology to collect the samples of personal management questionnaire, it shows that extroversion is related to financial behavior as a "risk seeker" [6]. The early warning model of Internet finance is of great significance for enterprises in the financial field to prevent and control risks. We propose an improved K-means algorithm based on quantum evolution, which combines initial value and risk value to determine the risk early warning interval, and introduce quantitative algorithm into this algorithm to improve the search efficiency, so as to get the accurate early warning interval. Finally, we calculate the risk value with GMDH prediction mining method. Comparing nearly 10,000 data of Internet financial companies with real financial institutions, it shows that its model is available and effective [7].

## 2. Adaptive Genetic Neural Network Algorithm

**2.1. Theory of Artificial Neural Networks.** Artificial neural network is a complex system composed of many processing units similar to biological neurons [8].

**2.1.1. Neuron Model.** Artificial neural network is composed of artificial neurons as many basic processing units [9]. To establish an artificial neural network, we must first decide the artificial neuron model. Figure 1 is a general model structure diagram of artificial neurons.

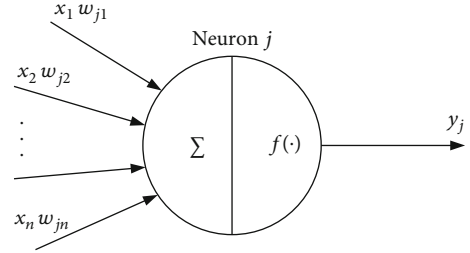


FIGURE 1: Neuron model.

**2.1.2. BP Algorithm.** BP algorithm is the most commonly used algorithm in neural network model learning. BP algorithm is a supervised learning algorithm. The idea of BP algorithm is that initial weights and thresholds are first provided to the network; an actual output value of the network is calculated from the input value [10, 11]; then, the desired output value is compared with the actual output value; such learning is repeated on the training samples based on the obtained weights and thresholds of the error correction network, and finally, the error between the actual output and the desired output is minimized.

The specific process is as follows:

It is assumed that the neural network is an  $I$  input unit and a  $K$  output unit, the implicit layer is a layer, and the  $J$  unit is shared. The BP algorithm is executed primarily to minimize the square error between the actual output, and the expected output obtained after the data is input into the network. The formula for the sum of squared errors is as follows.

$$E = \frac{1}{2} \sum_{k=1}^k (d_k - o_k)^2. \quad (1)$$

Among them,  $o_k = f(\text{net}_k)$  is the actual output value of neuron  $k$  in the output layer,  $d_k$  is the expected output value of neuron  $k$  in the output layer, and  $y_j$  is the output value of hidden layer neuron  $j$ .

For the  $E$  value, in order to achieve the goal of the ideal value, it is necessary to change the weight value of the network. First, adjust the connection weights between the implicit layer and the output layer.

$$w_{kj}(t+1) = w_{kj}(t) + \Delta w_{kj}. \quad (2)$$

In the above formula, the value obtained by the gradient method is the adjusted value of the connection weight between the implicit layer and the output layer.

$$\Delta w_{kj} = -\eta \frac{\partial E}{\partial w_{kj}} = \eta (d_k - o_k) f'(\text{net}_k) y_j. \quad (3)$$

In the above formula,  $\eta$  is the normal value, which is expressed as the iteration step.

In a similar manner, you can adjust the join weights between the input layer and the implicit layer. Formula

adjustment is as follows:

$$v_{ji}(t+1) = v_{ji}(t) + \Delta v_{ji}. \quad (4)$$

In the above formula,  $\Delta v_{ji}$  is the adjustment amount for determining the connection weight between the input layer and the implicit layer by the gradient method. It can be obtained from the following formula:

$$\Delta v_{ji} = -\eta \frac{\partial E}{\partial v_{ji}} = \eta \sum_{k=1}^k (d_k - o_k) f'(\text{net}_k) w_{kj} f'(\text{net}_j) x_i. \quad (5)$$

When there are samples, if there are  $P$  training samples, the total error sum form of the above calculation method is as follows:

$$E_p = \frac{1}{2} \sum_{p=1}^P \sum_{k=1}^K (d_k - o_k)^2. \quad (6)$$

As long as the operation is repeated for  $P$  samples as described above,  $E_p$  reaches the minimum requested value, and the algorithm ends.

**2.2. Adaptive Genetic Algorithm.** Adaptive genetic algorithm is evolved from basic genetic algorithm [12, 13]. It has strong global search performance and strong local search ability and accelerates the convergence speed to a certain extent. But it also has inherent defects.

**2.2.1. Improvement of Adaptive Genetic Algorithm.** The adaptive change formulas of crossover probability  $P_c$  and mutation probability  $P_m$  used in traditional adaptive genetic algorithm are as follows:

$$P_c = \begin{cases} k_1 \frac{(f_{\max} - f')}{f_{\max} - f_{\text{avg}}}, & f' \geq f_{\text{avg}}, \\ k_2, & f' < f_{\text{avg}} \end{cases}, \quad (7)$$

$$P_m = \begin{cases} \frac{k_3(f_{\max} - f)}{f_{\max} - f_{\text{avg}}}, & f \geq f_{\text{avg}}, \\ k_4, & f < f_{\text{avg}} \end{cases}. \quad (8)$$

Among them,  $f_{\text{avg}}$  is the average fitness value of all individuals in the population,  $f_{\max}$  is the maximum individual fitness value in the population,  $f'$  is the fitness value of the individual with the larger fitness value among the two individuals to be crossed, and  $f$  is the fitness value of the individual to be mutated, any number comes from  $k_1, k_2, k_3, k_4, 0$  and 1.

Srinivas et al., by proposing  $K_1 = K_2 = K, K_3 = K_4 = K'$ , represent adaptive adjustment curves for crossover probabilities and change probabilities in Figures 2 and 3.

As shown in the figure, in the early stage of evolution, individuals with higher fitness values may not be the global optimal solution.

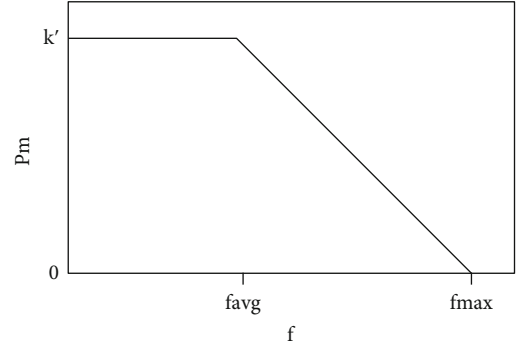


FIGURE 2: Variation curve of mutation probability.

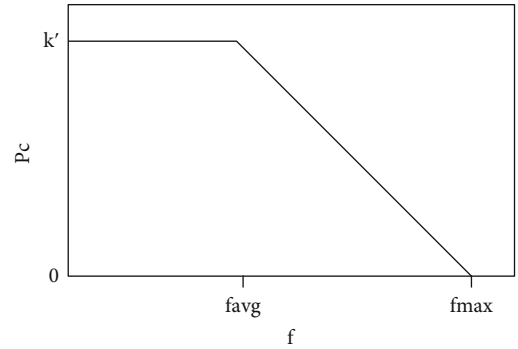


FIGURE 3: Cross probability change curve.

To solve this problem, this paper proposes an adaptive genetic algorithm. In addition, in order to maintain a better individual pattern after the evolution of the algorithm, the adaptive adjustment curve in  $f_{\max}$  should be smoothed as much as possible. The formulas of crossover probability and mutation probability are as follows.

$$P_c = \begin{cases} P_{c1} * \frac{1}{\exp\left(\frac{(f' - f_{\text{avg}})}{(f_{\max} - f_{\text{avg}})}\right)}, & f' \geq f_{\text{avg}}, \\ P_{c1}, & f' < f_{\text{avg}} \end{cases}, \quad (9)$$

$$P_m = \begin{cases} P_{m1} * \frac{1}{\exp\left(\frac{(f - f_{\text{avg}})}{(f_{\max} - f_{\text{avg}})}\right)}, & f \geq f_{\text{avg}}, \\ P_{m1}, & f < f_{\text{avg}} \end{cases}, \quad (10)$$

where  $f'$  is the fitness value of the larger of the two individuals to be crossed,  $f_{\text{avg}}$  is the average fitness value of all individuals in the population,  $f_{\max}$  is the largest individual fitness value in the population,  $f$  is the fitness value of the variant individual, and  $P_{c1}$  and  $P_{m1}$  are the largest crossover probability and mutation probability, respectively.

The adaptive adjustment curves of crossover probability and mutation probability are shown in Figures 4 and 5.



### 2.3. Adaptive Genetic Algorithm Evolutionary Neural Network

2.3.1. *Defects of Neural Networks.* BP neural network is the most widely used model of neural network in classification [14, 15], and this algorithm is simply analyzed here. BP algorithm is an effective algorithm, but it also has some defects in practical application:

- (1) Once a complex problem is solved, the result will fall into a local minimum, which will lead to the failure of learning
- (2) If the learning speed decreases, the convergence speed will definitely slow down, but if it increases, the correction will not only be excessive but also cause vibration and divergence
- (3) The number of input and output nodes of the network can be known according to the problem, and the selection of the number of hidden nodes is based on experience and lacks theoretical guidance
- (4) The robustness is poor, and the initial setting value of the network has great influence on the overall performance of the network

Because BP neural network still has a series of defects [16, 17], we need to make some improvements to optimize its performance in order to get more satisfactory results. In this paper, the improved adaptive genetic algorithm is combined with neural network to make up for the abovementioned one or two shortcomings of neural network and the shortcomings of genetic algorithm itself, such as the reduction of convergence efficiency in the early stage and the middle and late stage.

2.3.2. *Adaptive Genetic Neural Network.* Up to now, the combination direction of genetic algorithm and neural network can be roughly divided into the following three types [18, 19].

- (1) Optimizing network connection weights and thresholds
- (2) Optimizing the topological structure of the network
- (3) Optimize the learning rules of the network

The first optimization method is used most for BP neural network. This process corresponds to dividing the whole network into two steps. In the first step, genetic algorithm is used to derive the initial weights and thresholds of the network. In the second step, BP algorithm is applied to finally complete the training of the network. There are three key aspects in the optimization process: the expression of chromosome, the definition of fitness function, and the construction of genetic operator.

- (1) Chromosome expression (i.e., coding mode)

Real numbers are used here. Because the scope of network rights is unclear, using real numbers can avoid coding becoming difficult. In addition, the efficiency of the learning

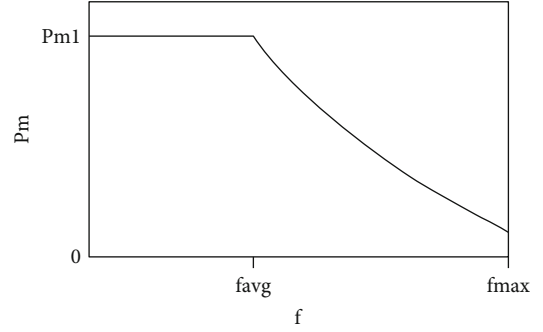


FIGURE 4: Variation curve of mutation probability after improvement.

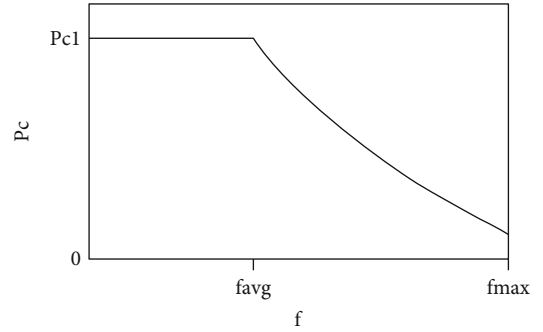


FIGURE 5: Modified curve of crossover probability.

algorithm can be improved without coding and coding. Real numbers are easy to retrieve in a large space, which can meet the accuracy requirements of genetic algorithm [20].

Taking a three-layer neural network as an example, chromosome length is as follows:

$$l = W_1 + b_1 + W_2 + b_2. \quad (11)$$

Chromosomes are composed of  $l$  random numbers between 0 and 1.

- (2) Definition of fitness function

After determining the initial weights and thresholds of the BP neural network, an estimate of the number of inputs for training can be used as an evaluation function of the chromosomes. The evaluation function may be expressed as the reciprocal of the absolute value of the error between the actual output value and the expected output value obtained by the adaptation function, namely,

$$f = \frac{1}{\sum_{i=1}^n \sum_{j=1}^k |y_{ij} - o_{ij}|}. \quad (12)$$

- (3) Construction of selection operator

By using the best individual preservation strategy, the individual with the highest adaptability in the current group

is prevented from participating in the subsequent cross-meaning and mutation operations. By replacing the individual with the lowest adaptability in the generation group, the best individual obtained so far will not be destroyed, and the convergence of the algorithm can be guaranteed.

- (4) Construction of crossover operator and mutation operator

Adaptive crossover operators and mutation operators change adaptively according to the evolution of groups [21, 22].

For BP neural network which determines the overall structure, the algorithm flow is as follows.

- (1) *Group Initialization.*  $N$  groups of initial network weights are randomly generated, and each group is used as a chromosome
- (2) *Select the Operation.* Calculate the proportion corresponding to the fitness value of each chromosome, and select  $N$  individuals to the next generation by roulette and the best individual preservation strategy
- (3) Cross operation
- (4) *Mutation Operation.* The number of iteration steps reached is (5), otherwise (2)
- (5) Substituting the best chromosome into the initial value and threshold value of BP neural network and continuing in the training group until the error accuracy, or the set maximum algebra is reached

The algorithm flow chart is shown in Figure 6:

### 3. Research on Classification and Preference of Enterprise Financial Customers Based on Adaptive Genetic Neural Network Algorithm

*3.1. Parameter Modification of BP Neural Network.* In this paper, the gradient descent method is mainly used to study the classification and preference of enterprise financial customers by using BP neural network, and the weight of each BP neuron in the network is adjusted [23]. The specific operation process is as follows.

Analyze the output of hidden nodes in the network

$$y_i = f\left(\sum_j \omega_{ij}x_j - \theta_i\right) = f(\text{net}_i). \quad (13)$$

Among them:

$$\text{net}_i = \sum_j \omega_{ij}x_j - \theta_i. \quad (14)$$

In the three-layer BP neural network structure, the input of output nodes is the output of hidden nodes.

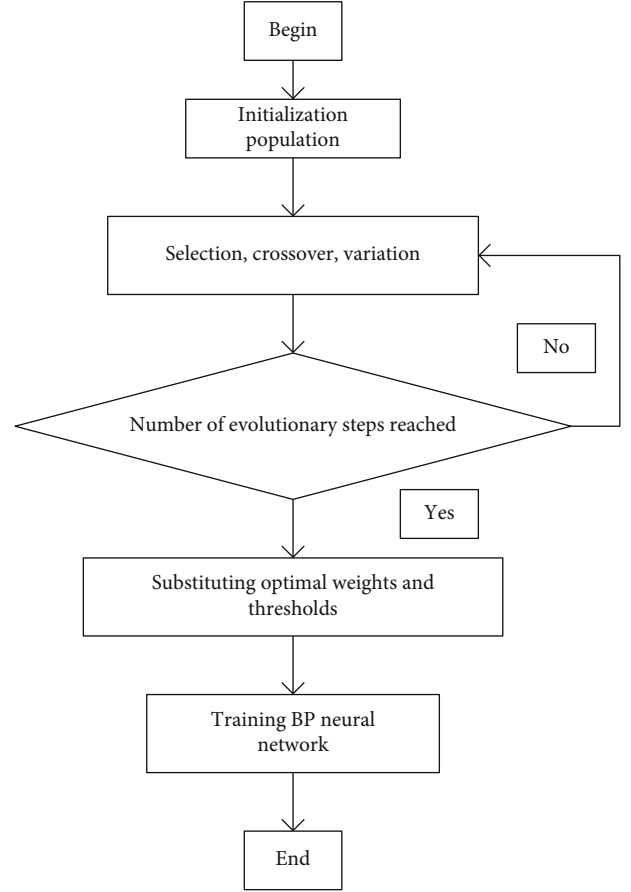


FIGURE 6: Flow chart of adaptive genetic neural network algorithm.

TABLE 1: Sample index numeralization.

Indicators	Default	Housing	Loan	Marital	Contact	Day
0	No	No	No	—	—	—
1	Yes	Yes	Yes	Married	Unknown	0-9
2	—	—	—	Divorced	Telephone	10-19
3	—	—	—	Single	Cellular	20-31

$$s_k = f\left(\sum_i u_{ij}y_i - \theta_k\right) = f(\text{net}_k), \quad (15)$$

$$\text{net}_k = \sum_i u_{ij}y_i - \theta_k. \quad (16)$$

The error between the output node of BP neural network and the actual value of training samples is calculated as follows.

$$E = \frac{1}{2} \sum_k (z_k - s_k)^2 = \frac{1}{2} \sum_k \left( z_k - f\left(\sum_i u_{ij}f\left(\sum_j \omega_{ij}x_j - \theta_i\right) - \theta_k\right) \right)^2. \quad (17)$$

TABLE 2: Sample index digitization (continued).

Indicators	Education	Balance	Month	Poutcome	Plays
1	Unknown	0以下	1-3	Unknown	-1
2	Secondary	0-999	4-6	Other	0-99
3	Primary	1000-4999	7-9	Failure	100-199
4	Tertiary	More than 5000	10-12	Success	200-299
5	—	—	—	—	More than 300

TABLE 3: Sample index digitization (continued).

Indicators	Age	Duration	Job
1	0-19	0-99	Admin
2	20-29	100-299	Unknown
3	30-39	300-499	Unemployed
4	40-49	500-599	Management
5	50-59	600-899	Housemaid
6	60以上	900-999	Entrepreneur
7	—	1000-1699	Student
8	—	More than 1700	Self-employed
9	—	—	Blue-collar
10	—	—	Retired
11	—	—	Technician
12	—	—	Services

The weights between output nodes, hidden nodes, and errors are analyzed. If the output nodes in BP neural network are independent of each other, the following relations exist.

$$\frac{\partial E}{\partial U_{ij}} = -\delta_i y_i. \quad (18)$$

**3.2. Sample Data Acquisition.** The experimental data comes from the enterprise financial customer data set in UCI machine learning database. This data is about whether the marketing products of financial enterprises can finally be purchased by customers. A total of 2000 sets of data samples were taken. Each sample consists of 16 attributes and 1 category. The 16 attributes can be divided into three categories.

*Demographic variables:* describe some basic information of customers.

*Demographic variables:* describe some basic information of customers, including age (age), work (job), marital status (marriage), education, default, annual average balance, housing, and personal loan (loan).

Some variables of communication between financial enterprises and customers about current marketing activities include communication mode (contact), the date of the last communication in a month, month of the last communication in a certain year, the last communication time (duration), and the number of communications with this customer during this activity.

Some variables that a financial enterprise communicates with a customer about the last event include the last event

and the last communication from the customer (pdays), the number of communications with the customer prior to the event (previous), and the result of the last marketing event (poutcome).

This category indicates whether the customer purchased the marketing products of the financial enterprise this time.

**3.3. Sample Data Preprocessing.** The steps of data preprocessing are as follows. Firstly, the nonnumerical attributes in the sample are numerized to discretize the continuous attributes. Then, the description and statistics of sample indicators are carried out to analyze the rationality of the application model. After that, principal component analysis is used to extract the hidden main features as input variables of neural network.

**3.3.1. Numerical Properties.** The nonnumerical attributes in the index are numerized, and the continuous attributes are discrete. The specific process is shown in Tables 1, 2, and 3, and the attributes are listed as the actual attribute values.

**3.3.2. Descriptive Statistics of Sample Indicators.** In order to explain whether the model is feasible, first of all, the sample indicators are explained and counted, and the statistical results are expressed in Table 4.

From the various values shown by the deviation and peak coefficients in Table 4, these coefficients of age, balance, and month are close to zero, that is, close to normal distribution, but other indicators hardly follow. Therefore, the traditional statistical model, which is constrained by many indexes, cannot be used to analyze and solve this problem. However, because these constraints cannot limit the model based on neural network technology, the classification and preference model based on genetic neural network can be applied here.

**3.3.3. Sample Impact Factor Analysis.** Factor analysis is a statistical technique, which can summarize a large number of indicators into a few factors and explain a large number of observed facts. When the main features are fuzzy and covered by redundant data, it is difficult for general neural networks to identify them [24, 25]. However, if the main features are clear and the same accuracy is obtained, the operation efficiency of the network model is greatly improved.

Principal component analysis is carried out on the numerical attribute data, and the eigenvalues and contribution rates of the correlation coefficient arrangement of variables are shown in Table 5.

TABLE 4: Sample index description statistics.

Variable	N	Minimum value	Maximum value	Mean value	Standard deviation	Skewness	Kurtosis
Age	2000	1	6	3.65	1.021	334	-0.540
Job	2000	1	12	7.06	3.493	-0.24	-1.181
Marital	2000	1	3	1.67	0.879	0.695	-1.346
Education	2000	1	4	2.70	0.947	0.301	-1.319
Default	2000	0	1	0.02	0.133	0.256	50.704
Balance	2000	1	4	2.32	0.725	0.534	0.174
Housing	2000	0	1	0.57	0.495	-0.275	-1.926
Loan	2000	0	1	0.16	0.365	1.877	1.524
Contact	2000	1	3	2.38	0.892	-0.823	-1.235
Day	2000	1	3	2.06	0.789	-0.115	-1.384
Month	2000	1	4	2.42	0.809	0.290	-0.395
Duration	2000	1	8	2.34	1.380	1.758	3.244
Campaign	2000	1	32	2.72	2.840	4.069	24.843
Pdays	2000	1	5	1.47	1.096	2.267	3.874
Previous	2000	0	20	0.54	1.607	5.191	38.656
Poutcome	2000	1	4	1.36	0.797	2.038	2.757

TABLE 5: Sample variance contribution rate table.

Composition	Total	Initial eigenvalue		Extract sum of squares and load			Rotation sum of square loading
		Variance%	Cumulative%	Total	Variance%	Cumulative%	Total
1	2.544	15.898	15.898	2.544	15.898	15.898	2.506
2	1.569	9.808	25.706	1.569	9.808	25.706	1.475
3	1.414	8.835	34.541	1.414	8.835	34.541	1.408
4	1.242	7.761	42.302	1.242	7.761	42.302	1.251
5	1.159	7.246	49.548	1.159	7.246	49.548	1.256
6	1.100	6.877	56.425	1.100	6.877	56.425	1.254
7	1.023	6.396	62.820	1.023	6.396	62.820	1.063
8	0.937	5.858	68.678				
9	0.880	5.499	74.176				
10	0.837	5.232	79.409				
11	0.803	5.018	84.427				
12	0.753	4.706	89.133				
13	0.620	3.877	93.010				
14	0.555	3.471	96.482				
15	0.397	2.483	98.965				
16	0.166	1.035	100.000				

It can be seen from Table 5 that the correlation coefficient matrix of variables has seven largest characteristic roots, which are 2.554, 1.599, 1.414, 1.242, 1.159, 1.100, and 1.023, respectively. The cumulative contribution rate of eigenvalue reaches 62.80%; that is to say, it contains most of the information of the original index. Based on the principle that the eigenvalue is greater than 1, seven main components can be extracted. In order to show the influence degree of principal components on the original index, it is necessary to establish their original factor load matrix. In order to facilitate the extraction of information and maximize the dispersion of principal components, the orthogonal

rotation method is used to further process the structurally simplified rotated factor load matrix, and the results are shown in Table 6. Finally, using these seven main component factors, instead of the original indicators, we can study the classification and preference of customers.

Table 6 only shows the load above 0.4, which clearly indicates the economic significance of each major component.

After determining the economic significance of the main component factors and calculating the score coefficient of the sample factors, the linear combination equation of 7 main component indexes and the original 16 indexes can

TABLE 6: Factor load matrix after sample rotation.

Attribute	Composition						
	1	2	3	4	5	6	7
Pdays	0.923						
Poutcome	0.913						
Previous	0.813						
Housing		-0.727					
Contact		0.687					
Month		0.584					
Marital			0.836				
Age			-0.800				
Balance				-0.656			
Default				0.635			
Loan				0.591			
Job					-0.806		
Education					0.742		
Day							0.744
Campaign							0.693
Duration							0.914

TABLE 7: Prediction errors corresponding to different hidden layer node numbers.

Number of hidden layer nodes	Prediction error	Number of hidden layer nodes	Prediction error
4	0.1176	9	0.0186
5	0.0933	10	0.0267
6	0.0658	11	0.1064
7	0.0872	12	0.0561
8	0.0143	13	0.0751

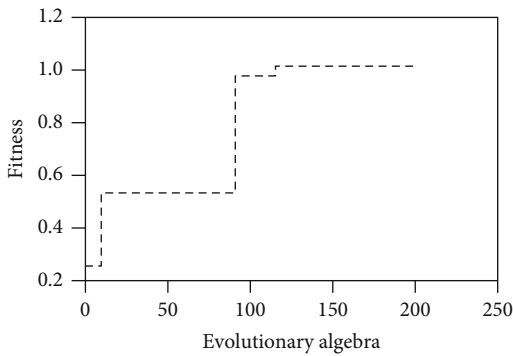


FIGURE 7: Variation diagram of fitness curve of traditional AGABP.

be obtained. These seven main component indicators can be replaced by the original 16 indicators as a new index system, which can be used as the input data of the follow-up model.

## 4. Experiment

4.1. *Definition of Model Structure and Selection of Parameters.* The sample data obtained from the principal

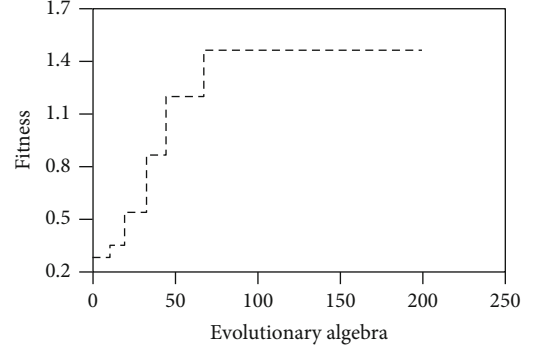


FIGURE 8: Change diagram of fitness curve of improved AGABP.

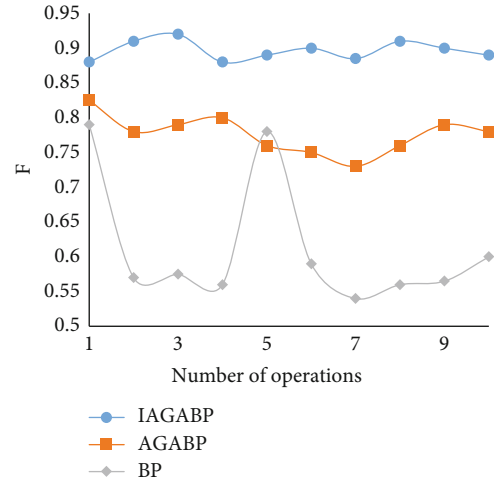


FIGURE 9: Comparison results of different algorithms.

component analysis of the original index of the sample is composed of 7 variables, so the number of input rows of the network is 7.

Determine the number of output layer nodes. The number of output layer nodes is determined by the number of desired output results of the network. This model divides the customer's output into two types, 1 for the customer's purchase and 0 for the customer's nonpurchase. Therefore, the number of output nodes of BP network model should be 1.

Determine the number of hidden layer nodes. Although there is no accepted standard so far, too much or too little is not appropriate. If the number is too large, the learning time will become longer, and the popularity of the network will decline. If the number is too small, the network may not be able to train or recognize new samples. Fault-tolerant performance is also greatly reduced. Here, the calculation is based on the following empirical equation (21).

$$n = \sqrt{a + b} + c. \quad (19)$$

Use estimates and show the results in Table 7.

The data in the table shows that when the number of implicit layer nodes is 8, the prediction error corresponding



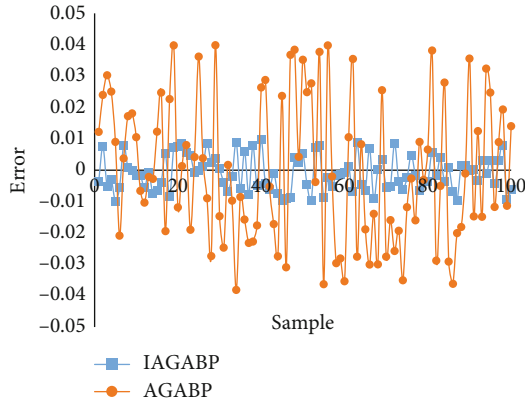


FIGURE 10: IAGABP and AGABP classification error result diagram of test set.

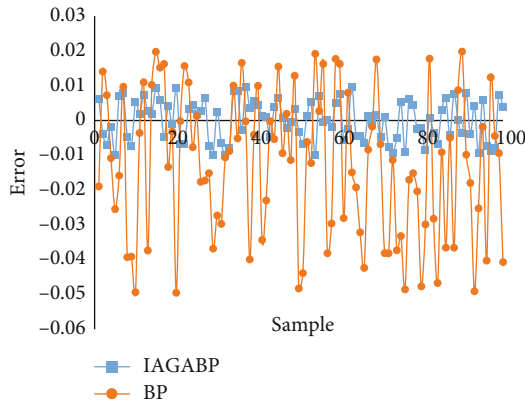


FIGURE 11: IAGABP and BP classification error result diagram of test set.

to BP neural network is the smallest, and 8 is selected as the number of implicit layer nodes. Make up a 7-8-1 network.

**4.2. Network Training and Result Verification.** In this paper, 2000 corporate financial customer data samples are randomly divided into two groups, and 1900 groups of data are used as training group training network. Another data set 100 examples detect the generalized performance of the network as a test set and predict customer categories and preferences.

**4.2.1. Algorithm Performance Analysis**

*(1) Comparison of Convergence Rate of Genetic Algorithm.* Set the end algebra to 200, and Figure 7 converges faster than Figure 8. This shows that the algebra of the latter should be much smaller than that of the former after setting a fixed convergence value, so the latter is much more efficient than the former.

People expect the same from all algorithms. I hope to converge early and realize overall optimization, but they are just a pair of contradictory requirements. As far as genetic algorithm is concerned, if it converges quickly, the

TABLE 8: Summary of prediction effect of each model.

Neural network type	BP neural network (BP)	Traditional adaptive genetic neural network (AGABP)	Improved adaptive genetic neural network (IAGABP)
Classification accuracy	73%	82%	97%

speed close to the best state will become faster, which cannot guarantee the diversity of combinations and makes it difficult to realize the overall optimization. In order to obtain the global optimum value, we must try our best to avoid falling into local extremum. This is because the population must keep the diversity of individuals as much as possible, so it cannot converge quickly. Therefore, if you want to combine the two, you should consider them comprehensively and choose from them. The method proposed in this paper not only pursues global optimization but also considers the operation speed of genetic algorithm, so as not to affect the global convergence speed as much as possible, thus finding a good balance between them.

*(2) Stability Analysis.* In order to verify the performance of the adaptive genetic neural network algorithm proposed in this paper, BP neural network algorithm, traditional adaptive genetic neural network algorithm, and improved adaptive genetic neural network algorithm are executed several times, respectively, and the correctness of the calculation method is evaluated according to  $F$  evaluation index. Here, the higher the  $F$  value, the higher the correctness of the result. The stability of the algorithm can be judged by whether the data has great changes. The experimental results are shown in Figure 9.

Through the above experimental results, it can be seen that the  $F$  value of the improved adaptive genetic neural network algorithm proposed in this paper is obviously higher than the other two algorithms in the global range, and the fluctuation in the global range is small, reflecting better stability. Among them, BP neural network algorithm has the smallest  $F$  value, which fluctuates greatly, and the lowest accuracy rate drops to less than 60%. As far as the traditional adaptive genetic neural network algorithm is concerned, its stability and accuracy have been improved to some extent, but compared with the improved adaptive genetic neural network algorithm, there are still some shortcomings, and the latter maintains better stability and higher accuracy.

From the above experimental results, it can be seen that the  $F$  value of the adaptive genetic neural network algorithm proposed in this paper is significantly higher than the other two algorithms in the global situation, and it fluctuates less in the global situation and shows better stability. The  $F$  number of BP neural network algorithm is the smallest, and it is easy to change greatly, and the lowest accuracy will reach below 60%. In the traditional adaptive genetic neural network algorithm, its stability and accuracy have been improved to some extent, but compared with the improved

adaptive genetic neural network algorithm, it is not sufficient, and the latter maintains better stability and high accuracy.

*4.2.2. Comparison of Classification Accuracy.* Figures 10 and 11 show the error results of classification test for 100 sets of data. It can be seen intuitively that the error of IAGABP is closer to 0 than that of AGABP and BP. To sum up, it can be concluded that IAGABP is more accurate than BP and AGABP in the application of corporate financial customer classification and preference.

According to the prediction results, if the indication with error within 0.01 is classified accurately, the prediction effects of each model on samples are summarized as shown in Table 8.

According to the data, the classification accuracy of adaptive genetic neural network is the highest, which is 24% and 15% higher than BP neural network and traditional adaptive genetic neural network, respectively.

## 5. Conclusion

Through the above research, we should provide targeted services to different types of customers.

### (1) Buy customers

Maintaining such customers plays a stable and important role in the income of financial enterprises. Therefore, financial enterprises must take measures to maintain long-term contact with them. For example, keep the communication channel smooth at all times. When issuing products or services, financial enterprises should let customers know in time, actively attract their opinions and actively improve to meet their needs. For example, the fee and annual fee of various cards are reduced, the agency business fees are eliminated, and the remittance fee rate and personal insurance rate are reduced.

### (2) Unpurchased customers

For such low-value customers, there is almost no contribution rate to financial products, but there are small deposits. For their needs, financial enterprises can reduce their counters and use the electronic equipment of financial enterprises. Such customers basically have no development value. The development cost is much higher than the income they create for the enterprise. Therefore, there is no need to carry out any marketing of products and services for such customers.

After analyzing the classification and preference of existing customers, financial enterprises should strive to provide corresponding services for different types of customers, maintain existing high-value customers to the maximum extent without wasting resources, and obtain more benefits for corporate finance. The future work needs to be carried out from the following points: (1) The data dimension of financial customers is insufficient, so we hope to analyze and predict the data under a large amount of data and adopt a deep multilayer learning complex model for learning and analysis; (2) intelligent algorithms can be applied to financial credit classification to dig deep into risky customers.

## Data Availability

The experimental data used to support the findings of this study are available from the corresponding author upon request.

## Conflicts of Interest

The authors declared that they have no conflicts of interest regarding this work.

## Acknowledgments

This work is supported by the Department of Education of Zhejiang Province.

## References

- [1] L. Zhang, T. Liu, Y. Xie, Z. Zeng, and J. Chen, "A new classification method of nanotechnology for design integration in biomaterials," *Nanotechnology Reviews*, vol. 9, no. 1, pp. 820–832, 2020.
- [2] O. Senvar, D. Akburak, and N. Yel, "Customer oriented intelligent DSS based on two-phased clustering and integrated interval type-2 fuzzy AHP and hesitant fuzzy TOPSIS," *Journal of Intelligent and Fuzzy Systems*, vol. 39, no. 5, pp. 6121–6143, 2020.
- [3] F. Pramaswari, A. P. Nasution, and S. L. Nasution, "The effect of branding quality and service quality on customer satisfaction through Financial Technology (FinTech) at PT. WOM Finance branch Rantauprapat," *Budapest International Research and Critics Institute (BIRCI-Journal) Humanities and Social Sciences*, vol. 4, no. 2, pp. 2995–3004, 2021.
- [4] X. Shi, G. Li, K. Li, J. Liu, and R. Wang, "Customer classification method of logistics enterprises based on BP-AdaBoost," *Journal of Physics Conference Series*, vol. 1670, 2020.
- [5] I. Raicu, "Financial banking dataset for supervised machine learning classification," *Informatica Economica*, vol. 23, pp. 37–49, 2019.
- [6] S. Thomas, M. Goel, and D. Agrawal, "A framework for analyzing financial behavior using machine learning classification of personality through handwriting analysis," *Journal of behavioral and experimental Finance*, vol. 26, p. 100315, 2020.
- [7] M. S. Dong, "Intelligent early warning of Internet financial risks based on mobile computing," *International Journal of Mobile Computing and Multimedia Communications*, vol. 11, no. 2, pp. 61–78, 2020.
- [8] S. Chavlis and P. Poirazi, "Drawing inspiration from biological dendrites to empower artificial neural networks," *Current Opinion in Neurobiology*, vol. 70, pp. 1–10, 2021.
- [9] C. M. Loo Christopher, T. Sasikumar, and T. Page, "Crack growth detection on Al/Sicp using acoustic monitoring and artificial neural network," *Materials Today: Proceedings*, vol. 16, no. P2, pp. 604–611, 2019.
- [10] S. Park, S. Seo, C. Jeong, and J. Kim, "The weights initialization methodology of unsupervised neural networks to improve clustering stability," *The Journal of Supercomputing*, vol. 76, no. 8, pp. 6421–6437, 2020.
- [11] M. V. Narkhede, P. P. Bartakke, and M. S. Sutaone, "A review on weight initialization strategies for neural networks," *Artificial Intelligence Review*, vol. 2, pp. 1–32, 2021.

- [12] S. Mirjalili, "Biogeography-based optimisation," in *Evolutionary Algorithms and Neural Networks* vol, pp. 57–72, Springer, 2019.
- [13] M. Zhou, Y. Long, W. Zhang et al., "Adaptive genetic algorithm-aided neural network with channel state information tensor decomposition for indoor localization," *IEEE Transactions on Evolutionary Computation*, vol. 25, no. 5, pp. 913–927, 2021.
- [14] V. Afzali Goroooh, S. Kalia, P. Nguyen et al., "Deep neural network cloud-type classification (DeepCTC) model and its application in evaluating PERSIANN-CCS," *Remote Sensing*, vol. 12, no. 2, p. 316, 2020.
- [15] S. Xu, N. Feng, K. Liu, Y. Liang, and X. Liu, "A weighted fuzzy process neural network model and its application in mixed-process signal classification," *Expert Systems with Applications*, vol. 172, no. 1, 2021.
- [16] Y. Ma, L. Li, Z. Yin, A. Chai, M. Li, and Z. Bi, "Research and application of network status prediction based on BP neural network for intelligent production line," *Procedia Computer Science*, vol. 183, no. 20, pp. 189–196, 2021.
- [17] D. Zhang, W. Li, X. Wu, and X. Lv, "Application of simulated annealing genetic algorithm optimized back propagation (BP) neural network in fault diagnosis," *International Journal of Modeling Simulation & Scientific Computing*, vol. 10, no. 4, pp. 1950024–1950049, 2019.
- [18] P. Mohamed Jebran and S. Gupta, "Pre-diabetic retinopathy identification using hybridGenetic algorithm-neural network classifier," *Journal of Physics: Conference Series*, vol. 1937, no. 1, 2021.
- [19] X. Feng, J. Zhao, and E. Kita, "Genetic algorithm-based optimization of deep neural network ensemble," *The Review of Socionetwork Strategies*, vol. 15, no. 1, pp. 27–47, 2021.
- [20] M. S. Kumar, "Image retrieval using heuristic approach and genetic algorithm," *The Journal of Computer Information Systems*, vol. 8, no. 4, pp. 1563–1571, 2019.
- [21] H. J. Lim, S. H. Choi, J. Oh, B. S. Kim, S. Kim, and J. H. Yang, "Adaptive ground control system of multiple-UAV operators in a simulated environment," *Aerospace Medicine and Human Performance*, vol. 90, no. 10, pp. 841–850, 2019.
- [22] S. Rani and B. Suri, "Investigating different metrics for evaluation and selection of mutation operators for Java," *International Journal of Software Engineering and Knowledge Engineering*, vol. 31, no. 3, pp. 311–336, 2021.
- [23] J. Wang, Y. Wen, Y. Gou, Z. Ye, and H. Chen, "Fractional-order gradient descent learning of BP neural networks with Caputo derivative," *Neural networks*, vol. 89, pp. 19–30, 2017.
- [24] E. Moulton, K. Bradbury, M. Barton, and D. Fein, "Factor analysis of the childhood autism rating scale in a sample of two year olds with an autism spectrum disorder," *Journal of Autism and Developmental Disorders*, vol. 49, no. 7, pp. 2733–2746, 2019.
- [25] L. Hou, Z. Zhang, Y. du, X. Wang, and C. Zhao, "An allergic risk factor analysis of extraordinary daytime only urinary frequency in children," *Risk Management and Healthcare Policy*, vol. 14, pp. 2683–2688, 2021.

## Research Article

# A Vehicle Detection Model Based on 5G-V2X for Smart City Security Perception

Teng Liu,<sup>1</sup> Cheng Xu ,<sup>1</sup> Hongzhe Liu ,<sup>1</sup> Xuewei Li,<sup>1</sup> and Pengfei Wang<sup>2</sup>

<sup>1</sup>Beijing Key Laboratory of Information Service Engineering, College of Robotics, Beijing Union University, Beijing, China

<sup>2</sup>Communication and Information Center of Ministry of Emergency Management of the People's Republic of China, Beijing, China

Correspondence should be addressed to Hongzhe Liu; liuhongzhe@buu.edu.cn

Received 23 September 2021; Accepted 10 November 2021; Published 27 November 2021

Academic Editor: Deepak Gupta

Copyright © 2021 Teng Liu et al. This is an open access article distributed under the Creative Commons Attribution License, which permits unrestricted use, distribution, and reproduction in any medium, provided the original work is properly cited.

Security perception systems based on 5G-V2X have become an indispensable part of smart city construction. However, the detection speed of traditional deep learning models is slow, and the low-latency characteristics of 5G networks cannot be fully utilized. In order to improve the safety perception ability based on 5G-V2X, increase the detection speed in vehicle perception. A vehicle perception model is proposed. First, an adaptive feature extraction method is adopted to enhance the expression of small-scale features and improve the feature extraction ability of small-scale targets. Then, by improving the feature fusion method, the shallow information is fused layer by layer to solve the problem of feature loss. Finally, the attention enhancement method is introduced to increase the center point prediction ability and solve the problem of target occlusion. The experimental results show that the UA-DETRAC data set has a good detection effect. Compared with the vehicle detection capability before the improvement, the detection accuracy and speed have been greatly improved, which effectively improves the security perception capability based on the 5G-V2X system, thereby promoting the construction of smart cities.

## 1. Introduction

With the continuous advancement of the construction of smart cities, the technology of intelligent networked vehicles has been greatly developed. They are equipped with sensors, controllers, actuators, and other devices on the basis of traditional vehicles. With the support of modern communication technology and network technology, information sharing and exchange between cars and everything is realized. To a certain extent, the intelligent networked vehicle realizes the organic unity of complex environment perception and intelligent decision-making and effectively realizes the control and execution management of the vehicle system. Improving the overall security of the smart city system has become a focal issue. V2X technology has different delay and coverage requirements in different business scenarios. For example, in active safety management such as collision avoidance and warning, the delay is required to be maintained at 20-100 ms. In business scenarios such as navigation, traffic lights, and road conditions, the delay should be controlled to 500 ms. Although the size of this type of data

packet is small, its coverage is relatively large. Generally, the communication coverage of V2X technology under this type of business is as high as 1000 m, standardized control of V2X technology, and reduce the time for perception and decision-making; expand the control range of navigation, traffic lights, etc., can effectively ensure the efficiency and safety of road traffic. At the perception level, it effectively improves the detection time of vehicles and other terminals on pedestrians, vehicles, traffic signs, and other targets. It can greatly reduce the processing time of the overall network, thereby improving the communication efficiency of the 5G-V2X network. The 5G-V2X-based technology effectively realizes the complementary advantages of each vehicle-mounted sensor system. Therefore, the improvement based on 5G-V2X perception technology provides an important guarantee for the safety of the entire system [1, 2].

In recent years, deep learning technology has continued to develop and has made huge breakthroughs, using convolutional neural networks to automatically extract target features. Thanks to the powerful feature extraction capabilities of the convolutional neural network, the detection accuracy



of the target detection algorithm is greatly improved, and it has stronger robustness and can adapt to more complex recognition scenarios. In the process of vehicle target detection, there are problems such as intervehicle occlusion, target deformation, and small target size, which make the detection accuracy not high. Therefore, the detection problem of small targets and occluded targets in vehicle detection is solved, and the detection accuracy and speed are improved. It has become a hot issue in the field of vehicle target detection. In response to the above problems, researchers have proposed feature extraction methods such as feature pyramids [3–5] and target detection algorithms without anchor frame [6, 7]. Some scholars [8] proposed a spatiotemporal event interaction model (STEIM) on this basis to solve the problem of time and data interaction in the V2X environment.

The improved method based on the feature pyramid can extract the features of small-scale targets well, but it requires a lot of computational overhead. The improved method based on the anchorless frame can directly extract the target features and classify them. The detection speed is faster than the previous method, but it cannot detect small-scale targets and adjacent targets well.

To solve the above problems, this paper proposes an improved algorithm based on the single-stage target detection algorithm CenterNet. Three improved methods are mainly used:

- (1) An adaptive feature extraction method is proposed to increase multiscale target features and improve the feature extraction capability of small targets
- (2) An adaptive feature fusion method is proposed, adding a feature branch to effectively fuse high-level and low-level features
- (3) A center point enhancement method is proposed to increase spatial information and effectively enhance the prediction ability of the target center point

The improved network I-CenterNet (Improved CenterNet) can fully extract low-level network location information, reduce the loss of feature map information in feature fusion, increase the attention of small targets, and improve the detection accuracy and speed of small targets and occluded targets.

The second chapter is related work, the third chapter is technical method, the fourth chapter is experiments and data set description, the fifth chapter is the analysis of experimental results, and the sixth chapter is the conclusion.

## 2. Smart City Security Perception Related Work

In recent years, the rapid development of deep learning has made significant breakthroughs in environmental perception technology. The proposal of AlexNet [9] in 2012 opened the curtain on the development of deep learning, and the proposal of VGGNet [10] in 2014 made the realization of deep neural networks possible. In 2015, ResNet [11] proposed to solve the gradient explosion problem through the residual connection method and reduce the model conver-

gence time. Shi et al. [12] propose a one-stage, anchor-free detection approach to detect arbitrarily oriented vehicles in high-resolution aerial images. The vehicle detection task is transformed into a multitask learning problem by directly predicting high-level vehicle features via a fully convolutional network. Nowadays, target detection algorithms are mainly divided into two categories: one-stage method and two-stage method. The two-stage method generates a series of candidate frames through algorithms and then performs regression and classification on the candidate frames. It is characterized by high accuracy but relatively low recognition speed.

In order to overcome the above problems, the researchers proposed a one-stage method, which mainly cancels the step of candidate frame generation, directly uses a convolutional neural network to perform convolution operations on image data, and detects and classifies the extracted features. In 2016, the YOLO (you only look once) [13] series of algorithms was proposed, which solved the real-time problem of the algorithm while ensuring the recognition accuracy. The SSD [14] detection algorithm combines the advantages of the Fast R-CNN series [15, 16] algorithm and the YOLO algorithm and realizes the detection of targets of various sizes by generating candidate frames of different sizes on the multiscale feature inspection map. Such as literature [17, 18] is used for vehicle target detection. Zheng and Chen [19] improved the cascading region of interest to increase the context information, which effectively improved the detection accuracy of small targets. Liang et al. [20] used an extra scaling branch of the deconvolution module with an average pooling operation to form a feature pyramid. The original feature fusion branch is adjusted to be better suited to the small object detection task. Chen [21] and others improved the feature extraction network by adding ResNet, deconvolution, and other methods to increase the detection ability of small target vehicles. Wang et al. [22] proposed a soft weighted average method, which “punishes” the detection result of the corresponding relationship through confidence attenuation, which improves the detection accuracy of road vehicles. Xu et al. [23] used deep learning models and blockchains in combination with blockchains and supporting intelligent hardware to achieve true recording and tracking of the entire fruit process. Improve the transparency and efficiency of the supply chain and reduce the cost of the supply chain.

In recent years, there has been an anchorless frame method [24, 25], which directly detects and locates the target through key points, which greatly reduces the network parameters and calculations, improves the detection speed, and its detection accuracy is also higher than that of the traditional one-stage and two-stage method. The one-stage method slides the complex arrangement of possible bounding boxes (anchors) on the image and then directly classifies the boxes without specifying the contents of the boxes. The two-stage method recalculates image features for each potential frame and then classifies those features. Postprocessing, namely, nonmaximum suppression (NMS), deletes duplicate detection frames of the same target by calculating the IOU between the bounding boxes. The method of the



anchorless target detection network is different from other networks. For example, the ConerNet [26] algorithm uses two corner points to predict the target, and the CenterNet [27] uses the target center point to present the target, and the image needs to be transferred to the volume. In the product neural network, a heat map is obtained, and the peak center point of the heat map is the center point. Then, return to the target's size, positions, and other attributes at the center point, thus turning the target detection problem into a standard key point estimation problem.

This type of algorithm is different from the traditional one-stage method. The anchor point of CenterNet is placed in a position, which can be regarded as an anchor of a shape and position. It does not need to manually set a threshold to distinguish between the foreground and the background, so the network does not need to prepare the anchor in advance. Each target has only one positive anchor, so there is no need for NMS operation to screen candidate frames, which greatly reduces network parameters and calculations. Its detection accuracy is also higher than the traditional one-stage and two-stage methods, and the detection speed meets the requirements of real-time detection, but there are still insufficient multiscale feature extraction, and the recognition of small-scale targets and occluded targets is not accurate. Insufficient context information at the time leads to the problem of false detection and missed detection of adjacent targets. Therefore, this article is based on the CenterNet network to improve, overcome the above problems in the small-scale vehicle detection problem, and propose the I-CenterNet vehicle target detection method.

### 3. Vehicle Detection Model Based on 5G-V2X

In order to solve the problem of insufficient low-dimensional feature extraction in the vehicle target detection problem in the 5G-V2X scene, adaptive context feature extraction is adopted. In order to overcome the problem that the network is more sensitive to high-dimensional features than low-dimensional features, the feature fusion method is improved, and the weight of small target features is increased. Aiming at the problem of inaccurate prediction of the target center point position in the detection method based on the anchorless framework, a center point position enhancement method is proposed. Improve the ability of the improved network to detect small-scale targets and occluded targets in vehicle small target detection, effectively improve the vehicle perception efficiency in the Internet of Vehicles environment, and reduce the operating pressure of the 5G-V2X system. The overall structure is shown in Figure 1.

**3.1. Adaptive Context Feature Extraction.** In the process of vehicle target detection, there are problems that the target is occluded, and the target is too small. During the detection process, a large amount of feature information will be lost after convolution and pooling operations, which will reduce the detection accuracy. And CenterNet only uses ResNet50/101 as the backbone network for feature extraction, which is prone to insufficient feature extraction.

In response to the above problems, this paper uses an adaptive context feature extraction method to improve the input layer of the network as follows. As shown in Figure 2, the input feature map of the Conv3-3 layer is pooled to  $3 \times 3$ ,  $7 \times 7$ , and  $9 \times 9$ , three different scales, to get different contextual information. Each pooled feature uses  $1 \times 1$  convolution for channel integration and then uses the deconvolution operation to separate each the feature map is upsampled to the same size as the shape.

The input traffic scene picture contains vehicles of various scales, and context features cannot be simply combined. Therefore, a scale fusion unit is added after the context feature extraction network, and the weights of each feature are added to increase the weight of small-scale targets. And use the jump connection method to fuse the original features into the upsampling features, the operation is as follows:

$$y_{ff} = a \cdot f^1 + b \cdot f^2 + c \cdot f^3 + d \cdot f^4. \quad (1)$$

Among  $y_{ff}$  is the output feature of the adaptive feature extraction network, which  $f^k (k \in \{1, 2, 3, 4\})$  represents the context feature map extracted at different levels after upsample and using the point multiplication operation to fuse the original features. For example, the  $f^1$  is as follows:

$$f^1 = f^{2 \times 2} \cdot f_2. \quad (2)$$

Among  $f^1$ , as mentioned above,  $f^{2 \times 2}$  is the original  $2 \times 2$  convolution feature, and  $f_2$  is the feature after upsampling.

The parameters  $a$ ,  $b$ , and  $c$ ,  $d$  represents scale weights, and the network can automatically learn these parameters, set  $a + b + c + d = 1$ ,  $a, b, c, d \in (0, 1)$ , and take the calculation formula  $a$  as an example, as shown below:

$$a = \frac{at(f^4)}{at(f^4) + at(f^3) + at(f^2) + at(f^1)}. \quad (3)$$

Among  $at$  is the composition of average pooling and sigmoid activation function, which can be calculated by the same calculation method to obtain  $b$ ,  $c$ , and  $d$ .

**3.2. Improved Feature Fusion Module.** After the context feature is extracted, it is integrated through  $1 \times 1$  convolution, followed by an improved feature fusion module. It can adaptively select important spatial location information and semantic information from the context feature extraction network by weighting, and complete the information fusion after fusing each feature. Among them, the features from the bottom layer contain a large amount of spatial information, which is suitable for target positioning. The high-level features contain a lot of semantic features, which are suitable for target classification. However, the original network cannot effectively use the spatial information of the underlying network and the semantic information of the high-level features, so this paper proposes an improved feature extraction module.

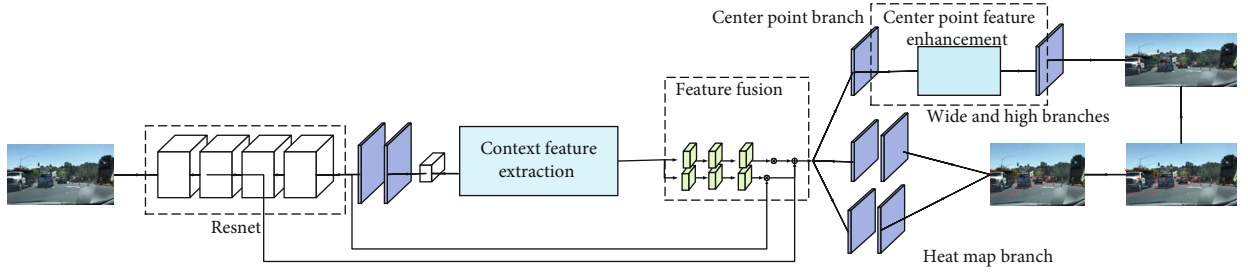


FIGURE 1: The overall network framework. The image has been improved feature extraction and feature fusion module, and the center point feature enhancement module of the attention mechanism is added when the center point and anchor frame are generated, and the obtained anchor frame and center point are matched to obtain the final result.

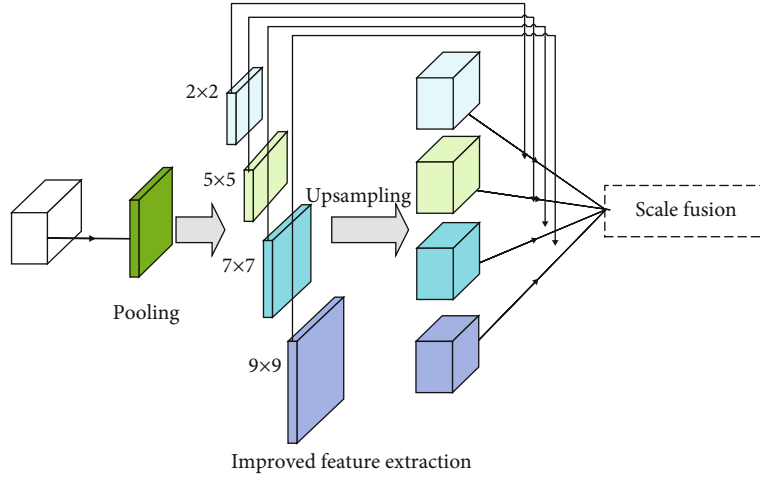


FIGURE 2: Feature fusion module. By pooling to different scales and using treaty links to get more features.

The improved feature extraction module proposed in this paper can adaptively perform feature fusion, as shown in Figure 3. Among them are the basic feature maps of each layer of feature extraction. Since the low- and high-level feature maps have different sizes of resolution and number of channels, bilinear interpolation is used to unify them to the same size. The input  $f_{in}$  is the original input and then enters the feature selection layer, uses  $1 \times 1$  convolution to continue feature smoothing, adjusts the resolution and the number of channels after a  $3 \times 3$  convolution layer, and then connects to the sigmoid activation function for output. Among them, the learning weight parameters are  $a$  and  $b$ , and feature fusion is performed in the manner shown in equation (4). Since low-dimensional and high-dimensional features mainly exist in the bottom and top layers of the network, this paper simply takes only the bottom features as the input low-dimensional features, and the highest-level output is taken as high-dimensional features.

$$y = a \otimes f_l + b \otimes f_h, \quad (4)$$

where  $y$  represents the final output feature of the feature fusion module,  $f_l$  represents the processed low-level feature, and  $f_h$  represents the processed high-level feature.  $\otimes$  means the corresponding position is multiplied, and  $\oplus$  means the

corresponding position is added. The improved feature fusion module weights the features of different layers through the learned weights and performs the screening and fusion of feature information, which not only strengthens the semantic features in the low-level features but also adds more spatial locations to the high-level feature information.

**3.3. Center Point Feature Enhancement.** In order to solve the problem that when the original network generates the heat map to predict the target center point, the center point position does not match the true center point position. The original network believes that the peak of the heat map is the center point, and the width and height information of the target at the peak point of each feature map is used. But in the actual picture, the geometric center of the object is not necessarily the peak point of the heat map, and there is a certain deviation. And when the network faces obstructed objects, it is easy to show that the predicted heat map has only one peak point. This leads to deviations between the predicted center point of the heat map and the actual target center point. In this paper, the problem of center point position offset is solved by the way of center point feature enhancement.

Like the CBAM (Convolutional Block Attention Module) module, the channel attention module structure in this

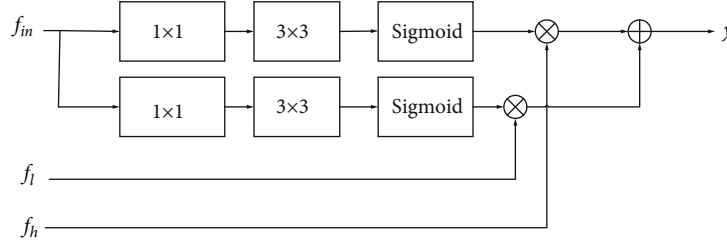


FIGURE 3: Feature fusion module. The input features go through two identical convolution modules and are, respectively, fused with the underlying and high-level semantic features, and the final fused feature is obtained.

paper is shown in Figure 4. First, the features are, respectively, passed through the maximum pooling and average pooling operations to obtain two one-dimensional vectors, and then the two channels' attention of the feature is obtained by fusing the features, which can reduce the complexity of the operation and maintain a high channel attention. The calculation can be expressed by the following formula.

$$M_c(F) = \sigma \text{AvgPool}(F) + \omega \text{MaxPool}(F). \quad (5)$$

Among them,  $F$  denotes the input feature map, AvgPool and MaxPool denote average pooling and maximum pooling, respectively, and  $\sigma$  and  $\omega$  denote the weights of the two operations, taking 1 and 0.5, respectively.

The spatial attention structure is shown in Figure 5. First, the input features are pooled to the maximum, and then, the pooled features are averagely pooled, followed by a convolution operation with a convolution kernel of  $3 \times 3$  and a skip connection. Fuse the original features of the input and the pooled features to increase the spatial feature attention, and finally output through the sigmoid function. The calculation formula is as follows:

$$M_s(F) = \partial(f^{3 \times 3}([\text{AvgPool}(F); \text{MaxPool}(F)]) \cdot F), \quad (6)$$

where  $\partial$  represents the sigmoid activation function and represents the input feature map, and *AvgPool* and *MaxPool* represent average pooling and maximum pooling, respectively.

In this paper, the improved channel and spatial attention are connected in series. Since the position of the center point is sensitive to spatial information, a spatial attention module is added, as shown in Figure 6.

By introducing the center point feature enhancement module, the accuracy of center point prediction is increased, and the problem that the position of the predicted target center point in the original network does not match the true center point is solved. In the vehicle detection, the accuracy of the center point prediction of obstructed vehicles and smaller vehicles in the distance is increased.

In summary, this paper proposes an adaptive feature extraction network, which can not only extract multiscale context features but also adaptively perform weighted fusion of features according to the different scale distributions of potential targets in the input image. The improved feature

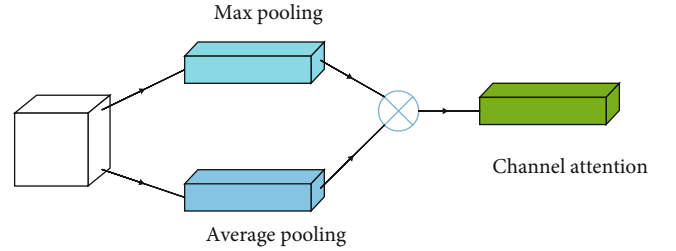


FIGURE 4: The channel attention module passes through the maximum pooling and average pooling layers, respectively, and the features obtained by the pathogenesis layers are multiplied to obtain the final channel attention.

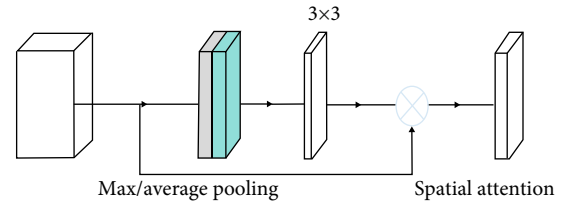


FIGURE 5: The spatial attention module adopts  $3 \times 3$  convolution after two maximum pooling and average pooling and superimposes the original features to obtain the final spatial attention output.

fusion module can combine low-level and high-level features. Features are weighted and fused to increase the weight of small targets. On this basis, the central point feature enhancement module is added, which effectively improves the accuracy of the target central point position. In summary, it effectively improves the network's ability to detect small vehicle targets and occluded targets.

## 4. Analysis of Experimental Results

**4.1. Experiment Environment.** The experimental platform of this article is as follows: Intel(R) Xeon E5@1.5 GHz, 32 G memory, Ubuntu 18 system, graphics card Nvidia GTX 1080ti, the program running python environment is Python 3.6, using PyTorch 1.5, CUDA 10.1, and the data set using UA-DETRAC data. When training, the following data enhancement methods are adopted for the original data during training, and the data is amplified to increase the diversity of training samples, including random angle rotation, brightness change, noise interference, and moderate transformation.

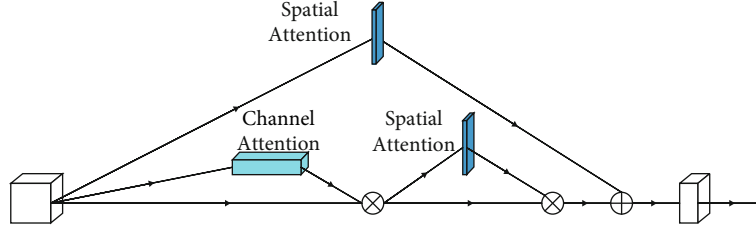


FIGURE 6: The center point feature enhancement passes through one spatial attention convolution module; the other uses the channel attention module first and then uses the spatial attention module. Output the two features through  $1 \times 1$  convolution.

4.2. *Results and Evaluation Indexes.* This paper uses  $P$  (precision),  $R$  (recall), and mean average precision (mAP) to test the performance of the model.

The accuracy rate  $P$  is actually the proportion of samples that are actually positive and predicted to be positive to all samples that are predicted to be positive. The formula is as follows:

$$P_{pre} = \frac{TP}{TP + FP}. \quad (7)$$

Among TP (true positives) refers to samples that were originally positive and classified as positive; FP (false positives) refers to samples that were originally negative but were classified as positive.

Recall rate  $R$  is the proportion of samples that are actually positive and predicted to be positive to all samples that are actually positive. The formula is as follows:

$$R_{re} = \frac{TP}{TP + FN}. \quad (8)$$

Among FN (false negative) refers to samples that were originally positive but classified as negative. The area enclosed by the P-R curve is the average accuracy mean mAP. The index to measure recognition accuracy in target detection is mAP. In multiple categories of object detection, each category can draw a curve based on recall and precision. AP is the area under the curve, and mAP is the average of multiple categories of AP.

Using the trained model to test the test set, the average accuracy can reach 89.9%, the accuracy rate  $P$  reaches 94.3%, the recall rate  $R$  reaches 93.7%, and the detection speed reaches 0.185/s. At the same time, the mainstream detection models are compared. As shown in Table 1, it can be seen from the table that the average accuracy of the method proposed in this paper is 7.7% higher than that of the original network, and the speed is relatively faster, and the detection speed is basically the same. In this case, the accuracy is higher than that of YOLOv4. The experimental effect is better and faster than Faster-RCNN.

The experimental results are shown in Figure 5. The results compare the I-CenterNet, Faster-RCNN, and CenterNet of this article. It can be seen from the figure that I-CenterNet effectively recognizes the smaller vehicles in the distance and successfully detects the occluded vehicles. Faster-RCNN and CenterNet cannot accurately identify

TABLE 1: Comparison of multiple detection algorithms.

Model	$P/\%$	$R/\%$	mAP/ $\%$	Time/s
Faster-RCNN [16]	93.2%	90.3%	91.5%	0.548
SSD [14]	85.6%	79.1%	82.3%	0.173
CenterNet [27]	87.8%	86.4%	87.2%	0.195
YOLOv3 [13]	86.3%	83.1%	84.8%	0.192
YOLOv4 [28]	89.2%	86.6%	87.4%	0.188
Ours	95.3%	92.7%	94.9%	0.185

small vehicles in the distance and recognize the two blocked vehicles as one target, and there are cases where individual vehicles cannot be detected.

The experimental results are shown in Figure 7. The results compare the I-CenterNet, Faster-RCNN, and CenterNet of this article. It can be seen from the figure that I-CenterNet effectively recognizes the smaller vehicles in the distance and successfully detects the occluded vehicles. Faster-RCNN and CenterNet cannot accurately identify small vehicles in the distance and recognize the two blocked vehicles as one target, and there are cases where individual vehicles cannot be detected.

4.3. *Comparison of Various Modules.* In this paper, an ablation experiment is performed on each module, and the detection method is the same as above. The original CenterNet network, CenterNet+ improved feature extraction and feature fusion (CenterNet\*), CenterNet+ center point feature enhancement (CenterNet\*\*), and CenterNet+ improved feature extraction and feature fusion + center point feature enhancement (I-CenterNet) were compared, respectively. And draw the PR curve of Bus, Truck, Car, and others category, as shown in Figure 8; it can be seen from the figure that under this data set, the detection effect of the “Bus” category has been improved, when  $R = 0.5$  and  $P = 0.16$  improved. The accuracy of the latter algorithm is 32% higher than that of the CenterNet network. And from the figure, it can be seen that P-R curve of the improved algorithm has more surrounding area, and the AP value of the proposed model (I-CenterNet) in Bus recognition is 87.6%, which is an increase of 1.4% compared to the original model. The model proposed in this paper has an AP value of 91.5% in the identification of the Truck class, which is an increase of 0.8% compared to the original model, and the detection effect is better.





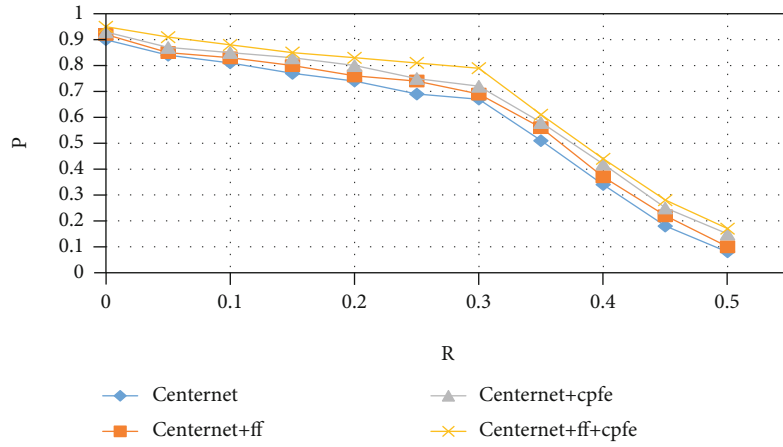
FIGURE 7: Experimental results of this article. Among them, (a) is the original input image, (b) is the improved result proposed in this paper, (c) is the output result of Faster-RCNN, and (d) is the output result of CenterNet. The model in this paper has identified more vehicles and effectively identified blocked vehicles.

The feature extraction and feature fusion methods proposed in this paper strengthen the extraction operation of the underlying features through skip connection and increase the spatial information of the target. On this basis, the low-level and high-level features are effectively integrated through feature fusion methods. The spatial and location information in the feature is improved, and the network's ability to extract small targets is improved. It can be seen from the comparative experiment that the improved method has greatly improved the detection performance of the network. Finally, the center point feature enhancement

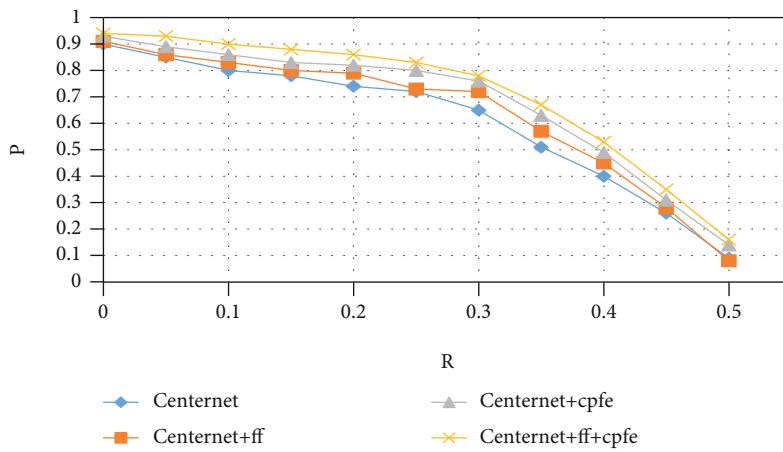
method is used to correct the center point position to improve the network's ability to detect current objects. The contribution rate of this part to network performance is close to 1%.

We also compared the results of center point enhancement. As shown in Figure 9, (a) represents the original image, (b) represents the result of applying center point enhancement, and (c) represents the result of the original network. The point on the vehicle in the figure is the predicted center point. It can be seen that compared with the center point predicted by the improved network, the

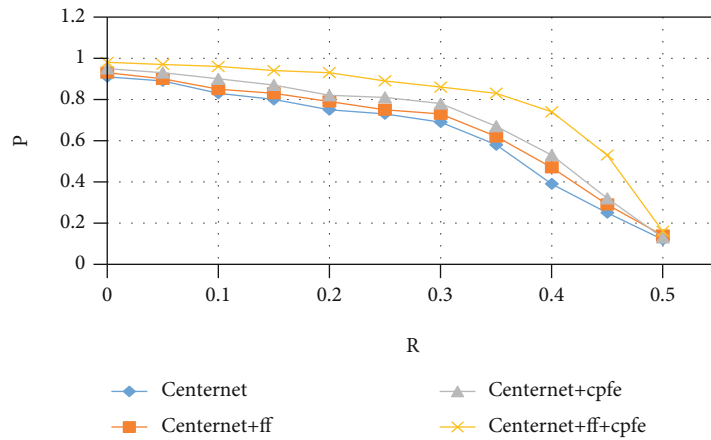




(a)



(b)



(c)

FIGURE 8: Continued.

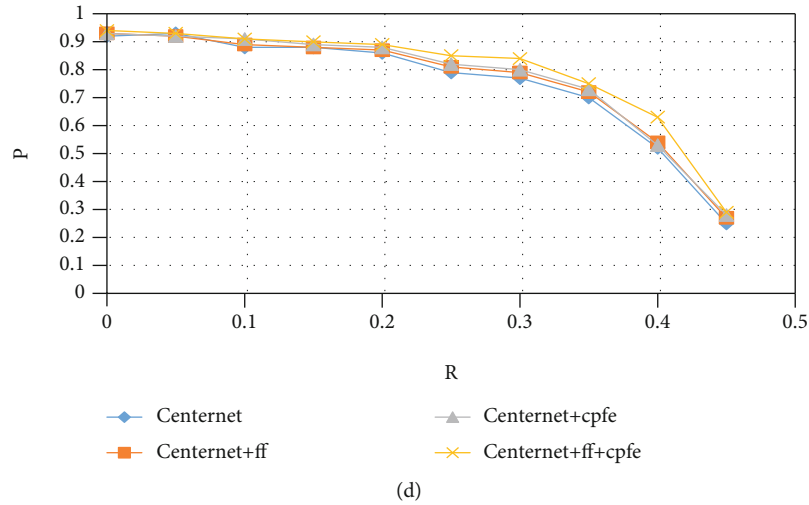


FIGURE 8: Comparison of the accuracy-call rate curves of different algorithms in this data set: (a) Bus; (b) Truck; (c) Car; (d) others. The results show that the curve enclosing area of the model in this paper is more.



FIGURE 9: Comparison of modules with enhanced center points: (a) the input image; (b) the result of the model in this paper; (c) the output result of CenterNet. It can be seen from the results that the center point enhancement model is used, and the predicted midline point is closer to the true center point of the target.

predicted center point in the original network is deviated from the obvious predicted point in individual vehicles, and it is not in the geometric center of the vehicle. In the smaller vehicles in the distance, the block and target are smaller. The center point of the original network prediction is often close or not predicted, which will cause the predicted target frame to be inac-

curate, and two vehicles that are very close together are recognized as one. The method in this paper avoids the problems of occlusion and inaccurate detection of small targets and accurately predicts the center point.

Table 2 compares and improves the detection effects of each module. It can be seen from the table that on this data

TABLE 2: Comparison and improvement of the detection effect of each module.

Model	P/%	R/%	mAP/%
CenterNet [27]	87.8%	86.4%	87.2%
CenterNet*	90.3%	87.3%	89.3%
CenterNet**	93.9%	89.6%	91.8%
I-CenterNet	95.3%	92.7%	94.9%

TABLE 3: Different backbone networks use the improved feature extraction method, and the results show that the method in this paper has a more obvious improvement effect on the ResNet network.

Model	Backbone	Feature extraction	Box AP/%
Faster-RCNN [16]	R-101	N	39.4%
	R-101	Y	41.5%
Dynamic R-CNN [29]	R-50	N	38.9%
	R-50	Y	40.3
ConerNet [26]	HourglassNet-104	N	40.4
	HourglassNet-104	Y	40.8

set, the improved model is compared with the original model in the same category of detection, and the model average of the feature extraction and feature fusion modules is added. The accuracy has increased by 1.5%, and the average accuracy of the model with the attention mechanism has increased by 1.0%. And the average frame rate meets the requirements of real-time detection. According to the experimental results, the improved CenterNet algorithm performs the best overall, which not only guarantees the real-time detection but also ensures the detection ability of small vehicle targets and occluded targets. We use the feature extraction method in this article for different backbone networks, where “N” means not using the method in this article and “Y” means using the method in this article. It can be seen from Table 3 that the method in this paper has an improvement effect on the mainstream backbone network, and the improvement of the backbone network of the ResNet series is more obvious. Using ResNet 50 network, Box AP value increased by 1.4%.

## 5. Conclusion

Aiming at the 5G-V2X-based smart city security perception vehicle detection problem, this paper proposes an improved vehicle target detection algorithm based on a deep learning target detection network. An adaptive feature extraction module is proposed to increase multiscale feature extraction capabilities for small vehicle targets. The feature fusion method is improved, and low-level features and high-level features are adaptively fused through weighting, which overcomes the problem that the network is more sensitive to

high-dimensional features than low-dimensional features. A center point feature enhancement method is proposed to improve the prediction accuracy of the center point position, which can improve the useful feature weight suppression and suppress the invalid weight and solve the problem of inaccurate prediction of the center point position of similar targets. The test results show that the overall performance of the model proposed in this paper is better than the original CenterNet network. The average accuracy rate is 94.9%, and the effectiveness of each module is verified through experiments. On the premise of ensuring the detection speed, the network’s ability to detect small vehicles and obstructed vehicles is improved. It can realize the detection of vehicles and other targets at the vehicle terminal, improve the operating efficiency of the perception layer, reduce the communication pressure of the 5G-V2X network in the network layer, reduce the transmission and processing pressure of cloud data, which can leave more computing resources for other tasks, and improve the operating efficiency and safety of the overall system.

## Data Availability

The data sets used and/or analyzed during the current study are available from the corresponding author on reasonable request.

## Conflicts of Interest

The authors declare that they have no conflicts of interest.

## Acknowledgments

This work was supported by the Beijing Municipal Commission of Education Project (Nos. KM202111417001 and KM201911417001), the National Natural Science Foundation of China (Grant Nos. 61871039, 62102033, 62171042, 62006020, and 61906017), the Collaborative Innovation Center for Visual Intelligence (Grant No. CYXC2011), and the Academic Research Projects of Beijing Union University (Nos. BPHR2020DZ02, ZB10202003, ZK40202101, and ZK120202104).

## References

- [1] C. Xu, H. Liu, Z. Pan, W. Li, and Z. Ye, “A group authentication and privacy-preserving level for vehicular networks based on fuzzy system,” *Journal of Intelligent & Fuzzy Systems*, vol. 39, no. 2, pp. 1547–1562, 2020.
- [2] C. Xu, H. Liu, Y. Zhang, and P. Wang, “Mutual authentication for vehicular network in complex and uncertain driving,” *Neural Computing and Applications*, vol. 32, no. 1, pp. 61–72, 2020.
- [3] T. S. Sharan, S. Tripathi, S. Sharma, and N. Sharma, “Encoder modified U-net and feature pyramid network for multi-class segmentation of cardiac magnetic resonance images,” *IETE Technical Review*, *Early Access*, pp. 1–13, 2021.
- [4] Q. Zhou, J. Wang, J. Liu, S. Li, W. Ou, and X. Jin, “RSANet: towards real-time object detection with residual semantic-guided attention feature pyramid network,” *Mobile Networks and Applications*, vol. 26, no. 1, pp. 77–87, 2021.

- [5] S. Chen, Z. Zhang, R. Zhong, L. Zhang, H. Ma, and L. Liu, "A dense feature pyramid network-based deep learning model for road marking instance segmentation using MLS point clouds," *IEEE Transactions on Geoscience and Remote Sensing*, vol. 59, no. 1, pp. 784–800, 2021.
- [6] S. Fan, F. Zhu, S. Chen et al., "FII-CenterNet: an anchor-free detector with foreground attention for traffic object detection," *IEEE Transactions on Vehicular Technology*, vol. 70, no. 1, pp. 121–132, 2021.
- [7] Z. He, Z. Ren, X. Yang, Y. Yang, and W. Zhang, "MEAD: a mask-guided anchor-free detector for oriented aerial object detection," *Applied Intelligence*, pp. 1–16, 2021.
- [8] C. Xu, H. Luo, H. Bao, and P. Wang, "STEIM: a spatiotemporal event interaction model in V2X systems based on a time period and a raster map," *Mobile Information Systems*, vol. 2020, Article ID 1375426, 20 pages, 2020.
- [9] A. Krizhevsky, I. Sutskever, and G. E. Hinton, "Imagenet classification with deep convolutional neural networks," *Advances in Neural Information Processing Systems*, vol. 25, pp. 1097–1105, 2012.
- [10] K. Simonyan and A. Zisserman, "Very deep convolutional networks for large-scale image recognition," *Computational and Biological Learning Society*, pp. 1–14, 2015.
- [11] K. He, X. Zhang, S. Ren, and J. Sun, "Deep residual learning for image recognition," in *Proceedings of the IEEE conference on computer vision and pattern recognition*, pp. 770–778, Las Vegas, Nevada, 2016.
- [12] F. Shi, T. Zhang, and T. Zhang, "Orientation-aware vehicle detection in aerial images via an anchor-free object detection approach," *IEEE Transactions on Geoscience and Remote Sensing*, vol. 59, no. 6, pp. 5221–5233, 2021.
- [13] J. Redmon, S. Divvala, R. Girshick, and A. Farhadi, "You only look once: unified, real-time object detection," in *Proceedings of the IEEE conference on computer vision and pattern recognition*, pp. 779–788, Las Vegas, Nevada, 2016.
- [14] W. Liu, D. Anguelov, D. Erhan et al., "October. SSD: single shot multibox detector," in *European conference on computer vision*, pp. 21–37, Springer, Cham, Amsterdam, Netherlands, 2016.
- [15] R. Girshick, "Fast R-CNN," in *Proceedings of the IEEE international conference on computer vision*, pp. 1440–1448, Santiago, Chile, 2015.
- [16] S. Ren, K. He, R. Girshick, and J. Sun, "Faster R-CNN: towards real-time object detection with region proposal networks," *Machine Intelligence*, vol. 39, no. 6, pp. 1137–1149, 2017.
- [17] J. Cao, C. Song, S. Song et al., "Front vehicle detection algorithm for smart car based on improved SSD model," *Sensors*, vol. 20, no. 16, p. 4646, 2020.
- [18] M. A. A. al-qaness, A. A. Abbasi, H. Fan, R. A. Ibrahim, S. H. Alsamhi, and A. Hawbani, "An improved YOLO-based road traffic monitoring system," *Computing*, vol. 103, no. 2, pp. 211–230, 2021.
- [19] Q. Zheng and Y. Chen, "Feature pyramid of bi-directional stepped concatenation for small object detection," *Multimedia Tools and Applications*, vol. 80, no. 13, pp. 20283–20305, 2021.
- [20] X. Liang, J. Zhang, L. Zhuo, Y. Li, and Q. Tian, "Small object detection in unmanned aerial vehicle images using feature fusion and scaling-based single shot detector with spatial context analysis," *IEEE Transactions on Circuits and Systems for Video Technology*, vol. 30, no. 6, pp. 1758–1770, 2020.
- [21] S. Chen, "A traffic scene target detection algorithm with dual attention module," *World Scientific Research Journal*, vol. 6, no. 9, pp. 99–107, 2020.
- [22] H. Wang, Y. Yu, Y. Cai, X. Chen, L. Chen, and Y. Li, "Soft-weighted-average ensemble vehicle detection method based on single-stage and two-stage deep learning models," *IEEE Transactions on Intelligent Vehicles*, vol. 6, no. 1, pp. 100–109, 2021.
- [23] C. Xu, K. Chen, M. Zuo, H. Liu, and Y. Wu, "Urban fruit quality traceability model based on smart contract for Internet of Things," *Wireless Communications and Mobile Computing*, vol. 2021, Article ID 9369074, 10 pages, 2021.
- [24] L. Jiao, S. Dong, S. Zhang, C. Xie, and H. Wang, "AF-RCNN: an anchor-free convolutional neural network for multi-categories agricultural pest detection," *Computers and Electronics in Agriculture*, vol. 174, article 105522, 2020.
- [25] Z. Sun, M. Dai, X. Leng et al., "An anchor-free detection method for ship targets in high-resolution SAR images," *IEEE Journal of Selected Topics in Applied Earth Observations and Remote Sensing*, vol. 14, pp. 7799–7816, 2021.
- [26] H. Law and J. Deng, "CornerNet: detecting objects as paired keypoints," *International Journal of Computer Vision*, vol. 128, no. 3, pp. 642–656, 2020.
- [27] K. Duan, S. Bai, L. Xie, H. Qi, Q. Huang, and Q. Tian, "CenterNet: keypoint triplets for object detection," in *Proceedings of the IEEE/CVF International Conference on Computer Vision*, pp. 6569–6578, Seoul, Korea, 2019.
- [28] A. Bochkovskiy, C. Y. Wang, and H. Y. M. Liao, "YOLOv4: optimal speed and accuracy of object detection," 2020, <https://arxiv.org/abs/2004.10934>.
- [29] H. Zhang, H. Chang, B. Ma, N. Wang, and X. Chen, "Dynamic R-CNN: towards high quality object detection via dynamic training," in *European Conference on Computer Vision*, pp. 260–275, Springer, Cham, Seoul, Korea, 2020.

## Research Article

# Evaluation Method of Chemical Technology Safety Practical Operation Ability Based on Stochastic Model

Xiaotong Wang 

School of Safety Engineering, Shenyang Aerospace University, Shenyang 110000, China

Correspondence should be addressed to Xiaotong Wang; lgxr381@163.com

Received 18 September 2021; Revised 28 October 2021; Accepted 1 November 2021; Published 26 November 2021

Academic Editor: Deepak Gupta

Copyright © 2021 Xiaotong Wang. This is an open access article distributed under the Creative Commons Attribution License, which permits unrestricted use, distribution, and reproduction in any medium, provided the original work is properly cited.

The current evaluation method does not consider the coordination and overall situation of various practical skills, which affects the evaluation contact degree and leads to hidden dangers of production safety. Therefore, an evaluation method of chemical technology safety practical operation ability based on a stochastic model is proposed. Using association rules to design the feature mining algorithm of practical operation ability, combined with crosslayer coding strategy, the mapping relationship between safety accidents and practical operation ability is established. The chemical safety practical operation skills are simulated by a random model, and the practical operation skills are classified and coordinated according to the simulation predictive control results. According to the coordination results, the evaluation index system is constructed, the index weight is determined, and the evaluation model of chemical technology safety operation ability is constructed. The experimental results show that the maximum connection degree of the evaluation method designed in this paper is 88.06%, and the evaluation results are more accurate, which is helpful to improve the production safety of chemical enterprises.

## 1. Introduction

Security issues are not only related to production but also related to the overall situation of China's economic development, political stability, social harmony, and people's happiness [1]. As a pillar industry of China's economic development, the chemical industry is also a high-risk industry with many accidents due to its complex production process, various equipment and instruments, large-scale equipment, raw materials, and products, and most of them are dangerous goods. At present, the situation of chemical safety production in China is grim. All kinds of accidents not only directly cause casualties and economic losses but also bring a great burden to society, enterprises, and countless families. It not only affects the stability and unity within the society but also seriously affects China's good market investment environment and international image. The emergence of new technologies, new processes, and new products not only meets the growing needs of people but also increases the risk factors and safety risks in the production and operation process of enterprises. The inherent characteristics of chemical production, such as complex

process, diverse raw materials, numerous equipment, fine operation, many hazardous chemicals, and dense distribution, have brought objective difficulties in risk management and control. Once an accident occurs, it is very easy to trigger a chain reaction, expand the harm of the accident, and even develop into a major safety accident, seriously threatening the personal safety of enterprise employees and residents near the plant [2]. It is an objective problem that chemical enterprise personnel must face to find and eliminate the potential safety hazard and accident risk in the process of production and operation.

Reference [3] proposed the research on the safety risk status index system of chemical enterprises based on analytic hierarchy process and investigated the safety risk status of chemical enterprises from the aspects of personnel technical level, equipment failure, major hazard sources, production process, environment, accidents, certification, safety assessment, and emergency response. The safety risk state index system of chemical enterprises is constructed from six aspects: personnel, equipment, materials, methods, environment, and safety management, and the key index system of safety risk state early warning is put forward. The analytic



hierarchy process is used to determine the index weight of safety risk status of chemical enterprises and finally determine the classification standard of safety risk status of chemical enterprises. Reference [4] proposed the research on safety early warning management of coal face based on expert system. Combined with the investigation of coal face in a large number of coal mines, a safety early warning expert system was constructed. This paper describes the classification, acquisition mechanism, and representation of knowledge and introduces the system structure, reasoning mechanism, and the establishment of knowledge base. In the process of construction operation in chemical enterprises, there are huge risks. Due to the complex procedures and various processes, it has a strong dependence on the safe operation behavior of workers. Once workers operate carelessly, it may cause serious accident consequences. It is of great practical significance to carry out the research on the evaluation of the practical operation ability of chemical technology safety to effectively improve the production safety of chemical enterprises. Nowadays and even in the future, the chemical industry will flourish. At present, China's relevant safety training, especially the practical training system, is not perfect, which leads to the lack of practical skills or unskilled chemical enterprise personnel, which easily produces unsafe behavior and leads to safety accidents. Therefore, it is necessary to evaluate the practical ability of chemical technical personnel, put forward the optimization angle of training system and specific measures to improve the practical ability, and apply it to practical training assessment and practice. The stochastic model can predict according to the current state, solve an open-loop optimization problem online according to the given objective function and constraints, and act the first element of the optimized control sequence on the controlled object. When it reaches a new state, it refreshes the optimization problem with the new measured value or estimated value and solves it repeatedly [5]. Therefore, the stochastic model can get good prediction optimization feedback results.

Therefore, this paper designs an evaluation method of chemical technology safety operation ability based on a random model. Through the correlation analysis between assessment items and safety accidents, this paper designs a feature mining algorithm of safety operation ability and obtains the correlation between data and safety accidents combined with crosslayer coding strategy. According to the random model, the construction safety operation skills are simulated, classified, and coordinated. When calculating the control strategy of a single safety operation skill, consider the behavior of other skills, so as to realize the global coordinated control of the whole operation ability and improve its connection degree. According to the coordination results, the evaluation index system is constructed, the evaluation index weight is determined, and the evaluation model of chemical technology safety operation ability is constructed [6–8], in order to continuously improve the practical training system, continuously improve workers' safety awareness and practical skills, reduce and control unsafe behaviors, and reduce the incidence of safety accidents.

## 2. The Evaluation Method of Chemical Technology Safety Practical Operation Ability Based on Stochastic Model

*2.1. Design of Security Operation Ability Feature Mining Algorithm Based on Association Rules.* In order to accurately evaluate the safety operation ability of technicians in chemical enterprises, firstly, the algorithm is used to mine the characteristics of operation ability. Through the correlation analysis between the assessment items and safety accidents, the importance of the assessment items and the correlation between the items are quantitatively evaluated, which provides valuable reference for the targeted training and assessment of practical skills. Association rule mining is one of the important branches of data mining, which is used to mine the correlation between valuable data items from a large number of data. The results of association rule mining mainly describe the association and degree between objects in the database or data warehouse [9]. Because the original data cannot directly reflect the correlation between chemical safety accidents and evaluation indexes, in order to better organize and summarize the correlation between existing capacity data and safety accidents, this paper proposes a crosslayer coding strategy. In this strategy, the original data is regarded as the bottom data of mining database, and the index item of practical ability is regarded as the middle layer. The original data is summarized to the corresponding middle layer through coding technology, and finally, the association rules between the target layer and the middle layer are found [10]. The flow chart of association rule mining algorithm is shown in Figure 1.

According to the analysis of Figure 1, first, through crosslayer coding, the original data is mapped from the basic item set to the interesting class item set in the form of coding. Class item sets are summarized from the original data and use the event sets of interest to objects. The binary sequence formed by the mapping from class to evaluation target is called basic antigen. In the process of class item mapping, the matching degree between basic item set index items and class item set index items is expressed by weight value, which is called mapping weight value [11]. For example, a "judgment error" in the basic item set and the corresponding index items in the category item set include "communication and communication ability," "decision-making ability," "stress and fatigue," and "situational awareness and risk assessment ability." Basic antigen and mapping weight value reflect the numerical relationship between basic item and category index. It can be expressed as

$$A_i = [W_i^T B_i]^T. \quad (1)$$

In formula (1),  $A_i$  represents the weighted value of the mapping;  $i$  represents the number of class items;  $T$  represents matrix transpose;  $W_i$  represents the mapping weight value; and  $B_i$  represents the basic antigen sequence of the class. Then, the numerical calculation formula of any class term is as follows:

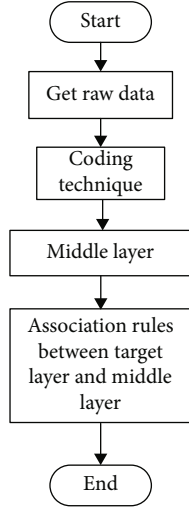


FIGURE 1: Algorithm flow of association rule mining.

$$z_i = \frac{A_i \beta}{\left( \sum_1^k c \alpha \right)_{\max}}. \quad (2)$$

In formula (2),  $z_i$  represents the class value;  $\beta$  represents the number of bits in the binary representation;  $k$  represents the number of basic items contained in the largest class item;  $c$  represents the weight value of nonzero mapping; and  $\alpha$  is the basic item. Then, we can mine the association rules of the coded class item set to find out the potential relationship between the interest index and the mining target [12]. Selecting the appropriate fitness function is a key problem of association rule mining algorithm, and it is also the key to the convergence speed of the algorithm [13]. The fitness function expression is as follows:

$$g(z_i) = \lambda_1 \frac{u(z_i)}{u_{\min}} + \lambda_2 \frac{d(z_i)}{d_{\min}}. \quad (3)$$

In formula (3),  $g$  represents the fitness value of the class item;  $\lambda_1, \lambda_2$  are adaptation coefficients, the sum of which is 1;  $u$  represents support;  $u_{\min}$  represents the support threshold;  $d$  represents the confidence level; and  $d_{\min}$  represents the confidence threshold. The above process establishes the mapping relationship between safety accidents and practical operation ability index, forms the data mining chain of this paper, and provides the basis for the evaluation of safety practical operation ability.

**2.2. Coordination of Chemical Safety Practice Skills Based on Stochastic Model.** Chemical safety accidents and disasters often occur suddenly, which could not be predicted before. In order to reduce the accident harm to the greatest extent, the most important thing is to do a good job with safety operations. Safety operation work runs through the whole chemical enterprise workflow. When there is no accident, it is necessary to regularly monitor the storage points of dangerous chemicals and storage tanks of inflammables and explosives in the chemical industry park or enterprise

production plant and take corresponding measures to eliminate risk factors and potential hazards, so as to prevent accidents. After the accident, it is necessary to know the situation of the accident, confirm the type of the accident, adjust the emergency plan according to the characteristics of the accident and the actual situation of the plant, carry out rescue, control the development trend of the accident, prevent the expansion of the harm of the accident and the occurrence of derivative disasters, and rescue the trapped personnel in time. After the accident is effectively controlled, it is necessary to help the enterprise to resume production as soon as possible, carry out strict safety hazard investigation in the plant, summarize the specific situation of the accident and the emergency rescue process, and timely repair the emergency plan and hazard protection measures for the existing problems. The evaluation of practical operation ability is based on state feedback, so it is only applicable to the situation of measurable state. However, due to the existence of uncertain factors in the operational capability, the state cannot be accurately estimated. In many cases, there may be conflicts before the control objectives of practical ability, leading to unsafe behavior. When there is a certain degree of coordination between the practical skills, it can effectively avoid unsafe behavior and improve the comprehensive practical ability. The random model is a group of random samples randomly selected everywhere, so the treatment effect is random and varies with different experiments. If the experiment is repeated, a new set of samples must be randomly selected from the population. The introduction of the random model can make individual observations have a certain correlation, improve the coordination between practical skills, and get good feedback results. According to the stochastic model, the chemical safety practical skills are simulated, and the practical skills are classified and coordinated according to the model predictive control results [14]. By considering the behavior of other skills when calculating the control strategy of a single safety practical skill, the global coordinated control of the whole practical ability is realized. For this reason, the feasible candidate solution of practical ability can be expressed as follows:

$$p = [v[n-1] \cdots v[n+m-1]0]^T. \quad (4)$$

In formula (4),  $p$  represents the augmented vector, that is, the feasible candidate solution;  $v$  represents the perturbation sequence of a single practical skill;  $n$  represents the number of skills that need to be coordinated; and  $m$  represents the number of skills that do not need to be coordinated [15]. In order to achieve the optimal coordination of operational capability, the weighted sum of local control functions is defined as follows:

$$f(v) = \min \theta_1 p + \sum_1^n \theta_2 l. \quad (5)$$

In formula (5),  $f(v)$  is the weighted sum of local control functions;  $\theta_1$  is weight matrix;  $\theta_2$  represents weighted cost; and  $l$  is the limit value of infinite time-domain control

function [16]. It can be seen that in order to promote the coordination among practical skills, the stochastic model designs a perturbation sequence for each coordination subskill [17]. At the same time, the weighted cost of each practical skill is considered in the local control function of comprehensive practical ability. Therefore, the comprehensive practical ability can predict and improve the comprehensive level of the whole practical ability by sacrificing the local ability of each subskill [18]. In order to optimize the output of the stochastic model, it is necessary to deal with the probability constraints. For any perturbed sequence, the following iterative feasible constraints need to be satisfied:

$$h(v) = pt(v) + e(v). \quad (6)$$

In formula (6),  $h(v)$  represents the feasible constraint matrix of iteration;  $t(v)$  is the displacement matrix; and  $e(v)$  represents the maximum element value of the matrix. In order to ensure the replaceability of the worst-case value, the perturbation sequence is decomposed to ensure that the probability constraint is satisfied, and under this constraint, the optimization result of iterative feasibility is obtained [19]. The above process can realize the simulation results of comprehensive practical ability under coupling constraints and realize the coordination among practical skills. The coupling probability constraints among multiple practical skills are transformed into deterministic local constraints; thus, the predictive control of the stochastic model is transformed into quadratic programming solution [20]. This method can ensure the iterative feasibility of the optimization problem for local constraints and coupling constraints and make the evaluation of practical operation ability more coordinated and global.

**2.3. Establish the Evaluation Index System of Practical Ability.** According to the coordination results, the evaluation index system is constructed and the weight of evaluation index is determined. According to the task and content of comprehensive practical skills, the first level evaluation index is divided into four types: prevention, preparation, response, and recovery [21]. In prevention ability, fully learn the professional knowledge and technology of hazardous chemicals and safety emergency, and improve their own quality and ability. Make clear all kinds of reactions, operation procedures, and safety protection measures in the production process of chemical industry park or enterprise, and understand the types, hazards, protection measures, and distribution of all kinds of hazard sources in the plant. Carry out regular inspection on the plant area, eliminate risk factors and potential safety hazards of accidents, and formulate emergency plans and protective measures for possible accidents [22]. In preparation ability, prepare for possible accidents or equipment containers with high risk coefficient, such as the establishment of emergency rescue command center, reasonable planning and design of internal emergency escape routes, and the development of risk management system. Only with the ability of preparation can we not panic; follow blindly, calmly, timely, and quickly; effec-

tively carry out emergency rescue; and ensure the safety of personnel [23]. In response ability, take measures immediately before the accident does not cause particularly serious harm to prevent the expansion of the scope and harm of the accident and effectively guarantee the safety of personnel and property [24], including accident and disaster identification, emergency rescue command and decision-making, and effective use of emergency equipment and materials. In recovery ability, after the accident is effectively controlled, it is necessary to carry out strict and comprehensive hidden danger investigation in the plant and help the enterprise to deal with the aftermath and recover, including potential safety hazard investigation, accident and disaster investigation and analysis, timely revision of emergency plan, strengthening enterprise accident protection measures, and resuming production [25, 26]. The above four first-level indicators are set as second-level indicators according to the specific situation to form the evaluation index system. After the evaluation index system is constructed, the index weight is further determined. When calculating the weight, it needs to meet the basic consistency and order consistency. That is, in an evaluation index system, if the relative importance of index  $x$  is twice of index  $y$  and the relative importance of index  $y$  is 3 times of index  $z$ , the relative importance of index  $x$  is 6 times of index  $z$ . At the same time, the weight coefficient of the evaluation index is determined. The calculation formula is

$$\omega_x = \left( 1 + \sum_2^x \prod_y^x \gamma_y \right)^{-1}. \quad (7)$$

In formula (7),  $\omega_x$  represents the weight of evaluation index;  $x, y$  represent any two evaluation indexes; and  $\gamma_y$  is the scale of relative importance among evaluation indexes. Based on the above evaluation index system and the weight coefficient, the evaluation model of chemical technology safety operation ability is further constructed.

**2.4. Construction of Evaluation Model for Practical Operation Ability of Chemical Technology Safety.** In the process of practical operation ability evaluation, there are often some situations that lack enough data or some indexes are difficult to quantify. It is difficult to use a quantitative index to express the evaluation results. At this time, the fuzzy evaluation method can be used to convert some qualitative indexes into quantitative indexes according to the membership theory in fuzzy mathematics thinking, which means that the concept of fuzzy mathematics can be used to make a general evaluation of the objects or objects affected by many factors. Therefore, this paper uses the concept of fuzzy mathematics to build a fuzzy rating model for the evaluation of safety practical operation capability and evaluates the safety practical operation ability of chemical technology. Because of the many factors, it involves a wide range of aspects, and the degree of influence in various aspects is different. When using the first-level model, it may be ignored because the weight of the one hand is small, so the results are not so accurate. Therefore, this paper uses a multilevel

TABLE 1: Evaluation index and its weight.

First-level indicators	Weight	Second level indicators	Weight
Preventive capacity	0.415	Monitoring and early warning	0.326
		Protective measures	0.458
		Operation process	0.216
Preparation ability	0.115	Use of emergency equipment	0.418
		Hidden danger investigation and control	0.201
		Emergency avoidance	0.381
Responsiveness	0.323	Accident identification and control	0.354
		Signal communication	0.286
		Rescue treatment	0.360
Resilience	0.147	Accident summary and analysis	0.392
		Dealing with the aftermath	0.133
		Restoration and reconstruction	0.475

model to evaluate fuzzy decisions. All factors are divided into several subsets according to the fields involved. Each subset is evaluated according to the first-order model first, and then, a corresponding number of first-order fuzzy evaluation vectors will be obtained. If each subset is regarded as an element, the first-order fuzzy evaluation vector can be evaluated as a single factor. By calculating the distributable weight, the multilevel fuzzy evaluation vector is obtained. The evaluation set is a set of evaluation results for the evaluation object, which is generally a degree description or a numerical interval. The number of comments in common evaluation sets is usually odd. The selected comment set in this paper is {very good, good, general, bad, very bad}. In the use of fuzzy evaluation method, the proper fuzzy operator should be selected for matrix composite calculation. In this paper, we choose weighted average operators, and by assigning values, all cases are considered according to weight, so as to avoid omission. In the process of fuzzy evaluation, membership function is also very important, because it can have a direct impact on the results. The expression of membership function is different in different situations, and its creation method is not fixed, so it needs to be modified constantly according to the actual situation. According to the steps of multilevel fuzzy evaluation, a fuzzy evaluation vector can be obtained. The evaluation index is processed by a weighted average principle. The five evaluation grades in the evaluation set are assigned. The final evaluation results can be expressed as follows:

$$F = \frac{\sum_{i=1}^s \phi_i p_i}{\sum_{i=1}^s \phi_i} \quad (8)$$

In formula (8),  $F$  represents the evaluation result;  $s$  is the number of evaluation vectors;  $i$  is the number of vector elements;  $\phi_i$  represents fuzzy evaluation vector; and  $p_i$  is the evaluation level assignment. The evaluation model is as follows: (1) factor set: according to the evaluation index system, the fuzzy evaluation factor set is established; (2) comment set: it is divided into five levels to evaluate the practical ability; (3) index weight set: the weight coefficient

of the determined evaluation index is used as the weight set of the evaluation; (4) membership degree: because most of the indexes in the evaluation index system of safety production emergency preparedness ability established in this paper are fuzzy, fuzzy judgment method is used to calculate the membership degree of the indexes; (5) operation model: the weighted average operator is used to fully consider the high weight index and low weight index; and (6) evaluation result processing: the final evaluation result is calculated by a weighted average method. Based on the above process, the evaluation method of chemical technology safety operation ability based on the stochastic model is designed.

### 3. Experiment

*3.1. Experimental Preparation.* In order to test the effectiveness of the evaluation method designed in this paper, the following experimental test was performed. Taking a chemical enterprise as the evaluation object, the safety operation ability was evaluated and analyzed. According to the evaluation method designed in this paper, the evaluation system is established and the weight is assigned. The specific results are shown in Table 1.

According to the established evaluation index system, the evaluation model is constructed. The safety data of technicians in chemical enterprises are input into the evaluation model to complete the test of the evaluation method.

*3.2. Experimental Results and Analysis.* The hardware of the test platform in the experiment is mainly composed of CPU, hard disk, etc. The framework is TensorFlow, and the software of the test platform is mainly composed of the kernel zImage and U-Boot.bin. The number of cores of the CPU is eight cores; the processor is AMD and has 16 threads. The hard disk has a capacity of 128 GB and uses a SATA interface.

Taking the safety practical operation ability evaluation method based on random model design as the experimental group and selecting the practical operation ability evaluation method based on AHP and expert survey method as the control group, the comparative experiment was carried out.



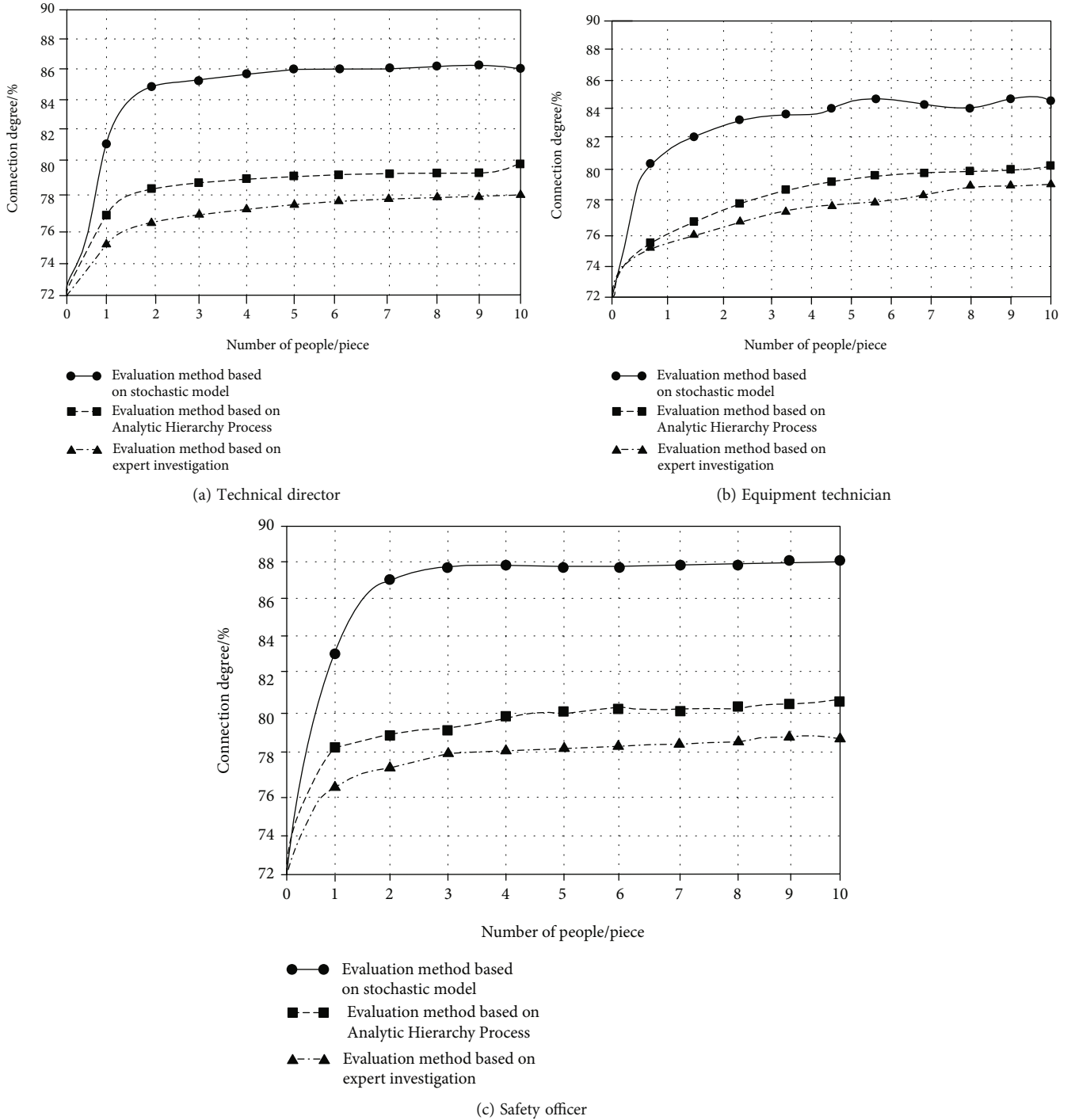


FIGURE 2: Evaluation results of practical ability.

In order to compare the evaluation accuracy of different methods, the value of connection degree is used to measure the correlation between evaluation objectives and evaluation grades. The calculation formula of the connection degree is as follows:

$$D = \eta_1 a + \eta_2 b + \eta_3 c. \quad (9)$$

In formula (9),  $D$  represents the connection degree of evaluation items;  $a$  is weighted degree;  $b$  is difference degree;

$c$  is opposite degree; and  $\eta_1, \eta_2, \eta_3$  represent the weight of secondary indicators. According to the above formula, the connection degree of evaluation target under different grades can be obtained. The larger the connection degree is, the more consistent the evaluation target is with the evaluation grade. Therefore, the greater the degree of connection, the more accurate the results of the method. In order to verify the feasibility, according to the determined index system, the results of the technical director, equipment technician, and safety officer are selected as the samples, and the



practical ability of the experimental group and the control group is evaluated by three methods. The results are shown in Figure 2.

According to the evaluation results in Figure 2, although the technical director, equipment technician, and safety officer have the same assessment hierarchy, due to their different management level and operation level, the evaluation results obtained by using the three evaluation methods are different. Using the evaluation method of this paper to evaluate the technical director, equipment technician, and safety officer, the contact degree is 86.13%, 84.22%, and 88.06%, respectively. Based on the analytic hierarchy process, the technical director, equipment technician, and safety officer were evaluated, and the contact degrees were 79.82%, 80.26%, and 80.46%, respectively. Based on the expert investigation method, the technical director, equipment technician, and safety officer were evaluated, and the contact degrees were 77.93%, 79.17%, and 78.68%, respectively. Compared with the evaluation results based on AHP and expert survey, the connection degree of the evaluation results based on the random model is higher, so the evaluation objective and evaluation grade of the design method in this paper are more relevant, and the evaluation results are more accurate. The evaluation method designed in this paper can realize the evaluation of practical ability of different chemical workers, help to train chemical technicians, and improve the production safety of chemical enterprises.

#### 4. Conclusion

The evaluation method of safety practical operation ability proposed in this paper can promote the improvement of practical operation training to a certain extent, which is conducive to the reform and innovation development of chemical enterprises, enhance the safety behavior of chemical technicians, and promote the prevention and safety control of operation accidents. With the rapid development of modern science and technology, it is necessary to establish an evaluation network technology platform with the combination of big data analysis and other modern scientific and technological achievements. And the real-time evaluation and dynamic analysis of the practical operation level of chemical technical personnel are carried out. In view of the problems in each stage, we can analyze the reasons in time and put forward the optimization path, so as to promote the practical ability of chemical technicians. The analysis of the results shows that the connection degrees obtained by the proposed method are 86.13%, 84.22%, and 88.06%, respectively. The connection degrees of the evaluation results are higher. The designed evaluation method can realize the evaluation of the practical operation ability of different chemical personnel, help to train chemical technicians, and improve the production safety of chemical enterprises.

Due to the complex factors affecting the safety practical operation ability of chemical technology, there may be some limitations. In terms of screening all factors that may affect the effectiveness of practical operation examination, more

comprehensive observation and further in-depth research are needed in the future.

#### Data Availability

The datasets used and/or analyzed during the current study are available from the corresponding author on reasonable request.

#### Conflicts of Interest

It is declared by the author that this article is free of conflict of interest.

#### References

- [1] G. C. Ta, M. Sultan, K. E. Lee et al., "A proposed integrated framework for chemical safety and chemical security," *Journal of Chemical Education*, vol. 97, no. 7, pp. 1769–1774, 2020.
- [2] S. Chen and S. Hu, "Safety integrity assessment and verification of typical chemical plant," *Modern Chemical Industry*, vol. 40, no. 5, pp. 10–13, 2020.
- [3] F. Wu, L. Cheng, Y. Yu, and J. Sun, "Research on the index system of chemical enterprise safety risk state based on analytic hierarchy," *E3S Web of Conferences*, vol. 245, no. 6, p. 03082, 2021.
- [4] F. Meng, Y. Fang, and C. Li, "Research on safety early warning management of coal mining face based on expert system," *IOP Conference Series Materials Science and Engineering*, vol. 490, no. 6, article 062056, 2019.
- [5] S. Golshan, R. Zarghami, and N. Mostoufi, "A hybrid deterministic-stochastic model for spouted beds," *Particulogy*, vol. 42, no. 1, pp. 104–113, 2019.
- [6] Z. Niu, B. Zhang, D. T. Li et al., "A mechanical reliability study of 3-dB waveguide hybrid couplers in submillimeter and terahertz bands," *Frontiers of Information Technology & Electronic Engineering*, vol. 22, no. 8, pp. 1104–1113, 2021.
- [7] B. Li, G. Xiao, R. Lu, R. Deng, and H. Bao, "On feasibility and limitations of detecting false data injection attacks on power grid state estimation using D-FACTS devices," *IEEE Transactions on Industrial Informatics*, vol. 16, no. 2, pp. 854–864, 2020.
- [8] Z. Lv, D. Chen, R. Lou, and H. Song, "Industrial security solution for virtual reality," *IEEE Internet of Things Journal*, vol. 8, no. 8, pp. 6273–6281, 2021.
- [9] F. Moslehi, A. Haeri, and F. Martínez-Lvarez, "A novel hybrid GA-PSO framework for mining quantitative association rules," *Soft Computing*, vol. 24, no. 6, pp. 4645–4666, 2020.
- [10] B. Shazad, H. U. Khan, F. M. Zahoor-ur-Rehman et al., "Finding temporal influential users in social media using association rule learning," *Intelligent Automation and Soft Computing*, vol. 26, no. 1, pp. 87–98, 2020.
- [11] G. Czibula, I. G. Czibula, D. L. Miholca, and L. M. Crivei, "A novel concurrent relational association rule mining approach," *Expert Systems with Applications*, vol. 125, no. JUL., pp. 142–156, 2019.
- [12] S. Nemet, D. Kukolj, G. Ostojic, S. Stankovski, and D. Jovanovi, "Aggregation framework for TSK fuzzy and association rules: interpretability improvement on a traffic accidents case," *Applied Intelligence*, vol. 49, no. 11, pp. 3909–3922, 2019.

- [13] P. D. Sheena Smart, K. K. Thanammal, and S. S. Sujatha, "A novel linear assorted classification method based association rule mining with spatial data," *Sādhanā*, vol. 46, no. 1, pp. 1–12, 2021.
- [14] F. M. Ibanez, I. Idrisov, F. Martin, and A. Rujas, "Design balancing systems for supercapacitors based on their stochastic model," *IEEE Transactions on Energy Conversion*, vol. 35, no. 2, pp. 733–745, 2020.
- [15] M. Lopez-Garcia, M. F. King, and C. J. Noakes, "A multicompartment stochastic model with zonal ventilation for the spread of nosocomial infections: detection, outbreak management, and infection control," *Risk Analysis*, vol. 39, no. 8, pp. 1825–1842, 2019.
- [16] E. Ferrero and D. Oettl, "An evaluation of a Lagrangian stochastic model for the assessment of odours," *Atmospheric Environment*, vol. 206, no. JUN., pp. 237–246, 2019.
- [17] T. Saravanakumar, N. H. Muoi, and Q. Zhu, "Finite-time sampled-data control of switched stochastic model with non-deterministic actuator faults and saturation nonlinearity," *Journal of the Franklin Institute*, vol. 357, no. 18, pp. 13637–13665, 2020.
- [18] E. Kianmehr, S. Nikkhal, and A. Rabiee, "Multi-objective stochastic model for joint optimal allocation of DG units and network reconfiguration from DG owner's and DisCo's perspectives," *Renewable Energy*, vol. 132, no. MAR., pp. 471–485, 2019.
- [19] G. Kermarrec, I. Neumann, H. Alkhatib, and S. Schon, "The stochastic model for global navigation satellite systems and terrestrial laser scanning observations: a proposal to account for correlations in least squares adjustment," *Journal of Applied Geodesy*, vol. 13, no. 2, pp. 93–104, 2019.
- [20] A. B. Kapranova, "Stochastic model of parallel or sequential processes of deaeration and mixing of granular media using the operation of a centrifugal device as an example," *Theoretical Foundations of Chemical Engineering*, vol. 53, no. 2, pp. 292–304, 2019.
- [21] C. M. Straut and A. Nelson, "Improving chemical security with material control and accountability and inventory management," *Journal of Chemical Education*, vol. 97, no. 7, pp. 1809–1814, 2020.
- [22] J. Zan, Y. Liu, X. Wang, and F. K. Zhang, "Assessment on emergency management capability of chemical industrial parks in Hubei Province," *Industrial Safety and Environmental Protection*, vol. 46, no. 1, pp. 64–66, 2020.
- [23] X. Liu, W. Mao, and G. Yu, "Research on safety deployment optimization technique of fire truck in petrochemical storage tank fire accident," *Industrial Safety and Environmental Protection*, vol. 45, no. 4, pp. 20–22, 2019.
- [24] K. Chen and Z. Deng, "Classification and analysis on the standardized system of occupational safety and health regulation in chemical industry," *China Occupational Medicine*, vol. 46, no. 2, pp. 239–242, 2019.
- [25] Q. Luo, Y. Li, B. Wu, and J. Tong, "Application of micro-reaction technology in improving safety of fine chemical process," *Modern Chemical Industry*, vol. 39, no. 4, pp. 63–66, 2019.
- [26] A. P. Essoh, F. Monteiro, A. R. Pena, M. Pais, M. Moura, and M. M. Romeiras, "Exploring glucosinolates diversity in Brassicaceae: a genomic and chemical assessment for deciphering abiotic stress tolerance," *Plant Physiology and Biochemistry*, vol. 150, pp. 151–161, 2020.

## Research Article

# Polygon Number Algorithm for Peak-to-Average Ratio Reduction of Massive 5G Systems Using Modified Partial Transmit Sequence Scheme

Hayder Alkatrani,<sup>1</sup> Muhammad Ilyas ,<sup>2</sup> Salam Alyassri,<sup>1</sup> Ali Nahar,<sup>3</sup> Fadi Al-Turjman ,<sup>4</sup> Jawad Rasheed ,<sup>5</sup> Ali Alshahrani,<sup>6</sup> and Basil Al-Kasasbeh<sup>6</sup>

<sup>1</sup>Electrical & Computer Engineering Department, University of Altinbas, Istanbul, Turkey

<sup>2</sup>Electrical & Electronics Engineering Department, University of Altinbas, Istanbul, Turkey

<sup>3</sup>Electrical Engineering Department, University of Technology, Iraq

<sup>4</sup>Artificial Intelligence Engineering Department, Research Center for AI and IoT, Near East University, Nicosia, Mersin 10, Turkey

<sup>5</sup>Department of Computer Engineering, Istanbul Aydin University, Istanbul, Turkey

<sup>6</sup>Arab Open University, Riyadh, Saudi Arabia

Correspondence should be addressed to Jawad Rasheed; jawadrasheed@aydin.edu.tr

Received 27 August 2021; Accepted 3 November 2021; Published 25 November 2021

Academic Editor: Deepak Gupta

Copyright © 2021 Hayder Alkatrani et al. This is an open access article distributed under the Creative Commons Attribution License, which permits unrestricted use, distribution, and reproduction in any medium, provided the original work is properly cited.

The high peak-to-average power ratio (PAPR) of the transmit signal is a major shortcoming of OFDM systems, which results in band radiation and distortion due to the nonlinearity of the high-power amplifier (H.P). To resolve the traditional OFDM high-PAPR issue, where the transmit sequence is designed to avoid similar data from being sent in the same order to reduce PAPR, there are numerous conventional ways for lowering the PAPR for OFDM system, such as selective mapping, tone reservation, block coding, filtering, clipping, and partial transmit sequence (PTS). This study proposes a new method called polygon number algorithm (PN) with conventional partial transmit sequence (C-PTS). This method (PN-PTS) processes the entered data before sending it, taking advantage of the number nonsimilarity according to the geometry of the number to prevent direct sending of similar data via PTS, and thus, this improved the level of PAPR rise in the proposed system. The amount of reduction that can be achieved in PAPR is up to 8 dB by different techniques. The best result obtained was the amount of reduction between the conventional method and the proposed method is 4.5683 where  $N=64$ . Besides this, there is no transmission of side information (SI), which improves transmission efficiency. Finally, this method is easy in the calculation process and the ciphering and deciphering of data, which adds a few calculations.

## 1. Introduction

The orthogonal frequency division multiplexing (OFDM) is a frequency division scheme in which the carrier frequencies are very close yet do not interfere with each other. The frequency spacing that is used in OFDM is very small, and its symbol period is bigger than or equal to the reciprocation of this spacing; OFDM usually has a high symbol duration, which reduces intersymbol interference (ISI) [1]. Multimedia communication systems necessitate a high data rate, which necessitates a large amount of transmission power

and bandwidth. As a result, high compression efficiency is required to transmit wireless multimedia information over a limited available bandwidth [2]. A common problem with wireless communications is especially in a multipath environment so that the ISI prevents high-speed communication. Therefore, OFDM allows high-productivity communication by increasing the number of carrier frequencies and maintaining high spectral efficiency. Nonetheless, it has challenges to implementation. OFDM signals have trouble with high peak-to-average power ratio (PAPR), to convert digital-to-analog (DAC) signal with high PAPR

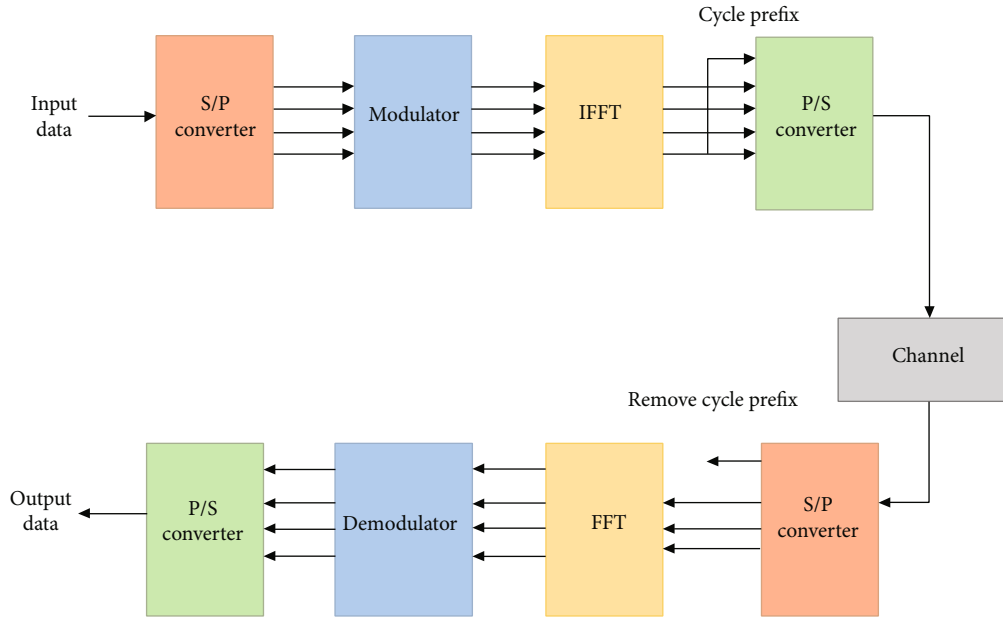


FIGURE 1: OFDM block diagram transmitter and receiver.

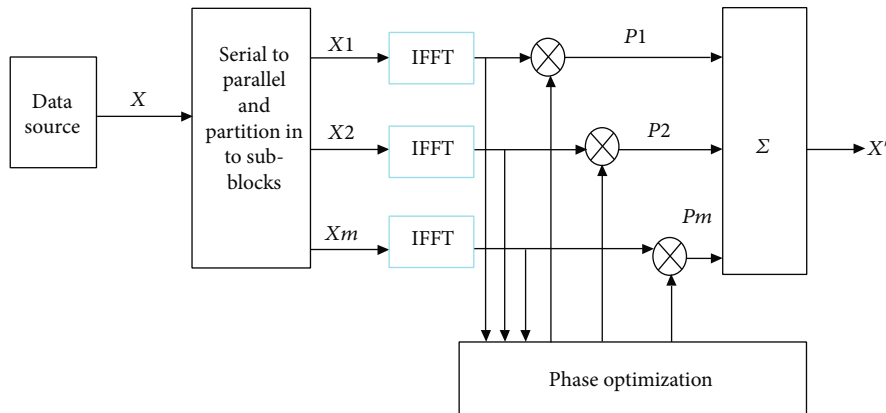


FIGURE 2: Block diagram of the conventional PTS scheme [23].

requires a high-speed and large dynamic range amplifier to forget perfect signal. These components are very expensive and lead to energy loss, shortening battery life in portable devices; besides, heat loss is not desirable in a fixed device [3].

One of the things to consider in the multicarrier transmission is the high-power ratio (PAPR) to normal signal transmission, as this is one of the OFDM signal negatives [4]. Therefore, this minimizes the range of the OFDM signal transmission. Furthermore, to avoid defects of the OFDM signal as a correction for burial between out-of-band radiation and subcarriers, the transmit power enhancer must be worked in its direct district. It is necessary to improve the transmission capacity in its immediate area. Therefore, the OFDM signal needs widespread backing, and this conversion is a waste of power [5]. OFDM is insensitive to the nonlinear effects of power amplifiers, due to the high peak-to-average power ratio (PAPR), and this is one of the major

problems in this system [6]. There are a lot of problems caused by high PAPR as it limits its wide use in some communications devices, and it is not preferred to use it in uplink transmission due to the restrictions in it [7]. It also leads to the consumption of large amounts of energy as the power amplifiers operate in the saturation region, and this leads to the deterioration of the bit error rate (BER) [8]. Also, high PAPR results in intermodulation and out-of-band radiation due to the nonlinearity in the power amplifier [9]. Therefore, many PAPR reduction schemes such as clipping and filtering [10, 11], block coding [12, 13], partial transmit sequence (PTS) [14], selected mapping (SLM) [15], tone injection (TI) [16], tone reservation (TR) [17], active constellation extension (ACE) [18], and random phase injection algorithms are used [19].

Despite the large number of methods used to reduce PAPR, where each method has pros and cons, there is still a problem of reducing complexity in the methods used, If

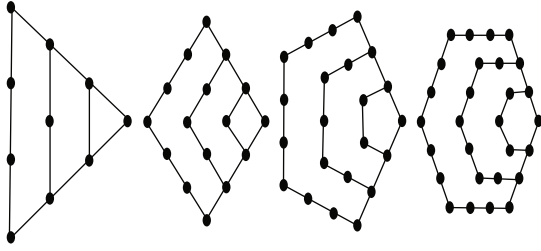


FIGURE 3: Type of polygon number: triangular, square, pentagonal, and hexagonal [25].

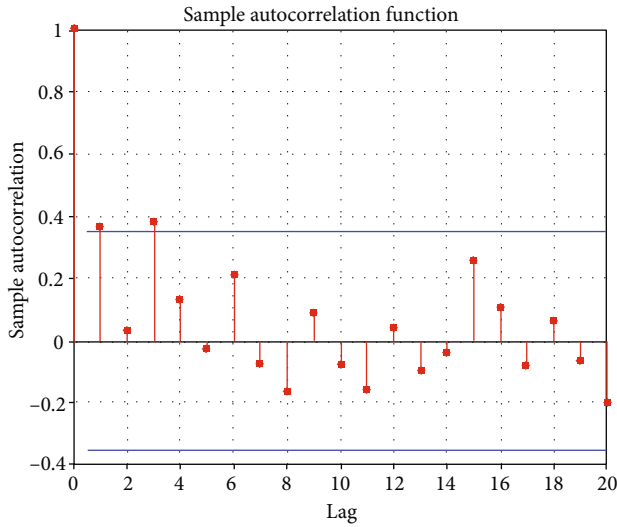


FIGURE 4: Input sequent numbers with different values.

we take, for example, the PTS and SLM methods, they have better performance in reducing PAPR and BER, but they have a problem with high computational complexity [20]. Among these theories that were used for reducing complexity in PTS is the ‘rotating phase shift technique,’ in which the signal was divided into groups, and this group was selected randomly. Moreover, choosing the low level of the PAPR depends on the different phase shifts according to a combination of factors [21]. The primary goal of source coding is to compress the original data intended for wireless transmission. Source coding techniques are used to greatly compress multimedia data [22]. A new method to reduce the PAPR value and complexity from the conventional PTS schemes is used. Polygon number is used to minimize the PAPR in the OFDM system, and good results are achieved when compared to the old method where the result was 4.7205, where  $N = 64$  and no.of signal = 1000. This method is one of the more recent methods used to improve OFDM defects. Moreover, when we compare the PN-PTS to the C-PTS or SLM, we can see how simple this algorithm is in comparison to the previous methods.

This paper is divided into seven sections. Section 1 outlines the introduction. Section 2 exposes the concept of the OFDM system and the peak-to-average power ratio (PAPR) and overviews the PAPR reduction scheme. Section 3 deals with the PTS scheme in the OFDM system, and Section 4

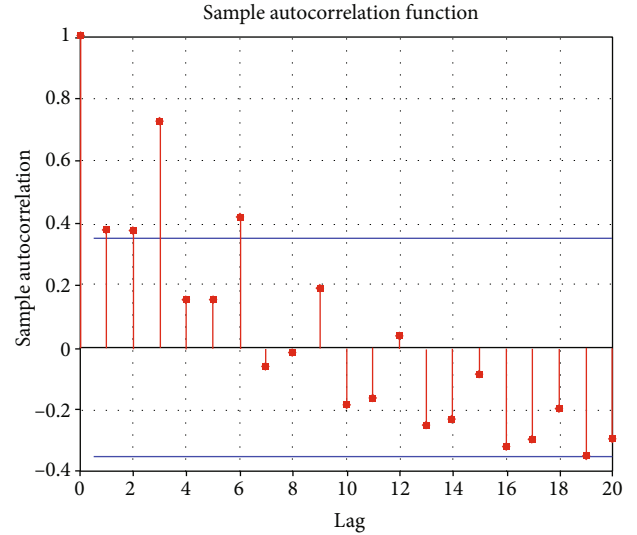


FIGURE 5: Processing number with autocorrelation.

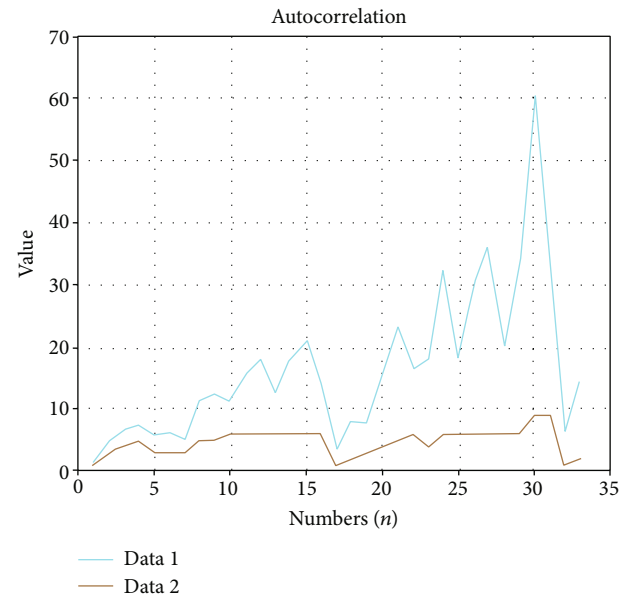


FIGURE 6: Autocorrelation with different values.

presents the concept of the number theory, while in Section 5 the proposed PTS scheme is indicated, Section 6 discussed the simulation results, and the conclusion and future work are discussed in Section 7.

## 2. OFDM System and PARP

In an OFDM scheme, the data symbols used by the  $N$  orthogonal subcarriers in the transmitter where  $X = [X(0), X(1) \dots X(N-1)]$  time domain sequence are as shown in Figure 1. An OFDM signal can be generated and written as in (1) for IFFT:

$$x(n) = \frac{1}{\sqrt{N}} \sum_{K=0}^{N-1} X_K e^{j\frac{2\pi kn}{N}}, n = 0, 1 \dots N-1. \quad (1)$$



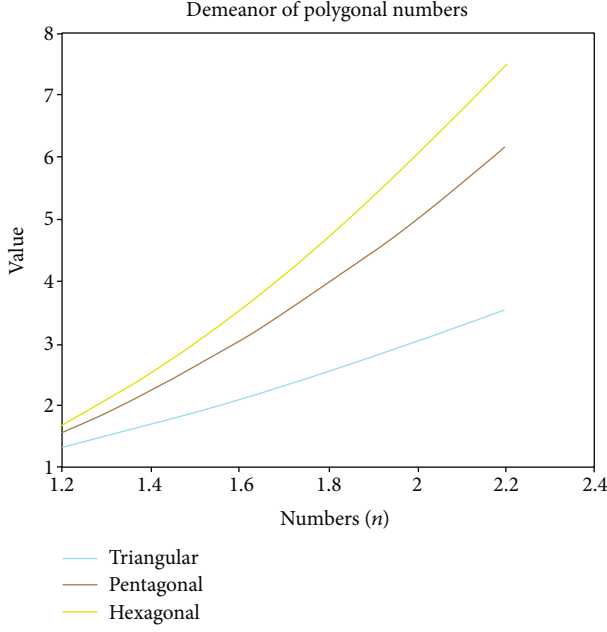


FIGURE 7: Demeanour of polygonal numbers for triangular, pentagonal, and hexagonal.

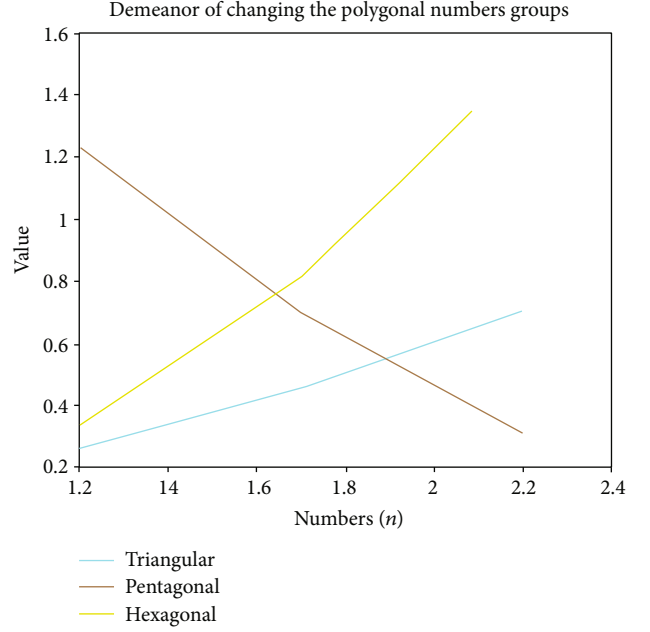


FIGURE 8: Demeanour of polygonal numbers when changing the value of a pentagonal number.

$X(n)$  is the discrete signal for the  $N$  orthogonal subcarriers. This is in the time domain, so the OFDM symbol is often the variations in the envelope will be as of PAPR, where PAPR is the ratio of the actual signal power to the mean signal power [17].

The OFDM signal series x PAPR is named as

$$\text{PAPR} = \frac{\max_{0 \leq n < N} |X(n)|^2}{E[|X(n)|^2]}, \quad (2)$$

where  $E[\cdot]$  stands for expectation. Complementary cumulative distribution function (CCDF) is used for the calculation value of PAPR level reduction performance in the OFDM system. PAPR CCDF can be described to given clip level PAPR as in (3) and (4).

$$\text{CDF PAPR} = \Pr(\text{PAPR} > \text{PAPR}_0), \quad (3)$$

$$\text{CCDF PAPR} = 1 - (1 - e^{-\text{PAPR}_0})^N, \quad (4)$$

where  $N$  is subcarrier numbers and  $\text{PAPR}_0$  is a certain threshold value.

### 3. PTS Scheme in OFDM System

In the conventional PTS scheme for the OFDM system, an input symbols vectors in the OFDM represent  $X = [X(0), \dots, X(N-1)]^T$ . The OFDM signal is generated by subcarriers  $N$ . The subcarrier generates a set of symbols. The subcarrier is separated from the adjacent subcarrier by

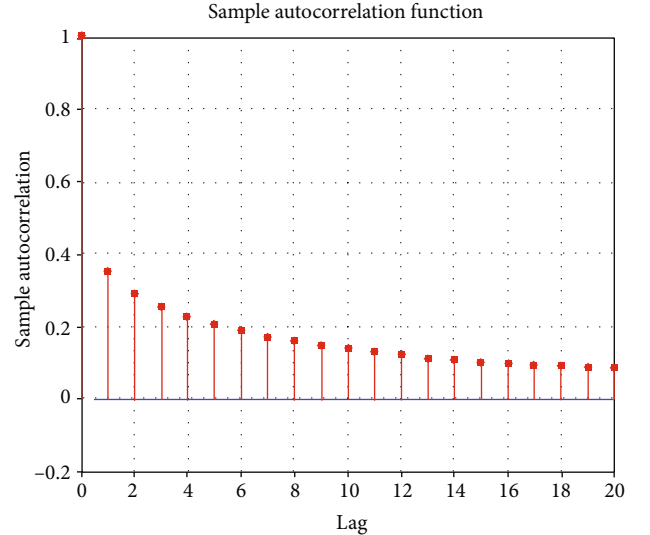


FIGURE 9: Data input with a range of magnitude 1.2-2.2.

the orthogonality of  $N$  when  $\Delta f = 1/T$ , where  $T$  is the signal duration of OFDM. The OFDM signal is expressed mathematically as follows:

$$x[n] = \frac{1}{\sqrt{LN}} \sum_{i=0}^{LN-1} \bar{X}(l) e^{j2\pi ln/N}, \quad 0 \leq n \leq LN - 1. \quad (5)$$

$X$  here is a subcarrier vector for  $N$  constellation symbols and  $\varepsilon$  constellation, according to quadrature phase shift keying modulation (QPSK). The ratio of the maximum

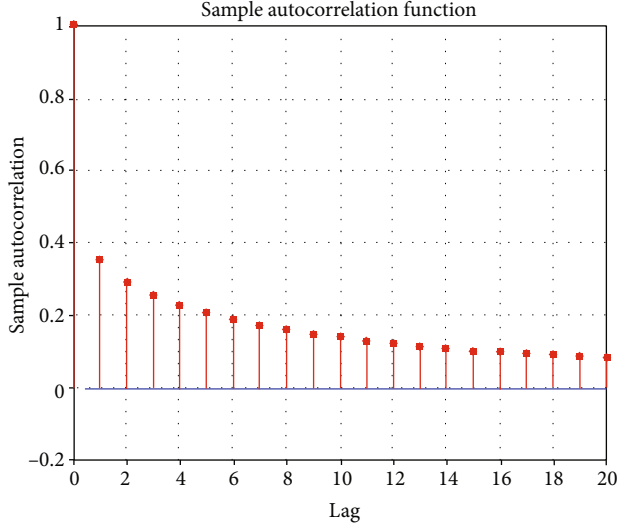


FIGURE 10: Data processing with a range of magnitude 1.2-2.2.

instantaneous power to the average power of the OFDM signal is known as the PAPR, and this can be expressed as in

$$\text{PAPR} = 10 \log_{10} \frac{\max_{0 \leq t < T} |X(t)|^2}{P(\text{av})}. \quad (6)$$

A sampling of the continuous-time signal  $X(t)$  produces the separate transmitted signal  $X[n]$  and often the Nyquist rate is taken; some information is lost at the height of  $X(t)$ , and therefore,  $X[n]$  is exceeded by a factor  $L$  to obtain the signal  $X(t)$  low value for PAPR. Factor  $L$  helps to sequence  $LN$ -point data by inserting  $N(L-1)$  zeros in the center of the  $N$ -point frequency domain signal and this is by  $LN$ -point IFFT and this gives IFFT, which can be expressed as

$$x[n] = \frac{1}{\sqrt{LN}} \sum_{i=0}^{LN-1} \bar{X}(l) e^{j2\pi ln/N}, \quad 0 \leq n \leq LN-1, \quad (7)$$

where  $\bar{X} =$

$$[X(0), \dots, X((N/2)-1), \underbrace{0, \dots, 0}_{(L-1)N}, X((N/2)), \dots, X(N-1)]^T. \quad \text{It}$$

shows that  $L = 4$  is enough to take the peak of the information  $X(t)$ .

The disjointed  $M$  submasses are the result of dividing the input data block into  $X$ , and this relationship can be represented by vectors according to Equation (8), and this is in the PTS system to reduce PAPR in OFDM:  $\{X_m, m = 1, 2, \dots, M\}$ . Therefore, we can get

$$X = \sum_{m=1}^M X_m. \quad (8)$$

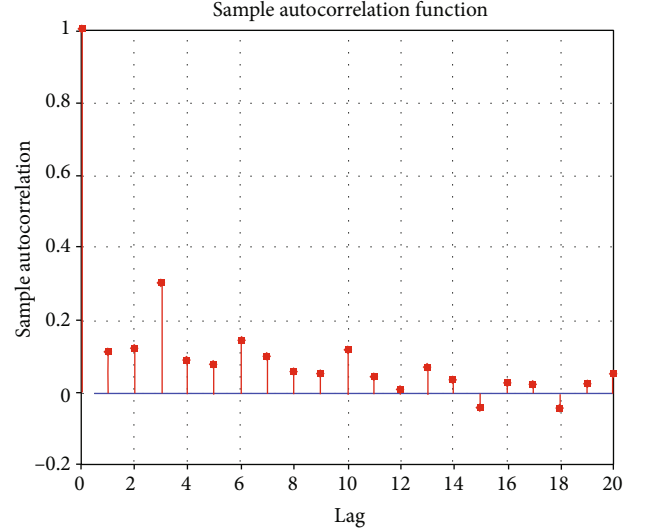


FIGURE 11: Data input with a range of magnitude 2.2-3.2.

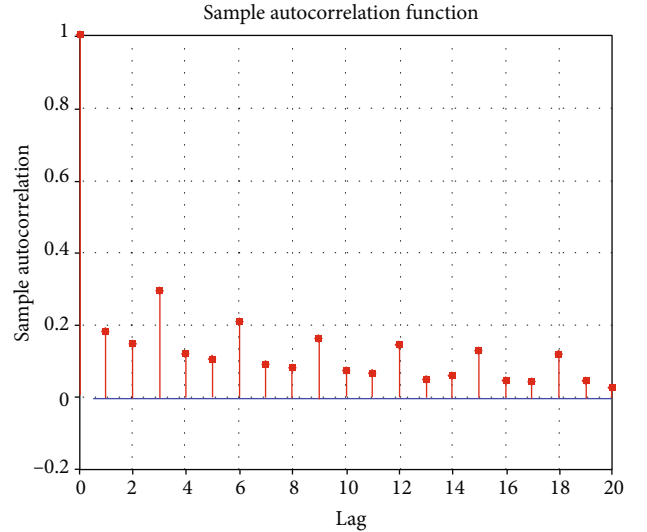


FIGURE 12: Data processing with a range of magnitude 2.2-3.2.

The sum of the subcarriers must be zero for the original signal which is displayed in another block. Then, the input symbol subblocks  $X$  are transformed into  $(M)$  time-domain partial transmit sequence. Therefore,  $X$  can be represented as

$$X_m = \text{IFFT}_{LN \times N} \{X_m\}. \quad (9)$$

By incorporating phase factors  $P = [P_1, P_2, \dots, P_m]$ , this results in a group of candidates when PTS rotated independently. It can be represented as

$$X = \sum_{m=1}^M P_m X_m = \sum_{m=1}^M \text{IFFT} \{P_m \otimes X_m\}. \quad (10)$$

It is possible to observe the special chart no. (4) for C-PTS and to know that the choice of the candidate with the

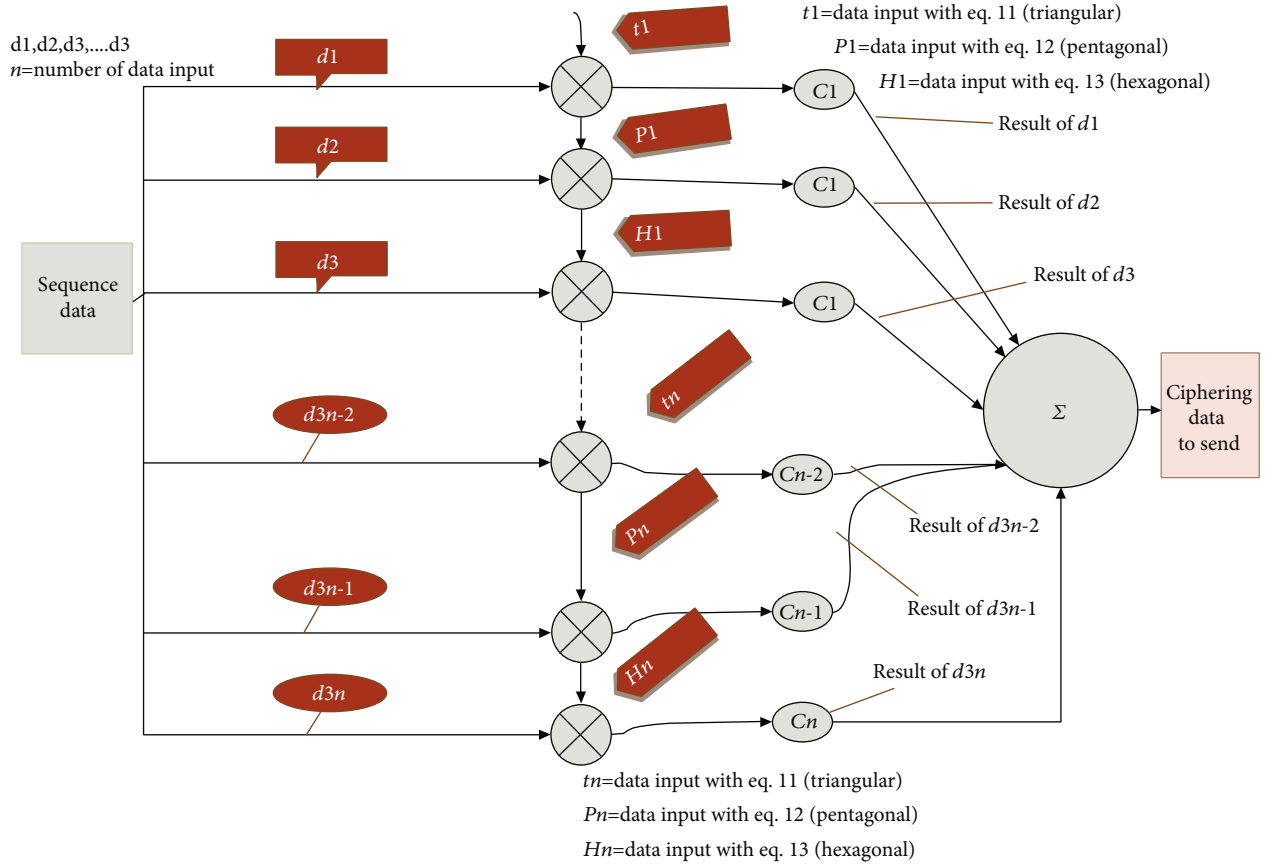


FIGURE 13: Principle of the polygonal numbers with data input and output to prevent similar data.

lowest PAPR is by searching the previous candidate for transmission, as to retrieve the original symbol  $X$  by sending the side information bits to indicate the improved phase sequence and then to the receiver, as seen in Figure 2.

#### 4. Number Theory

Number theory is a branch of pure mathematics mainly dedicated to studying the integral functions and integer. German mathematician Carl Friedrich Gauss (1777–1855) said: “A Queen of Sciences is Arithmetic — and the Queen of Arithmetic is the theory of numbers” [24]. Polygon numbers are a type of number theory. The diagrams in Figure 3 show how polygon numbers are geometrically constructed. The illustrated polygonal numbers are, respectively, triangular, square, pentagonal, and hexagonal [25]. In the proposed algorithm, we took advantage of this theory in preventing data similarities and reducing the value of PAPR. According to this theory, the numbers of polygons are characterized by their preventing similarity, and this leads to sequence similarities being prevented. This feature makes us think about applying it to our work to reduce PAPR.

#### 5. Proposed PTS Scheme

In this method, the geometric shape theory of numbers was used, and three sets of numbers 3, 5, and 6, for triangular,

pentagonal, and hexagonal numbers, respectively, were used. The following are the stages that have been implemented in applying this algorithm to the conventional scheme.

5.1. *Polygon Number Theory for Numbers 3, 5, and 6.* Three types of groups have been taken, and these groups of numbers are not equal if  $N$  is equal, as they depend on the geometry of the number. Below are the equations that were used in this proposed method in the form of each of these numbers:

$$t_n = \frac{1}{2} n(n+1), \quad (11)$$

$$p_n = \frac{1}{2} n(3n+1), \quad (12)$$

$$h_n = (2n-1), \quad (13)$$

where  $t_n$  is a triangular number,  $p_n$  refers to the pentagonal number, and  $h_n$  is a hexagonal number.

We took advantage of this feature in the input data when sending it; as this feature is highlighted on the input data, it prevents similar data. For example, when three consecutive values come one after the other equal in value, and when multiplying each of these equal values by a number from the group chosen (3, 5, and 6), the result of these numbers will be unequal according to the succession property, as seen

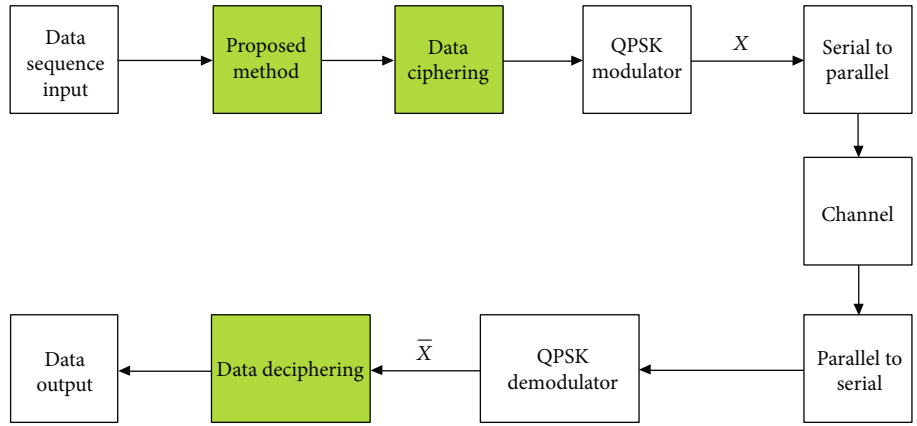


FIGURE 14: Principle block diagram of the proposed method.

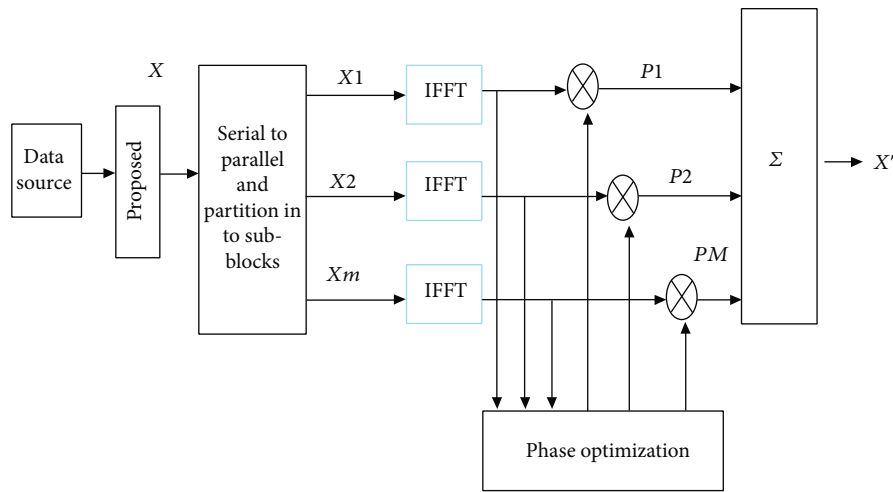


FIGURE 15: Block diagram of the proposed method with C-PTS scheme.

in Figures 4 and 5. This drawing, for the proposed method, shows the values that are not overlapping and preventing similar values from appearing. Moreover, Figure 6 depicts the amount of fluctuation that occurred due to similarities in numbers while they are progressing.

5.2. *Effect of Theory.* After knowing the effect of the theory on similar numbers, we made an experiment to analyse the effect on the shape of these three groups when increasing the value. This increase can be seen in Figure 7, whereas the amount of change that occurs when changing the value of each of these groups is shown in Figure 8.

5.3. *Set of Periods.* In this step, we made an experiment of a set of periods, which were divided into 10 values. After that, we chose a specific period from these periods, which is the selection of a portion of the abovementioned schemes, where we began to experiment with a period of (1.2-2.2) and another (2.2-3.2), etc. Meaning that the amount of the increase is 1, and we noticed that there was no big difference when changing these values between one group and another. This confirms the increase in fluctuation that was mentioned

in the previous clause, which was processed in the similarity of data. Figures 9–12 show these periods are taken.

These figures further demonstrate to us how to process similar data at different periods. Furthermore, it is clear from the figures that despite the fluctuation, it happens in all periods, but it differs in values. Therefore, to avoid amplifying the signal, we will choose one group over an average period for the rest of the work, which is (3.2-2.2).

5.4. *Mechanism for the Proposed Method.* After studying the effect of periods on data fluctuation, and to prevent amplification, the pentagonal number group was reversed (see Figures 9–12) to indicate the mechanism for the work of this algorithm by the proposed method. This can be observed in Figure 13, when the value of  $N$  is equal, the method is based on the premise that the three terms are not equal, and when the value of  $N$  is not equal, the algorithm is based on the progression property. According to Equations (11)–(13), the data do not overlap among them. We shed these data on the proposed algorithm, which can be observed in the sequence of this method as in Figure 14, where the data is entered on the algorithm, and then, it alternately changes

TABLE 1: The parameters for the simulation.

Parameter	Value
Number of OFDM signal	10000
Number of subcarriers $N$	64
Modulation	4, 32 QPSK
IFFT & FFT size	256
Oversampling factor ( $L$ )	4
Number of partition $p$	4

similar values to different values. The data generated is considered encrypted, and the resulting data is ready for the transmission process according to the conventional method steps in PTS shown in Figure 15. Upon receipt, decryption is performed to obtain the original data.

These figures show how to process similar data at different periods, and it is clear from the figures that despite the fluctuation, it happens in all periods, but it differs in values. Therefore, to avoid amplifying the signal, we choose one group over an average period for the rest of the work, which is (3.2-2.2).

Similarly, Figure 15 is showing the proposed method that was applied to the (C-PTS) method, as the old method characteristics (mentioned before) used modified PTS to improve the PAPR. The first block is the input data source to the OFDM system, which is synthesized by subcarriers represented by a sequence of input codes in  $X$  vector. The resultant is then converted into the  $M$  group by subblocks,  $X_m$ ,  $1 \leq m \leq M$ .

Then, the time field signal is converted to IFFT multiplied by the phase factors; after that, we get the OFDM and then pick the best  $X$  signal with the lowest PAPR point.

## 6. Simulation Results

In this research paper, we consider several simulation results to evaluate the performance in terms of PAPR reduction to demonstrate the effectiveness of the PN-PTS method. We used the MATLAB simulation program; the simulation results are based on the transmission of  $10^4$  randomly generated OFDM symbols with  $N = 64$  carriers and an oversampling factor  $L = 4$ . Table 1 lists the most important variables used in the simulation program to represent the PN-PTS method in which PTS was improved in reducing the PAPR.

The simulation results in Figure 16 show that when compared the PN-PTS with C-PTS, for 4QPSK,  $N = 32$ , no. of OFDM signal = 1000 symbols, and the original signal was 15.1263 dB. It was processed in the C-PTS, and the amount of reduction was calculated 6.4068 dB, The proposed scheme's (PN-PTS) PAPR performance is 4.6961 dB.

In Figure 17, the following are seen: no. of OFDM signal = 10000 symbols and the original signal was 15.1287 dB. The PAPR reduction with C-PTS is 6.3157 dB, and the PAPR performance for PN-PTS is 4.6826 dB. This is only the first stage of minimization; the rest of the enhancements

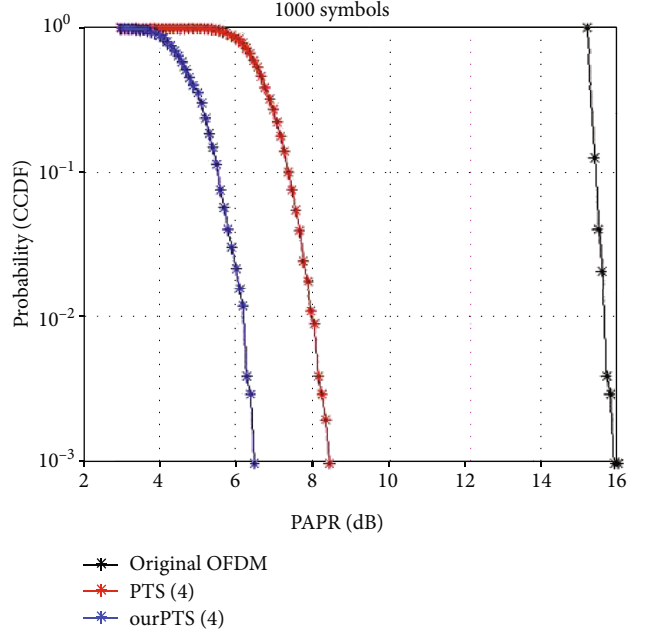


FIGURE 16: PAPR performance of the PN-PTS method with C-PTS for 4 QPSK with 1000 symbols.

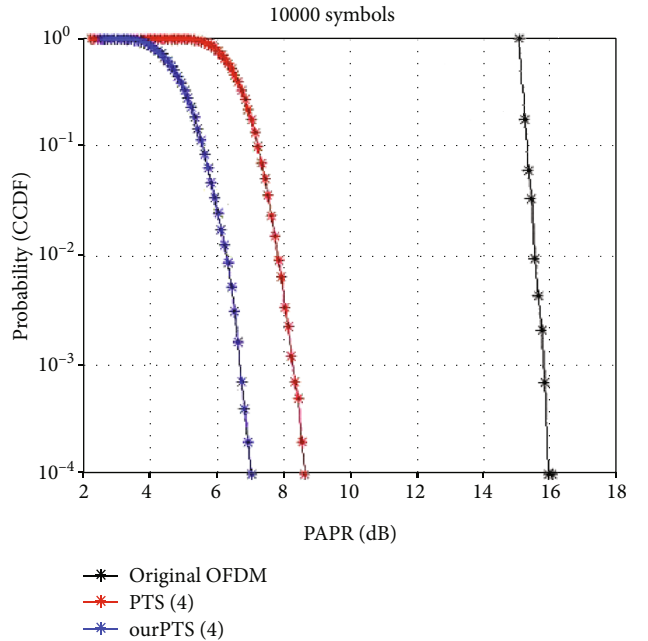


FIGURE 17: PAPR performance of the proposed scheme with C-PTS for 4 QPSK with 10000 symbols.

is shown in Table 2, which demonstrates the amount of progress made in reducing the PAPR.

In Figure 18 for simulation, 4 QPSK, the original signal is 15.1268 dB, the no. of OFDM signal = 10000 symbols, where the C-PTS gives 6.4376 dB, while PAPR performance for PN-PTS gives 4.5683 dB. In addition, when using 32 QPSK, the original signal is 17.9169 dB, where we see the most improvement between the two methods is clear where



TABLE 2: Computational complexity between the proposed and conventional schemes with a different number of subbands when  $N = 8, 32,$  and  $64$ .

$N$	No. of OFDM signal	Original signal (dB)	C-PTS	PN-PTS
8	1000	15.1263	6.4068	4.6961
	10000	15.1287	6.3157	4.6826
32	1000	15.1342	6.4473	4.7059
	10000	15.1288	6.4169	4.7125
64	1000	15.1268	6.4376	4.5683
	10000	15.1379	6.4503	4.7205

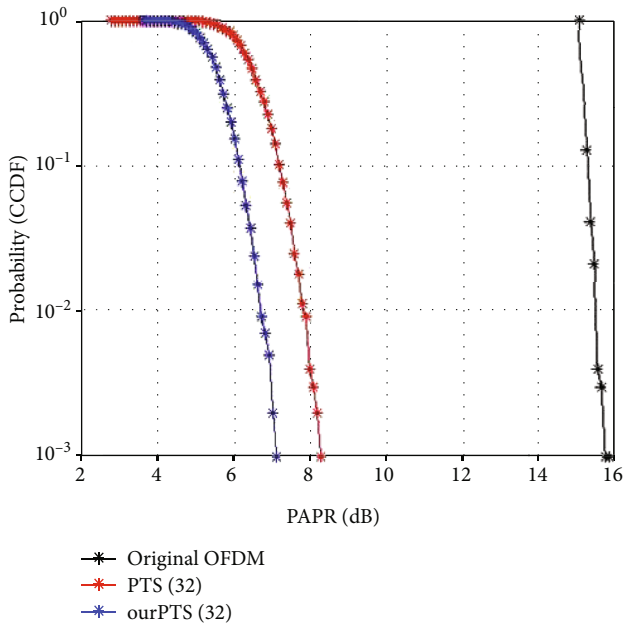


FIGURE 18: PAPR performance of the proposed scheme with C-PTS, 32 QPSK.

TABLE 3: Computational complexity between the proposed and conventional schemes with different modulations.

QPSK modulation	Original signal (dB)	C-PTS	PN-PTS
4	15.1268	6.4376	4.5683
32	17.9169	6.4363	5.5072

C-PTS gives worse PAPR performance 6.4363 dB, while the PN-PTS gives 5.5072 dB. Table 3 displays the results.

**6.1. Discussion.** When comparing the benefits of the proposed method to the conventional method and the previous methods that were used, we notice that this method is distinguished by an important feature, which has resulted in a reduction in the level of PAPR, which is the prevention of similar data when transmitting. In the conventional method, the selection of the candidate with the lowest PAPR is by searching for the previous candidate for transmission, which is accompanied by bits of the side information of the signal when retrieving the signal sent in the reception. The advan-

tage of PN-PTS being simple to encrypt and simple to decrypt when returning data for transmission. Furthermore, it is less complexity.

Many methods have been used to reduce PAPR, including SLM, clipping, tone reservation, rotating phase shift, and hybrid methods, but the method we are used had never been used before. Simulation results have shown that the proposed scheme is reliable to estimate the selection of the PAPR.

## 7. Conclusion

In this paper, we proposed a PAPR reduction scheme for OFDM signals based on an improved PTS with polygon number algorithm (PN-PTS). To achieve the best PAPR performance possible, the proposed method is based on preventing similar data from being input during transmission. This has improved transmission by preventing the transmission of side information and lowering the increase in the PAPR. In addition, the PN-PTS algorithm has the advantage of being simple to encrypt and simple to decrypt when returning data for transmission. It is clear from the above results that using PN-PTS reduces PAPR. In addition, the amount of the reduction was good as the reduction between the proposed method and the conventional method was done by a good percentage from (6.4068 to 4.6961).

In the future, it is planned to apply this algorithm to other methods such as the 'rotating phase shift technique.'

## Data Availability

Data sharing is not applicable to this article, as no new data were created or analysed in this study.

## Conflicts of Interest

The authors declare that there is no conflict of interest regarding the publication of this paper.

## Acknowledgments

The authors would like to thank Arab Open University and Oracle Saudi Arabia for supporting this study.

## References

- [1] K. Ramadan, M. I. Dessouky, and F. E. Abd El-Samie, "Modified OFDM configurations with equalization and CFO compensation for performance enhancement of OFDM communication systems using symmetry of the Fourier transform," *AEU - International Journal of Electronics and Communications*, vol. 126, article 153247, 2020.
- [2] A. Khalil, N. Minallah, M. A. Awan, H. U. Khan, A. S. Khan, and A. U. Rehman, "On the performance of wireless video communication using iterative joint source channel decoding and transmitter diversity gain technique," *Wireless Communications and Mobile Computing*, vol. 2020, 16 pages, 2020.
- [3] E. De Roux, M. Terosiet, F. Kölbl, M. Boissière, A. Histace, and O. Romain, "OFDM-based electrical impedance spectroscopy technique for pacemaker-induced fibrosis detection

- implemented in an ARM microprocessor,” *Microprocessors and Microsystems*, vol. 70, pp. 38–46, 2019.
- [4] A. A. Sharifi and M. Hosseinzadeh Aghdam, “A novel hybrid genetic algorithm to reduce the peak-to-average power ratio of OFDM signals,” *Computers and Electrical Engineering*, vol. 80, article 106498, 2019.
- [5] A. Kakkar, S. N. Garsha, O. Jain, and Kritika, “Improvisation in BER and PAPR by using hybrid reduction techniques in MIMO-OFDM employing channel estimation techniques,” in *2017 IEEE 7th International Advance Computing Conference (IACC)*, pp. 170–173, Hyderabad, India, 2017.
- [6] Y. C. Wang and Z. Q. Luo, “Optimized iterative clipping and filtering for PAPR reduction of OFDM signals,” *IEEE Transactions on Communications*, vol. 59, no. 1, pp. 33–37, 2011.
- [7] G. Wunder, R. F. H. Fischer, H. Boche, S. Litsyn, and J.-S. No, “The PAPR problem in OFDM transmission: new directions for a long-lasting problem,” *IEEE Signal Processing Magazine*, vol. 30, no. 6, pp. 130–144, 2013.
- [8] Y. Rahmatallah and S. Mohan, “Peak-to-average power ratio reduction in OFDM systems: a survey and taxonomy,” *IEEE Communication Surveys and Tutorials*, vol. 15, no. 4, pp. 1567–1592, 2013.
- [9] L. Yang, K. K. Soo, S. Q. Li, and Y. M. Siu, “PAPR reduction using low complexity PTS to construct of OFDM signals without side information,” *IEEE Transactions on Broadcasting*, vol. 57, no. 2, pp. 284–290, 2011.
- [10] X. Zhong, J. Qi, and J. Bao, “Using clipping and filtering algorithm to reduce PAPR of OFDM system,” in *2011 International Conference on Electronics, Communications and Control (ICECC)*, pp. 1763–1766, Ningbo, China, 2011.
- [11] S. Sengupta and B. K. Lande, “An approach to PAPR reduction in OFDM using Goppa codes,” *Procedia Computer Science*, vol. 167, pp. 1268–1280, 2020.
- [12] A. Idris, N. L. Mohd Sapari, M. Syarhan Idris, S. S. Sarnin, W. N. W. Mohamad, and N. F. Naim, “Reduction of PAPR using block coding method and APSK modulation techniques for F-OFDM in 5G system,” in *TENCON 2018 - 2018 IEEE Region 10 Conference*, pp. 2456–2460, Jeju, Korea (South), 2019.
- [13] H. A. Leftah, S. Boussakta, and S. Ikki, “Enhanced Alamouti space-time block-coding transmission based on a developed OFDM system,” in *2014 9th International Symposium on Communication Systems, Networks & Digital Sign (CSNDSP)*, pp. 591–595, Manchester, UK, 2014.
- [14] Z. Zhou, L. Wang, and C. Hu, “Low-complexity PTS scheme for improving PAPR performance of OFDM systems,” *IEEE Access*, vol. 7, pp. 131986–131994, 2019.
- [15] V. Sudha and D. Sriram Kumar, “Low complexity PAPR reduction in SLM-OFDM system using time domain sequence separation,” *Alexandria Engineering Journal*, vol. 57, no. 4, pp. 3111–3115, 2018.
- [16] J. Tellado, *Multicarrier Modulation with Low PAR: Applications to DSL and Wireless*, vol. 587, Springer Science & Business Media, 2006.
- [17] J. Wang, X. Lv, and W. Wu, “SCR-based tone reservation schemes with fast convergence for PAPR reduction in OFDM system,” *IEEE Wireless Communications Letters*, vol. 8, no. 2, pp. 624–627, 2019.
- [18] Y. Xiao, L. Zhang, and M. Imran, “Active constellation extension for peak power reduction based on positive and negative iterations in OFDM systems,” in *2019 UK/ China Emerging Technologies (UCET)*, pp. 1–5, Glasgow, UK, 2019.
- [19] H. Nikookar and K. S. Lidsheim, “Random phase updating algorithm for OFDM transmission with low PAPR,” *IEEE Transactions on Broadcasting*, vol. 48, no. 2, pp. 123–128, 2002.
- [20] J. Ji, C. Zhang, and W. Zhu, “Low-complexity PTS scheme based on phase factor sequences optimization,” *Journal of Systems Engineering and Electronics*, vol. 29, no. 4, pp. 707–713, 2018.
- [21] A. K. Nahar, A. N. Abdalla, A. Y. Jaber, and M. M. Ezzaldeen, “PAPR reduction using eight factors rotating phase shift technique based on local search algorithm in OFDM,” *Review of Computer Engineering Research*, vol. 4, no. 2, pp. 38–53, 2017.
- [22] N. Minallah, I. Ahmed, M. Ijaz, A. S. Khan, L. Hasan, and A. Rehman, “On the performance of self-concatenated coding for wireless mobile video transmission using DSTS-SP-assisted smart antenna system,” *Wireless Communications and Mobile Computing*, vol. 2021, 10 pages, 2021.
- [23] Y. A. Jawhar, L. Audah, M. A. Taher et al., “A review of partial transmit sequence for PAPR reduction in the OFDM systems,” *IEEE Access*, vol. 7, pp. 18021–18041, 2019.
- [24] T. Long Calvin, *Elementary Introduction to Number Theory*, vol. 77171950, Lexington, DC Heath Company, LCCN, 1972.
- [25] Gray, “Fermat's last theorem,” in *A History of Abstract Algebra: From Algebraic Equations to Modern Algebra*, pp. 15–21, Cham: Springer International Publishing, 2018.

## Research Article

# Optimization Method of Art Design Resource Scheduling for 6G Network Environment in Colleges and Universities

Meng Zhou <sup>1</sup> and Dong Yang<sup>2</sup>

<sup>1</sup>Department of Art and Product Design, Yibin University, Yibin 644000, China

<sup>2</sup>Department of Law and Public Administration, Yibin University, Yibin 644000, China

Correspondence should be addressed to Meng Zhou; 2003110001@yibinu.edu.cn

Received 30 September 2021; Revised 29 October 2021; Accepted 2 November 2021; Published 23 November 2021

Academic Editor: Deepak Gupta

Copyright © 2021 Meng Zhou and Dong Yang. This is an open access article distributed under the Creative Commons Attribution License, which permits unrestricted use, distribution, and reproduction in any medium, provided the original work is properly cited.

In order to solve the problem of low flexibility margin of traditional art and design resource scheduling in colleges and universities, an optimization method for art and design resource scheduling in the 6G network environment has been designed. By determining the flexibility margin index of university art and design resource scheduling, the scheduling optimization model is established, the scheduling communication parameters are set for the 6G network environment, the delay of university art and design resource scheduling is perceived, the period of insufficient flexibility is searched, and elimination measures are taken to realize the optimization of university art and design resource scheduling. The experimental results show that the margin of the designed scheduling method is always higher than that of the experimental control group in the same scheduling period, which can solve the problem of low scheduling flexibility margin of traditional methods.

## 1. Introduction

The curriculum resources of art design specialty include internal resources and external resources. The internal resources mainly refer to the effective combination of classroom subject knowledge and professional skills. External resources mainly refer to the use of extracurricular practical training and practical training resources as supplementary resources for classroom teaching resources. However, with the increasing demand for art and design talents, the problem of resource scheduling in the training of college students is becoming more and more obvious. Coupled with the impact of the network environment, the construction, sharing, and dissemination of curriculum resources are very limited. In order to ensure that students majoring in art and design can accurately obtain teaching resources inside and outside the school, relevant resource scheduling methods have attracted extensive attention of scholars.

The development of mobile communication has the rule of “use generation, construction generation, and R&D generation.” At present, although countries have not yet completed

5G deployment, they have already started 6G R&D. 6G will have three advantages: global signal coverage, faster transmission speed and higher intelligent level. The industry generally believes that 6G will go from the ground to the “sky” and integrate the ground wireless facilities with satellite communications to realize ubiquitous mobile communications. At that time, the signal will be seamlessly covered in the ground and air. Whether it is deep mountains, rainforests, deserts, or oceans, the signal can be searched. It is predicted that the theoretical download peak of 6G can reach 1 Tbps, and the network speed will be 500 times of 5G. At the same time, 6G wireless delay will be reduced to less than 100 microseconds, only 1/10 of 5G. In addition, the 6G data transmission speed is 100 GB/s. 6G can narrow the digital divide and further away from the interconnection of all things. 6G will be combined with computing and AI technology to achieve a higher level of intelligence.

In order to meet the requirements of art design resource scheduling in colleges and universities, an art design resource scheduling optimization method for a 6G network environment is proposed. By constructing the art design resource

scheduling model under the 6G network environment, calculating the marginal index of scheduling flexibility and analyzing the delay perception, the optimal scheduling of art design resources is realized, which provides a reference for the effective scheduling of internal and external resources of art design and further optimizes the teaching quality of art design courses.

## 2. 6G Network Environment

The core of the 6G network environment is 6G technology. 6G is the abbreviation of the sixth generation mobile communication system, which refers to the sixth generation mobile communication technology. It is the extension of 5G system and is in the development stage [1, 2]. Reducing the time delay effect is the goal of communication technology. The change of many communication technologies has brought about a significant increase in speed. The delay limit of 4G is 20 ms, while that of 5G is 1-10 ms. Although the delay is much lower than that of 4G, for some systems, such as driverless and VR/AR systems, the delay of 1-10 ms still does not meet the requirements. The 6G network reduces the delay to nanoseconds and enters the terabit era. Therefore, compared with 5G, the speed of the 6G network is increased by hundreds of times, which is basically close to the requirement of no delay, and achieves the real "online" goal [3]. 6G has a wider coverage. 4G network covers all people, thus forming the "Internet of people". 5G network combines the "Internet of things" with the "Internet of people." 5G seems to have exhausted everything by connecting people and things to the network, but there are still limitations. 6G makes up for the limitations of 5G in the following aspects: first, 5G is limited to the ground network, while 6G connects the ground network and satellites to form a network; second, the 5G network still has network blind areas in the sky, deep sea, desert, forest, and other places, while 6G network solves the coverage problem of these blind areas by combining a series of new technologies with satellites. The network coverage of 6G is wider than that of 5G, so that there is no dead angle in the network and the signal is fully covered. Therefore, this paper combines the advantages of the 6G network environment to optimize the art design resource scheduling in colleges and universities.

## 3. Establishing the Framework of Art Design Resource Scheduling Optimization in Colleges and Universities

This paper selects the hierarchical scheduling mode as the optimization framework of art design resource scheduling in colleges and universities and takes the demand side resource objectives as the scheduling basis. Two hierarchical structures are established, which are the agent layer for response and the center layer for scheduling. The centralized scheduling method is adopted in the scheduling layer, and the distributed scheduling method is adopted in the response agent layer. The optimization framework of university art design resource scheduling is shown in Figure 1.

As shown in Figure 1, in the university art design resource scheduling center, the hierarchical scheduling framework for the integration of demand side goals and university art design

resources from top to bottom is as follows: scheduling center layer, response agent layer, and demand side resource layer. The main functions of each layer in the framework are as follows: the dispatching center layer is used to ensure the safe and stable operation of multiple objectives. Collect the response data information of demand side targets, and supply side targets uploaded by the lower level through the dispatching center [4]. When there is a problem with the dispatching capacity of the dispatching center, the dispatching center shall timely make corresponding demand side response and adjust the demand side objectives according to the change of its communication rate or adjust the demand side objectives by directly sending communication signals. The response agent layer is used to optimize the scheduling of demand side and supply side objectives and communicate with the scheduling center. When the demand side responds, the response agent layer shall timely transfer the guidance of the dispatching center layer to the lower layer. The demand side resource layer is used to store university art and design resources. This layer provides data sources for the dispatching center layer and the response agent layer.

The main operation mode of the scheduling framework can be divided into two parts, which are the uplink of demand side target and supply side target response state and the dispatch instruction of the scheduling center [5, 6]. The specific processes of the two operation modes are as follows:

The former collects information from bottom to top according to the responsiveness information of demand side objectives and supply side objectives [7, 8]. In the collection process, it is necessary to measure and calculate the response capability, response time, and response rate of demand side targets and upload the calculation results to the corresponding agent layer [9]. Then, the response agent layer collects the response capability information of each corresponding demand side target and uploads it to the dispatching center through calculation to complete the uplink operation mode of the response status of demand side target and supply side target.

The latter issues instructions from top to bottom according to the issued response instructions. According to the dispatching center, calculate the response of the demand target, and send the calculation results to each corresponding response agent layer. The response agent layer calculates the response amount under specific conditions according to its own response ability and the constraints of the scheduling center and then sends the scheduling instructions to each demand side target, which executes the scheduling behavior according to the instructions.

## 4. Optimization Method of Art Design Resource Scheduling for 6G Network Environment in Colleges and Universities

*4.1. Determine the Flexibility Margin Index of Art Design Resource Scheduling in Colleges and Universities.* Before optimizing the art design resource scheduling of colleges and universities in the 6G network environment, it is necessary to determine the types of art design resources in colleges and universities. See Table 1 for details.



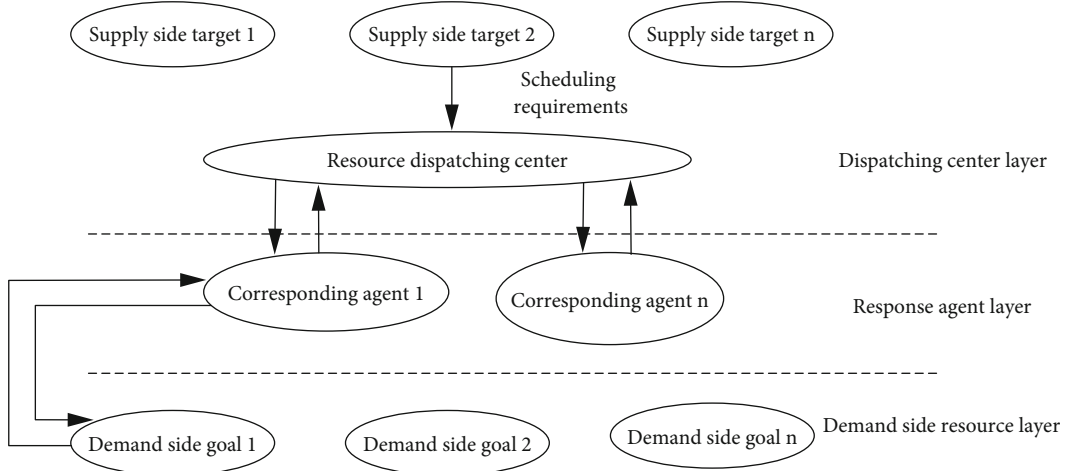


FIGURE 1: Framework of art design resource scheduling optimization in colleges and universities.

According to Table 1, after determining the types of art design resources in colleges and universities, the demand for flexibility of art design resource scheduling in colleges and universities is calculated [9]. Assuming that the expression is  $\Delta Pt^{du}$ , the calculation formula is as shown in

$$\Delta Pt^{du} = (Ct + 1 - Ct) + \eta u Ct + 1 + \eta e Ct + 1. \quad (1)$$

In Formula (1),  $Ct$  refers to the system cost of  $t$  period;  $Ct + 1$  refers to the system cost in  $t$  period of the next day;  $\eta u$  refers to the demand of the dispatching center for university art design resources; and  $\eta e$  refers to the demand of the dispatching center for university art design resources. According to the description of the demand for flexibility of university art and design resource scheduling in Formula (1), the coordination rolling scheduling flexibility margin index is defined as the difference between flexibility supply and flexibility demand [10]. Assuming that the flexibility margin index of art design resource scheduling in colleges and universities is  $\Delta Pt^{mu}$ , the calculation formula is as shown in

$$\Delta Pt^{mu} = C - \Delta Pt^{du}. \quad (2)$$

Through Formula (2), we can determine the flexibility margin index of university art design resource scheduling.

**4.2. Establishing the Optimization Model of Art Design Resource Scheduling in Colleges and Universities.** According to the resource scheduling flexibility margin index obtained above, the delay aware task scheduling of university art design resources is integrated into the scheduling model. Before establishing the scheduling model, we need to analyze the delay perception task of university art and design resources. In the 6G network environment, due to the high dynamic and random characteristics of user scheduling, the scheduling should be real-time, irregular, and independent. Supposing that the multitarget perception task set is  $\alpha$ , the single task in the task set is represented by  $\alpha 1$ , the arrival time of the task is represented by  $a$ , the 6G network length of the task is set as  $l$ , and the deadline for task completion is  $D$  [11]. Because the arrival

time and deadline of multiobjective delay aware tasks can only be obtained after the user publishes the scheduling task and the CPU processing capacity of virtual machine for the 6G network environment is heterogeneous, the calculation equation of  $\alpha$  is as shown in

$$\alpha = \frac{\alpha 1}{aD}. \quad (3)$$

Through Formula (3), the multitarget perception task set is obtained. Because the completion of the scheduling task needs to consume a certain amount of network resources, the resource consumption of the host CPU should be considered in the scheduling process. The resources consumed by virtual hosts are divided into idle resources and active resources, and the consumption of active resources is directly proportional to the working frequency. Assuming that the active resource consumed by the scheduling task is  $Z_1$ , the calculation formula is as shown in

$$Z_1 = v^2 \times f. \quad (4)$$

In Formula (4),  $v$  refers to the voltage of the main engine and  $f$  refers to the working frequency of the main engine. Since the voltage of the virtual host CPU is linearly related to the working frequency, the dynamic power  $H_d$  of the host is as shown in

$$H_d = Z_1 \propto f^3. \quad (5)$$

Assuming that the ratio of dynamic power consumed by the host to idle power is  $s$ , the power consumption  $H$  of the host is as shown in

$$H = Z_1 \times y \times f^3. \quad (6)$$

In Formula (6),  $y$  refers to the state of the virtual host. When the host is active,  $y = 1$ . When the host is idle,  $y = 0$  [12]. According to the above analysis, the resource model consumed by the virtual host to complete the task set is as shown in



TABLE 1: Types of university art and design resources.

Serial number	Types of art design resources in colleges and universities	Content
1	Text	Related concepts Related literature Related questions
2	Picture	Related legend Legend analysis Related people
3	Video	Analysis of related courses Relevant case analysis Demonstration of related techniques
4	Courseware	Courseware 1 Courseware 2

$$tec = \int s \times Z_1 \times y \times a \times d. \quad (7)$$

Based on the above task model and resource consumption model, the optimization model of art design resource scheduling in colleges and universities is as shown in

$$\begin{cases} \max & T = \sum \frac{l}{ad}, \\ \min & tec = \sum \int s \times Z_1 \times y \times a \times d. \end{cases} \quad (8)$$

The model considers the completion rate of maximizing the task set and the minimization of resource consumption [13]. Through the scheduling of the model, it provides sufficient resources for the virtual host of the scheduling center and ensures that the scheduling task is completed before the deadline. Combined with the actual demand of art design resource scheduling in colleges and universities, the lower limit of output of the scheduling model is set to 70%.

**4.3. Delay Perception of University Art and Design Resource Scheduling in 6G Network Environment.** On the basis of establishing the scheduling model, this paper designs a scheduling optimization algorithm with resource delay sensing ability for a 6G network environment to realize the value of the above model. The 6G network environment uses terahertz (THz) band, and the “densification” degree of the 6G network environment will reach an unprecedented level. Because of the high frequency of 6G network environment and the wide range of bandwidth allowed to be allocated, the larger amount of university art and design resources data can be transferred per unit time. In this paper, the 6G network environment is used as the communication parameter of art design resource

TABLE 2: Communication parameters of art design resource scheduling in the 6G network environment.

Serial number	Communication parameters of 6G network environment	Communication range
(1)	Communication speed: 20 Gbit/s	{0, 1}
(2)	Communication speed: 10 Gbps	{0, 1}
(3)	User experience rate: 100 Mbps	{0, 1}
(4)	Peak rate: 1Gbps	{0, 1}

scheduling in colleges and universities. The specific communication parameters of art design resource scheduling for 6G network environment are shown in Table 2.

As shown in Table 2, it is the basic parameter of communication in the process of art design resource scheduling. The delay perception of university art design resource scheduling for the 6G network environment design is composed of two constraints, as shown in

$$\begin{cases} r_x \geq t_x, & x \in cpu, \\ scheduleTask \leq t. \end{cases} \quad (9)$$

In Formula (9),  $r$  refers to the number of virtual hosts in the dispatching center and  $scheduleTask$  is the scheduling function. Algorithm 1 means that in the scheduling center, the resource available of virtual host is less than the resource demand of scheduling task. Algorithm 2 indicates that if the university art design resources are scheduled on a virtual host, the scheduling function is used to ensure that the task is completed before the deadline [14, 15]. In the university art design resource scheduling optimization algorithm, all the scheduling tasks are waiting in the rolling window RH; until the task starts to execute, it is transferred from the rolling window RH to the virtual host. When the system receives the new university art design resources, the algorithm will reschedule the unexecuted and new arrived tasks in the rolling window; the implementation process of the algorithm is shown in Algorithm 1.

In Algorithm 1, when a new task arrives in the system, the scroll window will delete all the art design resource scheduling schemes of colleges and universities and immediately update the virtual host ready time and running status and schedule the new art design resources of colleges and universities to the virtual host with enough available resources to schedule tasks and form a new art design resource scheduling scheme of colleges and universities [16]. When the university art and design resources arrive at the virtual host, Algorithm 2 is executed, and the execution process is shown in Algorithm 2.

Through the implementation of Algorithms 1 and 2, under the constraint of delay perception in Formula (9), the university art and design resources are reasonably scheduled to the virtual host in the system, improve the resource scheduling efficiency according to different execution processes, and realize the optimization of university art and the scheduling of design resources.

Input: real time task set  $t$ ;  
Output: mapping between each task and virtual host, mapping between virtual host and physical host;  
① RH; /\* Scroll through the task set  $t$  \*/;  
② When the new task  $T1 \in t$  reaches do;  
③ Delete the mapping relationship between waiting task and virtual host in RH, and update the ready time of virtual host;  
④ Task  $T1$  is added to RH;  
⑤ All tasks in RH are sorted by non decreasing deadline;  
⑥ For task  $T1$  belongs to RH do;  
⑦end for;  
⑧end whilr.

ALGORITHM 1: Execution process of the algorithm.

Function schedulertask  
Input: task  $T$ , available virtual host set;  
Output: mapping between task  $T$  and virtual host;  
① The resource status of virtual host is calculated;  
② Task  $t$  is assigned to a virtual host with sufficient resources and no tasks to be executed;  
③ Arrival time of task  $t$  on virtual machine  
④ Else /\* task completion scheduling results\*/  
⑤ end if

ALGORITHM 2: Execution process of the algorithm.

4.4. *Realizing the Optimization of Art Design Resource Scheduling in Colleges and Universities.* Using the delay perception of university art design resource scheduling, the specific implementation strategy can be implemented according to the response characteristics of demand side target and the matching characteristics of supply side target on time scale. The time period of art design resource scheduling in colleges and universities is divided into the day before, day in 2 hours, and day in 30 minutes [17, 18]. The daily scheduling is performed once every 24 hours, which is used to predict the demand of the demand side target and the supply side target in the dispatching center and adjust the demand side target according to the prediction results. The daily 2-hour scheduling is executed every 2 hours. The scheduling center forecasts the supply side target every 2 hours and adjusts the demand side target according to the result; The midday 30 minute scheduling is executed every 30 minutes. The scheduling center forecasts the demand side target every 30 minutes and adjusts the demand side target according to the prediction results. According to the art design resource scheduling strategy of colleges and universities, on the basis of ensuring the smooth operation of the scheduling center, the objective function of the day ahead 24-hour scheduling optimization is set as shown in

$$W1 = \sum \left[ \gamma1(s) \cdot \omega1(s) + \sum \left( \gamma1'(s) \cdot \omega1'(s) \right) \right]. \quad (10)$$

In Formula (10),  $\gamma1(s)$  refers to the execution time of a target schedule in the previous  $s$  period;  $\omega1(s)$  refers to the

length of the target in the  $s$  period before the day;  $\gamma1'(s)$  refers to the communication time between multiple targets in the  $s$  period before the day;  $\omega1'(s)$  refers to the response adjustment power of the dispatching center in the  $s$  period before the day. The constraints of the day ahead 24-hour dispatching are to ensure the normal power operation of the dispatching center and to adjust the quantity constraints. The optimization function of day to day scheduling is set as shown in

$$\min W2 = \sum \left[ \gamma2(s) \cdot \omega2(s) + \sum \left( \gamma2'(s) \cdot \omega2'(s) \right) \right]. \quad (11)$$

In Formula (11),  $W2$  refers to the total scheduling input cost under demand side target response;  $\gamma2(s)$  refers to the minimum value of total resource consumption in  $s$  period of the day;  $\omega2(s)$  refers to the total power of the dispatching center in  $s$  period between Japan and China;  $\gamma2'(s)$  refers to the response funds paid by the dispatching center to the agent during the  $s$  period between Japan and China;  $\omega2'(s)$  refers to the agent's response adjustment power during the  $s$  period of the day. The constraints of the day ahead 24-hour scheduling are as follows: the scheduling of art design resources in colleges and universities is limited by the characteristics of the load itself. After obtaining the art design resource scheduling model, the model is solved. Due to the large scale of the model, this paper divides the model into two scheduling layers: up and down. The flexibility margin is associated between the scheduling layers. Through problem decomposition, the model is transformed into multiple asynchronous long problems to simplify constraints. The optimization method is used for basic

TABLE 3: Experimental environment settings.

Parameter	Explain	Setting up
NCmax	Maximum iterations of task	200
Kerthe	Task scheduler	2
Number of host resources	Number of virtual host resources	860
Task consumption resources	Task resource consumption	30
Host geographic distance	Physical host geographic distance	20
Host update frequency	Host update constant	0.2
Network weight coefficient	Network weight coefficient	0.3

optimization, and the flexibility margin is updated in time [19, 20]. Based on the initial solution of the model, the art design resource scheduling particles that do not meet the constraints are modified to make them meet the constraints as much as possible. If the flexibility constraint is still not satisfactory when iterating to the last generation, we can search for the period of insufficient flexibility through the art design resource scheduling optimization algorithm in colleges and universities and take elimination measures, so as to realize the art design resource scheduling in colleges and universities. So far, we have completed the design of art design resource scheduling optimization method for the 6G network environment.

## 5. Experiment

*5.1. Experimental Preparation.* This case study selects a pilot university to study the art design major in the university. The university art design resources used in this experiment are all provided by the pilot universities, and their contents, functions, and teaching methods are evaluated by the professional review and appraisal team. The applicability, academic leadership, etc. are reviewed to confirm that they can be put into use. In this experiment, hardware facilities include the following: TYR3583589 host computer and CPUE5500 @ 2.80 GHz. The software environment is Twerfag operating system and YRjkle integrated development environment. The specific contents and parameters of the experimental environment are shown in Table 3.

According to Table 3, the scheduling cycle is set to 10 hours, and each hour is used as the test node. The traditional scheduling method and the scheduling method designed in this paper are used for comparative experiments. The experimental content is to test the scheduling flexibility margin of the two scheduling methods. The higher the scheduling flexibility margin is, the better the scheduling flexibility of the scheduling method is. The experimental results are recorded to judge the more flexible scheduling method.

*5.2. Analysis and Conclusion of Experimental Results.* Within 10 hours of the scheduling cycle, according to the calculation results of the flexibility margin index in Formula (2), the scheduling flexibility margin experimental results of the original art design resource scheduling method (control group) and the design method in this paper (experimental group) in

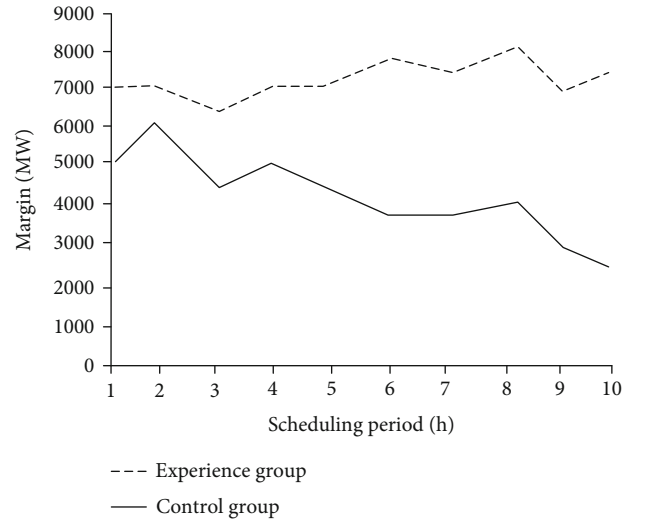


FIGURE 2: Comparison of dispatching flexibility margin.

colleges and universities are obtained, and the experimental results are sorted, as shown in Figure 2.

The following conclusions can be drawn from Figure 2: the scheduling flexibility margin of the scheduling method designed in this paper is higher than 6300 mw, which is more flexible than the scheduling of control group, and can realize the optimization of art design resource scheduling in colleges and universities, which shows that the function of the scheduling method designed in this paper can meet the design requirements. The main reason is that this method considers the high dynamic and random characteristics of user scheduling in 6G network environment and reduces the impact of real-time, irregular, and independent characteristics of scheduling on scheduling flexibility.

In order to further verify the overall effectiveness of the proposed method, the art design resource scheduling time of the two methods is compared, and the test results are shown in Figure 3.

By analyzing Figure 3, it can be seen that the time required to schedule the art design using the proposed method in multiple iterations is less than that required by the control group, because the 6G network environment of the proposed method expands the coverage, shortens the time required for task scheduling, and improves the scheduling efficiency of the proposed method.

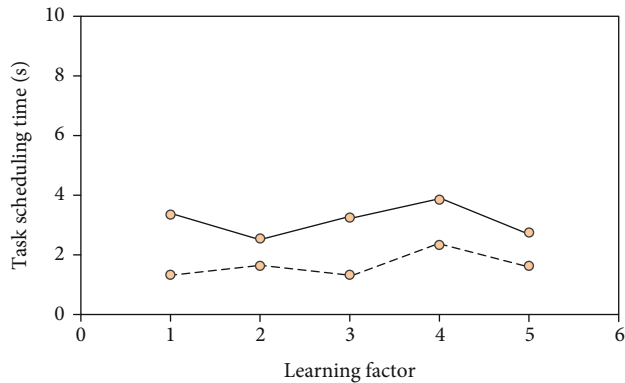


FIGURE 3: Task scheduling time.

## 6. Conclusions

Through the above research, it is proved that the design scheduling method has specific advantages in the scheduling of art design resources in colleges and universities. The art design resource scheduling method under the 6G network environment is the most practical and reliable means in art design resource scheduling in colleges and universities. It is reasonable to increase the application of design scheduling method in art design resource scheduling in colleges and universities. The experimental results show that this method takes design scheduling as the core, improves the scheduling flexibility margin, up to 6300 mw, and provides academic significance for the research in the field of art design resource scheduling in colleges and universities. The only deficiency of this paper is that there is no in-depth analysis of the genetic operator in the university art and design resource scheduling. I believe this can also be used as one of the future research directions in the university art and design resource scheduling. Hoping that through this study, we can contribute to the art design resource scheduling in colleges and universities.

## Data Availability

The data used to support the findings of this study are available from the corresponding author upon request.

## Conflicts of Interest

The authors declare that there is no conflict of interest regarding the publication of this paper.

## References

- [1] S. Han, T. Xie, and I. Chih-Lin, "Greener physical layer technologies for 6G mobile communications," *IEEE Communications Magazine*, vol. 59, no. 4, pp. 68–74, 2021.
- [2] F. Tariq, M. Khandaker, K. K. Wong, M. A. Imran, M. Bennis, and M. Debbah, "A speculative study on 6G," *IEEE Wireless Communications*, vol. 27, no. 4, pp. 118–125, 2020.
- [3] S. Han, T. Xie, C. L. I et al., "Artificial-intelligence-enabled air interface for 6G: solutions, challenges, and standardization impacts," *IEEE Communications Magazine*, vol. 58, no. 10, pp. 73–79, 2020.
- [4] H. Thiesen and C. Jauch, "Application of a new dispatch methodology to identify the influence of inertia supplying wind turbines on day-ahead market sales volumes," *Energies*, vol. 14, no. 5, p. 1255, 2021.
- [5] S. Qian, H. Wu, and G. Xu, "An improved particle swarm optimization with clone selection principle for dynamic economic emission dispatch," *Soft Computing*, vol. 24, no. 20, pp. 15249–15271, 2020.
- [6] N. B. Agaev and R. J. Abdullaev, "Using a fuzzy prognostic model in the operative-dispatch analysis of heat-supply systems' operation," *Thermal Engineering*, vol. 67, no. 9, p. 680, 2020.
- [7] Y. Chen, Q. Guo, H. Sun, Z. Pan, and B. Chen, "Generalized phasor modeling of dynamic gas flow for integrated electricity-gas dispatch," *Applied Energy*, vol. 283, no. 5, article 116153, 2021.
- [8] P. L. Chen Wieler, R. Kuiava, and F. Santana Souza, "Transient stability constrained optimal power flow based on trajectory sensitivity for power dispatch of distributed synchronous generators," *IEEE Latin America Transactions*, vol. 18, no. 7, pp. 1247–1254, 2020.
- [9] L. Wen, K. Zhou, S. Yang, and X. Lu, "Optimal load dispatch of community microgrid with deep learning based solar power and load forecasting," *Energy*, vol. 171, no. 15, pp. 1053–1065, 2019.
- [10] J. R. Xu and H. J. Zhu, "Multi-objective scheduling algorithm of DAG tasks in cloud computing," *Application Research of Computers*, vol. 36, no. 1, pp. 31–36, 2019.
- [11] I. G. Marnieris, C. G. Roumkos, and P. N. Biskas, "Towards balancing market integration: conversion process for balancing energy offers of central-dispatch systems," *IEEE Transactions on Power Systems*, vol. 35, no. 1, pp. 293–303, 2020.
- [12] M. L. Zhang, X. M. Ai, J. K. Fang, and J. Wen, "Two-stage stochastic programming for the joint dispatch of energy and reserve considering demand response," *The Journal of Engineering*, vol. 2019, no. 18, pp. 5172–5177, 2019.
- [13] M. Alramlawi, E. Mohagheghi, and P. Li, "Predictive active-reactive optimal power dispatch in PV-battery-diesel microgrid considering reactive power and battery lifetime costs," *Solar Energy*, vol. 193, pp. 529–544, 2019.
- [14] X. Xiang and J. Tian, "P2P transmission scheduling optimization based on software defined network," *Journal of Computer Applications*, vol. 40, no. 3, pp. 777–782, 2020.
- [15] Y. Jia, Z. Y. Dong, C. Sun, and K. Meng, "Cooperation-based distributed economic MPC for economic load dispatch and load frequency control of interconnected power systems," *IEEE Transactions on Power Systems*, vol. 34, no. 5, pp. 3964–3966, 2019.
- [16] J. G. Xiao and Y. X. Li, "University educational governance model and its optimization in the new era—based on the unity of instrumental rationality and value rationality," *Journal of Anhui Normal University (Humanities & Social Sciences Edition)*, vol. 48, no. 1, pp. 101–106, 2020.
- [17] J. T. Yu, C. H. Kim, A. Wadood, T. Khurshaid, and S. B. Rhee, "Jaya algorithm with self-adaptive multi-population and Lévy flights for solving economic load dispatch problems," *IEEE Access*, vol. 7, pp. 21372–21384, 2019.
- [18] L. Che, X. Liu, X. Zhu, Y. Wen, and Z. Li, "Intra-interval security based dispatch for power systems with high wind penetration," *IEEE Transactions on Power Systems*, vol. 34, no. 2, pp. 1243–1255, 2019.

- [19] M. Basu, "Dynamic economic dispatch incorporating renewable energy sources and pumped hydroenergy storage," *Soft Computing*, vol. 24, no. 7, pp. 4829–4840, 2020.
- [20] H. J. Li, L. Yang, and P. W. Zhang, "Method of online learning resource recommendation based on multi-objective optimization strategy," *Pattern Recognition and Artificial Intelligence*, vol. 32, no. 4, pp. 306–316, 2019.



## Research Article

# Automatic Roadblock Identification Algorithm for Unmanned Vehicles Based on Binocular Vision

Liang Fang <sup>1,2</sup>, Zhiwei Guan,<sup>1</sup> and Jinghua Li<sup>2</sup>

<sup>1</sup>School of Automobile and Transportation, Tianjin University of Technology and Education, Tianjin 300222, China

<sup>2</sup>School of Automotive Engineering, Tianjin Vocational Institute, Tianjin 300410, China

Correspondence should be addressed to Liang Fang; [fangliang@tute.edu.cn](mailto:fangliang@tute.edu.cn)

Received 22 September 2021; Revised 27 October 2021; Accepted 9 November 2021; Published 23 November 2021

Academic Editor: Deepak Gupta

Copyright © 2021 Liang Fang et al. This is an open access article distributed under the Creative Commons Attribution License, which permits unrestricted use, distribution, and reproduction in any medium, provided the original work is properly cited.

In order to improve the accuracy of automatic obstacle recognition algorithm for driverless vehicles, an automatic obstacle recognition algorithm for driverless vehicles based on binocular vision is constructed. Firstly, the relevant parameters of the camera are calibrated around the new car coordinate system to determine the corresponding obstacle position of the vehicle. At the same time, the three-dimensional coordinates of obstacle points are obtained by binocular matching method. Then, the left and right cameras are used to capture the feature points of obstacles in the image to realize the recognition of obstacles. Finally, the experimental results show that for obstacle 1, the recognition error of the algorithm is 0.03 m; for obstacle 2, the recognition error is 0.02 m; for obstacle 3, the recognition error is 0.01 m. The algorithm has small recognition error. The vehicle coordinate system is added in the camera calibration process, which can accurately measure the relative position information between the vehicle and the obstacle.

## 1. Introduction

With the wide popularity of automobiles, driverless vehicles have become a hot research topic. UAV is a complex mechanical product integrating a variety of technologies, and its key technologies include environment perception technology, positioning and navigation technology, path planning technology, and motion control technology [1–4]. In order to ensure the safe driving of unmanned vehicles, it is necessary to use environmental sensing technology to enable unmanned vehicles to automatically avoid obstacles on the road [5–9]. Therefore, as an important means of environmental perception, vision has been studied more and more [10]. Research on visual perception mainly includes vision-based positioning, vision-based road and traffic sign detection and recognition, and vision-based collision avoidance technology [11, 12]. The computer vision system usually requires two or more cameras for the same scene from two or more angles, in order to obtain a set of images in the same scene under different angles of view,

and then, through different images of the same scene, the parallax, calculation of the target space geometry, and position of the object are determined; this method is called stereo vision [13, 14]. The binocular stereo vision system uses two cameras to obtain two images of the same scene from two different perspectives, namely, the binocular stereo image pair. The gray-scale, shape, distance, and other information of the surface of the target object can be recovered by calculating the parallax of the target object in stereo image alignment. The binocular stereo vision system directly simulates the human eye to process the scene, which has important practical value and broad application prospect.

Compared with the binocular vision ranging system, the monocular vision ranging system cannot accurately obtain target distance because of less information acquired by monocular vision. Therefore, there are more and more researches on binocular ranging at home and abroad. However, although researchers have done a great deal of research on the measurement of vehicle distance ahead, reference [15] proposes a

monocular vision-based understanding of street view curves, and the use of autonomous vehicles to deliver medical and emergency supplies is a potential way to avoid unsafe and unpredictable factors. However, its implementation has been hampered by several key issues. A major difficulty was understanding the crooked alleys of the street scene. These can be seen as combinations of non-Manhattan structures that help us estimate their original posture in a three-dimensional scene. A new approach is proposed to understand curving alleys and bridge the gap between 2d scene understanding and monocular 3d environment reconstruction. The angular projection is assigned to the cluster. The curving alley scene approximates the Manhattan and non-Manhattan fold structures approximated in the alley scene reconstruction. This algorithm has geometric characteristics and does not require prior training or understanding of the internal parameters of the camera. The results show that the algorithm can successfully understand alley scenarios including Manhattan and curved non-Manhattan structures. Reference [16] proposed a monocular vision-based distance estimation method for a 3d detection workshop. In order to improve the accuracy and robustness of ranging results, the actual area of the vehicle rare visual field and the corresponding projection area in the image were obtained by 3d detection method. Then, an area-distance geometric model is established to restore the distance according to the camera projection principle. Our method shows its potential in complex traffic scenarios by testing test set data provided on KITTI, a real-world computer vision benchmark. The experimental results show better performance than the existing methods. In addition, the accuracy of shielding vehicle ranging results can reach about 98%, while the accuracy deviation between vehicles from different perspectives is less than 2%. However, the current distance measurement system is still based on monocular vision, and the accuracy of monocular vision image distance perception is low. Therefore, we should focus on the research of the binocular stereo ranging system, which can well simulate the function of human eyes and perceive the three-dimensional world. The binocular stereo ranging system mainly includes this method, which can effectively improve the accuracy of obstacle detection and accurately measure the relative position information with the object in front and has certain practical value [17]. On this basis, a road block automatic recognition algorithm based on binocular vision is proposed. Binocular vision is an important form of machine vision. It is a method to obtain the three-dimensional geometric information of the object by calculating the position deviation between the corresponding points of the image based on the parallax principle and using the imaging equipment to obtain two images of the measured object from different positions. Binocular vision fuses the images obtained by two eyes and observes the differences between them, so that we can obtain an obvious sense of depth, establish the corresponding relationship between features, and correspond the image points of the same spatial physical point in different images. The binocular vision method has the advantages of high efficiency, appropriate precision, simple system structure, and low cost. Binocular vision is one of the key technologies of computer vision. Obtaining the distance information of spatial 3D scene is also the most

basic content in computer vision research. By adding the vehicle coordinate system, the relative position information of the vehicle and obstacle can be obtained, and the accuracy of obstacle identification can be improved.

## 2. Design of Automatic Roadblock Identification Algorithm for Unmanned Vehicle Based on Binocular Vision

*2.1. Camera Calibration.* Through camera calibration, the mapping relationship between coordinates is generated, and the mapping relationship between world coordinates and image coordinates is expressed by projection matrix. The mapping relationship between the left camera image and the right camera image is represented by a homography matrix, in which the coordinate system of the whole vision system needs to be constructed, including the camera image coordinate system, the camera coordinate system, and the world coordinate system. The concrete content of coordinate system establishment is described as follows. The Cartesian coordinate system  $QOP$  is set as the image coordinate system, where the  $Q$  axis represents the number of columns of image pixels, the  $P$  axis represents the number of rows of image pixels, and the pixel point  $(q, p)$  represents the  $q$  row and the  $p$  column of this pixel on the image. Because it determines the position of pixel points according to the number of rows and columns, but does not reflect its position in the image through physical units, it is necessary to create an image coordinate system. The physical image coordinate system is set as  $XO_1Y$ , where the origin  $O_1$  is the intersection point of the camera optical axis and the plane where the image is located. The  $X$  axis and  $Y$  axis are parallel to the  $Q$  axis and  $P$  axis, respectively. The physical size of each pixel in the  $XO_1Y$  coordinate system is set as  $dx$  and  $dy$ , and the following relation can be obtained:

$$q = \frac{x}{dx} + q_0, p = \frac{y}{dy} + p_0. \quad (1)$$

Formula (1) is expressed in homogeneous coordinates and matrix form:

$$\begin{bmatrix} q \\ p \\ 1 \end{bmatrix} = \begin{bmatrix} \frac{1}{dx} & 0 & q_0 \\ 0 & \frac{1}{dy} & p_0 \\ 0 & 0 & 1 \end{bmatrix} \cdot \begin{bmatrix} x \\ y \\ 1 \end{bmatrix}. \quad (2)$$

The transformation from the image plane coordinate system to the image pixel coordinate system is completed by Formula (2). The coordinate system  $O_cX_cY_cZ_c$  is set as the camera coordinate system, which is the coordinate system of a single vision system in binocular vision. The origin  $O_c$  is the optical center of the camera; the  $X_c$  and  $Y_c$  axes are parallel to the  $X$  and  $Y$  axes in the image coordinate system  $XO_1Y$ , respectively; and the  $Z_c$  axes coincide with the optical axis of the camera. A reference coordinate system  $O_wX_wY_wZ_w$ , selected from the space environment, is set as the world coordinate system to represent the position of the camera and the car in the space

in the environment. The relation of any point  $A$  in the space in the camera coordinate system and the world coordinate system is shown in the following formula:

$$\begin{bmatrix} x_c \\ y_c \\ z_c \\ 1 \end{bmatrix} = \begin{bmatrix} R & T \\ 0 & 1 \end{bmatrix} \cdot \begin{bmatrix} x_w \\ y_w \\ z_w \\ 1 \end{bmatrix}. \quad (3)$$

In Formula (3),  $R$  represents an orthogonal rotation transformation matrix,  $T$  represents a three-dimensional translation vector,  $(x_c, y_c, z_c)$  represents the coordinates of point  $A$  in the camera coordinate system, and  $(x_w, y_w, z_w)$  represents the coordinates of point  $A$  in the world coordinate system. Through Formula (3), the space point  $A$  realizes the transformation from the world coordinate system to the camera coordinate system. According to the pinhole imaging model, the transformation from the camera coordinate system to the image plane coordinate system can be obtained by using geometric relations, as shown in the following formula:

$$\frac{f}{Z_c} = \frac{x}{X_c} = \frac{y}{Y_c}. \quad (4)$$

In Formula (4),  $f$  represents the focal length of the camera, which is expressed in homogeneous coordinate matrix form as follows:

$$Z_c \begin{bmatrix} x \\ y \\ 1 \end{bmatrix} = \begin{bmatrix} f & 0 & 0 & 0 \\ 0 & f & 0 & 0 \\ 0 & 0 & 1 & 0 \end{bmatrix} \begin{bmatrix} X_c \\ Y_c \\ Z_c \\ 1 \end{bmatrix}. \quad (5)$$

Using the above formula, the establishment and conversion of different coordinate systems (left and right camera calibration) are realized. After the calibration of the left and right cameras is completed, the binocular calibration also needs to know the relative positions between the left and right cameras. Therefore, two matrices are introduced, namely, the rotation matrix  $R_s$  and the translation matrix  $T_s$  of the left camera relative to the right camera. Then, the relationship between the two cameras is shown in the following formula:

$$\begin{bmatrix} X_{cl} \\ Y_{cl} \\ Z_{cl} \end{bmatrix} = R_s \begin{bmatrix} X_{cr} \\ Y_{cr} \\ Z_{cr} \end{bmatrix} + T_s. \quad (6)$$

In Formula (6),

$$T_s = \begin{bmatrix} T_1 \\ T_2 \\ T_3 \end{bmatrix}. \quad (7)$$

After considering camera calibration and once internal and external parameters are established, the world coordinate system and the location of the relationship between cars are relatively static. If the car is in motion, the world coordinate system is also doing the same movement, considering the factors, and in this system, only considering the relative position of car and obstacles. Therefore, a new coordinate system is selected, which is called the automobile coordinate system  $(X, Y, Z)$ , and its origin position is selected at the midpoint of the two cameras. Then, the homogeneous coordinated relationship is shown in the following formula:

$$\begin{bmatrix} X \\ Y \\ Z \end{bmatrix} = \frac{1}{2} \left( \begin{bmatrix} X_{cl} \\ Y_{cl} \\ Z_{cl} \end{bmatrix} + \begin{bmatrix} X_{cr} \\ Y_{cr} \\ Z_{cr} \end{bmatrix} \right). \quad (8)$$

In Formula (8),  $X_{cl}$ ,  $Y_{cl}$ , and  $Z_{cl}$ , respectively, represent the obstacle distance on the camera image corresponding to the  $X$  axis,  $Y$  axis, and  $Z$  axis, and  $X_{cr}$ ,  $Y_{cr}$ , and  $Z_{cr}$ , respectively, represent the relative position of the obstacle on the camera image corresponding to  $X$  axis,  $Y$  axis, and  $Z$  axis. Since the world coordinate system has changed, Formula (2) and Formula (5) are used to directly convert to the camera coordinate system. By calculating the coordinate of the obstacle on the left and right camera images, the relative position between the obstacle and the car is further calculated. Then, image matching is performed based on binocular vision.

**2.2. Binocular Matching.** The region matching algorithm is used to create a window centered on the point to be matched in the base graph, and the adjacent pixels in the window are used to represent the point to be matched. A sliding window of the same size is created as the center at a point on the polar line corresponding to the alignment diagram. The sliding window moved on the outer polar line and the window matching measure at each displacement point is calculated. The best matching point is obtained by searching the maximum or minimum value of the matching measure. For binocular image pairs, for a point in the left image, create a window centered on that point. A sliding window of the same size is created as the center at a point on the corresponding polar line in the alignment diagram. The sliding window moved on the outer polar line, and the window matching measure at each displacement point is calculated. The point with the maximum similarity or minimum difference is selected as the matching point of this point. The specific process is described below. First of all, when determining appropriate matching primitives, the obstacle target is uncertain. The obstacles could be pedestrians or other objects such as cars. Cars can also be divided into trucks, ordinary sedan, and so on; from the point of view of form, the difference is bigger and the relative characteristics of a single image are more complex, which is therefore difficult for feature matching [18]. By image segmentation, the target image is segmented from the background. The discussion is carried out if there is only one target in the image, and the target gray block in the left image is used as the base element to search in the right image. In the process of driving, the position of the obstacle on the horizontal plane directly determines the driving

result, while the vertical height of the obstacle has little influence on the driving decision. When the target is a pedestrian, the pedestrian's position on the horizontal plane will determine whether to stop or detour, and the pedestrian's height has no effect on this. Grayscale blocks in the two images are compared horizontally. The car is formed into a continuous gray block in the binary image, and the gray area registration in the horizontal direction can identify it as a matching target. Firstly, the background information is filtered out of the image by using threshold segmentation, and the target is highlighted. In the processed image, there are two obvious targets that can be matched: the car on the left of the center of the image and a narrow street line on the left of the car. Next, the gray block of the car target in the middle of the image is projected, and the projection line on the abscissa is used as the primitive for matching. Due to the existence of more than one target gray block in the image, due to the image illumination angle, shadow, overlay, and other adverse factors directly projected on the image, multiple targets will be fused together. Therefore, multiple targets should be extracted into a single target to facilitate matching. In order to reduce the amount of data to be processed, the whole image is cut into several banded regions, and the target of the gray block in each banded region is projected. After the projection processing, the target is transformed into several line segments in the image, the length of the line segments at the same height is calculated, and the similarity matching of the length of the line segments is carried out. If there are two line segments whose lengths are the closest, it can be considered as a target with the same name, and the two endpoints of the line segment are points with the same name. The smaller the interval is, the richer the information is and the more computation is needed. The larger the interval is, the less information is needed and the less computation is needed. The appropriate interval is selected according to the characteristics of the target. If the relative speed of the target is faster, the interval should be reduced; otherwise, it can be amplified to improve the real-time performance. If the height feature of the target is small, the interval should be reduced; otherwise, it can be enlarged. The length of the projected line segment is analyzed to get the length of the line segment. We list the matrix of the line segment length in both images and match the line segment with the closest length according to the rule from left to right to obtain three line segments with the same name. The two endpoints of the line segment are points with the same name. Through triangulation, the depth information of the points with the same name is calculated and obtained. The length of the line segment represents the width index of the target in the real world. Through the above process, the matching based on the region gray area is transformed into the feature matching based on the width of the projected line segment of the ribbon region. Three line segments and six points with the same name are obtained by matching the above pictures. Next, the six points are triangulated to calculate the three-dimensional coordinates of the points with the same name.

**2.3. Obstacle Identification.** After acquiring the characteristic points of the obstacles in the images captured by the left and right cameras, the position coordinates of the points in the

binocular vision system are calculated by using the method of depth information calculation of the points. Among them, in the calculation of the depth information of the point with the same name, the first step is to get the coordinates of the point with the same name in the image. The two images are taken by the left and right CCD cameras at the same moment by camera, and the position parameters  $(x_1, y_1)$  and  $(x_2, y_2)$  of the point with the same name in the two images are obtained by image processing. After the image coordinates of pixels to the coordinates into space coordinates of pixels corresponding to the physical, through the two image points with triangle to locate the implementation of physical points, since one side of the triangle (the connection between the two cameras) is known, so the second step to calculate as points to the physical connection with the angle of optical axis in the relative coordinates. Constants obtained from calibration measurement include the height from the origin to the ground, the distance between the two cameras, and the image width and height; parameters obtained from calibration include the focal length; and  $(x_1, y_1)$  and  $(x_2, y_2)$  of the same name point position parameters are detected in real time from the collected images. The coordinates of the target point in the relative coordinate system are calculated according to the determined geometric relation. After getting the coordinate information, through the analysis of the coordinate of the point with the same name, the type, color, and other details of the obstacle can be identified. For example, the width of the car in the original image can be calculated by comparing the abscissa of the left and right points with the same name. The left side of the car has a white door of the word line. The system can measure the width and vertical height information of the line. Use a series of points for complete matching as the most important target in the image information. The flow chart of driverless vehicle obstacle automatic recognition algorithm is shown in Figure 1.

Through further analysis of the information, the contour information of the target can be obtained, such as whether the target is the car, the pedestrian, or just the railing [19, 20]. Through the above process, the recognition of the target obstacle is realized.

### 3. Experiment

The proposed algorithm based on binocular vision is used to make a comparative experiment with two traditional identification algorithms. The specific content is as follows.

**3.1. Experimental Environment.** In the simulation experiment, the simulation platform of Pentium 42.8 GHz and 4G memory is used. The operating system model is XP SP2. The binocular vision hardware platform is composed of two identical USB3.0 industrial cameras, Jetson TX-1, camera support, and display. Binocular camera is used to collect images, and Jetson TX-1 is used to process the collected images. Specific parameters are shown in Table 1.

In the above experimental environment, the binocular calibration toolbox provided by MATLAB 2017b is used to calibrate the binocular camera.



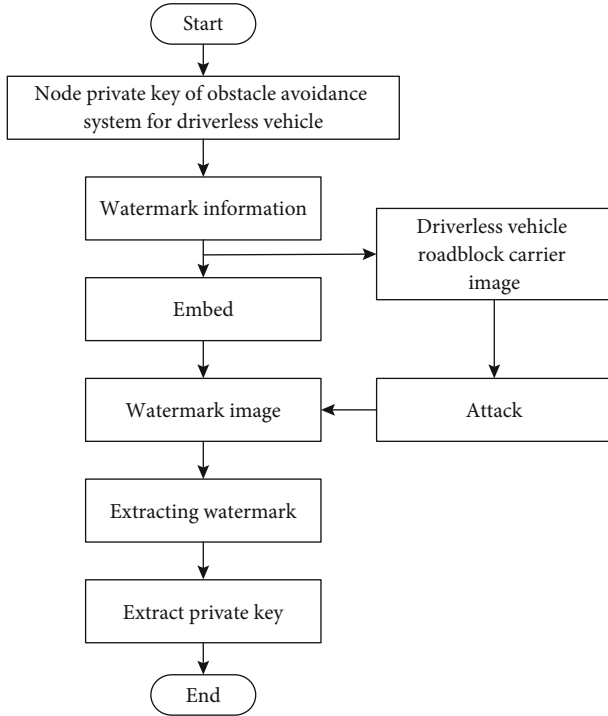


FIGURE 1: Flow chart of automatic obstacle recognition algorithm for driverless vehicle.

TABLE 1: Binocular camera and TX-1 parameters.

Instrument	Parameter	Parameter value
Binocular camera	Baseline	20.5 cm
	Focal length	3.1 mm
	Pixel	180 pixels
	Resolution ratio	2560 * 20
	System	Ubuntu14.04
Jetson TX-1	Memory	4 GB
	CPU	64-bit

**3.2. Experimental Process.** First of all, in order to ensure the smooth progress of the experiment, the binocular camera is used to carry out calibration work. Step 1, take the image. During shooting, the camera position should be fixed to shoot a group of images, and the direction and angle of the calibration plate should be changed at the same time, and all the corner points on the calibration plate should be included in the image, so as to facilitate the subsequent corner detection. Step 2, extract the corners. Input each checkerboard size 25 mm, then use MATLAB to extract checkerboard corner points. The third step is the calibration of the monocular camera. The camera calibration module of MATLAB 2017b is used to calibrate the left and right cameras, to obtain the internal parameters, rotation matrix, distortion coefficient, and translation vector of the left and right cameras. The fourth step is calibration error analysis. After the calibration of the monoc-

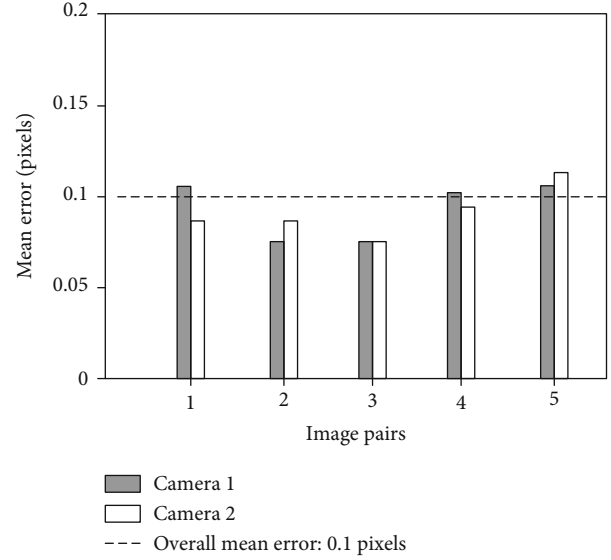


FIGURE 2: Calibration results of binocular camera.

ular camera is completed, the calibration results are analyzed based on the error pixel distribution. The fifth step is binocular camera calibration. The stereo camera is calibrated using the MATLAB 2017b camera calibration module to obtain the rotation matrix and translation vector of the binocular camera. Finally, the calibration results are outputted, as shown in Figure 2.

As can be seen from Figure 1, the average calibration errors of both monocular camera and binocular camera are within the range of 0.1 pixel, indicating high calibration accuracy and good calibration effect. After that, the obstacle identification is carried out automatically. The car went straight ahead at a speed of 30 km/h. Select the vehicle forward person as obstacle 1, the bicycle as obstacle 2, and the fork port as obstacle 3. The obstacles 1, 2, and 3 are set at 5 m, 10 m, and 20 m in front of the vehicle, respectively. Lighting conditions are natural light during the day. The simulation diagram of the experimental obstacles is shown in Figure 3, and the identification results are compared.

**3.3. Experimental Results.** The verification standard for effective obstacle avoidance is the verification standard that has no collision and can drive normally. With regard to failure to complete the avoidance or a collision with the obstacle, the verification standard of false avoidance is the behavior of avoiding obstacles on a road that is free of obstacles. The recognition results of the proposed binocular vision-based automatic recognition algorithm for UAV driving vehicle roadblocks, traditional algorithm 1, and traditional algorithm 2 are shown in Table 2.

As shown in Table 2, for obstacle 1, the recognition error of the proposed algorithm is 0.03 m; for obstacle 2, the recognition error of the proposed algorithm is 0.02 m; and for obstacle 3, the recognition error of the proposed algorithm is 0.01 m. In conclusion, the proposed algorithm has a smaller recognition error (higher recognition accuracy). Through analysis, it is found that the proposed obstacle recognition algorithm based



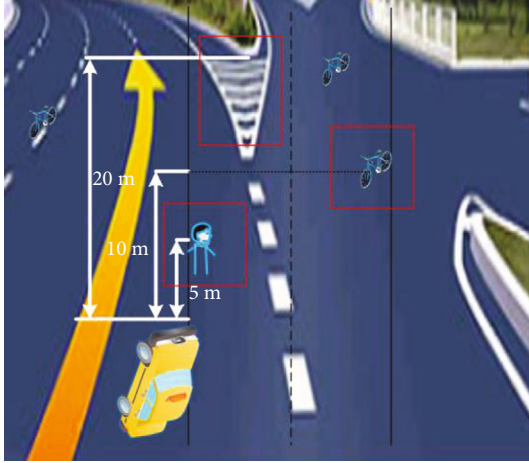


FIGURE 3: Simulation diagram of obstacle identification.

TABLE 2: Obstacle identification comparison results.

Items	Identification algorithm	Identification results	Error (m)
Obstacle 1	Proposed algorithm	5.03	0.03
	Traditional algorithm 1	5.24	0.24
	Traditional algorithm 2	5.16	0.16
Obstacle 2	Proposed algorithm	10.02	0.02
	Traditional algorithm 1	10.26	0.26
	Traditional algorithm 2	10.19	0.19
Obstacle 3	Proposed algorithm	20.01	0.01
	Traditional algorithm 1	20.51	0.51
	Traditional algorithm 2	20.33	0.33

on binocular vision can accurately measure the relative position information of the vehicle and the obstacle by adding the car coordinate system in the camera calibration.

#### 4. Conclusions

Computer vision has a broad application prospect; intelligent robot, medical image processing, and graphics search technology in all walks of life have their place; because the image contains abundant information, relative to other types of sensors, computer vision has obvious superiority, which will be applied to more and more engineering. Binocular stereo vision, as an important research branch of computer vision, has always been one of the focuses and hotspots of computer vision research. It simulates the process of human perception with both eyes and can measure the depth of a target using the parallax generated by multiple viewing angles. In this paper, binocular vision is applied for automatic identification of roadblocks of unmanned vehicles. By adding a car coordinate system, the relative position information of vehicles and obstacles can be obtained easily and the identification accuracy can be improved. It is hoped that the proposed algorithm can provide some reference value for the research in this field. Binoc-

ular vision processing system needs to be aimed at different applications because of its large information capacity and high complexity. Real time is the bottleneck of its engineering application. More in-depth research about how to solve the bottleneck of its engineering application is the key future research direction.

#### Data Availability

The data used to support the findings of this study are available from the corresponding author upon request.

#### Conflicts of Interest

The authors declare that there is no conflict of interest regarding the publication of this paper.

#### Acknowledgments

This work was supported by the Tianjin Artificial Intelligence Science and Technology Major Project (grant number 17ZXRGGX00070) and Key Tender Project of Tianjin Science and Technology Development Strategy Research Program (grant number 18ZLZDZF00390).

#### References

- [1] A. di Febbraro, F. Gallo, D. Giglio, and N. Sacco, "Traffic management system for smart road networks reserved for self-driving cars," *IET Intelligent Transport Systems*, vol. 14, no. 9, pp. 1013–1024, 2020.
- [2] M. Raue, L. A. D'Ambrosio, C. Ward, C. Lee, C. Jacquillat, and J. F. Coughlin, "The influence of feelings while driving regular cars on the perception and acceptance of self-driving cars," *Risk Analysis*, vol. 39, no. 2, pp. 358–374, 2019.
- [3] K. H. Lee, K. H. Baek, S. B. Choi et al., "Development of three driver state detection models from driving information using vehicle simulator; normal, drowsy and drunk driving," *International Journal of Automotive Technology*, vol. 20, no. 6, pp. 1205–1219, 2019.
- [4] A. Muralidharan and Y. Mostofi, "Statistics of the distance traveled until successful connectivity for unmanned vehicles," *Autonomous Robots*, vol. 44, no. 1, pp. 25–42, 2020.
- [5] A. Llamazares, J. M. Eduardo, and O. Manuel, "Detection and tracking of moving obstacles (DATMO): a review," *Robotica*, vol. 38, no. 5, pp. 761–774, 2020.
- [6] M. Cefalo and G. Oriolo, "A general framework for task-constrained motion planning with moving obstacles," *Robotica*, vol. 37, no. 3, pp. 575–598, 2018.
- [7] R. Reyes and R. Murrieta-Cid, "An approach integrating planning and image-based visual servo control for road following and moving obstacles avoidance," *International Journal of Control*, vol. 93, no. 10, pp. 2442–2456, 2020.
- [8] K. Mondal and P. S. Mandal, "Range-free mobile sensor localization and a novel obstacle detection technique," *Wireless Personal Communications*, vol. 92, no. 2, pp. 351–380, 2017.
- [9] D. M. Lyons, B. Barriage, and L. Del Signore, "Evaluation of field of view width in stereo-vision-based visual homing," *Robotica*, vol. 38, no. 5, pp. 787–803, 2020.
- [10] G. Y. Wan, F. D. Li, W. J. Zhu, and G. Wang, "High-precision six-degree-of-freedom pose measurement and grasping system

- for large-size object based on binocular vision,” *Sensor Review*, vol. 40, no. 1, pp. 71–80, 2020.
- [11] D. F. Jin and Y. Yang, “Sensitivity analysis of the error factors in the binocular vision measurement system,” *Optical Engineering*, vol. 57, no. 10, article 104109, 2018.
- [12] J. Xiong, S. D. Zhong, Y. Liu, and L. F. Tu, “Automatic three-dimensional reconstruction based on four-view stereo vision using checkerboard pattern,” *Journal of Central South University*, vol. 24, no. 5, pp. 1063–1072, 2017.
- [13] C. Li, C. H. Zhou, C. F. Miao, Y. Yan, and J. Yu, “Binocular vision profilometry for large-sized rough optical elements using binarized band-limited pseudo-random patterns,” *Optics Express*, vol. 27, no. 8, pp. 10890–10899, 2019.
- [14] T. Xue, L. S. Xu, and S. Z. Zhang, “Bubble behavior characteristics based on virtual binocular stereo vision,” *Optoelectronics Letters*, vol. 14, no. 1, pp. 44–47, 2018.
- [15] L. Wang and H. Wei, “Curved alleyway understanding based on monocular vision in street scenes,” *IEEE Transactions on Intelligent Transportation Systems*, vol. 6, no. 99, pp. 1–20, 2021.
- [16] T. Zhe, L. Huang, Q. Wu, J. Zhang, C. Pei, and L. Li, “Inter-vehicle distance estimation method based on monocular vision using 3D detection,” *IEEE transactions on vehicular technology*, vol. 69, no. 5, pp. 4907–4919, 2020.
- [17] S. Sharma and D. Shah, “Real-time automatic obstacle detection and alert system for driver assistance on Indian roads,” *International Journal of Vehicle Autonomous Systems*, vol. 13, no. 3, pp. 189–202, 2017.
- [18] R. Nakasone, N. Nagamine, M. Ukai, H. Mukojima, D. Deguchi, and H. Murase, “Frontal obstacle detection using background subtraction and frame registration,” *Quarterly Report of RTRI*, vol. 58, no. 4, pp. 298–302, 2017.
- [19] L. Priya and S. Anand, “Object recognition and 3D reconstruction of occluded objects using binocular stereo,” *Cluster Computing*, vol. 21, no. 1, pp. 29–38, 2018.
- [20] W. P. Ma, W. X. Li, and P. X. Cao, “Binocular vision object positioning method for robots based on coarse-fine stereo matching,” *International Journal of Automation and Computing*, vol. 17, no. 4, pp. 562–571, 2020.

## Research Article

# Green Product Market Development Strategy of Mobile Network Group Buying Community: Based on Three-Party Evolutionary Game and Simulation Analysis

Zhihong Ai 

College of Modern Economics & Management, Jiangxi University of Finance and Economics, Jiangxi 332020, China

Correspondence should be addressed to Zhihong Ai; 1200600439@jxufe.edu.cn

Received 29 September 2021; Accepted 1 November 2021; Published 20 November 2021

Academic Editor: Deepak Gupta

Copyright © 2021 Zhihong Ai. This is an open access article distributed under the Creative Commons Attribution License, which permits unrestricted use, distribution, and reproduction in any medium, provided the original work is properly cited.

With the advent of the 5G era, the mobile network group buying community dominated by focusing on social relations shows great development potential. However, in the mobile network group buying community, the mixed information makes the information environment of the community more complex. Information asymmetry will lead to “mistakes” in consumers’ choice, making it impossible for some important markets to be fully developed. Considering the gains and losses of three interest subjects—governments, enterprises, and consumers in the green product market under information symmetry, in this paper, an evolutionary game model involving governments, enterprises, and consumers was built. Numerical experiments and simulation were performed using SciPy, a scientific computing library of Python, to study the main factors influencing the healthy development of the green product market. The research results showed under information symmetry, when the governments’ benefit from increased government credibility was higher than the cost of governments for screening the information of enterprises’ products and identifying the green products, the expected fine of enterprises for producing high carbon products was higher than the difference between the actual cost increment and the actual income increment of enterprises for producing green products, and the utility perception of consumers from purchasing green products was higher than the cost of consumers for purchasing green products, the three-party game would evolve to a socially ideal stable state. The above conclusions provide useful policy suggestions for governments to vigorously develop the green product market.

## 1. Introduction

Green economy arouses wide concern among countries around the world amid growing environmental pollution, ecological environmental degradation, and global warming. In 2016, the State Council issued the opinions on establishing unified green product standards, certification, and identification system, which means that China is substantially promoting the certification and identification system of “Chinese green products.” Green product refers to the product with low toxicity and little harm, health and safety, and good ecological effects, which can reduce energy consumption and pollutant emissions [1]. The development of green

economy boosts people’s demand for green products. However, information asymmetry prevents enterprises from clearly conveying the attributes of their products and consumers from accurately distinguishing the green products. The “profit-driven” producers of high carbon products tend to provide false information for the low production cost of high carbon products, seriously hindering the development of the green product market.

Information asymmetry refers to the different product information owned by both the buyer and the seller in the incomplete information market, which hinders the buyer from making right choices, thus affecting the transaction behavior and market efficiency [2]. Especially information asymmetry

in the green product market will lead to so many “mistakes” in consumers’ choice that they will buy so-called “green products” damaging their health, such as the fake “green pork” incident of Wal-Mart exposed in 2011. It is difficult for the green product market to be formed and fully developed as consumers cannot accurately identify the key information of green products; so, governments need to control, identify, and disclose the information of green products and standardize the development of the green product market.

In the process of formation and development of the green product market, governments, enterprises, and consumers interact with one another. Enterprises, the supplier of green products, lack the enthusiasm to produce green products because of their high production cost and large number of false green products in the market. Consumers, the demander of green products, lose confidence in the green product market for paying high prices for fake green products resulting from information asymmetry. As a result, governments should identify and disclose the information of green products as an authority, which will play a crucial role in the formation and development of the green product market.

In recent years, scholars have conducted indepth research on the behavior of relevant stakeholders in the green product market. Liu [2] used the mathematical model to study the impact of information asymmetry on the green product market based on the relationship between manufacturers and consumers. Yan and Yu [3] used the imperfect information dynamic game theory to study the process of price game between producers and consumers in the green product market. Sun and Yu [4] analyzed the role of government subsidies in the development of green products using the two-stage game model. Liu et al. [5] analyzed the impact of environmental regulation and government subsidies on the production of green products of enterprises using the panel threshold model. However, there are deficiencies in the above studies. For example, some scholars studied the behavior of producers and consumers in the market using game models, but they ignored the key role of governments in the development of the green product market; some scholars took into account the role of governments by analyzing the impact of government subsidies on the production of green products of enterprises, but they ignored the impact on consumers. Therefore, in this paper, an evolutionary game model involving governments, enterprises, and consumers was built to discuss the factors of formation and development of the green product market that influences the socially ideal stable state where governments chose the strategy of information symmetry, enterprises chose the strategy of producing green products, and consumers chose the strategy of purchasing green products, with a view to providing feasible suggestions for cultivating green products and developing green economy in China.

## 2. Hypothesis and Construction of the Three-Party Evolutionary Game Model

Evolutionary game theory is to study the evolutionary stable state (ESS) of game groups in a competitive environment of survival of the fittest based on the hypothesis of bounded

rational man [6, 7]. Referring to the game assumptions of Cheng et al. [8], Xu and Lv [9], and Yu and Hu [10], this paper built an evolutionary game model involving governments, enterprises, and consumers.

To cultivate green industries, develop green economy, and protect ecological environment, governments need to search, identify, and publicly verify the information of green products in the trading market. Their behavior strategy space was (information symmetry, information asymmetry), with the probability of  $(x, 1 - x)$ , respectively. “Information symmetry” means governments identify and publicly verify the information of green products, which can help enterprises clearly convey the attributes of green products, and consumers accurately distinguish the green products and punish the high carbon products. Enterprises gain reputation by producing green products that requires huge costs and faces many uncertainty risks, and their production strategy is greatly influenced by the depth and breadth of governments’ information disclosure and consumers’ strategy of purchasing green products. Their behavior strategy space was producing (green products, high carbon products), with the probability of  $(y, 1 - y)$ , respectively. Consumers choose the strategy according to the purchase cost of green products and their utility perception from purchasing green products. Their behavior strategy space was (purchasing, not purchasing) green products, with the probability of  $(z, 1 - z)$ , respectively. Conforming to the hypothesis of bounded rational man, the three-party game players constantly changed their own strategy in the game so that the three-party game finally evolved to an evolutionary stable state (ESS). A game tree model of behavior strategy spaces of the three-party game players was built, as shown in Figure 1.

When choosing the strategy of information symmetry, governments will pay a cost  $C_g$  for screening the information of enterprises’ products such as R & D and production, transportation and distribution, material procurement, and identifying the green products, get a fine  $F_e$  from illegal enterprises, and gain a benefit  $U_g$  from increased government credibility. When choosing the strategy of information asymmetry, governments will pay a cost  $F_g$  for being punished by higher authorities or losing credibility because of enterprises producing high carbon products.

When choosing the strategy of producing green products, enterprises will pay an additional cost  $C_e$  such as R & D cost and uncertainty cost for producing green products, gain a market return  $U_{e1}$  from producing green products, and get an additional benefit  $U_e$  from producing green products, such as improved enterprise reputation for gaining consumer recognition. When choosing the strategy of producing high carbon products, enterprises will gain a market return  $U_{e2}$  from producing high carbon products, also the cost of consumers for purchasing high carbon products, and pay a fine  $F_e$  for producing high carbon products under information symmetry.

When choosing the strategy of purchasing green products, consumers will pay a cost  $U_{e1}$ , get the utility perception  $U_c$  such as physical health and psychological satisfaction from purchasing green products, and gain an additional benefit  $U_{gc}$  from improved consumer confidence

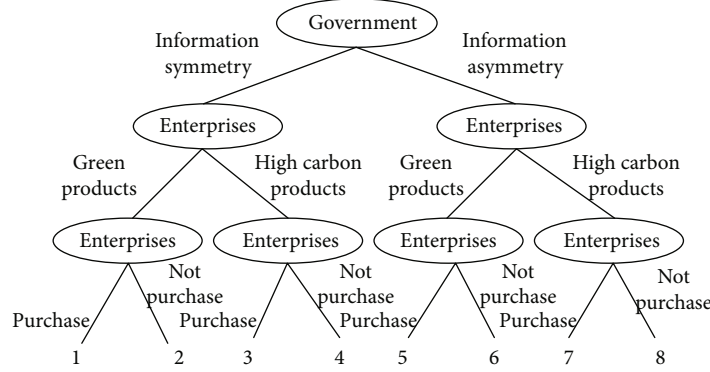


FIGURE 1: Game tree model of behavior strategy spaces of the three-party game players.

in the market products under information symmetry. Drawing on the views of Xu et al. [11], under the condition of information asymmetry, consumers are at a disadvantage and lack of understanding whether the purchased products are green products, which has hit consumers' purchase enthusiasm. If choosing green products, consumers can obtain the utility perception At the same time, pay a cost  $U_{e1}$ . When choosing the strategy of purchasing high carbon products, consumers will pay a cost  $U_{e2}$ , an additional cost  $C_c$  such as physical damage and psychological damage from purchasing high carbon products, and a negative impact  $C_{gc}$  such as environmental pollution from enterprises producing high-carbon products on consumers. The parameters of the three-party game players are shown in Table 1. According to the above assumptions and parameter settings, a payoff matrix of the three-party game players was obtained, as shown in Table 2.

### 3. Equilibrium Analysis of the Evolutionary Behaviors of the Three-Party Game Players

3.1. *Expected Benefits of the Three-Party Game Players.* According to Table 2, the expected benefits of the three-party game players were obtained:

Governments' expected benefit when choosing the strategy of "information symmetry," expected benefit when choosing the strategy of "information asymmetry," and average expected benefit were expressed as  $E_{g1}$ ,  $E_{g2}$ , and  $\bar{E}_g$ , respectively:

$$\begin{aligned}
 E_{g1} &= yz(U_g - C_g) + y(1-z)(U_g - C_g) \\
 &\quad + (1-y)z(U_g - C_g + F_e) \\
 &\quad + (1-y)(1-z)(U_g - C_g + F_e), \\
 E_{g2} &= (1-y)z(-F_g) + (1-y)(1-z)(-F_g), \\
 \bar{E}_g &= xE_{g1} + (1-x)E_{g2}. \tag{1}
 \end{aligned}$$

Enterprises' expected benefit when choosing the strategy of producing "green products," expected benefit when

choosing the strategy of producing "high carbon products," and average expected benefit were expressed as  $E_{e1}$ ,  $E_{e2}$ , and  $\bar{E}_e$ , respectively:

$$\begin{aligned}
 E_{e1} &= xz(U_{e1} + U_e - C_e) + x(1-z)(U_e - C_e) \\
 &\quad + (1-x)z(U_{e1} + U_e - C_e) \\
 &\quad + (1-z)(1-x)(U_e - C_e), \\
 E_{e2} &= xz(U_{e2} - F_e) + x(1-z)(-F_e) + (1-x)zU_{e2}, \\
 \bar{E}_e &= yE_{e1} + (1-y)E_{e2}. \tag{2}
 \end{aligned}$$

Consumers' expected benefit when choosing the strategy of "purchasing" green products, expected benefit when choosing the strategy of "not purchasing" green products, and average expected benefit were expressed as  $E_{c1}$ ,  $E_{c2}$ , and  $\bar{E}_c$ , respectively:

$$\begin{aligned}
 E_{c1} &= xy(U_c + U_{gc} - U_{e1}) \\
 &\quad + x(1-y)(U_{gc} - U_{e2} - C_c - C_{gc}) \\
 &\quad + (1-x)y(U_c - U_{e1}) \\
 &\quad + (1-x)(1-y)(-U_{e2} - C_c - C_{gc}), \\
 E_{c2} &= xyU_{gc} + x(1-y)(U_{gc} - C_{gc}) \\
 &\quad + (1-x)(1-y)(-C_{gc}), \\
 \bar{E}_c &= zE_{c1} + (1-z)E_{c2}. \tag{3}
 \end{aligned}$$

3.2. *Replicated Dynamic Analysis of the Three-Party Game Players*

(1) The replicated dynamic equation for governments to choose the strategy of information symmetry was

$$\begin{aligned}
 F(x) &= dx/dt = x(E_{g1} - \bar{E}_g) \\
 &= x(x-1)[y(F_g - F_e) - (F_g - F_e - C_g + U_g)]. \tag{4}
 \end{aligned}$$



TABLE 1: Parameters and their meanings of the three-party game players.

Parameters	Meanings
$C_g$	Cost of governments for screening the information of enterprises' products and identifying the green products under information symmetry
$U_g$	Benefit of governments from increased government credibility under information symmetry
$F_g$	Cost of governments for being punished by higher authorities or losing credibility because of enterprises producing high carbon products under information asymmetry
$C_e$	Additional cost of enterprises such as R & D cost and uncertainty cost for producing green products
$U_{e1}$	Market return of enterprises from producing green products, also the cost of consumers for purchasing green products
$U_e$	Additional benefit of enterprises from producing green products (such as improved enterprise reputation for gaining consumer recognition)
$U_{e2}$	Market return of enterprises from producing high carbon products, also the cost of consumers for purchasing high carbon products
$F_e$	Fine of enterprises for producing high carbon products under information symmetry
$U_c$	Utility perception (physical health, psychological satisfaction) of consumers from purchasing green products
$U_{gc}$	Additional benefit of consumers from improved consumer confidence in the market products under information symmetry
$C_c$	Additional cost (physical damage, psychological damage) of consumers from purchasing high carbon products
$C_{gc}$	Negative impact (environmental pollution) of enterprises producing high-carbon products on consumers

According to the stability theorem of replicated dynamic equation and a stable strategy,  $x$  should meet  $F(x) = 0$ , and  $F'(x) < 0$ .

If  $y = (F_g - F_e - C_g + U_g)/(F_g - F_e)$ , then  $F(x) \equiv 0$ ; that is, any strategy of governments was a stable strategy.

If  $y \neq (F_g - F_e - C_g + U_g)/(F_g - F_e)$ , set  $F(x) = 0$ , and then  $x = 0$  and  $x = 1$ , two quasievolutionary stability points, were obtained. The following equation was obtained by taking derivative of  $F(x)$ :

$$F'(x) = (2x - 1)[y(F_g - F_e) - (F_g - F_e - C_g + U_g)]. \quad (5)$$

If  $y > (F_g - F_e - C_g + U_g)/(F_g - F_e)$ , then  $(F'(x)|_{x=0}) < 0$  and  $(F'(x)|_{x=1}) > 0$ ; so,  $x = 0$  was a stable strategy; if  $y < (F_g - F_e - C_g + U_g)/(F_g - F_e)$ , then  $(F'(x)|_{x=0}) > 0$  and  $(F'(x)|_{x=1}) < 0$ ; so,  $x = 1$  was a stable strategy. This showed that the strategy selection of governments was closely related to that of enterprises. When the proportion of enterprises choosing the strategy of producing green products was higher than  $(F_g - F_e - C_g + U_g)/(F_g - F_e)$ , governments will choose the strategy of information asymmetry for effective use of social resources; when the proportion was lower than  $(F_g - F_e - C_g + U_g)/(F_g - F_e)$ , and governments will choose the strategy of information symmetry.

Figure 2 shows the strategy proportion  $x$  of governments was only related to that  $y$  of enterprises, but not to that  $z$  of consumers; that is, governments will not decide whether to choose the strategy of information symmetry based on consumers' willingness to purchase enterprises' products.

- (2) The replicated dynamic equation for enterprises to choose the strategy of producing green products was

$$F(y) = dy/dt = y(E_{e1} - \bar{E}_e) = y(1 - y)[z(U_{e1} - U_{e2}) - (C_e - xF_e - U_e)]. \quad (6)$$

If  $z = (C_e - xF_e - U_e)/(U_{e1} - U_{e2})$ , then  $F(y) \equiv 0$ ; that is, any strategy of enterprises was a stable strategy.

If  $z \neq (C_e - xF_e - U_e)/(U_{e1} - U_{e2})$ , set  $F(y) = 0$ , and then  $y = 0$  and  $y = 1$ , two quasievolutionary stability points, were obtained. The following equation was obtained by taking derivative of  $F(y)$ :

$$F'(y) = (1 - 2y)[z(U_{e1} - U_{e2}) - (C_e - xF_e - U_e)]. \quad (7)$$

With  $U_{e1} > U_{e2}$ , that is, enterprises can obtain higher benefit from producing green products, and  $C_e - U_e$  considered as the actual production cost of enterprises for green products, there were two different situations:

If  $xF_e > C_e - U_e$  or  $z(U_{e1} - U_{e2}) > (C_e - U_e)$ , then  $(F'(y)|_{y=0}) > 0$ ,  $(F'(y)|_{y=1}) < 0$ ,  $y = 1$ , was a stable strategy. This showed that if the fine of enterprises for producing high carbon products was higher than the actual production cost of enterprises for green products, enterprises will choose the strategy of producing green products.

If the above conditions were not met, there were two situations: if  $z > (C_e - xF_e - U_e)/(U_{e1} - U_{e2})$ , then  $(F'(y)|_{y=0}) > 0$ ,  $(F'(y)|_{y=1}) < 0$ ; so,  $y = 1$  was a stable strategy; that is, enterprises will choose the strategy of producing green products; if  $z < (C_e - xF_e - U_e)/(U_{e1} - U_{e2})$ , then  $(F'(y)|_{y=0}) > 0$ ,  $(F'(y)|_{y=1}) < 0$ ,  $y = 0$ , was a stable strategy; that is, enterprises will choose the strategy of producing high carbon products. This showed the strategy selection of enterprises was related to that of both governments and consumers.

TABLE 2: Payoff matrix of the three-party game players.

Game players		Consumers							
		Purchasing		Not purchasing					
Governments	Information symmetry	Enterprises	Green product	$U_g - C_g$	$U_{e1} + U_e - C_e$	$U_c + U_{gc} - U_{e1}$	$U_g - C_g$	$U_e - C_e$	$U_{gc}$
		Enterprises	High carbon products	$U_g - C_g + F_e$	$U_{e2} - F_e$	$U_{gc} - U_{e2} - C_c - C_{gc}$	$U_g - C_g + F_e$	$-F_e$	$U_{gc} - C_{gc}$
	Information asymmetry	Enterprises	Green product	0	$U_{e1} + U_e - C_e$	$U_c - U_{e1}$	0	$U_e - C_e$	0
		Enterprises	High carbon products	$-F_g$	$U_{e2}$	$-U_{e2} - C_c - C_{gc}$	$-F_g$	0	$-C_{gc}$

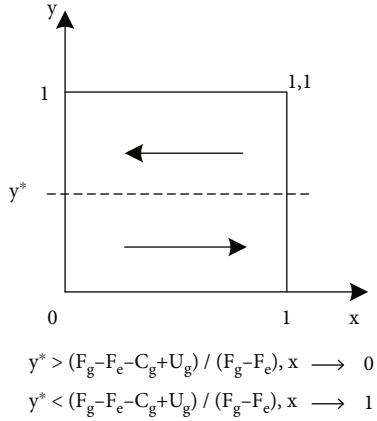


FIGURE 2: Schematic diagram of the dynamic evolution of governments' strategy.

Figure 2 shows the strategy proportion  $x$  of governments was only related to that  $y$  of enterprises, but not to that  $z$  of consumers,  $t$ .

Figure 3 shows the strategy proportion  $y$  of enterprises was related to both  $x$  of governments and  $z$  of consumers. In other words, the factors affecting enterprises' strategy were complex and multifaceted, which further showed the interaction among governments, enterprises, and consumers should be comprehensively taken into account in the formation and development of the green product market.

- (3) The replicated dynamic equation for consumers to choose the strategy of purchasing green products was

$$F(z) = dz/dt = z(E_{c1} - \bar{E}_c) = z(1-z)[y(U_c - U_{e1} + U_{e2} + C_c) - (U_{e2} + C_c)]. \quad (8)$$

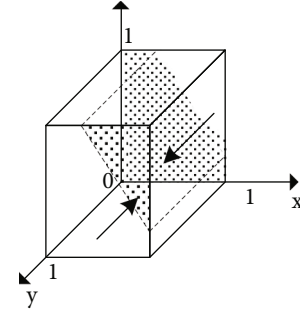
If  $y = (U_{e2} + C_c)/(U_c - U_{e1} + U_{e2} + C_c)$ , then  $F(z) \equiv 0$ ; that is, any strategy of consumers was a stable strategy.

If  $y \neq (U_{e2} + C_c)/(U_c - U_{e1} + U_{e2} + C_c)$ , set  $F(z) = 0$ , and then  $z = 0$  and  $z = 1$ , two quasievolutionary stability points, were obtained. The following equation was obtained by taking derivative of  $F(z)$ :

$$F'(z) = (1-2z)[y(U_c - U_{e1} + U_{e2} + C_c) - (U_{e2} + C_c)]. \quad (9)$$

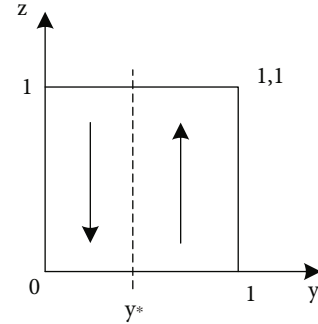
With  $U_{e2} + C_c > 0$ ,  $(U_c - U_{e1} + U_{e2} + C_c) = [U_c - (U_{e1} - U_{e2} - C_c)]$ , considered as the difference between the utility perception of consumers from purchasing green products and the additional cost, there were two different situations:

If  $[U_c - (U_{e1} - U_{e2} - C_c)] < 0$  and  $y(U_c - U_{e1} + U_{e2} + C_c) - (U_{e2} + C_c) < 0$ , then  $(F'(z)|_{z=0}) < 0$ ,  $(F'(z)|_{z=1}) > 0$ ; so,  $z = 0$  was a stable strategy. This showed if the utility perception of consumers from purchasing green products was lower than the additional cost, consumers will choose the strategy of not purchasing green products.



$z > (C_e - xF_e - U_e) / (U_{e1} - U_{e2}), y \rightarrow 1$   
 $z < (C_e - xF_e - U_e) / (U_{e1} - U_{e2}), y \rightarrow 0$

FIGURE 3: Schematic diagram of the dynamic evolution of enterprises' strategy



$[U_c - (U_{e1} - U_{e2} - C_c)] > 0$  and  $y^* > \frac{U_{e2} + C_c}{(U_c - U_{e1} + U_{e2} + C_c)} z \rightarrow 1$   
 $[U_c - (U_{e1} - U_{e2} - C_c)] > 0$  and  $y^* < \frac{U_{e2} + C_c}{(U_c - U_{e1} + U_{e2} + C_c)} z \rightarrow 0$

FIGURE 4: Schematic diagram of the dynamic evolution of consumers' strategy.

If  $[U_c - (U_{e1} - U_{e2} - C_c)] > 0$  and  $y > (U_{e2} + C_c)/(U_c - U_{e1} + U_{e2} + C_c)$ , then  $(F'(z)|_{z=0}) > 0$ ,  $(F'(z)|_{z=1}) < 0$ ; so,  $z = 1$ ; that is, purchasing green products was a stable strategy; if  $[U_c - (U_{e1} - U_{e2} - C_c)] > 0$  and  $y < (U_{e2} + C_c)/(U_c - U_{e1} + U_{e2} + C_c)$ , then  $(F'(z)|_{z=0}) < 0$ ,  $(F'(z)|_{z=1}) > 0$ ; so,  $z = 0$ ; that is, not purchasing green products was a stable strategy. It indicated when the utility perception of consumers from purchasing green products was large enough, the behavior strategy of consumers will depend on the probability of enterprises choosing to produce green products, that is, whether it was higher than  $(U_{e2} + C_c)/(U_c - U_{e1} + U_{e2} + C_c)$ .

Figure 4 shows the strategy proportion  $z$  of consumers was only related to that  $y$  of enterprises, but not to that  $x$  of governments.

**3.3. Evolutionary Stability Analysis of the Three-Party Game.** According to the evolutionary stability analysis of Friedman [6], the evolutionary stable strategy of the three-party game players can be judged by  $\text{Det}J > 0$  and  $\text{Tr}J < 0$ . The Jacobian matrix was obtained by taking partial derivatives of (4), (6), and (8) about  $x$ ,  $y$ , and  $z$ , respectively:

$$J = \begin{bmatrix} \frac{\partial F(x)}{\partial x} & \frac{\partial F(x)}{\partial y} & \frac{\partial F(x)}{\partial z} \\ \frac{\partial F(y)}{\partial x} & \frac{\partial F(y)}{\partial y} & \frac{\partial F(y)}{\partial z} \\ \frac{\partial F(z)}{\partial x} & \frac{\partial F(z)}{\partial y} & \frac{\partial F(z)}{\partial z} \end{bmatrix} = \begin{bmatrix} J_{11} & J_{12} & J_{13} \\ J_{21} & J_{22} & J_{23} \\ J_{31} & J_{32} & J_{33} \end{bmatrix}, \quad (10)$$

where

$$\begin{aligned} J_{11} &= (2x-1)[y(F_g - F_e) - (F_g - F_e - C_g + U_g)], \\ J_{12} &= x(x-1)(F_g - F_e), \\ J_{13} &= 0, \\ J_{21} &= 0, \\ J_{22} &= (1-2y)[z(U_{e1} - U_{e2}) - (C_e - xF_e - U_e)], \\ J_{23} &= y(1-y)(U_{e1} - U_{e2}), \\ J_{31} &= 0, \\ J_{32} &= z(1-z)(U_c - U_{e1} + U_{e2} + C_c), \\ J_{33} &= (1-2z)[y(U_c - U_{e1} + U_{e2} + C_c) - (U_{e2} + C_c)], \end{aligned} \quad (11)$$

so that

$$\begin{aligned} DetJ &= (2x-1)[y(F_g - F_e)(F_g - F_e - C_g + U_g)] \\ &\quad \cdot \{(1-2y)[z(U_{e1} - U_{e2}) - (C_e - xF_e - U_e)] \\ &\quad \cdot (1-2z)[y(U_c - U_{e1} + U_{e2} + C_c) - (U_{e2} + C_c)] \\ &\quad - z(1-z)(U_c - U_{e1} + U_{e2} + C_c)y(1-y)(U_{e1} - U_{e2})\}, \\ TrJ &= (2x-1)[y(F_g - F_e) - (F_g - F_e - C_g + U_g)] \\ &\quad \cdot (1-2y)[z(U_{e1} - U_{e2}) - (C_e - xF_e - U_e)] \\ &\quad \cdot (1-2z)[y(U_c - U_{e1} + U_{e2} + C_c) - (U_{e2} + C_c)]. \end{aligned} \quad (12)$$

The evolutionary stability of the three-party game system is shown in Table 3.

## 4. Model Simulation and Sensitivity Analysis

**4.1. Case Simulation.** This paper is aimed at promoting the evolution of the three-party game to an ideal stable state. According to Equations (4), (6), (8), and Table 3,  $U_g > C_g$  can make  $x$  show a trend of monotonic increasing and evolving to  $x \rightarrow 1$ . Thus, the evolutionary conditions can be maintained by limiting the initial threshold of  $x$ , making the three-party game evolve to (1,1,1). If  $x = 0.4$ , that is, the superior government required 40% of governments in the region to choose the strategy of information symmetry as the lower limit, the three-party game will eventually evolve to a socially ideal stable state, as shown in Table 4.

Because the python scientific computing library SciPy has a more convenient 3D drawing toolkit and computing ecology, numerical experiments and simulation were performed using SciPy, a scientific computing library of Python, to verify the above inferences. If the initial parameter setting met  $U_g > C_g$ ,  $xF_e > [(C_e - U_e) - (U_{e1} - U_{e2})]$ , and  $U_c > U_{e1}$ , then the game may eventually evolve to a socially ideal stable state where all the three parties chose an active strategy. So, the following initial values were set:  $F_g = 70$ ,  $F_e = 60$ ,  $C_g = 40$ ,  $U_g = 80$ ,  $C_e = 70$ ,  $U_e = 65$ ,  $U_{e1} = 100$ ,  $U_{e2} = 40$ ,  $C_c = 40$ , and  $U_c = 200$ . This paper verified the strategy selection of the three-party game players under the premise that the lower limit of proportion of governments choosing the strategy of information symmetry was  $x = 0.4$ . In Figure 5, the initial values  $x = 0.4$ ,  $y = 0.6$ , and  $z = 0.7$ , and  $x = 0.5$ ,  $y = 0.5$ , and  $z = 0.3$  were taken for an example, respectively. The simulation results showed the three-party game eventually evolved to a socially ideal stable state of (1, 1, 1), verifying the inference.

Evolutionary results are as follows:  $x \rightarrow 1$ ,  $y \rightarrow 1$ , and  $z \rightarrow 1$ .

Restrictive conditions are as follows:  $U_g > C_g$ ,  $xF_e > [(C_e - U_e) - (U_{e1} - U_{e2})]$ , and  $U_c > U_{e1}$ .

Figure 5 shows under information symmetry, when the benefit of governments from increased government credibility was higher than the cost of governments for screening the information of enterprises' products and identifying the green products  $U_g > C_g$ , the expected fine of enterprises for producing high carbon products was higher than the difference between the actual cost increment and the actual income increment of enterprises for producing green products  $xF_e > [(C_e - U_e) - (U_{e1} - U_{e2})]$ , and the utility perception of consumers from table purchasing green products was higher than the cost of consumers for purchasing green products  $U_c > U_{e1}$ , the three-party game would evolve to a socially ideal stable state where governments chose the strategy of information symmetry, enterprises chose the strategy of producing green products, and consumers chose the strategy of purchasing green products.

**4.2. Sensitivity Analysis.** In order to explore the influence of different parameters on the formation and healthy development of the green product market, this paper analyzed the sensitivity of some parameters to study the influence of change in restrictive conditions on the evolution trajectory of the three-party game players.

Situation 1: set  $C_g = 65$  and  $U_g = 60$ , and parameter setting met the evolution conditions of  $U_g < C_g$ ,  $xF_e > [(C_e - U_e) - (U_{e1} - U_{e2})]$ , and  $U_c > U_{e1}$ . In Figure 6, the three-party game eventually evolved to a stable state of (0, 1, 1), verifying the inference.

Evolutionary results are as follows:  $x \rightarrow 0$ ,  $y \rightarrow 1$ , and  $z \rightarrow 1$ .

Restrictive conditions are as follows:  $U_g < C_g$ ,  $xF_e > [(C_e - U_e) - (U_{e1} - U_{e2})]$ , and  $U_c > U_{e1}$ . Figure 6 shows when parameter conditions changed, that is, when the benefit of governments from increased government credibility was lower than the cost of governments for screening the information of enterprises' products and identifying the green

TABLE 3: Local stability analysis of the equilibrium points.

Equilibrium points	DetJ	TrJ
(0, 0, 0)	$-(U_{e2} + C_c)(U_e - C_e)(F_g - F_e - C_g + U_g)$	$-(U_{e2} + C_c) + (U_e - C_e) + (F_g - F_e - C_g + U_g)$
(0, 0, 1)	$(U_{e2} + C_c)(U_e - C_e + U_{e1} - U_{e2})(F_g - F_e - C_g + U_g)$	$C_c + (U_e - C_e + U_{e1}) + (F_g - F_e - C_g + U_g)$
(0, 1, 0)	$-(C_e - U_e)(C_g - U_g)(U_c - U_{e1})$	$(C_e - U_e) - (C_g - U_g) + (U_c - U_{e1})$
(0, 1, 1)	$-(C_g - U_g)(U_c - U_{e1})(U_e - C_e + U_{e1} - U_{e2})$	$-(C_g - U_g) - U_c - (U_e - C_e - U_{e2})$
(1, 0, 0)	$-(U_{e2} + C_c)(C_e - F_e - U_e)(F_g - F_e - C_g + U_g)$	$-(U_{e2} + C_c) - (C_e - F_e - U_e) - (F_g - F_e - C_g + U_g)$
(1, 0, 1)	$(U_{e2} + C_c)(C_e - F_e - U_e - U_{e1} + U_{e2})(F_g - F_e - C_g + U_g)$	$C_c - (C_e - F_e - U_e - U_{e1}) - (F_g - F_e - C_g + U_g)$
(1, 1, 0)	$-(C_g - U_g)(U_c - U_{e1})(F_e + U_e - C_e)$	$(C_g - U_g) + (U_c - U_{e1}) - (F_e + U_e - C_e)$
(1, 1, 1)	$(C_g - U_g)(U_c - U_{e1})(C_e - F_e - U_e - U_{e1} + U_{e2})$	$(C_g - U_g) - U_c + (C_e - F_e - U_e + U_{e2})$

TABLE 4: Socially ideal stable state of the three-party game model for enterprises' green product innovation.

Strategy behaviors of game players	Parameter conditions	Trends of probability change
Governments choosing the strategy of information symmetry	$U_g > C_g$	$x \rightarrow 1$
Enterprises choosing the strategy of producing green products	$x F_e > [(C_e - U_e) - (U_{e1} - U_{e2})]$	$y \rightarrow 1$
Consumers choosing the strategy of purchasing green products	$U_c > U_{e1}$	$z \rightarrow 1$

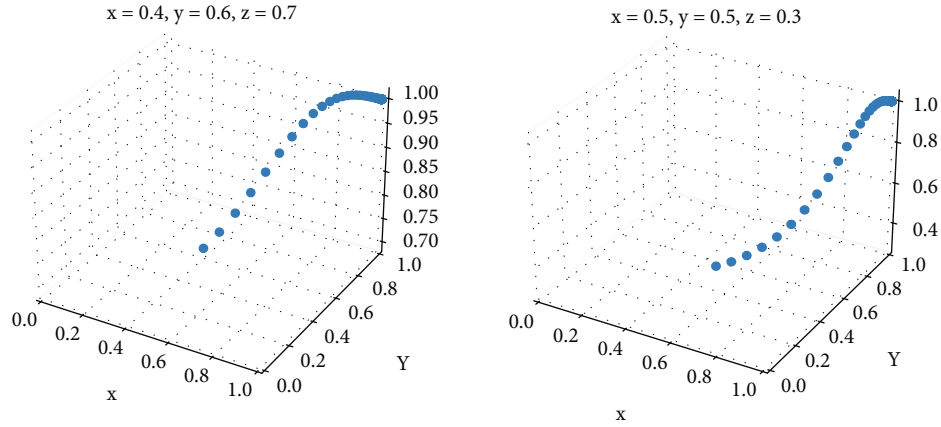


FIGURE 5: Evolutionary path diagram of the three-party game system.

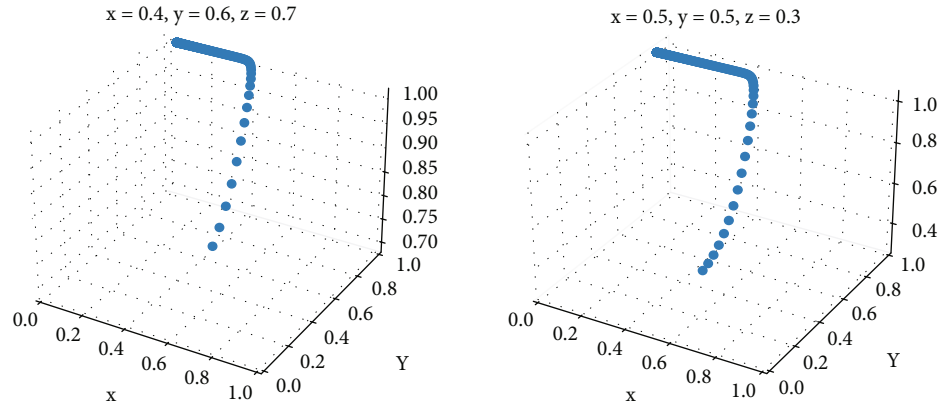


FIGURE 6: Evolutionary path diagram of the three-party game system.



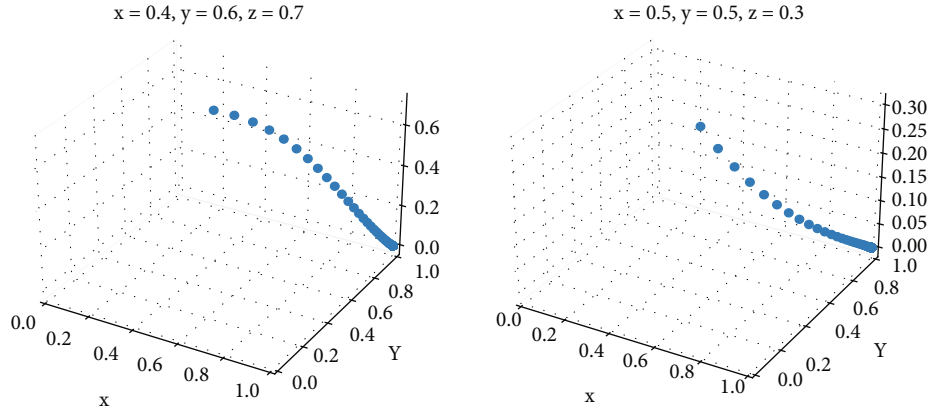


FIGURE 7: Evolutionary path diagram of the three-party game system.

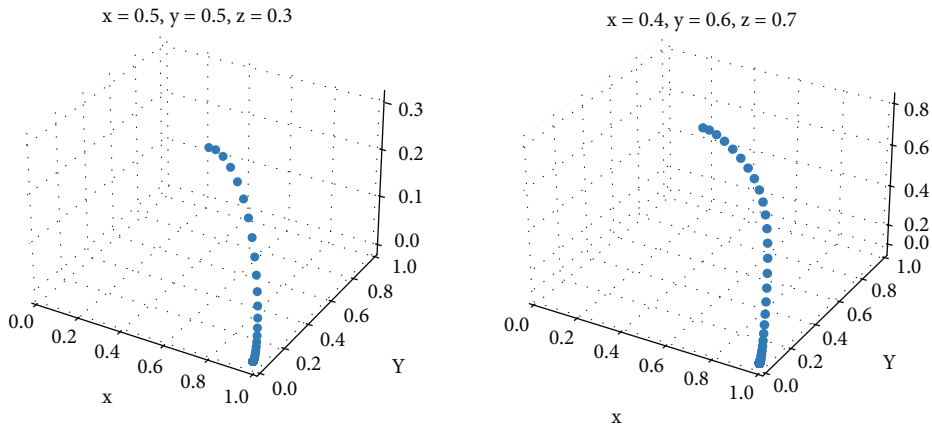


FIGURE 8: Evolutionary path diagram of the three-party game system.

products  $U_g < C_g$ , the expected fine of enterprises for producing high carbon products was higher than the difference between the actual cost increment and the actual income increment of enterprises for producing green products  $x F_e > [(C_e - U_e) - (U_{e1} - U_{e2})]$ , and the utility perception of consumers from purchasing green products was higher than the cost of consumers for purchasing green products  $U_c > U_{e1}$ , the three-party game would evolve to a stable state where governments chose the strategy of information asymmetry, enterprises chose the strategy of producing green products, and consumers chose the strategy of purchasing green products.

Situation 2: set  $U_{e1} = 150$ ,  $U_c = 100$ , and parameter setting met the evolution conditions of  $U_g > C_g$ ,  $x F_e > [(C_e - U_e) - (U_{e1} - U_{e2})]$ , and  $U_c < U_{e1}$ . In Figure 7, the three-party game eventually evolved to a stable state of (1, 1, 0), verifying the inference.

Evolutionary results are as follows:  $x \rightarrow 1$ ,  $y \rightarrow 1$ , and  $z \rightarrow 0$ .

Restrictive conditions are as follows:  $U_g > C_g$ ,  $x F_e > [(C_e - U_e) - (U_{e1} - U_{e2})]$ , and  $U_c < U_{e1}$ .

Figure 7 shows when parameter conditions changed, that is, when the benefit of governments from increased govern-

ment credibility was higher than the cost of governments for screening the information of enterprises' products and identifying the green products  $U_g > C_g$ , the expected fine of enterprises for producing high carbon products was higher than the difference between the actual cost increment and the actual income increment of enterprises for producing green products  $x F_e > [(C_e - U_e) - (U_{e1} - U_{e2})]$ , the utility perception of consumers from purchasing green products was lower than the cost of consumers for purchasing green products  $U_c < U_{e1}$ , the three-party game would evolve to a stable state where governments chose the strategy of information symmetry, enterprises chose the strategy of producing green products, and consumers chose the strategy of not purchasing green products. This also showed consumers pay more attention to the gains and losses of their own interests than green consumption in the spotlight when choosing to purchase green products, and consumers with higher green value perception are more willing to purchase green products.

Situation 3: set  $F_e = 20$ ,  $C_e = 100$ ,  $U_e = 30$ ,  $U_{e1} = 60$ , and  $U_{e2} = 50$ , and parameter setting met the evolution conditions of  $U_g > C_g$ ,  $x F_e < [(C_e - U_e) - (U_{e1} - U_{e2})]$ , and  $U_c > U_{e1}$ . In Figure 8, the three-party game eventually evolved to a stable state of (1, 0, 0), verifying the inference.

Evolutionary results are as follows:  $x \rightarrow 1$ ,  $y \rightarrow 0$ , and  $z \rightarrow 0$ .

Restrictive conditions are as follows:  $U_g > C_g$ ,  $x F_e < [(C_e - U_e) - (U_{e1} - U_{e2})]$ , and  $U_c > U_{e1}$ .

Figure 8 shows when parameter conditions changed, that is, when the expected fine of enterprises for producing high carbon products was lower than the difference between the actual cost increment and the actual income increment of enterprises for producing green products  $x F_e < [(C_e - U_e) - (U_{e1} - U_{e2})]$ , no matter whether the utility perception of consumers from purchasing green products was higher than the cost of consumers for purchasing green products, consumers will chose the strategy of not purchasing green products, suggesting a long-term production of high carbon products by enterprises is unrealistic.

## 5. Conclusions and Suggestions

In view of the difficulties in the formation and healthy development of Chinese green product market, in this paper, an evolutionary game model involving governments, enterprises, and consumers was built. And numerical experiments and simulation were performed. The research results showed the relation between the governments' benefit from increased government credibility and the cost of governments for screening the information of enterprises' products and identifying the green products, between the expected fine of enterprises for producing high carbon products and the difference between the actual cost increment and the actual income increment of enterprises for producing green products, as well as the gains and losses of consumers from purchasing green products played a decisive role in the healthy development of the green product market. The above conclusions provide useful policy suggestions for governments to vigorously develop the green product market. In order to promote the healthy development of Chinese green product market, the following suggestions were drawn:

- (1) Take measures to reduce the cost of governments for identifying the green products. Through extensive participation of all kinds of nongovernmental organizations such as the public and media in supervising the production process of green products of enterprises, establish and improve the mechanisms of industry collection, information disclosure, and social supervision and reduce the identification and certification fees of governments. Through the indepth cooperation among governments, industries, universities, and research institutes, establish a unified green product information platform for use and collection by the whole society
- (2) Strengthen policy support for the R & D and production, transportation and distribution, consumption, and procurement of green products of enterprises, increase subsidies for green manufacturing, and green procurement to effectively reduce the burden of enterprises producing green products. Strictly implement the main responsibility of producers for

product quality, establish a joint punishment mechanism for those who are serious trust breaking, and establish a blacklist system for enterprises violating laws and regulations

- (3) Vigorously carry out the public welfare publicity of green products through the media, network and social publicity, spread the theory of green development, guide the green lifestyle, and improve the utility perception of consumers from purchasing green products. Affect consumers' negative attitude towards environmental crisis by truly reporting the harm of production of high carbon products. Reduce the purchase cost of green products through various means (such as guidance and support) and popularize the green consumption pattern

## Data Availability

The datasets used and/or analyzed during the current study are available from the corresponding author on reasonable request.

## Conflicts of Interest

It is declared by the author that this article is free of conflict of interest.

## Acknowledgments

This study was supported by the Science and Technology Project of the Education Department of Jiangxi Province "Research on the Improvement of Absorption Capacity of Latecomer Enterprises from the Perspective of Global-Local Innovation Network" (GJJ209201), Humanities and Social Science Project of Universities in Jiangxi Province "Influence and Action Mechanism of Innovative Network Technology Diversification on Enterprise Innovation under the Background of High-quality Development" (GL20155), Preferential Funding of Postdoctoral Research Projects in Jiangxi Province "Double Embedding of Knowledge Network and Enterprise Transformation and Upgrading" (2019KY37), and Daily Funding for Postdoctoral Researchers in Jiangxi Province "Cross-border Search, Absorption Capacity and Innovation Performance Research of Technological Small and Medium-sized Enterprises" (2018RC28).

## References

- [1] G. H. Ma and J. L. Xia, "Analysis on the multi-subject evolutionary game of green product technology innovation under the background of environmental regulation," *Ecological Economy*, vol. 36, no. 5, pp. 50–56, 2020.
- [2] G. L. Liu, "Impact of information asymmetry on the green product market—research based on relation between manufacturers and consumers," *Journal of Shanxi University of Finance and Economics*, vol. 29, no. 8, pp. 68–72, 2007.
- [3] Y. Yan and J. Yu, "Role of consumer organizations in preventing the risk of reverse selection in the green product market—

- analysis based on bivalent game model,” *Consumer Economics*, vol. 29, no. 3, pp. 43–45, 2013.
- [4] D. Sun and Y. M. Yu, “Determination of the optimal government subsidy policy in the green product market,” *Chinese Journal of Management*, vol. 15, no. 1, pp. 118–126, 2018.
- [5] J. R. Liu, X. F. Zeng, and Q. Zeng, “Impact of environmental regulation and government innovation subsidy on the green product innovation of enterprises,” *Research on Economics and Management*, vol. 40, no. 6, pp. 106–118, 2019.
- [6] D. Friedman, “Evolutionary games in economics,” *Econometrica*, vol. 59, no. 3, pp. 637–666, 1991.
- [7] D. K. Levine and W. Pesendorfer, “The evolution of cooperation through imitation,” *Games and Economic Behavior*, vol. 58, no. 2, pp. 293–315, 2007.
- [8] M. Cheng, Y. Q. Liu, and H. Q. Wang, “Analysis of the three-party evolutionary game of the PPP projects of NIMBY facility based on system dynamics,” *Operations Research and Management Science*, vol. 28, no. 10, pp. 39–49, 2019.
- [9] J. Z. Xu and X. C. Lv, “Research on the strategic behavior evolution of the government, manufacturing enterprises and consumer groups under the low-carbon economy,” *Operations Research and Management Science*, vol. 23, no. 6, pp. 81–91, 2014.
- [10] J. R. Yu and D. L. Hu, “Study on the improvement strategy of brand authenticity under the three-party game scenario,” *Journal of Business Economics*, vol. 10, pp. 20–29, 2019.
- [11] W. C. Xu, J. H. Xue, and Y. J. Miao, “Asymmetric information and organic food consumption behavior,” *Journal of Central University of Finance and Economics*, vol. 3, pp. 59–67, 2017.

## Research Article

# Research on the Application of Internet of Things and VR Technology in the Protection and Development of Shouzhou Kiln

Xuelian Yu <sup>1,2</sup> and Yajun Zhang <sup>2,3</sup>

<sup>1</sup>Graduate School, University of Perpetual Help System DALTA, Philippines

<sup>2</sup>School of Art, Anhui University of Finance and Economics, Bengbu, China

<sup>3</sup>Faculty of Design and Architecture, University Putra Malaysia, Malaysia

Correspondence should be addressed to Yajun Zhang; [120081521@aufe.edu.cn](mailto:120081521@aufe.edu.cn)

Received 30 September 2021; Accepted 3 November 2021; Published 18 November 2021

Academic Editor: Deepak Gupta

Copyright © 2021 Xuelian Yu and Yajun Zhang. This is an open access article distributed under the Creative Commons Attribution License, which permits unrestricted use, distribution, and reproduction in any medium, provided the original work is properly cited.

The Internet of things (IoT) has changed the information transmission mode of people, things, and services. The new functional experience will bring users an efficient, convenient, and safe lifestyle. Virtual reality (VR) technology, also known as spiritual environment technology, is a new stage of the development of computer and information technology. It is an important auxiliary tool in the fields of R & D, production, education, and so on. As one of the six most famous kilns in the Tang Dynasty (618–907 BC), Shouzhou kiln plays an important role in the history of ceramics in China and even in the world. However, due to the long history, incomplete site preservation, fragile ceramic materials, and lack of effective promotion and publicity, it has been difficult to make a breakthrough in the protection and development of Shouzhou kiln. VR technology makes comprehensive use of computer software and hardware, breaks the barrier between virtual and reality, and provides a new idea for the protection and development of Shouzhou kiln. On the basis of fully combing the principle of VR technology and analyzing the application possibility of VR technology, firstly, focusing on the history and from the perspective of archaeological research of Shouzhou kiln, this paper discusses how to use VR technology to realize the restoration of ancient kiln sites, ancient ceramics, ancient ceramics technology, and relevant data preservation of Shouzhou kiln. Secondly, focusing on the present, this paper discusses the application of VR technology and Internet of things technology in Shouzhou kiln ceramic product design, Shouzhou kiln process technology improvement, Shouzhou kiln ceramic product display, and Shouzhou kiln marketing. Finally, focusing on the future, this paper discusses the application prospect of VR technology in the inheritance of Shouzhou kiln technology and the promotion of Shouzhou kiln ceramic culture. It is expected to explore feasible paths and methods for the protection, inheritance, and development of ancient ceramic culture in China and even the world through the discussion of VR technology involved in the protection and development of Shouzhou kiln.

## 1. Introduction

The Internet of things (IoT) is realized and developed on the basis of the Internet, telecommunication network, and radio and television network. It is an extension and expansion on the basis of three networks. User application terminals have expanded from information interaction and communication between people to communication and connection between people and things, things and things, and things and people. Therefore, the Internet of things technology can make objects more intelligent. It has increasingly become a new

point of technological innovation and economic growth. Many American colleges and universities, such as the University of California, Berkeley, Massachusetts Institute of Technology, and Auburn University, and well known enterprises such as, IBM, Crossbow Technology, have put forward relevant solutions for the Internet of things technology. The U.S. government policies to encourage the development of the Internet of things technology are mainly reflected in energy, broadband, and healthcare three areas of medical treatment. In August 2009, the Japanese government upgraded the “U-Japan” plan to the “I-Japan” strategy 2004,

which is committed to building an intelligent Internet of things service system. Meanwhile, countries such as Australia, Singapore, South Korea, France, Germany, and Australia are also stepping up the deployment of the Internet of things technology. Many countries are gradually promoting construction of the next-generation ubiquitous network infrastructure.

Virtual reality technology is a new stage in the development of computer and information technology. It refers to “in the computer software and hardware, various sensors, graphics and image generation systems, as well as special clothing, three-dimensional environment with certain audio-visual touch and smell, users can communicate with this computer-generated virtual reality in a concise and natural way with the support of these software and hardware equipment” interact with objects in the real world. It is the result of the comprehensive integration of modern high-performance computer system, artificial intelligence, computer graphics, man-machine interface, three-dimensional image, three-dimensional sound, measurement control, simulation, and other technologies. The purpose is to establish a more harmonious artificial environment [1].

In the 1960s and 1970s, VR technology was in the brewing stage of ideas, concepts, and technologies. In 1965, Dr. Suther [2], an important founder of computer graphics, published a short article “the ultimate display”, describing a new display technology. Users were directly immersed in the virtual environment controlled by computers. At the same time, users can also interact with objects in the virtual environment. In the 1980s, with the development of personal computer technology and computer network, the development of VR technology accelerated. During this period, the VR system with practical value appeared and a relatively complete reality simulation was realized through a VR helmet. In 1987, Foley published “interfaces for advanced computing” in *Scientific American* magazine. The magazine also published articles on data gloves, which attracted people’s attention. In 1989, Lanier, the founder of the American VPL company, first proposed the word “virtual reality,” which became a special name in this field of science and technology. After the 1990s, with the breakthrough and rapid development of computer technology and high-performance computing, computer network and communication, human-computer interaction equipment, and other scientific and technological fields, as well as the huge demand in application fields, VR technology has entered a period of rapid development. In 1993, Heim [3] proposed that “VR is an event or entity in effect rather than in fact” and described the seven characteristics of VR: simulation, interaction, artificial reality, immersion, telepresence, whole-body immersion, and network communication. In 1994, Burdea et al. [4] published “Virtual Reality Technology,” in which they summarized the basic characteristics of VR with 3I (immersion, interaction, and imagination). The software platform and modeling language for VR system development are developed. Quantum 3D developed open GVS in 1989 and sensors launched WTK in 1992. VRML was first proposed at the first WWW conference held in Geneva in March 1994, and the formulation of relevant international standards began. In 2005, ITU formally

defined the concept of the “Internet of things” at the World Summit on the Information Society (WSIS) held in Tunis and then issued “ITU Internet Reports 2005—the Internet Things,” which introduced the characteristics, related technologies, challenges, and future market opportunities of the Internet of things, pointing out the direction for the rapid development of the Internet of things. The Internet of things enables us to obtain a new communication dimension in the world of information and communication technology, and also enables the virtual world of VR technology to finally become a reality.

China’s research on VR technology began in the 1970s, when it was mainly concentrated in the field of aerospace. In the early 1990s, some Chinese universities and scientific research institutes began to study VR from different angles. In 1996, Chengcheng et al. of Tsinghua University and other three people published China’s first book on VR, “The Theory, Implementation and Application of Spiritual Environment (Virtual Reality) Technology” [5]. In the same year, Qiping and others published the overview of VR research [6]. The ministry of science and technology of the People’s Republic of China and the National Natural Science Foundation of China began to give key grants to the research in the field of VR. The national “863” plan identified the “distributed virtual environment” as a key project in 1996 and implemented the DVENET plan. With the maturity of China’s technology and theory in the field of VR, after 2010, its discussion scope has rapidly expanded to the fields of ancient ceramic protection, ceramic product design, and ceramic culture inheritance in China. In 2012, Cheng and others proposed VR-based modeling and reverse restoration technology of ancient ceramic relics. In 2014, Hu analyzed the feasibility of VR technology to support ancient ceramic cultural relics. Taking Jingdezhen ancient kiln as an example, this paper discusses the use of VR technology to display ancient ceramic sites, so as to promote the inheritance and dissemination of the ceramic culture [7]. In terms of ceramic product design and technology, He discussed the role of virtual reality in the traditional nonrelic firing technology of Jun porcelain in his paper “Innovative Exploration of VR Ceramic Firing Simulation Technology” in 2019. In 2021, Wang summarized the value of VR interactive technology in ceramic cultural and creative product design in his paper.

## **2. Application of VR Technology in Ancient Ceramic Restoration, Ancient Kiln Site Restoration, and Related Data Preservation of Shouzhou Kiln**

In terms of cultural heritage protection at home and abroad, with the help of VR technology and digital synthetic image and other technical frameworks, the cultural heritage and sites are digitally copied and simulated and the simulated reproduction of cultural relics is realized by digital means. The core of virtual reality technology is modeling and simulation. Digital technology is used to effectively preserve cultural relics, realize the three-dimensional or model establishment of data, and scientifically, effectively, accurately,



and permanently preserve endangered cultural relics. [8] Using VR technology for restoration and reproduction can shorten the restoration period of Shouzhou kiln cultural relics, establish an online virtual museum through computer network, and provide the public with novel and intuitive Shouzhou kiln cultural relic resources. In addition to the above points, the role of VR technology in Shouzhou kiln archaeology is also reflected in the sensory impact. If VR technology can be applied during the exhibition of ancient ceramic relics of Shouzhou kiln, the exhibition environment of ancient ceramic relics will become more open and intuitive. In this way, it can be ensured that after the ancient ceramic relics of Shouzhou kiln are displayed by using VR technology, visitors can more clearly and intuitively contact the relics and feel the strong impact of different aspects such as vision and perception.

In terms of specific application, VR reverse engineering technology can be used to restore the fragments of ceramic relics of Shouzhou kiln and the Shouzhou kiln site. The methods are briefly introduced as follows:

*Step 1.* Measure and scan the existing ceramic relics, fragments, or ancient kiln sites of Shouzhou kiln with CMM and 3D laser scanner to obtain their data point clouds and align them quickly.

*Step 2.* Use data optimization software such as surface to analyze results, optimize data points, remove useless information, and quickly extract product feature point cloud.

*Step 3.* According to the convenience of drawing, intercept the profile of the restored object in an all-round way, draw the product surface by using 3D CAD software such as Pro/E and UG, and complete the virtual reconstruction of 3D product modeling.

*Step 4.* The surface can be repaired and restored by software according to the condition of the surface, and then, it can be output into an STL format file, which can be processed and manufactured by connecting the ceramic 3D printer and other processing equipment, or use an ordinary 3D printer to print it out and make the mold after equal scale amplification. Alternatively, it can be exported to STL or IGES format files, imported into 3DMAX or rhino for rendering and 3D data saving, or transferred to Virtools and Cult3D software for interactive virtual demonstration, as shown in Figure 1.

### **3. Application of VR Technology in Shouzhou Kiln Ceramic Product Design, Shouzhou Kiln Process Technology Improvement, Shouzhou Kiln Ceramic Product Display, and Shouzhou Kiln Marketing**

*3.1. VR Technology Involved in the Design and R & D of Shouzhou Kiln Ceramic Products.* VR technology can convey the design scheme of Shouzhou kiln products through virtual reality and comprehensively check the shape and color of product design with the help of relevant hardware, VR glasses, data pen, etc. Through simulated firing, the possible

defects of Shouzhou kiln products in the firing process can be further reduced. VR technology not only strengthens the interactive virtual experience of designers when observing products, so that they can more effectively feel the performance of products. It can also copy, repair, and save data of existing products. It can also be used as a performance testing tool for Shouzhou kiln products for all-round evaluation and correction before production. Using VR technology to realize the virtual detection and evaluation of Shouzhou kiln ceramic products can further simulate its production process and build a virtual detection and evaluation system, so that its quality can be monitored and guaranteed more effectively before it is officially put into production.

The specific method is to use the modeling software to construct the digital three-dimensional modeling and paste the material. Through the signal transformed from Virtools into virtual reality, the designer can modify the design draft through virtual reality hardware and then feedback the modified data to the modeling or color texture stage to improve the product. Finally, the detection module is used to detect, analyze whether the hidden dangers and defects are within the allowable error range, and then make necessary corrections, so as to effectively ensure the quality requirements of the product and improve the efficiency. See Figure 2 for the specific process.

*3.2. VR Technology Involved in Raw Material Improvement of Shouzhou Kiln.* Shouzhou kiln has a long history of using materials nearby as tire and glaze of ceramic products. As early as the Northern and Southern dynasties (420~589), the clay of Shangyao town in Huainan was developed and utilized for manufacturing Shouzhou porcelain. According to the records of Huaiyuan County annals, “sixty miles to the south of the county, near the Luohe River, there are two winding peaks, under which there are coal kilns, Aboriginal stone burning ash, Bo mud filling, burning basin, and other utensils. Red chalk soil is also produced, and the glaze is taken by those who paint it” [9]. Until the beginning of the Ming dynasty (1368–1644), Shangyao people used the clay and mountain glaze from crow mountain, cave mountain, Wu family memorial archway, and other places to burn pottery jars and other pottery products. In the late 1950s, clay was found in Datong, Dongshan, Bagongshan, and other places, which was later developed and utilized by Datong bowl factory, municipal ceramic factory, and Bagongshan refractory factory. In the early 1960s, minerals such as clay, feldspar, and purple shale were found in Xiejiaji, Bagongshan, and Shangyao, respectively, which were developed and utilized by Huainan porcelain factory, Fengtai pot and bowl factory, and Shangyao cylinder factory.

The element composition of ancient Shouzhou kiln porcelain was determined by energy-dispersive X-ray fluorescence (EDXRF) technology. The results are shown in Table 1.

The results of the determination of the composition of the tire glaze of Shouzhou kiln ceramic products are as follows: the main components of the tire are silicon dioxide, aluminum oxide, and iron oxide. The glaze is mainly composed of silicon dioxide, aluminum oxide, calcium oxide, and phosphorus pentoxide. There are two groups of data

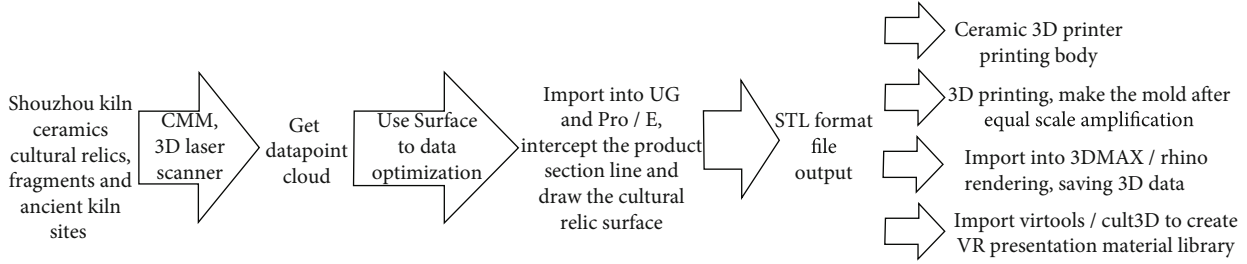


FIGURE 1: Reproduction, restoration, and data preservation of ceramic relics in Shouzhou kiln.

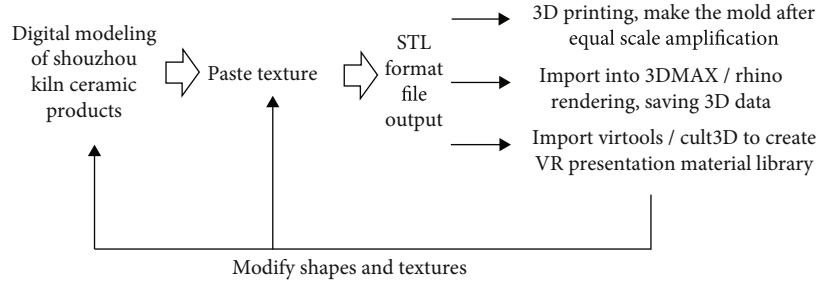


FIGURE 2: Flow chart of VR intervention in Shouzhou kiln ceramic product design.

TABLE 1: Chemical composition analysis of ancient Shouzhou kiln fragments [10].

Kiln site	Sample		SiO <sub>2</sub>	Al <sub>2</sub> O <sub>3</sub>	Fe <sub>2</sub> O <sub>3</sub>	TiO <sub>2</sub>	CaO	MgO	K <sub>2</sub> O	Na <sub>2</sub> O	P <sub>2</sub> O <sub>5</sub>	MnO <sub>2</sub>
Guanzuizi	Grayish-brown buttress		56.11	20.33	4.58	2.73	0.95	4.95	2.77	2.25	0.05	0.11
		Body	56.06	25.05	3.51	1.29	0.78	4.94	2.01	2.99	0.14	0.037
Guanzuizi	Blue-glazed porcelain	Engobe	56.39	23.98	3.09	1.23	1.73	4.29	4.04	1.83	0.14	0.04
		Glaze	45.89	15.38	2.81	0.85	19.46	4.9	3.74	1.06	1.4	0.54
		Body	55.54	25.49	3.4	1.27	0.88	5.01	1.91	3.43	0.087	0.047
Guanzuizi	Blue-glazed porcelain	Engobe	54.38	21.9	2.4	0.92	5.48	5.23	3.48	2.66	0.33	0.77
		Glaze	46.49	13.69	3.88	0.81	20.44	4.95	2.6	1.22	1.18	0.42
		Body	54.66	26.69	2.69	1.19	0.91	4.97	1.25	4.36	0.23	0.057
Guanzuizi	Blue-glazed porcelain	Engobe	55.43	23.93	2.11	0.94	1.37	5.06	4.16	3.97	0.17	0.043
		Glaze	47.4	12.6	2.38	0.73	19.87	5.38	4.01	1.43	1.26	0.42
Inpatient department	Gray buttress		57.03	23.61	3.33	1.43	1.11	4.9	2.32	3.06	0.18	0.06
		Body	59.37	20.37	4.7	0.96	1.06	4.8	2.54	2.64	0.18	0.083
Inpatient department	Yellow-glazed porcelain	Engobe	60.31	19.73	2.67	1.03	1.21	5.35	2.63	3.31	0.22	0.063
		Glaze	48.88	11.94	3.8	0.77	17.92	5.07	4.35	1.57	1.47	0.52
		Body	57.24	21.25	4.53	1	0.87	5.19	2.78	3.4	0.37	0.093
Inpatient department	Yellow-glazed porcelain	Engobe	62.24	18.75	3.24	1.21	0.84	4.98	2.87	3.1	0.18	0.037
		Body	57.86	20.39	5.25	1.02	1.25	4.8	2.93	2.89	0.11	0.083
Inpatient department	Yellow porcelain	Engobe	63.36	16.81	3.36	0.67	1.73	5.56	2.22	2.51	0.1	0.053
		Glaze	47.48	11.25	5.48	0.63	17.94	5.27	3	2.11	1.25	0.51

for the determination and analysis of chemical composition of Shouzhou kiln yellow glaze porcelain: dl-01 fetal material: silica 66.51%, aluminum oxide 25.2%, and iron oxide 3.48%; glaze: silicon dioxide 61.21%, aluminum oxide 14.45%, calcium oxide 14.52%, and phosphorus pentoxide 1.33% and Dl-02 tire material: silica 68.33%, aluminum oxide 24.3%, and iron oxide 3.17%; glaze: silica 59.23%, aluminum oxide

14.06%, calcium oxide 15.15%, and phosphorus pentoxide 1.28%.

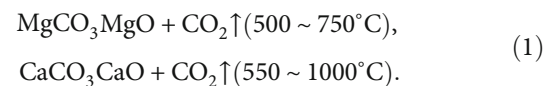
Systematically sort out the historical data of raw materials around Shouzhou kiln and establish the corresponding raw material database according to the chemical element content and composition data of various carcass raw materials. Specifically, it includes the following: first, the plasticity

and fluidity test of ceramic slurry: the forming process of Shouzhou kiln includes the wheel forming process, grouting forming process, and rolling forming process. The corresponding mud data is established according to the methods and characteristics of Shouzhou kiln blank forming process; second, the temperature test of raw materials: the firing process of Shouzhou kiln has strict requirements on temperature, and the fire resistance of raw materials should reach 1300°C. Therefore, a certain proportion of high-temperature-resistant raw materials should be added to the raw material formula of Shouzhou kiln and the relevant raw material temperature data should be established after the experiment; and thirdly, the glaze configuration technology of Shouzhou kiln: the key to the unique yellow glaze of Shouzhou kiln lies in the glaze formula technology. The glaze technology of Shouzhou kiln includes glaze classification, raw materials of glaze, glaze formula calculation, etc. According to the data of chemical element content and composition of raw materials in the glaze color of traditional Shouzhou kiln, the corresponding glaze database is established. The raw material database is input into the VR system developed by Shouzhou kiln ceramic products to realize that the material type, composition, and location can produce the final firing effect in combination with different firing temperatures and firing atmospheres. In the system, the designer can constantly try to replace the green body and glaze according to the green body thickness, fire resistance, glaze hardness, and glaze finish of the product and determine the final material ratio and combination from the final firing form reflected in VR.

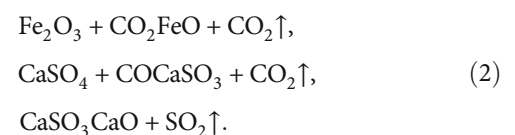
**3.3. VR Technology Involved in Shouzhou Kiln Firing Process Improvement.** Ancient Shouzhou kiln had mastered advanced firing technology as early as the Sui Dynasty (581~618), and the glaze of ancient ceramic products excavated is still as bright as new. The reason why Shouzhou kiln has achieved such great success in history is mainly due to its early mastery of advanced firing technology and the glaze of utensils is fully melted, which is very suitable for daily life. What kind of atmosphere system is used to burn ceramic products? It shall be determined according to the composition of raw materials in the product formula and the physicochemical reaction in each stage of the firing process. When the raw material contains less organic matter and carbon, low viscosity, weak adsorption, and high iron content, it is suitable to choose the reducing atmosphere for sintering. On the contrary, it is suitable to choose the oxidation atmosphere. The firing atmosphere of ceramic products refers to the percentage of free oxygen and reducing components contained in the combustion products in the kiln during the firing process. Generally, the firing atmosphere is divided into oxidation atmosphere and reduction atmosphere. The atmosphere with free oxygen content above 8% is called a strong oxidation atmosphere. The atmosphere with free oxygen content of 4%~5% is called an ordinary oxidation atmosphere. The atmosphere with a free oxygen content of 1%~1.5% is called medium atmosphere. When the content of free oxygen is less than 1%. And when the content of CO is less than 3%, it is called a weak reduction atmosphere. The atmosphere with a CO content above 5% is called a

strong reduction atmosphere. The content of iron in the glaze of Shouzhou kiln is high (2.38%~5.48%), and the content of titanium and manganese is low (0.63%~0.85% and 0.42%~0.54%, respectively). The main coloring element in the glaze is iron. Through the analysis of the ceramic fragments of ancient Shouzhou kiln, it is found that the content of coloring elements in the porcelain body and glaze of each sample is basically the same. It can be inferred that there are no additional coloring elements iron and titanium in the process of glaze making. The contents of coloring elements iron and titanium in the fetus and glaze of Guanzuizi green glaze sample and the yellow glaze sample of the inpatient department are basically the same. Therefore, the green glaze and yellow glaze are likely to be formed due to different firing atmospheres. The green glaze is formed in a reducing atmosphere and the yellow glaze is formed in an oxidizing atmosphere. The divalent iron ions in the green glaze are more than the yellow glaze, and the trivalent iron ions are less than the yellow glaze. Scholars speculate that the traditional firing method of Shouzhou kiln is oxidation, weak reduction, oxidation, strong reduction [11].

In the low-temperature stage of the firing process, the green body of Shouzhou kiln is mainly to remove water and carry out oxidative decomposition. In order to ensure the full oxidation of organic matter, carbon, and sulfide and the full decomposition of carbonate, a strong oxidation atmosphere is generally selected. In addition to the oxidation reaction described above, carbonate decomposition is also accompanied by ceramic products in the low-temperature stage of the firing process.



The speed and completeness of these reactions are affected by the atmosphere. When the oxidizing atmosphere is sufficient, the reaction will be faster and more complete. On the contrary, the reaction speed becomes slow and incomplete. When the firing process enters the high-temperature stage, the gas produced by the liquid-phase reaction can not be freely discharged from the billet, so there are pinholes, bubbles, and other defects. It is impossible to oxidize and decompose all the gas components in the billet at the low-temperature stage, because carbonate and  $\text{Fe}_2\text{O}_3$  decompose above 1300°C in an oxidizing atmosphere. However, in such a high-temperature region, the green body already has liquid a phase. When the viscosity decreases, the decomposed bubbles will break through the liquid phase and escape, resulting in uneven glaze or remaining in the glaze layer to form bubble defects. In order to solve this problem, the firing atmosphere should be controlled to a reducing atmosphere before high temperature (about 1000°C), so that  $\text{Fe}_2\text{O}_3$  and sulfate can undergo the following reduction decomposition:



The first reaction is strong at 1100°C in a reducing atmosphere. The latter reaction reacts strongly at 800°C in a reducing atmosphere. This ensures that such substances are fully reduced and decomposed before the glaze layer closes the green body [11]. Therefore, in order to eliminate the pinhole and bubble defects of Shouzhou kiln ceramic products, it is necessary to ensure that there is a strong oxidizing atmosphere in the preheating and a reducing atmosphere in the firing zone. Combined with multiple firing experiments, the firing atmosphere control of Shouzhou kiln can be adjusted as follows: strong oxidation (960–1030°C)-strong reduction (1030–1280°C)-weak reduction (1280–1300°C).

VR ceramic firing simulation technology uses a computer to simulate a three-dimensional virtual visual traditional kiln, providing users with a visual, tactile, and auditory environment. Users can observe and control the ceramic products fired in the kiln from all angles without restrictions. Its fidelity and real-time interaction provide a strong support for the ceramic firing process of Shouzhou kiln. The main function of VR ceramic firing simulation technology is to truly simulate the whole process of ceramic molding, glaze configuration, firing system, and so on in the process of the traditional Jun porcelain intangible cultural heritage firing technology. It provides valuable reference data for the R & D and innovation of contemporary Jun porcelain glaze.

Exploration and Application of Simulation Technology in the Production Process of Shouzhou Kiln. The simulation of Shouzhou kiln firing technology by virtual reality technology can not only shorten the R & D cycle of Shouzhou kiln products and reduce R & D costs but also reduce the environmental pollution caused by long-term experiments. Using VR virtual reality, 3D glasses, and other auxiliary equipment, ceramic engineers can directly observe the real-time state of the glaze color in the firing process of Shouzhou kiln in the laboratory without going to the kiln workshop and find problems in the process of simulating temperature, reducing atmosphere, and glaze color, so as to timely and efficiently adjust various components of ceramic materials before mass production of ceramic products and accurately grasp the ceramic raw materials, temperature curve, reduction atmosphere data, product shrinkage ratio, and other data in the production of ceramics, so as to solve various problems found in R & D.

The involvement of VR technology in the Shouzhou kiln firing process includes the following contents: first, fuel simulation: through the data analysis of chemical elements contained in firewood fired in Shouzhou kiln, the data analysis of the combustion value of various firewood, and the data analysis of metal substances contained in wood ash, the fuel database is established; second, temperature simulation: (1) temperature rise curve database: according to the characteristics of traditional firewood burning technology, analyze the temperature rise changes and firing time in each stage of the firing process and establish the corresponding firewood burning temperature curve data, (2) type of temperature sensor: firewood combustion is characterized by long flame, and the flame is in direct contact with utensils (naked combustion), so the contact temperature sensor is adopted, and

(3) number and distribution of temperature sensors: the number of temperature sensors is calculated according to the space size in the virtual Chai kiln, and the distributed structure is used for temperature sensing deployment in the kiln [12]; third, firing system simulation: (1) carbon dioxide database: according to the reduction reaction formula in the ceramic firing process ( $\text{Fe}_2\text{O}_3 + 3\text{CO} = 2\text{Fe} + 3\text{CO}_2$ ), analyze the  $\text{CO}_2$  content and distribution position in the reduction stage of Shouzhou kiln and establish the corresponding carbon dioxide concentration database and (2) furnace atmosphere pressure and flow rate database: test and analyze the atmosphere pressure and flow rate at different positions in the process of traditional Shouzhou kiln firing technology and establish the corresponding database.

*3.4. VR Technology Involved in the Exhibition and Marketing of Shouzhou Kiln Ceramic Products.* Build a VR display platform of Shouzhou kiln ceramic products based on e-commerce. With the continuous development of modern society, people's demand for ceramic products is gradually developing in the direction of multivariety and personalization. The design of traditional Shouzhou Kiln ceramics is generally formed in batches by ceramic craftsmen after making molds through grouting, extrusion, and other methods. Therefore, it is inevitable to have the following two shortcomings: first, the elements such as product shape and color are determined according to the craftsman's own aesthetic taste and cultivation. Therefore, the product characteristics are inevitably limited and it is difficult to realize multivariety and personalization. Second, it is impossible to establish communication channels with consumers, so it is somewhat blind in design, and it is difficult to flexibly adapt to the ever-changing market demand. In view of this, with the help of VR technology, we can build a virtual Shouzhou kiln ceramic product display platform based on the e-commerce system, so that consumers can customize the shape, color, and other personalized elements of products according to their own needs without leaving home and truly experience the fun of customized products through interactive methods.

After completing the construction of the e-commerce website, it is necessary to refine the VR display platform of each virtual ceramic product. The steps are as follows and Figure 3:

*Step 1.* Construct the initial product model in 3D Max and other 3D software and convert it into a grid object (the number of points and surfaces should not be too large; otherwise, the subsequent operation will be affected), copy the initial model (keep the number of points and surfaces unchanged), and modify it into the end model B.

*Step 2.* Assign materials and maps to the two models (UV coordinates must be specified to ensure correct model mapping). You can also choose the shell material in Virtools. The map is best refined with the unwrap UVW command to prevent aliasing when the model is changed in the future.

*Step 3.* Construct elements such as the background, environment, and lighting (the simpler the better). After the



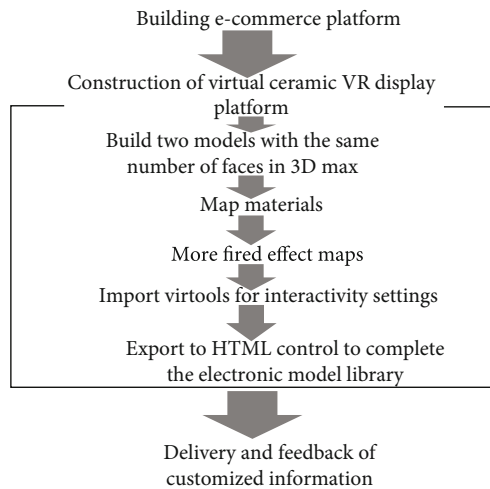


FIGURE 3: Construction flow chart of the Shouzhou kiln e-commerce system supported by VR technology.

rendering effect meets the requirements, use the “bake” command to generate the first set of colors, save the burned map, reassign its UV coordinates to the model, and render again to observe the effect. Change the map from the shader and use the bake command again to get the second set of maps. By analogy, multiple sets of baked maps are obtained.

*Step 4.* Import the generated model together with the baked map into the VIR tools software. You can add the shader provided by Virtools to debug and get the highlight and glaze effect of ceramics. Then, first formulate the basic operations such as zoom, translation, and rotation, and then, use the building block module to set two buttons, one to control the selection and replacement of colors (the thumbnail of each color can be placed below) and the other to control the change of the transition of the model from the initial state to the end point, which can be set into the form of the slider and digital display, The user can control the change of the product shape and record the numerical points through the slider.

*Step 5.* Complete other subsequent operations in Virtools and export them into HTML controls. Classify and sort out all the generated virtual ceramic product modules, use the website database to produce the electronic model library, and use ASP or PHP language to generate dynamic web page files to complete the production.

We are standing on the edge of a new communication era. The goal of information and communication technology (ICT) has developed from meeting the communication between people to realizing the connection between people and things, things, and things. The ubiquitous Internet of things communication era is coming. The Internet of things extends the traditional information and communication network to a wider physical world. Although the “Internet of things” is still a developing concept, bringing “things” into the “network” is a general trend of information development [13]. If VR is a virtual reality, the production of Shouzhou kiln is a complete reality. The necessary bridge between the

two in line with the characteristics of information is the Internet of things technology. The combination of VR technology and the Internet of things provides a very broad development and imagination space for the product marketing and promotion of Shouzhou kiln. Using RFID technology as a substitute for bar code identification to realize the intelligent management of Shouzhou kiln product logistics system can realize the personalized customization of Shouzhou kiln ceramic products from users’ high participation in design to blank forming and then to product firing, packaging, and logistics distribution, so as to realize the whole process real-time monitoring and users’ participation in the whole process. The Internet of things is the “last mile” to realize the marketing of Shouzhou kiln products supported by VR technology.

#### 4. VR Technology Is Involved in the Inheritance of Shouzhou Kiln Technology and the Promotion of the Shouzhou Kiln Ceramic Culture

Cultural promotion has become an important application field of VR technology. Now VR technology has become the core support technology of digital museums, science and technology museums, large-scale event opening and closing ceremony rehearsal simulation, digital museums, science and technology museums immersive interactive games and other application systems. It can be used for the recording, digitization and display of various documents, manuscripts, photos, movies, collections and other cultural relics. The high-precision modeling of these cultural relics also continuously puts forward higher requirements on VR modeling methods and data acquisition equipment, which promotes the development of VR. Many countries have actively carried out this work, such as the Metropolitan Museum in New York, the British Museum Russia’s Winter Palace Museum, and France’s Louvre which have established their own digital museums. China has also developed and established university digital museums, digital science and technology museums, and virtual Dunhuang and virtual Forbidden City [14].

As the dominant cultural and historical attribute, Shouzhou kiln must build a good cultural space and clear cultural identity in order to get a place in the current social space [15]. Combining traditional elements with modern aesthetics, while modern design injects vitality into the contemporary development of Shouzhou kiln, we must use effective scientific and technological means to realize the dissemination of Shouzhou kiln cultural identity. The core or main spiritual connotation of the living inheritance content of various traditional art and cultural activities is the collective aesthetic experience of specific cultural groups [16]. How to strike a balance between the two is an important issue in the development of Shouzhou kiln.

VR technology makes virtual scenes based on the real environment through the computer. Through VR technology, it can provide visitors with real-time interaction and realistic feeling, improve the speed of cultural relics display



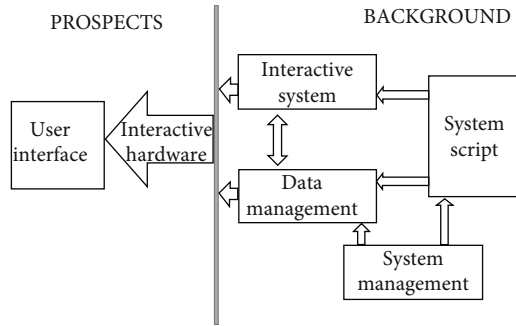


FIGURE 4: Shouzhou kiln VR display system structure.

and repair, reduce the use and operation cost, and provide a new idea for site display. As a world-famous category of ancient ceramics, Shouzhou kiln is not only an important production and export base of craft ceramics but also a window of the Chinese ceramic culture. At present, its display mode is mainly traditional entity, picture, and sample exhibition. It is a pity that this traditional display mode lacks interaction with tourists and can only provide static experience, but tourists spend time and energy but can not be satisfied. VR technology can well solve this problem and let visitors experience visiting the virtual space. By using VR technology, the exhibition can provide Shouzhou kiln with a virtual ceramic exhibition hall with friendly interaction and roaming functions. Customers can walk freely and watch freely in this virtual exhibition hall. At the same time, they can also observe more details of a single product with the help of interactive operation. The structure diagram of the Shouzhou kiln VR display system is shown in Figure 4. The system includes the user interface, interactive system, data management, system script, system management and other modules.

## 5. Conclusion

Culture is the sum of material civilization and spiritual civilization created by human beings. Shouzhou kiln is the crystallization of human spiritual and material creation and the materialized form of people's wisdom in the region. Technology is a method where people use existing things and knowledge to change the function and performance of existing things. VR technology is a bridge for human beings to shuttle freely between the imaginary space and the real space. The emergence of new technology will inevitably bring new development opportunities and space to the old cultural form. Similarly, the application of VR technology also brings new development opportunities for the ancient Shouzhou kiln. This opportunity comes from the comprehensive involvement of VR technology in Shouzhou kiln archaeology, Shouzhou kiln industry development, and Shouzhou kiln ceramic culture promotion. Technology and culture are never antagonistic. On the contrary, appropriate technology application can inject fresh vitality into the development of culture. With the unique 3I (immersion, interaction, and imagination) attribute of VR technology and the interconnection attribute of the Internet of things

technology, the ancient Shouzhou kiln will have the opportunity to reenter the vision of today's people from the historical dust and glow with vigorous vitality. At the same time, VR technology's all-round involvement in the historical research, current development, and future inheritance of Shouzhou kiln also provides reference experience for the protection, development, and inheritance of human traditional ceramic culture.

## Data Availability

Data sharing is not applicable to this article as no datasets were generated or analyzed during the current study.

## Conflicts of Interest

The authors declared no potential conflicts of interest with respect to the research, authorship, and/or publication of this article.

## Acknowledgments

The authors acknowledge Anhui Provincial Quality Engineering Project (2019jyxm0190), the scientific research project of Anhui University of Finance and Economics (ackyc20065), and Provincial Ideological and Political Demonstration Courses (2020szsfkc0014).

## References

- [1] Heim and J. Wulun, *From Interface to Cyberspace: Metaphysics of Virtual Reality*, L. Gang, Ed., Shanghai Science and Technology Education Press, Shanghai, 2000.
- [2] I. Suther, "The ultimate display," in *Proceedings of the International Federation of Information Congress*, pp. 506–508, New York, 1965.
- [3] M. Heim, *Metaphysics of Virtual Reality*, Oxford University Press, Oxford, 1993.
- [4] G. Burdea and P. Coiffet, *Virtual Reality Technology*, John Wiley and Sons, NJ, 1994.
- [5] C. Wang, W. Gao, and X. Wang, *The Theory, Implementation and Application of Lingjing (Virtual Reality) Technology*, Qinghua University press, Beijing, 1996.
- [6] Z. Qinpeng, H. Jinpeng, L. Bo, and S. Xukun, "Overview of virtual reality research," *Computer Research and Development*, vol. 33, no. 7, pp. 493–500, 1996.
- [7] Z. Hu and L. Li, "Research and application of VR technology to the restoration and display of ancient ceramics," *Information and Communication*, vol. 3, 2014.
- [8] L. Jun and G. Guohua, "3D realistic modeling and virtual display technology of cultural sites," *Computer Engineering*, vol. 36, 2010.
- [9] S. Rangxiu, *Qing Dynasty: Huaiyuan County Annals*, wood movable type reprint, 1998.
- [10] Y. Ruochun, Y. Zhengzheng, L. Yinghua, and C. Wang, "Test and preliminary analysis of Shouzhou kiln porcelain," *Journal of China University of Science and Technology*, vol. 1, pp. 22–28, 2011.

- [11] H. Yundong, "Influence of firing atmosphere on defects of ceramic products and control analysis," *Ceramics*, vol. 6, pp. 33–35, 2002.
- [12] P. Wang, "Application of orthogonal experimental method in the experiment of improving ceramic glaze hardness," *Shandong Ceramics*, vol. 4, pp. 22–23, 2013.
- [13] International Telecommunication Union, *Internet Reports 2005: The Internet of Things*, ITU, Geneva, 2005.
- [14] Z. Qiping, S. Xukun, and Q. Yue, "Research on some key technologies of digital museum," *Journal of System Simulation*, vol. 19, Supplement 2, pp. 1–6, 2007.
- [15] Z. Yajun, X. Yu, and Z. Yongxi, "Development and thinking of Shouzhou kiln from the perspective of living inheritance," *Journal of Liaoning University of Science and Technology*, vol. 2, pp. 49–52, 2019.
- [16] X. Gao, "Living protection of traditional art and construction of contemporary aesthetics," *Literature and Art Research*, vol. 7, pp. 5–13, 2013.

## Research Article

# A Real-Time and Long-Term Face Tracking Method Using Convolutional Neural Network and Optical Flow in IoT-Based Multimedia Communication Systems

Hanchi Ren,<sup>1,2</sup> Yi Hu ,<sup>2</sup> San Hlaing Myint,<sup>3</sup> Kun Hou ,<sup>1</sup> Xiuyu Zhang,<sup>4</sup> Min Zuo,<sup>1</sup> Chi Zhang ,<sup>2</sup> Qingchuan Zhang ,<sup>1</sup> and Haipeng Li <sup>5</sup>

<sup>1</sup>National Engineering Laboratory for Agri-Product Quality Traceability, Beijing Technology and Business University, Beijing 100048, China

<sup>2</sup>Swansea University, Swansea SA1 8EN, UK

<sup>3</sup>Global Information and Telecommunication Institute, Waseda University, Tokyo 169-8050, Japan

<sup>4</sup>Guizhou Academy of Testing and Analysis, Guiyang 550000, China

<sup>5</sup>Capinfo Company Ltd., Beijing 100010, China

Correspondence should be addressed to Kun Hou; [hokun@btbu.edu.cn](mailto:hokun@btbu.edu.cn)

Received 12 August 2021; Accepted 1 October 2021; Published 31 October 2021

Academic Editor: Deepak Gupta

Copyright © 2021 Hanchi Ren et al. This is an open access article distributed under the Creative Commons Attribution License, which permits unrestricted use, distribution, and reproduction in any medium, provided the original work is properly cited.

The development of the Internet of Things (IoT) stimulates many research works related to Multimedia Communication Systems (MCS), such as human face detection and tracking. This trend drives numerous progressive methods. Among these methods, the deep learning-based methods can spot face patch in an image effectively and accurately. Many people consider face tracking as face detection, but they are two different techniques. Face detection focuses on a single image, whose shortcoming is obvious, such as unstable and unsmooth face position when adopted on a sequence of continuous images; computing is expensive due to its heavy reliance on Convolutional Neural Networks (CNNs) and limited detection performance on the edge device. To overcome these defects, this paper proposes a novel face tracking strategy by combining CNN and optical flow, namely, C-OF, which achieves an extremely fast, stable, and long-term face tracking system. Two key things for commercial applications are the stability and smoothness of face positions in a sequence of image frames, which can provide more probability for face biological signal extraction, silent face antispoofing, and facial expression analysis in the fields of IoT-based MCS. Our method captures face patterns in every two consequent frames via optical flow to get rid of the unstable and unsmooth problems. Moreover, an innovative metric for measuring the stability and smoothness of face motion is designed and adopted in our experiments. The experimental results illustrate that our proposed C-OF outperforms both face detection and object tracking methods.

## 1. Introduction

With the development of AI technology [1–3], IoT [4–7] is receiving more and more attention from academia. It emphasizes that all objects connected to the internet (including people and machines) have unique addresses and communicate through wired and wireless networks and have been deeply integrated into humans' daily life. For example, a doctor can conduct the diagnosis remotely or even complete the surgery via a telemedical system [8, 9]; by collecting personal

information, smart devices may provide personal recommendations which are most suitable for him/her [3, 10]; and even the satellite in the universe can be utilized more efficiently for better serving mankind [11]. However, the smarter the humans' life is, the more dangerous the privacy is. Every smart device is "monitoring" you, so personal data protection and privacy-preserved problems should be paid more attention to. Especially the release of GDPR in EU and EEA in 2016, more and more researchers have been digging into privacy-related works [12–19].

The development of IoT-based MCS drives a sharp increase of human face-related techniques, such as face detection, face tracking, and face recognition. Applications of beauty cameras, security access, surveillance and tracking suspect, etc., have been widely used around people's life, for example, smart city and smart campus. It is with no doubt that accurately detecting and tracking faces are essential steps for the aforementioned missions. Additionally, stably and smoothly tracking face bounding boxes from a sequence of continuous images is also required for some special missions in the field of IoT-based MCS, e.g., face biological signal extraction, silent face antispoofing, and facial expression analysis, as stable and smooth face bounding boxes captured along frames can reduce the signal noise significantly.

Regarding the traditional visual methods, a lot of prior face tracking methods [20–25] take tremendous spirits on feature engineering and color spaces. For the long-term tracking of human faces in the unconstrained video, face tracking has been generally treated as common object tracking, e.g., [26] is a typical method which comes from TLD [27, 28] and also is one of the earliest attempts to apply the tracking-by-detection diagram for the face tracking task. Although common TLD can also deal with face tracking work, [26] upgraded it to be more robust even when view-points change. In detail, it adapted a frontal face detector from [29] which is the state-of-the-art method at that time. A validator was deployed on the top of the detector outputting confidence that is how the current image patch corresponds to a face. [30] proposed a face tracking approach where optical flow information is incorporated into the *Viola-Jones* face detection algorithm [31]. Its outputs proceed to build a likelihood map where face bounding boxes are extracted. FT-RCNN [32] is an efficient face tracking method based on Faster R-CNN [33]. A tracking branch is conducted into Faster R-CNN and jointly performs face detection and tracking, but its running time cost is expensive.

Face detection methods are eligible to do face tracking. However, face tracking turns to more concentrate on frame-wise face pattern connection. Thus, as for face tracking, the relationships of the patterns between frames are taken into consideration rather than detecting faces in each individual frame naively. In this paper, we present a novel method for super real-time and long-term face tracking by combining CNN and optical flow (see Figure 1). There are three principal components: a cascade lightweight face detector that takes responsibility for generating an initial face bounding box, a face tracker based on optical flow [28], and a face identifier (a very shallow FCN) who provides face confidence for binary classification. The face identifier guarantees that the face tracker does not focus on nonface patch. The optical flow field is always continuous and uniform; the face bounding boxes generated from our method are extraordinarily stable and smooth. Additionally, C-OF can be easily transferred to any other missions which meet the stable tracking requirement, such as object tracking and person reidentification. Overall, we make five main contributions:

- (i) We novelly combine lightweight deep CNN with the optical flow to substantially reduce the running

time cost, which achieves stable, smooth, super real-time, and long-term face tracking on both CPU and edge computing devices

- (ii) Compared with the deep CNN face detection method, C-OF output fairly stable and smooth bounding boxes and enhance the performance of many applications, such as face biological signal extraction, silent face antispoofing, and facial expression analysis
- (iii) A lightweight FCN which only contains five convolutional layers is designed for face identification to guarantee the tracking accuracy
- (iv) We innovatively design a metric to quantify bounding box stability and smoothness regarding the scale and position changing of bounding boxes. The experimental results illustrate that our proposed C-OF outperforms both face detection and object tracking methods
- (v) The implementation of C-OF is released on GitHub (<https://github.com/HandsomeHans/C-OF>) for those who are interested in further research work and application on the commercial product

The rest of the paper is organised as follows: in the next section, related work on face detection and object tracking is presented. Our method of how to combine optical flow on a CNN face detection method and insert a lightweight FCN to identify the face box is described in Proposed Method. The details of the experiment and discussion on the results are provided in Experiment and Discussion followed by Conclusion.

## 2. Related Work

*2.1. Face Detection.* As the huge success of deep learning, traditional methods face a tough situation in some particular missions. However, they still matter and have many advantages that are worth to be learnt from. Commonly, they extract hand-crafted features to train a classifier and then deploy a kind of sliding-window method to locate the face. For example, with the combination of Haar features and AdaBoost [34], Viola and Jones [35] deployed a cascaded face detector, which performs high recognition accuracy and fast running time. Benefitting from [34], many excellent methods [36–38] are proposed afterwards. Felzenszwalb et al. [39] used mixtures of multiscale models to detect an object, which inspires many face detection approaches, e.g., [40–42]. As the aforementioned methods use hand-crafted features, they all have bad generalization. That is to say, in complex scenarios, the performance of those methods slumps sharply.

Since Krizhevsky et al. [43] won the ILSVRC, deep learning and CNN have had explosive progress on vision missions. CMS-RCNN [44], Face R-CNN [45], and FNet [46] adopt many novel strategies with regard to face detection based on Faster R-CNN [33]. SSD [47] is another commonly used way of face detection. Methods based on SSD

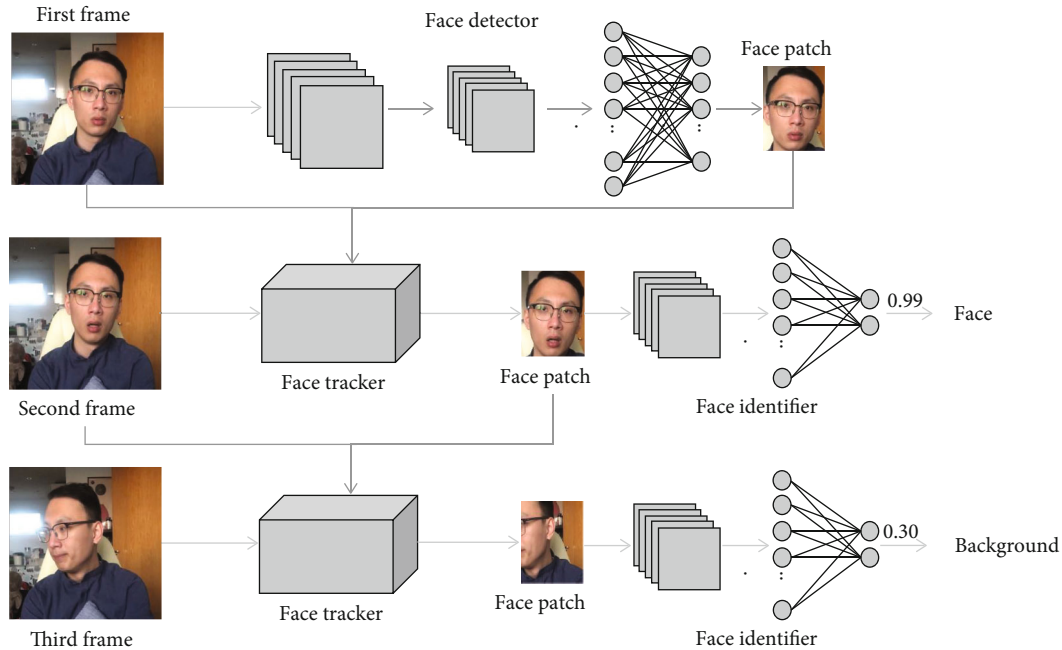


FIGURE 1: The overall architecture of C-OF.

usually lead to high accuracy and efficiency, e.g., a tiny network is designed in FaceBoxes [48], which attain real-time performance on CPU; FANet [49] uses FPN [50] and merges high-level and low-level features in a low computing cost to train a face detector. On the other hand, cascade CNN methods also show their superiority on the face detection mission. MTCNN [51] consists of three lightweight cascade CNN models to jointly detect face and landmark. PCN [52] upgrades MTCNN by adding an orientation branch to be able to output the face rotated angle. Deng and Xie [53] proposed a nested CNN-cascade learning algorithm that adopts shallow CNN architectures. All these are face detection methods, which all focus on single image representation only. That is why on a continuous video, bounding boxes generated by them are unstable and unsmooth.

**2.2. Object Tracking.** Face tracking can be considered to be a special category of object tracking. Most scientists implement object tracking methods for face tracking as control experiments. In the beginning, an initial state such as a bounding box of a target object is given, and then, feature extracting and pattern matching methods are conducted in all the subsequent frames. Object tracking has been progressing all the time, as the release of many benchmark datasets and competitions including RGB-T [54], MOT16 [55], and Lasot [56], as well as the development of deep learning. CF [57] has been widely used and inspired a lot of good work in tracking missions. It proved, for the first time, that there is a connection between ridge regression and classical correlation filters. The work accelerated the cost expensive matrix algebra to fast Fourier transforms with  $O(n \log n)$  computational complexity. In the meantime, the KCF was first presented and a solution of computing kernels on shifts was proposed as well based on radial basis and dot product. [58] proposed MOSSE which

greatly improved the performance of tracking methods with respect to CF. It reduced the computational complexity, and the accuracy increased at the same time. However, it only concerned gray-scale features that this kind of low dimension feature space does not have a good representation. On the other hand, it is unable to adapt object scale variance as it concentrates on translational motion of the center point of the target object between frames and does not take into consideration the scale change of the target object reflected on the screen in the process of moving scale variance. To this end, Danelljan et al. proposed DSST [59] making an improvement on MOSSE by deploying fhOG [39] features instead of gray-scale features to increase the dimension of features from 2 to 28. What is more, the object scale variance is concerned in DSST.

Apart from traditional object tracking methods, CNN-based methods have had great progress and outperform traditional methods a lot on the public benchmarks. [60] introduced a generic object tracking network using a regression mechanism by watching videos offline of objects moving in the world. To be specific, the regression-based tracking network only requires a single feed-forward pass through the network to directly regress the location of the target object. Zhu et al. [61] made progress on Siamese networks, which conduct tracking through similarity comparison strategy, by learning distractor-aware Siamese networks for accurate and long-term tracking. MDNet [62] is one of the most successful generic object tracking methods. It consists of a shared CNN, which is trained on a large set of videos with tracking ground truths, for feature representation extraction. After training, all the branches of domain binary classification layers are replaced. Then, the model was fine-tuned online during tracking to adapt to the new domain. Regarding bounding box regression, they set up an online training linear model to generate the final bounding box.



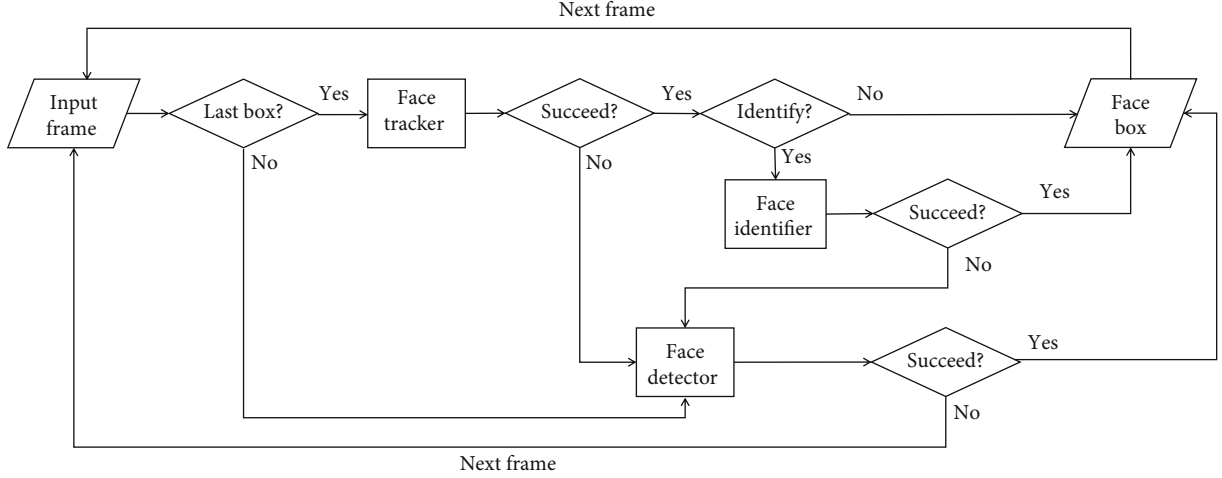


FIGURE 2: The proposed C-OF face tracking system.

TABLE 1: Architectures of cascade convolutional networks. “ $k$ ” stands for kernel size, “ $s$ ” means stride, and “ $p$ ” is padding number.

Stage 1	
Input	Color-scale image
Convolution	Outputs: 10, $k: 3 \times 3$ , $s: 1$ , $p: 1$
MaxPooling	$k: 3 \times 3$ , $s: 2$
Convolution	Outputs: 16, $k: 3 \times 3$ , $s: 1$ , $p: 1$
Convolution	Outputs: 32, $k: 3 \times 3$ , $s: 1$ , $p: 1$
Convolution	Outputs: 6, $k: 1 \times 1$ , $s: 1$ , $p: 1$
Stage 2	
Input	Color-scale image
Convolution	Outputs: 28, $k: 3 \times 3$ , $s: 1$ , $p: 1$
MaxPooling	$k: 3 \times 3$ , $s: 2$
Convolution	Outputs: 48, $k: 3 \times 3$ , $s: 1$ , $p: 1$
MaxPooling	$k: 3 \times 3$ , $s: 2$
Convolution	Outputs: 64, $k: 2 \times 2$ , $s: 1$ , $p: 1$
Dense	Outputs: 128
Dense	Outputs: 6
Stage 3	
Input	Color-scale image
Convolution	Outputs: 32, $k: 3 \times 3$ , $s: 1$ , $p: 1$
MaxPooling	$k: 3 \times 3$ , $s: 2$
Convolution	Outputs: 64, $k: 3 \times 3$ , $s: 1$ , $p: 1$
MaxPooling	$k: 2 \times 2$ , $s: 2$
Convolution	Outputs: 128, $k: 2 \times 2$ , $s: 1$ , $p: 1$
Dense	Outputs: 256
Dense	Outputs: 6

### 3. Proposed Method

The details of the proposed C-OF face tracking method are shown in Figure 2. It consists of three principal components: face detector, face tracker, and face identifier. In the following parts of this section, the first part presents the lightweight face

detector. In the second part, the implementation logistics of optical flow are given. The face identifier is provided in the last part.

**3.1. Lightweight Face Detector.** Same with other face tracking methods, a face detector is essential to figure out an initial face bounding box. We adopt a cascade CNN referring to [51], which is only for face detection without facial landmark prediction. In the first stage, a FCN [63] is deployed to obtain the candidate face bounding boxes. As the networks output not only vast bounding boxes but also confidence density for binary classes of face and background, we predefine a threshold to filter some boxes which have low confidence. Then, highly overlapped boxes are merged by NMS. In stage two, the candidate faces cropped from the input image are fed into the second CNN. Abundant false positive faces are dropped out, and NMS is conducted again. In the last stage, the output is generated the same way as stage two. After NMS, we have the final face box. In our face detector, each part takes its own attention on tackling the detection problem. The first part more focuses on outputting vast face candidates. Then, for the second part, it has to filter false positive faces which means this part is concentrated on face identification. The last part not only focuses on face identification but also puts a lot of attention on box regression. More details of the three CNNs are shown in Table 1.

**3.2. Optical Flow Face Tracker.** Once the initial face bounding box is obtained, it comes into the tracking part. For the general face detection methods, every frame is handled separately, and there is no more temporal information taken considered, so face bounding boxes perform to be very unstable. The sharp shaking of face bounding boxes makes it more difficult to tackle the problem of critical face analysis missions. To this end, a Median-Flow tracker is deployed and collaborates with a bounding box regression module to locate the position of the face in the current frame with respect to the last frame. Basically, a grid of  $10 \times 10$  points is uniformly selected from the last face patch, namely,  $P^l$ .

TABLE 2: Architectures of face identifier. “ $k$ ” stands for kernel size, “ $s$ ” means stride, and “ $p$ ” is padding number.

Input	Color-scale image
Convolution	Outputs: 28, $k: 3 \times 3$ , $s: 1$ , $p: 1$
MaxPooling	$k: 3 \times 3$ , $s: 2$
Convolution	Outputs: 48, $k: 3 \times 3$ , $s: 1$ , $p: 1$
MaxPooling	$k: 3 \times 3$ , $s: 2$
Convolution	Outputs: 64, $k: 2 \times 2$ , $s: 1$ , $p: 1$
Convolution	Outputs: 128, $k: 1 \times 1$ , $s: 1$ , $p: 1$
Convolution	Outputs: 2, $k: 1 \times 1$ , $s: 1$ , $p: 1$

TABLE 3: Stability values with respect to Equation (3) for MDNet, MTCNN, and C-OF on aforementioned four videos with different conditions.

Method	Active camera				
	Clip 1	Clip 2	Clip 3	Clip 4	Clip 5
MDNet	4.106844	4.387077	5.088164	5.704352	4.977256
MTCNN	6.679212	6.522255	6.166027	8.261213	9.037096
C-OF (ours)	2.936315	3.350025	3.372295	3.907079	3.864539

Method	Active human				
	Clip 1	Clip 2	Clip 3	Clip 4	Clip 5
MDNet	3.045595	2.81129	3.305667	3.098207	3.322302
MTCNN	4.064902	3.55413	3.513855	4.050621	3.746015
C-OF (ours)	0.851283	0.993135	0.728653	1.208135	1.403328

Method	Static human				
	Clip 1	Clip 2	Clip 3	Clip 4	Clip 5
MDNet	1.425355	1.47768	1.453236	1.518395	2.260055
MTCNN	1.994141	2.51177	2.318275	2.333235	2.237117
C-OF (ours)	0.310882	0.308686	0.295996	0.245097	0.321575

Method	Active illumination				
	Clip 1	Clip 2	Clip 3	Clip 4	Clip 5
MDNet	1.961921	2.130076	2.3661	3.036336	2.243076
MTCNN	2.831262	2.758897	3.116406	4.073383	2.963807
C-OF (ours)	0.452622	0.579371	0.696979	1.006401	0.392867

Then, the motions of these points between the current frame and last frame are estimated by the pyramidal Lucas-Kanade tracker [64] in two directions.  $P^f = [p_1^f, p_2^f, \dots, p_N^f]$  and  $P^b = [p_1^b, p_2^b, \dots, p_N^b]$ , where  $p_n^f$  and  $p_n^b$  represent the predicted points in forward (from last to current frame) and backward (from current to last frame) directions, respectively, from pyramidal Lucas-Kanade tracker, where  $N$  is the number of points. In other words, the forward predicted points  $P^f$  is calculated from the last frame, current frame, and last frame’s uniformly selected points  $P^l$ ; the backward predicted points  $P^b$  are from the two frames and the current frame’s uniformly selected points  $P^c$ . As for the pyramidal Lucas-Kanade tracker, we set the size of the search window at each pyramid level to be 4 by 4, and two pyramid levels are used. The termination criteria of the iterative search algorithm are set to have a 20 maximum iteration number and 0.03 con-

TABLE 4: Smoothness values with respect to Equation (5) for MDNet, MTCNN, and C-OF on four videos with different conditions.

Method	Active camera				
	Clip 1	Clip 2	Clip 3	Clip 4	Clip 5
MDNet	0.152312	0.146476	0.303847	0.270567	0.088137
MTCNN	1.071629	0.683341	0.650429	0.581538	0.656829
C-OF (ours)	0.005137	0.011361	0.010636	0.005119	0.009432

Method	Active human				
	Clip 1	Clip 2	Clip 3	Clip 4	Clip 5
MDNet	0.678967	0.491966	0.586164	0.699405	0.402297
MTCNN	1.145627	0.847167	0.93854	0.977966	0.971969
C-OF (ours)	0.001103	0.003444	0.001304	0.004872	0.021336

Method	Static human				
	Clip 1	Clip 2	Clip 3	Clip 4	Clip 5
MDNet	0.393428	0.43518	0.444789	0.521464	0.612867
MTCNN	0.5484	0.673217	0.729767	0.625556	0.566896
C-OF (ours)	0.004908	0.000072	0.0	0.000008	0.0

Method	Active illumination				
	Clip 1	Clip 2	Clip 3	Clip 4	Clip 5
MDNet	0.417814	0.3991	0.564509	0.531881	0.48117
MTCNN	1.020253	0.616373	0.805697	1.110985	1.045736
C-OF (ours)	0.010921	0.000995	0.0	0.007117	0.000901

vergence threshold. In order to filter the points  $P^l$  and  $P^f$  to estimate the offset of face patch, normalization cross-correlation between last and current frames is performed firstly. Any point whose value is smaller than the median similarity value is dropped out. Then, the median value of  $P^b$  is used to further filter points in sets  $P^l$  and  $P^f$ . The point whose value is larger than the median value is dropped out. While having the filtered points  $\hat{P}^l$  and  $\hat{P}^f$ , the coordinate offset of the current face box against the last face box is the median *Euclidean* distance between  $\hat{p}_n^l$  and  $\hat{p}_n^f$ :

$$\text{offset}(\hat{P}^l, \hat{P}^f) = \text{median}\left(\left\|\hat{p}_m^l - \hat{p}_m^f\right\|\right); \forall m \in M, M \leq N. \quad (1)$$

Hence, from the last face box and coordinate offsets, we have the current face box. In this way, face boxes are significantly stable and smooth along with frames than those generated from the common face detection method.

**3.3. Face Identifier.** Face recognition is in general brought into vast focus by the success of CNN on vision missions, and various methods have been presented already. In order to filter the representation in the bounding box generated by the optical flow face tracker, we show a very simple face identifier that works very well in distinguishing the background. Table 2 shows the architecture of the proposed face identifier which has a minor difference against the second part of the aforementioned face detector. The second part of the face detector outputs six values, four for face box coordinate and two for face and background probabilities. We

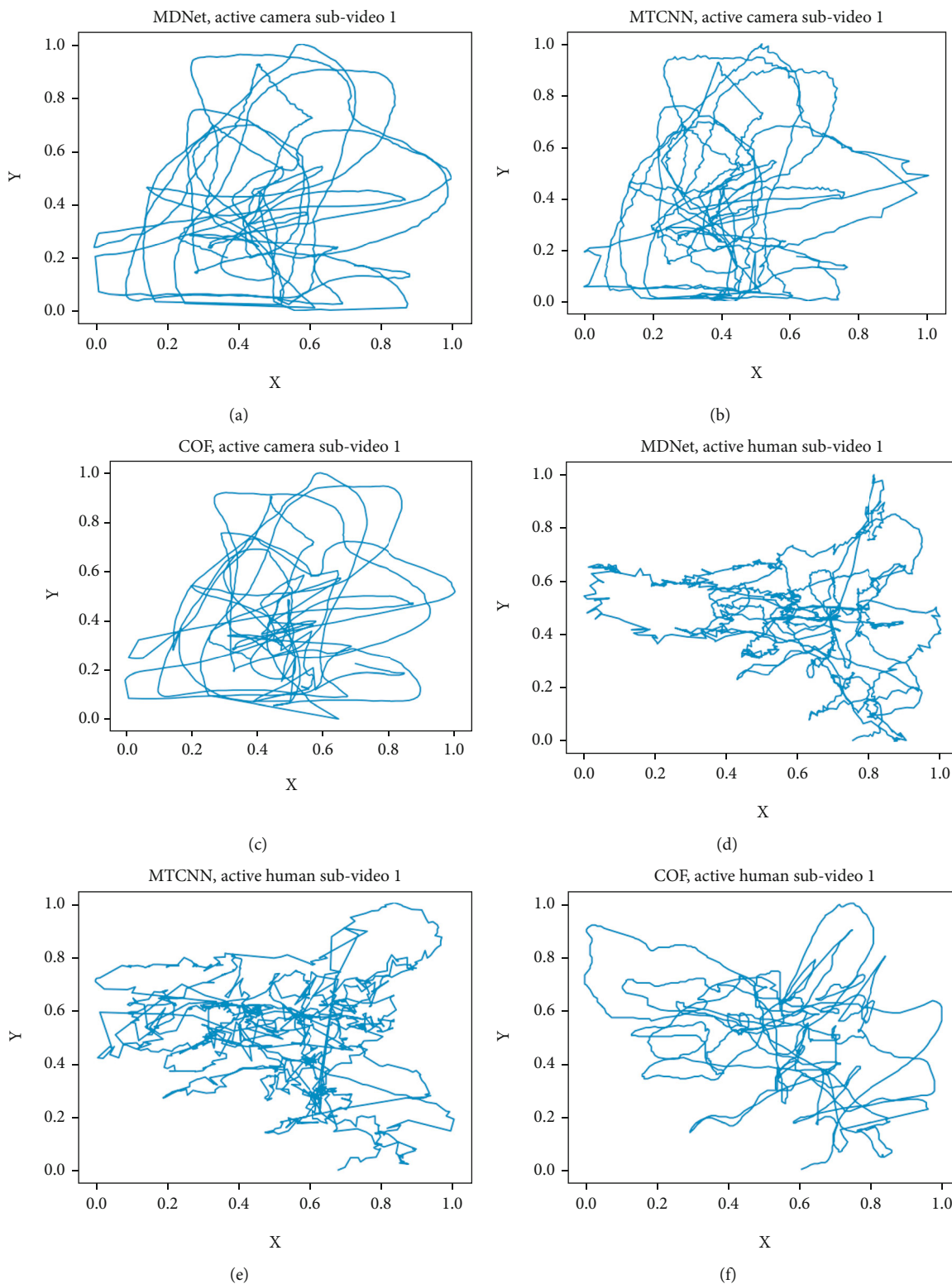


FIGURE 3: Continued.

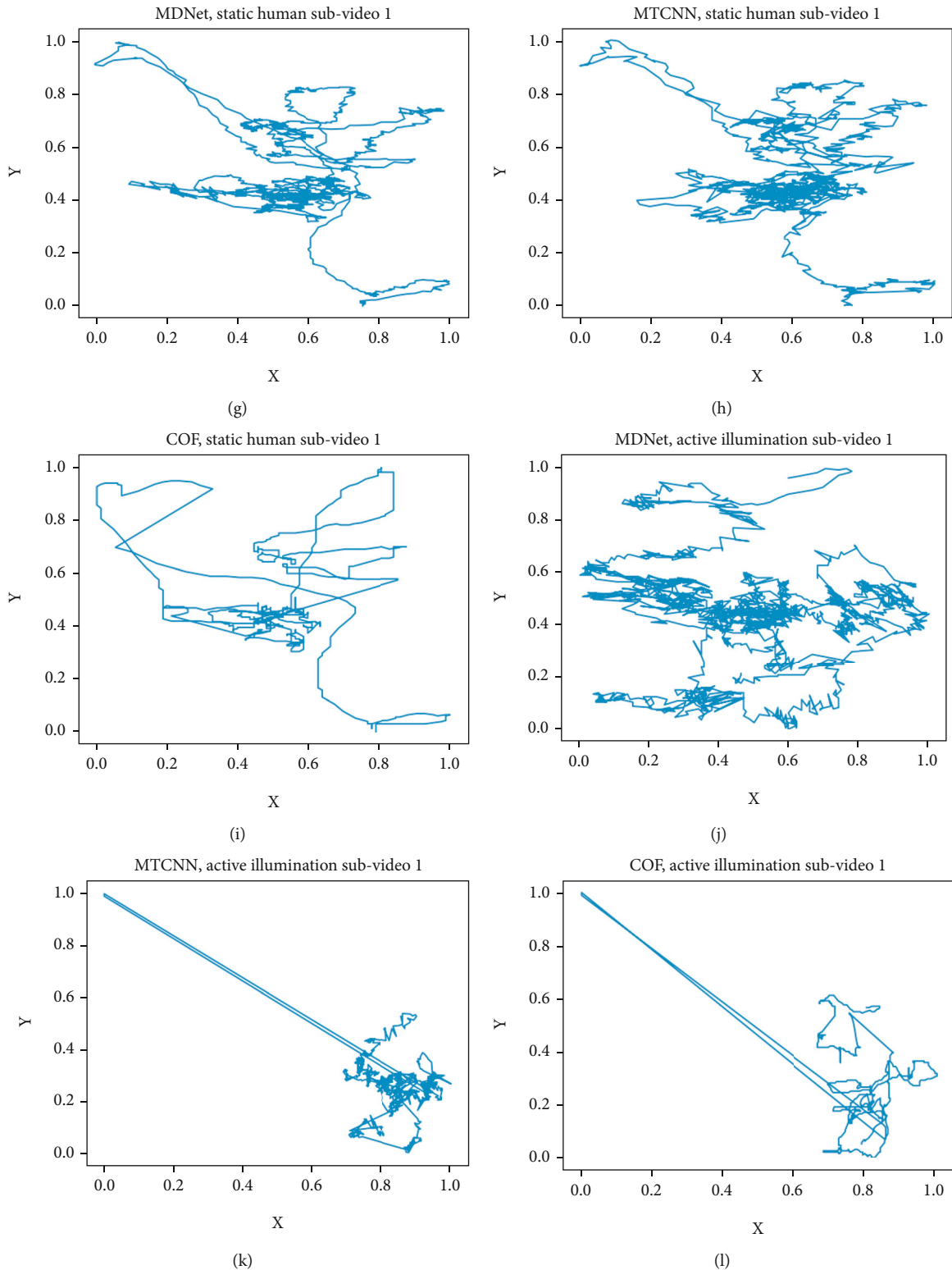


FIGURE 3: Selected visualization for the motion tracking of center point in the bounding box.

change the output layer to only generate binary probabilities. As the face in a sequence of frames may vary a lot, the face tracker may fail in tracking the face and output a wrong object. So, the face identifier is essential; the main goal of it is to filter the false positive candidates to fit well with its

motivation. Therefore, we change the number of output values to two, and the probability distribution for face and background is obtained by a *Softmax* layer which follows the last convolutional layer. In order to make the face identifier capable of dealing with different sizes of face bounding



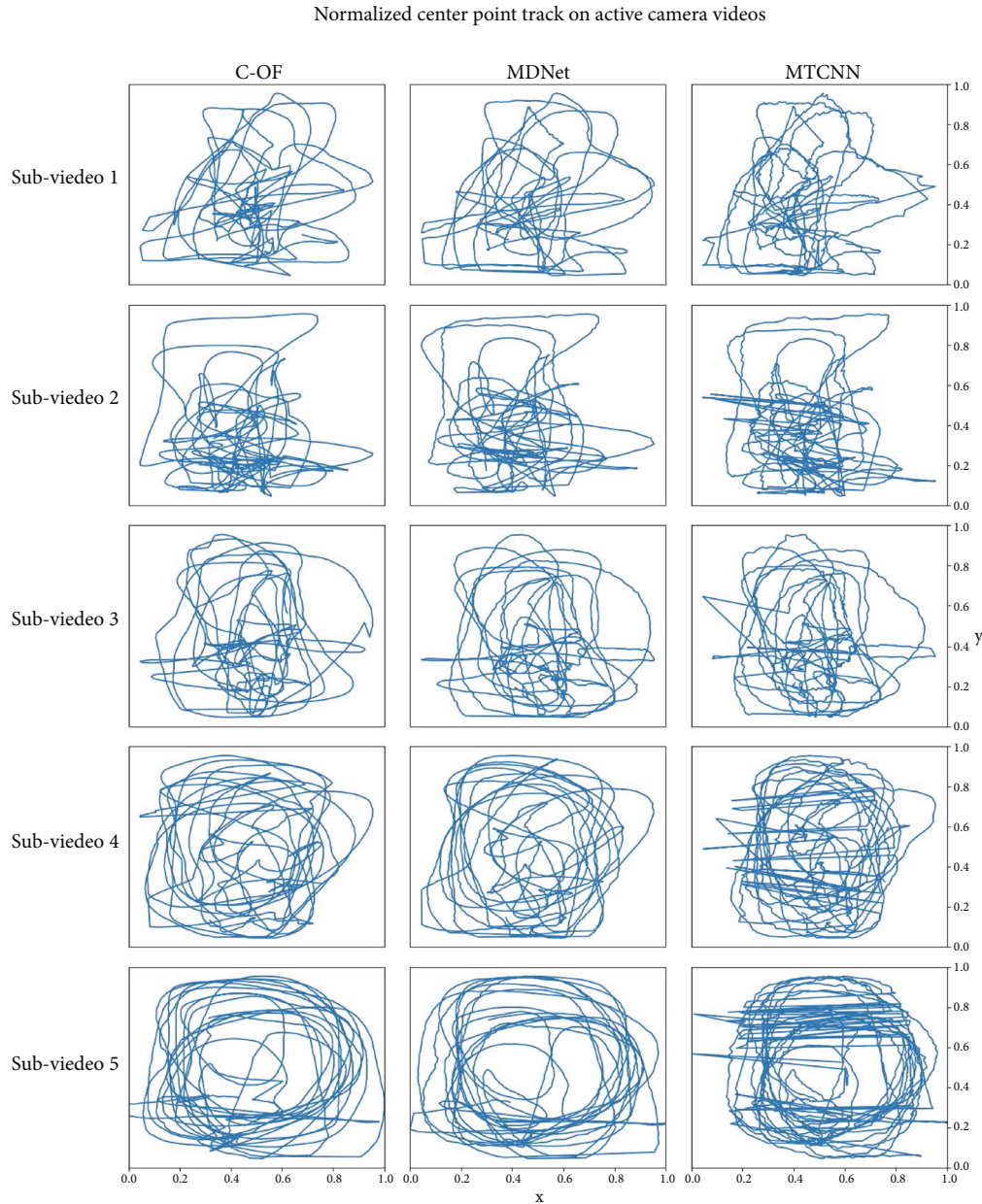


FIGURE 4: Center point motion tracking on active camera videos.

boxes, we replace two fully connected layers with two convolutional layers to make the model be a FCN [63]. FCN is a specially designed neural network for semantic segmentation. By replacing all the fully connected layers with convolutional layers, FCN breaks the limitation of fixed input size. That is because a fully connected layer needs an input with a fixed dimension to fit with its weights, while a convolutional layer with a 1 by 1 kernel size has no need of fixing the input's dimension. Let the kernel number in a convolutional layer be the same as the hidden node number in a fully connected layer; then, this convolutional layer can replace the fully connected layer directly and break the limitation of fixed input size. Its ability to deal with the arbitrary scale of input images has been spread to other vision missions, such as object classification and detection.

## 4. Experiment and Discussion

**4.1. Experimental Setting and Dataset.** A number of experiments on face tracking were conducted to evaluate our proposed C-OF. Other than C-OF, we reproduced MTCNN [51] and MDNet [62] for comparing the tracking performance. For Python implementation, all neural network models are implemented using PyTorch [65] framework, and the source code has been made publicly available (<https://github.com/HandsomeHans/C-OF>) for reproducing the results. The hyperparameters for MDNet and MTCNN are the same as their official implementation. We also implement C-OF via C++ with ncnn (<https://github.com/Tencent/ncnn>) which is a high-performance neural network inference computing framework optimized for mobile



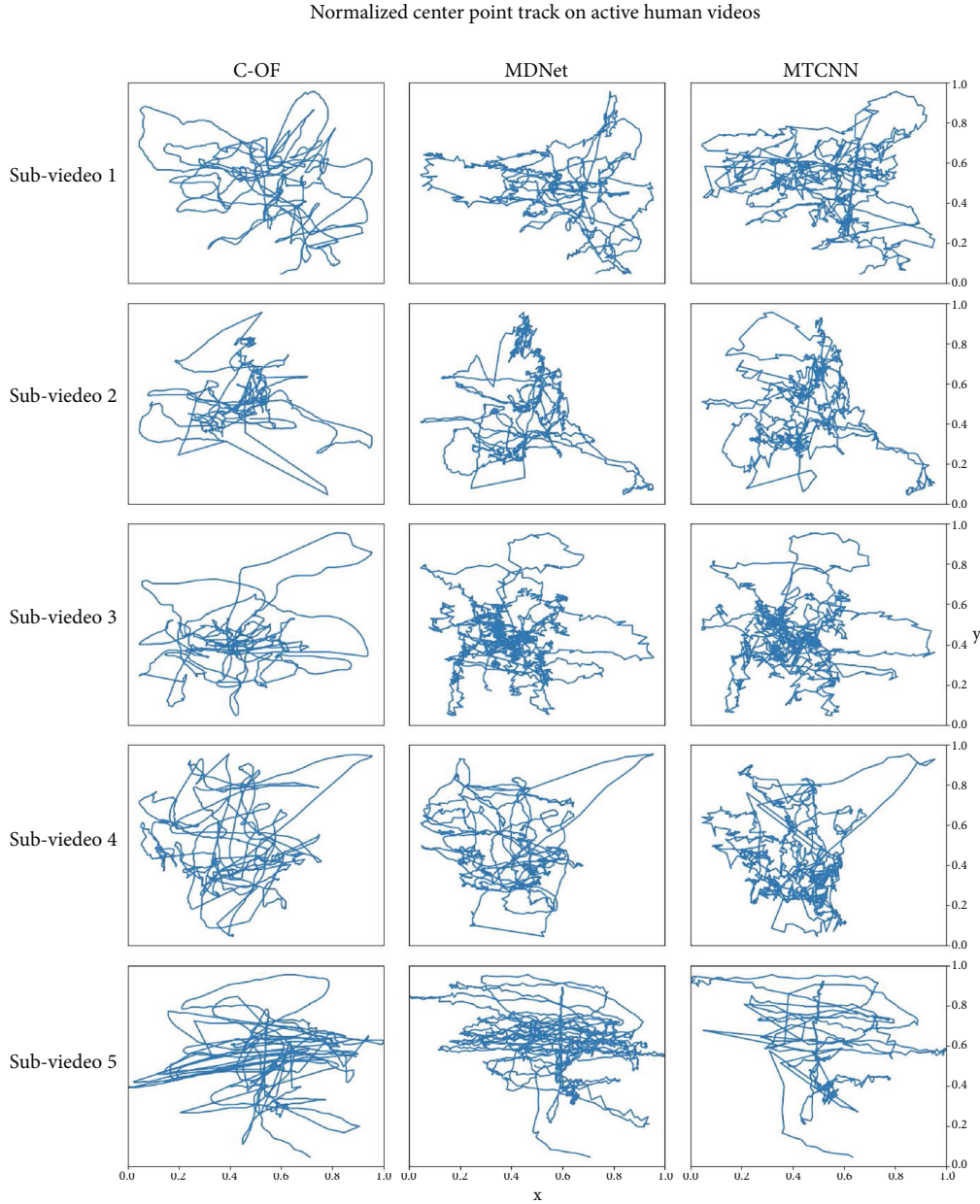


FIGURE 5: Center point motion tracking on active human videos.

platforms. The devices we used in the experiments are *Intel Core i7-8700K* and *Nvidia GTX TITAN X*. Details of running time using Python and C++ implementations are presented in Running Time.

In terms of the dataset, four long-term videos are recorded for the experiments, as there are no public benchmark aims for stable face tracking. The four videos are recorded via different conditions: active camera, active human, static human, and active illumination, respectively. As for the active camera and illumination, we let the actor be static and randomly move the camera and light source in front of the face. And for the active and static human, we first ask the actor to talk to the cameraman and act in a freestyle. Then, we ask the actor to stop acting and sit statically in front of the camera. We split each video into five

clips, each clip is about one-minute long. The recording device is iPhone X with a 12-megapixel rear camera. We resize each frame to 1080 \* 608 resolution. The three different methods can detect and track faces all the time in each clip. So, the only difference is the scale and position changes of bounding boxes frame by frame. The download link of this testing dataset can be found in the GitHub repository as well.

#### 4.2. Result Discussion

**4.2.1. Stability.** In the perspective of evaluating the stability and smoothness of face boxes from a frame sequence, comparing with ground truth is not the principal aspect. Besides, to the best of our knowledge, there is no general metric to

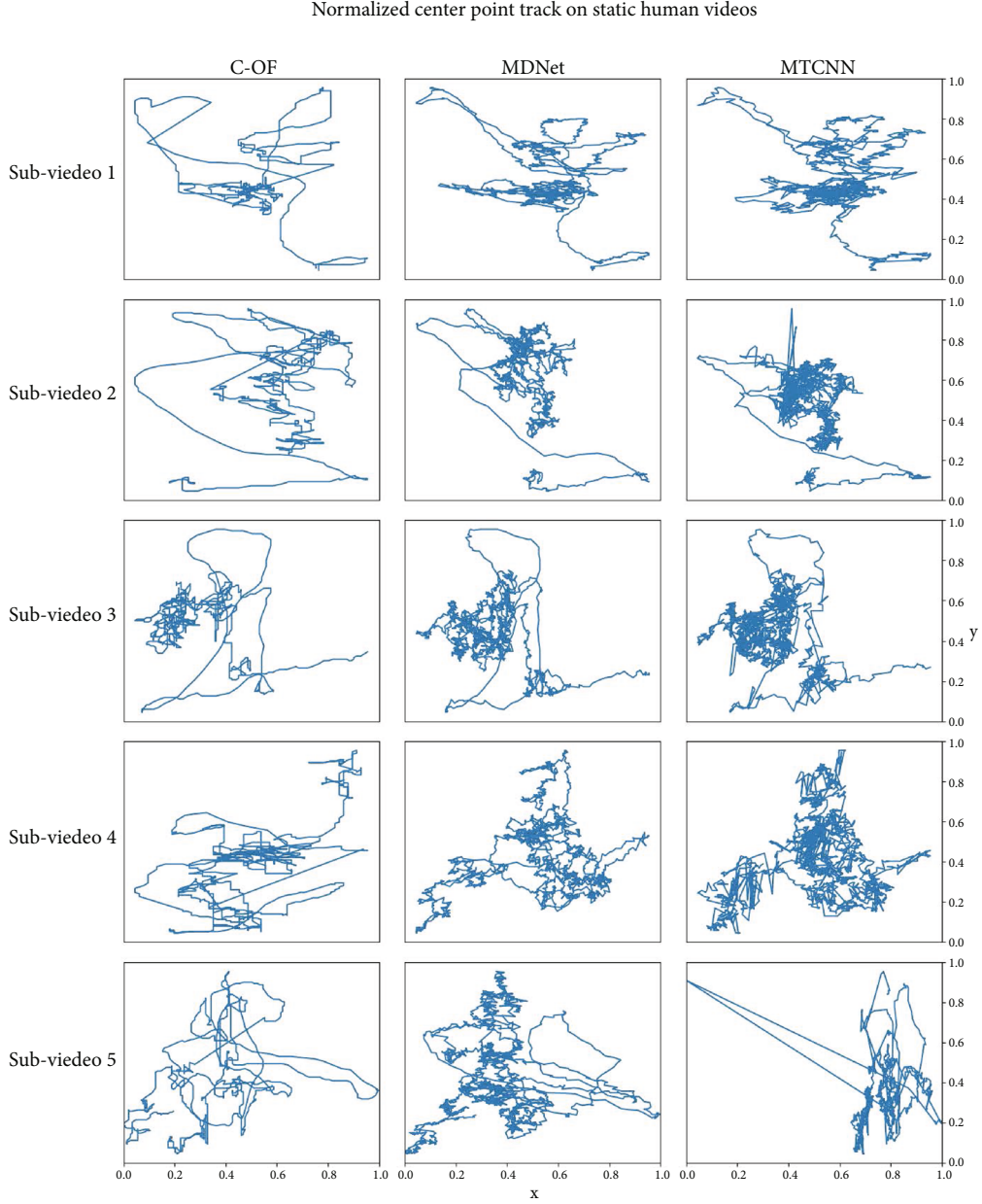


FIGURE 6: Center point motion tracking on static human videos.

quantificate the stability and smoothness of the bounding box. Hence, we naively consider the moving route of the bounding box's corner and center points to evaluate how the bounding box changes along with frames regarding scale and position. We first quantificate the stability by judging the change of width and height and position of the center point:

$$r_n^c = \sqrt{(x_n^c - x_{n-1}^c)^2 + (y_n^c - y_{n-1}^c)^2}, \quad (2)$$

$$\text{Stability} = \frac{1}{3N} \sum_{n=0}^N (|w_n - w_{n-1}| + |h_n - h_{n-1}| + r_n^c), \quad (3)$$

where  $x^c$  and  $y^c$  are the  $x, y$  coordinate of the center point, respectively,  $r^c$  is the absolute moving route of the center

point,  $N$  is the total number of frames, and  $w$  and  $h$  are width and height of the bounding box, respectively. The summation offsets of width, height, and center point illustrate the change of scale and position of bounding box collaboratively. A smaller value means the box moves a short distance or has a little change of width or height. Table 3 gives all the results of stability for MDNet, MTCNN, and C-OF, respectively, on aforementioned four videos with different conditions. It can be viewed that our proposed C-OF significantly outperforms the other two methods in all experiments. Faces in static human videos are the more stable, where the minimum values take in place; for example, MDNet gains its minimum value of 1.425355, MTCNN's is 1.994141, and C-OF's is 0.245097 which is the global minimum value as well. Also, the maximum value of C-OF, which is 0.321575, on static human

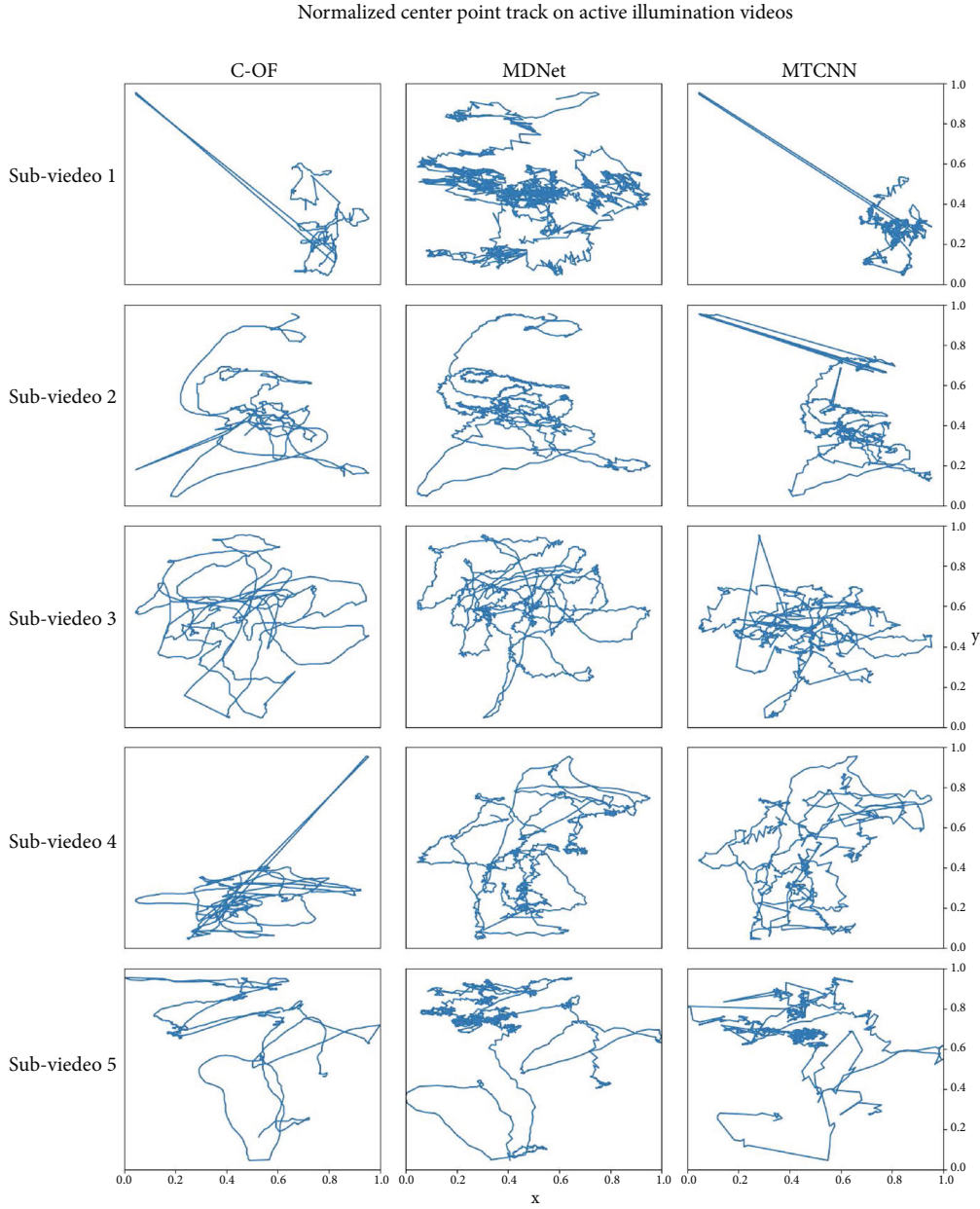


FIGURE 7: Center point motion tracking on active illumination videos.

videos is even smaller than the minimum values of MDNet and MTCNN, which are 1.425355 and 1.994141, respectively.

**4.2.2. Smoothness.** On the other hand, to further quantify the smoothness, we design another function, which mostly focuses on the scale change of the bounding box:

$$R_n = \frac{r_n^{tl} + r_n^{tr} + r_n^{br} + r_n^{bl}}{4}, \quad (4)$$

$$\text{Smoothness} = \frac{1}{N} \sum_{n=0}^N \ln \left( \frac{e^{R_n}}{e^{r_n^c}} \right), \quad (5)$$

where  $r_n^{tl}$ ,  $r_n^{tr}$ ,  $r_n^{br}$ , and  $r_n^{bl}$  are the absolute moving route of top left, top right, bottom right, and bottom left points, respec-

tively. In this function, we empirically consider the ratio of corner and center points' absolute moving routes. By observation, we found that a bounding box that moves a long distance usually comes with a change of its scale. In Equations (4) and (5),  $e^r$  is larger than 1, as  $r$  is a nonnegative value. The mean route of corner point  $R_n$  is larger than the route of center point  $r_n^c$ , so logarithm of the ratio of  $e^{R_n}$  and  $e^{r_n^c}$  is always a nonnegative value. In conclusion, we say that the box that moves a short distance without or with little scale change may gain a smaller value. We report the smoothness values in Table 4, where our proposed C-OF is superior to MDNet and MTCNN all the time.

**4.2.3. Motion Tracking.** The stability and smoothness can be observed clearly on the image sequence, but it is not

TABLE 5: Approximate running time for MDNet, MTCNN, and C-OF on different computing devices and resolutions. CPU refers to *Intel Core i7-8700K*; GPU is *Nvidia GTX TITAN X*.

Method	Language & framework	CPU		GPU	
		320 * 240	640 * 480	320 * 240	640 * 480
MDNet	Python & PyTorch	1362 ms	1334 ms	269 ms	270 ms
MTCNN		15 ms	32 ms	17 ms	22 ms
C-OF (ours)		10 ms	11 ms	11 ms	11 ms
MDNet	C++ & ncnn	—	—	—	—
MTCNN		10 ms	31 ms	—	—
C-OF (ours)		2 ms	3 ms	—	—

convenient to show out the image sequence in a paper. To this end, visualizing the motion tracking of any specific point from the bounding box is a feasible way. Figure 3 shows some visualization examples for the motion tracking of the center point in the bounding box from three methods. It is obvious that the proposed C-OF has far more smooth lines than MDNet and MTCNN, which illustrates that motion tracking of face boxes generated by C-OF is more smooth. In graphs (k) and (l), the outlier means a wrong face box is taken in place. All of the visualization examples are presented in Figures 4–7 for your reference.

**4.2.4. Running Time.** Running time is another principal aspect that commercial applications mostly take into account. Benefitting from lightweight models and optical flow method, our proposed C-OF is super real-time even on CPU, while the typical deep learning model commonly depends on GPU to attain a sufficient performance. Table 5 shows all the experimental results of approximate running time for MDNet, MTCNN, and C-OF on different computing devices and resolutions. The input image is resized to 320 \* 240 resolution. Regarding Python implementations, as MDNet needs to fine-tune the model online, its running time is far slower than the other two methods. Our proposed C-OF is super real-time of approximately 200 FPS and spends 5 ms and 6 ms less than MTCNN on CPU and GPU, respectively. Note that both MTCNN and C-OF have no massively parallel computing, in which case PyTorch using GPU performs worse than using CPU. That is why the running time of MTCNN and C-OF conducted on CPU (15 ms and 10 ms) is faster than GPU (17 ms and 11 ms). Typically, C++ implementation is more common than Python implementation in the industry field, so we also provide a C++ version of C-OF, which is also publicly available. We say C-OF is hyper real-time when using C++ and ncnn. Although benefitting from C++ and ncnn, MTCNN has a speedup from 15 ms to 10 ms on CPU; C-OF has a five times progress from 10 ms to 2 ms and achieves 500 FPS. If we change the input resolution from 320 \* 240 to 640 \* 480, MDNet and C-OF have little running time increment or even a reduction. For MDNet, all the candidate face boxes are cut off, resized to a fixed resolution, and then fed into the model for fine-tuning. So the size of the input image does not matter, cause the number and the size of the candidate face boxes are predefined. In terms of C-OF, the resolution increment definitely may slow down the detector part; how-

ever, it only runs very limited times in one experiment. Other than the detector, optical flow is insensitive to the size of the image, and the identifier is too light to present out the performance loss. On the other hand, MTCNN has a normal running time increment from 15 ms to 32 ms on CPU and 17 ms to 22 ms on GPU as the input image’s resolution changes. For the C++ version, MTCNN has a normal running time increment as well from 10 ms to 31 ms. Same as the Python version, C-OF runs 1 ms more than 320 \* 240 resolution (3 ms vs. 2 ms). Overall, no matter what implementation language or computing devices we use, our proposed C-OF is the fastest one, and the running time is more than sufficient for the commercial application.

## 5. Conclusion

In this paper, we proposed a stable, smooth, super real-time, and long-term face tracking system using lightweight CNN and optical flow, namely, C-OF, which consists of a face detector, face tracker, and face identifier. The method is aimed at solving the bounding box shaking problem, which commonly occurs in deep learning methods. We also optimize the system to make it run faster than most face detection and tracking methods. The experimental results show that C-OF can produce stable and smooth face boxes on a long-term face sequence with super even hyper real time. We design two functions to quantificate the stability and smoothness individually, and C-OF is superior to both MDNet and MTCNN. Meanwhile, we visualize the center point motion tracking of face boxes to observe the path the box goes and conclude that C-OF has a far more stable and smooth path line with a little crook. In the end, we make the Python and C++ implementations of C-OF public available for people who are interested in the work.

## Data Availability

The testing data (20 mp4 files) used to support the findings of this study are included within the article, which also can be downloaded from <https://www.dropbox.com/sh/fcks3k2l9xs36ze/AABlXm3FY3pMzStNrPktYKdRa?dl=0>.

## Conflicts of Interest

The authors declare that they have no conflicts of interest.



## Acknowledgments

This study is supported by the National Key Technology R&D Program of China (No. 2019YFC1606401), Beijing Natural Science Foundation (No. 4202014), and Humanity and Social Science Youth Foundation of Ministry of Education of China (No. 20YJ CZH229).

## References

- [1] Z. Guo, S. Yu, A. K. Bashir, K. Yu, and J. C.-W. Lin, "Graph embedding-based intelligent industrial decision for complex sewage treatment processes," *International Journal of Intelligent Systems*, 2021.
- [2] Z. Guo, K. Yu, A. Jolfaei, A. K. Bashir, A. O. Almagrabi, and N. Kumar, "A fuzzy detection system for rumors through explainable adaptive learning," *IEEE Transactions on Fuzzy Systems*, p. 1, 2021.
- [3] Z. Guo, K. Yu, L. Yu, G. Srivastava, and J. C.-W. Lin, "Deep learning-embedded social internet of things for ambiguity-aware social recommendations," *IEEE Transactions on Network Science and Engineering*, 2021.
- [4] S. K. Lakshmanprabu, K. Shankar, A. Khanna et al., "Effective features to classify big data using social internet of things," *IEEE access*, vol. 6, pp. 24196–24204, 2018.
- [5] Y. Gong, Z. Lin, R. Liu, K. Yu, and G. Srivastava, "Nonlinear mimo for industrial internet of things in cyber-physical systems," *IEEE TII*, vol. 17, no. 8, pp. 5533–5541, 2021.
- [6] W.-L. Shang, J. Chen, H. Bi, Y. Sui, Y. Chen, and H. Yu, "Impacts of covid-19 pandemic on user behaviors and environmental benefits of bike sharing: a big-data analysis," *Applied Energy*, vol. 285, p. 116429, 2021.
- [7] F. Ding, G. Zhu, M. Alazab, X. Li, and Y. Keping, "Deep-learning-empowered digital forensics for edge consumer electronics in 5g hetnets," *IEEE Consumer Electronics Magazine*, p. 1, 2020.
- [8] K. Yu, L. Tan, L. Lin, X. Cheng, Z. Yi, and T. Sato, "Deep-learning-empowered breast cancer auxiliary diagnosis for 5gb remote e-health," *IEEE Wireless Communications*, vol. 28, no. 3, pp. 54–61, 2021.
- [9] Y. Sun, J. Liu, K. Yu, M. Alazab, and K. Lin, "PMRSS: privacy-preserving medical record searching scheme for intelligent diagnosis in iot healthcare," *IEEE Transactions on Industrial Informatics*, p. 1, 2021.
- [10] K. Yu, Z. Guo, Y. Shen, W. Wang, J. C.-W. Lin, and T. Sato, "Secure artificial intelligence of things for implicit group recommendations," *IEEE Internet of Things Journal*, 2021.
- [11] L. Zhen, Y. Zhang, K. Yu, N. Kumar, A. Barnawi, and Y. Xie, "Early collision detection for massive random access in satellite based internet of things," *IEEE Transactions on Vehicular Technology*, vol. 70, no. 5, pp. 5184–5189, 2021.
- [12] K. Yu, M. Arifuzzaman, W. Zheng, D. Zhang, and T. Sato, "A key management scheme for secure communications of information centric advanced metering infrastructure in smart grid," *IEEE Transactions on Instrumentation and Measurement*, vol. 64, no. 8, pp. 2072–2085, 2015.
- [13] K. Sharma, A. Aggarwal, T. Singhania, D. Gupta, and A. Khanna, "Hiding data in images using cryptography and deep neural network," 2019, arXiv preprint arXiv:1912.10413.
- [14] T. Liang, K. Yu, F. Ming, X. Chen, and G. Srivastava, "Secure and resilient artificial intelligence of things: a honeynet approach for threat detection and situational awareness," *IEEE CEM*, p. 1, 2021.
- [15] H. Li, K. Yu, B. Liu, C. Feng, Z. Qin, and G. Srivastava, "An efficient ciphertext-policy weighted attribute-based encryption for the internet of health things," *IEEE Journal of Biomedical and Health Informatics*, 2021.
- [16] L. Tan, K. Yu, N. Shi, C. Yang, W. Wei, and H. Lu, "Towards secure and privacy-preserving data sharing for covid-19 medical records: a blockchain-empowered approach," *IEEE Transactions on Network Science and Engineering*, 2021.
- [17] C. Feng, K. Yu, and M. Aloqaily, "Attribute-based encryption with parallel outsourced decryption for edge intelligent iov," *IEEE TVT*, vol. 69, no. 11, pp. 13784–13795, 2020.
- [18] L. Liu, J. Feng, and Q. Pei, "Blockchain-enabled secure data sharing scheme in mobile-edge computing: an asynchronous advantage actor-critic learning approach," *IEEE Internet of Things Journal*, vol. 8, no. 4, pp. 2342–2353, 2021.
- [19] C. Feng, B. Liu, Z. Guo, K. Yu, Z. Qin, and K.-K. R. Choo, "Blockchain-based cross-domain authentication for intelligent 5g-enabled internet of drones," *IEEE Internet of Things Journal*, 2021.
- [20] J. L. Crowley and F. Berard, "Multi-modal tracking of faces for video communications," in *In Proceedings of IEEE Computer Society Conference on Computer Vision and Pattern Recognition*, pp. 640–645, San Juan, PR, USA, 1997.
- [21] G. R. Bradski, "Real time face and object tracking as a component of a perceptual user interface," in *In Proceedings Fourth IEEE Workshop on Applications of Computer Vision. WACV'98 (Cat. No. 98EX201)*, pp. 214–219, Princeton, NJ, USA, 1998.
- [22] R. J. Qian, M. I. Sezan, and K. E. Matthews, "A robust real-time face tracking algorithm," in *In Proceedings 1998 International Conference on Image Processing. ICIP98 (Cat. No. 98CB36269)*, vol. 1, pp. 131–135, Chicago, IL, USA, 1998.
- [23] K. Schwerdt and J. L. Crowley, "Robust face tracking using color," in *In Proceedings Fourth IEEE International Conference on Automatic Face and Gesture Recognition (Cat. No. PR00580)*, pp. 90–95, Grenoble, France, 2000.
- [24] H. Stern and B. Efron, "Adaptive color space switching for face tracking in multi-colored lighting environments," in *In Proceedings of Fifth IEEE International Conference on Automatic Face Gesture Recognition*, pp. 249–254, IEEE, 2002.
- [25] P. Vadakkepat, P. Lim, L. C. De Silva, L. Jing, and L. L. Ling, "Multimodal approach to human-face detection and tracking," *IEEE Transactions on Industrial Electronics*, vol. 55, no. 3, pp. 1385–1393, 2008.
- [26] Z. Kalal, K. Mikolajczyk, and J. Matas, "Face-ld: tracking-learning-detection applied to faces," in *In 2010 IEEE International Conference on Image Processing*, pp. 3789–3792, Hong Kong, China, 2010.
- [27] Z. Kalal, J. Matas, and K. Mikolajczyk, "Online learning of robust object detectors during unstable tracking," in *In 2009 IEEE 12th International Conference on Computer Vision Workshops, ICCV Workshops*, pp. 1417–1424, Kyoto, Japan, 2009.
- [28] Z. Kalal, K. Mikolajczyk, and J. Matas, "Tracking-learning-detection," *IEEE Transactions on Pattern Analysis and Machine Intelligence*, vol. 34, no. 7, pp. 1409–1422, 2012.
- [29] Z. Kalal, J. Matas, and K. Mikolajczyk, "Weighted sampling for large-scale boosting," in *BMVC*, 2008.
- [30] A. Ranftl, F. Alonso-Fernandez, and S. Karlsson, "Face tracking using optical flow," in *In 2015 International Conference*



- of the Biometrics Special Interest Group (BIOSIG), pp. 1–5, Darmstadt, Germany, 2015.
- [31] P. Viola and M. Jones, “Rapid object detection using a boosted cascade of simple features,” in *In Proceedings of the 2001 IEEE computer society conference on computer vision and pattern recognition. CVPR 2001*, vol. 1, Kauai, HI, USA, 2001.
- [32] Y. Lin, J. Shen, S. Cheng, and M. Pantic, “Ft-rcnn: real-time visual face tracking with region based convolutional neural networks,” in *In 2020 15th IEEE International Conference on Automatic Face and Gesture Recognition (FG 2020)(FG)*, pp. 267–274, Buenos Aires, Argentina, 2020.
- [33] S. Ren, K. He, R. Girshick, and J. Sun, “Faster r-cnn: towards real-time object detection with region proposal networks,” *IEEE Transactions on Pattern Analysis and Machine Intelligence*, vol. 39, no. 6, pp. 1137–1149, 2017.
- [34] Y. Freund and R. E. Schapire, “A decision-theoretic generalization of on-line learning and an application to boosting,” in *In European conference on computational learning theory*, pp. 23–37, Springer, 1995.
- [35] P. Viola and M. J. Jones, “Robust real-time face detection,” *International Journal of Computer Vision*, vol. 57, no. 2, pp. 137–154, 2004.
- [36] S. Charles Brubaker, J. Wu, J. Sun, M. D. Mullin, and J. M. Rehg, “On the design of cascades of boosted ensembles for face detection,” *International Journal of Computer Vision*, vol. 77, no. 1-3, pp. 65–86, 2008.
- [37] S. Liao, “A fast and accurate unconstrained face detector,” *IEEE Transactions on Pattern Analysis and Machine Intelligence*, vol. 38, no. 2, pp. 211–223, 2016.
- [38] M.-T. Pham and T.-J. Cham, “Fast training and selection of haar features using statistics in boosting based face detection,” in *In 2007 IEEE 11th International Conference on Computer Vision*, pp. 1–7, IEEE, 2007.
- [39] P. F. Felzenszwalb, R. B. Girshick, D. McAllester, and D. Ramanan, “Object detection with discriminatively trained part-based models,” *IEEE Transactions on Pattern Analysis and Machine Intelligence*, vol. 32, no. 9, pp. 1627–1645, 2009.
- [40] X. Zhu and D. Ramanan, “Face detection, pose estimation, and landmark localization in the wild,” in *In 2012 IEEE conference on computer vision and pattern recognition*, pp. 2879–2886, Providence, RI, USA, 2012.
- [41] M. Mathias, R. Benenson, M. Pedersoli, and L. Van Gool, “Face detection without bells and whistles,” in *In European conference on computer vision*, pp. 720–735, Springer, 2014.
- [42] J. Yan, Z. Lei, L. Wen, and S. Z. Li, “The fastest deformable part model for object detection,” in *In Proceedings of the IEEE Conference on Computer Vision and Pattern Recognition*, pp. 2497–2504, Columbus, OH, USA, 2014.
- [43] A. Krizhevsky, I. Sutskever, and G. E. Hinton, “ImageNet classification with deep convolutional neural networks,” *Communications of the ACM*, vol. 60, no. 6, pp. 84–90, 2017.
- [44] C. Zhu, Y. Zheng, K. Luu, and M. Savvides, “Cms-rcnn: contextual multi-scale regionbased cnn for unconstrained face detection,” in *In Deep learning for biometrics*, pp. 57–79, Springer, 2017.
- [45] H. Wang, Z. Li, X. Ji, and Y. Wang, “Face r-cnn,” 2017, arXiv preprint arXiv:1706.01061.
- [46] C. Zhang, X. Xu, and T. Dandan, “Face detection using improved faster rcnn,” 2018, arXiv preprint.arXiv:1802.02142.
- [47] W. Liu, D. Anguelov, and D. Erhan, “Ssd: single shot multibox detector,” in *In European conference on computer vision*, pp. 21–37, Springer, 2016.
- [48] S. Zhang, X. Zhu, Z. Lei, H. Shi, X. Wang, and S. Z. Li, “Face-boxes: a cpu real-time face detector with high accuracy,” in *In 2017 IEEE International Joint Conference on Biometrics (IJCB)*, pp. 1–9, Denver, CO, USA, 2017.
- [49] J. Zhang, X. Wu, S. C. H. Hoi, and J. Zhu, “Feature agglomeration networks for single stage face detection,” *Neurocomputing*, vol. 380, pp. 180–189, 2020.
- [50] T.-Y. Lin, P. Dollár, and R. Girshick, “Feature pyramid networks for object detection,” in *In Proceedings of the IEEE conference on computer vision and pattern recognition*, pp. 2117–2125, 2017.
- [51] K. Zhang, Z. Zhang, Z. Li, and Q. Yu, “Joint face detection and alignment using multitask cascaded convolutional networks,” *IEEE Signal Processing Letters*, vol. 23, no. 10, pp. 1499–1503, 2016.
- [52] X. Shi, S. Shan, M. Kan, S. Wu, and X. Chen, “Real-time rotation-invariant face detection with progressive calibration networks,” in *In Proceedings of the IEEE Conference on Computer Vision and Pattern Recognition*, pp. 2295–2303, Salt Lake City, UT, USA, 2018.
- [53] J. Deng and X. Xie, “Nested shallow cnn-cascade for face detection in the wild,” in *In 2017 12th IEEE International Conference on Automatic Face & Gesture Recognition (FG 2017)*, pp. 165–172, Washington, DC, USA, 2017.
- [54] C. Li, X. Liang, Y. Lu, N. Zhao, and J. Tang, “Rgb-t object tracking: benchmark and baseline,” *Pattern Recognition*, vol. 96, p. 106977, 2019.
- [55] A. Milan, L. Leal-Taixé, I. Reid, S. Roth, and K. Schindler, “Mot16: a benchmark for multi-object tracking,” 2016, arXiv preprint arXiv:1603.00831.
- [56] H. Fan, H. Ling, L. Lin et al., “Lasot: a high-quality benchmark for large-scale single object tracking,” in *In Proceedings of the IEEE conference on computer vision and pattern recognition*, pp. 5374–5383, Long Beach, CA, USA, 2019.
- [57] F. João, R. C. Henriques, P. Martins, and J. Batista, “Exploiting the circulant structure of tracking-by-detection with kernels,” in *In European conference on computer vision*, pp. 702–715, Springer, 2012.
- [58] D. S. Bolme, J. R. Beveridge, B. A. Draper, and Y. M. Lui, “Visual object tracking using adaptive correlation filters,” in *In 2010 IEEE computer society conference on computer vision and pattern recognition*, pp. 2544–2550, San Francisco, CA, USA, 2010.
- [59] M. Danelljan, G. Häger, F. S. Khan, and M. Felsberg, “Discriminative scale space tracking,” *IEEE Transactions on Pattern Analysis and Machine Intelligence*, vol. 39, no. 8, pp. 1561–1575, 2017.
- [60] D. Held, S. Thrun, and S. Savarese, “Learning to track at 100 fps with deep regression networks,” in *In European Conference on Computer Vision*, pp. 749–765, Springer, 2016.
- [61] Z. Zheng, Q. Wang, and B. Li, “Distractor-aware Siamese networks for visual object tracking,” in *In Proceedings of the European Conference on Computer Vision (ECCV)*, pp. 101–117, 2018.
- [62] H. Nam and B. Han, “Learning multi-domain convolutional neural networks for visual tracking,” in *In Proceedings of the IEEE conference on computer vision and pattern recognition*, pp. 4293–4302, Las Vegas, NV, USA, 2016.

- [63] J. Long, E. Shelhamer, and T. Darrell, "Fully convolutional networks for semantic segmentation," in *In Proceedings of the IEEE conference on computer vision and pattern recognition*, pp. 3431–3440, Boston, MA, USA, 2015.
- [64] J.-Y. Bouguet, "Pyramidal implementation of the affine Lucas Kanade feature tracker description of the algorithm," *Intel corporation*, vol. 5, 2001.
- [65] A. Paszke, S. Gross, and F. Massa, "Pytorch: an imperative style, high-performance deeplearning library," 2019, arXiv preprint arXiv:1912.01703.

## Research Article

# Internet of Things-Based Smart Electricity Monitoring and Control System Using Usage Data

Mohammad Kamrul Hasan <sup>1</sup>, Musse Mohamud Ahmed,<sup>2</sup> Bishwajeet Pandey <sup>3</sup>,  
Hardik Gohel,<sup>4</sup> Shayla Islam <sup>5</sup> and Izzul Fitrie Khalid<sup>2</sup>

<sup>1</sup>Network and Communication Lab, Center for Cyber Security, Faculty of Information Science and Technology, Universiti Kebangsaan Malaysia (UKM), 43600 UKM, Bangi, Selangor, Malaysia

<sup>2</sup>Department of Electrical and Electronics Engineering, Universiti Malaysia Sarawak, 94300 Kota Samarahan, Sarawak, Malaysia

<sup>3</sup>Department of Computer Science and Engineering, Gyancity Research Ltd., India

<sup>4</sup>Department of Computer Science, University of Houston-Victoria, 3007 N. Ben Wilson, St. Victoria, TX 77901, USA

<sup>5</sup>Institute of Computer Science and Digital Innovation, UCSI University, 56000 Kuala Lumpur, Malaysia

Correspondence should be addressed to Mohammad Kamrul Hasan; [hasankamrul@ieee.org](mailto:hasankamrul@ieee.org) and Shayla Islam; [shayla@ucsiuniversity.edu.my](mailto:shayla@ucsiuniversity.edu.my)

Received 5 June 2021; Accepted 14 September 2021; Published 27 October 2021

Academic Editor: Deepak Gupta

Copyright © 2021 Mohammad Kamrul Hasan et al. This is an open access article distributed under the Creative Commons Attribution License, which permits unrestricted use, distribution, and reproduction in any medium, provided the original work is properly cited.

In everyday life, electricity is necessary, and proper use is critical. To strengthen home electricity control, the existing systems have been examined over the years. However, the existing PMAS method's error ratio is higher and does not allow for a remote monitoring system. Therefore, this study proposes a smart monitoring and control system (SMACS) for household appliances. The application's significance is to monitor household appliances' electricity usage using hardware and the Internet of Things (IoT) methods. The prototype of the proposed system is designed and developed considering Arduino UNO, a liquid crystal display (LCD), an ACS712 current sensor module, relays, and AC sources. The components are selected from the software library, and the simulation results are found the same as the prototype. WiFi module ESP8266 is not included in the design because it is not provided in the system. The data is recorded in cloud storage using Thing-speak. A mobile application (Virtuino) also accesses the data to visualize it through the graphical and numerical display. This study provides users with an easy system to monitor and control household appliances' power consumption using mobile applications. Results show that the proposed system provides 0.6% current errors for the hairdryer appliance, whereas the existing Power Monitoring and Switching (PMAS) system provides 7.8% current errors.

## 1. Introduction

In Malaysia, electricity has the highest demand as it is expected to increase gradually in years to come, in line with the expansion of urbanization, rapid industrialization, and the growing population of the country. Statistically, residential sectors consume up to 48% of the energy globally [1]. Around 40% of Malaysia's buildings' energy is divided into commercial buildings and residential buildings [1]. In this modern era, people utilize household appliances with new technologies. In Malaysia, on average, 20 to 30 electrical

household appliances are used in homes [2]. A vast majority of household appliances consume a large amount of power and energy. Consumers mostly tend to leave their lights, fans, freezer, air conditioner, and other appliances turned on when they are not in use, resulting in energy wastage, a tendency of human behaviour [3].

This negligence concerning the consumers' behaviour can lead to excessive power consumption and wastage of the electrical energy needed, and it can shorten the life span of household appliances such as hair dryer, dry iron, induction and rice cooker, water heater, microwave oven, air

conditioner, and television. It has been identified that old appliances contribute to higher energy consumption than newer ones.

This paper presents an integration of both hardware and software. The software is used to monitor power usage and the consumption of household appliances and control systems through overcurrent relay and notification of any mismatches. The developed system consists of Arduino UNO, a WiFi module (ESP8266), a relay, a low current sensor breakout (ACS712), and a liquid crystal display (LCD). Arduino UNO is a microcontroller used to program customized coding for executing output at any instant time. It is also a very capable microcontroller that receives and sends information over the Internet with various modules and shield platforms. However, in this case, the ESP8266 WiFi module is used as the platform. The ESP8266 WiFi module is famous for its IoT applications. The relay function performs the cut-off current and the isolation of input and output operations and performs switching functions. The outputs are shown in 2 ways: LCD and IoT implementation based on the web server or mobile application (APPS). LCD is used to display the voltage, current, and power consumption where the web or mobile application is used to visualize the data and trigger alarm, when necessary. In the web and mobile application systems, the energy usage statistics of power consumption parameters are determined. It displays the detailed monitoring of electrical quantities such as voltage, current, power, and energy.

IoT attaches the internet connectivity and remote control of mobile devices, integrated with a range of sensors, to the smart home appliances. Sensors can be embedded in the refrigerator, air conditioner, and lighting, and other environmental sensors can be connected to home-related gadgets. The overcurrent or circuit overloading can be detected earlier based on advanced IoT applications where consumers' alarm triggers.

The significance of SMACS is that it creates an opportunity for consumers to control their power consumption practices and help them manage their power and energy usage. It also creates an opportunity for the consumers to practice energy saving and to keep track of their household appliance's performances and current behaviour to prevent overcurrent. Therefore, the main challenge will be designing an efficient technique that can monitor power consumption in residential buildings.

## 2. Literature Review

A brief overview of the related techniques and literature on the study's scope is discussed in this section. Four (4) components are discussed, such as a monitoring system, a control system, IoT implementation, and other related techniques.

Nowadays, people's dependency on electricity is extreme, as power consumption has increased for the past few years [4]. It is imperative to consider monitoring and measuring the electric system or appliances that operate every day for residential and commercial buildings. As the focus of this article, the residential sectors are made up of

small energy consumers and users, such as houses and apartments. The research suggested that the residential energy consumers [5] waste 41% of the power supplied to their homes. Various research and trials have been shown that on average, savings of 7.8% to 16.7% home energy can be achieved by using a home energy monitoring system [6, 7]. Several case studies have been shown that energy consumption can be reduced by modifying the lifestyle with proper habits/behaviours [8–10].

A node microcontroller unit (NodeMCU) with a WiFi-based gateway has been used to connect different sensors and update their data to the Adafruit IO cloud server [11]. A power monitoring system can help users or consumers monitor their usage of electricity efficiently. Improvement of electricity efficiency usage can be made by reduction due to changing habits [12]. In this modern era, monitoring systems must sort the data, record data in the system, exploit them to get the intrinsic information shown in legit and innovative ways, and access the Internet to efficiently visualize it [13]. A power monitoring system can be considered a user-friendly and unified solution for reliable electricity management [14]. This system can help users to change their use by providing real-time feedback [15].

The control system is a system that can control other things depending on what needs to be controlled. Local and remote control are included in the control application. Local control is an action that the control unit will take on its own, and remote control is a mechanism that remotely controls the IoT-based system [15]. Electrical equipment operational status monitoring will reduce the cost of building power consumption and increase buildings' electrical energy to a reasonable and efficient ratio [16]. As all can be managed, control systems can help consumers handle their energy more effectively and efficiently. The control system controls the current in this study, which will be cut off if an overcurrent is found. This control system can raise awareness of the consumption of household appliances among users.

Technology is one of the main reasons for a country to become a well-developed country. Innovations and technology can likely change people's lives and make the world more sustainable and inclusive. Internet of Things, known as IoT, is a new and ever-growing network that is becoming a hot topic in people's conversations in the era of modern technology. IoT is a wide-open and complete network of smart and intelligent objects that has the full capability and capacity to autoorganize; share information, data, and resources; and act and react to any circumstances or atmosphere of the changing environment [17–22]. IoT is growing and needs to be sustained so that it will be the expanded, innovative concept in the IT world. IoT advancement controls the real Thing that will transform the Internet into a fully integrated Future Internet [23]. Future information communication technology is to be used with embedded sensors. The target applications are smart metering, Internet-connected sensor devices for household appliances, emphasizing the benefits of remote real-time monitoring for household energy consumption appliances [13, 24–30]. The IoT applications have already brought attention to and shown the

performance of monitoring modern household appliances' energy usage toward a sustainable and improved quality of urban lifestyle. IoT is beneficial and recommended in smart home applications [31–33]. It has improvised our quality of life and also can reduce the unnecessary costs of daily life. This wellness system has been implemented for many great things and monitoring and controlling the electricity at home. The information is uploaded to the website by a server using the cloud server's local home gateway. However, security and privacy challenges have been raised due to the reliability and dependability issues of the Internet. This is because of some connections between the cyber environment and physical environment to fulfill the consumers' demands. It is presumed that these problems will indeed be solved in the future [34], as shown in Figure 1.

Even though IoT is an intelligent technology that makes people's lives more comfortable, IoT-connected systems might lack a comprehensive platform if applications of individual items are not transformed. These separate individual applications are combined into a single infrastructure, where a platform can be used in the future for data mining and extraction of knowledge [32]. As far as IoT is concerned, the future of IoT will be the best and advanced in the sensing services; communications; and in monitoring, controlling, and producing information from vast amounts of data [8]. Gartner, a technology consulting company, is concerned in predicting the future of technology trends, especially the Internet of Things for smart homes, smart industries, agriculture, healthcare, and autonomous vehicle applications [35–40].

The energy that is mainly being used and consumed in the residential areas is primarily on water heating, lighting, air conditioner, refrigerator, and more. Precisely, in Malaysia, it can be predicted that only a small amount of energy is consumed during office hours between 0800 hours and 1700 hours. However, peak demand reaches mainly at night, where all the people gather around having dinner, watching television, and more. Yet, their power rating can be categorized as household appliances, where Table 1 shows the average household item power rating [39–42].

Moreover, household appliances can also be divided into three (3) parts: inductive, capacitive, and resistive. Resistive load-based heating appliances have the highest energy consumption as compared to inductive and capacitive household appliances. Air conditioners and washing machines use inductive and capacitive loads that can be considered reactive loads. They have lower consumption than the resistive-based loads, but the resistive load's power factor is one. The load needs more current to satisfy the real power requirement if the power factor is low, and most consumers are not aware of it as the electricity bills are basically in energy (kWh) [43].

**2.1. Related Works and the Research Challenges.** In this section, related IoT-based electricity monitoring systems are discussed and explained. The development of these projects has led the world to a better future in saving electricity, practicing energy saving, and making electricity usage very effective and efficient.

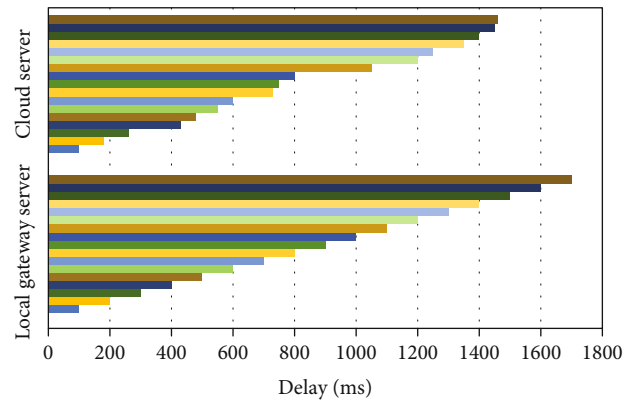


FIGURE 1: Final information uploading delay for cloud and local home gateway approach [34].

Smart Power Monitoring and Analysis is aimed at developing a solution to keep track of every electrical appliance and monitor the energy used consumed by an Android device. As mentioned, this study's main problem statement is that most of the power meters installed in any residential buildings showed the total consumption of the electricity used. It does not mention which appliances contributed to the usage of most electricity. The goal is at least to lower the electricity bills and energy consumption by 30% to 40%. This can be achieved by a proper monitoring system that allows item-wise energy consumption monitoring and can regulate lifestyle with usage habits [9]. The architecture used only current sensors to measure all the parameters needed and a microcontroller as the system. The data collected and monitored were stored in a central cloud server instantly for some analysis. The IoCare IoT module has been used on the WiFi board with a microcontroller [44]. Authors have presented a system with mobile apps to collect energy consumption data. This study's performance was satisfied as the electricity consumption is successfully shown in their smartphone apps in meters and numeric form; however, a real-time analytical value of the energy or the power consumed has not existed in the system. This application can help a single user forecast energy use and billing with reliable accuracy comprehensively, manage the unnecessary waste of energy consumption and optimize electricity use from a mass-user perspective [44].

As mentioned in this paper, the primary source of the development and advancement of technology in this world is electric energy. There is a demand for it from both domestic and industrial sectors. As stated in the annual energy report, the demand for electricity in homes is expected to increase by 24% [30]. As in recent years, wireless sensor networks (WSNs) have experienced rapid growth. WSNs are incredibly flexible and provide an exciting opportunity to advance the future of home automation. An IoT-based intelligent energy management system using WSN is a project implemented as IoT for a home appliance monitoring system and real-time power management system. This system integrates WSN and Web Service communications to comprehend the management of a power and information



TABLE 1: Average household item power rating [39–42].

No	Item	Rating (Watt)
1	Television—Samsung	150.00
2	Television—Sony	125.00
3	Air conditioner—Panasonic	600.00
4	Air conditioner—Panasonic 2	500.00
5	Air conditioner—Daikin	800.00
6	WiFi modem	10.00
7	Cable TV setup box	25.00
8	Internet modem	10.00
9	Refrigerator	150.00
10	Water heater	1,000.00
11	Microwave	600.00
12	Dispenser	600.00
13	Dishwasher	1,200.00
14	LED light bulbs—7	7.00
15	LED light bulbs—9	9.00
16	Incandescent light bulbs—60	60.00
17	Incandescent light bulbs—80	80.00
18	Washing machine	500.00
19	Vacuum cleaner	200.00
20	Electric iron	400.00
21	Rice cooker	400.00
22	Toaster	600.00
23	Laptop	50.00
24	Printer	20.00
25	Scanner	10.00
26	Desktop computer—Apple	100.00
27	Mobile phone charger—Samsung	3.00
28	Mobile phone charger—iPhone	3.00
29	Water pump	400.00
30	Electric saver	15.00
31	Lawn mower	1,000.00
32	Food blender	300.00
33	Hair dryer	400.00
34	Coffee maker	600.00

provider using the IoT platform. The proposed system for this project is to use the current sensor and voltage sensors for calculation purposes. Figures 2 and 3 refer to the functional description of the system developed. Data is transferred wirelessly with ZigBee (ZigBee Ethernet shield receivers via serial port). The data collected from the Ethernet shield is sent using the WiFi router to the LAN. The system is controlled and monitored remotely [45].

The aim of this research is consistent with SMACS, but this method uses ZigBee and Ethernet.

Ethernet is able to connect to an Ethernet network as either a client or a server [37]. The proposed project uses WiFi module ESP8266, which is a transceiver module compared to the ZigBee module.

Electrical engineers have to conserve energy in this world as everyone demands electrical energy at any point in the

human life cycle. The proposed system designs an autonomous system capable of controlling electricity flow, reducing consumption, and collecting and transmitting maximum and dynamic loads. The system consists of five parts: tracking, calculating, monitoring, regulating, and electrical safety of the power system.

Power system monitoring is a robust, reliable, and highly accurate energy management system, while metering is the important system in which data and information are acquired and presented in the database in real time. The measurements indicate the voltage, current, frequency, active power, reactive power, and apparent power. Monitoring and control is the management of information, and the application of a control system involves the maintenance of information.

Electrical protection is also included in this system to protect the equipment and the personnel and avoid extensive damage caused by faults as it can monitor a large-scale system that is a substation. The proposed system for this project is as follows:

- (1) Voltage sensing by using a voltage transformer
- (2) Measure current via current sensors
- (3) Zero crossing technique used for sensing frequency
- (4) Voltage and current signal are used for power factor estimation
- (5) The load will be tripped when the current event exceeds the set value
- (6) A generator will be switched on and the load will be shifted when there is a shutdown

There are two parts of this study that are crucial for references: the voltage divider circuit and the current divider circuit. The voltage divider circuit is used to scale down the waveform, and an offset is added when there is no harmful component. Single-phase voltage is monitored and calculated by stepping down to 12 V of 240 V [14]. On the other hand, the current is measured using the current transformer sensor where the current transformer sensor with burden resistors and biasing voltage dividers (R1 and R2) is used to achieve the wave of the current divider [14]. Therefore, the system design uses the Arduino microcontroller, where a single-phase voltage and current are measured. The corresponding frequency (50 Hz), power factor, apparent power (KVA), reactive power (KVAR), and real power (KW) are found by calculating the value shown in the LCD [14].

This proposal is close to SMACS as the system for both similar. The main difference between this work [16] and SMACS is that the existing system focused on a bigger scale of the electrical system, a substation, whereas SMACS is narrowed down to the minor part in household electrical appliances. The significance of a microcontroller-based power monitoring and switching device for appliances over a ZigBee Network is the development of a system that can help users be more aware of their appliances' consumption. Another focus of PMAS is storing data and monitoring

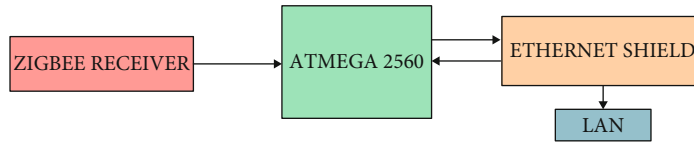


FIGURE 2: Receiver section of smart power management system [32].

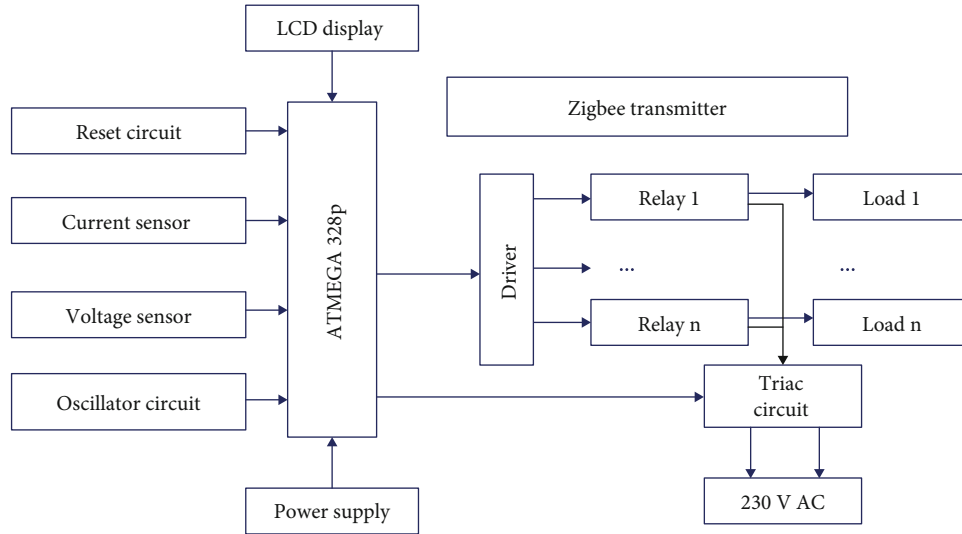


FIGURE 3: Transmitter section of smart power management system [45].

consumption based on the android app. The microcontroller will read the current and transverse parameters on the android app: voltage, current, and power. Zigbee is used to transmit data but in a small range of frequencies. The gateway sends and receives data to the web server and mobile application [46]. The design is partly divided into adapters, central hubs, databases, and android applications. The adapter consists of the current sensor ACS712, the same current module used in the proposed system. The data is shown in Table 2, where the data collected are based on four appliances.

Table 2 shows the reading from the multimeter compared to the reading with the PMAS converter. It was not far from accurate, but there were some errors in the system. Developing Arduino-based IoT measurement system for energy on-demand monitoring is a system that offers cost optimization for energy use in Nigeria. The solution expected in the residential area of Nigeria is supposed to monitor the use of energy that can be stored in a database to access historical data to create awareness [47]. The primary component used in this paper is the ACS712 current sensor which measures both the alternating current and the direct current. The components used include Arduino UNO, an LCD, a ACS712 current sensor, a  $4 \times 4$  matrix calculator, and a GSM module. This system can be monitored on the LCD screen and also on the Cloud Application Consumer web server.

It was designed using the HTML/PHP script. The GSM module can also monitor the data, where the data will be texted to the numbers installed. The system was limited to a small communication range.

TABLE 2: Average current reading on a multimeter without PMAS and on one with a PMAS adapter [46].

Appliances	Current reading from multimeter (A)	Current reading with PMAS adapter
Air conditioner	12.5	12.9
Hair dryer	5.1	5.5
Induction cooker	3.7	3.8
Microwave	5.05	5.1

The authors have designed a home control and monitoring system where this system was developed as an embedded micro web server and a remote application by using a smartphone. This project is aimed at reducing costs and saving energy. Other than that, the authors wanted to control the device and the home environments were also being monitored to maintain the amount of desired energy consumption. Arduino UNO with the ESP 8266 WiFi module and the clamp current transformer with relay have been used for the appliances. A different AT command should also be presented by GSM-based communications as well as home control. The disadvantage of the system is that consumers are not given any user interface to display, and users have to remember the AT command to control the connected device. The architecture is shown in Figure 4 [48].

The implementation of the system is divided into two parts that are implemented and combined. It consists of

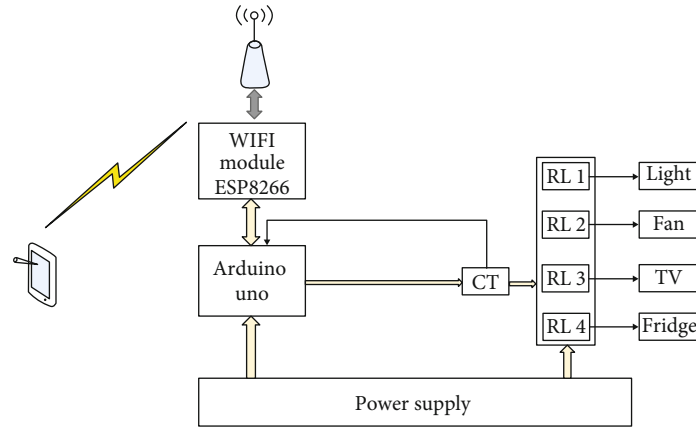


FIGURE 4: The block diagram of IoT-based control [48].

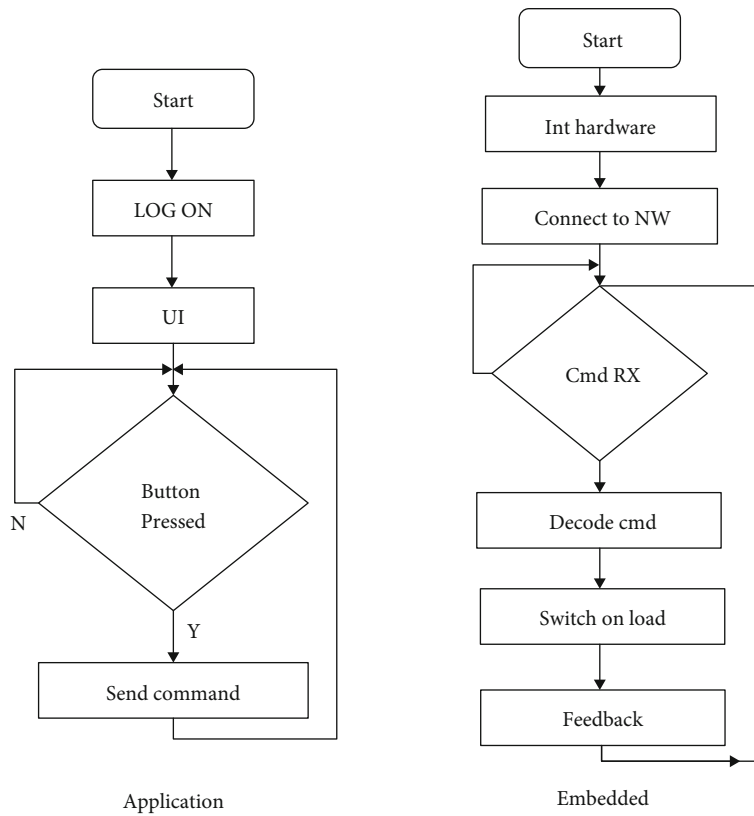


FIGURE 5: The flowchart of the IoT-based control.

mobile phones, an android application for the app part, and an Arduino board with a WiFi module in the home gateway for the second embedded part. Figure 5 shows the suggested flow diagram for both systems, respectively.

This study’s advantages are that it can reduce human efforts, save power, and low cost. This project’s application is a control and monitoring system using different home appliances based on IoT, and this system can be improved further for industrial purposes. It can also be used in offices by using the mobile application [46]. The authors found that a current transformer is not efficient because the reading was

not directly from the cable. The impacts of this research in comparison with the proceeding technology in the context of sustainability are summarized below:

- (i) Bigger data storage that increases the communication speed by using the WiFi module ESP8266 instead of using ZigBee communication technology
- (ii) Targeting IoT sustainable technology that evolves with future upgrading
- (iii) Low cost and less complicated technology

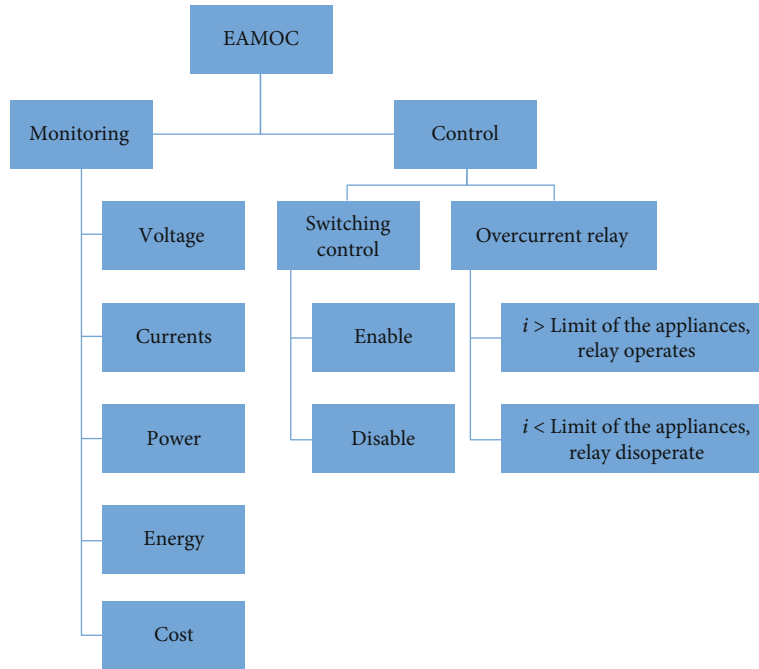


FIGURE 6: Flow diagram of a low-cost Smart HAMCoS based on IoT.

(iv) Real-time usage and fulfilling customer requirements

IoT application to the electrical systems opens the opportunities for short, medium, and long-term adaptation processes, which takes its course as smart technology can be driven from household appliances to the large-scale industry. As seen from the results achieved from this research work, IoT proves real practical application capabilities, leading to sustainable and mature technology.

**2.2. Research Gaps.** Based on the literature review, the electricity usage monitoring system is aimed at creating awareness for users to be more concerned with energy consumption in the home in general and every appliance specifically. The research was conducted for the monitoring system in which monitoring rules on IoT can be more efficient and manageable. Based on the papers reviewed, there are conflicting results among the authors. The WiFi communication unit used in the monitoring system is the Zigbee transmitter as it is designed to transmit a small amount of data over a short distance from the network. It is considered to be slow as the maximum speed is 250 kbps. However, Zigbee has an inoperability problem where it can interfere with one and another. The main research question is what design considerations and techniques need to be focused on controlling the power consumption in residential buildings. More studies are needed to find a better solution that can handle bulk data in the long-distance network and efficiently monitor the energy of house appliances. The existing works using sensors in the system are yet to function efficiently as the sensor in direct contact. As a result, the percentage of error increases in monitoring the current units for the household appliances. A more in-depth study is required to find a better solution to get accurate results.

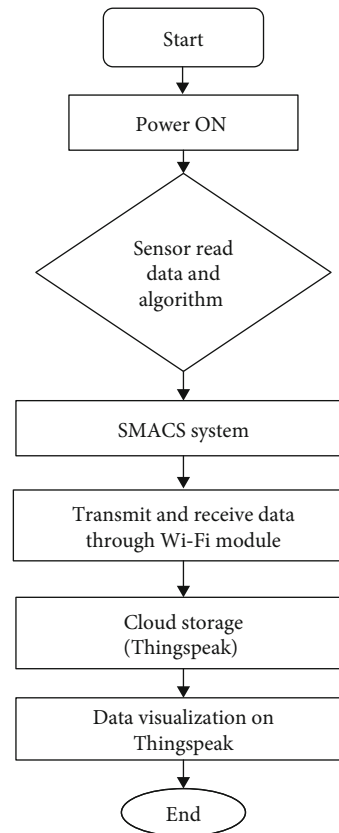


FIGURE 7: The flowchart of SMACS system.

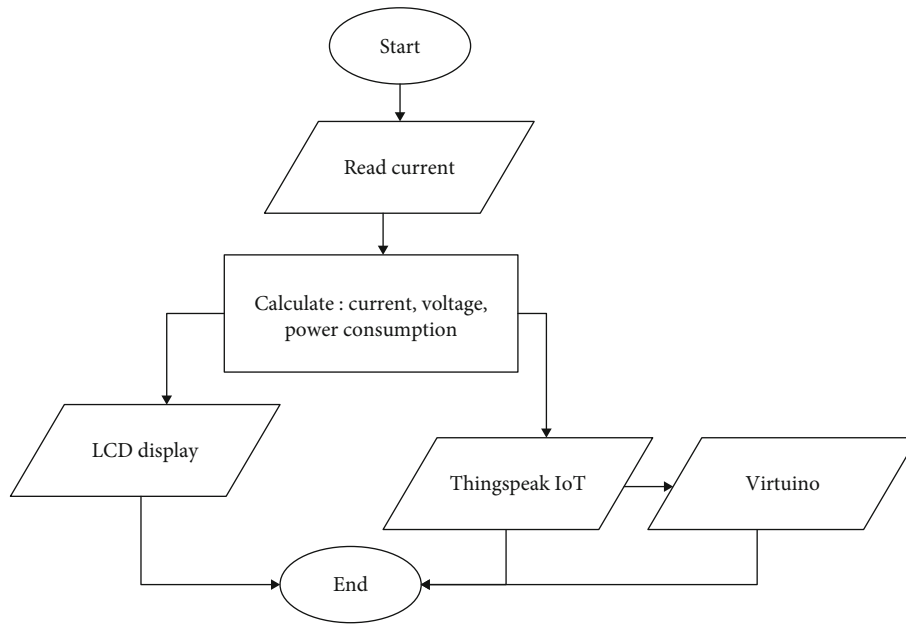


FIGURE 8: Monitoring system of SMACS flowchart.

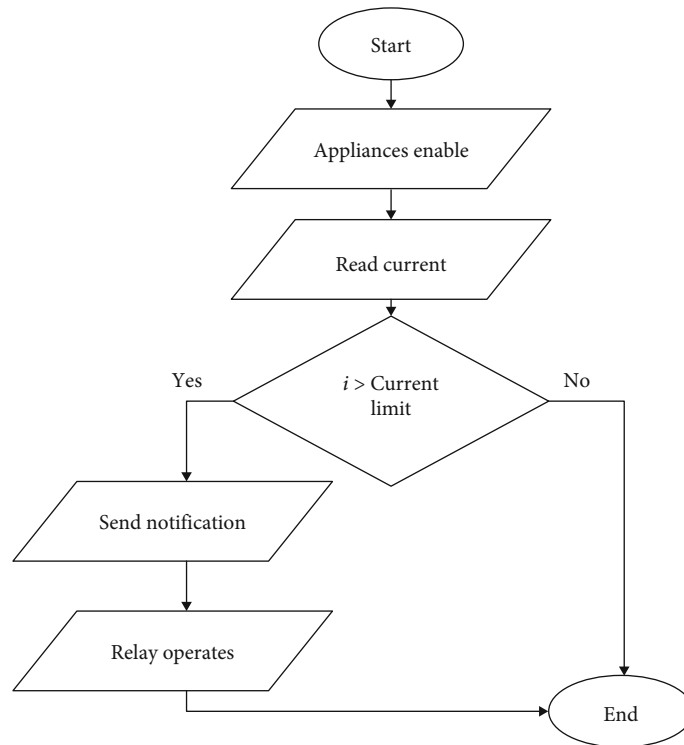


FIGURE 9: Control system of SMACS.

### 3. Materials and Methods

The developed SMACS in this paper discussed the monitoring system, control system, implementation of IoT, appliances, and basic electrical theory. Figure 6 presents the proposed flow diagram, consisting of five specific parts that are explained in the following discussion.

*3.1. Monitoring System.* Since the user appliances and the power consumption have increased in residential and commercial sectors, it is imperative to monitor and measure the electric system and appliances. As the focus of this study, the residential sectors are made up of small energy consumers and users, such as houses and apartments [34]. A power monitoring system can help users or consumers to



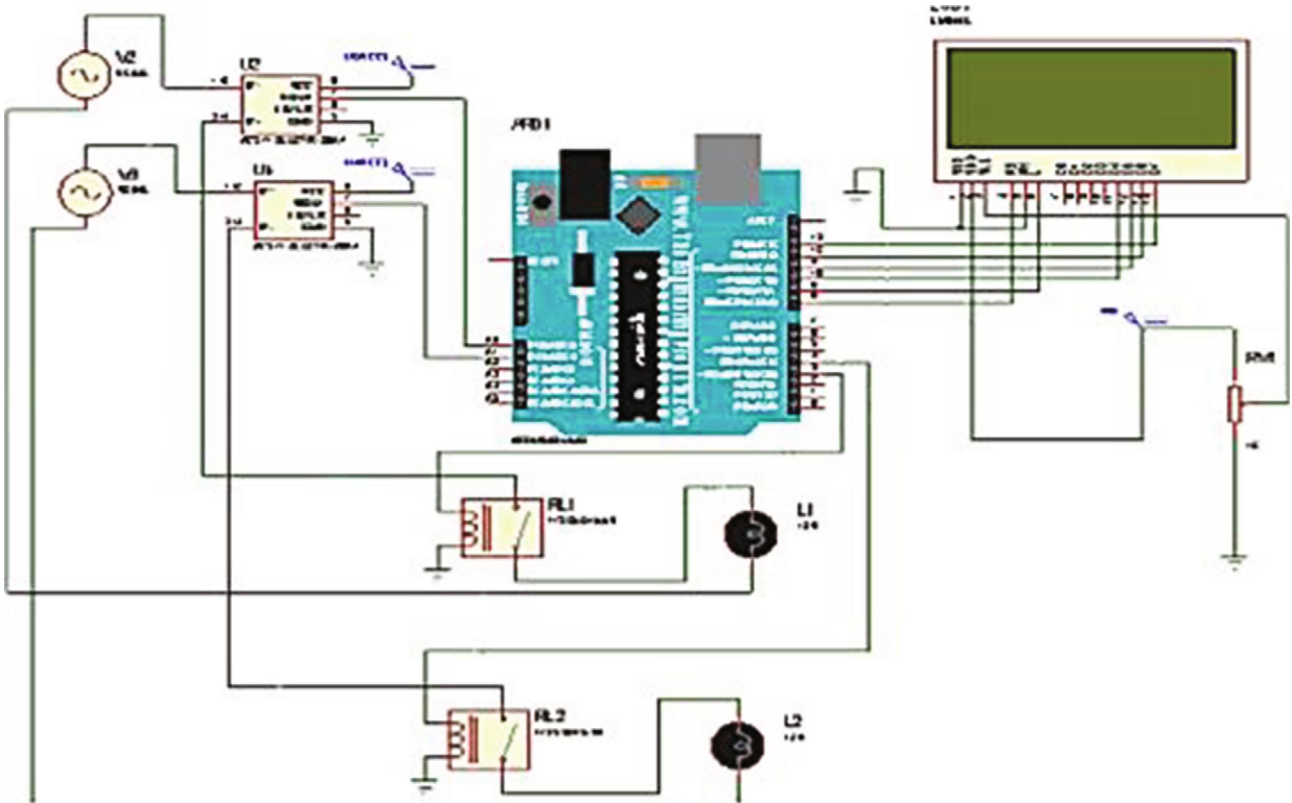


FIGURE 10: System design of SMACS.

monitor their usage of electricity efficiently. Improvement of electricity efficiency usage can be achieved by reduction due to changing habits [8].

In this modern era, monitoring systems must sort the data and record and exploit them to get the intrinsic information shown in legit and innovative ways and access the Internet to visualize it anywhere [4]. The monitoring system can be considered a user-friendly and unified solution for reliable electricity management [5]. This system can help users to change their usage by providing real-time feedback [6].

**3.2. Control System.** Electric equipment’s operational status control can reduce buildings’ power consumption cost and improve the buildings’ electrical energy to an effective and reliable ratio. The power control system can help the user manage their electricity more effectively and efficiently as everything can be controlled. This system can give commands directly from the remote control device [5].

**3.3. Implementation of IoT.** Thing-speak has been used for the development of IoT which is compatible with the ESP 8266 WiFi module. It can also show, analyze, and calculate the required data and store them publicly or privately in the cloud. Thing-speak is used as a medium to analyze and store data from the sensor-based IoT. It can be analyzed remotely via either a laptop or cell phone as long as WiFi is attached. To integrate Thing-speak with Arduino and the ESP8266 WiFi module, some prerequisites need to be done. The most crucial process is the command. Before the

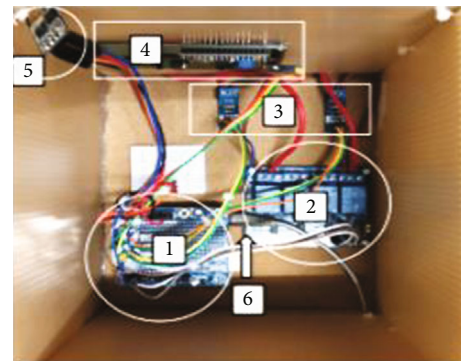


FIGURE 11: Testbed scenario of SMACS.



FIGURE 12: Complete SMACS prototype.

command is done, the Thing-speak account needs to be created. Only authorized persons can access the IoT application through Arduino and the ESP8266 WiFi module using the account created.

#### 4. Design Consideration

The first step of this research work is system design. A flow-chart is constructed to visualize the project flow, and the process is clearer and more understandable. Figure 7 presents the general system flow of SMACS which shows that, when the system is powered up, the sensors will read the data and all the processes will be executed. The data will be transmitted and received through the WiFi module and then stored on the cloud storage. The data will be visualized in both web servers and mobile applications. As far as SMACS is concerned, it is a system that monitors the current, voltage, and power consumption usage of the appliances that can be monitored on LCD and also based on the Internet of Things by using Thing-speak. The WiFi module ESP8266 is used as a medium to transmit and receive data using WiFi. SMACS for household appliances is divided into 2 parts: one major part for the monitoring system and one minor part for the control system. This system is supplied using 12 Vdc or 240 Vac with an AC to DC converter. The ACS712 current sensor module is used to measure the current, and the value of the current is used to calculate the power consumption. Relay is used in the control system part where it acts as protection, and it cuts off and delays the current when overcurrent occurs. Figures 8 and 9 show the flowchart of the monitoring system and control system, respectively. As shown in Figure 10, the design of SMACS consists of Arduino UNO, a liquid crystal display (LCD), an ACS712 current sensor module, relays, and AC sources. The components can be selected from the library of the software so that the simulation result will be the same as the prototype.

**4.1. System Configuration (Thing-Speak).** Thing-speak is an Internet of Things open-source application. It stores data and retrieves it via HTTP protocol over the Internet or Local Area Network (LAN) [44]. Thing-speak is compatible with the ESP 8266 WiFi module, and it is also used to show, analyze, and calculate the data and store it publicly or privately in the cloud. In this project, Thing-speak is used to analyze and store data from the sensor based on IoT. It was analyzed through both laptops and mobile phones anywhere and in any place as long as WiFi is connected. To integrate Thing-speak with Arduino and the ESP8266 WiFi module, some prerequisites need to be done. The most crucial process is the command. Before the command is done, the Thing-speak account was created.

Figure 8 presents the SMACS monitoring system, where it first reads the current status then calculates the current, voltage, and total power consumption. These estimations can be monitored in the LCD and also in the apps using the Thing-speak IoT module. Figure 9 shows the flowchart of the proposed SMACS control system, enabling the appliances to read the current and check its limit. If the expected

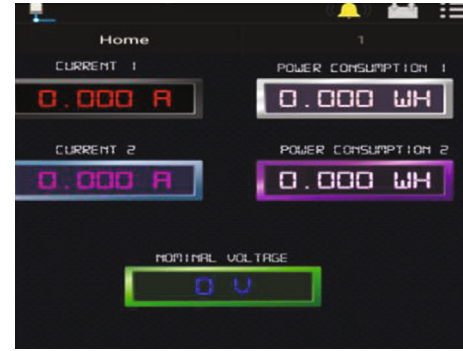


FIGURE 13: Numerical display from Thing-speak.

TABLE 3: Component shown in numbering.

Number	Component
1	Arduino UNO
2	5 V relay
3	ACS712 current sensor
4	LCD 20 × 4 I2C
5	ESP8266 WiFi module
6	Power adapter

TABLE 4: Voltage level.

Voltage level	Supply voltage
Low voltage	
Single phase	240 V
Three phases	415 V

current is greater than the limit, then it sends the notifications to the relay operation.

**4.2. Hardware Configuration.** The circuitry diagram is shown for the proposed SMACS in Figure 10. After designing and simulating the system using Proteus and Arduino IDE, the next step is to build and fabricate the prototype using the correct configurations. The first fabrication is developed to test and make sure the system is functioning. Figures 11 and 12 show the experimental testbed of SMACS. All the connections are based on the design created on Proteus. Two supply sockets are used as the power source for the appliances, and LCD and Thing-speak are used to display and store data, respectively. As shown in Figure 11, the hardware testbed scenario of SMACS is stated in numbering; the details are shown in Figure 13, and the data is presented in Table 3. This testbed was conducted at the university laboratory with load variations.

**4.3. System Parameters.** The main system parameters used for the performance evaluation and calculation are discussed here. The residential voltage rating with the configuration is presented in Table 4, where the voltage levels from the low side to the high side for a single phase and for three phases are shown.

TABLE 5: Comparison between ESP8266 and Zigbee transmitter.

ESP8266 WiFi module	Zigbee module	Comparison
Wireless local area network (WLAN) area networks with an average range between 30 and 100 meters	Restricted to wireless personal area networks (WPAN), reaching 10-30 meters in usual applications	Network range
2.4 GHz, 5 GHz	900-928 MHz, 2.4 GHz	Operating frequencies
Up to 54 mbps	250 kbps low data rate	Data rate

TABLE 6: Current comparison and percentage error of proposed SMACS.

Appliances	Actual current (A)	Current reading from Thing-speak (A)	Percentage error of current (%)
Hair dryer	2.461	2.476	0.60
Dry iron	4.175	4.190	0.41
Induction cooker	3.905	3.890	0.38
Water heater	6.78	6.80	0.29

As shown in Table 4, a low voltage side is selected for this system where a single-phase housing of the scope of SMACS is a 240 Vac from the power supply. The crucial part of the household appliances is not on the voltage side but on the current side. Current is an electrical charge that carries flow. A simple way of defining this is that current is a charge over time. Current can be categorized into 2 parts: direct current (DC) and alternating current (AC). DC flows only in one direction, whereas AC periodically changes in direction. The root mean square (RMS) current is used in the calculation since AC is constantly changing its value. The RMS current is calculated as follows:

$$I_{r.m.s.} = \frac{I_{max}}{\sqrt{2}}, \quad (1)$$

where  $I_{r.m.s.}$  is the root mean square of the current in A,  $I_{max}$  is the maximum value of current in A.

Other than that, the other important parameter in SMACS is power consumption. Power is an electrical energy flow for the unit time. It can also be defined as the multiplication of voltage, current, and power factors. The formula for power is shown in equation (2) and equation (3):

$$P = VI \cos \theta, \quad (2)$$

$$Z = \frac{V}{I} \cos \theta, \quad (3)$$

where  $P$  = power in W,  $I$  = current in A,  $\cos \theta$  = power factor,  $Z$  is the impedance of the system.

Voltage and power factors are assumed in SMACS, where it is fixed to 240 Vac and 90%, respectively. It is the nominal value for residential areas, where all the values are based on active power.

## 5. Result and Discussions

Most researchers have been using the Zigbee transmitter as a medium to transmit and receive data and cloud storage in

the current work. Smart monitoring and control system (SMACS) for household appliances have chosen the ESP8266 WiFi module as a WiFi connection medium. ESP8266 has shown a great work of transmitting and receiving data in this study compared to the Zigbee transmitter. The comparison between the Zigbee transmitter and the WiFi module is shown in Table 5.

Table 6 shows that the ESP8266 WiFi module can facilitate higher data rates at 54 Mbps, and the operating frequencies are 2.4 GHz and 5 GHz. Whereas, the Zigbee operates in 900-928 Mhz and also 2.4 GHz, and the data rate is 250 kbps. Therefore, it can be summarized that ESP8266 is better than Zigbee in terms of range, data rate, and operating frequencies. It is also very efficient and accurate in current sensing, as the current sensor is the most crucial in this module.

*5.1. Accessing ESP8266 WiFi Module with Thing-Speak in Web Server.* SMACS was tested with the Thing-speak using the WiFi module to transmit and receive the data from the sensors and Arduino UNO. The first step was to sign up for the Thing-speak account to have ownership of the system. Then, the channel is created to know the amount of data to be monitored. As in this system, four data were visualized and listed as follows: field 1—current 1; field 2—power consumption 1; field 3—current 2; field 4—power consumption 2; and field 5—nominal voltage. It is shown in Figures 14 and 15 that the channel status is either in the form of a chart and numerical display. Figure 14 displays the chart from Thing-speak.

*5.2. Mobile Application.* Virtuino mobile application was made to monitor the usage wirelessly and remotely. The mobile application that was used in this is Virtuino. It is an application that can be used as a monitoring system for SMACS. Virtuino can be linked with the Thing-speak web server. It reads the real-time data from Thing-speak and visualizes it on the mobile application; however, Virtuino cannot visualize historical data itself. The data can be read on the mobile application as long as the mobile or WiFi

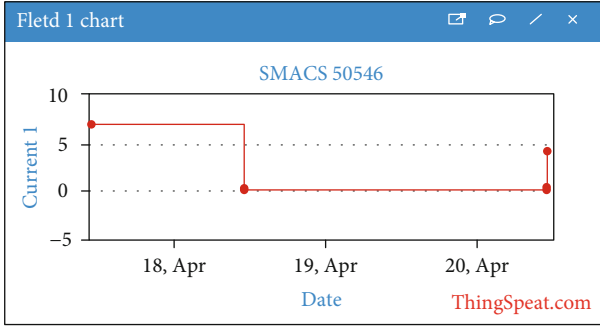


FIGURE 14: Chart display from Thing-speak.

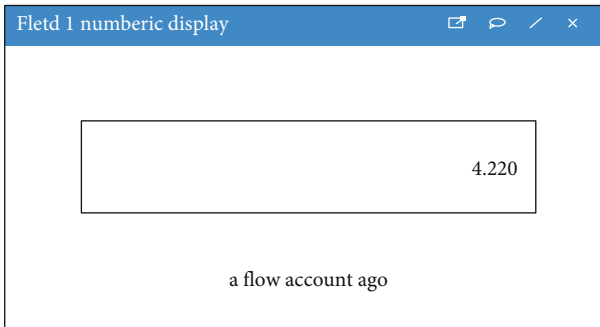


FIGURE 15: Complete visualization of SMACS in Virtuino.

network connection is fast. Historical data can only be accessed on the Thing-speak web server. Figure 16 showed the completed visualization of Virtuino on mobile phones. On the other hand, Virtuino can trigger an alarm whenever an overcurrent occurs. The alarm will produce a sound to trigger awareness to the users about the overcurrent. The value set in this system was 12 A, where it triggered the alarm before the limit of the current value reaches 13 A. This is done to create awareness and avoid any damage or danger to either the appliances or the users themselves. When the value surpasses 13 A, the relay will operate, where the switch will be disabled for a few seconds.

**5.3. Data Comparison with Different Household Appliances.** A comparison between different types of household appliances were accomplished to identify the accuracy of the proposed system. A few appliances were selected with varying values of current. Table 7 shows the appliances that have been chosen for system testing.

The higher the current value, the more accurate the result of SMACS is presented in Figures 16–23. The percentage of error for the bulb is 2.5%, where the current is the smallest among the appliances chosen. In comparison to the highest value of current among the appliances chosen, which is the water heater, the percentage error is only 0.15%. The value is approaching zero, which is considered to be accurate. This proposed system is considered to be efficient and successful. The data gathered from the monitoring system were tested for 5 minutes for every 30 seconds. The percentage error is calculated.

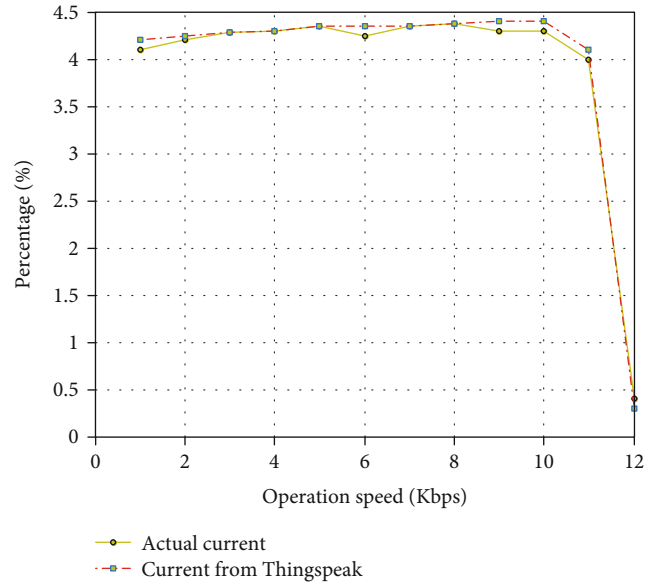


FIGURE 16: Current percentage error of SMACS.

TABLE 7: Household appliances used for testing.

Appliances	Power rating
Bulb	100 W
Hair dryer	900 W
Dry iron	1000 W
Rice cooker	1000 W
Water heater	1500 W

As presented in Figure 21, the higher the value of the current, the more accurate the result will be using SMACS. The percentage of error for the bulb is 2.5%, where the current is the smallest among the appliances chosen.

According to the paper on microcontroller-based power monitoring and switching device (PMAS) for appliances over a ZigBee network [46], the system called PMAS as shown in Figures 22 and 23 show the percentage error of each system. It can be seen that the performance of the proposed SMACS is preferably accurate and has very low error compared to the existing PMAS. The detailed comparison is presented in Table 8, where it can be seen that the existing PMAS has chosen a few appliances quite similar to the proposed system. The data can be analyzed to show that PMAS is considered successful, but according to Table 7, the percentage error of currents is relatively large compared to SMACS. Table 6 shows the average value of current and its percentage error of SMACS.

**5.4. Discussion and Limitation of This Work.** The results obtained are based on a constructed circuit that is simulated using real-life power system data and hardware prototype trials at the power socket. Monitoring power consumption problems are pervasive in household electric appliances. Therefore, a sustainable design and implementation of smart



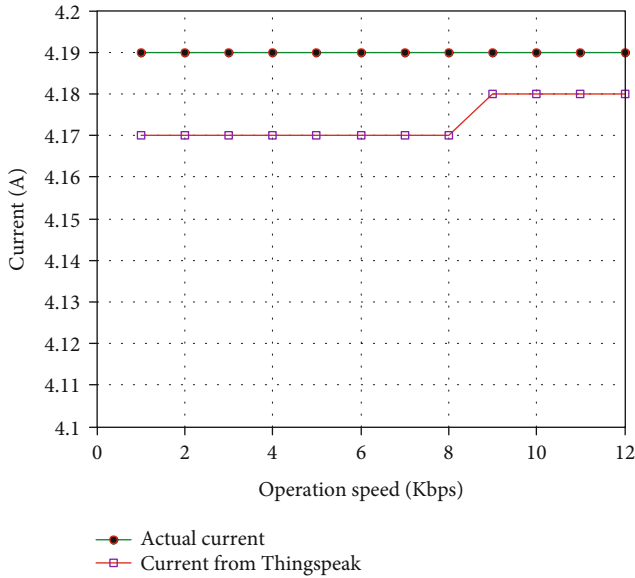


FIGURE 17: Current test comparison for rice cooker appliance.

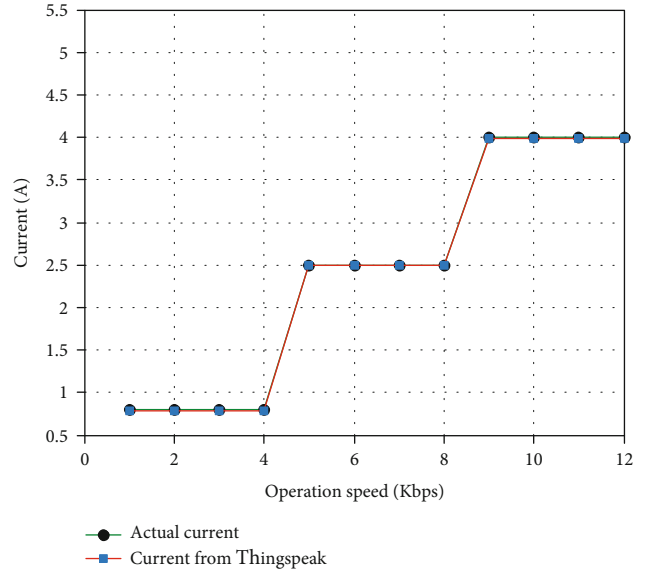


FIGURE 19: Current test comparison for 100 W lighting appliance.

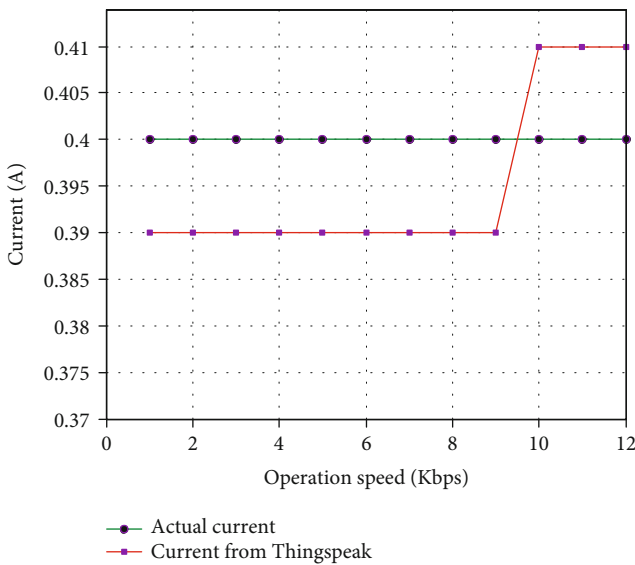


FIGURE 18: Current test comparison for water heater appliance.

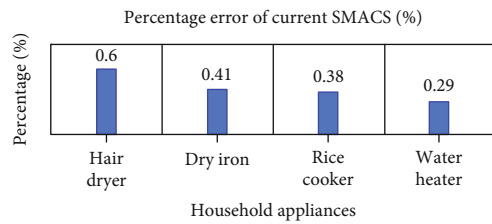


FIGURE 20: Current test comparison for hairdryer appliance.

electricity management of every consumption have been top prioritized to reduce usage and cost for a sustainable society [9, 11]. The proposed smart home electricity monitoring system is sustainable that utilizes the most advanced Internet technologies to impact electric consumption monitoring performance. Monitoring the consumption of electrical appliances, including advanced digital appliances, can directly regulate the usage of the air conditioner, water heaters, heaters, dry iron, washing machine, music systems, and lighting systems. Therefore, the proposed system can positively improve lifestyles and habits for a sustainable urban lifestyle with the accessible functionalities that can connect the house to an extraordinary remote monitoring center or to a mobile device through a mobile app; it is environmentally friendly. Using the proposed system can create

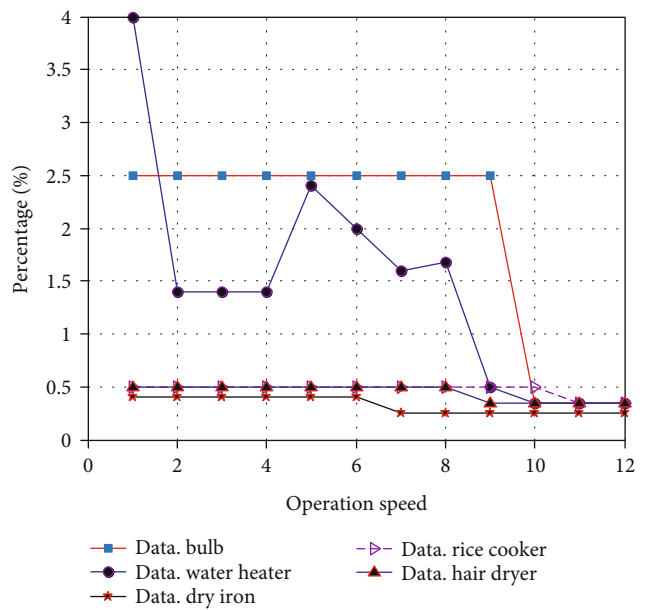


FIGURE 21: Percentage error comparison with different appliances.



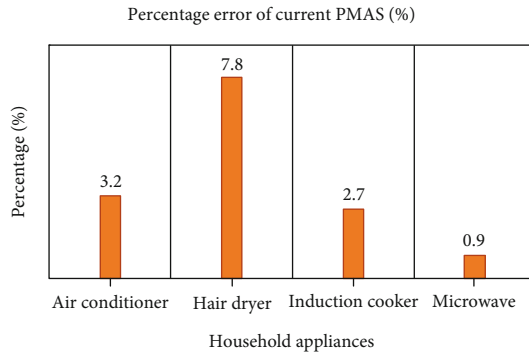


FIGURE 22: Percentage error of PMAS.

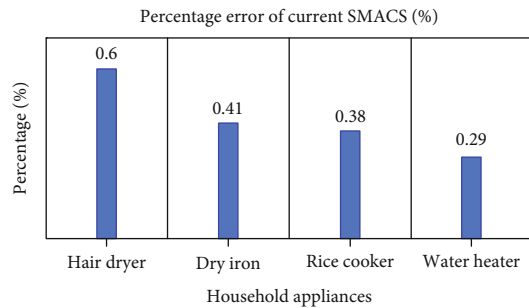


FIGURE 23: Percentage error of SMACS.

TABLE 8: Current comparison and percentage error of PMAS [44].

Appliances	Current reading from multimeter (A)	Current reading with PMAS adapter (A)	Percentage error of current (%)
Air conditioner	12.5	12.9	3.2
Hair dryer	5.1	5.5	7.8
Induction cooker	3.7	3.8	2.7
Microwave	5.05	5.1	0.9

awareness of energy usage for the appliances like air conditioners, bulbs, and other home appliances. The significant advantage is that the proposed system can be customized at the controller for future expansion. However, IoT-based systems for the smart home have a few disadvantages, especially with regard to the challenge of privacy, bandwidth, and Internet security.

Some limitations for this work, such as the voltage, were assumed to be 240 Vac since no sensor was included for the voltage sensor. However, in our future study, a voltage sensor is considered to measure the real-time voltage from the incoming voltage supply. Thus, the accuracy of the result can be improved further. Other than that, undervoltage and overvoltage detection can also be included if the voltage sensor is used. The control system can be improved further by considering time scheduling, remote switching, automatic switching, temperature switching, and sensor controlling. This will help the users to reduce electricity consumption as well as to make life easier.

## 6. Conclusions

This paper has proposed and developed an IoT-based smart monitoring and control system for household appliances. The methodology and processes are designed and created to provide a useful and crucial solution in a monitoring and control system. The proposed system performed better in measuring and monitoring the current, voltage, and power consumption. This is because the proposed SMACS considered the system process design with the hardware selection of the ESP8266 WiFi module, ACS712 current sensors, and 5 V relays. The entire communication has been done through the WiFi module to display the data on web servers, Thing-speak, and mobile applications like Virtuino. The data are also monitored in real time and historically, where the data were stored in the cloud database. The monitoring system makes the system more accessible for customers to view consumption rates clearly in real time. The control system of SMACS can fulfill the requirement of safety, can monitor appliances in the household individually or collectively, and can create awareness on electricity consumption. The voltage and current will be monitored in a wider scale in the smart house environment in future work.

## Data Availability

All data has been supplied with the manuscript.

## Conflicts of Interest

The authors declare no conflict of interest.

## Acknowledgments

This paper was funded by Universiti Kebangsaan Malaysia (UKM) under grant nos. FRGS/1/2020/ICT03/UKM/02/6 and GGPM 2020-028.

## References

- [1] J. S. Hassan, R. M. Zin, M. Z. A. Majid, S. Balubaid, and M. R. Hainin, "Building energy consumption in Malaysia: an overview," *Jurnal Teknologi*, vol. 70, no. 7, pp. 33–38, 2014.
- [2] S. Engineering and D. Systems, "Monitoring and reducing the consumption of home electric appliances December 2013," *Monitoring and reducing the consumption of home electric appliances*, p. 53, 2013.
- [3] E. Effah, F. L. Aryeh, W. K. Kehinde, and E. Effah, "GSM-Based Home Appliances Control System for Domestic Power Users in Ghana," *Ghana Journal of Technology*, vol. 1, no. 1, pp. 25–30, 2016.
- [4] T. Teng-Fa and K. Cheng-Chien, "A smart monitoring and control system for the household electric power usage," in *2013 IEEE PES Asia-Pacific Power and Energy Engineering Conference (APPEEC)*, Hong Kong, China, 2013.
- [5] Y. R. Tan, F. W. Akashah, and N. Mahyuddin, "The analysis of fire losses and characteristics of residential fires based on investigation data in Selangor, 2012-2014," in *MATEC Web of Conferences*, vol. 66, p. 00109, 2016.

- [6] S. S. van Dam, C. A. Bakker, and J. D. M. van Hal, "Home energy monitors: impact over the medium-term," *Building Research & Information*, vol. 38, no. 5, pp. 458–469, 2010.
- [7] W. A. Jabbar, T. K. Kian, R. M. Ramli et al., "Design and Fabrication of Smart Home With Internet of Things Enabled Automation System," *IEEE Access*, vol. 7, pp. 144059–144074, 2019.
- [8] K. Gram-Hanssen, "Efficient technologies or user behaviour, which is the more important when reducing households' energy consumption?," *Energy Efficiency*, vol. 6, no. 3, pp. 447–457, 2013.
- [9] A. G. Paetz, E. Dütschke, and W. Fichtner, "Smart homes as a means to sustainable energy consumption: a study of consumer perceptions," *Journal of Consumer Policy*, vol. 35, no. 1, pp. 23–41, 2012.
- [10] J. Walzberg, T. Dandres, N. Merveille, M. Cheriet, and R. Samson, "Assessing behavioural change with agent-based life cycle assessment: application to smart homes," *Renewable and Sustainable Energy Reviews*, vol. 111, pp. 365–376, 2019.
- [11] J. M. Batalla, A. Vasilakos, and M. Gajewski, "Secure Smart Homes," *ACM Computing Surveys*, vol. 50, no. 5, pp. 1–32, 2017.
- [12] E. Carroll, E. Hatton, and M. Brown, *Residential Energy Use Behavior Change Pilot*, CMFS project code B 21383, 2009.
- [13] M. Trejo-Perea, G. J. R. Moreno, A. Castañeda-Miranda, D. Vargas-Vázquez, R. V. Carrillo-Serrano, and G. Herrera-Ruiz, "Development of a Real Time Energy Monitoring Platform User-Friendly for Buildings," *Procedia Technology*, vol. 7, pp. 238–247, 2013.
- [14] U. G. Scholar, "Smart Power Flow Monitoring and Control," *International Journal of Science Technology & Engineering*, vol. 2, no. 10, pp. 1159–1165, 2016.
- [15] E. Mohamed and M. Ibrahim, *Smart Energy Monitor*, Infinity Tech of Embedded Solution, Mansoura, 2018.
- [16] M. J. Watts and S. P. Worner, "Comparing ensemble and cascaded neural networks that combine biotic and abiotic variables to predict insect species distribution," *Ecological Informatics*, vol. 3, no. 6, pp. 354–366, 2008.
- [17] M. Shafiq, Z. Tian, A. K. Bashir, X. Du, and M. Guizani, "CorrAUC: a malicious bot-IoT traffic detection method in IoT network using machine learning techniques," *IEEE Internet of Things Journal*, vol. 8, no. 5, pp. 3242–3254, 2021.
- [18] A. H. Bagdadee, L. Zhang, and M. S. Remus, "A brief review of the IoT-based energy management system in the smart industry," in *Artificial Intelligence and Evolutionary Computations in Engineering Systems*, pp. 443–459, Springer, 2020.
- [19] Z. Ibrahim and R. Hassan, "The implementation of Internet of Things using Test Bed in the UKMNET environment," *Asia Pacific Journal of Information Technology and Multimedia*, vol. 8, no. 2, pp. 1–17, 2019.
- [20] Q.-V. Pham, M. Liyanage, N. Deepa et al., "Deep Learning for Intelligent Demand Response and Smart Grids: A Comprehensive Survey," 2021, <http://arxiv.org/abs/2101.08013>.
- [21] N. Sakib, E. Hossain, and S. I. Ahamed, "A qualitative study on the United States internet of energy: a step towards computational sustainability," *IEEE Access*, vol. 8, pp. 69003–69037, 2020.
- [22] Z. E. Ahmed, M. K. Hasan, R. A. Saeed et al., "Optimizing energy consumption for cloud Internet of Things," *Frontiers of Physics*, vol. 8, 2020.
- [23] R. B. Gubbi and S. Marusic, "Internet of Things (IoT): a vision, architectural elements, and future directions," *Future generation computer systems*, vol. 29, no. 7, pp. 1645–1660, 2013.
- [24] M. B. Rivera, E. Eriksson, and J. Wang, "ICT practices in smart sustainable cities—in the intersection of technological solutions and practices of everyday life," in *EnviroInfo and ICT for Sustainability 2015*, Atlantis Press, 2015.
- [25] B. Vanderborgh, "Technology is not neutral (from the Editor's desk)," *IEEE Robotics & Automation Magazine*, vol. 25, no. 1, pp. 4–4, 2018.
- [26] Y. Strengers, "Smart energy in everyday life: are you designing for resource man?," *Interactions*, vol. 21, no. 4, pp. 24–31, 2014.
- [27] M. K. Hasan, A. F. Ismail, S. Islam, W. Hashim, M. M. Ahmed, and I. Memon, "A novel HGBBDSA-CTI approach for subcarrier allocation in heterogeneous network," *Telecommunication Systems*, vol. 70, no. 2, pp. 245–262, 2019.
- [28] S. Islam, A. H. Abdalla, and M. Kamrul Hasan, "Novel multihoming-based flow mobility scheme for proxy NEMO environment: a numerical approach to analyse handoff performance," *ScienceAsia*, vol. 43S, no. 1, pp. 27–34, 2017.
- [29] R. A. Mokhtar, R. A. Saeed, H. Alhumyani, M. Khayyat, and S. Abdel-Khalek, "Cluster mechanism for sensing data report using robust collaborative distributed spectrum sensing," *Cluster Computing*, vol. 4, pp. 1–6, 2021.
- [30] M. K. Hasan, M. M. Ahmed, S. S. Musa et al., "An improved dynamic thermal current rating model for PMU-based wide area measurement framework for reliability analysis utilizing sensor cloud system," *IEEE Access*, vol. 9, pp. 14446–14458, 2021.
- [31] B. L. Risteska Stojkoska and K. V. Trivodaliev, "A review of Internet of Things for smart home: challenges and solutions," *Journal of Cleaner Production*, vol. 140, pp. 1454–1464, 2017.
- [32] T. Kılıç and E. Bayır, "An investigation on Internet of Things technology (IoT) in smart houses," *International Journal of Engineering Research and Development*, vol. 9, no. 3, pp. 196–207, 2017.
- [33] H. Ghayvat, S. Mukhopadhyay, J. Liu, A. Babu, E. Elahi, and X. Gui, "Internet of Things for smart homes and buildings: opportunities and challenges," *Australian Journal of Telecommunications and the Digital Economy*, vol. 3, no. 4, p. 33, 2015.
- [34] S. A. Hashmi, C. F. Ali, and S. Zafar, "Internet of things and cloud computing-based energy management system for demand side management in smart grid," *International Journal of Energy Research*, vol. 45, no. 1, pp. 1007–1022, 2021.
- [35] S. Wang, X. Mao, and H. Khodaei, "A multi-objective home energy management system based on Internet of Things and optimization algorithms," *Journal of Building Engineering*, vol. 33, article 101603, 2021.
- [36] M. K. Hasan, S. Islam, M. Shafiq et al., "Communication delay modeling for wide area measurement system in smart grid Internet of Things networks," *Wireless Communications and Mobile Computing*, vol. 2021, pp. 1–10, 2021.
- [37] S. Sharad, P. Bagavathi Sivakumar, and V. Anantha Narayanan, "A novel IoT-based energy management system for large scale data centers," in *Proceedings of the 2015 ACM Sixth International Conference on Future Energy Systems*, New York, 2015.
- [38] Z. S. Ageed, S. R. Zeebaree, M. A. Sadeeq et al., "A state of art survey for intelligent energy monitoring systems," *Asian Journal of Research in Computer Science*, vol. 27, pp. 46–61, 2021.

- [39] D. P. Rani, D. Suresh, P. R. Kapula, C. M. Akram, N. Hemalatha, and P. K. Soni, "IoT based smart solar energy monitoring systems," in *Materials Today: Proceedings*, Elsevier, 2021.
- [40] M. K. Hasan, M. M. Ahmed, A. H. Hashim, A. Razzaque, S. Islam, and B. Pandey, "A novel artificial intelligence based timing synchronization scheme for smart grid applications," *Wireless Personal Communications*, vol. 23, pp. 1–8, 2020.
- [41] M. K. Hasan, S. H. Yousoff, M. M. Ahmed, A. H. A. Hashim, A. F. Ismail, and S. Islam, "Phase offset analysis of asymmetric communications infrastructure in smart grid," *Elektronika ir Elektrotechnika*, vol. 25, no. 2, pp. 67–71, 2019.
- [42] A. Ponniran, E. Sulaiman, S. A. Jumaat, M. Ishak, M. A. Chulan, and S. Saiman, "A study on electric energy usage at the residential area," in *Engineering Conference*, pp. 27–28, 2007.
- [43] V. Tadavarthy and A. Broota, "Smart power monitoring & analysis," *International Journal of Science and Research*, vol. 5, no. 7, pp. 1627–1630, 2016.
- [44] P. R. Joshi and M. S. Prof, "IoT based smart power management system using WSN," *International Research Journal of Engineering and Technology*, vol. 4, no. 6, pp. 783–786, 2017.
- [45] M. G. E. Ante, K. A. N. Garcia, B. A. A. Gonzales, J. T. D. Mendoza, and A. C. Roque, "Microcontroller-based power monitoring and switching device for appliances over a ZigBee network," *Journal of Telecommunication, Electronic and Computer Engineering*, vol. 10, no. 1, pp. 93–97, 2018.
- [46] K. C. Okafor, G. C. Ononiwu, U. Precious, and A. C. Godis, "Development of Arduino based IoT metering system for on-demand energy monitoring," *International Journal of Mechatronics, Electrical and Computer Technology*, vol. 7, pp. 3208–3224, 2017.
- [47] P. Dasan, A. Prabhu, S. Sundaram, and S. Rajan, "A ubiquitous home control and monitoring system using android based smart phone," *International Journal Of Computer Science And Mobile Computing*, vol. 2, no. 12, pp. 188–197, 2013.
- [48] M. Thomas, *13 examples of IoT in environmental sustainability you should know*, 2019, <https://builtin.com/internet-things/iot-environment-sustainability-green-examples>.

## Research Article

# A Recommendation Model for College Career Entrepreneurship Projects Based on Deep Learning

Yuan Feng<sup>1</sup> and Weixian Huang<sup>2</sup> 

<sup>1</sup>Employment Guidance Teaching and Research Office, Yellow River Conservancy Technical Institute, Kaifeng, Henan 475004, China

<sup>2</sup>School of Entrepreneurship and Innovation, Shenzhen Polytechnic, Shenzhen Guangdong Province 518000, China

Correspondence should be addressed to Weixian Huang; [cxcyhwx@szpt.edu.cn](mailto:cxcyhwx@szpt.edu.cn)

Received 24 August 2021; Revised 25 September 2021; Accepted 1 October 2021; Published 21 October 2021

Academic Editor: Deepak Gupta

Copyright © 2021 Yuan Feng and Weixian Huang. This is an open access article distributed under the Creative Commons Attribution License, which permits unrestricted use, distribution, and reproduction in any medium, provided the original work is properly cited.

The recommendation system is an active, personalized, and real-time technology platform proposed in the 1990s to solve the problem of information overload. The recommendation system can constantly adjust the recommendation results according to the real-time behaviors of users. In other words, if the user's interest changes, the recommendation system can present different information to the user. Therefore, the recommendation system is the best way to solve the problem of information overload in entrepreneurial projects. Based on the ConvMF algorithm, this paper proposes an entrepreneurial project recommendation algorithm based on a deep neural network and matrix decomposition. A deep neural network was established for the extraction of the hidden features of entrepreneurial projects, and a convolution neural network was used to process the text description information of entrepreneurial projects. One-hot coding was used to process the regional characteristics and financing round characteristics of entrepreneurial projects, and word embedding was used to process the label features of entrepreneurial projects. The implicit features of users are extracted from the user's rating matrix using matrix decomposition technology. Finally, recommendations are made according to the implicit characteristics of users and the items learned.

## 1. Introduction

Nowadays, China's universities have become the front line of innovation. The government and schools encourage college students to carry out innovative and entrepreneurial practice activities, apply teaching theoretical knowledge to extracurricular practice, and guide students to cultivate the ability of independent thinking and problem-solving, which improve the quality of personnel training and increase the employment rate. In the process of participating in innovation and entrepreneurship projects, students have accumulated a lot of knowledge, experience, and project data [1]. However, at present, the resource pool of innovation and entrepreneurship projects in colleges and universities is huge, the utilization rate of resources is low, and it is difficult to search for resources. We study the commonly used recommendation algorithms and build a personalized recommendation model suitable for college students' innovation

and entrepreneurship resource library system, which can help users quickly find interesting resources [2].

The investigation of college students' entrepreneurship mainly investigates their entrepreneurial purposes and activities, while the GUESSS project is a global research, which has positive homework for understanding college students' entrepreneurship. The survey also covers a wide range, with about 200,000 students in 54 countries [3]. To study the factors of women's entrepreneurship development, we first list the important determinants and create a matrix to show the relationship at each level in the process, and we then quantify and define the above factors. Through this research method, it is helpful to encourage women to have entrepreneurial intentions and careers [4]. There are roughly three kinds of factors that affect women's entrepreneurship, namely, individual, environment, and, most importantly, politics. Nowadays, college graduates are more common, so it is particularly important to train and cultivate personal



abilities and the motivation and ability to effectively participate in entrepreneurial activities during school. The entrepreneurial intention model for higher education came into being, which has a positive effect on improving students' entrepreneurial intention. The model is implemented as a practical digital application, mainly in three aspects: skill awareness, entrepreneurial resources, and network [5]. In view of the research of college students' entrepreneurial career and their adaptive behavior in occupations, this paper adopts the social cognitive model of career self-management [6]. We use 380 students who are about to graduate, based on the data, and use this model to verify and find the relationship between social cognitive career theory and adaptive exploration, which fills this unknown and has a certain influence on the education of career research and counseling in the future. It is helpful to study the time and type of individual entrepreneurship based on the opportunity to collect entrepreneurs' experiences. Using the data of Danish university graduates and employees, individuals are tracked. Compared with those who never started a business in terms of time, experience, and type of starting a business, early entrepreneurs earn higher wages and suffer fewer losses than late entrepreneurs [7]. This shows that the time type of entrepreneurial experience determines the subsequent career trajectory and the uncertainty of employers' value to it. Based on the data of college graduates and the theory of social cognitive career, this paper establishes a model of how different levels of contextual influence can help or inhibit the transformation of entrepreneurial intention into new entrepreneurial creation, which can evaluate the direct and larger background that affects the creation of new enterprises [8]. Entrepreneurship education for students is attracting attention from all walks of life, and it is also a factor affecting students' entrepreneurial intention, and it is also increasing significantly in schools around the world. Through the in-depth study and review of relevant literature, as the basic background of knowledge, and then relying on narrative as a means of understanding and a form of communication, this research is positioned as a qualitative and explanatory phenomenological research [9]. With the advancement of education, rural students and young people are often not interested in engaging in agriculture as a career, MoMo, and prefer to work in cities. This paper studies this prominent phenomenon. Collecting 345 graduate students as samples, this paper analyzes the decisive factors of their ideas and intentions for agricultural entrepreneurship and shows that intention is the decisive factor, which is directly proportional to career planning and so on [10]. On the other hand, career planning, entrepreneurial ability, and agricultural family background (FB) can significantly predict agricultural entrepreneurial intention. This analysis has reference value for future teaching reform. Through investigation and study, college students' interest in entrepreneurship is closely related to their gender and race. This paper analyzes and compares their different attitudes and motives and then judges their interest points. For example, immigrant boys are much more enthusiastic about starting a business than local boys, girls are generally lower than boys, and boys will be greatly influenced by external factors, such as family,

friends, and economic interests; girls are more motivated to use "internal factors" such as their skills and abilities. Entrepreneurship is equally important for both men and women to be flexible and independent [11]. College students are an important and valuable human force in a country. What is often discussed in society is the employability of graduates and whether they are willing to start entrepreneurial activities. The professional willingness of social entrepreneurs should be spread and cultivated during their student years, and entrepreneurship can be used as the starting point of their career, which requires college students to have the opportunity to get in touch with the concepts and opportunities of social entrepreneurship [12].

## 2. Recommendation Process

This paper designs a recommendation algorithm for entrepreneurial projects based on a deep neural network and matrix decomposition. This algorithm integrates the content information of entrepreneurial projects into the recommendation algorithm. Figure 1 shows the overall flow chart of the algorithm shown in this chapter. As can be seen from the figure, the recommendation flow mainly includes the following parts:

(1) *Data Processing*. It mainly includes the following: (i) scoring, calculating the score data of the user's entrepreneurial project according to the historical behavior data of the user's entrepreneurial project; (ii) sampling negative samples to generate negative samples based on the historical behavior data of users; and (iii) generation of the scoring matrix.

(2) *Recommendation Model Construction*. The construction of the recommendation model is the construction of the entrepreneurial project recommendation algorithm based on a deep neural network and matrix decomposition.

(3) *Recommendation Result Generation*. Use the trained model to generate recommendation results for users.

## 3. Data Processing

*3.1. Processing of Implicit Feedback Data*. In the research of personalized recommendation, users' interest in items is usually reflected by user rating data. For example, the well-known MovieLens dataset and Netflix Prize dataset have clear user movie ratings [13]. However, in many practical application scenarios, there is often no clear user rating data, such as ordinary e-commerce websites such as JD.com and Taobao and news websites such as Today's Headlines and Baidu News. In this case, the user's implicit feedback data is usually used to measure the user's interest in the project [14]. User action data in the entrepreneurial project recommendation system is implicit feedback data. Next, the processing method of implicit feedback data is introduced.

Generally speaking, implicit feedback data is extracted from the interaction history between users and websites, for example, user clicks, browses, collections, and interaction time. For example, on e-commerce websites, users' reading,



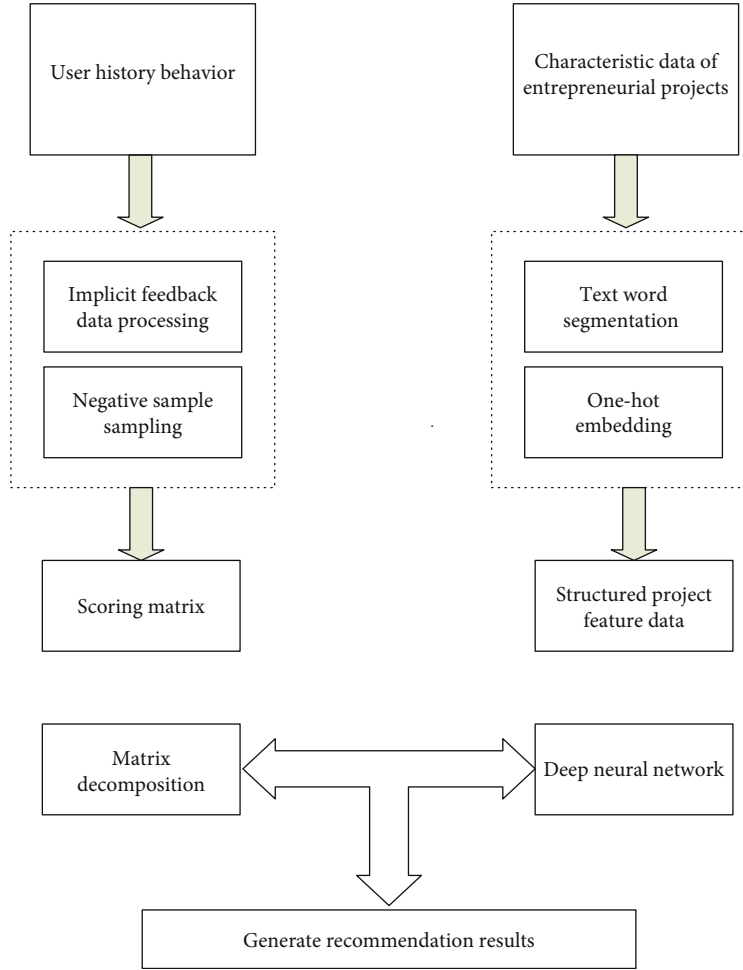


FIGURE 1: Recommendation flow chart.

TABLE 1: User interaction record table.

Users	Project 1	Project 2	.....	Project $n$
Browse	$I_{11}$	$I_{12}$	.....	$I_{1n}$
Attention	$I_{21}$	$I_{22}$	.....	$I_{2n}$
Comments	$I_{31}$	$I_{32}$	.....	$I_{3n}$

clicking, shopping cart addition, collection, purchase, and other behaviors reflect users' interest in goods [15].

In view of the research problem of this paper, the personalized recommendation system for entrepreneurial projects also has no specific user rating information. For users, the interaction history can be represented by Table 1: each row represents an action type (including reading, paying attention, and commenting, which are represented by 1, 2, and 3, respectively), each column represents an entrepreneurial project, and  $I_{ij}$  represents the number of rows  $i$  of users on entrepreneurial projects  $j$ .

However, this raw interaction history cannot be used directly and needs to be processed before it can be used. The data type in Table 1 is the number of times, which refers to the number of times users browse, pay attention to, and comment on items, which is implicit feedback data. On the

other hand, it can analyze the attention degree of users to the project, which reflects the personalized preference degree.

Users' interest in entrepreneurial projects is mainly reflected in two dimensions: the number of interactions and the types of interactive behaviors. First of all, in terms of the number of interactions, the more interactions the user has with the startup project, the more interest the user has in the project. For example, if the user browses item A five times and item B once, it indicates that the user is more interested in item A. Second, different interactive behaviors reflect different interests of users. For example, if a user comments on Project A and clicks Project B, it indicates that the user is more interested in Project A than Project B. Using the historical behavior of users, you can get the user score of starting the project. See Equation (1) for the calculation method:

$$r_{wi} = \sum_{j=1}^k a_j q_{ni,j}, \quad (1)$$

where  $a_j$  denotes the number of comments made by user  $a$ ,  $q_{ni,j}$  denotes the degree of interest in comments, and the

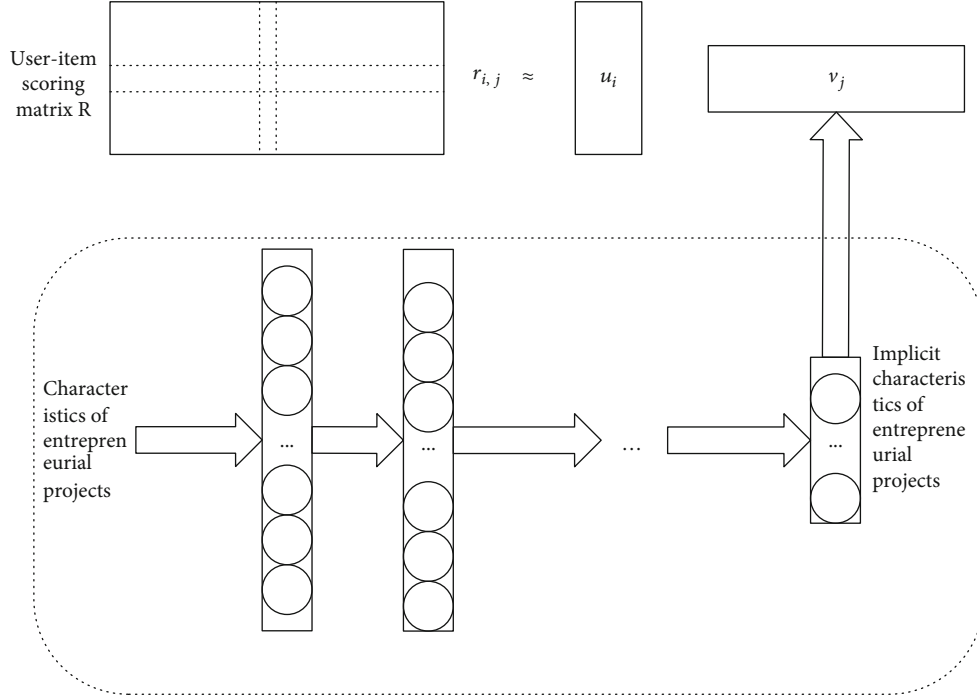


FIGURE 2: Structure diagram of the entrepreneurial project recommendation algorithm based on a matrix decomposition and deep neural network.

product of the different comment times and interest degree is the degree of interest in items in comments.

**3.2. Negative Sampling.** In a score-based recommendation system, users show their goodwill towards an item by scoring. For example, MovieLens and Netflix Prize datasets have user rating data on movies. If a user gives a movie a score of 5, it means that the user likes the movie. If the user does not like a movie, the user will give the movie a very low score. Therefore, the score-based dataset contains both positive samples (items that the user likes) and negative samples (items that the user does not like) [16]. For the recommendation system of entrepreneurial projects, the user's action data is implicit feedback data. One of the characteristics of internal hidden feedback data is that there are only positive samples and no negative samples [17].

For the sampling of negative samples, Xiang Liang put forward the following sampling scheme in the book *Practice of Recommendation System* and achieved good results:

- (1) For each user, it is necessary to ensure the balance of positive and negative samples
- (2) For the negative sampling of users, select those elements that are very popular but have no user behavior

Generally speaking, websites will have columns similar to popular items, so popular items are easier for users to find. If the project is very popular and the user has no behavior, it can better indicate that the user is not interested in the project. For unpopular items, the exposure on the website may not be high, and users may not find them at all during browsing the

website, so it is impossible to judge whether users are interested in the item. Therefore, aiming at the research problem [18], this paper adopts the sampling method proposed by Xiang Liang to carry out the negative sampling.

## 4. Recommendation Algorithm Description

As shown in Figure 2, the business project recommendation algorithm based on a deep neural network is constructed and decomposed into two parts: the business project recommendation algorithm based on a deep neural network and matrix decomposition. As an input element of a business project, the output is used to extract the implicit features of the project.

**4.1. Deep Neural Network and Probability Matrix Decomposition Algorithm.** The probability matrix factorization (PMF) algorithm is a matrix factorization algorithm [19]. The purpose of probability matrix factorization is to decompose the hidden characteristics of elements and users from the score matrix [20] and then introduce the probability matrix factorization algorithm used in this Table 1.

Assuming that there are  $N$  users and  $M$  items, the scoring matrix  $R = R^{N \times M}$  can be obtained. The goal of matrix decomposition is to calculate the hidden features of users and items  $U = R^{K \times N}$  and  $V = R^{K \times M}$  by using the scoring matrix  $R$ . With the hidden features  $U$  and  $V$  of users and items, on the contrary, the unknown scores in the evaluation matrix  $R$  are calculated by  $U^T V$ .

Firstly, the probability matrix decomposition algorithm assumes that the hidden feature vectors of users and items follow Gaussian distribution, and its expressions are shown in

$$P(U | \sigma_U^2) = \prod_{i=1}^N N(u_i | 0, \sigma_U^2 I), \quad (2)$$

$$P(V | \sigma_V^2) = \prod_{j=1}^N N(V_j | 0, \sigma_V^2 I), \quad (3)$$

where  $N(x|\mu, \sigma^2)$  represents the probability density function of Gaussian distribution,  $\mu$  represents the mean value,  $\sigma^2$  represents the variance,  $U$  and  $V$  represent the implicit feature evidence of users and items,  $U_i$  and  $V_j$  represent the implicit feature vectors of users and items, and  $I$  represents the unit matrix.  $U$  and  $V$  are obtained by matrix decomposition, which can better calculate the hidden characteristics of users and projects.  $P$  represents the probability density function of Gaussian distribution.

In addition, it is assumed that the conditional probability of observation score data also follows Gaussian prior distribution, and the expression is shown in

$$P(R | U, V, \sigma_R^2) = \prod_{i=1}^n \prod_{j=1}^m [N(R_{i,j} | U_i^T, V_j \sigma_R^2)]^{r_{i,j}}. \quad (4)$$

The Bayesian formula can be used to obtain the postinspection probability of users and projects with hidden characteristics, as shown in

$$P(U, V | R, \sigma_R^2, \sigma_U^2, \sigma_V^2) \propto P(R | U, V, \sigma_R^2) P(U | \sigma_U^2) P(V | \sigma_V^2). \quad (5)$$

Assuming that  $W$  is the parameter set of the deep neural network and follows Gaussian distribution and that  $X_j$  is the characteristic input of term  $j$ , the calculation method of term  $j$ ,  $V_j$ , is shown in

$$V_j = \text{dnn}(W, X_j) + \epsilon_j. \quad (6)$$

In addition,  $\text{dnn}(\cdot)$  denotes the deep neural network, and  $\epsilon_j$  denotes the random error and expresses the equation shown in Equation (7) according to Gaussian distribution:

$$\epsilon_j \sim N(0, \sigma_V^2)I. \quad (7)$$

Assuming that the parameter set  $W$  also obeys Gaussian distribution, the probability distribution of  $W$  is shown in

$$P(W | \sigma_W^2) = \prod_{k=1}^P N(W_k | 0, \sigma_W^2). \quad (8)$$

The conditional probability distribution of the implicit feature  $V$  of the item is shown in

$$P(V | W, X, \sigma_V^2) = \prod N(V_j | \text{dnn}(W, X_j), \sigma_V^2 I). \quad (9)$$

The probability distribution can be calculated by the Bayesian formula, as shown in

$$\begin{aligned} P(U, V, W | R, X, \sigma^2, \sigma_U^2, \sigma_V^2, \sigma_W^2) \\ = P(R | U, V, \sigma^2) P(U | \sigma_U^2) P(V | R, W, X) P(W | \sigma_W^2). \end{aligned} \quad (10)$$

*4.2. Extraction of Implicit Features of Entrepreneurial Projects.* Entrepreneurial projects contain a lot of specific information, especially the description of commercial projects, brand names and signature characteristics of commercial projects, regional characteristics of commercial projects, and advantages of commercial projects, including structured data of project content such as regions, domains and labels, and structured data such as project description texts. When using the traditional word-back model to simulate entrepreneurial projects, there are certain boundaries. On the other hand, the word-back model has many limitations, such as not finding the context information of text data and extracting very little feature data. On the other hand, using the same method to process all feature data indiscriminately will also affect the recommendation results.

In order to extract more effective features from these content data, this paper combines the convolution neural network, word embedding technology, and one-hot technology to establish a deep neural network to extract hidden features of entrepreneurial projects. The convolution neural network is used to deal with the text description of entrepreneurial projects, word embedding technology is used to deal with the label data of entrepreneurial projects, and one-hot is used to deal with the regions and regional characteristics of entrepreneurial projects. Figure 3 is the structure diagram of the deep neural network established in this paper. Next, the network structure will be described in detail.

In Figure 3, the text input, region, domain, and label are of different data types or have different attribute requirements. Different inputs are the result of processing for the performance of attribute characteristics. Different input attributes in Figure 3 need to process different attribute values. After processing, all attributes will be converted into a unified processing attribute format. The input data of different attribute formats are unified into a unified data type after different processing, which is convenient for the application of the deep learning model.

*4.2.1. Input Layer.* The input layer inputs the characteristic data of the collated project, including label data input, text data input, company field data input, and regional data input (four parts). The input data is as follows.

*Step 1* (item label data input). The number of item labels is between 3 and 10.

*Step 2* (text description data entry for business projects). Text description data must separate words and enter them into the network in word order.

*Step 3* (regional data input). Regional data input is a single discrete value, such as Beijing and Shanghai.

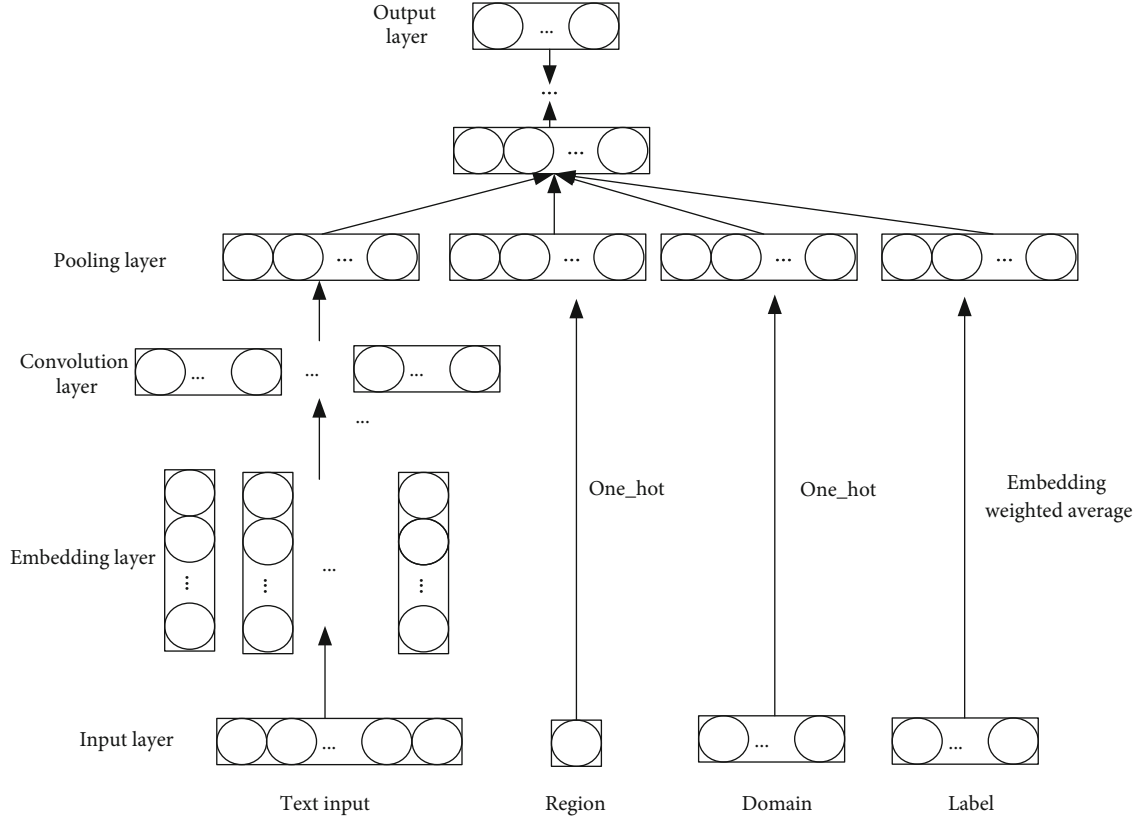


FIGURE 3: Deep neural network structure for extracting project features.

TABLE 2: The 10 tags most similar to the label “finance.”

Label	Similarity
Insurance business	0.8180
Wealth management	0.8172
Nonperforming assets	0.8161
Fund	0.8140
Banking services	0.8082
Quantitative investment	0.8064
Asset securitization	0.8047
Foreign exchange	0.8039
Bill financing	0.8027
Microfinance	0.8008

*Step 4* (domain data input). The domain information of the company is a sequence value, which can contain one or two values.

**4.2.2. Label Data Processing of Entrepreneurial Projects.** Each label is represented by a  $k$ -dimensional vector. The principle of the same vector is the same. The more similar the labels are, the closer the spatial distance is. Table 2 shows the 10 labels closest to “finance” and their similarity. In this paper, cosine similarity is used to calculate the similarity between different tags.

Because each item has multiple tags, the trained tag vector cannot be directly used as the input of the neural net-

TABLE 3: Content information of an item.

Item number	50000
Project name	Business Information Technology
Project area	Enterprise services
Project brief introduction	Business Information Technology is committed to providing efficient solutions for the catering and entertainment industry
Item label	Enterprise services, SAAS, APP, platform, solutions, performance management

work. Assuming that the item has a tag set, then using the method  $T = \{t_1, t_2, \dots, t_l\}$  of adding and averaging tag vectors, where  $t_i \in p^{l \times k}$ , then the processed  $p$  of the tag for each item can be expressed as

$$p = \frac{1}{l} \sum_{i=1}^l t_i, \quad (11)$$

where  $l$  represents the number of tags for the project and  $p$  represents the processing result in Table 3.

Finally,  $p$  is input into the deep neural network as the feature of item tag information. Table 4 shows the content information of the item with item number 50000, and the tag vector display of the item can be calculated using calculation formula (15). Table 4 shows the 10 tags closest to the item tag vector.

TABLE 4: Labels similar to Project 50000.

Label	Similarity
Performance management	0.9346
IT operation and maintenance	0.9298
PAAS	0.9167
Enterprise mobility	0.9088
CMS	0.9080
Call center	0.8976
Mobile device management	0.8972
Server	0.8901
Customer service	0.8731
ERP	0.8706

4.2.3. *The Processing Method of Text Description Data of Entrepreneurial Projects.* In order to improve the accuracy of feature extraction of entrepreneurial projects, this paper uses a convolution neural network to process the file description information of entrepreneurial projects. The structure of the neural network containing text is shown in Figure 4. Next, the working mode of the text convolution neural network will be introduced in detail.

(1) *Embedding Layer.* An important concept of the embedding layer is embedded language, that is, distributed representation. The purpose is to use dense vectors to represent words to avoid the data sparsity problem of one-hot.

The purpose of the embedding layer is to transform the sequence of word segmentation results of text into the matrix and input it into the convolution neural network. The input of the embedding layer is in the order shown in

$$D_j = (w_1, w_1, \dots, w_{nj}). \quad (12)$$

For example, “Today’s weather is fine” after the word segmentation order is as follows: “Today’s weather is fine”; this word order can be used as the input of the embedding layer.

In the embedding layer, each word is represented by a  $k$ -dimensional vector (for example, 100 dimensions). After each word is represented by a  $k$ -dimensional vector, the results are spliced together, and each text sequence input can be converted into a matrix  $D \in R^{N \times K}$  (where  $N$  represents the length of the sequence and  $K$  represents the dimension of the word vector), which can be expressed by

$$D_{n \times k} = \begin{bmatrix} -w_1 - \\ -w_2 - \\ \dots \dots \\ -w_{n-1} - \\ -w_n - \end{bmatrix}, \quad (13)$$

where  $k$  represents the dimension of the word vector,  $n$  represents the number of words in the text, and  $w_i$  represents the word vector.

After the input text sequence is converted into the matrix, it can be used as the folding neural network input of text, in addition, how to quantify the words. In other words, there are two main ways to convert a word into a dense high-order vector:

- (a) Pretrained word vectors can quantitatively express the relationship between words, such as the similarity between words. Vectorization of words is also beneficial to the modeling of natural language processing problems and reduces the sparsity of data. Therefore, word vectorization is a research hotspot in recent years. In recent years, many algorithms represented by word vectors have been proposed, such as Word2Vec, FastText, and WordRank. Here, the Word2Vec algorithm is the most widely used, which was proposed by Mikolov and others. The algorithm includes the CBOW language model and Skip-Gram language model. Because this part is not the main content of this paper, it will not be explained here. The word vector training tool in this paper is Word2Vec
- (b) At the beginning of network training, the word vector is initialized randomly, and the word vector is always optimized and adjusted during training

(2) *Convolution Layer.* The main purpose of the convolution layer is to extract local features. Figure 5 folds a schematic diagram of the local field of view of a neural network with an input of the  $8 \times 8$  matrix, with a local perceptual range of  $2 \times 2$ . All inputs in each local perceptual field are connected to the same hidden neuron, and  $K$  and  $L$  hide the original output, as shown in

$$f \left( b + \sum_{i=0}^n \sum_{j=0}^m w_{i,j} a_{i+kl+j} \right). \quad (14)$$

The convolution kernel of the text convolution neural network is  $P \times K$ , the number of rows per convolution of  $P$  is variable, and  $K$  represents the dimension of the word vector, which is constant.

Therefore, the convolution operation of the text convolution neural network can be expressed by

$$c_i^j = f \left( b_c^j + \sum_{i=0}^p \sum_{j=0}^m w_{i,j} D_{i+k,d+j} \right), \quad (15)$$

where  $c_i^j$  represents the activation value on a convolution kernel,  $b_c^j$  is the offset term,  $w_i$  and  $j$  are the shared weights,  $f$  is the activation function, and  $D$  represents the input of the convolution layer.



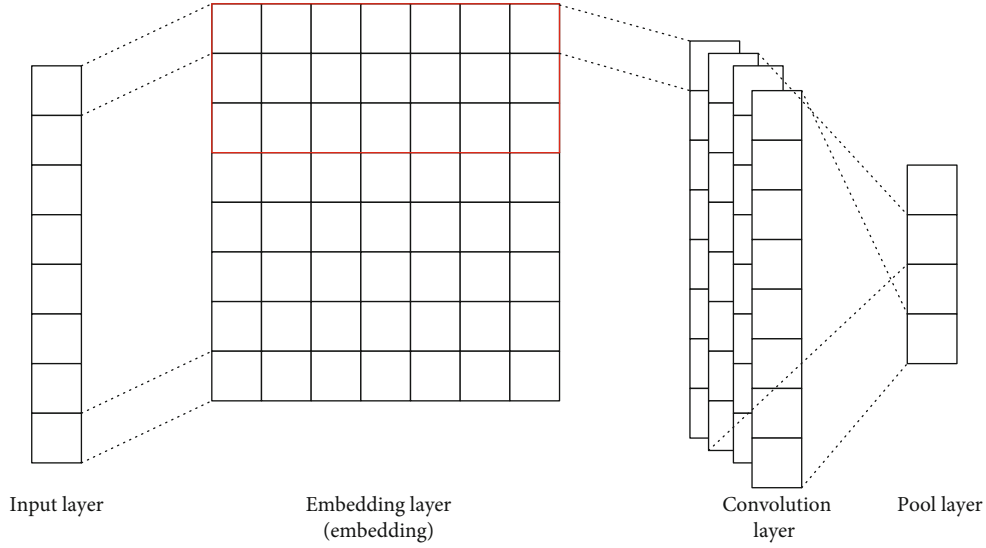


FIGURE 4: Structure diagram of the text convolution neural network.

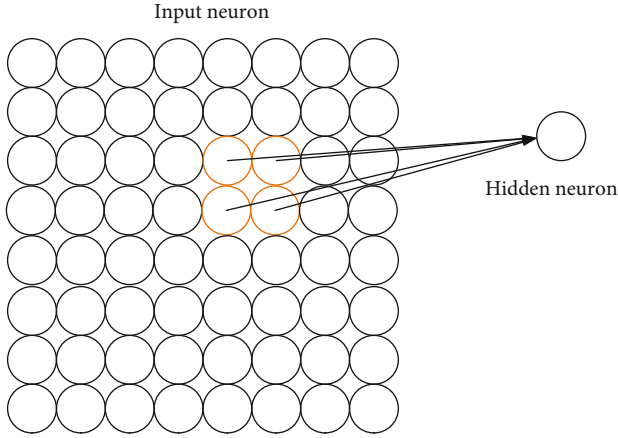


FIGURE 5: Schematic diagram of the local perceptual visual field of the convolution neural network.

After the above convolution operation, the output of the convolution layer can be expressed by

$$c^j = [c_1^j, c_2^j, \dots, c_i^j, \dots, c_l^j]. \quad (16)$$

In this paper, using the ReLU activation function, the ReLU function can avoid the gradient disappearance problem and avoid falling into the local optimal solution.

(3) *Pool Layer.* In a convolution neural network, the pool layer follows the convolution layer closely. Its goal is to simplify the output of the convolution layer. In fact, this is a downsampling operation. Pooling can reduce the size of data space, thus reducing the number of parameters and calculations.

The pool layer takes the output of the convolution layer as an input and converts the input into a fixed feature map. The most commonly used operation is max-pooling, which takes the maximum value in the local sensory field of a specific size

so as to achieve the purpose of dimensionality reduction. The specific operation method can be expressed by

$$d_f = [\max(c^1), \max(c^2), \dots, \max(c^i), \dots, \max(c^n)]. \quad (17)$$

4.2.4. *Regional Characteristics of Entrepreneurial Projects and Domain Characteristics of Entrepreneurial Projects.* The regional characteristics and domain characteristics of entrepreneurial projects are coded by one-hot. Taking the region feature processing method as an example, assuming that there are  $Q$  region information, the region information of the project is mapped into a  $Q$ -dimensional vector. Assuming that the region set can be expressed as  $a = \{a_1, a_2, \dots, a_q\}$ , the region information of the item can be encoded as

$$[\dots 0 \dots \dots 0 \dots]_{ixq}. \quad (18)$$

Similarly, the domain information of the project can be encoded in this way.

In addition, you can use one-hot encoding to handle lost data. There are a few missing values in the project area information. In this case, the missing value can be incorporated as a code directly into a one-hot encoding. For example, if there are  $Q$  regions, adding a "missing" region will become a  $Q + 1$  region, and the region vector of each item will become a  $Q + 1$  dimension vector accordingly.

4.2.5. *Fusion Layer.* In this paper, the horizontal stitching method is adopted directly, and the output of the text convolution neural network is directly stitched into region information, domain information, and label information as the input of the next layer, as shown in

$$X = [X_1, X_2, \dots, X_k], \quad (19)$$

where  $X_1, X_2, \dots, X_k$  represents the output of various features after corresponding processing.

```

Input:  $R$ : user rating matrix
       $X$ : item attribute feature data
Output:
       $U$ : user implicit feature vector
       $V$ : implicit feature vector of items
Initialization:
      Regularization parameter:  $\lambda_U, \lambda_V, \lambda_W$ 
      Maximum number of iterations: max_iter
      Dimension of implicit features: latent_dim
      Proof of implicit characteristics of randomly generated users and projects:  $U$ 
      Parameter set of the deep neural network:  $W$ 
      Calculate the loss value according to the formula:  $L$ 
For  $k$  from 1 to max_iter do:
  For each  $\langle i, j \rangle$  in trainset
    Update  $u_i, u_j \leftarrow (VI_iV^T + \lambda_U I_K)^{-1} VR_i$ 
    Update  $v_i, v_j \leftarrow (UI_iU^T + \lambda_V I_K)^{-1} (UR_j + \lambda_V \text{dnn}(W, X_j))$ 
  End for
  Training DNN (deep neural network)
  Calculate the loss value  $L'$  according to the formula
  If  $\|L - L'\| < \varepsilon$ 
    Termination of iteration
  End for

```

ALGORITHM 1: Optimization algorithm based on the deep neural network and matrix decomposition.

TABLE 5: Schematic diagram of entrepreneurial project data.

Field	Data
Item number	10005
Project name	VICO Smart Car Box
Project area	Automobile traffic/vehicle networking and hardware
Financing rounds	Angel wheel
Project description	VICO Smart Car Box provides car networking equipment and services
Item label	Equipment/traffic/vehicle networking
Region	Haiding District, Beijing
Project status	Not online

4.2.6. *Full Connection Layer.* The combined features need to extract the abstract features of the project through the whole connection layer, and the calculation formula of all connection layers is as shown in

$$X_{fc} = f(W_{fc}X + b_{fc}), \quad (20)$$

where  $f$  represents the activation function,  $W_{fc}$  represents the parameter set, and  $b_{fc}$  represents the offset set.

4.2.7. *Output Layer.* The purpose of the output layer is to transform the output of the previous layer into feature vectors contained in items with specific dimensions. The calculation method is shown in

$$\text{output} = f(WW_{fc} + b). \quad (21)$$

TABLE 6: Sample table of user information.

Field	Data
User number	75
User region	Sichuan Chengdu
User profile	After graduating from college, I have been starting a business and setting up overseas projects, and now I am transforming to make an investment
Areas of concern	Automobile/advertisement/hardware/culture/sports/software
User's purpose on the website	Find an investment target/understand new companies and new products

## 5. Model Optimization

To optimize the above model, the optimization objectives are shown in

$$\begin{aligned}
& \max_{U, V, W} P(U, V, W | R, X, \sigma^2, \sigma_U^2, \sigma_V^2, \sigma_W^2) \\
& = \max_{U, V, W} [P(R | U, V, \sigma^2) P(U | \sigma_U^2) \\
& \quad \cdot P(V | W, X, \sigma_V^2) P(W | \sigma_W^2)]. \quad (22)
\end{aligned}$$

By optimizing formula (22), the optimal  $U$ ,  $V$ , and  $W$  can be obtained. In this paper, the gradient descent algorithm is adopted, and the first partial derivative of  $U$  and  $V$  in formula (22) is obtained so that it is equal to 0, and the gradient descent direction can be obtained, such as

$$u_i \leftarrow (VI_iV^T + \lambda_U I_K)^{-1} VR_i, \quad (23)$$

$$u_j \leftarrow (UI_j U^T + \lambda_U I_K)^{-1} (UR_j + \lambda_U \text{dnn}(W, X_j)), \quad (24)$$

where  $W$  represents the parameter set of the depth neural network, which cannot be solved directly by the above formula, but when  $U$  and  $V$  are determined, the depth neural network can be established.

The above optimization process can be described by Algorithm 1.

Using the algorithm in the third part, we can get the hidden features  $u$  and  $v$  of the optimal user and scheme and use  $u$  and  $v$  to predict the missing score information in the score matrix  $R$ . The score of user  $I$  on item  $J$  can be calculated by

$$r_{ij} \approx \widehat{r}_{ij} = u_i^T v_j. \quad (25)$$

Calculate the user's scores of all items, sort the predicted scores from big to small, and take the first  $k$  results as the user's top  $k$  recommendation results.

## 6. Experiment and Evaluation

**6.1. Data Acquisition and Data Processing.** In this paper, a Python crawler is used to capture data from a network information platform. Different information needs to be processed separately, and the processing methods are as follows.

**6.1.1. Missing Data Processing.** After deleting the data of users with too little action, users with too much data, and entrepreneurial projects, there are 7762 entrepreneurial projects and 7765 users. With the implicit feedback data processing method, the sparsity of 248605 scoring data of users is 99.59%.

**6.1.2. Data Processing of Entrepreneurial Projects.** Among the entrepreneurial projects, only a few projects have a loss value. Table 5 is an example of entrepreneurial project information.

**6.1.3. User Data Processing.** The characteristics of the user mainly include the user number, the user area, the user profile, the area of interest of the user, and the purpose on the user's website. Table 6 is an example table representing the characteristic data of the user.

As shown in Table 7, the loss rate of each field of user-specific information can be seen from the table whether the loss rate of user information is large or not. The main reason is that the user's characteristic data is filled in by himself when registering the user, which is unnecessary information. Among them, the missing rate of the user profile is 75.83%, which is too large to be used. The missing rate of user areas, areas of interest, and purposes on the user's websites is about 20%. Because these fields are processed using one-hot encoding, one-hot encoding has the characteristic of being able to handle missing data. Keep these three fields.

**6.2. Evaluation Criteria.** In this paper, two algorithms of the recommendation system, RMSE and Recall@M, are used to evaluate the experimental results. RMSE represents the

TABLE 7: Missing ratio of each field of user information.

Field	Deletion rate
User number	0
User region	23.26%
User profile	75.83%
Areas of concern to users	23.38%
User's purpose on the website	19.80%

mean square error, which is mainly used to evaluate prediction problems. The calculation method is shown in

$$\text{RMSE} = \sqrt{\frac{1}{|T|} \sum_{i=1}^{|T|} (r_i - \widehat{r}_i)^2}. \quad (26)$$

Recall@M is often used in the evaluation of top  $N$  recommendations. The calculation method is shown in

$$\text{Recall@M} = \frac{\sum_u |R(u) \cap T(u)|}{\sum_u T(u)}. \quad (27)$$

### 6.3. Data Preprocessing

**6.3.1. Text Data Processing.** The text introduction information and user description information of business projects need word segmentation.

**6.3.2. Word Vector and Pretraining.** Use Stanford Segmenter for word segmentation. Then, the wordERC tool provided by Python's Gensim wrapper is used to train the word vector, and finally, about 2.7 million word vectors are obtained.

**6.3.3. Feature Extraction.** In regional information processing, the data is indeed encoded separately, and finally, there are 44 regions. There are 21 areas of concern to users. There are 9 purposes on the user's website.

**6.4. Experimental Results.** In this paper, the PMF algorithm and ConvMF algorithm are selected and compared with the recommendation algorithm proposed in this paper. As can be seen from Table 8, RMSE is 9.83% higher than that of the PMF algorithm and is 2.97% higher than that of the CovMF algorithm. As can be seen from Table 8 and Figure 6, the DNN-MF algorithm significantly improves the other two algorithms in the recall indicator.

The recall rate of the DNN-MF algorithm from Figure 6 varies from 50-300, and the DNN-MF has an obvious upward trend, which is higher than the other two algorithms.

**6.5. Influence of Adding Different Numbers of Features on Recommendation Results.** In this paper, the DNN-MF model is experimented with adding various quantities of item feature information in stages, as shown in Table 9 and Figure 7.

From Table 9, the RMSE index of the DNN-MF1 model is increased by 1.73% compared with that of the ConvMF model. Compared with the DNN-MF1 model, the RMSE index of the DNN-MF2 model increased by 1.26%.

TABLE 8: Overall experimental results.

Indicators	RMSE	Recall@50	Recall@100	Recall@200	Recall@300
PMF	0.6889	0.0425	0.0736	0.1164	0.1556
ConvMF	0.6402	0.0869	0.1446	0.2422	0.3181
DNN-MF	0.6212	0.1385	0.2044	0.2975	0.3711

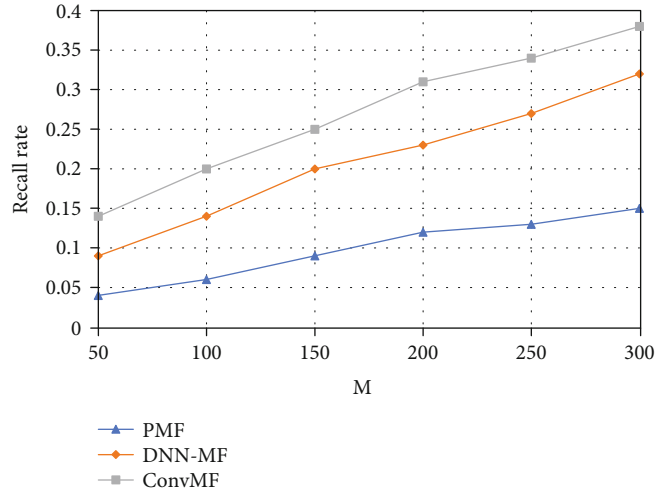


FIGURE 6: Recall rate line chart.

TABLE 9: Influence of adding different numbers of content characteristics on results.

Indicators	RMSE	Recall@50	Recall@100	Recall@200	Recall@300
ConvMF	0.6402	0.0869	0.1446	0.2421	0.3181
DNN-MF1	0.6291	0.1221	0.1861	0.2772	0.3469
DNN-MF2	0.6212	0.1385	0.2044	0.2975	0.3710

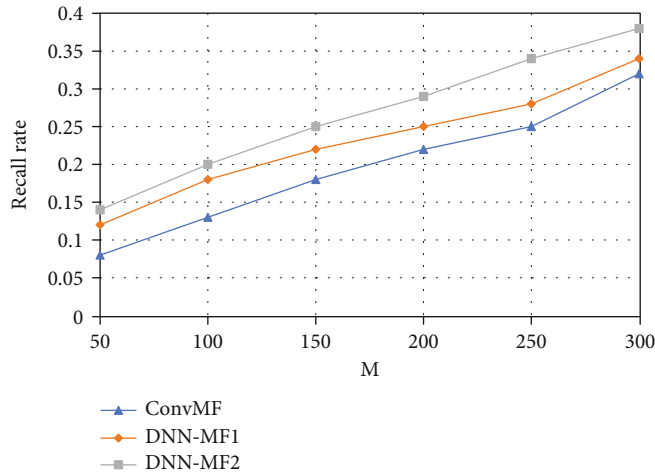


FIGURE 7: Recall rate line chart.

From the above experimental results, it can be seen that by adding more content features, the recommendation accuracy of the model can be effectively improved. This is mainly because the characteristics of project content can reflect users' interests to a certain extent. For example, for the financing rounds of entrepreneurial projects, some users

may pay more attention to the projects in the seed round, while others may pay more attention to the projects after Round A.

6.6. Influence of the Number of Implicit Features and the Length of the Word Vector on Recommendation Results. In

TABLE 10: Influence of the length of the implicit feature number and word vector number on RMSE.

Implicit feature number	50	100	150	200	250
100	0.6376	0.6279	0.6252	0.6255	0.6232
200	0.6331	0.6265	0.6237	0.6212	0.6264
300	0.6313	0.6316	0.6260	0.6246	0.6258

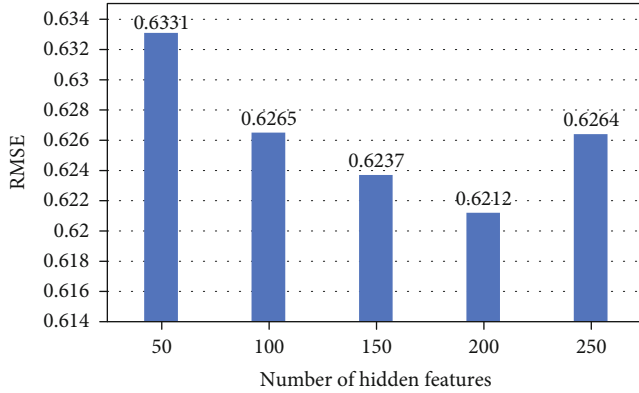


FIGURE 8: Influence of the number of hidden features on RMSE (word vector length: 200).

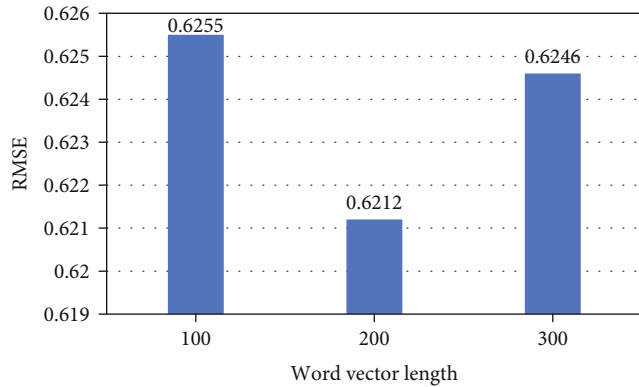


FIGURE 9: Influence of word vector length on recommendation results (number of hidden features: 200).

this paper, the grid search method is adopted. Table 10 and Figures 8 and 9 are experimental results implicitly containing the number of features and the length of the word vector. It can be seen from Table 10 that if the number of features is 200 and the length of the word vector is 200, the RMSE value obtained is the smallest and the recommendation effect is the best.

As you can see from Figure 8, if the word vector dimension is 200, the RMSE value is the smallest. When the number of implicit features increases from 50 to 200, the RMSE value of the algorithm decreases continuously.

Figure 9 is a diagram of the relationship between word vectors of different dimensions and RMSE when the dimension of implicit feature is 200. As can be seen from the figure, the recommendation effect is best when the length of the word vector is 200, so the best length of the word vector is 200.

## 7. Conclusion

Firstly, this paper introduces the basic process of an entrepreneurial project recommendation system based on a deep neural network and matrix decomposition and introduces the internal feedback data processing method and negative sampling method related to this study. Moreover, this paper introduces the principle of the entrepreneurial project recommendation algorithm based on a deep neural network and matrix factorization proposed in this paper. We introduce the principle of probability matrix decomposition and the extraction of hidden features of entrepreneurial projects. Finally, the optimization method of the model and the generation method of recommendation results are introduced.

## Data Availability

The experimental data used to support the findings of this study are available from the corresponding author upon request.

## Conflicts of Interest

The authors declared that they have no conflicts of interest regarding this work.

## References

- [1] C. Carrer, G. A. Plonski, C. Carrer, and C. E. L. . Oliveira, "Innovation and entrepreneurship in scientific research," *Revista Brasileira de Zootecnia*, vol. 39, suppl spe, pp. 17–25, 2010.
- [2] X. Hu and Y. Tan, "A study on the reasons of insufficiency of entrepreneurship initiative of Chinese college students," in *Communications in Computer and Information Science*, vol. 208, pp. 348–352, Springer Berlin Heidelberg, Dalian, China, 2011.
- [3] J. A. Cano and A. Tabares, "Determinants of university students' entrepreneurial intention: GUESSS Colombia study," *Espacios*, vol. 38, no. 45, p. 22, 2017.
- [4] W. Ragmoun, "WR A descriptive analysis of entrepreneurial female career success determinants on Saudi Arabia along entrepreneurial process," *Archives of Business Research*, vol. 7, no. 11, pp. 119–129, 2019.
- [5] J. Wichmann, "Grundideen und internationale Rezeption des Modells einer Service University," *Zeitschrift für Erziehungswissenschaft*, vol. 3, no. 1, pp. 81–96, 2000.
- [6] M. C. Pérez-López, M. J. González-López, and L. Rodríguez-Ariza, "Applying the social cognitive model of career self-management to the entrepreneurial career decision: the role of exploratory and coping adaptive behaviours," *Journal of Vocational Behavior*, vol. 112, pp. 255–269, 2019.
- [7] A. L. Merida and V. Rocha, "It's about time: the timing of entrepreneurial experience and the career dynamics of university graduates," *Research Policy*, vol. 50, no. 1, p. 104135, 2021.
- [8] K. D. Cassidy, K. A. Quinn, and G. W. Humphreys, "The influence of ingroup/outgroup categorization on same- and other-race face processing: the moderating role of inter- versus intra-racial context," *Journal of Experimental Social Psychology*, vol. 47, no. 4, pp. 811–817, 2011.



- [9] K. M. Fems, "Entrepreneurship education in Nigeria tertiary institutions and its impact on students' entrepreneurial career intentions. A study of students at Federal Polytechnic Ekowe," *Open Science Journal*, vol. 5, no. 4, 2020.
- [10] M. Banerjee, S. Biswas, P. Roy, S. Banerjee, S. Kunamaneni, and A. Chinta, "Does career planning drive agri-entrepreneurship intention among university students?," *Global Business Review*, vol. 4, 2020.
- [11] T. Baycan, "Entrepreneurial interest of university students in a multicultural society," in *A Broad View of Regional Science*, vol. 47, pp. 137–159, 2021.
- [12] S. F. F. Binti Shamsudin, A. A. Mamun, N. B. Che Nawi, N. A. B. Md Nasir, and M. N. Bin Zakaria, "Factors affecting entrepreneurial intention among the Malaysian university students," *The Journal of Developing Areas*, vol. 51, no. 4, pp. 423–431, 2017.
- [13] Z. K. Zhang, T. Zhou, and Y. C. Zhang, "Personalized recommendation via integrated diffusion on user-item-tag tripartite graphs," *Physica A Statistical Mechanics & Its Applications*, vol. 389, no. 1, pp. 179–186, 2010.
- [14] Y. Guo, M. Wang, and X. Li, "Application of an improved Apriori algorithm in a mobile e-commerce recommendation system," *International journal of entrepreneurial behaviour & research*, vol. 23, no. 2, pp. 287–303, 2017.
- [15] Y. Wang, H. Y. Ou, and J. M. Zhang, "Design and implementation of e-commerce recommendation system based on ontology technology," *Advanced Materials Research*, vol. 978, pp. 244–247, 2014.
- [16] J. Huang, B. Jiang, J. Pei, J. Chen, and Y. Tang, "Skyline distance: a measure of multidimensional competence," *Knowledge and Information Systems*, vol. 34, no. 2, pp. 373–396, 2013.
- [17] L. Liu, J. Xu, S. S. Liao, and H. Chen, "A real-time personalized route recommendation system for self-drive tourists based on vehicle to vehicle communication," *Expert Systems with Applications*, vol. 41, no. 7, pp. 3409–3417, 2014.
- [18] O. Khalid, M. Khan, S. U. Khan, and A. Y. Zomaya, "OmniSuggest: a ubiquitous cloud-based context-aware recommendation system for mobile social networks," *IEEE Transactions on Services Computing*, vol. 7, no. 3, pp. 401–414, 2014.
- [19] G. Chen and S. Li, "Research on location fusion of spatial geological disaster based on fuzzy SVM," *Computer Communications*, vol. 153, pp. 538–544, 2020.
- [20] S. Li, Y. Zhang, M. Xie, and H. Sun, "Belief reasoning recommendation –mashing up web information fusion and FOAF," *Journal of Computers*, vol. 5, no. 12, pp. 1885–1892, 2010.

## Research Article

# Resource Sharing of Smart City Based on Blockchain

**Tao Huang** 

*The University of Queensland, St Lucia Campus, Brisbane, St Lucia QLD 4072, Australia*

Correspondence should be addressed to Tao Huang; [tao.huang2@uq.net.au](mailto:tao.huang2@uq.net.au)

Received 30 August 2021; Revised 23 September 2021; Accepted 25 September 2021; Published 20 October 2021

Academic Editor: Deepak Gupta

Copyright © 2021 Tao Huang. This is an open access article distributed under the Creative Commons Attribution License, which permits unrestricted use, distribution, and reproduction in any medium, provided the original work is properly cited.

The concept of smart city refers to the improvement of the quality of life of the city by making full use of idle resources by sharing. However, limited by the technical level, the current resource sharing system mostly adopts centralized data storage mode. Systems managed in this way are vulnerable to multiple threats. The tested blockchain technology with the characteristics of decentralization and tamper resistance can effectively prevent various risks. Starting with the architecture of blockchain intelligent contract, this paper puts forward a structural optimization factor model of intelligent contract. To optimize the structure of blockchain intelligent contract, the gas optimization theory is put forward by changing the order, reducing the use of costly EVM data fields, reducing redundant fields, and optimizing intelligent contract codes. Experimental analysis of the proposed model is carried out, and the effectiveness of the proposed method is verified by comparing the transaction execution time of cost calculation with the cost of executing gas, which can provide reference for the selection of intelligent contract organization structure of smart city resource sharing system.

## 1. Introduction

The concept of smart city refers to the improvement of the quality of life of the city by making full use of idle resources by sharing. Due to the limitation of technical level, most of the current resource sharing systems adopt centralized data storage mode. Systems managed in this way are vulnerable to multiple threats. In addition, the traditional sharing method cannot establish an objective and true credit mechanism for bad users, which leads to potential safety hazards. The tested blockchain technology with the characteristics of decentralization and tamper resistance can effectively prevent various risks. This paper proposes an algorithm to predict transaction execution time and gas execution cost and verifies the effectiveness of the algorithm by experiments, which can provide reference for the selection of intelligent contract organization structure in smart city resource sharing system.

Literature [1] proposes a method based on network tomography to realize low-cost, scalable, and flexible monitoring deployment of the road network system. It can complete the path matching of smart city system. Literature [2] studies the specific positioning and components of data cen-

ter. Based on the construction requirements of data center, it constructs an architecture of smart city, related contents, and construction ideas that data center should contain in it and discusses the application of data center in smart city. Literature [3] proposes an infrastructure based on blockchain to realize sustainable Internet of Things (IoT) sharing economy in super smart cities, so as to support space-time intelligent contract services for security and privacy. Literature [4] constructs the smart city blockchain vehicle information network system. By running the system in a decentralized way, a multipoint collaborative transportation management system can be built. Literature [5] proposes an efficient, scalable, and blockchain-based distributed smart city network architecture-light-fidelity (Li-Fi) communication technology. In order to solve the rapid increase in the number and diversity of smart devices connected to the Internet, literature [6] establishes a new multi-interconnection system framework of smart cities. Through the design of hybrid architecture, the architecture is divided into two parts: core network and edge network, which improves the efficiency and solves the limitations of the current architecture. Literature [7] proposes a multivariate system model which is divided into core network and edge

network and puts forward a working proof scheme in the model. Literature [8] uses blockchain technology to take a global view of the security policy in the system and integrate it into the FIWARE platform. Literature [9] deeply explores the association between sensor networks and blockchain smart contracts. The concept of “rolling blockchain” is put forward, which can be used as a network node to build wireless sensor networks with the participation of smart cars. Literature [10] puts forward a workflow chart of technical experiment to explore how blockchain technology can protect the integrity of sensor data when the Internet of Things is the infrastructure. A data management framework of Internet of Things is constructed, which can strengthen data-driven operation. Literature [11] identifies the basic elements of smart cities, then provides a detailed literature on the existing technologies for realizing smart cities, highlights their shortcomings, and explains how blockchain can help the effective implementation of these technologies. Literature [12] proposes a decentralized architecture using blockchain, which can run ledger services on distributed networks. Literature [13] proposes a blockchain-based power transaction (B-ET) ecosystem and designs an intelligent contract to ensure that the transaction is conducted in a safe and reliable way. Literature [14] proposes an infrastructure based on blockchain to support space-time intelligent contract services for security and privacy, which can be used for sustainable sharing economy in megasmart cities. Literature [15] proposes a smart city information exchange blockchain network, which is helpful to establish sharing among several untrusted organizations. The proposed approach enables one organization to safely use data from another organization to participate in business operations without having to access the data.

According to the research status proposed in this paper, there is no description of the differences in contracts in blockchain. However, there is no intelligent contract method for resource sharing mechanism. The intelligent contract method proposed in this paper can reduce the operating cost and improve the overall performance.

## 2. Brief Introduction of Blockchain Intelligent Contract

### 2.1. Brief Introduction of Blockchain Technology

*2.1.1. Blockchain Technology.* Blockchain is a distributed ledger, which can provide verifiable evidence of transactions between sender and receiver. It has no central repository, and it is continuously maintained by many investors (possibly individuals or organizations).

From the perspective of discipline boundary, the research topics of blockchain include mathematics, cryptography, data network, and many other directions. In practical application, blockchain plays its sharing function, which can be applied to the network architecture where multiple individuals interact, and has antitampering function. Blockchain can reduce the probability of omitting all transaction information in the network and complete the necessary repair and maintenance work at the necessary time. Blockchain is

essentially a distributed database. Bitcoin, Ethereum, etc. use blockchain as the underlying technology and use the Hasi specification method to generate a series of data fields. These data blocks all have data messages that generate the next block, and they all contain a record of the complete error process, which is used to verify whether the information is valid and ensure its security.

The three types of blockchain are private chain, alliance chain, and public chain. All data in the public chain is accessible to the public, including Bitcoin and Ethereum. However, alliance chain and private chain will have access restrictions in Table 1.

The relationship between blockchain and multiple data blocks can be understood as the relationship between record list and record chain. Blockchain network can be regarded as a decentralized account book of public network. The ledger is also publicly shared among users. Blockchain creates a constant database for transactions between individuals in the network. Each item stores data with a timestamp and is linked to the previous item, and each digital record or transaction can be reorganized into a block linked to a particular participant. At a certain level, these individual data blocks together constitute an information network that is difficult to modify and attack, and only when there is consensus among individuals can it be maintained and updated. Blockchain technology ensures the credibility of information in the matching system by this method. In short, you can think of blockchain as a record-based repository, which can replicate data on a large peer-to-peer computer network instead of a central server.

Blockchain uses the Secure Hash Algorithm (SHA) or Hash Encryption Method. Hashing algorithms do not use secrets such as passwords or keys to provide security. A hashing algorithm can convert any part of information data such as numbers (such as text and pictures) into data fields having a prescribed length. The National Institute of Standards and Technology (NIST) has developed a hash specification, which is publicly available to government and private users.

*2.1.2. P2P Networks.* P2P (peer-to-peer) network is a peer-to-peer network architecture. At present, the dominant network structure is client-server mode. In this network structure, there are two roles: client and server, and the server serves the client as a center. Through the P2P network, the traditional top-down structure is broken, but each node provides services to each other, and each node is both a client and a server. This decentralized approach allows permissions to be distributed over multiple network nodes instead of centralizing on a single central server.

Because of the decentralized propagation of the P2P network, the blockchain technology can distribute data fields to each node through intelligent contracts to realize distributed accounting. In this manner, multiple copies of the data fields are provided and stored in each node where consensus is reached. When the ledger is threatened by tampering, attack, etc., only the data nodes stored on a single node are maliciously attacked, and the whole blockchain network will not be affected. Therefore, by increasing the geometric

TABLE 1: Differences between block chains.

Property	Private chain	Alliance chain	Public chain
Participant	Members within the organization	Alliance member	Anyone
Read permission	Restricted	Public or restricted	Public
Consensus mechanisms	Solo and PBFS	PBFS, Kafka, Raft	PoW, PoS, and DpoS
Efficiency	High	Low	Low
Represents	Multichain	Hyperledger fabric	Bitcoin and Ethereum

multiples of attack cost and difficulty, the blockchain network meets the requirements of tamper resistance and transaction security, and the blockchain network has the characteristics of decentralization and extensibility.

Each node in a peer-to-peer network has two functions, one is to maintain its own data information, and the other is to verify and propagate the data information of other nodes. Blockchain spreads the transaction data to individuals in each regional network, and after being tested by preset judgment conditions, it continuously spreads effective information in the network. It is this mechanism that ensures the accuracy and effectiveness of data information stored in blockchain network. Individuals in the regional chain network are distinguished by their own accommodation limits and are divided into all nodes with all information data from the establishment of the whole network to the current time, and light nodes with relatively weak accommodation capacity, such as various hard disks, which can only retain some information associated with themselves. There is interactive function between full node and light node. The decision mechanism of each individual in the local area network is formulated by the asymmetric encryption algorithm, so as to judge the transaction data. During the transaction, the public key (used to validate the transaction data) is paired with the private key (used to encrypt the transaction data).

The node uses the private key to sign the transaction information and then initiates the transaction. Once the transaction is accepted by the corresponding node, the initiator's public key is used to verify the received transaction. In blockchain technology, two parties who do not know each other do not need to be certified by centralized certification bodies but only need to trust the algorithm-based trading rules to establish mutual trust and reach consensus.

The emergence of the P2P technology provides an efficient and fast way for users to download network resources. Adding recommendation algorithm to the P2P sharing platform can enable users to capture the resources they are interested in in a small range, so as to effectively improve the utilization rate of resources and realize the rapid use and sharing of resources.

**2.1.3. Consensus Mechanism.** The blockchain network has decentralized and scalable data storage mode, which requires high trust between nodes, which needs to be realized by different consensus methods. At present, common consensus methods mainly include proof of rights and interests, proof of workload, proof of entrusted rights and interests, and practical byzantine fault tolerance in Table 2.

Among the four common blockchain consensus mechanisms, this paper adopts the consensus mechanism of entrusted rights and interests proof. In cryptocurrency technology, the consensus algorithm of entrusted rights proof is used to ensure the security and reliability of the whole blockchain network.

**2.2. Smart Contracts.** Intelligent contract is the core of resource sharing system. The research on intelligent contract operation mechanism and Ethernet gas mechanism can provide reference for the selection of intelligent contract organization structure of smart city resource sharing system. Smart contract can help make decisions, provide verification and execution functions, store data and trade functions for the system, and realize the applications needed by a variety of resource sharing systems. Figure 1 shows how smart contracts work. With the spread of transaction data, intelligent contracts are constantly taking effect at various nodes in the blockchain network. Smart contracts can be preinstalled with relevant condition settings and corresponding rules. When the conditions are met, corresponding operations can be performed when relevant functions are automatically triggered, thus realizing comprehensive management and control of physical and digital assets.

**2.3. Encryption Algorithm.** Encryption can protect data from theft or tampering. This key can be used for user authentication. There are three general and widely used encryption schemes: symmetric encryption, asymmetric encryption, and hash function. This paper introduces the homomorphic encryption algorithm.

Homomorphic encryption is regarded as a bright pearl in the field of cryptography, which is a method of processing data without accessing the data itself, that is, the result of processing ciphertext in encrypted state is the same as that of corresponding plaintext operation. Homomorphic encryption can realize ciphertext addition and multiplication at any time. In 2009, Pascal Paillier proposed a provable additive homomorphic secure encryption system. This scheme allows any computable function to operate the encrypted data, but it needs to be improved in practical application.

Assuming that  $M$  represents a set of plaintext and  $C$  represents a set of ciphertext, for a given key  $k$  satisfying formula (1), it is called homomorphic encryption scheme.

$$\forall m_1, m_2 \in M, E(m_1 \odot_M m_2) \leftarrow E(m_1) \odot_C E(m_2). \quad (1)$$

Among them, the symbol can be calculated directly in

TABLE 2: Common blockchain consensus mechanism.

Consensus method	Proof of rights and interests	Proof of workload	Proof of entrusted rights and interests	Practical byzantine fault tolerance
Consensus efficiency	General	Low	High	High
The trust environment used	Untrusted	Untrusted	Untrusted	Semitrusted
Computing power/resource consumption	General	High	Low	Low
The ratio of fault-tolerant nodes	As the case may be	Less than or equal to 25%	As the case may be	Less than or equal to 33.3%
Security threat	Candidate cheating	Computing power centralization	Candidate cheating	Master node failure

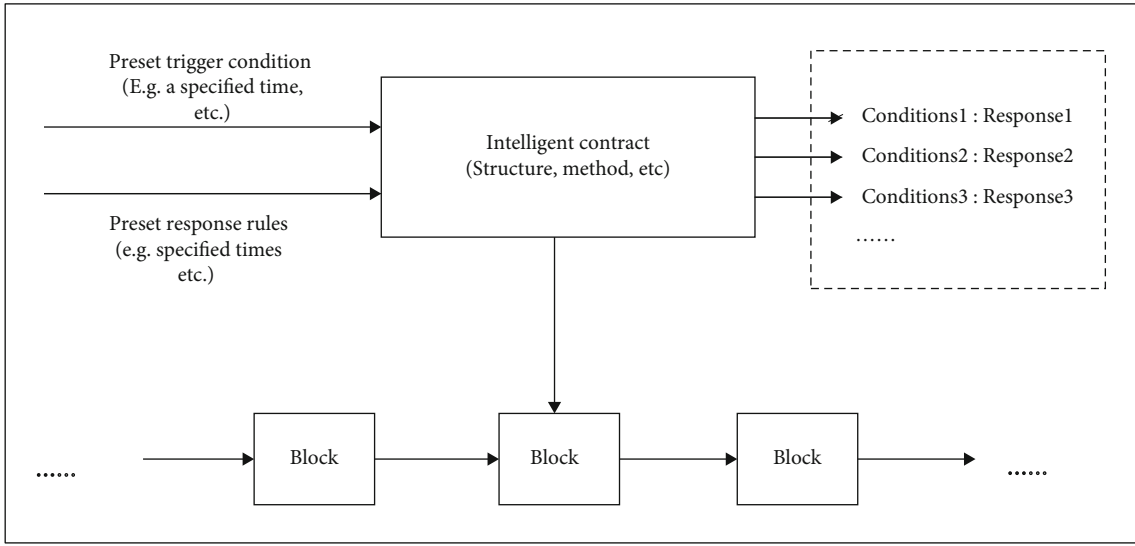


FIGURE 1: Operation mechanism of smart contract.

the set  $M$  and can be calculated directly in the set  $C$ , and neither calculation process needs any encryption and decryption.

At present, the additive homomorphism schemes are mainly Paillier, the multiplicative homomorphism schemes are RSA and ElGamal, the hybrid encryption schemes are BGV, EHC, NEHE, etc. and are given, and the ciphertext of  $+$  can be calculated. The principle of the algorithm is as follows:

Key generation section is as follows:

*Step 1.*  $p$  and  $q$  are two independent large prime numbers randomly selected, and  $\gcd(pq, (p-1)(q-1)) = 1$ , where  $\gcd$  denotes finding the greatest common divisor.

*Step 2.* Calculate the parameter  $n = pq$ ,  $\lambda = \text{lcm}(p-1, q-1)$ , where  $\text{lcm}$  is the least common multiple.

*Step 3.* Choose a random integer  $i$ , and  $i \in Z_{n^2}^*$ .

*Step 4.* Calculate  $\mu = (L(i^\lambda \bmod n^2))^{-1} \bmod n$ , where  $L(u) = (u-1)/n$ .

*Step 5.* The public key is  $(n, i)$ , and the private key is  $(\lambda, \mu)$ .

Data encryption process is as follows:

*Step 1.* Choose  $P$  as plaintext, and  $0 \leq p < n$ .

*Step 2.* Choose the random number  $r$ , and  $0 < r < n, r \in Z_n^*$ .

*Step 3.* Calculate the ciphertext  $C = i^p \cdot r^n \bmod n^2$ .

Homomorphic computation is as follows:

*Step 1.* Additive homomorphism of ciphertext:  $D(E(m_1, r_1) \cdot E(m_2, r_2) \bmod n^2) = m_1 + m_2 \bmod n$ .

*Step 2.* The ciphertext is multiplicative homomorphism with the constant  $k$ :  $D(E(m_1, r_1)^k \bmod n^2) = kmk_1 \bmod n$ .

Decryption process is as follows:

*Step 1.* The data ciphertext is  $C \in Z_{n^2}^*$ .

*Step 2.* The data plaintext  $P = L(C^\lambda \bmod n^2) \cdot \mu \bmod n$  is calculated.



### 3. Research on the Factor Model of Structural Optimization of Smart Contract

*3.1. Research on Gas Optimization Theory.* The execution of each transaction in Ethereum has the attribute of transaction cost, that is, the gas consumed by transaction execution. When a transaction contains data fields, transaction costs consist of execution costs and additional costs per byte in the data fields. If the transaction cost is  $G_t$ , the execution cost is  $G_e$ , and the data cost is  $G_d$ , there are

$$G_t = G_e + G_d. \quad (2)$$

Ethereum foundation predefines the consensus rule of gas benchmark measurement according to opcodes, so the gas consumed by each EVM opcode is fixed. The execution cost is available in the transaction log and can be debugged in a debug manner, such as in the online compilation environment Remix, to obtain all the opcodes during the execution of the transaction in sequence. Let each opcode cost  $Gas$  be  $G$ , and there are

$$G_e = \sum G_o. \quad (3)$$

In the data cost, except that each transaction has a fixed value  $Gas$  cost, the  $Gas$  cost is different according to the byte type of the data field. The fixed cost per transaction is 21,000  $Gas$ , 68  $Gas$  is required for each nonzero byte of data or code in the transaction, and 4  $Gas$  is required for each zero byte of data or code. Then, let the number of nonzero bytes and zero bytes of the additional data field of the transaction be  $N_x$  and  $N_y$ ; then there are

$$G_d = 21000 + 68N_x + 4N_y. \quad (4)$$

According to formula (1), the transaction cost of each transaction in Ethereum is positively correlated with the data cost and execution cost. From formula (2) and formula (3), we know the formation mode of data consumption and execution consumption in Ethernet Square and put forward the optimization methods from these two aspects to reduce gas consumption.

According to the above theory, the smart contract code is optimized by reducing gas cost from three aspects: changing the order of variables, reducing the use of expensive EVM opcodes, and reducing redundancy and unreasonable design of smart contract codes.

*3.1.1. Change the Order of the Quantities.* The EVM virtual machine executes in a 32-byte group each time, so the compiler will try to merge variables into 32 bytes for execution. However, the compiler cannot automatically optimize variable grouping, and it divides 32 bytes into groups according to variables of static size. According to the different byte types of different variables, the access order can be adjusted to optimize.

*3.1.2. Reduce the Use of Expensive EVM Opcodes.*  $Gas$  of EVM opcode has been defined in advance. For example,

```
contract SingleContractModel{
  uint cnt;
  struct Dealing{
    uint dealingValue; }
  mapping(uint => Dealing) private Dealings;
  function buildDealing(uint _dealing Value){
    cnt += 1;
    var newDealing = Dealing({
      dealingValue:_dealingValue });
    Dealings[ent] = newDealing;
  }
}
```

CODE 1: Simplified code for a single smart contract.

TABLE 3: Offsets between predicted events and test time.

Trading volume	200000	400000	600000	800000	1000000
Test time (s)	0.289	0.265	0.214	0.336	0.346
Forecast events (s)	0.318	0.336	0.346	0.354	0.360
Offset value (s)	0.029	0.071	0.132	0.018	0.014

adding ADD opcode consumes 3  $Gas$ , dividing DIV opcode consumes 5  $Gas$ , while SSTORE opcode means writing data, which requires 20000  $Gas$  for the first writing and 5000  $Gas$  for remodification. Therefore, taking SSTORE opcode as an example, it is expensive to modify it again, and the optimization direction needs to avoid repeated writing, that is, it can write as much data as possible at one time.

*3.1.3. Optimize Smart Contract Code to Reduce Redundancy and Unreasonable Design Code.* Reducing redundant and unreasonable code design can reduce the gas cost caused by code transmission and also reduce the use of EVM opcodes, thus reducing the gas cost more effectively. Therefore, it is necessary to try our best to remove redundant and unreasonable codes in the system with intelligent contract as the core.

*3.2. Algorithm Establishment.* Different from Bitcoin, the Ethernet platform uses Merkle Patricia tree instead of Merkle tree. By modifying the block structure, it avoids the fact that the original node can only obtain the global state of the system through the processed transactions, so that each region can clearly give the global state of the system. The structure of the MPT tree (that is, the Merkle Patricia tree) is the organizational structure of the Patricia tree. Ethernet uses the MPT tree to store the account Trie for special processing of key values and uses a special hexadecimal prefix (HP) encoding for key values, which corresponds to 16 characters in the alphabet. And before the node is inserted into the MPT tree, the key value is hashed once again by sha3 ( ), so that the key value is random, so the MPT tree used in the global state of Ethernet can be regarded as a random 16-fork Patricia tree. According to the relationship between tree height expectation and node size of randomly asymptotic Patricia tree, the relationship between tree height expectation and node number of binary Patricia tree is as

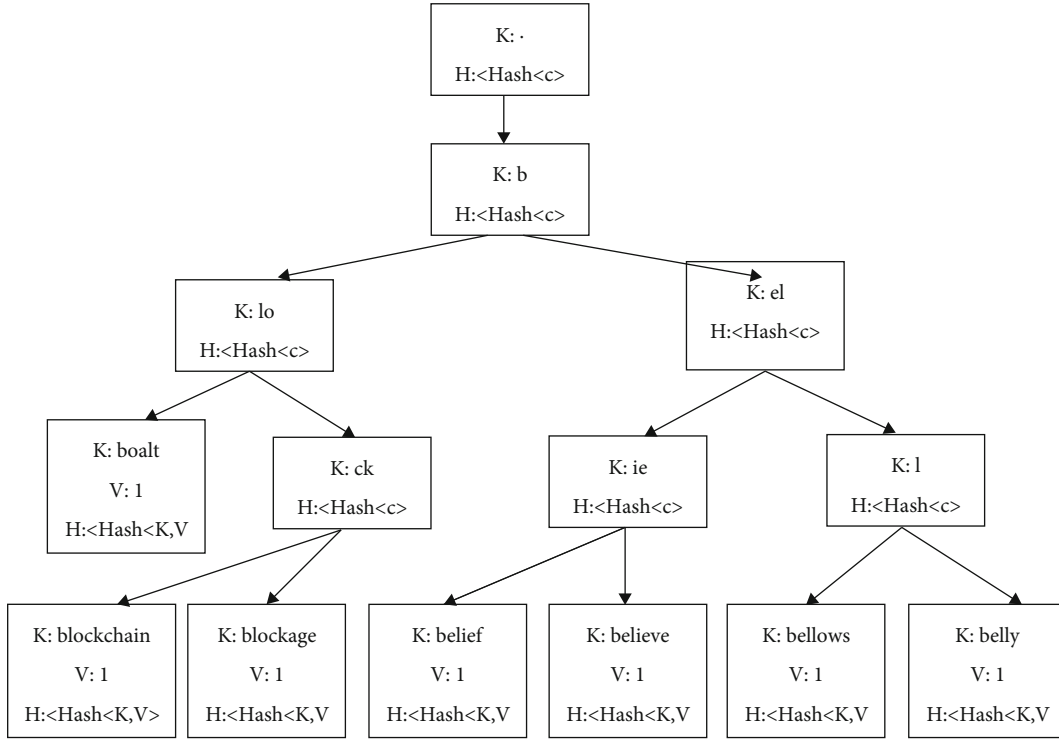


FIGURE 2: Ethernet MPT tree in gas theory.

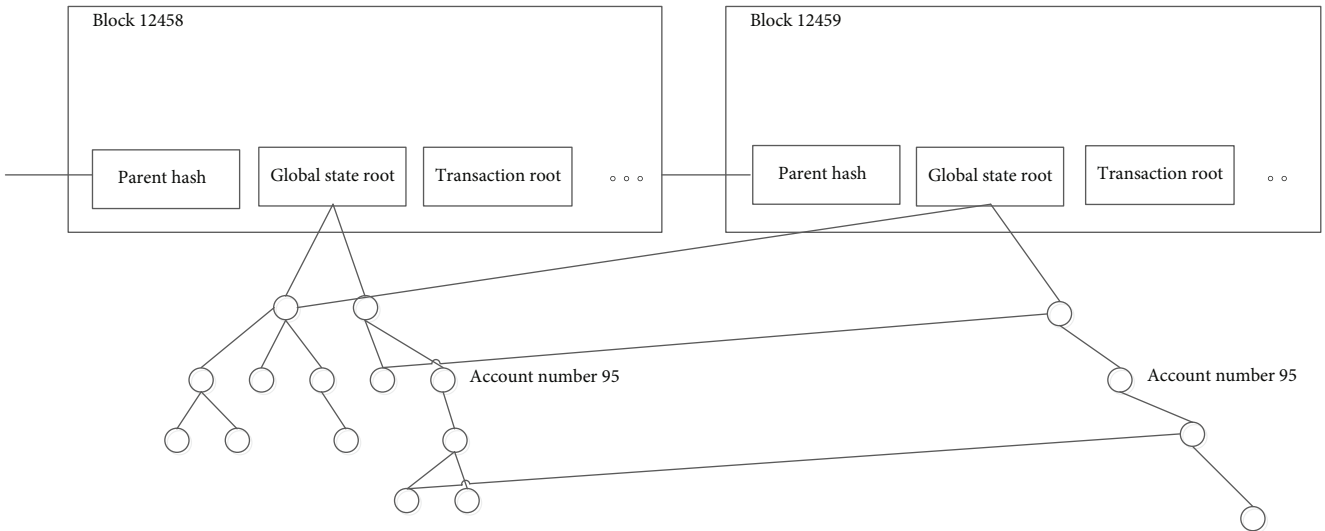


FIGURE 3: Transition of global state Trie of Ethereum.

follows:

$$E\{H_n\} \sim c \log n, \tag{5}$$

$$\text{where } c = \frac{2}{\log_2\left(1/\sum_j P_j^2\right)}.$$

Since the MPT tree in the global state can be regarded as a random Patricia tree with 16 forks ( $P_j = 1/16, 1 \leq j \leq 16$ ),

according to formula (4), we can deduce the following:

$$E\{H_n\} \sim \log(n)/2. \tag{6}$$

When an intelligent contract executes a new transaction, i.e., inserting or modifying leaf nodes in an MPT tree, all hash values on the path will be updated because of the characteristics of the Merkle tree, that is, all nonleaf node values of tree height will be updated. And because the MPT node is stored in LevelDB, the database needs to be read and updated. Assuming that the average time of each node in

MPT is  $t$  (including the time of calculating Hash and accessing database), then when the transaction scale reaches  $r$  and then executes another transaction, it can be concluded that the average time required to modify MPT tree is

$$T_{mpt}(n) = t \log(n)/2. \quad (7)$$

Set the deployment intelligent contract consumption gas to  $G_{deploy}$  and the one-time transaction consumption gas to  $G_{tran}$ ; then the total consumption gas when the transaction amount is  $n$ :

$$G(N) = G_{deploy} + \sum G_{tran}. \quad (8)$$

By analyzing the MPT tree of the underlying structure of Ethernet Square as a 16-fork Patricia tree, the relationship between transaction volume and tree height is determined. Since updating the transaction node will result in updating the  $\log n$  node, the relationship between transaction volume and time is derived. Gas cost, additional data size, and EVM opcode have definite calculation formulas, so gas cost can also be derived from transaction volume.

When the data is dispersed into the newly created smart contract, the read time is positively correlated with the height of the global state tree. But with it, there is a lot of gas expenditure, which is used to create new smart contracts. Therefore, according to the actual system, the transaction execution time and gas consumption can be predicted from the transaction scale, and these two factors can be considered to choose different intelligent contract organization structures for the system.

**3.3. Algorithm Verification.** Any one of the three organizational architectures of intelligent contract is based on MPT tree, so it can be used for algorithm verification. This verification chooses a single intelligent contract. Considering the execution time and execution cost, the smart contract with code simplification is adopted, as shown in Code 1; this code uses the structure Dealing, links the structure with a mapping index, and then executes build Dealing, saving the Dealing information in the Single Contract Model's storage space, and the newly added Dealing storage will enter the Single Contract Model's storage Trie.

If the transaction volume is  $n$ , the successful execution time of the transaction is  $t$  (including calculating the sha30 hash function and the time of database access), and  $a$  data structure is changed in one transaction; the average time of the next transaction after  $n$  transactions that have been executed is

$$T(n) = t \log(an)/2 \quad a > 0. \quad (9)$$

Each transaction changes the data structure  $a = 1$ , and the average time to access the database  $t = 0.12$  ms (since LevelDB random access dramatically degrades performance with the increase of data volume,  $t$  will continue to increase, which is only an average in the simple use test here). When  $G_{deploy} = 119799$  and the control input data is always 1, then

```
Struct Dealing {
    address userAddress;
    Uint256 date;
    Uint64 dealingNo;
    Uint64 publishingNo;
    Address publisherAddress;
    Uint64 price;
    State state;
    String newTime;
}
Enum State {Created, Pending, Completed, Stopped}
```

CODE 2: before manual optimization of specified structure.

```
'Struct Dealing {
    Uint64 dealingNo;
    Uint64 publishingNo;
    Uint64 price;
    Address publisherAddress;
    address userAddress;
    State state;
    String newTime;
    Uint256 date;
}
Enum State {Created, Pending, Completed, Stopped}
```

CODE 3: Code after manual optimization of specified structure.

$G_{tran1} = 62319$  and  $G_{tran} = 47319$  are measured. The next transaction after  $n$  transactions are executed:

$$T_{predict}(n) = 0.06 \log(n). \quad (10)$$

After the transaction volume is  $n$ , the consumption gas is

$$G_{predict}(n) = 47319n + 87480. \quad (11)$$

In this experiment, a dedicated Ethernet chain is built on the server, and 10 Ethernet nodes are deployed. Deploy the above simplified contract, which generates transaction structure data every time it is called. Execute transactions randomly in the system. The Ethernet node prints logs internally and records the consumption of transaction time, gas consumed by transactions, and transaction volume in the global intelligent contract account. When the transaction volume reaches millions, stop the above experiment, write data analysis scripts, and extract data such as processing log time. Under different transaction volumes, the offset value between the forecast time and the test transaction execution time is shown in Table 3.

By comparing the error between the predicted value and the test time, the blockchain method in this paper can have little correlation with the actual business occurrence time. It shows that the test time is safe and reasonable, which can represent the good performance of the system.

Because the prediction curve in this paper is calculated with a fixed  $t$  value, the  $t$  value in the real environment is

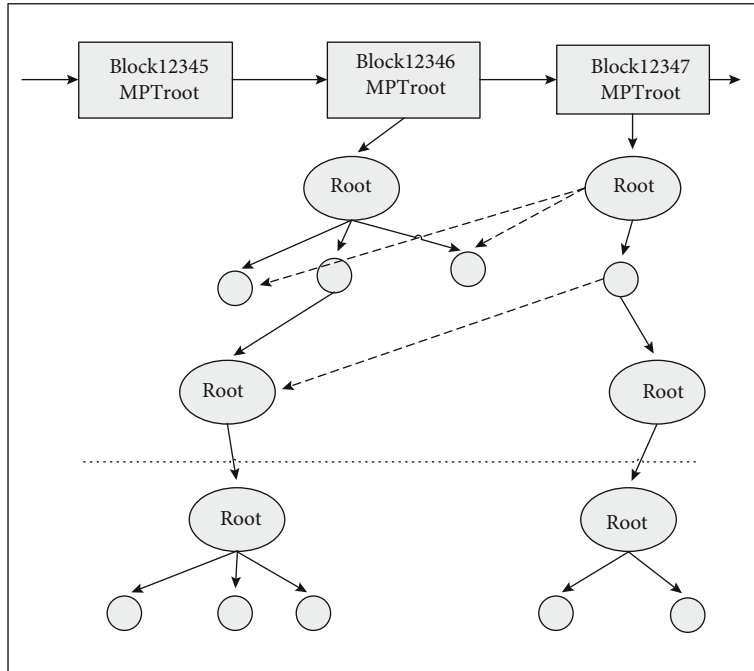


FIGURE 4: Organizational architecture of smart contract.

from small to large, which is mainly determined by the reading performance of LevelDB. Within 200000 data, the predicted value is significantly larger than the experimental data, because the actual time is smaller than the fixed value used in calculation. With the increase of trading volume, the distribution of experimental data on both sides of the curve is more obvious, and the prediction is effective. The overall offset value is less than 0.1s, which is acceptable and proves the effectiveness of the algorithm. Once the smart contract structure is fixed and the input data is fixed, it can be seen from the above that the consumption of gas is fixed and can be completely calculated, so the algorithm is correct.

After the above verification, it can be seen that the prediction algorithm is effective. Then, according to the system transaction volume and the implementation of the specific system intelligent contract code, we can choose the time and gas cost and then choose different intelligent contract organization modes.

#### 4. Performance Test

Gas is the consumption unit for deploying and executing smart contracts in Ethereum, which represents the amount of computation required to execute transaction operations. Therefore, the constraint of gas factor must be considered when designing related business process contracts. Gas mechanism can encourage computing nodes to participate in negotiation mechanism to create transactions, thus ensuring that Ethernet can continue to be decentralized without trust under increasingly complex intelligent contracts in Figure 2.

Gas is an important performance index in Ethernet Square system. Therefore, the next step will be to analyze

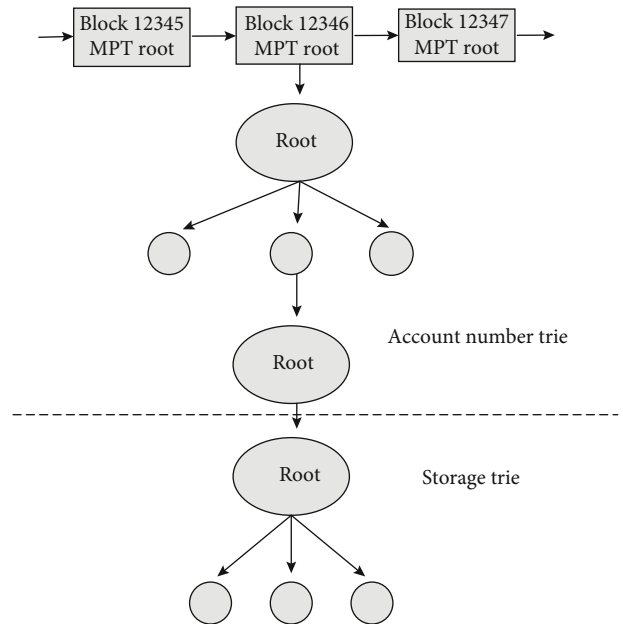


FIGURE 5: Account Trie and storage Trie.

and test from the perspective of gas consumption. First, the function code was specified for the gas optimization analysis, the detailed optimization method was elaborated, and then for the function for the Gas test, and the Gas trend graph and optimization percentage were drawn to verify whether the gas optimization method is effective. Finally, according to the optimization theory, the code of the whole intelligent contract is processed by these three methods in turn, and the optimization results are checked by comparing the gas test values before and after optimization in Figure 3.

TABLE 4: Formulating function gas consumption.

Gas consumption	Transaction cost	Execution cost	Date cost
Original distribution	84177	62905	21272
Change sequence variable	83576	61347	21274
Reducing high energy consumption directive	76862	56727	21272
Redundant code cut	72022	51750	20270

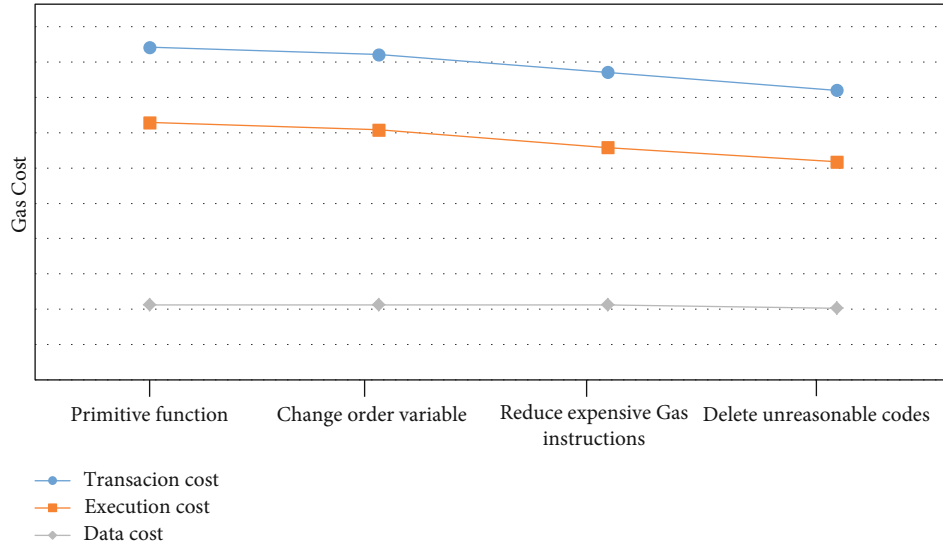


FIGURE 6: Line chart of gas consumption of function.

**4.1. Gas Optimization Analysis.** According to the gas optimization theory proposed in section 3, the intelligent contract code is optimized by reducing gas cost from three aspects: changing the order of variables, reducing the use of expensive EVM opcodes, and reducing redundancy and unreasonable design of intelligent contract codes. The following is a detailed explanation and example of manual optimization for specific functions.

**4.1.1. Change the Order of the Quantities.** The EVM virtual machine can only read sequentially and process variables in a group of 32 bytes. The declared variable type `unit64` occupies 64 bits, that is, 8 bytes, `unit256` occupies 256 bits, that is, 32 bytes, the variable type address occupies 160 bits, that is, 20 bytes, string is a variable length variable, that occupies different bytes according to the stored variable length, and state occupies 8 bits, that is, 1 byte according to the defined type of enumeration. Then, considering the unreasonable order of variables, try to sort them in a group of 32 bytes, and put the variables updated at the same time together to effectively reduce gas consumption. The manually optimized code is shown in Codes 2 and 3.

**4.1.2. Reduce the Use of Expensive EVM Opcodes.** Call the function `personAllDealing()`, `tempNo` as a temporary variable, get the total number of orders for the user, and write that number to the return value result. The global variables `cntDealing` and `tempNo` are counted in a self-growing way and are used in their functions. However, `cntDealing` has a

better way, that is, after `tempNo++` gets the final result, it directly assigns a value to `cntDealing` once. That is, `cntDealing = tempNo` is used instead of `cntDealing` for optimization purposes in Figures 4 and 5.

**4.1.3. Optimize Smart Contract Code to Reduce Redundancy and Unreasonable Design Code.** The function of `tempNo` is to obtain all the orders of the user. This operation can be calculated after the client obtains all the order information. There is no need to consume gas calculation in the intelligent contract, so this part of unreasonable design code is removed to reduce gas consumption.

As shown in Table 4 and Figure 6, it is the change trend of consuming gas by manually optimizing the specified function `personAllDealingO` in three ways in turn and initiating the same order data information query. It can be seen from the chart that the consumption of gas has dropped significantly. After three optimizations, the transaction cost of gas has dropped by 12.9%, so it can be proved that it is effective to optimize smart contracts from three aspects: changing sequence variables, reducing expensive gas instructions, and reducing unreasonable codes.

**4.2. Gas Optimization Test.** Functions in blockchain intelligent contract architecture consume gas with the selection of associated bytes or the distributed output of contracts. Therefore, by integrating the information contained in contracts into EVM function codes, the gas consumption of contract-related function codes is tested and improved.



TABLE 5: Gas expenditure for smart contract deployment.

Gas consumption	Transaction cost	Execution cost	Date cost
Original distribution	4873802	3670188	1203614
Variable sequence	4863592	3662582	1201010
Control modify variable operation	4860415	3662063	1198352
Reduce useless code	4473174	3357074	1116100

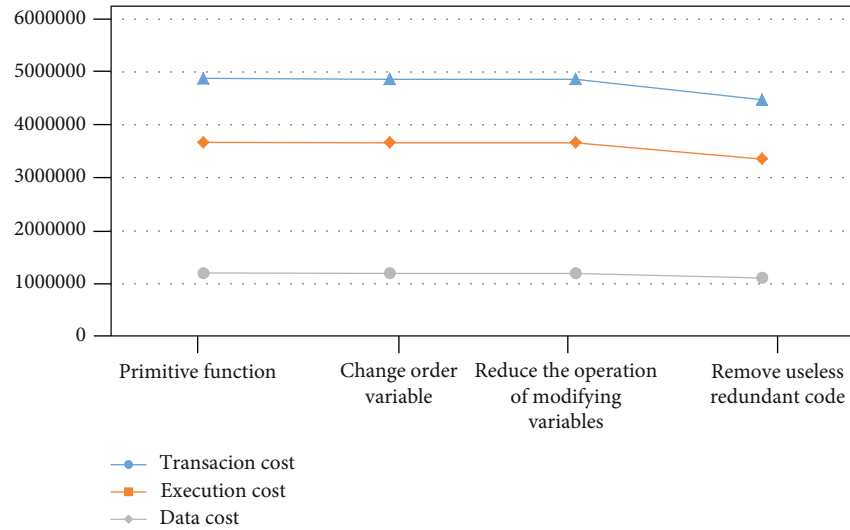


FIGURE 7: Gas consumption trend chart of smart contract deployment.

Table 5 and Figure 7 show the trend chart of gas cost for deploying smart contracts. It can be seen that the consumption of gas in millions has decreased. Because the smart contract has been written as concise and reasonable as possible, the cost of gas transaction has decreased by 8.22% after the final three methods, thus completing the gas optimization and testing of smart contract.

As can be seen in Figure 7, the execution cost can be reduced a lot through blockchain. Among all indicators, the execution cost of blockchain is lower than the conversion cost. The greater the change, the better the performance, and the lower the cost of the proposed method.

## 5. Conclusion

In this paper, the optimization factors of intelligent contract structure of smart city sharing system are studied. The structure of intelligent contract can be divided into two situations: the code structure of intelligent contract and the organizational structure of intelligent contract. The key factor affecting the performance of intelligent contract includes gas cost. Firstly, based on the composition of gas cost of transaction, the gas optimization theory is put forward, and the way to optimize intelligent contract code by changing the order of variables, reducing the use of expensive EVM opcodes, and reducing redundant codes is put forward, which provides a basis for the optimization of intelligent contract code in the final system. In addition, an algorithm for predicting transaction execution time and gas execution cost is proposed. According to the different

transaction volume of specific systems and the implementation mode of intelligent contracts, the reference of intelligent contract organization structure is given, and the effectiveness of the algorithm is verified by experiments, which provides the implementation basis for intelligent contract organization structure and the basis for the implementation of smart city sharing system.

## Data Availability

The experimental data used to support the findings of this study are available from the corresponding author upon request.

## Conflicts of Interest

The author declared no conflicts of interest regarding this work.

## References

- [1] R. Zhang, S. Newman, M. Ortolani, and S. Silvestri, "A network tomography approach for traffic monitoring in smart cities," *IEEE Transactions on Intelligent Transportation Systems*, vol. 19, no. 7, pp. 2268–2278, 2018.
- [2] J. Su, "The research of data center construction for smart city," *IOP Conference Series: Materials Science and Engineering*, vol. 490, pp. 1–6, 2019.
- [3] M. A. Rahman, M. M. Rashid, M. S. Hossain, E. Hassanain, M. F. Alhamid, and M. Guizani, "Blockchain and IoT-based

- cognitive edge framework for sharing economy services in a smart city,” *IEEE Access*, vol. 7, pp. 18611–18621, 2019.
- [4] P. K. Sharma, S. Y. Moon, and J. H. Park, “Block-VN: a distributed blockchain based vehicular network architecture in smart city,” *Journal of Information Processing Systems*, vol. 13, no. 1, pp. 184–195, 2017.
- [5] S. P. Kumar, R. Shailendra, and P. J. Hyuk, “DistArch-SCNet: blockchain-based distributed architecture with li-fi communication for a scalable smart city network,” *IEEE Consumer Electronics Magazine*, vol. 7, no. 4, pp. 55–64, 2018.
- [6] P. K. Sharma and J. H. Park, “Blockchain based hybrid network architecture for the smart city,” *Future Generation Computer Systems*, vol. 86, pp. 650–655, 2018.
- [7] S. Guo, Y. Qi, P. Yu, S. Shao, and X. Qiu, “Edge network resource synergy for mobile blockchain in smart city,” in *2020 International wireless communications and Mobile computing (IWCMC)*, pp. 1272–1277, Limassol, Cyprus, 2020.
- [8] C. Esposito, M. Ficco, and B. B. Gupta, “Blockchain-based authentication and authorization for smart city applications,” *Information Processing & Management*, vol. 58, no. 2, p. 102468, 2021.
- [9] S. Fan, L. Song, and C. Sang, *Research on Privacy Protection in IoT System Based on Blockchain*, vol. 11911, Springer, Cham, 2019.
- [10] U. Saxena, J. S. Sodhi, and R. Tanwar, “Augmenting smart home network security using blockchain technology,” *International Journal of Electronic Security and Digital Forensics*, vol. 12, no. 1, p. 99, 2020.
- [11] K. B. Adolphe, “Privacy protection issues in blockchain technology,” *International Journal of Computer Science and Information Security*, vol. 17, pp. 119–123, 2020.
- [12] J. Liu, M. Xie, S. Chen, C. Ma, and Q. Gong, “An improved DPoS consensus mechanism in blockchain based on PLTS for the smart autonomous multi-robot system,” *Information Sciences*, vol. 575, no. 12, pp. 528–541, 2021.
- [13] N. Kawaguchi, “Application of blockchain to supply chain: flexible blockchain technology,” *Procedia Computer Science*, vol. 164, pp. 143–148, 2019.
- [14] M. H. Joo, Y. Nishikawa, and K. Dandapani, “Cryptocurrency, a successful application of blockchain technology,” *Managerial Finance*, vol. 46, no. 6, pp. 715–733, 2020.
- [15] G. Lin and J. Tao, “A privacy protection method of lightweight nodes in blockchain,” *Security and Communication Networks*, vol. 2021, no. 10, 17 pages, 2021.

## Research Article

# Synchronized Information Acquisition Method for Virtual Geographic Scene Image Synthesis in Cities Based on Wireless Network Technology

Tianfang Ma<sup>1</sup> and Shuoyan Liu<sup>2</sup>

<sup>1</sup>School of Microelectronics, Tianjin University, Tianjin 300072, China

<sup>2</sup>Qiushi Honors College, Tianjin University, Tianjin 300072, China

Correspondence should be addressed to Tianfang Ma; [matianfang@tju.edu.cn](mailto:matianfang@tju.edu.cn)

Received 10 August 2021; Accepted 20 September 2021; Published 19 October 2021

Academic Editor: Deepak Gupta

Copyright © 2021 Tianfang Ma and Shuoyan Liu. This is an open access article distributed under the Creative Commons Attribution License, which permits unrestricted use, distribution, and reproduction in any medium, provided the original work is properly cited.

At present, in the process of image synthesis information acquisition of urban virtual geographic scene, there is information complexity. The existing acquisition technology is easy to disturb in the process of information positioning and transmission, resulting in large acquisition delay and affecting the final synthesis quality of the image. In response to the above problems, the method of synchronous information acquisition for urban virtual geographic scene image synthesis based on wireless network technology is studied. Based on the construction of an urban virtual geographic environment, the spatial localization of the sign target of geographic scene image synthesis is carried out, and the optical flow method is used to register the urban geographic scene images. Based on the greedy algorithm of the beacon to design the synchronous wireless network route for urban virtual scene image synthesis, and after the grid division of the wireless network in the synthesis information acquisition area, the packets of each acquisition node are acquired and transmitted according to the designed wireless network route to realize the synchronous acquisition of image synthesis information. The comparison experimental data show that the acquisition delay of the studied information synchronization acquisition method is less than 0.5 s, the acquisition synchronization rate is significantly improved, and the quality of the synthesized images is better by applying the information acquired by the method, and the practical use is better.

## 1. Introduction

Urban virtual geographic scene image synthesis is an important technology in computer vision applications, and the quality of its synthesis results will directly affect the effect of urban virtual scene construction. In the construction of urban virtual geographic scenes, it is necessary to combine the synthesis information with the geographic scene information acquired by the camera for parameter resolution and other operations, in order to improve the authenticity of the virtual geographic scene. For virtual geographic scene image synthesis, the most important thing is the efficiency and accuracy of synthesis information acquisition [1, 2]. Current research results related to the synchronous acquisition of image synthesis information are mainly applied to

medical images, and the synchronous acquisition of medical imaging synthesis information is achieved by establishing techniques such as ultrahigh field, weighted imaging, and time encoding or by combining RF communication technology [3–7]. These methods have a high synchronization rate and relatively high information acquisition accuracy, but when applied to virtual geographic scene image synthesis information acquisition, it is difficult to achieve a high information acquisition rate and accuracy due to the large amount of information to be acquired and the data being complicated, and there are limitations in the use. Synthetic information acquisition using NFC technology and wireless mobile networks requires a certain amount of manual effort to assist in achieving synthetic information acquisition [8]. This leads to the high cost of this method and is not suitable for wide-

scale use. Synthetic information acquisition using synthetic adversarial networks requires the establishment of synthetic adversarial networks, which has the problem of large delays [9–11].

Wireless sensor network is an infrastructure-free self-organized, multihop wireless network, which can sense, collect, and process various monitoring object information in real time and has wide application prospects in the military, industrial automation, intelligent transportation, environmental monitoring, etc. It is also one of the international research hotspots that have received much attention. Image synthesis requires sensors to monitor a large number of geographical parameters to enrich the virtual scene detail information and improve the quality of synthesized images. The use of wireless sensor networks in wireless network technology can effectively enhance the data transmission and processing speed and reduce the acquisition delay. Based on the above analysis background, this paper will study the method of synchronous acquisition of image synthesis information of urban virtual geographic scenes based on wireless network technology.

## 2. Research on the Method of Synchronous Information Acquisition of Urban Virtual Geographic Scene Image Synthesis Based on Wireless Network Technology

*2.1. Geographical Scene Image Synthesis Sign Target Spatial Localization.* Target location in a virtual geographic environment is the key to realize the combination of reality and virtual. Before collecting the image synthesis information of an urban virtual geographic scene, this paper first constructs the urban virtual geographic environment and then locates the sign target of geographic scene image synthesis.

Therefore, in order to improve the accuracy of scene image synthesis information acquisition, it is necessary to locate the target synthesis symbol of geographic scene image. When taking urban geographical images, the internal orientation element in photogrammetry is the parameter to determine the relevant position between the camera lens center and the image, namely, the vertical distance between the camera center,  $S$ , and the image,  $f$ , and the position coordinate  $(x_0, y_0)$  of the image main point (the vertical foot of the main optical axis on the image surface) relative to the image center. The external orientation element is the position and attitude of the photography center, including six parameters, among which three straight elements  $(X_s, Y_s, Z_s)$  are used to describe the coordinate value of the photography center in the spatial coordinate system, and the other three angle elements  $(\alpha, \beta, \gamma)$  are used to determine the spatial attitude of the photography beam at the moment of photography [12]. According to the schematic diagram of the OpenGL projection principle shown in Figure 1, the relationship between internal and external azimuth elements and the transformation matrix of the OpenGL imaging process can be determined.

When internal azimuth elements such as width and height  $(L_x, L_y)$ , focal length  $f$ , and coordinate of main point

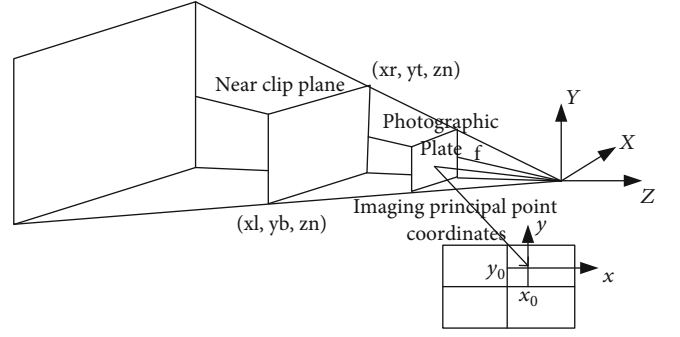


FIGURE 1: Schematic diagram of OpenGL projection principle.

$(x_0, y_0)$  of the photographic plate (CCD) are determined, the internal orientation elements are set as parameters to the function parameters of OpenGL's imaging function `glFrustum` using the isometric relationship to simulate the real camera imaging process, which corresponds to the following [13]:

$$\begin{cases} x_1 = -\frac{Z_n}{f} \left( \frac{1}{2} L_x + x_0 \right), \\ x_r = \frac{Z_n}{f} \left( \frac{1}{2} L_x - x_0 \right), \\ y_1 = -\frac{Z_n}{f} \left( \frac{1}{2} L_y + y_0 \right), \\ y_b = \frac{Z_n}{f} \left( \frac{1}{2} L_y - y_0 \right). \end{cases} \quad (1)$$

Substitute the above equation into the projection transformation formula of OpenGL, and the following projection matrix can be obtained.

$$P = \begin{bmatrix} \frac{2f}{L_x} & 0 & -\frac{2x_0}{L_x} & 0 \\ 0 & \frac{2f}{L_y} & -\frac{2y_0}{L_y} & 0 \\ 0 & 0 & -\frac{Z_f + Z_n}{Z_f - Z_n} & -\frac{2Z_f Z_n}{Z_f - Z_n} \\ 0 & 0 & -1 & 0 \end{bmatrix}. \quad (2)$$

In the above formula,  $Z_f$  and  $Z_n$ , respectively, determine the near and far cutting surfaces of the projection cone. In OpenGL, model transformation and view transformation have duality, so the model transformation matrix can also be realized by `glLookAt()`. Assuming that the camera position parameter in the external orientation element is  $(X_s, Y_s, Z_s)$  and the angle element of the space attitude is  $(\varphi, \omega, k)$ , the external parameter matrix can be calculated. According to the quantitative relationship between OpenGL perspective imaging view functional parameters and internal and external orientation elements, the projection matrix and model view required for camera imaging of urban virtual

geographic scene image are calculated through camera position, attitude, and internal parameters. According to the inverse process of OpenGL urban virtual geographic scene imaging, the imaging projection ray of the target in three-dimensional space is calculated, and the intersection of the ray and the three-dimensional scene is obtained, that is, the actual coordinates of the synthetic recognition target in the real world, where the calculation formula of pixel coordinates of the monitoring target imaging on the simulation image is as follows [14]:

$$\begin{cases} \text{winX} = \frac{w_v}{w_r} * u, \\ \text{winY} = \frac{h_v}{h_r} * v. \end{cases} \quad (3)$$

In the above formula, winX and winY are screen coordinates,  $w_r$  and  $w_v$  are the width and height of the actual image,  $w_v$  and  $h_v$  are the width and height of the virtual simulation image, and  $u$  and  $v$  are the pixel coordinates of the target on the actual image. Through the screen coordinates of the target in the simulation image, the intersection points of its projection rays on the near and far cropping surfaces in the projection cone can be obtained, and the corresponding coordinates are  $(\text{winX}, \text{winY}, 0)$  and  $(\text{winX}, \text{winY}, 1)$ , respectively. According to the inverse process of OpenGL imaging, through screen coordinates and the corresponding depth value winZ, the real world coordinates in three-dimensional space can be calculated by pressing the following formula:

$$[X \ Y \ Z \ 1]^T = M^{-1} \cdot P^{-1} \cdot V^{-1} [\text{winX} \ \text{winY} \ \text{winZ}]^T. \quad (4)$$

In the above equation,  $M$  is the transformation relation matrix between the virtual scene and the view in OpenGL and  $V$  is the OpenGL viewport transformation matrix. Finally, the imaging projection ray of the target in 3D space can be obtained in the virtual geography scene. The ray is intersected with the digital surface model in the virtual scene. The intersection position is the spatial coordinate of the target located on the surface of the earth. After locating the spatial coordinates of the composite mark target of the geographic scene image, the scene image is registered.

**2.2. Image Registration Processing of Virtual Geographic Scene.** On the basis of recording urban virtual geographic scene images, in order to retain more original urban geographic scene information and improve the accuracy of the image information synthesis, this study uses an optical flow method to register urban geographic scene images. Let the three input images with different exposure levels be  $I_1$ ,  $I_2$ , and  $I_3$ , and their exposure times are  $t_1$ ,  $t_2$ , and  $t_3$ , respectively. The optical flow method detects the brightness when the constant flow of the motion is the most accurate, so in order to accurately calculate the optical flow between  $I_1$  and  $I_2$ ,  $I_1$ 's first exposure must be consistent with  $I_2$ ; at the same time, transfer  $I_2$ 's exposure to be consistent with  $I_3$ ,

then for subsequent optical flow computing, this process can be expressed as [15]

$$\begin{aligned} I_{1,2} &= \text{clip}\left(I_1 \Delta_{1,2}^{1/\gamma'}\right), \\ I_{2,3} &= \text{clip}\left(I_2 \Delta_{2,3}^{1/\gamma'}\right), \end{aligned} \quad (5)$$

where  $\Delta_{1,2}$  is the exposure ratio between  $I_1$  and  $I_2$ ;  $\Delta_{2,3}$  is the exposure ratio between  $I_2$  and  $I_3$ ;  $I_{1,2}$  is the image that matches the exposure value of image  $I_2$  after exposure correction of image  $I_1$ ;  $I_{2,3}$  is the image that matches the exposure value of image  $I_3$  after exposure correction of image  $I_2$ ;  $\gamma'$  is the gamma coefficient, with a value of 2.2; and function clip is a clipping function whose purpose is to ensure that the pixel value of the image is within the range [0,1]. The calculation formula of exposure ratio  $\Delta$  is as follows:

$$\Delta_{i,j} = \frac{t_j}{t_i}. \quad (6)$$

In order to obtain a consistent structure of the image magnitude sequence of the urban geographic scene, it is necessary to find the optical flow from  $I_2$  to  $I_{1,2}$  and from  $I_2$  to  $I_{2,3}$ . Firstly, the optical flow from  $I_2$  to  $I_{1,2}$  is calculated assuming that the coordinate system in which  $I_2$  is located is  $\Omega = \{z_k : z_k \in R^2\}_{k=1}^N$ , and  $z_k$  is a two-dimensional coordinate in the coordinate system. In the optical flow method, the mapping relationship between images is represented by the error between feature points, and the objective function can be expressed as [16]

$$\begin{aligned} E(\{w_k\}) &= \sum_{k=1}^N \sum_{q \in N_k} r_k(q) \|I_1(z_k + w_k + q) - I_{2,1}(z_k + q)\|^2 \\ &\quad + a \sum_{k=1}^N h_k \|w_k - w_{k+1}\|^2, \end{aligned} \quad (7)$$

where  $\{w_k\}$  is the optical flow vector from  $I_2$  to  $I_{1,2}$  at each pixel position and defines  $w_{N+1} = w_1$ .  $h_k$  is the weight parameter that regulates the distance between points  $z_k$  and  $z_{k+1}$ ,  $N_k$  is a square neighborhood of point  $z_k$ ,  $a$  is the regularization factor, and  $r_k$  is the weighting function for each pixel point. The defined equation is as follows [17]:

$$r_k(q) = 1[q + z_k \in \Omega] \exp\left\{-\frac{\|q\|}{2\sigma_r^2}\right\}, \quad (8)$$

where  $1[q + z_k \in \Omega]$  means that the value is 1 if  $q + z_k$  is in the range  $\Omega$  and 0 otherwise.  $\sigma_r$  is the pixel point pixel variance;  $q$  is the pixel value of the image pixel point.

Assuming that there is a preliminary estimate for  $\{w_k\}$ , the feature points can be adjusted to obtain the optimal value. In this study, the coarse-to-fine search method is adopted to update the optical flow quantity iteratively.



Taking the linear minimization of the above function as the optimization objective, the conjugate gradient method is used to solve the optimization objective function, and the corresponding optical flow estimation from  $I_2$  to  $I_{1,2}$  is obtained. In the same way, the optical flow estimation from  $I_2$  to  $I_{2,3}$  is obtained. After the optical flow between the images is obtained, images  $I'_{1,2}$  and  $I'_{2,3}$  that are consistent with the  $I_2$  structure can be obtained by conversion. Finally, the bicubic interpolation method is used to adjust the pixel points in the images to complete the registration processing of the urban geographical scene images [18]. In order to realize the synchronous acquisition of synthetic information of city virtual geographic scene, the wireless sensor network synchronous acquisition route is designed.

**2.3. Build Wireless Network to Realize Image Synthesis Information Acquisition.** The acquisition and transmission of image synthesis information of urban virtual geographic scenes mainly rely on multiple sensors and wireless communication networks to be realized, while the computational capacity, storage capacity, and communication capacity of nodes in wireless sensor networks and the energy carried are very limited, so the routing algorithm of wireless sensor networks is particularly important. Based on the geographic location information of the image synthesis markers positioned above, a beacon-based greedy algorithm is used to design the synchronous wireless network routing for image synthesis of urban virtual scenes.

When building a wireless network to obtain image synthesis information, the target area of urban scene image synthesis information covered by the wireless network is divided into equal length grid sets, and the division results are stored in the database table. The specific division steps are as follows [19]:

- (1) Determine the parameters for dividing the grid. Specify the grid distribution range, including the minimum longitude and longitude and maximum latitude and longitude of the wireless network coverage area. The coverage area is divided into square cells with specified grid side lengths, and the grid cell side length is set to 30-50 m according to the actual urban geographic scenario
- (2) Record the geographic information of each grid, including the horizontal coordinates, vertical coordinates, minimum longitude, minimum latitude, maximum longitude, maximum latitude, central longitude, and central latitude of each grid. And label the network location information of the image synthesis markers. The purpose of dividing the grid is achieved by executing a quadratic loop system, i.e., the maximum latitude minus the minimum latitude of the network coverage area and dividing it by the grid edge length to get the number of rows of the grid table maximum longitude minus minimum longitude and dividing it by the grid edge length to get the number of columns of the grid table. The boundary value of the outer loop is used as the boundary

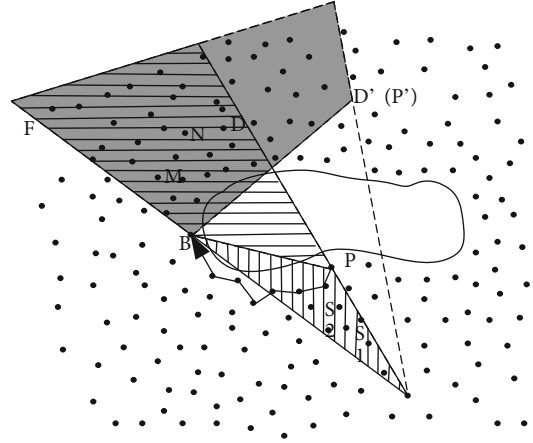


FIGURE 2: Target node shaded area and source node shaded area.

value of the inner loop, and the loop body calculates the geographic information of the grid in the current row of the current front to get the divided wireless network

According to the actual demand of urban virtual geographic scene establishment, a certain number of nodes are selected from the divided wireless network to build the source nodes for image synthesis information acquisition and transmission. Hardware devices such as cameras and sensors are placed at the image synthesis identification points to collect multiple geographic information in real time. The control and transmission of synchronous information data acquisition is realized through the wireless network source nodes. Influence the design of wireless network communication routing in order to reduce the delay of information acquisition.

As shown in Figure 2, source nodes  $s$ ,  $s_1$ , and  $s_2$  send packets to target nodes  $D$ ,  $M$ , and  $N$ . When the source node  $s$  sends a packet to the target node  $D$ , the packet is first sent to the local smallest node from  $s$  in the greedy algorithm mode, and then, it enters the surrounding algorithm mode to the beacon node  $P$ , and then, it recovers from  $B$  to the greedy mode and sends to  $D$ . If the source node knows the beacon cache  $\langle B, P \rangle$ , the next time when point  $S$  sends data to the target node  $M$  and  $N$ , it directly takes a route through point  $B$  instead of passing through point  $P$ , so that the number of routing hops can be saved. Point  $S$  will send the information of beacon cache  $\langle B, P \rangle$  to  $s_1$  and  $s_2$ , then  $s_1$  and  $s_2$  will also directly bypass point  $B$  when sending messages to  $D$ ,  $M$ , and  $N$ , which can reduce the return length of the path when bypassing the void and save the number of routing hops for them to bypass the void [20].

Based on Figure 2, when sending data packets to the target node of urban virtual geographic scene image synthesis, first, query the target node to see whether it is located in the shadow area of the target node characterized by local beacon cache. If there is a shadow area of the target node, the indirect target node is directly extracted from the beacon cache, and the grouping mode is set to data greedy mode. The data packet is sent directly to the indirect target node, that is, the beacon node. After reaching the indirect target

node, query the target node to see if it is located in one of the shadow areas of the target node characterized by the beacon cache of the node. If so, continue to the indirect destination address. If it does not exist, the urban virtual geographic scene image synthesis packet is sent directly to the target address. If the target node receives the urban virtual geographic scene image synthesis packet with this mode, the whole data transmission process is completed here. If the target node receives a packet sent in the mode of DATA|FLD, the target node also needs to send back the beacon information found during the beacon discovery process to the source node and the nodes in the shadow area of the source node. When no route hole is found in the whole routing process, the sending process is all done by greedy algorithm and the size of beacon cache  $\langle B, P \rangle$  in the packet is zero, then the target node has no beacon node information to be returned and the data sending process is completed. According to the above designed wireless network communication route transmission of each hardware device to obtain synthetic information. So far, under the transmission communication network architecture built by wireless network technology, the synchronous acquisition of synthetic information of urban virtual geographic scene images is realized by the above process.

### 3. Experimental Study

The above paper addresses the problems of the current geographic scene image synthesis information acquisition method and uses wireless network technology to build a communication network in order to improve the acquisition speed of image synthesis information. In this section, the experimental study on the method of synchronous acquisition of image synthesis information of urban virtual geographic scenes based on the wireless network technology proposed above will be conducted by setting up the corresponding experimental environment with reference to the actual situation. The following contents are the specific experimental scheme design and the experimental result analysis.

*3.1. Experimental Protocol Design.* In order to verify the application performance of this method in the synchronous acquisition of the image synthesis information of an urban virtual geographic scene, experimental analysis is carried out. The experimental tool is matlab2016, the size of image sample is 120, the training set is 50, the scale of image segmentation is 12, the gray coefficient of the image is 0.34, the similarity coefficient is 0.38, and the scale of wavelet decomposition is 18. The synchronous collection of image synthesis information of the urban virtual geographic scene is set according to the above parameters. In this experiment, the NFC-based information synchronization acquisition method and the time-coding-based information synchronization acquisition method are selected as the comparison method 1 and the comparison method 2, respectively, with the acquisition methods studied above. The practical application of the three methods is evaluated by comparing the latency of the images captured by the three methods and

TABLE 1: Synthetic information acquisition delay comparison/s.

Number	Synthetic information data volume (G)	Method for this paper	Comparison method 1	Comparison method 2
1	0.5	0.152	0.167	0.171
2	1	0.156	0.192	0.189
3	1.5	0.183	0.243	0.251
4	2	0.212	0.308	0.298
5	3	0.267	0.426	0.396
6	5	0.299	0.571	0.547
7	7	0.369	0.724	0.735
8	10	0.456	0.859	0.866

the quality of the images synthesized by applying the captured synthetic information.

*3.2. Experimental Data and Analysis.* Using three synthetic information acquisition methods to acquire the same amount of data for image synthetic information, the average latency comparison of the data acquired at each acquisition point is shown in Table 1.

Analyzing the data in Table 1, we can see that the acquisition delay of both comparison methods grows more obviously as the amount of synthetic information data increases, and the larger the amount of data increases, the faster the growth rate of the acquisition delay of both comparison methods tends to accelerate. Although the acquisition delay of this paper shows a small fluctuation, the overall value is less than 0.5 s, which can meet the demand of synthetic information acquisition of a large range of geographical scene images. The smaller the synthetic information acquisition delay, the higher the synchronization rate of the acquisition method and the better the performance. The reason for the small delay of this method is that before collecting the image synthesis information of urban virtual geographic scene, the urban landmark building target is located first, which improves the collection efficiency.

The image quality comparison after applying the synthesized information collected by the three methods for virtual city scene image synthesis is shown in Table 2, and the four indexes of the average gradient, spatial frequency, information entropy, and peak signal-to-noise ratio (PSNR) of the image are selected for image quality evaluation in this experiment.

By analyzing the data in Table 2, it can be seen that the synthesized images collected by the three methods all meet the lowest standard, and the generated images have no obvious distortion compared with the true value. However, compared with the data collected by the method in this paper, the value of the image quality evaluation index for the synthesized images is more superior. From the value of the peak signal-to-noise ratio (PSNR), the image synthesized by using the information collected by the method in this paper has a larger value in both the case of hue mapping and the case of linearization, and the synthesis effect is better. The peak signal-to-noise ratio of this method is 47.5427. The main reason is that this method constructs

TABLE 2: Comparison of composite image quality.

Method	Information entropy	Average gradient	Spatial frequency	PSNR
Method for this paper	7.2365	8.5879	22.9407	47.5427
Comparison method 1	7.1519	8.3152	20.1742	42.3145
Comparison method 2	7.1601	8.2471	22.5683	45.7431

the network topology, realizes full coverage, and improves the image acquisition quality in the process of synchronous acquisition of image synthesis information of urban virtual geographic scene.

The above experimental data analysis shows that the urban virtual geographic scene image synthesis information synchronous acquisition method studied in this paper based on wireless network technology has a low acquisition delay, a higher synchronization rate, and a better application effect compared with other methods.

#### 4. Conclusion

Due to the massive, multisource, and heterogeneous characteristics of urban geospatial data, real-time rendering of large-scale urban 3D scene has always been the difficulty of 3D geographic information technology. In order to establish a highly realistic and reliable virtual scene for urban planning, this paper studies the synchronous acquisition method of image synthesis information of virtual urban geographical environment based on wireless network technology, verifies the feasibility of this method through experiments, and verifies that this method greatly improves the quality of composite images. Firstly, locate the target space of geographical environment image synthesis signature, then register the obtained virtual geographical environment image, and, finally, build a wireless network to realize the synchronous collection of image synthesis information. In this paper, there is still room to improve the synchronization speed of the network. We can try to improve the performance of the network from the perspective of hardware optimization to further reduce the acquisition delay.

#### Data Availability

The datasets used and/or analyzed during the current study are available from the corresponding author on reasonable request.

#### Conflicts of Interest

The authors declare no competing interests.

#### References

- [1] L. Gyu-cheol and Y. Jisang, "Real-time virtual-viewpoint image synthesis algorithm using kinect camera," *Journal of Electrical Engineering & Technology*, vol. 9, no. 3, pp. 1016–1022, 2014.
- [2] C. Li, "Research on synchronous acquisition method of image synthesis information in virtual reality," *Computer Simulation*, vol. 38, no. 1, pp. 316–320, 2021.
- [3] S. Kawin, A. F. David, and R. P. Jonathan, "Rapid brain MRI acquisition techniques at ultra-high fields," *NMR in Biomedicine*, vol. 29, no. 9, pp. 1198–1221, 2016.
- [4] S. U. Dar, M. Yurt, L. Karacan, A. Erdem, E. Erdem, and T. Cukur, "Image synthesis in multi-contrast MRI with conditional generative adversarial networks," *IEEE Transactions on Medical Imaging*, vol. 38, no. 10, pp. 2375–2388, 2019.
- [5] Y. Liu, W. Wang, X. B. Qin et al., "The applied research of simultaneous image acquisition of T2-weighted imaging (T2WI) and diffusion-weighted imaging (DWI) in the assessment of patients with prostate cancer," *Asian Journal of Andrology*, vol. 21, no. 2, pp. 177–182, 2019.
- [6] S. Yuriko, H. Michael, K. Peter, V. C. Marc, and J. P. V. O. Matthias, "Simultaneous acquisition of perfusion image and dynamic MR angiography using time-encoded pseudo-continuous ASL," *Magnetic Resonance in Medicine*, vol. 79, no. 5, pp. 2676–2684, 2018.
- [7] D. Dean, C. Jonathan, R. Fraser, W. S. Allen, and T. Trong-Kha, "Integrated radio-frequency/wireless coil design for simultaneous MR image acquisition and wireless communication," *Magnetic Resonance in Medicine*, vol. 81, no. 3, pp. 2176–2183, 2019.
- [8] S. J. Peng, Z. T. Zhang, C. L. Wu, and G. Liu, "Research on synchronization technology of geological data acquisition system based on NFC and mobile internet," *Journal of Circuits, Systems and Computers*, vol. 27, no. 14, p. 1850225, 2018.
- [9] P. Shamsolmoali, M. Zareapoor, E. Granger et al., "Image synthesis with adversarial networks: a comprehensive survey and case studies," *Information Fusion*, vol. 72, no. 1, pp. 126–146, 2021.
- [10] R. Cyprien, H. Romain, L. Eric, and G. Gilles, "Pixel-wise conditioned generative adversarial networks for image synthesis and completion," *Neurocomputing*, vol. 416, no. 1, pp. 1–28, 2019.
- [11] K. Y. Cheng, R. Tahir, L. K. Eric, and M. Z. Li, "An analysis of generative adversarial networks and variants for image synthesis on MNIST dataset," *Multimedia Tools and Applications*, vol. 79, no. 19–20, pp. 13725–13752, 2020.
- [12] W. L. Ryan and J. M. Jonathan, "Grasping a 2D virtual target: the influence of target position and movement on gaze and digit placement," *Human Movement Science*, vol. 71, no. 3, 2020.
- [13] K. Matwey, M. Kornilov, and K. Malanchev, "Fips: an OpenGL based FITS viewer," *Journal of Physics: Conference Series*, vol. 1525, no. 1, article 012047, 2020.
- [14] V. Sowmya, D. Govind, and K. P. Soman, "Significance of processing chrominance information for scene classification: a review," *Artificial Intelligence Review*, vol. 53, no. 2, pp. 811–842, 2020.
- [15] A. Kushwaha, A. Khare, O. Prakash, and M. Khare, "Dense optical flow based background subtraction technique for object segmentation in moving camera environment," *IET Image Processing*, vol. 14, no. 14, pp. 3393–3404, 2020.

- [16] R. T. Wei, S. C. Chee, E. A. Hernan, and T. Kiyoshi, "Improved ArtGAN for conditional synthesis of natural image and artwork," *IEEE Transactions on Image Processing*, vol. 28, no. 1, pp. 394–409, 2018.
- [17] D. Kawahara, S. Ozawa, T. Kimura, and Y. Nagata, "Image synthesis of monoenergetic CT image in dual-energy CT using kilovoltage CT with deep convolutional generative adversarial networks," *Journal of Applied Clinical Medical Physics*, vol. 22, no. 4, pp. 184–192, 2021.
- [18] P. Costa, A. Galdran, M. I. Meyer et al., "End-to-end adversarial retinal image synthesis," *IEEE Transactions on Medical Imaging*, vol. 37, no. 3, pp. 781–791, 2018.
- [19] D. Andrei, D. Lucian, and U. Petru, "Classification of soil types using geographic object-based image analysis and random forests," *Pedosphere*, vol. 28, no. 6, pp. 913–925, 2018.
- [20] A. S. Wahyul, A. A. S. Yosua, and B. P. Agung, "Smart agent and modified master-backup algorithm for auto switching dynamic host configuration protocol relay through wireless router," *International Journal of Communication Networks and Information Security*, vol. 12, no. 2, pp. 248–255, 2020.

## Research Article

# An Effective Fault-Tolerant Intrusion Detection System under Distributed Environment

Bo Hong , Hui Wang , and Zijian Cao

School of Computer Science and Engineering, Xi'an Technological University, Xi'an 710021, China

Correspondence should be addressed to Bo Hong; hongbo123@xatu.edu.cn

Received 19 August 2021; Accepted 20 September 2021; Published 19 October 2021

Academic Editor: Deepak Gupta

Copyright © 2021 Bo Hong et al. This is an open access article distributed under the Creative Commons Attribution License, which permits unrestricted use, distribution, and reproduction in any medium, provided the original work is properly cited.

Traditional intrusion detection system is limited to a single network or several hosts, which has been seriously unable to fulfill the growing information security problems. This paper uses the distributed technology to design and implement an intrusion detection system (IDS) based on the hybrid of Hadoop with some effective open-source technologies. On the one hand, it can efficiently realize the data acquisition and analysis under distributed environment. On the other hand, it can solve the problems of single-point fault-tolerant and the insufficient data processing capacity of the traditional intrusion detection system. In this IDS, RabbitMQ, Flume, and MongoDB are utilized to act as the middleware of this system to build the system environment which includes the collector, analyzer, and data storage. By detecting the CPU and memory usage of hosts, TCP connections, network bandwidth, web server operation logs, and the logs of user behavior, the proposed IDS especially focuses on monitoring the first four parts, which can better detect external distributed denial of service attacks and intrusions and send automatically alarm service information to the administrators.

## 1. Introduction

The wide application of Internet and the heterogeneity of the interconnection network are limited to a single host-based traditional intrusion detection technology that has become increasingly difficult to meet the current security requirements. In addition, the forms of network intrusions and attacks have become very hidden and gradually tend to be distributed, coordinated, and diverse [1–4]. Therefore, intrusion detection system also needs to meet the new application requirements, such as easy expansion, reuse, cross-platform, and collaborative detection [3, 5–7]. Therefore, it is very urgent to study and utilize distributed technology to realize the distributed intrusion detection system. Hadoop is an open-source distributed system infrastructure based on cloud computing [4, 5, 8, 9] and can perform large-scale cluster distributed parallel programming calculations. Based on Hadoop, many cheap hardware devices can be formed into a cloud computing cluster and make full use of those cluster computing environment and fast storage advantages to develop a distributed system that handles large-scale data suitable for user needs. Hadoop is developed and imple-

mented based on the object-oriented programming language Java, which has good fault tolerance, data analysis balance, and portability. Hence, the application of Hadoop in the intrusion detection of network data can effectively solve the problem of insufficient data analysis ability of the current intrusion detection system and realize a real distributed intrusion detection system. Based on the above analysis, this paper intends to design and implement a distributed intrusion detection system based on Hadoop and some open-source technologies.

Intrusion detection technology enables the security system to make real-time response to intrusion events and intrusion processes by studying the process and characteristics of intrusion behaviors. In terms of detection methods, there are roughly two kinds: misuse intrusion detection and anomaly intrusion detection [10–12]. In the former, it can be assumed that all intrusion behaviors and skills can be expressed as a pattern or feature; all known intrusion methods can be found by matching methods. The key idea of it is how to express the pattern of invasion and to distinguish the real invasion from the normal behavior, and its advantage is to identify the known attack false positives less;



the limitation is the unknown attack that can do nothing. In abnormal intrusion detection, all intrusion behaviors are assumed to be different from normal behaviors. Thus, if a trajectory of the normal behavior of the system is established, then theoretically, all system states that are different from the normal trajectory can be regarded as one suspicious behavior. For example, abnormal network traffic at unusual times is considered suspicious through traffic statistical analysis. The limitation of anomaly intrusion detection is that not all intrusion is abnormal, and the system trajectory is difficult to calculate and update.

By comparing the above two intrusion detection methods, it can be clearly seen that the abnormal detection is difficult to be quantitatively analyzed, and this detection method has inherent uncertainties. Unlike this, the misuse detection follows a defined pattern and can be detected by pattern matching on audit records or network real-time data streams, but only known intrusion methods can be detected. Thus, neither of these detection mechanisms is perfect. In terms of specific detection methods, there have been many intrusion detection methods, but any method has its limitations and cannot solve all intrusion problems [8, 13–19]. The main reason for choosing Hadoop is as follows. Spark is not applicable for applications that update the state asynchronously and finely, such as web service storage or incremental web crawler and index; that is, the application model of incremental modification is not suitable. Spark is also not suitable for processing super large amounts of data. The super large here is relative to the memory capacity of the cluster, because spark needs to store data in memory. In a word, Spark is mainly used for big data calculation, while Hadoop is mainly used for big data storage. Because the requirement of real-time calculation about IDS system is not high, Hadoop is the better choose. Therefore, the research of intrusion detection method is still a difficult point in the current intrusion detection research. Based on the above analysis, this paper designs a distributed intrusion detection system in combination with the structural characteristics of Hadoop cluster. The main contributions of this paper can be summarized as follows.

- (1) To better detect external distributed denial of service attacks, Hadoop which has good fault tolerance, data analysis balance, and portability is used in the IDS system to solve the problem of insufficient data analysis ability of the current intrusion detection system and realize a real distributed IDS
- (2) The open-source technologies, RabbitMQ, Flume, and MongoDB which, respectively, act as the collector analyzer and data storage, are utilized to construct the IDS system. It is not only free of copyright problems, but also it is efficient

The rest of this article is organized as follows. Section 2 represents the framework of IDS with effective techniques incorporated into Hadoop for different functions. The system implementation of the proposed IDS is given in Section 3. In Section 4, the system testing and analysis are discussed, followed by conclusions in Section 5.

## 2. The Framework of the Proposed IDS

Through the research on the process and characteristics of intrusion behavior, the intrusion detection technology enables the security system to make real-time response to intrusion events and intrusion process. There are two detection methods: misuse intrusion detection and abnormal intrusion detection. But these two kinds of detection mechanisms are not perfect. As for specific detection methods, there are many intrusion detection methods, but any method has its limitations and cannot solve all problems. Therefore, the research on intrusion detection methods is still a focus of current intrusion detection research. Based on the existing problems of intrusion detection methods, we design this intrusion detection system. The structure of the proposed IDS system is shown in Figure 1, which consists of data collector, data detector, data transceiver middleware, data analysis center, system monitoring, and alarm service.

In Figure 1, this system refers to the design idea of checklist (checklist is an online system operating status monitoring function, which can be a single-point monitoring or distributed monitoring) system and adds data detector, system monitoring page, alarm service, and other functions on the basis of the checklist system. In addition, some other functions of the system are realized by open-source software. The reason is that these open-source software are widely used in large enterprise applications and have undergone a lot of tests, which is conducive to the stability and long-term operation of the system. Based on the basic framework of checklist, this paper develops a distributed intrusion detection system based on Hadoop distributed computing framework.

*2.1. Data Detector.* The data detector is the system data acquisition and event analysis unit, distributed at the bottom of the system. A detector is a detection subject that runs independently on the host. The system has no restrictions on the detector; that is, the detector runs as a root user. According to the classification of data sources, the data detector can be divided into the detector of the host and the detector of the base network.

For this IDS system, the host-based detector is used to mainly detect the host CPU utilization rate, TCP connection number, MEM utilization rate, network bandwidth, user behavior log, web server operation log, which are the six indicators. CPU, TCP, MEM, network bandwidth are the four general indicators for each host, by fetching service to grab the four indicators, fetching the data for the unit with the minute, and writing the data directly into the data transceiver middleware; then, these data are feedbacked to the data center, for the user behavior and system log information through journal monitoring service time to grab the latest information and regular cleaning. For the network data detector, this system uses the host's own firewall and other protection procedures. The operation process of the data monitor is shown in Figure 2.

*2.2. Data Collector.* The data acquisition agent controls all detectors on the local host, and the detector does not send

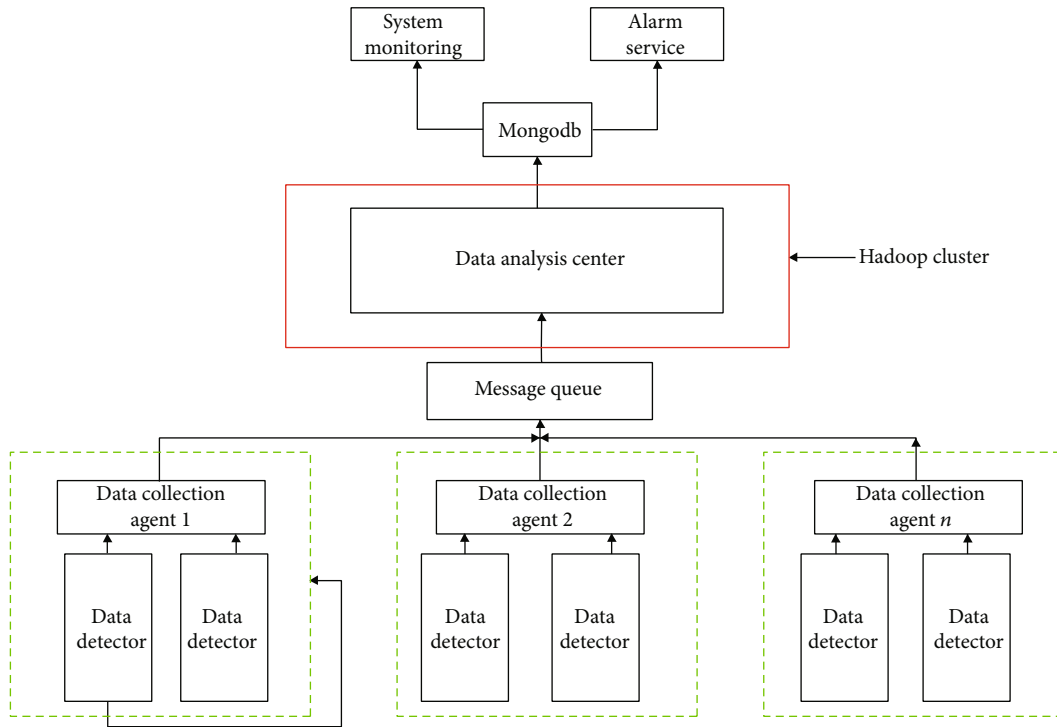


FIGURE 1: IDS structure diagram.

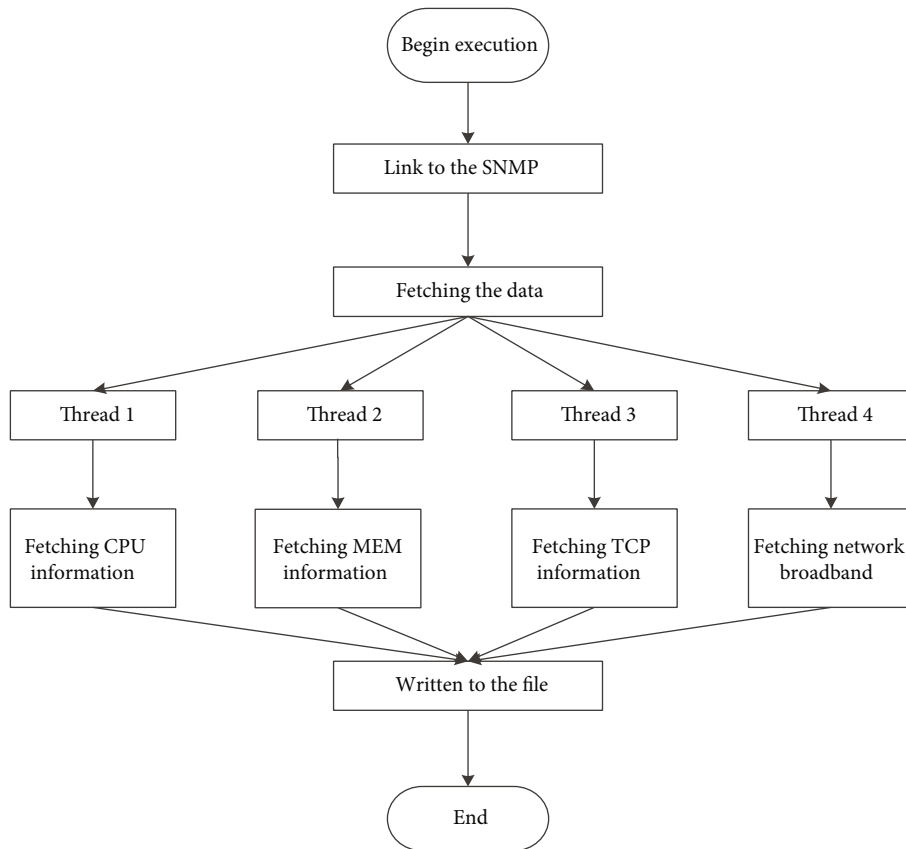


FIGURE 2: Flow chart of data detector.

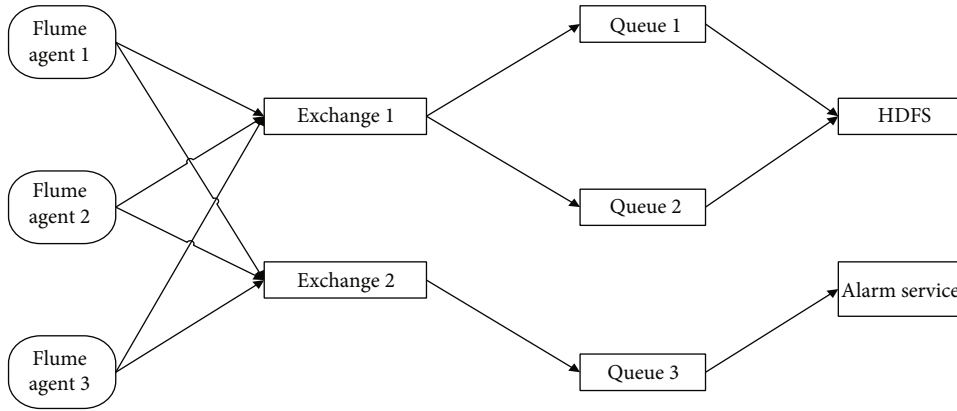


FIGURE 3: Data transceiver middleware structure diagram.

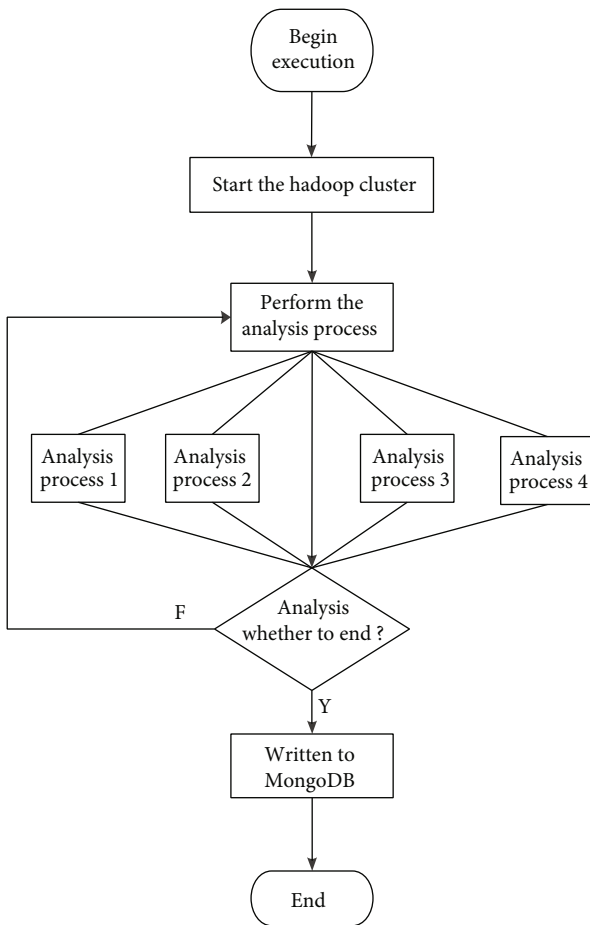


FIGURE 4: Flow chart of data analysis center.

data directly to the transceiver. When the detector wants to transmit data, the data acquisition agent connects to the transceiver to transmit. Flume is used as the data collector in this system. Flume listens for the data detector to write data to the file. If the file has new content, the new content is sent out on a line basis and sent to Flume's collector. Collector aggregates the collected data and writes it to Rab-

bitMQ. The Flume agent listens to files such as CPU, MEM, TCP connection count, network bandwidth, web server access logs, and user behavior logs. If these files are updated, the agent sends the updates line by line to Flume's collector, which writes the aggregated logs to the responding RabbitMQ exchange.

*2.3. Data Transceiver.* The reason why this system uses the data transceiver middleware is that a monitoring system may need to monitor multiple regions or networks. Different types of tasks are processed in different regions, and the data generated are used for different purposes. The use of the data transceiver middleware can classify the unnecessary data and facilitate the analysis of data by the data analysis center. This system uses the RabbitMQ as the data transceiver middleware, the RabbitMQ is a kind of message queue and will be written to the log information of different queues, data collector as the data producer just writes different types of data into the corresponding queue, and data analysis center data read from the queue as a data consumer end, analysis, and calculation. The RabbitMQ mechanism used in this system is shown in Figure 3.

*2.4. Data Analysis Center.* As the core module of the system, the data analysis center adopts the mode of centralized storage, distributed detection, and centralized analysis. When the analysis of the data of detector is sent back according to different need, we can customize different data analysis process, and give full play of the Hadoop cluster computing ability. By analysing the collected data, we can also find the underlying detect intrusion behavior. Then, the feedback of the intrusion detection results is timely made to the system administrator, to adjust each host firewall policy. The analysis process in the data analysis adopts different analysis processes for different logs. Through the analysis of the web server access logs, we can get the number of IP visits to the monitored system per unit time, which the IP address has the highest access frequency in 24 hours, the IP source, and other information. By analyzing the analysis of the user behavior log, we can get the information about what a user did after entering the system, which services he visited, etc. Through this information, it can be analyzed out the illegal

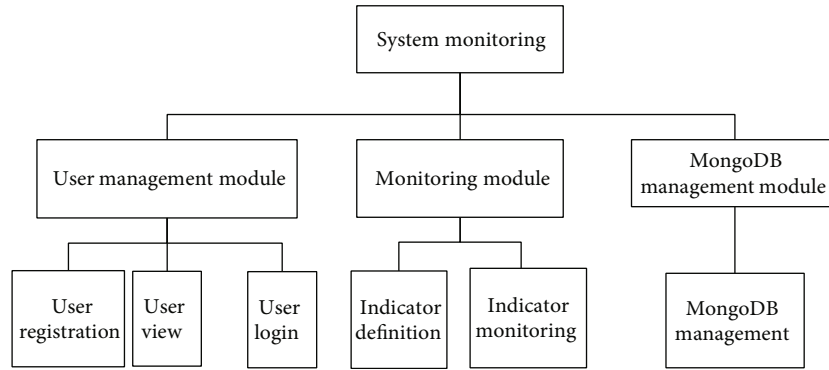


FIGURE 5: System monitoring function diagram.

operation of the user and the timely discovery of intrusion behavior. The analysis center uses the cluster of Hadoop as the basic framework, which is expansible. The MapReduce computing framework of Hadoop is sufficient to deal with massive data, which completely solves the problem that the single-point processing capacity of the traditional intrusion detection system is not out of the question. According to the actual situation, users define their own analysis process for the information to be analyzed and obtain the required analysis results. The basic flow of the data analysis center is shown in Figure 4.

**2.5. System Monitoring.** The system monitoring module is used to display the running state of each host of the monitored system, as well as the running state of the Hadoop cluster. By monitoring the running state of each host, traces of external intrusion can be found, discovered, and handled in a timely manner. Monitoring system is mainly to monitor each host CPU, MEM, TCP connection, network bandwidth, and other basic information; this information is every machine must have information; they can clearly reflect the running status of each host. The function diagram of system monitoring is shown in Figure 5.

In Figure 5, the user management module consists of three functions: user registration, user view, and user login. The user must log in before entering the monitoring system. If the user does not logged in, the user cannot enter the system. User registration function can only be made if the system administrator has this permission; ordinary users cannot be registered; it must be the administrator to add users; user view function can see how many users exist in the monitoring system. The monitoring module has two functions: indicator definition and indicator monitoring. The indicator definition defines the indicator to be monitored by the user, the name of the set stored in MongoDB, the indicator is discrete or continuous and other information. Metric monitoring shows only the collected data, in the form of a trend chart. It can be viewed the recent one hour, six hours, and the whole day trend chart; the system's operation status is intuitively displayed in front of the user. MongoDB management module is mainly designed for the convenience of online MongoDB management. In general, MongoDB is deployed in the production environment in enterprise-level applications, and the development machine

cannot access MongoDB in the production environment. The problem that the development machine cannot access the online environment is solved by accessing the online environment through HTTP protocol.

**2.6. Alarm Service.** The alarm service is at the top of the system. On the one hand, the data distraction center analyzes the collected data to find out whether the system has been attacked and whether the operation is normal. When the data analysis center analyzes some information anomalies, it sends alarm information to the relevant administrators through the alarm service, including SMS alarm and email alarm. On the other hand, when the monitoring system monitors the abnormal running state of a host, it will alarm in time, such as high CPU utilization rate and other problems.

It is through the alarm service administrators can find the problems of the system in time and deal with them in time to ensure the long-term operation of the system. For the four indicators monitored by this system (CPU, MEM, TCP connection number, and network bandwidth), the alarm strategy adopted is that when the value of an indicator appears  $n$  times in a continuous  $m$  minutes, the alarm can be set at different levels. If the level is low, the alarm will be sent by email, and if the level is high, the alarm will be sent by SMS and mail. Considering that the staff cannot check the email in time after work, the use of short message alarm is beneficial after work. The flow chart of alarm service is shown in Figure 6.

**2.7. Data Storage.** This system uses MongoDB, an open-source NoSQL database. MongoDB is a database based on distributed file storage and has the ability of massive data processing [20, 21]. It has the following characteristics: set oriented and data is stored in the dataset. Schema-free means that users of the files we store in the database do not need to know the format of the data stored. Documents stored in a collection exist as key-value pairs for easy lookup. This system mainly processes data collector gathering up the log data, such as a large amount of data and format is not fixed; the traditional relational database is not good at dealing with huge amounts of data, so we use MongoDB as a database to store data analysis center after analysis of data, and it will facilitate system monitoring read data from the

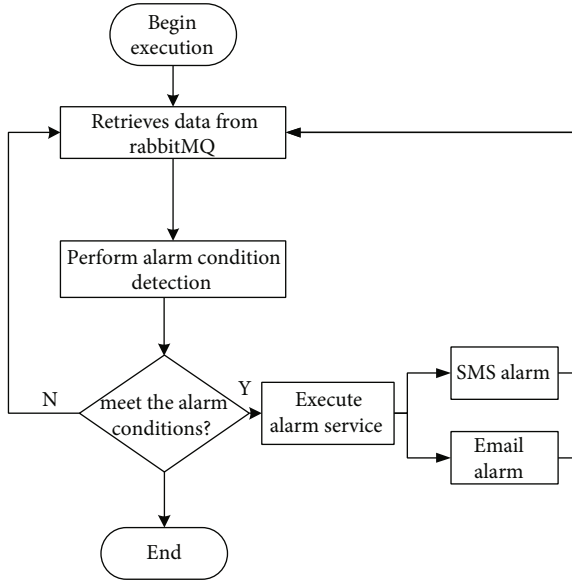


FIGURE 6: Alarm service flow chart.

```

{
  "_id": "49902cde5162504500b45c2c",
  "serverName": "server001",
  "quotaName": "CPU",
  "quotaValue": 1,
  "currentTime": "yyyy-MM-dd hh:mm:ss"
}
  
```

ALGORITHM 1

```
Hadoop jar /xxx/xxx/xx.jar arg1 arg2
```

ALGORITHM 2

MongoDB. The data format of CPU, MEM, TCP connection number, and network bandwidth monitored by this system in MongoDB is as follows in Algorithm 1.

The corresponding set names of each index are as follows: quota\_cpu, quota\_mem, quota\_tcp, and quota\_network\_width, respectively. \_id: Produced by MongoDB is a unique identifier for each document; ServerName: Server name. QuotaName: Indicator name; the names of these four indicators are CPU, MEM, TCP\_CONN, and network\_width. quotaValue indicates the current value of this indicator. CurrentTime identifies the time when this piece of data was written to MongoDB, enabling MongoDB to be queried by time dimension.

### 3. System Implementation

**3.1. Hadoop Cluster Operation.** After the Hadoop cluster is set up, it will be executed all the time after starting the Hadoop cluster. Developers can submit their written Java programs into JAR packages to the Hadoop cluster for execution; it can commit multiple JAR packages for execution in Algorithm 2.

```

while(recVB.getOid().toString().indexOf(cpuOid)>=0){
  pdu.clear();
  pdu.add(new VariableBinding(recVB.getOid()));
  pdu.setType(PDU.GETNEXT);
  ResponseEvent respEvt = snmp.send(pdu, target);
  if (respEvt != null && respEvt.getResponse() != null) {
    for (int i =0; i < recVBs.size(); i++) {
      recVB = recVBs.elementAt(i);
      if(recVB.getOid().toString().indexOf(cpuOid) >=0){
        cpuInfo+=recVB.getVariable().toInt();
        cpuCoreNum += 1;
        tcpConn += recVB.getVariable().toInt();
      }
    }
  }
}
  
```

ALGORITHM 3

where xxx represents the path of the JAR package and arg1 and arg2 are the parameters of the execution jar package.

**3.2. Data Collector Implementation.** Data acquisition can collect a variety of data, such as the system operation of the log information and the system operation of the data. This paper mainly realizes the collection of CPU utilization rate, memory, TCP connection number, network bandwidth, and other information when the host is running. The following mainly uses CPU utilization and TCP connection number as an example to introduce the implementation; other information is the same principle. The data detector is implemented in JAVA language, and the protocol is SNMP protocol. SNMP is a network management standard based on TCP/IP protocol family. Its predecessor is Simple Gateway Monitoring Protocol (SGMP), which is used to manage communication lines. The data detector is connected to SNMP service through the SNMP driver package of Java, and it is connected to port 161. By sending the corresponding SNMP OID to the server to obtain the corresponding information, the OID of CPU utilization is 1.3.6.1.2.1.25.3.3.1.2. The method for SNMP to obtain data is GetNext method, which uses recursive query to query the corresponding values of all OIDs under the current OID tree.

Taking the development machine as an example, the development machine uses a 4-core CPU. Hence, there should be 4 subtrees under the OID tree. The GetNext method is used to recursively obtain the utilization rate of all cores for 4 times to find the average value. The OID of the number of TCP connections is 1.3.6.1.2.1.6.9. Since the number of TCP connections in the system has only one value, the OID tree has only one, and the current number of TCP connections in the system can be obtained only by recursing once. The core workflow of the data detector is shown as follows in Algorithm 3.

**3.3. Realization of System Monitoring.** System monitoring is developed based on B/S structure, and the entire system monitoring module can be configured using Spring MVC



```

<bean id="initDashBoard"
  class = "com.elong.dashboard2.dashboard.InitDashBoardController">
</bean>
<bean id="velocityConfig"
  class="org.springframework.web.servlet.view.velocity.VelocityConfigurer">
  <property name="configLocation">
    <value>/WEB-INF/views/velocity/velocity.properties</value>
  </property>
</bean>
<bean id="viewResolver"
class="org.springframework.web.servlet.view.velocity.VelocityLayoutViewResolver">
  <property name="cache" value="false" />
  <property name="layoutUrl" value="/layout/main.vm" />
  <property name="prefix" value="/templates/" />
  <property name="suffix" value=".vm" />
  <property name="exposeSpringMacroHelpers" value="true" />
  <property name="contentType" value="text/html;charset=UTF-8" />
  <property name="viewClass"
    value="org.springframework.web.servlet.view.velocity.VelocityLayoutView" />
<bean id="handlerMapping"
class="org.springframework.web.servlet.mvc.annotation.DefaultAnnotationHandlerMapping">
  <property name="interceptors">
    <ref bean="localeChangeInterceptor" />
  </property>
</bean>

```

ALGORITHM 4

```

#RABBITMQ_NODE_PORT=8088 //The port number
#HOSTNAME=http://www.ddsnort.com
RABBITMQ_NODENAME=mq
RABBITMQ_CONFIG_FILE=/etc/rab.conf //Configuration file path
RABBITMQ_MNESIA_BASE=/rabbitmq/data
// MNESIAPath to the database
RABBITMQ_LOG_BASE=/rabbitmq/log //log The path
RABBITMQ_PLUGINS_DIR=/rabbitmq/plugins//The plugin path

```

ALGORITHM 5

framework in `servlet.xml` file in Spring, which determines the functions of using the framework, as well as the combination of Spring MVC and Velocity [12, 22, 23]. The main functions of the system monitoring module include user management module, monitoring module, and MongoDB management module. Under normal conditions, the development machines cannot access the online database. Through the MongoDB management module, the inaccessible problem can be solved by using HTTP protocol access. The following code configures how Velocity parses the view page, and Velocity configures the path of the page. The `servlet.xml` file is the key of the entire MVC framework. If this file is configured incorrectly, a web application will not run in Algorithm 4.

**3.4. Main Configuration of RabbitMQ.** The data detector, system monitoring, and alarm service of the system need to be realized by ourselves. Other modules are realized by open-source software. The data collector uses the open-source mass log collection tool Flume to collect the data.

The data delivery middleware uses RabbitMQ, where users write different data streams to different queues. Some of the common RabbitMQ environment variables are as follows in Algorithm 5.

The above section is the main configuration of the RabbitMQ. For more details, please refer to the RabbitMQ website.

## 4. System Testing and Analysis

DDoS (distributed denial of service) attack tool is used to test the system and launch a DDoS attack on the monitored. There are many TCP links in the machine system, and then, the number of TCP connections in the system monitoring can be seen to surge. As shown in Figure 7, under normal circumstances, the number of TCP connections in the system tends to be stable, and it can be seen from Figure 7 that the number remains between 0 and 50. When the system is attacked by DDoS, the number of TCP connections

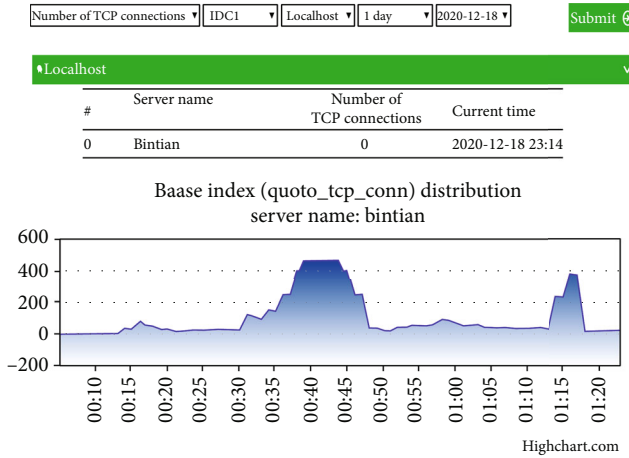


FIGURE 7: Schematic diagram of TCP network connection number when system is attacked.

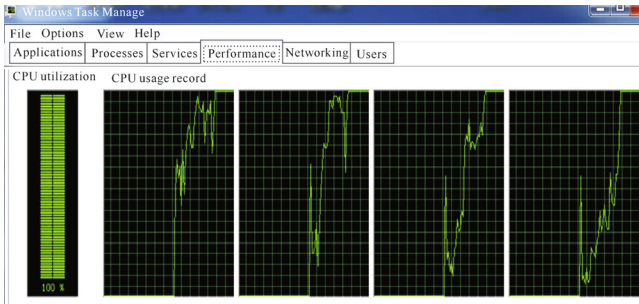


FIGURE 8: CPU utilization.

increases sharply to about 450. For external attack monitoring system, we can timely detect external attacks and intrusions. This is also shown in Figure 7.

To verify the correctness of the data detector, we intercepted the CPU utilization graph in the task manager of the Windows system at this time, as shown in Figure 8.

## 5. Conclusions

The distributed intrusion detection system based on Hadoop is a relatively practical system. This paper adopts distributed technology and open-source software to change the shortcomings of traditional intrusion detection system, such as insufficient computing power. Using distributed computing technology, through the network, the huge need to deal with the data will be automatically split and delivered by the server cluster consisting of a large system; after the search, calculation, and analysis, data mining, the optimized results, the corresponding treatment scheme, and reliable and stable update results stored in the database, through data detector of CPU, MEM, TCP, network bandwidth, and other four indicators test, can better find external DDoS attack and intrusion alarm and provide service function. Because the Hadoop is based on the distributed environment, the proposed IDS system with Hadoop and other effective open-source technologies is fault-tolerant according to the system testing and analysis.

## Data Availability

The datasets used and/or analyzed during the current study are available from the corresponding author on reasonable request.

## Conflicts of Interest

It is declared by the authors that this article is free of conflict of interest.

## Acknowledgments

This research was partially funded by the Shaanxi Natural Science Basic Research Project (Grant No. 2020JM-565), the Project of Department of Education Science Research of Shaanxi Province (Grant No. 18JK0383), the Innovation and Entrepreneurship Training Program for College Students (Grant No. S202010702108), the Teaching Reform Research Project of Xi'an Technological University (Grant No. 20JGY38), and the General Cultivation Project of President Fund of Xi'an Technological University (Grant No. XGPY200207).

## References

- [1] R. Z. Yang, T. Y. Chen, and Y. P. Li, "Broad-scale distributed intrusion detection system," *Network and Information Security*, vol. 39, no. 7, pp. 31–35, 2020.
- [2] D. Song, E. Shi, I. Fischer, and U. Shankar, "Cloud data protection for the masses," *IEEE Computer*, vol. 45, no. 1, pp. 39–45, 2012.
- [3] S. Chen and V. P. Janeja, "Human perspective to anomaly detection for cybersecurity," *Journal of Intelligent Information Systems*, vol. 42, no. 1, pp. 133–153, 2014.
- [4] S. Deng, A. H. Zhou, D. Yue, B. Hu, and L. P. Zhu, "Distributed intrusion detection based on hybrid gene expression programming and cloud computing in a cyber physical power system," *IET Control Theory & Applications*, vol. 11, no. 11, pp. 1822–1829, 2017.
- [5] S. Deng, A. H. Zhou, and D. Yue, "Algorithms. Study data from Nanjing University update understanding of algorithms (distributed intrusion detection based on hybrid gene expression programming and cloud computing in a cyber physical power system)," *Journal of Engineering*, vol. 8, 2017.
- [6] N. M. Ibrahim and A. Zainal, "A distributed intrusion detection scheme for cloud computing," *International Journal of Distributed Systems and Technologies*, vol. 11, no. 1, pp. 68–82, 2020.
- [7] G. de la Torre Parra, P. Rad, K. R. Choo, and N. Beebe, "Detecting Internet of Things attacks using distributed deep learning," *Journal of Network and Computer Applications*, vol. 163, article 102662, 2020.
- [8] S. Zhou and P. Yang, "Risk management in distributed wind energy implementing analytic hierarchy process," *Renewable Energy*, vol. 150, pp. 616–623, 2020.
- [9] H. Han, H. Kim, and Y. Kim, "Evaluation of distributed intrusion detection system based on MongoDB," *KIPS Transactions on Computer and Communication Systems*, vol. 8, pp. 287–296, 2019.

- [10] A. M. Riyad, M. S. I. Ahmed, and R. L. R. Khan, "An adaptive distributed intrusion detection system architecture using multi agents," *International Journal of Electrical and Computer Engineering*, vol. 12, 2019.
- [11] D. L. Li, "Exploring the application of intrusion detection technology in computer database," *Digital Technology & Application*, vol. 37, no. 3, 2019.
- [12] K. Xie, Y. X. Yang, Y. Xin, and G. Xia, "Cellular neural network-based methods for distributed network intrusion detection," *Mathematical Problems in Engineering*, vol. 2015, Article ID 343050, 10 pages, 2015.
- [13] J. F. Colom, D. Gil, H. Mora, B. Volckaert, and A. M. Jimeno, "Scheduling framework for distributed intrusion detection systems over heterogeneous network architectures," *Journal of Network and Computer Applications*, vol. 108, pp. 76–86, 2018.
- [14] J. C. McEachen and C. Wai Kah, "An analysis of distributed sensor data aggregation for network intrusion detection," *Microprocessors and Microsystems*, vol. 31, no. 4, pp. 263–272, 2007.
- [15] T. E. Simos and C. Tsitouras, "Evolutionary derivation of Runge–Kutta pairs for addressing inhomogeneous linear problems," *Numerical Algorithms*, vol. 87, no. 2, pp. 511–525, 2021.
- [16] M. A. Medvedev, T. E. Simos, and C. Tsitouras, "Explicit, eighth-order, four-step methods for solving  $Y''=F(X,Y)$ ," *Bulletin of the Malaysian Mathematical Sciences Society*, vol. 43, no. 5, pp. 3791–3807, 2020.
- [17] Y. Sarac and S. S. Sener, "Identification of the initial temperature from the given temperature data at the left end of a rod," *Applied Mathematics and Nonlinear Sciences*, vol. 4, no. 2, pp. 469–474, 2019.
- [18] Y. X. Wang, S. R. Behera, J. Wong et al., "Towards the automatic generation of mobile agents for distributed intrusion detection system," *The Journal of Systems & Software*, vol. 79, no. 1, pp. 1–14, 2006.
- [19] A. Fagiolini, G. Dini, and A. Bicchi, "Distributed intrusion detection for the security of industrial cooperative robotic systems," *IFAC Proceedings Volumes*, vol. 47, no. 3, pp. 7610–7615, 2014.
- [20] J. Manan, A. Ahmed, I. Ullah, L. Merghem-Boulahia, and D. Gaïti, "Distributed intrusion detection scheme for next generation networks," *Journal of Network and Computer Applications*, vol. 147, article 102422, 2019.
- [21] M. Himi, J. Tapias, S. Benabdelouahab et al., "Geophysical characterization of saltwater intrusion in a coastal aquifer: the case of Martil-Alila plain (North Morocco)," *Journal of African Earth Sciences*, vol. 126, pp. 136–147, 2017.
- [22] H. Tang, L. Chen, J. Lu, and C. K. Tse, "Adaptive synchronization between two complex networks with nonidentical topological structures," *Physica A*, vol. 387, no. 22, pp. 5623–5630, 2008.
- [23] Z. Sui, "Large-scale network intrusion detection based on multi-point and multi-task decomposition mapping technology," *Computer Simulation*, vol. 31, no. 2, 2014.

## Research Article

# Lightweight Automatic Identification and Location Detection Model of Farmland Pests

Kunpeng Li,<sup>1</sup> Junsheng Zhu,<sup>2</sup> and Nianqiang Li <sup>1</sup>

<sup>1</sup>University of Jinan, Jinan 250000, China

<sup>2</sup>Plant Protection Station, Jinan 250000, China

Correspondence should be addressed to Nianqiang Li; ise\_linq@ujn.edu.cn

Received 23 August 2021; Revised 15 September 2021; Accepted 20 September 2021; Published 15 October 2021

Academic Editor: Deepak Gupta

Copyright © 2021 Kunpeng Li et al. This is an open access article distributed under the Creative Commons Attribution License, which permits unrestricted use, distribution, and reproduction in any medium, provided the original work is properly cited.

Automatic identification and location of farmland pests are an important direction of target detection research. The wide variety of pests and the similarity between pest categories make the automatic identification of farmland pests have some problems, such as high error rate and difficult identification. In order to achieve a better target for automatic identification and location of farmland pests, this paper proposes a lightweight pest detection model, and the network is the EfficientNet proposed by Google, which achieves the detection of 26 pests, the idea based on the classical Yolo target detection algorithm. First of all, features were extracted through the lightweight backbone, and then multiscale feature fusion is performed by PANet; finally, three feature matrices with different sizes were output to predict pests of different sizes. Using CIOU as the loss function of regression prediction better reflects the relative position of the prior box and the real box. The experimental results are compared with other lightweight algorithms, and the results show that the accuracy rate of the algorithm for identification and localization of agricultural pest in this paper is the highest and could reach 93.73%. Moreover, the model is lightweight and can be deployed on low-cost equipment, which reduces the cost of equipment and accurately predicts the status of pests and diseases in farmland. In practice, it is shown that the algorithm can effectively solve the problems of large number of pests, pest accumulation, background interference, and has strong robustness.

## 1. Introduction

Wheat and corn are the main food crops in North China. The growth of crops often suffers from pests, which cause enormous economic losses to wheat and corn yields every year. There are many kinds of pests on agricultural crops, which attack the growth of crops and often erupt into disasters; so, there is a need for real-time and accurate monitoring of wheat and corn pests, develop reasonable prevention, and control measures to reduce economic losses. Traditional wheat versus corn pest detection primary methods still require staff from the base layer to enter the field to observe pest type characteristics, visually observe, and diagnose pest status in the area. This method has the characteristics of heavy workload and low efficiency. It cannot predict the occurrence of diseases and insect pests in real time, meet the needs of current pest monitoring, reduce the accuracy

of agricultural pest monitoring, and is not conducive to the scale and automation of pest detection [1–3].

With the growth of computing resources, deep learning has developed rapidly, especially in the field of image, which provides a technical basis for lightweight farmland pest detection [4]. In the early stage of pest identification, artificial neural network, support vector machine, and other methods were used to realize pest identification, mainly based on the color, texture, morphology, and other characteristics of pests. It has high requirements for the body shape characteristics of pests in the data set and can only complete several categories. The identification results are very unstable. This method is essentially a classification problem. Only one pest can be solved in one picture, which is not in line with the actual environment [5]. With the growing maturity of deep learning technology [6, 7], a large number of excellent detection models have emerged in the field of target

detection, such as SSD, Fast-RCNN, and Yolo [8–10]. These excellent target detection models extract features through convolutional neural networks. These algorithms are based on anchors to achieve target positioning. Recently, some target detection algorithms without anchors have emerged, such as Centernet [11]. However, for small target objects such as pests, the performance of no a priori frame algorithm is not very ideal. The target detection model has been widely used in pedestrian detection, vehicle detection, face detection, driverless, and other fields. It is also applicable to the target detection of pests. For example, Wei Yang and others have realized the automatic identification of pests by using the two-stage faster-RCNN detection model [12]. Yuan and others have realized the automatic recognition and counting of 8 types of insects by using the yolov3 model, and the recognition rate can reach 70.98% [13], while the accuracy of pest recognition still needs to be improved.

Most of the existing recognition methods use network pictures as datasets for training. Although they have good recognition rate, the pictures collected on the network can only identify one side of the pests [14]. There is a big gap in practical applications. The robustness of the model is not high, and the deployment needs a high computing resources device, which cannot meet the current actual needs [15]. In this paper, a lightweight detection model is proposed to solve the problem that the existing target detection model requires a large amount of computing resources. The model is deployed on low-cost devices, mainly to monitor pests in farmland, so as to achieve the scale and automation of pest monitoring. The detection model in this paper mainly refers to the idea of the Yolo algorithm. Because each pest has a different size, the model outputs three different size feature matrices, and sets three anchors with different size for each feature matrix, and the regression predicts pests with different size. The deployment of the detection model on the local device is implemented, which reduces the waste of computing resources and greatly reduces the cost.

## 2. Related Work

*2.1. Image Processing.* The nature of depth learning is end-to-end; so, the construction of datasets is the basis of in-depth learning. Because of the scarcity of public pest datasets, there is a big difference from the actual situation. The pest dataset used in this paper was obtained by using a telemetry lamp device in Shandong Province. The device mainly uses light to attract pests, kills pests through heating chamber, falls on the insect board, and takes pictures of pests through high-definition camera. A total of 10,000 pictures of pests were collected. 6,144 useful pictures of pests were manually screened out. A total of 26 pests were identified. Some of the samples were shown in Figure 1. The category and number distribution of pests were shown in Table 1 below. The labelling tool was used for labeling manually to generate VOC2007 format [16].

The input of the pest detection model in this paper is a  $416 \times 416$  size picture, while the size of the data set is not the same, the data need to be adjusted to a uniform size to be the input of the network, if the direct resize the picture

is distorted, and may lose the original characteristics of the picture; so, the method of adding padding to the picture is adopted to prevent the distortion of the data set. For a good target detection model, it requires massive data sets for training to avoid overfitting of the network and enhance the robustness of the model, while the number of this data set is obviously insufficient, a total of seven methods have been used to further augment the data set, namely, rotation, horizontal translation, vertical translation, perspective transformation, and scaling horizontal inversion as well as brightness enhancement, thereby enhancing the generalization ability of the model, and the dataset was expanded to more than 20000 sheets [17].

In order to further improve the robustness of the model and enhance its generalization ability, the mosaic data enhancement method is used when loading the data set. The mosaic data enhancement refers to the data enhancement method of Cutmix [18]. The Cutmix data enhancement method is to splice two images, but mosaic uses four images to enrich the background of the object and increase the diversity of the data. When calculating in BN (batch normalization) layer, the larger the setting of batch size is, the closer the mean value and variance of the whole data set will be, and the better the effect will be. Due to the limitation of GPU memory, it is impossible to train multiple pictures at one time. When we put four pictures together and input them into the network, the batch size of the input network will be increased in disguise. As shown in Figure 2, the image is enhanced by mosaic data.

*2.2. Target Detection Algorithm.* The object detection algorithm in deep learning consists of three parts: backbone, neck, and head. Backbone is mainly used for feature extraction to generate feature map, such as VggNet, ResNet, and Densenet [19–21]. The function of neck is to fuse feature maps of different scales for further feature extraction, such as FPN, PAN, and BiFPN [22–24]. Finally, the head is used for classification and regression prediction to complete the target recognition and positioning. The head is mainly divided into two parts. One is based on anchor, such as SSD, Yolo, and Retinanet. It sets anchor box in feature points in feature map in advance and locates the target by adjusting the size and position of anchor box. There are two main problems: the preset anchor box size is fixed, and the other is based on anchor free, such as Cornernet [25] and Centernet. When building the model, it takes the target as a point; that is, the center point of the target BBox uses key points to find the center point and returns to other target attributes; in the experimental study, the accuracy of anchor is higher than that of anchor free; so, this paper proposes a lightweight target detection algorithm based on Yolo's idea and improves the two shortcomings of two anchor bases.

*2.3. Model Structure.* The network architecture draws lessons from the Yolo model structure and uses the one stage method to build the model. The Yolo series detection model has been very perfect after three generations of iteration. It has the advantages of high calculation speed and high accuracy and is widely used. In this paper, the network





FIGURE 1: Insect samples of each classification target.

TABLE 1: Sample and target quantity of each classification.

No.	Name	Sample quantity	No.	Name	Sample quantity
0	Corn borer	545	13	Amata emma	492
1	Cotton bollworm	1565	14	Gryllotalpa spp	167
2	Chafer	1799	15	Chiasmia cinerearia	221
3	Macdunnughia crassigna	159	16	Eupolyph	256
4	Athetis lepigone	928	17	Callambulyx tatarinovi	340
5	Mamestra brassicae linnaeus	727	18	Scarites	229
6		265	19	Cricket	179
7	Striped sorghum borer	73	20	Diaphania quadrimaculalis	238
8	Agrotis ypsilon	624	21		200
9	Mythimna Separata	189	22	Agrius convolvuli	200
10	Latoia sinica Moore	366	23	Smeritus planus walker	203
11	Beet armyworm	183	24	Parum colligata	190
12	Agrotis segetum	374	25	Bremer et Grey	147
	Ladybug			Butler	

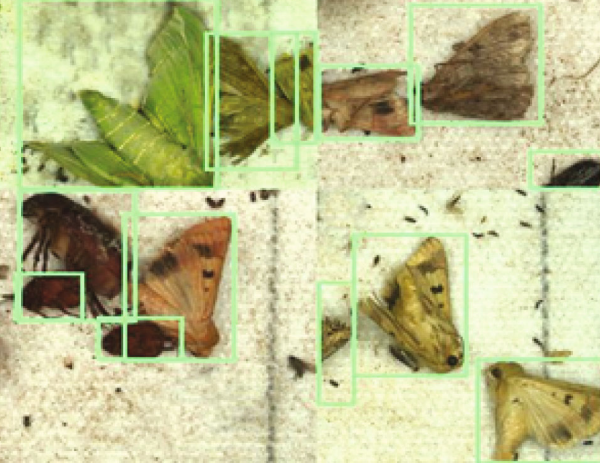


FIGURE 2: Mosaic enhanced image.

architecture constructed by the algorithm according to its idea is shown in Figure 3. The darknet-53 of the backbone in yolov3 is replaced by the improved Efficientnet [26], and the PAN is replaced by the FPN in neck to improve the feature fusion.

The backbone in this algorithm is based on Efficientnet-B2 [26] network, which was proposed by Google in 2019 for image classification. The input of the Efficientnet-B2 network is  $260 \times 260$ . In order to better extract the characteristics of the image, the input size is changed to  $416 \times 416$ , and the SPP network structure is added in the last block, so as to further sample the feature map. The Efficientnet-B2 network is mainly composed of seven MBConv blocks. The structure is shown in Figure 4. It uses  $1 \times 1$  ordinary convolution for dimension raising, then BN and swish activation functions, and then uses deep separable volume for down sampling. After an SE module, it uses a  $1 \times 1$  convolution for dimension reduction, and normalizes through a BN layer. Finally, the input characteristic matrix is added with the main channel characteristic matrix through the shortcut branch to complete the output of the characteristic matrix. Only when the dimension of the input MBConv structure characteristic matrix is the same as that of the output characteristic matrix, the splicing operation is carried out. In the first ascending dimension of  $1 \times 1$  convolution layer, the input MBConv structure characteristic matrix is connected with the output characteristic matrix, and the number of convolution kernels is  $N$  times of the input characteristic matrix channel.

The changed network parameters are shown in Table 2, rechanging the input size and adding the SPP structure, enhancing the generalization ability of the algorithm and having a broader vision of features.

Deep separable convolution [27] is a deformation of traditional convolution. It is different from traditional convolution in that the number of channels of its convolution core is equal to the number of channels of the input characteristic matrix, the number of channels of the output characteristic matrix, the number of convolution cores, and the size of the convolution core is a matrix of  $1 \times 1$ . The structural schematic of the ordinary convolution is shown in

Figure 5, the deep separable convolution is shown in Figure 6, assuming that  $D_F$  represents the size of the input feature matrix,  $M$  is the number of feature matrices,  $D_K$  is the size of the convolution kernel,  $N$  is the number of output feature matrices, and the computational comparison of the deep separable convolution with ordinary convolution is shown by equation (1).

$$\frac{D_k \cdot D_k \cdot M \cdot D_F \cdot D_F + M \cdot N \cdot D_F \cdot D_F}{D_K \cdot D_K \cdot M \cdot N \cdot D_F \cdot D_F} = \frac{1}{N} + \frac{1}{D_K^2}. \quad (1)$$

Assuming that the size of the convolutional kernel is  $3 \times 3$ , the formula is equal to  $1/N + 1/9$ ; so, the computation of the ordinary convolution is theoretically 8 to 9 times the depth, which is visible to be much less than the ordinary convolution.

The structure of SE module is shown in Figure 7. The feature map performs a global average pooling and transforms the size of the feature matrix to  $1 \times 1$ , which performs two full connection layers. The first full connection uses the swish activation function, and the number of channels becomes  $1/4$  of the original number. The second full connection uses the sigmoid activation function, the number of nodes is equal to the number of channels of the output characteristic matrix of the depth separable convolution layer, and the final output is obtained by multiplying with the input feature map. The SE module is similar to the self-attention [28] mechanism and increases the interesting features through the output of the sigmoid function.

In the main feature network, a SPP (spatial pyramid pooling) structure is added; that is, three maximum pooling samplings are conducted after the last MBConv block, because the stride is all one, the size of the padding, and feature matrix in the feature matrix is added not to change. The three obtained feature matrices and the input feature matrix are splicing to obtain the feature matrix of 4 times the depth. The structure is shown in Figure 8.

In the stage of feature fusion, the idea of the PANet (path aggregation network) structure is used for multiscale feature fusion. In the backbone feature network, three feature matrices with different sizes are collected, as shown in Figure 3. The three feature matrices are MBConv5, MBConv7, and MBConv8. First, convolution and SPP operations with convolution kernel size of  $3 \times 3$  are performed on MBConv8, and then up sampling and stacking with MBConv7 are performed. The feature layer continues to perform up sampling and fusion stacking with MBConv5. Through two times of length and width expansion, the up sampling operation is completed, and the feature layer with high semantics is obtained. The convolution operation with convolution kernel size of  $5 \times 5$ , and down sampling are carried out, respectively, to ensure the feature information of the target, which is more conducive to detecting objects of different sizes.

In neck, after completing the fusion stack, the three characteristic matrices perform the convolution operation with the convolution kernel size of  $5 \times 5$ , respectively, and output three characteristic matrices with different sizes, namely, (13,13,93), (26,26,93), and (52,52,93). The first two

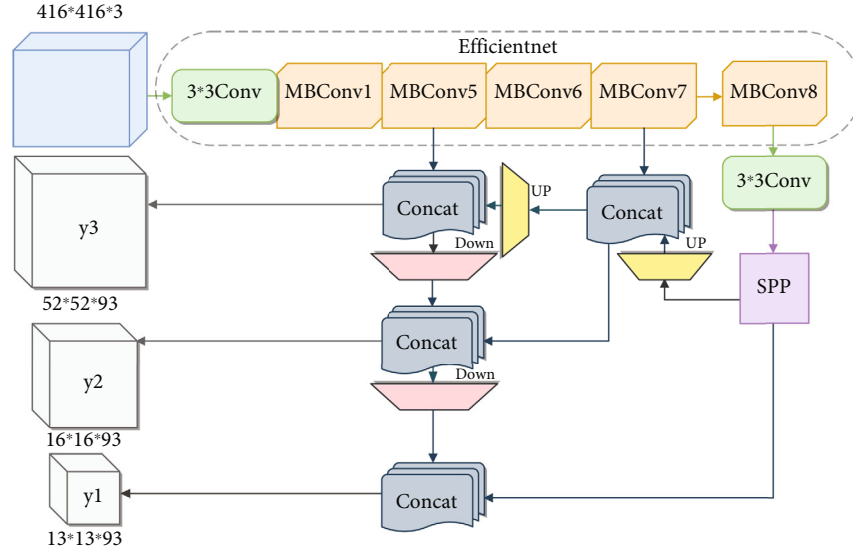


FIGURE 3: Model structure.

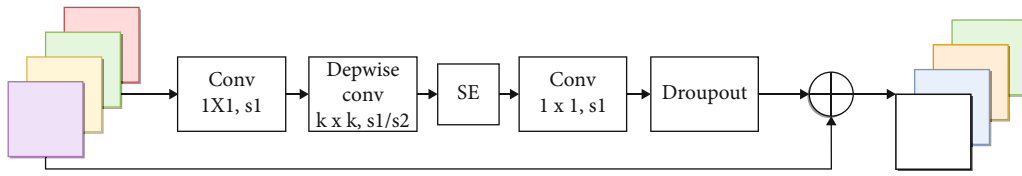


FIGURE 4: MBConv structure.

TABLE 2: Network parameters of features extraction.

Stage	Operation type/ convolutional core size	Matrix size	Number of channels	Number of repetitions
1	Conv, $k3 \times 3$	$416 \times 416$	32	1
2	MBConv, $k3 \times 3$	$208 \times 208$	16	1
3	MBConv, $k3 \times 3$	$208 \times 208$	24	2
4	MBConv, $k5 \times 5$	$104 \times 104$	48	2
5	MBConv, $k3 \times 3$	$52 \times 52$	80	3
6	MBConv, $k5 \times 5$	$26 \times 26$	120	3
7	MBConv, $k5 \times 5$	$26 \times 26$	192	4
8	MBConv, $k3 \times 3$	$13 \times 13$	350	1
9	SPP, $k5, k9, k13$	$13 \times 13$	1408	1

dimensions represent the size of the feature layer and are used to detect objects of different sizes, while 93 represents that each feature point has three a priori boxes. Each a priori box contains five parameters, namely, length, width, center point, and classification probability. A total of 26 pests are detected this time; so, this dimension is  $3 \times 31$ .

Swish activation function is used in MBconv block. Swish is an improved version of sigmoid and Relu, similar to the combination of Relu and Sigmoid, which contains a parameter  $\beta$ , and  $\beta$  can be set as a constant or a trainable parameter. It has the characteristics of no upper bound but

lower bound, smoothness, and nonmonotonicity, as shown in formulae (2) and (3).

$$\text{Sigmoid}(x) = \frac{1}{1 + e^{-x}}, \quad (2)$$

$$f(x) = x \cdot \text{sigmoid}(\beta x). \quad (3)$$

The Swish activation function not only has the advantages of the Relu and Sigmoid functions but also is superior to Relu in the deep model. It can be seen as a smoothing function between the linear function and the Relu function.

**2.4. Loss Function.** The loss function in target detection can be roughly divided into three parts: confidence loss, classification loss, and location loss. In the confidence loss function, IOU (intersection over union) is used to judge the relative position relationship between the prediction frame and the real frame, but IOU cannot judge the overlapping area, center distance, and aspect ratio between the prediction frame and the real frame. Therefore, this paper uses CIOU (complete, IOU) [29] to replace IOU and adds a penalty term, so that the regression loss function tends to converge and reduce the divergence of loss function in the training process. The loss function of the model is shown in formula (4).

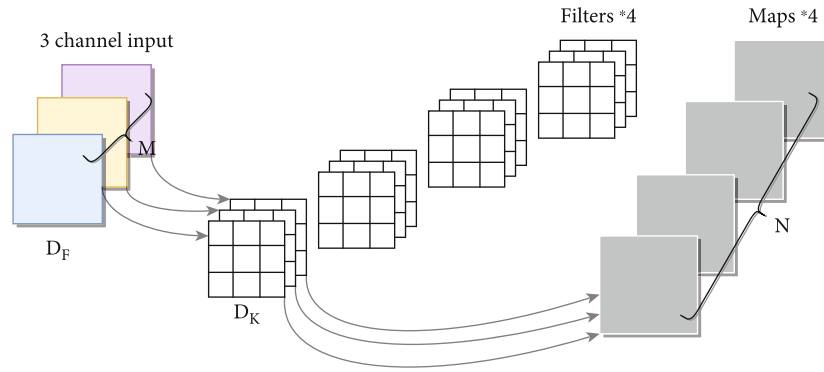


FIGURE 5: Ordinary convolution.

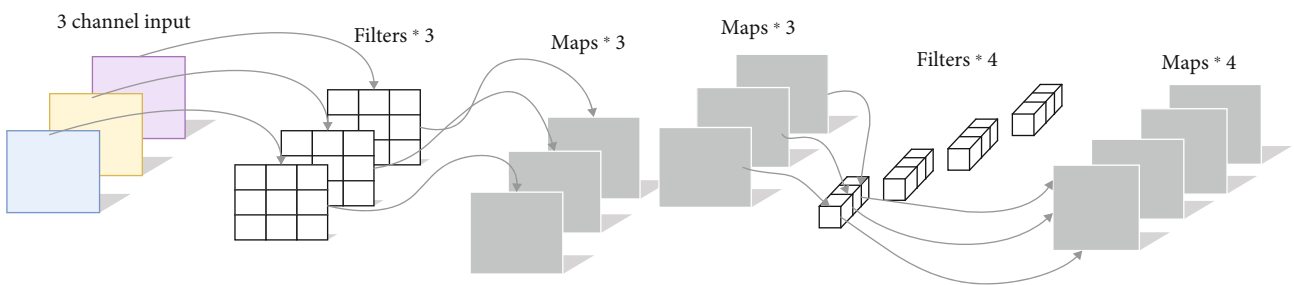


FIGURE 6: Depthwise separable convolution.

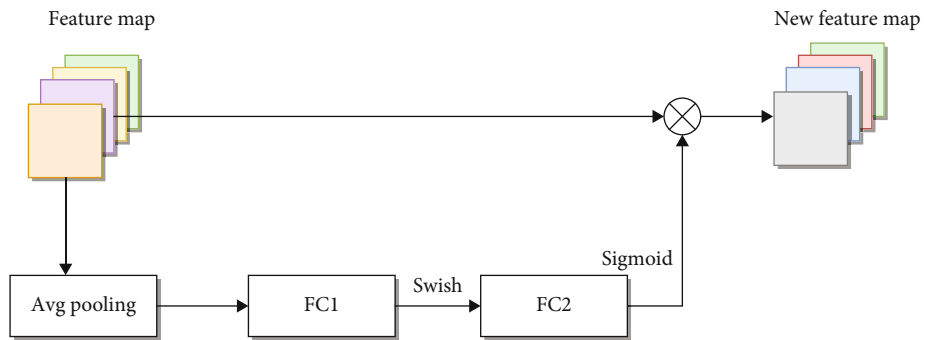


FIGURE 7: SE block.

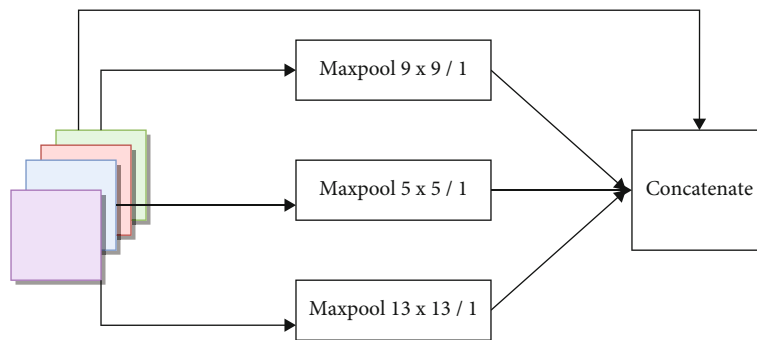


FIGURE 8: Spatial pyramid pooling.



$$L(o, c, O, C, l, g) = \lambda_1 L_{\text{conf}}(o, c) + \lambda_2 L_{\text{cla}}(O, C) + \lambda_3 L_{\text{loc}}(l, g). \quad (4)$$

Among them,  $\lambda_1$ ,  $\lambda_2$ , and  $\lambda_3$  are equilibrium coefficients. The weight of each loss function is adjusted by setting the size of each  $\gamma$ . The specific formulas of confidence loss, classification loss, and positioning loss are shown in formula (5), (6), and (7).

$$L_{\text{conf}}(o, c) = -\frac{\sum_i (o_i \ln(\hat{c}) + (1 - o_i) \ln(1 - \hat{c}_i))}{N}, \quad (5)$$

$$L_{\text{cla}}(O, C) = -\frac{\sum_{i \in \text{pos}} \sum_{j \in \text{cla}} (O_{ij} \ln(\hat{C}_{ij}) + (1 - O_{ij}) \ln(1 - \hat{C}_{ij}))}{N_{\text{pos}}}, \quad (6)$$

$$L_{\text{loc}}(l, g) = \frac{\sum_{i \in \text{pos}} \sum_{m \in \{x, y, w, h\}} (l_i^m - g_i^m)^2}{N_{\text{pos}}}. \quad (7)$$

In formula (5),  $o_i \in [0, 1]$ , which represents the CIOU between the prediction frame and the real frame,  $c$  is the prediction value,  $\hat{c}$  is the prediction confidence obtained by  $c$  through the Sigmoid function, and  $N$  is the number of positive and negative samples. In formula (6),  $O_{ij} \in \{0, 1\}$  indicates whether there is a class  $j$  target in the prediction frame  $i$ ,  $C_{ij}$  is the prediction value,  $\hat{C}_{ij}$  is the target probability obtained by  $C_{ij}$  through the Sigmoid function, and  $N_{\text{pos}}$  is the number of positive samples. In formula (7),  $l_i^m$  is the center point coordinate and length and width in the prediction frame, and  $g_i^m$  is the information of the real frame. The formula of CIOU is shown in (8).

$$\text{CIOU} = \text{IOU} - \frac{\rho^2(b, b^{gt})}{c^2} - \alpha v, \quad (8)$$

where  $b$  represents the coordinates of the distance between the center point of the prediction box,  $b^{gt}$  represents the coordinates of the distance between the center point of the real box,  $\rho(\cdot)$  represents the calculation of Euclidean distance,  $c$  represents the distance between the prediction box and the diagonal line of the minimum bounding box of the real box, and penalty factors  $\alpha$  and  $v$  are added to it, as shown in (9) and (10).

$$\alpha = \frac{v}{1 - \text{IOU} + v}, \quad (9)$$

$$v = \frac{4}{\pi^2} \left( \arctan \frac{w^{gt}}{h^{gt}} - \arctan \frac{w}{h} \right)^2. \quad (10)$$

$w^{gt}$  and  $h^{gt}$  represent the width and height of the real box.  $w$  and  $h$  are the width and height of the prediction box. This penalty is mainly to make the width of the prediction box as fast as possible to be close to the width and height of the real box. Finally, we get the regression loss function as shown in formula (11).

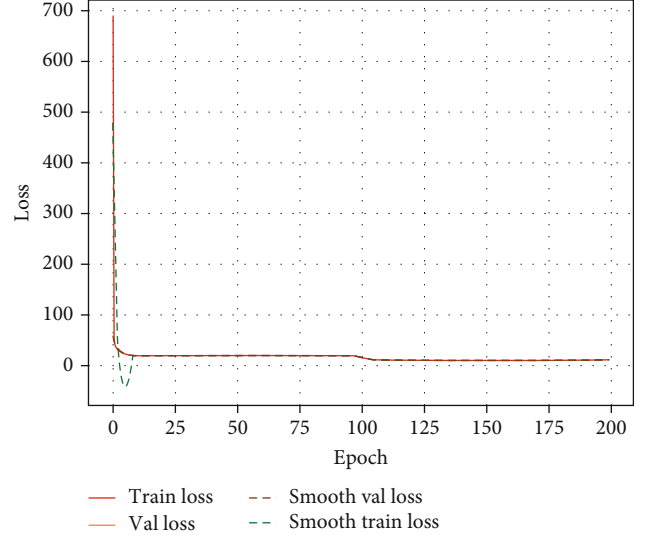


FIGURE 9: Training loss function curve.

$$L_{\text{ciou}} = 1 - \text{IOU} + \frac{\rho^2(b, b^{gt})}{c^2} + \alpha v. \quad (11)$$

The present algorithm uses anchor base to predict the target position of the object. The main idea is to set anchor, of different sizes in each feature point in the feature matrix, although the problem of positive and negative sample imbalance during training, leading to reduced model accuracy. For example, an image may produce tens of thousands of candidate boxes, but only few parts contain the target; the target box is positive sample, and the negative sample with no candidate box. The focal loss [30] function solves the problem of positive and negative sample imbalance and also controls the weights of easily classified and difficult classified samples. The formula of the focal loss function is as follows: (12), (13), and (14).

$$p_t = \begin{cases} p & \text{if } y = 1 \\ 1 - p & \text{otherwise} \end{cases}, \quad (12)$$

$$\alpha_t = \begin{cases} \alpha & \text{if } y = 1 \\ 1 - \alpha & \text{otherwise} \end{cases}, \quad (13)$$

$$\text{FL}(p_t) = -\alpha_t (1 - p_t)^Y \log(p_t). \quad (14)$$

Among them,  $(1 - p_t)^Y$  is called the adjustment coefficient. When  $p_t$  tends to 0, the adjustment coefficient tends 1, the contribution to loss increases, and the adjustment coefficient tends 0, equivalent to a small contribution to the total loss. When the coefficients  $Y = 0$ , the traditional crossentropy loss function realizes the adjustment coefficient by adjusting the  $Y$ .

### 3. Results and Discussion

3.1. *Experimental Environment.* This experiment uses Pytorch as a deep learning framework to accelerate the



TABLE 3: Prediction effect of target detection model in this paper on insects in each test set.

Name	AP (%)	Name	AP (%)
Corn borer	99.36	Amata emma	99.13
Cotton bollworm	99.27	Gryllotalpa spps	95.50
Chafer	99.59	Chiasmia cinerearia	96.56
Macdunnoughia crassisigna	71.43	Eupolyph	96.67
Athetis lepigone	99.01	Callambulyx tatarinovi	99.58
Mamestra brassicae Linnaeus	96.15	Scarites	94.85
Striped sorghum borer	98.20	Cricket	100.00
Agrotis ypsilon	62.86	Diaphania quadrimaculalis	97.50
Mythimna Separata	98.32	Agrius convolvuli	99.58
Latoia sinica Moore	99.94	Smeritus planus walker	86.96
Beet armyworm	92.75	Parum colligata	88.60
Agrotis segetum	81.90	Bremer et Grey	89.81
Ladybug	95.82	Butler	97.66
mAP			93.73

training model. The hardware configuration is: R5-3600 processor, 16GB memory, and Nvidia RTX3070 graphics card; the software environment is Windows10 system, Python3.7, Pytorch1.9, CUDA version 11.0, and cuDNN version 8.0.1.

**3.2. Evaluation Criteria.** Average precision (AP) is a main-stream measure of the target detection model. AP is calculated by calculating the AP of each target category. AP is calculated by using the area under precision-recall (P-R) curve as the AP value, where precision and recall formulas (15) and (16) show.

$$\text{Recall} = \frac{\text{TP}}{\text{TP} + \text{FN}}, \quad (15)$$

$$\text{Precision} = \frac{\text{TP}}{\text{TP} + \text{FP}}. \quad (16)$$

TP (true positives) represents the correct target class classification and is a positive sample, FN (false negatives) represents the wrong result of model classification, and the sample is negative, FP (false positives) represents the wrong model classification, the sample is negative, and map has become a recognized method of target detection and is widely used.

**3.3. Results and Analysis.** In the process of regression prediction, nine candidate frames are set according to three characteristic matrices with different sizes. Because of different training data sets, the sizes of candidate frames are also different. In this paper,  $K$ -means clustering algorithm is used to find the appropriate size of prior frames in the training set. The  $K$ -means clustering algorithm is different from the standard one. It calculates the distance between candidate frames through CIOU, and the final nine candidate frames are (29, 35), (55, 70), (72, 117), (87, 83), (94, 149), (115, 110), (124, 186), (145, 146), and (182, 220), which fit 81% of the frames of the dataset. During training, the transfer learning method is adopted. The preloaded model is the model of VOC data set, and the partially frozen backbone

method is used to iterate 50 times, then thaw the training, and then iterate 50 times. As shown in Figure 9, the decline curve of the loss function after 200 times of model training is displayed. The cosine annealing method is used to reduce the learning rate. Among them, the learning rate adopts the cosine annealing method to reduce the learning rate through the cosine function. In the cosine function, with the increase of  $x$ , the cosine value first decreases slowly, then accelerates the decline and decreases slowly again. It is easier for the model to find the best advantage, and the label smoothing method is added, which is mainly to punish the classification so that the model cannot be classified too accurately and prevent overfitting

We divide the dataset into training set, validation set, and test set according to 7:1:2 ratio and then calculate the AP value of the pest species through the test set. Table 3 shows that the mAP value of the model can reach 93.73%, which proves that the detection model has good performance. We can see that the accuracy of Scarite pests can reach 100%, while the AP of Agrotis ipsilon pests is only 62.86%. From the table, we can know that this may be caused by the uneven distribution of pest species, or it may make the characteristics of pests have little difference, the number of samples is small, and the model is not enough to extract the features. To further demonstrate the robustness of the model, we tested the detection of the algorithm in real-world situations. As shown in Figure 10, the algorithm detection results in different scenarios. In Figure 10(a), there is little background interference, the number of pests is always constant, and there is no stacking. The algorithm accurately predicts the type and location of pests. In Figure 10(b), although the number of pests has decreased, the background has been seriously disturbed, and the pests have been flipped. The model still finds the location and classification of pests accurately. In Figure 10(c), stacks of pests appear, and the number and species increase. Although pests are identified as two species, this may be due to the low IOU threshold, but most pests are accurately identified. In Figure 10(d), there are a large number of pests, and some

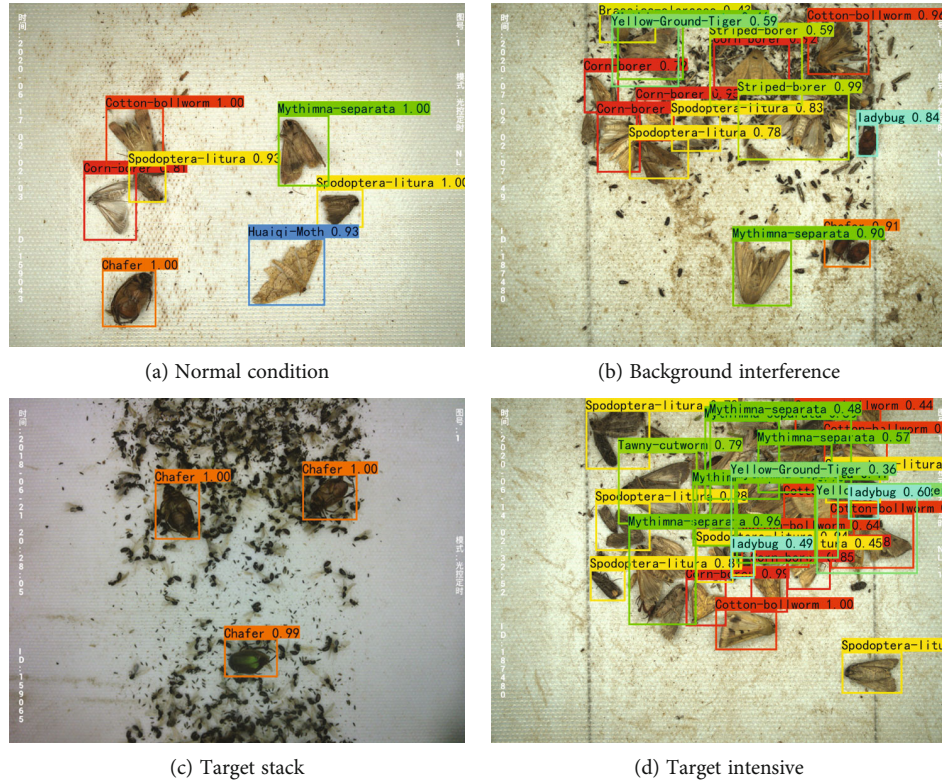


FIGURE 10: Model detection results in different scenarios.

TABLE 4: Average recognition accuracy, detection speed, and model size of different models for insects.

Models	mAP(%)	Speed (s)	Parameters (million)	Size (MB)
Yolov3	89.71	1.90	61.66	235.21
ShuffleNet-yolo	75.71	0.42	9.60	36.60
MobileNetv1-yolo	84.66	0.60	12.40	47.31
MobileNetv2-yolo	81.65	0.63	10.51	40.09
MobileNetv3-yolo	81.93	0.54	11.13	43.63
GhostNet-yolo	82.49	0.53	11.14	42.49
EfficientNet-yolo	88.16	0.69	15.12	59.23
Our model	93.73	0.72	15.66	59.78

of them are stacked, which is compared with the actual number. Despite the missed pest detection, the model still detects the location of pests and their corresponding species. Through these complex cases, it can be shown that the target detection algorithm has excellent robustness, can cope with a variety of complex environments, and has wide application.

*3.4. Comparison of Several Models.* To evaluate the performance of the algorithm, this paper is compared with yolov3, yolov3 algorithm adopts Darknet-53 as the backbone feature network, it uses the original EfficientNet-B2, for comparison, and finally, on the basis of this algorithm replaced different lightweight backbone, such as Google MobileNet [31, 32] series, and more lightweight ShuffleNet [33, 34] and Huawei GhostNet [35], these are lightweight classification networks. The same training set is used in the experi-

ments, finally, test evaluation using the same test set. Finally, the model is deployed on industrial tablets, its CPU is adopted as a J1900 processor, 4GB of running memory, and test the inference speed of the model, and results are shown in Table 4. We can see that the yolov3 model has high accuracy, but the number of participants can reach 60 million, the inference of the model is the longest time-consuming, high performance requirements for the equipment, not convenient for practical deployment, and using a lightweight backbone, we can see that the ShuffleNet parameter is minimal, the model is only 36 MB, and the detection speed is also the fastest, but the model really has the lowest accuracy. Compared with MobileNet series and GhostNet, the comprehensive performance of explicit GhostNet is the best, with the volume size of only 42 MB, the accuracy can be up to 82%, and the detection speed can basically reach two pictures per second, with good timeliness. Although these

models are small, the accuracy does not meet the commercial standard. For this algorithm compared with EfficientNet-B2, the accuracy rate can reach 93% and improve by almost 5 percentage points, and the volume of the algorithm is only a quarter more than GhostNet; so, this algorithm has lightweight and high sex characteristics.

#### 4. Conclusion

In order to achieve automatic recognition and classification of farmland pests, a lightweight target detection model is proposed. Based on the idea of yolov3, the EfficientNet-B2 classification network is used as the main feature extraction network and improved. PANet is added to THE neck, and CIOU is used as the loss function of target detection to highlight the relative position between the prediction box and the real box. The problem that the low confidence prediction box is filtered due to the overlap of the target box, and the prediction box is avoided. Focal loss function is used to solve the imbalance between positive and negative samples during training. In order to increase the diversity of datasets, the Mosaic data enhancement method is used to increase the diversity of data and improve the robustness of the model. Experiments show that the mAP value of this algorithm can reach 93% accuracy, and it has good recognition ability. The algorithm also has strong recognition ability in complex environment. Compared with other algorithms, this algorithm not only recognizes many kinds of classes but also has high accuracy and wide application.

#### Data Availability

The experimental data used to support the findings of this study are available from the corresponding author upon request.

#### Conflicts of Interest

The authors declared that they have no conflicts of interest regarding this work.

#### Acknowledgments

This work is supported by the Major Agricultural Application Technology Innovation Project of Shandong Province. The project number is SD2019ZZ007.

#### References

- [1] H. Liu, "Driving agricultural modernization with photography agriculture to accelerate the digital transformation of modern agriculture," *China Agricultural Resources and Regional Planning*, vol. 40, 2019.
- [2] Y. Peng, Y. Yang, W. Yang, and S. Chen, "Design of intelligent agricultural management system based on Internet of Things technology," *Modern Agricultural Science and Technology*, vol. 4, no. 19, 2020.
- [3] J. Nie, R. Sun, and X. Deng, "Processing of uncertain complex events in precision agriculture based on data lineage management," *Transactions of the Chinese Society of Agricultural Machinery*, vol. 47, no. 5, pp. 245–253, 2016.
- [4] H. Feng and Q. Yao, "Automatic identification and monitoring technology of agricultural pests," *Plant Protection*, vol. 44, no. 5, 2018.
- [5] X. Shi, M. Zhao, H. Li, and Z. Wen, "Research on corn pest species recognition system based on image processing," *Agriculture and Technology*, vol. 41, no. 12, pp. 28–31, 2021.
- [6] Y. Shen, *Research on stored-grain pest detection algorithm based on deep learning*, Master thesis, Beijing University of Posts and Telecommunications, 2018.
- [7] Y. Zhang, M. Jiang, and P. Yu, "Image recognition method of agricultural pests based on multi-feature fusion and sparse representation," *China Agricultural Sciences*, vol. 51, no. 11, pp. 67–76, 2018.
- [8] W. Liu, D. Anguelov, and D. Erhan, "SSD: Single shot multi-box detector," in *in Proc. European conference on computer vision*, pp. 21–37, Springer, Cham, 2016.
- [9] S. Ren, K. He, and R. Girshick, "Faster R-CNN: towards real-time object detection with region proposal networks," *IEEE Transactions on Pattern Analysis & Machine Intelligence*, vol. 39, no. 6, pp. 1137–1149, 2017.
- [10] J. Redmon, S. Divvala, and R. Girshick, "You only look once: unified, real-time object detection," in *in Proc. Proceedings of the IEEE Conference on Computer Vision and Pattern Recognition*, pp. 779–788, Las Vegas, USA, 2016.
- [11] X. Zhou, D. Wang, and P. Krähenbühl, *Objects as points*, 2019, <https://arxiv.org/abs/1904.07850>.
- [12] Y. Wei, B. I. Xiu-Li, and B. Xiao, "Agricultural insect pest detection method based on regional convolutional neural network," *Computer Science*, vol. 45, no. 11A, pp. 226–229, 2018.
- [13] Z. Yuan, H. Yuan, Y. Yan, S. Liu, and S. Tian, "Automatic recognition and classification algorithm of field Insects Based on lightweight deep learning model," *Journal of Jilin University (Engineering and Technology Edition)*, vol. 51, no. 3, pp. 1131–1139, 2021.
- [14] W. An, L. Zhao, X. Zhang, and Y. Han, "Phenological prediction and prediction of major pests in orchards in Baoding area," *Modern rural Science and Technology*, vol. 12, no. 3, pp. 36–37, 2020.
- [15] X. Liu, *Research on lightweight insect detection model based on deep learning*, Mater thesis, Beijing Forestry University, 2019.
- [16] M. Everingham, L. V. Gool, and C. K. I. Williams, "The pascal visual object classes (voc) challenge," *International journal of computer vision*, vol. 88, no. 2, pp. 303–338, 2010.
- [17] Y. Gao, B. Zhou, and X. Hu, "Research on convolutional neural network image recognition based on data enhancement," *Computer Technology and Development*, vol. 28, no. 8, pp. 62–65, 2021.
- [18] J. Xing, M. Jia, F. Xu, and J. Hu, "Recognition method of small defects on workpiece surface based on Cut Mix and YOLOv3 (English)," *Journal of Southeast University (English Edition)*, vol. 37, no. 2, pp. 128–136, 2021.
- [19] K. Simonyan and A. Zisserman, "Very Deep Convolutional Networks for Large-Scale Image Recognition," *Computer Science*, 2014, <https://arxiv.org/abs/1409.1556v6>.
- [20] K. He, X. Zhang, and S. Ren, "Deep residual learning for image recognition," in *in Proc Proceedings of the IEEE Conference on Computer Vision and Pattern Recognition*, pp. 770–778, Las Vegas, USA, 2016.



- [21] G. Huang, Z. Liu, and L. Van Der Maaten, "Densely connected convolutional networks," in *in Proc. Proceedings of the IEEE Conference on Computer Vision and Pattern Recognition*, pp. 4700–4708, Hawaii, USA, 2017.
- [22] T. Y. Lin, P. Dollar, and R. Girshick, "Feature pyramid networks for object detection," in *in Proc. 2017 IEEE conference on computer vision and pattern recognition (CVPR)*, IEEE Computer Society, Hawaii, SA, 2017.
- [23] S. Liu, L. Qi, and H. Qin, "Path aggregation network for instance segmentation," in *in Proc. Proceedings of the IEEE Conference on Computer Vision and Pattern Recognition*, pp. 8759–8768, Salt Lake City, USA, 2018.
- [24] M. Tan, R. Pang, and Q. V. Le, "Efficientdet: scalable and efficient object detection," in *in Proc. Proceedings of the IEEE/CVF conference on computer vision and pattern recognition*, pp. 10781–10790, Seattle, USA, 2020.
- [25] H. Law and J. Deng, "CornerNet: detecting objects as paired keypoints," *International Journal of Computer Vision*, vol. 128, no. 3, pp. 642–656, 2020.
- [26] M. Tan and Q. Le, "Efficientnet: rethinking model scaling for convolutional neural networks," in *in Proc. International Conference on Machine Learning*, pp. 6105–6114, PMLR, 2019.
- [27] A. G. Howard, M. Zhu, and B. Chen, "Mobilenets: efficient convolutional neural networks for mobile vision applications," 2017, ar Xiv preprint ar Xiv: 1704.04861.
- [28] S. Khan, M. Naseer, and M. Hayat, "Transformers in vision: a survey," 2021, ar Xiv preprint ar Xiv: 2101.01169.
- [29] Z. Zheng, P. Wang, and D. Ren, "Enhancing geometric factors in model learning and inference for object detection and instance segmentation," 2020, ar Xiv preprint ar Xiv: 2005.03572.
- [30] T. Y. Lin, P. Goyal, and R. Girshick, "Focal loss for dense object detection," in *in Proc. Proceedings of the IEEE international conference on computer vision*, pp. 2980–2988, Hawaii, USA, 2017.
- [31] A. Howard, A. Zhmoginov, and L. Chen, "Inverted residuals and linear bottlenecks: Mobile networks for classification, detection and segmentation," 2018, <https://arxiv.org/abs/1801.04381v2>.
- [32] A. Howard, M. Sandler, and G. Chu, "Searching for mobilenetv 3," in *in Proc. Proceedings of the IEEE/CVF International Conference on Computer Vision*, pp. 1314–1324, Long Beach, USA, 2019.
- [33] X. Zhang, X. Zhou, and M. Lin, "Shufflenet: an extremely efficient convolutional neural network for mobile devices," in *in Proc. Proceedings of the IEEE Conference on Computer Vision and Pattern Recognition*, pp. 6848–6856, Salt Lake City, USA, 2018.
- [34] N. Ma, X. Zhang, and H. Zheng, *Shuffle Net V2: Practical Guidelines for Efficient CNN Architecture Design*, in Proc. Springer, Cham. Springer, Cham, 2018.
- [35] K. Han, Y. Wang, and Q. Tian, "Ghostnet: more features from cheap operations," in *in Proc. Proceedings of the IEEE/CVF Conference on Computer Vision and Pattern Recognition*, pp. 1580–1589, Seattle, USA, 2020.

## Research Article

# Dynamic Gesture Contour Feature Extraction Method Using Residual Network Transfer Learning

Xianmin Ma and Xiaofeng Li 

Department of Information Engineering, Heilongjiang International University, Harbin 150025, China

Correspondence should be addressed to Xiaofeng Li; [lixiaofeng@hiu.net.cn](mailto:lixiaofeng@hiu.net.cn)

Received 2 August 2021; Revised 10 September 2021; Accepted 24 September 2021; Published 13 October 2021

Academic Editor: Deepak Gupta

Copyright © 2021 Xianmin Ma and Xiaofeng Li. This is an open access article distributed under the Creative Commons Attribution License, which permits unrestricted use, distribution, and reproduction in any medium, provided the original work is properly cited.

The current dynamic gesture contour feature extraction method has the problems that the recognition rate of dynamic gesture contour feature and the recognition accuracy of dynamic gesture type are low, the recognition time is long, and comprehensive is poor. Therefore, we propose a dynamic gesture contour feature extraction method using residual network transfer learning. Sensors are used to integrate dynamic gesture information. The distance between the dynamic gesture and the acquisition device is detected by transfer learning, the dynamic gesture image is segmented, and the characteristic contour image is initialized. The residual network method is used to accurately identify the contour and texture features of dynamic gestures. Fusion processing weights are used to trace the contour features of dynamic gestures frame by frame, and the contour area of dynamic gestures is processed by gray and binarization to realize the extraction of contour features of dynamic gestures. The results show that the dynamic gesture contour feature recognition rate of the proposed method is 91%, the recognition time is 11.6s, and the dynamic gesture type recognition accuracy rate is 92%. Therefore, this method can effectively improve the recognition rate and type recognition accuracy of dynamic gesture contour features and shorten the time for dynamic gesture contour feature recognition, and the  $F$  value is 0.92, with good comprehensive performance.

## 1. Introduction

Gesture is an intuitive and convenient way of communication, and natural and comfortable human-computer interaction can be realized through gesture recognition [1]. At present, dynamic gestures are more intuitive than static gestures and are widely used in flexible human-computer interaction applications. It can not only manipulate virtual objects in a virtual reality environment but also can be widely used in smart home appliances and corresponding automatic control fields [2–3]. However, due to the complexity of the human hand structure, dynamic gestures are presented as diverse. The recognition of dynamic gestures has always been one of the difficulties in research. Traditional gesture recognition methods are usually implemented by background filtering and feature extraction. They are easy to be affected by external factors such as light, reduce the performance of the algorithm, and are difficult to obtain satisfactory results.

In recent years, with the rise of deep learning algorithms, a deep residual network has been widely used as a new deep learning algorithm. This learning algorithm adopts end-to-end learning strategy, which can efficiently and independently realize image feature analysis, explore the internal features of images, and help improve the effect of image analysis. However, the deep learning model is complicated for sample training and learning process. Therefore, transfer learning is introduced to migrate the learned sample data or model parameters to the new model to avoid the lack of zero learning in the deep learning network [4]. There are many related studies on the transfer learning of residual network. The literature [5] proposes the method of combining wide residual and long-term and short-term memory network. Convolutional neural network is used to extract features synchronously in space and time dimensions, respectively, and the long-term and short-term memory network is used to analyze features synchronously and input them into the residual network, so as to finally realize gesture recognition.



The literature [6] uses deep neural network and residual learning technology to study nonlinear wavefront sensing. The deep residual learning method expands the usable range of Lyot-based low order wavefront sensors (LLOWFS) by more than one order of magnitude and can improve the closed-loop control of the system with large initial wavefront error. This paper shows the advantages of residual network. The literature [7] proposes a deep residual convolutional neural network (CNN) model to self-learn the hidden median filter traces in JPEG lossy compressed images. In order to alleviate the over fitting problem of the deeper CNN model, this paper adopts a data enhancement scheme in training to increase the diversity of training data, so as to obtain a more stable median filter detector.

To solve the above problems, this paper proposes a dynamic gesture contour feature extraction method based on residual network transfer learning.

- (1) The sensor is used to integrate the dynamic gesture information. The distance between the dynamic gesture and the acquisition device is detected by transfer learning, and the dynamic gesture image is segmented in the background
- (2) The feature contour image is initialized, the dynamic gesture feature contour image was replaced, and the dynamic gesture feature recognition model was trained. The residual network method is used to accurately identify the contour and texture features of dynamic gestures
- (3) The processing weights are fused to obtain a significant contour response, and the contour features of dynamic gestures are traced frame by frame. According to the geometric features of the dynamic gesture region, the dynamic gesture part is projected longitudinally, and the dynamic gesture contour area is processed by gray and binarization to realize the dynamic gesture contour feature extraction

## 2. Related Work

At present, a large number of scholars in this field have conducted research on it and achieved certain research results. The literature [8] proposes a multitask-based recurrent residual network, a multitask-based method that performs gesture recognition and time detection at the same time. It adopts a double loss function, which assigns the category of each frame of video to a gesture class, and determines the frame interval related to each gesture, so as to extract gesture contour and gesture motion features to complete dynamic gesture recognition. The dynamic gesture recognition speed of this method is fast, but the contour and texture of dynamic gesture recognition are not considered, resulting in low accuracy of dynamic gesture recognition. The literature [9] proposed a dynamic gesture recognition method based on a feature fusion network and variant convolution Long Short-Term Memory (ConvLSTM) and designed the gesture recognition architecture. The architecture extracts spatiotemporal feature information from local, global, and deep

and combines feature fusion to reduce the loss of feature information. The local spatiotemporal feature information is extracted from video sequences by using the three-dimensional residual network of channel feature fusion. The variation ConvLSTM is used to learn the global temporal and spatial information of dynamic gestures, and the attention mechanism is introduced to change the gate structure of ConvLSTM to realize dynamic gesture recognition. This method can effectively improve the accuracy of dynamic gesture recognition, which has the problem of long time of dynamic gesture recognition. The literature [10] proposed dynamic gesture recognition based on selective spatiotemporal feature learning, combined with the dynamic selection mechanism of selective spatiotemporal feature learning of ResC3D network and ConvLSTM, improved the architecture of dynamic gesture fusion model, adaptively adjusted dynamic gesture data, extracted short-term and long-term spatiotemporal features of dynamic gesture learning, and recognized dynamic gestures. The dynamic gesture recognition rate of this method is high, but the accuracy of dynamic gesture type recognition is low. The literature [11] proposes a dynamic gesture recognition method based on short-time sampling neural network. The short-time sampling neural network is used to integrate verified modules to learn short-term and long-term features from video input. Each video input is divided into a fixed number of frame groups, one frame is selected and represented as RGB image and optical flow snapshot, and the convolution neural network is input to extract features and output long-term short-term memory network to recognize dynamic gestures. This method has good robustness. However, the recognition efficiency is low. The literature [12] proposed a dynamic gesture recognition algorithm based on simultaneous detection and classification of wide residual network and long-term and short-term memory network. Firstly, the spatiotemporal features are extracted from the fine-tuning three-dimensional convolutional neural network. Secondly, the bidirectional convolutional long-term and short-term memory network is used to further consider the time aspect of image sequence. Finally, these advanced features are sent to a wide range of residual networks for final gesture recognition. The success rate of gesture recognition is high, but the accuracy of gesture recognition is low.

Relevant achievements have also been made in China. The literature [13] proposes a multifeature dynamic gesture recognition method, which uses the somatosensory controller leap motion to track the dynamic gesture to obtain data, extract the displacement vector angle and inflection point judgment count, train the dynamic gesture using the hidden Markov model, and recognize the multifeature dynamic gesture according to the matching rate of the gesture to be tested and the model. This method can effectively improve the recognition rate of similar gestures, but the recognition time is long. Literature [14] proposed a feature extraction method based on the geometric distribution of gestures, normalized the segmented gesture image, calculated the width length ratio of the minimum circumscribed rectangle of the gesture main direction and the gesture contour, preliminarily identified it by using the similarity function, counted

the distribution of gesture contour points by using the contour segmentation method, and recognized the gesture contour according to the modified Hausdorff distance similarity measurement method. The recognition time of this method is shorter, but the recognition accuracy is lower.

In order to solve the shortcomings of research, a dynamic gesture contour feature extraction method based on residual network transfer learning is proposed, and the performance of the proposed method is verified by experiments. The results show that the proposed method has high dynamic gesture contour feature recognition rate and gesture type recognition accuracy rate, and the recognition time is short, only 11.6s, and the average  $F$  value of feature extraction is as high as 0.92.

### 3. Dynamic Gesture Contour Feature Extraction Method Based on Residual Network Transfer Learning

*3.1. Dynamic Gesture Segmentation Image.* Complicated background and external lighting can easily affect the acquisition of dynamic gesture images, so it is particularly important to choose a suitable gesture collection device. The sensor is used to segment the depth information of the palm gesture from the complex background. The distance between the dynamic gesture and the collection device is detected by transfer learning.

Assume that the source domain data sample of transfer learning is expressed as  $D_s$ , the label of the source domain data sample is expressed as  $L_s$ , the target domain data sample is expressed as  $D_t$ , and the label of the target domain data sample is expressed as  $L_t$ . Nonlinearly change the characteristics of the source and target domains, and align the source and target domain characteristics to perform second-order statistics. If the dynamic gesture contour feature covariance matrix is expressed as  $C_t$ , the loss between the contour features of the dynamic gesture on each feature layer of the source domain and the target domain is

$$l_s = \frac{1}{4C_t} \|D_s - D_t\|^2 \|L_s - L_t\|^2. \quad (1)$$

For the classification model, the feature adaptation method is adopted, if the source domain data sample classifier is  $U_f$ , the target domain data sample classifier is  $U_t$ , and then the classification loss  $P(D_s)$  of the source domain data sample  $D_s$  of transfer learning can be expressed as

$$P(D_s) = \min \frac{1}{C_t} P(U_f, U_t), \quad (2)$$

where  $P(U_f, U_t)$  is cross entropy function. The classification loss  $P(D_s)$  of the target domain data sample  $D_t$  of transfer learning can be expressed as

$$P(D_t) = \min \frac{1}{C_t} K(U_t), \quad (3)$$

where  $K(U_t)$  is entropy function. Thus, the loss function of constructing the migration learning architecture is expressed as

$$S(h) = \min \frac{1}{C_t} P(D_s) + \frac{1}{\gamma} P(D_t) + \chi l_s, \quad (4)$$

where  $\gamma$  is the trade-off parameters of the target domain data sample and  $\chi$  is loss trade-off parameters between dynamic gesture contour features. In gesture human-computer interaction, the palm is always in front of the camera, so by selecting an appropriate depth distance threshold, the palm gesture information can be separated from the background. However, the selection of the distance threshold is very difficult, and the threshold selection is inappropriate, which easily leads to the segmented gestures including arms. Or when the gesture is close to the body, the palm information cannot be segmented [15]. In order to overcome the influence caused by the selection of the threshold, the depth mining of image information is carried out by detecting the information of the gesture skeleton node. The sensor is used to collect the gesture bone node data, find the position of the palm node, and search for dynamic gestures in the palm node range. When all the pixels on the entire palm are close to the camera, setting a distance difference threshold can separate the gesture information from the background, and the dynamic gesture segmentation process. It is shown in Figure 1.

As the collector tracks the dynamic gesture skeletal node, the phenomenon of node drift is prone to occur. At this time, the distance between the palm node and the collector is not the actual distance between the palm node and the collector. When the distance difference threshold is segmented, the gesture segmentation will fail. Therefore, an approximate method for determining the position of the palm node is designed [16]. The position coordinates of all self-color pixels are averaged in a circle with the palm node as the center and the distance  $r$  between the palm node and the wrist node as the radius. This can be calculated by using the mean value to represent the position coordinates of the palm node. Therefore, the  $(x_p, y_p)$  equation of the palm node collection is

$$(x_p, y_p) = \left( \frac{1}{T} \sum_{i=1}^T x_i, \frac{1}{T} \sum_{i=1}^T y_i \right), \quad (5)$$

where  $T$  is the number of self-color pixels in the circle,  $x_i$  is the horizontal vector of the  $i$  self-color pixel, and  $y_i$  is the vertical vector of the  $i$  self-color pixel. After the position of the palm node is found, the gesture is segmented by judging the distance difference between the palm node and the pixels in the surrounding area to the collector. When the palm node is found, the gesture pixels need to be divided around the palm node [17]. In order to prevent the deviation of the gesture pixel points due to the drift of the palm node, the gesture pixel points are segmented in a large rectangular area centered on the palm node. The algorithm process is as follows: suppose the distance from the bone palm node

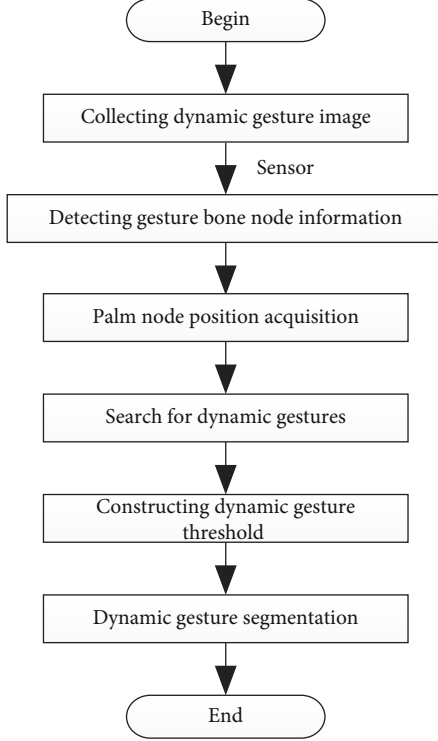


FIGURE 1: Dynamic gesture segmentation process.

extracted by the collector to the camera of the collector is  $d$ , the position of the palm node is  $(x_p, y_p, d_p)$ , and the position of the ankle node is  $(x_r, y_r, d_r)$ . Perform dynamic gesture pixel segmentation in a rectangular pixel centered on the palm node with a width of  $W$  and a height of  $H$ . It is shown in

$$W = \frac{1}{X(x_p, y_p)} H d \sqrt{(x_p - x_r)^2 + (y_p - y_r)^2}. \quad (6)$$

The dynamic gesture segmentation is carried out through equation (6), and the basic pixel points of each dynamic gesture image are obtained, so that the subsequent recognition of the dynamic gesture contour feature is more unified, thereby increasing the rate of dynamic gesture extraction.

**3.2. Recognize the Characteristic Contours of Dynamic Gestures.** Recognize the segmented dynamic gesture image. First, initialize the value of the feature contour image, output the network model of the last layer of the training connection layer, and replace it with the dynamic gesture feature contour image. On this basis, the dynamic gesture feature recognition model is trained, the training set is recognized by the model obtained during each training, and the training accuracy is obtained. The dynamic gesture feature contour image is recognized to obtain the accuracy of the test set. When the current method performs dynamic gesture feature contour recognition, it cannot accurately recognize the contour and texture of the dynamic gesture, resulting in a low

accuracy of dynamic gesture recognition. This is caused by the deep learning neural network layer of the recognition machine. Introduce the residual network model, before the level output, through the use of identity mapping, let the output layer cross the previous layer for data entry, and execute the identity mapping signal to avoid the network layer being too deep [18].

If the residual network has a total of  $l$  layers, the fully connected layer belongs to the last layer in the residual network, and the output of the residual mapping is expressed as

$$F(x^{l-1}) = g(\sigma_i \otimes g(\sigma_i \otimes x^{l-1})). \quad (7)$$

Then, the output of the residual unit in the residual network model is expressed as

$$H(x^{l-1}) = g(F(x^{l-1}) + \kappa_i \otimes x^{l-1}). \quad (8)$$

where  $\sigma_i$  is convolution kernel parameters,  $x^{l-1}$  is  $l-1$  layer input,  $\kappa_i$  is convolution kernel parameters for convolution operation,  $\otimes$  is the convolution operation, and  $g(x)$  is activated function. It is shown in

$$g(x) = \begin{cases} x & \text{if } x > 0, \\ 0 & \text{if } x \leq 0, \end{cases} \quad (9)$$

Due to the clever structure of each residual unit, when the gradient is transmitted backward, the error transmission mode is converted from the form of continuous multiplication to the form of addition to the upper level error sensitive items, thereby avoiding the gradient explosion and gradient caused by continuous multiplication. The disappearance of the problem ensures the effectiveness of error transmission.

The actual label and the model predicted label error are expressed as  $J$ . When parameters at layer  $l-1$  are updated, the gradient of the current layer needs to be passed to this layer, and the back propagation algorithm is used to calculate the error sensitive term of this layer as

$$g^{l-1} = \frac{\partial J}{\partial x^{l-1}}, \quad (10)$$

If the gradient transfer error sensitive term of the  $l+1$  layer is expressed as

$$g^{l+1} = \frac{\partial J}{\partial H(x^{l-1})}, \quad (11)$$

then, in the residual network model, when the shortcut is not connected,  $H(x^{l-1}) = F(x^{l-1})$ ,  $g^{l-1}$  can be expressed as

$$g^{l-1} = \frac{\partial J}{\partial H(x^{l-1})} \frac{\partial H(x^{l-1})}{\partial x^{l-1}}. \quad (12)$$

When the shortcut is connected,  $H(x^{l-1}) = F(x^{l-1}) + x^{l-1}$ ,

in back transmission,  $\vartheta^{l-1}$  can be expressed as

$$\vartheta^{l-1} = \frac{\partial J}{\partial H(x^{l-1})} \left( \frac{\partial H(x^{l-1})}{\partial x^{l-1}} + 1 \right). \quad (13)$$

During the transfer process, due to the residual unit structure of the residual network, the gradient of the previous layer can be directly transferred to the next layer and will not disappear due to the continuous multiplication of the transfer. In order to expand the scale of the training and recognition of dynamic gesture feature contours, the residual network's processing of the training set images is enhanced. The processing process includes flipping, rotating, filtering, cropping, and deformation. Because the difference of dynamic gesture changes is small, it needs to rely on a certain subtle feature to distinguish. Therefore, the focus of dynamic gesture feature contour recognition is to use the residual network to accurately identify the various features of dynamic gestures. However, if data enhancement methods such as cropping and deformation are used, important features may be lost, and the image after data enhancement may become unreliable. For different gestures, take the center node of the wrist as the relative coordinate, and set the wrist coordinate point as  $(x, y, z)$ , and suppose the coordinates corresponding to the feature points of the gesture are  $p = (x_i, y_i, z_i)$ ,  $i = 1, 2, 3, 4 \dots n$ . Therefore, the distance ( $S_i$ ) between the wrist coordinates and the dynamic gesture feature is

$$S_i = \sqrt{(x - x_i)^2 + (y - y_i)^2 + (z - z_i)^2}. \quad (14)$$

According to the above equation, within a certain time  $T$ , the motion sequence of the dynamic gesture skeleton node is expressed as  $(D = S_i^1, S_i^2, S_i^3, \dots, S_i^n)$ , and the time series of the test gesture is  $(Y = T_1, T_2, T_3, \dots, T_n)$ . Find the best point pair between the two sequences so that the sum of the distances between the corresponding points is the smallest, expressed as

$$Q(x, y) = \vartheta^{l-1} S_i \sum_n^{i=1} \omega(x_i, y_i, z_i), \quad (15)$$

where  $\omega$  is the corresponding node coefficient. The coordinates corresponding to the feature points of the gesture are  $p = (x_i, y_i, z_i)$ . Through the optimal sum of the distances of the points, the dynamic gesture images of the training set are recognized, and three methods are used for enhancement processing: rotation, flip, and filtering. Rotation is a random selection between -300 and 300. After rotation, the margins of the edge are filled with the adjacent background; the image is flipped horizontally. Image filtering adopts Gaussian filtering method, and the filtered image adds noise and is clearer than the original image [19]. After the original dynamic gesture images were enhanced in three ways, the training set image data set was expanded to 7044 images. After processing, there are many kinds of gesture recogni-

tion methods, such as neural network, SVM, and convolutional neural network. SVM has obvious effects on the two-classification processing, and the data outside the training set can achieve accurate prediction, low generalization error rate, and good real-time performance. Therefore, the residual network transfer learning is used to recognize the segmented gesture image and evaluate the normality of the gesture. The residual network migration learns the results of dynamic gesture recognition, tests the credibility of gestures and standard gestures, and provides a basis for dynamic gesture trace points.

**3.3. Scan Feature Contour Frame by Frame.** By identifying the feature contours of dynamic gestures, the basic data of dynamic gesture images and the skeleton data of gesture nodes are obtained. Consider the physiological characteristics of a single perception field in the visual pathway or the contextual adjustment between optic nerves [20]. For the same image, preserving contour information and removing background texture are usually contradictory. In this paper, the salient contour information of some spatial frequency tuning channels is transferred to the primary visual cortex in parallel, and the weight fusion processing is realized, and the salient contour response total -  $r(x, y)$  is finally obtained. It is shown in

$$\text{Total} - r(x, y) = \sum_j^{n'} (\beta_j \cdot R_j(x, y)), \quad (16)$$

where  $X$  is the value of the contour feature point of the dynamic gesture on the  $x$ -coordinate axis,  $y$  is the value of the contour feature point of the dynamic gesture on the  $y$ -coordinate axis,  $\beta_j$  is the reference parameter of the node,  $R_j$  is the error parameter of the node, and  $n'$  is band fusion weight of the contour response on the frequency tuning channel of the  $n$  space, whose value is  $[0, 1]$ . Considering that on the low-frequency spatial frequency tuning channel, the contour map mainly represents the overall contour of the image [21]. Therefore, based on the fusion coding of the frequency-divided visual information stream under the primary visual cortex, and considering the influence of the frequency-divided characteristic parameters on the fusion weight, a value model for drawing points is proposed. It is shown in

$$\beta_j = [\text{total} - r(x, y)] \frac{e^{-\delta_j}}{\sum_{j=1}^{n'} e}, \quad (17)$$

where  $e^{-\delta_j}$  is the outer value of feature trace node and  $e$  is inner value of feature trace node. Through equation (7), the contour feature of the dynamic gesture is traced, and the coordinate data of the skeleton node of the contour of the dynamic gesture is extracted to realize the feature trace of the dynamic gesture. Next, there is a need to go through the standard dynamic gesture detection of the dynamic gesture sample library, and the contour features of the dynamic



gesture by matching the optimal residual network transfer learning method were extracted.

**3.4. Extract Contour Features of Dynamic Gestures.** The color space model is used to check the area of the dynamic gestures. After obtaining the dynamic gesture region, according to the geometric features in the dynamic gesture sample library, the dynamic gesture region is traced a second time, and the gesture region square is extracted. According to the color characteristics between the images, grayscale changes and binarization remove the brighter interference items such as the background and then remove the darker interference items such as nails and dark backgrounds. Finally, the projection filtering operation is performed, and the vertical projection operation is performed on the dynamic gesture part. Set a certain threshold. If the vertical projection is less than the threshold, it will be set to black to remove interference items such as irrelevant lines [22, 23]. Perform skin color model processing on the obtained dynamic gesture contour area window to detect the approximate range of the dynamic gesture area. Determine the skin area; it is shown in

Suppose  $A$  is the area of the skin area of the dynamic gesture contour and  $B$  is to identify the total area of the image. Then, it is determined that the skin area is a dynamic gesture contour area. The area of the filtered area was sorted, and the largest value is the area square of the final detection. Assign 0 to the nondynamic gesture contour area in the original image, that is, paint it in black. The method is to first assign the original image to 0 and black it, and then the detected dynamic gesture contour area window to 1 white was assigned, and then the AND operation was performed with the unprocessed original image to obtain an image with only the dynamic gesture contour area square. Perform grayscale processing on the above image, and then binarize it; only the dynamic gesture contour area exists, and it is white. After multiplying by the unprocessed original image, a picture with only dynamic gesture outline area (including nails and darker background) is obtained [24–25]. Perform grayscale processing on the image obtained above (set a certain threshold). The white area obtained after binarization is the dynamic gesture contour area. According to the method process of the image projection filtering operation, the white connected areas of the dynamic gesture area are labeled, and each line of each area is traversed. Add each row of the area and project the image longitudinally to obtain the processed dynamic gesture contour feature image, which realizes the dynamic gesture contour feature extraction.

**3.5. Method for Feature Recognition of Dynamic Gesture Contours.** The residual network migration learning is used to realize dynamic gesture contour feature and dynamic gesture type recognition; the dynamic gesture contour feature recognition method is described as

- (i) Input: obtain the loss function of the migration learning architecture through the source and target domains with or without labels in the migration learning  $S(h)$ . Set the input of a layer in the residual

network to  $\tau$ . After passing some convolutional layers and activation functions, a residual mapping  $F(x^{l-1})$  is obtained.

- (ii) Output: extraction result of dynamic gesture contour feature potential  $T(\lambda)$ .
  - (1) The sensor is used to segment the depth information of the palm gesture from the complex background. The distance between the dynamic gesture and the collection device is detected by transfer learning. Construct the loss function of the transfer learning architecture  $S(h)$ . Calculate the position coordinates of the palm nodes, and segment the pixels of the dynamic gesture image
  - (2) Initialize the contour image of the dynamic gesture feature, and use the residual network method to calculate the error-sensitive items  $\mathcal{G}^{-1}$ . Obtain the distance between the wrist coordinate and the dynamic gesture feature, and accurately identify the contour and texture feature of the dynamic gesture through the optimal sum of the distances of the points
  - (3) Obtain significant contour response total  $-r(x, y)$  through weight fusion processing. Considering the influence of the frequency-division characteristic parameters on the fusion weight, the  $\beta_j$  is constructed to draw the point value model, and the dynamic gesture contour features are drawn frame by frame
  - (4) The gray scale and binarization process the dynamic gesture contour area, detect the approximate range of the dynamic gesture area, and obtain the dynamic gesture contour feature extraction result as  $T(\lambda)$

$$T(\lambda) = \frac{1}{S(h)} F(x^{l-1}) \beta_j r(x, y) \quad (18)$$

- (5) End

In summary, to achieve the feature extraction of dynamic gesture contours, the specific process is shown in Figure 2.

## 4. Experimental Analysis and Results

**4.1. Experimental Environment and Data Set.** In order to verify the effectiveness of the dynamic gesture contour feature extraction method based on residual network migration learning, the experimental hardware configuration is i72.6GHz processor, 16 GB RAM graphics workstation, and Kinect 2.0 sensor. VS2008, OpenCV, and WindowsSDK2.0



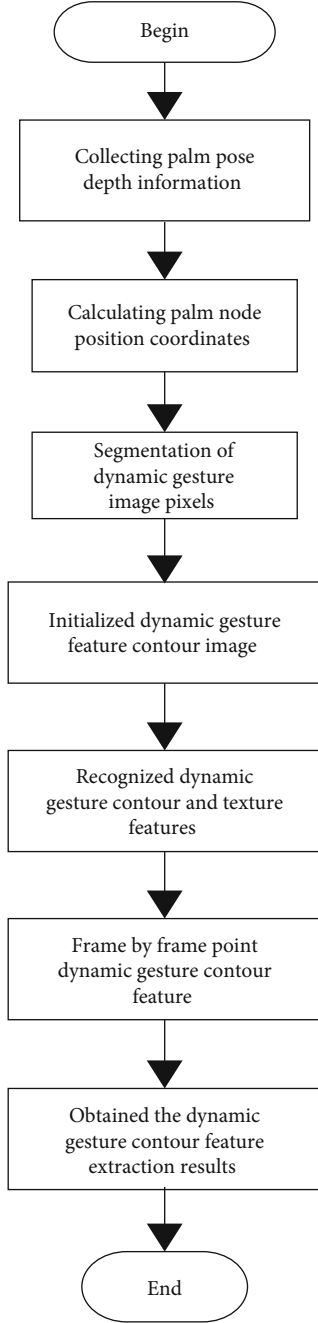


FIGURE 2: Dynamic gesture contour feature extraction process.

software development platforms are used to conduct simulation experiments.

The experiment uses CGD gesture recognition data set, 11k Hands data set, and HandNet data set as data sources:

- (1) CGD gesture recognition data set: this data set mainly includes 24-letter images, collected by 5 people under different illumination and different height conditions.
- (2) 11k Hands data set: this data set covers 11,076 hand images, the age of the collected objects is between 18 and 75 years old, and the pixels are  $1600 \times 1200$

pixels. The gesture images in this data set are all taken from the back and palm sides of the hand.

- (3) HandNet data set: gesture images in this data set are taken at different locations, and they are all taken from different directions using RGB-D cameras to form nonrigid deformed images.

After obtaining data from the above three data sets, distinguish similar or nonstandard gestures, and calculate the bone feature point data obtained by the proposed method, select 4 dynamic gestures with larger differences for analysis, and establish a sample library. At the same time, 18 3D feature points such as the palm, wrist, elbow, shoulder, and shoulder center were selected to analyze the gesture changes, and the influence of other regional feature points on gesture recognition was not considered. The established sample library contains human palm movements with different illumination and different heights, and a total of 400 sets of gesture image data are selected.

#### 4.2. Evaluation Criteria

- (1) Taking the first image of the hand as the object, the computer is used to draw the process of gesture image segmentation, contour recognition, contour tracing, and feature recognition, in order to show the intuitive effect of using the proposed method to extract the contour features of dynamic gestures
- (2) Dynamic gesture contour feature recognition rate refers to the ratio of the number of relevant dynamic gesture contour feature points to the total number in the gesture recognition database. The calculation equation is

$$D_s = \frac{\alpha_z}{\sigma_z} \times 100\%, \quad (19)$$

where  $\alpha_z$  is the number of identified contour feature points of related dynamic gestures and  $\sigma_z$  is the total number of contour features of dynamic gestures to be recognized

- (3) In the recognition time of dynamic gesture contour feature, taking the recognition time of dynamic gesture contour feature as a criteria, combine the proposed method with Bastos et al.'s [8] method, Peng et al.'s [9] method, Tang et al.'s [10] method, Zhang et al.'s [11] method, and Liang and Liao's [12] method which are compared to verify the performance of the proposed method
- (4) Dynamic gesture type recognition accuracy refers to the correctness of dynamic gesture type recognition, which reflects the accuracy of dynamic gesture contour feature recognition

$$D_z = \frac{\beta_z}{\sigma_z} \times 100\%, \quad (20)$$

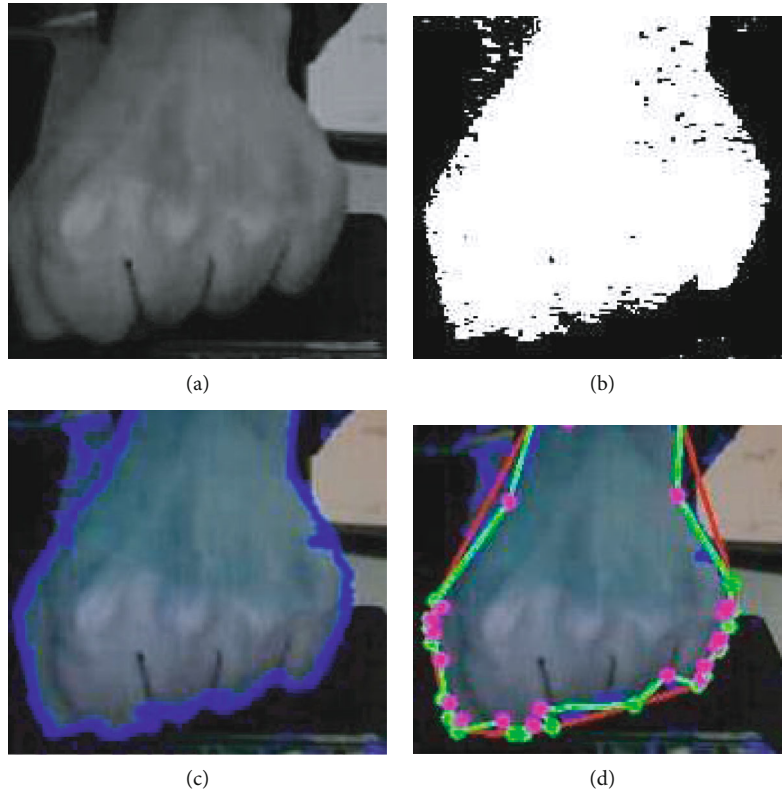


FIGURE 3: Dynamic gesture contour feature extraction.

where  $\beta_z$  is the number of correctly identified dynamic gesture contour features.

- (5) The  $F$  value of dynamic gesture contour feature extraction is the weighted harmonic average of the precision rate and the recall rate, which can take into account the precision and recall rate of the method, and is a comprehensive evaluation criteria

**4.3. Results and Discussion.** Taking a fist holding gesture image as the original image, the proposed method is used to segment and recognize the gesture image and finally realize the contour feature extraction. The process diagram is shown in Figure 3.

It can be seen from Figure 3 that the proposed method can be input to the computer to draw the overall dynamic gesture contour feature extraction process and can effectively trace the feature contour to complete the feature extraction.

Select 800 dynamic gesture contour feature points and 4 dynamic gesture types. Among them, there are 150 contour feature points for the dynamic gesture type of hand grasping fist with index finger and middle finger extending, 230 contour feature points for the dynamic gesture type of hand grasping fist with thumb up, and the contour feature of hand grasping fist with thumb and little finger extending dynamic gesture. There are 220 points, and there are 200 contour feature points of the five-finger open palm dynamic gesture type. Select 90 sets of data as the training set, 4 sets of average values as the test samples, respectively, using the pro-

posed method and Bastos et al.'s [8] method, Peng et al.'s [9] method, Tang et al.'s [10] method, Zhang et al.'s [11] method, and Liang and Liao's [12] method which are compared, and the recognition rate of dynamic gesture contour features of different methods is obtained. It is shown in Figure 4.

According to Figure 4. When there are 800 dynamic gesture contour feature points, the average dynamic gesture contour feature recognition rate of Bastos et al.'s [8] method is 60%, and the average dynamic gesture contour feature recognition rate of Peng et al.'s [9] method is 57%, the average dynamic gesture contour feature recognition rate of Tang et al.'s [10] method is 82%, the average dynamic gesture contour feature recognition rate of Zhang et al.'s [11] method is 76%, and the average dynamic gesture contour feature recognition rate of Liang and Liao's [12] method is 10%. The average recognition rate of dynamic gesture contour features is 91%. It can be seen that the dynamic gesture contour feature recognition rate of the proposed method is relatively high. Because the proposed method uses transfer learning to segment dynamic gesture images, feature contour images were initialized, and dynamic gesture feature recognition models were trained. Using the residual network method, each feature of the dynamic gesture contour is accurately recognized, and the influence caused by the excessively deep network layer is avoided, thereby improving the recognition rate of the dynamic gesture contour feature.

On this basis, the dynamic gesture contour feature recognition time of the proposed method is further verified, using Bastos et al.'s [8] method, Peng et al.'s [9] method,

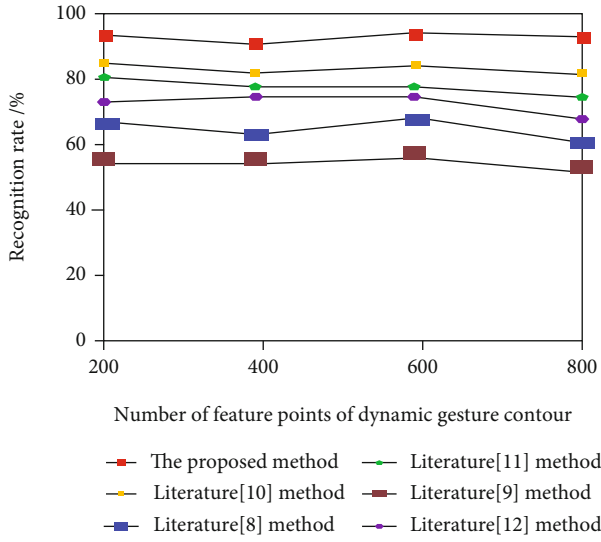


FIGURE 4: Comparison results of dynamic gesture contour feature recognition rate with different methods.

Tang et al.'s [10] method, Zhang et al.'s [11] method, and Liang and Liao's [12] method for dynamic gesture contour feature recognition. The comparison results of different methods of dynamic gesture contour feature recognition time are obtained. It is shown in Figure 5.

According to Figure 5, as the number of contour feature points of dynamic gestures increases, the recognition time of dynamic gesture contour features increases. When the number of dynamic gesture category recognition feature points is 800, the dynamic gesture contour feature recognition time of Bastos et al.'s [8] method is 18.8s, and the dynamic gesture contour feature recognition time of Peng et al.'s [9] method is 25.3s, the dynamic gesture contour feature recognition time of Tang et al.'s [10] method is 19.5s, the dynamic gesture contour feature recognition time of Zhang et al.'s [11] method is 23.8s, and the dynamic gesture contour feature recognition time of Liang and Liao's [12] method is 16.9s. The dynamic gesture contour feature recognition time of the proposed method is only 11.6s. It can be seen that the dynamic gesture contour feature recognition time of the proposed method is shorter. Because the proposed method detects the distance between the dynamic gesture and the acquisition device through transfer learning and divides the dynamic gesture image to obtain the basic pixel points of each dynamic gesture image, the dynamic gesture extraction rate is increased, and the dynamic gesture contour feature recognition time is shortened.

In order to verify the accuracy of the dynamic gesture type recognition of the proposed method, Bastos et al.'s [8] method, Peng et al.'s [9] method, Tang et al.'s [10] method, Zhang et al.'s [11] method, and Liang and Liao's [12] method are compared with the proposed method, respectively. Thus, the comparison results of the accuracy of dynamic gesture type recognition of different methods can be obtained. It is shown in Figure 6.

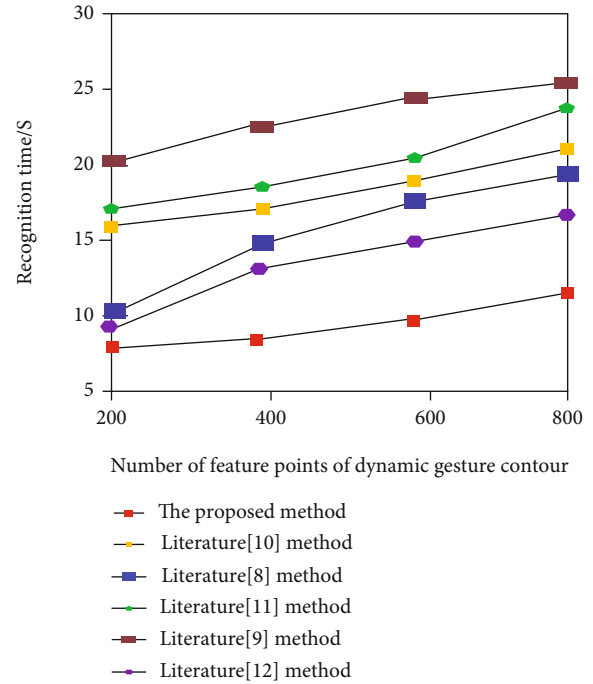


FIGURE 5: Recognition time comparison results of dynamic gesture contour feature with different methods.

According to Figure 6, for different dynamic gesture types, the average dynamic gesture type recognition accuracy of Bastos et al.'s [8] method is 42%, the average dynamic gesture type recognition accuracy of Peng et al.'s [9] method is 71%, and the average dynamic gesture type recognition accuracy of Tang et al.'s [10] method. The recognition accuracy rate is 81%, the average dynamic gesture type recognition accuracy rate of Zhang et al.'s [11] method is 61%, and the average dynamic gesture type recognition accuracy rate of Liang and Liao's [12] method is 56%. The average dynamic gesture type recognition accuracy of the proposed method is 92%. It can be seen that the dynamic gesture type recognition accuracy of the proposed method is relatively high. Because the proposed method adopts the residual network method through transfer learning, the dynamic gesture contour is accurately recognized, and the processing weight is merged to obtain a significant contour response. According to the geometric characteristics of the dynamic gesture drawing area, the dynamic gesture part is projected longitudinally, and the dynamic gesture contour area is binarized, so as to effectively improve the accuracy of dynamic gesture type recognition.

In order to further verify the comprehensiveness and accuracy of the method proposed, the  $F$  value is selected as a criteria, and the proposed method is compared with the method of [8], method of [9], method of [10], method of [11] and method of [12], and the results are shown in Table 1.

The value range of  $F$  value is  $[0, 1]$ , and the larger the value of  $F$  in the value range, the better the output effect of the proposed method. According to Table 1, it can be seen that the average  $F$  value of the dynamic gesture contour feature extraction proposed method is 0.92, the average  $F$  value

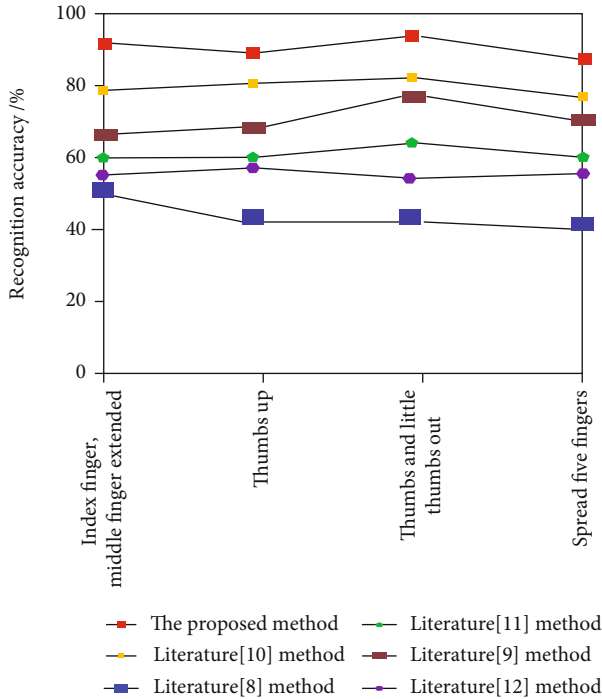


FIGURE 6: Comparison results of dynamic gesture type recognition accuracy with different methods.

TABLE 1: Comparison results of  $F$  values of different methods.

Method	$F$ values
The proposed method	0.92
Literature [8]	0.84
Literature [9]	0.72
Literature [10]	0.84
Literature [11]	0.67
Literature [12]	0.68

of [8] is 0.84, the average  $F$  value of [9] is 0.72, and the average  $F$  value of [10] is 0.84, the average  $F$  value of [11] is 0.67, and the average  $F$  value of [12] is 0.68. It can be clearly seen that this method has absolute advantages, and the  $F$  value is large, which shows that this paper uses residual network transfer learning to extract dynamic gesture contour features, which can balance the accuracy and recall of the method and obtain better feature extraction effect.

## 5. Conclusions

In order to improve the recognition rate of dynamic gesture contour features and the accuracy of dynamic gesture type recognition and shorten the recognition time of dynamic gesture contour features, a dynamic gesture contour feature extraction method based on residual network migration learning is proposed. Sensors are used to integrate dynamic gesture information, transfer learning is used to detect the distance between dynamic gestures and the collection device, and dynamic gesture images are segmented in the back-

ground to obtain basic pixels of each dynamic gesture image, which shortens the time for dynamic gesture contour feature recognition. Initialize the feature contour image, train the dynamic gesture feature recognition model, and use the residual network method to accurately identify the dynamic gesture contour and texture feature, merge the processing weights, and get a significant contour response. The contour features of dynamic gestures are traced frame by frame, and the contour area of dynamic gestures is processed by gray scale and binarization, which improves the accuracy of dynamic gesture type recognition. However, the proposed method can fully suppress the contour texture and cannot achieve better results. In the future, the research on contour texture should be enhanced. Based on the frequency division characteristics of the perception field, visual processing mechanisms such as peripheral texture suppression guided by multifeature information, and frequency division visual flow fusion of the primary visual cortex should be proposed. This can not only ensure the continuity and completeness of the contour to the greatest extent but also effectively suppress texture noise.

## Data Availability

The data used to support the findings of this study are included within the article. Readers can access the data supporting the conclusions of the study from CGD data set and 11k Hands data set and HandNet data set.

## Conflicts of Interest

The authors declare that they have no conflicts of interest.

## Acknowledgments

This work was supported by the Ministry of Education Science and Technology Development Center Fund under grant number 2020A050116 and the Natural Science Foundation of Heilongjiang Province of China under grant number LH2021F040.

## References

- [1] D. Pandey, V. Namdeo, and P. Kshirsagar, "Motor imagery feature extraction cum optimization for detection of ALS disease," *Solid State Technology*, vol. 64, no. 1, pp. 739–758, 2021.
- [2] F. Ye, Y. Guo, Z. Xia, Z. Zhang, and Y. Zhou, "Feature extraction and process monitoring of multi-channel data in a forging process via sensor fusion," *International Journal of Computer Integrated Manufacturing*, vol. 34, no. 1, pp. 95–109, 2021.
- [3] L. Zhu, G. Wang, F. Huang, Y. Li, W. Chen, and H. Hong, "Landslide susceptibility prediction using sparse feature extraction and machine learning models based on GIS and remote sensing," *IEEE Geoscience and Remote Sensing Letters*, pp. 1–5, 2021.
- [4] B. Espejo-Garcia, N. Mylonas, L. Athanasakos, E. Vali, and S. Fountas, "Combining generative adversarial networks and agricultural transfer learning for weeds identification," *Biosystems Engineering*, vol. 204, pp. 79–89, 2021.

- [5] Z. Liang and S. Liao, "Research on dynamic gesture recognition integrating wide residual and long-term and short-term memory networks," *Computer application research*, vol. 36, no. 12, pp. 3846–3852, 2019.
- [6] G. Allan, I. Kang, E. S. Douglas, G. Barbastathis, and K. Cahoy, "Deep residual learning for low-order wavefront sensing in high-contrast imaging systems," *Optics Express*, vol. 28, no. 18, pp. 26267–26283, 2020.
- [7] S. Luo, A. Peng, H. Zeng, X. Kang, and L. Liu, "Deep residual learning using data augmentation for median filtering forensics of digital images," *IEEE Access*, vol. 7, no. 99, pp. 80614–80621, 2019.
- [8] L. O. Bastos, V. H. C. Melo, and W. Robson Schwartz, "Multi-loss recurrent residual networks for gesture detection and recognition," in *2019 32nd SIBGRAPI Conference on Graphics, Patterns and Images (SIBGRAPI)*, pp. 170–177, Rio de Janeiro, Brazil, 2019.
- [9] Y. Peng, H. Tao, W. Li, H. Yuan, and T. Li, "Dynamic gesture recognition based on feature fusion network and variant ConvLSTM," *IET Image Processing*, vol. 14, no. 11, pp. 2480–2486, 2020.
- [10] X. Tang, Z. Yan, J. Peng, B. Hao, H. Wang, and J. Li, "Selective spatiotemporal features learning for dynamic gesture recognition," *Expert Systems with Applications*, vol. 169, 2021.
- [11] W. Zhang, J. Wang, and F. Lan, "Dynamic hand gesture recognition based on short-term sampling neural networks," *IEEE/CAA Journal of Automatica Sinica*, vol. 8, no. 1, pp. 110–120, 2021.
- [12] Z. Liang and S. Liao, "Dynamic gesture recognition based on wide residual networks and long short-term memory networks," *Application Research of Computers*, vol. 36, no. 12, pp. 3846–3852, 2019.
- [13] G. Yu, H. Xiaohai, W. Xiaohong, W. Zhengyong, and Z. Yukun, "Dynamic gesture recognition method based on leap motion," *Computer system application*, vol. 28, no. 11, pp. 208–212, 2019.
- [14] H. Xiao, Z. Jing, and L. Yuelong, "Gesture recognition based on geometric distribution of gestures," *Computer science*, vol. 46, no. S1, pp. 246–249, 2019.
- [15] H. Huan, P. Li, N. Zou et al., "End-to-end super-resolution for remote-sensing images using an improved multi-scale residual network," *Remote Sensing*, vol. 13, no. 4, p. 666, 2021.
- [16] Y. Qing and W. Liu, "Hyperspectral image classification based on multi-scale residual network with attention mechanism," *Remote Sensing*, vol. 13, no. 3, p. 335, 2021.
- [17] Y. Li, S. Wang, H. He, D. Meng, and D. Yang, "Fast aerial image geolocalization using the projective-invariant contour feature," *Remote Sensing*, vol. 13, no. 3, p. 490, 2021.
- [18] G. Song, "Accuracy analysis of Japanese machine translation based on machine learning and image feature retrieval," *Journal of Intelligent and Fuzzy Systems*, vol. 40, no. 2, pp. 2109–2120, 2021.
- [19] M. Kowdiki and A. Khaparde, "Automatic hand gesture recognition using hybrid meta-heuristic-based feature selection and classification with dynamic time warping," *Computer Science Review*, vol. 39, 2021.
- [20] L. Hao, Y. L. Lin, and Z. X. Li, "Train driver dynamic gesture recognition method based on machine vision," *Transducer and Microsystem Technologies*, vol. 40, no. 2, pp. 34–37, 2021.
- [21] S. B. Reed, T. Reed, and S. M. Dascalu, "Spatiotemporal recursive hyperspheric classification with an application to dynamic gesture recognition," *Artificial Intelligence*, vol. 270, pp. 41–66, 2019.
- [22] B. Huang, T. Xu, Z. Shen, S. Jiang, B. Zhao, and Z. Bian, "SiamaATL: online update of Siamese tracking network via attentional transfer learning," *IEEE Transactions on Cybernetics*, vol. 1, pp. 1–14, 2021.
- [23] C. Chao, "Contour feature extraction of moving image based on multi threshold optimization," *Journal of Shenyang University of technology*, vol. 41, no. 3, pp. 315–319, 2019.
- [24] G. Krishnan, R. Joshi, T. O'Connor, F. Pla, and B. Javidi, "Human gesture recognition under degraded environments using 3D-integral imaging and deep learning," *Optics Express*, vol. 28, no. 13, pp. 19711–19725, 2020.
- [25] Z. Xia, J. Xing, C. Wang, and X. Li, "Gesture recognition algorithm of human motion target based on deep neural network," *Mobile Information Systems*, vol. 2021, Article ID 2621691, 12 pages, 2021.



## Research Article

# Influence of Hayao Miyazaki's Animation on the Cross-Cultural Spread of Japanese Traditional Culture under the Background of 5G and Wireless Communication

Chenmei Li 

*School of Foreign Languages, Guangzhou Huashang College, Guangzhou 511300, China*

Correspondence should be addressed to Chenmei Li; [li\\_chenmei@outlook.com](mailto:li_chenmei@outlook.com)

Received 13 August 2021; Revised 16 September 2021; Accepted 20 September 2021; Published 11 October 2021

Academic Editor: Deepak Gupta

Copyright © 2021 Chenmei Li. This is an open access article distributed under the Creative Commons Attribution License, which permits unrestricted use, distribution, and reproduction in any medium, provided the original work is properly cited.

The development of 5G technology has brought tremendous changes to all areas of social life, especially in the external communication of culture; the increasing effect of 5G technology has become more obvious. All kinds of new media are constantly emerging, and the expression of cultural products is more diversified, and they also have certain characteristics of their own national cultural symbols. As one of the important representatives of Japanese modern and contemporary culture, animation works have made extremely outstanding contributions in promoting the spread of Japanese culture. Japanese animation is not only second to none in Asia but has also many fans all over the world. This article takes the characteristics of Hayao Miyazaki Animation's external communication under the background of 5G as the starting point and deeply analyzes the impact of technological background changes on the external communication of Japanese traditional culture. Through data comparison, it is found that with the support of 5G technology, people's habit of watching videos has changed a lot, from mobile terminals and short videos in the 4G era to large-screen projections and long animations in the 5G era. In a certain sense formed the return of the animation viewing form to the television era at the end of the last century. The number of video clicks on major websites shows that the number of Japanese animation products represented by Hayao Miyazaki Animation has increased significantly. Moreover, the age and occupation coverage of the audience is also very wide. The survey shows that people's appreciation of Hayao Miyazaki's animation at this stage is not only the attractiveness of the plot itself, but the deep meaning behind the animation is also the focus of attracting them. This gives Hayao Miyazaki Animation a higher level of appreciation value, that is, guiding countries that have suffered from the side effects of industrial civilization to rethink the relationship between ruleism and development speed. The research results suggest that the development of 5G technology has given traditional Japanese animation new characteristics in the dissemination of it and directly affected the cross-cultural dissemination effect of Japanese traditional culture. Discover the essence of respecting nature and observing rules in Japanese traditional culture to better serve our social development.

## 1. Introduction

The cultural integration between various ethnic groups has shown a trend of more frequent and in-depth development in contemporary times. This trend becomes more rapid with the advent of the 5G era. When writing literature, writers from various countries will almost deliberately learn from the essence of other cultures. Therefore, how to make better use of the output of cultural products to achieve cultural dissemination, so that the outside world can better understand their own culture, has become the focus of the governments

of all countries. The animation industry is one of Japan's important means for foreign cultural exchanges. At the beginning of the 21st century, the Japanese government launched a key training and support plan for cultural products such as animation. After nearly two decades of hard work, Japanese animation has achieved an industry status similar to that of automobiles and electrical appliances.

It can be seen from Table 1 that in the five years from 2013 to 2017, the market share of the Japanese animation industry has achieved rapid growth. Because Japanese animation has absorbed the characteristics of a variety of

TABLE 1: 2013-2017 Japan's animation industry market total market (unit: 100 million yen).

Year	Total market
2013	14709
2014	16299
2015	18215
2016	19924
2017	21527

foreign cultures in its creation, the process of appreciating and evaluating it is smoother for the audience. Among the numerous animation works, Hayao Miyazaki's works have always been regarded as classics.

It can be seen from Table 2 that although Hayao Miyazaki's works were mainly created at the turn of the 21st century, which is the early stage of the Japanese government's try hard to cultural strategy, it still has a very strong influence today, and the box office has become insurmountable for the latter. During the peak, his works are not only well-made but also reflect Japanese traditional culture in different aspects, such as the ubiquitous ruleism in Miyazaki's works and the simple love of the world. When the audience appreciates Hayao Miyazaki's animation works, they can not only bring visual pleasure but also have a certain understanding of Japanese traditional culture. From this perspective, the dissemination of Hayao Miyazaki's animation works represents the Japanese traditional culture to a large extent.

The changes caused by the development of 5G technology in the field of cross-cultural communication of national cultures have attracted the attention of scholars. Seiple and Hoover pointed out that the cross-cultural dissemination of national culture is a double test of the content and cultural connotation of cultural works, and the dissemination effect reflects which aspect between pluralism and narrow nationalism occupies the active position [1]. Mirzaei Abbasabadi and Soleimani pointed out that with the rapid advancement of communication technology, people have very different ways of contacting other ethnic cultural products, and they have a deeper understanding of the depth of their cultural connotations, which puts forward higher requirements for the quality of cultural products [2]. Yin pointed out that cross-cultural communication ability has a very direct impact on the effect of communication, and the establishment of a scientific evaluation system can effectively improve the quality of cultural exchange products [3]. Chen believes that "cultural discount" is inevitable when all ethnic cultures communicate with each other. Its production is closely related to the quality of cultural products and the compatibility with the own culture of audience, and it is also restricted by the technical level of cultural media. The higher the technical level, the stronger the audience's sense of experience, and the better the effect of cultural exchanges [4]. Duan discussed the contemporary reconstruction of the relationship between cosmopolitanism and nationalism in this field from the perspective of the construction of an ethical system of cross-cultural communication [5]. It is pointed out that the cross-cultural communication of

TABLE 2: The top three box office of Hayao Miyazaki's animation works and Douban scores.

Anime title	Box office	Release year	Douban score
Spirited Away	30.8 billion yen	2001	9.4
The Mobile Castle of Harbin	19.6 billion yen	2004	9.1
Princess Mononoke	19.3 billion yen	1997	8.5

national culture should respect the cultural habits of the audience, strengthen communication and exchanges, and enhance the equality of exchanges, so as to achieve the goal of enhancing the value of their own cultural products [6].

## 2. Interpretation of Japanese Traditional Cultural Elements in Hayao Miyazaki's Animation

At the beginning of the twentieth century, a famous French film critic predicted that cartoons would become a symphony of hearts with multiple cultural elements in the future. Seventy years later, Miyazaki made this prediction a reality. In his animation creation, he perfectly integrates visual, auditory, and cultural elements to form a unique and diverse and unified animation style. In his animation works, you can see both the ancient Japanese mythological elements, the quaint buildings with Western style, and the thinking about where humans should go under the invasion of industrial civilization. The reason why Miyazaki Animation can form such a rich connotation is inseparable from the inheritance of Japanese traditional culture [7]. This connection will inevitably be reflected in the content of his animation creation. The name Hayao Miyazaki not only has a pivotal position in the Japanese animation industry but also has a high reputation even in the world. This has made many animation production companies invite him to participate in their own animation production in order to "catch the heat." In order to ensure the scientificity of the research, this article restricts the research objects: specifically referring to the feature-length movies in which Hayao Miyazaki is the director or other important positions alone, which is best known as "Castle in the Sky" and "Spirited Away," ten classic animation works represented by etc.

*2.1. Persistence to the Beauty of Things.* The sorrow of things is a unique aesthetic consciousness in Japanese traditional culture, and it is an atypical aesthetic experience that arises from the long-term blending of subjectivity and self-discipline [8, 9]. In this kind of culture, "wu sorrow" is not the literal "sorrow of things"; sorrow is a commonly used modal auxiliary word in Japanese, and the beauty of sorrows is the description and transmission of "beauty of objects." It originated in "The Tale of Genji" and has deeply influenced Japanese literature for thousands of years. The expression of this cultural tradition can be seen everywhere in Hayao Miyazaki's animation.

For example, the animation “Castle in the Sky” shows the unremitting pursuit of the beauty of dreams. The process by which Cedar and Bass look for their dreams is the process by which Hayao Miyazaki externalizes their inner perseverance and perseverance into perceivable beauty. Almost every dream catcher can find his own shadow in this animation. Although the ending may not be satisfactory, this dream-seeking process is also what makes people moving. This makes the whole movie immersed in an aesthetic state. In *Nausicaä of the Valley of the Wind*, the carrier of grief and beauty presents completely different characteristics. The environment for human existence has been severely damaged due to its own desires, and the ravages of the sea of rot and insects have caused humans to fall into a constant extinction, in an endless loop. And the protagonist Nausicaä is transformed into a “man in blue” who leads mankind to break the game, leading mankind to find hope of survival in the process of growing up.

*2.2. The Pursuit of the Harmonious Unity of Industrial Civilization and Nature.* Although the Japanese government has made a series of wrong decisions on environmental protection at this stage, the country’s cultural traditions are striving for the harmonious coexistence of human development and nature. Miyazaki believes that the development of mankind should not be arbitrary from nature but should seek a coexistence node between the two, otherwise it will inevitably encounter natural revenge. For example, in “*Nausicaä*,” Hayao Miyazaki showed the audience a beautiful picture of the harmonious coexistence of man and nature. Huge windmills can be seen everywhere standing in the valley. The highly developed industrial civilization of mankind has been captured by insects and destroyed, and the relatively “primitive” farming civilization has preserved the fire for human survival. The guardians of the forest are docile, but when the forest is damaged, it will immediately burst out with destructive power, so that the groups that destroy nature will receive the punishment they deserve. In “*The Valley of Ghosts*,” this kind of thinking is also more obvious. Ebbsey went to open up the forest for the development of mankind and started a long-term battle with the forest god. In the end, although he defeated the mountain beast god, he was also hit by the latter’s dying blow and paid the price of his life. In this cartoon, although Ebbsey appears as a villain, it also represents to a large extent the pioneers who conquered nature under the demands of the development of industrial civilization.

*2.3. Devotion to Life and Work.* At the same time that Hayao Miyazaki’s animation was created, information equipment has been widely used in the animation industry. The animation produced by high-tech means can not only save costs but also upgrade the image quality and production cycle. However, Hayao Miyazaki has always adhered to the traditional animation production method, thinking that only by adhering to the tradition can he better express the creator’s ideological characteristics. Therefore, the most important tools for Hayao Miyazaki’s animation production are traditional paper and pencils, and information equipment has

to be used only when performing postproduction special effects. It is precisely by relying on this “original” production tool that Hayao Miyazaki has beaten European and American high-tech animations at the box office and word of mouth time and time again. For example, “*Spirited Away*” and “*Goldfish Princess on the Cliff*” have more than 100,000 drawings. Miyazaki’s pursuit of traditional animation production technology is highly compatible with the persistence and dedication of work in traditional Japanese culture.

*2.4. Blending of Multiple Cultural Elements.* Japanese traditional culture originates from multiple systems, such as Chinese culture and Western culture. This allows Hayao Miyazaki to achieve a perfect combination of multiple cultures in his animation works. His animation works can be said to be based on Japanese traditional culture, supplemented by various cultural system elements. This format not only enhances the appreciability of the work but also expands the audience. What is commendable is that Hayao Miyazaki combines these different styles together, but it is not obtrusive, thus forming a unique Miyaji manga. Looking at Hayao Miyazaki’s animation from the perspective of cross-cultural communication, we can find that his works are deeply rooted in Japanese traditional culture and have achieved innovation in expression.

### **3. The New Characteristics of Hayao Miyazaki’s Animation Cross-Cultural Communication under the Background of 5G**

*3.1. It Is Easier to Help the Audience Resonate with the Writer.* The development of 5G technology has brought a violent impact on the life that people have become accustomed to, and all industries are on the eve of a comprehensive upgrade. In the 4G era, mobile phones have replaced traditional televisions and other media as the main medium of cultural consumption. People use smart phones or tablets for much longer than traditional media such as televisions. However, due to the limitations of network transmission rate and cell phone screen size, people seldom appreciate long-form film and television works but prefer fast-paced short videos or film excerpts. In this fragmented appreciation mode, it is difficult for people to think deeply about the cultural meaning behind the video. In the 5G era, information terminals are more intelligent, and people increasingly prefer large-screen smart devices when they enjoy film and television works [10, 11].

As can be seen from Figure 1, in areas where 5G signals are used, people’s mobile phone habits have changed a lot. In the 4G era, the average daily viewing time of short videos, which occupy the peak of traffic, is gradually shortening, while the viewing time of regular film and television dramas is constantly increasing. More advanced technology and equipment will bring the audience a more comprehensive sensory enjoyment. For example, through smart VR devices, viewers can experience the immersive feeling. Surrounded by beautiful animation scenes, it resonates with Miyaji Animation’s love and cherishment of nature [12, 13].

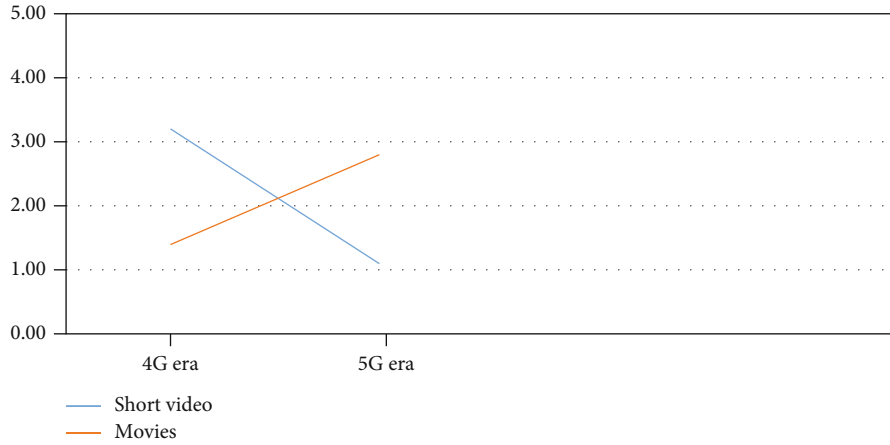


FIGURE 1: Market comparison of content watched by smart devices everyday (unit: hour).

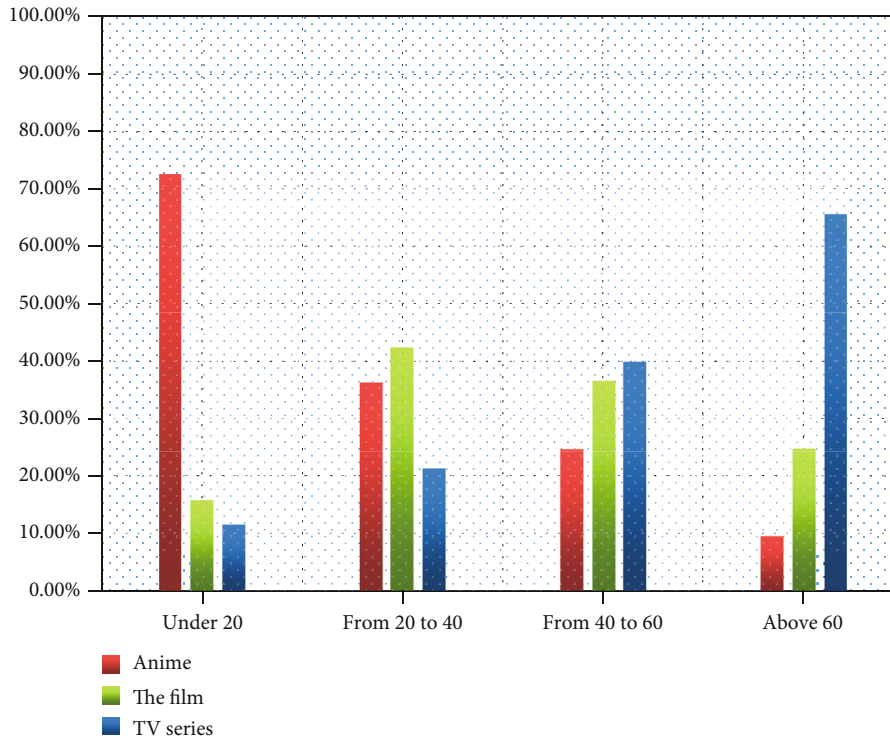


FIGURE 2: Comparison of the market for viewing smart device content by age groups.

3.2. *The Change in the Mode of Communication Has Broadened the Scope of the Audience.* After the popularization of 5G equipment, network traffic will inevitably show a spurt of growth. The faster transmission speed of 5G equipment allows people to watch videos with shorter waiting times and clearer effects. The survey results show that more and more middle-aged people and even the elderly are now using wireless smart terminals to watch video content [14]. When watching animation, Japanese animation is the main focus. Although domestic animation has developed rapidly in recent years, there is still a big gap with Japanese animation in terms of the number of boutiques and the update time. Japanese animation represented by Hayao Gong Miyazaki Animation covers a wide range of

ages, which has played a very positive role in the spread of the traditional Japanese culture.

It can be seen from Figure 2 that the audiences of animation at this stage cover almost all age groups. In the past, only teenagers watched animation and the pattern of audiences was further expanded.

3.3. *Bringing Greater Challenges to the Cross-Cultural Communication of Japanese Animation.* Although Hayao Miyazaki Animation has maintained its high competitiveness for nearly two decades, as the current integration of 5G technology and animation production has gradually improved, many Internet companies have regard animation production as an important entry point for increasing



income. Big IP series of animations are constantly being released, such as China's "Nezha: Devil Boy Comes into the World" and "Jiang Ziya" and the United States' "How to Train Your Dragon 3" and "Angry Birds 2," which have caused a lot of problems worldwide and great response. These animations all have outstanding performance in representing their own national culture. The cross-cultural communication of these opponents will inevitably have a great impact on the overseas broadcasting of Hayao Miyazaki Animation. Coupled with Hayao Miyazaki's insistence on hand-made animation, it is difficult to establish a branch plot that conforms to the trend of the times, which will have a certain impact on the interaction between the audience and the animation film, and this impact will inevitably further affect the traditional Japanese culture, cross-cultural communication.

#### 4. Conclusion

All in all, in the context of 5G and wireless communication, Japanese traditional culture represented by Hayao Miyazaki Animation has ushered in an excellent opportunity in the process of cross-cultural communication, which has greatly improved the scope of the audience and the depth of cultural communication. But at the same time, the strength of competitors also makes it face greater challenges.

At this stage, my country has entered a period of high production of animation works, and many big IP productions have been released one after another. These characters are beautiful in appearance and exquisite pictures, but they have a high degree of convergence. Almost all of them are adapted from popular online novels, such as "Martial Universe" and "God of War." These animation works are not only in the "shell." Outside of a certain national culture, they are almost all superficial visual works, generally lacking in-depth thinking and display of Chinese traditional culture. In the 5G era, the use of technical means to produce animation is understandable, but works that do not pay attention to cultural connotations cannot become classics that will last forever. If we want to further enhance the cultural temperament of our animation works, we must deeply explore the connotation of traditional culture in the process of animation design and production, realize the fit of animation works and cultural temperament, and reflect cultural reflection. Only in this way can we better arouse the emotional resonance of the audience.

#### Data Availability

The datasets used and/or analyzed during the current study are available from the corresponding author on reasonable request.

#### Conflicts of Interest

The author declares no competing interests.

#### Acknowledgments

Fund projects "Research on Hayao Miyazaki's Animation Works from the Perspective of Traditional Culture Inheritance" were funded by the tutorial system project of Guangzhou Huashang College (Project No. 2020HSDS22).

#### References

- [1] C. Seiple and D. R. Hoover, "A case for cross-cultural religious literacy," *The Review of Faith & International Affairs*, vol. 19, no. 1, pp. 1–13, 2021.
- [2] H. Mirzaei Abbasabadi and M. Soleimani, "Examining the effects of digital technology expansion on unemployment: a cross-sectional investigation," *Technology in Society*, vol. 64, no. 2, article 101495, 2021.
- [3] G. H. Yin, "The cross-cultural development direction of American dramas in China," *Media Forum*, vol. 4, no. 11, pp. 125–126, 2021.
- [4] P. Chen, "The historical development and cross-cultural communication of Chinese media in Europe," *Overseas Chinese and Chinese History Studies*, vol. 2, pp. 14–22, 2021.
- [5] L. J. Duan, "The dilemma and optimized path of cross-cultural communication in my country," *People's Forum*, vol. 14, pp. 98–100, 2021.
- [6] L. K. Gong, "Analysis of the cross-cultural communication of internet meme-taking the overseas popularity of "Yijianmei" as an example," *Audiovisual*, vol. 5, pp. 140–142, 2021.
- [7] S. M. Wang and E. L. Du, "Foreign influencers" short video research from the perspective of cross-cultural communication," *China Media Technology*, vol. 4, pp. 52–56, 2021.
- [8] Y. F. Yang, "An analysis of the cross-cultural communication of TV dramas," *Cultural Industry*, vol. 10, pp. 63–64, 2021.
- [9] J. Chen, "Analysis of cognitive differences in cross-cultural communication of the animation film "Ne Zha"," *Media Forum*, vol. 4, no. 7, pp. 103–104, 2021.
- [10] Z. H. Lv, A. K. Singh, J. H. Li, and H. B. Song, "Deep learning for security problems in 5G heterogeneous networks," *IEEE Network*, vol. 35, no. 2, pp. 67–73, 2021.
- [11] S. Q. Qu and F. Z. Liu, "National image construction and dissemination in domestic science fiction movies," *Science and Technology Think Tank*, vol. 5, pp. 41–48, 2021.
- [12] J. F. Lin, "Comparison of the narrative characteristics of Chinese and Japanese documentaries from the perspective of cross-cultural communication: taking the traditional cultural documentaries of China Central Television and Japan's NHK Broadcasting Corporation as examples," *Putian University Journal*, vol. 3, pp. 68–73, 2019.
- [13] X. Lan and X. Wang, "Strategies for the integrated development of Chinese martial arts and animation from the perspective of cross-cultural communication," *External Communication*, vol. 3, pp. 35–37, 2020.
- [14] R. Yang, "International expression and meaning sharing in the cross-cultural communication of video games: taking the mobile game "Onmyoji" as an example," *Comparative Research on Cultural Innovation*, vol. 3, no. 18, pp. 18–20, 2019.



## Research Article

# The Application of Virtual Reality Technology on Intelligent Traffic Construction and Decision Support in Smart Cities

Gongxing Yan<sup>1</sup> and Yanping Chen<sup>2</sup> 

<sup>1</sup>Center for Mechanics and Materials Science, Chongqing Vocational Institute of Engineering, Chongqing 402260, China

<sup>2</sup>School of Management, Wuhan Donghu University, Wuhan 430000, China

Correspondence should be addressed to Yanping Chen; [chenyanping927@163.com](mailto:chenyanping927@163.com)

Received 15 July 2021; Revised 10 September 2021; Accepted 17 September 2021; Published 5 October 2021

Academic Editor: Deepak Gupta

Copyright © 2021 Gongxing Yan and Yanping Chen. This is an open access article distributed under the Creative Commons Attribution License, which permits unrestricted use, distribution, and reproduction in any medium, provided the original work is properly cited.

The core of smart city is to build intelligent transportation system. An intelligent transportation system can analyze the traffic data with time and space characteristics in the city and acquire rich and valuable knowledge, and it is of great significance to realize intelligent traffic scheduling and urban planning. This article specifically introduces the extensive application of urban transportation infrastructure data in the construction and development of smart cities. This article first explains the related concepts of big data and intelligent transportation systems and uses big data to illustrate the operation of intelligent transportation systems in the construction of smart cities. Based on the machine learning and deep learning method, this paper is aimed at the passenger flow and traffic flow in the smart city transportation system. This paper deeply excavates the time, space, and other hidden features. In this paper, the traffic volume of the random sections in the city is predicted by using the graph convolutional neural network (GCNN) model, and the data are compared with the other five models (VAR, FNN, GCGRU, STGCN, and DGCNN). The experimental results show that compared with the other 4 models, the GCNN model has an increase of 8% to 10% accuracy and 15% fault tolerance. In forecasting morning and evening peak traffic flow, the accuracy of the GCNN model is higher than that of other models, and its trend is basically consistent with the actual traffic volume, the predicted results can reflect the actual traffic flow data well. Aimed at the application of intelligent transportation in an intelligent city, this paper proposes a machine learning prediction model based on big data, and this is of great significance for studying the mechanical learning of such problems. Therefore, the research of this paper has a good implementation prospect and academic value.

## 1. Introduction

With the rapid development of social economy, the process of industrialization and urbanization has been continuously promoted, people's living standards continue to rise, all kinds of means of transportation are becoming more and more popular, the popularity of domestic cars is constantly improving, the supply of urban infrastructure is in short supply, the limited traffic resources cannot meet the growing traffic needs, and the contradictions between people and vehicles, vehicles and roads, and roads and people are increasingly obvious; the imbalance of traffic structure leads to the limitation of urban sustainable development. At present, various cities have appeared to have traffic congestion;

traffic congestion is spreading from the first-level cities to the second- and third-level cities, gradually affecting the travel safety and living standards of most people. For this contradiction, it is not an efficient way to increase the number of traffic channels by relying on traditional methods. Only an efficient transportation system can truly solve a series of problems such as traffic safety, vehicle supervision, traffic congestion, and traffic flow supervision caused by road vehicle conflicts. Intelligent transportation involves the full application of information technology. On the basis of communication and electronic traffic management technology, a set of complete coverage, accurate results, and efficient operation management system is established. An intelligent transportation system can effectively utilize the

existing traffic resources, improve the operating efficiency and safety factor of the entire transportation system, and reduce congestion and environmental pollution [1, 2]. Therefore, in facing the future, intelligent transportation should be a necessary choice to strengthen urban traffic construction. The core of an efficient transportation system is intelligent, so how to build and improve the intelligent transportation system has become an urgent problem. A good road environment can give users a clear and pleasant feeling, thereby increasing the fun of the journey, eliminating fatigue, and reducing traffic accidents.

The research on an intelligent transportation system abroad mainly includes the intersection of transportation planning, information technology, traffic information technology, and so on; the theory of the intelligent transportation system is applied to guide the construction of the urban transportation system. Sedjelmaci et al. proposed an intelligent transportation system evaluation index system, using big data to comprehensively evaluate six kinds of indicators, including traffic structure, traffic information service, traffic efficiency, traffic safety, energy saving and emission reduction, and social inclusion. The traffic big data includes license plate recognition (LPR), GPS, and automatic vehicle location (AVL), and smartphone data provide a more scientific theoretical basis for the evaluation of these indicators. But they did not provide specific data to support [3]. Hanapi et al. have designed a public transport charging proposal system. By analyzing the subway card data, it can predict the future travel mode of the public, so as to guide the travel time, ticket purchase method, and other information, so as to save the capital and time cost. However, they only aimed to improve public transport and could not fully cover road traffic [4]. Tourani proposed a decision support model for urban traffic planning based on traffic big data, which is divided into three stages: the location data of taxi passengers entering and leaving, the definition of alternative public transport routes, and the comparison of alternative schemes to scientifically calculate the public transport lines that the government should increase [5].

Based on the research of the intelligent transportation industry in our city, this paper analyzes and summarizes the benefits and risks of smart city management capability big data crash research method circulation. Through the improvement of the city's intelligent transportation system, improve the city's traffic quality, promote urban economic development, and accelerate the construction of smart cities.

## 2. Big Data Application of the Intelligent Transportation System in a Smart City

### 2.1. Role of Intelligent Transportation in a Smart City

*2.1.1. Definition of a Smart City.* A smart city is the product of the new generation of information technology revolution and knowledge economy. It is based on the Internet and the Internet of things, combined with the telecommunications network, broadcasting network, and broadband network. A smart city will further promote the development and construction of the basic information system and implementa-

tion information system and form a network-based, information-based, intelligent, and modern city. A smart city is characterized by highly integrated information integration and deep integration of information application; it is to use communication and information media to detect and integrate key information of the central city system. Wisdom responds to various needs such as life, environmental protection, public security, and urban services [6–8]. A smart city pays more attention to intelligent discovery and problem solving and has stronger innovation and development ability. The road model is mainly used to describe the geometric characteristics of the road, the lane division, the width of the isolation belt and the shoulder, the type of the road surface, and the location of fixed traffic signs.

*2.1.2. Definition of Intelligent Transportation.* An intelligent transportation system (ITS) is an efficient, accurate, and integrated real-time traffic management system developed on the basis of traditional road facilities; by studying the basic theoretical model, the advanced information technology and sensor technology are effectively integrated; and information technology, electronic control technology, and mechanical system technology are the development direction of modern transportation systems and have become the development direction of modern transportation systems, the best way to solve traffic problems in modern society. It includes all existing vehicles. By collecting, processing, analyzing, providing, and using traffic information, the transformation from traffic system construction to traffic management is an important part of China's high-tech industry.

*2.1.3. Connection between a Smart City and Intelligent Transportation.* The development of intelligent transportation conforms to the inner needs of the construction of smart cities. On the one hand, traffic congestion and traffic pollution are the main "urban diseases." Through the effective integration of high and new technologies, intelligent transportation can reduce road congestion and road accidents and indirectly reduce vehicle exhaust emissions, which is an important and effective means to control urban traffic diseases. On the other hand, due to the demand development based on intelligent transportation, governments at all levels and transportation departments have implemented calculation application of cloud. Application of Internet of things and other advanced technologies in daily traffic management operation [9, 10]. Obviously, the development of intelligent transportation will inevitably drive the development of emerging industries such as the mobile Internet to better meet the needs of smart city construction.

Intelligent transportation accelerates the construction of smart cities. The development of smart transportation has promoted the development of smart public transportation, smart parking, and information services. It has improved people's living standards and embodies the characteristics of smart cities. Therefore, intelligent transportation plays an important role in the construction of smart cities and can promote the construction of smart cities. The rapid

development of the intelligent transportation industry has contributed to the construction of smart cities.

The construction of smart cities provides huge opportunities for the development of smart transportation. Improving the efficiency of smart city construction has laid a good foundation for the development of smart transportation. At the same time, the modernization of other smart city systems will also accelerate the pace of smart transportation construction [11].

#### 2.1.4. Application of Big Data in Intelligent Transportation

(1) *Big Data Classification in Traffic Management.* The situation of road traffic management is becoming more and more serious. The management design is wide and the number of participants is large. Various behaviors and traffic management methods produce a lot of basic data. Road is the carrier of traffic flow. The true description of road network topology and road geometric conditions and the establishment of a reasonable and scalable road traffic network data structure are the basis for traffic flow simulation. From the perspective of operators, the main traffic data mainly includes the following basic data types:

- (1) Dynamic traffic information collection data, for example, data collected through road monitoring, intersection flow collection, etc. As far as the city is concerned, the daily traffic behavior of nearly 600000 motor vehicles will be uploaded to the monitoring system and data acquisition equipment to generate astronomical basic road traffic data. These traffic behaviors are widely distributed in urban, suburban, and county traffic arteries
- (2) Static traffic management statistics, for example, basic parking management data. In this regard, the main elements of transportation especially include the following aspects: first, the location of a parking lot, the internal regional planning of a parking lot, the classification of parking lot nature, and the number of parking spaces and second, the parking state of the vehicle, the specific parking time of the vehicle, etc. [12]. In addition, there are a series of data about parking management, such as administrator status, time charge, or one-time charge
- (3) Basic data of driving management service, such as the number of motor vehicles and the number of drivers. There are millions of motor vehicle drivers in this city; a large amount of basic data is generated in every connection related to the driver, including driving license application, renewal, verification, and cancellation. Similarly, the registration, annual inspection, scrapping, and other related procedures of more than 600000 vehicles will also generate huge basic data. The sum of the two data has reached the level of 10 million
- (4) Traffic management data summary, for example, traffic violation data processing, off-site road traffic

violation data processing, road accident data processing, road traffic basic data processing, and traffic illegal behavior data processing. In recent years, the number of traffic violations is positively correlated with the development speed of traffic participants. Among them, each traffic violation involves at least one traffic participant, motor vehicle or nonmotor vehicle, and one or more families. In the process of handling traffic and accident infringement, a large number of basic data have also been generated [13, 14]

- (5) Auxiliary data of road traffic management. Just like the component of the regional traffic management department, it includes the number of traffic police, the number of assistants, traffic, and civilized traffic counselor data. In the case of further subdivision, it can be specific to the basic situation of these traffic controllers, personality characteristics, specific preferences, attendance status, administrative effect, and other quantitative indicators. In addition, with the support of traffic management, basic data such as road network structure and traffic monitoring, traffic signs and points, and basic data such as flow collectors are also provided
- (6) Road traffic management information. This paper mainly deals with the relevant units and aspects that directly affect traffic management. For example, the police patrol, public security, and other parts share defense data, such as multifleet and hazardous chemical operation data, for example, the peak period of pedestrian and vehicle flow in the market, the time of school and holiday, as well as the number of students and details of traffic violation fines collected by banks [15].

(2) *Benefits of Big Data in Intelligent Transportation.* Big data is not only a social phenomenon but also a scientific and technological achievement, which is the inevitable result of the historical development trend of information science and technology and knowledge economy. The availability of mining, power transmission, and large-scale data technology and the corresponding technical processing methods are technical means for massive data collection and processing, as well as a large amount of structured, semistructured, and unstructured data sets by systematically using nontraditional existing hardware and software tools, to obtain survey results and analysis. Big data technology mainly includes data extraction technology, data maintenance technology, calculation and processing technology, data research technology, and result display technology [16, 17]. At the same time, in the application of large-scale data technology, it mainly involves data sorting and merging, data storage, data mining, and other multilevel and all-round content. Big data technology has become the infrastructure guarantee of big data and its implementation, so it plays an important role.

Based on the above theoretical basis, the benefits brought by big data injection into public management decision-making can be divided into the following benefits:

(1) Improve traffic operation efficiency

Because big data is real-time, distributed, efficient and predictive, it improves the effectiveness of emergency traffic management. Managers can call real-time data from the big data background at any time. The distribution of big data solves the problem of cross regional management and has unique advantages in information integration and combination [18]. Big data improves the command, dispatch, and guidance ability of traffic managers in an all-round way and improves the response and processing efficiency of traffic violations.

(2) Improve traffic safety

Big data can improve traffic safety. On the macro level, by improving the data processing capacity of the traffic safety system, it can provide road accident early warning and efficient emergency decision-making assistance for managers and avoid traffic accidents as far as possible. On the micro level, the comprehensive safety performance monitoring of vehicles and drivers is carried out. The monitoring contents include the real-time relationship between the vehicle and the complex traffic environment during driving, and whether the driver may drive drunk or fatigue.

(3) Enhance the decision-making ability of the government

A large amount of data can improve the scientific nature of government decision-making and governance capabilities. Scientific decision-making mainly benefits from the coexistence of new and traditional data sources, through some accurate, detailed, and fast updated data. Traffic decision-makers can find the information flow that cannot be detected in the past and hidden development patterns and relationships. Rich data provide a window for observing the real social operation and support the decision-making based on evidence of the government.

(4) Improving the Environment and Saving Energy

Big data can improve the environment and save energy. On the one hand, big data can be used for effective environmental monitoring. Big data is comprehensive, detailed, and rapidly updated data, which has advantages in monitoring and forecasting traffic emissions. At the same time, it can also associate environmental data and establish a data platform for the exchange and sharing of traffic big data and environmental data, so as to carry out causal analysis. On the other hand, by improving the traffic operation efficiency and shortening the congestion time, the emission of vehicle pollutants is indirectly reduced [19].

*2.2. Traffic Flow Prediction Model Based on Machine Learning.* A traffic prediction task is the basis of its stable

operation. Accurate and reliable traffic prediction results can assist active and dynamic traffic control. In recent years, prediction methods based on deep learning have received considerable attention [20]. Some research attempts to use deep repetitive neural networks (RNN) and vaccine neural networks (CNN) to predict traffic flow. However, these methods are not suitable for data points with irregular graph relations [21]. Because a traffic network can be represented by graph, a graph convolution neural network (GCNN) naturally becomes a very suitable choice in this scenario. Research shows that GCNN with a deep structure is very effective in short-term traffic prediction. The basic model of GCNN is shown below.

(1) Graph Convolution Neural Network

The graph convolution neural network uses  $M = (\nu, \varepsilon, w)$  to express a directed graph, where  $\nu$  represents all the  $P$  vertex sets in the graph,  $\varepsilon$  represents the set of all edges in the directed graph, and  $w$  represents the weight matrix corresponding to  $M$ . The signal values of all vertices in the graph are expressed as a vector  $a \in \mathbb{R}^P$ , where  $A_i$  is the signal value at the  $i$ -th vertex. The Laplacian matrix of a digraph is expressed as  $L = D - W$ , and the corresponding feature decomposition can be expressed as  $L = U \Lambda U^T$ . When  $D$  is the diagnosis matrix, the value of the  $i$ -th element of the graph is equal to the number of times of the  $i$ -th rotation in the graph, that is,  $D_{ii} = \sum_j w_{ij}$ .  $U$  is an orthogonal matrix. The Fourier transform of vector  $a$  can be expressed as  $\hat{A} = U^T A$ . Therefore, the graph convolution operation of signals  $A_1$  and  $A_2$  in the Fourier domain can be expressed as follows:

$$A_1 * M A_n = U((U^T A_1) \cdot (U^T A_2)), \quad (1)$$

A signal is convoluted by  $g_\theta$  and can be expressed as

$$y = g_\theta(L)A = g_\theta(U \Lambda U^T)A = U g_\theta(\Lambda)U^T A. \quad (2)$$

In order to realize  $K$  localization and reduce computational complexity, formula (2) can be further expressed as follows:

$$y = U g_\theta(\Lambda)U^T A = U \left( \sum_{k=0}^{k-1} \theta_k \Lambda^k \right) U^T A = \sum_{k=0}^{k-1} \theta_k L^k A, \quad (3)$$

where parameter  $\theta \in \mathbb{R}^K$  is the vector of the polynomial Fourier coefficients. The convolution operation makes the distance  $DG(I, J)$  between nodes  $I$  and  $J$  limited to  $K$  hops. At that time,  $d_g(i, j) \geq K$  and  $L_{i,j}^K = 0$ . Therefore, convolution operation on the spectral domain of  $k$ -order polynomial expressed as the Laplacian matrix can realize  $k$ -localization [22, 23].

Assuming that each vertex contains CIN features, the signal values of the  $P$  nodes in graph  $M$  can be represented by a matrix with the size of  $CIN * P$ . When the matrix is used as the input of a graph convolution layer, the



convolution operation with tensor of size  $(C_{in}, c_{out}, K)$  as a convolution kernel can be expressed as follows:

$$y_j = \sum_{ie[1, c_{in}], ke[1, K]} \theta_{ijk} K^k x_i, \quad j = 1, 2, \dots, c_{out}, \quad (4)$$

Among them,  $c_{in}$  and  $c_{out}$  represent the size of the input and output characteristic graph of the graph neural network, respectively.

## (2) Figure signal processing

In the graph signal processing area, the signal forms a function at the top of the weighted graph. The main challenge in this area is to learn graph structures from data. The chart read must have a substantial explanation and be useful for analysis. Given a set of  $V$  nodes and a set of corresponding labels on these nodes, the graph structure is learned by estimating the matrix  $L$ . the nonzero mode defines the connectivity at both ends of the graph.

Given a  $p$ -dimensional random graph signal  $x$  and its  $N$  observations  $x_1, \dots, x_N$ , its sampling covariance is  $Q = 1/N \sum_{i=1}^N x_i x_i^T$ . A graph structure learning problem is often transformed into a matrix optimization problem, and an effective solution is found. According to the maximum likelihood estimation of  $L$ ,

$$\min_{L \geq 0; L_{ij} \leq 0, \forall i \neq j} -\log \det(L) + \text{tr}(QL). \quad (5)$$

Minimizing  $\text{tr}(QL)$  is equivalent to improving the average smoothness. The logarithmic function  $\det$ , as the obstacle of the minimum eigenvalue of  $L$ , is used to enforce the semidefinite constraint. Symbolic constraints can be handled using Lagrange multipliers [24, 25].

## 3. Simulation Experiment

**3.1. Environment Configuration.** For road planning and design in a three-dimensional virtual city, due to the need to test and compare different design schemes, it will involve modifying the number of lanes, road width, and other attributes. As shown in Table 1, it includes the system configuration required by the experimental platform, such as CPU, memory, hard disk, and other hardware information. The model algorithm is programmed with the Java language and operates on a computer with the Windows 10 operating system.

**3.2. Experimental Data Collection.** In this paper, we collect the traffic data in the morning and evening of the same road section in the city. The data collection time is the first three days of the experimental simulation, and the data sampling medium is 5 minutes. This paper randomly selects 6 sensor tracking data from the urban transportation department. From the morning peak time (7:00-10:00) and the evening peak time (17:00-20:00), each sensor collects and outputs the traffic data every 5 minutes and adds the daily weather data.

TABLE 1: System configuration.

Configuration	Software and hardware
CPU	Intel Core i5
Frequency	2.5 GHz
RAM	8 G
Hard disk	256 G
Operating system	Windows 10
Program development environment	Visual Studio 2015

**3.3. Experimental Evaluation Index.** In the process of designing roads, this article through intuitive understanding of the surrounding environment of the road is conducive to a more comprehensive consideration of the relationship between the road and the environment and the impact on traffic safety. In order to verify the appropriateness and accuracy of the prediction model, we should use performance evaluation indicators to evaluate the prediction model. Commonly used performance evaluation indicators are mean square error (MSE), average absolute percentage error (MAE), and average absolute percentage error (MAPE). In this paper, MAE and MAPE are used as the evaluation indexes of the prediction results. The average absolute error (MAE) can directly reflect the difference between the actual value and the predicted value; the average relative error (MAPE) is an error in the actual value, which is a dimensionless value that can reflect the level of error and the measured value reliability.

$$\text{MSE} = \frac{1}{N} \sqrt{\sum_{i=1}^N (y_i - \hat{y}_i)^2}, \quad (6)$$

$$\text{MAE} = \frac{1}{N} \sum_{i=1}^N |y_i - \hat{y}_i|, \quad (7)$$

$$\text{MAPE} = \frac{1}{N} \sum_{i=1}^N \left| \frac{y_i - \hat{y}_i}{y_i} \right| \times 100\%, \quad (8)$$

where  $y_i$  is the actual traffic volume at time  $i$ ,  $\hat{y}_i$  is the expected traffic volume over a period of time  $i$ , and  $N$  is the total number of individuals of the predicted value. Four other models are selected for performance comparison: VAR, FNN, GCGRU, and STGCN.

## 4. Statistics and Comparison of Experimental Results

**4.1. Prediction Accuracy of Each Model.** In this paper, five models (VAR, FNN, GCGRU, STGCN, and DGCNN) were run for 15 times, and the average prediction error was obtained to obtain the accuracy of each model in the traffic flow prediction. In the way of using virtual urban traffic to simulate actual urban traffic, it can be observed in a realistic three-dimensional urban traffic scene with various control methods from viewpoints, and various scenes can be



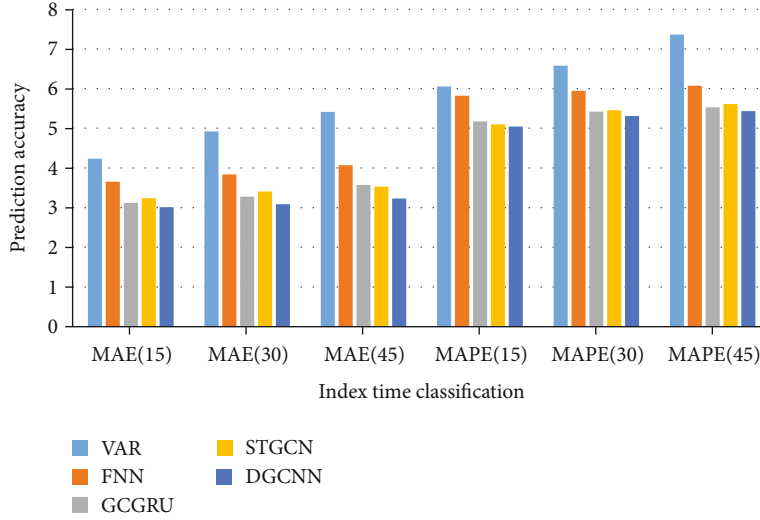


FIGURE 1: Accuracy of model prediction.

generated through changes to ultimately establish an effective city. Traffic control and management provide an effective basis.

As shown in Figure 1, the GCNN model presented in this paper achieves the lowest RMSE and MAE in traffic prediction accuracy on both datasets, which is better than all other comparison models. It can be clearly seen from the forecast results that the traditional linear prediction method VAR is the worst because it cannot deal with the variability of traffic data. Compared with the other three deep learning models, GCNN also performs better, with an average prediction error of 8%-10%. The traffic mode and spatial dependence of urban road network are dynamic. By ignoring the dynamic change of the road network spatial dependence, the prediction error of the other three models is large.

**4.2. Prediction Fault Tolerance of Each Model.** Due to sensor failure or traffic accidents on some road sections, local anomalies may exist in real-time traffic samples. In order to test the fault tolerance ability of the model in extreme environment, this paper randomly selects the designated road section to destroy some historical observations.

As shown in Figure 2, the DGCNN model shows higher fault tolerance, with an average prediction error reduction of 10%-25% compared with the two most advanced models based on graph CNN. Even if the failure rate of all road sections reaches 90%, DGCNN still shows strong prediction ability. The DGCNN model can detect the change of spatial dependence hidden in the “polluted” traffic samples and adjust the perceptual domain of graph convolution operation. With the increase in the training period, DGCNN achieves the lowest verification error compared with GCNN and STGCN, which shows the training effect. The reason is that the dynamic Laplace matrix estimator increases the performance and flexibility of the prediction model to capture the influence of various factors in the road network. In the urban traffic simulation system, the road network model is not only a simple geo-

metric figure, but more importantly, it should be able to play the role of a traffic simulation carrier. Through effective data organization, the road network model must actively and efficiently reflect its dynamics. The effect of entity-vehicle constraints improves the efficiency of simulation operation.

**4.3. Comparison of Early Peak Model Prediction.** As shown in Figure 3, the prediction effect of the DGCNN model is better than that of the other two models in the morning peak hours of weekdays. The prediction curve is more suitable for the actual traffic flow curve, and its changing trend is basically consistent with the actual traffic flow. Although other models are closer to the actual value at certain two points, their change trend is not consistent with the actual value, indicating that DGCNN can effectively reduce the adverse effects of accidental errors.

**4.4. Comparison of Late Peak Model Prediction.** As shown in Figure 4, the predicted value of the DGCNN model differs very little from the actual value, almost in agreement, while the predicted value of other models always has a certain deviation. Therefore, in this article, due to the selection of the characteristics of the DGCNN algorithm and the optimization of the parameters, the prediction accuracy of the DGCNN model is higher than that of other models. By intuitively understanding the environment around the road, the coordination relationship between the road and the environment and the impact on traffic safety can be considered more comprehensively.

To sum up, through the comparison results of each model, we can know that due to the introduction of more influential factors, such as weather conditions, the feature selection process and parameter optimization process have been improved; the prediction accuracy and error tolerance of the DGNN short-term traffic flow prediction model in the morning and evening hours of the peak working day are better than those of the traditional model.

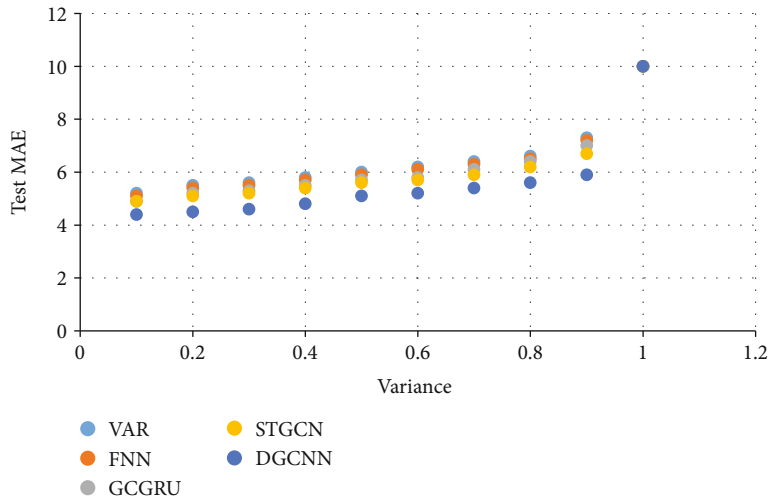


FIGURE 2: Model fault tolerance comparison.

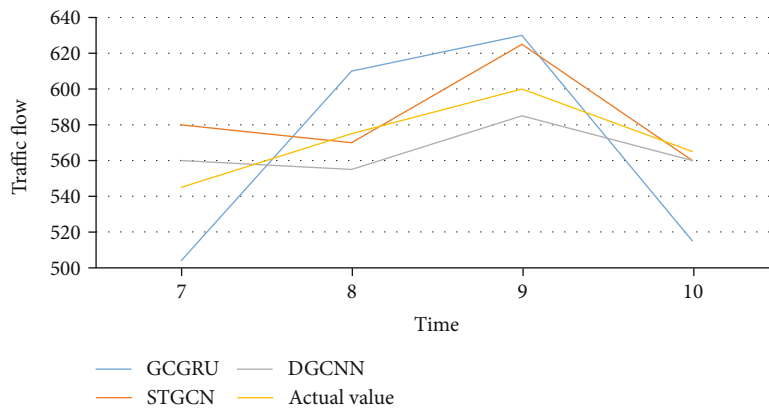


FIGURE 3: Early peak forecast.

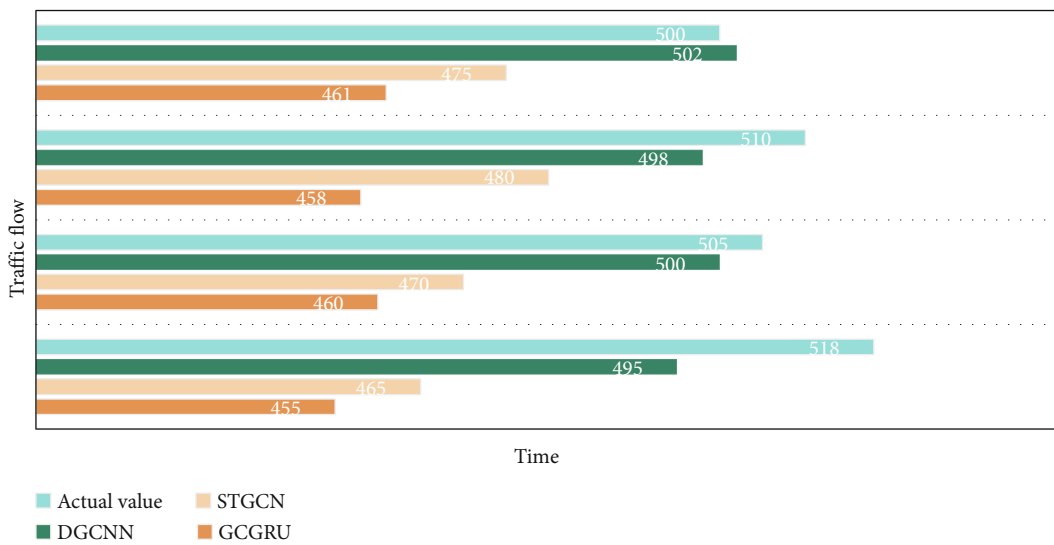


FIGURE 4: Late peak forecast.

## 5. Conclusions

With the development of urban economy and the improvement of residents' living standards, the number of urban vehicles in our country is increasing year by year. With the development of urban economy, the contradiction between transportation supply and demand, environmental pollution, and immeasurable economic losses has emerged. After realizing that the traditional traffic management mode cannot solve the modern traffic problems, the governments domestically and internationally began to control public transport since the 1960s. The continuous exploration and innovation of management mode and tools are aimed at creating a travel environment with high efficiency, safety, comfort, energy conservation, and environmental protection for the people. The emergence of big data is widely concerned by people. In the field of transportation, the rapid development of detection technology provides the possibility for efficient and high-quality high-flow data collection, and the continuous improvement of big data analysis ability can transform massive data into public value. With the real-time collection of information of traffic elements such as people, vehicles, and roads, big data has been formed and developed. Big data has been proven to be a favorable tool for urban traffic management in practice.

In this paper, systematic literature review is used to sort out the relevant literature, extract the benefits and risks of big data application in urban intelligent transportation, and summarize and analyze the application of big data in intelligent transportation. In this paper, a machine learning method is applied to urban intelligent transportation scene to solve practical problems, and in the process of solving problems, an innovative model is proposed combining with the characteristics of traffic spatial-temporal data. In this paper, the DGCNN model is used to predict the morning and evening peak traffic flow data and compared with other models. The experimental results show that the DGCNN model has good performance for traffic prediction.

To sum up, we can draw the following conclusions: the intelligent transportation systems were combined, there are many kinds of big data combination modes, and transportation informatization and intellectualization are the fundamental trend of urban transportation system transformation and upgrading in the future; only by effectively integrating the analysis technology of big data with other relevant data of urban management and development can the city be effectively promoted (intelligent transportation construction and development).

## Data Availability

The data that support the findings of this study are available from the corresponding author upon reasonable request.

## Conflicts of Interest

The authors declared no potential conflicts of interest with respect to the research, authorship, and/or publication of this article.

## Acknowledgments

This work was supported by the Youth Fund Project of Wuhan Donghu University: Research on the construction of consumer purchase decision function based on live broadcast with goods, and Science and Technology Research Project of Chongqing Education Commission (KJQN2020 03404).

## References

- [1] X. Cheng, L. Yang, and X. Shen, "D2D for intelligent transportation systems: a feasibility study," *IEEE Transactions on Intelligent Transportation Systems*, vol. 16, no. 4, pp. 1784–1793, 2015.
- [2] C. Y. Hsu, C. S. Yang, L. C. Yu et al., "Development of a cloud-based service framework for energy conservation in a sustainable intelligent transportation system," *International Journal of Production Economics*, vol. 164, pp. 454–461, 2015.
- [3] H. Sedjelmaci, S. M. Senouci, N. Ansari, and M. H. Rehmani, "Recent advances on security and privacy in intelligent transportation systems (ITSs)," *Ad Hoc Networks*, vol. 90, p. 101846, 2019.
- [4] Z. M. Hanapi, Z. Vahdati, M. Salehi, and Z. Vahdati, "Using traffic control scheme in intelligent transportation system," *International Journal of Advanced Trends in Computer science and Engineering*, vol. 8, pp. 165–172, 2019.
- [5] A. Tourani, A. Shahbahrami, A. Akoushideh, S. Khazaei, and C. Y. Suen, "Motion-based vehicle speed measurement for intelligent transportation systems," *International Journal of Image, Graphics and Signal Processing*, vol. 11, no. 4, pp. 42–54, 2019.
- [6] A. Gaur, B. Scotney, G. Parr, and S. McClean, "Smart city architecture and its applications based on IoT," *Procedia Computer science*, vol. 52, no. 1, pp. 1089–1094, 2015.
- [7] N. Kim and S. Hong, "Automatic classification of citizen requests for transportation using deep learning: case study from Boston City," *Information Processing & Management*, vol. 58, no. 1, p. 102410, 2021.
- [8] H. M. Moftah and T. M. Mohamed, "A novel fuzzy bat based ambulance detection and traffic counting approach," *Journal of Cybersecurity and Information Management*, vol. 1, no. 2, pp. 41–54, 2021.
- [9] Y. Li, W. Dai, Z. Ming, and M. Qiu, "Privacy protection for preventing data over-collection in smart city," *IEEE Transactions on Computers*, vol. 65, no. 5, pp. 1339–1350, 2016.
- [10] M. Centenaro, L. Vangelista, A. Zanella, and M. Zorzi, "Long-range communications in unlicensed bands: the rising stars in the IoT and smart city scenarios," *IEEE Wireless Communications*, vol. 23, no. 5, pp. 60–67, 2016.
- [11] M. Rath and B. Pati, "Communication improvement and traffic control based on V2I in smart city framework," *International Journal of Vehicular Telematics & Infotainment Systems*, vol. 2, no. 1, pp. 18–33, 2018.
- [12] X. Zheng, W. Chen, P. Wang et al., "Big data for social transportation," *IEEE Transactions on Intelligent Transportation Systems*, vol. 17, no. 3, pp. 620–630, 2016.
- [13] F. Ghofrani, Q. He, R. M. P. Goverde, and X. Liu, "Recent applications of big data analytics in railway transportation systems: a survey," *Transportation research*, vol. 90, pp. 226–246, 2018.

- [14] C. Li and P. Xu, "Application on traffic flow prediction of machine learning in intelligent transportation," *Neural Computing and Applications*, vol. 33, no. 2, pp. 613–624, 2021.
- [15] M. Saki, M. Abolhasan, and J. Lipman, "A novel approach for big data classification and transportation in rail networks," *IEEE Transactions on Intelligent Transportation Systems*, vol. 21, no. 3, pp. 1239–1249, 2020.
- [16] C. An and C. Wu, "Traffic big data assisted V2X communications toward smart transportation," *Wireless Networks*, vol. 26, no. 3, pp. 1601–1610, 2020.
- [17] S. K. Roy, S. Midya, and G. W. Weber, "Multi-objective multi-item fixed-charge solid transportation problem under twofold uncertainty," *Neural Computing and Applications*, vol. 31, no. 12, pp. 8593–8613, 2019.
- [18] A. Sukoco, A. S. Prihatmanto, R. Wijaya, I. Sadad, and R. Darmakusuma, "SEMUT: next generation public transportation architecture in the era IoT and big data," *Journal of Engineering and Applied Sciences*, vol. 14, no. 12, pp. 4052–4059, 2019.
- [19] T. B. A. Isabel, D. S. Javier, L. Ibai, M. Ilardia, M. N. Bilbao, and S. Campos-Cordobés, "Big data for transportation and mobility: recent advances, trends and challenges," *IET Intelligent Transport Systems*, vol. 12, no. 8, pp. 742–755, 2018.
- [20] D. Chen, M. Hu, H. Zhang, and J. Yin, "Forecast method for medium-long term air traffic flow considering periodic fluctuation factors," *Xinan Jiaotong Daxue Xuebao/Journal of Southwest Jiaotong University*, vol. 50, no. 3, pp. 562–568, 2015.
- [21] L. Zhao, D. Wei, Y. Dong-Mei, G. Chai, and J.-h. Guo, "Short-term traffic flow forecast based on combination of K nearest neighbor algorithm and support vector regression," *Journal of Highway and Transportation Research and Development*, vol. 12, no. 1, pp. 89–96, 2018.
- [22] T. Xie and J. C. Grossman, "Crystal graph convolutional neural networks for an accurate and interpretable prediction of material properties," *Physical Review Letters*, vol. 120, no. 14, pp. 145301.1–145301.6, 2018.
- [23] V. Korolev, A. Mitrofanov, A. Korotcov, and V. Tkachenko, "Graph convolutional neural networks as "general-purpose" property predictors: the universality and limits of applicability," *Journal of Chemical Information and Modeling*, vol. 60, no. 1, pp. 22–28, 2020.
- [24] D. Bone, C.-C. Lee, and T. Chaspari, "Signal processing and machine learning for mental health research and clinical applications [perspectives]," *IEEE Signal Processing Magazine*, vol. 34, no. 5, p. 196, 2017.
- [25] A. Deleforge, D. Di Carlo, M. Strauss, R. Serizel, and L. Marcenaro, "Audio-based search and rescue with a drone: highlights from the IEEE signal processing cup 2019 student competition [SP competitions]," *IEEE Signal Processing Magazine*, vol. 36, no. 5, pp. 138–144, 2019.

## Research Article

# An Efficient Method for Choosing Digital Cluster Size in Ultralow Latency Networks

Alexander Paramonov <sup>1</sup>, Mashael Khayyat <sup>2</sup>, Natalia Chistova,<sup>1</sup> Ammar Muthanna <sup>1</sup>, Ibrahim A. Elgendy <sup>3,4</sup>, Andrey Koucheryavy <sup>1</sup> and Ahmed A. Abd El-Latif <sup>5</sup>

<sup>1</sup>The Bonch-Bruевич Saint-Petersburg State University of Telecommunications (SPbSUT),  
Department of Telecommunication Networks and Data Transmission, Russia

<sup>2</sup>Department of Information Systems and Technology, College of Computer Science and Engineering, University of Jeddah,  
Jeddah, Saudi Arabia

<sup>3</sup>School of Computer Science and Technology, Harbin Institute of Technology, Harbin 150001, China

<sup>4</sup>Department of Computer Science, Faculty of Computers and Information, Menoufia University, Shibin el Kom 32511, Egypt

<sup>5</sup>Department of Mathematics and Computer Science, Faculty of Science, Menoufia University, Al Minufiyah 32511, Egypt

Correspondence should be addressed to Ahmed A. Abd El-Latif; a.rahiem@gmail.com

Received 9 August 2021; Accepted 17 September 2021; Published 4 October 2021

Academic Editor: Deepak Gupta

Copyright © 2021 Alexander Paramonov et al. This is an open access article distributed under the Creative Commons Attribution License, which permits unrestricted use, distribution, and reproduction in any medium, provided the original work is properly cited.

The paper proposes a solution to the problem of choosing the size of a cluster in an ultralow latency network. This work is aimed at designing a method for choosing the size of the digital cluster in an ultralow latency network taking into account the lengths of connecting lines. If the linear dimension calculation is based only on the latency requirements without specifics of building the communication line, it negatively affects timing characteristics. This paper shows the method taking into account the communication line features and basing on the fractal dimension estimation of the road network. The proposed method could be used in planning and designing networks with ultralow latencies. Finally, a numerical experiment was carried out, based on the data of electronic maps, which showed that the assessment of the fractal dimension of roads in the network's service area makes it possible to increase the accuracy of the size of the formed cluster. Moreover, the proposed method can allow you to reduce the error in estimating the length of connecting lines, which without using it can be on average about 30%.

## 1. Introduction

The development of services with high latency requirements of data delivery in the network leads to a change of approaches to determining the network structure. As shown in works, [1, 2] describe in detail the reasons leading to an increase in the requirements for the value of the delay in the delivery of packets in promising communication networks. In [1], the tasks of the Tactile Internet and target requirements for the amount of latency are given; in [2], a structure with the use of border calculations is proposed, which provides a decrease in latency. In [3], the prospects for the application of edge

computing in sixth-generation networks are considered. The paper [4] presents the results of an analysis of the use of d2d technologies for direct connections to devices, which can also serve as a means of reducing the delay. In [5], the author proposes a territorial division into digital clusters according to the distribution of users. There should be a data center at the center of such clusters. In [6], the authors propose the use of multiple computing systems and the distribution of tasks between them. In [7], a method for the formation of digital clusters in networks of the first and subsequent generations is proposed. In [8], the use of edge computing for blockchain implementation is considered.



Mentioned above requires a change in the network structure, as the numerical values of the delay are already commensurate with the propagation time of an electromagnetic or optical signal [9, 10]. This limitation necessitates shifting the service point provision closer to the end-user. It is possible by promising communication networks by organizing local cloud services located at a sufficiently small distance from users, making it possible to meet the requirements for data delivery time [11, 12].

As the works [2, 4, 5] show, the formation of such structure is associated with the task of allocating a certain number of user clusters in the serviced area according to the cluster size, and access points (service provision) can then be located in the centers of the selected clusters. The work [7] shows that clusters of different sizes can be formed for users with different requirements for latency time. The work proposes a method that considers the road's characteristics and the laying of communication lines on the territory of the cluster.

Depending on the magnitude of the delay, the cluster radius varies from several tens to several hundred kilometers. At such distances, the connection between the point of service provision (the clusters' center) with the elements of the cluster (for example, settlements) is carried out by cable communication lines. The length of these lines determines the real propagation delay of the signal. In most cases, the link is longer than the straight line connecting the points on the map.

Currently, there is an intensive growth of interest in services requiring low and ultralow delays, such as telemedicine, telecontrol of vehicles, and unmanned aerial vehicles. To solve such problems, it is often proposed to use local mobile edge computing nodes (edge computing). However, in many cases, when there is a stable demand for services, it is advisable to build a stationary network structure containing data processing centers located close enough to service consumers. The construction of such a structure requires the development of methods for optimizing the structure in order to increase the efficiency of resource use and ensure the delay requirements for subscribers.

The purpose of this article is to present the method developed for assessing the real length of cable communication lines in digital clusters, which will make it possible to determine the required size of these clusters. The main contributions of this paper are summarized as follows:

- (i) The formation of digital clusters in an ultralow latency network based on the distance from the point of service provision is necessary in order to meet the requirement for the delay introduced by the signal propagation time
- (ii) When forming a cluster, it is necessary to consider the fact that communication lines are laid along roads, which most often differ from straight lines
- (iii) It will be shown in the work that this feature can be taken into account by using the fractal dimension, estimated for the road network in the service area of the communication network

## 2. Problem Statement

The work [7] proposes to use the FOREL clustering method to solve the problem of choosing positions for placing the service provision points. When using this method, the cluster boundary is defined by a circle of a given radius. In other words, the maximum possible distance of a cluster element from its center does not exceed the specified radius of the circle. Figure 1(a) shows an illustration of the performed clustering, in which two cluster elements are very close to the cluster boundary.

The more significant density (an amount of the elements on the one square unit) corresponds with the higher probability for such an event. That is quite acceptable for modeling, but the distance between the cluster center and the element is determined by the existing cable route in the real condition. Moreover, the cable route is laid along the existed road.

Figure 1(b) shows the possible example of choosing the route on the real map (the map was obtained from Google Earth [13]). As you can see from the example, the real route could be significantly different from the straight line connecting the cluster center and the element. The route distance was more considerable than the straight line from 15 to 37%. Also, the length to 3 out of 4 selected for the example points exceeded a radius of 50 km.

Thus, the implementation of the clustering algorithms is complicated by choosing the actual roadways as metrics, but not the straight distance between two points. Of course, there might be more than one option for selecting the route.

Another approach to solving the problem of choosing clusters can be determining a smaller value of the radius  $R$  by some value  $\Delta$ , which would consider the increase in the length of the communication lines due to the choice of routes for their laying.

Even from the given examples, you can notice that the spread of the path length increments is quite large. However, the real situation is far from being limited to this example and can have a greater variety.

This study is aimed at developing a method for choosing the parameters for solving the clustering problem (selecting the size of the cluster), taking into account the peculiarities of the road infrastructure of the target region.

## 3. Related Work

The clustering task is the most common task when building a communication network. In general, the task of clustering is to divide network objects into groups (clusters) according to some criterion. This general setting is good for any context. However, in practical applications, specific clustering problems differ significantly from each other both in the formulation and in the method of solution.

The statement of the problem and the method of its solution depend on the applied area and the purpose of its solution. The most striking example is the problem of clustering subscribers in a mobile network (in a somewhat simplified interpretation). In this case, the number of clusters will be equal to the number of base stations, and the criterion is the

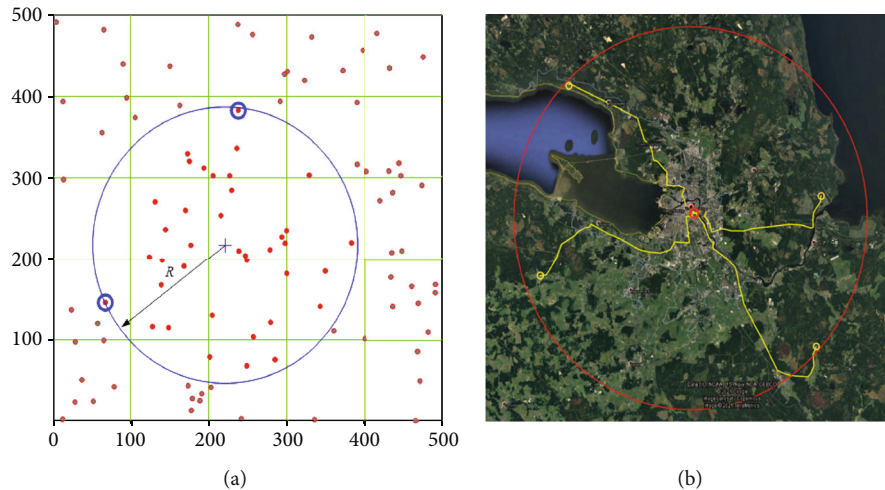


FIGURE 1: Example of applying the FOREL clustering method.

highest quality of service. In this case, a cluster is understood as a group of subscriber units served by one base station [14].

A second example of clustering would be the distribution of users across access nodes, for example, on an access network in a large apartment building. In this case, the criterion can be both the length of the subscriber line and the bandwidth guaranteed to the user. It should be noted that despite the existence of many approaches and methods for solving these problems, one cannot be completely sure that the problems are solved in an optimal way. In general, these problems are multiobjective optimization problems and their exact solution is often unattainable. Most of the methods used make it possible to obtain partial solutions that are not the worst or close to optimal ones. In this sense, clustering problems always attract the attention of researchers.

Device clustering is also used when using direct connections between devices (D2D connections) [4, 15, 16]. In this case, it is also required to select a group of users by the criterion of traffic quality of service, only one of the users of the group, which has a connection with the base station, acting as an access point. Other scenarios for forming a group of D2D users are also possible, but in any case, one of the criteria is the quality of service.

In this paper, the clustering problem is considered in relation to the problem of minimizing the data delivery delay. The component of the delay introduced by the propagation time of an electromagnetic or optical signal in the propagation medium is specifically considered. We consider cable communication lines, most likely optical lines, as a distribution medium. In advanced communication systems, signal propagation time is important for the organization of connections with ultralow URLLC delays. Such connections are required to provide services with increased latency requirements, such as telecontrol, telemedicine (in terms of medical equipment control), and the industrial Internet of things. The solution of the clustering problem according to the propagation delay criterion is practically equivalent to its solution according to the distance criterion; however, the complexity of the solution lies in the fact that the distance, defined as the geometrical or geographical distance

between points on a plane or a geographic map, does not give an unambiguous characteristic of the length of the communication line between the points under consideration. The reason for this is that cable lines are laid along existing roads that cannot be described by a straight line. In this sense, it is also not efficient to determine, for example, the length of the route between points, since there is absolutely no certainty that the route of the communication line will be close to this route.

In [5, 17], a method of network clustering is proposed, taking into account the signal propagation time, based on the assumption of the presence of direct (rectilinear) connections between network elements. The method considered in the work is based on the use of the FOREL clustering algorithm and allows you to select clusters of elements by the criterion of the distance between these elements and the center of the cluster. In this case, the maximum distance between the center of the cluster and its element is determined along a straight line. This method makes it possible to obtain a solution in which the distances between the centers of the obtained clusters and the most distant elements of these clusters do not exceed a given value.

In [7], a development of the method proposed in the mentioned work is proposed, taking into account the existence of various requirements for the magnitude of the delay, i.e., when providing several time-critical services, the points of provision of which it is desirable to combine in the same network nodes. The proposed by the authors allows you to distinguish clusters of various sizes, depending on the set of services and requirements for the amount of delay. An important feature of this method is that the centers of these clusters are aligned. This is done because when implementing a network, it is advisable to combine the functions of providing several services in one network node. This method, like the one mentioned above, assumes that the points of service are located in the centers of the found clusters.

Both of these methods, as noted above, give a significant overestimation of the cluster sizes, since the actual lengths of the connecting lines will be significantly greater than the linear distances between the points. When choosing the size of

the clusters according to the above methods, the actual lengths of communication lines will exceed the calculated values, which will lead to an overestimation of the delay. In other words, when using them, there is a high probability that the calculated amount of delay will be exceeded. This is an extremely unpleasant situation, since it is possible to reduce the amount of delay only by changing the length of the communication lines, which is associated with significant material costs. Thus, in this case, the quality of solving the clustering problem directly affects the quality of the provision of latency-critical services.

The proposed method makes it possible to take into account the peculiarities of the road network, which make it possible to take into account the “curvature” of existing roads and, on the basis of this knowledge, make adjustments to the solution of the clustering problem. The advantage of the proposed method is that it allows one to obtain a solution that, in terms of the quality of the solution, surpasses the methods described above, due to the fact that the cluster size in this case will be smaller; therefore, the probability of exceeding the delay standard will also be less. The proposed method makes it possible to make a reasonable choice of the cluster size reduction factor.

#### 4. Solution

Assume that cable routes between the service provision point and the endpoint (cluster element) are laid along the existed road. In other words, cable routes are not making a straight line between elements. That the real length of the route  $L_T$  will be not smaller than the straight line  $L_0$  that connects the elements:

$$L_T \leq L_0. \quad (1)$$

Also, assume that the road infrastructure is sufficiently developed. So, the cable route still tends to a straight line between points and does not “loop” endlessly within the cluster, for example, like a fractal line [18–21]. This assumption is possible because the points in the model coincide with settlements, each of which is reachable by a route of a finite length.

If  $L_{\max}$  is the maximum length of the route, so the following condition must be met:  $L_T \leq L_{\max}$ . The radius of the assumed cluster should also be less than this value (see Figure 2):

$$R \leq L_{\max}. \quad (2)$$

The value of  $R$  should ensure the fulfillment of these conditions. We will proceed from the assumption that the increase in the length of the route is proportional to the fractal dimension of the roads in the territory of the proposed cluster:

$$\Delta L = L_T - L_0 \propto D. \quad (3)$$

Equation (3) shows that  $D$  is the fractal dimension. If  $L_0 = L_{\max}$ , then  $\Delta L = \Delta R$ .

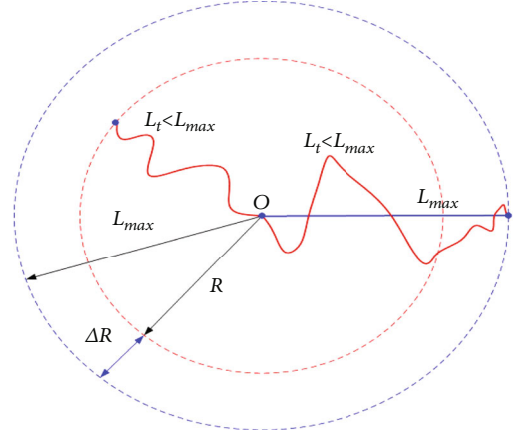


FIGURE 2: Cluster model.

To clarify the method for assessing the fractal dimension, Figure 3 shows an example in which two points located at equal distances are connected in the first case by a straight line and in the second case by an arbitrary curve.

Both lines are covered with some amount of squares with side size  $\tau$ . There are various methods for estimating the fractal dimension [20]. In particular, circles with the radius  $\tau$  could be used instead of the square. However, in most practical implementations (programs) of the fractal dimension estimation, the Minkowski method (box-counting) is used, which involves the construction of a grid and counting the cells through which the line  $n(\tau)$  passes, which in this case is equivalent to covering with squares.

According to the definition, the fractal dimension (FD) of the line is equal to the following limit [19, 20]:

$$D = \lim_{\tau \rightarrow 0} \frac{\ln n(\tau)}{\ln \tau}, \quad (4)$$

where  $n(\tau)$  is the number of elements of the covering of size  $\tau$ .

Figure 3 shows that the bigger line requires a bigger number of elements to cover. Also, the line size might be measured in the numbers of these elements. The smaller element size brings the smaller measured error  $n(\tau)\tau \rightarrow L$ .

However, if the measurement is performed for a fractal object (i.e., not a model, but an object of the real world), then, according to the theory of fractals, the number of coverage elements and the total length of the coverage will tend to infinity:

$$n(\tau) \xrightarrow{\tau \rightarrow 0} \infty. \quad (5)$$

The fundamental relation [19, 20] which caused Equation (4) established the correlation between the line length and the size of the coverage element as

$$L \propto \frac{1}{\tau^D}. \quad (6)$$

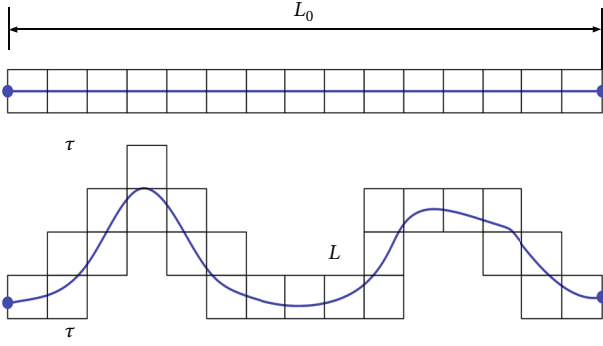


FIGURE 3: The fractal dimension estimation illustration.

Let us introduce the variable  $a$  into expression (6) to pass to the equal sign:

$$L = \frac{a}{\tau^D}. \quad (7)$$

It is known from [20] that for a straight line of FD  $D = 1$ , then based on Formula (7), it is possible to write a system of two equations:

$$\begin{cases} a\tau^{-1} = R, \\ a\tau^{-D} = L_{\max}, \end{cases} \quad (8)$$

where  $R$  is the desired cluster radius,  $L_{\max}$  is a maximum route length,  $D$  is a fractal dimension, and  $a$  is an unknown variable.

The first equation in the system is written for a straight line segment connecting the center of the cluster with a point on its edge, i.e., a line whose length equals the radius. Therefore, the exponent  $t$  is minus 1, i.e., equal to a straight line's fractal dimension.

The second equation is written for a line, which is a trace with fractal dimension  $D$ . In this case, the trace length is equal to the maximum route length  $L_{\max}$ .

The system solution is the following:

$$R(D) = L_{\max} \tau^{D-1}, \quad (9)$$

where  $\tau$  is the coverage element size.

Figure 4 shows two examples: straight routes from the cluster center to the edge (see Figure 4(a)) and joggle lines (see Figure 4(b)). The fractal dimension estimation for Figure 4(a) is  $D = 1.002$  and for Figure 4(b) is  $D = 1.108$ . The fractal dimension was estimated using the program [21].

In the first case (Figure 4(a)), the routes are straight lines, and the FD of straight lines should be equal to one, which is confirmed with sufficiently high accuracy by measurement. In this case, the cluster radius coincides with  $L_{\max}$ . In the second case (Figure 4(b)), the FD is greater than one, and according to Equation (9), the radius should be 0.62 of  $L_{\max}$ .

Figure 4(b) also shows a circle, which results from a decrease in the cluster size due to the "curvature" of the traces.

For greater generality, let us assume that  $L_{\max} = 1$ ; the dependence of the radius of the assumed cluster on the fractal one will look as shown in Figure 5.

The range of the fractal dimension is selected from 1 to 2, which corresponds to the possible values for the lines, i.e., from a straight line to a line filling the entire plane. As can be seen from the figure, the cluster radius decreases with increasing fractal dimension. It is especially worth noting the role of the  $\tau$  in this dependence.

In Figure 5, the red curve presents the route length  $L_0 = 50$  km at intervals of 1 km ( $\tau = 0.02$ ), the black curve the same route length at intervals of 1 m, and the blue at intervals of 45 km. The dependence on  $\tau$  is obvious and is explained by the fractal nature of the measured objects.

The cable route is outwardly different from the coastline, but this difference does not affect the essence, i.e., these objects are objects of the surrounding world. Therefore, the "coastline paradox" [19, 20, 22], which consists in the fact that when the length of the metric  $\tau$  decreases, its length tends to infinity, to the same extent, applies to this problem.

This is shown in Figure 5. When  $\tau = 1$ , i.e., when the length of the metric is equal to the length  $L_0$ , naturally, there is no dependence; the graph will coincide with the abscissa axis.

With the length of the metric  $\tau \rightarrow 0$ , the cluster size also tends to zero  $R(\tau) \rightarrow 0$ . So, by definition, the length of the fractal line tends to infinity.

All applications essential for practice must operate with  $\tau$  values between these boundaries. In other words, it is necessary to determine such a value  $\tau$  that corresponds to the real possibilities and needs for each task. Within the framework of this work, it is advisable to choose  $t$ , proceeding from the permissible error in estimating the magnitude of the delay.

If the permissible error in estimating the delay is  $\Delta t$ , then, this will correspond to the value of the permissible error in a distance equal to

$$d = \Delta t C, \quad (10)$$

where  $C$  is the speed of light propagation (m/sec).

Then, it is advisable to choose  $\tau$  based on the  $d$  value since this is the size of the metric, and the error is equal to 1/2 of this value. We get the following:

$$\tau = \frac{2d}{L_0}. \quad (11)$$

For example, at  $L_0 = 50000$  m,  $\Delta t = 1 \mu\text{s}$ ,  $d \approx 600$  m, and  $\tau \approx 0.012$ . But if we increase  $\Delta t = 10 \mu\text{s}$ , then  $d \approx 6000$  m, and  $\tau \approx 0.12$ .

Figure 6 illustrates these results.

As shown in Figure 6, with real values of the fractal dimension (1-1.3), the cluster size can be more than half the line length  $L_{\max}$ .



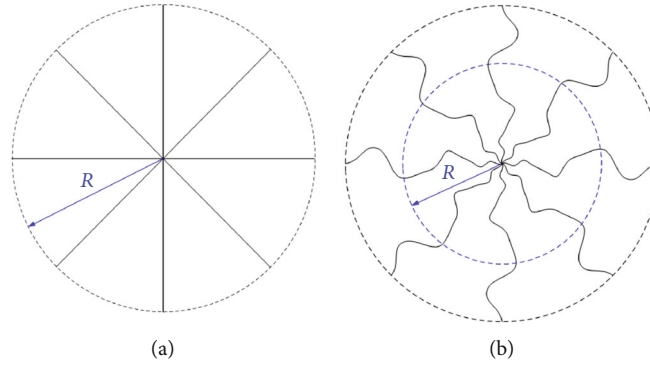


FIGURE 4: Examples of various cluster structures.

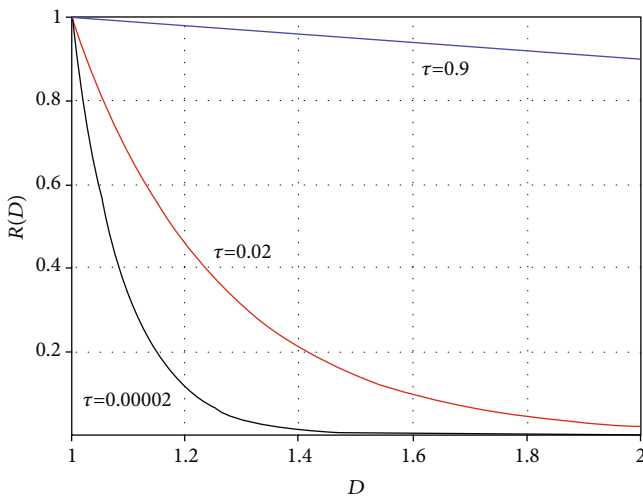
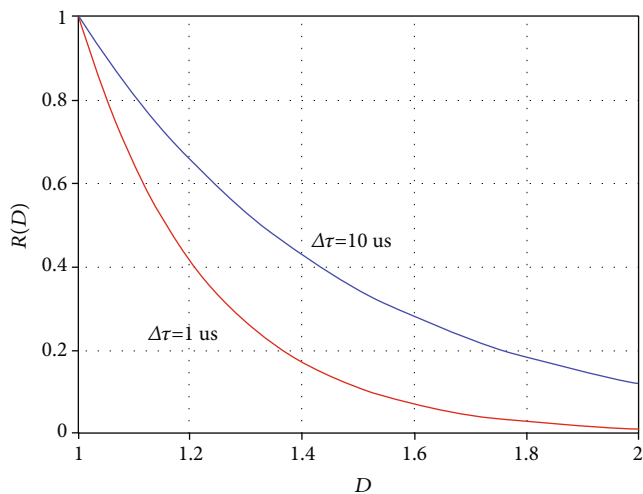


FIGURE 5: The dependence of the cluster radius on the fractal dimension (FD).

FIGURE 6: The dependence of the cluster radius to the fractal dimension (FD) (with a permissible error of the delay estimation of 1 and 10  $\mu$ s).

The redundancy of the trace length is assumed to be unchanged when the size (radius) of the cluster changes and the fractal dimension of the roads. With the uneven distribution of road properties within the original cluster, after adjusting its size (9), the length of the tracks may be underestimated or overestimated. To reduce the error, it is advisable to assess the fractal dimension in the cluster before adjusting the size and taking the fractal dimension's average value as the target value.

The model algorithm is shown in Figure 7.

The computational complexity of the given algorithm is determined by the complexity of the operations for estimating the fractal dimension of the road network. In practice, the assessment of the fractal dimension of an image depends on the size of the image (the number of pixels) and the features of the algorithm implementation. For example, for a  $1080 \times 720$  image, the algorithm can be implemented by organizing cycles of counting the number of squares containing the points of the curves, starting from  $72 \times 72$  (10 squares along the short side of the image) to 1 by 1 (this is the maximum number of cycles; usually, it is less). Each cycle requires about  $1080/s \cdot 720/s$  operations, where  $s$  is the size of the side of the square. Then, for given image size, a maximum of about 1.3 million operations will be required.

Taking into account the performance of modern computers, the solution to this problem is not a significant problem. In practice, the time to solve it, when implementing the method for estimating fractal dimension in Java, is about one second.

The presented algorithm allows estimating the cluster size, taking into account the lengths of the existed cable routes. The clustering process itself can be implemented by complementing the method proposed in [7], based on the FOREL algorithm. The additions are to incorporate the above algorithm into the specified method before the next cluster search step. In contrast to the original method, in which the size of the cluster is chosen constant, this addition provides for the adaptation (change) of the size of each formed cluster, taking into account the peculiarities of the terrain in order to meet the requirements for the amount of delay.



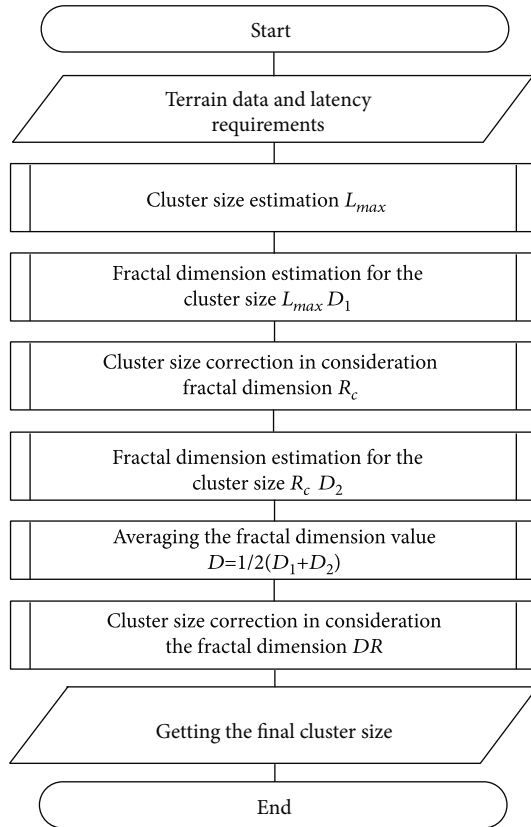


FIGURE 7: Cluster estimation algorithm.

The parameters of the proposed algorithm are selected in accordance with the requirements for the accuracy of estimating the delay value. According to the analysis and modeling performed, the following numerical values of the parameters can be recommended, which can be used in solving most practical problems. The parameter values are given in Table 1.

The proposed algorithm in Figure 7 contains two modules that require a significant investment of time: a block for estimating the size of a cluster and a block for estimating a fractal dimension. Cluster size estimation includes the clustering method, which in the worst case requires  $n^3$  operations, where  $n$  is the number of clustered objects. The complexity of the fractal dimension estimation method depends on the image parameters and does not exceed  $d^2$ , where  $d$  is the number of pixels.

Furthermore, this algorithm is applicable in cases where the area under consideration already contains a sufficiently developed network of roads. This condition is quite natural, since the method and algorithm are based on the assumption of cable laying along existing roads. If the considered area is devoid of roads or their construction is assumed, then the problem becomes degenerate. In this case, either it is impossible to assume in advance the plan for laying the cable or it is absolutely known, therefore, the solution to the problem is also known. Since the construction of a road network, as a rule, precedes the development of an infocommunication system, this algorithm is applicable in most cases for solving such problems.

TABLE 1: Algorithm parameters.

Fractal dimension	$R$ reducing factor		
	Delay error ( $\Delta = 10 \mu s$ )	Delay error ( $\Delta = 5 \mu s$ )	Delay error ( $\Delta = 1 \mu s$ )
1.2	0.654	0.573	0.413
1.4	0.428	0.329	0.170
1.6	0.280	0.189	0.070
1.8	0.183	0.108	0.029
2.0	0.120	0.062	0.012

## 5. Experimental Environment and Setup

To carry out this work, we used Google Earth electronic maps [13], the Image Processing and Analysis in Java program for image processing and fractal dimension estimation [23], and the Mathcad program.

They were obtaining digital images of the plan of the area where the construction of a communication network is supposed to be realized by various means. These can be scans of paper maps or plans of the area or digital images obtained in another way. The simplest and most affordable way to obtain digital images, at present, is the use of digital maps of the area. Google Earth is perhaps the most advanced geographic system available. It allows you to receive images of various scales, make measurements, and enable or disable various map elements. However, in most cases, the resulting digital images require additional processing. The fact is that the parameters of the road structure are subject to assessment, but the digital image also contains other map elements. These elements must be excluded when evaluating the fractal dimension. When performing the experiments, the results of which were given above; we used Google Earth processing tools, a graphics editor, and an image processing program [23]. The processing process was not fully formalized. At the first step, on the digital image, the roads were highlighted in color, which was taken into consideration. Also, all labels and unrelated map elements were turned off on the map, which could be excluded by means of Google Earth. A digital image was formed in the form of a separate graphic file. On the second template, this image was processed in a graphical editor, where the roads were highlighted, and all other elements of the map were deleted. At the third stage, the Image Processing and Analysis in Java program [23] was used, in which the final image processing (setting the contrast threshold) and the evaluation of the fractal dimension were performed.

It should be noted that the process described above is not entirely formal since the second step is human editing of the image. The amount of uncertainty introduced by the actions of the editor is very small, since these actions are aimed at highlighting well-defined objects and removing unnecessary objects in the image and are mainly determined by erroneous actions. To a greater extent, this process is reflected in the complexity, which is determined by the stage of manual editing. Note also that the entire described sequence of operations can be fully formalized and implemented in the form of software. This will eliminate the factor of errors introduced by

manual image editing. Since this work was research work, such a task was not set in it.

Full formalization of image processing will be implemented in the course of further work.

The analytical dependencies shown in Figures 5 and 6 were obtained using the Mathcad program.

## 6. Conclusions

Choosing the cluster size of an ultralow latency network, one should consider the specifics of laying communication lines between the point of service provision and the points of connection of users. This feature, as a rule, consists in the fact that the route of laying communication lines runs along existing roads. Therefore, the structure of the existing road route influences the choice of routes for laying communication lines. Given this feature, the length of the communication line, in most cases, turns out to be greater than the distance between the connected points. For a cluster, this leads to an overestimation of the delay relative to the target values. In addition, it is necessary to select the cluster size to consider the length of the cable routing to avoid overestimating the delay. The proposed algorithm assesses the cluster size and considers route lengths based on assessing the fractal dimension of the road in the area. The value of the fractal dimension makes it possible to assess the degree of difference between the laying routes and straight lines and, as a result, determine the coefficient by which it is necessary to reduce the size of the assumed cluster. Moreover, the road's route unevenness may affect the underestimation or overestimation of the cluster size. It is essential to estimate the fractal dimension for the initial and corrected cluster sizes for its compensation. Then, use the averaged value of the fractal dimension for the final estimate of the cluster size.

Although the fractal dimension is estimated to improve the accuracy of the formation of digital clusters, its value significantly depends on the image processing method. Therefore, in ongoing and future work, the proposed method will be further improved to include the processing of digital images with the objective of maximizing the formalization of the method to highlight roads as lines and exclude the influence of other image elements.

## Data Availability

The datasets generated during and analysed during the current study are available from the corresponding author upon reasonable request.

## Conflicts of Interest

The authors declare that they have no conflicts of interest.

## Acknowledgments

This research is based on the Applied Scientific Research under the SPbSUT state assignment 2021.

## References

- [1] G. Fettweis, H. Boche, T. Wiegand et al., *The Tactile Internet-ITU-T Technology Watch Report*, Int. Telecom, Union (ITU), Geneva, 2014.
- [2] ITU-T, "Signalling requirements and architecture of intelligent edge computing," <https://www.itu.int/rec/T-REC-Q.5001/en>.
- [3] A. al-Ansi, A. M. al-Ansi, A. Muthanna, I. A. Elgendy, and A. Koucheryavy, "Survey on intelligence edge computing in 6g: characteristics, challenges, potential use cases, and market drivers," *Future Internet*, vol. 13, no. 5, p. 118, 2021.
- [4] A. Muthanna, P. Masek, J. Hosek et al., "Analytical evaluation of d2d connectivity potential in 5g wireless systems," in *Internet of Things, Smart Spaces, and Next Generation Networks and Systems*, vol. 9870, pp. 395–403, Springer International Publishing, 2016.
- [5] V. I. Blanutsa, "Territorial structure of the russian digital economy: preliminary delimitation of smart urban agglomerations and regions," *Regional Research of Russia*, vol. 9, no. 4, pp. 318–328, 2019.
- [6] A. Alshahrani, I. A. Elgendy, A. Muthanna, A. M. Alghamdi, and A. Alshamrani, "Efficient multi-player computation offloading for vr edge-cloud computing systems," *Applied Sciences*, vol. 10, no. 16, p. 5515, 2020.
- [7] A. Paramonov, N. Chistova, M. Makolkina, and A. Koucheryavy, "The method of forming the digital clusters for fifth and beyond telecommunication networks structure based on the quality of service," in *Internet of Things, Smart Spaces, and Next Generation Networks and Systems*, vol. 12525, pp. 59–70, Springer, 2020.
- [8] A. A. Abd el-Latif, B. Abd-el-Atty, I. Mehmood, K. Muhammad, S. E. Venegas-Andraca, and J. Peng, "Quantum-inspired blockchain-based cybersecurity: securing smart edge utilities in iot-based smart cities," *Information Processing & Management*, vol. 58, no. 4, article 102549, 2021.
- [9] A. A. A. el-Latif, B. Abd-el-Atty, A. Belazi, and A. M. Iliyasu, "Efficient chaos-based substitution-box and its application to image encryption," *Electronics*, vol. 10, no. 12, p. 1392, 2021.
- [10] A. Alanezi, B. Abd-El-Atty, H. Kolivand, and A. A. Abd El-Latif, "Quantum based encryption approach for secure images," in *2021 1st International Conference on Artificial Intelligence and Data Analytics (CAIDA)*, pp. 176–181, Riyadh, Saudi Arabia, 2021.
- [11] I. A. Elgendy, W.-Z. Zhang, H. He, B. B. Gupta, and A. A. Abd El-Latif, "Joint computation offloading and task caching for multi-user and multi-task mec systems: reinforcement learning-based algorithms," *Wireless Networks*, vol. 27, no. 3, pp. 2023–2038, 2021.
- [12] W.-Z. Zhang, I. A. Elgendy, M. Hammad et al., "Secure and optimized load balancing for multitier iot and edge-cloud computing systems," *IEEE Internet of Things Journal*, vol. 8, no. 10, pp. 8119–8132, 2021.
- [13] The world's most detailed globe, "Google earth," <https://earth.google.com/web/>.
- [14] A. Jajszczyk, "Cognitive wireless communication networks (Hossian, E. and Bhargava, V.; 2007) [book review]," *IEEE Communications Magazine*, vol. 46, no. 11, pp. 18–18, 2008.
- [15] A. Paramonov, O. Hussain, K. Samouylov, A. Koucheryavy, R. Kirichek, and Y. Koucheryavy, "Clustering optimization for out-of-band D2D communications," *Wireless*

*Communications and Mobile Computing*, vol. 2017, Article ID 6747052, 11 pages, 2017.

- [16] R. Kirichek, A. Paramonov, A. Vladyko, and E. Borisov, "Implementation of the communication network for the multi-agent robotic systems," *International Journal of Embedded and Real-Time Communication Systems*, vol. 7, no. 1, pp. 48–63, 2016.
- [17] X. Li, A. Gani, R. Salleh, and O. Zakaria, "The future of mobile wireless communication networks," in *2009 International Conference on Communication Software and Networks*, pp. 554–557, Chengdu, Sichuan, China, 2009.
- [18] A. Paramonov, E. Tonkikh, A. Koucheryavy, and T. M. Tatarnikova, "High density internet of things network analysis," in *Internet of Things, Smart Spaces, and Next Generation Networks and Systems*, vol. 12525, pp. 307–316, Springer, 2020.
- [19] B. B. Mandelbrot and B. B. Mandelbrot, *The Fractal Geometry of Nature*, vol. 1, WH Freeman, New York, 1982.
- [20] A. Paramonov, A. Muthanna, O. I. Aboulola et al., "Beyond 5g network architecture study: fractal properties of access network," *Applied Sciences*, vol. 10, no. 20, p. 7191, 2020.
- [21] K. Falconer, *Fractal Geometry: Mathematical Foundations and Applications*, John Wiley & Sons, 2003.
- [22] Wolfram MathWorld Coastline Paradox, "Coastline paradox," <https://mathworld.wolfram.com/CoastlineParadox.html>.
- [23] ImageJ Disclaimer, "Image processing and analysis in java," <https://imagej.nih.gov/ij/>.

## Research Article

# Key Technologies of Cache and Computing in 5G Mobile Communication Network

**Yanfang Zha** 

*School of Artificial Intelligence, Suzhou Industrial Park Institute of Services Outsourcing, Suzhou Jiangsu 215000, China*

Correspondence should be addressed to Yanfang Zha; zhayf@siso.edu.cn

Received 18 August 2021; Revised 10 September 2021; Accepted 15 September 2021; Published 26 September 2021

Academic Editor: Deepak Gupta

Copyright © 2021 Yanfang Zha. This is an open access article distributed under the Creative Commons Attribution License, which permits unrestricted use, distribution, and reproduction in any medium, provided the original work is properly cited.

The deployment of cache and computing resources in 5G mobile communication networks is considered as an important way to reduce network transmission delay and redundant content transmission and improve the efficiency of content distribution and network computing processing capacity, which has been widely concerned and recognized by academia and industry. Aiming at the development trend of cache and computing resource allocation in 5G mobile communication networks, in order to improve the efficiency of content cache and reduce network energy consumption, a 5G network cache optimization strategy based on Stackelberg game was proposed, which modeled network operators and content providers as multimaster and multislave Stackelberg game model. Providers buy base station storage space from network operators to cache popular content. In this paper, we construct the strategy space and profit function of the two sides of the game and prove the existence of Nash equilibrium solution among content providers given a set of base station rental prices of network operators. In this paper, distributed iterative algorithm is used to solve the game model, and the optimal base station pricing of network operators and the optimal base station occupancy rate of content providers are obtained.

## 1. Introduction

The network caching strategy reduces the user's request waiting time and content sending waiting time by caching the content of the content provider to the caching node or base station of the 5G network in advance, reduces the sending energy consumption in the network, and improves the experience quality of network users [1]. The performance of caching strategy directly affects the caching efficiency of network content and the quality of user experience, which is one of the hot spots in the current 5G network research. The traditional content caching strategy is relatively simple to expand in the network, but it has some shortcomings such as low integration, low cache hit rate, and low utilization rate of network resources [2]. At the same time, due to the limited cache resources in the network, there are conflicts among content providers. Previous strategies lack of consideration of the competitive relationship between content providers, there are high cost of network operators, low utilization of cache space, and other drawbacks. For the above problems, some scholars have studied the cache strategies

of 5G networks, but most of these algorithms and strategies only consider a single network performance index and do not consider the competitive relationship between network operators and content providers, and the comprehensive consideration of cache hit rate, network cost, resource utilization, and other factors is insufficient [3]. Therefore, the cache strategy needs further research and optimization.

With the combination of UAV communication and edge caching, coupled with network deployment, resource allocation is very important to the quality of experience (QoE) of content distribution application users [4]. The optimization problem of maximizing QoE is proposed and evaluated by MOS. In the first step, greedy algorithm and Lagrange duality algorithm are used to obtain the optimal position and association. In the second step, the iterative algorithm of optimization is proposed, which achieves the best way of computational complexity and optimization. Network edge caching for D2D can reduce the burden of transmission, which is a more promising technology [5]. But it relies too much on the content preferences of individual users, so we must take some proactive measures if we want to give full

play to its advantages. In the research, the recommendation algorithm has a great impact on caching decision, so we further study how to improve the caching efficiency of D2D wireless content caching network. According to the requirements of personalized recommendation quality and quantity, including cache capacity, the cache hit rate maximization problem of general network model is adopted to solve the cache efficiency problem. Two criteria in cache-assisted MEC networks are relay link channel gain and direct link channel gain, both of which can greatly improve the computing power [6]. Similarly, there are three criteria for cache-free MEC networks. Based on the outage probability defined by transmission plus computation time, cache can alleviate the impact of heavy computation, while the improvement of cache in high signal-to-noise ratio (SNR) area is not as significant as that of cache-free network adopting the destination with the largest channel gain of direct link. Literature [7] is aimed at the restrictive problem that the development of smart grid technology depends on the convenient data transmission service provided by Power Line Communication (PLC), mainly the channel environment and the increasing traffic load in the backhaul, which is a high energy consumption work. A PLC network with high cache is proposed, which can reduce load energy consumption. Literature [8] is aimed at the increase of network traffic caused by the increase of population, but metropolis adopts local cache to reduce traffic, which is a traditional method and will be limited by storage space. Therefore, researchers put forward data mining technology based on clustering concept. This technology is a pattern of collecting feedback data to reduce traffic, and then, grouping it and redeploying it can achieve the effect of traffic reduction. On the experimental surface, it can indeed reduce the flow rate by about 8%.

As mentioned above, the current cache policy has some problems, such as high cache cost, large network energy consumption, and low cache hit rate. In view of the above problems, this chapter uses the Stackelberg game method to model and analyze the content caching process of 5G network and comprehensively considers the popularity of content, user preferences, cache hit rate, etc. and puts forward an optimization strategy of 5G network caching based on Stackelberg game, which is used for network content caching and provides users with high-quality network services.

## 2. 5G Network Content Caching

Router nodes and network base stations in 5G networks have storage capacity. By setting the cache strategy and cache replacement strategy, the content of the content provider is cached to the router node or network base station of 5G network in advance, which can effectively reduce the transmission delay and network energy consumption of 5G network by reducing the retrieval delay of content and the backhaul load of 5G network [9] and at the same time improve the experience quality of netizens.

Cache technology mainly includes three stages: cache policy determination, online user request, and cache replacement. The so-called caching decision refers to making caching

strategies based on network traffic changes or content hit rate and caching content into the network in advance. User request is a way to decide the request and send the request content by judging whether the file needed by the user is stored in the cache. Cache replacement refers to replacing cache contents and determining what to update when the cache space reaches a threshold [10].

Caching technology can divide cache into core cache and edge cache according to cache location. Core caching strengthens the overall scheduling ability of the network by caching the network content to the router of the core network, but it enhances the storage load of the core network to a certain extent. Edge caching caches network content to routers close to users' edge networks, which reduces the delay of video search. When the next request is received, the network can respond to users' needs in time, improve the efficiency of users' content acquisition, and increase the transmission speed of network content [11].

Caching technology can be divided into active caching and passive caching according to caching methods. In the case of passive caching, the content within the network is cached in the corresponding location only after being sent through the node. If no data is requested from the responding node, the node does not cache the data. However, due to the high diversity of user preferences, multiple users no longer request exactly the same content, and caching content in passive cache may not meet the needs of future network users [12]. An effective way to improve the efficiency of network caching is to activate the requested content before the user's request arrives. Thus, the active cache can anticipate user requirements and fetch content from the content provider before being requested.

User demand and user mobility are two factors to consider activating and caching network users in 5G networks.

The advantages of applying caching technology in 5G networks are as follows:

- (1) It can reduce the demand of nodes for backhaul links, so it can increase the deployment density of nodes and improve spectrum utilization and network throughput
- (2) Hot data can be cached in advance in the cache node to balance the traffic in the network, thus avoiding the occurrence of network congestion during the peak traffic period
- (3) It can reduce the network occupation of backhaul bandwidth and reduce the deployment cost of backhaul link of base station to a certain extent
- (4) It can effectively reduce the retrieval delay and transmission delay for users to obtain content, because users can directly obtain the requested content from the cache node and do not need to obtain it from the core network
- (5) It can effectively avoid duplicate contents transmitted on the backhaul link, thereby reducing the energy consumption of the network and improving the energy efficiency



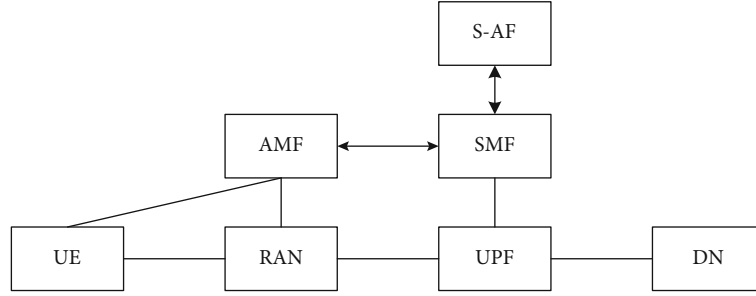


FIGURE 1: 5G network architecture.

### 3. System Model of Content Caching

The focus of this paper is to model and analyze the content caching system. Firstly, the network architecture of content caching in 5G network is summarized, and then, the system is modeled in this network architecture. Finally, the popularity of content, user preference, and cache hit rate are introduced in detail.

As shown in Figure 1, the 5G network architecture [13] mainly includes modules such as UE, AMF, RAN, S-AF, SMF, UPF, and DN. The functions of each module are as follows.

- (1) *UE*. The module mainly includes 5G user terminals requesting network content.
- (2) *AMF*. AMF module is mainly responsible for user mobility management and network access control. The 5G core access and mobility management function (AMF) receives all connection and session-related information from user equipment, but is only responsible for handling connection and mobility management tasks. All messages related to session management are forwarded to the session management function through the reference interface.
- (3) *RAN*. It is mainly responsible for the terminal access function of 5G network, and the base stations of network operators are distributed in the layer of wireless access network.
- (4) *Stackelberg Game Application [14] Function*. S-AF module mainly interacts with the implementation of cache optimization strategy, the processing of network information, and the core network of 5G network presented in this section to provide corresponding services.
- (5) *SMF*. This module is mainly responsible for the management and control of end-user sessions.
- (6) *UPF*. The user interface function completes the related operations of the user interface, including the retrieval and root functions of the data content of the user interface.
- (7) *DN*. The content provider is located in this location, mainly providing the content required by users.

**3.1. System Model.** Network operators in wireless access networks and content providers in data networks are combined as a system model. Figure 2 shows the system model of cache optimization strategy.

The system model in this paper includes  $M$  network operators  $\{1, 2, \dots, M\}$ ,  $N$  content providers  $\{1, 2, \dots, N\}$ , and 5G network [15] end users. Each network operator may lend base station space to the content provider to precache content specified by the content provider. Here, the base station distribution of network operators follows the distribution density. The different  $\lambda$  is arranged neatly, and the users follow the uniform distribution of berthing points with different properties of distribution density  $n$ .

In the system model, the specific process for completing content request and download is the first step: the network operator first sets the price of its base station and notifies the content provider through the 5G network. Second step: The content provider leases a certain percentage of the base stations based on the type of network operator and the pricing of the base stations and caches popular or popular content to the base stations for request by the end user. Step 3: The end user downloads the required content from the base station.

**3.2. Content Popularity.** In practical applications, users have different preferences for different contents (for example, some people like football videos, scientific messages, or music), and part of the contents that the next user may request is cached and provided to the user based on the user's historical browsing records, thus reducing the request waiting time and transmission waiting time of the content [16]. The contents of popular files on the network are set to  $C$ , the set represents  $C = \{F_1, F_2, F_c\}$ , and the popularity of the  $C$  content is set to  $D_c, c = \{1, 2, \dots, C\}$ .

$$D_c = \frac{1/c^\alpha}{\sum_{j=1}^C (1/j^\alpha)}, \forall c. \quad (1)$$

As can be seen from Equation (1), content  $F_1$  is the most popular and content  $F_c$  is the least popular.

In this paper, the adjustment coefficient is introduced based on Formula (1). For  $\sigma$ , in order to adjust the cached content, the base station caches the popular content of the content provider and improves the income of the content

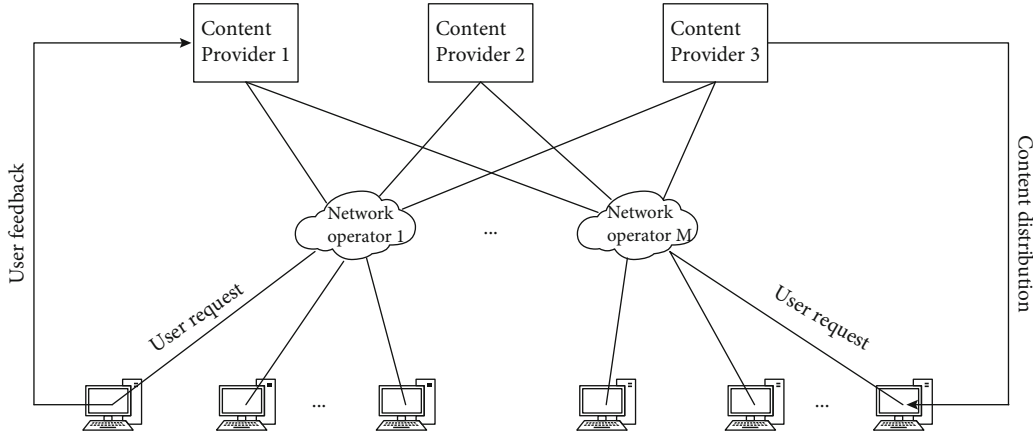


FIGURE 2: System model.

provider. The popularity of imported  $\sigma$  modified content is expressed in Formula (2).

$$D_c = \frac{\sigma/c^\alpha}{\sum_{j=1}^C (1/j^\alpha)}, \forall c. \quad (2)$$

**3.3. User Preference Degree.** According to users' usage habits, users have different preferences for content providers. For example, for video providers, Tencent, Youku, and eye contact use groups are different. User preference indicates the user's experience level with the content provider, and the higher the preference, the higher the user's access frequency. Therefore, in this specification, by introducing a user preference indicator, content provided by a content provider with a high user preference degree is cached in advance in a network in order to improve the revenue of the content provider. Assuming there are  $N$  content providers  $n = \{1, 2, \dots, N\}$ , the user preferences are  $e = \{E_1, E_2 \dots E_N\}$ , respectively. Since the user's content provider preferences follow the Zipf distribution,  $E_n$  is defined as Formula (3).

$$E_n = \frac{1/n^\beta}{\sum_{i=1}^n (1/i^\beta)}, \forall n. \quad (3)$$

Among them,  $\beta$  benchmark index,  $\beta > 0$ . The larger the beta, the more popular the content provider is among users and the more frequently it is accessed. According to Formula (3), it can be seen that content provider 1 is the most popular and content provider  $N$  is the least popular.

The cache hit ratio of content providers is an indicator that content caching must consider. The cache hit ratio  $P_{hit}$  is shown in Formula (4).

$$P_{hit} = \frac{\pi \lambda P_c R_{th}^2 \tau e^{-\lambda \pi P_c R_{th}^2}}{\epsilon \tau + \mu}, \quad (4)$$

where  $\mu$  represents the normalization factor and  $e^{-\lambda \pi P_c R_{th}^2}$  is the adjustment factor for the cache hit ratio.

## 4. Creation of Stackelberg Game

The standard game model should include three elements: game participants, game strategy space, and game income function. Among them, Stackelberg is a game suitable for master-slave relationship [17, 18]. The participants of the game are generally instructors and followers, and the instructors and followers have their own game strategies and profit functions. The process of the game is as follows:

- (1) Leaders make decisions based on their own benefits
- (2) Followers make corresponding decisions according to leaders' decision-making actions
- (3) Maximize the income value of both parties through the game process

**4.1. Composition of Stackelberg Game.** In this paper, the game model is established as a multimaster and multislave Stackelberg game [19, 20], and the constituent elements of the game are as follows:

- (1) *Participants in the Game.* The leaders are  $N$  content providers  $\{1, 2, \dots, N\}$ . Followers are  $M$  network operators  $\{1, 2, \dots, M\}$ .
- (2) *Strategy Space of Game.* The leader's strategy is the proportion of content provider renting network operator's base station  $t_{mn}$ , or the follower's strategy is to set the rental price of network operator's base station, which is expressed as  $P = \{P_1, P_2, \dots, P_M\}$ .
- (3) *The Return Function of the Player.* Revenue from caching content

$$U_n^{cache} = \sum_{m=1}^M \sum_{c=1}^C K \eta Q E_n D_c P_{hit}, \quad (5)$$

where  $Q$  is the unit price of each content and  $K$  is the average number of users' requests for content. The

other part is the rent for renting the base station of the network operator:

$$U_n^{\text{rent}} = \sum_{m=1}^M \tau_{mn} \lambda_m P_m. \quad (6)$$

The revenue function for content providers is as follows:

$$U_n = U_n^{\text{cache}} - U_n^{\text{rent}}. \quad (7)$$

For network operators, the revenue mainly comes from the rental fee  $P_m$  charged by the content provider for renting the base station and the cost  $C_m$  of managing the base station by the network operators. Therefore, the revenue function of network operators is as follows:

$$U_m = \sum_{n=1}^N (P_m - C_m) \tau_{mn} \lambda_m. \quad (8)$$

**4.2. Problem Creation of Stackelberg Game.** For a single network operator, the optimization problem can be created as a revenue maximization problem for the network operator, namely,

$$\max_{p \geq 0} U_m(p, \tau). \quad (9)$$

Special attention should be paid to the fact that the content storage capacity must not exceed the total cache space of the base station.

For each content provider, the optimization problem is created as the revenue maximization problem of the content provider. By substituting Formulas (5) and (6) into Formula (7) and deducing calculation, the revenue of the content provider can be obtained as follows:

$$\begin{aligned} U_n &= \sum_{m=1}^M \sum_{c=1}^C K \eta Q E_n D_c P_{\text{hit}} - \sum_{m=1}^M \tau_{mn} \lambda_m P_m \\ &= \sum_{m=1}^M \left[ \frac{\sum_{c=1}^C K \eta Q E_n D_c \pi \lambda_m P_c R_{nh}^2 \tau e^{-\lambda \pi P_c R_{nh}^2}}{\varepsilon \tau + \mu} - \tau_{mn} \lambda_m P_m \right] \#. \end{aligned} \quad (10)$$

The optimization problem for the content provider is created as follows:

$$\max U_n(p, \tau). \quad (11)$$

Among them,  $0 \leq 1$ .

According to the above game model, the goal of the network operator is to maximize the benefits specified in Formula (8). The content provider leases the network operator's base station in a proportion  $\tau$  depending on the network operator's leased price  $P_m$  of the base station. The

purpose of the game is to find Stackelberg's Nash equilibrium point, discourage leaders and followers from deviating from the best strategy, and achieve the goal of maximizing the interests of both parties.

**4.3. Stackelberg's Nash Equilibrium.** The purpose of the game [21, 22] is to let the participants choose the best strategy. Whether the game ends or not determines whether the game process has a stable state. It is worth studying to play games only at the end of the game process. The steady state in game is usually described by Nash equilibrium.

Nash equilibrium refers to a combination of strategies called Nash equilibrium, which can make the strategies of all players correspond to those of other players. Once Nash equilibrium is reached, the strategy chosen by any participant is the most appropriate, and it is impossible to obtain higher benefits by adjusting his own strategy. Nash's equilibrium strategy is divided into "pure strategic Nash equilibrium" and "mixed strategic Nash equilibrium." Mixed strategy means that game participants choose response strategies randomly through probability distribution, while pure strategy means that game participants choose a single strategy determined in the current strategy space.

It is worth noting that before solving any nanoequilibrium, it is necessary to prove whether nanoequilibrium exists in the game process. For noncooperative games, Nash equilibrium is defined as no operating point, and participants can change their strategies to increase returns.

For noncooperative games, in general, if the game satisfies the following conditions,

- (1) The set of players in the game is limited
- (2) The strategy space set of game belongs to the bounded closed set of Euclidean space
- (3) The profit function of noncooperative game is continuous in strategy space and satisfies the characteristics of concave function

It can be concluded that there is Nash equilibrium in the game process, and the utility of each player will be maximized, and any participant cannot obtain higher returns by changing his own strategy privately.

If there are Nash equilibrium solutions in both game processes, then there must be Nash equilibrium solutions in their combined game.

The Nash equilibrium of Stackelberg game is obtained by looking for the perfect Nash equilibrium. In the game set here, after the lease price of the base station of the network operator set is given, a noncooperative game relationship is provided between the content providers. However, in a practical case, a plurality of nanoequilibrium solutions may exist even if there is not necessarily a nanoequilibrium solution among content providers. Therefore, this paper analyzes and proves the existence of Nash's equilibrium solution.

The return function satisfies the strict concave function characteristic, and the return function  $U_n$  is calculated as

the first derivative and the second deflection derivative of the strategy space.

$$\begin{aligned} \frac{dU_n}{d\tau_{mn}} &= \sum_{m=1}^M \left[ \frac{\mu \sum_{c=1}^C K\eta Q E_n D_c \pi \lambda P_c R_{th}^2 e^{-\lambda \pi P_c R_{th}^2}}{(\varepsilon \tau + \mu)^3} \right] - \lambda_m P_m, \\ \frac{dU_n}{d\tau^2} &= \sum_{m=1}^M \left[ \frac{-2\mu \sum_{c=1}^C \pi K\eta Q E_n D_c \lambda P_c R_{th}^2 e^{-\lambda \pi P_c R_{th}^2}}{(\varepsilon \tau + \mu)^3} \right] < 0. \end{aligned} \quad (12)$$

Through solving, it is found that the result of quadratic partial differential is negative. The income function  $U_n$  satisfies strict sag function characteristics. Therefore, the game between content providers has Nash equilibrium, which ensures the existence of perfect Nash equilibrium in the Stackelberg game model. The Nash equilibrium proposed in this paper is mainly aimed at the balance between content providers, and it is also the main function of the Stackelberg game model.

## 5. Optimization of Stackelberg Game

In the process of solving game optimization, it is necessary to consider the actual situation, such as the space size of the base station, the high price, and the low adjustment. First, the maximum and minimum values of the rental price are determined by determining the pilot frequency without considering the limitation of the storage space size of the base station. After that, the theory is expanded and the base station space is limited. Considering the actual situation of the lease ratio, it is solved in detail by the Lagrange multiplier method. Finally, the best rental ratio and the best pricing of the base station are obtained. The process of solving the game is as follows.

It is assumed that the limitation of the storage size  $S$  of the network operator is not considered. Firstly, the network operator gives a set of base station renting prices  $P = \{P_1, P_2, \dots, P_M\}$ , and then, by deriving  $dU_n/d\tau_{mn} = 0$ , the optimal solution  $\tau$  of the content provider renting base station ratio is solved:

$$\tau = \frac{1}{\varepsilon} \sqrt{\frac{\mu K \eta \pi Q E_n \lambda P_c R_{th}^2 e^{-\lambda \pi P_c R_{th}^2} \sum_{c=1}^C D_c}{\lambda_m P_m}} - \mu. \quad (13)$$

When  $\tau = 0$ , because the price of the base station is too high, the content provider chooses which base station not to rent to store the content, and because of the large delay of content request and search, the experience quality of the user is reduced. Therefore, there is a maximum rental price of the base station. Substituting  $\tau = 0$  into Equation (14), the maximum rental price is as follows:

$$P_{\max} = \frac{\pi K Q \eta E_n \lambda P_c \mu R_{th}^2 e^{-\lambda \pi P_c R_{th}^2} \sum_{c=1}^C D_c}{\mu \lambda_m}. \quad (14)$$

When  $\tau = 0$  in one case, the content provider chooses to lease all the base stations to store the content because the price of the base stations is too low, thus reducing the revenue of the network operator. Therefore, the base station price has a minimum value. Substituting  $\tau = 1$  into Equation (14), the minimum value of the rental price is as follows:

$$P_{\min} = \frac{\pi K Q \eta E_n \lambda P_c \mu R_{th}^2 e^{-\lambda \pi P_c R_{th}^2} \sum_{c=1}^C D_c}{\lambda_m (\mu + \varepsilon)^2}. \quad (15)$$

By the above solver process, the maximum and minimum values of the rental price of the base station are determined. If the price of the base station is lower than  $P_{\min}$ , the network operator should increase the price of the current base station. If the base station price is higher than  $P_{\max}$ , the network operator should reduce the current base station price. Through multiple games to modify the price strategy, the network operators and content providers ultimately maximize the benefits of both sides.

The above situation is only theoretical analysis. In practical application, the cache space of base station is limited. Therefore, the storage space size  $S_m$  is limited, and the specific constraints are as follows:

$$S_m = \sum_{n=1}^N \tau_{mn} \lambda_m \leq S_{\max}, \quad (16)$$

where  $S_{\max}$  is the maximum storage space.

In the actual solver, considering the limitation of storage space, the lease ratio of base station must meet  $0 < T \leq 1$ . Therefore, this paper seeks a solution by choosing the Lagrange multiplier method. First, a Lagrangian function of the formula is created, that is, Formula (17).

$$\begin{aligned} L_v &= \sum_{m=1}^M \sum_{c=1}^C K \eta Q E_n D_c P_{hit} - \sum_{m=1}^M \tau_{mn} \lambda_m P_m \\ &\quad + A \tau_{mn} + B \tau_{mn} + \theta \tau_{mn} \lambda_m, \end{aligned} \quad (17)$$

where  $A$ ,  $B$ , and  $\theta$  are Lagrange multipliers. According to the constraint conditions, the sufficient and necessary KKT (Karush-Kuhn-Tucher) condition of this function is as follows:

$$\begin{cases} \frac{dL_U}{d\tau} = 0, \\ A, B \geq 0, \\ A\tau = 0, \\ B(\tau - 1) = 0. \end{cases} \quad (18)$$

The optimum value  $\tau^*$  of the base station lease ratio is derived from the KKT condition, as shown in Formula (19).

$$\tau^* = \begin{cases} 0, \theta > \frac{KQ\pi\lambda\eta E_n P_c R_{th}^2 e^{-\lambda\pi P_c R_{th}^2} \sum_{c=1}^C D_c}{\varepsilon\lambda_m P_m} - 1, \\ 1, \theta < \frac{\varepsilon KQ\pi\lambda\eta E_n P_c R_{th}^2 e^{-\lambda\pi P_c R_{th}^2} \sum_{c=1}^C D_c}{(\varepsilon + \mu)^2 + \lambda_m P_m} - 1, \\ \frac{1}{\mu} \left( \sqrt{\frac{\varepsilon KQ\pi\lambda\eta E_n P_c R_{th}^2 e^{-\lambda\pi P_c R_{th}^2} \sum_{c=1}^C D_c}{1 + \theta}} - \varepsilon \right), \text{ other.} \end{cases} \quad (19)$$

The variable  $\theta$  is a constraint condition set to satisfy the space limitation of the base station, as shown in Formula (20).

$$\theta = \left( \frac{1}{\mu \left( S - \sum_{m=1}^M \lambda_m P_m \right)} \right)^2 - 1. \quad (20)$$

After solving the optimal value  $\tau^*$ , the best solution of base station price must be determined. The maximum value is obtained from Equation (20), the conductance result is shown in Equation (21), the derivative of Equation (8) is set to 0, the inverse solution is  $P_m$ , and the best price of the base station is set to  $P_m$  (Formula (22)).

$$\frac{dU_m}{dP_m} = \tau_{mn}^* \lambda_m + \lambda_m (P_m - C_m) \frac{d\tau^*}{dP_m}, \quad (21)$$

$$P_m^* = C_m - \frac{\tau^*}{d\tau^*/dP_m}. \quad (22)$$

The above solution shows that the best solution of base station price does not have a closed form, because the best price of a single network operator's base station is closely related to the prices of other base stations. That is, after the network operator's price changes, other network operators need to update their base station rental prices. Therefore, the price of network operators needs to be solved iteratively. The repetition is as follows:

$$P_m^{t+1} = C_m^t - \frac{\tau^*(P_m^t)}{d\tau^*/dP_m^t}, \quad (23)$$

where  $t$  represents the number of iterations,  $C_m^t$  represents the cost price of the base station managed by the network operator during the  $t$  iteration, and  $P_m^t$  represents the rental price of the base station during the  $T$  iteration.

If the revenue of the network operator and content provider is maximized at the time point  $T + 1$ , the repetitive process is stopped. Otherwise, the next iteration period will proceed until the two benefits reach the maximum value. Stop repeating the process.

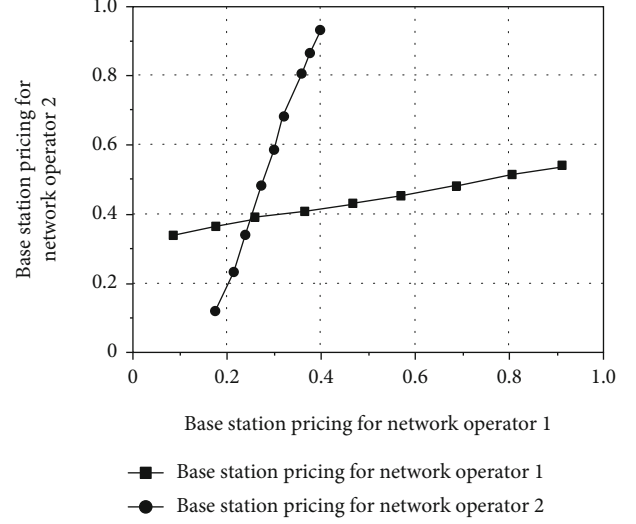


FIGURE 3: Relationship between optimal base station pricing of network operators.

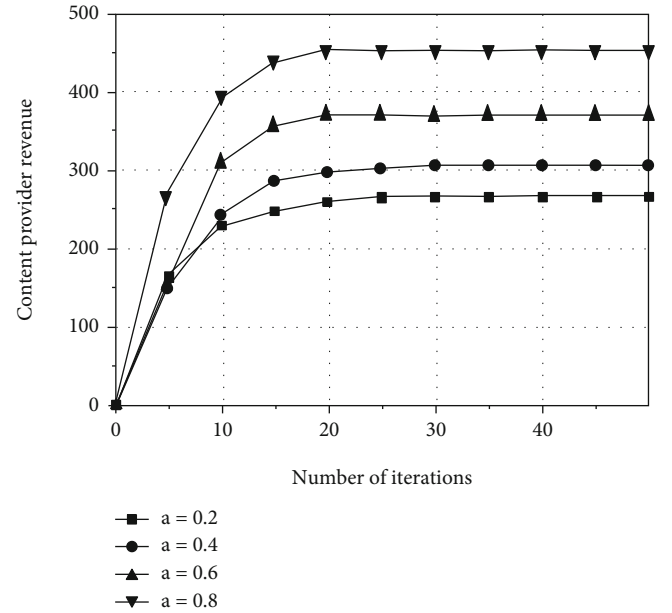


FIGURE 4: Relationship between iteration times and content provider revenue.

## 6. Analysis of Simulation Results

In this paper, we use the simulation tool MATLAB to verify and analyze the proposed algorithm. The simulation of this paper is a network environment composed of two network operators and three content providers. The content provider conflicts with the cache space resources of the network operator to cache the content. The setting values of the simulation parameters set the initial cache requirement policy for each network operator to 1.2 GB, where the available cache space for two network operators is 500 GB.  $\alpha = 2.3$ ,  $\beta = 0.7$ ,  $C = 3$ ,  $6 = 15$ ,  $\mu = 8$ ,  $R_n = 10$ ,  $P_c = 0.8$ ,  $\lambda = 8$ ,  $\eta = 20$ , and  $K = 50$ . The income value of this paper is dimensionless,



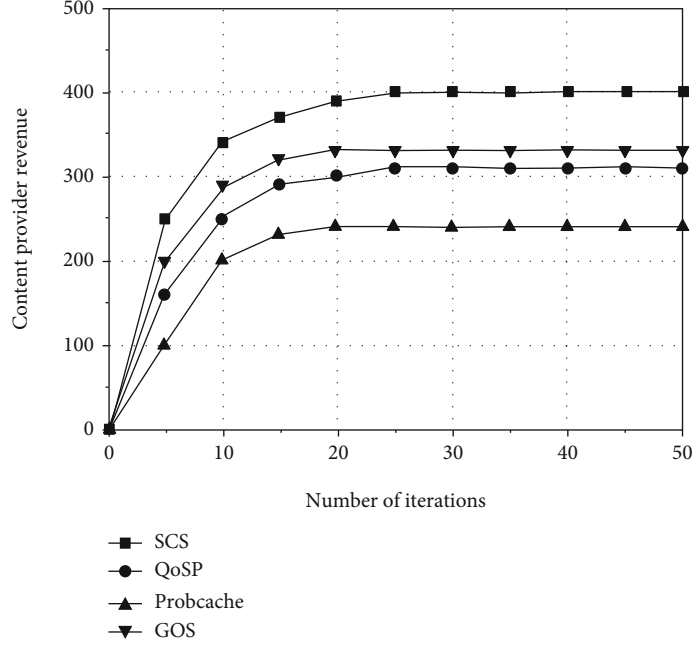


FIGURE 5: Relationship between iteration times and content provider revenue.

and the larger the value, the higher the corresponding income. In the simulation, the algorithm (SCS) compares the user QoS priority algorithm (QOSP) [23] and ProbCache ( $P = 0.38$ ) with the Global Optimization Scheme (GOS) [24] and compares the average energy consumption reduction rate, network cost, and average cache hit rate, where the average cache hit rate and the average energy consumption reduction rate are defined as follows:

- (1) *Average Cache Hit Ratio*  $P_{hit}$ . It represents the average hit probability of users requesting cached content in the network and is used to measure the rationality of content caching strategy in the network. The cache hit ratio is defined as follows:

$$P_{hit} = \frac{\sum_B \text{hit}_{c,i}^{\text{count}}}{\sum_B \text{request}_{\text{sum},i}^{\text{count}}}, \quad (24)$$

where  $\sum_B \text{hit}_{c,i}^{\text{count}}$  denotes the total number of times the user requests the content file from the cache base station  $i$  and  $\text{request}_{\text{sum},i}^{\text{count}}$  denotes the total number of times the user successfully obtains the content from the cache base station  $i$ .

- (2) *Average Energy Consumption Reduction Rate*  $E_{ave}$ . It represents the change of energy consumption between simulation comparison algorithm and classical LCE, as shown in Formula (25).

$$E_{ave} = \frac{E_{LCE} - E_{\text{other}}}{E_{LCE}}. \quad (25)$$

The energy consumption of the algorithm is composed of the cache energy consumption  $E_{\text{cache}}$  and the transmission

energy consumption  $E_{\text{tran}}$ ,  $f_n$  represents the number of cached files, and  $e_{\text{cache}}$  represents the energy consumption required for caching each file. Energy consumption is defined as follows:

$$E_{\text{other}} = E_{\text{tran}} + E_{\text{cache}} = E_{\text{tran}} + f_n e_{\text{cache}}. \quad (26)$$

Figure 3 is a diagram illustrating the relationship between the best base station pricing of the network operator 1 and the best base station pricing of the network operator 2. The points on the two curves in the graph, respectively, represent the best pricing strategy of the network operator to other network operators. It can be seen from the figure that the two curves have an intersection (0.28, 0.36), which is the Nash equilibrium point of the game, where the benefits of both can be maximized. Once the price of the network operator 2 is determined, the size of the revenue value of the network operator 1 is affected by the change of base station pricing, and the revenue itself is maximized according to the optimal pricing of the base station. If the price of the network operator 2 is changed, although the optimal base station pricing of the network operator 1 is changed, there is an optimal pricing that maximizes its revenue.

The intersection point in Figure 3 is (0.28, 0.36), and the intersection point is the Nash equilibrium point of the game, where the benefits of both can be maximized.

Figure 4 is a diagram showing popularity indices of different contents: the relationship between the number of repetitions and the revenue of the content provider in the case of  $\alpha$ . As can be seen from Figure 4, with the increase of repetition times, the rental ratio of content providers and the base station pricing of network operators gradually repeat to the optimal value. Therefore, the revenue value of

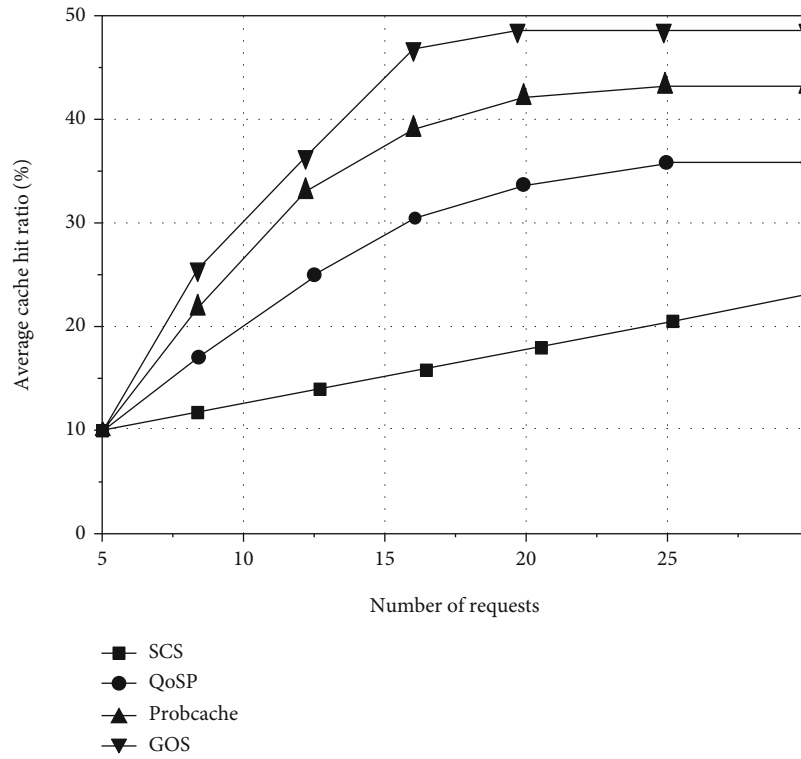


FIGURE 6: Number of requests vs. average cache hit ratio.

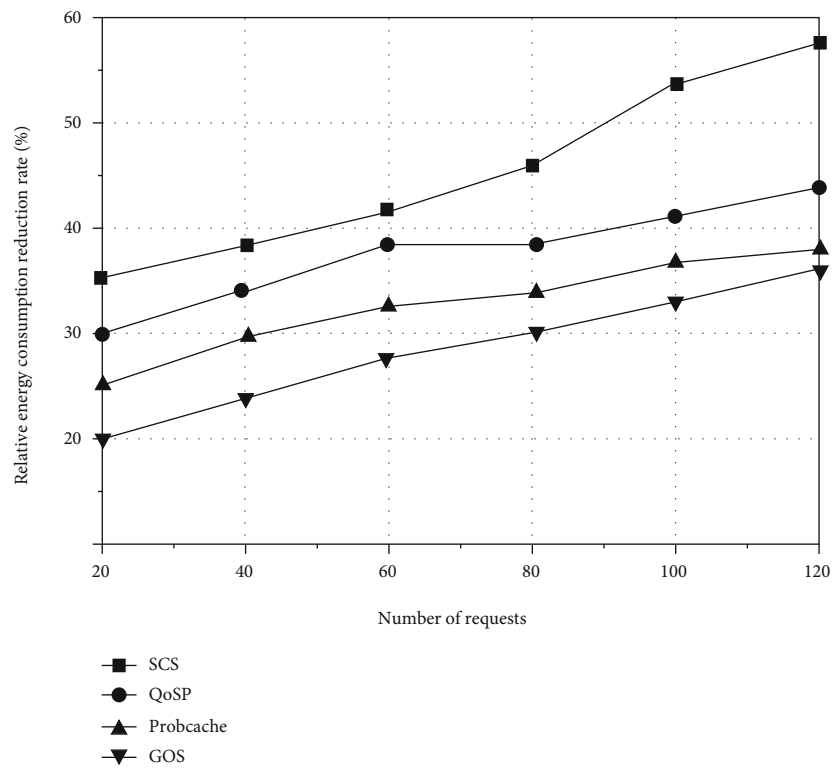


FIGURE 7: Relationship between content request times and relative energy consumption reduction rate.

the content provider continues to increase, and when the number of repetitions reaches about 24 times, the revenue function value of the content provider converges to the

optimal value. Displaying the  $\alpha$  value in the figure will also directly affect the revenue of the content provider. The larger the  $\alpha$  value, the more popular the content provided by the

content provider, and thus the higher the revenue value of the content provider within the network.

Figure 5 is a diagram illustrating the number of repetitions of different algorithms and alpha's revenue relationship with the content provider. As can be seen from Figure 5, in the case of different algorithms, the ProbCache policy only determines the content cached by the network based on the weighted probability value of the content and does not fully consider the conflict relationship between the content providers in the network. QoSP policy caches content according to users' QoS requirements, which improves the revenue of content providers to a certain extent. However, GOS policy fully considers the competitive relationship among content providers in the network, and the revenue of content providers is higher than QoSP policy. Because the GOS strategy has some limitations in taking global revenue as the objective function of the strategy, the revenue value of content providers is lower than that of this strategy.

Figure 6 is a diagram illustrating the relationship between the number of content requests and the average cache hit rate in different algorithms. As shown in Figure 6, the number of requests increases and the cache hit ratio increases gradually. ProbCache determines the content of cache according to the weighted probability value, which effectively improves the cache hit rate of content, so the cache hit rate is the highest. The lowest hit rate of GOS cash is because GOS strategy only considers the overall income and does not consider the index of cash hit rate in detail. QoSP considers content hit ratio, but because of the request for latency value in user QoS, it can sacrifice a part of the revenue of content provider to meet the latency limit. The strategy of this paper fully considers the cash hit rate. The game model introduces the popularity and preference of content into the income function and effectively improves the cache hit rate of the network by influencing the income of content providers through the feedback of cash rate index.

Figure 7 shows a small relationship between the number of content requests and the relative energy consumption in different algorithms. As can be seen from Figure 7, with the increase of requests, the reduction rate of relative energy consumption also increases. Compared with other schemes, the reduction rate of energy consumption of the algorithm adopted in this paper has obvious advantages. Because other strategies do not consider the index of energy consumption, the energy consumption performance is relatively poor.

## 7. Conclusion

According to the development trend of caching and computing resource allocation in 5G mobile communication networks, in order to improve the efficiency of content caching and reduce network energy consumption, this paper proposes a strategy of optimizing 5G network caching based on Stackelberg game, which models network operators and content providers as the multimaster and multislave Stackelberg game model. Providers purchase base station storage space from network operators to cache popular content, so as to achieve high-performance computing of 5G communi-

cation network and optimize resources, and the reduction rate of energy consumption has obvious advantages compared with other schemes.

## Data Availability

The data used to support the findings of this study are available from the corresponding author upon request.

## Conflicts of Interest

The author declares no conflicts of interest.

## References

- [1] R. Torre, I. Leyva-Mayorga, S. Pandi, H. Salah, G. T. Nguyen, and F. H. P. Fitzek, "Implementation of network-coded cooperation for energy efficient content distribution in 5G mobile small cells," *IEEE Access*, vol. 8, pp. 185964–185980, 2020.
- [2] Q. Zhou, L. Chen, G. Li, and Z. Zhang, "Research on Internet of Things technology," in *Computer, Informatics, Cybernetics and Applications. Lecture Notes in Electrical Engineering*, X. He, E. Hua, Y. Lin, and X. Liu, Eds., vol. 107, pp. 253–260, Springer, Dordrecht, 2012.
- [3] S. Maharjan, Y. Zhang, and S. Gjessing, "Economic approaches for cognitive radio networks: a survey," *Wireless Personal Communications*, vol. 57, no. 1, pp. 33–51, 2011.
- [4] T. Zhang, Y. Wang, Y. Liu, W. Xu, and A. Nallanathan, "Cache-enabling UAV communications: network deployment and resource allocation," *IEEE Transactions on Wireless Communications*, vol. 19, no. 11, pp. 7470–7483, 2020.
- [5] Y. Fu, L. Salaun, X. Yang, W. Wen, and T. Q. S. Quek, "Caching efficiency maximization for device-to-device communication networks: a recommend to cache approach," *IEEE Transactions on Wireless Communications*, p. 1, 2021.
- [6] J. Xia, C. Li, X. Lai et al., "Cache-aided mobile edge computing for B5G wireless communication networks," *EURASIP Journal on Wireless Communications and Networking*, vol. 2020, no. 1, 2020.
- [7] Y. Qian, L. Shi, L. Shi, K. Cai, J. Li, and F. Shu, "Cache-enabled power line communication networks: caching node selection and backhaul energy optimization," *IEEE Transactions on Green Communications and Networking*, vol. 4, no. 2, pp. 606–615, 2020.
- [8] L. Kang, R. S. Chen, Y. C. Chen, C. C. Wang, X. Li, and T. Y. Wu, "Using cache optimization method to reduce network traffic in communication systems based on cloud computing," *IEEE Access*, vol. 7, pp. 124397–124409, 2019.
- [9] I. Shayea, M. Ergen, M. Hadri Azmi, S. Aldirmaz Colak, R. Nordin, and Y. I. Daradkeh, "Key challenges, drivers and solutions for mobility management in 5G networks: a survey," *IEEE Access*, vol. 8, pp. 172534–172552, 2020.
- [10] F. H. Sun, "Research on key technologies of optimal routing design in ad hoc networks," *Applied Mechanics & Materials*, vol. 380–384, pp. 2312–2315, 2013.
- [11] M. Lou and J. Xiao, "Dynamic, tagless cache coherence architecture in chip multiprocessor," *Advances in Intelligent Systems and Computing*, vol. 277, pp. 201–209, 2014.
- [12] N. Li, Y. Wang, S. Li, and Z. Wang, "Research on relations between Two PWM technologies and system performance optimization," in *Proceedings of the 7th International Power*

- Electronics and Motion Control Conference*, pp. 2333–2337, Harbin, China, 2012.
- [13] A. Gupta and R. K. Jha, “A survey of 5G network: architecture and emerging technologies,” *IEEE Access*, vol. 3, pp. 1206–1232, 2015.
- [14] H. Sedghani, D. Ardagna, M. Passacantando, M. Z. Lighvan, and H. S. Aghdasi, “An incentive mechanism based on a Stackelberg game for mobile crowdsensing systems with budget constraint,” *Ad Hoc Networks*, vol. 123, article 102626, 2021.
- [15] M. Luo, Y. Pei, and W. Huang, “Mutual heterogeneous sign-cryption schemes with different system parameters for 5G network slicings,” *Wireless Netw*, vol. 27, no. 3, pp. 1901–1912, 2021.
- [16] X. Wang, P. Sun, and Y. Zhang, “Notice of retraction: research on key technologies of polymorphous and heterogeneous data collection for ocean ship,” in *International conference on logistics Engineering and intelligent transportation systems*, pp. 1–5, Wuhan, China, 2010.
- [17] X. Kang, R. Zhang, and M. Motani, “Price-based resource allocation for spectrum-sharing femtocell networks: a Stackelberg game approach,” *IEEE Journal on Selected Areas in Communications*, vol. 30, no. 3, pp. 538–549, 2012.
- [18] M. He, Y. Jin, H. Zeng, and J. Cao, “Pricing decisions about waste recycling from the perspective of industrial symbiosis in an industrial park: a game model and its application,” *Journal of Cleaner Production*, vol. 251, article 119417, 2020.
- [19] L. Xia and L. Hai, “A seamless transfer strategy based on multi-master and multi-slave microgrid,” in *2018 9th IEEE International Symposium on Power Electronics for Distributed Generation Systems (PEDG)*, pp. 1–5, Charlotte, NC, USA, 2018.
- [20] J. Ma and H. Ren, “The impact of variable cost on a dynamic Cournot-Stackelberg game with two decision-making stages,” *Communications in Nonlinear Science and Numerical Simulation*, vol. 62, pp. 184–201, 2018.
- [21] S. V. Melnikov, “Stackelberg-Nash equilibrium in the linear city model,” *Automation and Remote Control*, vol. 81, no. 2, pp. 358–365, 2020.
- [22] Y. T. Zhan, X. S. Li, and N. J. Huang, “A Stackelberg-population competition model via variational inequalities and fixed points,” *Carpathian Journal of Mathematics*, vol. 36, no. 2, pp. 331–339, 2020.
- [23] S. Sharma, V. Sharma, and A. Goyal, “QoS analysis of multi priority DCF algorithm in wireless local area network,” *International Journal of Computer Sciences and Engineering*, vol. 7, no. 6, pp. 291–294, 2019.
- [24] S. Tang, J. Yuan, Z. Zhang, and D. Z. Du, “iGreen: green scheduling for peak demand minimization,” *Journal of Global Optimization*, vol. 69, no. 1, pp. 45–67, 2017.

## Research Article

# A Machine Learning Approach for Improving the Movement of Humanoid NAO's Gaits

**Fatmah Abdulrahman Baothman** 

*Faculty of Computing and Information Technology, King Abdulaziz University, Jeddah 21431, Saudi Arabia*

Correspondence should be addressed to Fatmah Abdulrahman Baothman; [fbaothman@kau.edu.sa](mailto:fbaothman@kau.edu.sa)

Received 22 April 2021; Revised 16 May 2021; Accepted 4 September 2021; Published 22 September 2021

Academic Editor: Deepak Gupta

Copyright © 2021 Fatmah Abdulrahman Baothman. This is an open access article distributed under the Creative Commons Attribution License, which permits unrestricted use, distribution, and reproduction in any medium, provided the original work is properly cited.

A humanoid robot's development requires an incredible combination of interdisciplinary work from engineering to mathematics, software, and machine learning. NAO is a humanoid bipedal robot designed to participate in football competitions against humans by 2050, and speed is crucial for football sports. Therefore, the focus of the paper is on improving NAO speed. This paper is aimed at testing the hypothesis of whether the humanoid NAO walking speed can be improved without changing its physical configuration. The applied research method compares three classification techniques: artificial neural network (ANN), Naïve Bayes, and decision tree to measure and predict NAO's best walking speed, then select the best method, and enhance it to find the optimal average velocity speed. According to Aldebaran documentation, the real NAO's robot default walking speed is 9.52 cm/s. The proposed work was initiated by studying NAO hardware platform limitations and selecting Nao's gait 12 parameters to measure the accuracy metrics implemented in the three classification models design. Five experiments were designed to model and trace the changes for the 12 parameters. The preliminary NAO's walking datasets open-source available at GitHub, the NAL, and RoboCup datasheets are implemented. All generated gaits' parameters for both legs and feet in the experiments were recorded using the Choregraphe software. This dataset was divided into 30% for training and 70% for testing each model. The recorded gaits' parameters were then fed to the three classification models to measure and predict NAO's walking best speed. After 500 training cycles for the Naïve Bayes, the decision tree, and ANN, the RapidMiner scored 48.20%, 49.87%, and 55.12%, walking metric speed rate, respectively. Next, the emphasis was on enhancing the ANN model to reach the optimal average velocity walking speed for the real NAO. With 12 attributes, the maximum accuracy metric rate of 65.31% was reached with only four hidden layers in 500 training cycles with a 0.5 learning rate for the best walking learning process, and the ANN model predicted the optimal average velocity speed of 51.08% without stiffness:  $V_1 = 22.62$  cm/s,  $V_2 = 40$  cm/s, and  $V = 30$  cm/s. Thus, the tested hypothesis holds with the ANN model scoring the highest accuracy rate for predicting NAO's robot walking state speed by taking both legs to gauge joint 12 parameter values.

## 1. Introduction

Engineers have investigated humanoid walking in the area related to control, stability, and speed in simulated or real environments, focusing on hardware design and functions. Walking is a complicated process that involves several domains in different planes such as sagittal, frontal, and transverse; it requires vision, several joints, muscles, and awareness, and the speed cycle varies with human body structure, strength, stability, and others. Humanoid NAO

provides a good research platform for bipedal locomotion to perform different walking styles such as static, forward, and sideways. Aldebaran builds NAO for an international football competition based on movements and collaboration between robot agents, and speed is crucial for football sports. Although walking is a complex problem, the author simplifies the assumption to determine which classification techniques can improve NAO's gaits' speed and, if so, which one is the most successful without applying any mechanical changes to the structure. The hypothesis is as follows:



$H_0$  is the humanoid NAO speed that can be improved without changing its physical configuration.

$H_1$  is the humanoid NAO speed can be improved without changing its physical configuration.

In this research, the author tests if the  $H_0$  hypothesis holds. If " $H_0$ " is true, the inference would be that the humanoid robot NAO's speed velocity can be improved without changing its physical structure. If " $H_0$ " is false, the conclusion would be that there is no need to concentrate on classification techniques without changing the physical design. The Robotic Industries Association (RIA) [1] defined "a robot as a reprogrammable multifunctional manipulator designed to move material, parts, tools or specialized devices through variable programmed motions for the performance of a variety of tasks." Sometimes, robots are categorized in production according to the time frame and characteristics. The first robot generation in the 1970s was stationary, non-programmable, and described as electromechanical devices without sensors [2]. The second robot generation appeared in the 1980s and included sensors plus programmable controllers. The third robot generation was developed in the 1990s with some intelligence characteristics, while the fourth generation is under the R&D phase [3], embedding advanced intelligent features of miniaturization, growth, autoreplication, and autoassembly. The word "Robot" was first introduced in 1890 and used by Karel Capek; in 1921, it was mentioned in his known play (Rassum's Universal Robots) and entered the English dictionary in 1923. Six years later, Westinghouse, Electric introduced the robot "Elektro," with some walking capabilities. After a few years, Walter completed the two autonomous robots called Elmer and Elsie. In 1968, Stanford Research Institute (SRI) created "Shakey" who can plan and move objects [4]. In the 80s, Honda produced its first robot called H0 by 2000, and "Asimo" went to the market and has walking capabilities.

Robots are created in many shapes and structures, such as an ant-like tiny structure [5, 6]. Some are as huge as the Japanese giant robot Gundam, which weighs 24 tons and 60 feet high. Robots can perform a particular task or multi-tasks for industry, security, service, research, education [7], or entertainment purposes. For example, the ancient Japanese created the robot kimono-clad for entertainment and Chahakobi Ningyo for tea-serving. They enabled the Robot Buddha to learn from nature's law and Astroboy to go to a regular school with human children [8–10]. Thus, robots became socially interactive, mimicked human behavior, and understanding [11], such as Sophia, the first robot granted a Saudi nationality. Such behaviors highlighted the advancement and versatility in the artificial intelligence (AI) field to improve robots' value to replace humans in repetitive tasks and services. For example, KUKA, the Lightweight Robot [12], with a control architecture, unlike Jijo-2, was designed to serve in an office environment [13]. These robots need special training to attain the specific task's knowledge and sense to employ walking in an environment. Empowering robots with walking capabilities by teaching them to advance their performance requires ethical standards, laws, and regulations to match human values. In the 40's, Asimov [14] described three basic laws for controlling

robots' behaviors, a robot must not destroy a human being, a robot must abide by the orders given, and a robot must protect its own existence. Chien et al. argued the necessity of modifying the three rules for robot home services and ethical purposes [15, 16]. Recently, a superior professor of artificial intelligence, Frank Pasquale, argued that Asimov rules should be updated by four more principles regarding the concept of augmented AI [17]:

"Law 1: AI should complement professionals, not replace them.

Law 2: Robotic systems and AI should not counterfeit humanity.

Law 3: Robotic systems and AI should not intensify zero-sum arms races.

Law 4: Robotic systems and AI must always indicate the identity of their creator (s), controller (s), and the owner (s)."

Although robots were invented in the last century, robotic designers are still facing significant challenges, and continuous developments are required for creating autonomous walking robots to perform multitasks service. Different materials were used to overcome such design challenges, for example, robots such as Manav, Mitra, INDRO, and Daksh are made of 3D-printer, fiberglass, wood, cardboard, plastic, and aluminum. Intelligent living robots are innovative inventions mimicking humans' behavior, and some can even perform tasks that seem impossible for humans to accomplish as fast with high accuracy. The robotic era of 2020 has also covered many sectors, including education and research supporting humanoid walking robots, for example, a robot agent presented by [18] named "Interactive Phantom" supported medical education in orthopedic for knee joint clinical inspection training. The International Federation of Robotics (IFR) indicated that the robot market in education, research, and entertainment would significantly increase [19]. Robots with moving capabilities can now work in car shops, production industries [20], packaging, medical services [21], and hotel services, leading to complete replacements of humans with the robots dentist, surgeon, and nurse. Such [22] humanoid robots can perform tasks and move like humans. This type of robot represents a challenging approach in the area of multicontrol, intelligent, and evolutionary robots. Nowadays, some humanoid robots accomplish extraordinary responsibilities that are considered even challenging for humans to perform.

According to Ray Kurzweil, computers will be as smart as humans by 2029, and by 2045, they would be billions of times more powerful than humans [23]. In the 21st century, intelligent humanoid robots were produced to imitate humans' capabilities to communicate, sing, dance, perform detailed tasks better than humans, and even design or manufacture another robot. The word humanoid robot describes a physical structure similar to a human having a head, body, hands, and two legs (biped). Some humanoid robots have one or more parts of the body: upper or lower torso and a head equipped with human facial features. A humanoid robot's main characteristic is its autonomous adaptation in changing its environments and imitating humans' physical and mental tasks in intelligence, cognition, behavior, and

actions. The humanoid robots are one of the greatest inventions of the century; designing them to move, walk, and run like humans, or faster is essential even in evolutionary robotics (ER). The ER robots [24] require autonomous design and implementation for robot control and structure to develop comprehensive knowledge about itself, its walking behavior, and the environment, but the speed of gaits is still an issue for robots to perform human-like jobs. Thus, the robot's legs and feet should be designed carefully with full functionalities.

Developing intelligent humanoid robot characteristic is challenging and too complicated. For example, babies take several months before they learn their first step and start walking, due to gravity effects, the body weight, and the learning technique, which is self-developed by the child at an early stage. The process of human walking is highly complicated and dynamic in nature; it involves 29 Degree of Freedom (DoF) and 48 muscles for coordination. It includes the eyes, legs, joints, hip, knees, ankles, the upper body, and the basin. With such complexities of a walking cycle, [25] identified sixteen states. NAO walking technique has been evaluated and a trapezoid function augmented by [24] for implementing an improved dynamic walk. [26] introduced an omnidirectional walk, using ZMP [27, 28] centered on low motor stiffness to help fast movements. The current research mainly focuses on NAO's walking and movement learning without changing the hardware configuration. The author focused only on gaits and speed/velocity, excluding vision, navigation, uneven floor, turning around, or going up or down. The main idea is to implement AI, classification, and learning techniques to test the robot NAO walking speed. Such characteristics are considered to add an intelligence flavor to any humanoid robot. The advantages of the proposed methods are small number of parameters, low memory requirements during the testing and training process, and most importantly, the optimal average velocity speed obtained of  $V_2 = 40$  cm/s for the humanoid real robot NAO and the improved average velocity speed of 51.08% without stiffness during walking.

The research contributions are as follows:

- (i) Analyzing NAO's gaits with only 12 parameters to improve the real robot walking speed of 9.52 cm/s
- (ii) Applying three classifications techniques, an ANN model with 12 parameters accomplished an improved average velocity speed of 51.08% without stiffness
- (iii) Achieving an optimal average velocity speed of  $V_2 = 40$  cm/s for the humanoid the real robot NAO
- (iv) NAO's gait speed can be improved without changing its physical structure configurations

This paper is structured to cover six primary sections. Section 2 briefly presents the NAO platform and architectural limitations. Section 3 discusses the biped robots and gaits control. Following this, Section 4 introduces the methodology and techniques, and in Section 5, the author discusses the experiment's design, implementation, and results. Finally, Section 6 summarizes the work and proposes future directions.

*1.1. NAO Platform and Architecture Limitations.* Humanoid biped robots such as NAO are used in the Robot World Cup Initiative, which started in 1992 as the Robot J-League (Japan). The initiative objective is "By the year 2050, a team of fully autonomous humanoid robots can win the world soccer champion against the human" [1]. The initiative areas are AI, machine learning (ML), machine vision, image processing, natural language processing, multiagents, team planning, electronics, and control. Aldebaran created the NAO humanoid robot's evolution several generations (V3+, V3, 2, V4, V5, V6) of NAO existed. The latest generation is considered the most powerful, stronger, and smarter autonomous and programmable robots specially designed for educational and research purposes [29]. NAO became famous, and more than 70 countries have been using NAO for computer and science classes either in schools, colleges, or universities. This research focuses on the NAO humanoid robot, and (Table 1) below lists the joints chains of the 12 legs and feet parameters that are only related to this work:

The NAO robot consists of a head, torso, motors, actuators, multiple sensors, sonar, and bump sensors in hands and feet, gyrometer, accelerometer, and infrared. The body's structure is made of plastic, which lacks movement flexibility. "Nao has 25 Degrees of Freedom (DoF) (Head: 2 DoF; Arm: 5 DoF x 2; Pelvis: 1 DoF; Leg: 5 DoF x 2; Hand: 1 DoF x 2)" [30] as visualized in (Figure 1) describing 24 joints. NAO weight 5.4 kg, 574 mm in height, Intel Atom E3845 processor, built-in Linux (Gentoo) OS, and equipped with two CPUs located on the head and the torso. NAO can see via two OV5640  $2592 \times 1944$  digital cameras and has loudspeakers and microphones to hear and talk in two default languages but can be upgraded to 21 languages; the author was among the pioneers of building and activating the Arabic language in human-robot interaction (HRI). The robot NAO can also connect over Ethernet or Wi-Fi. It is equipped with rechargeable battery powers that work only 60 minutes in active use and 90 minutes in regular use. Although its obstacle detection capability and battery power have improved to 30 percent [28, 31] in the latest generation, NAO still needs more development to match an adult human's walking patterns and time duration. However, NAO's velocities, accelerations, and inclinations are measured dynamically.

The software platform supports Linux, Windows, and Mac operating systems. The NAO robot can be programmed in several languages: C++, MATLAB, Urbi, JAVA, LabVIEW, Python, and JavaScript. The Choregraphe is a multiplatform supported with a visual programming language to create unprogrammed animations and behaviors with Python and C++ for testing, simulation, interaction, control, and monitoring the physical robot NAO with the NAOqi tool (see Figure 2). The NAOqi is a middleware that connects with the main broker via modules [32]; it interfaces with motor joints, interacts with the Linux-Geode operating system, and performs many actions using (ALMotion).

A screenshot of the Choregraphe software (see, Figure 3) represents a graphical user interface to initiate behaviors by connecting boxes of preprogrammed code to support testing the robot's joint angles control via the ALMotion proxy. The

TABLE 1: NAO 12 leg joint chains [Aldebaran documentation].

The chain	LLeg	RLeg
The joints	LHipYawPitch	RHipYawPitch
	LHipRoll	RHipRoll
	LHipPitch	RHipPitch
	LKneePitch	RKneePitch
	LAnklePitch	RAnklePitch
	RAnkleRoll	LAnkleRoll

monitor software allows users to record or watching the robot’s eyesight perception and his encountered action in real-time. The simulator software is called Naosim and is used to test NAO behaviors and build new algorithms for the virtual environment, enabling object insertion and shapes modification [33]. The Linux-Geode OS offers a safety interface layer for preserving the motor joints’ durability [34]. The NAOqi software is based on a distributed system, and its components can be executed in the robot’s system or between systems. One limitation in the distributed system is that the primary process referred to as main broker must be executed on the NAO robot’s physical structure when using actuators or sensors [21].

Featuring NAO’s technical capabilities, its mechanical architecture, including hearing, speaking, walking, or seeing, has several limitations. For example, the default walking speed for NAO is limited to 9.52 cm/s. Additional constraints are related to the plastic material covering the robot’s shape; the number of fingers is only three in each hand, NAO has no toes in his feet, and the size of memory is minimal and its inability to simulate multicomplex human movements. For example, NAO could not bend his torso to 90° toward the front and keeping his balance and could not sit down while bending the knee and feet behind the body. According to Aldebaran, as in Figure 4, LHipYawPitch and RHipYawPitch cannot be controlled independently because a single motor physically controls them, and by default, in case of order conflict, LHipYawPitch has priority.

Furthermore, NAO’s initial position is required to sit down before starting any new behavior to reduce the motors’ heating. “Nao’s motion module is based on generalized inverse kinematics, which handles cartesian coordinates, joint control, balance, redundancy, and task priority” [2]. Therefore, the NAO movement is limited by its degree of freedom. There are also anticollision limitations for both right and left ankles resulting from the roll motion range limitation by the pitch value as indicated by the Aldebaran documentation in Table 2 [30] below for the left ankle joint parameters. The joints’ motor is controlled every 10 ms. Böckmann [17] proved a time delay caused by controlled joint angles between 30 ms and 40 ms.

NAO also faces frequent joint stiffness, which requires enslaving the motors, and if NAO is not in a self-stable pose, it usually loses its balance and falls. The only way to maintain the robot’s stability is by setting the walking speed to 0.2 m/s, which is very slow. Additionally, NAO requires unique standard floor surfaces to maintain its balance for a

more extended period. The best measured enabled walking distance for NAO was estimated by 3 meters.

*1.2. Biped Walking and Gaits’ Control Techniques.* Humanoid robotics is similar to humans in talking, walking, emotions, and so forth. Their way of movements covers gaits’ speed, stability, and steps’ generation. Walking robots [7] can be classified into three main classes: static, dynamic, and passive. Static walkers have regular languid walks. Passive walkers react to the forces of gravity [20, 35]. Dynamic walkers [3, 6] plan their steps with a high level of accuracy. Waseda University’s laboratories introduced WL-10, a revolutionary dynamic continuous walking robot for 1.3 seconds, using Zero Moment Point (ZMP) control; since then, several results were recorded [36, 37] in the area of passive and active walkers, parameter settings for successful walking gaits, balance, and locomotion. For example, [38] Light Adaptive-Reactive biPed (LARP) was created for modeling human lower limbs walking style within an environment using artificial feet, knees, and limbs. According to [39], three planes exist during walking for body movements within an environment: (1) “Sagittal plane - divides the body into left and right sides into a vertical plane” [40]. (2) “Frontal plane - divides the body into the front and back, related to legs and arms” [41]. (3) “Transverse plane - divides the body horizontally” in an upper and lower half associated with twisting rotation [41]. Humanoid robots implement several techniques to overcome the environments’ difficulty, such as nonlinear dynamics, multivariable dynamics, limited foot-ground interaction, hybrid dynamics during steps, quick detection of a push, fast reaction speed, and relatively large actuator power. Classification of locomotion based on swing legged has discrete contact with the ground for a walker. The popular locomotion concepts that support biped are the swing-legged discrete and big-footed (SDB) applied in most of today’s robots using flat ground with stability [37]. Generally, the gaits consist of 3 phases, and each has different frames and defined actions. Table 3 below summarizes the phases.

According to [42], there are nine gait parameters for the controller on flat ground: step length, step height, knee bending, step time, stretch time, torso pitch inclination, quadratic Bezier point, torso roll inclination, and proportion of single support duration. They defined a fitness for the gait’s stability and gait’s energy consumption and implemented a policy gradient reinforcement learning (PGRL) for optimization. The results showed that exploiting the physical robot’s hardware positively impacts without implementing complex deep learning or complex mathematical models. Previous research [36] applied to three walking humanoids Priscilla, ELVIS, and ELVINA reported improved forward walking speed. Reinforcement learning in robots [34] using different techniques [37, 43] surveyed learn from demonstration (LfD) methods. [44] illustrated artificial neural network (ANN) to extract parameters, predict walking patterns, and identify robot’s gait learning errors. In this research, the author shows that the humanoid NAO speed can be improved without changing its physical structure using machine learning techniques.

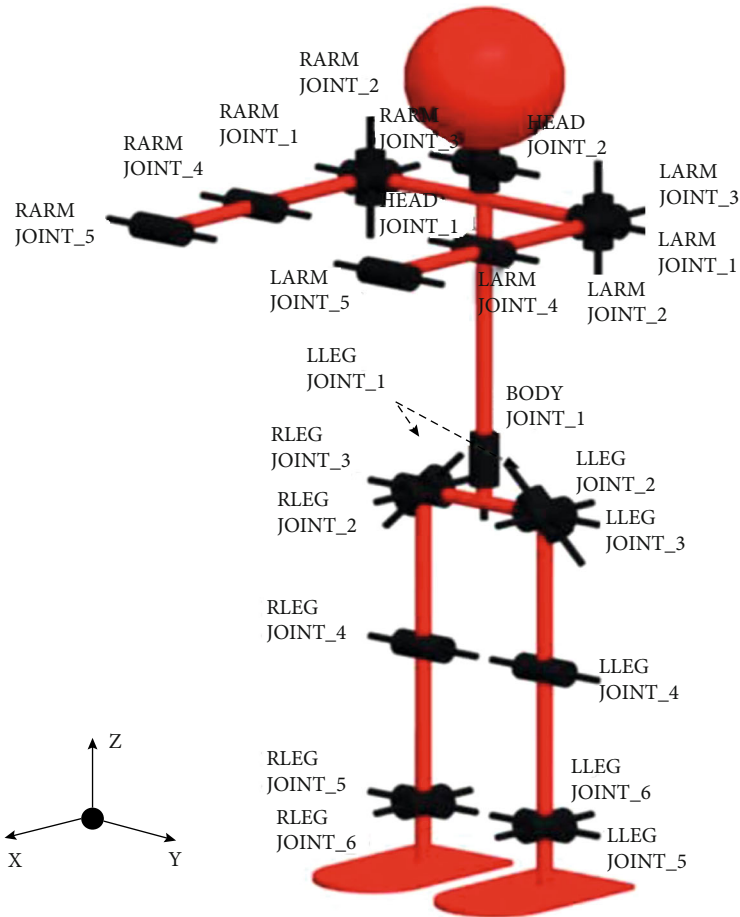


FIGURE 1: NAO 24 joints: 12 parameters for legs and feet and 12 for hands and arms.

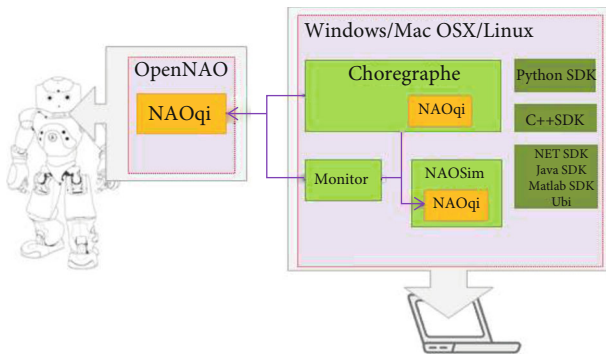


FIGURE 2: Aldebaran NAO NAOqi tool structure [32].

## 2. Materials and Methods

Some machine learning (ML) techniques do not require extensive training, offer quicker time execution for training models, and operate on any machine. ML uses algorithms such as XGBoost, which is impossible to understand its details. There are three main types of ML. Supervised learning is known as classification techniques; the data are labeled for the classification observations process’s training phase. Unsupervised learning is known as clustering techniques, in which the model is fed with unknown unlabeled data to

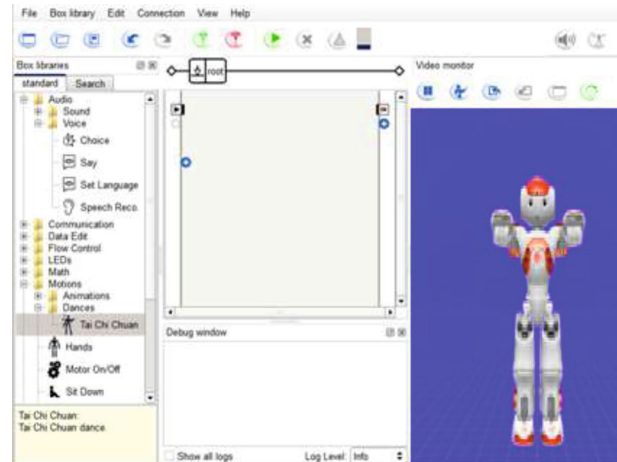


FIGURE 3: Choregraphe graphical interface.

form clusters, involving cluster analysis based on similarity metric, estimated density, and graph connectivity for financial systems [45]. Reinforcement learning implements dynamic programming techniques, for example, used in autonomous cars. ML needs models to operate such as artificial neural networks (ANNs), decision trees, support vector machines (SVMs), regression analysis, Bayesian network,



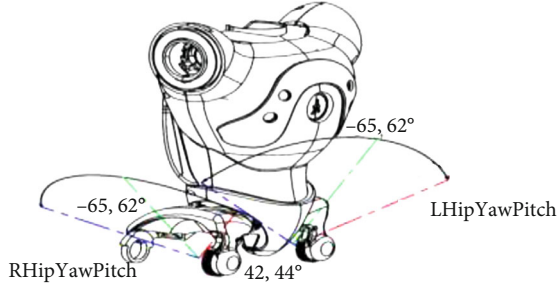


FIGURE 4: Single motor control for LHip and RHip.

and genetic algorithm (GA). Usually, model performance and validation for accuracy are measured using the holdout method,  $K$ -fold crossvalidation, sensitivity, and specificity. The ML algorithms are related to building a computational model to train sample data to assist in predictions or decision-making. The classification is a two-step process that involves model construction and model usage. Figure 5 describes the process for NAO's walking pattern.

The first phase is model construction and defines a data set of NAO's walking parameters, represented by two classes: distance and speed of the step cycle walking. The data is divided into two sets for model construction (training set and testing set). The model usage is implemented for classifying unknown walking patterns; it estimates the model's accuracy metrics. The previously defined label for testing is paired with the model classification outcome. The model accuracy metric is determined by the correct percentage of the classified testing data, which is the focus of this work. The test dataset consists of 25% of all the data, while the training set is equal to 75%. The optimization of the training process has to be carefully determined; otherwise, an overfitting will occur. Using the model to classify unknown data for distance and speed classes is the primary concern of this stage. For example, in the first step, the training data (see, Table 4) is collected for each step cycle for the robot Noa concerning (distance, speed time), and the classification algorithm is invoked to complete the model construction with a defined conditional set of rules such as (IF NAO distance/ $m$  = "3" OR time/ $s$  > 6 then the return value = "success"), which results in a success score for step cycle two, three, and four.

A new dataset was introduced during model usage (see Table 5), and the classifier is tested for unseen data records (11, 1, 9). The results indicate a successful step cycle according to the model construction rules. Thus, prediction models estimate and forecast unknown values.

Robot walking requires path planning algorithms; planning is either static or dynamic depending on how often the robot's map reading updates. The author implements three ML models for NAO's walking: (1) decision tree, (2) Naive Bayes, and (3) artificial neural network. Figure 6 below shows the walking learning pattern's overall design for this work.

The decision tree is based on a root node and branches. Each node represents a test, and the branch refers to the

result, with each node leaf holds a class label. The tree is constructed in a top-down approach with an iterative technique. All the training data starts at the top, which is called the tree root. The algorithm recursively selects the attributes and partitions. The test attributes are chosen according to statistical measures such as information gain. The stopping condition is set if all samples end up in the same class, or no more attributes can be further partitioning, or there are no samples left. The most critical issue with the decision tree is determining the best splitting criteria for the records. Usually, one of the three measures is applied: Gini index, entropy, or information gain. The Gini index for the ( $t$ ) node is defined by [46]:

$$\text{GINI}(t) = 1 - \sum_j [p(j|t)]^2. \quad (1)$$

$p(j|t)$  represents the probability of the  $j$  class at node  $t$ , while  $(1-1/n_c)$  calculates the maximum number of distributed records indicating the minimum least interesting information becomes (0.0) if all records fall in a single class, which means the most interesting information.

The entropy measure at a given node  $t$  is defined by [46]:

$$\text{Entropy}(t) = - \sum_j p(j|t) \log p(j|t) \quad (2)$$

$p(j|t)$  represents the probability of the  $j$  class at node  $t$ . For measuring the node's homogeneity, the minimum (0.0) is reached if all records fall in a single class, and the maximum ( $\log n_c$ ) is calculated if records are equally disseminated within all classes implying the most information.

Thus, information gain (IF) selects the split that maximizes the GAIN; it prefers splits with a large number of partitions and is defined by [46]:

$$\text{GAIN}_{\text{split}} = \text{Entropy}(p) - \left( \sum_{i=1}^k \frac{n_i}{n} \text{Entropy}(i) \right), \quad (3)$$

where the root node  $p$  defined by the entropy is divided into  $k$  classes, and  $n_i$  represents the record number in class  $i$ .

The second classification technique implemented is the Naive Bayes, based on a statistical probabilistic classifier using Bayes' theorem features strongly independent. It requires a small amount of data for training, and it is extremely fast compared to other classification techniques. Given  $X$  as the data training set, the posteriori probability of  $H$ ,  $P(H|X)$ , comes from the Bayes theorem [46].

$$P(H|X) = \frac{P(X|H)P(H)}{P(X)}, \quad (4)$$

where  $X$  belongs to class  $C_2$  if the probability  $P(C_i|X)$  is the highest for all the  $k$  classes in  $P(C_k|X)$ . The maximum posteriori of  $P(C_i|X)$  can be found from the following



TABLE 2: Left joint ankle parameter values [30].

LAnklePitch (degrees)	LAnkleRoll min	LAnkleRoll max	LAnklePitch (degrees)	LAnkleRoll min (radians)	LAnkleRoll max (radians)
-68.15	-2.86	4.30	-1.189442	-0.049916	0.075049
-48.13	-10.31	9.74	-0.840027	-0.179943	0.169995
-40.11	-22.80	12.61	-0.700051	-0.397935	0.220086
-25.78	-22.80	44.06	-0.449946	-0.397935	0.768992
5.73	-22.80	44.06	0.100007	-0.397935	0.768992
20.05	-22.80	31.54	0.349938	-0.397935	0.550477
52.87	0.00	2.86	0.922755	-0.000000	0.049916

TABLE 3: Gaits' phases.

Phase	Name	Frame numbers	Repetition	Action
One	Start	11	0	Define a state from inactive to an active state, causing the robot to go into the next phase
Two	Walk	44	Many times	Take two steps to go again into an inactive position
Three	Stop	11	0	The robot moves to the start inactive situation

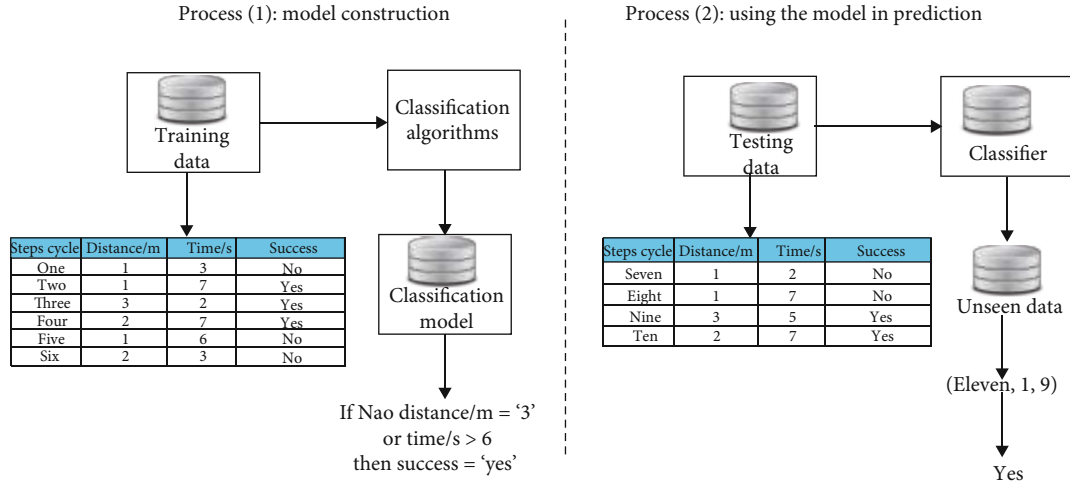


FIGURE 5: Two-step classification process for NAO's walking pattern.

TABLE 4: Conversion of sample data model building.

Steps cycle	Distance/m	Time/s	Success
One	1	3	No
Two	1	7	Yes
Three	3	2	Yes
Four	2	7	Yes
Five	1	6	No
Six	2	3	No

TABLE 5: Conversion of sample data model usage.

Steps cycle	Distance/m	Time/s	Success
Seven	1	2	No
Eight	1	7	No
Nine	3	5	Yes
Ten	2	7	Yes

Bayes' theorem equation:

$$P(C_i | X) = \frac{P(X | C_i)P(C_i)}{P(X)}. \quad (5)$$

Since  $P(X)$  is the constant number for all given classes, then

$$P(C_i | X) = P(X | C_i)P(C_i) \text{ can be maximized.} \quad (6)$$

The ANN is a mathematical model that emulates a biological neural network in design, processing, learning, etc. It can solve engineering problems using classification, clustering, and regression. The architecture is described by a set of neurons arranged in three primary layers (input, hidden, and output). A nonlinear function defines

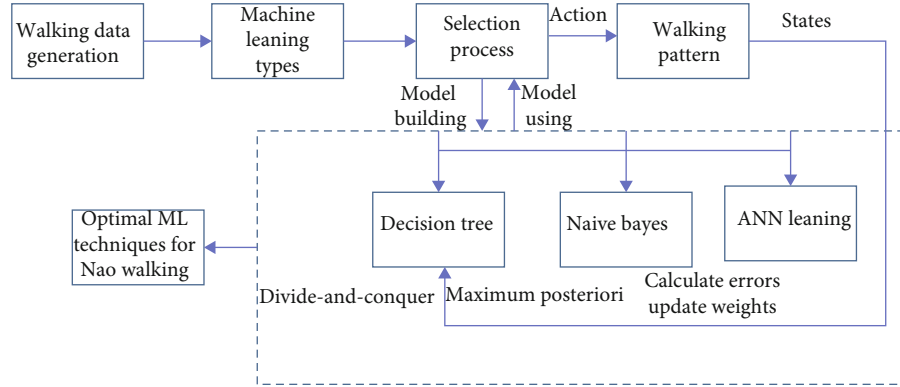


FIGURE 6: Diagram of ML for NAO's walking pattern.

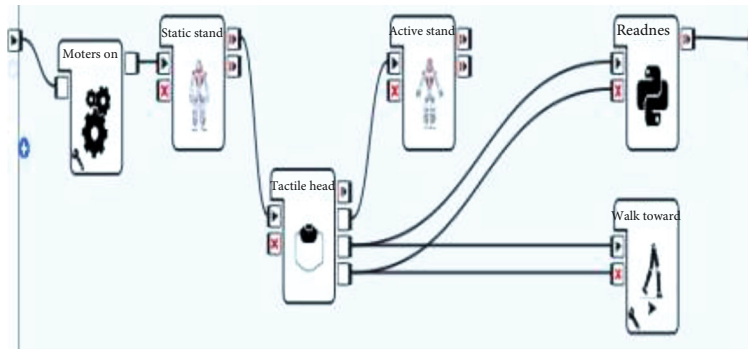


FIGURE 7: Choregraphe screenshot for activating NAO's walking data collection.

it as follows [47]:

$$\text{net}_j = \sum_i W_{ij}x_{ij} = W_{0j}x_{0j} + W_{1j}x_{1j} + \dots + W_{Ij}x_{Ij}, \quad (7)$$

where for node  $j$ ,  $x_{ij}$  is the  $i$ th input,  $W_{ij}$  is the weight related to the  $i$ th node,  $i + 1$  inputs to node  $j$ ,  $x_1, x_2, \dots, x_I$  are inputs from upstream nodes,  $x_0$  is the constant input value = 1.0, and each input node has extra input  $W_{0j} \times 0j = W_{0j}$ .

The complete designed methodology in this work is represented in Figure 6 above. The preliminary training data robot's walking data was collected automatically using the Choregraphe software (see Figure 7 below). Walking gaits are constructed by developing visual boxes representing the walking Python code, the joint movements, and speed activity.

This study used different ML types to test the fastest walking technique. The two-step process model building and model using implemented to calculately divide and conquer in the case of the decision tree, maximum posterior in the case of Naive Bayes, and errors minimization with weights updates in the ANN's case. The walking pattern was learned and generated based on every classification technique. The learning process is repeated until the physical robot NAO shows improving performance. The idea is to find the optimal walking algorithm, as in humans, to measure improvement when simulating a human walking pat-

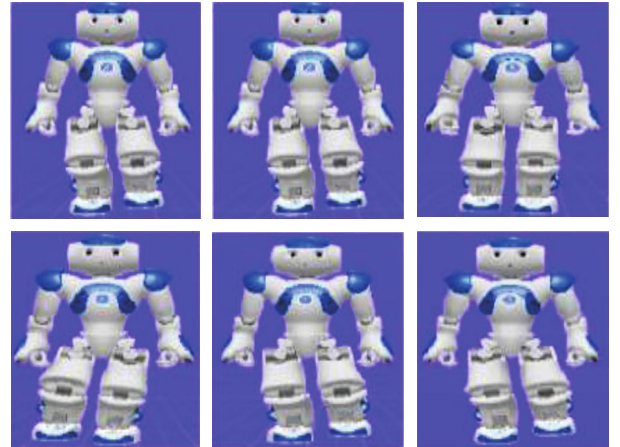


FIGURE 8: NAO humanoid movement records.

tern. The practical experiments were carried out, as explained in Section 5 below. This study had several limitations. First, it was impossible to check all classification techniques; so, the authors limited the techniques to the three abovementioned most researched ones. Second, the domain knowledge includes engineering, medical, mathematics, computer science, artificial intelligence, planning, machine learning, and data mining; therefore, the author focused on AI/ML techniques to limit the searched domain. The study covered only the humanoid robot NAO platform because

TABLE 6: Max-min list of collected walking attributes.

Right leg values	Variables	Min-max	Left leg values	Variables	Min-max
Right ankle roll	RAr	-44.1 to 22.8	Left ankle roll	LAr	-22.8 to 44.1
Right ankle pitch	RAp	-68.0 to 53.4	Left ankle pitch	LAp	-68.1 to 52.9
Right knee pitch	RKp	-5.3 to 121.0	Left knee pitch	LKp	-5.3 to 121.0
Right hip pitch	RHp	-88.0 to 27.7	Left hip pitch	LHp	-88.0 to 27.7
Right hip yaw pitch	RHyp	-65.6 to 42.4	Left hip yaw pitch	LHyp	-65.6 to 42.4
Right hip roll	RHR	-45.3 to 21.7	Left hip roll	LHR	-21.7 to 45.3

of the research budget limitation. The NAO platform has its limitation, as discussed in the NAO platform.

### 3. Results and Discussion

NAO is taken for the collection of data associated with its gaits joint parameter. In total, there are 26 joints, including the head, arm, and leg, which further split in the right and left sides. The author focuses on the walking pattern only on the first stage of the physical NAO's different actions during data capturing are shown in Figure 8.

Using NAO robots connected with the Choregraphe interface, only 12 attributes were selected to prepare the feeding for ANN. The list and details of each attribute presented in Table 6 [48]. The selection of attributes is based on NAO's movement, parts' connection, and the association between leg joints. Each attributes, high, and low values, as recorded in Table 6, depending on its maximum and minimum stretching of both legs. The selection of gaits has shown in Figure 9.

**3.1. Data Preparation.** The experiment starts by collecting all gaits joints' parameters for the NAO robot generated by both legs and analyzes the walking and standing patterns. Altogether, there are 12 attributes listed in Table 7 below; each row represents the standing or walking position of the robot. A new column was added to classify the data named "Position" based on the integer values extracted from gaits parameters. This column has two values assigned according to the remaining attribute's specification, where "0" denotes standing while "1" denotes the robot's waking state, respectively. The collected datasets are 5000 records altogether. The data has been shuffled randomly after the assignment of its position. The datasets are preprocessed through different techniques, such as outlier treatment and finding missing datasets to apply neural networks to predict their states and performance vector. To work further, 75% of the total datasets selected as training datasets to "Train" the model, while the remaining 25% associated with "Testing" the model. While selecting datasets for training and testing, the model was performed randomly using a "Validation" operator in RapidMiner [49] (see Table 7, representing RapidMiner values).

**3.2. Experiment Design, Results, and Discussion.** Several experiments were applied to discover the walking pattern and to predict the accuracy by testing the model. For this,

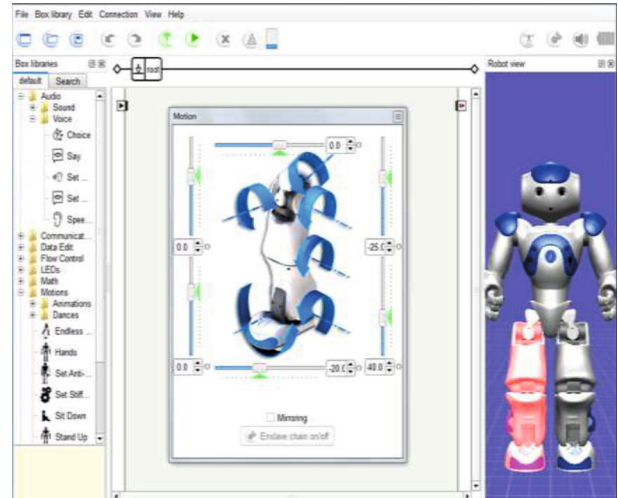


FIGURE 9: Selection of gaits.

RapidMiner has taken for building, testing, and validating the model and finally extracts the accuracy of the model. A RapidMiner is an open-source tool specially designed for data mining and applying different AI and statistical methods [45]. In this research, the classification technique implemented to construct, predict, and measure the performance of the model. Therefore, the first data sliced into two sections, "Training" and "Testing," using split validation operator, further discussed in each experiment section as follows:

**3.3. Classification Using Naïve Bayes (Experiment 1).** Many ML methods have been used in this study to provide accurate implementation due the capacity of theses to use in many applications and adapted to provide accurate solutions. The Naïve Bayes classifier is used in the first experiment as a learner to identify the independent variables characterization for building models. The trained model was then reattempted for testing the model. Screenshots are taken during model building and experiment designing shown in Figures 10(a)–10(d). The results of all experiments are shown in Table 8. Altogether, 12 attributes were selected for learning the model for NAO's walking pattern. 70% of the whole data sets used to train the model. It requires the mean and variance of all attributes necessary for classification to perform the task. Finally, all independent variables, including the dependent variable "Label" column, regulated

TABLE 7: RapidMiner gait parameter metadata.

Name	Type	Statistic	Range	Missing
Position	Binomial	Mod = 1(2574), least = 0(2426)	0(2426), 1(2574)	0
Rar	Integer	Avg = -10.641 + / - 19.402	[-44.000; 22.000]	0
Rap	Integer	Avg = -7.723 + / - 35.331	[-68.000; 53.000]	0
RKp	Integer	Avg = -58.660 + / - 36.803	[-5.000; 12.000]	0
Rhp	Integer	Avg = -30.235 + / - 33.373	[-88.000; 27.000]	0
Rhyp	Integer	Avg = -11.801 + / - 30.985	[-65.000; 42.000]	0
RHr	Integer	Avg = -11.797 + / - 19.270	[-45.000; 21.000]	0
Lar	Integer	Avg = 11.193 + / - 19.473	[-22.000; 44.000]	0
Lap	Integer	Avg = -8.681 + / - 34.768	[-68.000; 52.000]	0
Lkp	Integer	Avg = 57.728 + / - 36.911	[-5.000; 121.000]	0
Lhp	Integer	Avg = -30.139 + / - 33.628	[-88.000; 72.000]	0
Lhyp	Integer	Avg = -12.507 + / - 31.111	[-65.000; 42.000]	0
LHr	Integer	Avg = 12.228 + / - 19.228	[-21.000; 45.000]	0

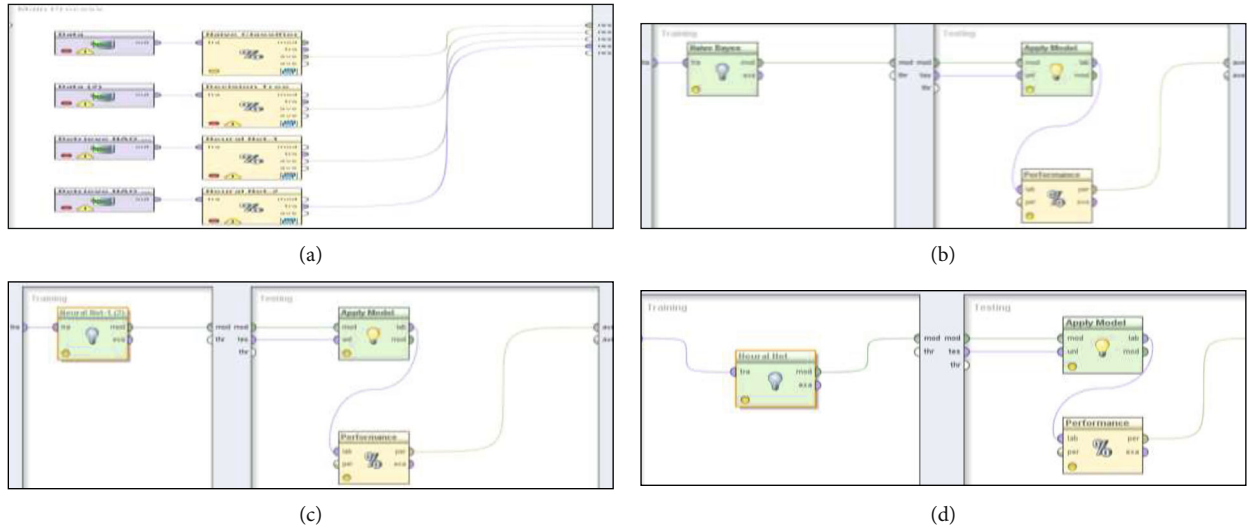


FIGURE 10: (a) Screenshots of experiment design (b). Screenshots of experiment design. (c). Screenshots of experiment design (d). Screenshots of experiment design.

TABLE 8: Result summary for all experiments.

Experiment#	List of attributes	Techniques used	Data set training	Data set testing	Prediction accuracy	Hidden layers	Learning rate	Training cycle
1	12	Naïve Bayes	70%	30%	48.20%			
2	12	Decision tree	70%	30%	49.87%			
3	12	ANN	70%	30%	55.12%	1	0.3	500
4	12	ANN	70%	30%	65.17%	2	0.5	500
5	12	ANN	70%	30%	65.31%	3	0.5	500

together based on each attribute’s individual representation. The further developed model has to follow by testing and validation processes using unseen testing datasets, which consist of 30% of the entire data sets. The purpose is to measure the model’s accuracy metric and check the Naïve Bayes algorithm’s performance for NAO’s gait parameters. This

model’s accuracy metric is calculated as 48.20%, shown in Table 9 from the system, which means the model predicted somewhere 48% correctly by using all independent attributes for deciding its states as walking or standing. The measured accuracy is not considered as optimal as the model predicted less than 50% correctly.

TABLE 9: Classification using Naïve Bayes.

Accuracy: 48.20%			
	True 0	True 1	Class precision
Pred.0	182	207	46.79%
Pred.1	570	541	48.69%
Class recall	24.20%	72.33	

TABLE 10: Classification using Decision Tree.

Accuracy: 48.87%			
	True 0	True 1	Class precision
Pred. 0	0	0	0.0%
Pred. 1	752	748	48.87%
Class recall	0.0%	100.00%	

3.4. *Classification Using Decision Tree (Experiment 2)*. The accuracy metric measured in the previous experiment was not good enough, but not the best. Therefore, another experiment was designed to improve the results and accuracy metric of the model. In this test, we applied a decision tree, another algorithm of classification on the same datasets. As mentioned in Section 4, a decision tree is a tree-like classification learning algorithm. Its top branch considers the primary classes (distinct values) of the datasets; it grows downwards according to the learning scheme or attributes of the independent variables. The training dataset was set to 70% randomly and considered unseen data for testing the model. From RapidMiner, the screenshot captured is shown in Figures 10(a)–10(d). The current tree model has improved slightly from the last result, and the accuracy metric recorded 49.87% or 50%, as in Table 10 copied from the system. It helped and improved the prediction level with more accuracy than the previous test.

As discussed, the data has been divided into two categories standing and walking states of the NAO robot based on 12 independent attributes associated with its gaits' joint parameters. This work intends to construct a model that can predict NAO's walking speed/velocity state more accurately. According to this research's purpose, the result was not the best while using the most common classification methods, Naïve Bayes, and Decision Tree.

3.5. *Artificial Neural Network (AI) (Experiments 3, 4, and 5)*. The last segment of this work is building an ANN model for the NAO humanoid robot to learn the dataset generated by its gaits' joint. The algorithm used for preparing the ANN is a feedforward technique trained using a back-propagation algorithm known as the multilayer perceptron. Figure 11 represents a generic design for NAO's walking using 12 parameters. Basically, this ANN follows a general structure of three layers: input, hidden, and output. The technique was applied three times with different combinations to get the optimal accuracy of the model. The primary purpose of building an ANN is to determine the difference between the previous two (naïve Bayes and

decision tree) implementation and ANN. A first static neural network was designed with only one hidden layer with a 0.3 learning rate with 500 training cycles, as shown in Figure 12. The input layer consists of 12 attributes that relates to NAO's gait parameters. Splitting of datasets into training and testing used 70% and 30%, respectively, to validate the model. The model's result showed 55.12% accuracy, which proved that the prediction was more than 50% correctly the first time in this research (Hidden layer: 1; learning rate: 0.3; training cycle: 500. Hidden layer: 3; learning rate: 0.5; training cycle: 500. Hidden layer: 4; learning rate: 0.5; training cycle: 500 (experiments 3 to 5).

The process repeats two more times with hidden layers with 3 and 4, respectively, while the learning rate also changed by 0.5. Moreover, both times, the accuracy metric measured after the implementation was around 65%, which was supposed to stand the highest and optimal accuracy metric of the learning model for NAO robot's walking pattern during the whole experiment process. Therefore, the learning cycle was stopped at this point as there is no more improvement even by changes in the learning rate and the number of hidden layers, see Figures 10(a)–10(d).

Finally, the results show that the last model can predict new and unseen datasets as accurately as 65%. The summary and features of all the experiments are shown in Table 8 below, which indicates that the ANN model scored the highest metrics accuracy.

The Aldebaran library enables the NAO robot for a maximum straight-line speed of 9.52 cm/s. The best speed NAO records are 32 cm/s, 28 cm/s, 22 cm/s, and 44.47 cm/s [46] achieved during the RoboCup challenge in 2009-2010 by four teams: HTWK, B-human, rUNS-Wift, and Devils. This work adapts [46] calculation by taking the average of two-time measures for  $t_1$  and  $t_2$ , for the steps satisfying the average distance  $d_1 = d_2 = 3$  m, instead of exact measure as in [46] to calculate the average speed as follows:

$$V_1 = d_1/t_1, \quad (8)$$

$$V_2 = d_2/t_2 - t_1, \quad (9)$$

$$V = (d_1 + d_2)/t_2. \quad (10)$$

The calculated maximum speed shows that ANN accomplished 51.08% improved walking speed than Aldebaran NAO's default straight-line speed, scoring  $V_1 = 22.62$ ,  $V_2 = 40$ , and  $V = 30$ . Future work using ANN or deep learning is expected to improve the speed velocity further by including NAO's hand pattern and parameters during the walk. The main limitations of our study are limited dataset due not dataset available online and the privacy of the case study. Also, it requires larger data and would be more efficient for a greater number of parameters, 100, and more. A humanoid robot's development requires an incredible combination of interdisciplinary work from engineering to mathematics, software, and machine learning. Furthermore, it is related to the design structure of the robot and the materials used to build it. The robot



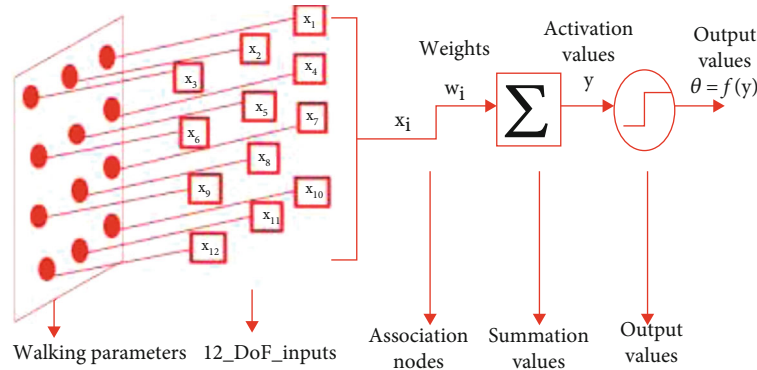


FIGURE 11: Generic artificial neural network for NAO's walking.

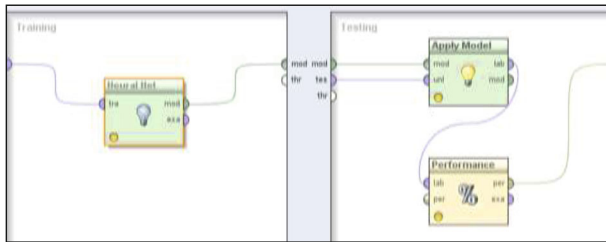


FIGURE 12: Neural net learning rate 0.3; training cycle 500.

cannot walk on any surface, and the motor stiffness is an issue to consider. The current research limitation supports only walking in a straight line and on even surface, and data collection is limited only to the 12 selected parameters.

#### 4. Conclusions

The research investigates the understanding and predicting of NOA humanoid gaits' joint 12 parameters in two states (walking and standing). Therefore, the right and left legs contribute to generating numerous datasets for feeding the model as an input. Naive Bayes, decision tree, and artificial neural net classification techniques were applied for learning and predicting the unseen observables. The accuracy metric was recorded for predicting new data generated from the NOA robot in the two different positions. Five experiments were designed where neural net training represents the maximum accuracy with 3 and 4 hidden layers for learning the whole learning process. The maximum accuracy metric rate of 65.31% was reached with only four hidden layers in 500 training cycles with a 0.5 learning rate for the best walking learning process. The optimal average velocity speed of 51.08% was achieved without stiffness. Thus, the tested hypothesis holds with the ANN model scoring the highest accuracy rate for predicting NAO's robot walking state speed of  $V_1 = 22.62$  cm/s,  $V_2 = 40$  cm/s, and  $V = 30$  cm/s, taking both legs to gauge joint 12 parameter values. For future work, experimental techniques, both gaits, and hand movement behaviors, apply ANN and deep learning techniques to measure NAO's predictive walking pattern and improved speed model and stability performance.

#### Data Availability

The preliminary data was used from the open-source at GitHub, the NAL dataset, and RoboCup datasheets.

#### Conflicts of Interest

The author declares that there is no conflict of interest regarding the publication of this paper.

#### Acknowledgments

The author thanks the Science and Technology Unit at King Abdulaziz University. The project is funded by the National Plan for Science, Technology, and Innovation (MAARI-FAH), King Abdulaziz City for Science and Technology, the Kingdom of Saudi Arabia (award number (03-INF188-08)).

#### References








- [1] Osha Technical Manual (OTM), Section IV: Chapter 4, Industrial robots and robot system safety (2017), Occupational Safety and Health Administration, 2015.
- [2] K. Wolff and P. Nordin, "Evolution of efficient gait with humanoids using visual feedback," in *Proceedings of the 2nd IEEE-RAS International Conference on Humanoid Robots, Humanoids*, pp. 99–106, Tokyo, Japan, 2001 November.
- [3] K. Dautenhahn, "Getting to know each other—artificial social intelligence for autonomous robots," *Robotics and Autonomous Systems*, vol. 16, no. 2-4, pp. 333–356, 1995.
- [4] S. K. Saha, *Denavit and Hartenberg (DH) Parameters*, Introduction to Robotics, 2008.
- [5] R. Beekers, O. E. Holland, and J. L. Deneubourg, "From local actions to global tasks: stigmergy and collective robotics," in *Proceedings of Artificial Life IV*, vol. 26, pp. 1008–1022, Dordrecht, 2000.
- [6] J.-L. Deneubourg, S. Goss, N. Franks, A. Sendova-Franks, C. Detrain, and L. Chrétien, "The dynamics of collective sorting robot-like ants and ant-like robots," in *Proceedings of the International Conference on Simulation of Adaptive Behavior*, Beijing, China, 2000.
- [7] T. Brogardh, "Present and future robot control development—an industrial perspective," *Annual Reviews in Control*, vol. 31, no. 1, pp. 69–79, 2007.

- [8] F. L. Shodt, *Inside The Robot Kingdom: Japan, Mechatronics, and the Coming Robotopia*, Kodansha International, Tokyo: New York, 1988.
- [9] “Rinri: an incitement towards the existence of robots in Japanese Society,” *The International Review of Information Ethics*, vol. 6, pp. 78–83, 2006.
- [10] Y. Sone, “Japanese Robot Culture Performance,” in *Imagination, and modernity*, Palgrave Macmillan, New York, 2017.
- [11] T. Fong, I. Nourbakhsh, and K. Dautenhahn, “A survey of socially interactive robots,” *Robotics and autonomous systems*, vol. 42, no. 3–4, pp. 143–166, 2003.
- [12] G. Schreiber, A. Stemmer, and R. Bischoff, “The fast research interface for the kuka lightweight robot,” in *IEEE workshop on innovative robot control architectures for demanding (Research) applications how to modify and enhance commercial controllers (ICRA 2010)*, pp. 15–21, Shanghai, China, 2010, May.
- [13] J. Fry, H. Asoh, and T. Matsui, “Natural dialogue with the jijo-2 office robot,” in *Proceedings. 1998 IEEE/RSJ International Conference on Intelligent Robots and Systems. Innovations in Theory, Practice and Applications (Cat. No. 98CH36190)*, vol. 2, pp. 1278–1283, Victoria, BC, Canada, 1998.
- [14] I. Asimov, “*Runaround*,” *Science Fiction Short Story*, Published in *Astounding Science Fiction*, 1942.
- [15] <https://www.brookings.edu/opinions/isaac-asimovs-laws-of-robotics-are-wrong/>.
- [16] C. Van Dang, M. Jun, Y.-B. Shin, J.-W. Choi, and J.-W. Kim, “Application of modified Asimov’s laws to the agent of home service robot using state, operator, and result (Soar),” *International Journal of Advanced Robotic Systems*, vol. 15, no. 3, 2018.
- [17] Böckmann, Arne: *development of a dynamic shot motion with the humanoid robot NAO [PhD Thesis]*, university of Bremen, Germany, 2015.
- [18] R. Riener, M. Frey, T. Proll, F. Regenfelder, and R. Burgkart, “Phantom-based multimodal interactions for medical education and training: the Munich knee joint simulator,” *IEEE Transactions on Information Technology in Biomedicine*, vol. 8, no. 2, pp. 208–216, 2004.
- [19] K. Dan, *Sizing and seizing the robotics opportunity*, vol. 17, no. 1, 2003RoboNexus, 2003.
- [20] P. van der Smagt, M. Grebenstein, H. Urbanek et al., “Robotics of human movements,” *Journal of Physiology-Paris*, vol. 103, no. 3-5, pp. 119–132, 2009.
- [21] N. Hockstein, C. Gourin, R. Faust, and D. Terris, “A history of robots: from science fiction to surgical robotics,” *Surgery*, vol. 1, no. 2, pp. 113–118, 2007.
- [22] K. Wolff and P. Nordin, “Evolution of efficient gait with an autonomous biped robot using visual feedback,” in *Proceedings of the Mechatronics Conference. University of Twente, Enschede, the Netherlands*, 2002.
- [23] R. Kurzweil, “The Singularity is Near: When Humans Transcend Biology,” in *Viking*, Penguin, 2005.
- [24] A. L. Nelson, G. J. Barlow, and L. Doitsidis, “Fitness functions in evolutionary robotics: a survey and analysis,” *Robotics and Autonomous Systems*, vol. 57, no. 4, pp. 345–370, 2009.
- [25] N. Rokbani, B. A. Cherif, and A. M. Alimi, *Toward intelligent biped-humanoids gait generation, humanoid robots*, B. Choi, Ed., INTECH, 2009.
- [26] D. Gouaillier, C. Collette, and C. Kilner, “Omni-directional closed-loop walk for NAO,” in *2010 10th IEEE-RAS International Conference on Humanoid Robots*, pp. 448–454, Nashville, TN, USA, 2010.
- [27] J. Strom, G. Slavov, and E. Chown, “Omnidirectional walking using ZMP and preview control for the NAO humanoid robot,” in *RoboCup 2009: Robot Soccer World Cup XIII*, vol. 5949 of Lecture Notes in Computer Science, pp. 378–389, Springer, Berlin, Germany, 2010.
- [28] J. Kulk and J. Welsh, “A low power walk for the NAO robot,” in *Proceedings of the Australasian Conference on Robotics and Automation (ACRA’ 08)*, Pasadena, California, December 2008.
- [29] [http://www.robotictrends.com/consumer\\_education/article/Nao\\_evolution\\_humanoid\\_robot\\_smarter\\_stronger/](http://www.robotictrends.com/consumer_education/article/Nao_evolution_humanoid_robot_smarter_stronger/).
- [30] NAO Hardware — NAO Software 1.12 documentation (cmu.edu).
- [31] D. Gouaillier and P. Blazevic, “A mechatronic platform, the Aldebaran robotics humanoid robot,” in *IECON 2006-32nd Annual Conference on IEEE Industrial Electronics*, Paris, France, 2006.
- [32] <http://www.cs.cmu.edu/~cga/nao/doc/reference-documentation/software/index.html/>.
- [33] <http://www.cse.unsw.edu.au/~robocup/2009site/reports/TayThesisB.pdf>.
- [34] J. Kober, J. A. Bagnell, and J. Peters, “Reinforcement learning in robotics: a survey,” *The International Journal of Robotics Research*, vol. 32, no. 11, pp. 1238–1274, 2013.
- [35] R. Mitnik, M. Recabarren, M. Nussbaum, and A. Soto, “Collaborative robotic instruction: a graph teaching experience,” *Computers & Education*, vol. 53, no. 2, pp. 330–342, 2009.
- [36] K. Capek, *RUR (Rossum’s Universal Robots)*, Penguin Group, New York, 2004.
- [37] B. D. Argall, S. Chernova, M. Veloso, and B. Browning, “A survey of robot learning from demonstration,” *Robotics and Autonomous Systems*, vol. 57, no. 5, pp. 469–483, 2009.
- [38] G. C. Gini, M. Folgheraiter, U. Scarfogliero, and F. Moro, *A biologically founded design and control of a humanoid biped*, vol. 33, Humanoid Robots, 2009.
- [39] Crossfitwebsite, 2019, <https://www.crossfit.com/essentials/planes-of-the-body/>.
- [40] P. Nordin and M. G. Nordahl, “An evolutionary architecture for a humanoid robot,” in *Proceedings of the Fourth International Symposium on Artificial Life and Robotics (AROB 4th 99)*, Oita, Japan, 1999.
- [41] K. Adistambha, S. J. Davis, C. H. Ritz, and D. Stirling, “Limb-based feature description of human motion,” in *2011 5th International Conference on Signal Processing and Communication Systems (ICSPCS)*, pp. 1–6, Honolulu, HI, USA, 2011.
- [42] <http://www2.informatik.uni-freiburg.de/~wurm/papers/hornung10iros.pdf>.
- [43] A. L. Thomaz and C. Breazeal, “Teachable robots: Understanding human teaching behavior to build more effective robot learners,” *Artificial Intelligence*, vol. 172, no. 6-7, pp. 716–737, 2008.
- [44] M. Umar Suleman and M. M. Awais, “Learning from demonstration in robots: Experimental comparison of neural architectures,” *Robotics and Computer-Integrated Manufacturing*, vol. 27, no. 4, pp. 794–801, 2011.
- [45] B. Y. Tchaleu, *Effective Algorithms to Predict Customer Churn in Financial Services*, University of Johannesburg (South Africa), ProQuest Dissertations Publishing, 2019.

- [46] D. T. Larose and C. D. Larose, *Discovering Knowledge in Data: An Introduction to Data Mining*, John Wiley & Sons Inc, 2005.
- [47] J. Cristiano, D. Puig, and M. A. García, *On the maximum walking speed of NAO humanoid robots*, XIV Workshop of Physical Agents, Madrid - España, 2011.
- [48] [http://doc.aldebaran.com/2-1/family/robots/joints\\_robot.html/](http://doc.aldebaran.com/2-1/family/robots/joints_robot.html/).
- [49] M. Hofmann and R. Klinkenberg, *Rapidminer*, Internet resource, 2016.

## Research Article

# Study and Analysis of Multiconnectivity for Ultrareliable and Low-Latency Features in Networks and V2X Communications

**Alexander Paramonov** <sup>1</sup>, **Jialiang Peng** <sup>2</sup>, **Dmitry Kashkarov**,<sup>1</sup> **Ammar Muthanna** <sup>1</sup>,  
**Ibrahim A. Elgendy** <sup>3,4</sup>, **Andrey Koucheryavy** <sup>1</sup>, **Yassine Maleh** <sup>5</sup>,  
and **Ahmed A. Abd El-Latif** <sup>6</sup>

<sup>1</sup>Department of Telecommunication Networks and Data Transmission,

The Bonch-Bruевич Saint-Petersburg State University of Telecommunications (SPbSUT), Russia

<sup>2</sup>School of Data Science and Technology, Heilongjiang University, Harbin 150080, China

<sup>3</sup>School of Computer Science and Technology, Harbin Institute of Technology, Harbin 150001, China

<sup>4</sup>Department of Computer Science, Faculty of Computers and Information, Menoufia University, Shibin el Kom 32511, Egypt

<sup>5</sup>LaSTI Laboratory, ENSAK, Sultan Moulay Slimane University, Beni Mellal, Morocco

<sup>6</sup>Department of Mathematics and Computer Science, Faculty of Science, Menoufia University, Al Minufiyah 32511, Egypt

Correspondence should be addressed to Jialiang Peng; [jialiangpeng@hlju.edu.cn](mailto:jialiangpeng@hlju.edu.cn)

Received 25 May 2021; Accepted 14 August 2021; Published 31 August 2021

Academic Editor: Deepak Gupta

Copyright © 2021 Alexander Paramonov et al. This is an open access article distributed under the Creative Commons Attribution License, which permits unrestricted use, distribution, and reproduction in any medium, provided the original work is properly cited.

Ultrareliable and low-latency connection (URLLC) is one of the novel features in 5G networks and subsequent generations, in which it targets to fulfill stringent requirements on data rates, reliability, and availability. Moreover, the multiconnectivity concept is introduced to meet these requirements, where multiple different technologies are connected simultaneously, and the data packet is duplicated and transmitted from multiple transmitters. To this end, in this paper, we present an analysis, model, and method to ensure the reliability of data delivery when organizing URLLC in 5G networks. In addition, a new approach based on the organization of multiple connections (multiconnectivity) and duplication of transmitted data is considered. Further, an analytical model is presented for assessing the probability of failure, taking into account the traffic intensity, the probability of failure of elements, and the number of used connections. Moreover, an efficient method is proposed for increasing the reliability of data delivery by optimizing the number of connections. Further, a multiconnectivity-based URLLC model has been built for evaluating the proposed method and verifies that the optimal number of routes for data delivery between the user and the point of service can be obtained, where the probability of losses and equipment reliability are jointly considered. Finally, detailed analysis of results shown that with “equal” routes in terms of load (with an equally probable traffic distribution) and the probability of equipment failure, the optimal number of routes can be found, at which the minimum probability of losses is achieved.

## 1. Introduction

Fifth-generation (5G) communication network customarily distinguished three main groups of services, namely, eMBB (enhanced mobile broadband), mMTC (massive machine type communications), and URLLC (Ultrareliable low-latency communications)—ultrareliable connections with ultralow-latency [1–6]. In addition, eMBB and mMTC are focused on services with high data rate and high and ultrahigh device density, while URLLC is focused on applications requiring

ultrareliable ultralow-latency data delivery. Further, URLLC is considered as one of the key features of 5G technology and subsequent generations [4, 7–9].

Furthermore, as shown in Figure 1, the main parameters of the 4G and 5G networks are compared and realized that set of improvements in 5G key metrics which can normally reflect the achievable data rates, density of subscriber devices, energy efficiency, and delivery times [10, 11]. However, URLLC implementation requires a delay to be decreased from 10 ms to 1 ms. This is achieved by the technical features

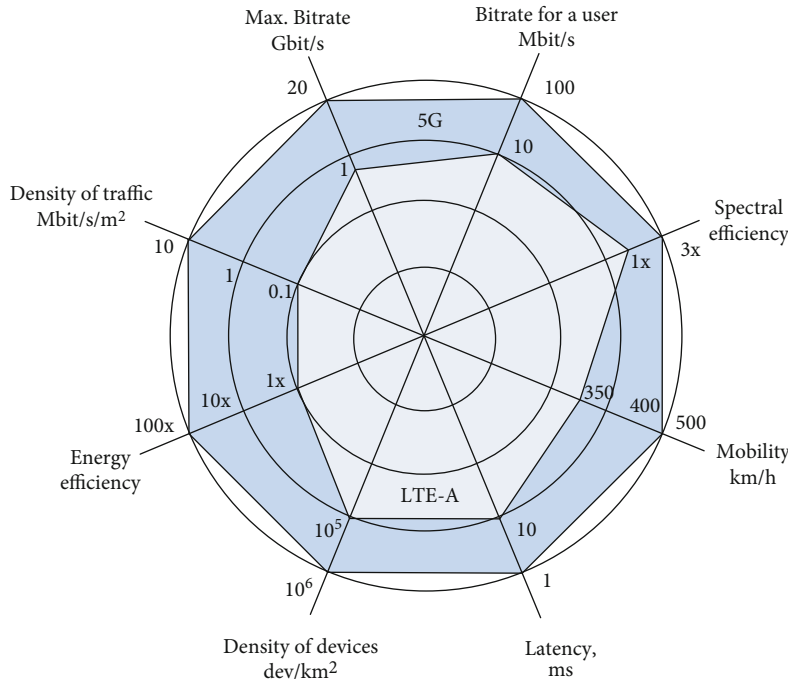


FIGURE 1: Basic parameters of 4G and 5G networks.

involved in building a network at the level of access [12–15], in particular by changing the format of transmitted frames or by changing the structure of the network at other levels [3] primarily because of the “approaching” point of service provided by the user (cloud and edge organization) [16–20].

Recently, significant efforts have been made to address the challenges related to ensuring the delay requirements through efficient interaction with base stations [21–23]. More specifically, the division of resources (slicing) is utilized in the implementation of services with different requirements for the parameters of functioning to provide various services through virtual network organization [24, 25].

The organization of multiple (parallel) connections and duplication of transmitted data are considered one of the dominant solutions to address this problem and fulfill the requirements for ultralow latency and ultrahigh reliability [3, 21, 26]. This approach ensures that the probability of packet loss is reduced to the target level due to the maintenance of redundancy. Moreover, the concept of reliability is interpreted as the probability of successful data delivery in the overwhelming majority of works devoted to URLLC, in which the requirements for this probability depend on the applied problems that are also significantly higher than modern ones (e.g., the probability of successful delivery is 0.99999 in [22] while it reaches to 0.999999999 in [3]).

Indeed, the probability of data delivery is the ultimate goal of the functioning of the network. However, this probability is influenced not only by probabilistic processes associated with the transmission and reception of messages (i.e., equipment functioning processes) but also by the probabilistic processes associated with equipment failures (i.e., failure of network elements) in connection with which its normal functioning is disrupted.

Subsequently, it should be noted that the concept of reliability is associated with this process in domestic literature. However, the process of technical failures (equipment failures) is virtually ignored in the aforementioned literature. In addition, the overwhelming majority of publication cite research results for equipment that is fully trustworthy and tolerant of failures. For example, in [27], the hardware reliability is considered with packet losses, in which the requirements are higher than existing ones (e.g., the requirement for the probability of a good state in the aforementioned work is defined as 0.9999).

Consequently, based on this interpretation and the generally accepted approach in the domestic literature, URLLC should be given as connections to ultralow losses and delays, as defined in Russian. However, this will be a narrower definition because, in the absence of additional reservations regarding hardware reliability, the term reliability includes the concept of losses.

More recently, a new multiconnectivity scheme is proposed in [28] for 5G networks, in which virtual network functions, local servers within MEC, and communication link failures are formulated as an integer problem whose object of optimally deploying network slices with the minimum cost. Then, an efficient algorithm based on a genetic algorithm is proposed to solve this problem and derive the close-optimal solution, whereas, in [29], an end-to-end latency approach has been reduced for downlink communication using cooperation among multiple access points. In addition, the proactive radio resource allocation is formulated as an optimization problem for open-loop uplink. Finally, Lyapunov optimization-based technique is developed to solve this problem in an efficient manner.

It is also worth noting that the only reason to lose data (i.e., a hardware or program failure or random events during



the transmission process) is very difficult to be obtained in a modern network (interference leading to errors, resource shortage or hardware failure). In other words, the reason is complex, and the more possible reasons the model takes into account, the more accurately it describes the real network. It is, therefore, logical to use the term URLLC in a general interpretation and add more factors to the model that take into account the equipment fault tolerance.

In the above-mentioned work [27], the concept of hardware reliability is stated, and even numerical requirements for the probability of failure are provided. Therefore, motivated by such considerations, in this paper, we proposed a novel approach based on multiple connections (multiconnectivity) for improving the system reliability, in which the hardware reliability of network elements is considered. This work proved that the implementation of URLLC using multiconnectivity in 5G networks allows to increase the reliability of data delivery but at the same time increases the load on the network. An efficient model is proposed that makes it possible to estimate the optimal number of parallel connections at which the maximum connection reliability is achieved. The distribution function of the message delivery time in the URLLC network is investigated. A simulation model was built, which confirmed the proposed analytical models. The main contributions reported in this study can be summarized as follows:

- (i) The multiple connections obtained by increasing the number of delivery routes and “propagating” data are considered, which provides increased reliability both by reducing the likelihood of data loss due to congestion and by reducing the likelihood of losses due to technical malfunctions of the route elements
- (ii) The duplication (multiplication) of data, namely, the impact on the probability of losses, the amount of delay, and traffic intensity in the network, is analyzed
- (iii) The data delivery routes using a queuing system model with a combined service discipline is simulated
- (iv) The optimal number of routes is defined, in which the minimum probability of losses is achieved, and this solution is obtained for both “equal” and “unequal” routes
- (v) A simulation model was built, which confirmed the proposed analytical models

## 2. Model and Problem Statement

Heterogeneity is the key feature of 5G networks, which allows the implementation of URLLC and allows several ( $k$ ) parallel connections (routes) to be organized between customer’s device and the point of service delivery using different technology networks (seen in Figure 2).

In the general case, these connections can be implemented in different ways and passed through various network elements; therefore, we will call them routes below.

Furthermore, the use of multiple routes allows the parallel transmission of one data packet through different network elements. First, it enables the reliability of delivery to be increased; as in this case, the probability of packet loss is less than the smallest value for each route used.

$$P_L = \prod_{i=1}^k p_i, \quad (1)$$

where  $p_i$  denotes the data loss’s probability on the  $i$ th route.

Secondly, this makes it possible to reduce the delivery time of the package, due to the fact that only the first of the arriving packages will be used at the point of service provision (i.e., delivery time will be equal to the minimum time for all routes used).

$$t_D = \min \{t_1, t_2, \dots, t_k\}, \quad (2)$$

where  $t_1, t_2, \dots, t_k$  are the delivery times for each of the  $k$  routes. In this case, under the assumption that the delivery time is independent and if its distribution function for all routes is the same and has a distribution function  $F(t)$ , the delivery time distribution function for  $k$  routes operating in accordance with (2) will be defined as

$$F(t)_k = 1 - (1 - F(t))^k. \quad (3)$$

From (3), it is easy to see that if this is an exponential distribution, then it is also an exponential distribution, the mathematical expectation of which differs by a factor of  $k$ . This qualitative example shows that the expected delivery time decreases in proportion to the number of routes.

It is evident from expression (1) that the probability of data delivery loss also decreases with an increase in the number of parallel routes  $k$ .

However, when considering the routing system in a single communication network, it is also evident that the transmission of the same packet along  $k$  routes increases the traffic intensity in this network by a factor of  $k$ .

Thus, with an even distribution of traffic along routes, if the system serves the traffic of  $n$  users,  $m$  of which uses URLLC and uses multiple connections (multiconnectivity), the resulting traffic intensity can be defined as

$$a = (n - m)a_0 + mka_0. \quad (4)$$

If the share of URLLC users is  $\eta = m/n$ , then the traffic intensity of each of the routes can be expressed as

$$\hat{a}_i = [1 - (k - 1)\eta]a_i, \quad (5)$$

where  $k$  is the number of parallel channels,  $\eta$  is the share of clients using URLLC, and  $a_i$  is the traffic intensity in the  $i$ th route without using URLLC.

Each of the routes is a sequence of several network sections (channels) and, in the general case, can be described as a multiphase queuing system. In this case, we will assume that the most significant contribution to the probability of

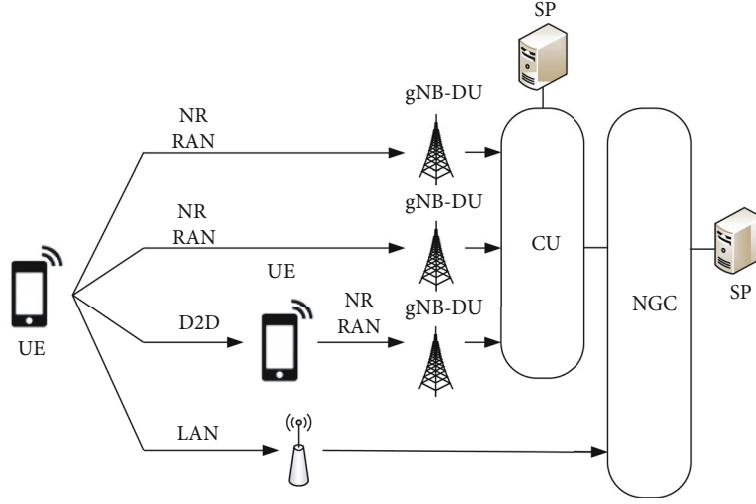


FIGURE 2: Parallel data delivery routes in the 5G network.

losses and the amount of delay is made only by one of the route sections; the influence of the remaining sections will be considered negligible. This simplification is probably acceptable if the subscriber access section is considered the most “complex.”

Considering the accepted assumption, we describe the channel model as a single-phase queuing system of the G/G/1/R type. As noted above, data loss can also occur for technical reasons in case of failure of route elements. Consider a model that takes into account both of these factors. A formalized model of  $k$  routes between a plurality of users of a UE and an SP is shown in Figure 3.

In this model, each of the routes is a sequence of three elements, two of which ( $Q$  and  $t$ ) describe the queuing system G/G/1/R, and element  $A$  takes into account the finite reliability of the route elements.

The probability of packet loss due to the finite size of the buffer in each of the routes will be described by an approximate expression [18]:

$$p \approx \frac{1 - \rho}{1 - \rho^{SR+1}} \rho^{SR}, \quad (6)$$

where  $\rho$  is the load intensity and  $R$  is the buffer size.

The value of  $S$  in expression (6) depends on the properties of the traffic flow and the service (transmission) time of the data packet:

$$S = \frac{2}{C_A^2 + C_B^2}, \quad (7)$$

where  $C_a$  is the coefficient of variation of the time intervals between the moments of arrival of traffic packets and  $C_b$  is the coefficient of variation of the service (transmission) time of the data packet.

For example, for the Poissonian flow model,  $S = 1$ .

We will also assume that the organization of the URLLC does not affect the size of the data packets in any way. Tak-

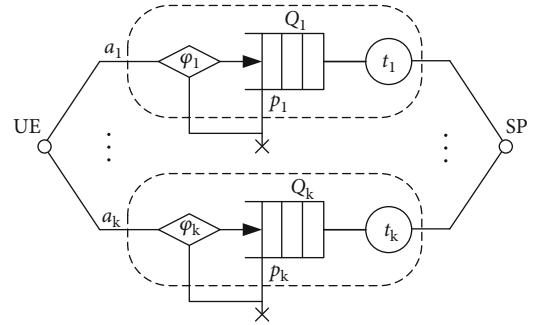


FIGURE 3: Model of traffic routes.

ing into account this assumption, from expression (5), a similar expression will follow for the intensity of the load in each of the routes:

$$\widehat{\rho}_i = [1 + (k - 1)\eta]\rho_i. \quad (8)$$

Then, taking into account (6) and (8), we can estimate the probability of losses in each of the  $k$  routes:

$$p_i = \frac{1 - \widehat{\rho}_i}{1 - \rho \wedge_i^{SR+1}} \rho \wedge_i^{SR}. \quad (9)$$

Taking into account (1) and (9), we can obtain an expression for the probability of losses in a system with  $k$  routes.

$$p_L = \prod_{i=1}^k \left[ \frac{1 - \widehat{\rho}_i}{1 - \rho \wedge_i^{SR+1}} \rho \wedge_i^{SR} \right]. \quad (10)$$

Figure 4 shows the dependence of the probability of packet loss on the number of routes used for parallel packet transmission. In this model, it is assumed that routes are chosen randomly, i.e., traffic is equally likely (evenly) distributed between routes.

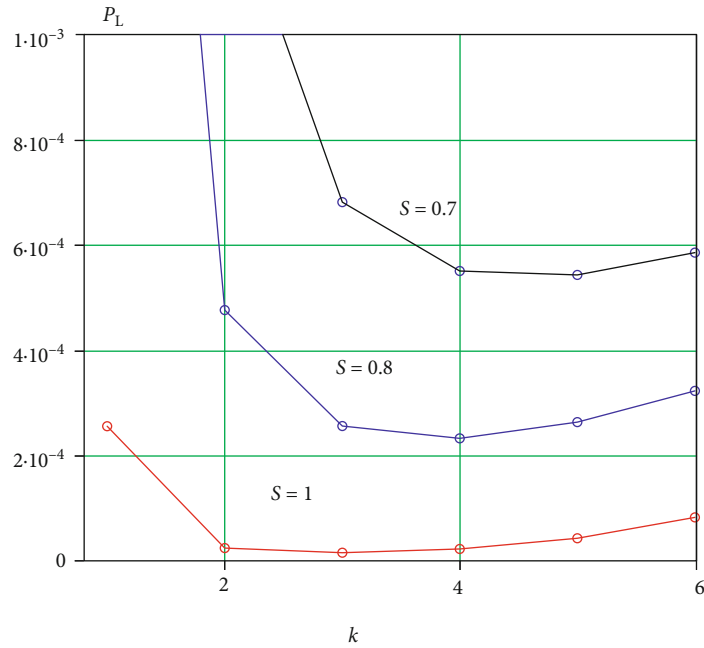


FIGURE 4: Dependence of the probability of losses (10) on the number of routes for sending a packet.

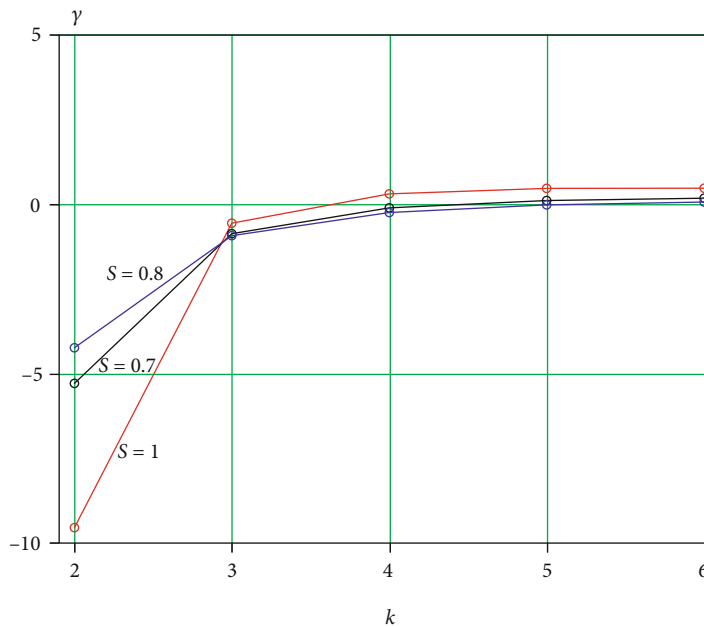


FIGURE 5: Dependence of the coefficient of change in the probability of losses on the number of routes.

As shown in the above graph, the probability of losses due to a limited buffer size has a nonlinear dependence on the number of routes for sending a packet. This dependence is obvious, since an increase in the number of delivery routes  $k$  leads to an increase in traffic (as can be seen from (5)). With an increase in  $k$  to a certain value, a decrease in losses in accordance with the parallel model (1) dominates; however, further growth leads to a dominance of an increase in losses in the channel in accordance with the model (9).

Thus, there is a number of routes for which system losses are minimal. For the given example, the optimal values of  $k$  were 3, 4, and 5 for traffic with different properties:  $S = 1$ ; 0.8 ; and 0.7, respectively, i.e., this value is different for streams with different properties.

It should be noted that the degree of influence of an increase in the number of routes on the probability of losses sharply decreases with an increase in  $k$ . Figure 5 shows the dependence of the coefficient of change in the probability of losses on the number of delivery routes.

As can be seen from the above graph, the greatest decrease in the probability of losses occurs when the second route is switched on (3  $\cdots$  10 times). Moreover, the addition of the third route changes the probability of loss by less than half.

As noted above, equipment reliability also affects the likelihood of data loss. We will characterize the reliability of the data delivery route by its availability factor, i.e., the likelihood of a good condition. In turn, the probability of the healthy state of the route is determined by the probabilities of the healthy state of each of its elements.

The probability of packet loss due to technical failure can be defined as:

$$p_U = p_d \varphi, \quad (11)$$

where  $p_d$  is the probability that data is transmitted through the network element and  $\varphi$  is the probability of route failure.

$p_d$  is numerically equal to the traffic intensity.

Taking into account (8) and (11), we can determine the probability of packet loss in the  $i$ th route due to a technical malfunction as

$$p_i^{(U)} = \hat{p}_i \varphi_i, \quad (12)$$

where  $\varphi_i$  is the probability of failure of the  $i$ th route.

Taking into account (10) and (12), we can calculate the probability of losing a data packet, which depends both on the number of traffic delivery routes and on the probability of a healthy state of each of the routes:

$$\tilde{p}_L = \prod_{i=1}^k \left[ 1 - \left( 1 - p_i^{(U)} \right) \left[ 1 - \frac{1 - \hat{p}_i}{1 - \rho \Lambda_i^{SR+1}} \rho \Lambda_i^{SR} \right] \right], \quad (13)$$

where  $p_i^{(U)}$  is the probability of data loss due to failure of route elements.

Figure 6 shows an example of the dependence of the probability of losses (5) on the number of routes, provided that all the probabilities of route failure are equal  $p_i^{(U)} = 0.05$ ;  $i = 1 \cdots 8$ . The choice of a relatively high probability of failure is due to the fact that the elements of the route can be not only the equipment of the telecom operator, which has relatively high-reliability rates, but also the devices of users in the case of organizing D2D connections; the performance of which can be limited by a simple discharge of the battery or a software failure.

From the given example, it can be seen that the probability of data delivery losses has a dependence on the number of routes, similar to (10) with a difference in numerical values, which is due to taking into account the reliability of the route.

The optimal number of routes is determined by the load intensity (8) and flow properties (7). For the given example with  $S = 1$ ; 0.8; and 0.7, the optimal value is achieved at  $\hat{p}_i = 0.56$ ; 0.58; 0.80, respectively. As shown from the obtained results and the given examples, the optimal number of routes depends on the intensity and properties of the packet flow and is determined from the model (13). However, the solution to

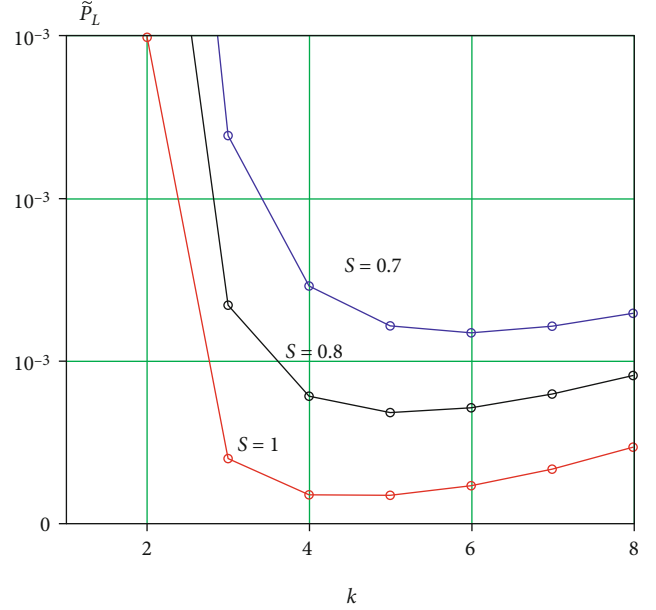


FIGURE 6: Dependence of the probability of losses, taking into account reliability, on the number of routes.

this problem is not expressed in the final form. Therefore, numerical optimization methods are necessarily required to solve this problem.

### 3. Experimental Environment and Software

To obtain numerical results, we used the Mathcad software for solving analytical modeling problems and the AnyLogic simulation system for solving multiconnectivity simulation problems. AnyLogic is a general purpose simulation system. It includes a system of discrete event modeling and allows you to create models of systems based on models of queuing systems. This system allows you to flexibly choose the degree of detail of the simulated processes, simulate random processes with different properties, and accompany the modeling process by collecting the necessary statistics. The system has a sufficiently high performance, which makes it possible to collect the required amount of data in a reasonable time and obtain sufficiently accurate estimates of the simulated processes. One of the undoubted advantages of this system is a very simple and intuitive user interface that allows you to implement the necessary functionality by combining a fairly rich library and the necessary additions in the Java Language, entered by the user.

The results shown in Figures 4–6 were obtained in Mathcad by analytical modeling.

Figure 7 shows a simulation model built in AnyLogic.

The model contains a source of user (users) traffic that is implemented on UE elements,  $RT1, \dots, RT5$ , each of the routes is modeled by a queuing system consisting of a queue  $q1, \dots, q5$ , and a delay element transfer1,  $\dots$ , transfer5, simulating the process of transmitting a data packet. Both the observed traffic and the background traffic served by this direction, which are produced by the elements  $BT1, \dots, BT5$ , arrive at the inputs of the channels. The introduction of

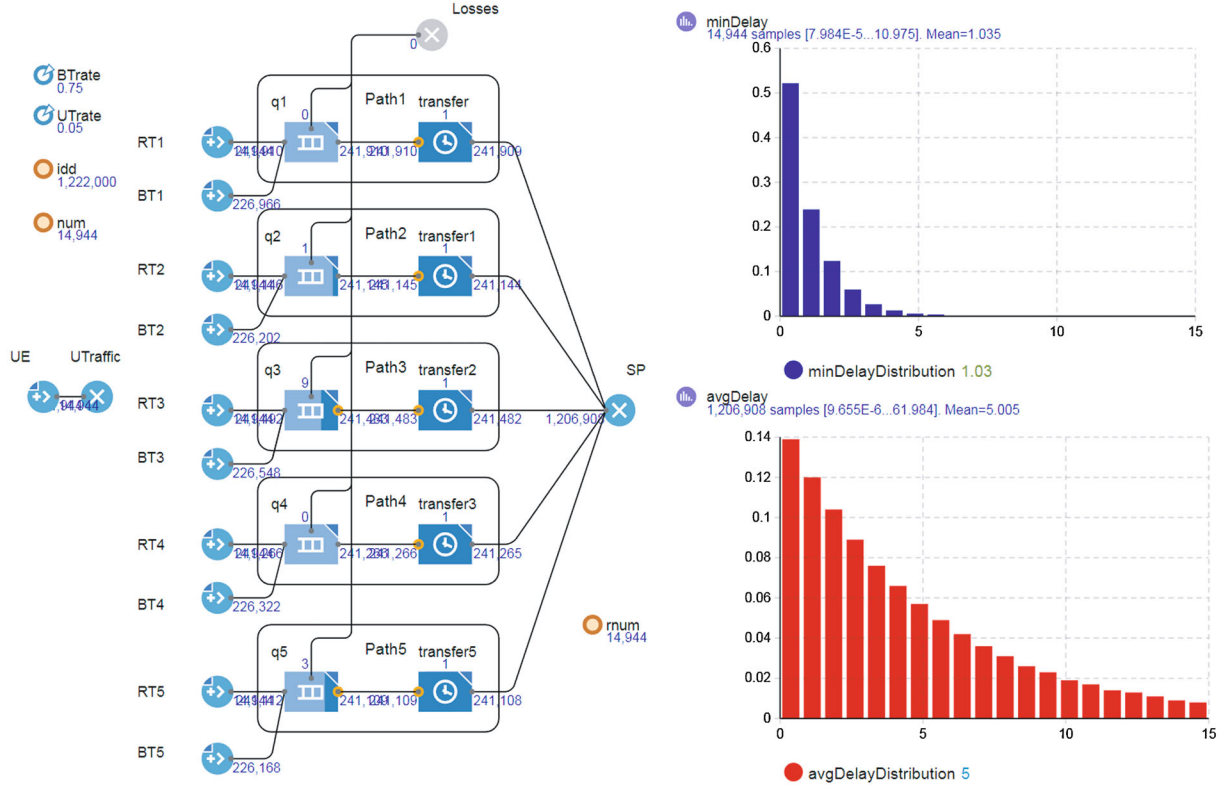


FIGURE 7: Multiconnectivity model in AnyLogic.

background traffic into the model is necessary in order to reduce the dependence of the delivery time in different routes.

The example simulation shown in Figure 7 demonstrates the difference in delivery times. The upper histogram (blue bars) shows the probability density of the minimum delay for the route group. The bottom bar graph (red bars) shows the average delivery time for all routes. From the given example, it can be seen that the minimum delivery time for a group of routes is less than the average value by a factor of the number of routes (in this case, 5 times).

In the given example, the share of user traffic was 7% of the total traffic in each of the routes. In this simulation example, the parameters of the routes were identical.

The results obtained confirm the expression for the distribution of the minimum delivery time (3), as well as the above conclusions for the exponential distribution of the delivery time.

When the distribution of delivery time changes (if it differs from exponential), the results change. For example, with an increase in the probability of losses in each of the routes, the distribution of delivery time becomes different from exponential and the ratio between the minimum delivery time and its average value changes.

It should be noted that with an increase in the dependence between flows in different routes, the effect of decreasing the delay decreases. The effect of reducing the delivery time when using a group of routes is the higher and the higher the independence of flows, i.e., when the share of traf-

fic is not large in relation to the total traffic of the routes, as well as when the routes themselves differ from each other.

The given model was also used to optimize the choice of the number of routes, which will be considered below.

#### 4. Method for Choosing the Optimal Number of Routes

The problem of minimizing losses for equal values of the probability of failure  $p_i^{(U)}$  and equiprobable distribution of traffic over  $k$  routes can be written as

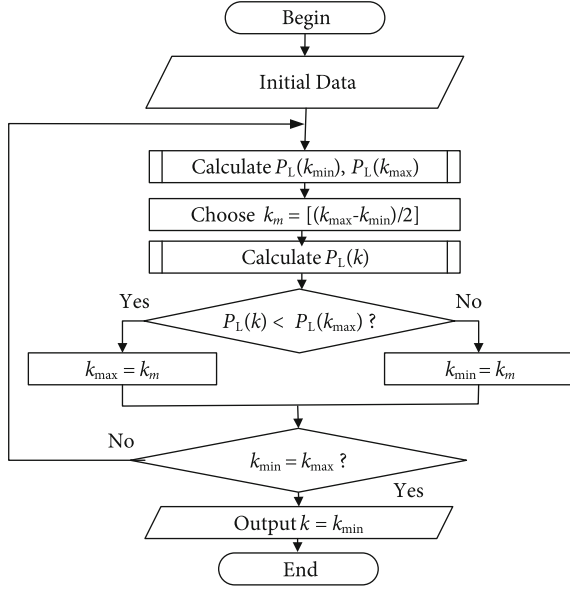
$$k = \arg \min_k \{ \tilde{p}_L \mid k = 1, \dots, k_{\max}; 0 \leq \tilde{p}_i < 1 \}. \quad (14)$$

The analytical solution of the problem (14) is complicated by the fact that it is not expressed in the final form from (13). However, in practical problems, the number of possible routes  $k_{\max}$  is not too large, and then problem (14) is an integer optimization problem. In many cases, with real values of  $k_{\max}$ , it can be easily solved by a simple search of  $k$ .

For the general case and to improve the efficiency of searching for an extremum, it is proposed to use an integer binary search algorithm [19].

The proposed algorithm in Figure 8 consists of cyclically dividing the entire set of possible values of  $k$  and discarding the half in which there cannot be an extremum until the search range is narrowed down to a single value at the next



FIGURE 8: Algorithm for finding the optimal value of  $k$ .

iteration. The idea of the method is similar to the dichotomy method [19], with the difference that the search for a solution is performed on the set of integer values of the argument.

If the routes are not equal, for example, the probabilities of data loss due to the failure of route elements or the load are not equal to each other, then the choice problem arises. To solve this problem, it is proposed to use the dynamic programming method. In this case, the solution to the problem is not the number of routes  $k$ , but the set of route numbers. Theoretically, such a solution can be obtained for each data packet sent, but in practice, it will require too much computation. Therefore, in this case, it is proposed to consider separate traffic flows  $a_i, i = 1, \dots, n$ , where  $n$  is the number of flows produced by devices, and to find a set of routes for each of these flows  $R_i$ .

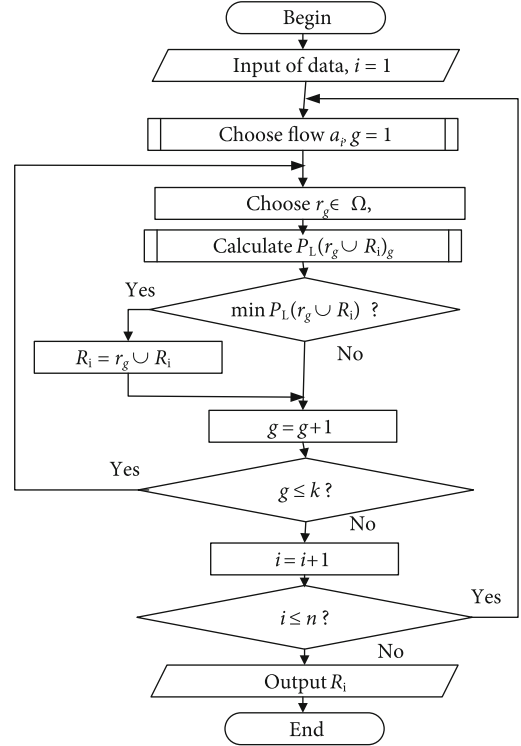
In this case, the objective function looks like this:

$$\{r_{i,j}\} = \arg \min_{R_i} \left\{ \begin{array}{l} r_{i,j} \in \Omega, \quad j = 1, \dots, m_i; \\ \tilde{p}_L, \quad i = 1, \dots, n; \quad 0 \leq \hat{\rho}_g < 1; \quad g = 1, \dots, k \end{array} \right\}, \quad (15)$$

where  $R_i = \{r_j\}$  is the set of routes for serving the  $i$ th flow,  $r_j$ ,  $j$  is the  $j$ th route serving the  $i$ th flow, what is this symbol is the set of available routes,  $m_i$  is the number of routes serving the  $i$ th flow,  $n$  is the number of flows, and  $k$  is the total number of routes and is the load of the  $g$ th route.

The proposed algorithm is shown in Figure 9.

The given algorithm consists of executing two cycles: external—according to the number of flows; internal—according to the number of available routes. In the inner loop, a plurality of routes is selected to serve the flow. The choice of a route is made by its inclusion in the set of selected routes for a given flow, if its choice leads to the largest decrease in

FIGURE 9: Algorithm for finding the optimal value of  $k$ .

the value of the objective function. The objective function is calculated, taking into account the traffic of the flow in question.

## 5. Discussion

The results obtained show, firstly, that the use of multiconnectivity can increase the likelihood of data delivery and, secondly, reduce the delay in their delivery. The graphs shown in Figures 4–6 show that the nature of the dependence is preserved when changing the properties of the flow. All dependencies for different values of  $S$  have the same character. The probability of losses has a pronounced minimum (Figures 4 and 6), which indicates the existence of an optimal number of parallel routes, exceeding which, on the contrary, reduces the probability of delivery due to an increase in the generated load.

Thus, the effectiveness of the use of multiconnectivity is ensured only under certain conditions, which should be selected based on the requirements for the probability of delivery and the magnitude of the load on the communication directions. Such a choice requires performing a certain number of operations to analyze the state and make a decision, which is very problematic given that the time to complete this work should be significantly less than the allowable delivery time. We propose to use traffic analysis and forecasting methods for this purpose, as well as to use preprepared sets of routes. This will reduce the time spent on this work. The solution to this problem is a further direction of research in this area.

## 6. Conclusions

In this paper, we conducted an analysis that showed that multiple connections, obtained by increasing the number of delivery routes and “propagation” of data, provide increased reliability both by reducing the likelihood of data loss due to congestion and by reducing the likelihood of data loss. For technical malfunctions of route elements, we have also shown that multiple connections can reduce the average delivery time of data, and this approach is most effective when streams are independent, i.e., when the share of “useful” traffic is relatively small in the total traffic of the route. It was also shown that duplication (multiplication) of data and their transmission along several routes, along with a decrease in the probability of losses and the amount of delay, leads to an increase in traffic in the network, which in turn can lead to the opposite effect, i.e., increase the likelihood of losses due to traffic growth. We proposed a model of data delivery routes, described using a queuing system model with a combined service discipline, which allows us to estimate the dependence of the loss probability on the number of routes chosen for data delivery. As a result of the analysis, it was shown that with “equal” routes in terms of load (with an equally probable traffic distribution) and the probability of failure, the optimal number of routes could be found, at which the minimum probability of losses is achieved. To solve this problem, it is proposed to use the integer binary search method. It was also shown that with “unequal” routes, the problem of traffic distribution arises. To solve this problem, it is proposed to consider traffic flows generated by users and select delivery routes for each of these flows. To solve this problem, we proposed to use a dynamic programming method, and the result is a set of delivery routes for each of the flows.

In ongoing and future work, the privacy and security requirements related to the communication channel will be discussed, in which blockchain technology will be utilized.

## Data Availability

The datasets generated during and analysed during the current study are available from the corresponding author upon reasonable request.

## Conflicts of Interest

The authors declare that they have no conflicts of interest.

## Acknowledgments

This work is supported by the Heilongjiang Province Natural Science Foundation of China (Grant no. LH2020F044); the 2019-“Chunhui Plan” Cooperative Scientific Research Project of Ministry of Education of China (Grant no. HLJ2019015); and the Fundamental Research Funds for Heilongjiang Universities, China (Grant no. 2020-KYYWF-1014). Also, this research is based on the Applied Scientific Research under the SPbSUT state assignment 2021.

## References

- [1] M. Series, “Minimum requirements related to technical performance for imt-2020 radio interface,” International Telecommunication Union, 2017.
- [2] G. T. Draft, “Feasibility Study on New Services and Markets Technology Enablers Stage 1 (Release 14),” International Telecommunication Union, 2016.
- [3] M. Bennis, M. Debbah, and H. Vincent Poor, “Ultrareliable and low-latency wireless communication: tail, risk, and scale,” *Proceedings of the IEEE*, vol. 106, no. 10, pp. 1834–1853, 2018.
- [4] A. Paramonov, A. Muthanna, O. I. Aboulola et al., “Beyond 5G network architecture study: fractal properties of access network,” *Applied Sciences*, vol. 10, no. 20, article 7191, 2020.
- [5] D. Patra, S. Chavhan, D. Gupta, A. Khanna, and J. J. P. C. Rodrigues, “V2X communication based dynamic topology control in VANETs,” in *Adjunct Proceedings of the 2021 International Conference on Distributed Computing and Networking*, pp. 62–68, New York, NY, USA, January 2021.
- [6] A. Khakimov, A. Loborchuk, I. Ibdullokhodzha, D. Poluektov, I. A. Elgendy, and A. Muthanna, “Edge computing resource allocation orchestration system for autonomous vehicles,” in *The 4th International Conference on Future Networks and Distributed Systems (ICFNDS)*, pp. 1–7, New York, NY, USA, November 2020.
- [7] A. Koucheryavy, A. Vlydyko, and R. Kirichek, “State of the art and research challenges for public flying ubiquitous sensor networks,” in *Internet of Things, Smart Spaces, and Next Generation Networks and Systems*, pp. 299–308, Springer, 2015.
- [8] V. Artem, M. Al-Sveiti, I. A. Elgendy, A. S. Kovtunencko, and A. Muthanna, “Detection and recognition of moving biological objects for autonomous vehicles using intelligent edge computing/LoRaWAN mesh system,” *Internet of Things, Smart Spaces, and Next Generation Networks and Systems*, 2020, pp. 3–15, Springer, 2020.
- [9] B. A. Y. Alqaralleh, S. N. Mohanty, D. Gupta, A. Khanna, K. Shankar, and T. Vaiyapuri, “Reliable multi-object tracking model using deep learning and energy efficient wireless multimedia sensor networks,” *IEEE Access*, vol. 8, pp. 213426–213436, 2020.
- [10] W. Mohr, “The 5G infrastructure association,” ITU-R, 2017, March 2019, <https://www.itu.int/en/ITU-R/study-groups/rsg5/rwp5d/imt-2020/Documents/S03-15GPPP>.
- [11] M. Khayyat, I. A. Elgendy, A. Muthanna, A. S. Alshahrani, S. Alharbi, and A. Koucheryavy, “Advanced deep learning-based computational offloading for multilevel vehicular edge-cloud computing networks,” *IEEE Access*, vol. 8, pp. 137052–137062, 2020.
- [12] A. Paramonov, O. Hussain, K. Samouylov, A. Koucheryavy, R. Kirichek, and Y. Koucheryavy, “Clustering optimization for out-of-band D2D communications,” *Wireless Communications and Mobile Computing*, vol. 2017, Article ID 6747052, 11 pages, 2017.
- [13] A. Paramonov, E. Tonkikh, A. Koucheryavy, and T. M. Tatarnikova, “High density internet of things network analysis,” in *Internet of Things, Smart Spaces, and Next Generation Networks and Systems*, pp. 307–316, Springer, 2020.
- [14] Y. Liu, J. Peng, J. Kang, A. M. Ilyyasu, D. Niyato, and A. A. A. el-Latif, “A secure federated learning framework for 5G networks,” *IEEE Wireless Communications*, vol. 27, no. 4, pp. 24–31, 2020.

- [15] A. A. A. el-Latif, B. Abd-el-Atty, S. E. Venegas-Andraca, and W. Mazurczyk, "Efficient quantum-based security protocols for information sharing and data protection in 5G networks," *Future Generation Computer Systems*, vol. 100, pp. 893–906, 2019.
- [16] I. A. Elgendy, W.-Z. Zhang, C.-Y. Liu, and C.-H. Hsu, "An efficient and secured framework for mobile cloud computing," *IEEE Transactions on Cloud Computing*, vol. 9, no. 1, pp. 79–87, 2018.
- [17] A. Paramonov, N. Chistova, M. Makolkina, and A. Koucheryavy, "The method of forming the digital clusters for fifth and beyond telecommunication networks structure based on the quality of service," in *Internet of Things, Smart Spaces, and Next Generation Networks and Systems*, pp. 59–70, Springer, 2020.
- [18] I. A. Elgendy, W.-Z. Zhang, Y. Zeng, H. He, Y.-C. Tian, and Y. Yang, "Efficient and secure multi-user multi-task computation offloading for mobile-edge computing in mobile IoT networks," *IEEE Transactions on Network and Service Management*, vol. 17, no. 4, pp. 2410–2422, 2020.
- [19] I. A. Elgendy, A. Muthanna, M. Hammoudeh, H. Shaiba, D. Unal, and M. Khayyat, "Advanced deep learning for resource allocation and security aware data offloading in industrial mobile edge computing," *Big Data*, 2021.
- [20] I. Elgendy, W.-Z. Zhang, H. He, B. B. Gupta, and A. A. Abd el-Latif, "Joint computation offloading and task caching for multi-user and multi-task MEC systems: reinforcement learning-based algorithms," *Wireless Networks*, vol. 27, no. 3, pp. 2023–2038, 2021.
- [21] N. H. Mahmood, A. Karimi, G. Berardinelli, K. I. Pedersen, and D. Laselva, "On the resource utilization of multi-connectivity transmission for URLLC services in 5G new radio," in *2019 IEEE Wireless Communications and Networking Conference Workshop (WCNCW)*, pp. 1–6, Marrakech, Morocco, April 2019.
- [22] S. R. Pokhrel, J. Ding, J. Park, O.-S. Park, and J. Choi, "Towards enabling critical MMTC: a review of URLLC within MMTC," *IEEE Access*, vol. 8, pp. 131796–131813, 2020.
- [23] W.-Z. Zhang, I. A. Elgendy, M. Hammad et al., "Secure and optimized load balancing for multitier IoT and edge-cloud computing systems," *IEEE Internet of Things Journal*, vol. 8, no. 10, pp. 8119–8132, 2021.
- [24] P. Popovski, K. F. Trillingsgaard, O. Simeone, and G. Durisi, "5G wireless network slicing for eMBB, URLLC, and MMTC: a communication-theoretic view," *IEEE Access*, vol. 6, pp. 55765–55779, 2018.
- [25] T. Ma, Y. Zhang, F. Wang, D. Wang, and D. Guo, "Slicing resource allocation for eMBB and URLLC in 5G RAN," *Wireless Communications and Mobile Computing*, vol. 2020, Article ID 6290375, 11 pages, 2020.
- [26] Evolved Universal Terrestrial Radio Access Network, *3rd Generation Partnership Project; Technical Specification Group Radio Access Network; Evolved Universal Terrestrial Radio Access Network*, EUTRA Network, 2011.
- [27] M. F. Zhani and H. ElBakoury, "FlexNGIA: a flexible internet architecture for the next-generation tactile internet," *Journal of Network and Systems Management*, vol. 28, no. 4, pp. 751–795, 2020.
- [28] P. K. Thiruvassagam, A. Chakraborty, and C. S. R. Murthy, "Resilient and latency-aware orchestration of network slices using multi-connectivity in MEC-enabled 5G networks," *IEEE Transactions on Network and Service Management*, vol. 28, no. 4, pp. 751–795, 2021.
- [29] Y. Zhang, L. Zhao, G. Zheng, X. Chu, Z. Ding, and K.-C. Chen, "Resource allocation for open-loop ultra-reliable and low-latency uplink communications in vehicular networks," *IEEE Transactions on Vehicular Technology*, vol. 70, no. 3, pp. 2590–2604, 2021.

## Retraction

# Retracted: A Detailed Research on Human Health Monitoring System Based on Internet of Things

### Wireless Communications and Mobile Computing

Received 8 August 2023; Accepted 8 August 2023; Published 9 August 2023

Copyright © 2023 Wireless Communications and Mobile Computing. This is an open access article distributed under the Creative Commons Attribution License, which permits unrestricted use, distribution, and reproduction in any medium, provided the original work is properly cited.

This article has been retracted by Hindawi following an investigation undertaken by the publisher [1]. This investigation has uncovered evidence of one or more of the following indicators of systematic manipulation of the publication process:

- (1) Discrepancies in scope
- (2) Discrepancies in the description of the research reported
- (3) Discrepancies between the availability of data and the research described
- (4) Inappropriate citations
- (5) Incoherent, meaningless and/or irrelevant content included in the article
- (6) Peer-review manipulation

The presence of these indicators undermines our confidence in the integrity of the article's content and we cannot, therefore, vouch for its reliability. Please note that this notice is intended solely to alert readers that the content of this article is unreliable. We have not investigated whether authors were aware of or involved in the systematic manipulation of the publication process.

In addition, our investigation has also shown that one or more of the following human-subject reporting requirements has not been met in this article: ethical approval by an Institutional Review Board (IRB) committee or equivalent, patient/participant consent to participate, and/or agreement to publish patient/participant details (where relevant).

Wiley and Hindawi regrets that the usual quality checks did not identify these issues before publication and have since put additional measures in place to safeguard research integrity.

We wish to credit our own Research Integrity and Research Publishing teams and anonymous and named external

researchers and research integrity experts for contributing to this investigation.

The corresponding author, as the representative of all authors, has been given the opportunity to register their agreement or disagreement to this retraction. We have kept a record of any response received.

### References

- [1] L. Ru, B. Zhang, J. Duan et al., "A Detailed Research on Human Health Monitoring System Based on Internet of Things," *Wireless Communications and Mobile Computing*, vol. 2021, Article ID 5592454, 9 pages, 2021.

## Research Article

# A Detailed Research on Human Health Monitoring System Based on Internet of Things

Lei Ru <sup>1</sup>, Bin Zhang <sup>2</sup>, Jing Duan <sup>3</sup>, Guo Ru <sup>4</sup>, Ashutosh Sharma <sup>5</sup>, Gaurav Dhiman,<sup>6</sup>  
Gurjot Singh Gaba <sup>7</sup>, Emad Sami Jaha,<sup>8</sup> and Mehedi Masud <sup>9</sup>

<sup>1</sup>College of Physical Education, Fuyang Normal University, Fuyang 236041, China

<sup>2</sup>Anhui University of Chinese Medicine, Hefei 230012, China

<sup>3</sup>Middle School Affiliated to Fuyang Normal University, Fuyang 236037, China

<sup>4</sup>Graduate School, Beijing Sport University, Beijing 100084, China

<sup>5</sup>Institute of Computer Technology and Information Security, Southern Federal University, Russia

<sup>6</sup>Government Bikram College of Commerce, Punjab, India

<sup>7</sup>School of Electronics and Electrical Engineering, Lovely Professional University, Punjab 144411, India

<sup>8</sup>Department of Computer Science, Faculty of Computing and Information Technology, King Abdulaziz University, Jeddah 21589, Saudi Arabia

<sup>9</sup>Department of Computer Science, College of Computers and Information Technology, Taif University, P. O. Box 11099, Taif 21944, Saudi Arabia

Correspondence should be addressed to Bin Zhang; [binzhang231@outlook.com](mailto:binzhang231@outlook.com) and Mehedi Masud; [mmasud@tu.edu.sa](mailto:mmasud@tu.edu.sa)

Received 25 February 2021; Revised 7 April 2021; Accepted 3 May 2021; Published 15 May 2021

Academic Editor: Deepak Gupta

Copyright © 2021 Lei Ru et al. This is an open access article distributed under the Creative Commons Attribution License, which permits unrestricted use, distribution, and reproduction in any medium, provided the original work is properly cited.

The technological advent in smart sensing devices and the Internet has provided practical solutions in various sectors of networking, public and private sector industries, and government organizations worldwide. This study intends to combine the Internet of Things (IoT) technology with health monitoring to make it personalized and timely through allowing the interconnection between the devices. This work is aimed at exploring various wearable health monitoring modules that people wear to monitor heart rate, blood pressure, pulse, body temperature, and physiological information. The information is acquired using the wireless sensor to create a health monitoring system. The data is integrated using the Internet of Things for processing, connecting, and computing to achieve real-time monitoring. The temperature of three people measured by the temperature thermometer is 36.4, 36.7, and 36.5 (°C), respectively, and the average acquired by the monitoring system of the three people is 36.5, 36.4, and 36.5 (°C), respectively, indicating that the system demonstrated relatively accurate and stable testability. The user's ECG is displayed clearly and conveniently using the ECG acquisition system. The pulse rate of the three people tested by the system is 78, 78, and 79 (times/min), respectively, similar to the medical pulse meter results. The physiological information acquired using the semantic recognition, matching system, and character matching system is relatively accurate. It concludes that the human health monitoring system based on the Internet of Things can provide people with daily health management, instrumental in heightening health service quality and level.

## 1. Introduction

In 2017, the *Report on the Status of Chinese Residents' Nutrition and Chronic Diseases* issued by the Ministry of Health pointed out that the mortality rate of chronic diseases, represented by cardiovascular diseases and diabetes, is about 85.5% each year, and chronic diseases account for about

75% of all diseases in China [1]. Internet healthcare focuses on chronic high-risk diseases and subhealthy groups due to many subhealthy groups, together with the long course, complex etiology, and high treatment costs of chronic diseases. It follows that human health monitoring based on the Internet of Things (IoT) is popularized. As a result of the rapidly expanded aging population in China and the improvement



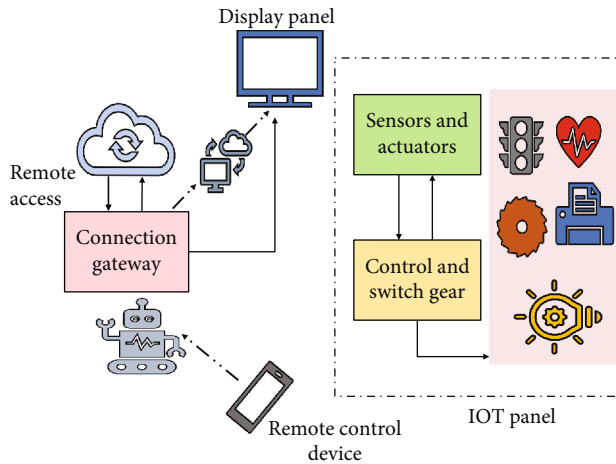


FIGURE 1: IoT architecture.

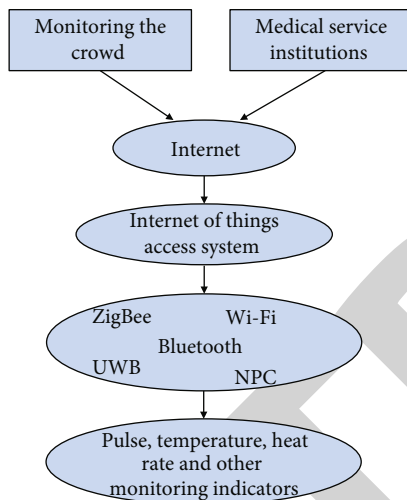


FIGURE 2: The framework of health monitoring and medical information system based on the Internet of Things.

of living standards, the subhealthy population increases with chronic diseases. Creating efficient, convenient, safe, and reliable healthcare conditions and services is a basic need for Chinese people. It is highly urgent to develop a health monitoring system to achieve remote real-time health monitoring [2–4].

IoT technology uses smart sensing devices and the Internet to provide an effective solution to the challenges faced by the networks, public and private sector industries, and government organizations worldwide [5]. The IoT innovations have emerged a new paradigm in using smart systems and intelligent devices to analyze data for various applications [6–10]. A basic IoT structure with generalized architecture is presented in Figure 1.

The various applications [11–15] in which IOT can comprise security and surveillance, automation of agriculture, healthcare, traffic management, the emergence of smart cities, etc. [16–19]. At present, there has not been a unified concept of the Internet of Things. Li Hang defines the Internet of

Things as a kind of Internet that is based on various information sensors, radio frequency identification technology, global positioning system, infrared sensors, light, heat, electricity, machinery, chemistry, biology, location, and other information of a target [20]. Health monitoring is the continuous collection of individual health-related physiological parameters and related influence factors through a certain monitoring system. That follows the process, analysis, and summarization of data to generate health-related information spread to the corresponding individuals or groups, guiding disease prevention and control, promoting health management, and accelerating health conditions.

At present, there is a variety of studies on human health monitoring systems based on the Internet of Things worldwide. The development of human health monitoring systems based on the Internet of Things in foreign countries is earlier than that in China. Significant progress has been made in remote consultation and remote monitoring of blood pressure, blood glucose values, and some medical data (long-distance transmission). Rezaeibagha and Mu [21] designed an Agent system that can monitor vital signs such as blood pressure, pulse, respiratory rate, and body temperature, which was connected to wireless sensors. Agnisarman et al. [22] have designed a remote video medical diagnosis system, which used the Internet of Things technology to facilitate the doctor's medical diagnosis process, with multifunctional modes such as online consultation and video dialogue. Mugica et al. [23] designed an ECG monitor matched with the Android system's intelligent terminal to realize remote monitoring. Tamilselvi et al. [24] proposed a health monitoring system that can assess patients' primary symptoms like their oxygen level, body temperature, and eye movement using the IoT platform. Acharya et al. [25] developed a kit for healthcare monitoring using the IoT platform to assess the parameters like a heartbeat, ECG, temperature, and respiration using various intelligent sensors. The major limitation of this system is that data visualization is ineffective due to the lack of interface. A pulse rate detection system was presented by Banerjee et al. [26] using a noninvasive method. This method uses a real-time monitoring platform for interactive IoT applications. Gregoski et al. [27] presented a smartphone-based technique for heart rate monitoring using mobile and camera interaction. Oresko et al. [28] developed a smartphone interactive tool for identifying cardiovascular diseases to monitor the level of heart rate during the progression of time. Trivedi et al. [29] developed a mobile-based method for monitoring analog data for surveillance applications. The Arduino platform is used for digital conversion, and Bluetooth transmission is required to transmit physical quantities to the device. Kumar et al. [30] suggested a safety device incorporating the IoT platform at three separate layers: control, device, and transport layer. The information is uploaded on the cloud platform using Wi-Fi and Ethernet. Desai et al. [31] proposed a wireless sensor network-based approach to track smart homes and heartbeat monitoring using the Spartan3 and FPGA interface.

IoT's evolution has increased nowadays with smart devices' tremendous ability to share information between them [32]. The reliance on IoT on various applications has

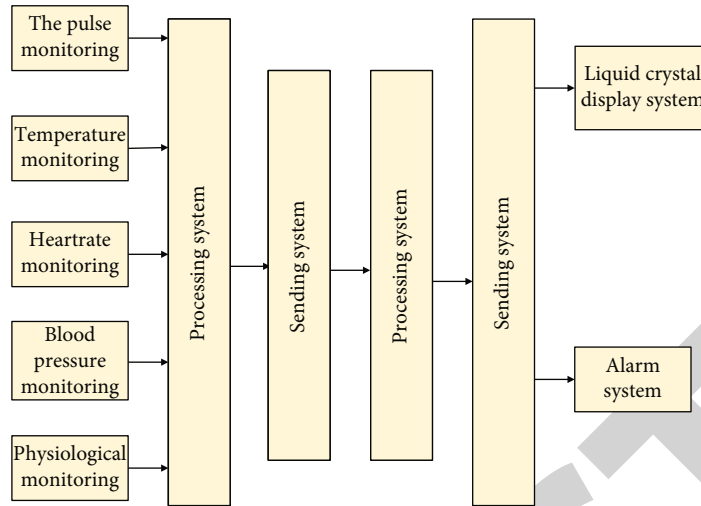


FIGURE 3: The framework of the human health monitoring terminal system.

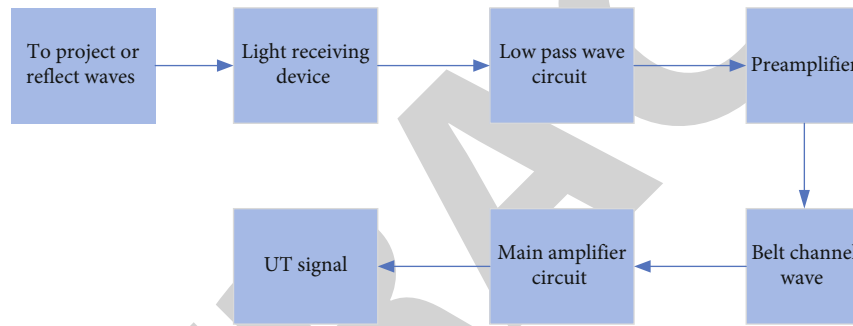


FIGURE 4: The pulse acquisition module diagram.

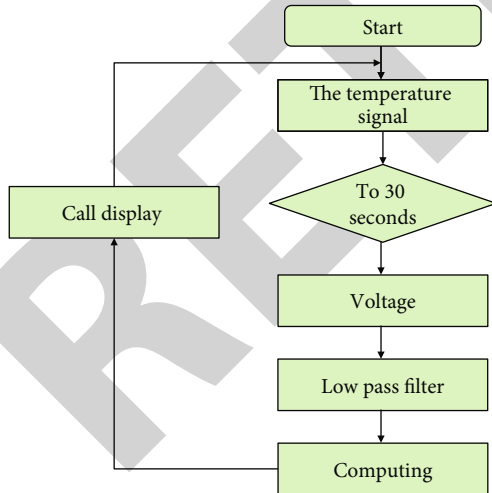


FIGURE 5: The structure diagram of the body temperature collection module.

widened its importance in the healthcare sector for remote monitoring of patients' criticality levels [33, 34]. This technological advent has come across various domains of safety, health, and human wellbeing [35, 36]. IoT is advantageous in computation, processing, and storage utilizing cloud-based solutions [35–37]. It is also beneficial in processing

and storing the geographical data on the cloud platform, which can be shared between the devices for various applications [38, 39]. The current human health monitoring system based on the Internet of Things has some limitations, such as increasing users and uploaded databases, no guarantee for users, poor real-time performance, and low data utilization. A human health monitoring system based on the Internet of Things is designed in this work. The system can uninterruptedly and accurately monitor the human body's heart rate, blood pressure, pulse, body temperature, physiological information, and other vital sign parameters. This work uses wireless sensors to retain the information for health monitoring. The data is integrated using the Internet of Things for processing, connecting, and computing to achieve real-time monitoring. The proposed system demonstrated relatively accurate and stable test ability improving deficiencies in the existing health monitoring platform [40, 41]. This article contributes in daily health management using the human health monitoring system based on the Internet of Things which is instrumental in heightening health service quality and level.

This article is organized as follows: Section 2 presents the material and methods defining the various modules designed for the health monitoring framework. Section 3 presents the results and discussion of the analysis done in this study, followed by the article's concluding remarks in Section 4.

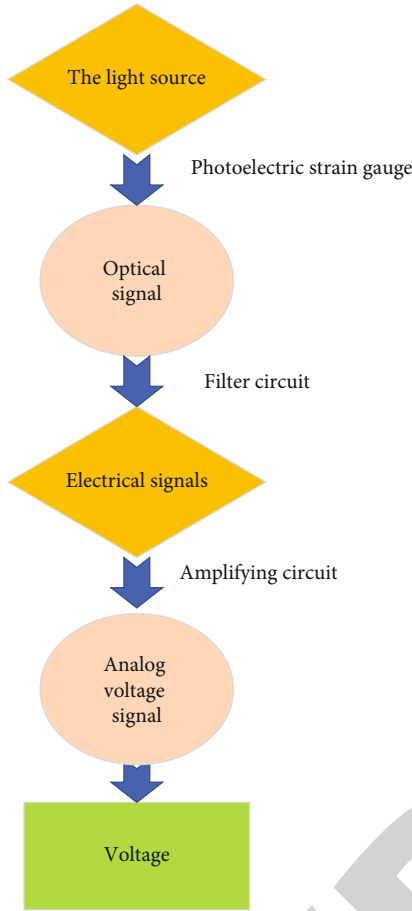


FIGURE 6: The diagram of the heart rate acquisition module.

## 2. Materials and Methods

The health monitoring system using IoT consists of various modules like pulse acquisition module, body temperature acquisition module, heart rate acquisition module, and blood pressure acquisition module. All these frameworks are elaborated in this section.

**2.1. The Framework of the Health Monitoring System Based on the Internet of Things.** The health monitoring and medical information system based on the Internet of Things integrate technologies such as wireless networks and mobile computing, aiming to provide patients with remotely receivable sensing, sound, image, and video multimedia information, enhancing medical diagnosis accuracy the quality of clinical services. The patient's blood pressure, heart rate, body temperature, pulse, and other information can be collected accurately by wearing related equipment. Information is transmitted using sensor network technologies such as Zigbee, Wi-Fi, Bluetooth, ultrawideband, and short-range wireless transmission, as shown in Figure 2.

**2.2. The Framework of Health Monitoring Terminal System Based on Internet of Things Human.** In the human health monitoring system based on the Internet of Things, the terminal system is mainly responsible for collecting and moni-

toring normal human health data. When abnormal data occurs, the terminal's alarm system will raise the alarm. At this time, it is necessary to conduct research and analysis on abnormal data and perform timely data processing. For example, the monitor's specific situation is confirmed first, and then, emergency rescue measures are carried out. Therefore, monitoring various indexes of the subjects is highly critical. To sum up, based on the existing research state quo and results and the market demand, the terminal system's hardware framework is designed for human health monitoring based on the Internet of Things. The terminal is mainly divided into a health monitoring project module, a data acquisition module, a data receiving module, a data transmission module, a data processing module, and a display and alarm module, as shown in Figure 3.

**2.3. Pulse Acquisition Module.** Generally speaking, the photoelectric pulse sensor is divided into two types: transmitted wave monitoring and reflected wave monitoring according to how to detect light [42]. Their key components are the same (i.e., stable light source and light-receiving sensor). The impulse data sensor of Rohm Semiconductor Group is selected in the study, as shown in Figure 4.

**2.4. Body Temperature Acquisition Module.** In this study, the voltage output integrated temperature sensor is selected for the health monitoring system terminal, and the hardware circuit is designed. The digital conversion of the output analog signal is realized through the displayer, as shown in Figure 5.

The temperature sensor converts the temperature signal into a voltage output, performs low-pass filtering on the output signal to remove noise, and then amplifies the temperature sensor output voltage to a voltage level by the amplifier circuit [43].

**2.5. Heart Rate Acquisition Module.** The light volume method's principle is to measure the heart rate using the difference in the blood vessel's light transmittance caused by the pulse's beating [44]. The light source is converted into an optical signal using a photoelectric sensor, and the optical signal is then converted into an electrical signal by a filter circuit. The selected wavelength is 650 nm-750 nm. The signal flow of the heart rate sensor is shown in Figure 6.

When the light passes through human peripheral blood vessels, the volume change caused by pulse congestion affects the light source's light transmittance. The light signal reflected by the photoelectric converter through the human body's peripheral blood vessels is converted and output by the amplifier circuit. The heart rate is output in analog voltage. This value is acquired using the heart rate acquisition module.

**2.6. Blood Pressure Acquisition Module.** Blood pressure monitoring methods can be divided into the direct method and indirect method (Oscillometric method). The indirect method avoids the direct method's shortcomings, such as being complicated and traumatic [45]. It monitors the pressure value on the body surface using the relationship between the vessel's pressure and the FM flow change. It is easy to operate, hygienic and concise without particularly severe

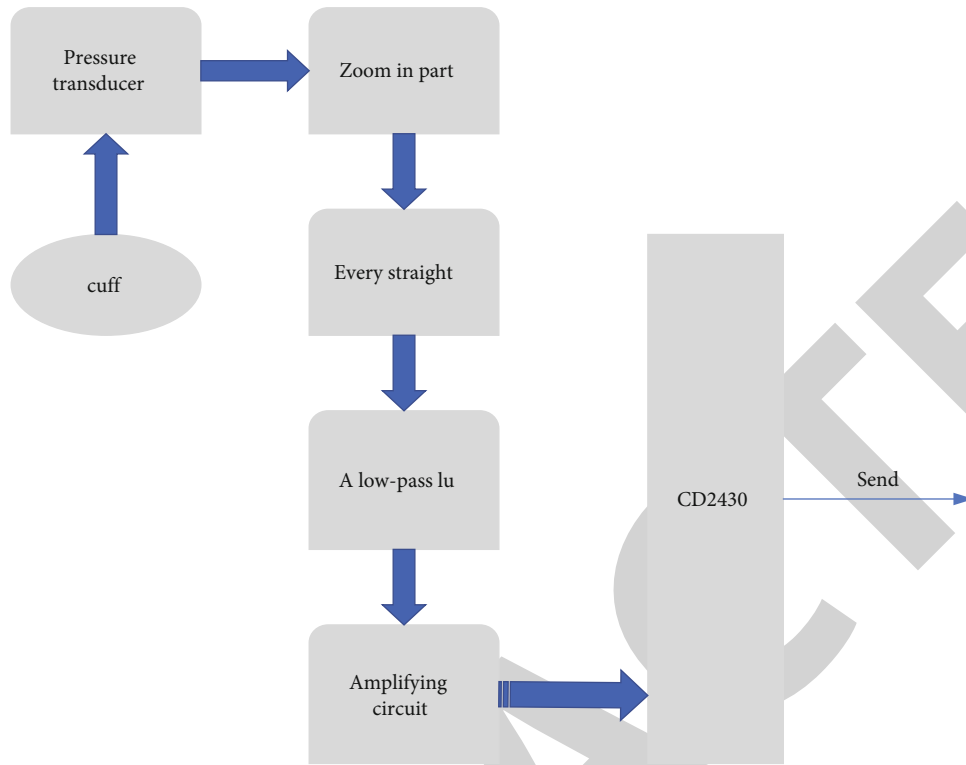


FIGURE 7: The diagram of the blood pressure acquisition module.

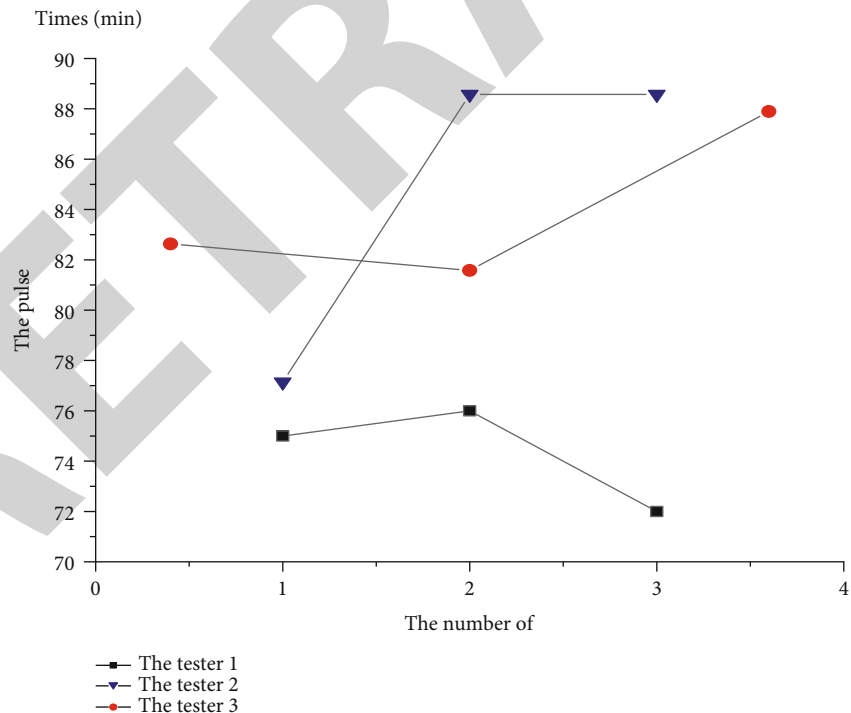


FIGURE 8: The pulse test results.

medical restrictions, and does not harm health. As a result, the indirect method is more commonly used. Not only is the blood pressure monitored without any trauma to the human body but the monitored values are also more accurate [6–15]. The system diagram is shown in Figure 7.

The signal acquisition and processing are dependent on the op-amp LM324. The sensor is a BP300 sensor, which is sensitive, accurate, and precise. Besides, air pumps, resistors, and capacitors are also necessary components. The pressure sensor converts the pressure signal by converting the blood

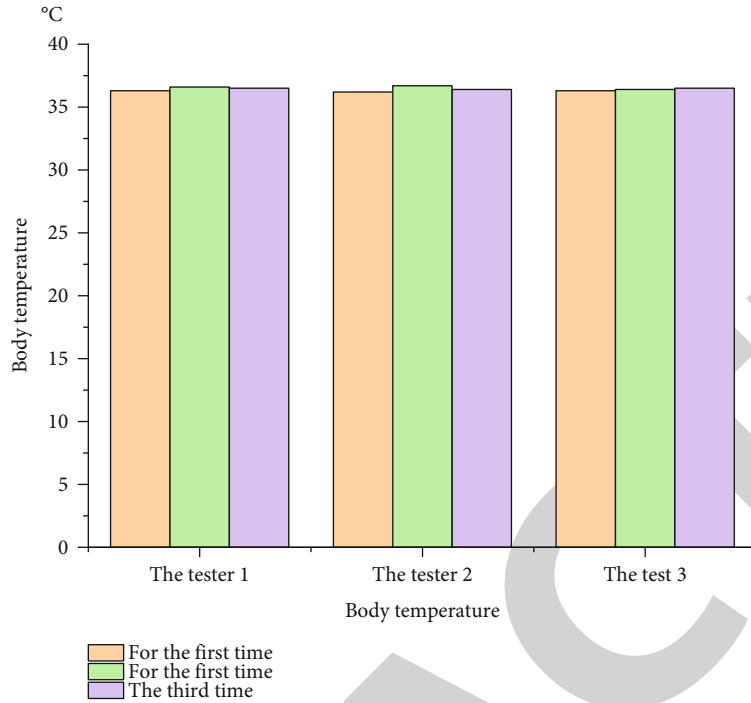


FIGURE 9: The temperature test results.

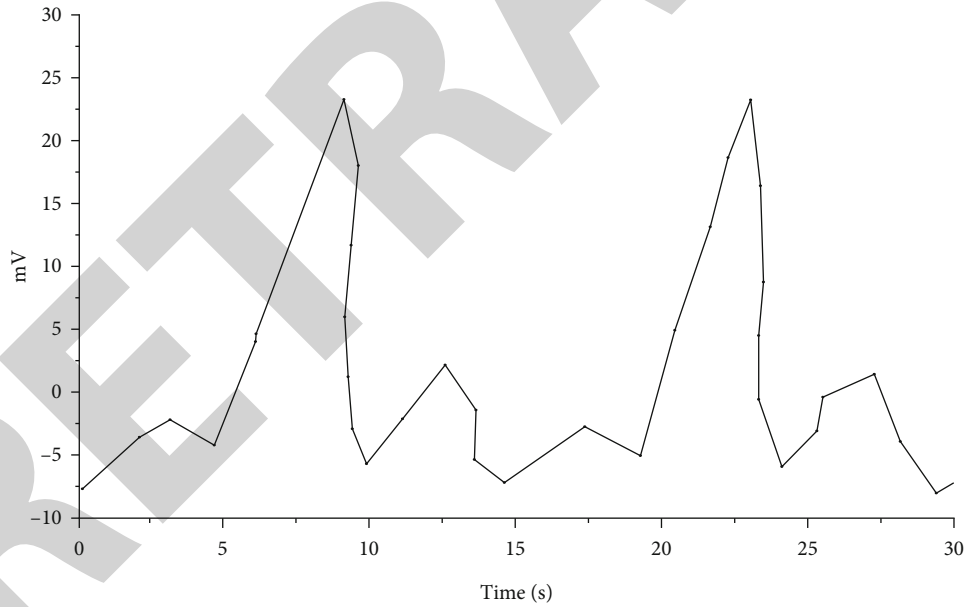


FIGURE 10: The 30-second ECG.

flow pressure signal in the inflatable bandage into a voltage signal close to the microcontroller’s voltage amplitude. The one-chip computer collects and processes the signal and is responsible for the control of the entire circuit.

### 3. Results and Discussion

The experimentation outcomes are analyzed in this section discussing various compliances and assessing outcomes obtained from their implementation. Various modules like

pulse acquisition, body temperature monitoring, ECG, and physiological information acquisition are observed in the upcoming subsections.

*3.1. Compliance Test of the Pulse Acquisition Module.* It is evident from the pulse test results that the three subjects’ pulse values are all within the normal range (the pulse rate of an average adult is 70~90 beats/min). The pulse signal acquisition test is performed three times for each person, and the average pulse value acquired is 78, 78, and 79 (beats/min),



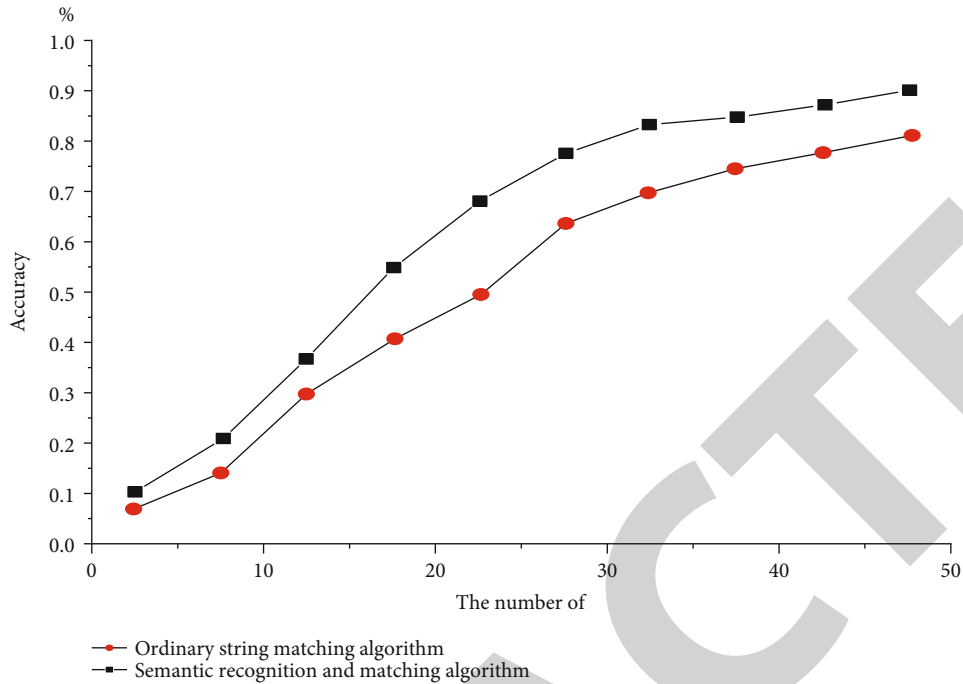


FIGURE 11: The comparison of keyword matching.

respectively. The thermometer's corresponding values are 77, 79, and 78, indicating that the system's test results are relatively accurate, as shown in Figure 8.

Although there is deviation sometimes, it is within the acceptable range. This is because the sensor of the pulse acquisition module is associated with the circuit design. It can be further improved in the future to acquire more accurate results.

**3.2. Compliance Test of Body Temperature Acquisition Module.** Three people were selected as test subjects to conduct temperature measurements to make reasonable judgments on the temperature monitoring module's performance to evaluate the system's accuracy more rigorously.

As shown in Figure 9, three persons' temperature using a thermometer is 36.4°C, 36.7°C, and 36.5°C, respectively. The temperature test was carried out three times for each person, and the average of each person acquired by the system is 36.5°C, 36.4°C, and 36.5°C, respectively. It is evident that this system's measurements are very close to those of a thermometer and can monitor body temperature. It also indicates that the temperature test of this system is relatively stable.

**3.3. Compliance Test of ECG Information Acquisition Module.** In monitoring the ECG information collection module, the first step is to update or load the user's latest ECG measurement record information. Simultaneously, the corresponding detailed operation page will be displayed so that the real-time ECG image is acquired. Considering that the ECG data points are complicated, slight adjustments can be performed in the image's functional area to achieve the best

results to view a particular segment's image curve. The ECG operation interface is shown in Figure 10.

**3.4. The Compliance Test of the Physiological Information Acquisition Module.** It is found that as the number of keywords input by users increases, whether it is a traditional character matching system or not, the accuracy to obtain information is further raised, as shown in Figure 11, to verify the rationality of the semantic recognition and matching system and improve the traditional character matching system, through simulation experiments.

Therefore, in addition to measuring pulse and temperature, users should also be provided with more physiological-related information to understand their physical condition better.

## 4. Conclusion

In the study, the wireless sensor technology is combined with the human health monitoring terminal based on the Internet of Things to test the health-related indexes. The test results are analyzed. It is observed that the human health monitoring system of the Internet of Things is relatively stable and has functions such as an accurate collection of human health data, real-time monitoring and alarming, and evaluation of subjects. The subjects were assessed for temperature using the thermometer, which provides the temperature values of 36.4, 36.7, and 36.5 (°C), respectively, demonstrating relatively accurate and stable testability. Similarly, the pulse rate monitoring module employing the ECG observes the test outcomes of 78, 78, and 79 (times/min), respectively, similar to the medical pulse meter results.

The human health monitoring system based on the Internet of Things designed in this study has completed collecting the user's blood pressure, pulse, body temperature, heart rate, physiological information, and other vital sign data, which is suggested in practice. After long-term data collection, factors related to a potential risk prediction should be further explored in the future to expand the application of human health monitoring systems based on the Internet of Things. This will provide a scientific and effective basis for preventing and controlling chronic high-risk diseases in the near future.

## Data Availability

All data is shared in the manuscript.

## Conflicts of Interest

The authors declare that they have no conflicts of interest.

## Acknowledgments

The authors would like to thank for the support of the Taif University Researchers Supporting Project (No. TURSP-2020/10), Taif University, Taif, Saudi Arabia.

## References

- [1] C. O'Brien and C. Heneghan, "A comparison of algorithms for estimation of a respiratory signal from the surface electrocardiogram," *Computers in Biology and Medicine*, vol. 37, no. 3, pp. 305–314, 2007.
- [2] R. E. Nappi, E. Martini, L. Cucinella et al., "Addressing vulvovaginal atrophy (VVA)/genitourinary syndrome of menopause (GSM) for healthy aging in women," *Frontiers in Endocrinology*, vol. 10, p. 561, 2019.
- [3] A. Bansal, S. Kumar, A. Bajpai et al., "Remote health monitoring system for detecting cardiac disorders," *IET Systems Biology*, vol. 9, no. 6, pp. 309–314, 2015.
- [4] G. Dhiman, D. Oliva, A. Kaur et al., "BEPO: a novel binary emperor penguin optimizer for automatic feature selection," *Knowledge-Based Systems*, vol. 211, p. 106560, 2021.
- [5] K. Gatsis and G. J. Pappas, "Wireless control for the IoT," in *Proceedings of the Second International Conference on Internet-of-Things Design and Implementation*, pp. 341–342, 2017 Apr 18.
- [6] S. Kaur, L. K. Awasthi, A. L. Sangal, and G. Dhiman, "Tunicate swarm algorithm: a new bio-inspired based metaheuristic paradigm for global optimization," *Engineering Applications of Artificial Intelligence*, vol. 90, p. 103541, 2020.
- [7] G. Dhiman and A. Kaur, "Spotted hyena optimizer for solving engineering design problems," in *2017 International Conference on Machine Learning and Data Science (MLDS)*, pp. 114–119, Noida, India, 2017.
- [8] G. Dhiman and A. Kaur, "STOA: a bio-inspired based optimization algorithm for industrial engineering problems," *Engineering Applications of Artificial Intelligence*, vol. 82, pp. 148–174, 2019.
- [9] G. Dhiman and A. Kaur, "A hybrid algorithm based on particle swarm and spotted hyena optimizer for global optimization," in *In Soft computing for problem solving*, pp. 599–615, Springer, Singapore, 2019.
- [10] A. Kaur and G. Dhiman, "A review on search-based tools and techniques to identify bad code smells in object-oriented systems," in *In Harmony search and nature inspired optimization algorithms*, pp. 909–921, Springer, Singapore, 2019.
- [11] G. Dhiman and A. Kaur, "Optimizing the design of airfoil and optical buffer problems using spotted hyena optimizer," *Designs*, vol. 2, no. 3, p. 28, 2018.
- [12] A. Kaur, S. Kaur, and G. Dhiman, "A quantum method for dynamic nonlinear programming technique using Schrödinger equation and Monte Carlo approach," *Modern Physics Letters B*, vol. 32, no. 30, p. 1850374, 2018.
- [13] P. Singh, G. Dhiman, and A. Kaur, "A quantum approach for time series data based on graph and Schrödinger equations methods," *Modern Physics Letters A*, vol. 33, no. 35, p. 1850208, 2018.
- [14] G. Dhiman and A. Kaur, "HKn-RVEA: a novel many-objective evolutionary algorithm for car side impact bar crashworthiness problem," *International Journal of Vehicle Design*, vol. 80, no. 2/3/4, p. 257, 2019.
- [15] A. Kaur, S. Jain, S. Goel, and G. Dhiman, "A review on machine-learning based code smell detection techniques in object-oriented software system(s)," *Recent Advances in Electrical & Electronic Engineering (Formerly Recent Patents on Electrical & Electronic Engineering)*, vol. 14, no. 3, pp. 290–303, 2021.
- [16] M. Poongodi, M. Hamdi, A. Sharma, M. Ma, and P. K. Singh, "DDoS detection mechanism using trust-based evaluation system in VANET," *IEEE Access*, vol. 7, pp. 183532–183544, 2019.
- [17] J. Dogra, S. Jain, A. Sharma, R. Kumar, and M. Sood, "Brain tumor detection from MR images employing fuzzy graph cut technique," *Recent Advances in Computer Science and Communications*, vol. 13, no. 3, pp. 362–369, 2020.
- [18] G. Rathee, A. Sharma, R. Kumar, F. Ahmad, and R. Iqbal, "A trust management scheme to secure mobile information centric networks," *Computer Communications*, vol. 151, pp. 66–75, 2020.
- [19] H. B. Hassen, N. Ayari, and B. Hamdi, "A home hospitalization system based on the Internet of things, Fog computing and cloud computing," *Informatics in Medicine Unlocked*, vol. 20, p. 100368, 2020.
- [20] M. M. Islam, A. Rahaman, and M. R. Islam, "Development of smart healthcare monitoring system in IoT environment," *SN Computer Science*, vol. 1, no. 3, 2020.
- [21] F. Rezaeibagha and Y. Mu, "Practical and secure telemedicine systems for user mobility," *Journal of Biomedical Informatics*, vol. 78, pp. 24–32, 2018.
- [22] S. O. Agnisarman, K. Chalil Madathil, K. Smith, A. Ashok, B. Welch, and J. T. McElligott, "Lessons learned from the usability assessment of home-based telemedicine systems," *Applied Ergonomics*, vol. 58, pp. 424–434, 2017.
- [23] F. Mugica, À. Nebot, S. Bagherpour, L. Baladón, and A. Serrano-Blanco, "A model for continuous monitoring of patients with major depression in short and long term periods," *Technology and Health Care*, vol. 25, no. 3, pp. 487–511, 2017.
- [24] V. Tamilselvi, S. Sribalaji, P. Vigneshwaran, P. Vinu, and J. GeethaRamani, "IoT based health monitoring system," in *2020 6th International Conference on Advanced Computing and Communication Systems (ICACCS)*, pp. 386–389, Coimbatore, India, 2020.